

Preface



International Conference on Industrial Engineering has taken place on October 22-23, 2015. The event was organized by South Ural State University (national research university), Chelyabinsk, Russian Federation. The Conference was held at two venues, with the main venue at South Ural State University, Chelyabinsk, and an additional venue at Platov South-Russian State Polytechnic University, Novocherkassk, Rostov region, Russian Federation. Throughout the course of the Conference, both venues were connected via a televised communication link. Besides, an online broadcast of its panels was organized for both days of the event.

This brand new feature enabled Conference-wide communication without any need for long trips. At jointly-held panels, the participants at both venues delivered their presentations by turns. The attendees could ask each other questions regardless of anyone's particular location.

The Conference was truly international and magnificent in scale. The Program Committee elected 194 reports out of more than 260 submissions. The event had participants from the UK, Germany, India, Kazakhstan, Kyrgyzstan, Ukraine, Russian cities of Barnaul, Volgograd, Yekaterinburg, Magnitogorsk, Moscow, Murom, Novosibirsk, Novocherkassk, Omsk, Perm, Rostov, St. Petersburg, Ufa, and Chelyabinsk.

The participants presented their research on the latest state-of-the-art developments in Industrial Engineering, in English and Russian. The Conference consisted of 10 panels, including:

Part 1. Research and development of machines and mechanisms:

- 1.1. Dynamics of machines and workings processes;
- 1.2. Design-engineering issue of industrial facilities;
- 1.3. Surface transport production machines.

Part 2. Materials engineering and technologies for production and processing:

- 2.1. New functional materials and technologies;
- 2.2. Innovation and cost-effective use of resources of metallurgy industry.

Part 3. Systems of control and automation for manufacturing in the areas of industrial production:

- 3.1. Automotive electromechanical systems;
- 3.2. Power supply systems;
- 3.3. Electrotechnological complexes and systems;
- 3.4. Industrial mechatronics and robototronics systems;
- 3.5. Control systems and control technologies;
- 3.6. Simulation and computing technologies.

As a result, the Program Committee elected 161 papers to be published in the *Procedia Engineering* journal (Elsevier Ltd.).

Organising committee would like to express our sincere appreciation to everybody who has contributed to the conference. Heartfelt thanks are due to authors, reviewers, participants and to all the team of organizers for their support and enthusiasm which granted success to the conference.

Conference Chair, prof. Andrey A. Radionov and Program Co-Chair, prof. Oleg A. Kravchenko.



International Conference on Industrial Engineering

Improving electric power quality within the power supply system of wide-strip hot-rolling mill stand

Karandaev A.S.^{a,b}, Kornilov G.P.^b, Khramshin V.R.^b, Khramshin T.R.^{b,*}

^aSouth Ural State University, 76, Lenin Avenue, Chelyabinsk, 454080, Russian Federation

^bNosov Magnitogorsk State Technical University, Lenina Av. 38, Magnitogorsk, 455000, Russia

Abstract

The paper proposes studies of electric power quality indexes for 10 kV network supplying electric drives of the wide-strip hot-rolling mill stand equipped with thyristor electric drives. It provides the power supply diagram of the plate rolling shop. Information on the methods of experimental studies of the current and voltage spectral distribution with the use of a standard measuring device and software is provided. The paper shows the nature of higher-order harmonics content for units of the 10 kV distribution substation. It considers the method and system for reactive power control in the load center that ensures a step power change of the reactive-power compensator batteries and the following smooth fine adjustment by automatic control of synchronous motor excitation current. According to the algorithm proposed condenser batteries shall be operated in the basic mode and compensate a semi-constant component of reactive power.

© 2015 The Authors. Published by Elsevier Ltd. This is an open access article under the CC BY-NC-ND license (<http://creativecommons.org/licenses/by-nc-nd/4.0/>).

Peer-review under responsibility of the organizing committee of the International Conference on Industrial Engineering (ICIE-2015)

Keywords: electric network; hot-rolling mill; thyristor electric drive; spectral current distribution; measuring device; experimental researches; reactive power; compensation; control systems; algorithm.

1. Introduction

An essential condition for fault-free power supply of the industrial enterprise is a stable power consumer supply of the required amount and quality specified by national and international standards. Here, power consumers with

* Corresponding author. Tel.: +79049759803.
E-mail address: hvrngn@gmail.com

non-linear current/voltage diagrams (thyristor converters used for supply of high-power DC electric drives) mainly effect electric power quality [1, 2].

Typical examples are power supply systems of the plate rolling shops where one power supply source provides electric power for quiescent loads (descaler pumps, vents, etc.) and stands of the rolling mill featuring Thyristor-Converter-Motor electric drives. That is why, voltage fluctuation and deviations may be observed within the distribution shop networks; their sources are thyristor converters [3]. Furthermore, these networks have a low power factor resulting in reactive-power shortage of the system [4]. These specific parameters of power supply are fully characteristic for the plate rolling shop No. 10 (PRS-10) at OJSC Magnitogorsk Iron and Steel Works (OAO MMK) with its major unit – the 2,000 mm hot-rolling mill.

The PRS-10 power supply system is shown in Fig. 1. The following voltages are used for supply of power equipment:

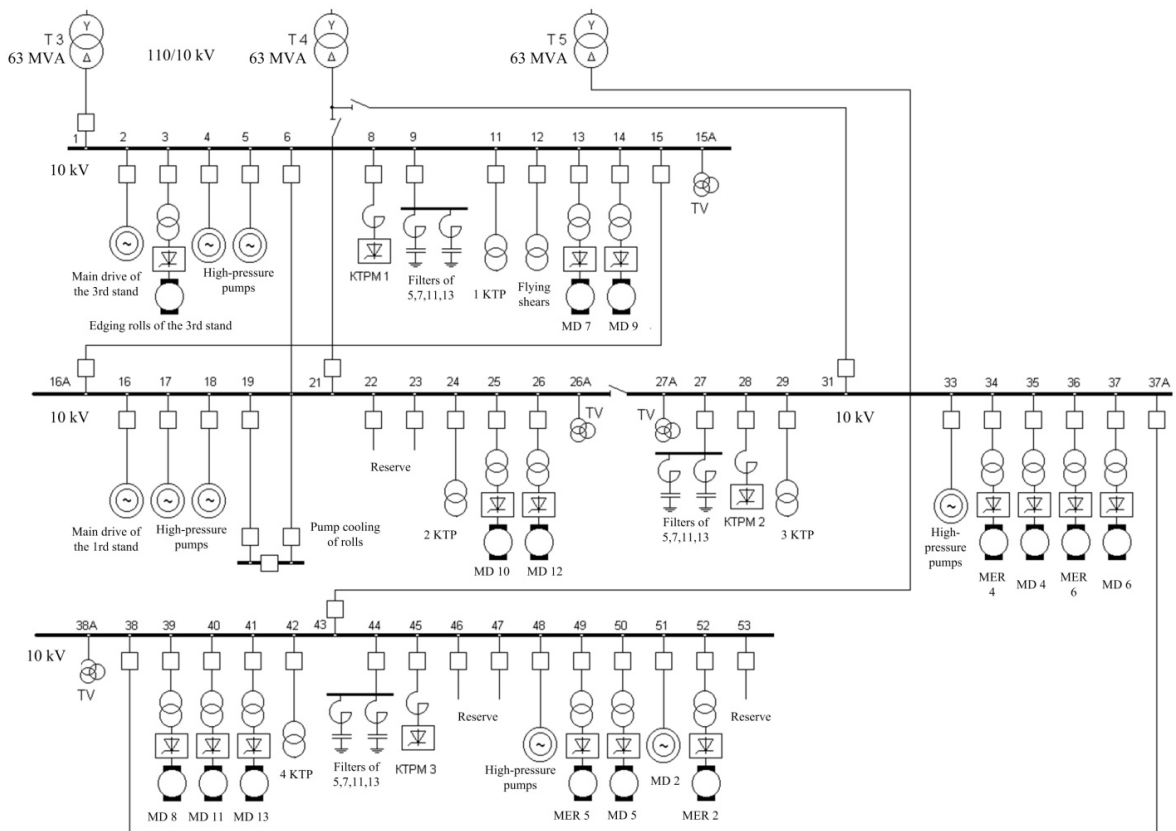


Fig. 1. Diagram of power supply for the 10 kV distribution substation (DS) of PRS-10

- 10 kV – for three synchronous motor of main electric drives of roughing stands No. 1-3, pumps for roll cooling, high-pressure pumps as well as thyristor converters of main electric drives of stands No. 4-13 and flying shears;
- 6 kV – for supply of asynchronous and synchronous 200–1600 kW motors as well as thyristor converters of auxiliary electric drives and step-down transformers of the complete transformer substations.

Total capacity of power consumers at 10 kV voltage is as follows:

- synchronous motors: 35 MW;
- thyristor electric drives: 140.6 MW;

Total capacity of power consumers at 6 kV voltage is as follows:

- synchronous motors: 24.5 MW;
- asynchronous motors: 21.5 MW;
- thyristor electric drives: 29.2 MW;

According to the technical project for the 10 kV network of the 2,000 mm mill, 3 packages of VAR compensators were provided; each of them contains a 20 MVAR thyristor and reactor set as well as filters of the 5th, 7th, 11th and 13th 6.3 MVAR harmonics. Gross capacity of condenser batteries should be about 90 MVAR to provide the following data in accordance with the project:

- increasing the power factor to 0.93 at 10 kV busbars and to 0.91 – at 6 kV busbars;
- reducing voltage fluctuations within the 10 kV network to the $\delta U \leq 5.0\%$ value, within the 110 kV network to $\delta U \leq 1.0\%$.
- decrease of the voltage non-sinusoidality at 6-10 kV busbars to the level of 4–5%.

Unfortunately, these compensation filter devices are not being operated at present. Their absence results in the current and voltage harmonic content deterioration and raise of losses, so, is intolerable. Based on calculations, the reactive-power shortage is more than 120 MVAR while non-sinusoidality of the voltage waveform is as high as 16–18%.

In view of the foregoing, of special interest is estimation of an actual current harmonic content and voltage distortion at 10 kV units of the 2,000 mm mill. Its results shall be a foundation for elaboration of measures to improve electric power quality indexes. Moreover, there is a challenge to develop a quick-response system providing compensation of reactive power.

2. Main Part

Distortions of supply voltage at thyristor converter operation are known to be caused by valve switching that is followed by a short-term phase short circuit. The distortion form and amplitude depend on the rectification circuit, converter output and parameters of the supply main. These distortions occurs periodically; this enables their harmonic analysis.

Switching processes in the thyristor converters accompanied by step changes of circuit parameters are known to result in voltage distortion of the supply main [5].

2.1. Experimental study of voltage in the power supply main of the rolling mill

Electric signal were logged with RES-3 recorder with sampling frequency of 4.5 kHz. The connection diagram of the device is shown in Fig. 2. Then, signals were processed with specifically developed applications within the Matlab framework.

Oscyllograph analysis established current and voltage form deviations from the sine-wave ones at all units of the 10 kV DS resulting from the non-linear load predomination. By means of the harmonic analyzer, the most significant harmonics being present in the current curve were determined, that is, the 5th, 11th and 13th harmonics (Fig. 3). The operating principle of the harmonic analyzer is based on the short-time Fourier transform of the examined signal at the set interval which duration amounts 10–15 periods of the fundamental frequency [6]. The application of the pickup signal superposition (so termed "Hann window") enables impairing the edge effect appearing at inequality of the elementary frequency period to the sampling one.

However, the harmonic analyzer helps only to distinguish the most essential harmonics but not to follow their alternation in time. Resonance filters configured to the frequency of the harmonics to be distinguished and implemented within the Matlab Simulink software framework should solve this task.

Fig. 4 shows oscyllographs of the effective range of current and its harmonic constituents at the time interval of 5 minutes for the unit under consideration. Similar oscyllographs were obtained for four units of the 10 kV DS shown in Fig. 1 (units 1, 2A, 2B, 3). The analysis of the oscyllographs provided in [7] enables the following conclusions:

1. In the current curves of the fundamental harmonic, we may observe cyclic variations with 50–100 sec. period connected with rolling process cycle.

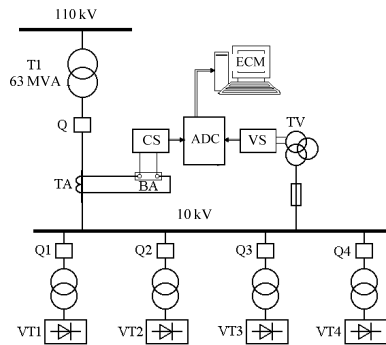


Fig. 2. Connection diagram of the RES-3 device for recording current and voltage oscillographs: T1 – 110/10 kV main transformer; TA, TV – current transformer and voltage transformer, CS, VS– current and voltage sensors; BA –shunt; RES-3 – electric signal recorder; ECM – electronic computing machine (industrial computer); VT – thyristor converter; Q – circuit breaker.

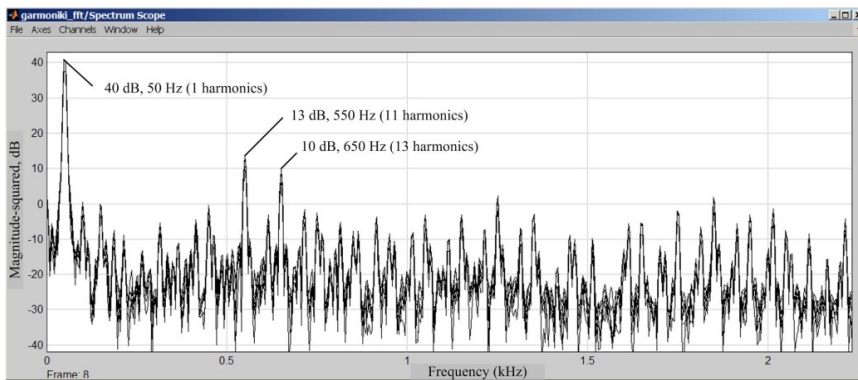


Fig. 3. Current spectrogram of the first unit of the 10 kV DS

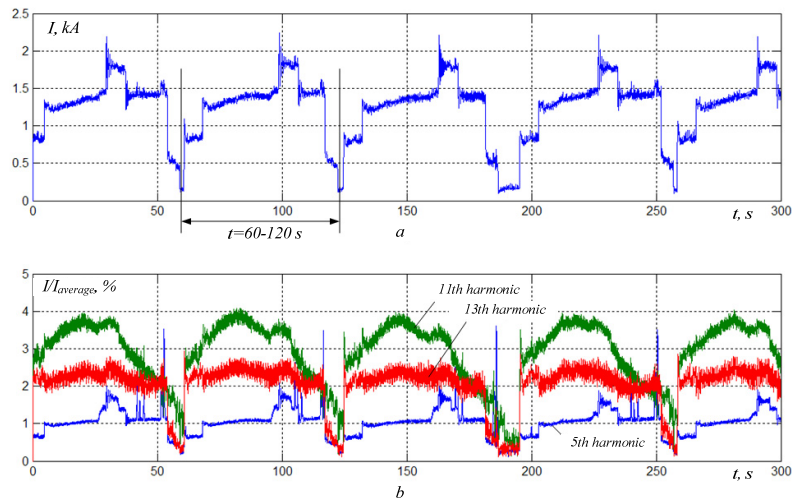


Fig. 4. Fragment of effective range of current of 10 kV DS unit No. 1 (a) and its 5th, 11th and 13th harmonic constituents (b)

2. The nature of the level change of the higher-order harmonics mainly correspond to the current alteration of the fundamental harmonic. Considering all sections, the level of the 5th harmonics does not exceed 1%, the 13th one–2%, the 11th one –5%. The level of the 7th harmonics is less than 1% , so it was not taken into consideration.

3. There is an explicit dependence between currents of the 5th and fundamental harmonics at unit No.1, yet current surges of the 5th harmonic appear in some chart areas at load relief. At this, these processes do not influence on the 11th and 13th harmonics explicitly. The behavior of these harmonics features more stability, so filters may be selected and configured according to the average current values of these harmonics only.

2.2. Development of the system for main voltage quality control

Based on the conducted researches, we offer the method for reactive power control in the load center that ensures a step power change of the reactive-power compensator batteries and the following smooth fine adjustment by automatic control of synchronous motor (SM) excitation current. We have developed the system for automatic control of the power factor compensation devices and improvement of the harmonic voltage content; its diagram is shown in Fig. 5 [8]. System input signals comes from outputs of the voltage and reactive current sensors installed at bus-bars of the 10 kV DS as well as of the current sensors of the finishing stands' thyristor converters and exciting current sensors of the roughing stands' SM. These elements constitute the first (lower) level of the control system. As a logic-control unit, the industrial controller with corresponding software is used.

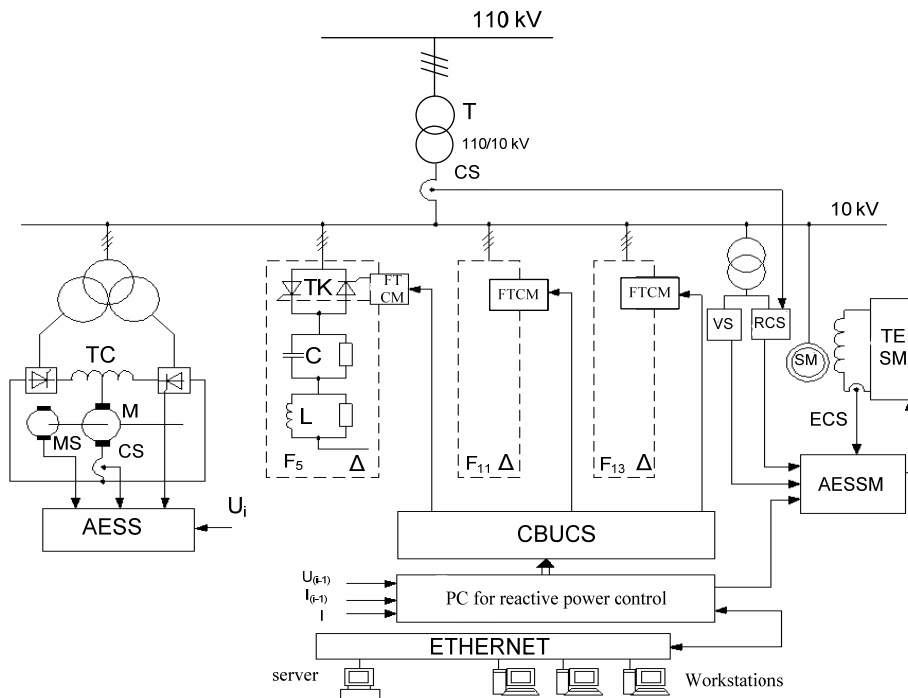


Fig. 5. Structural diagram of the reactive power control system at 10 kV busbars: T – 110/10 kV main transformer; TC– thyristor converter; M – DC motor; TK – thyristor key; L – reactor coil; C – capacitor battery; TE – thyristor exciter; SM– synchronous motor; VS– voltage sensor; RCS – reactor current sensor; CS– current sensor of the stand electric drive; ECS – SM's exciter current sensor; IC– industrial controller; AES– automated exciter system of the SM; CBUCS– capacitor battery unit control system; FT-CM– filter thyristor control modules

It processes received data in the real-time mode, compares reactive-power balance and issues commands to the system of automated control of synchronous motor excitation and capacitor battery control system [9]. As a result, capacitor output is established due to the selection of the required step number and time of their actuation.

The system is based on the three-level principle; it consists of power components, the system controlling the SM excitement, thyristor key control system, industrial controller, devices for data capture and processing as well as data and command communication channels [10]. Components of the higher level are existing servers and workstations of the automated energy resource control system (AERCS) and process control system (PCS) of the mill.

When setting the rolling shape known beforehand, active power according to the stands and control preferences (voltage stability, minimum level of reactive power consumption, etc.), one can implement a feed-forward adaptive control within the proposed system and improve information awareness of the electrical and process personnel, thus, to add functionality of existing AERCSs and PCSs.

If there are two and more reactive power sources (compensating device and synchronous motor) with different operating principles, their simultaneous control will be difficult due to various response times. Therefore, static and dynamic errors are possible. They result in reactive power and voltage fluctuations causing failures of the equipment. In connection with these facts, there is a challenge to develop a control algorithm considering the response time and switching sequence.

The main control principle is explained with time diagrams presented in Fig. 6. Capacitor batteries are operated in the basic mode and provide compensating a semi-constant component of reactive power corresponding to the rolled strip gauge. Reactive power fluctuations caused by stand load alteration are eliminated due to the excitement current control of SM operating in the mode of an additional controller with constantly changing reactive power for smooth adjustment of the main controller. The gross capacity is specified by the general reactive power compensation setting where the main controller sets generation of lacking power only under power shortage condition.

The step number and power of each of them are selected so as gross power of the capacitor battery shall be less than that of the thyristor converter by the value not exceeding the SM reactivity worth under steady-state operational mode of electric drives of one stand or two. This mode is conditioned by the need to provide stability of the synchronous motor. The reason for this is that its operation with excitement current being less than no-load current (i.e. at the left of U-diagram) is inadmissible under the specified operating conditions.

To establish feasibility of the proposed reactive power control method, the compensating capabilities of the 2,000 mm mill roughing train SM were estimated. The estimation relied on the analysis of electrical load charts and preliminary calculation of the compensating device power according to the 10 kV units. Levels of available reactive power of SM were determined at various rolling programs given that root-mean-square excitement current does not exceed the rated value ($Q_{av100\%}=4.4$ MVar) and 75% of the rated one ($Q_{av75\%}=1.6$ MVar) for an operational cycle. More accurate values for reactive powers generated and SM excitation current settings in the developed system are calculated automatically in the real-time mode depending on the actual rolling gauge and active power load of the SM.

Before commissioning, filters are adjusted to the acceptor resonance by changing tun number of the air reactor coil. Filters are connected to the network through the substation integration modules and devices in the electric control room consequently, in increasing order of harmonic numbers.

3. Conclusions

1. Oscillographic testing currents and voltages of 10 kV units of PRS-10 at OJSC Magnitogorsk Iron and Steel Works has proved a significant effect of non-linear loads on voltage deviations, fluctuations and non-sinusoidality of the supplying network. Here, available compensating devices do not provide a full compensation of reactive power and voltage level control.

2. To examine current and voltage harmonic content of the 10 kV units, an ingenious software and hardware suit has been developed; it ensures recording and analyzing momentary load current and main voltage values on the basis of the PC's RES-3 electric signal recorder. Software include the Matlab Simulink package enabling estimation of present higher-order harmonic components as well as tracing their trends during operation of the power consumers.

3. Voltage non-sinusoidality and harmonic current content of four 10 kV distributing units have been experimentally studied. As a result, the most significant harmonics in the current curve have been determined: the 5th, 11th and 13th. It helps to substantiate the parameter selection of compensating devices to be developed.

4. We propose the method and system for reactive power control in the load center that ensures a step power change of the reactive-power compensator batteries and the following smooth fine adjustment by automatic control of synchronous motor excitation current.

5. The control algorithm has been offered and implemented; according to this algorithm, the capacitor batteries provide compensating a semi-constant component of reactive power corresponding to the rolled strip gauge while its fluctuations caused by load alteration of separate stands are eliminated due to the excitement current control of the synchronous motor operating in the mode of an additional controller.

Acknowledgements

This research was performed with financial support in the form of a grant from the President of the Russian Federation (Grant No. MD-3395.2015.8)

References

- [1] A.S. Karandaev, G.P. Kornylov, A.A. Nikolaev, P.A. Pushkarev, Peculiarities of reactive power compensation at large iron and steel works, *Industrial Power Engineering*. 12 (2010) 43–49.
- [2] A.S. Maklakov, A.A. Radionov, EMC evaluation of three level NPC converter based on space vector PWM, *Proceedings of the 2015 IEEE North West Russia Section Young Researchers in Electrical and Electronic Engineering Conference, EIConRusNW 2015*. (2015) 236–240. DOI: 10.1109/EIConRusNW.2015.7102269
- [3] G.P. Kornylov, A.N. Shemetov, T.R. Khrumshin, Ju. P. Zhuravlev, E.A. Semenov, Reactive power control in power supply systems with mill heavy-duty thyristor converters, *Industrial Power Engineering*. 1 (2008) 39–44.
- [4] A.S. Maklakov, A.A. Radionov, Integration prospects of electric drives based on back to back converters in industrial smart grid, *2014 12th International Conference on Actual Problems of Electronic Instrument Engineering, APEIE 2014 – Proceedings*. (2014) 770–774. DOI: 10.1109/APEIE.2014.7040790
- [5] V.R. Khrumshin, R.R. Khrumshin, A.S. Karandaev, V.N. Medvedev, Methodic of calculation of the non-sinusoidal voltage index within electrical networks with high-voltage frequency convertors. *Proceedings of the 2015 International Siberian Conference on Control and Communications (SIBCON–2015)*. (2015) 6. DOI 10.1109/SIBCON.2015.7147262.
- [6] M.M. Fotiev, Power losses within circuits with thyristor converters, *Higher School Bulletin. Power Engineering*. 2 (1976) 43–48.
- [7] Yu.P. Zhuravlev, G.P. Kornylov, A.S. Karandaev, Study of voltage and current harmonic content at 10 kV busbars of wide-strip hot-rolling mill, *Bulletin of Nosov State Technical University*. 2 (2007) 65–68.
- [8] G.P. Kornylov, A.S. Karandaev, A.A. Nikolaev, A.N. Shemetov, T.R. Khrumshin, V.R. Khrumshin, A.G. Medvedev, *Compensating devices in industrial power supply systems*, Nosov Magnitogorsk State Technical University, Magnitogorsk, 2012.
- [9] A.A. Radionov, A.S. Maklakov, E.A. Karyakina, New control method of back to back converter, *2015 International Siberian Conference on Control and Communications, SIBCON 2015 – Proceedings*. (2015). DOI: 10.1109/SIBCON.2015.7147135
- [10] A.A. Radionov, A.S. Maklakov, V.R. Gasiyarov, Smart Grid for main electric drive of plate mill rolling stand, *Proceedings of 2014 International Conference on Mechanical Engineering, Automation and Control Systems, MEACS 2014*. (2014). DOI: 10.1109/MEACS.2014.6986842

International Conference on Industrial Engineering

Study of self-starting high-voltage variable frequency electric drives

Khramshin V.R.^a, Karandaev A.S.^{a,b}, Khramshina E.A.^a, Kosmatov V.I.^{a,*}

^aNosov Magnitogorsk State Technical University, Lenina Av. 38, Magnitogorsk, 455000, Russia

^bSouth Ural State University, 76, Lenin Avenue, Chelyabinsk, 454080, Russian Federation

Abstract

The paper compares transient processes of self-starting non-controlled and variable frequency electric drives (VFED) at short-term power supply interruptions. It offers simplified dependencies for calculating duration of transient processes of the individual self-starting asynchronous motor. The study defines reasons for increasing speed recovery time of this assembly. It distinguishes main differences of self-starting the variable frequency and non-controlled electric drives with or without the Flying Start function in the algorithms of the frequency converter. Results of the experimental studies of self-starting high-voltage VFED with the Power Flex 7000 frequency converter are presented. The paper proposes guidelines to provide continuous operation of the essential units at the power supply interruptions. It also emphasizes developments aimed to improve VFED self-starting conditions.

© 2015 The Authors. Published by Elsevier Ltd. This is an open access article under the CC BY-NC-ND license (<http://creativecommons.org/licenses/by-nc-nd/4.0/>).

Peer-review under responsibility of the organizing committee of the International Conference on Industrial Engineering (ICIE-2015)

Keywords: high-voltage asynchronous motor; variable frequency electric drive; power supply interruptions; individual self-starting; transient processes; duration; analytical dependencies; experimental studies.

1. Introduction

The modes of group and individual asynchronous motor (AM) self-starting were subject matters of many detailed studies and scientific papers. However, the issues of self-starting AMs supplied by the frequency converter have not been adequately addressed. At the variable frequency control, particular features of this transient process are

* Corresponding author. Tel.: +79049759803.

E-mail address: hvrnmg@gmail.com

connected with increasing break time after power supply recovery as well as response of the fast-speed internal protection of the frequency converter configured to the maximum available self-protection mode [1].

An accurate calculation of the electric motor self-starting is possible only due to the coordinated solution of differential equations describing electromechanical and electromagnetic processes which number significantly exceeds the number of electric motor involved in self-starting. This calculation is time-consuming and requires numerous initial parameters of the network, transformers and all motors involved in run-down and self-starting. Thereinafter, simplified analytical dependencies are considered that may be used for revised calculation of AM individual self-starting mode.

2. Main part

1.1. Simplified calculation of asynchronous motor individual start

Practically all auxiliary local power station units have a speed-torque characteristic being similar to the vent (square-law) one. When ignoring a friction moment, the run-down of these units may be defined with the following dependence [2, 3]:

$$\omega = 1 / (1 + t / \tau_j) \quad (1)$$

where ω – normalized angular velocity taken relative to synchronous angular one; t – time from voltage loss; τ_j – mechanical time constant at motor load factor $K_{load} \approx P / P_{rated}$.

$$\tau_j = \tau_{j\,rated} / K_{load}; \quad \tau_{j\,rated} \approx J_{eq} \omega_{synchr}^2 / P_{rated}; \quad J_{eq} = J_M + J_{unit},$$

where J_{eq} – equivalent moment of unit inertia, kg·m²; J_M – motor inertia moment; J_{unit} – unit inertia moment.

If we know the time of power supply interruption and assume that at the power supply interruption the unit was rotating at angular velocity being equal to the synchronous motor velocity, we may calculate the angular velocity at the voltage recovery according to the proposed relations and with relative high accuracy.

A successful self-starting and its duration greatly depend on the supply interruption persistence. With decreasing time-gap, electric motors are slowed and self-starting currents are limited to a lower degree, while voltage at bus bars is enhanced at power supply recovery. Therefore, the dynamic moment is increased and recovery of the rated speed is promoted too.

1.2. Specific features of self-starting variable frequency electric drive

The VFED self-starting features a number of specific characteristics depending on the topology of the frequency converter, control principles, converter's network connection diagram (an individual VFED or a group control diagram).

Fig. 1 shows schematic processes within the district heating grid at a short-term power supply interruption of the line pipe with estimation of absolute time interval values being close to real ones [3, 4]. The time axis shows events in their sequential order and an approximate nature of the electric drive speed alteration in respect to the line pump. At t_1 time moment, the power supply was interrupted, thus, resulting in reduction of the motor speed form ω_{init} initial value and water flow through the boiler. At t_3 moment the flow is fully interrupted due to the actuation of the return valve at the pump head, while a bit earlier, at t_2 moment, the countdown t_{emerg} boilers' emergency protection starts. If water flow is not recovered to the minimum setting all operating boilers shall be simultaneously shut off (t_{emerg} is the same for all boilers). After interruption t_{interr} the power supply shall be recovered at t_4 time moment, for instance, due to actuation of the built-in automatic transfer switch (ATS).

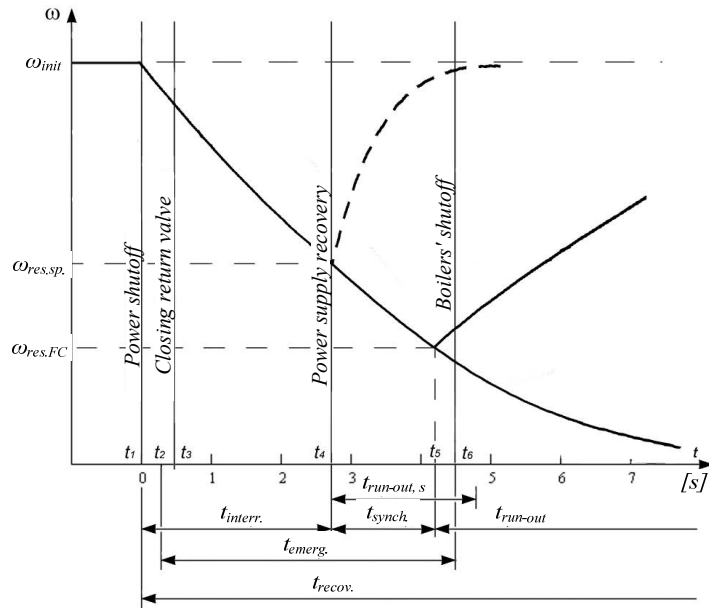


Fig. 1. Nature of process within the district heating grid at a short-term power supply interruption and automatic restart of the line pump.

If the rotating main-supplied electric drive is energized at t_4 moment its run-out (dash line on Fig. 1) starts afterwards ($t_{run-out,s}$) water flow shall be recovered. The total time $t_{recov.}$ amounts:

$$t_{recov.} = t_{interr.} + t_{run-out, s} \quad (2)$$

where $t_{run-out, s}$ – time of the electric drive run-out from the residual speed $\omega_{res.sp.}$ at its main-supply.

Obviously, a non-stop operation of boilers is provided with the inequality $t_{recov.} < t_{emerg.}$.

Almost all modern frequency converters (FCs) has an electric motor load pickup Flying Start function. This function enables the reconditioning technological parameters at recovery of a normal power supply.

The load pickup of the rotating drive supplied from the FC differs from the described self-starting with main-supply. Within the time interval $t_4 - t_5$, the ready-to-start condition of the converter is recovered; it is specified as a synchronizing time $t_{synch.}$ in Fig. 1. If self-starting at t_5 is successful, the run-out starts, which rate, shall be defined with overload capacitance of the frequency converter. A total time of the mode recovery contains an additional constituent in contrast to (2) and a longer run-out time $t_{FC run-out}$:

$$t_{recov.} = t_{interr.} + t_{synch.} + t_{FC run-out} \quad (3)$$

Furthermore, for $t_{synch.}$ the electric drive speed continues decreasing to $\omega_{res. FC}$ value, thus, complicating the issue of mode recovery due to the raise of the required run-out time.

According to the manufacturer specifications for various types of frequency converters, almost all FCs provide the motor self-starting. In practice, however, they do not offer the opportunity of load pickup from the rotating motor as well as VFED restart at practical zero or near-to-zero speed in a number of cases. It is evident that a total time of self-starting essential units will unacceptably raise.

Processes appearing at supply voltage dips at VFEDs of the boiler draft units are similar to the above ones for line pump but have the following specific characteristics:

- a high inertia moment of the smoke exhauster or forced-draught fan does not permit essential reduction of the unit speed for voltage depression time.
- actuation time of the blast air and draft pressure protection system in the boiler furnace is 3–5 s.

1.3. Differences between variable frequency and non-controlled electric drives

Based on the analysis of reviewed scientific papers and VFED operating experience of several power plants, we may distinguish the following major differences between non-controlled and variable frequency electric drive self-starting:

1. Under real conditions, VFED self-starting occurs in 90% cases without the Flying Start function. It can be explained either by its lack or by faulty algorithm implementing this function. The known studies of this function consider the high-voltage VFEDs with supply sources only; there is no available information on similar studies dealing with low-voltage FCs with the voltage inverter.

2. About 30 ms after voltage depressions, the FC is unenergized and then the AM coasting to stop follows at absence of the above function. Afterwards, the run-out from zero to steady speed occurs. At the absence of the Flying Start function, interruption duration of over 30 ms and voltage depression depth do not effect a transient process practically as the motor is not connected to the network. At high rotating masses at the electric motor shaft, the speed alterations for time 30 ms are negligible.

3. Under real conditions, the following should be compared in 90% cases: self-starting the uncontrolled electric drive (with due regard to the run-out time and residual main voltage) coasting to zero speed and the further AM start by underfrequency relay at recovered voltage level. An intolerable pressure loss is followed by the actuation of the water (for line pumps), supplied air or draft pressure protection system in the boiler furnace (for draught units) and emergency shutdown of the boiler.

4. As the FC is not connected to the network the EMF is not induced at the variable frequency AM coasting. At group coasting non-controlled AMs connected to the same bus bar section, the induced EMF shall be considered although it is considerably lower compared to that at the run-down of synchronous motors.

5. If the Flying Start function is ensured an additional break shall be borne in mind that is required for self-testing and synchronizing the FC rate with vertical frequency of the motor stator. Thereby, duration of the time gap after voltage recovery to the VFED connection will be involuntarily increased. Its duration depends on the FC internal protection setting, software version and a number of other factors [1].

6. A specific feature of motor self-starting at supply form the FC is in reduced maximum permissible currents (up to 1.1–1.5 of the rated value) whilst the permissible in-rush starting current of the uncontrolled AD may be five-fold as high as the rated one. Low in-rush starting current affects favorably the main voltage recovery but significantly decelerates recovery of the operational mode. To compensate this disadvantage, [2] proposes an automatic change of the run-out rate. It should provide switching to the mode before power supply interruption for minimum time within the overload range of 1.1–1.5 of the rated value.

1.4. Experimental studies of high-voltage VFED self-starting

To determine possible reasons of the high-voltage VFED shutdown at short-term power supply interruption, we have carried out experimental studies of 630 kW/5 kV line pump electric drives equipped with Power Flex 7000 frequency converters.

The oscillographs in Fig. 2, a, show transient processes at 6 kV input shutoff with duration of 0.74 sec. at 28 Hz operational frequency. As a result, the VFED tried to restart but was shut off by the MOTOR STALL protection system 22 seconds after voltage recovery. Fig. 2, b, shows similar oscillographs at 6 kV input shutoff after 1.56 sec. at 40 Hz operational frequency. In this case, the motor was accelerated to a steady speed for 24 sec. after voltage at the input had been recovered.

Fig. 3 demonstrates a restart after shutoff of the infeed unit, ATS pickup and automatic switching to the standby unit in 0.58 sec. The shutoff was followed by a successful restart: the motor was accelerated to a steady speed for 10 sec. after voltage at the input had been recovered. The VFED control system performed a preliminary internal testing for 1 sec., the run-out occurred for the rest time. At voltage recovery, motor speed was decreased by 7 % (FC output of about 37 Hz at an initial value of 40 Hz). Speed was increased by 50 % at the run-out start (in 1 sec.): FC output was about 20 Hz.

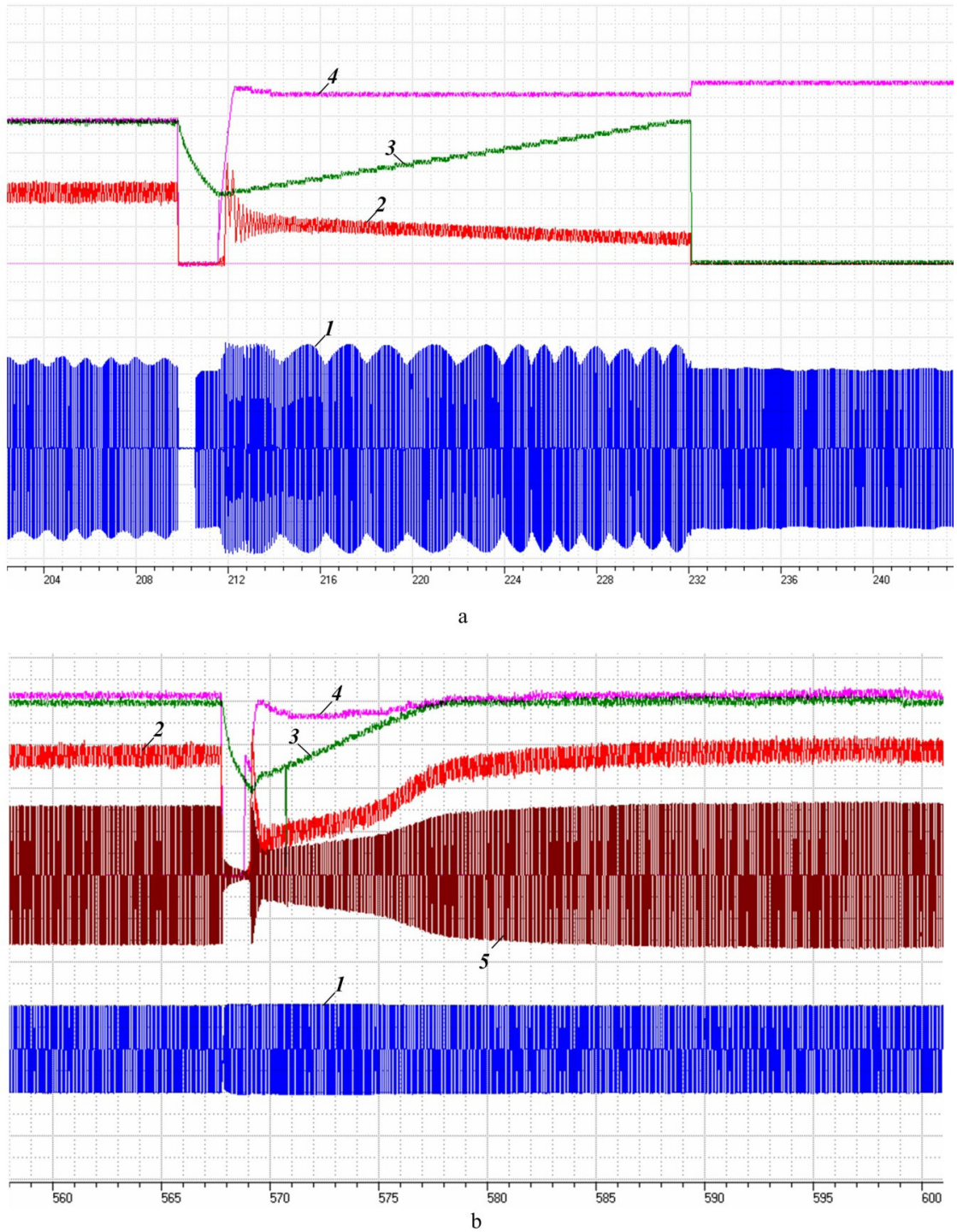


Fig. 2. Oscylographs of a faulty (a) and successful (b) high-voltage VFED self-starting at input shutoffs for 0.74 and 1.56 sec., correspondingly:
 1 – network voltage; 2 – current in DC link; 3 – rotational speed; 4 – calculated magnetic flux; 5 – motor current.

3. Outcome summary

Ongoing experimental studies have proved that the automated self-starting the high-voltage VFED with the self-excited current inverter is provided at short-term supply voltage depressions approximately in 50 % cases. At this, duration of the power supply interruption is not the only factor determining condition of a successful self-starting. This is because protection systems of modern frequency converters are set to the above maximum available self-protection condition in any abnormal situations [5, 6].

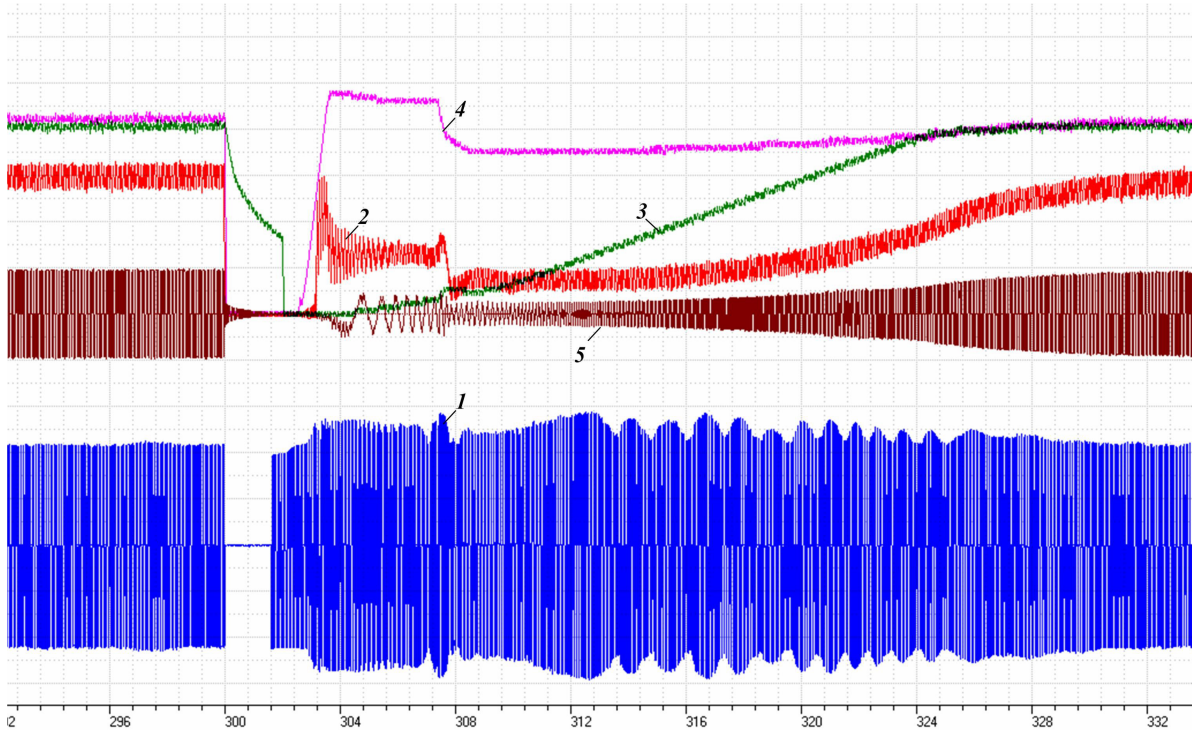


Fig. 3. Electric drive restart through shutoff at power supply interruption of 1.56 sec.

The total outcome of Power Flex 7000 electric drive studies takes form of recommended measures for each type of power supply interruption that are given in tabular form hereafter (Table 1). Only one measure of them is time- and cost-consuming and requires an additional elaboration: establishment of the own high-speed ATS. However, without its implementation the issue of non-stop operation of essential unit would be unsolved.

Table 1. Recommendation for providing continuous VFED operation with Power Flex 7000 converters at power supply interruptions

Type of power supply interruption	Recommended measures	Activities for implementation
Rapid 40–200 ms power supply interruptions	Optimal self-starting configuration	Provision of ATS response delay of at least 0.2 sec.
Power supply interruption for more than 0.2 sec.	1. Optimal self-starting configuration 2. Establishment of the own high-speed ATS with response time of less than 0.3 sec. from the voltage loss.	1. Solving problem of coordinated ATS selectivity. 2. Design solutions involving generation of additional power supply units with ATS for each electric drive
Voltage reduction to 30%	Provision of 6.7 kV voltage at FC	Ensuring voltage at FC by switching outputs of the transformer operation in a set with FC

Based on the outcome of theoretical and experimental studies, we have specified the condition of continuous boiler operation at power supply interruption: a total time of interruption, synchronization and run-out to an initial speed of electric drives of each essential unit shall be less than settings of response time for the emergency protection systems. The main challenge at implementation of the Flying Start function is presence of a residual magnetic field of running-down electric motor after its deenergizing. Preliminary field suppression by short circuit of the stator winding to dropping resistors proposed in [7] appeared to be ineffective with respect to the dropping intense as well as the additional time of switching system response.

[8–10] consider procedures and equipment providing switching the frequency converter to the rotating motor without in-rush currents for a minimum time after the line voltage recovery. The offered technical solutions should provide improving VFED resistance to short-term power supply interruptions. The result of this is enhancing operational reliability of essential units of boiler assemblies as well as the whole power plants.

Obviously, the main issues are comparison of technical possibilities and analysis of benefits and drawbacks of all developed means for enhancing VFED stability. For this purpose, studies by means of mathematical modeling and experiments at the facilities in operation are required. Moreover, development of mathematical models becomes more challenging because of nonavailability of algorithms implemented in the control systems of frequency converters offered by the most manufacturers. Experiments at essential operating facilities of the power plants are connected with substantial feasibility demonstration, extensive preparation works and executive problems. At present, researches in this field are under way and provide a positive outcome resulting in publishing in the scientific serials. Unfortunately, we cannot reflect and discuss all of them within margins of one paper provided.

Acknowledgements

Work is performed within the state job number 2014/80 of the Ministry of Education and Science of the Russian Federation.

References

- [1] Yu.A. Krylov, A.S. Karandaev, V.N. Medvedev, Power savings and production automation at the urban heat and power facilities. Variable frequency electric drive, Lan Publishing House, Saint Petersburg, 2013.
- [2] A.T. Sultanov, G.B. Lazarev, Requirements to variable frequency electric drives related to self-starting mode provision. specific characteristics of self-starting asynchronous and synchronous motors without frequency-related control. URL: <http://www.center-enel.ru/publ4.html>.
- [3] Yu.A. Krylov, I.A. Selivanov, A.S. Karandaev, A.R. Gubaydullin, V.V. Rovneyko, R.R. Galyamov, Issues of introduction of the variable frequency electric drives at essential units of the thermal power plant, Higher School Bulletin. Electromechanics. 4 (2011) 19–25.
- [4] V.R. Khramshin, K.E. Odintsov, A.R. Gubaydullin, O.I. Karandaeva, Yu.N. Kondrashova, Analysis of fault rate of variable frequency electric drives of local thermal power plants at power supply interruptions, Bulletin of the South-Ural State University. Power Engineering Series. 14(2) (2014) 68–79.
- [5] A.A. Radionov, A.S. Maklakov, E.A. Karyakina, New control method of back to back converter, 2015 International Siberian Conference on Control and Communications, SIBCON 2015 – Proceedings. (2015). DOI: 10.1109/SIBCON.2015.7147135
- [6] A.S. Maklakov, A.A. Radionov, EMC evaluation of three level NPC converter based on space vector PWM, Proceedings of the 2015 IEEE North West Russia Section Young Researchers in Electrical and Electronic Engineering Conference, ElConRusNW 2015. (2015) 236–240. DOI: 10.1109/ElConRusNW.2015.7102269
- [7] P.J. Lawrenzon, J.M. Stephenson, Variable-speed switched reluctance motors, IEEE Pros. 127 (1980) Pt. B N4.
- [8] A.S. Karandaev, R.R. Khramshin, T.R. Khramshin, V.R. Khramshin, A.R. Gubaydullin, Means enhancing stability of variable frequency electric drives at power supply interruptions, Russian Internet Journal of Industrial Engineering. 1 (2013) 62–69.
- [9] A.A. Radionov, A.S. Karandaev, R.R. Khramshin, A.R. Gubaydullin, O.I. Karandaeva, E.A. Khramshina, Estimation of power saving resource of electric drive of forced-draught fan with two-speed electric motor, Bulletin of the South-Ural State University. Power Engineering Series. 14(3) (2014) 61–70.
- [10] A.S. Karandaev, G.P. Kornilov, T.R. Khramshin, V.R. Khramshin, A variable-frequency electric drive with power supply by two independent inputs, Russian Electrical Engineering. 86(4) (2015) 201–207. DOI 10.3103/S1068371215040045.



International Conference on Industrial Engineering

Mathematical description of AFE rectifier closed loop system

Radionova L.V.^a, Chernyshev A.D.^{a*}

^aSouth Ural State University, Chelyabinsk, Russia

Abstract

This article address a mathematical description of a closed loop system of an active front-end (AFE) rectifier. The AFE rectifier has been considered as a two-dimensional linear object and its mathematical description has been presented. Synthesis of regulators have been carried out by the step-by-step correction principle. The mathematical model has been made in Matlab/Simulink program. The mathematical description of AFE rectifier as an object of controlling allows us to conclude that it is complex nonlinear system, and the synthesis of control system should be carried out based on the linear model for referents operation conditions.

© 2015 The Authors. Published by Elsevier Ltd. This is an open access article under the CC BY-NC-ND license (<http://creativecommons.org/licenses/by-nc-nd/4.0/>).

Peer-review under responsibility of the organizing committee of the International Conference on Industrial Engineering (ICIE-2015)

Keywords: power converter, active front end rectifier, closed loop system, step-by-step correction;

1. Introduction

There are a lot of consumers requiring adjustable voltage or current and bidirectional power flow. These consumers are used in electric drives and automated systems of technological processes [1, 2]. Power frequency converters are a famous part of automation control systems of industrial installations. These converters are designed to regulate difference parameters of electric drives and an operation of power systems. A lot of modern power converter topologies work based on pulse wide modulation (PWM) methods [3, 4]. Currently, the power frequency converters for powerful industrial installations include active front end (AFE) rectifiers, which convert an alternation current (AC) voltage to a direct current (DC) voltage. The main reasons of a wide application of the AFE rectifiers at industry are the following advantages [5]: bidirectional power flow, acceptable electromagnetic capability (EMC), power factor correction, and high dynamic accuracy of regulating current and DC voltage [6].

* Corresponding author. Tel.: +7-912-476-2921.
E-mail address: fis6en@gmail.com

Nomenclature

i_{abcAFE}	three phase current of AFE rectifier
u_{abcAFE}	three phase voltage of AFE rectifier
L_{abcAFE}	equivalent inductance at the input of AFE rectifier
R_{abcAFE}	equivalent active resistance at the input of AFE rectifier
$u_{abcgrid}$	three phase voltage of the grid
i_{dcAFE}	DC current of AFE rectifier
i_{dload}	DC current of a load
i_{dc}	DC current on the capacitor
C_{dc}	equivalent capacitance of DC
u_{dc}	DC voltage
p	Laplace operator
u_{dqgrid}	voltage of the grid in dq reference frame
u_{dqAFE}	voltage of AFE rectifier in dq reference frame
i_{dqAFE}	current of AFE rectifier in dq reference frame
ω_{grid}	rotation speed of dq reference frame (rotation speed of voltage grid vector)
S_{AFE}	apparent power of AFE rectifier
K_I	linearization factor

2. Problem definition

Currently, AFE rectifier as a linear object of controlling is not considered at scientific works and synthesis of a closed loop system is a difficult task. The main aim of this paper address issues of mathematical description of AFE rectifier, the synthesis of closed loop system and modelling in the Matlab/Simulink.

3. AFE rectifier as a linear object of controlling

The schematic circuit of AFE rectifier is presented in Fig. 1. This circuit is simple to synthesis a control system and develop mathematical description. The main elements of AFE are a three-phase bridge based on semiconductor modules, a reactor, a filter at the AC mains and a direct current (DC).

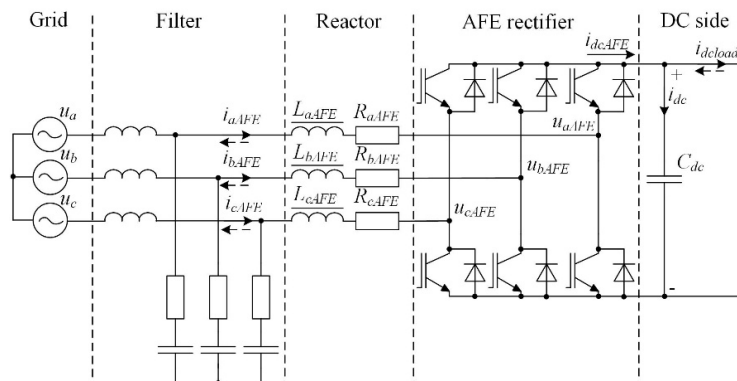


Fig. 1. Schematic circuit of AFE rectifier

A system of equations has been made based on the second laws of Kirchhoff and the ideal power semiconductor switches, a symmetric system of the grid voltages, and an equality of active resistance and inductance have been taken. The system of equations is as the following:

$$\begin{cases} u_{abcgrid} = i_{abcAFE} \cdot R_{abcAFE} + L_{abcAFE} \cdot p \cdot i_{abcAFE} + u_{abcAFE} \\ i_{dcAFE} - i_{dload} = i_{dc} \\ C_{dc} \frac{du_{dc}}{dt} = i_{dcAFE} - i_{dload} \end{cases} \quad (1)$$

The rotating reference frame dq is common used to develop a mathematical description for symmetrical three phase systems. If the dq transformation is applied for the system (1), a new system of equations will be as the following:

$$\begin{cases} u_{dgrid} = R_{dAFE} \cdot i_{dAFE} + L_{dAFE} \cdot p \cdot i_{dAFE} - \omega_{grid} \cdot L_{qAFE} \cdot i_{qAFE} + u_{dAFE} \\ u_{qgrid} = R_{qAFE} \cdot i_{qAFE} + L_{qAFE} \cdot p \cdot i_{qAFE} + \omega_{grid} \cdot L_{dAFE} \cdot i_{dAFE} + u_{qAFE} \\ i_{dcAFE} - i_{dload} = i_{dc} \\ C_{dc} \frac{du_{dc}}{dt} = i_{dcAFE} - i_{dload} \end{cases} \quad (2)$$

The power balance equation between AC and DC side is as the following:

$$S_{AFE} = u_{dgrid} \cdot \sqrt{i_{dAFE}^2 + i_{qAFE}^2} = u_{dc} \cdot i_{dc} \quad (3)$$

On the basis of the equation (3) the magnitude of DC current is defined as the following:

$$i_{dc} = \frac{3 \cdot u_{dgrid}}{2 \cdot u_{dc}} \cdot \sqrt{i_{dAFE}^2 + i_{qAFE}^2} \quad (4)$$

The block diagram of AFE rectifier as an object of controlling is shown in Fig. 2 based on the equations (2), (3), and (4).

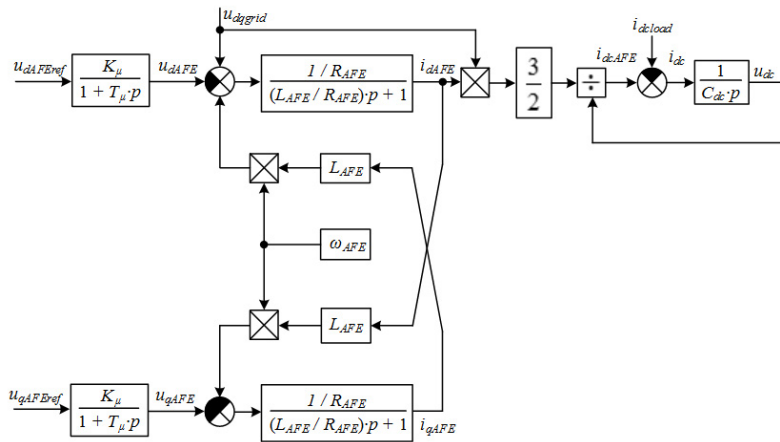


Fig. 2. Block diagram of AFE rectifier as an object of controlling

The block diagram consists of two parts: The first part is linear dimensional current loop with antisymmetric cross-connection and the second part is DC voltage loop based on an integer transfer function. A relationship

between reference voltage signal and output AFE voltage is determined by transfer function with small time constant T_μ and gain K_{PWM} .

Transient process in the DC at unit power factor are described based on the following equation:

$$C_{dc} \cdot \frac{du_{dc}}{dt} = \frac{3 \cdot u_{dgrid}}{2 \cdot u_{dc}} \cdot i_{dAFE} - i_{dload} \quad (5)$$

Taylor series expansion of three variables non-linear function $F(x, y, z)$ around a set conditions $F(x_0, y_0, z_0)$ can be used to approximate the equation (5). The formula of linear approximation is as the following:

$$\frac{dx}{dt} = F(x, y, z) \Rightarrow \frac{d\Delta x}{dt} = \left. \frac{\partial f}{\partial x} \right|_{\substack{y=y_0 \\ z=z_0}} \cdot \Delta x + \left. \frac{\partial f}{\partial y} \right|_{\substack{x=x_0 \\ z=z_0}} \cdot \Delta y + \left. \frac{\partial f}{\partial z} \right|_{\substack{x=x_0 \\ y=y_0}} \cdot \Delta z \quad (6)$$

Linear approximation of the equation (6) for a dependence between DC voltage and DC current around the set point, which is determined by the rated DC voltage, is as the following:

$$C_{dc} \cdot \frac{d\Delta u_{dc}}{dt} = \frac{3 \cdot u_{dgrid}}{2 \cdot u_{dcref}} \cdot \Delta i_{dAFE} = \frac{3}{2} \cdot K_l \cdot \Delta i_{dAFE} \quad (7)$$

4. AFE rectifier closed loop system in Matlab/Simulink

Synthesis of regulators is carried out by the step-by-step correction principle. Transfer functions of the closed current loops in axes d and q are as follows:

$$W_{idq}(p) = \frac{1}{2 \cdot T_\mu^2 \cdot p^2 + 2 \cdot T_\mu \cdot p} \quad (8)$$

The transfer functions of current regulators d and q are as follows:

$$W_{Regidq}(p) = K_{pdq} + \frac{K_{idq}}{p} = \frac{L_{AFE}}{2 \cdot T_\mu} + \frac{R_{AFE}}{2 \cdot T_\mu} \cdot \frac{1}{p} \quad (9)$$

Transfer function of the closed DC voltage loop is as follows:

$$W_{DC}(p) = \frac{8 \cdot T_\mu \cdot p + 1}{64 \cdot T_\mu^4 \cdot p^4 + 64 \cdot T_\mu^3 \cdot p^3 + 32 \cdot T_\mu^2 \cdot p^2 + 8 \cdot T_\mu \cdot p + 1} \quad (10)$$

The transfer function of DC voltage regulator is as follows:

$$W_{RegDC}(p) = K_{pDC} + \frac{K_{iDC}}{p} = \frac{C_{dc} \cdot K_l}{6 \cdot T_\mu} + \frac{C_{dc} \cdot K_l}{48 \cdot T_\mu^2} \cdot \frac{1}{p} \quad (11)$$

For example, closed current loops and closed DC voltage loop in Matlab/Simulink are shown in Fig. 3 and Fig. 4.

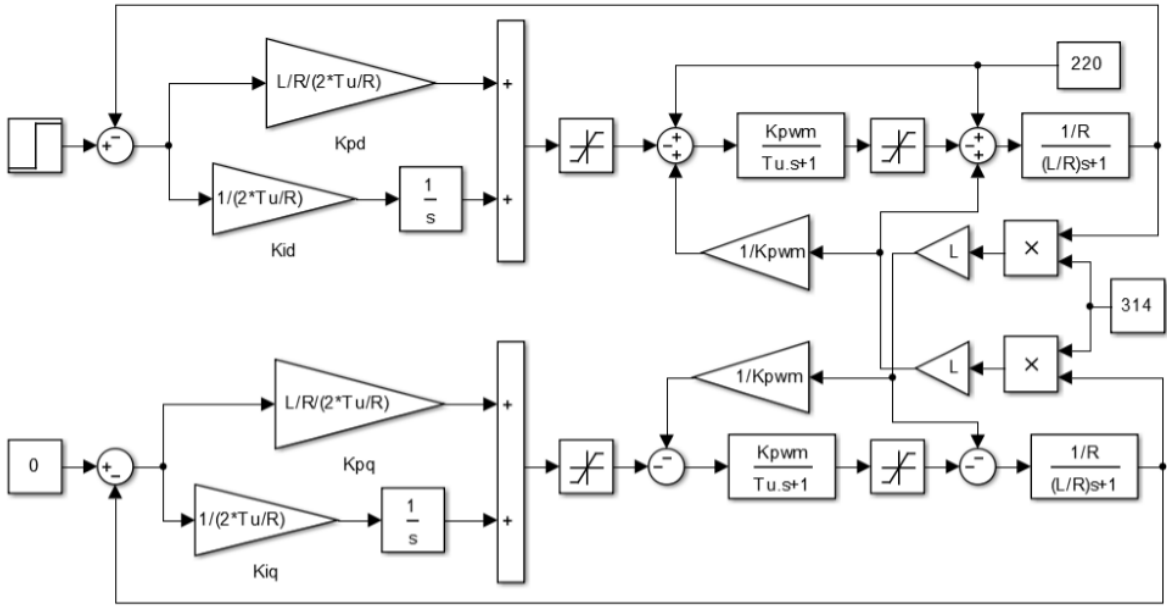


Fig. 3. Closed current loops in axes *d* and *q* of AFE rectifier

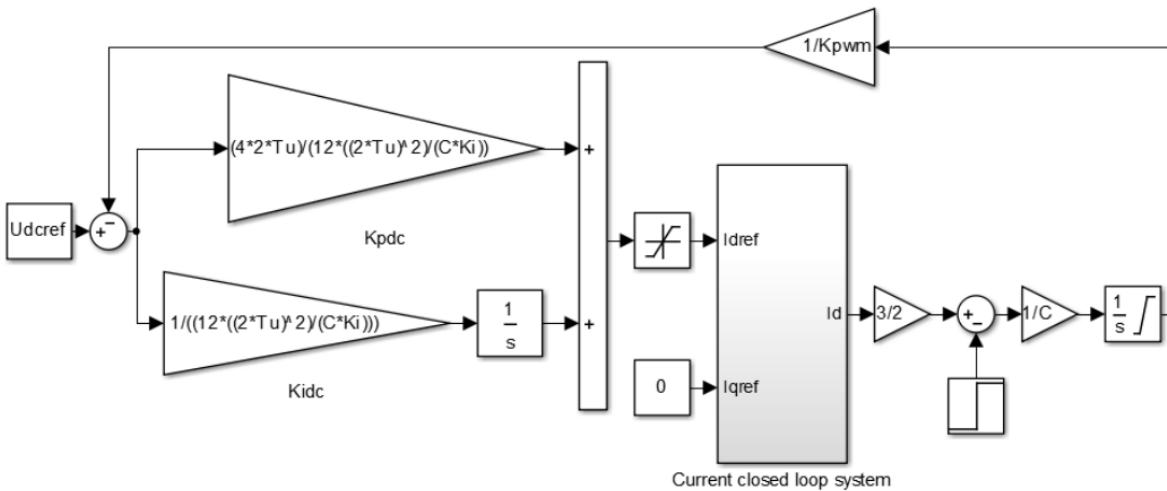


Fig. 4. Closed DC voltage loop of AFE rectifier

Conclusions

The mathematical description of AFE rectifier as an object of controlling allows us to conclude that it is complex nonlinear system. The AFE rectifier has been considered as a two-dimensional linear object, and the synthesis of regulators have been carried out by the step-by-step correction principle. Control system should be set based on the linear model for referents operation conditions.

References

- [1] A.A. Radionov, A.S. Maklakov, E.A. Karyakina, New control method of back to back converter, 2015 International Siberian Conference on Control and Communications, SIBCON 2015 - Proceedings, (2015). DOI: 10.1109/SIBCON.2015.7147135[2] W. Strunk Jr., E.B. White, *The Elements of Style*, third ed., Macmillan, New York, 1979.
- [2] A.S. Maklakov, A.A. Radionov, EMC evaluation of three level NPC converter based on space vector PWM, Proceedings of the 2015 IEEE North West Russia Section Young Researchers in Electrical and Electronic Engineering Conference, EIConRusNW 2015, (2015) 236–240. DOI: 10.1109/EIConRusNW.2015.7102269
- [3] A.S. Maklakov, A.A. Radionov, Integration prospects of electric drives based on back to back converters in industrial smart grid, 2014 12th International Conference on Actual Problems of Electronic Instrument Engineering, APEIE 2014 - Proceedings, (2014) 770–774. DOI: 10.1109/APEIE.2014.7040790
- [4] A.A. Radionov, A.S. Maklakov, V.R. Gasiyarov, Smart Grid for main electric drive of plate mill rolling stand, Proceedings of 2014 International Conference on Mechanical Engineering, Automation and Control Systems, MEACS 2014, (2014). DOI: 10.1109/MEACS.2014.6986842
- [5] V.R. Khramshin, A.S. Evdokimov, G.P. Kornilov, A.A. Radionov, A.S. Karandaev, System for speed mode control of the electric drives of the continuous train of the hot-rolling mill, 2015 International Siberian Conference on Control and Communications, SIBCON 2015 – Proceedings. DOI: 10.1109/SIBCON.2015.7147264
- [6] A. S. Maklakov, "Analysis of PWM boost rectifier in modes of reactive power compensation," *Russian Internet Journal of Industrial Engineering*, 21, (2013) 43–50.



International Conference on Industrial Engineering

Application of subtractive clustering for power transformer fault diagnostics

Radionov A.A.^a, Evdokimov S.A.^b, Sarlybaev A.A.^b, Karandaeva O.I.^{b,*}

^aSouth Ural State University, 76, Lenin Avenue, Chelyabinsk, 454080, Russian Federation

^bNosov Magnitogorsk State Technical University, Lenina Av. 38, Magnitogorsk, 455000, Russia

Abstract

The issue of developing methods and implementation of hardware and software for power transformer state control is relevant due to the need for enhancing stability and durability of essential expensive equipment. A promising diagnostic condition control technique for the high-voltage oil-filled electrical facilities is the method of positioning partial discharges (PDs) and their intense measuring. The paper provides outcome of experiments enabling acoustic PD positioning at the transformers of the power plant units. It considers the methods and algorithm of processing results of the periodical acoustic PD positioning based on the subtractive clustering technique. These methods provides a fault tracing and identification as well as assessment of their trend.

© 2015 The Authors. Published by Elsevier Ltd. This is an open access article under the CC BY-NC-ND license (<http://creativecommons.org/licenses/by-nc-nd/4.0/>).

Peer-review under responsibility of the organizing committee of the International Conference on Industrial Engineering (ICIE-2015)

Keywords: power plant; power transformer; technical state; fault; diagnostics; tracing; methods; subtractive clustering method; algorithm; use.

1. Introduction

Implementation of means for fault diagnostics of oil-filled power transformers is challenging and highly urgent. This is due to a number of intrinsic reasons one of which is a physical equipment wear being as high as 50–70% in the Russian power sector. Furthermore, development of means and systems of technical diagnostics is the most essential condition of the Smart Grid technology introduction into the industrial electric networks [1-3].

One of the advanced and intensively developing methods of condition monitoring without deenergization (in on-line mode) is the partial discharge positioning. PDs have been recorded at the high-voltage facilities for diagnostics

* Corresponding author. Tel.: +73519012367.

E-mail address: radionov.mail@gmail.com

over the last 20 years. However, this method is used today mainly for monitoring power systems, large power plants and heavy-duty arc steel-making furnaces [4–6]. This fact may be explained by technical, research and methodical problems. One of substantial reasons is a lack of methods of transformer condition diagnostics based on processing and analyzing results of the periodic PD intense measurements.

2. Main part

We propose the engineering practice for identification of power transformer faults by analyzing complex partial discharge parameters. Fig. 1 shows the functional structure explaining the essence of the procedure developed.

It includes the following methods of mathematical analysis of PD parameters:

- analysis of PD intensity dependency upon the limit values;
- PD cluster analysis based on generation of uniform characteristics of the power equipment condition;
- amplitude and phase analysis of the time-dependent behavior of PD signals;
- spectrum analysis of harmonic content of PD signals.

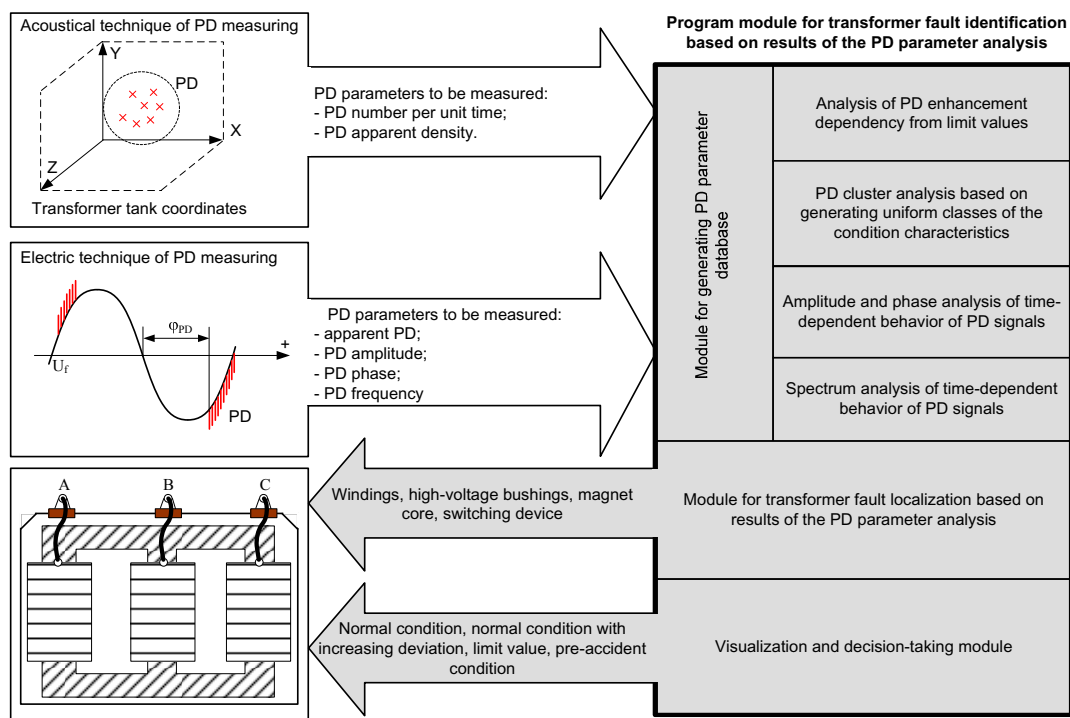


Fig. 1. Functional structure explaining the developed technique of transformer fault identification.

2.1. Experimental research of discharge activity

Within the framework of engineering implementation of the developed technique, acoustic tracing and processing data of partial discharges in the transformer tanks of the power sub-stations of industrial power plants were performed. Measuring was carried out with portable device for PD analysis and tracing defect zones in the insulation of the AR-700 high-voltage facilities [8]. For this, acoustic sensors were installed on the outer sides of the tank. Their location was chosen with methods specified by GOST 20074-83.

Fig. 2 shows intrinsic flow charts obtained at the transformer. Acoustic spikes recorded in pickup signals provided by sensors characterize the PD amplitude, frequency and duration [9].

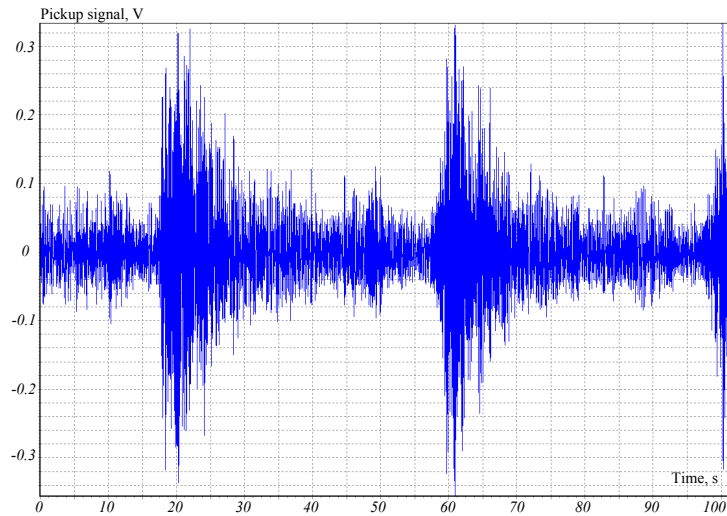


Fig. 2. Acoustic signal oscillographs.

Fig. 3 shows results of PD recording during the set time period. Points outlined within the volumetric tank envelope visualize the number and location of discharges recorded during 1 minute. There are geometrical coordinates of all recorded discharges in the right part of the picture. During experiment at relatively high noise levels (0.45 V), a significant number of discharges distributed practically in the whole tank envelope was recorded. Experiments were carried out at six transformers of the power generating sets.

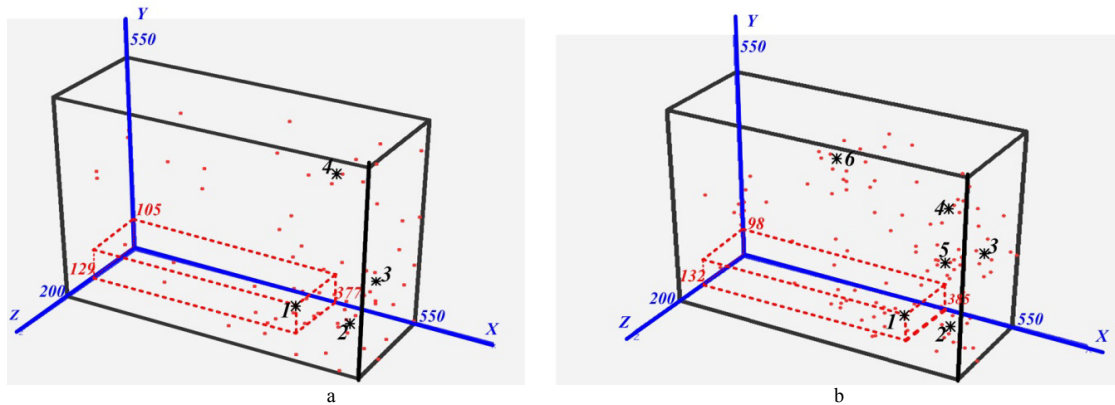


Fig. 3. Three-dimensional circuits of PD distribution in transformer No.5.

For estimation of discharge activity development, three-dimensional PD circuits obtained with measuring results at the margin of 6 months were compared (Fig. 3, a and Fig. 3, b, correspondingly). As a result, it was found out that at later measuring operations an increase of discharge activity can visually be observed; this fact confirms the change of their condition. At this, volume PD distribution in separate tank zones is changed too, thus, reflecting defect growth in these zones.

As may be inferred from the results provided, a large PD location data file may be accumulated at diagnosing transformers with acoustic tracing method. Data file processing is required for diagnostics; here, application of statistic analysis methods is not advisable as it requires a priori knowledge of distribution laws.

2.2. Application of subtractive clustering method

Measuring result processing is proposed to be performed with cluster analysis method enabling division of pooled data under consideration into groups of similar objects (clusters) and record distribution into different groups or segments. Most clustering algorithms may be used under conditions of almost the whole unavailability of information on data distribution laws. Objects with quantitative (numerical), qualitative or mixed attributes are subject to clustering. Division of sampled information into groups of similar objects simplifies further data processing and decision-making as a specific analysis method may be used for each cluster. The clustering algorithm is the a -function: $X \rightarrow Y$ that assigns to all $x \in X$ objects numbers of $y \in Y$ clusters. The Y range is known in advance in some cases but normally the objective is to determine an optimum cluster number in terms of the specified criterion of clustering quality.

Based on the analysis of conceptual theoretical issues of the clustering analysis, the subtractive (mountain) clustering algorithm may reasonably be applied for processing outcome of the PD acoustic tracing; here, each point of the data array is assumed to be a center for a potential cluster. For the later, the objective function-density of other points around the considered one shall be calculated. The algorithm enables formalization of expert estimation of any electric machine condition with data obtained at measuring PDs and tracing its temporal variation trend.

As elements of the observation matrix, the PD coordinates (x_i, y_i, z_i) in the volumetric transformer envelope (see Fig. 3) were proposed to be used immediately. Geometric X -, Y - and Z -coordinates of each PD are stored into AR-700 memory and may be output as numerical arrays for processing with the Fuzzy Logic Toolbox package of the MATLAB system being most convenient for processing experimental data [10-12].

The technique of PD analysis using subtractive clustering has been developed based on studies [13]. It includes the following provisions.

1. As reference parameters we propose the x_{ij}, y_{ij}, z_{ij} PD coordinates recorded during experiments in the tank for all considered transformers. The X_{Tj} observation matrices of dimensions $[nj \times 3]$ are formed:

$$X_{Tj} = \begin{bmatrix} x_{(Tj)1} & y_{(Tj)1} & z_{(Tj)1} \\ x_{(Tj)2} & y_{(Tj)2} & z_{(Tj)2} \\ \dots & \dots & \dots \\ x_{(Tj)nj} & y_{(Tj)nj} & z_{(Tj)nj} \end{bmatrix}, \quad (1)$$

where i and n_j – number of the recorded discharge and PD impulses at the frequency level 10 imp./sec. for transformer No. j .

2. Potentials of clusters' n -centers shall be calculated with the following dependence

$$P(Z_h) = \sum_{k=1, M} \exp(-\alpha D(Z_h, X_k)), \quad h = \overline{1, S},$$

where $Z_h = (z_{1,h}, z_{2,h}, \dots, z_{n,h})$ – a potential center of cluster No. h ; $h = \overline{1, S}$; α – positive constant; $D(Z_h, X_k)$ – distance between a potential center of the Z_h cluster and X_k clustering object.

3. The potential shall be recalculated with the following dependence

$$P_2(Z_h) = P_1(Z_h) - P_1(V_1) \cdot \exp(-\beta \cdot D(Z_h, V_1)),$$

where $P_1()$, $P_2()$ – potentials at the 1st and 2nd iterations, correspondingly;

V_1 – center of the first detected cluster: $V_1 = \arg_{Z_1, Z_2, \dots, Z_Q} \max(P_1(Z_1), P_1(Z_2), \dots, P_1(Z_Q))$;

β – a positive constant.

Recalculation occurs as long as the rated potential value is higher then the set limit value P_{lim} .

F_{Tj} matrices of detected PD cluster centers are formed for each transformer. They correspond to the first steady-state operation mode:

$$F_{Tj} = \begin{bmatrix} x_{(Tj)1} & y_{(Tj)1} & z_{(Tj)1} \\ x_{(Tj)2} & y_{(Tj)2} & z_{(Tj)2} \\ \dots & \dots & \dots \\ x_{(Tj)Lj} & y_{(Tj)Lj} & z_{(Tj)Lj} \end{bmatrix},$$

where Lj – the number of the PD clusters detected in transformer No. j in the first steady-state on-load operation mode.

Vectors of corresponding cluster potentials $S_{Tj} = [P_{(Tj)1} \ P_{(Tj)2} \ \dots \ P_{(Tj)Lj}]$ are formed separately.

4. When the load mode or temperature of the transformer are changed, that is, additional factors appear that may result in variation of the insulation PD intensity, the X'_{Tj} observation matrices for a new load mode are generated according to (1).

5. Calculations as per sub-s. 2 and 3 of this algorithm are carried out and F'_{Tj} matrices of the detected centers of PD clusters for the altering mode and corresponding S'_{Tj} potential vectors are determined.

6. For each transformer, the M'_j dimension of rows (number of detected clusters) of F'_{Tj} matrices is compared with the M_j dimension of F_{Tj} matrix rows of the previous mode. The number of additionally generated clusters (additional PD sources) $\Delta M_j = M'_j - M_j$ is specified. If $\Delta M_j < 0$ that means a normal condition of the transformer insulation.

7. If $\Delta M_j > 0$ the coordinates of $x_{(Tj)k}$, $y_{(Tj)k}$, $z_{(Tj)k}$ cluster centers and vectors of $S_{\Delta Tj}$ potentials of additionally generated PD clusters shall be defined (here, k – number of the cluster generated).

With due regard to the potential values, the hazard rate of recent sources of partial discharges may be estimated while pursuant to cluster center coordinates, the location and so, reasons and mechanism of occurring damage inside the transformer tank are derived.

The schematic algorithm of PD analysis by means of the technique under consideration is provided in Fig. 4. With this algorithm and the Fuzzy Logic Toolbox applications, changing discharge activity of electricity works (EW) transformers has been analyzed. The coordinates of the detected clusters for transformer No. 5 are outlined in Fig. 3 by points with corresponding numbers. For the first measuring (Fig. 3, a), 4 clusters are pronounced, for the second one (Fig. 3, b) – 6. As an example, both figures show plotting the center of cluster No. 1 with coordinates of F_{Tj} , F'_{Tj} matrix rows of the cluster centers.

The coordinates of clusters with the highest intensity established with results of the first measuring and of newly generated clusters carry inference about development of discharge processes near B and C high-voltage phase inputs. The newly generated PD clusters (No. 5 and 6) are determined to have rather high potentials (higher PD density compared to the centers) in comparison with proportional's of clusters recorded during the previous measuring. This conclusion served as a recommendation for operating personnel to continue capturing and processing data with the AR-700 device and additional transformer examinations with other methods.

3. Conclusion

The example provided proves that the developed technique enables comparing discharge focal points (cluster centers) directly with packaging transformer assembly units (windings, high-voltage inputs, RUL etc.), so fault localizing and identifying. It is obsequiously that drawing firm conclusions on condition of the examined transformers based on only two measuring operations may be difficult. However, the obtained results provide an

opportunity to show the application of the proposed algorithm and its efficiency at diagnostics under operational conditions [14].

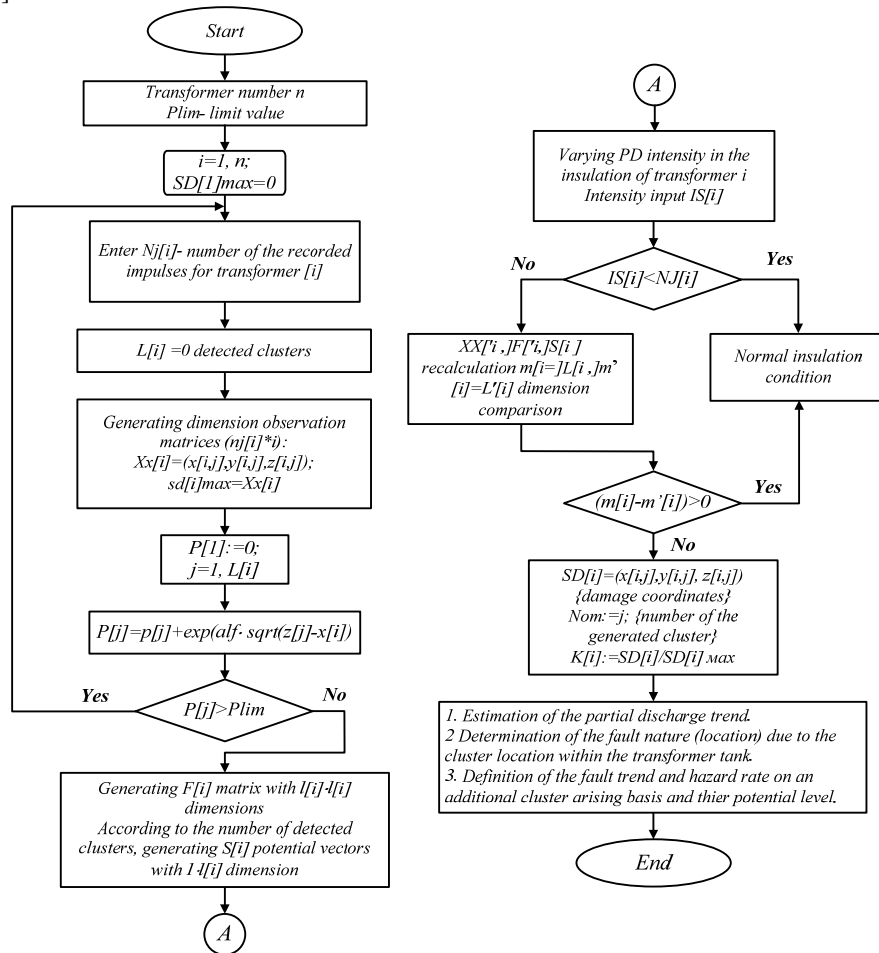


Fig. 4. Algorithm of transformer condition analysis based on the subtractive clustering method.

The key point of the developed technique is the use of two methods of measuring PD parameters – an acoustic and electric one. A simultaneous application of these methods enables:

- significant expansion of the initial PD data base for further analysis and tracing incipient insulation damages;
- application of mathematical analysis methods using as initial data parameter of acoustic radiation and electric generation signals due to partial discharges;
- enhancing fidelity of measuring PD parameters.

The advantage of the developed technique is in possibility to estimate transformer insulation condition timely due to the dynamic examination of discharge processes for a relatively short term. Globally, it ensures more objective estimation of condition of the transformer windings insulation.

References

- [1] V.R. Khramshin, S.A. Evdokimov, An.A. Nikolaev, Ar.A. Nikolaev, A.S. Karandaev, Monitoring technical state of the power transformers is a necessary condition of the smart-grid technology introduction within the industrial electric networks, Proceedings of the 2015 IEEE NW Russia young researchers in electrical and electronic engineering conference (EIconRusNW), St. Petersburg. (2015) 214–220. DOI 10.1109/EIconRusNW.2015.7102265.
- [2] A.S. Maklakov, A.A. Radionov, Integration prospects of electric drives based on back to back converters in industrial smart grid, 2014 12th International Conference on Actual Problems of Electronic Instrument Engineering, APEIE 2014 – Proceedings. (2014) 770–774. DOI: 10.1109/APEIE.2014.7040790
- [3] A.A. Radionov, A.S. Maklakov, V.R. Gasiyarov, Smart Grid for main electric drive of plate mill rolling stand, Proceedings of 2014 International Conference on Mechanical Engineering, Automation and Control Systems, MEACS 2014. (2014). DOI: 10.1109/MEACS.2014.6986842
- [4] A.S. Karandaev, S.A. Evdokimov, V.R. Khramshin, R.A. Lednov, Diagnostic functions of a system for continuous monitoring of the technical condition of the transformers of arc steelmaking furnaces, Metallurgist. 58(7-8) (2014) 655–663. DOI 10.1007/s11015-014-9972-5.
- [5] A.S. Karandaev, S.A. Evdokimov, V.R. Khramshin, A.A. Sarlybaev, System for real-time monitoring of the technical state of a transformer on an ultrahigh-power electric-arc steelmaking furnace, Metallurgist. 58(9-10) (2014) 872–879. DOI:10.1007/s11015-015-0010-z.
- [6] A.S. Karandaev, S.A. Evdokimov, V.R. Khramshin, O.I. Karandaeva, Information and measuring system for electric arc furnace transformer monitoring, 12th International Conference on Actual Problems of Electronic Instrument Engineering (APEIE-2014), Novosibirsk.1 (2014) 273–279. DOI 10.1109/APEIE.2014.7040896.
- [7] A.S. Karandaev, S.A. Evdokimov, O.I. Karandaev, S.E. Mostovoy, A.A. Chertousov, Control of power transformer technical state using acoustic diagnostics, Bulletin of the South-Ural State University. Power Engineering Series.10 26(126) (2008) 26–31.
- [8] A.S. Karandaev, S.A. Evdokimov, D.Kh. Devyatov, B.N. Parsunkin, A.A. Sarlybaev, Power transformer diagnostics using acoustic tracing partial discharges, Bulletin of the Novosibirsk State Technical University. 1 (2012) 105–108.
- [9] S.D. Shtovba, Introduction to fuzzy set and logic theory. Designing control systems, Fuzzy Logic Toolbox, http://matlab.exponenta.ru/fuzzylogic/book1/12_2.php.
- [10] A.A. Radionov, A.S. Maklakov, E.A. Karyakina, New control method of back to back converter, 2015 International Siberian Conference on Control and Communications, SIBCON 2015 – Proceedings. (2015). DOI: 10.1109/SIBCON.2015.7147135
- [11] A.S. Maklakov, A.A. Radionov, EMC evaluation of three level NPC converter based on space vector PWM, Proceedings of the 2015 IEEE North West Russia Section Young Researchers in Electrical and Electronic Engineering Conference, EIconRusNW 2015. (2015) 236–240. DOI: 10.1109/EIconRusNW.2015.7102269
- [12] O.N. Agmalov, Cluster analysis of partial discharges for estimation of condition of electric machine insulations, Electricity. 6 (2006) 56–62.
- [13] A.S. Karandaev, V.R. Khramshin, S.A. Evdokimov, Yu.N. Kondrashova, O.I. Karandaeva, Methodology of calculation of the reliability indexes and life time of the electric and mechanical systems. Proceedings of 2014 International Conference on Mechanical Engineering, Automation and Control Systems (MEACS). (2014) 6. DOI 10.1109/MEACS.2014.6986866.
- [14] V.R. Khramshin, A.S. Evdokimov, S.A. Evdokimov, A.S. Karandaev, Development and industrial introduction of systems for monitoring technical state of the rolling mills' electrical equipment. Proceedings of the 2015 IEEE NW Russia Young Researchers in Electrical and Electronic Engineering Conference (EIconRusNW). (2015) 208–213. DOI 10.1109/EIconRusNW.2015.7102264.

International Conference on Industrial Engineering

Synthesis of an object moving control system with flexible suspension under the action of external forces

Pyatibratov G.Ya.^a, Bogdanov D.Yu.^a, Bekin A.B.^{a*}

^a *Electromechanical Faculty, Platov South-Russian State Polytechnic University (NPI), 132, Prosvyashcheniya Str., 346428 Novocherkassk, Russia*

Abstract

The paper presents electromechanical systems with flexible linkage, which movement parameters shall be specified by external force impact. The approaches to the compound movement division of such systems into components are given. The requirements to the control system of object horizontal moving with flexible suspension are formulated. The block diagram of electromechanical part of object horizontal moving system to research the impact of disturbing effect on its work is presented. The feasibility of using grapho-analytical methods and inverse frequency characteristics of control system synthesis is proved. The structure of corrective device is defined and a guideline for its parameters for its selection is given. The results of control system operation simulation with the synthesized corrective device are described. The recommendations for using adaptive control of object horizontal movement systems with flexible suspension are given. The results of system operation are compared with the recommended rational parameters of the corrective device and with application of adaptive control.

© 2015 The Authors. Published by Elsevier Ltd. This is an open access article under the CC BY-NC-ND license (<http://creativecommons.org/licenses/by-nc-nd/4.0/>).

Peer-review under responsibility of the organizing committee of the International Conference on Industrial Engineering (ICIE-2015)

Keywords: flexible suspension; control system; mathematical model; corrective device; adaptation.

1. Introduction

By studying various production machines and complexes it is possible to allocate electromechanical systems (EMS), which movement parameters shall be defined not by control, but by external force impact. The controlled electric drive (ED) of such systems is to monitor efforts with high precision in executive body and to compensate friction forces, elastic and gravitational forces, inertia forces of the joined masses affecting an object. While performing compensating condition of all effort components blocking the object moving, by applying to it insignificant additional efforts it starts moving which parameters (acceleration, speed, movement) are defined by

* *E-mail address:* g.pyatibratov@mail.ru; bogdanov_dmitr@mail.ru; azamatbekin@gmail.com

value and duration of adding external force impact. The specified performance features are contained in:

- balanced manipulators used for automation of manual work by moving freights of considerable weight [1];
- medical training machines used for restoration of broken functions of patient's musculo-skeletal system and activation of their rehabilitation during walking [2];
- special benches for adjusting of space equipment products on the Earth [3];
- simulators for cosmonauts training to work in non-gravity and reduced gravity conditions [4].

In studied systems the required spatial movements of an object are assured by their division into components in the horizontal and vertical planes, and also onto rotation and swinging of an object relative to its center of masses. In practice the most frequently division of object movements into components in the vertical plane is carried out with application of rope transmission and the required horizontal movements of an object are executed with use of bogies and bridges.

Attempts to minimize mass of studying mechanisms result in decreasing of their transmission and designs rigidity that defines requirement of negative impact accounting of mechanical linking elasticity on EMS operation.

The analysis of various approaches to execution of objects spatial movements detected that for developing of considered EMS it is necessary to apply the multiaxis control systems providing required mobility degrees [5]. Thus for high-quality control of compound object movement it is advisable to solve a problem of local systems synthesis.

Frequently a design feature of the considered mechanisms is use of flexible suspension for vertical movement of objects, necessity to estimate elasticity of mechanical transmissions and change of controlled object parameters that complicates synthesis of control systems. The design concepts and implementation features of objects' vertical movements systems (VMS) are reviewed in the paper [6]. The synthesis problem of efforts control system in rope transmission of VMS via use of optimal control theory is solved in [7].

For the development of theory and implementation experience of considered EMS the problem solution of control impacts synthesis is of interest to the system of object horizontal movements system (HMS) on flexible suspension via adding to it of external force influences.

2. Statement of the problem

Generally speaking the purpose of HMS control is object movement on flexible suspension without swings and rotations with the demanded movement parameters determined by external power influence. Thus the required performances of HMS are assured by coordinated control of bogie and bridge moving.

The analysis detected that the problem of HMS control is solved in the most complicated way at developing of advanced simulators for imitation of cosmonauts moving in non-gravity or reduced gravitation conditions [8]. We will study the features of the synthesis solution problem of HMS corrective device structure and parameters of the simulator providing cosmonaut movement in a space suit under the influence of his own muscular efforts with movement parameters as in actual practice. The system of object horizontal movements of the advanced simulator shall have the following parameters: the maximum mass of an object (a cosmonaut in a space suit) 200 kg, his required movement in any direction of 8 m with the maximum speed of 2.1 m/sec and acceleration up to 7 m/sec².

To solve the problem it is necessary to consider the features of controlled object which define the methodology of control effects synthesis:

- a cosmonaut moving in working space of the simulator can only happen under the influence of his muscular efforts that defined the requirement to research of disturbing effect system;
- high-precision compensation of friction forces and inertial forces from additionally joined masses to an object will demand considerable coefficients of strengthening that causes a problem to ensure stability of control system;
- impact on HMS operation of flexible suspension defines need of active damping via use of ED of object elastic vibration;
- by changing suspension length the parameters are modified which consider elastic-dissipative properties of the controlled object in the function of a cosmonaut position and it can require adaptive control of HMS.

3. Mathematical description of researched system

Taking into account the features of considered EMS in the paper [9] it is given the generalized linearized mathematical description of HMS formed by accounting elasticity of mechanical transmissions and swings of an object on flexible suspension. At the description of the system mechanical part (SMP) the following allowances were used: forces and torques are applied to not deformable lumped masses; elements of the bridge and bogie design under the influence of external forces aren't deformed, the bridge and the bogie have the same degree of mobility; directives assured the movement of bridge and bogie are located in the horizontal plane, friction forces don't depend on the position of bridge and bogie; the rope is weightless and in the course of work is always tensed; during VMS mechanism operation the radius of a drum and a point of descending from it rope remains constant; the mass center of weightlessness object is always on the straight line continuing a rope.

In Fig. 1 EMS block diagram of HMS disturbing effect is given via use of Laplace transformation. The direct channel is presented in the form of SMP structure considering impact of the elastic linkages defining swing of an object, and in the reverse channel the electric part of system is shown which properties are considered by transfer functions of current control closed loop (CCL) $W_{CCL}(s)$, synthesized corrective device (CD) $W_{CD}(s)$ and an angle transmitter $W_{AT}(s)$ of a rope deflection of an object suspension from a vertical position.

To have an opportunity of general conclusion for research results we apply relative units to make EMS mathematical description. For this purpose the engine torque M_D , the torque of an elastic element M_{el} , external torque M_{Ex} is defined relates to the nominal engine torque M_N ; the speed of mechanism shaft rotation Ω_M – relates to the speed of ideal engine hole shaft Ω_0 ; an angle α of an object deflection from a vertical position – relates to a basic deflection angle α_b equal to an angle of object deflection under fixed bogie and bridge by acting of external effort determined by torque basic value.

$$\alpha_b = M_N / \rho \cdot P_O \quad (1)$$

where ρ – reduction radius; P_O – object weight.

In Fig. 1 it is designated: T_M , T_O – mechanical constants of mechanism and object time; T_C , T_d – time constants specifying equivalent rigidity and damping properties of control object.

SMP features are described by transfer function

$$W_{SMP}(s) = \frac{1/\gamma}{T_{el}^2 s^2 + T_d s + 1} \quad (2)$$

where $\frac{1}{\gamma} = \frac{T_M}{T_M + T_O}$ – SMP amplification coefficient;

$$T_{el} = \sqrt{\frac{T_C T_M T_O}{T_M + T_O}} \text{ – time constant of own object elastic vibrations.}$$

For the solution of synthesis problem the simplification of ED control system was executed, due to this fact current control loop was folded and its properties are considered by transfer function $W_{CCL}(s) = 1/(T_{CCL} \cdot s + 1)$, where T_{CCL} – a time constant of current control closed loop. Sensor dynamic properties of an object deflection angle from a vertical are also described by transfer function of a periodic link with time constant T_{AT} .

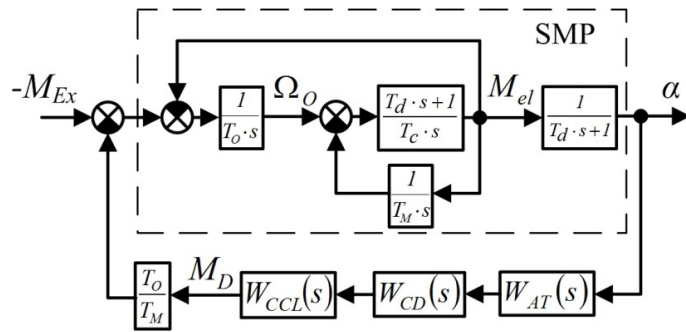


Fig. 1. The block diagram of researched EMS.

4. Problem solving

The studied features of HMS design and performance considerably complicate synthesis problem solving of required control effect. In the paper [10] we proved applicability and application methodology of frequency characteristics is given for research and synthesis of EMS with considerable vibrations at resonant frequencies. Analysis of CD possible structures detected that in general case it must have integro-differential properties. The researches executed in the paper [6] showed that in general case at sufficient high-speed action of CCL of an angle sensor when their signal transmission frequency exceeds own object vibration frequency on flexible suspension by several times, the high-quality functioning of HMS can be ensured via application of CD with transfer function.

$$W_{CD}(s) = k_{CD} \left(1 + \frac{k_I}{k_c T_I s} \right) \frac{k_c T_D s + 1}{k_c T_A s + 1} \tag{3}$$

The peculiarity of researched HMS is time constants T_C and T_d changing in process of its work which describes elastic and dissipative properties of the system. Researches detected that T_C and T_d values are changed depending on length of object suspension in compliance with the nonlinear law that it can demand HMS adaptive control by its implementation it is required to change CD time constants due to this fact k_c coefficient is entered into transfer function (Eq. 3).

The coefficient k_{CD} determines control precision of an angle, its required value can be estimated by given droop $\delta_A = \alpha(0)M_{Ex}(0)$ according to equation $k_{CD} = (T_M/T_O)(1/\delta_A - \gamma)$.

In control law there is the integral component with time constant T_I that gives droop to angle control system. It is recommended to apply $T_I \geq (2-4)T_{el}$. However it should be kept in mind that by using such method of increasing control precision of an angle high stability of angle measuring instruments is required and it causes considerable difficulties with system stability ensuring. That's why it is advisable to apply $k_I = 0$ while CD implementing.

Time constants T_D , T_A and their equation $k_\omega = T_D/T_A$ mostly impact on angle control quality in the researched system. That's why it is required to choose them in terms of condition providing maximum possible margin of system stability during its operation in substantial disturbances environment. It is recommended to use such T_D value, EMS resonant frequency of HMS taking into account CD action will be in the middle of frequency range from $\omega_D = 1/T_D$ to $\omega_A = 1/T_A$ where an angle sensor signal is differentiated. Taking into account these recommendations we will receive

$$T_D = (T_O T_C / k_{ACC})^{1/2} k_\omega^{1/4} \tag{4}$$

It is advisable to accept $k_\omega = 4-8$.

Time constant $T_A = T_D/k_\omega$ defines value of transmission coefficient of an angle control channel (ACC) relates to $\omega \gg \omega_{cr}$. By implementation and adjustment of CD T_A shall be specified in terms of working conditions of this system, electromagnetic compatibility of its elements and disturbances impact caused by substantial electric and magnetic fields. At a choice of coefficient k_ω we should seek to improve system noise immunity.

5. Research of horizontal movement system

We investigate HMS operation on the example of bogie control mechanism of the advanced simulator with a suspension length when elastic linkage has the minimum rigidity. In this case SMP properties are defined by time constants $T_O = 3.017$ sec, $T_M = 0.407$ sec, $T_Y = 0.311$ sec, $T_C = 0.270$ sec and $T_d = 0.003$ sec.

By HMS implementation of variable-frequency ED of Sinamics-S120 series (produced by Siemens company) was applied with Simotiond435i control system and angle sensor realized with use of the digital photo-electric angle converter LIR-237A (produced by “Special Design Bureau IS” in St. Petersburg).

The results of synthesis problem solving providing the required horizontal movements of an object with flexible suspension without vibrations should be carried out for EMS with single integration system of ED coordinates subordinate control while adjusting of current control for a modular optimum. In this case ED properties will be considered by CCL with frequencies bandwidth ω_{CCL} . Such engineering solution will assure ED and AS frequencies bandwidth several times exceeding frequency of swings of an object in closed HMS ω_{cr} .

In compliance with the requirements imposed to considered HMS simulator the control system should provide frequency drop of an angle $\delta_A = 0.02$ at amplitude minimization of an angle deflection resonant vibrations of rope transmission from a vertical.

To obtain necessary frequency characteristics of studied HMS we should apply Fourier transformation to transfer functions of the block diagram given on Fig. 1. According to the methodology presented in the work [11] by problem solving of synthesis structure and channel parameters of active damping of object swings with flexible suspension it is advisable to compare the logarithmic amplitude frequency characteristic (LAFC) of SMP $L_{SMP}(\omega) = 20\lg[\text{mod}W_{SMP}(j\omega)]$ and reverse LAFC of active damping channel of object swings $L_{ACC}^{-1}(\omega) = -20\lg[\text{mod}W_{ACC}(j\omega)]$ where transmission complex coefficient $W_{SMP}(j\omega)$ is defined by the equation (1), and $W_{ACC}(j\omega)$ according to the equation: $W_{ACC}(j\omega) = (T_O/T_M)W_{CCL}(j\omega)W_{CD}(j\omega)W_{AT}(j\omega)$.

At the initial stage of problem solving of CD synthesis it is advisable to define ACC required amplification coefficient. Depending on specified frequency drop of an angle δ_A the required value $k_{ACC} = 1/\delta_A - \gamma$ is actual in considered EMS $\gamma < 1/\delta_A$ and therefore reverse LAFC L_{ACC}^{-1} will pass much lower than abscissa axis and cross LAFC L_{SMP} at frequency ω_{cr} which is much higher than SMP resonant frequency ω_{el} , it allows to use asymptotical LAFC $L_{A\ SMP}$ at CD synthesis. In the considered range of frequencies at CD synthesis of HMS the asymptotical LAFC of SMP $L_{A\ SMP}$ and reverse LAFC of ACC L_{ACC}^{-1} can be defined by the following equations:

$$L_{ASMP}(\omega) = 20\lg(1/\gamma) - 40\lg\left(\sqrt{(T_{el}\omega)^2 + 1}\right) \quad (5)$$

$$L_{ACC}^{-1}(\omega) = -20\lg(k_{ACC}) - 20\lg\left(\text{mod}\left[\left[1 + \frac{k_I}{k_c T_I(j\omega)}\right] \frac{k_c T_D(j\omega) + 1}{k_c T_A(j\omega) + 1}\right]\right) \quad (6)$$

In Fig. 2 the frequency characteristics of studied HMS are presented illustrating the synthesis problem solution of required CD: precise LAFC of SMP $L_{SMP}(\omega)$, the asymptotical LAFC of SMP $L_{ASMP}(\omega)$ and ACC $L_{ACC}(\omega)$ and also resultant LAFC $L_{REZ}(\omega)$ showing change of an angle in studied HMS with CD synthesized. The integrate component of LAFC L_{ACC}^{-1} is indicated by the dash-dotted line.

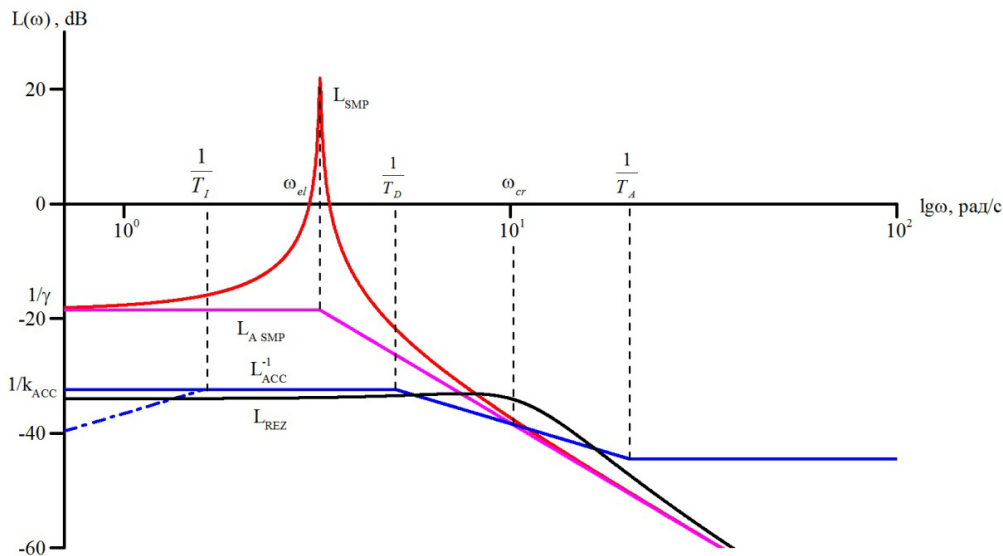


Fig. 2. Frequency characteristics of corrective device synthesis.

In this example $1/\gamma = 0.12$; $\omega_{el} = 3.21$ rad/s. As a result of CD synthesis problem solving we received its following parameters $k_{CD} = 5.62$; $k_I = 0$; $T_D = 0.20$ sec; $T_A = 0.05$ sec.

In Fig. 3 the simulation results of studied HMS are given. In Fig. 3 a transient processes in initial mechanical part of the system are presented and in Fig. 3 b in the system with synthesized CD. Transient processes are received via adding external stepped impact relates to 200 N effort

The static error of an angle control in opened HMS reaches 12% and in system with synthesized CD is 2%. Thus the time of transient process decreased from 189 sec to 0.52 sec. Over control in HMS with CD ranged 14.5%.

At considerable modification of suspension length in EMS operation process we should apply adaptive control realized via change of coefficient k_C , for example, reducing it by rope shorting of mechanical transmission while object moving.

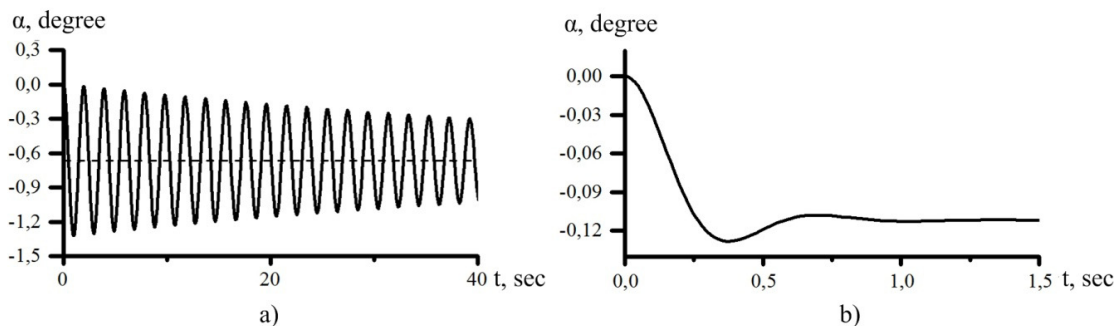


Fig. 3. Transient processes (a) in initial mechanical part of the system and (b) in the system with synthesized CD.

In case of the minimum transfer rigidity characterized by time constant T_{Cmax} we should take into account $k_C = 1$, by implementation of adaptive control it is required to change k_C together with T_C reduction according to the formula $k_C = (T_C / T_{Cmax})^{1/2}$.

If we don't apply adaptive control, it is recommended to define CD parameters at maximum T_{Cmax} value. In this case the acceptable results can be received at minimum T_{Cmin} values. In Fig. 4 the simulation results of studied HMS are given for the minimum suspension length with $T_{Cmin} = 0.0169$ sec via application of adaptation and without it.

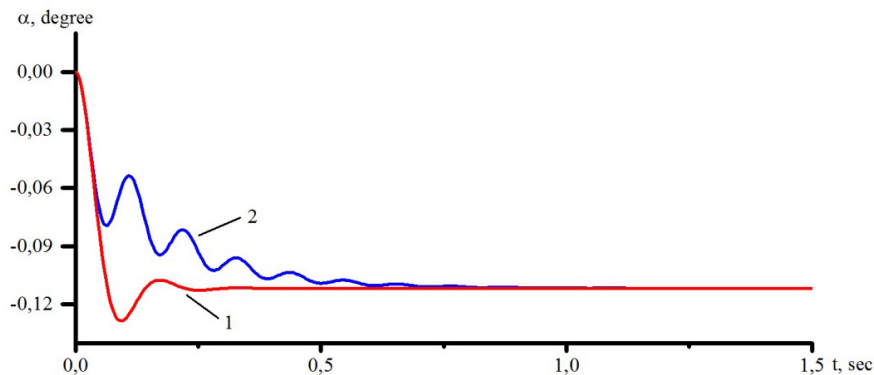


Fig. 4. Transient processes at minimum suspension length:
1 – via application of adaptive control; 2 – by setting minimum suspension length.

Researchers detected that at insufficient high-speed action of ED or considerable lag of force sensor it is advisable to apply CD with differentiation of higher order. The methodology of structure and parameters determination of such CD is given in papers [6, 12].

Conclusion

The results study of executed researches makes possible to do the following key findings:

1. In mechanisms implemented via use of objects flexible suspension while changing external force impact low damped vibrations appear complicating HMS operation.
2. To remove object swings with flexible suspension it is required to control electric drives of executing mechanisms via use of the monitoring principle of object moving.
3. For high-quality control of horizontal movements of an object with flexible suspension it is advisable to implement control system with feedback of rope deflection angle from a vertical.
4. The channel synthesis of angle deflection control of flexible suspension from a vertical is recommended to execute with application of reverse frequency characteristics of the electric drive control system.
5. In case of considerable change of suspension length in object vertical movements process CD should have adaptive properties. When adaptive control can't be carried out, CD adjustment is reasonable to apply on the smallest rigidity of rope transmission to corresponding maximum suspension length.
6. The horizontal movements system of an object with the synthesized CD assures high-quality control of object moving with flexible suspension under abrupt changes of external force impact.

The paper results are obtained with the support of project № 2878 "Theory development and implementation of electro-technical systems of simulator complexes and mobile objects" performed in terms of basic part of State assignment № 2014/143.

References

- [1] G.Ya. Pyatibratov, N.A. Sukhenko, Electromechanical force-compensating systems of lift-and-carry manipulators, Bulletin SUSU "Power Engineering" part. 14(4) (2014) 67–75.
- [2] L.L. Altunyan, A.A. Danshina, N.A. Sukhenko, Problems and objectives of medical simulators modification with electromechanical systems of patient's weight removal, Mechanical engineering: network electronic scientific journal. 2(3) 1–7.

- [3] G.Ya. Pyatibratov, V.P. Papirnyak, V.G. Polezhaev, A.I. Supchev, State, problems and modification methods of zero-gravity simulation for ground testing of space products, HEI news. North Caucasus reg. Engineering sciences. 3(4) (1995) 39–49.
- [4] O.A. Kravchenko, G.Ya. Pyatibratov, Implementation and operation experience of force-compensating systems assuring multifunctional training of cosmonauts to work in zero-gravity environment, HEI news. Electro mechanic. 2 (2008) 42–47.
- [5] O.A. Kravchenko, G.Ya. Pyatibratov, Design concepts, implementation and development prospects of multiaxis force-compensating systems of simulation complexes, AEP 2012 tr. VII Intern. (XVIII Russian) scien. conf. of automated electric drive. (2012) 495–499.
- [6] G.Ya. Pyatibratov, Design concepts and implementation of efforts control systems in elastic transmissions of electromechanical complexes, HEI news. Electro mechanic. 5-6 (1998) 73–83.
- [7] O.A. Kravchenko, G.Ya. Pyatibratov, Synthesis of optimal efforts controller in electromechanical systems with elastic linkages, HEI news. Electro mechanic. 4 (1998) 58–63.
- [8] G.Ya. Pyatibratov, N.A. Sukhenko, D.U. Bogdanov, N.A. Bachmanovskiy, Problems and development prospects of the simulator for training cosmonauts to work in planets with reduced gravitation, Manned space missions: mater. 10 Intern. scien. conf. (2013) 256–258.
- [9] O.A. Kravchenko, D.U. Bogdanov, D.V. Barilnik, Mathematical model of electromechanical multiaxis force-compensating system, Bulletin SUSU "Power Engineering" part. 14-1 (2014) 71–78.
- [10] G.Ya. Pyatibratov, The synthesis of electric drive subordinate control system minimizing dynamic loads in elastic mechanical transmissions, HEI news. Electro mechanic. 3 (1982) 296–303.
- [11] G.Ya. Pyatibratov, The compound research and design methodology of effort electromechanical control systems inn elastic transmissions of mechanisms, Dep. in VINITI 29.06.1999, №2119-B99.
- [12] G.Ya. Pyatibratov, O.A. Kravchenko, Implementation of effort control systems in elastic transmissions and executed devices of electromechanical complexes, HEI news. Electro mechanic. 1 (2008) 45–56.



International Conference on Industrial Engineering

The work roll bending control system of the hot plate rolling mill

Maklakova E.A., Maklakov A.S., Gasiyarov V.R., Voronin S.S.*

South Ural State University, 76, Lenin Avenue, Chelyabinsk, 454080, Russian Federation

Abstract

This article describes the kinds of thickness deviation arising during hot plate rolling process. The ways to determine thickness deviation by measuring the thickness of the sheet at various points are shown. The reasons of rolls bending under the rolling pressure are found. Examples of using the different structures for the implementation of the roll bending system are shown. The results of the system were considered in the hot rolling plate mill conditions.

© 2015 Published by Elsevier Ltd. This is an open access article under the CC BY-NC-ND license (<http://creativecommons.org/licenses/by-nc-nd/4.0/>).

Peer-review under responsibility of the organizing committee of the International Conference on Industrial Engineering (ICIE-2015)

Keywords: hot rolling, roll bending, sheet thickness, sheet flatness.

1. Introduction

The quality of the final rolled sheet greatly depends on its thickness deviation. This statement is applicable for thin and thick sheets, rolled on hot and cold rolling mills. Sheet thickness falls into two categories: longitudinal and cross (transverse) thickness. Both of these parameters define the final flatness of the sheet. The initial reduction of the slab, taking place on hot rolling, makes a significant influence on the geometric parameters of the metal. No matter the rolled plate is the final product or just the first step in getting a thin strip - the longitudinal and cross variation in thickness is laid in primary rolling passes.

* Corresponding author. Tel.: +7-922-013-27-72;
E-mail address: stsvoronin@gmail.com

2. Determination of the thickness deviation

The most common schemes of hot plate rolling are "longitudinal", "cross" and "angular" [1-3]. In these schemes all types of thickness deviation occur mostly in the cross passes. Thus, the cross component of the sheet thickness should be paid an attention. First of all, it is necessary to define what does "thickness deviation" mean?

The actual measurement of the sheet thickness n times at regular intervals of length and the mark their numbers $i = 1, 2, \dots, n$ gives a sheet thickness at every point h_i [4]. In this case the thickness difference means the deviation on the absolute value

$$\Delta_i = |h_i - h_{cp}|, \quad (1)$$

where $h_{cp} = \frac{1}{n} \sum_{i=1}^n h_i$ - the average thickness of the sheet.

Then, the average thickness variation of the sheet can be calculated by the next formula

$$\Delta = \frac{1}{n} \sum_{i=1}^n \Delta_i. \quad (2)$$

As shown on formulas (1,2) the accuracy of the thickness deviation value depends on the number of measurements. It is very difficult to make a large number of measurements under real conditions. Therefore, the sheet thickness measured at the three points: at the center and at the lateral edges (at some distance from the edge). The values obtained on the edges are averaged, and the difference between this two values is the desired value.

During the rolling process it's difficult to take into account all parameters impact on the cross thickness deviation of the rolled sheet. The same difficulties take place in developing of the automated rolling control system. More than 10 different factors may counted in the first approximation, including deformations as sheet metal, as rolling equipment. The temperature of the rolling play a central role, also the force and speed of rolling. In this situation it's better to avoid a complex approach and separately calculate the influence of each component. The component combination and development of the control system are carried out after finishing all mathematical calculations and its improvement on the computer models.

3. The work roll bending

One of the most influential parameter on the hot plate geometry is the bending of the work rolls. The consideration that all rolls in the main rolling cage have an ideal geometric form of cylinder (in the case of rolling in "quarto" stand) allows to determine a "work roll bending" (figure 1, a). Another assumption is the constant roll-gap during work roll width. In such condutions, at the rolling moment, the rolls bend takes place under the metal impact, that has a negative influence on the sheet geometry (figure 1, b). A value of the bending can be identified by rolling force "P". A dependence between the bending value and the cross-section of the work roll is called "bending curve". The form of the "bending curve" is complex, vaguely resembling a parabolic.

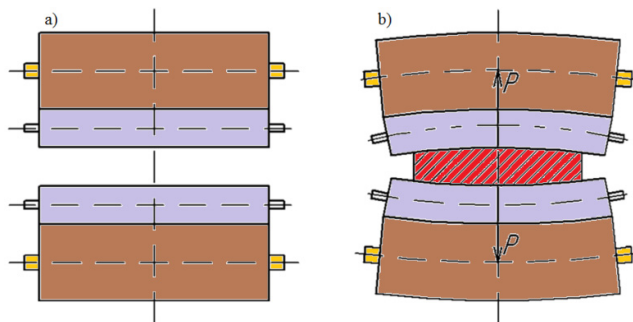


Fig. 1. Rolls of the "quarto" stand without the force (a) and under the rolling metal pressure (b).

Some hot rolling mills have work rolls with special-curved cross section. Nevertheless, the "curved rolls" can compensate the rolling pressure just under a particular set of parameters, like a rolling force, rolling speed and initial sheet profile. A majority of modern rolling mills to eliminate the roll bending value during the operation, are equipped with a work roll bending system (WRBS) [4].

WRBS has a hydraulic cylinders at the roll edges, which create a compensation force. The value of this force must convert the bending curve into constant roll-gap. Figure 2 shows an example of WRBS realization.

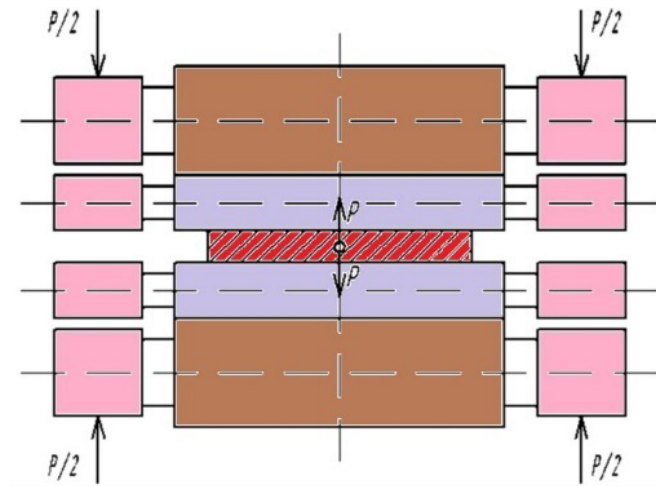


Fig. 2. The typical scheme of WRBS.

Another way to avoid the roll bending is the rolling with rolls put in the electromagnetic field [5]. External rolls are made hollow. Special pistons are mounted into the rolls with ability to move along the roll axis both jointly and separately (figure 3). In this way, rolls can form different forms and sheet thickness depending on pistons position. It allows to increase the accuracy and quality of finished product using simple design of roll stand. However, using the pistons has own weaknesses. One of them is the lack of relation between some electromagnetic parameters leading to the complex modelling process.

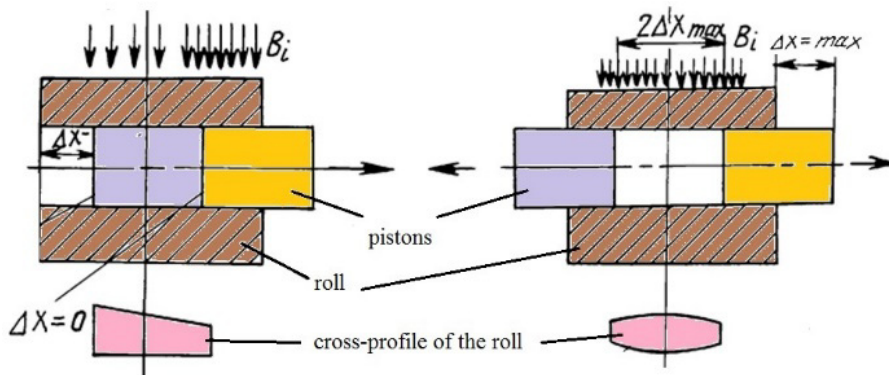


Fig. 3. A method of the cross-profile roll formation.

One more method of the sheet flatness control includes the dependence of the roll bending in the change of electromagnetic, physical and mechanical parameters of the rolling process. Authors [6] suggest how the independent electromagnetic, physical and mechanical properties of rolling influence on the sheet bending (equation 3).

$$y_{\Sigma \zeta=0 \rightarrow 1} = \frac{3 \cdot 9315}{13440 + 38,5\alpha_g} \cdot \frac{B_x^2 \cdot S \cdot \cos\alpha}{\mu_0 \cdot L_v} \cdot \frac{B_n \cdot \alpha_g \cdot (1 - \mu_{01}^2)}{\pi \cdot E_0 \cdot v} \cdot \left\{ \frac{1}{72} (\zeta - 2\zeta^3 + \zeta^4) + \frac{1}{8!} [7 - 420\zeta + 420\zeta^2 - 448 \cdot (\zeta - 0,5)^6] \right\} - \frac{B_x^2 \cdot S \cdot \cos\alpha}{\mu_0 \cdot L_v} \cdot \frac{(L_v - B_n)^2 \cdot \alpha_g \cdot (1 - \mu_{01}^2)}{24 \cdot \pi \cdot E_0 \cdot v \cdot B_n} \cdot (\zeta - \zeta^3), \quad (3)$$

where $\zeta = \frac{x}{B_n}$, ($X = 0; 0.1B_n; \dots; 0.9B_n, B_n$); $\frac{B_x^2 \cdot S \cdot \cos\alpha}{\mu_0 \cdot L_v} = \frac{\Phi_{ax}^2 \cdot \cos\alpha}{S \cdot \mu_0 \cdot L_v} = \frac{P_{ax}}{L_v} = q_x$; $\frac{B_x^2 \cdot S \cdot \cos\alpha}{\mu_0} = P_{ax}$;
 $\cos\alpha$ – an angle between the force of gravity of the roll to the pole and the vertical plane; $\mu_0 = 4\pi \cdot 10^{-7} = 12.57$ – magnetic permeability of vacuum; $\mu_{01} = 0.5$ – Poisson's ratio; $E = 2 \cdot 10^8$ – elasticity modulus of the roll; $\sigma_s = 500 \cdot 10^3$ – the yield point; L_v – the length of the work roll; B_n – sheet width; H – sheet thickness; h – sheet thickness after rolling pass; B_x – magnetic induction; $S = \frac{L_b \cdot D_n \cdot \pi}{4}$ – the contact area of the electromagnet poles with a roll (the air gap area); D_n – the diameter of the pressure roll; k – the density coverage pole ratio of the surface electromagnet and the roll; $\alpha_g = \frac{\pi \cdot E_0 \cdot v \cdot B_n^3}{(1 - \mu_0^2) \cdot E \cdot J}$ – roll flexibility; $J = 0.8R_p^4 = 0.05D_p^4$ – roll moment of inertia; $E_0 = \frac{\sigma_s}{\varepsilon}$ – deformation module of the sheet; $\varepsilon = \frac{H-h}{H}$ – relative reduction; $v = \sqrt{0.5D_p \cdot \Delta h} = \sqrt{0.5D_p(H-h)}$ – the arc length of capture; $\zeta_0 = 0$; $\zeta_1 = 0.1$; $\zeta_2 = 0.2$; $\zeta_3 = 0.3$; $\zeta_4 = 0.4$; $\zeta_5 = 0.5$; $\zeta_6 = 0.6$; $\zeta_7 = 0.7$; $\zeta_8 = 0.8$; $\zeta_9 = 0.9$; $\zeta_{10} = 1$; P_{ax} – active electromagnetic force applied to the roll (the result of an electromagnetic pressure); D_p, R_p – diameter and radius of the work roll; Δh – absolute reduction; Φ_{ax} – magnetic flux.

Changes of the roll bending and the sheet profile occur due to the change of the magnetic flux with the extent of the roll gap. Thus, the magnetic induction and distribution of the active electromagnetic load changes along the work roll. As a result, the different configurations of the roll gap and changes in the thickness and profile of the sheet during rolling can be obtained.

4. Results of the WRBS operation

In practice, the widely used mechanisms to control the WRBS are servo and proportional valves. For example, the mill 5000 of Magnitogorsk Stel Works is equipped with eight cylinders - four on each work roll [7-10]. The operation of the WRB system is shown on figure 4.

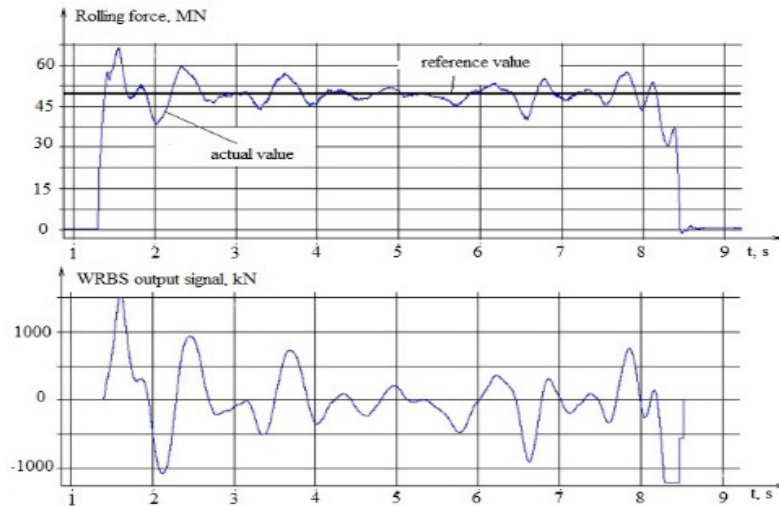


Fig. 4. WRB system operation.

Pressure sensors are used to measure the pressure in the piston rod and the stock cavity. Different handling of valve groups are used to control the pressure in the work-roll bending mode. The WRBS is used for rolling force control and works as follows: the actual value of the rolling force is subtracted from the expected value, then the difference is multiplied by a gain, which is determined by rolling model. The resulting value is used as an additional signal to force regulator. In case of a deviation of rolling force from target value, the output signal of the control system is corrected.

References

- [1] S.S. Voronin, D.U. Usatyi, The range of rolling mills and basic schemes of sheet reduction on the hot plate rolling mill, Achievements of university research, Novosibirsk, 2013, pp. 99–105.
- [2] V.R. Gasiyarov, D.U. Usatyi, The thickness control system of the hot plate mill 5000, Technology and production automation processes in metallurgy, 2012, pp. 126–130.
- [3] S.S. Voronin, D.U. Usatyi, A variable compression slab technology in the vertical and horizontal rolling cages of the hot plate mills, Actual problems of modern science, technology and education. 71 (2013).
- [4] A.I. Rudskoy, V.A. Lunev, Theory and technology of rolling production, Saint-Peterburg, 2005.
- [5] V.I. Abramenko, G.L. Kochi, A.M. Sorokin, L.G. Delusto, V.Y. Antonov and P.B. Gorelik, Russian Patent 2,146,971 (2000).
- [6] S.V. Soldatov, L.G. Delusto, A.I. Nikiforov, V.M. Benenson, G.V. Evilin and V.N. Ulanov, Russian Patent 2,216,417 (2002).
- [7] V. R. Gasiyarov, O. A. Zalogin, A. A. Radionov, The strip thickness, profile and flatness control systems of the Magnitogorsk steel works hot plate mill 5000, Urals science and industry, 2010, pp. 107–112.
- [8] V. R. Gasiyarov, A. A. Radionov, L. V. Radionova, D. U. Usatyi, Automatic control of the geometry of the hot plate rolling mill 5000, All-Russian multiconference on control problems. 4 (2011) pp. 307–309.
- [9] S. S. Voronin, D. U. Usatyi, Work roll bending as a parameter that affects the lateral variation in thickness of the sheet and work roll bending control system of the hot rolling mill, Russian Internet Journal of Industrial Engineering. 1 (2013), pp. 51–55, URL: <http://www.indust-engineering.ru>
- [10] Radionov, A.A., Gasiyarov, V.R., Gasiyarova, O.A., Automatic gap control of Plan View Pattern Control Mechatronics System, Source of the Document 2015 International Siberian Conference on Control and Communications, SIBCON Proceedings, 2015, pp. 1–4.



International Conference on Industrial Engineering

Retrofit simulator to train cosmonauts for working in non-gravity and reduced gravity environment

Pyatibratov G.Y., Bekin A.B., Bogdanov D.Y.*

Electromechanical Faculty, Platov South-Russian State Polytechnic University (NPI), 132, St. Prosvescheniya, Rostov region, Novocherkassk, 346428, Russian Federation

Abstract

The paper describes implementation and operational features of the object transfer systems in the working space of simulators for training cosmonauts to fulfill extravehicular activity in non-gravity and reduced gravity environment. The control system design concepts of cosmonauts' horizontal movements under non-gravity and reduced gravity environment simulation were studied. It was proved necessary to apply electromechanical systems for friction and inertial force compensation by additionally joined masses to the non-gravity object while implementing advanced simulators. The control system structure was developed; it contains feedbacks on current, speed and electric drive shaft accelerations, as well as on belt transmission force and power drive cable deflection angle from the perpendicular position. The paper presents the results of synthesizing the cosmonauts' movement control system structure in the working space of simulators, as well as of correcting device parameters to provide damping of springy oscillations in machinery.

© 2015 Published by Elsevier Ltd. This is an open access article under the CC BY-NC-ND license (<http://creativecommons.org/licenses/by-nc-nd/4.0/>).

Peer-review under responsibility of the organizing committee of the International Conference on Industrial Engineering (ICIE-2015)

Keywords: simulator; non-gravity simulation; electric drive; synthesis; efforts control system.

* Corresponding author. Tel: +7-918-544-12-34;
E-mail address: bogdanov_dmitr@mail.ru

1. Introduction

To perform long-range programs for development of near-Earth space, the surfaces of the Moon and Mars cosmonauts should gain required experience and be trained on simulator complexes specially made for this. It is necessary to have simulators with high quality performance and high functionality in order to increase cosmonauts' training level to work in non-gravity and reduced gravity environment.

While training cosmonauts items of extravehicular activity (EVA) during long term occupation in mission-ready suits by using variable equipment designed to operate in outer space or in the planets with gravity forces lower than on the Earth it is reasonable to apply simulators with electromechanical object transfer systems (OTS) [1]. In such simulators cosmonaut's movement imitation in non-gravity or reduced gravity environment is assured by compensation system of gravity force and other effort components blocking cosmonauts' movement.

While implementing OTS cosmonaut's complex spatial movement in simulator working space is divided into vertical and horizontal components, as well as into rotating and rolling motions towards mass center. Vertical movements simulation of an cosmonaut in the spacesuit (m_0) with required speeds and accelerations, as well as his weight compensation (full or partial) is assured by the vertical movements system (VMS) implemented by using a flexible suspension usually in the form of steel-cable. The horizontal movements system (HMS) provides horizontal movements simulation of a cosmonaut in the spacesuit.

In simulators with electromechanical OTS a cosmonaut's movement in the spacesuit with required speeds and accelerations is specified only by cosmonaut's muscular efforts. Herewith the important task of HMS is to neutralize friction forces in its mechanisms and to minimize impact on cosmonaut's movement parameters in the spacesuit, inertial torques additionally joined masses (m_{AM}) to the non-gravity object.

2. Actuality of the research

At present time, "Vykhod-2" simulator is exploited in FSBEI "Y.A. Gagarin SRI CTC" (Zvezdny gorodok, Moscow Region). This simulator is used for adjustment of cosmonauts operations on open space going and extravehicular activity in non-gravity environment, and also for working on space suit system control in standard and non-nominal situations [2]. Outward appearance of "Vykhod-2" simulator is presented on Fig. 1.



Fig. 1. Outward appearance of "Vykhod-2" simulator.

"Vykhod-2" simulator contains two independently working VMS and HMS, which separates space movement of cosmonaut in space suit on vertical and horizontal intensity. The moving of cosmonaut in space suit total mass less than 250 kg in non-gravity conditions on "Vykhod-2" simulator can be executed on minimum effort values (30–40) N, and it allows cosmonaut to move with maximum speed under 0.4 m/sec and acceleration under 0.2 m/sec² [3].

Every VMS of “Vykhod-2” simulator is realized with the use of variable-frequency electric drive (ED) with synchronous engine with permanent magnets (SMPM). High-accuracy effort regulation system inside space suit cable suspension provides required degree of weight deprivation and vertical moving of cosmonaut in space suit with required speed and acceleration in working area only due to the muscular force. Executed tests showed, all technical solutions on VMS realization of “Vykhod-2” simulator might be successfully applied while prospective simulator developing [4].

Bridge and bogie transfer mechanisms of “Vykhod-2” simulator are made via pneumatic support on air cushion, that allows providing friction coefficient as 0.004–0.005 and to decrease starting force while cosmonaut horizontal moving. Studies indicated, while acceleration increasing during horizontal moving of a cosmonaut in space suit, bogie and, especially, bridge inertial forces influence on transfer parameters is significantly increased. That is why HMS of prospective simulators is necessary to execute via using of active methods of inertial forces compensation by additionally masses joined to the weight derivate objects.

Prospective issues of cosmonauts training analysis demonstrated, “Vykhod-2” simulator is not able to provide required transfer imitation of a cosmonaut in space suit similarly to the transfer in gravity conditions of the Moon and Mars [5]. Therefore, there is a need to create HMS of providing movement of cosmonauts with increased speeds and accelerators for new generation simulators creation for cosmonauts training on Moon and Mars programs realization.

3. Statement of the problem

Executed analysis [6] demonstrated prospective simulator for cosmonauts training should supply cosmonaut transfer in space suit with maximal vertical speeds and accelerators up to 1.8 m/sec and up to 5.8 m/sec², and horizontal – respectively, up to 2.1 m/sec and up to 7.4 m/sec².

In the research [7], for masses minimization additionally joined to the weight derivate object, it is recommended to use ED with belt transmission in HMS of developed simulators; it will permit to raise the quality of cosmonaut transfer imitation which is in line with real conditions. There are following recommended ways of VMS and HMS realization:

- VMS of electromechanical unit is advised to be on bridge construction, reeving rope should be made with polyspast using;
- HMS of electromechanical unit of bogie is advised to be on bridge construction;
- HMS of electromechanical unit of bridge is advised to be on OTS.

Mentioned constructive solution enables to essentially decrease mechanical lag of drives HMS, but can be a reason of elastic vibrations appearance in belt transmission. Due to this fact, there is a rising necessity of researching of electric drive HMS control system taking into account elastic properties of mechanisms. At the same time, change of belt transmission equivalent stiffness becomes a reason of change of controlled object combined parameter which are depends on cosmonaut position inside simulator working space. Besides, a complicated kinematic scheme of mechanisms HMS with great gear ratio implies significantly frictional forces. Taking into account the fact that mechanical inertia of electrical drives of bogie and bridge is different, it is necessary, inside HMS control system, to foresee ways and tools for faults alignment on speed and accelerator for these coordinates. Cosmonaut swinging on flexible suspension is exists owing to belt transmission application in VMS. Moving of cosmonaut in space suit is realized only by his muscular force, and this fact defines the need of HMS synthesis task solution while external disturbances.

Subjected to HMS of functioning features, we can determine efficient control system structure which might the provision of prospective issues on cosmonaut testing in non-gravity and reduced gravity conditions.

4. Proof of effective control system structure of horizontal moving of cosmonauts

All While problem solving of HMS structure synthesis, a complicated object containing several internal cross feedbacks, non-linear characteristics and variable control parameters, having vibration properties, and working in accidental force conditions, is necessary to be reviewed. To upgrade transfer imitation quality of cosmonaut in space suit in non-gravity and reduced gravity conditions, there is a need to resolve the following interjoined issues:

- to provide the decrease of elastic vibrations influence in HMS belt transmissions of bogie and bridge;
- to compensate static and dynamic frictional forces of mechanisms;
- to minimize the impact of mechanical lag of bogie and bridge electric drive on acceleration fault;
- to eliminate the cosmonaut swinging on flexible suspension.

Structural synthesis problem of automatic control system is complex, and there is no general solution. And so, determination of HMS structure and proof of application of necessary feedback is executable, but taking into account their functional purpose and possibility of its practical realization.

As a case in point, we consider HMS of bogie in which electrical drive is realized with employ of SMPM made by Siemens AG, High Dynamic series, 1FK7033-5AF21 type (380 W; 314 rad/sec; 1.2 N·m; $J_{EE}=0.27 \cdot 10^{-4} \text{ kg} \cdot \text{m}^2$; $m_{EE}=3.1 \text{ kg}$). A belt transmission is performed using ALPHA Linear H50 saw-tooth belt made by Optibelt.

To have an opportunity of general conclusion for research results, we apply relative units. For this case, all speeds relates to idle speed of SMPM – ω_{E0} , all moments and forces – to nominal engine torque – M_{EN} , and based value for deflection angle reduction of rope VMS, from the vertical while bogie transfer to relative units, is accepted as following:

$$\alpha_{B_X} = \frac{M_{EN_X}}{(m_0 + m_{AJM}) \cdot g \cdot \rho_X} \quad (1)$$

Table 1 brings parameters of generalized mathematical model of bogie HMS which are necessary for horizontal transfer control system synthesis issue resolving of cosmonaut in space suit.

Table 1 Parameters of generalized mathematical model of bogie HMS.

Name of parameter	Designation	Value
Mechanical time constant of EMM, sec	T_X	0.039
Mechanical time constant of bogie, sec	T_T	0.368
Mechanical time constant of object, sec	T_{0_X}	3.017
Time constant considering dissipative properties of belt transmission, sec	T_{d_BT}	0.006
Time constant considering elastic properties of belt transmission, sec	T_{c_BT}	0.005
Time constant considering dissipative properties of object swinging, sec	T_{d_os}	0.001
Time constant considering object swinging, sec	T_{c_os}	0.27
Time constant considering converter lag, sec	T_{c_X}	0.00075
Electrical time constant of electrical engine, sec	T_{E_X}	0.0049
Electrical coefficient of electrical engine transmission, r.u.	k_{E_X}	29.73

To decrease influence of ED of electromagnetic lag, to weaken undesirable impact of anti-EMF, to stable electromagnetic moment of electric engine (EE), and to realize current limitation, there is a need to use negative feedback (NFB) on EE current. At the same time, it is recommended to use current proportional-integral controller (PI-controller), which ensures ED quick-action, necessary for active damping of elastic vibrations in belt transmission [8].

To realize active method of elastic vibrations damping of effort using ED, current PI-controller parameters should have the following values:

$$W_{PI_X}(s) = \frac{0.0049 \cdot s + 1}{0.0446 \cdot s} \tag{2}$$

To decrease vibrations of effort dynamic component in belt transmission, there is a need to use flexible NFB on the effort which will allow promoting reliability and durability of mechanism operating. The choice of structure and parameters of Compensative Device (CD) are defined in accordance with recommendations mentioned in the research [9]:

$$W_{CDI_X}(s) = \frac{0.03 \cdot s}{0.005 \cdot s + 1} \tag{3}$$

Advised block diagram for control system of bogie horizontal transfer with NFB on EE current, and with NFB on effort in belt transmission, is presented on Fig. 2.

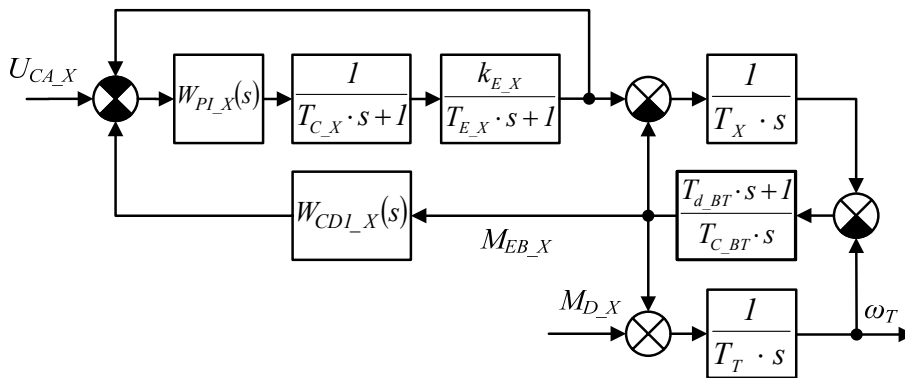


Fig. 2. The block diagram of bogie HMS with NFB on effort in belt transmission.

In Fig. 3 it is presented the application results of active damping way of springy oscillations efforts in HMS belt transmission of the bogie with actual value of external step disturbance $M_{D_X} = 1.23$ p.u. with 1 sec duration acting on the bogie.

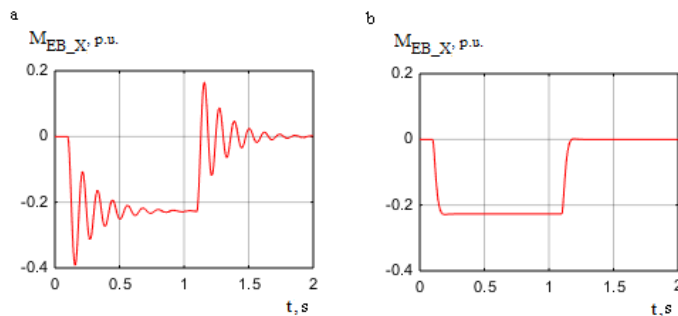


Fig. 3. Transient processes of the torque in the springy element of belt transmission M_{EB_X} in HMS of the bogie: (a) without negative force feedback; (b) with springy negative force feedback.

In Fig. 3a the highest peak value of oscillations effort in the belt transmission is 72% of steady state value, but the time of transient one is 0.5 sec. Application of negative force feedback in the belt transmission and corrective devices with specified parameters is capable for complete damping of oscillations (Fig. 3b). Herewith the time of the transient process is 0.08 sec that is 6.25 times less than in the system without negative force feedback.

In Fig. 4 it is presented the block diagram of the control system of cosmonaut’s horizontal movements in the spacesuit, it shall be implemented with considerable rigidity of the belt transmission HMS of the bogie by using the belt ALPHA Linear H150. In this case the main negative feedback of VMS cable deflection angle out of perpendicular position shall assure required static and dynamic performance of HMS operation. Structure and parameters synthesis of the corrective device with transfer function $W_{CD2_X}(s)$ should be performed with application of reverse frequency response in compliance with the methodology presented in the paper [10] or using methods of optimal control studied in [11].

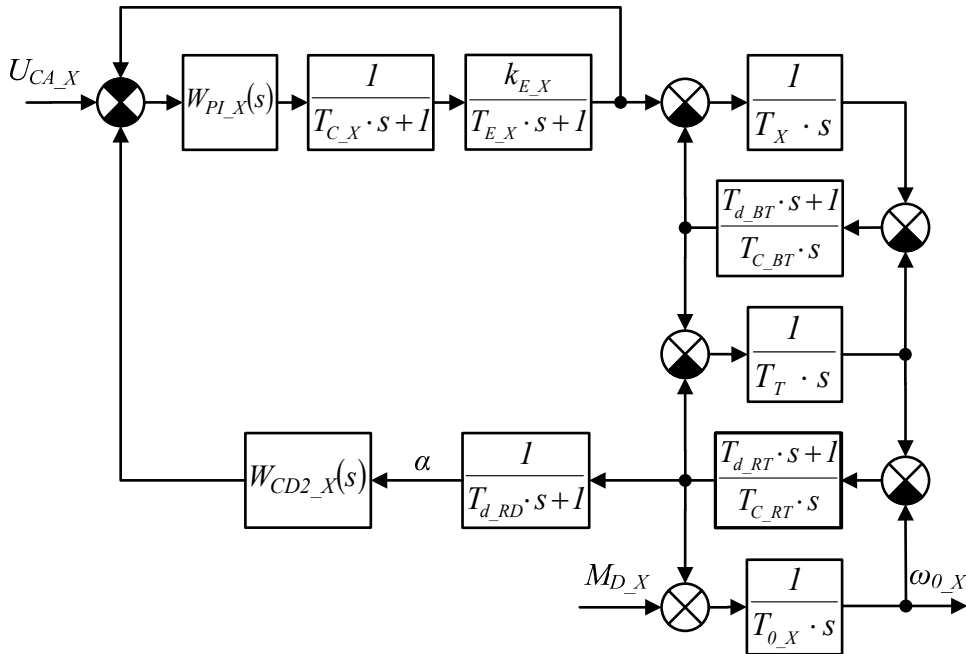


Fig. 4. The block diagram of HMS of the bogie with NFB of cable deflection angel of VMS out of perpendicular position.

In compliance with the synthesis methodology presented in [10] we can detect the transfer function of the corrective device in terms of VMS cable deflection angle out of perpendicular position

$$W_{CD2_X}(s) = 4 + 4.5 \frac{I}{s} + \frac{2 \cdot s}{0.005 \cdot s + 1} \tag{4}$$

In Fig. 5 it is presented the results of reducing springy oscillations of the cable deflection angle under step disturbance $M_{D_X} = 1.23$ p.u. with 10 sec duration forced on the weight derivate object.

In Fig. 5a the steady-state value of the cable deflection angle is 0.16 p.u., the transient overshoot index reaches 96%. In this case the angle springy oscillations have weak decaying nature. Application of angle negative feedback and corrective devices with recommended settings gives the possibility to minimize deflection of VMS cable out of perpendicular position (Fig. 5b). The transient overshoot index reaches 4%, but the time of transient process is 3 sec.

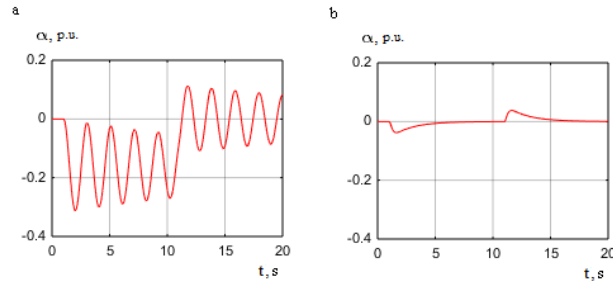


Fig. 5. Transient processes of cable deflection angle: (a) without negative angle feedback; (b) with negative angle feedback.

By using in the drive mechanism of bogie in HMS the belt ALPHA Linear H50 with lower rigidity it is recommended to apply the control system block diagram of cosmonaut’s horizontal movements presented in Fig. 6. In this case it is reasonable to use effort feedback in belt transmission and corrective device with transfer function

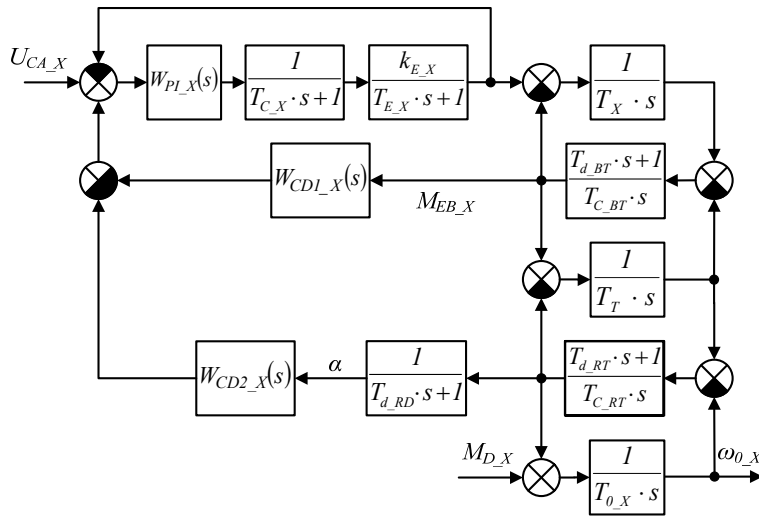


Fig. 6. The control system block diagram of cosmonaut’s horizontal movements.

In Fig. 7 it is presented the transient processes of effort in the belt transmission under external step disturbance of the weight derivate object.

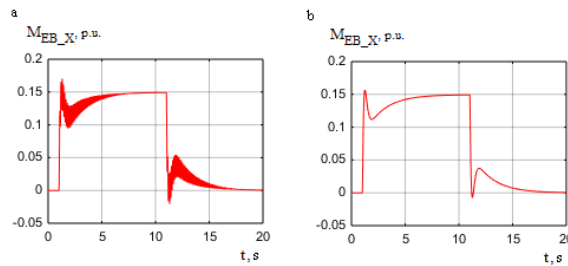


Fig. 7. Transient processes of effort torque in belt transmissions $M_{EB,X}$ in HMS of the bogie with NFB of the angle:
(a) without NFB of force; (b) with NFB of force.

In the system with NFB cable deflection angle of VMS without effort NFB there are oscillations in belt transmission HMS of bogie with frequency 4.1 Hz (Fig. 7a). By implementing effort NFB with CD of the type (3) belt springy oscillations are completely removed (Fig. 7b).

To improve operating quality of HMS it is reasonable to use auxiliary feedbacks. To neutralize adverse impact of engine counter EMF on control processes in HMS it is advisable to apply positive feedback of electric engine implemented according to the recommendations given in [10].

To assure cosmonaut's movement parameters identity in simulator working space for variable directions activated by electric drives of bogie and bridge it is advisable to use engine acceleration feedback [11], it makes possible to assure the same acceleration errors for all coordinates of the system.

To neutralize the viscous friction forces impact of the mechanisms on HMS operation it is required to use positive feedback of engine speed and to reduce unlubricated friction forces it is proposed to use nonlinear control with switching structure. Guidelines for system implementation and adjustment while neutralizing friction forces of power transmissions are given in the paper [12].

Practical implementation of multicircuit control system of HMS requires approving of high-speed operation of all control circuits. Implementation of proposed methods and technical solutions helps to design modern simulators for cosmonauts training to solve problems of space exploration.

Conclusion

The results study of executed researches makes possible to do the following key findings:

- While HMS developing of advanced simulators to train cosmonauts for working in non-gravity and reduced gravity conditions it is required to apply active methods of friction and inertial force compensation by additionally added masses to the weight derivate object.
- Generally speaking the control system of astronaut's horizontal movements in spacesuit shall have feedbacks of engine current, belt transmission force of bogie and bridge moving mechanism, speed and acceleration of electric drive, as well as key feedback of cable deflection angle of VMS mechanism out of perpendicular position.
- The described structure of HMS with advisable parameters of controllers and corrective devices makes possible to assure the required quality of cosmonaut's movement control in working space of advanced simulator designed to train cosmonauts for performing Moon and Mars programs.

The paper results are obtained with the support of project № 2878 "Theory development and implementation of electro-technical systems of simulator complexes and mobile objects" performed in terms of basic part of State assignment № 2014/143.

References

- [1] G.Y. Pyatibratov, O.A. Kravchenko, V.P. Papirnyak, Implementation Methods and Ways of Simulators Improvement to Train Cosmonauts for Working in Non-gravity Conditions [Sposoby Realizatsii i Napravleniya Sovershenstvovaniya Trenazherov dlya Podgotovki Kosmonavtov k Rabote v Nevesomosti], *Izv. vuzov. Elektromekhanika*. 5 (2010) 70–76.
- [2] Information on <http://www.getc.ru/main.php?id=2894>
- [3] D.V. Baryl'nik, G.Y. Pyatibratov, O.A. Kravchenko, Force Balancing Systems with AC Electric Drives of Cosmonauts' Training Complexes [Silikompensiruyushchie Sistemy s Elektroprivodami Peremennogo Toka Trenazhernykh Kompleksov Podgotovki Kosmonavtov], *Yu.-Ros. gos. tekhn. un-t (NPI), Novocherkassk: Red. zhurn. «Izv. vuzov. Elektromekhanika»*. (2012) 176.
- [4] G.Y. Pyatibratov, N.A. Sukhenko, D.V. Bogdanov, N.A. Bachmanovskiy, Challenges and Opportunities of Simulator Development to Train Cosmonauts for Working on the Planets with Reduced Gravity [Problemy i Perspektivy Sozdaniya Trenazhera dlya Podgotovki Kosmonavtov k Deystviyam na Planetakh s Ponizhennoy Gravitatsiey], *Manned space missions [Pilotiruemye polity v kosmos]: mater. 10-y Mezhdunar. nauch.-prakt. konf.* (2013) 256–258.
- [5] G.Y. Pyatibratov, D.V. Baryl'nik, A.B. Bekin, N.R. Zhamaletdinov, Retrofit Objectives of the Simulator "Vikhov 2" for Solving Problems of

- Cosmonauts' Physical Readiness Evaluation to Work on Mars [Zadachi Sovershenstvovaniya Trenazhera "Vikhov 2" dlya Resheniya Zadach po Otsenke Fizicheskoy Gotovnosti Kosmonavtov k Deyatelnosti na Marse], [Pilotiruemye polity v kosmos]: mater. 10-y Mezhdunar. nauch.-prakt. konf. (2013) 258–260.
- [6] G.Y. Pyatibratov, A.M. Kivo, O.A. Kravchenko, Electromechanical Systems of Special Simulators Providing Cosmonauts' Training to Move on Planets with Reduced Gravity [Electromekhanicheskie Sistemy Specialnykh Trenazherov, Obespechivayushchikh Otrabotku Kosmonavtami Peremeshcheniy na Planetakh s Ponizhennoy Gravitatsiyey], AEP- 2012: tr. VII Mezhdunar. (XVI II Vseros.) nauch. konf. po avtomatizirovannomu elektroprivodu. (2012) 612–616.
- [7] A.B. Bekin, G.Y. Pyatibratov, O.A. Kravchenko, D.Y. Bogdanov, Justification of Rational Design and Option of Simulator Electric Drives for Training Cosmonauts to Work in Reduced Gravity Conditions [Obosnovanie Razionalnoy Konstruktsii i Vybora Elektroprivodov Trenazherov dlya Podgotovki Kosmonavtov k Deystviyam v Usloviyakh Ponizhennoy Gravitatsii], 2015 International Siberian Conference on Control and Communications (SIBCON). Proceedings. (2015).
- [8] G.Ya. Pyatibratov, Feasibility of Electric Drives Application of Active Oscillation Limitations of Springy Power Transmissions [Vozmozhnosty Primeneniya Elektroprivodov dlya Aktivnogo Ogranicheniya Kolebaniy Uprugikh Mekhanicheskikh Peredach], Izv. vuzov. Elektromekhanika. 10 (1990) 89–93.
- [9] G.Ya. Pyatibratov, System Synthesis of Electric Drives Subordinate Control Minimizing Dynamic Loads of Springy Power Transmissions [Sintez Sistem Podchinennogo Regulirovaniya Elektroprivodov, Minimiziruyushchikh Dinamicheskie Nagruzki v Uprugikh Mekhanicheskikh Peredachakh], Izv. vuzov. Elektromekhanika. 3 (1982) 296–303.
- [10] G.Ya. Pyatibratov, Design Concepts and Implementation of Force Control Systems in Springy Transmissions of Electromechanical Complexes [Printsipy Postroeniya i Realizatsii System Upravleniya Usiliyami v Uprugikh Peredachakh Elektromekhanicheskikh Kompleksov], Izv. vuzov. Elektromekhanika. 5-6 (1998) 73–83.
- [11] O.A. Kravchenko, G.Ya. Pyatibratov, N.A. Sukhenko, A.B. Bekin, Design Concepts and Implementation of Gravitation Force Balancing System [Printsipy Postroeniya i Realizatsii System Kompensatsii Sily Tyazhesti], Izv. vuzov. Severo-Kavkazskiy region. Tekhnicheskie nauki. 2 (2013) 32–35.
- [12] O.A. Kravchenko, G.Ya. Pyatibratov, Impact Compensation of Friction Forces on Electromechanical Complexes Performance [Kompensatsiya Vliyaniya Sil Treniya na Kachestvo Raboty Elektromekhanicheskikh Kompleksov], Novye tekhnologii upravleniya dvizheniem tekhnicheskikh obyektov: Materialy II Mezhdunar. nauch.-tekhn. konf., SRSPU (NPI) New control technologies of technical objects moving: Materials of II Internat. scien.-techn. conf. (1999) 26–28.



International Conference on Industrial Engineering

The determination of energy-power parameters of hot plate mill mechatronic system

Voronin S.S., Maklakova E.A., Maklakov A.S., Gasiyarov V.R.*

South Ural State University, 76, Lenin Avenue, Chelyabinsk, 454080, Russian Federation

Abstract

The paper considers issues of energy-power parameters determination of mechatronic system of hot plate mill. The dependence of the calculation of roll torque on features of high deformation zone is given. Based on the obtained expressions the structural diagram of the deformation zone model has been developed. The adequacy of specified method for calculation of energy-power parameters was checked and proved. Results of the experimental studies proved the correctness of conclusions to use specified method during rough rolling as well as finish rolling on the hot plate mill.

© 2015 The Authors. Published by Elsevier Ltd. This is an open access article under the CC BY-NC-ND license (<http://creativecommons.org/licenses/by-nc-nd/4.0/>).

Peer-review under responsibility of the organizing committee of the International Conference on Industrial Engineering (ICIE-2015)

Keywords: hot plate mill; hot rolling; reliability; mechatronic system; deformation zone; electric drive

1. Introduction

The hot plate mills are destined to produce hot-rolled plates. Moreover they must accommodate varying industrial needs such kinds of industries as pipe and tube production, building and construction industry and shipbuilding industry. Commissioning of the modern hot plate mills and the necessity to develop the technological regimes for carrying out of a wide range of rolled products require to create the mathematical models, including energy-power parameters calculation.

The main idea of this article is to develop an engineering method for calculating the roll force and the roll torque in view of the deformation-zone geometry on the hot plate mill 5000 in OJSC "Magnitogorsk Iron and Steel Works" (hereafter "MMK").

* Corresponding author. Tel.: +79068503892.

E-mail address: gasiyarovvr@gmail.com

2. Main Part

The energy-power parameters of hot rolling include total roll force and the roll torque. It is necessary to determine these values of hot rolling under steady conditions and under profiling mode in horizontal stand. It should be done to estimate the features of the screw-down mechanisms and the main electric drives, likewise to develop the mathematical models of these mechanisms.

2.1. Analysis of the well-known methods for calculating the roll force and the roll torque

A number of methods to determine roll force and torque have been currently known and developed. Most methods for calculating roll force are obtained by solving differential equations of the contact stresses acting on the metal in the deformation zone.

These ratios do not have the generalized character, and the applications is limited by conditions in which constituent factors was obtained. An unambiguous choice of the best methods of calculation for a particular mill is almost impossible; we can only determine the preference of a number of methods to calculate the roll force of the hot plate mill.

The calculation of energy-power parameters on each pass of plate rolling on mill 2000 and 5000 OJSC "MMK" was done to test the applicability of the known methods. Furthermore the error of experimental data was calculated that was obtained by recording the coordinates of the mill electric drives for each pass. The calculation results are summarized in [1-3]. Analysis of the results shows that the direct application of simplified methods is unacceptable during the rough rolling, i.e. when a plate thickness is more than 150 mm. The most acceptable method is the method of academic A.I. Tselikov, which gives a deviation in the calculations under rough rolling to 38% and with decreasing of the plate thickness reduces this deviation to 2 ... 6%.

Thus, it is necessary to analyze the causes that lead to such miscalculations of energy-power parameters at plate rolling, and as a result, a new specified technique should be developed.

2.2. The development of the specified method for calculating the roll torque and roll force for hot plate mill 5000

The distinction of the rough rolling in hot plate mill is a high deformation zone and as a result a large angle of nip. Thus concerning hot plate mill 5000 the maximum thickness of the slab is 300 mm and the diameter of the work roll 1210 mm, the angle of nip can reach 20°. In this regard, the neglects, which were made by A.I. Tselikov in his method, are the main reasons leading to significant miscalculations [4-6]. The scheme of the stress state of the deformation zone is shown in Fig.1.

The mathematical model of deformation zone is developed on the basis of an improved method of A.I. Tselikov, which is proposed and developed taking into an account the peculiarity of rolling plates [2, 7-9]:

$$\frac{dP_x}{dx} \pm \frac{dt_x}{dx} \cdot \frac{dy}{dx} - \frac{k \mp t_x \cdot \operatorname{tg} \varphi_x}{y} \cdot \frac{dy}{dx} \pm \frac{t_x}{y} = 0 \quad (1)$$

where P_x is the specific pressure on the rolls rolled metal; φ_x is the angle between the tangent to the arc ab and the horizontal plane in Fig. 1; t_x is the specific friction force between the rolled metal and the surface of rolls; y is a half of height of the cross section bd ; $k = 1,15 \cdot k_f$; k_f is the yield strength or the resistance to plastic deformation under simple tension. The "plus" in the first and before the third member of this equation refers to the zone of slippage on the delivery side, and the sign "minus" refers to the zone of slippage on the entry side. In the second term, on the contrary, "plus" refers to the zone of slippage on the entry side and "minus" refers to the zone of slippage on the delivery side.

As a result of the integration of this equation constants are obtained, they can be determined from the initial conditions. For this purpose it is necessary to find the specific pressure at points A and B . In this case the rolled strip at the entrance to the stand and at the exit from the stand is not in tension.

then the equation (5) can be written as

$$\sigma_x = P_x \pm t_x \cdot y_x' - k \quad (8)$$

consequently

$$\sigma_x' = P_x' \pm t_x \cdot y_x'' \quad (9)$$

substituting (9) in (1) the equation takes the form

$$P_x' \pm t_x \cdot y_x'' - \frac{P_x}{y} \cdot y_x' + \frac{P_x \pm t_x \cdot y_x' - k}{y} \cdot y_x' \pm \frac{t_x}{y} = 0 \quad (10)$$

after all transformations the roll force in polar coordinate system is found as follow

$$P_\varphi = \mp \int \frac{t_x}{\cos^2 \varphi} \cdot d\varphi \mp t_x \cdot \int \frac{R_r}{(h/2 + R_r \cdot (1 - \cos \varphi)) \cdot \cos \varphi} \cdot d\varphi + \int \frac{k \cdot R_r \cdot \sin \varphi}{h/2 + R_r \cdot (1 - \cos \varphi)} \cdot d\varphi \quad (11)$$

Then finally the general solution to the differential equation takes the form

$$P_\varphi = \mp t_x \cdot \operatorname{tg} \varphi \mp \frac{8 \cdot R_B^2}{(h + 2 \cdot R_B) \cdot \sqrt{h \cdot (h + 4 \cdot R_B)}} \cdot \operatorname{arctg} \left(\frac{h + 4 \cdot R_B}{\sqrt{h \cdot (h + 4 \cdot R_B)}} \cdot \operatorname{tg} \left(\frac{\varphi}{2} \right) \right) \mp \quad (12)$$

$$\mp \frac{2 \cdot R_B}{h + 2 \cdot R_B} \cdot \ln \left| \frac{\operatorname{tg}(\varphi/2) + 1}{\operatorname{tg}(\varphi/2) - 1} \right| + k \cdot \ln |h/2 + R_B \cdot (1 - \cos \varphi)| + k \cdot (1 - \ln(h/2))$$

The relationship between the rolling torque and the roll force may be defined as

$$T_{\text{tr}} = 2 \cdot P \cdot \psi \cdot \sqrt{R_r \cdot (h_0 - h_1) - \frac{(h_0 - h)^2}{4}} \quad (13)$$

where $\psi = \beta/\alpha$ is the position coefficient of the resultant roll force P Fig. 1; α is the nip angle; β is the angle of point of roll force application; R_r is the radius of rolls; h_0, h_1 is the slab thickness before and after rolling.

A series of experiments at the hot plate mill 5000 OJSC "MMK" were done to solve the problem of changing the angle of point of roll force [10]. The results showed in Fig.2 [8, 11] that the angle β for each steel grade contained in one area with respect to the angle of bite α , therefore, it can be concluded that angle β does not depend on the steel grade and size of deformation zone

The dependence of angle β is as follows:

$$\beta = 0,391 \cdot \alpha^{1,1459} \quad (14)$$

Then the rolling torque can be determined as:

$$T_{\text{tr}} = 2 \cdot P_x^* \cdot \frac{0,391 \cdot \alpha^{1,1459}}{\alpha} \cdot \sqrt{R_r \cdot (h_0 - h_1) - \frac{(h_0 - h)^2}{4}} \quad (15)$$

2.3. Check the adequacy of the developed specified method for calculating the roll torque of hot plate mill 5000 at OJSC "MMK"

As a result, based on obtained expressions the models for calculating energy-power parameters were made up in accordance with two methods: simplified that is recommended by A.I. Tselikov and a new specified method. The calculation of the energy-power parameters of rolling was carried out on each pass the rolled steel grades and the error of experimental data, which was obtained by recording the coordinates of the mill electric drives for each pass, was counted up. The results of calculations are shown in Table 1.

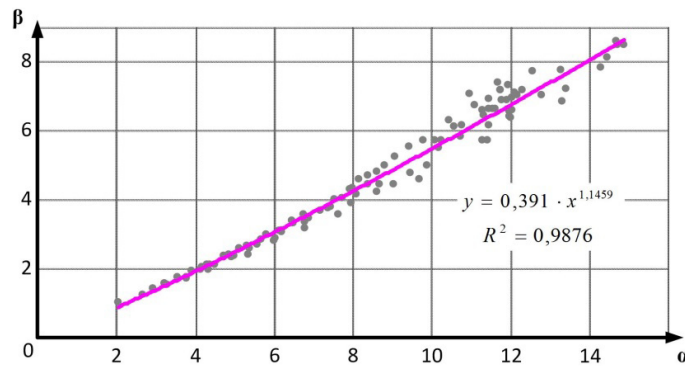


Fig.2. The experimental dependence $\beta = f(\alpha)$

Table 1. Check the adequacy of the developed specified method for calculating the roll torque of hot plate mill 5000

Number of pass	h_0, m	error, %		Number of pass	h_0, m	error, %		Number of pass	h_0, m	error, %	
		Method 1	Method2			meth. 1	meth.2			meth. 1	meth.2
Steel grad K52				Steel grade X70				Steel grade K60			
1	0,3	2,56	33,86	1	0,3	3,29	29,83	1	0,3	4,28	37,91
2	0,26076	2,40	34,22	2	0,25978	3,11	34,64	2	0,28252	4,93	36,63
3	0,23488	6,70	36,33	3	0,23285	5,40	35,08	3	0,2573	2,98	34,77
4	0,21004	1,71	31,83	4	0,20412	3,37	31,53	4	0,23335	4,81	35,48
5	0,18546	1,37	30,48	5	0,17196	2,60	26,29	5	0,21085	1,39	29,08
6	0,16208	4,20	23,90	6	0,14591	4,08	23,23	6	Dummy pass		
7	0,13569	4,16	19,24	7	Dummy pass			7	0,18321	4,50	31,58
8	0,10962	6,01	14,94	8				0,16281	2,94	23,95	
9	Dummy pass			9	0,12203	1,47	23,25	9	0,14173	4,81	29,73
10				10	0,10572	3,49	26,57	10	0,1255	4,96	28,15
11	0,08636	3,70	14,76	11	0,09291	3,31	24,36	11	0,11045	4,15	25,78
12	0,07146	3,47	12,45	12	0,08081	3,09	21,49	12	0,0963	3,28	22,01
13	0,05947	1,64	10,84	13	0,0693	1,97	13,68	13	0,08271	2,20	14,30
14	0,04938	2,22	6,18	14	0,05841	2,30	9,84	-	-	-	-
15	0,04099	4,80	0,83	15	0,0485	2,72	3,79	-	-	-	-
16	0,03431	1,45	1,58	16	0,03985	5,47	4,18	-	-	-	-
17	0,02902	1,47	1,90	17	0,0328	2,95	5,84	-	-	-	-
18	0,0246	2,42	3,26	18	0,02712	1,50	6,48	-	-	-	-
19	0,02092	5,39	5,19	19	0,02259	5,04	5,00	-	-	-	-

Analysis of these data shows that the method A. I. Tselikov gives an error in the calculations in the first passes up to 38%, but specified method, which is developed with taking an account the features of a high-deformation zone. This method enables to make calculation of energy-power parameters on all passes with an error up to 6 ... 7%.

3. Outcome summary

To summarize this research paper, it can be concluded that the direct application of the simplified method of academic A.I. Tselikov is inadmissible during rough on hot plate mill 5000, because it gives miscalculations in the first passes to 38%. With the reduction of the sheet thickness miscalculation is reduced to 2...6%. Specified method, which is developed by the authors in accordance with the view of features of a high deformation zone, gives the accuracy of calculation of energy-power parameters on all passes more than 95%.

Thus, as a result of the research, analytical dependences for specified calculation of roll torque on the motor shaft of hot plate mill 5000 are obtained. Experimental verification has proved the adequacy of the design data, that lets to recommend the developed method for use.

References

- [1] V.R. Khramshin, I.Yu. Andryushin, A.N. Gostev, A.S. Karandaev, A.A. Radionov, Dynamic loads reduction of mechanical and electrical equipment of the hot rolling mill roughing train, Russian internet journal of Industrial Engineering 2 (2013) 69-77.
- [2] V.R. Gasiyarov, Development of the plan view pattern automatic control system of drives of hot plate mill, Nosov Magnitogorsk State Technical University Publ., Magnitogorsk, 2012.
- [3] V.R. Gasiyarov, E.A. Puzankova, A.A. Radionov, The method of the calculation of the roll torque at the hot plate mill, Electrical systems and complexes, Nosov Magnitogorsk State Technical University Publ., Magnitogorsk, 16 (2009) 100-106.
- [4] A.S. Karandaev, Improvement of automatic electric drives for rolling machinery, Russian internet journal of Industrial Engineering 1 (2014) 3-15.
- [5] V. Galkin, A. Karandaev, V. Golovin, A. Rodionov, V. Khramshin, V. Gasiyarov, O. Zalogin, Algorithm of calculation of high-speed and loading modes of electric drives of cages of the rolling mill at the rolling of thick strips, Journal Tula State University. Technical sciences, 2-3 (2010) 12-17.
- [6] A.A. Radionov, A.S. Karandaev, A.S. Evdokimov, I.Yu Andryushin., A.N. Gostev, A.G. Shubin, Mathematical modelling of the interrelated electric and mechanical systems of continuous sub-group of the rolling mill stands. Part 1. development of the mathematical model. Bulletin of the South Ural State University. Ser. power engineering, 1 (15) (2015) 59–73. DOI: 10.14529/power150108
- [7] A.A. Radionov, V.R. Gasiyarov, D.Yu. Usatiy, Develop an improved method of calculating the rolling torque on the motor shaft of hot plate mill and check its adequacy, Sci. Electromechanics, 4 (2011) 78-81.
- [8] A.A. Radionov, V.R. Gasiyarov, D.Yu. Usatiy, Experimental determination of the position of the resultant rolling force at plate mill 5000, Electrical systems and complexes, Magnitogorsk, 2010, vol. 18, pp. 3-6
- [9] A.A. Radionov, A.S.Maklakov, Integration prospects of electric drives based on back to back converters in industrial smart grid, 2014 12th International Conference on Actual Problems of Electronic Instrument Engineering, APEIE 2014 – Proceedings,
- [10] A. A. Radionov, A. S.Maklakov, V. R. Gasiyarov, Smart grid for main electric drive of plate mill rolling stand. Paper presented at the Proceedings of 2014 International Conference on Mechanical Engineering, Automation and Control Systems, MEACS 2014, (2014). doi:10.1109/MEACS.2014.6986842
- [11] A. A. Radionov, V. R. Gasiyarov, O. A. Gasiyarova, Automatic gap control of plan view pattern control mechatronics system. Paper presented at the 2015 International Siberian Conference on Control and Communications, SIBCON 2015, (2015) – Proceedings, doi:10.1109/SIBCON.2015.7147027

International Conference on Industrial Engineering

Automatic control system of speed of synchronous motor

Gasiyarov V.R., Maklakov A.S., Voronin S.S., Maklakova E.A.*

South Ural State University, 76, Lenin Avenue, Chelyabinsk, 454080, Russian Federation

Abstract

The article deals a mathematical model of an automatic control system on the basis of field oriented control method of a synchronous motor. The synchronous motor with electromagnet excitation as object control has been considered by a system of differential equations. The proposed the automatic control system consists of two closed current loop, closed torque loop and model of synchronous motor. Experimental results of the automatic control system are presented in this paper.

© 2015 The Authors. Published by Elsevier Ltd. This is an open access article under the CC BY-NC-ND license (<http://creativecommons.org/licenses/by-nc-nd/4.0/>).

Peer-review under responsibility of the organizing committee of the International Conference on Industrial Engineering (ICIE-2015)

Keywords: closed-loop system, synchronous motor, electric drive, dynamical mode, mathematical model.

1. Introduction

A modern automatic AC electric drives have found application in metallurgy industry, e.g. of rolling mills. These AC electric drives are implemented as a system «frequency converter – synchronous motor». Stator winding of the synchronous motor is usually supplied by the back-to-back convertor, which consist of active front end (AFE) rectifier and voltage source inverter (VSI). Both the AFE and VSI operate on the principle pulse-width modulation (PWM) [1, 2]. Rotor winding is supplied by a nonreversible thyristor converter.

Synchronous motors are selected for high power systems at a wide range of adjustable speed. The main advantages of synchronous drives are high energy efficiency [3] and good energy characteristics.

A research object is the automatic control system of speed of synchronous motor with parameters: $U=3000$ V; $P=12000$ kW; $I_s=2379$ A; $\omega=6.28$ rad/s; $J=145000$ kgm²; $M=1909.9$ kNm; $f=10$ Hz; $R_s=0.00954$ ohm.

* Corresponding author. Tel.: +7-951-244-75-06
E-mail address: karyakina-katya@yandex.ru

Nomenclature

u_{sd}, u_{sq}, u_{rd}	d-q stator winding voltage and rotor winding voltage
i_{sd}, i_{sq}, i_{rd}	d-q stator current and rotor current
R_s, R_f	phase stator active resistance and rotor active resistance
L_{sd}, L_{sq}, L_{rd}	d-q stator winding inductances and rotor winding inductance
M_{df}	coefficient of mutual inductance between stator winding and rotor winding
$\Psi_{sd}, \Psi_{sq}, \Psi_{rd}$	d-q stator flux and rotor flux
ω	rotation speed of d-q system
p	Laplace operator
T_μ	small time constant
x_{sd}, x_{sq}	d-q stator winding reactance resistances
K_{if}	stator current feedback coefficient
K_c	the convertor coefficient
ω_c	break frequency
Z_p	quantity of pole pairs
K_ω	speed feedback coefficient
K_{nd}, K_{nq}	d-q stator flux feedback coefficients
K_f	rotor current feedback coefficient
K_{if}	coefficient current sensor
K_M	coefficient speed sensor
M	torque
I_{0f}	no-load rotor current

2. Mathematical description for synchronous motor

Operation of all electric motors is determined on the basis of laws of electromagnetic induction. It makes the possible of generalizing properties of electric motors into one model. A typical AC motor is described non-linear differential equations on the basis of a movement equation of electrodynamic system. Solution the system of differential equations is complex because of variable coefficients. In the world literature such equations are simplified by Park's transformation a-b-c/d-q-0 and Clarke's transformation a-b-c/ α - β - γ . The transformation a-b-c/d-q-0 is a mathematical transformation of the reference frame of system a-b-c in the rotating system d-q-0. The transformation a-b-c/ α - β - γ is a mathematical transformation of the reference frame of system a-b-c in the reference frame of system α - β - γ . Thus, it allows one to replace the three-phase AC motor by the two-phase unified electrical machine and consider synchronous motor in the frame d-q [4].

$$\begin{cases} u_{sd} = R_s \cdot i_{sd} + p \cdot \Psi_{sd} - \omega \cdot \Psi_{sq}; \\ u_{sq} = R_s \cdot i_{sq} + p \cdot \Psi_{sq} + \omega \cdot \Psi_{sd}; \\ u_{rd} = R_f \cdot i_f + p \cdot \Psi_f; \\ \Psi_{sd} = L_{sd} \cdot i_{sd} + M_{df} \cdot i_f; \\ \Psi_{sq} = L_{sq} \cdot i_{sq}; \\ \Psi_f = L_f \cdot i_f + M_{df} \cdot i_{sd}; \end{cases} \quad (1)$$

3. Model for closed-loop system of synchronous motor

3.1. Model for a closed current loop and a closed flux loop

The synchronous motor is considered in the frame d-q, because the closed-loop system has two closed current loops which are located on d-axis and q-axis. Formation of electromagnetic torque in a transient process is required determined response of both the closed current loop and the closed flux loop [5]. However, crucial importance for response is has the closed current loop. Turning of the closed current loop and the closed flux loop is carried out by standard transient process, which accords to the Butterworth filter [6].

Transfer functions of current controllers on d-axis and q-axis are presented as follows:

$$W_{id}(p) = \frac{1 + (x_{sd} / R_s) \cdot p}{2 \cdot T_\mu \cdot p \cdot (K_{if} \cdot K_c / R_s)}; \tag{2}$$

$$W_{iq}(p) = \frac{1 + (x_{sq} / R_s) \cdot p}{2 \cdot T_\mu \cdot p \cdot (K_{if} \cdot K_c / R_s)}. \tag{3}$$

There is compensation unit of cross-connection on electromotive force rotation in the system. It is applied in order to oscillation of the system reduced when speed increases. Due to compensation unit, isolation the closed current loops in the frame d-q and the closed flux loop is achieved in the system [7].

The block diagram of closed current loops, transient process and bode plot of the frequency response of a system is shown Fig. 1. The closed current loops in the frame d-q which have been tuned using the magnitude optimum method have a step-response overshoot 4.3% [8]. Bode plot of the closed current loops in the frame d-q appears an asymptote with gradient -20 dB and cutoff frequency $\omega_c = 1/2 \cdot T_\mu = 1/2 \cdot 0.01 = 50$ rad/s, and phase margin is equal to 15°. It confirms stability of the closed current loops.

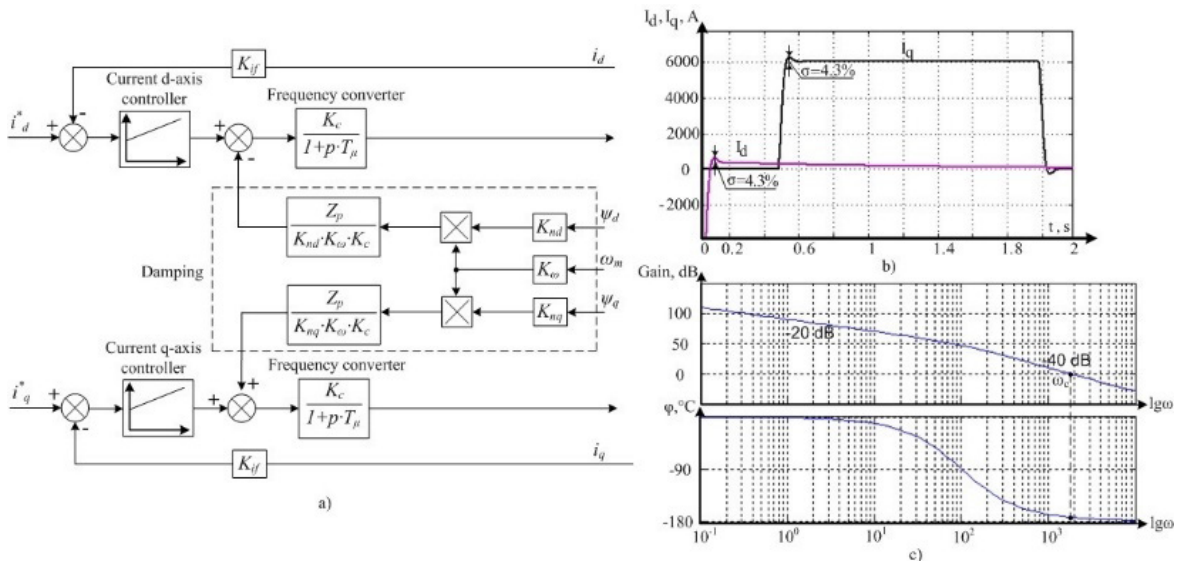


Fig. 1. a) The block diagram of closed current loops; b) transient process of the closed current loops in the frame d-q; c) bode plot of the frequency response of the closed current loops in the frame d-q

The closed flux loop is built similar of closed current loops. Transfer functions of flux controller are presented as follows:

$$W_f(p) = \frac{1 + (L_f / R_f) \cdot p}{2 \cdot T_{df} \cdot p \cdot K_f \cdot K_{df} \cdot (L_f / R_f)}. \quad (4)$$

3.2. Model for a closed speed loop

Torque is necessary to create on motor shaft for adjustment of synchronous motor speed. The speed controller performs such function. The output voltage of the speed controller acts on nonlinearity units 1, 2, 3 forming necessary magnitude of torque [9]. Signal of the nonlinearity units 1, 2 act on the current controllers and the flux controller. The functions the nonlinearity units 1, 2, 3 have the form [10]:

$$i_{sq} = \frac{1}{\psi_s \cdot \sqrt{1 + \frac{M^2}{(3/2 \cdot Z_p \cdot \psi_s)^2} \cdot \frac{L_{sq}^2}{\psi_s^2}}} \cdot \frac{M}{3/2 \cdot Z_p \cdot \psi_s}; \quad (5)$$

$$i_{sd} = - \frac{L_{sq}}{\psi_s \cdot \sqrt{1 + \frac{M^2}{(3/2 \cdot Z_p \cdot \psi_s)^2} \cdot \frac{L_{sq}^2}{\psi_s^2}}} \cdot \frac{M^2}{(3/2 \cdot Z_p \cdot \psi_s)^2}; \quad (6)$$

$$\psi_f = \frac{1}{\sqrt{1 + \frac{M^2}{(3/2 \cdot Z_p \cdot \psi_s)^2} \cdot \frac{L_{sq}^2}{\psi_s^2}}} \times \left[L_f \cdot I_{0f} + \frac{L_{sd} \cdot L_{sq}}{(M_{df} / L_f) \cdot \psi_s} \cdot \frac{M^2}{(3/2 \cdot Z_p \cdot \psi_s)^2} \right]. \quad (7)$$

A closed speed loop is tuned both the magnitude optimum method and the symmetrical optimum depending upon requirements for the droop of the system automatic control [11]. Transfer function of speed controller, which is tuned using the magnitude optimum method is presented as follows:

$$W_\omega(p) = \frac{J}{8 \cdot T_\mu \cdot K_M \cdot K_\omega}; \quad (8)$$

Transfer function of speed controller, which is tuned using the symmetrical optimum is presented as follows:

$$W_\omega(p) = \frac{1 + 16 \cdot T_\mu \cdot p}{16 \cdot T_\mu \cdot p} \cdot \frac{J}{8 \cdot T_\mu \cdot K_M \cdot K_\omega}. \quad (9)$$

The block diagram of the automatic control system of synchronous motor is shown Fig. 2. The transient process of torque and speed is shown Fig. 3.

The closed speed loop, which has been tuned using the symmetrical optimum method, has a step-response overshoot 43% [12].

References

- [1] A.S. Maklakov, A.A. Radionov, EMC evaluation of three level NPC converter based on space vector PWM, Proceedings of the 2015 IEEE North West Russia Section Young Researchers in Electrical and Electronic Engineering Conference, ElConRusNW 2015. (2015) 236–240. DOI: 10.1109/ElConRusNW.2015.7102269
- [2] A.A. Radionov, A.S. Maklakov, E.A. Karyakina, New control method of back to back converter, 2015 International Siberian Conference on Control and Communications, SIBCON 2015 - Proceedings, (2015). DOI: 10.1109/SIBCON.2015.7147135
- [3] A.A. Radionov, O.S. Malakhov, S.N. Baskov, A.S. Konkov, M.S. Davydkin, The design features of the converters for synchronous motors vector-pulsed launch control, Proceedings - 2010 IEEE Region 8 International Conference on Computational Technologies in Electrical and Electronics Engineering, SIBIRCON-2010. (2010) 608–610. DOI: 10.1109/SIBIRCON.2010.5555140
- [4] O.V. Slezhanovskij, L.H. Dackovskij, I.S. Kuznecov, Sistemy podchinennogo regulirovaniya jelektroprivodov peremennogo toka s ventil'nymi preobrazovateljami, Energoatomizdat, Moscow, 1983.
- [5] A.A. Radionov, S.A. Evdokimov, A.S. Karandaev, V.R. Khramshin, Information and measurement system for control of technical state of asynchronous electric motors with group supply from frequency converter, 12th International Conference on Actual Problems of Electronic Instrument Engineering, APEIE 2014 – Proceedings. (2014) 280–285. DOI: 10.1109/APEIE.2014.7040897
- [6] P.V. Shilyaev, I.Yu. Andryushin, V.V. Golovin, A.A. Radionov, A.S. Karandaev, V.R. Khramshin, Algorithms of a digital automatic system for tension and loop control in a wide-strip hot-rolling mill, Russian Electrical Engineering. 84(10) (2013) 533–541. DOI: 10.3103/S106837121310009X
- [7] A.A. Radionov, V.R. Gasiyarov, O.A. Gasiyarova, Automatic gap control of Plan View Pattern Control Mechatronics System, 2015 International Siberian Conference on Control and Communications, SIBCON 2015 – Proceedings. (2015). DOI: 10.1109/SIBCON.2015.7147027
- [8] J. Weidauer, R. Messer, Electrical drives, Siemens Aktiengesellschaft, Berlin and Munich, 2010.
- [9] V.R. Khramshin, A.S. Evdokimov, G.P. Kornilov, A.A. Radionov, A.S. Karandaev, System for speed mode control of the electric drives of the continuous train of the hot-rolling mill, 2015 International Siberian Conference on Control and Communications, SIBCON 2015 – Proceedings. DOI: 10.1109/SIBCON.2015.7147264
- [10] V.R. Gasiyarov, E.A. Maklakova, Mathematical Description of Main Electric Drive of Hot Plate Mill 5000, Russian Internet Journal of Electrical Engineering. 2(3) (2015) 62–66.
- [11] P.C. Krause, O. Wasynczuk, S.D. Sudhoff, Analysis of Electric Machinery and Drive Systems: books in the IEEE press series on power engineering, IEEE, USA, 2002.
- [12] A.S. Maklakov, A.A. Radionov, Integration prospects of electric drives based on back to back converters in industrial smart grid, 2014 12th International Conference on Actual Problems of Electronic Instrument Engineering, APEIE 2014 - Proceedings, (2014) 770–774. DOI: 10.1109/APEIE.2014.7040790
- [13] A.A. Radionov, A.S. Maklakov, V.R. Gasiyarov, Smart Grid for main electric drive of plate mill rolling stand, Proceedings of 2014 International Conference on Mechanical Engineering, Automation and Control Systems, MEACS 2014, (2014). DOI: 10.1109/MEACS.2014.6986842



International Conference on Industrial Engineering

Energy-efficient power supply system for mines

Linkov S.A.^a, Olizarenko V.V.^a, Radionov A.A.^b, Sarapulov O.A.^{a,*}

^aNosov Magnitogorsk state technical University, 38, Lenin Avenue, Magnitogorsk, 455000, Russia

^bSouth Ural State University, 76, Lenin Avenue, Chelyabinsk, 454080, Russian Federation

Abstract

The research group developed an independent power supply system for a mine, which generates electrical power to supply electrical loads inside the mine. The electrical power is generated from kinetic energy of gangue material transported from the upper level of the mine to the lower one and thanks to the improved operation of fan exhausters controlling air flows inside the mine. A new design of the turbine for electric power generation in the process of slurry transportation was suggested and its pilot sample was produced.

© 2015 Published by Elsevier Ltd. This is an open access article under the CC BY-NC-ND license (<http://creativecommons.org/licenses/by-nc-nd/4.0/>).

Peer-review under responsibility of the organizing committee of the International Conference on Industrial Engineering (ICIE-2015)

Keywords: turbine, generator, self-commutated inverter, slurry, backfilling material, mine, mine water

Introduction

The wide range of ore mining electrical machinery for mines requires an extensive power network with various voltage ratings, current and consumed power. Electrical machinery for mines usually consists of alternating current power consumers based on a squirrel-cage induction motor: exhausters fans, deep well pumps for pumping water out of mines, grinding machines for ore reduction, drilling machines, hoisting equipment, etc. Electric power supply of this equipment is provided by 0.4 and 6 kV network by means of cables laid both at grass and on all levels inside the mines. Mine electrical equipment is characterized by abruptly variable loads with high starting currents. That is why a separate supply substation with equipment for power compensation, which is connected with the main transmission line, [1].

* Corresponding author. Tel.: +7-906-851-0091; fax: +0-000-000-0000.
E-mail address: xx_linkov@rambler.ru

Capital costs of mine development as well as huge electric energy consumption by mining equipment result in the increase of the unit cost and, consequently, in the decrease of competitiveness of the whole enterprise. Development and maintenance of some remote deposits, which are located far from the infrastructure and from the national grid of the Russian Federation, could even become unprofitable [2, 3]. The issues of ecology and preservation of environment, the increase of tax levies on industrial enterprises for harmful emissions into atmosphere encourages the study of the problem of energy saving by making use of renewable energy sources, [4, 5]. Each deposit is a unique object with its special features, that is why an individual approach should be applied in each case to solve this problem.

Modern projects of ore deposit development do not take into account the capabilities of electric power generation by low and medium power generators making use of energy of flows to drive auxiliary equipment of the mine. The following moving flows could be used for the purpose: underground water flowing out of cracks in the ceilings or mine sides; underground, surface and process water contaminated with ore particles incoming from the upper levels into the main water collector, which is later pumped out to the surface by the mine drainage complex; backfilling material flowing under gravity along vertical and sloping stowage pipelines into the empty mined-out spaces; slurry of mill tailings in the process of hydraulic filling of mined-out spaces of open-pit mines; outside air blown by the main fan into tunnels of the mine to provide their ventilation and further evacuation of contaminated dust and gas flow of mine air into the atmosphere, [6].

The authors of the article offer original engineering solutions to a number of problems aimed at energy saving in mines:

1. Generation of electric energy for auxiliary equipment from kinetic energy of slurry descending into the mine to fill the mined-out spaces and from water descending from the upper level of the mine to the lower ones.
2. Compensation of reactive power of the mine power network.
3. Energy saving due to optimized control of air flow rate on various levels of the mine

Electric energy generation from the slurry (backfilling material) going down the mine

The developed turbine for slurry (Fig. 1) is unique as no turbine has ever been used for such an aggressive material, that is why the authors applied for a useful model patent of the turbine used for slurry. The backfilling material contains fine ground ore (slag) and has high abrasive properties, that is why the turbine wheel will be subjected to increased wear and breakdown. The offered design of the turbine consists of a wheel with blades (Fig. 1b), strengthened reinforcement ribs, as the blades will be subjected to high pressure. The number of reinforcement ribs can be from one to two depending on the area of the blade and diameter of the pipe with slurry. The material of the wheel must have high resistance to rupture resulting in the high cost of the turbine and capital costs, [7, 8]. The second variant is to use cheaper materials but to shorten the service life of the turbine wheels. As backfilling is a discontinuous process, the worn out turbine can be quickly changed during out-of-service time, while welded metal wheels for the turbine can be manufactured by one of the departments of the enterprise. The bottom part of the turbine shell must be elongated (Fig. 1a) to provide cleaning of the blade from slurry due to the centrifugal effect. This will prevent the wheel from jamming during the turbine operation.

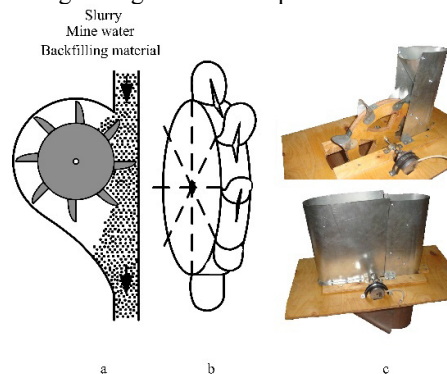


Fig. 1. The turbine for slurry (a), the wheel (b) and the pilot sample of the turbine for laboratory tests (c)

At present, slurry and backfilling material is transported to the mined-out spaces through pipelines with elevation difference from 50 to 500 meters, [2]. Dissipation of kinetic energy of the falling slurry is provided by the assembly of pipe knee joints on various levels of the mine (Fig. 2a). Frequent failures of these joints increase the time of the backfilling process and is a very important problem at present. It seems reasonable to install hydraulic turbines instead of knee joints (Fig. 2b), thus solving two problems: electric energy generation due to the decrease in velocity of the falling slurry (backfilling material) and elimination of the possibility of pipeline failure in the knee joints of the transportation pipeline.

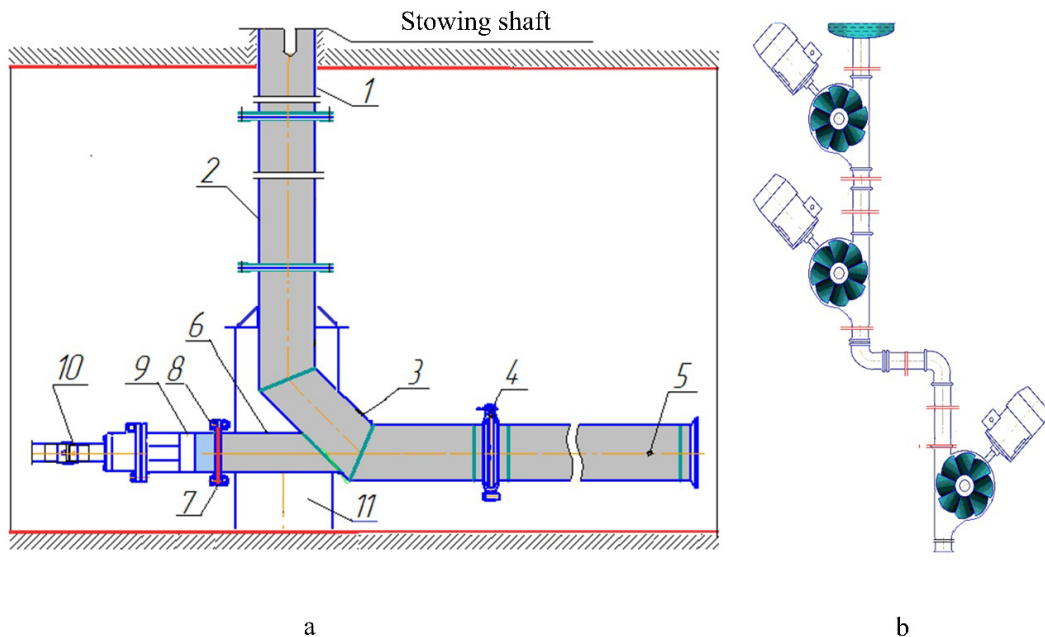


Fig. 2. Stowing pipeline design (a): 1- surface pipe; 2-vertical insertion piece; 3-welded knee joint with 90° bend; 4-make-and-break joint; 5-horizontal pipeline; 6-connecting pipe; 7-diaphragm; 8-flange coupling; 9-hydraulic cylinder with a piston; 10-a fixed joint of the piston rod with the vibration source; 11-seating unit; (b) – installation diagram of hydraulic turbines on the stowing pipe.

Energy saving due to control of air flow rate

The problem of optimized control and air flow circulation in mines has been only partially solved. The exhaust fan stations on the surface providing air supply and air exhaust operate with the nominal rating and at a uniform rate 24 hours a day. Such stations consume up to 30% of the total energy supplied to the mine electrical installations.

Air flow rate is different on different mine levels. On lower levels air circulation is weak, which makes it necessary to install additional exhaust fan stations. On upper levels the air flow rate is so high, that it makes it difficult to for miners and operating staff to work. At present, in order to reduce the air flow rate, special dampers are installed, which slow down the air velocity, thus making the working environment more comfortable. The offered measures aimed at optimization and control of air flow in a mine include installation of a wind turbine instead of the dampers, which will generate electric energy from excessive air flow and feed it into the mine network. Capital costs of such an installation are not very high because it is not necessary to design a special air turbine with a generator, [9]. It is only necessary to install an industrial fan with an induction motor. The complete circuit diagram of air flow rate control in the mine is given in Fig. 3. The fan turbine is supplied with an air collector, which is mounted into the damper opening. The frame of the air collector will increase the density of the air flow going through the turbine, thus improving the energy efficiency of the wind turbine. In the process of air injection, the induction motor is switched to the generator mode by means of a controlled inverter [10, 11], which controls the speed of the fan blades.

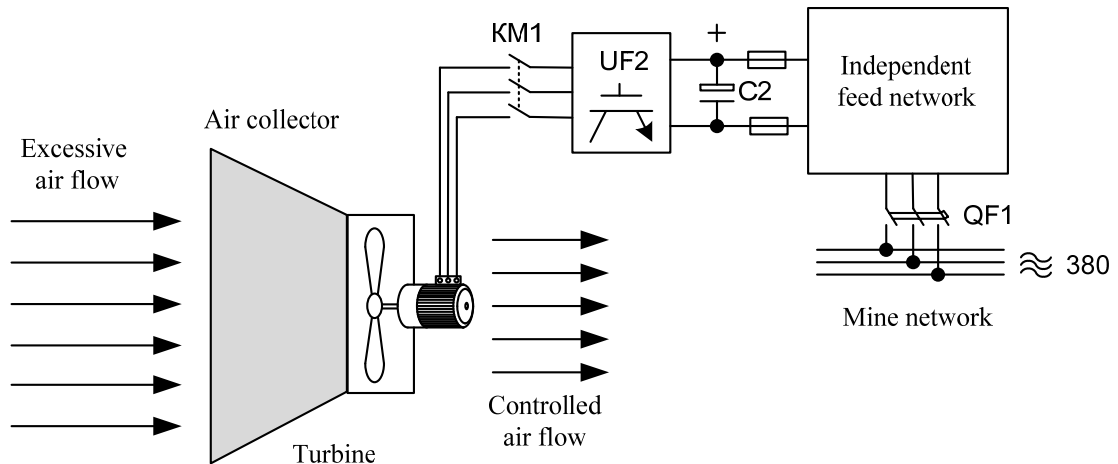


Fig. 3. The complete circuit diagram of air flow rate control with regeneration of current into the mine network

Air flow rate is controlled by the inverter current. The higher the inverter current, the weaker the air flow at the turbine exit and, subsequently, the more electric energy is generated and fed into the mine network. If the air flow in the mine shaft is low, the inverter switches off and the turbine fan is allowed to rotate freely without changing the air flow rate. Modern inverters have microprocessor modules capable of calculating and setting the necessary generator speed on a real-time basis depending on the preset scheme or by means of remote control.

Circuit diagram of the energy saving power supply system of a mine

The circuit diagram of the independent power supply system of a mine is given in Fig. 4. In the process of slurry (water) transportation along the pipeline to the worked-out spaces, the blade turbine drives a low-speed generator, which generates three-phase alternating voltage, [5]. The independent controlled inverter converts alternating voltage into direct constant one. Direct voltage is supplied to each consumer by cable. Thus, the mine gets an independent direct current network with the voltage of up to 400 V. This network has lower electric energy loss compared to the alternating current network, because it has no losses caused by reactive power. Electric energy consumers require alternating current, that is why they are equipped with additional independent controlled inverters, which are capable of speed control. For example, to control the air flow in the shaft, the inverter feeding the induction motor can change the fan speed and, consequently, electric energy consumption rate. The smoothness of speed control effects the reactive power consumption from the main, for example, it eliminates the risk of voltage sags at the moment of motor starts. Electric energy generation in the redundant circuit is not constant and depends mainly on kinetic energy of slurry in the backfilling process, while mine equipment must be constantly supplied by electricity. If the turbine does not rotate, voltage value in the redundant circuit decreases, and the circuit automatically switches to the mine network either by means of a UD diode bridge or by means of a UF6 inverter. Thus, power consumers will be constantly supplied by electric power. If the UF6 inverter is used instead of the UD diode bridge, it makes it possible to feed electric power into the 380 V mine network.

Conclusion

The developed independent power supply system is capable of satisfying more than 50% of power demand of the mine facilities both inside and outside the mine. The new set of energy saving measures in the process of mining can significantly reduce the operating costs of the mining enterprise.

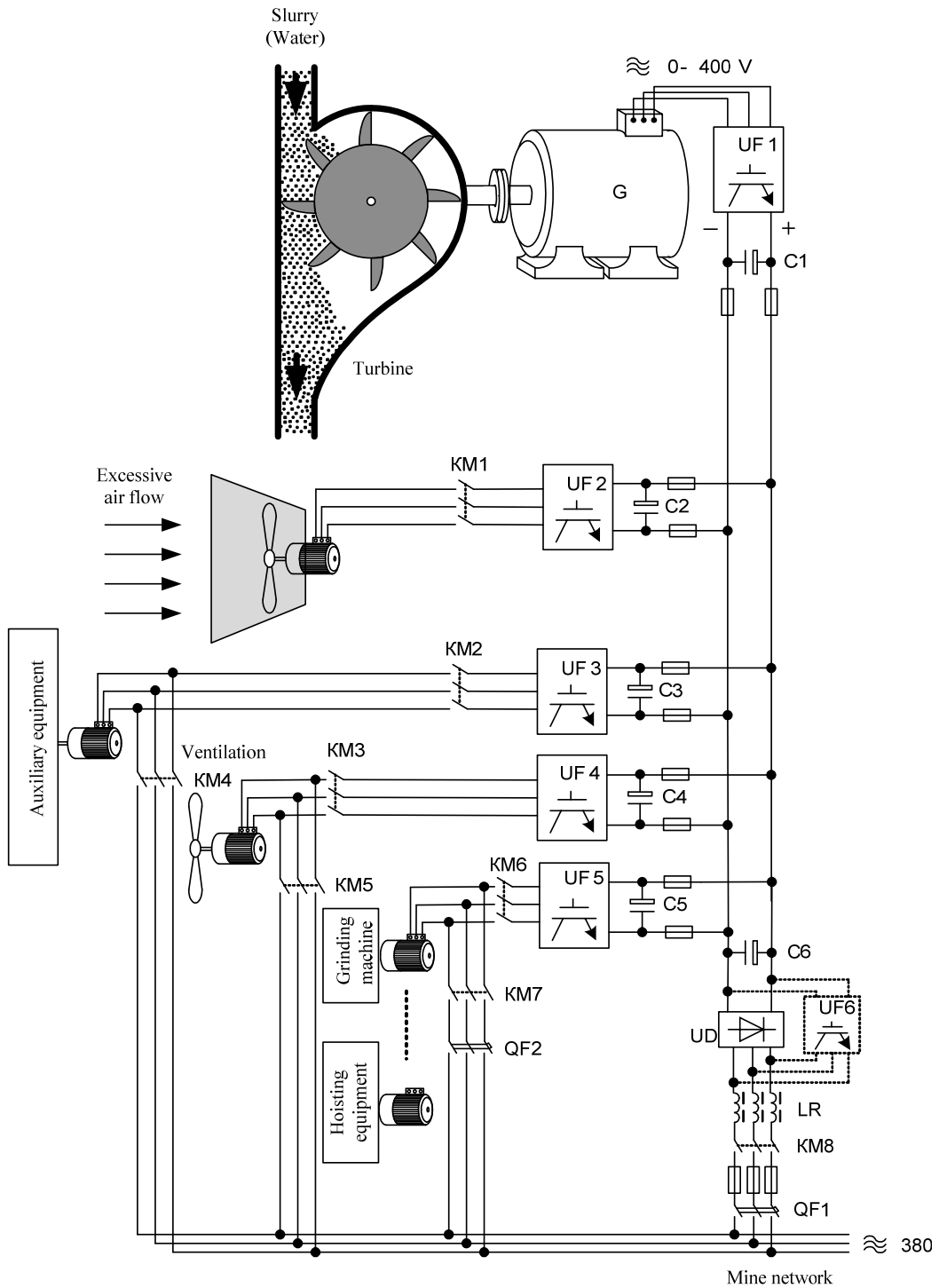


Fig. 4. The scheme of the independent power supply system of the mine

Acknowledgements

The research was carried out within the framework of the government contract of the Russian scientific fund – grant № 14-17-00255.

References

- [1] D.R. Kaplunov, M.V. Rylnikova, D.N. Radchenko, Application of renewable energy sources in the process of hard minerals mining, *Physical and engineering issues of mineral mining*. 1 (2015) 88–96.
- [2] A.S. Maklakov, A.A. Radionov, Integration prospects of electric drives based on back to back converters in industrial smart grid, 2014 12th International Conference on Actual Problems of Electronic Instrument Engineering, APEIE 2014 – Proceedings. (2014) 770–774. DOI: 10.1109/APEIE.2014.7040790
- [3] A.A. Radionov, A.S. Maklakov, V.R. Gasiyarov, Smart Grid for main electric drive of plate mill rolling stand, Proceedings of 2014 International Conference on Mechanical Engineering, Automation and Control Systems, MEACS 2014. (2014). DOI: 10.1109/MEACS.2014.6986842
- [4] M.V. Rylnikova, V.A. Angelov, I.S. Turkin, Some features of engineering solutions and design of recycling wastes from ore mining and processing in worked-out spaces of open-pit mines, *Proceedings of Universities, Mining Journal*. 2 (2015) 59–66.
- [5] M.V. Rylnikova, V.A. Angelov, I.S. Turkin, Justification of manufacturing scheme and equipment system for utilization of mill tailings in underground worked-out spaces, *Mining research and information journal*. S41 (2014) 138–149.
- [6] M.V. Rylnikova, V.A. Angelov, I.S. Turkin, Prospects of underground hydroelectric station construction in areas with worked out mines, *Surveyor bulletin*. 5 (2014) 24–27.
- [7] A.A. Kuzmenko, Control system of hydraulic turbine speed: integrated adaptation, *Proceedings of YuFU, Engineering sciences*. 4(129) (2012) 175–181.
- [8] A.P. Barabanova, T.N. Skorobogatova, Simulation of load distribution along hydraulic turbine blade as a system with distributed constants, *Young scientist*. 14(2) (2015) 92–94.
- [9] S.A. Linkov, A.S. Sarvarov, I.V. Bachurin, Development prospects of wind power generation in Russia and abroad, *Electrical systems and complexes*. 21 (2013) 220–225.
- [10] A.A. Radionov, A.S. Maklakov, E.A. Karyakina, New control method of back to back converter, 2015 International Siberian Conference on Control and Communications, SIBCON 2015 – Proceedings. (2015). DOI: 10.1109/SIBCON.2015.7147135
- [11] A.S. Maklakov, A.A. Radionov, EMC evaluation of three level NPC converter based on space vector PWM, Proceedings of the 2015 IEEE North West Russia Section Young Researchers in Electrical and Electronic Engineering Conference, EIConRusNW 2015. (2015) 236–240. DOI: 10.1109/EIConRusNW.2015.7102269



International Conference on Industrial Engineering

Analytical model of soil pulverization and tillage tools

Blednykh V.V.^a, Svechnikov P.G.^a, Troyanovskaya I.P.^{a, b *}

^a South Ural State Agrarian University, Lenin's avenue, 75, Chelyabinsk, Russia

^b South Ural State University, Lenin's avenue, 76, Chelyabinsk, Russia

Abstract

The paper deals with the pulverization (fracture) model that is not based on soil elastic properties but on the physical processes of the wedge interaction with soil. The presented model agrees with the experimental data better than other models, including those based on soil elastic properties, and the tests of flat tillage tools with a variable cutting angle have proved this.

Published by Elsevier Ltd. This is an open access article under the CC BY-NC-ND license (<http://creativecommons.org/licenses/by-nc-nd/4.0/>).

Peer-review under responsibility of the organizing committee of the International Conference on Industrial Engineering (ICIE-2015)

Keywords: fracture model, tractive resistance, soil pulverization, two-sided wedge, interaction, optimal parameters.

1. Introduction

Up to the present moment, there are no universally accepted models of soil pulverization. A significant number of well-known soil pulverization (fracture) models resort to fracture patterns of an elastic body. Numerous attempts of using the investigation methods of elastic materials for soil pulverization have not yielded practical results yet, since the relationship between the force acting on the soil and the soil deformation is the function of the soil condition. Therefore, the use of the mathematical apparatus for fracturing elastic bodies in its classical form when designing working bodies is ineffective. Thus, this paper is concerned with one of feasible approaches to investigating the process of soil pulverization (fracture) with tillage tools.

* Corresponding author. Tel.: +7-951-113-76-30;
E-mail address: tripav@rambler.ru

2. Metodology

The basics of the approach are:

- the pulverization of the soil and its elements happens when the acting force exceeds the soil resistance force;
- the value and direction of the acting force can be determined through analysing the tillage tool interaction with the soil;
- the soil resistance force can be estimated on the basis of its aggregate-size distribution and humidity at the time of tillage.

Now let's consider some of the elements of the pulverization process exemplified with a two-sided wedge (Figure 1).

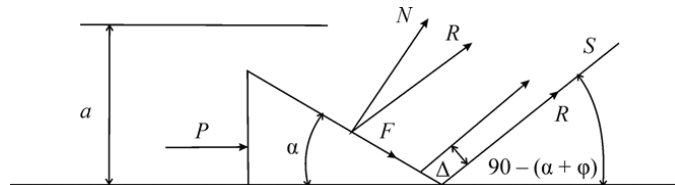


Figure 1 The soil fracture with a two-sided wedge

When moving in the soil the wedge interacts with the soil normal, declined at a friction angle of the soil movement on the wedge surface. In this direction the wedge moves the soil along the plane and the soil area is:

$$S = \frac{ab}{\sin(90 - (\alpha + \varphi))} = \frac{ab}{\cos(\alpha + \varphi)}, \quad (1)$$

where S is the pulverization plane of the soil;

a is the depth of the wedge movement;

α is the two-sided wedge angle;

φ is the friction angle when the soil slides on the wedge;

b is the wedge width.

And the value of the force R should be equal to:

$$R = \frac{\mu ab}{\cos(\alpha + \varphi)}, \quad (2)$$

where μ is the friction coefficient of the soil particles over the area S .

This coefficient, of course, can hardly be considered as the ultimate soil shearing resistance τ with a number of assumptions.

The action of the force R can manifest itself only when a soil layer of the Δ thickness is formed on the wedge. The wedge penetrates into the soil without breaking it up until the thickness of the soil layer becomes Δ . The value of the layer thickness can be determined from the condition:

$$R = \Delta b \sigma, \quad (3)$$

where σ is the ultimate normal stress on the layer.

Solving the equations (2) and (3) together we have:

$$\Delta = \frac{a\tau}{\sigma \cos(\alpha + \varphi)} \quad \text{or} \quad \Delta = \frac{\mu a}{\sigma \cos(\alpha + \varphi)}, \quad (4)$$

Figure 2 shows the dependence of the pulverization element thickness Δ on the setting angle of the wedge to the furrow bottom, provided: $\sigma = 10\tau$.

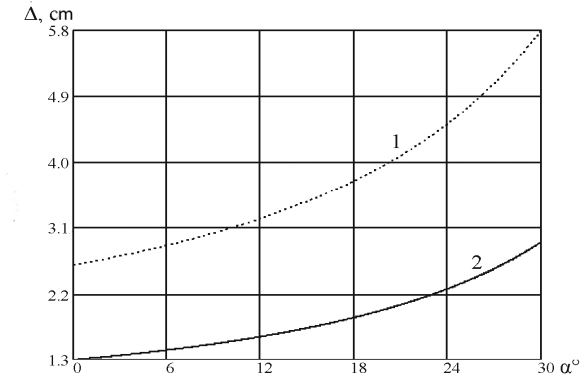


Figure 2 The thickness of the soil fracture elements depending on the setting wedge angle to the furrow bottom ($\sigma_c=10\tau$; $1 - a = 20$; $2 - a = 10$ cm)

Applying the value Δ to the equation 3, we get:

$$R = \frac{\mu ab}{\cos(\alpha + \varphi)} \quad \text{or} \quad R = \frac{\tau ab}{\cos(\alpha + \varphi)}, \tag{5}$$

The power of the tractive resistance P is determined by the obtained fracture force R and the friction force of the soil movement on the wedge at the pulverization point F when ignoring the efforts necessary to move the obtained soil layer on the wedge of the length L (Figure 3, 4):

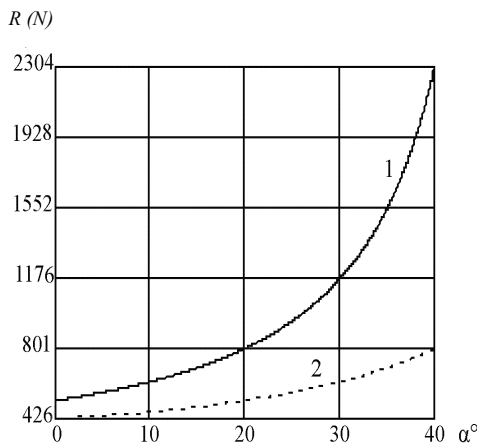


Figure 3 The power on the wedge when pulverizing the soil of the thickness Δ :
 1 – the depth of the wedge movement 0,2 m;
 2 – the depth of the wedge movement 0,1 m

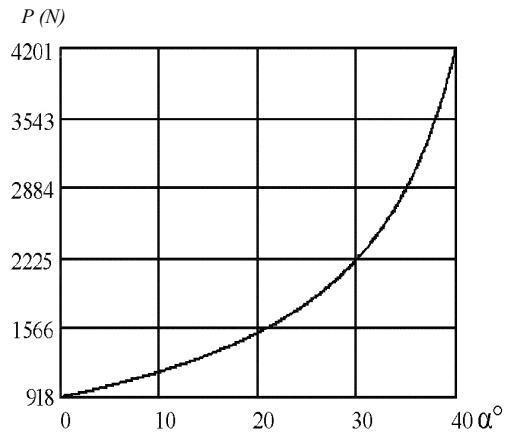


Figure 4 The wedge resistance force when pulverizing the soil $\mu=40000\text{N/m}^2$, $a=0,1\text{m}$, $b=0,1\text{m}$, $\varphi=40^\circ$

$$P = R \cos(90 - (\alpha + \varphi)) + F \cos \alpha, \tag{6}$$

where F is the friction force when moving the soil on the wedge at the pulverization point of the continent layer:

$$F = N \text{tg} \varphi, \tag{7}$$

where φ is the friction angle,

N is the force of the normal pressure on the soil surface when pulverization the continent soil:

$$N = \frac{R}{\cos \varphi} = \frac{\mu ab}{\cos \varphi \cos(\alpha + \varphi)}. \quad (8)$$

When applying F to the equation 6 we get:

$$P = R \left(\sin(\alpha + \varphi) + \frac{\cos \alpha \operatorname{tg} \varphi}{\cos \varphi} \right). \quad (9)$$

The numerical values of the component of the tractive resistance force (R and F) are shown in Figure 5.

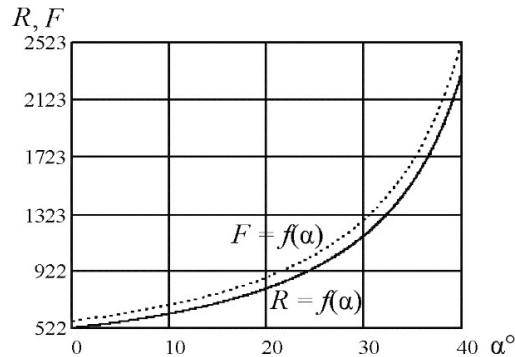


Figure 5 The components of the wedge tractive resistance force when pulverizing the soil (F is the upper curve, R is the low curve: $\mu=4000N/m^2$; $a=0,1m$; $b=0,1m$; $\varphi=40^\circ$)

3. Results

These theoretical findings were applied to the operating parts of flat-cutting and mouldboard ploughs, with the results of laboratory and experimental tests being presented below.

Thus, the foregoing caused to put forward the following scientific hypothesis: the variable cutting angle along the blade length improves the soil layer pulverization. To confirm this scientific hypothesis the above mentioned theoretical and laboratory-industrial experiments were conducted.

The laboratory tests needed a specially made soil channel and a set of two-sided wedges that differ from each other in cutting edge angles set to the furrow bottom. Moreover, the tests were carried out in different physical and mechanical properties (typical chernozem, sand, peas, clay), with the influence of the variable cutting angle on the bending of clay, plasticine and wet chernozem being determined.

The laboratory tests proved the following:

- despite the differences in physico-mechanical properties and the formation appearance of the outer layer, all environments when interacting with the wedge have some common characteristics dependant on the wedge parameters,
- the blade with a variable cutting angle causes the stress state in the soil layer more than the blade with a constant cutting angle.

As a result, there were obtained [1] mathematical formula for determining the equivalent stress (the stress state) produced by a blade with a variable and constant cutting angle.

$$\frac{\sigma^{III}}{\sigma^{II}} = \frac{1}{2} + \frac{1}{2} \sqrt{1 + 1,5\rho^2 \left(\frac{\Delta \varepsilon}{l} \right)^2}, \quad (10)$$

where σ^{III} is the stress state caused with a blade with a varying cutting angle in the soil layer;

σ^{II} is the stress state caused with a blade with a constant cutting angle in the soil layer;

ρ is the radius of the soil layer bending;

$\Delta\varepsilon$ is the intensity of the cutting angle changing along the length of the blade (in $\Delta\varepsilon$ experiments varied from 200 to 450);

l is the blade length.

When analyzing the results it can be noted that the wedge with a variable cutting angle causes a greater stress state in the soil layer than the wedge with a constant cutting angle. When the pulverization is in proportion to stresses, the wedge with a variable cutting angle is proved to ensure a better pulverization.

The theoretical and laboratory studies have helped to create the operating parts of cultivators and subsurface ploughs with variable cutting angles.

The nature of stresses that occur in the soil layer varies. When the soil is tilled with a machine with a constant angle along the cutting ploughshare, the stress state occurs because of bending deformation, and when the soil is tilled with a machine with a variable angle, the stress state is caused by bending-torsion deformation.

The experimental data on pulverization and tractive resistance prove the validity of our scientific hypothesis (Figure 6).

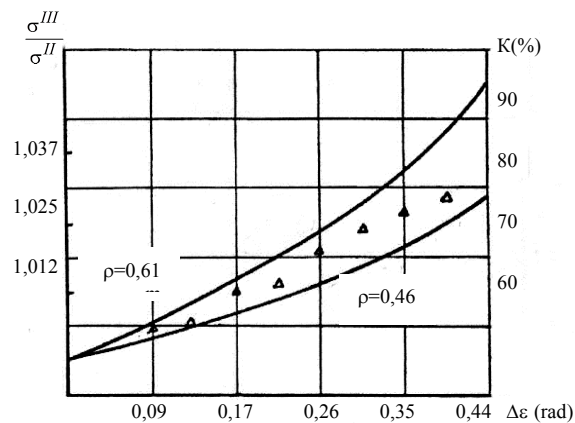


Figure 6 The influence of the intensity of changing cutting angles along the ploughshare ($\Delta\varepsilon$) on the equivalent stress and the soil layer pulverization: Δ is the experimental data concerning the tilled soil layer pulverization

Thus, the model of soil pulverization can be considered to be in good agreement with physical processes of the wedge interaction with soil, and the calculated data in Figures 2-5 correspond to the experimental ones obtained by many scientists in Russia and abroad [2, 3, 4, 5, 6, 7, 8, 9].

The presented models with the experimental data is much more convergent as compared with others, including those based on the elastic properties of soil.

To obtain the necessary quality of soil pulverization this paper offers operating parts for cultivator-subsurface ploughs with variable cutting angles.

4. Conclusions.

The experimental data prove operating parts for cultivator-subsurface-ploughs with variable cutting angles along the ploughshare to cause a 20-50% better soil pulverization than traditionally produced ones, with the economic effect of the former operating parts to be 200-1300 roubles per 1 ha of cultivated area higher as compared with the latter ones.

References

- [1] P.G. Svechnikov, Justification of parameters of the flat hoe with a variable cutting angle for deep soil loosening, Dissertation of the doctor of technical sciences (Engineering), Chelyabinsk, 1984
- [2] V. Blednykh, The structure, calculation and design of tillers, CSAA, Chelyabinsk, 2010.
- [3] V. Goryachkin, Collected Works, third ed., Moscow, 1968.
- [4] A. Kulen, H. Kuipers, Modern agricultural mechanics, Moscow, 1986.
- [5] V. Blednykh, P. Svechnikov, Theoretical Foundations of Tillage. Tillers and Aggregates, Nova Science Publishers, Science Publishers Inc, New York, 2014.
- [6] V. Blednykh, P. Svechnikov, Economic reasons of tillage quality, *Journal European Science Review*. 7-8 (2014) 103–105.
- [7] V. Blednykh, P. Svechnikov, Soil pulverization with a moldboard plough, *Vestnik CSAA*. 65 (2014) 68–73.
- [8] V. Blednykh, P. Svechnikov, Theory of a Tillage Wedge and its Applications, Logos Verlag Berlin GmbH, Berlin, 2013.
- [9] V. Blednykh, I. Sinyavsky, P. Svechnikov, Designing technological processes in plant growing, *Vestnik CSAA*. 70 (2014) 219–223.



International Conference on Industrial Engineering

Estimation of residual stresses influence on oscillation modes of welded housing part

Yaushev A.A.^{a*}, Taranenko P.A.^a, Zhestkov A.V.^b

^aSouth Ural State University, Chelyabinsk, Russian Federation, 454080

^bElmetro Grupp, Chelyabinsk, Russian Federation, 454106

Abstract

The article is devoted to the calculation and experimental determination of Coriolis flowmeter case vibrations modes. The case of the flowmeter is welded of thin steel plates 12H18N10T. It is determined that calculated and experimental modes of vibrations of some elements of a case free from welded joints vary by 3%. After all the elements are welded the modes of case vibration vary by over 50%. Such great variation can be explained by two reasons, i.e., influence of residual stresses after welding and case deformation due to the mentioned stresses. By means of coordinate measuring manipulator “Stinger II” highly precise surface measurement is held. Then finite-element calculation of model is performed with consideration to the real geometry of the object. To check the influence of residual stresses on case vibration modes one employs stress relieving.

© 2015 The Authors. Published by Elsevier Ltd. This is an open access article under the CC BY-NC-ND license (<http://creativecommons.org/licenses/by-nc-nd/4.0/>).

Peer-review under responsibility of the organizing committee of the International Conference on Industrial Engineering (ICIE-2015)

Keywords: Coriolis flowmeter, finite element method, experimental analysis of modes, Modal Assurance Criterion MAC, residual stresses

1. Introduction

Coriolis flowmeter is designed to measure mass flow rate of gases and liquids. It consists of a case and two U-shaped oscillating pipes where liquid flows. The overview of various Coriolis flowmeters is given in [1, 2], and precise description of operation in [3].

* Corresponding author. Tel.: +7-351-272-37-44.
E-mail address: iaushevaa@susu.ac.ru

Relative position of vibration modes housing and pipes of a flowmeter can influence the precision of liquid flowrate. That is why the research task of the dynamic characteristics of the housing seems up-to-date.

It is determined that oscillation modes of pipes obtained through finite element method and experimentally practically, coincide, so the case of the flowmeter is free from pipes.

The housing of the flowmeter is made of steel 12H18N10T. It consists of a massive base, two plates and boards 2 mm thick. For more structural stiffness two bushes are inserted between the plates 2 mm thick. All elements of the housing are welded in shielding gas with non consumable electrode. The housing plan is given in Fig. 1.

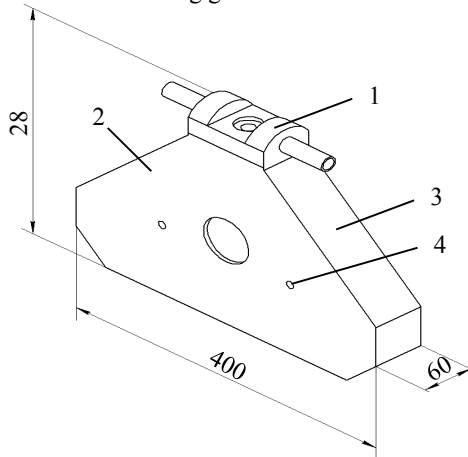


Fig. 1. The plan of a housing: 1 – base; 2 – plate; 3 – board; 4 – bush.

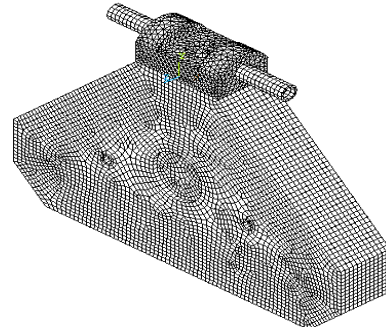


Fig. 2. Finite element mesh.

2. Methods

For calculation of vibration modes of the housing shell-type and volumetric finite element models are formed (Fig. 2). The difference between modal frequencies of both models shall not exceed 3%, so in further calculations only shell-type model is employed being less time-consuming from the point of view of calculation [4, 5]. To verification of the finite element model experimental determination of oscillation modes of the case was held [6, 7].

At experimental determination of modal characteristics of the housing impact excitation of vibrations is employed [8, 9, 10]. In the experiment the housing is hung on flexible mounts against the pipes of the housing base.

Tests are held upon the employment of program hardware system which includes:

- measuring equipment LMS SCADAS Recorder to acquisition and processing dynamic signals, 40 channels;
- program module LMS Test.Lab Impact Testing for modal impact testing and processing its results;
- impact hammer PCB 086C03 with an in-built sensor of the force;
- triaxial accelerometers PCB 356A32 with sensitivity level 100 mV/g.

To estimate the conformity of experimental and calculated eigenforms the criteria of modal assurance is selected (Modal Assurance Criterion) MAC [11, 12]. The MAC between two mode shape vectors $\{\psi\}_e$ (experiment) and $\{\psi\}_c$ (calculation) is defined as

$$MAC_{ij} = \frac{|\{\psi\}_i^{cT} \{\psi\}_j^e|^2}{(\{\psi\}_i^{eT} \{\psi\}_j^e)(\{\psi\}_i^{cT} \{\psi\}_j^c)}, \quad (1)$$

where i, j – numbers of modes.

If vectors $\{\psi\}_e$ и $\{\psi\}_c$ are estimation of one and the same mode shape, then the modal assurance criterion aims for 1, if mode shape vectors are estimation of two various mode shape then the value of criterion must aim for 0. This conclusion is based upon the feature of orthogonality of eigenmode shapes.

In Figure 3 and in table 1 the comparison between calculated modes of vibrations and experimental ones are given as per MAC. The difference between calculated (f_c) and experimental (f_e) eigenfrequency is determined as

$$\delta = \frac{f_e - f_c}{f_e} 100\%. \tag{2}$$

3. Results and discussion

From table 1 one concludes that the oscillation modes of housing determined in the course of the experiment and calculation differ over 50%. To research the reasons of divergence of results in experiment and calculation the housing is examined as separate parts.

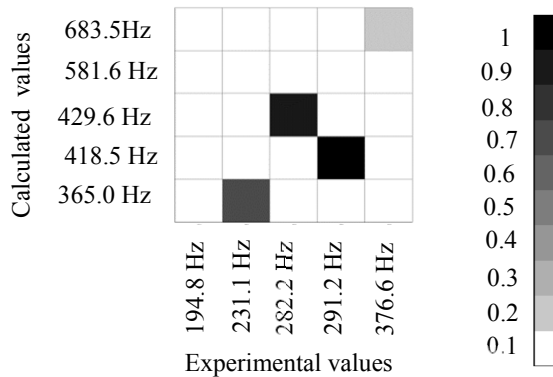


Fig. 3. Comparison between calculated and experimental shapes of housing oscillation according to MAC.

Table 1. Comparison between calculated and experimental modes of housing oscillation.

No.	f_c , Hz	f_e , Hz	δ , %	MAC
1	365.0	231.1	58	0.69
2	418.5	291.2	44	0.95
3	429.6	282.2	52	0.85
4	581.6			
5	683.5	376.6	81	0.13

In Fig. 4 the geometry of the plate free from welded parts is shown (position 2 in Fig. 1). The thickness of plate is 2 mm, the plate has a forged cavity 72 mm in diameter, and 5 mm depth in the middle and two holes 13 mm in diameter. The first seven oscillation modes of the plate received by finite element method and experimentally differ less than by 3%. MAC is given in Fig. 5. So, judging by coincidence of vibration modes of the plate the conclusion comes that the geometry of the model and material properties (thickness and elasticity modulus) in the calculation are given correctly.

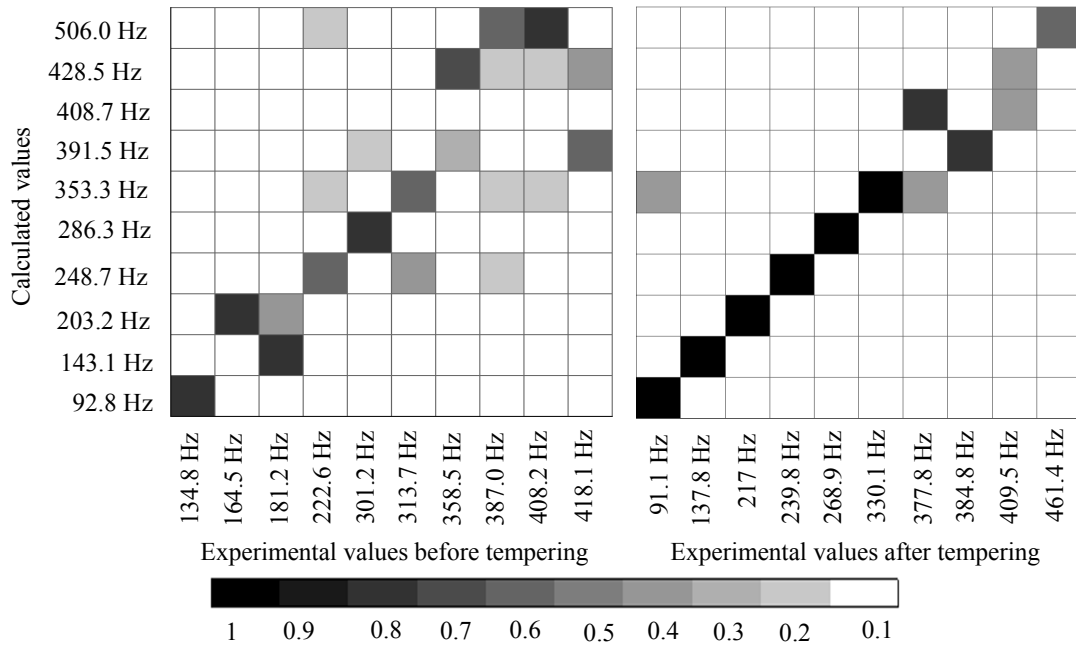


Fig. 7. Comparison between calculated and experimental forms of case vibration according to MAC.

So, the main reason of difference between calculation and experiment lies in failure to consider residual stresses after welding. Thermal physical properties peculiar to highly alloyed steel determine some of their qualities of welding. The reduced heat conduction coefficient at other equal conditions varies considerably the distribution of temperatures in the seam and conjoint area. And considering the heightened thermal expansion coefficient the shape distortion of product raises [14].

The impact of residual stresses on eigenfrequencies is considered by the example of a beam at works [15, 16]. The impact of residual stresses on resonance frequency of sensor membranes is researched at works [17, 18]. Ways of determining residual stresses are considered at works [19, 20]. From the overview of these works and results obtained in the article one can conclude that residual stresses can have a lot of impact on structure oscillation modes.

Table 2. Comparison of calculated and experimental oscillation modes of a housing part.

Calculation		Before tempering			After tempering		
No.	f, Hz	f _i , Hz	δ ₁ , %	MAC ₁	f ₂ , Hz	δ ₂ , %	MAC ₂
1	92.8	134.8	31.2	0.78	91.8	1.1	0.86
2	143.1	181.2	21	0.79	137.8	3.8	0.9
3	203.2	164.5	23.5	0.76	217	6.4	0.91
4	248.7	222.6	11.7	0.51	239.8	3.7	0.81
5	286.3	301.2	4.9	0.78	268.9	6.5	0.86
6	353.3	313.7	12.6	0.58	330.1	7	0.82
7	391.5	358.5	9.2	0.2	384.8	1.7	0.72
8	408.7				377.8	8.2	0.61
9	428.5	418.1	2.5	0.3	409.5	4.6	0.37
10	506	408.2	2	0.73	461.4	9.7	0.59

4. Conclusion

In the paper the main reason of difference between calculated and experimental oscillation modes of thin-walled welded case of Coriolis flowmeter was found out and proved. It is determined that residual stresses after welding in the housing part influence its own mode shapes, and lead to change of eigenfrequencies by 10 – 30%.

References

- [1] T. Wang, R. Baker, Coriolis flowmeters: a review of developments over the past 20 years, and an assessment of the state of the art and likely future directions, *Flow Measurement and Instrumentation*. 40 (2014) 99–123.
- [2] K.O. Plache, Measuring mass flow using the Coriolis principle, in: R. Loxton, P. Pope, *Instrumentation: A Reader*, Springer US. (1990) 55–62.
- [3] H. Raszillier, F. Durst, Coriolis-effect in mass flow metering, *Archive of Applied Mechanics*. 61(3) (1991) 192–214.
- [4] L.J. Segerlind, *Applied finite element analysis*, second ed., Wiley, New York, 1984.
- [5] K.J. Bathe, E.L. Wilson, *Numerical Methods in Finite Element Analysis*, New Jersey, Prentice-Hall, 1976.
- [6] J. Melcer, Experimental Verification of a Computing Model, *Applied Mechanics & Materials*. 732 (2014) 345–348.
- [7] V.S. Mezhin, V.V. Obukhov, The Practicel of Using Modal Tests to Verify Finite Element Models of Rocket and Space Hardware, *Space technics and technology*. 1(4) (2014).
- [8] O. Dossing, *Structural Testing, Part 1, Mechanical Mobility Measurements*, Brüel & Kjær, Denmark, 1989.
- [9] O. Dossing, *Structural Testing, Part 2, Modal Analysis and Simulation*, Brüel & Kjær, Denmark, 1989.
- [10] D.J. Ewins, *Modal Testing: Theory, Practice and Application*, Hertfordshire: Research Studies Press, 2000.
- [11] R.J. Allemang, The Modal Assurance Criterion – Twenty Years of Use and Abuse, *University of Cincinnati, Sound and Vibration*. (2003) 14–21.
- [12] W. Heylen, S. Lammens, P. Sas, *Modal Analysis Theory and Testing*, Katholieke Universiteit Leuven, 1997.
- [13] K. Ostrowska, A. Gaska, J. Śladek, Determining the uncertainty of measurement with the use of a Virtual Coordinate Measuring Arm, *Int J Aut Technol*. 17 (2014) 529–537.
- [14] I. Hrivnak, *Theory of weldability of metals and alloys*, Elsevier Science, 1992.
- [15] S. Abbasion, A. Rafsanjani, R. Avazmohammadi, A. Farshidianfar, Free Vibration of Microscaled Timoshenko Beams. 95 (2009) 5.
- [16] V.L. Biderman, *Teorija mehanicheskikh kolebanij (Theory of mechanical oscillations)*, The higher school, Moscow, 1980.
- [17] S. Lee, T. Tanaka, K. Inoue, J.M. Kim, Y.E. Shin, Stress Influences on the Ultrasonic Transducers, *Sensors Actuators*. 119(2) (2005) 405–411.
- [18] N.S. Rossini, M. Dassisti, Methods of measuring residual stresses in components, *Materials and Design*. 35 (2012) 572–588.
- [19] J.Zhao, S. Yu, Effects of Residual Stress on the Hydro-Elastic Vibration of Circular Diaphragm, *World Journal of Mechanics*. 2 (2012) 361.
- [20] I.A. Birger, *Ostatochnye napryazheniya (Residual Stresses)*, Mashgiz, Moscow, 1963.



International Conference on Industrial Engineering

Engineering design technique development of continuous loading modules

Otrokov A.V.^{a,*}, Khazanovich G.S.^a, Afonina N.B.^a

^a *Shakhty institute (branch) of Platov South-Russian state polytechnic university (NPI), 1, Lenin Square, Shakhty, Rostov region, Russia*

Abstract

The problem of improvement of mined rock loading system efficiency in drifting faces is stated in the paper, as well as the necessity to develop an up-to-date methodology of continuous loading module design is revealed, which considers dynamic and stochastic loading processes. Essential differences in resolving problems of loading module design are given for tunneling machines and mine loaders. Basic approaches to an objective function and constraint-functions are determined. A generalized design-functional construction of loading modules is developed.

© 2015 The Authors. Published by Elsevier Ltd. This is an open access article under the CC BY-NC-ND license (<http://creativecommons.org/licenses/by-nc-nd/4.0/>).

Peer-review under responsibility of the organizing committee of the International Conference on Industrial Engineering (ICIE-2015)

Keywords: continuous loading module; system “loading module – pile – control assembles”; process dynamics of mined rock flow formation and loads; design-parametric synthesis.

1. Introduction

Strategic purposes of coal-mining industry development in Russia are as follows:

- reliable supply of economy and population of the country with high quality solid fuel and products of its processing;
- support of competitiveness in conditions of market saturation with alternative energy resources;
- stable and safe development of coal-mining industry in terms of up-to-date advances in science and technology, meeting the environmental protection standards.

* Corresponding author. Tel.: +7-918-509-03-07; fax: +7-8636-22-30-88.

E-mail address: oav711@gmail.com

Scientific-technical and innovative policy in coal-mining industry in Russia focuses on launching and implementing a technology program of competitive domestic mining machinery.

Loading modules are thought to be a compulsory element in up-to-date highly efficient tunnelling machinery (loading machines, road headers, tunnelling systems and shields). A loading module forms a flow of mined rock from the working face and influences on the efficiency of the entire tunnelling system. Hence, improvement of technical and economic parameters of excavation depends considerably on efficiency of loading processes and face transport.

In view of the fact, that “A system is considered as such complex of selectively involved components, whose interaction and interrelation are characterized by inter-assistance of components aimed at attaining a focused usable result” [1, 2, 3] a continuous loading module is thought of as a system including:

- A) a loading organ (element) of a separate loader, loader-transporter, operating as a part of tunnelling equipment set, drilling and blasting modularized complex or selective road header;
- B) supply and manipulation mechanism, constructively connected with the loading element;
- C) “external” environment, which a loading element is operated in and interacts with – a pile of mined rock and supporting surface of supply and manipulation mechanism;
- D) control loop (control sub-system) over mined rock loading.

PNB-series double pallet handle loaders are widely used in coal mines of Russia and some other countries. A lot of selective road headers are equipped with similar loading elements (Fig. 1, a). After this machinery had been modernized loading elements with reverse rotating wedge gathering arms were designed (Fig. 1, b). Wedge arms of various designs are used in loading machine MPNK and in road header KP-21 [4]. Road headers have been equipped recently with loading elements designed as two rotating stars of various design (Fig. 1, c).

Main factors, which determine the difference in numerous series-manufactured continuous loading modules of loading machines and road headers, are as follows: kinematic characteristics of operating assembly gripping elements relatively to the delivery table; characteristics of transmission arrangement; the type of engine and that of energy supplied to the gathering components; the type of engine and that of energy of the running gear; the form of gathering element motor – running gear connection; the type of supply regulator.

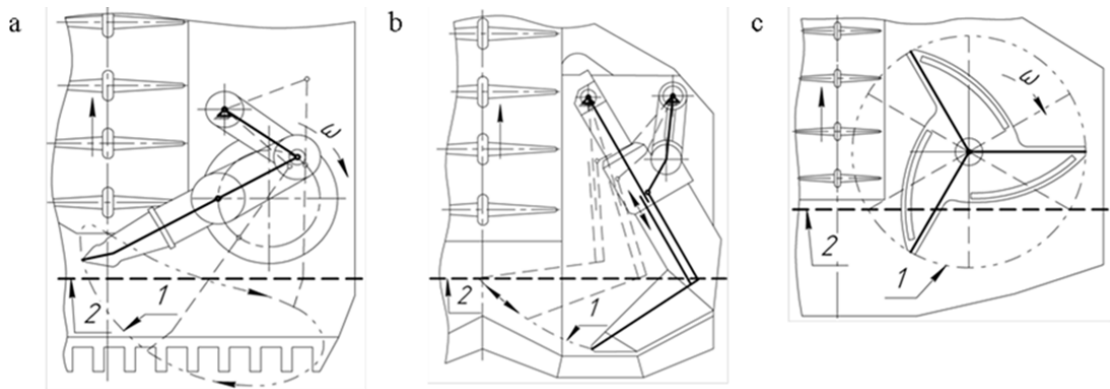


Fig. 1. Diversity of continuous loading modules (the right halves of loading elements are depicted): 1 – edge path of a gathering element; 2 – front edge of rock pile.

2. The need for development of modern-day design technique of continuous loading modules

Continuous loading modules considered as a part of tunnelling systems are currently designed on the basis of the principle of engineering analogues. In terms of this principle a loading module is developed according to a prototype. Theoretical capacity is calculated [5-13] regarding a provisional standard pile, and a flow formation together with the system state in the further cycles are not assessed, that is, the flow developed by continuous loading module is not viewed dynamically.

The capacity of continuous loading modules depends on loading module, pile and control loop interacting dynamically. The relative position of operating assemble components and a pile is changing constantly, as the result, the form and dimensions of the latter are subjected to transformation. Regarding the information on the state of the system a control unit or an operator takes a decision concerning further actions. The results of the next cycle or those of the sub-period of material gathering can differ from the planned ones because of the influence of random factors. As the consequence, controlling action in the next cycle can be entirely different than that in the previous cycle.

Dynamic character of the working process, determining all the performance qualities of continuous loading modules (grabbing cubature, forces and torque moment in elements of power unit and non-rotational parts) is caused by the following external factors:

- random change in time and functions of instantaneous attributes of operating element and a pile – its form, dimensions, granulometric composition in the area of its interaction with the operating element [14, 15];
- variability of reduced mass of moving parts of the system, including that of the load transported together with the loading element;
- character of operator or automatic unit actions to control the engine sub-systems of loading element and supply on a pile.

Therefore, it necessitates the study of the system including interrelated supporting running gear, continuous loading module, a pile and a control loop in a dynamical process, involving formation of mined rock flow at each moment of time at the system output, as well as energy consumption over the whole line from the operating element up to the engine and loading in the components of the system.

3. The issue of research into continuous loading modules general statement

Conceptual approaches to continuous loading module design are not available now, which take into consideration, first, a loading module, a pile and a control loop as an entire system involving numerous degrees of freedom, second, methodology of selecting rational parameters of machines in terms of their efficiency of application and operation.

Although previously conducted research admitted the random character of capacity and labour intensity formation, available computing formulas are determined by proportions. Over the period of research into various types of continuous loading modules information on such stochastic characteristics has been accumulated as distribution according to the coarseness of mined rock, formation of failure and repair flow of the equipment. However, a contradictory situation is observed, on one hand, regularities of working processes formation in continuous loading module have been found out according to a vast amount of information, on the other hand, these regularities are not applied for design of new machinery and for determination of suitability of available machines to real operational conditions.

Currently applied simulation methods of continuous loading modules working processes and mathematical models, they are based on, are to simulate and assess processes taking place when flow of mined rock is formed in transmissions under different modes of work in terms of varying mass of grabbed load. They are also to find possibilities to reduce dynamic loads, therefore, to correct requirements for the strength of particular components and assemble; selection of the best parameters of mechanisms and control schemes over machines in order to improve their efficiency, reliability and longevity. Solution of this problem is a burning scientific and practical issue.

4. Problem, resolved for different continuous loading modules

When designing up-to-date continuous loading modules it is necessary to take into consideration engineering peculiarities of mined rock transport.

All components of a loading module are connected with each other either in terms of construction or technology. For continuous loading module, for instance, for manually controlled elements, the interrelation “loading module – pile - operator” is of a technological character. Provided that automatic units of control over loading process are applied, rigid construction dependence occurs, meanwhile loading module – pile connection is a technological one.

For a loading machine the initial form of a pile is exactly determined by drilling and blasting operations. For a tunnelling machine a pile is continuously formed alongside with face destruction, whereas the process of loading can be controlled over by changing operation mode of destructing element only.

All the listed peculiarities will effect on selected objective function and constrain-functions, because in a tunnelling machine continuous loading module is included into a technological line right after the cutting unit. Hence, when designing a continuous loading module of this kind a process of mined rock pile formation is to be taken into account, which depends on the type of deconstructing unit and scheme of its running [16]. For a loading machine primary pile formation and its further loading are to be viewed as separate processes.

5. Objective function selection

The main distinctive feature of a system is a result of its performance, that's why as an objective function such factor is to be selected, which will [17]: A) depend on the system functioning; B) be easily calculated according to the mathematical description of the system; C) make one of the system properties evident; D) assume a simplified approximate assessment according to experimental data.

When selecting an index of efficiency of continuous loading module operation it is to consider the construction of the module, its parameters, regularities of environmental influence, internal and external random factors, that is, the index of efficiency is determined by module operating.

Loading module operation results in removal of mined rock, output factors of this process include capacity or cost of mined rock loading. Provided that acceptable values of these indexes are obtained characteristics of lower level can be considered: power-intensity, steel intensity, reliability. Continuous loading module is noted to be an element of technical tunnelling system and its capacity can not exceed throughout performance of transport sub-system of a mining enterprise and is to be in line with the capacity of face deconstructing while mined rock pile forming constantly. Therefore, when designing new continuous loading modules specific power-intensity of mined rock loading, entirely meeting standards of efficiency indexes is reasonable to use for assessment of efficiency of taken technical decisions. In terms of super-system, which includes the continuous loading module its minimization has no restriction. A designer, who succeeds in reducing specific power-intensity, decreases loads, arising in transmission of continuous loading module, and increases efficiency of mined rock loading.

6. Justification of the system of constrains

The parameters of loading module the objective function depends on include the width of the operating area, dimensions of operating elements and their arrangement, kinematic characteristics of the operating element, the mode of machine supply to the pile, and power available.

Geometrical and physical-mechanical characteristics of the pile have a significant effect on efficiency, but they are not among the structural parameters of a loading module, therefore, they are thought of as constrain-functions. Moreover, constrains include those of power and energy, influencing on the drive and propeller of the gathering element (for example, heating and maximum torque), on the drive and propeller of the running gear (frequency of powering on, crowding power), standards of allowed geometrical arrangement of loading module elements (for example, arrangement of drive plates of pallet handles and receiving boom to form an entire front of gathering), stable work of control loop and so on.

7. System engineering

When developing general approaches to selection of parameters and engineering design of multi-purpose loading modules systematic methodology is used. Viewing a complex technical object it finds important interrelations [18, 19]. To grasp the principles of various loading module operation constructional models of mined rock loading systems are designed.

All continuous loading module elements performing physical operations form flows of matter, energy, and signals (stream connections). In addition, continuous loading module elements have definite functional connections with each other, forming a design-functional structure [20]. A model of continuous loading module [21] thought of

as a part of tunnelling systems is developed to form stream and design-functional structures. Regarding design-functional structures of particular continuous loading modules, a generalized functional structure of a continuous loading module, as well as on the basis of available classification schemes of loading elements, a generalized design-functional structure of loading modules is developed (Fig. 2), which helps to resolve problems of their design-parametric synthesis [14].

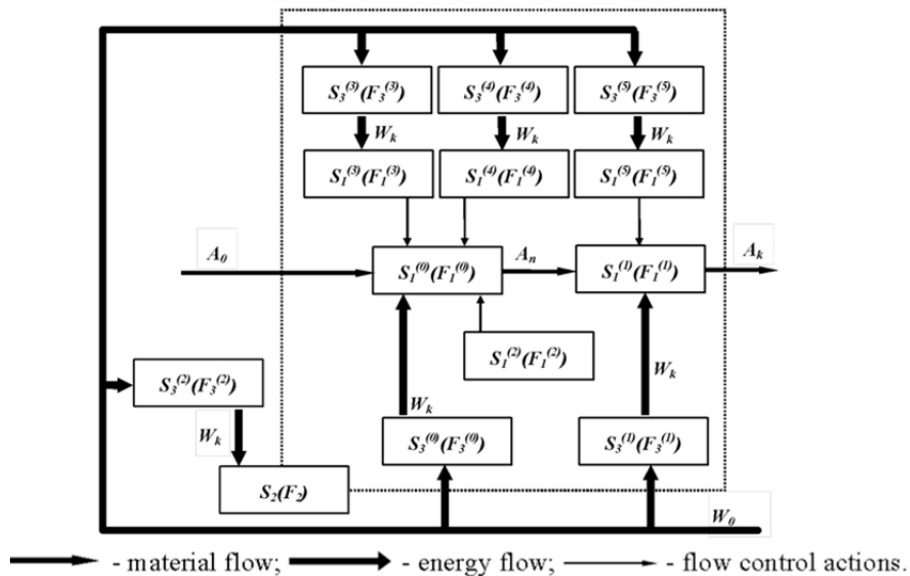


Fig. 2. Generalized design-functional structure of continuous loading modules.

The following conventional symbols are used in Fig. 2: $F_1^{(0)}$ – function of mined rock grabbing from the pile A_0 (sub-system of mined rock grabbing) $S_1^{(0)}$ and its transfer into the system of accumulation or mined rock re-loading $S_1^{(1)}$ (position A_n); $F_1^{(1)}$ – function of accumulation and re-loading to the transport vehicle A_k of a gathered mined rock slug; $F_1^{(2)}$ – function of removing mined rock slug from the sub-system $S_1^{(0)}$; $F_1^{(3)}$ – function of pile deep-unloading, providing by the sub-system $S_1^{(3)}$ face deep-servicing; $F_1^{(4)}$ function of pile front uploading, providing by the sub-system $S_1^{(4)}$ face front-servicing; $F_1^{(5)}$ – function of contact keeping with the transport vehicle; F_2 – function of machine short-distance movement near the face; $F_3^{(0)}...F_3^{(5)}$ – energy functions (and sub-systems $S_3^{(0)}...S_3^{(5)}$ respectively), transforming external energy W_0 into mechanic energy W_k , necessary to implement functions $F_1^{(0)}...F_1^{(5)}$.

When design-parametric synthesizing continuous loading modules their construction is not known in advance, both construction and parameters of a module are alternated, therefore, parameter vector length is not known in advance, it is searched for among constructions and parameters. Moreover, peculiarities of continuous loading modules are to be taken into consideration the motor of loading elements, that of moving mechanism of continuous loading module effect on forming a flow of mined rock, a working (damaging) element is involved in this process for loading module of tunneling machines. A running gear is used as a thrust mechanism and to provide maneuvers along the field of loading. Mechanisms of damaging, grabbing and running interact as an entire sub-system forming a grabbing cubature; their parameters are to be selected in the total process of optimization.

One of the algorithms to find a design of continuous loading module is a methodology of technical appliance synthesis on and-or-tree [20, 21]. Its basis is formed by a generalized design-functional construction of continuous loading module, containing classification characteristics [21]. As when design-functional synthesizing the number of parameters of a loading module is not known beforehand, after the design of continuous loading module is developed, the length of parameter vector is to be calculated for further optimization of selected design parameters.

8. Conclusion

Complex theoretical and experimental research into the continuous loading module is carried out at Shakhty Institute (branch) (NPI) of Platov South-Russian State polytechnic University to resolve the problems mentioned above: experimental-model complex is manufactured, which affords to simulate main operation processes to form mined rock flow, dynamic loads, programs of theoretical and experimental research of definite continuous loading modules are developed, a generalized methodology of design-parametric optimization of continuous loading modules is made up.

References

- [1] P.K. Anokhin, Outlines on physiology of functional systems, Moscow, 1975.
- [2] McCloskey, F. Joseph, David D. Debeau, Systems: Research and Design / Operations Research. 10(4).
- [3] J.C. Wetherbe, Systems analysis and design: traditional, structured, and advanced concepts and techniques, West Pub. Co., 1984.
- [4] A.V. Otrokov, G.Sh. Khasanovich, I.E. Kolesnichenko, V.G. Khasanovich, On systematization of constructions and kinematic schemes of continuous loading modules, Modern-day problems of science and education. 4 (2014). URL: <http://www.science-education.ru/118-13857>.
- [5] N.V. Gontar, About improvement of grasping element of the machine C-153, Scientific papers. 49 (1959) 29–46.
- [6] I.D. Marian, Standards of operating element of loading machine equipped with pallet handles, Scientific papers, Design and research Institute Hypronickel. 2 (1958) 133–161.
- [7] Ya.B. Kalnitsky, A.T. Filimonov, Self-propelled loading and transporting equipment in underground mines, Undergrounds, Moscow, 1974.
- [8] B.G. Gorbachev, Calculation of motor power for loading machines equipped with pallet handles, Transport of mining enterprises. (1963) 100–105.
- [9] E.A. Krisachenko, Research into the process of loading machine operating element with coupled pallet handles – pile of coarse rock interaction: PhD in engineering thesis: 05.174: defended 23.06.71, 1971.
- [10] V.A. Turushin, Research into the dynamics of operating element transmission of loading machines with coupled pallet handles: PhD in engineering thesis: defended 26.03.71, 1971, 146.
- [11] A.V. Otrokov, G.S. Khasanovich, Problem designing of loading machines with grasping claws, III International Symposium ENERGY MINING, Energy mining, new technologies, sustainable development : proceedings. (2010) 343–352.
- [12] LI Xiaohuo, Simulation and Analysis of a Two-raking Pawl Loading Mechanism, Journal of Heilongjiang Institute of Science. 3 (2002).
- [13] QIN Feng, LI Chun-ying, Influence of the Turntable Size and Rotation Rate and the Materials Depth on the Loading Efficiency of Roadheader, Mechanical Management and Development. 2 (2011).
- [14] G.Sh. Khasanovich, G.V. Lukyanova, A.V. Otrokov, Imitative simulation of wedge loader operation in conditions of random external influence, Research in design, operating processes and maintenance of technological machinery: collected scientific papers. (2006) 8–11.
- [15] G.Sh. Khasanovich, G.V. Lukyanova, E.A. Revyakina, A.V. Otrokov, Simulated operation processes of loading-transport modules in terms of random external influence: monograph, SEI HPE SRSTU, Shakhty, 2010.
- [16] V.G. Khasanovich, Development and selection of rational parameters of hydroficated loading element in selective tunneling machine: PhD in Engineering thesis. (1996).
- [17] N.P. Buslenko, V.V. Kalashnikov, I.N. Kovalenko, Lectures on the theory of complex systems, Soviet radio, Moscow, 1973.
- [18] S. Ahmed, M. Štorga, Merged ontology for engineering design: contrasting an empirical and a theoretical approach to develop engineering ontology. Artificial Intelligence for Engineering Design, Analysis and Manufacturing. 23(4) (2009) 391–407.
- [19] V. Hubka, W.E. Eder, Theory of technical systems and engineering design synthesis, Engineering design synthesis – understanding, approaches and tools, Springer-Verlag. (2002) 49–65.
- [20] A.I. Polovinkin, Fundamentals of engineering creativity: Students book for higher technical educational institution students, Machinebuilding, Moscow, 1988.
- [21] A.V. Otrokov, Rational set selection of design-functional characteristics of mine loaders: PhD in Engineering thesis: 05.05.06. (2001) 216.



International Conference on Industrial Engineering

Kinematic analysis of mechanism for converting rotational motion into reciprocating rotational motion

Prihodko A.A.^a, Smelyagin A.I.^{a*}

^a*Kuban State Technological University, 2 Moskovskaya st., Krasnodar, 350072, Russian Federation*

Abstract

The authors propose a distinctive construction of the planetary mechanism with elliptical gears designed to convert rotational motion into reciprocating rotational (oscillating) one. We conducted a kinematic analysis of the mechanism, found the variation of the rotation angle, the angular velocity analogue and angular acceleration analogue of the mechanism output shaft. The developed mechanism is a classic planetary mechanism and is more reliable and compact in comparison with the lever and electromagnetic inverters.

© 2015 The Authors. Published by Elsevier Ltd. This is an open access article under the CC BY-NC-ND license (<http://creativecommons.org/licenses/by-nc-nd/4.0/>).

Peer-review under responsibility of the organizing committee of the International Conference on Industrial Engineering (ICIE-2015)

Keywords: rotational motion; reciprocating rotational motion; elliptical gears; planet gear mechanism; kinematic analysis; angular velocity analogues; angular acceleration analogues.

1. Introduction

Converters of rotational motion into reciprocating rotation (oscillating) motion are widely used in engineering [1-4]. Transfer mechanisms, sewing and planing machines, non-traditional internal combustion engines, stirrers and others are created on their principle. Most often, these converters are the coulisse mechanisms or four-bar linkages [3, 4]. Also, electromagnetic mechanisms can be used as such converters [5].

The most compact and highly reliable converters of rotational into reciprocating rotational motion can be obtained by creating them using only gear units. Since the use of spur gears does not allow to develop such

* Corresponding author. Tel.: +7-861-251-87-05.

E-mail address: asmelyagin@yandex.ru, sannic92@gmail.com

converters there we propose a planetary gear mechanism which contains spur and elliptical gears with properly chosen parameters [6].

Planetary mechanism (Fig. 1) consists of a rack 0, the input shaft 1, the carrier 2, the output shaft 3, the sun circular stationary gear 4, the elliptical gear 5, based on output shaft, a spur planet gear 6, the elliptical planet gear 7, a shaft 8, connecting planet gears.

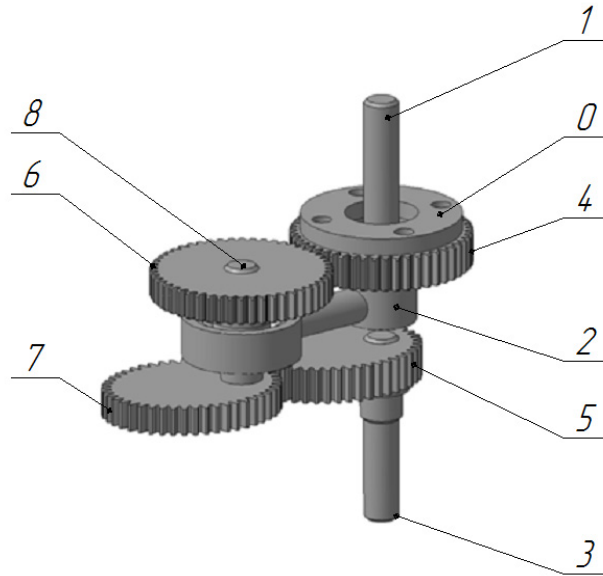


Fig. 1. Planetary mechanism with spur and elliptical gears.

In this mechanism, the gears 4 and 6 have the same diameters, and elliptical gears 5 and 7 have the same semiaxis, and the axle base distances of spur and elliptical gears are equal. Reciprocating rotational motion is provided by the variable transmission ratio of elliptical gears.

2. Kinematic analysis of the mechanism

To carry out the kinematic analysis we construct linear velocities plans of all mechanism links [7] (Fig. 2). The angular velocity analogue of the output shaft 3 is defined as:

$$\varphi_3' = \frac{d\varphi_3}{d\varphi_1} = \frac{\omega_3}{\omega_1} = \frac{v_C \cdot BO}{v_B \cdot CO} = \frac{CC' \cdot BO}{BB' \cdot CO}, \quad (1)$$

where φ_3 , ω_3 is the angle of rotation and the angular velocity of the output shaft 3; φ_1 , ω_1 is the angle of rotation and the angular velocity of the input shaft 1.

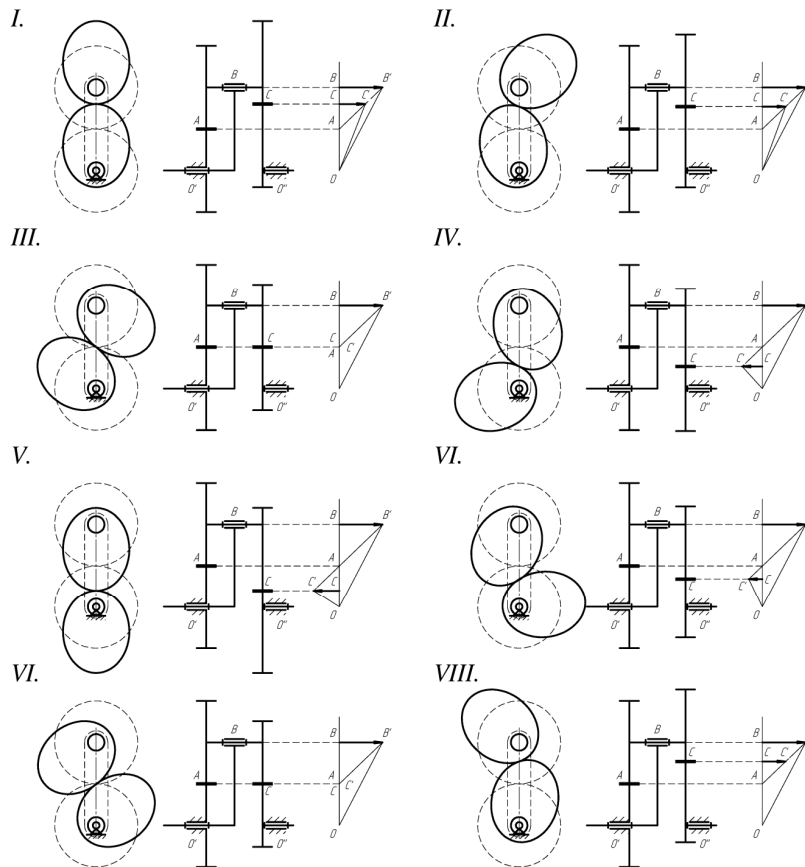


Fig. 2. Linear velocities plans.

As we can see from figure 2, point C changes its position relatively to the point A , at the same time the velocity vector CC' changes its direction and value. In order to determine distances BC and CO , let's consider the equation of the ellipse in polar coordinates [8]. The focus of the driving ellipse 1 will be taken as the pole, and the major axis will be taken as the polar axis (Fig. 3), then we will get the following ellipse equation [9]:

$$\rho(\varphi_x) = \frac{p}{1 - e \cos \varphi_x}, \tag{2}$$

$$p = a(1 - e^2), \tag{3}$$

where φ_x is a drive gear (indicated by pos. 7 in fig. 1) rotation angle; p is a ellipse focal parameter; e is eccentricity of the ellipse; a is a semi-major axis of the ellipse.

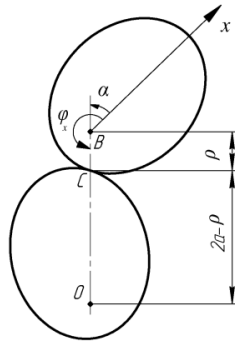


Fig. 3. Elliptical gear.

Considering that $CO=2a-\rho(\varphi_x)$, we get the following equation (1):

$$\varphi'_3 = \frac{\operatorname{tg}\varphi_{b'a} \cdot AC \cdot BO}{\operatorname{tg}\varphi_{b'a} \cdot AB \cdot CO} = 1 - \frac{\rho}{2a - \rho}. \tag{4}$$

By substituting (2) to (4) with transformations, we get:

$$\varphi'_3 = 1 - \frac{p}{2a(1 - e \cos \varphi_x) - p}. \tag{5}$$

Since the diameters of the gears 4 and 6 are identical, then the angle α in Fig. 3 is equal to the angle of rotation of the input shaft φ_1 . Thus, the angles φ_x and φ_1 are associated with:

$$\varphi_x = \varphi_1 + \pi. \tag{6}$$

By substituting (6) to (5), we get the equation to calculate the angular velocity analogue $\varphi'_3(\varphi_1)$:

$$\varphi'_3(\varphi_1) = 1 - \frac{p}{2a(1 - e \cos(\varphi_1 + \pi)) - p}. \tag{7}$$

To determine the law of motion of the output shaft $\varphi_3(\varphi_1)$ we integrate (7) according to the generalized coordinate φ_1 :

$$\varphi_3(\varphi_1) = \varphi_1 - \frac{(1-e^2)}{\sqrt{(1+e^2)^2 - 4e^2}} \cdot \left[\operatorname{arctg} \left(\frac{(1+e^2) \cdot \operatorname{tg}(\varphi_1 + \pi)}{\sqrt{(1+e^2)^2 - 4e^2}} \right) + \operatorname{arctg} \left(\frac{2e \cdot \sin(\varphi_1 + \pi)}{\sqrt{(1+e^2)^2 - 4e^2}} \right) \right]. \tag{8}$$

We find the angular acceleration analogue after differentiation of equation (7) according to the generalized coordinate φ_1 :

$$\varphi_3''(\varphi_1) = \frac{2p \cdot a \cdot e \cdot \sin(\varphi_1 + \pi)}{(2a(1 - e \cos(\varphi_1 + \pi)) - p)^2} \quad (9)$$

Thus, equations (6)-(8) perform the kinematic model of the designed mechanism.

3. Results and discussion

As an example let's investigate a planetary mechanism, shown in Fig. 1, having the following geometrical parameters: $d_4=d_6=50\text{mm}$ – diameter of spur gears; $a_5=a_7=25\text{mm}$ – semi-major axes of elliptical gears; $b_5=b_7=20\text{mm}$ – semi-minor axes of elliptical gears; $c_5=c_7=15\text{mm}$ – focal length; $p_5=p_7=16\text{mm}$ – focal parameter; $e_5=e_7=0,6$ – the eccentricity of elliptical gears; $a=d_4+d_6=2a_5=2a_7=50\text{mm}$ – axle base distance.

Using the equations (7)-(9), we construct the function of the output shaft position, angular velocity analogue, and angular acceleration analogue (Fig. 4).

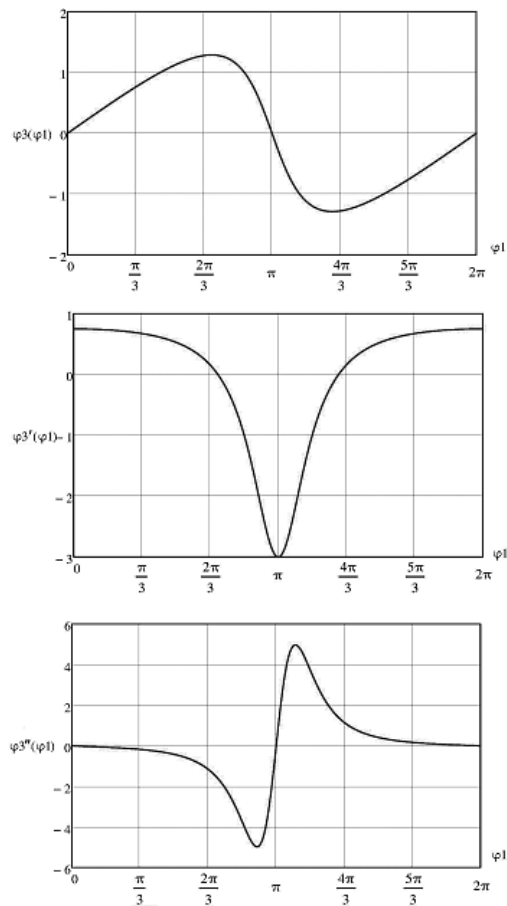


Fig. 4. The functions $\varphi_3(\varphi_1)$, $\varphi_3'(\varphi_1)$, $\varphi_3''(\varphi_1)$.

Analysis of charts shown in Figure 4 testifies that an output shaft of the studied planetary mechanism at the unidirectional rotation of an input shaft will make a reciprocating rotational motion. This allows us to use this mechanism in machines whose actuators make reciprocating rotational motion.

4. Conclusion

We proposed planetary mechanism for converting rotational into reciprocating rotational motion and conducted its kinematic analysis. Since the designed mechanism consists of spur and elliptic gears and is a classic planetary gear, it is compact and reliable. This proves the perspective to apply the proposed mechanism in various machine-tools, stirred tanks, alternative internal combustion engines, drilling rigs and other devices and machines where converting rotational into reciprocating rotational motion is necessary.

Acknowledgements

The research is done using scientific equipment of the Center of Shared Usage “The research center of engineering, materials, construction, and transportation systems” in Kuban State Technological University.

References

- [1] I.I. Artobolevski, *Mechanisms in modern engineering design*, MIR Publishers, Moscow, 1986.
- [2] N. Sclater, N.P. Chironis, *Mechanisms and mechanical devices sourcebook*, fourth ed., McGraw-Hill, New York, 2001.
- [3] A.G. Ambekar, *Mechanism and machine theory*, Prentice-Hall of India Private Limited, NewDelhi, 2007.
- [4] A.A. Prikhodko, A.I. Smelyagin, RU Patent 2,528,843. (2014)
- [5] A.I.Smelyagin, Maximal efficiency of an electromagnetic drive, *Journal of mining science*. 23(2) (1987) 154–158.
- [6] A.I. Smelyagin, I.V. Yukhnevich, RU Patent 2,528,493. (2014)
- [7] N.I. Levitskiy, *Theory of mechanisms and machines*, Nauka, Moscow, 1979.
- [8] F.L. Litvin, A. Fuentes, *Gear geometry and applied theory*, second ed., Cambridge University Press, 2004.
- [9] H.S.M. Coxeter, *Introduction to Geometry*, second ed., Wiley, New York, 1969.



International Conference on Industrial Engineering

Detailed dynamic modeling of common rail piezo injector

Pogulyaev Y.D., Baitimerov R.M.*, Rozhdestvenskii Y.V.

South Ural State University, 76 Lenina Avenue, Chelyabinsk 454080, Russian Federation

Abstract

A mathematical model of Bosch 3rd generation Common Rail fuel injection system with piezoelectric injector has been created. The numerical calculations for third different accumulator pressures (30, 80 and 160 MPa) and third energizing times ET (0.5, 1 and 2 ms) have been carried out. The results of calculations of total injected mass per cycle have been compared with the experiment with good agreement. The maximum error for ET=0.5 ms is 10.4% and for ET \geq 1 ms is less than 5 %.

© 2015 The Authors. Published by Elsevier Ltd. This is an open access article under the CC BY-NC-ND license (<http://creativecommons.org/licenses/by-nc-nd/4.0/>).

Peer-review under responsibility of the organizing committee of the International Conference on Industrial Engineering (ICIE-2015)

Keywords: Fuel injection system; Common rail; Piezo injector; Mathematical model.

1. Introduction

Modern diesel fuel injection systems (FIS) are characterized by complex dynamic hydromechanical processes. Also, an electromagnetic processes on drives of injector's control valves significant influence on fuel injection process.

Optimization of developed fuel injection system design has an important role [1], then, an adequate mathematical modeling, that allows fast and flexible change of varying parameters and get simulation results in optimization criteria form, is very actual.

Now, one of the most perfect of FIS is common rail fuel injection system with piezoelectric indirect-acting injector.

This paper is devoted to modeling of common rail piezo injector from Bosch.

* Corresponding author. Tel.: +7-351-267-9057; fax: +7-351-267-9083.

E-mail address: baitimerovrm@susu.ac.ru

2. Mathematical modeling

2.1. Bosch Common Rail piezo injector

The design of a piezoelectric injector essentially differs from hydraulic injectors of the previous generations besides that the electromagnetic operating valve has been replaced with the piezoelectric. Developers have refused the locking piston, thereby having excluded the mechanical forces operating on a needle and having reduced moving weights. The management chamber is directly over a needle that, in a compartment with speed of operation of a piezoelement and reduction of moving weights, allows to lower a delay of lifting of a needle to 0,15 ms [2]. The principle of the injector working described in detail in [2-7].

2.2. Mathematical model

For modeling of hydromechanical processes the Astakhov-Golubkov method was used [8,9]. This method consists of a solution of unsteady fuel flow in high pressure line problem by D'Alembert method with boundary conditions in form of volume or mass balance.

The simulation scheme of piezo injector is presented in Fig. 1.

Mass balance equation (for control chamber as an example):

$$\frac{dp_3(t)}{dt} = B_3 \frac{\frac{\sigma_{13}}{\rho_3} G_{13} - \frac{\sigma_{34}}{\rho_3} G_{34} + A_3 \frac{dx_n(t)}{dt}}{V_3 - A_3 x_n(t)}, \quad (1)$$

where t - time; p_3 - pressure in chamber 3 (control chamber) (see Fig. 1); B - bulk modulus of fuel с учетом деформации стенок камеры [10]; ρ_3 - current fuel density in chamber 3; V_3 - initial volume of chamber 3; A_3 - geometrical area of area 3; x_n - current lift of needle; $\sigma_{13} = \text{sign}(p_1 - p_3)$; $\sigma_{34} = \text{sign}(p_3 - p_4)$; G - fuel mass flow through orifice, for example:

$$G_{13} = C_{d13} A_{13} \sqrt{\rho_1 (p_1 - p_3)}, \quad (2)$$

where C_{d13} - discharge coefficient of orifice 13; A_{13} - cross-sectional area of orifice 13.

For solution of unsteady fuel flow in high pressure line problem D'Alembert method was used [8,9]. For example, equations for line 1 is written as:

- for inlet:

$$\begin{cases} p_0 + F_1(t) - W_1(t) \cdot e^{-k_1 \frac{L_{line1}}{a}} = P_A; \\ \frac{1}{a\rho} \left[F_1(t) + W_1(t) \cdot e^{-k_1 \frac{L_{line1}}{a}} \right] = u_{1in}; \end{cases} \quad (3)$$

- for outlet:

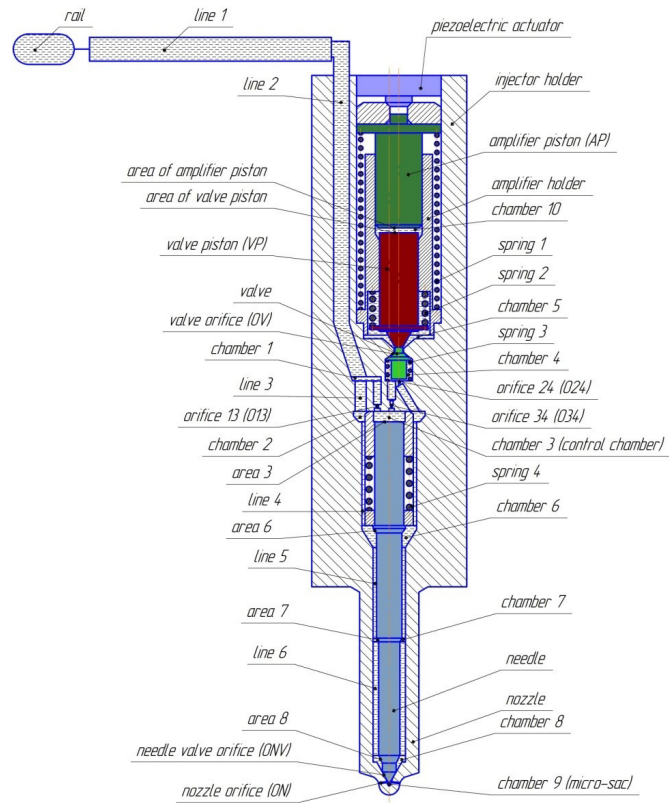


Fig. 1. Schematic cross-section of piezo injector.

$$\begin{cases} p_0 + F_1 \left(t - \frac{L_{line1}}{a} \right) \cdot e^{-k_1 \frac{L_{line1}}{a}} - W_1 \left(t + \frac{L_{line1}}{a} \right) = p_0 + F_2(t) \cdot e^{-k_1 \frac{L_{line1}}{a}} - W_2(t) \cdot e^{-k_2 \frac{L_{line2}}{a}} ; \\ \frac{A_{line1}}{a\rho} \left[F_1 \left(t - \frac{L_{line1}}{a} \right) \cdot e^{-k_1 \frac{L_{line1}}{a}} - W_1 \left(t + \frac{L_{line1}}{a} \right) \right] = \frac{A_{line2}}{a\rho} \left[F_2(t) + W_2(t) \cdot e^{-k_2 \frac{L_{line2}}{a}} \right] ; \end{cases} \quad (4)$$

where p_0 - initial pressure in high pressure line; P_A - pressure in rail; F , W - direct and backward pressure waves in high pressure lines respectively; A_{line1} - cross-sectional area of line 1; a - fuel speed of sound; ρ - fuel density; L_{line1} - length of line 1; k - friction factor.

Discharge coefficients of orifices was determined by using ANSYS CFX software taking into account the flow regime and cavitation phenomenon [11].

The mathematical model was realised by using of Matlab/Simulink software [12]. The dynamic model of piezoelectric actuator was created as a subsystem in the Simulink environment by using the U. Mezon's thermodynamic condition equations [13].

3. Results of modeling and discussion

For check of adequacy of mathematical model comparison of results of calculation with experiment has been made. Experimental data are taken [3] from work and represent sizes of total injected fuel mass cyclic giving of fuel for three levels of pressure in the accumulator (300, 800 and 1600 bar) and three values of energizing time ET: 0,5; 1 and 2 ms. Results of comparison are presented in Table 1.

Table 1. Comparison results of calculation of injected mass with experiment.

ET (ms)	300 (bar)		800 (bar)		1600 (bar)	
	Calculation	Experiment	Calculation	Experiment	Calculation	Experiment
0.5	5.85	5.3	16.33	17.3	36.47	33.8
1	19.50	20.3	52.49	51.8	86.36	84.8
2	47.02	47.4	96.45	96.1	134.71	134.0

Maximal error for ET=0.5 ms is 10.4% and for ET≥1 ms - less than 5 %.

Feature of the given injector is high lifting of a needle - to 0,9 mm [14], unlike other injectors where courses do not exceed 0,2-0,3 mm [15,16]. Such injector is called ballistic injector [17].

So high lifts of a needle have lacks:

- negatively affects a resource of a spray [18];
- for decrease in fluctuations of a needle and accuracy increase its positioning is necessary to carry out the powerful directing;
- accuracy of dispensing owing to high duration of uncontrollable sites of lifting and needle landing decreases;
- occurrence nonmonotonicity on schedules of dependence of cyclic giving from duration of an operating impulse.

Sites nonmonotonicity on dependence of cyclic giving on duration of an operating impulse at pressure in 800, 1200 and 1600 bar are shown on Fig. 2. At pressure in 300 bar such site is not present, this results from the fact that the needle at such pressure and duration of an operating impulse does not reach against the stop.

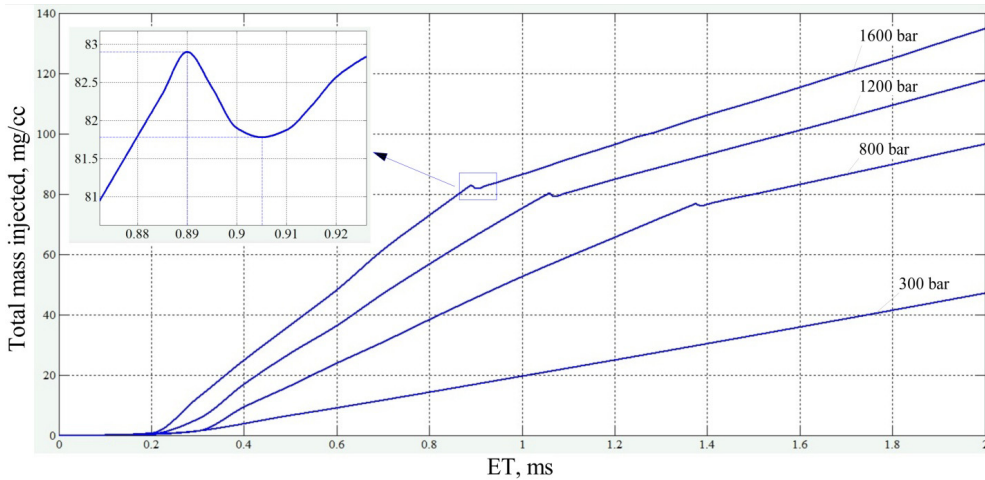


Fig. 2. Total mass injected influence on ET.

On Fig. 2 on the increased fragment of a site nonmonotonicity it is visible that at ET=0,89 ms giving more than at longer ET=0,905 ms, accordingly 82,9 and 81,8 mg.

On Fig. 3 are shown needle lifts, valve lifts, injected masses and injected rates history lines for ET=0,89 and 0,905 ms.

At $ET=0,89$ ms the needle does not reach against the stop, therefore for change of a direction of its movement it is necessary for more time to extinguish its inertia. At $ET=0,905$ ms the needle reaches against the stop, its kinetic energy at blow is transferred to an emphasis owing to what, the needle begins movement downwards earlier.

However so big courses of a needle have also advantages:

- owing to high lifts of a needle at injection decreases choking fuel under a needle thanks to what pressure of injection increases;
- work ballistic injector assumes absence of a contact of a needle of an emphasis, deterioration of a shaft of a needle therefore decreases;
- ballistic injector in comparison with conventional injector spends fuel for management less, as at identical ET to a needle ballistic injector it is necessary for more time for being closed and consequently will be more injected fuel, thus fuel consumption on the managements, defined ET, it will be identical.

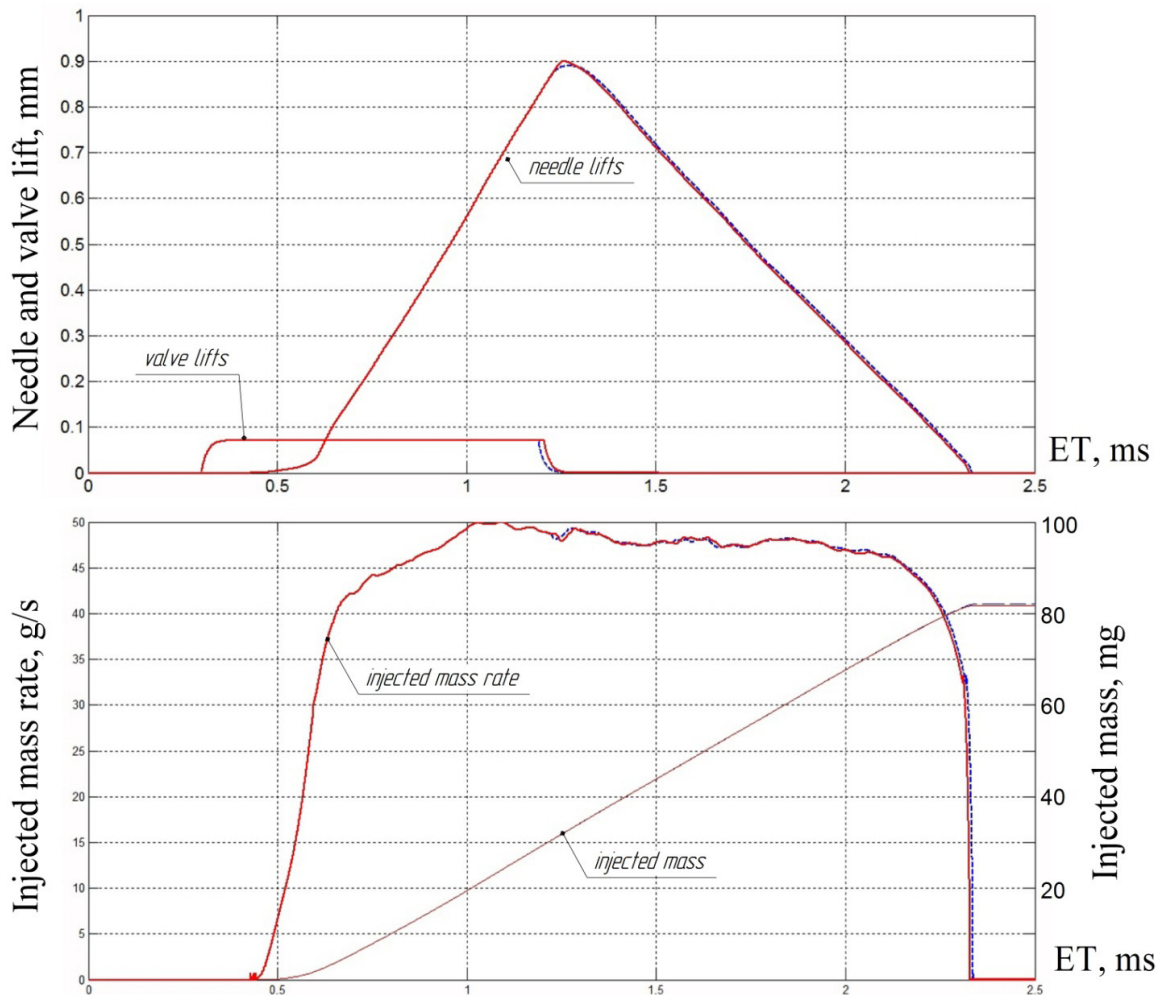


Fig. 3. Needle lifts, valve lifts, injected masses and injected rates for $ET=0.89$ ms (dashed line) and $ET=0.905$ ms (solid line).

4. Conclusions

Common Rail piezo injector has been studied in this paper and conclusions are obtained as follows:

1. The mathematical model of hydrodynamic processes of fuel system Common Rail of firm Bosch of 3 generations with a piezoelectric injector which can be used for studying and optimization of fuel supply systems of the given type.
2. Comparison of results of calculations with experiment largely changes of pressure in the accumulator and duration of operating impulses has shown satisfactory coincidence that proves adequacy of the developed mathematical model.

References

- [1] A.A. Prokhorenko, D.E. Samoilenko, D.V. Meshkov, Optimizatsiya konstruktivnykh parametrov p'yezoelektricheskoy dizel'noy forsunki, Vesti Avtomobil'no-dorozhnogo instituta. 1 (2010) 47–53.
- [2] K. Reif, *Moderne Diesel-Einspritzsysteme*, Vieweg+Teubner Verlag, Wiesbaden, 2010.
- [3] F.J. Salvador, A.H. Plazas, J. Gimeno, M. Carreres, Complete modelling of a piezo actuator last-generation injector for diesel injection systems, *International Journal of Engine Research*. 15(1) (2014) 3–19.
- [4] F. Boecking, U. Dohle, J. Hammer, S. Kampmann, Passenger Car Common Rail Systems for Future Emissions standards, MTZ worldwide. 66(7-8) (2005) 14–16.
- [5] K. Hummel, F. Boecking, J. Gross, J. Stein, U. Dohle, Third-Generation Common Rail System with Piezo Inline Injectors from Bosch for passenger Cars, MTZ worldwide. 65(3) (2004) 9–12.
- [6] V. Caika, P. Sampl, D. Greif, Integrated 1D/2D/3D Simulation of Fuel Injection and Nozzle Cavitation, *SAE Int. J. Engines*. 6(3) (2013) 1–9.
- [7] V. Caika, P. Sampl, D. Greif, Coupled 1D/2D/3D Modeling of Common Rail Injector Flow and Nozzle Cavitation, in: *Proceedings of the FISITA 2012 World Automotive Congress, Advanced Internal Combustion Engines (I)*, Springer-Verlag, Berlin. 1 (2013) 375–386.
- [8] I.V. Astakhov, V.I. Trusov, A.S. Khachiyani, L.N. Golubkov, Podacha i raspylivanie topliva v dizelyakh, Mashinostroenie, Moscow, 1971.
- [9] L.V. Grekhov, I.I. Gabitov, A.V. Negovora, *Konstruktsiya, raschet i tekhnologicheskii servis toplivopodayushchikh sistem dizeley*, Legion-Avtodata, Moscow, 2013.
- [10] Yu.D. Pogulyaev, R.M. Baytimerov, Opredelenie koeffitsienta deformatsii polostei sistem toplivopodachi dizelei, Stroitel'nye i Dorozhnye Mashiny. 8 (2015) 11–14.
- [11] Yu.D. Pogulyaev, R.M. Baytimerov, Opredelenie koeffitsientov raskhoda raspylivayushchikh otverstiy raspylitateley dizel'nykh forsunok s ispol'zovaniem ANSYS CFX, Stroitel'nye i Dorozhnye Mashiny. 1 (2014) 47–53.
- [12] V.P. D'yakov, MATLAB 6.5 SP1/7 + Simulink 5/6. Osnovy primeneniya, SOLON - Press, Moscow, 2005.
- [13] A.A. Bobtsov, V.I. Boykov, S.V. Bystrov, V.V. Grigor'yev, *Ispolnitel'nye ustroystva i sistemy dlya mikroperemeshcheniy*, ITMO University, Saint Petersburg, 2011.
- [14] V. Caika, P. Sampl, Nozzle Flow and Cavitation Modeling with Coupled 1D-3D AVL Software Tools, *SAE Technical Paper 2011-24-0006*. (2011) 1–12.
- [15] A.A. Prokhorenko, D.E. Samoilenko, D.V. Meshkov, Matematicheskaya model protsessa toplivopodachi sistemoi Common Rail s pezoelektricheskoi forsunkoi, Vesti Avtomobil'no-dorozhnogo instituta. 1 (2009) 6–12.
- [16] F.J. Salvador, J. Gimeno, J. De la Morena, M. Carreres, Using one-dimensional modeling to analyze the influence of the use of biodiesels on the dynamic behavior of solenoid-operated injectors in common rail systems: Results of the simulations and discussion, *Energy Conversion and Management*. 54 (2012) 122–132.
- [17] F.J. Salvador, P. Marti-Aldaravi, M. Carreres, D. Jaramillo, An Investigation on the Dynamic Behaviour at Different Temperatures of a Solenoid Operated Common-Rail Ballistic Injector by means of a One-Dimensional Model, *SAE Technical Paper 2014-01-1089*. (2014) 1–17.
- [18] V.E. Lazarev, *Povysheniya resursa raspylitateley topliva v dizeliakh snizheniem nagruzhennosti precizionnykh sopriazhenii: avtoreferat dis. ... doktora tekhn. nauk*, Barnaul, 2008.



International Conference on Industrial Engineering

A method of improving fiber-reinforced composite workpiece surface quality during the machining on 5-axis CNC machines

Shchurov I.A.*

South Ural State University, Lenina, 76, Chelyabinsk, 454080, Russia

Abstract

Fiber-reinforced composite parts are often finally processed by machining. Complex-shaped surfaces are often cut using the CNC machines. The resulting composite workpiece surface quality is essentially dependent on angles between two vectors: the resultant cutting direction and the fiber direction. As 5-axis CNC machines support every imaginable tool movement it is reasonable to guide these movements so that the specified angles were the most favorable to obtain the best surface quality. The proposed method enables to secure the required tool movements. Computer software has been developed and a cutting simulation has been executed. The verification of the designed CNC-program with CAM systems has proven the efficiency of the method.

© 2015 The Authors. Published by Elsevier Ltd. This is an open access article under the CC BY-NC-ND license (<http://creativecommons.org/licenses/by-nc-nd/4.0/>).

Peer-review under responsibility of the organizing committee of the International Conference on Industrial Engineering (ICIE-2015)

Keywords: Fiber-reinforced composite, surface quality, 5-axis CNC machining, CAM system.

1. Introduction

Composite materials are widely used in industry. Among them metal-matrix unidirectional fiber-reinforced composite materials (FRC) are at the utmost interest. In particular, such materials can be used for turbine blade production [1]. But it is well known, that precise blades mentioned above may not be produced by ordinary composite production methods. So machining of composite workpieces is still used in practice. However, these machining processes present problems to obtain good surface quality, especially if composite fibers are found in the

* Corresponding author. Tel.: +7-351-267-9111; fax: +7-351-267-9111.
E-mail address: igor_shurov@mail.ru

cutting zone [2-4]. Previous researches have shown that the best quality is obtained if the angle between two vectors: resultant cutting direction and fiber direction is equal to 45 ± 15 degrees [5].

CNC machine tools are widely used to make complex surfaces. Obviously, the most favorable to provide the best machining conditions are 5-axis machines. Now CAM systems are usually applied to develop CNC programs for these machines. However, modern CAM systems generating CNC programs have not provided required cutting angles for fiber reinforced composites yet. Voxel-based models are appropriate to realize such conditions for CAM systems with the fact that fiber directions may vary at different workpiece points [6-8]. Now CNC program preparation by using voxel models is not an extraordinary fact. Based on these models solution of a problem how to improve surface quality for the unidirectional fiber reinforced composites by using 5-axis CNC milling machines is presented in this article.

2. A method to develop CNC programs for 5-axis fiber-reinforced composite workpiece milling

2.1. Input data

As an example, a case of a complex-shape surface workpiece finishing by ball end milling is considered. Such ball or spherical surface will be referred to as spherical tools surface or STS. Let us assume that at machining start time all corresponding axes of a workpiece coordinate system X_1, Y_1, Z_1 and a tool coordinate system X_2, Y_2, Z_2 are parallel, and the origin of the second coordinate system is located at the STS center (Fig. 1). Then the equation of the nominal machined surface (NMS) for the workpiece coordinate system is $Z_1 = F_1(X_1, Y_1)$. Furthermore, a set of vectors $\{\vec{f}\}$, which tangent to fibers axes at places of their intersection with NMS, is given as input data. The equation of each such fiber vector is $\vec{f} = \vec{i}X_{1f} + \vec{j}Y_{1f} + \vec{k}Z_{1f}$. It is well known, that trajectory calculation for 3-axis milling of a steel workpiece, for example, is a routine process now. So this task may be solved in advance. Then a set of point coordinates $\{C_1\}$ - $C_1(X_{1c}, Y_{1c}, Z_{1c})$ of the STS centers in workpiece coordinate system may be obtained. Also, there is a set $\{M_1\}$ of contact points where STS and NMS are touchdown. Coordinates of these contact points are $M_1(X_{1M}, Y_{1M}, Z_{1M})$. This set $\{M_1\}$ is corresponded to set $\{C_1\}$. Further, we will define the same point set $\{M_1\}$ in the tool coordinate system as $\{M_2\}$, where point coordinates are $M_2(X_{2M}, Y_{2M}, Z_{2M})$. Later we will assume that a suitable angle between two vectors: resultant cutting direction \vec{V}_M of contact tool point and fiber direction \vec{f} is equal to 45. Thus, further the given task will be solved on the basis of these data and assumptions.

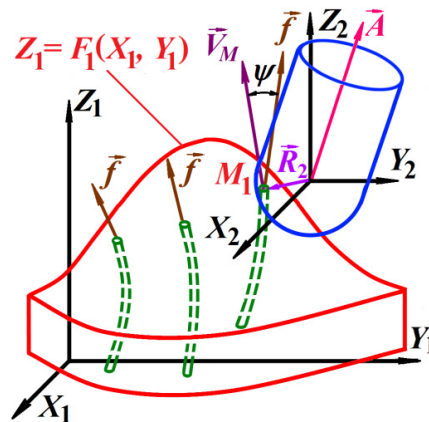


Fig. 1. Nominal machined surface, tool, fibers and vectors.

2.2. Calculation method

As STS and NMS are touchdown, so planes tangent to them at the point of their contact are coinciding too. $\vec{V}_M(X_{1V}, Y_{1V}, Z_{1V})$ vector is placed in this common plane. In the tool coordinate system, which axes are parallel to the

workpiece system axes, there is located the same $\vec{V}_M(X_{2V}, Y_{2V}, Z_{2V})$ vector, where $X_{1V} = X_{2V}$, $Y_{1V} = Y_{2V}$, $Z_{1V} = Z_{2V}$. Therefore, the milling-cutter longitudinal axis $\vec{A}(X_{1A}, Y_{1A}, Z_{1A})$ has to be perpendicular to \vec{V}_M and placed in the parallel plane (see Fig. 1).

As STS is touchdown to NMS, so its radius-vector at the contact point $\vec{R}_2(X_{1R}, Y_{1R}, Z_{1R})$ is parallel to \vec{N} vector, which is perpendicular to NMS at the same point. Thus, there are three conditions for calculation:

$$\vec{f} \vec{V}_M = \cos(\psi), \quad (1)$$

$$\vec{V}_M \vec{R}_2 = 0, \quad (2)$$

$$\vec{A} = \vec{V}_M \times \vec{R}_2. \quad (3)$$

These conditions show that \vec{V}_M vector is the result of the intersection of a cone (its angle is ψ and axis is \vec{f}) with a plane, which is perpendicular to \vec{R}_2 . \vec{A} vector is a perpendicular vector to \vec{R}_2 and \vec{V}_M simultaneously.

From (1), using the well-known equation, we obtain:

$$\cos(\psi) = \frac{X_{1f}X_{1V} + Y_{1f}Y_{1V} + Z_{1f}Z_{1V}}{\sqrt{(X_{1f}^2 + Y_{1f}^2 + Z_{1f}^2)}\sqrt{(X_{1V}^2 + Y_{1V}^2 + Z_{1V}^2)}}. \quad (4)$$

From (2), using the known equation, we obtain:

$$X_{2M}X_{2V} + Y_{2M}Y_{2V} + Z_{2M}Z_{2V} = 0. \quad (5)$$

Let us denote:

$$Q_1 = \frac{X_{1f}}{\cos(\psi)\sqrt{(X_{1f}^2 + Y_{1f}^2 + Z_{1f}^2)}}, \quad Q_2 = \frac{Y_{1f}}{\cos(\psi)\sqrt{(X_{1f}^2 + Y_{1f}^2 + Z_{1f}^2)}}, \quad Q_3 = \frac{Z_{1f}}{\cos(\psi)\sqrt{(X_{1f}^2 + Y_{1f}^2 + Z_{1f}^2)}}. \quad (6)$$

Considering that \vec{V}_M vector has identical coordinates in both coordinate systems, then from (4) and (5) we obtain:

$$Q_1 \frac{-Y_{2M}}{X_{2M}} Y_{2V} + Q_1 \frac{-Z_{2M}}{X_{2M}} Z_{2V} + Q_2 Y_{2V} + Q_3 Z_{2V} = \sqrt{\left(\frac{-Y_{2M}}{X_{2M}} Y_{2V} + \frac{-Z_{2M}}{X_{2M}} Z_{2V}\right)^2 + Y_{2V}^2 + Z_{2V}^2}. \quad (7)$$

To solve this equation we define the following notations:

$$Q_4 = \left(Q_1 \left(\frac{-Y_{2M}}{X_{2M}}\right) + Q_2\right)^2 + \left(\frac{-Y_{2M}}{X_{2M}}\right)^2 - 1, \quad (8)$$

$$Q_5 = Z_{2V} \left[\left(Q_1 \left(\frac{-Y_{2M}}{X_{2M}}\right) + Q_2\right) \left(Q_1 \left(\frac{-Z_{2M}}{X_{2M}}\right) + Q_3\right) - \left(\frac{Y_{2M}Z_{2M}}{X_{2M}^2}\right) \right], \quad (9)$$

$$Q_6 = Z_{2V}^2 \left[\left(Q_1 \left(\frac{-Z_{2M}}{X_{2M}} \right) + Q_3 \right)^2 - \left(\frac{-Z_{2M}}{X_{2M}} \right)^2 - 1 \right]. \quad (10)$$

In that case from the equation (7) the next equation is obtained

$$Q_4 Y_{2V}^2 + 2Q_5 Y_{2V} + Q_6 = 0, \quad (11)$$

where

$$Y_{2V} = \frac{-Q_5 \pm \sqrt{Q_5^2 - Q_4 Q_6}}{Q_4}. \quad (12)$$

Two unknown component of the speed vector, Y_{2V} and Z_{2V} are present at this equation. As for this case not the vector size but the vector direction is the important fact, so we accept $Z_{2V} = 1$. After Y_{2V} и Z_{2V} evaluation from the formula (5) the value of X_{2V} may be found easily. Thus, all necessary components of \vec{V}_M vector are assessed.

Here, it should be noted that solutions with $X_{2M} = 0$ are possible. In this case expressions in brackets in formulas for Q_4 , Q_5 and Q_6 may slightly change. Besides that, solution does not always exist if \vec{f} vector is parallel to the normal to STS vector. In this case it is offered to increase the angle ψ from the demanded value up to 90 degrees gradually until the conditions (1) and (2) are satisfied.

$\vec{A}(X_A, Y_A, Z_A)$ vector may be determined by vectors \vec{R}_2 and \vec{V}_M :

$$\vec{A} = \begin{vmatrix} \vec{i} & \vec{j} & \vec{k} \\ X_{2M} & Y_{2M} & Z_{2M} \\ X_{2V} & Y_{2V} & Z_{2V} \end{vmatrix}. \quad (13)$$

It should be noted that this tool axis vector is received from the condition of the NMS and STS touchdown at STS "spherical equator", and this way is not always rational. To change the contact point position on spherical surface it is reasonable to rotate milling-cutter axis on an angle η in plane of \vec{A} and \vec{R}_2 vectors. Obviously, this will be a rotation around an axis, which is parallel to \vec{V}_M vector. Then well-known equations give us vector coordinates for a new milling-cutter axis:

$$X_{AN} = X_A (\cos\theta + \alpha^2 (1 - \cos\theta)) + Y_A (\gamma \sin\theta + \alpha\beta (1 - \cos\theta)) + Z_A (-\beta \sin\theta + \alpha\gamma (1 - \cos\theta)), \quad (14)$$

$$Y_{AN} = X_A (-\gamma \sin\theta + \alpha\beta (1 - \cos\theta)) + Y_A (\cos\theta + \beta^2 (1 - \cos\theta)) + Z_A (\alpha \sin\theta + \beta\gamma (1 - \cos\theta)), \quad (15)$$

$$Z_{AN} = X_A (\beta \sin\theta + \alpha\gamma (1 - \cos\theta)) + Y_A (-\alpha \sin\theta + \beta\gamma (1 - \cos\theta)) + Z_A (\cos\theta + \gamma^2 (1 - \cos\theta)), \quad (16)$$

where:

$$\theta = \arctg(Z_{2V} / \sqrt{X_{2V}^2 + Y_{2V}^2}), \quad \alpha = \arctg(X_{2V} / \sqrt{X_{2V}^2 + Y_{2V}^2 + Z_{2V}^2}), \quad \beta = \arctg(Y_{2V} / \sqrt{X_{2V}^2 + Y_{2V}^2 + Z_{2V}^2}), \quad (17)$$

$$\gamma = \arctg(Z_{2V} / \sqrt{X_{2V}^2 + Y_{2V}^2 + Z_{2V}^2}).$$

Thus, the equations (5) – (17) give a set of milling-cutter axis vectors. Location of such milling-cutter will always provide the required value of angle ψ .

3. Implementation

A computer program has been developed on the base of the obtained equations (Fig. 2). This program generates a new CNC program. This CNC program contains both trajectory points (STS centers) coordinates and tools axis tilt angles. A part with a convex form and with vertical fibers arrangement is used as an example. The obtained CNC program has been verified by using of Vericut and SIMCO software (Fig. 3).

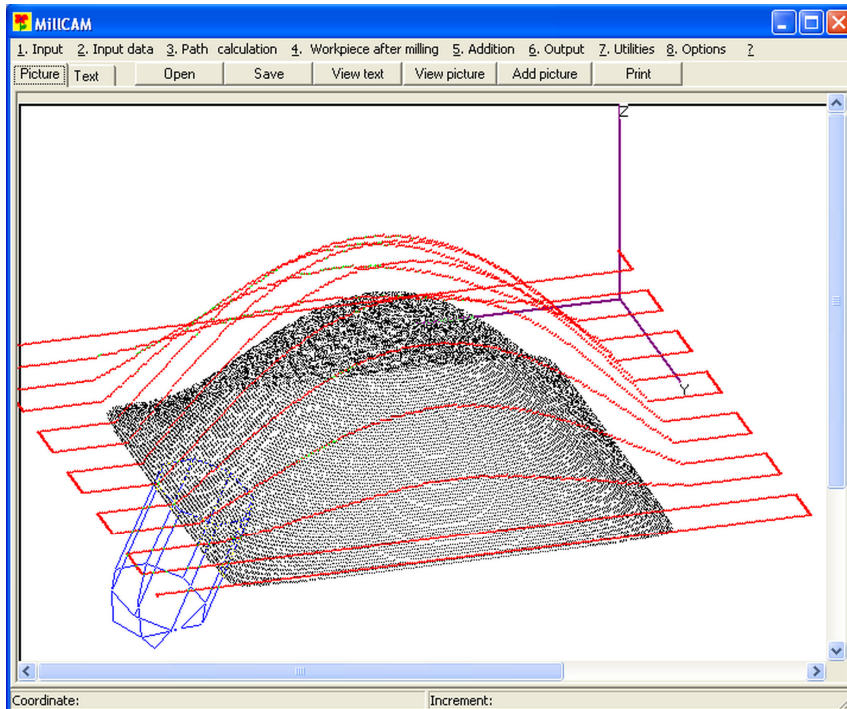


Fig. 2. Author's CAM program for CNC program generation.

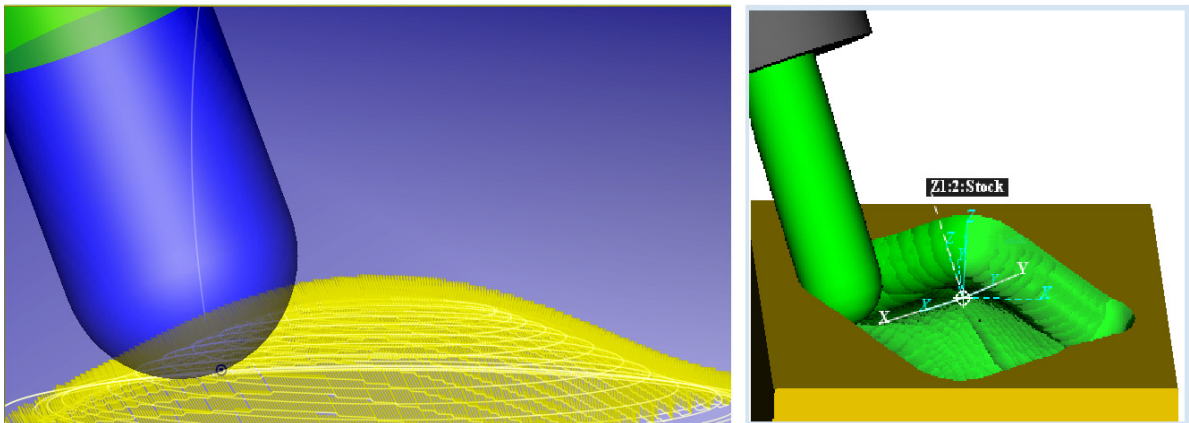


Fig. 3. Obtained trajectory verification with SIMCO and Vericut software.

4. Analysis and discussion

Proposed research suggests that required angles between two vectors: resultant cutting direction and fiber direction do not always exist. In some points (if the normal to NPD coincides with a fiber vector) demanded angle is not achievable, so it has to be equal to 90 degrees. There are zones on a workpiece surface where machining is limited by machine tool technological parameters, which are usually caused by tool axis rotation. It is obvious, that there is a limitation that is caused by collisions between machine components, clamping fixtures, and non-machining parts of workpiece surface.

5. Conclusions

1. Machining of fiber-reinforced composite materials may be limited by increased part surface hairiness and fiber-matrix debonding. Partial hairiness declining may be obtained by using of rational angles between fiber and resultant cutting vectors. This may be performed on 5-axis CNC machine tools.

2. The existing voxel modeling method is the most flexible one for such composite description. This article proposes the method of CNC program development using such voxel approach.

3. Verification of elaborated CNC programs with well-known CAM systems has confirmed the adequacy of the obtained equations and proposed method.

References

- [1] S.A. Singerman, J.J. Jackson, Titanium metal matrix composites for aerospace applications, Superalloys. Proceedings of Eighth Int. Symp. on Superalloys. (1996) 579–586.
- [2] K. Palanikumar, L. Karunamoorthy, R. Karthikeyan, Assessment of factors influencing surface roughness on the machining of glass fiber-reinforced polymer composites, *Materials and Design*. 27 (2006) 862–871.
- [3] A.C. Basheer, U.A. Dabade, S.S. Joshi, V.V. Bhanuprasad, V.M. Gadre, Modeling of surface roughness in precision machining of metal matrix composites using ANN, *J. of Materials Processing Technology*. 197 (2008) 439–444.
- [4] Y. Fujisawa, M. Komori, Method for removing burrs and pits from small gears using a gear-shaped tool composed of glass-fiber-reinforced plastic, *J. of Materials Processing Technology*. 210 (2010) 1159–1170.
- [5] R. Teti, Machining of Composite Materials, *CIRP Annals - Manufacturing Technology*. 51(2) (2002) 611–634.
- [6] R.B. Jerard, J.M. Angleton, R.L. Drysdale, P.Su, The Use of Surface Points Sets for Generation, Simulation, Verification and Automatic Correction of NC Machining Programs, Proceedings of NSF Design and Manufacturing Systems Conf., Tempe, Az, Jan. 8(12) (1990) 143–148.
- [7] S. Hauth, Y. Murtezaoglu, L. Linsen, Extended linked voxel structure for point-to-mesh distance computation and its application to NC collision detection, *Computer-Aided Design*. 41(12) (2009) 896–906.
- [8] W. Zhu, Y.S. Lee, Dixel-based force-torque rendering and volume updating for 5-DOF haptic product prototyping and virtual sculpting, *Computers in Industry*. 55 (2004) 125–145.
- [9] O. Ilushin, G. Elber, D. Halperin, R. Wein, M.-S. Kim, Precise global collision detection in multi-axis NC-machining, *Computer-Aided Design*. 37 (2005) 909–920.
- [10] S.Q. Liu, S.K. Ong, Y.P. Chen, A.Y.C. Nee, Real-time, dynamic level-of-detail management for three-axis NC milling simulation, *Computer-Aided Design*. 38 (2006) 378–391.
- [11] I. Blasquez, J.-F. Poiraudau, Undo facilities for the extended z-buffer in NC machining simulation, *Computers in Industry*. 53 (2004) 193–204.

International Conference on Industrial Engineering

A new file format to describe fiber-reinforced composite workpiece structure for additive technology machines

Shchurova E.I.^{a,*}, Shchurova A.V.^a

^aSouth Ural State University, Lenina, 76, Chelyabinsk, 454080, Russia

Abstract

Additive manufacturing is mostly used to produce homogeneous parts. Soon fiber-reinforced composite materials which let to crowd fibers at the maximal stress locations will be available for additive manufacturing. However, the existing file formats such as STL-format describing the composites on micro-level require incredible data volume. To overcome this problem the authors propose a file format with a description of domains, representative volume elements, and voxels in the first file section. The second section includes the information on the part surfaces. The third one consists of the polynomial coefficients for domains on each part layer. This approach gives a real opportunity to produce FRC parts by additive manufacturing.

© 2015 The Authors. Published by Elsevier Ltd. This is an open access article under the CC BY-NC-ND license (<http://creativecommons.org/licenses/by-nc-nd/4.0/>).

Peer-review under responsibility of the organizing committee of the International Conference on Industrial Engineering (ICIE-2015)

Keywords: Additive technologies, fiber-reinforced composite, file format, domain structure, voxel.

1. Introduction

Additive technologies (AT) have come to stay in modern production. Their advantages are obvious: any forms of parts, including closed interspaces with complex internal structures, are practicable to be produced. Also, such parts can be made in one operation directly from CAD-model that gives high production flexibility and efficiency. The important fact is that every part is not made from given workpiece with its present structure, but this part and its structure can be simultaneously formed on additive manufacturing machine (AMM). Obviously, such advantage may be used in composite material part production. It is well known that modern 3D printers form parts with separate

* Corresponding author. Tel.: +7-351-267-9111; fax: +7-351-267-9111.

E-mail address: shchurova_ei@mail.ru

one-piece areas consisting of different materials [1-3]. Selective laser sintering/melting (SLS/M) [4], electron beam melting (EBM) or laser beam melting (LBM) [5], direct metal deposition (DMD) [6] technologies produce structures from different materials, including particle-reinforced composites. This lets to expect that very soon technological machines and technologies to produce parts with internal structures consisting of various materials with particles located under the special law will come into existence. Obviously, such law has to be determined by the demanded part functionality. Each assembly part has not just to locate an adjoining part (form and size function), but also has to take a specified load from this part without exceeding upper stress and deformation limits. Such composite part design approaches are well known in practice. However, they have limited application and are used only for homogeneous materials or materials with laminate or honeycomb structures [7, 8]. It is obvious that fiber reinforced composites (FRC) with fibers crowded at the locations of the maximal stress offer the greatest reinforcement opportunities. AT that sinter high-strength components in special places afford such opportunities.

However, the problem to design machines for multicomponent materials is not the only difficulty to get over for production of previously described parts. Another difficulty is design of the corresponding software and formats of data files which sizes are acceptable for modern computers. Some specifics of such design are discussed in one of the earlier published works [9]. It describes a model for a part made of 50 various materials for AMM. One of the first articles devoted to computer description of multicomponent structures is the publication by F. Zhu and K.Z. Chen [10]. The authors describe multicomponent parts as structures and substructures. At the top level areas with their specific materials are selected. These areas are divided into subareas with periodic microstructures which further are described using their specific materials and location functions. Such periodic microstructures are also known as representative volume elements (RVE). RVE are often used by applied mechanical specialists to calculate composite structures and are described in previous publications [11 – 13]. Modeling structures presented in these articles are periodic and are absolutely identical with size and shape. Other specific of this approach is the description of each subarea of each area. Obviously, such approach will require an essential volume of information to describe complex composite structures.

Similar discretization approach and following information storage optimization is proposed by J. Vanek, etc. [14]. Authors separate area into subareas and then detect similar ones and unite them to macro areas. Such approach does not only accelerate part production but also gives a way to product parts from segments made of different materials. However, the authors do not discuss opportunities of composite structures micro-level modeling. The same approach with part body separation into subareas of different materials is proposed by S.P. Gurusamy and B. Koc [15].

Another approach is associated with gradient changing of material properties into separate part areas, but these areas and subareas have constant characteristics, too [13, 16, 17]. Such separation is made narrowly and so material changing is realized rather gradually. Obviously, this approach is insufficient to describe fiber reinforced composite at micro-level. One of the mentioned works considers this approach and also file formats for AT [18]. Disadvantages of widely used STL format are marked in this article. The X3D, STEP, PLY, SAT, OBJ formats and other formats applied for AT are discussed there. All of them are not suitable to describe internal part microstructures. AMF file format offered by the author is the peculiarity of this work. This peculiarity is that file structure provides the ordinary area description (for example, by triangles and their vertexes) and also includes equations and voxel structure associations. The file is based on XML format and, therefore, may be used universally for any operating system and AMM. But the solution of the problem to describe composite at the micro level is not proposed in this article, too.

Voxel modeling has increasing application for composites description at micro level. One of the latest works dealing with use of voxel modeling for AT is the article by E.L. Doubrovski, etc. [19]. Authors note that approximately 4000 layers are required to describe a 130 mm high part at 845 dpi resolution. Thickness of each layer has not to exceed the thickness of one voxel. Assuming that the part sizes in two other directions are nearly the same the description of all model requires about 64 billion of voxels. If each voxel should represent whether fiber or matrix particle then voxel association into a XML structure will require to record to the file not only their coordinates and parameters as usual, but also the corresponding keywords. If each coordinate reserves about 6 bytes, and each symbol – 2 bytes, so the specified structure should reserve not less than 100 bytes, and all ASCII format file will require about 10 Terabytes. Obviously, this size is not inappropriate for modern AMM.

The solution of this problem is presented in a lot of publications. Many of them are based on octree voxel models and are often used for computer graphics [20]. There are solutions based on dixel models and etc. All of them are

aimed at file size reduction by association of similar part subareas. The authors of this article have designed the file format to produce composite parts with fiber reinforced non-uniform structures on AMM. Methodological aspects and the main modules of three-dimensional raster and vector editors were worked out for this purpose [21-23].

«Domains» with constant structures and variable sizes which are modeled automatically or semi-automatically in part areas are the main basis of this approach. However, the voxel method used in these works does not allow to reduce the sizes of output files. So the aim of the present article is the development of file formats for the non-uniform fiber-reinforced composite parts description to produce them by AMM.

2. Ground Rules and Assumptions

To develop file formats for AMM consideration should be given to AMM and appropriate processes. Probably, non-uniform RFC parts may be made by selective laser melting (SLM) process. Now some examples of production of regular honeycomb structures with one millimeter sizes are known [24, 25]. Such structure may be represented as matrix with pores. Fibers are located in these pores. In this case delivery system with matrix powder should be placed in one direction and the similar fiber powder system should be placed in perpendicular direction (Fig. 1). Each workpiece layer should be made in two cycles. During the first cycle fiber layer (the first part-layer) should be made in traditional way. Then brush and vacuum cleaner has to remove all particles which are not bounded with top surface layers. During the second cycle matrix powder should be placed at the same layer and bounded between fiber particles. If necessary, pores may be made in desired places by switching off laser beam. Then brush and vacuum cleaner have to remove all not bounded matrix particles too. Pattern of each layer may be constant or variable from layer to layer and this pattern provides fibers curvature. According to this technology and voxel modeling of composite parts laser beam has to be controlled for each voxel. Thus, each voxel corresponds to a powder particle or to beam diameter and its sizes have not to be changed. AMM are equipped with CNC systems like usual CNC machine tools and so similar G-code programs are in use [26, 27]. This program guides a laser beam, which has to move from voxel to voxel and to bind appropriate workpiece places only.

Thus, CNC system has to read out data from file, which should be prepared by 3D graphic editor, and to convert data into G-codes in real time. Obviously, in that case is not necessary to produce large files containing information about each voxel. It is sufficient to apply files with metadata. Then CNC system itself should count movement trajectories of a laser beam from voxel to voxel. Thus, it is offered to use metadata files similar to described above ones [18]. In that case, every file has to contain three sections. In the head section domains, representative volume elements with fibers and matrix and pores which can be spread in composite have to be described. In the second file section part surface has to be described as usual. In the third file section records with information about domain locations have to be used. As domains are larger than RVE and RVE are larger than voxels, metafile size may be much less than ordinary voxel file size. Based on this approach, required format files are described further.

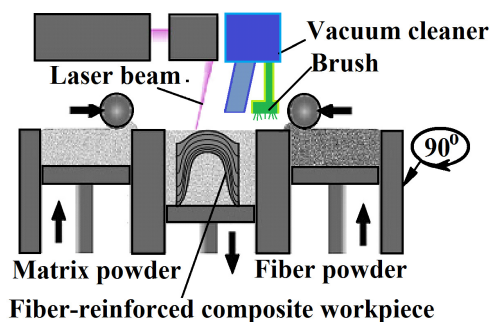


Fig. 1. Additive manufacturing machine for composite parts.

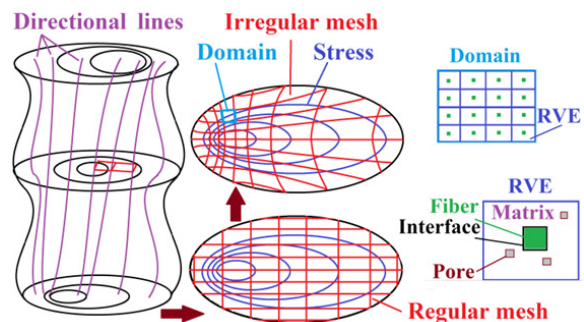


Fig. 2. Part, directional lines, domains and RVE placed between them.

3. Realization

For purposes of AT and AMM it is reasonably to keep voxel sizes constant and equal to the sizes of the powder particle or (more nearly) to the laser beam diameter. Voxel parameter is an integer value and should be equal to the material number (fiber, matrix or pore). In that case, fiber and matrix voxels have to form similar RVE. Quantity of matrix voxels may vary depending on RVE sizes. As fiber sizes are usually constant, so quantity of fiber voxels is constant too (see Fig. 2). Each RVE may have one fiber or several ones as it is described in known programs [11]. Subsequently, RVE have to be assembled in domains – more complex structures. Examples of sections specified above are given in the Table 1 below. Using this file format, domains, RVE and pores should be described first.

Originally directional lines can be specified by a regular constant step mesh and after stress determination in the required planes mesh steps will be defined by relevant functions (see Fig. 2.) It has been suggested to specify such functions like second order polynomial:

$$\sigma = C_0 + C_1X + C_2X^2 + C_3XY + C_4Y^2 + C_5Y .$$

So the file for AMM should have records with z-coordinates and polynomial coefficients. In this case each part layer should be described by such line: **LAYER, SIZE_Z, C0, C1, C2, C3, C4, C5**, where: **SIZE_Z** – is the layer position coordinate; **Ci** – coefficients of the second order polynomial evaluated according to stresses file data for the specified section multiplied by the constant.

Table 1. Descriptions and examples of file sections.

File formats		
<i>DESCRIPTION, Domain, NUM</i>	<i>DESCRIPTION, RVE, NUM</i>	<i>DESCRIPTION, PORES</i>
<i>Begin</i>	<i>Begin</i>	<i>Begin</i>
<i>RVE, NUM_1, NUM_2, ... NUM_9</i>	<i>FIBER, MAT, R_X, R_Y, SIZE_X, SIZE_Y</i>	<i>PORE, NUM_1, SIZE_X1, SIZE_Y1, SIZE_Z1</i>
<i>RVE, NUM_1, NUM_2, ... NUM_9</i>	...	<i>PORE, NUM_2, SIZE_X2, SIZE_Y2, SIZE_Z2</i>
...	<i>FIBER, MAT, R_X, R_Y, SIZE_X, SIZE_Y</i>	...
<i>RVE, NUM_1, NUM_2, ... NUM_9</i>	<i>INTERFACE, MAT, SIZE_TOP, SIZE_BOTTOM, SIZE_LEFT, SIZE_RIGHT</i>	<i>PORE, NUM_9, SIZE_X9, SIZE_Y9, SIZE_Z9</i>
<i>End</i>	<i>MATRIX, MAT</i>	<i>End</i>
	<i>PORE, MAT, NUM, QUAN</i>	
	<i>End</i>	
File examples		
<i>DESCRIPTION, Domain, 1</i>	<i>DESCRIPTION, RVE, 2</i>	<i>DESCRIPTION, PORE</i>
<i>Begin</i>	<i>Begin</i>	<i>Begin</i>
<i>RVE,1,1,1,1,1</i>	<i>FIBER, 1, 0.33, 0.33, 8.0E-6,8.0E-6</i>	<i>PORE, 1, 1.0E-7, 2.0E-7, 6.0E-7</i>
<i>RVE,1,2,2,2,1</i>	<i>FIBER, 1, 0.66, 0.66, 8.0E-6, 8.0E-6</i>	<i>PORE, 2, 2.0E-7, 4.0E-7,8.0E-7</i>
<i>RVE,1,2,2,2,1</i>	<i>INTERFACE, 3, 2.0E-7, 2.0E-7, 2.0E-7, 2.0E-7</i>	<i>End</i>
<i>RVE,1,2,2,2,1</i>	<i>MATRIX, 3</i>	
<i>RVE,1,1,1,1,1</i>	<i>PORE, 1, 2, 10</i>	
<i>End</i>	<i>End</i>	
Domain №1 with 25 RVE of 2 types.	RVE №2 with 2 fibers (material №1) in diagonal position (ratio) with their sizes, their interface material and sizes, matrix №3 and 10 pores with material №1 and sizes of number 2.	Pore descriptions. Sizes №1 and №2 in x and y directions.

4. Conclusions

1. The description of the fiber reinforced composite parts for AMM by description of each particle is not possible because of large file sizes.

2. Such description is possible if the part is separated into domains which consist of RVEs and whereas RVEs consist of voxels which correspond to fibers or matrix powder particles and to pores.

3. Crowding of composite fibers at the locations of the maximal stress may be achieved by the polynomial that is corresponded to such stresses. Each polynomial should be relevant to some part layer. Other layers have to be calculated by interpolation. Such polynomial gives domain key node coordinates and domain sizes. Thus, fiber density depends on the domains and RVE sizes in each part locality.

4. Files for AMM have to include three sections. The first consists of the parameters of domain, RVE and pore descriptions. The second section has to include the same data as usual STL file, i.e. information about part surfaces. The third file section consists of the coefficients of the polynomial describing every domain key node for each part layer.

References

- [1] H.H. Cheung, S.H. Choi, Digital fabrication of multi-material biomedical objects, *Biofabrication*. 1(4) (2009) 1–22.
- [2] R.R. Ma, J.T. Betler, A.M. Dollar, Hybrid Deposition Manufacturing: Design Strategies for Multimaterial Mechanisms Via Three-Dimensional Printing and Material Deposition, *J. of Mechanisms and Robotics*. 7(4) (2015) 1–10.
- [3] J. Hergel, S. Lefebvre, Clean color: Improving multi-filament 3D prints, *Eurographics. Computer Graphics Forum. Strusbourg*. 33(2) (2014) 469–478.
- [4] D. Manfredi, F. Calignano, M. Krishnan, R. Canali, E.P. Ambrosio, S. Biamino, D. Ugues, M. Pavese, P. Fino, Additive Manufacturing of Al Alloys and Aluminium Matrix Composites (AMCs), in W.A. Monteiro (Edr.), *Light Metal Alloys Applications*, InTech, 2014.
- [5] T. Laumer, M. Karg, M. Schmidt, Laser beam melting of multi-material components, *Physics Procedia*. 39 (2012) 518–525.
- [6] D. Novichenko, A. Marants, L. Thivillon, Ph. Bertrand, I. Smurov, Metal Matrix Composite Material by Direct Metal Deposition, *Physics Procedia*. 12 (2011) 296–302.
- [7] L. Lu, A. Sharf, H. Zhao, Y. Wei, Q. Fan, X. Chen, Y. Savoye, C. Tu, D. Cohen-Or, B. Chenly, Build-to-Last: Strength to Weight 3D Printed Objects, *ACM Transactions on Graphics*. 33 (2014) 1–10.
- [8] F. Rissa, J. Schilpa, G. Reinharta, Load-dependent Optimization of Honeycombs for Sandwich Components – New Possibilities by Using Additive Layer Manufacturing, *Physics Procedia*. 56 (2014) 327–335.
- [9] S.H. Choi, H.H. Cheung, A multi-material virtual prototyping system, *Computer-Aided Design*. 37 (2005) 123–136.
- [10] F. Zhu, K.Z. Chen, A CAD modeling system for the components made of multi heterogeneous materials, *IEEE Int. Conf. on Emerging Technologies and Factory Automation Proceedings*. 1 (2003) 559–565.
- [11] T. Belytschko, K. Mish, N. Moes, C. Parimi, Structured Extended Finite Element Methods of Solids Defined by Implicit Surfaces. Report of LLNL, Evanston, 2002.
- [12] J. Segurado, J. Llorca, A numerical approximation to the elastic properties of sphere-reinforced composites, *J. of the Mechanics and Physics of Solids*. 50 (2002) 2107–2121.
- [13] V. Gupta, K.S. Kasana, P. Tandon, Computer Aided Design Modeling for Heterogeneous Objects, *IJCSI Int. J. of Computer Science Issues*. 7-2(5) March (2010) 31–38.
- [14] J. Vanek, J.A. Garcia Galicia, B. Benes, R. Mech, N. Carr, O. Stava, G.S. Miller, PackMerger: A 3D Print Volume Optimizer, *Computer Graphics Forum, The Eurographics Association and John Wiley & Sons Ltd.* (2014) 1–11.
- [15] S.P. Gurusamy, B. Koc, Geometric algorithms for manufacturing of freeform multi-material objects using reconfigurable tools, *Int. J. Manufacturing Technology and Management*. 14(1/2) (2008) 145–173.
- [16] S.H. Choi, H.H. Cheung, A topological hierarchy-based approach to layered manufacturing of functionally graded multi-material objects, *Computers In Industry*. 60(5) (2009) 349–363.
- [17] D.J. Yoo, Heterogeneous Object Modeling Using the Radial Basis Functions, *Int. J. Of Precision Engineering And Manufacturing*. 14(7) (2013) 1133–1140.
- [18] J.D. Hiller, H. Lipson, STL 2.0: A Proposal For A Universal Multi-Material Additive Manufacturing File Format, *Proceeding of the 20th annual Int. Solid freeform fabrication symposium, Austin.* (2009) 266–278.
- [19] E.L. Doubrovski, E.Y. Tsai, D. Dikovskiy, J.M.P. Geraedts, H. Herr, N. Oxman, Voxel-based fabrication through material property mapping: A design method for bitmap printing, *Computer-Aided Design* 60 (2015) 3–13.
- [20] S. Laine T. Karras, Efficient Sparse Voxel Octrees – Analysis, Extensions, and Implementation, *Analysis, NVIDIA Technical Report, NVR-2010-001.* (2010) 1–30.
- [21] E.I. Shchurova, 3D raster graphics based on algebra of sets and voxel modeling, *Scientific works of young researchers of the «Step to the future» program: 11 Russian scientific and engineering exhibition and 14 Russian scientific conference, APFN.* 11 (2008) 60–62.
- [22] E.I. Shchurova, 3D raster editor and voxel approach for computer simulation of the composite structure parts to produce them by additive

- technology, Technological support of machine-building production: Scientific works of the First Int. science and technical teleconference. Russia, Chelyabinsk: SUSU. (2013) 600–606.
- [23] E.I. Shchurova, Raster and vector 3D editor modeling and three-dimensional display presentation of the fiber-reinforced composite parts for their additive technology methods production, in *The automated design in mechanical engineering. The Second Int. Dist. Sci-pr. Conf. Novokuznetsk. 2* (2014) 69–73.
- [24] S. Lohfeld, M.A. Tyndyk, S. Cahill, N. Flaherty, V. Barron, P.E. McHugh, A method to fabricate small features on scaffolds for tissue engineering via selective laser sintering, *J. Biomedical Science and Engineering. 3* (2010) 138–147.
- [25] C. Gao, T. Liu, C. Shuai, S. Peng, Enhancement mechanisms of graphene in nano-58S bioactive glass scaffold: mechanical and biological performance, *Sci. Rep. 4*(4712) (2014) 1–10.
- [26] A.C. Brown, D. de Beer, P. Conradie, Development of a stereolithography (STL) input and computer numerical control (CNC) output algorithm for an entry-level 3-D printer, *South African J. of Industrial Engineering. 25*(2) (2014) 39–47.
- [27] O. Topçu, Y. Taşcıoğlu and H. Ö. Ünver, A Method for Slicing CAD Models in Binary STL Format, *6th Int. Adv. Technologies Symp. (IATS'11)*. (2011) 141–145.



International Conference on Industrial Engineering

On the mechanism of ferromagnetic materials wear reduction

Borisova E.A.^{a*}, Zelinskiy V.V.^a

^a*Murom Institute of Vladimir State University, Orlovskaya Street, Murom, 602264, Russia*

Abstract

The article proposes a hypothesis on the nature of anti-adhesion processing method by the magnetic field of cutting and deformation tools based on the analysis of operating experience and experimental studies of a wide range of tools. The results of the wear process experimental and mathematical modeling in terms of increasing the magnetic impact are presented. It is found that with the increasing number of impulses, the external magnetic field decreases wear and increases the residual magnetic induction of the samples processed by the magnetic field, and the quantification of changes in the intensity of these processes is showed. A new mechanism of influence is proposed of processing magnetic field on the wear, from which is concluded the appearance of an electronic system with a modified energy level that is resistant to the formation of chemical bonds, causing the adhesion.

© 2015 The Authors. Published by Elsevier Ltd. This is an open access article under the CC BY-NC-ND license (<http://creativecommons.org/licenses/by-nc-nd/4.0/>).

Peer-review under responsibility of the organizing committee of the International Conference on Industrial Engineering (ICIE-2015)

Keywords: wear, adhesion, sample, impulse, magnetic field, magnetic induction, wear intensity, energy.

1. Introduction

One of the new physical methods of improving the wear resistance of cutting and deforming tools is processing by the magnetic field (PMF). However, despite the existing effect of the PMF of ferromagnetic materials, the mechanism and factors influencing processing on the wear are still poorly understood. Therefore, the practicability technology of the PMF based on the previously proposed mechanisms [1, 2, 3, 4, 5] does not give a reliable result. This constrains the extended use of this method.

The research conducted by the authors of this article analyzes the operating experience and experimental research on the wear of a large range of instruments based on structural and technological factors. This allows for the

* Corresponding author. Tel.: +7-920-904-5693; fax: +7 (49234) 77-128
E-mail address: Catherine.b2011@yandex.ru

establishment of [6] the prevailing aspect and causes of wear to cutting tools, to identify causal relationships, and the ratio of total tool wear to the causes for their occurrence. It is revealed that the largest proportion of the cause is the adhesive wear, which may be up to 85%. In practice a significant reduction of tool wear processed by the magnetic field was established (up to 3.5 times). In this regard, the hypothesis about the nature of the anti adhesion effect of this method is given.

The purpose of this work is an experimental and mathematical modeling of the processing of wear in the tribosystem of the tool material - processed material under increasing external magnetic impact.

2. Assessment of influence of the magnetic field on the wear

In the experiments, we used a modernized friction machine such as MI, which provides the testing scheme friction through a "roller-sample". The samples were rectangular prisms of high speed steel R6M5 and alloy steel CVM, hardened by appropriate technologies. A separate roller from steel 45, hardened to a hardness of 44-46 HRC served as the counterbody for each sample. The wear of the samples was evaluated by the weight loss shall be determined by weighing them on laboratory analytical scales. The level of the experimental load for all samples was 300 N.

The samples were exposed to the external magnetic field with of the different the numbers of pulses from 1 to 7, with a pulse duration of 2 seconds caused by setting the tenseness of the magnetic field of 400 kA/m with an adjustable pulse duration. One sample of each steel was not magnetized. They were the control samples.

Diagrams of the dependence of the amount of wear on the samples on the number of pulses of the external magnetic field are presented (Fig. 1). In these graphs, a steady decrease in the amount of wear by increasing the number of pulses of the magnetic effects of the gradual weakening of its influence can be traced, presumably due to the magnetic saturation of the samples/ material.

Moreover, for steel CVM multiplicity, the reduction the amount of wear of most of the magnetized sample compared to the control sample was 2.9 - 3.6; R6M5 steel multiplicity of the reduction of the value lies in the range 2.42 - 2.66.

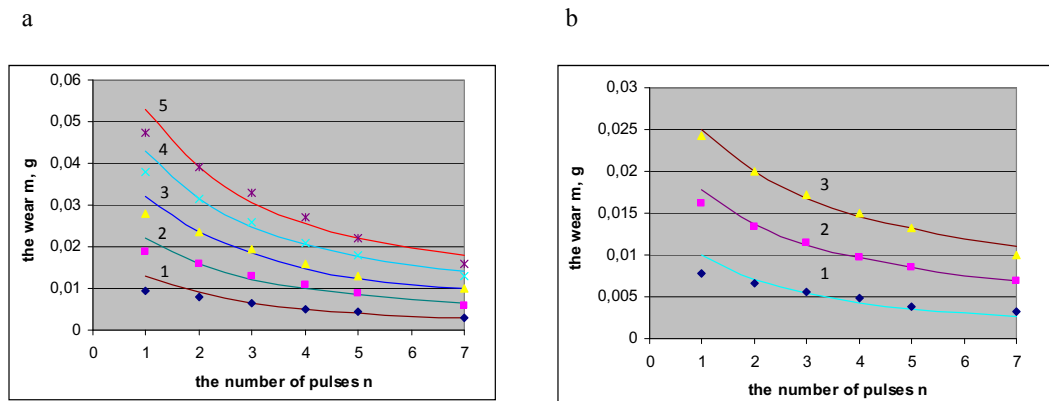


Fig. 1. The dependence of wear amount m from the number of pulses of the magnetic influence n and duration of the friction t ;
 (a) – steel CVM (1 – $t = 30$ min, 2 – $t = 60$ min, 3 – $t = 90$ min, 4 – $t = 120$ min, 5 – $t = 150$ min),
 (b) – steel R6M5 (1 – $t = 60$ min, 2 – $t = 120$ min, 3 – $t = 180$ min).

One of the approaches to the assessment of wear is an approach based on the Archard equation wear of resulting from the mathematical modeling of adhesive wear [7].

$$dW = K_a \frac{qV}{H} dA, \quad (1)$$

where W – is a volumetric wear; K_a – is a dimensionless coefficient of adhesion; q – is a contact pressure; V – is a

sliding velocity; H – is a hardness of the material; A – is an area of friction contact.

From the experimental conditions adopted, this equation of wear takes the form [8, 9]

$$m = K_a \gamma A V \frac{q}{H} t, \quad (2)$$

where γ – is a density of the material of the wear particles, t – is a duration of the friction.

The analysis of the equation shows that at constant values of γ , A , V , q , and H (realized in experiments with the same duration of friction), the value of weight wear is determined only by the coefficient of adhesion K_a .

3. Assessment of influence of magnetic field on the residual magnetic induction

For this reason, we assume that the magnetization gives some new properties to the samples, which influence the adhesive interaction of the modified samples with a counterbody. Consequently, the coefficient of adhesion K_a in the equation of wear is the most powerful internal factor of wear processing.

In the development of the hypothesis about giving new properties by magnetizing samples, experiments were conducted to determine the dependence of the residual magnetization from the impact of the number of pulses by an external field. For this purpose, 3 samples of steel subjected to magnetization modes with the number of pulses of 3, 6, 9 and 15 with the same duration of exposure to the magnetic field of 2 seconds were examined. The magnetic induction B of the residual magnetic field at the surface of the magnetized samples was measured by the magnetometer. These surfaces in the following experiments were friction surfaces.

From the measurement results presented in Figure 2 it follows that with increasing the number of pulses of an external magnetic field, the level of residual magnetic induction (and therefore, the tensions of the residual magnetic field) on the friction surface of the samples increased steadily with some weakening at large quantities of pulses.

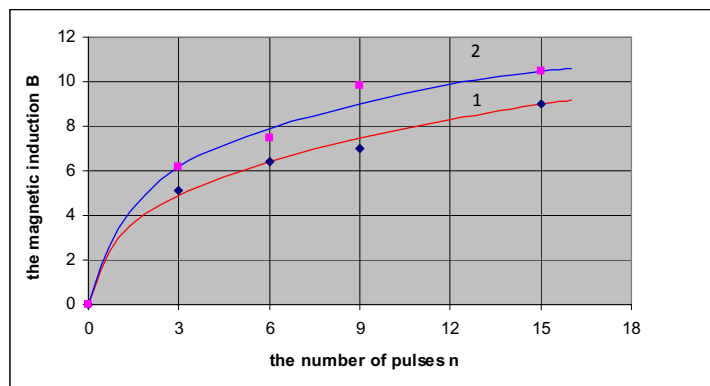


Fig. 2. The dependence of residual magnetic induction of friction surfaces of samples from the number of pulses of external magnetic field (1 – is a sample from steel R6M5; 2 – is a sample from steel CVM; $n = 0$ – without PMF)

4. Assessment of the influence of residual magnetic induction by an amount of wear

From a comparison of the experimental dependences of wear (Figure 1) and the residual magnetic induction (Figure 2) from the number of pulses n , it can be seen that while in the process of pumping the samples' material by the energy of the magnetic field, two processes take place simultaneously the residual magnetic induction increases and decrease the wear decreases amount.

We think that the growth process of the residual magnetic induction in the interaction of the friction surfaces leads and initiates the reduction rate of wear. In this case, the degree of conditionality of the second process

(reducing the rate of wear), by the first (increasing residual magnetic induction) is important.

The computer processing of the experimental results allowed both processes to be represented as functions of the same variable, rather accurately reproducing the experimental dependence (divergence less than 10%).

$$B = An^{0.35}, \tag{3}$$

$$m = Cn^{-0.67}, \tag{4}$$

where A, C – are the constant coefficients.

Comparison of functions (3) and (4) in the exponent of the variable values (differing by almost 2 times) shows a lack of full conditionality of reducing the rate of wear by the process of increasing residual magnetic induction. It can be seen that in the process of pumping the samples by the magnetic energy, the rate of reducing wear exceeds the growth rate of the residual magnetic induction.

A quantitative estimate of the difference in the rates of passage of both processes as a function of the number of pulses of the magnetization can be done by comparing the absolute values of the current intensities changes of the residual magnetic induction J_1 and reducing the rate of wear J_2 of the processes considered, presented in the form

$$J_1 = \frac{\Delta B}{\Delta n}, J_2 = \frac{\Delta m}{\Delta n}, \tag{5}$$

where $\Delta B, \Delta m, \Delta n$ - are the absolute values of the current changes of the magnetic induction and the wear amount at the corresponding value of change of the number of pulses.

The results of comparing J_1 and J_2 , shown in Fig. 3, illustrate that the intensity of wear reduction is more than the intensity of increasing the residual magnetic induction throughout the range of increasing the number of pulses. The intensity reduction of wear is always higher than the intensity of accumulation of magnetic induction by 1.5-2 times (Fig. 4).

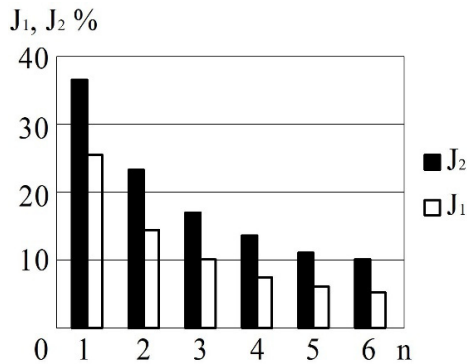


Fig. 3. Changes in the current intensities of wear reduction m and increases in magnetic induction B

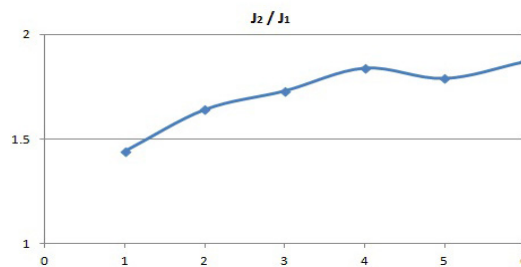


Fig. 4. The ratio of current intensities of wear reduction m and increases in magnetic induction B

5. Discussion of the research results

From the above, it follows that the material of the pump energy to the wear process affects not only the magnetization factor, but also affects additional factor which is anti-adhesive in nature and in its manifestation also expands the part of the pumped energy. Moreover, the accumulation of magnetic induction in the material is a contributing and necessary process.

Thus, in principle it is possible to use the following mechanism of influence PMF on the wear. The external magnetic field in the ferromagnetic material orients the domains in a direction that create magnetization of the solid material. In accordance with the theory of quantum-mechanical structure of the atom, the external magnetic field changes the energy state of the molecular orbitals of the interacting crystal lattices. When the magnetic field is removed, the residual magnetization, together with part of the energy of the friction phenomena, supports energy changes. This electronic system is more resistant to the formation of chemical bonds, causing the adhesion. Reduced activity of adhesion processes helps reduce the amount of wear.

The proposed mechanism corresponds to the quantitative assessment (85%) of causes of tool wear in practice and on this basis a hypothesis is put forward about the anti-adhesive nature of the influence of the magnetic impact on the wear resistance of tools.

Conclusion

- The studied steels are predisposed to increased wear resistance by the using the PMF, and the multiplicity of reducing wear amounted for steel CVM from 2.9 to 3.6, for steel R6M5 - from 2.42 to 2.66.
- It has been established experimentally that in reducing the wear, the anti-adhesive factor plays a leading role and the role of the magnetization is secondary.
- A new mechanism of reducing wear as a result of PMF was proposed and one of the leading factors of influence was found to be the number of pulses of the magnetic field. The optimal values for impact (6 ... 7) were installed.

References

- [1] F.P. Bowden, D. Tabor, *The Friction and Lubrication of Solids*, Oxford University Press, Clarendon Press, second corrected ed., Oxford classic text in the physical sciences edition, 1986.
- [2] D. Tabor, Friction as a dissipative process, *Proc. Fundamentals of friction: macroscopic and microscopic processes*. Dordrecht – Boston – London, NATO ASI Series E: Applied sciences, Kluwer Academic Publisher. 220 (1992) 3–24.
- [3] D.P. Markov, A.D. Kelly, Establishment of a new class of wear: adhesion initiated catastrophic wear, *International journal of applied mechanics and engineering*. 7(3) (2002) 887–901.
- [4] H.M. Pollock, Surface forces and adhesion, *Proc. Fundamentals of friction: macroscopic and microscopic processes*. Dordrecht – Boston – London, NATO ASI Series E: Applied sciences. Kluwer Academic Publisher, 1992.
- [5] E. Rabinowicz, *Friction and Wear of Materials*, Wiley, 1995.
- [6] El.M. Mansori, K. Lafdy, D. Palmer, Enhanced wear resistance and tools durability using magnetization, *Metal Cutting and High Speed Machining*. Kluwer Academic. Plenum Publishers. (2002) 301–310.
- [7] J.F. Archard, Contact and rubbing of flat surfaces, *Journal of applied physics*. 24 (1953) 981–988.
- [8] M.K. Mohamed, Effect of Magnetic Field on The Friction and Wear Displayed by The Scratch of Oil Lubricated Steel, *International Journal of Engineering & Technology IJET-IJENS*. 12(6) (2012).
- [9] F.J. Giessibl, M. Herz, J. Manhart, Friction traced to the single atom, *PNAS*. 99(19) (2002) 12006–12010.



International Conference on Industrial Engineering

Determining the effective conditions for machining fabrication procedures based on the cutting process energy patterns

Karpov A.V.^{a*}

^a*Murom Institute of Vladimir State University, Orlovskaya Street, Murom, 602264, Russia*

Abstract

The article is devoted to the rational consumption of energy resources during the metal-cutting tools processing blanks of machine component parts in machine-building production. A scientific and methodological approach to the establishment of energy-efficient processing conditions is proposed, being based on the optimization of fabrication procedures according to new energy efficiency criterion. A study of advantages and disadvantages of known methods of fabrication procedures optimization according to the criterion of the lowest specific energy intensity has been conducted. A new integral indicator of energy efficiency of cutting operation is defined as a ratio of constructional material specific energy intensity to the specific energy consumption in the cutting area. The methods of determining the energy efficiency figure with respect to the properties of the processed material, the behaviors of its deformation and fracture, type of formed chippings and technological purpose of processing are offered. The optimization of machining fabrication procedures with the new criterion in place permits the 18-22% reduction of energy costs in the cutting area in comparison to the applied processing conditions.

© 2015 The Authors. Published by Elsevier Ltd. This is an open access article under the CC BY-NC-ND license (<http://creativecommons.org/licenses/by-nc-nd/4.0/>).

Peer-review under responsibility of the organizing committee of the International Conference on Industrial Engineering (ICIE-2015)

Keywords: Machining fabrication procedures, cutting system, optimization of fabrication procedures, energy intensity, energy efficiency, optimal cutting conditions

1. Introduction

In comparison with other industries mechanical engineering is characterized by high materials consumption and energy intensity of products. The proportion of the energy component in the costs of engineering products that were manufactured previously in the Soviet Union, did not exceed 5-7 per cent, and in the last decades in Russia and some Eastern European countries the one has increased up to 20-25 per cent with the trend to further increase. The

* Corresponding author. Tel.: +7-492-347-7125; fax: +7-492-347-7128.
E-mail address: krash75@mail.ru

significant part of the manufacturing stage of machine-building productions the machining fabrication procedures occupy - they have 60-70 percent of the total labor intensity of manufacturing of machine parts. Formation of one ton of chippings is accompanied by average consumption of 450-600 kW·h of electricity, and according to this indicator the products of Russian enterprises is 1.5-2.5 times more expensive than similar products of Largest Economies of Western Europe. In Germany, Sweden, France, at the stage of development and certification of fabrication procedures, along with the criterion of the lowest costs, already a lot of decades such criteria as specific energy intensity and metal removal per power unit are applied [5, 9]. Thus, increase of machining of fabrication procedures by optimization of the energy costs to implement them is relevant task for the machine-building complex of Russia and number of European countries. However, up to now the unified methodology that permits to carry out such optimization in terms of operating production is not built up.

2. Purpose of Research

To create scientific and methodological approach to defining such conditions of machining fabrication procedures under which the required quality degree of the produced surfaces, cutting tool durability and the performance will be ensured due to sufficient (minimum required) amount of power consumption.

3. Results and Discussion

We think that the complex task of increase of the energy efficiency of machining fabrication procedures shall be resolved on the basis of three trends:

- reduction of energy consumption in the cutting area by means of both determining and applying of economic conditions of execution of each manufacturing operation, manufacturing step and tool travel;
- reduction of power wastes in the mechanical part of a drive of metal-cutting machinery;
- reduction of power wastes in the electrics of a drive of metal-cutting machinery.

The first trend is subject matter of this article, because in particular this work that is performed by the cutting tool in the cutting area, and determined by the rules of chip production, sets ultimately, the total amount of energy, consumed by the motor of the machine tool station from the mains [4].

The intensity of the cut work depends primarily on the type and physic-mechanical properties of process material. However, the constructional material is usually given by drawing of part, in consequence of which the one is uncontrollable factor as for cutting system.

Except for type and properties of process material, the following factors have an effect on intensity of cutting work: the state of the surface layer of the blank, the thickness and width of the shear layer, the type and properties of tool material, geometrical parameters of active part of cutting tool, cutting conditions, characteristics of lubricating processing means and other conditions of execution and parameters of the cutting operation, which together form the group of controllable factors of cutting system. Effective values of controllable factors of any system, including cutting system, shall be determined on the basis of on optimization techniques [7, 8, 13].

Specific energy intensity of the cutting process (valid synonyms - "specific cutting work," "specific energy consumption of cutting", "density of the cutting work") numerically characterizes the quantity of energy, expended by the cutting tool to separate as chippings the unit volume of the sheared off layer of blank (preliminary ("rough") stages of processing), or to form area unit of new surface of part (final ("finishing") stages of processing) [13, 15].

Specific power consumption is, in fact, universal physical efficiency factor of the cutting operation. The less value of the specific energy intensity when maintaining the desired processing results (performance, tool life, processed surface quality) is, the more effective the values of controllable factors cutting systems are. The advantages of the specific energy intensity of the cutting operation include simplicity of its definition by means of both theoretical and experimental methods.

We will give a number of disadvantages that we found at time of approbation of methods of fabrication procedures optimization in accordance with criterion of the least specific energy intensity.

Firstly, the specific energy intensity is dimensional indicator and the one does not permit to determine what part of the energy is spent directly on the deformation and (or) the destruction of unit volume of the sheared off layer, or formation of unit area of new surface, and some portion of energy is spent on the mechanical and physic-chemical processes that inevitably accompany the chip formation.

Secondly, using the factor of the specific energy intensity, it is difficult to compare the level of energy, developed in the cutting area, with the marginal energy state of constructional material that is determined by rules of its deformation and damage.

Thirdly, the manipulation with specific energy intensity, represented by the ratio of cutting work to the volume of the sheared layer, assumes isotropy of material per cross-section of chippings (the outer layer of the chippings is "equaled" in the properties with near-cutter one) [11]. So, in the most energy-consuming small-scale production when the blanks with considerable allowances and lapping (rolled metal, castings, forged forgings, welded constructions) are used, the specific energy intensity of individual operating stroke shall be determined by the following ratio [6]:

$$e = \frac{A}{V} = \frac{N}{V_0}, \quad (1)$$

where A – is a cutting work; V – is a volume of the material, separated in the form of chippings; N – is a cutting power (work of cutting per unit time); V_0 – is a productivity (volume of chippings, separated per unit time).

The fourth, the specific energy intensity is proportional one to the cutting power, at that the power is assumed to be constant during the entire time of operating stroke that is true only for stationary cutting and it occurs rarely [10].

Taking into account presented comments as an integral characteristic of the effectiveness of machining, we propose the dimensionless factor K - "Energy Efficiency of the cutting operation" [4, 8]

$$K = \frac{\Delta w \cdot V}{n_c \cdot A_c} = \frac{\Delta w \cdot V}{n_c \cdot \int_0^{\tau_c} N(\tau) d\tau}, \quad (2)$$

where Δw – is a specific energy intensity of processed material; V – is a volume of processed material that was exposed; n_c – is a number of cycles of cutting power changes $N(\tau)$ during the tool travel; A_c – is a cutting work for time τ_c of one cycle of power change.

Applied in machine building the methods of blanks processing with metal-cutting tools it is possible to divide into 4 groups, depending on the pattern of change of cutting power during the time of tool travel:

pattern 1 - steady mode (power is constant);

pattern 2 - power increases monotonically up to the maximum value and then the one decreases rapidly;

pattern 3 - power increases intensively up to the maximum value and then the one decreases monotonically;

pattern 4 - power changes according to parabolic law.

Under duration of one cycle of change τ_c of cutting power, we mean either full-time of tool travel during steady mode (pattern 1), or period of time during which there is complete single change of cutting power during non-steady behavior (patterns 2-4). On the basis of the proposed schemes of change of power, the expressions of the cutting power A_c that is carried out by machining tool during τ_c time that made possible to calculate factor K and thereby quantify the energy efficiency of different methods of machining.

Specific energy intensity of process able material Δw , we will interpret as a critical excess of internal energy of unit volume of the material, i.e. as the difference between the limit $[u]$ level and initial u_0 one of volumetric density of the internal energy

$$\Delta w = [u] - u_0. \quad (3)$$

As basis of determination of the value of $[u]$ for wide range of constructional materials, we put energy concept of destruction: the volume of the material is destroyed, if the accumulated in it energy has reached the limit value as a result of external influence. The body is considered as destroyed one if at least one of its local volumes of the internal energy density has increased up to critical value $[u]$.

Critical delta of internal energy can be determined from different points, such as with usage of indicators of thermo physical properties of the material [3, 14]:

$$\Delta w = [u] - u_0 = \int_{T_0}^{T_s} (C_p \cdot \rho) dT \approx C_p \cdot \rho \cdot (T_s - T_0), \quad (4)$$

where C_p - average specific heat capacity of the material; ρ - density; T_s - melting point; T_0 - initial temperature. Calculation of the specific energy intensity of material Δw through thermo physical properties we recommend to use for grinding [12], as well as at time of final (finishing) edge cutting machining, accompanied by the formation of continuous chip and occurrence of area of plastic contact of chippings with cutter face (cutting of blanks of low-carbon steel or nonferrous wrought alloy, the thickness of sheared layer is 0.1-0.5 mm, cutting velocity is 300 m/min or more).

Interpretation and definition of value Δw during preliminary edge cutting machining we offer to carry out depending on the type of produced chippings, since the type of chippings is stipulated by the mechanism and intensity of deformation of the material of the sheared layer. When cutting materials with formation of shearing chip we assume Δw that will equal to maximum density of work of tangential stresses in the conventional shear area. So, during semi finishing work of carbon and alloy-treated steel the value Δw can be calculated as the work of tangential stresses in the conventional shear area, if we take the value of relative shear $\varepsilon = 2.5$:

$$\Delta w = \tau \cdot \varepsilon = \frac{1.5 \cdot \sigma}{1 - 1.7 \cdot \psi}, \quad (5)$$

where $\tau = \frac{0.6 \cdot \sigma}{1 - 1.7 \cdot \psi}$ - is the resistance of the processed material against flow shear; ψ - uniform relative necking of material.

The proposed figure of energy efficiency of the cutting operation K meets requirements, maintained as to the criteria of fabrication procedures optimization. Firstly, this figure represents the "Energy Efficiency" of the cutting operation and, consequently, the one has the physical meaning. Secondly, it is simply and unambiguously described in mathematical form. Third, the one can be reduced to the objective function of $K \rightarrow \max$ pattern, the arguments of which are the controllable factors of cutting system.

Thus, the optimization of machining fabrication procedures per $K \rightarrow \max$ criterion permits to determine the energy-saving values, driven by factors of cutting operation.

In terms of K figure it is possible to compare the effectiveness of alternative methods of surface treatment, design the optimal structure of fabrication procedure of manufacturing of part. With respect to the individual manufacturing step or operating stroke it is possible to assign the brand of tool material, the values of the geometric parameters of active part of cutting tool, cutting depth, feed velocity, cutting velocity, and other conditions, related to the highest value of K .

Algorithm of optimization per criterion of the highest energy efficiency of the cutting operation was implemented by us in the form of software package in Delphi environment, when used in respect of lathe turning, drilling, milling of blanks made of carbon and alloy-treated steels, gray and ductile iron.

4. Conclusion

Fulfillment of $K \rightarrow \max$ condition at the preliminary stages of processing corresponds to such values of the geometric parameters of active part of cutting tool and cutting parameters under which due to minimum required energy costs, it is possible to provide required performance and durability of machining tool.

Fulfillment of $K \rightarrow \max$ condition at the finishing stages of processing corresponds to such values of the geometric parameters of active part of cutting tool and cutting parameters under which due to minimum required energy costs, it is possible to provide required quality rating of machined surface of part.

Power consumption reducing in the cutting area at time of switch to the optimal cutting conditions runs to 18-22% in comparison with used at present time technological conditions of specified processing techniques.

References

- [1] A.V. Karpov, The Definition of Structural Engineering Materials Cutability on the Basis Of The Chip Formation Energy Patterns, *Modern Problems of Science and Education*. 3 (2014). URL: <http://www.science-education.ru/117-13311>.
- [2] A.V. Karpov, To the Question Of Decrease In Power Consumption of Technological Processes of Materials Cutting, *Modern Problems of Science and Education*. 2 (2013). URL: <http://www.science-education.ru/108-8697>.
- [3] B.F. Turkovich, Calvos, Some Applications Of Physical Metallurgy In Metal Cutting, *Advances Maching Toll Design And Resistans*. 2 (1968) 1051–1071.
- [4] E.M. Trent, P.K. Wright, *Metall Cutting*, fourth ed., Butterworth-Heinemann, Boston, 2000.
- [5] F. Maitre, Relations Entre Eneries De Coupe Et Endommagement Des Outils, *Wear*. 1(62) (1980) 139–160.
- [6] J.T. Black, On the Fundamental Mechanism of Large Strain Plastic Deformation. *Electron Microscopy Of Metal Cutting Chips*, ASME, 1970.
- [7] K. Iwata, Y. Murotsu, F. Oba, Optimization Of Cutting Condition For MultiPass Operations Considering Probabilistic Natur In Machining Processes, *Transection ASME*. 1 (1977) 152–159.
- [8] K. Iwata, Y. Murotsu, T. Iwatsubo, S. Fujii, A Probabilistic Approach To The Determination Of The Optimum Cutting Conditions, *Transection ASME*. 4 (1972) 137–146.
- [9] *Manufacturing Technology*, *Annals of CIRP*, Elsevier. 51(1) (2007).
- [10] S. Ramalingam, B. Thomann, K. Basu, J. Hazra, The Role Of Sulphide Type And Of Refractory Inclusions In The Machinability Of Free Cutting Steels, Influence Of Metallurgy On Machinability, *American Society For Metals*. 1 (1975) 111–129.
- [11] U. Kunio, K. Yuichi, Identification of Chip Formation Mechanism through Acoustic Emission Measurement, *Annals of the CIRP*. 1 (1984) 71–74.
- [12] V.A. Yashkov, L.V. Silin, Internal Grinding Without Thermal Effects, *Russian Engineering Research*. 32 (2012) 601–603.
- [13] V.K. Starkov, *Physics And Optimization Of Cutting Of Materials*, Mashinostroenie, Moscow, 2009.
- [14] V.S. Ivanova, *The Destruction of Metals*, Metallurgia, Moscow, 1979.
- [15] W. Pegner, H. Lutze, E. Smejkal, *Spanende Formung. Theorie Berechnung Richtwerte*, Veb Verlag Technik, Berlin, 1989.



International Conference on Industrial Engineering

Automatic cycles multiparametric optimization of internal grinding

Pereverzev P.P.^a, Akintseva A.V.^b *

^aSouth Ural State University, 76, Lenin Avenue, Chelyabinsk, 454080, Russian Federation

^bKyshtym Branch, South Ural State University, Respublk Street 10, Kyshtym, 456870, Russian Federation

Abstract

An important and intractable problem of domestic engineering industry is the low productivity of operations performed on CNC machines. The reason for this is the absence of standards and methodologies for the design of optimal cycles for CNC machines. As a result, in practice, one has to manually choose processing modes which presents no solution to the problem of low productivity, as this method generates losses, particularly in relation to automated production intra grinding processing on CNC machines in series production.

To solve this problem the research, primarily, proposes a methodology for the design of optimal multivariable stepwise cycles internal grinding processing, allowing to calculate as follows: optimal values of the radial flow at all stages of the cycle; the optimum value of the axial feed at all stages of the cycle; optimal allocation deduct allowance on the steps of the cycle for radial and axial feeds, which provide the minimum cycle time, given the technological constraints of the objective function.

As a mathematical method of optimization of grinding cycles, applied dynamic programming method (DPM) is used. The application of the DPM is permissible due to the fact that this method does not require constructing an a priori bounds of the permissible restrictions and is not sensitive to the properties of management models and constraints. The optimality criterion is adopted, the minimum cycle time of grinding. The optimality criterion is adopted being the minimum cycle time of grinding. The use of DPM allows taking into account any number of technological limitations of the objective function (limitations on the accuracy and other quality indicators; performance properties of a circle; design parameters of the machine).

The designed internal grinding cycles of processing are multi-dimensional and reflect the dependence interdependence speed axial flow, radial flow and amount of removed stock. The method of optimization cycles allows expanding the number of optimized parameters and performing multivariable optimization in multidimensional space, which makes it use CAD to create engineering standards for cutting data for internal grinding operations that meet the requirements of modern production.

© 2015 The Authors. Published by Elsevier Ltd. This is an open access article under the CC BY-NC-ND license (<http://creativecommons.org/licenses/by-nc-nd/4.0/>).

Peer-review under responsibility of the organizing committee of the International Conference on Industrial Engineering (ICIE-2015)

Keywords: internal grinding; process optimization; cutting parameters, automatic cycles, CNC machines;

* Corresponding author. Tel.: +8-922-633-56-57;
E-mail address: akintseva_av@mail.ru

1. Introduction

One of the leading trends of modern machinery is equipment with the latest CNC machines, enabling processing at higher speeds by set cycles [1-3]. Design cycles on modern machines continue to be made on the basis of data taken from reference literature 60, 70, 80-ies. This literature was developed for universal machines based on static data from that period and was intended mainly for the valuation of transactions. The use of software and technical support of modern equipment «outdated» data on the cutting conditions and the structure of the cycle leads to its inefficient use. The practice of using in the production of modern CNC machines shows that their performance is used only by 40-60% and often the performance is lower than on universal machine tools especially for small batches of parts. In an effort to increase the productivity of modern machine tools, enterprises are forced to carry out the selection of cutting parameters by processing of several test pieces with gradual increase of intensity of processing. This method is not cost-effective for the most common at the moment, the type of production – serial. All of the above fully applies to the operations of grinding internal cylindrical surfaces on modern CNC machines.

The currently known computational techniques design cycles [4-10] have one common drawback – they do not use mathematical optimization techniques. The result using these methods, cycles is rational, if not optimal, which in turn leads again to an inefficient use of productive resources: equipment, tools, etc. It should also be noted that in the above-mentioned methods is missing one of the most important models of the performance limitations of the model the accuracy of the treatment, i.e. the methodology of design cycles do not guarantee the accuracy of machined surfaces. Thus, poor performance of internal grinding operations due to the lack of standards and techniques for design of control programs for CNC machine tools is a pressing concern within the engineering industry.

Nomenclature

V_{Soc}	axis feed rate, mm/min
S_{pad}	radial flow, mm/dv.course
II	allowance, mm
n	the number of radial flow
m	the number of the discrete unit allowance
b	the number of speed axial flow
z	number of stages of the cycle

2. Methods of optimizing internal grinding cycles

In the 90-ies in the Chelyabinsk school grinding under the guidance of S. N. Korchak developed theory and methods of calculation of optimal cycles machining on cylindrical grinding machines [11-13]. In this work, we first applied a mathematical optimization method – the method of dynamic programming (MDP) [14], which found their application in works of many scientists [15, 16]. The application of the MDP due to the fact that this method does not require constructing an a priori bounds of the permissible restrictions and is not sensitive to the properties (differentiability and continuity) management models and constraints. The optimality criterion is adopted, the minimum cycle time of grinding, as it is a variable part of the costs, depending on the processing modes. The determination of the minimum cycle time in the process of optimization of the grinding cycle is performed with the mandatory accounting major technological constraints: quality and precision, operational characteristics, circle, design parameters of the machine, etc. Projected processing cycles for the operations round mortise grinding are two-dimensional and reflect the dependence of the radial velocity measurement of flow removed from the value of the allowance.

By its structure and the complexity of the control loops internal grinding processing are more complex compared to the above-mentioned outer infeed grinding as it takes control not only radial flow, but the axial velocity. Additionally, require management and other processing parameters that have a significant impact on the process itself: the diameter and height of the circle, the speed of rotation of the work piece, the characteristic of a circle, radius grinding mandrel, overrun, and many others. As a consequence, application of the technique of optimization

cycles of the external plunge grinding process cannot directly be used to design internal grinding cycles. Therefore, it is necessary to develop a new methodology for the design of optimal cycle's internal grinding treatment that balances all of the above control parameters. The underlying basis of the new methodology is the development of the dynamic programming method for the multidimensional space of control parameters.

Optimization of operating conditions is made in mesh radial flow (S_{rad} , mm/dv.course) – axis feed rate (V_{Soc} mm/min) – allowance (Π_M , mm). A graphical representation of the relationship of the listed operating parameters shown in Fig. 1. To facilitate understanding of the methodology for the design of optimal cycles internal grinding processing, the number of the units operating parameters reduced to the lowest possible value. MDP requires discretization of the governing parameters, as it relates to the methods of discrete optimization. We shall divide the scale of the radial flow on the $N-1$ pixels, where N is the number of radial feed of the machine) in the range from minimum to maximum radial feed. The scale of allowance will be divided into $M-1$ (M is the maximum number of discrete allowance at which the magnitude of the remaining portion of the allowance is equal to zero) in the range from the maximum value of the allowance to zero. The third coordinate axis (axis feed rate) divide $B-1$ discret (B – number of speeds axial feeds on the passport of the machine) in the range from minimum to maximum speed axial flow of the circle. For the purpose of fulfilling the constraints of the objective function by the number of valid steps of the cycle the state of the process introduces an additional z coordinate – number of stages of the cycle. That is, the process state will be characterized on the grid coordinates $[m, n, b, z]$, which will henceforth be called the state coordinates of the grinding process. At each intersection of the grid placed «information cell» containing the following data: the optimal (minimal) time to reach the state, the current size of the surface finish, cutting forces, etc. The determination of the minimum time attaining the state is determined by means of brute-force options switch (changes) of filing within a projected cycle of competitive moves (Fig. 1). The number of competitive moves depends on the following factors: the rate of axial flow and radial flow are switched simultaneously or not simultaneously in the z -th level; the number of suitable feeds the discrete unit with its allowance, etc.

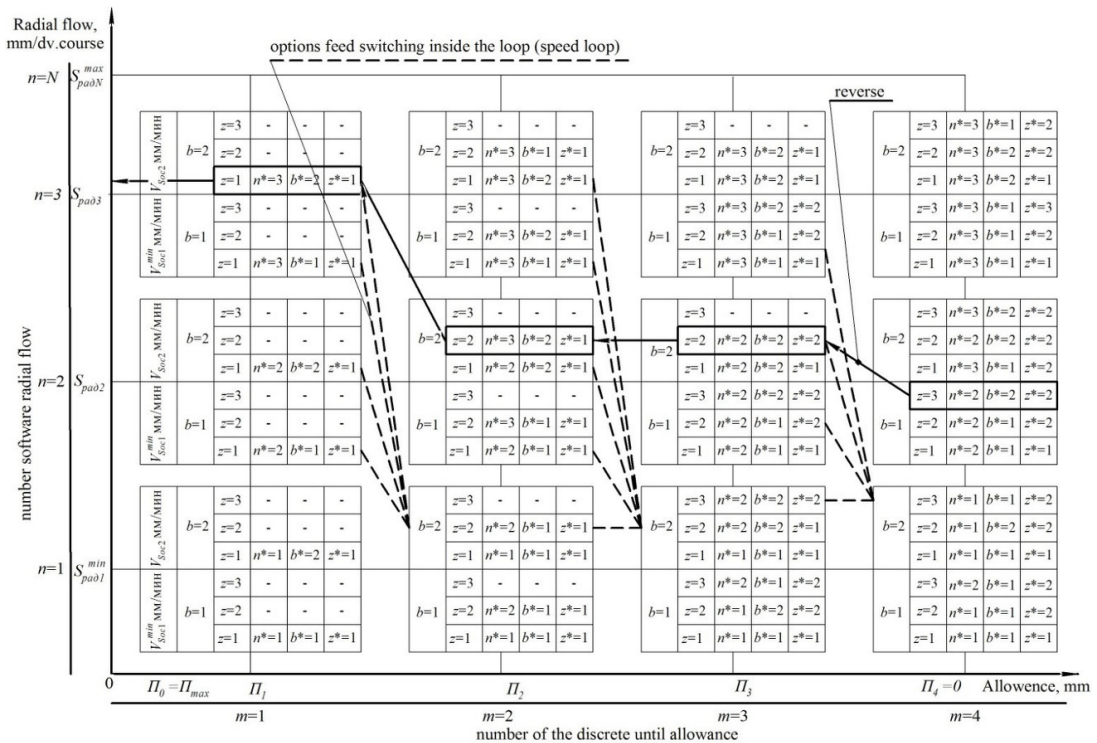


Fig. 1. Grid to optimize cycle internal grinding processing using dynamic programming when taking into account restrictions on the number of switching's innings

According to the principle of optimality of the competing moves, you must choose the best course with the best time to reach state. The choice of the optimal move is carried out by means of modeling of removal rate of the m -th discrete unit allowance for each contention turn. In modeling the process of metal removal calculated values actually recorded in the allowance, the current values of the radii of the processed holes, the cutting force, time of removal of the discrete unit of allowance, the time to reach the States, etc. More detailed modeling of metal removal for internal grinding can be found in [17-20].

Competing the course involved in choosing the best move, if made in the state $[m, n, b, z]$ are all constraints on the target function. Constraints are divided into two groups. The first group includes the constraints in the end of the cycle (precision, respirologist, the roughness of the processed surface). The second group of limitations during the entire grinding cycle (on the flow properties of the circle, drive power, admissibility feed rate, etc.).

The amount actually filmed allowance is in direct proportion to the radial feed control limit which is determined by the allowable range of the machine. As a result, we can assume that the most rapid decrease in the value of the actually-recorded allowance possible with the minimum permissible value of radial flow and speed of the axial flow. Then check how the restrictions in the final state of the process is to answer the question (principle validation of stroke) – possible after removing the m -th part of an allowance of time to reduce the amount actually recorded an allowance of time for removal of the remaining portion of the allowance with minimal radial and axial feed up to the value at which executed the limitations of the first group? If the answer to this question is negative, then the removal of the remaining portion of the allowance under any other large values of the radial and axial feeds from the acceptable range of flows to meet these constraints it is even more impossible. As a result, validation of progress on the limitations of the first group (accuracy, cauterization and roughness) is reduced to the following typical procedure. After modeling metal removal-coordinates $[m, n, b]$ (make a move) made a similar simulation of the removal of the remaining portion of the allowance, if admissible under the machine feeds – coordinates $[m_{max}, n_{min}, b_{min}]$. Thus, of all the competing moves are selected, only the valid moves. And from a set of valid moves selected optimum speed, with the optimal (minimal) time to reach the state and allowed by all constraints. Then, in the «information cell» contains the radial and axial feeds, number of steps, produced where the optimal move. Memorized the level value, where the produced optimal speed, is fixed for each state $[m, n, b, z]$ and is stored in the variable n^* , b^* , and z^* (Fig. 1). The exceptions are the intersection coordinates $[m, n, b, z]$, which do not have any valid moves.

The optimization process begins with the implementation of the totality of moves straight to the first discrete mating. Then made the transition from the previous discrete allowance ($m-1$) for n -th radial feed of the circle at the m -th one of the discrete mating. Each competing progress checks for valid according to the specified constraints. When reaching $[m, n, b, z]$ condition of the grinding process with one or more valid competing moves by the selection of the best move, providing the minimal time to reach the state. In the «information cell» is written to the coordinates of the previous state of the process from which the transition is optimal. After reviewing recent discrete allowance $m=M$ of the optimal number of moves which are located in different rooms of radial feeds, selects one move that has the minimum time to reach the end state (minimum cycle time).

For fixation of optimal trajectory control of a grinding cycle, you must perform the reverse procedure, which starts from the process of having the minimum time to reach the end state. Recovery trajectory control cycle occurs on the coordinates of the previous process state n^* , b^* and z^* , going from a finite discrete unit allowance to primary, while remembering the value of feeds and allowances. In Fig. 1 shows a graphical representation of the example procedure reverse that form the trajectory of the optimal control program. After the compulsory procedure-reverse cycle is formed internal grinding processing, is presented in Fig. 2 in the coordinates of the «Radial flow (S_{rad} , mm/dv.course) – axis feed rate (V_{soc} , mm/min) – allowance (Π_M , mm)» a spatial trajectory of the control program and its projections. In Fig. 2 you can also see the spatial path control program, change the values actually recorded in the allowance, spatial representation changes the values actually recorded in the allowance, the projection of the trajectory cycle in planes S_{rad} and $\Pi - A_1B_1C_1D_1E_1$, S_{rad} and $V_{soc} - A_2B_2C_2D_2E_2$, V_{soc} and $\Pi - A_3B_3C_3D_3E_3$.

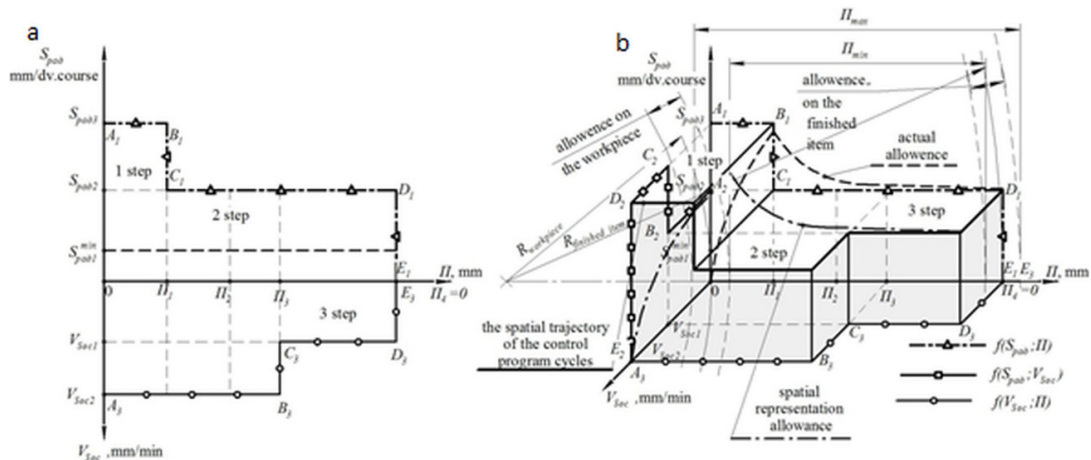


Fig. 2 – Example of a three-cycle internal grinding processing in two-dimensional (a) and three-dimensional (b) the space of control parameters

3. Conclusion

This paper proposes a method of calculating the optimum internal grinding cycles of processing:

- allows with mathematical precision to design the optimal internal grinding cycles using dynamic programming method;
- not sensitive to the form of mathematical models (linearity, differentiability) of the process and constraints of the target function;
- allows to take into account any number of technological constraints on the target function;
- provides multi-parameter optimization of the control program for CNC machines on the internal grinding operations. The results of the optimization are: optimal values of the radial flow S_{rad} at all stages of the cycle; the optimum value of the axial feed V_{sec} at all stages of the cycle; optimal allocation deduct allowance on the steps of the cycle for radial flow S_{rad} and axial flow V_{sec} , which provide the minimum cycle time (or other objective function).
- allows you to expand the number of optimized parameters and perform multivariable optimization in multidimensional space.

References

- [1] J.F.G. Oliveira, E.J. Silva, C. Guo, F. Hashimoto, Industrial challenges in grinding, *CIRP Annals, Manufacturing Technology*. 58 (2009) 633–680.
- [2] W.B. Rowe, *Principles of Modern Grinding Technology*: second ed., Elsevier Inc, Liverpool, 2013.
- [3] D.V. Ardashev, Definition of Abrasive Grain Wear upon Grinding from the Standpoint of the Kinetic Theory of Strength, *Journal of Friction and Wear*, Allerton Press. 36 (2015) 266–272.
- [4] V.N. Mikhelkevich, *Automatic control of grinding*, Mechanical Engineering, Moscow, 1975.
- [5] A.A. D'yakonov, L.V. Shipulin, Complex process modeling of plane grinding by the periphery of a circle, *Science Intensive Technologies in Mechanical Engineering*. 6 (2013) 14–18.
- [6] R.D. Nathan, L. Vijayaraghavan, R. Krishnamurthy, Intelligent estimation of burning limits to aid in cylindrical grinding cycle planning, *Heavy Vehicle Systems*. 80 (2001) 48–59.
- [7] T. Nishimura, I. Inasaki, N. Yamamoto, Study on optimization of internal grinding cycle, *Nippon Kikai Gakkai Ronbunshu, C Hen/Transactions of the Japan Society of Mechanical Engineers, Part C*. 55 (1989) 1808–18013.
- [8] O. Horiuchi, T. Shibata, Computer simulations of cylindrical plunge grinding – Influence of work stiffness on grinding accuracy, *Key Engineering Materials*. 329 (2007) 51–56.
- [9] I. Inasaki, Monitoring and Optimization of Internal Grinding Process, *CIRP Annals – Manufacturing Technology*. 400 (1991) 359–363.

- [10] J. Alvarez, D. Barrenetxea, J.I. Marquinez, I. Begiaga, I. Gallego, Continuous variable feed rate: A novel method for improving infeed grinding processes, *International Journal of Advanced Manufacturing Technology*. 73 (2014) 53–61.
- [11] P.P. Pereverzev, Simulation and optimization of the controlling programs in automated machine-building production, *Bulletin of the South Ural State University. Ser. Mashinostroenie*. 12 (2012.) 152–157.
- [12] P.P. Pereverzev, Modeling technological constraints in the optimization of automatic grinding cycles, *Bulletin of the South Ural State University. Ser. Mashinostroenie*. 12 (2012) 165–170.
- [13] P.P. Pereverzev, D.Yu. Pimenov, Optimization of control programs for numerically controlled machine tools by dynamic programming, *Russian Engineering Research*. 35 (2015) 135–142.
- [14] R. Bellman, *Dynamic programming*, Foreign Literature Publishing House, Moscow, 1960.
- [15] C.W. Lee, Dynamic optimization of the grinding process in batch production, *Journal of Manufacturing Science and Engineering, Transactions of the ASME*. 131 (2009) 61–66.
- [16] P. Krajinik, R. Drazumeric, J. Badger, F. Hashimito, Cycle optimization in cam-lobe grinding for high productivity, *CIRP Annals – Manufacturing Technology*. 630 (2014) 333–336.
- [17] P.P. Pereverzev, A.V. Popova, Analytical modeling of interrelation of force of cutting at internal grinding with the key technological parameters, *Metalloobrabotka*. 3 (2013) 24–30.
- [18] P.P. Pereverzev, A.V. Popova, D.Yu. Pimenov, Relation between the Cutting Force in Internal Grinding and the Elastic Deformation of the Technological System, *Russian Engineering Research*. 35 (2015) 215–217.
- [19] A.V. Popova, Design of Optimal Internal_Grinding Cycles, *Russian Engineering Research*. 35 (2015) 378–380.
- [20] P.P. Pereverzev, A.V. Popova, Development of a method of optimization of internal grinding cycles of processing in multidimensional space, *Modern problems of theory of machines*. 3 (2015) 22–25.



International Conference on Industrial Engineering

Dynamic model of material deforming under Microgrinding

Sopeltzev A.V.^a, Dyakonov A.A.^{a*}, Karali Patra^b

^aSouth Ural State University, 76, Lenin Avenue, Chebysinsk, 454080, Russian Federation

^bIndian Institute of Technology Patna, Patliputra Colony Patna-800013, Bihar, India

Abstract

Model of the process of the dynamic contact interaction of a single abrasive grain with processed material was generated on the basis of the microgrinding process physical parameters analysis. Model is implemented on the basis for the finite elements method, using LS-DYNA software. Following is considered to be condition of destruction - achieving limit deformation of the element with further removing the element.

Suggested model is universal in relation to materials under examination, which contact is simulated. If we know strength parameters of the specific processed material and a single grain, we can calculate stresses and deformations in the sample and cutting forces components on a single grain.

Performed calculations resulted in obtaining new data on spreading stress and pressure fields in a sample, as well as cutting forces components values on a single grain.

© 2015 The Authors. Published by Elsevier Ltd. This is an open access article under the CC BY-NC-ND license

(<http://creativecommons.org/licenses/by-nc-nd/4.0/>).

Peer-review under responsibility of the organizing committee of the International Conference on Industrial Engineering (ICIE-2015)

Keywords: modeling, dynamic interaction, microgrinding, strain, stress, components of cutting forces

1. Introduction

Mechanical micromachining – microgrinding [1-3] – is one of the main production processes of producing micro-electro-mechanical systems (MEMS) mechanical parts [1-3]. It should assure accuracy of the dimensions, geometrical accuracy of components arrangement [4-5], as well, as machined surface quality under maximum effectiveness of the machining process [6, 7].

* Corresponding author. Tel.: +7-351-272-32-94, fax: +7-351-267-92-73.

E-mail address: sigma-80@mail.ru

Analysis of the up-to-date research in the field of the high-speed processes modeling, including microgrinding, demonstrates that practically all research is aimed on performing experimental studies, receiving data, and empirical relationships developing [8-17].

It is obvious that this approach will lead to necessity of performing models coefficients clarification experiments for every material, component configuration, tool parameters, cutting mode, etc.

Modeling of high-speed processes in the form of physical models is a quite time consuming task. We need not only a process physical model, but also a whole complex of measuring equipment, as well, as manufacturing of processed material work pieces and abrasion striking grains.

Nomenclature

t	cutting depth
V_d	detail speed
V_w	wheel speed
ρ	density
v	speed
\ddot{x}	acceleration
σ	Cauchy stress tensor
g	acceleration of gravity
\dot{u}	internal energy change speed
D	speed deformation tensor
r	volumetric heat source intensity
q	heat flow
∇	Hamilton operator
$\langle\langle \cdot \rangle\rangle$	scalar multiplication
$\langle\langle \cdot \rangle\rangle$	double scalar multiplication

2. Problem description

Evolution of hardware and software complexes allows passing from physical modeling to modeling in CAE-systems on effective IT complexes. It allows decreasing physical modeling system design, manufacturing and installation operations scope, as well, as allows generating multiparameters models with wide range of parameters changing.

Previously received data or few proving experiments are enough for verification of this model validity.

Microgrinding process is a high-speed process with interacting speeds of up to 50-80 m/s and deformation speeds of $10^{-6} \dots 10^{-7}$ s [18, 19] This process is considered as process of multiple micro-cutting by microgrinding wheel grains, where each grain is a micro-cutter, performing cutting process [20].

Due to indicated advantages of processes modeling in CAE-systems, it makes sense to overview process of contact interaction of the abrasive microgrinding wheel with a processed detail.

Process design scheme is presented on Fig. 1.

In order to implement provided design scheme it is necessary to perform preliminary analysis of the process modeling possibility. Beside this it is necessary to have a physical model of contact interacting for comparing with design data.

Physically, when abrasive grain cuts into the sample, later deforms, forming a groove. Chip also forms during this process. Fig. 2 presents a picture after cutting the sample with a single grain at speed of 35 m/s and intrusion depth of 5 mkm.

Physically, when abrasive grain cuts into the sample, later deforms, forming a groove. Chip also forms during this process. Fig. 2 presents a picture after cutting the sample with a single grain at speed of 35 m/s and intrusion depth of 5 mkm.

Preliminary analysis of the microgrinding wheel and detail contact modeling possibility revealed following difficulties and task specialties:

- quite big quantity of interacting elements;
- big difference between dimensions of interacting bodies and these bodies overlapping during contact;
- bodies contact at a tangent to the detail;
- high level of symmetry.

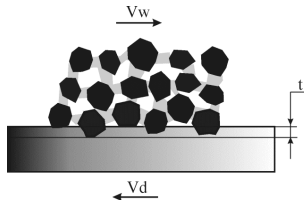


Fig. 1. Design scheme of microgrinding wheel and detail contact

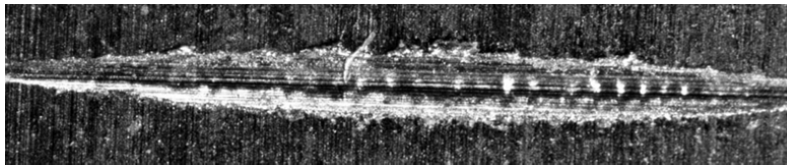


Fig. 2. Sample picture after single cut with an abrasive grain

Due to this following simplifications and assumptions are used on the first modeling stage:

- single grain interacting with a detail was considered instead of the microgrinding wheel;
- reduced sector of the detail was considered instead of the whole detail;
- detail does not move (used reflection plane on the plane, opposite to contact plane);
- abrasive grain moves straight against the detail with determined ingress value;
- abrasive grain - absolutely rigid body with constant speed.

We also need to take into account, that materials strength parameters depend on contacting bodies interaction speed, contact area temperature and deformation speed [18], so material model is functionally dependant.

Task is as follows:

Single grain with speed of 50 m/s tangentially cuts into the fixed sample and deforms it, forming a notch or groove (Fig. 2). Cutting depth is 5 mkm (corresponds to abrasive microgrinding). Grain material – zirconium electrocorundum, detail material – steel 45.

Modeling is aimed on determining process energy parameters and sample volume changing, as well, as numerical expression of power and contact interaction of the abrasive grain and detail, namely, cutting force on the grain and deformation in a detail.

First stage – generating geometry of interacting elements. We can use any CAD-system, able to store information in transition data formats, suitable for CAE-system.

Then received geometry is passed to CAE-system, where all initial task parameters are set, finite elements grid is formed, etc. ANSYS software preprocessor is used as a CAE-system.

Mathematically this task is based on following methods and input parameters:

Lagrange approach is used for describing solid deformed media moving.

It includes:

a) mass conservation equation:

$$\dot{\rho} + \rho \cdot \text{div}(\mathbf{v}) = 0, \quad (1)$$

b) movement quantity conservation equation:

$$\rho \ddot{\mathbf{x}} = \rho \mathbf{g} + \text{div}(\boldsymbol{\sigma}), \quad (2)$$

c) energy conservation equation:

$$\rho \dot{u} = \boldsymbol{\sigma} : \mathbf{D} + \rho \cdot \mathbf{r} - \nabla \cdot \mathbf{q}, \quad (3)$$

Input task parameters are described later:

1. Geometry

Reduced sector is used as a sample; reduced hollow cone is used as a grain. Using hollow cone decreases grain model scope, leading to decreasing finite elements grid nodes and elements quantity, leading to decreasing task resource intensity and calculating period.

2. Separating to finite elements.

Two types of finite elements are used: for sample these are 8 nodes volumetric cube type elements, for grain – 10 nodes volumetric tetrahedron elements.

Materials models: for sample – Plastic_Kinematic with kinematic strengthening, material – steel 45; for grain – Rigid material model with strength parameters, typical for zirconium electrocorundum.

3. Border conditions.

Sample has reflection plane on the surface, opposite to contact; this allows minimizing model scope and assures results reliability. Target sample has symmetry plane in the direction of striker moving. Implementing this plane allowed decreasing sample design scope twice.

Grain has only one degree of freedom – ability of moving along determined moving direction.

4. Moving

Sample is stable, grain moves with constant speed.

5. Contact

Eroding (ESS) type contact is used. This is a contact with destructing of one of the contacting bodies, with determining friction coefficient for steel-electrocorundum, also taking into account sample symmetry plane.

Following is considered to be condition of destruction – achieving limit deformation of the element with further removing the element.

3. Numerical implementation of the solution

Fig. 3 presents grid of finite elements, over imposed on geometry, generated in CAD system. For this model finite elements grid includes about 40000 elements and 48000 nodes, accordingly.

After inputting all initial parameters of the task ANSYS software complex preprocessor forms initial file for calculating in software complex LS-DYNA.

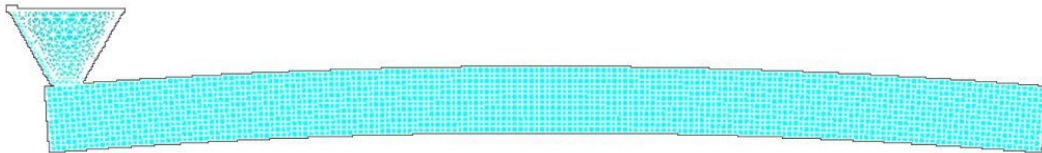


Fig. 3. Finite elements grid over model axial section.

Deformations and moving all over sample volume, as well, as spreading stresses and elastic waves are determined based on calculation results. Power parameters of the process are also determined. Calculation results are presented on Fig. 4, 5, and 6.

As we can see from Figure 5, deformation center in a sample is identical to deformed physical sample, presented on Fig. 2, proving validity of presented model, as well, as correctness of chosen models of material and destruction criteria.

After performing primary calculations and analyzing results for deformed sample, we have performed calculations for determining components of forces, acting on a single grain under contact interaction with processed material. In order to do this model geometry was added with a resistant element, single grain was added with a freedom degree in radial direction against the single grain moving axis. Resistant element moves synchronously with a grain and is connected with it through the axial element. Generated process model allowed obtaining (based on calculation results) data on cutting forces components, acting on the grain from the processed material, i.e. work piece. Results of the cutting forces components calculations are presented on Fig. 7.

As we can see from Figure 7, compression forces (X and Y components are negative) act on a grain. Beside this due to calculation was performed for half of a grain and detail, obtained values of cutting forces components should be doubled.

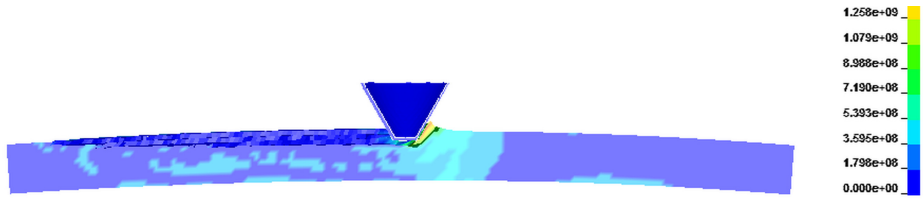


Fig. 4. Spreading stresses in a sample over axial section.

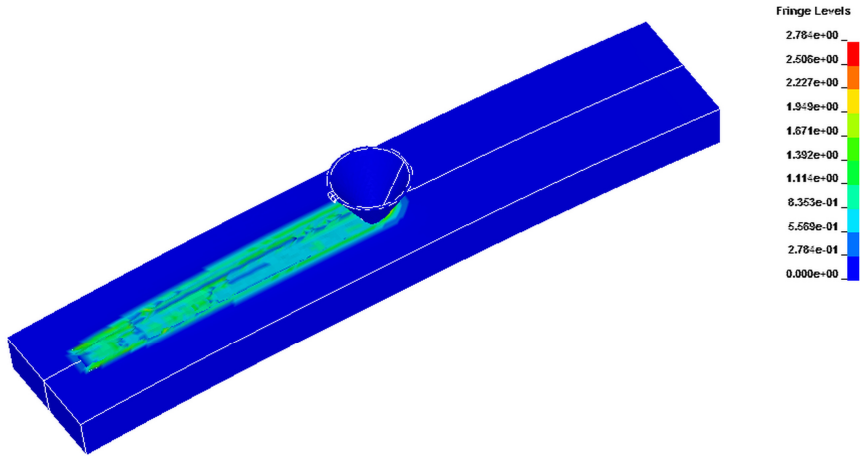


Fig. 5. Deformation in sample.



Fig. 6. Spreading stresses in a sample over axial section.

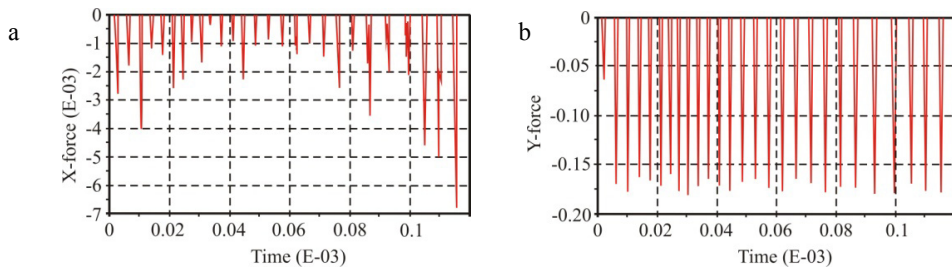


Fig. 7. Cutting forces components on a single grain (a) X-component; (b) Y-component.

4. Conclusion

Performed work resulted in creating model of the process of the dynamic contact interaction of a single abrasive grain with processed material. We obtained data on spreading deformations in a work piece. They are identical to deformations in a physical sample, presented on Fig. 2. Obtained new data on spreading stress and pressure fields in a sample, as well as cutting forces components on a single grain.

Now we perform verifying model validity and possibility to use calculations results in further activity. Beside this we review changing material destruction criteria for deformed body material, and possibility to change stress design schemes.

It should be noted that obtained model, operating on the finite elements method, is universal to materials, whose contact is modeled. So, if we know strength parameters of the processed material and a single grain, we can easily calculate stresses and deformations in the sample and cutting forces components on a single grain.

In the situation of quick development and upgrading of different materials manufacturing and processing methods, implementing such models significantly decreases timeframes of materials strength parameters studies and, accordingly, their implementation and using at production plants.

5. Acknowledgement

This article is a part of the bilateral research project «Modeling and analysis of high speed hybrid micromachining»:

1. The reported study was partially supported by DST, Govt. of India, research project No. INT/RUS/RFBR/P-226.
2. The reported study was partially supported by RFBR, research project No. 15-58-45017 ИИД_а.

References

- [1] M. Dickerhof, Paving the ground for the next generation of micro nano enabled products in europe. MINAM Position Paper, Chap.2, 2011.
- [2] J.L. Liow, Mechanical Micromachining: A Sustainable Micro-Device Manufacturing Approach, *J. of Cleaner Production*. 17 (2009) 662–667.
- [3] M.A. Camara, J.C.C.Rubio, A.M. Abrao and J.P. Davim, State of the Art on Micro-milling of Materials, A Review, *J. of Materials Science & Technology*. 28 (2012) 673-685.
- [4] C.W. Liu, C. Gau, H.S. Ko, C.S. Yang and B.T. Dai, Fabrication challenges for a complicated micro-flow channel system at low temperature process, *J. Sensors and Actuators A*. 130–131 (2006) 575–582.
- [5] K. Malecha, L.J. Golonka, Microchannel fabrication process in LTCC ceramics, *J. of Microelectronics Reliability*. 48 (2008) 866–871.
- [6] D.V. Ardashev, Group Abrasive Machining in Flexible Production, *J. Russian Engineering Research*. 35(4) (2015) 305-306.
- [7] D.V. Ardashev, Predicting the performance of abrasive tools in Process design for diversified production, *J. Russian Engineering Research*. 35(3) (2015) 206-208.
- [8] G. Bissacco, H.N. Hansen, J. Slunsky, Modelling the cutting edge radius size effect for force prediction in micro milling, *J. CIRP Annals - Manufacturing Technology*. 57 (2008) 113-116.
- [9] A. Aramcharoen, P.T. Mativeng, Size effect and tool geometry in micromilling of tool steel, *J. Precision Engineering*. 33 (2009) 402-407.
- [10] R.S. Anand, K. Patra, M. Steiner, Size Effect in Micro Drilling of Carbon Fiber Reinforced Plastic Composite, *Production Engineering Research and Development*, Springer, 2014, DOI 10.1007/s11740-014-0526-2.
- [11] Y. Altintas, X. Jin, Mechanics of micro-milling with round edge tools, *J. CIRP Annals – Manuf. Tech*. 60 (2011) 77-80.
- [12] S. Rao, M.S. Shunmugam, Analytical modeling of micro end-milling forces with edge radius and material strengthening effects, *J. Mach. Sci. and Tech*. 16 (2013) 205-227.
- [13] A. Dikshit, J. Samuel, R.E. DeVor, S.G. Kapoor, Microstructure-Level Machining Simulation of Carbon Nanotube Reinforced Polymer Composites – Part I: Model Development and Validation, *ASME J. of Manuf. Sci. and Eng*. 130 (2008) 031114.
- [14] M.P. Vogler, R.E. DeVor, S.G. Kapoor, On the Modeling and Analysis of Machining Performance in Micro-Endmilling, Part I: Surface Generation, *ASME J. of Manuf. Sci. and Eng*. 126 (4) (2004) 685-694.
- [15] V. Bajpai, R.K. Singh, A.K. Kushwaha, Burr formation and surface quality of high speed micromilling of titanium alloy, *ASME Conference proceedings*, 2013.
- [16] V. Horch, V. Schulze, D. Lohe, Deburring and surface conditioning of micromilled structures by abrasive and non-abrasive micro-peening, *ICSP9*. (2009) 191-196.
- [17] D.J. Yun, T.I. Seo and D.S. Park, Fabrication of biochips with micro fluidic channels by micro end-milling and powder blasting, *Sensors*. 8 (2008) 1308-1320.
- [18] A.A. D'yakonov, Blank-cutter interaction in high-speed cutting, *J. Russian Engineering Research*, 34(12) (2014) 775-777.

- [19] A.A. Dyakonov, Simulated stochastic thermo-physical model of grinding process, *Lecture Notes in Engineering and Computer Science*. 2 (2014) 914-917.
- [20] A.A. D`yakonov, L.V. Shipulin, Selecting the Cutting Conditions for Plane Grinding by the Wheel Periphery, *J. Russian Engineering Research*. 34(12) (2014) 814-816.



International Conference on Industrial Engineering

Modeling Cutting Force in Micro-Milling of Ti-6Al-4V Titanium Alloy

Tej Pratap^a, Karali Patra^{a*}, Dyakonov A.A.^b

^aIndian Institute of Technology Patna, Patliputra Colony Patna-800013, Bihar, India

^bSouth Ural State University, 76, Lenin Avenue, Chelyabinsk, 454080, Russian Federation

Abstract

This work presents a finite element method (FEM) based micro-end milling cutting force modeling of Ti-6Al-4V titanium alloy microchannels. Ti-6Al-4V is one of the widely acceptable titanium based alloys for medical as well as aerospace applications due to its advantageous properties like; corrosion resistance, larger strength to weight ratio, non-toxic nature and bio-compatibility. Johnson-Cook constitutive equation is used for the FEM model with due consideration of effects of strain, strain rate and temperature on the material property and failure parameters considered as the chip separation criterion. Simulation of stress distribution, temperature distribution and cutting forces prediction during micro-end milling of Ti-6Al-4V alloy is performed by ABAQUS/Explicit 6.12 software with incorporation of tool edge radius effect, which is more common in downscaling of the process. Predicted cutting forces model results are validated by conducting micro-end milling experiments. The trend of the predicted cutting forces results shows in good agreement with experimental results.

© 2015 Published by Elsevier Ltd. This is an open access article under the CC BY-NC-ND license (<http://creativecommons.org/licenses/by-nc-nd/4.0/>).

Peer-review under responsibility of the organizing committee of the International Conference on Industrial Engineering (ICIE-2015)

Keywords: Micro-end milling, titanium alloy, microchannel, finite element method, von-Mises stress, size effect

1. Introduction

The need for production of micro components is increasing with increasing demand for enhancement of product performance and reduction of weight and cost in many industries such as medical instrumentation, aerospace, automobile, electronics, etc [1]. In general, micro components can be produced by various methods such as

* Corresponding author. Tel.: +91-612-255-2012; fax: +91-612-227-7383.
E-mail address: kparta@iitp.ac.in

lithography, laser machining, ion beam machining, electro-discharge machining, electro-chemical machining and mechanical micromachining [1,2]. Among these mechanical micromachining methods such as; micro-end milling shows a great promise in the manufacturing of these micro components with 3D features, higher aspect ratio, tolerable surface quality and applicability to wide range of engineering materials such as metals, metal alloys, non-metals, composites, ceramics, etc [3,4]. Titanium alloy Ti-6Al-4V is one of such ideal materials that provides the excellent properties like; high specific strength, corrosion resistance, fracture resistance, non-toxicity and biocompatibility; which makes it suitable for micro-feature based applications in aerospace, chemical, medical and many more [5,6]. However, Ti-6Al-4V alloy also possesses difficulty in machining due to its high temperature strength, relatively low modulus of elasticity, low thermal conductivity and high chemical reactivity which promotes reactivity of titanium with tool and leads to accelerated tool wear and uneven micro-burr formation [7,8].

Moreover, downscaling of conventional milling to micro-milling brings several problems related to size effects, micro-burr formation, tool wear and sudden tool breakage, etc [6,8]. Since micro-milling tool stiffness is low due to high aspect ratio (length/diameter), increase of forces in the micro cutting process will cause tool deflection or cause imperfection on the final product and even cause tool breakage if not minimized [9]. Therefore, an accurate prediction of cutting forces in micro-milling is essential. In micro-milling, uncut chip thickness is comparable to the tool edge radius known as size effect. This size effect associated with ploughing and elastic recovery causes nonlinear increase of specific cutting forces at low feed rates [10,11].

Therefore, micro-milling of Ti-6Al-4V alloy is a two-fold challenge: one due to unfavourable material properties for machining and another due to downscaling of the process. FEM based techniques are good compliments with the advancement of recent computational speed to experimental intensive, mechanistic approaches and offer a reasonable insight to the machining process for selection of cutting parameters to avoid premature wear and breakage of the tool [10-12]. There are several examples of 2D and 3D finite element method simulation of macro-milling process of Ti-6Al-4V alloy to study cutting forces, chip formation, cutting temperature and cutting tool wear under different process parameters [13-15]. However, there are limited applications of finite element based modeling and simulation of micro-milling of Ti-6Al-4V alloy, so far. Özel et al. [6] utilized FE simulation to predict temperature and wear development in micro-milling of Ti-6Al-4V alloy.

In the present study, a FEM model is proposed for prediction of cutting forces, stress generation and temperature distribution in micro-end milling of Ti-6Al-4V. Micro-end milling experiments have been performed for manufacturing of microchannels on Ti-6Al-4V workpiece using 400 μm diameter two fluted uncoated tungsten carbide micro flat-end mills. Experimental results are verified with proposed model predicted results in order to assess the validity of the FEM model.

2. Micro-end milling cutting force modeling an FEM approach

A plane strain based orthogonal cutting force model with tool edge radius effect has been performed for micro-end milling process as shown in Fig. 1 using ABAQUS/Explicit 6.12 software. Fig. 2 shows the schematic representation of cutting process by a micro-end mill cutter.

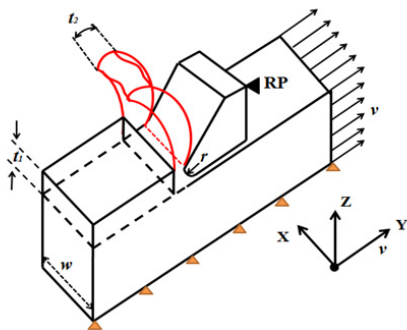


Fig. 1 FEM model of orthogonal cutting

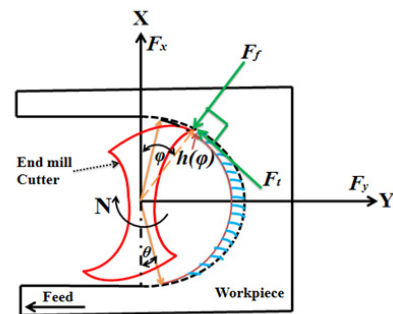


Fig. 2 Micro-end milling with two fluted cutter

The cutting tool used for the modeling purpose is considered as an isothermal rigid body and represented by the reference point (RP) to acquire the data value [12]. The size of the generated mesh is comparable with tool edge radius in order to maintain the simulation precision. The tool is restricted in all directions and workpiece travels towards the tool with uniform velocity v in Y-direction. The uncut chip thickness (h) in micro-end milling process varies with cutter rotation angle and calculated by Eq. 1.

$$h(\varphi) = f_i \sin(\varphi), \quad (1)$$

where, φ is related to positioning angle of the tool and f_i is feed per tooth. Cutter rotation, feed direction and cutting force directions were also shown in Fig. 2.

3. Material properties and damage criterion for chip formation

Generally two types of approach are used to simulate the chip formation in Ti-6Al-4V titanium alloy: (a) material damage criterion or (b) modified material model with temperature dependent material softening approach [16]. However, literature also suggests about higher temperature generation during machining of titanium alloy due to low thermal conductivity of the material and effect of flow softening and strain hardening effect reduces as temperature increases [17]. As high strain and high temperature occur during machining of titanium alloy [15], flow stress will not be affected much by the flow softening phenomenon. Therefore, the more popular traditional Johnson-Cook material constitutive model [18] with material damage criterion [19] has been used for the proposed model. The Johnson-Cook model is described by the expression of average flow stress given by Eq. 2.

$$\bar{\sigma}_{JC} = \left[A + B(\varepsilon)^n \right] \times \left[1 + C \ln \left(\frac{\dot{\varepsilon}}{\dot{\varepsilon}_0} \right) \right] \times \left[1 - \left(\frac{T - T_0}{T_m - T_0} \right) \right], \quad (2)$$

where ε is the equivalent plastic strain, ε and $\dot{\varepsilon}_0$ are the equivalent and reference plastic strain rates, T , T_m and T_0 are the material's cutting zone, melting and room temperature, respectively, n is the strain hardening index, and m is the thermal softening index. Johnson-Cook Parameters A , B and C represent the yield strength, strain and strain rate sensitivities of the material. The material properties Table 1 from Wu and Zang test results were used for the FEM modeling [15].

Table 1. Mechanical properties and Johnson-Cook parameter of Ti-6Al-4V alloy [15].

Details		Parameters			
Mechanical properties	Density [Kg/m ³]	Elastic modulus [MPa]	Poisson's ratio	T_m [°C]	T_0 [°C]
Value	4430	123	0.34	1570	20
Johnson Cook model	A [MPa]	B [MPa]	n	C	m
Value	1000	780	0.47	0.033	1.02

Johnson-Cook failure model [19] was used as a damage initiation criterion. This model takes into account the influence of stain, strain rate, and temperature on material failure shown in Eq.3. The five failure parameters of the Johnson-Cook model are shown in Table 2 [15].

$$\varepsilon_{f\ failure} = \left[d_1 + d_2 \exp \left(d_3 \frac{P}{\bar{\sigma}_{JC}} \right) \right] \times \left[1 + d_4 \ln \left(\frac{\dot{\varepsilon}}{\dot{\varepsilon}_0} \right) \right] \times \left[1 + d_5 \left(\frac{T - T_0}{T_m - T_0} \right) \right]. \quad (3)$$

Table 2. Johnson-Cook failure parameter of Ti-6Al-4V alloy [15]

Details		Parameters				
Fracture parameters	d_1	d_2	d_3	d_4	d_5	
Value	-0.09	0.25	-0.5	0.014	3.87	

The main cause of the heat generation and its thermal aspect in contact problem is friction. The coefficient of friction μ has been taken as 0.5 for contact problem simulation purpose [15].

4. Micro-end milling simulation of Ti-6Al-4V titanium alloy

FEM simulations of the micro-end milling process for Ti-6Al-4V alloy were performed under different cutting conditions (spindle speed of 15000 rpm to 35000 rpm; feed rate of 1-5 $\mu\text{m}/\text{tooth}$; and constant axial depth of cut of 30 μm). Tool edge radius of 2 μm is used for the modeling purpose. Workpiece material is assumed to be viscoplastic material, as this assumption is more practical and reduces the computational time significantly with very small deviation in the results of cutting forces, tool wear and temperature [20]. von-Mises stress calculates the yield criterion and fracture strength of the material and once its value exceeds the average flow stress value, yielding takes place. However, experimental measurement of these simulation variables like; stress, strain, temperature are very difficult and numerical simulation or analytical simulation is more preferred as alternatives of direct measurement. Therefore, von-Mises stress distribution and temperature distribution is simulated for the micro-end milling of titanium alloy Ti-6Al-4V. One of simulation results at uncut chip thickness 1 μm and cutting depth of 30 μm at cutting speed of 31.415 m/min (corresponding to 25000 rpm spindle speed) is shown in Fig. 3. The stress distribution also shows that lower value of von-Mises stress occurs on the machined surface and it is increasing towards the cutting edge of the tool. This is due to the higher force required at the cutting edge of the tool in the shear zone for chip formation [21]. The maximum stress occurred in the primary shear band and the value was 2467 MPa. However, the increase of stress value may be due to the size effect of the micro-milling process. The maximum value of temperature is 845.3 $^{\circ}\text{C}$ which is quite high. This value is in the range of the temperature of macro-milling of Ti-6Al-4V alloy [15] and results of this higher temperature leads to accelerated tool wear in micro-milling process [6].

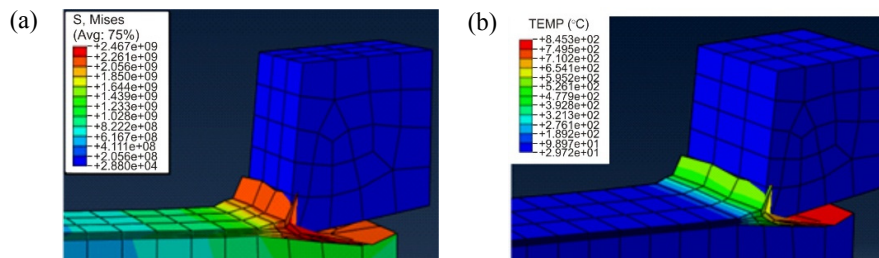


Fig. 3. Predicted (a) von-Mises stress distribution and (b) Temperature distribution at cutting speed of 31.415 m/min feed rate of 1 $\mu\text{m}/\text{tooth}$ with depth of cut of 30 μm

5. Model validation through experimental results

The experimental setup for validation of FEM model results is shown in Fig. 4 (a). SEM image of the used tool and microscopic image of fabricated microchannels at spindle speed of 25000 rpm, feed rate of 1 $\mu\text{m}/\text{tooth}$ with depth of cut of 30 μm are shown in Fig. 4 (b) and (c) respectively.

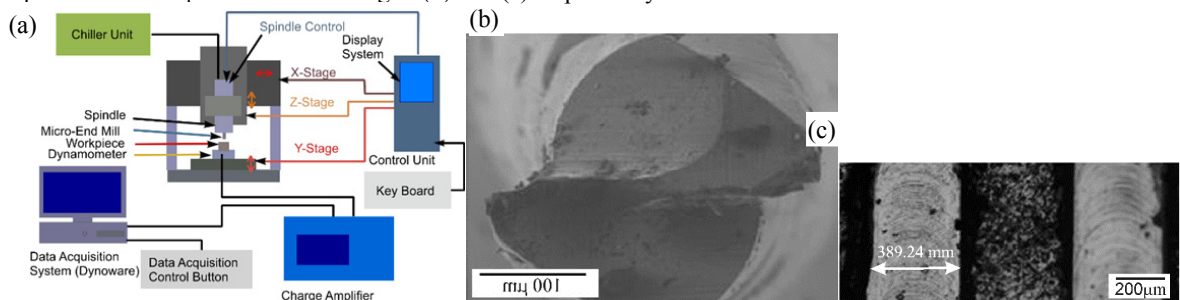


Fig. 4. (a) Experimental setup; (b) SEM image of micro-end mill after manufacturing of microchannels;

(c) Microscopic images of microchannels at spindle speed of 25000 rpm, feed rate of 1 $\mu\text{m}/\text{tooth}$ with depth of cut of 30 μm

Experiments are performed on a multi-purpose micro machining center (Model No. DT-110, Mikrottools Ltd.) having a maximum spindle speed of 60000 rpm and run out of less than 1 μm . Two-flute tungsten carbide micro-end mill with 400 μm tool diameters and 2 μm of tool edge radius is used to produce microchannels on Ti-6Al-4V workpiece having dimension of 75 mm x 45 mm x 3 mm. Table 3 shows the values of different cutting parameters (cutting speed, feed and axial depth of cut) used for microchannel fabrication. Cutting forces are acquired by piezo electric type force dynamometer (Kistler Type 9256C2) with sampling rate of 6000 Hz. The dynamometer having high natural frequency of over 5 kHz in all the three force directions makes it more reliable for measuring low cutting forces. However, tool wear and micro burr formation are not analyzed in the present work.

Table 3. Cutting condition used for fabrication of microchannels on titanium alloy Ti-6Al-4V

Details	Cutting parameters for dry cutting		
	Spindle speed [rpm]	Feed value [$\mu\text{m}/\text{tooth}$]	Axial depth of cut [μm]
Value	15000, 25000, 35000	0.5, 1.0, 1.5	30

6. Experimental validations of predicted results

To analyze the utility of proposed model, experimental cutting forces are used for validation. The experimental and FEM simulated cutting forces at spindle speed of 25000 rpm, feed rate of 0.5, 1.0 and 1.5 $\mu\text{m}/\text{tooth}$ and depth of cut of 30 μm are compared in Fig. 5 (a), (b), (c) and 6 (a), (b), (c).

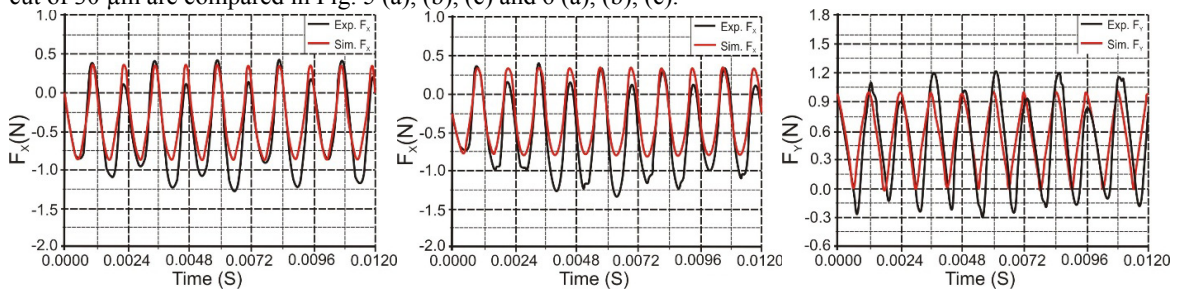


Fig. 5. Comparison of cutting force F_x (a) 0.5 $\mu\text{m}/\text{tooth}$ (b) 1.0 $\mu\text{m}/\text{tooth}$ (c) 1.5 $\mu\text{m}/\text{tooth}$

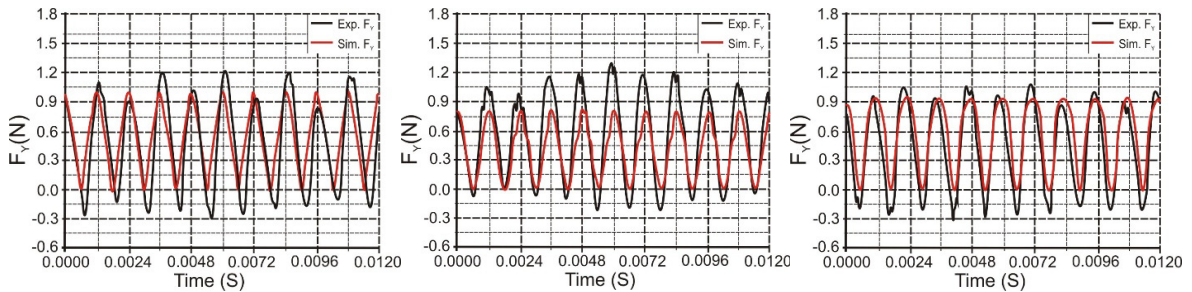


Fig. 6. Comparison of cutting force F_y (a) 0.5 $\mu\text{m}/\text{tooth}$ (b) 1.0 $\mu\text{m}/\text{tooth}$ (c) 1.5 $\mu\text{m}/\text{tooth}$

The simulated cutting forces F_x and F_y show good agreement with experimental results. However, small discrepancy of simulated and experimental forces is observed as tool dynamics, tool wear affects during the milling process are not considered in the model, which always predicts same force in each pass of the cutting edge. However, in actual experimental scenario tool dynamics and tool wear of the material will cause variations of cutting forces in different passes of the cutting edge. From Fig.5 and Fig. 6 it can also be observed that experimental cutting forces increase with increase in number of cutter rotation. This may be because of the accelerated tool wear and edge rounding due to high cutting temperature created in the micro-end milling of Ti-6Al-4V alloy.

7. Conclusions

The present paper described the cutting force modeling in micro-end milling of titanium alloy Ti-6Al-4V using ABAQUS/Explicit finite element method. The proposed FEM model simulated stress distribution, temperature distribution and cutting force generation considering the effects of tool edge radius, uncut chip thickness, cutting speed and feed rate. Maximum Von-Mises stress and cutting temperature were found to be more than those of macro-milling of Ti-6Al-4V alloy. These can be related to the effect of tool edge radius and low feed values applied in micro-end milling. The finite element simulation of specific cutting forces showed the size effects in micro-end milling process. The simulated cutting forces were successfully validated with experimental results.

8. Acknowledgement

This article is a part of the bilateral research project «Modeling and analysis of high speed hybrid micromachining»:

1. The reported study was partially supported by DST, Govt. of India, research project No. INT/RUS/RFBR/P-226.
2. The reported study was partially supported by RFBR, research project No. 15-58-45017 ИИД_a.

References

- [1] J. Chae, S.S. Park, T. Freiheit, Investigation of micro cutting operations, *Int. J. Mach. Tools. Manuf.* 46(2006) 313-332.
- [2] R.S. Anand, K. Patra, M. Steiner, Size effects in micro drilling of carbon fiber reinforced plastic composite, *Prod. Eng. Res. Devel.* 8 (2014) 301–307.
- [3] D.Dornfeld, S.Min, Y.Takeuchi, Recent advances in mechanical micromachining, *Ann. CIRP: Manuf. Technol.* 55 (2006) 745-768.
- [4] M.A. Camara, J.C.C. Rubio, A.M. Abrao, J.P.Davim, State of the Art on Micromilling of Materials A Review, *J. Mater. Sci. Technol.* 28(8)(2012) 673-685.
- [5] Y.Su, N.He, L.Li, X.L.Li, An experimental investigation of effects of cooling/lubrication conditions on tool wear in high-speed end milling of Ti-6Al-4V, *Wear.* 261 (2006) 760–766.
- [6] T.Özel, T.Thepsonthi, D.Ulutan, B.Kaftanoglu, Experiments and finite element simulations on micro-milling of Ti–6Al–4V alloy with uncoated and cBN coated micro tools, *Ann. CIRP: Manuf. Technol.* 60 (2011) 85–88.
- [7] G.M. Schueler, J. Engmann, T. Marx, R. Haberland, J.C. Aurich, Burr Formation and Surface Characteristics in Micro-end milling of Titanium Alloys, *Burrs-Analysis, Control and Removal*, Springer, Berlin, 2010, pp. 129–138.
- [8] V. Bajpai, A.K. Kushwaha, R.K. Singh, Burr formation and surface quality of high speed micro-milling of titanium alloy, *ASME Conference International Manufacturing Science and Engineering*, Madison, Wisconsin, USA, 2013.
- [9] M. Malekian, S.S. Park, M.B.G. Jun, Modeling of dynamic micro-milling cutting forces, *Int. J. Mach. Tools. Manuf.* 49 (2009) 586–598.
- [10] X. Lai, H. Li, C. Li, Z. Lin, J. Ni, Modelling and analysis of micro scale milling considering size effect, micro cutter edge radius and minimum chip thickness, *Int. J. Mach. Tools. Manuf.* 48 (2008) 1-14.
- [11] X. Liu, R.E. DeVor, S.G. Kapoor, K.F. Ehmann, The mechanics of machining at the micro-scale: assessment of the current state of the science, *J. Manuf. Sci. Eng.* 126 (2004) 666-678.
- [12] X. Jin, Y. Altintas, Prediction of micro-milling forces with finite element method, *J. Mater. Process. Technol.* 212 (2012) 542-552.
- [13] D. Umbrello, Finite element simulation of conventional and high speed machining of Ti6Al4V alloy, *J. Mater. Process. Technol.* 196 (2008) 79-87.
- [14] Y.Karpat, Temperature Dependent Flow Softening of Titanium Alloy Ti6Al4V: An Investigation Using Finite Element Simulation of Machining, *J.Mater. Process. Technol.* 211 (2011)737-749.
- [15] H.B. Wu, S.J. Zhang, 3D FEM simulation of milling process for titanium alloy Ti6Al4V, *Int. J. Adv. Manuf. Technol.* 71 (2014) 1319–1326.
- [16] M. Sima, T.Özel, Modified material constitutive models for serrated chip formation simulations and experimental validation in machining of titanium alloy Ti-6Al-4V, *Int. J. Mach. Tools. Manuf.* 50 (2010) 943-960.
- [17] S. Nemat-Naser, W.G. Guo, V.F. Nesterenko, S.S. Indrakanti, Y.B. Gu, Dynamic response of conventional and hot isostatically pressed Ti-6Al-4V alloy: experiments and modeling, *Mech. of Mater.* 33 (2011) 425-439.
- [18] G.R.Johnson, W.H.Cook, A constitutive model and data for metals subjected to large strains, high strain rates and high temperature, In: *Proceedings of the Seventh International Symposium on Ballistics*, The Hague, The Netherlands, 1983, pp.541-547.
- [19] G.R. Johnson, W.H. Cook, Fracture characteristics of three metals subjected to various strains, strain rates, temperatures and pressures, *Eng. Fract. Mech.* 21 (1985) 31–48.
- [20] T. Thepsonthi, Modeling and optimization of micro-end milling process for micro-manufacturing, PhD Thesis, Rutgers, The State University of New Jersey (2014).
- [21] K. Kadirgama, R.A. Bakar, M. Rahman, M. Bashir, Modeling of Residual Stress, Dr. David Moratal (Ed.), *InTech*, 2012, pp. 369-378.



International Conference on Industrial Engineering

The research of influence characteristics of heat-storage material on thermodynamic process in heat storage, installed in system of waste-heat recovery of internal combustion engines

Raznoshinskaia A.V.*

38B - 40 Let Pobedy Str., Apt 82, Chelyabinsk, Russia. 454021

Abstract

The article outlines the results of the research of influence characteristics of heat-storage material on thermodynamic process in heat storage, installed in system of waste-heat recovery of internal combustion engines. It is shown that the highest average temperature and dampening effect among 4 analyzed heat-storage materials is reached by means of utilization of tripartite eutectic mixture $7\text{NaNO}_3/40$, $\text{NaNO}_2/53$ KNO_3 and LiNO_3 , due to appropriate thermophysical properties.

© 2015 The Authors. Published by Elsevier Ltd. This is an open access article under the CC BY-NC-ND license (<http://creativecommons.org/licenses/by-nc-nd/4.0/>).

Peer-review under responsibility of the organizing committee of the International Conference on Industrial Engineering (ICIE-2015)

Keywords: internal combustion engine, exhaust gases, heat storage of transition curve, heat-storage material, thermophysical properties, temperature, temperature variations.

1. The research of influence characteristics of heat-storage material on thermodynamic process in heat storage.

The article outlines the results of the research of influence characteristics of heat-storage material on thermodynamic process in heat storage, installed in system of waste-heat recovery of internal combustion engines. It is shown that the highest average temperature and dampening effect among 4 analyzed heat-storage materials is reached by means of utilization of tripartite eutectic mixture $7\text{NaNO}_3/40$, $\text{NaNO}_2/53$ KNO_3 and LiNO_3 , due to appropriate thermophysical properties.

* Corresponding author *. Tel.: +7-951-810-24-11.
E-mail address: razn.alenal@yandex.ru

During last years the humanity witnesses the dramatic boost of automobiles. Thus, due to the analytic centre “Alfastrakhovanie”, the number of registered cars has grown twice for the last 10 years. Motor park increase leads to augmentation of influence on the environment. Main ecological problems of car utilization are: high toxicity of exhaust gases, heat and noise pollution, natural energy resources depletion. It is extremely important to introduce new technologies in auto industry to decrease the harmful influence of exhaust gases on the atmosphere in the future.

It is a well-known fact that up to 45% of heat energy, generated by an engine is extracted into the atmosphere with exhaust gases. There are groundbreaking reserves of amplification of engine performance in case of energy utilization by systems based on the Stirling engines, steam engines, gas turbines, thermoelectric generators, air expansion machines, etc.

The operation of waste treatment plants and oxidation catalyst demand stable and high temperature of air inflow, regardless engine operating condition [1,2]. However the temperature of exhaust gases of conventional engines changes in wide range depending on engine operating condition. So, on the basis of the research it is proven that the temperature of exhaust gases of KamAZ-740 engine on different engine operating conditions varies from 80 to 650 C [3].

It is possible to lower the oscillatory amplitude of the exhaust gases temperature by means of installation in car exhaust system device, containing heat-storage material of transition curve.

The device can be named as damper of temperature variations of exhaust gases.

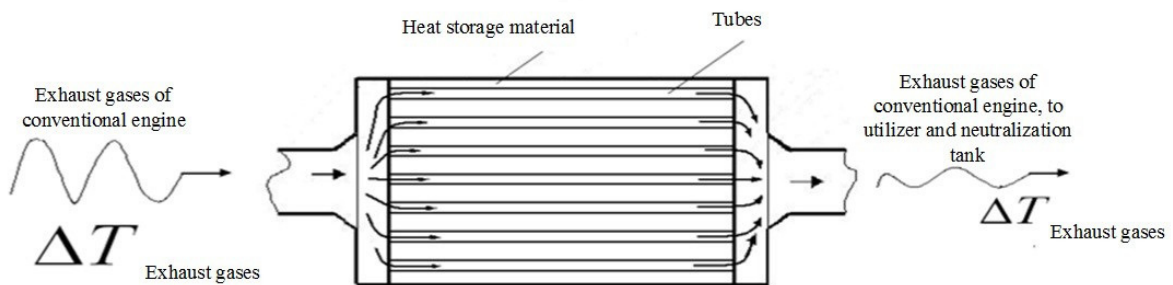


Fig.1. Damper of temperature variations of exhaust gases.

Dampers of temperature variations of exhaust gases of shell and tube type with transition curve are the most acceptable for the target implementation. The construction of damper of temperature variations of exhaust gases consists of frame with built in metal tubes, conducting exhaust gases of internal combustion engine. The space between the tubes is heat-storage material of phase transition.

In case the temperature of exhaust gases, flowing through the vibration damper is higher than the heat-retaining material's then the emission of heat takes place, consequently the temperature falls down. If exhaust gas is cooler than the heat-storage material, it gives some warmth to gas, boosting their temperature. Thus, damping vibrations of exhaust gases temperature takes place, flowing through the device.

The main structural component of damper of temperature variations – is heat storage material. Thus, the paramount priority is to choose the most suitable one.

It is worthwhile to choose substances for heat storage material, which are not degradable in smelting and not dissolvable in spill water. They are crystallizing as separate crystals, featuring comfortable melting temperature from the exploitation point of view, high definitions of latent heat of transition curve, heat conduction coefficient and specific heater in solid and liquid phases, low price, sufficient level of safety during operation, etc. Optional limitations connected with the damper construction are possible [4].

New materials are offered by now, providing approximately any level of melting temperature within the range of exhaust gases temperatures. Salinas and bases – are the most numerable and investigated substances for heat storage. They are used for heat accumulation for both exhaust gases and chemical reactor of oxidation catalyst. Moreover in the original form, binary and trinary systems of salinas and bases, the melting temperature can be more suitable. Finally, the price of such composed substance is much lower than the pure one, as it consists of the composition of expensive and cheap substances [5].

For heat energy accumulation the following bases are appropriate: lithium, sodium, potassium hydroxide, different binary systems composed of bases. Lithium hydroxide is considered to be the best among 400 analyzed heat-storage substances [6]. However, while choosing salinas and bases, it is important to take into account their excessive corrosion aggressiveness, typical for crystalline hydrates, alteration of volume during smelting and low conductivity. Nitrates are also used, as they are low-melt and resistible in the air molecular entity, nevertheless their fundamental defect –is explosive risk. From the point of view of productive heat transmission, it is possible to use alloys as heat-storage material. In comparison with salinas, alloys possess the same melting equivalent.

Except for inorganic compound in working systems with the temperatures up to 120C, different organic materials, as heat storage materials, can be used, for example: polyoxyethylene glycol, octadecane.

Nowadays, mixtures and alloys of organic and nonorganic substances are considered for usage, allowing to provide necessary melting temperature and longtime working lifespan. Slastilova S.V. [7] and some other researchers investigate heat-storage materials on the basis of aluminium, cuprum, silicon, magnesium alloys. Tests results showed the concordance of such heat-storage material to major requirements.

While examining exhaust gases, on the output of conventional engine and then following through damper of temperature variations, we deal with flow of matter, which means – open thermodynamic system. As the gas flow through the damper of temperature variations is accompanied with heat transmission from exhaust gases to working medium of damper of temperature variations (heat-storage material) or vice versa, from heat-storage material to exhaust gases, and their movement is rather fast, so basically the process is unbalanced. However making a suggestion about quasi-equilibrium (the following suggestion concerning exhausting process is related to the second order of approximation [8], one can use thermodynamic relations for stationary state and obtain major processes characteristics, free of nonequilibrium state.

2. Experimental results of usage of heat-storage material.

During the development of numerical scheme, we got the simultaneous differential equations, which described heat exchanging process in damper of temperature variation with phase transition. Adequacy of the suggested physico- mathematical model is proved with help of testing researches [9]. The experiment with the help of software suit MathCAD was made to estimate characteristics of heat-storage material for thermodynamic processes in damper of temperature variations.

The detailed formula depends on type of tasking and bank of initial data. While obtaining the observed characteristics of operation mode in actual environment of exploitation of conventional engine, the research discovered the influence of major design values of damper of temperature variations and features of some heat-storage materials on temperature smoothing of exhaust gases and their energy datum.

Characteristics of researched heat-storage materials are depicted in table 1.

Table 1. Major characteristics of researched heat-storage materials

Type of Heat-storage material	Melting temperature, K	specific thermal heat capacity of heat-storage material J/(kg·K)		Heat-transfer capacity of heat-storage material W/ (M·K)		mass density of heat-storage material kg/ m3
		Liquid state	Hard phase	Liquid state	Hard phase	
LiNO ₃	525	2040	2020	2,7	1,35	2360
LiOH	744	3900	3300	2,6	1.3	1460
NaOH	591	2090	2100	1,8	0,92	2170
7NaNO ₃ /40NaNO ₂ /53KNO ₃	415	1860	1340	0,5	0,5	2146

Fig. 2 presents the average temperature and its variations of the researched heat-storage materials and exhaust gases on the output from the damper in 3 minutes from the working point of damper of temperature variations. The determined range (ΔT) shows corresponding thermophysical properties of heat-storage material and exhaust gases.

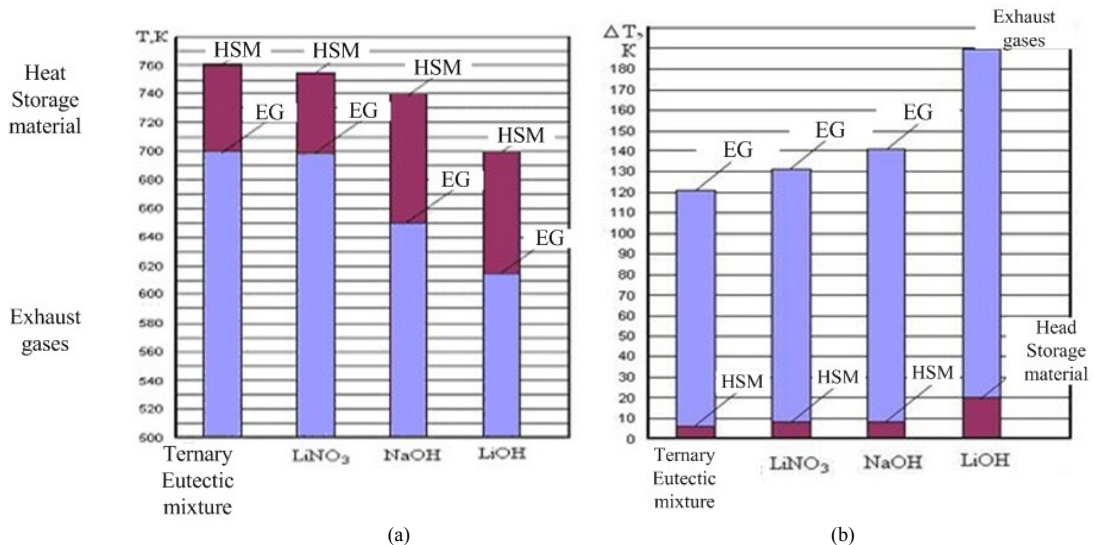


Fig.2. The average temperature and its variations of some heat-storage materials and exhaust gases on the output from the damper in 3 minutes from the working point of damper of temperature variations, a) – average values; b) – variations.

Obviously, the temperature of the heated heat-storage material is higher in case its thermal heat capacity is lower, under the conditions of the same temperature of exhaust gases and heat-transfer environment. The investigations discovered that the highest average temperature and dampening effect among viewed 4 heat-storage materials is reached by using ternary eutectic mixture $7\text{NaNO}_3/40\text{NaNO}_2/53\text{KNO}_3$ (760 K) и LiNO_3 (755 K).

The level of an average temperature of exhaust gases on the output from the damper of temperature variations is disproportional in correspondence with an average temperature of the considered heat-storage materials. Probably, it is connected with diverse heat transfer capacity of the used materials. Determined ranges ΔT are due to corresponding thermophysical properties of heat-storage materials and exhaust gases.

Thus, we can conclude that heat-storage material has an influence on dampening of temperature variations and energy datum of exhaust gases. Considered characteristics of temperature variations of different heat-storage materials and exhaust gases on the output from damper of temperature variations mostly depend on thermophysical properties of heat-storage material and they are extremely important for dampening of temperature variations of combustion material before their penetration into the oxidation catalyst. Dampening of temperature variations is of main interest in case the heat on the output of damper of temperature variations of exhaust gases is used for starting the utilization engine.

References.

- [1] V.S. Kukis, *Sistemno-termodynamicheskie osnovy primeniya dvigatelya Stirlinga dlya povysheniya effektivnosti silovyykh i teploispolzuiuschiykh ustanovok mobilnoy tekhniki*. Thesis, D.Sc. of engineering, Chelyabinsk, 1989.
- [2] V.A. Romanov, V.S. Kukis, *Povyshenie moshnostnykh, ekonomicheskikh i ekologicheskikh pokazateley porshnevuykh DVS putem ispolzovaniya sistem akkumulirovaniya energii*, *Dvigately vnutrennego sgoraniya*, kharkiv: University of Science and technology. 1 (2007) 53–56.
- [3] V.A. Kozminykh, *Issledovanie ellemenov sistemy utilizatsii teploty na baze dvigatelya Stirlinga dlya avtomobilnoy tekhniki*, Thesis, Cand. Tech. Sc., Chelyabinsk, 1994.
- [4] V.D. Levenberg, *Akkumulirovanie tepla*, Nauka, Moscow, 1991.
- [5] G. Bekman, P. Gilli, *Teplovoe akkumulirovanie jenerгии*, Mir, Moscow, 1987.
- [6] M.M. Kenisarin, *High-temperature phase change materials for energy storade*, *Renew Sustain Energy Rev.* (2009). DOI: 10.1016/j.rser.2009.11.011.
- [7] S.V. Slastilova, *Razrabotka materialov dlya teplovykh akkumulyatorov s ispolzovaniem teploty phasovogo perekhoda*, ThesisCand.Tech.Sc., Moscow, 2000.
- [8] A.M. Gorshkov, Z.N. Nestratova, A.G. Podolskiy, *Processy v otkrytykh termodynamicheskikh sistemakh*, *Mashinosroeniie*. 9 (1987)

45–51.

- [9] A.V. Raznoshinskaia, Povyshenie effektivnosti utilizatsii teploty I neutralizatsii otrabotavshikh gazov porshnevykh DVS putem demphirovaniya kolebaniy ikh temperatury: thesis, Cand.Tech.Sc., Chelyabinsk, 2005.
- [10] V.A. Kozminykh, A.V. Raznoshinskaia, V.A. Shibanova, Programma rascheta termodinamicheskikh processov v teplovom akkumuliatore, ustanovlennom v sisteme utilizatsii teploty otrabotavshykh gazov DVS, Nauchnyi vestnik. 16 (2003) 16–20.



International Conference on Industrial Engineering

Mathematical modeling of fuel flow in channels cone spray

Goun V.S.*, Morozova V.S., Polyacko V.L.

South Ural State University, 76 Lenina Avenue, Chelyabinsk 454080, Russian Federation

Abstract

The method of numerical flow simulation in diesel engine spray devices channels is reviewed in the article. The efficiency of conformal mappings use for converting the flow domain to a parametric rectangle with orthogonal grid is declared and illustrated. In this method, the reduced boundary value problem for Navier-Stokes equations for velocity and pressure fields is solved in this rectangle. The numerical conformal mapping, based on Finite Element Method (FEM) is described. Boundary value problems of Laplace equations for real and imaginary component of mapping function are solved by FEM algorithm. The proposed simulation and qualitative estimation method for various configurations of the flow channel of the spray head is analyzed in the article. The influence of the angle of deflection from the axis channel sprayer nozzle on the flow velocity in the channel is described. The capacities of a software package for numerical conformal mapping are presented.

© 2015 The Authors. Published by Elsevier Ltd. This is an open access article under the CC BY-NC-ND license (<http://creativecommons.org/licenses/by-nc-nd/4.0/>).

Peer-review under responsibility of the organizing committee of the International Conference on Industrial Engineering (ICIE-2015)

Keywords: spray cone, viscous flows, Navier-Stokes equations, conformal mapping

1. Introduction

Fuel system is an important element affecting the quality of the working process of a diesel engine. Improvement of this system allow improve the flow and fuel spraying in the cylinders to enlarge performance, cost efficiency and reduce emissions. Currently, in the calculation of the flow of the spray devices is widely used the methods of numerical experiment (Computational Fluid Dynamic - CFD). It can take the place of additional analysis approach to the methods

*Corresponding author. Tel. +7 902 612 7854; fax: +8 351 267 9416.

E-mail address: gunvs@susu.ac.ru

and software, based on the calculation of the one-dimensional unsteady flow in pipelines and fuel balance equations with corresponding boundary conditions [1]. Methods of numerical experiments allow for a closer look at those elements of the equipment of fuel supply in which the possibility of one-dimensional approach is not enough [1 – 7].

2. Methods

The CFD is possible to estimate the flow rates and spray nozzles for a whole variety of structures: with the holes in the channel and cone injector nozzle. It is known that with an increase speed of stream the separation of the boundary layer is formed. It becomes substantially dependent on phase transitions and in the areas of gas at a pressure close to zero This phenomenon is close to the cavitations regime. Isolated in the vortex zones gases increase their volume, decreasing the real net area of the main stream. The check of applicability of the software ANSYS CFX [2] for the numerical calculation of the flow in the channels of the fuel injector [16] showed that the CFD-simulation gives good results, which is especially valuable for individual geometry nozzles. According to the results of this work it can be concluded that the calculations allow analyze unconventional geometry, but so far with low accuracy. In particular, the main error of the accuracy of the assessment should be considered as the field of joining separated boundary layer in the spray hole [1,3,10,15].

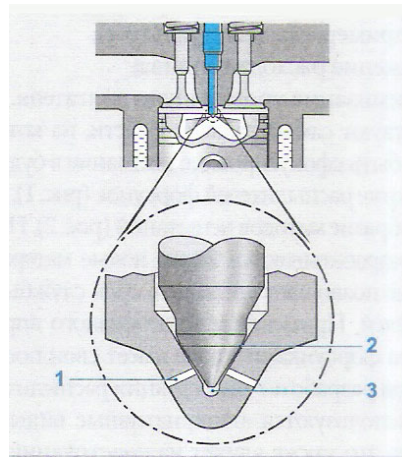


Fig. 1. 1.- channels spray, 2.- stop needle, 3.- a sub-space.

In the most general case for hydrodynamic problems it is necessary to solve a system of four Navier-Stokes equations expressing the basic laws of conservation of mass, momentum, and energy in differential form [8,9].

In this paper we summarize the implementation of one of the subsystems of the simulation of such processes - numerical conformal mapping of an arbitrary simply connected region on the parametric rectangle. It is necessary to note the advantages of the proposed approach [11,15].

Separately solved complex accounting issues form the source region and the choice of computational models of processes. They are designed for a standard parametric area - rectangle with a wide range of proven numerical schemes. It's not necessary to transfer boundary conditions in the nodes of difference nets on the borders of a complex shape

- the advantages of the method of finite differences are manifested. The coordinate splitting scheme (variable direction, subincremental method, etc.) with a high degree of parallelism are applicable;
- different equations describing numerical model of the flow (the Navier - Stokes equations, thermal conductivity, and others.) can be solved by the best way for them, each in its own grid of high order of accuracy;
- it is possible to enter a specialized grid with the dramatic changes in the decision-time different areas (for example, the boundary layer at the boundary of the flow jumps up-compacting, etc.);

- it is convenient to perform various operations with fields calculated values (temperatures, pressures, velocities), to display various graphics systems, to differentiate, interpolate, integrate, calculate the gradients, translate into a different, etc.

The mapping function (Fig. 2) is sought in the form of a set of values of the coordinates (x, y) points of the transition region at the grid box parameter plane (φ, ψ), so that every point with the coordinates (x, y) moves the conformal mapping at the position (φ, ψ). On the contrary, every point with the coordinates (φ, ψ) goes in the reverse conformal mapping to the point with the coordinates (x, y). This formulation does not require an explicit expression implementing such a map, assuming that the image of any point of the rectangular area (φ, ψ) may be obtained by interpolation on the grid nodes.

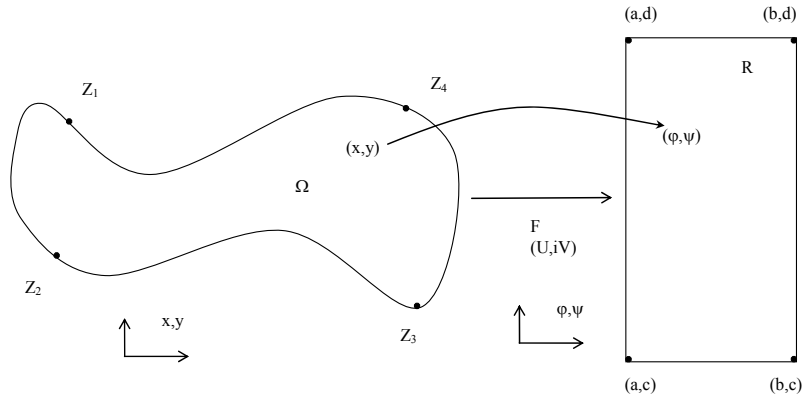


Fig. 2 Transition to the parametric computational domain - a rectangle.

We define a mapping analytical function as solutions of boundary value problems for the Laplace equation in the form of a numerical calculation of harmonic functions that make up its real and imaginary components.

Suppose that the desired map region $Z_1Z_4Z_2Z_3$ plane coordinates (x, y) on the rectangle (a, c), (b, c), (b, d), (a, d) coordinates (φ, ψ) is implemented by the functions $\phi = \phi(x, y)$ $\psi = \psi(x, y)$.

Solve the following boundary value problems:

- a) for the imaginary component of the mapping function

$$\begin{cases} \Delta \psi = 0 & : Z_1Z_4Z_2Z_3 \\ \psi = \psi_1 & : Z_2Z_3 \\ \psi = \psi_2 & : Z_1Z_4 \\ \frac{\partial \psi}{\partial n} = 0 & : Z_1Z_2 \\ \frac{\partial \psi}{\partial n} = 0 & : Z_3Z_4 \end{cases} \quad (1)$$

where: ψ_1 and ψ_2 – ordinates of the rectangle in the parametric region Δ – Laplace operator: $\Delta = \frac{\partial^2}{\partial x^2} + \frac{\partial^2}{\partial y^2}$

The first two boundary conditions of the system (1) reflect the assignment of the ordinate component in the upper and lower boundaries of the region $\Omega:Z_1Z_4Z_2Z_3$, passing into the upper and lower limits direct-rectangle (a, d), (b, d), (a, c), (b, c), the next two the condition of orthogonal lines-level functions of the left and right borders of the region $Z_1Z_4Z_2Z_3$, passing to the left and right sides of the rectangle. These values are based on the characteristics of the processes in the region Ω .

b) for the real components of the mapping function:

$$\begin{cases} \Delta\varphi = 0 & : Z_1Z_4Z_2Z_3 \\ \varphi = \varphi_1 & : Z_1Z_2 \\ \varphi = \varphi_2 & : Z_3Z_4 \\ \frac{\partial\varphi}{\partial n} = 0 & : Z_1Z_4 \\ \frac{\partial\varphi}{\partial n} = 0 & : Z_2Z_3 \end{cases} \quad (2)$$

It is similar to (a), the first two boundary conditions of the system (2) express reference abscissa components φ on the left and right borders of the region Ω : $Z_1Z_4Z_2Z_3$, passing to the left and right sides of the rectangle (a, d), (b, d), (a, c), (b, c). The next two boundary conditions of the lines orthogonally level functions $\phi = \phi(x, y)$ of the upper and lower boundaries of the region $Z_1Z_4Z_2Z_3$, transitions in the upper and lower bounds of the rectangle. The value of the abscissa the left side of the rectangle can also be set arbitrarily, the preferences of the problem being solved.

The boundary problem (1) – (2) are solved software package, designed for both work in the systems of numerical modeling of processes in two-dimensional (flat and with axial symmetry) range and autonomously. Components of the mapping function sought by solving the boundary value problems (1) – (2) by the Finite Element Method [12,13,14]. In particular, by means of the software package the following tasks:

- finding images of the points (x, y) the physical plane, passing under the mapping in a given grid (ϕ, ψ) on a parametric rectangle;
- finding images of points (ϕ, ψ) given grid on parametric rectangle on the physical plane (x, y) ;
- calculation of partial derivatives $\frac{\delta X}{\delta \phi}, \frac{\delta X}{\delta \psi}, \frac{\delta Y}{\delta \phi}, \frac{\delta^2 X}{\delta \phi^2}, \frac{\delta^2 X}{\delta \psi^2}, \frac{\delta^2 Y}{\delta \phi^2}$ and Lamé coefficients at these points.

In developed using this approach, the software package is solved full system Navier-Stokes equations, supplemented by \square supplemented rheological equations, regarding the pressure, density, velocity and temperature in the flow of the fuel mixture (channel with the spray nozzle hole). This allows to obtain the distribution of pressures, temperatures and flow rates at any point in the region Ω , without limit its geometry, boundary conditions (friction, adhesion) and in a sufficiently wide range of fuel mixtures.

3. Results

Examples of opportunities of this method (Fig. 3-5).

The proposed method allows to directly evaluate the quality of profiling channel nozzles preliminary design without solving boundary value problems in a "viscous" approximation to the calculation of the real mass and heat transfer in the channels of the nozzles.

Evenly, without sudden expansion and contraction of the distribution of the current lines with a small change of vectors in magnitude and direction indicates a low variability of flow, "smooth" flow through the channel of the nozzle. The uneven, with areas of expansion, and contraction about the difficulties during the high hydraulic resistance of stagnant zones, possible cavitation and phase transformations boiling, the emergence and collapse of gas (cavitation) cavities. It allows preliminary assessment of the operation of the projected channel injector without a precise calculation of the flow.

The specifics of solutions of such problems is the presence of the point of rapid change in velocity of flow both in direction and magnitude. Therefore, for the calculation of the flow in such areas in the developed software package is used a number of measures, giving improved accuracy solutions.

- local mesh refinement of finite element at the points of rapid change solutions;
- the use of special types of finite element interpolation function ("singular" functions).

For the calculation of the current applied both techniques. Note that the estimated time example (≈ 2500 nodes 400 elements) is 1.5 min (Celeron 3 GHz, 1 core, 2 GB DDR – 1 RAM).

Fig. 3–5 – illustrate the simulation of fuel injectors in the channel at different angles channel sprayer. speed (flow) in the left section adopted the same (section A-B).

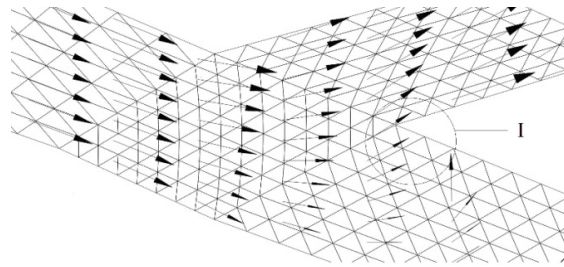


Fig. 3. The velocity field of the flow of fuel to the nozzle channel while changing the tilt spattering holes (small angle of inclination).

Fig. 3 shows a relatively uniform, with low turbulence flow at small angles of inclination (I) channel from the axis of the sprayer nozzle. Grading speeds (shown by the magnitude of the vector velocity field) is relatively minor. Noteworthy leaking the mixture in a sub-part of the nozzle to form a reverse flow in it. Chance cavitation is negligible. The velocity field is relatively uniform, and in the section marked deceleration of the flow does not occur.

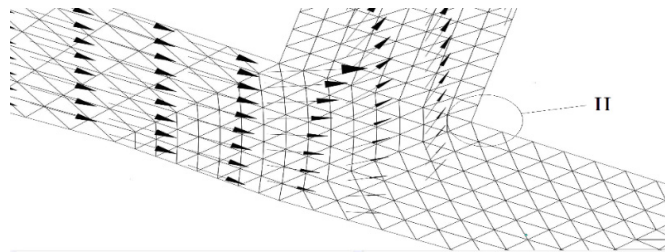


Fig. 4. The velocity field of the flow of fuel to the nozzle channel while changing the tilt spattering holes (average angle of inclination).

Fig. 4 shows the flow at the growth angle (II) from the axis of the channel spray nozzle. Growing unequal distribution of velocity over the cross section of the channel interface. □ Reduced leaking the mixture in a sub-part of the nozzle to form in it the return flow. It increases the likelihood of cavitation. The velocity field loses uniform, observed flow breakdown at the interface point between the channel from the current flow streams with pursed.. Noticeable deceleration of the flow with an increase in resistance and a decrease in the flow.

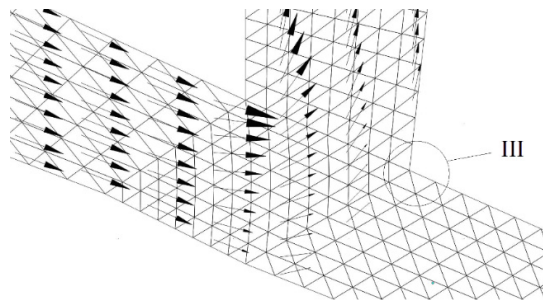


Fig. 5. The velocity field of the flow of fuel to the nozzle channel while changing the tilt spattering holes (tilt angle is maximum)

Fig. 5 shows the flow at the maximum angle of inclination (III) from the axis of the channel spray nozzle. The uneven distribution of velocities over the cross section channels is maximum. Leaking the mixture into a sub-nozzle portion to form therein backflow is absent. High probability of cavitation in place stall. The velocity field is very fragmented, there is separation of the flow at the point of cross section channels from the current high preload effective flow. Large value inhibition with increasing flow resistance and a decrease in the flow.

4. Conclusions

- 1) A method for the calculation of viscous flow in channels of complex shape. The efficiency of the method of conformal mappings to convert the flow region in a parametric rectangle with orthogonal grid. Demonstrate the application of the proposed method for the calculation and qualitative evaluation of various configurations of the flow channels of the cone spray.
- 2) The proposed method of formation of "computational domain" to solve the basic boundary value problems, an assessment of the quality grading channel nozzles. This capability is based on the hydrodynamic interpretation of analytic functions of two variables realizing the conformal mapping.

References

- [1] L. Sin, N.A. Ivashchenko, V.I. Markov, LV fuel equipment and diesel engine management systems, Legion Avtodata, 2005.
- [2] ANSYS CFX v.12. Release. Theory Reference.
- [3] J.H. Ferziger, M. Perić, Computational Methods for fluid Dynamics, third ed., Springer, Berlin, 2002.
- [4] B.I. Trusov, V.P. Dmitrienko, Injectors automotive diesel, Mashinostroenie, Moscow, 1977.
- [5] L. Sin, N.A. Ivashchenko, V.A. Markov, Fuel equipment and diesel engine management systems: a textbook for high schools, Legion Avtodata, 2004.
- [6] N.A. Ivashchenko, V.A. Wagner, L. Sin, Modeling of fuel and design of diesel fuel equipment, Publishing House of the Altai State Technical University them. Polzunov, Moscow, 2002.
- [7] I.I. Gabitov L. Sin, A.B. Negovora, Maintenance and diagnostics of fuel equipment for auto-tractor diesel engines: a tutorial, Izd BSAU, Ufa, 2008.
- [8] Y.E. Dragan, The treatment of the compressibility of the fuel rods and deformation in the mathematical modeling of electro-injectors, Ukrainian scientific and technical journal "Internal combustion engines". 2 (2007) 35–39.
- [9] I.V. Astakhov, V.I. Trusov, A. Khachiyan L.N. Golubkov, Podacha and atomization of fuel in diesel, Mechanical Engineering, Moscow, 1971.
- [10] V.S. Morozova, Returnless fuel process: dis. ... Dr. tehn, MSTU. NE Bauman, Moscow.
- [11] V. Goun, V. Bunov, A. Goun, Modelling of Time-Depending Heat Transfer in complex Shaped Axi-Symmetrical Bodies for Automotive Applications, SAE. (1996) 960377.
- [12] J.F. Thompson, B. Soni, N. Weatherill, Handbook of grid generation, CRC Press, NY, 1998.
- [13] L. Segerlind, Application of the finite element method, Mir, Moscow, 1979.
- [14] A.I. Markushevich, Brief course in the theory of analytic functions, Mir, Moscow, 2006.
- [15] K.N. Ryss, A.A. Denisov, L. Sin, Y.A. Grishin, Estimated forecasting flow characteristics of diesel spray-term fuel equipment, Proceedings of Volgograd State Technical University. 5-12(115) (2013).
- [16] V.S. Morozova, V.S. Gong, V.L. Polyatsko, The method of calculation of viscous media channels odds spray-ures diesel, Bulletin of the South Ural University endowment gosu-Series Engineering. 13(2) (2013) 75–80.
- [17] N. Papamichael, Lectures on Numerical Conformal Mapping, University of Cyprus, 2008



International Conference on Industrial Engineering

Results of vortex tube usage in diesel exhaust gas recirculation system

Kukis V.S.^{a*}, Omelchenko E.A.^b, Raznoshinskaia A.V.^c

^a18 - L. Chaikinoy Str., Apt 3, Chelyabinsk, Russia. 454129

^b63 - 2 Poselkovaya Str., Apt 149, Omsk, Russia. 644050

^c38B - 40 Let Pobedy Str., Apt 82, Chelyabinsk, Russia. 454021

Abstract

The article outlines the results of vortex tube usage in exhaust gas recirculation system of diesel 4ЧН13/15. It presents main functional features of a vortex tube. It is shown that the usage of the tube allows reducing the temperature of recirculated gas up to 60 °C and significantly diminishes the content of nitrogen oxide and particulate matter in exhaust gases of an engine at general operation modes, conforming to the Rule of Economic Commission for Europe Organization of United Nations #96.

© 2015 The Authors. Published by Elsevier Ltd. This is an open access article under the CC BY-NC-ND license (<http://creativecommons.org/licenses/by-nc-nd/4.0/>).

Peer-review under responsibility of the organizing committee of the International Conference on Industrial Engineering (ICIE-2015)

Keywords: Diesel, exhaust gas, noxious substances, toxicity, vortex tube, temperature.

1. The research of vortex tube usage in exhaust gas recirculation system

In virtue of some diesels working processes peculiarities actions, aimed at wastes diminution of unburnt combustibles, carbon oxide, hydrocarbon and harmful particles are accompanied by the growth of nitrogen oxide emissions and vice versa. Then to provide an appropriate diesel work in accordance with functioning and long-term standards of toxicity, there is an urge to use methods of reduction of noxious substances, including the combination of exhaust gas recirculation system with cooling of recirculated gas and exhausted gas aftertreatment [1].

It is worth mentioning that the creation of a reliable and effective heat transfer device for recirculated gas cooling is a challenge due to the stratum and pollutants, extracted from exhausted gas of diesel.

* Corresponding author. Tel.: +7-951-810-24-11.
E-mail address: idem37@mail.ru

From this perspective the vortex tube is of considerable interest, which can be used for cooling the recirculated gas [2,3]. Vortex tubes, presenting the devices where Ranque-Hilsch Effect takes place, allow to divide the stream of compressed liquid (dripping and elastic) in 2 constituents: cold and warm, widely used in different spheres of engineering [4]. These are simple, reliable and cheap devices, with no nonferrous metal in it (as common regenerative heat-exchange units), featuring insignificant water resistances, demanding simple maintenance.

An important feature of applying vortex tube in exhaust system is both cooling of recirculated gas and provision of comfort temperature of exhaust gas on the input in oxidation catalyst to provide an efficient operation at all diesel functioning modes.

The article presents the results of experimental estimate of usage of vortex tube to increase the efficiency of exhaust gas recirculation system on the diesel 4FH13/15.

Experimental assembly. System diagram of exhaust gas recirculation and after treatment with placement locations of sensors (Fig. 1).

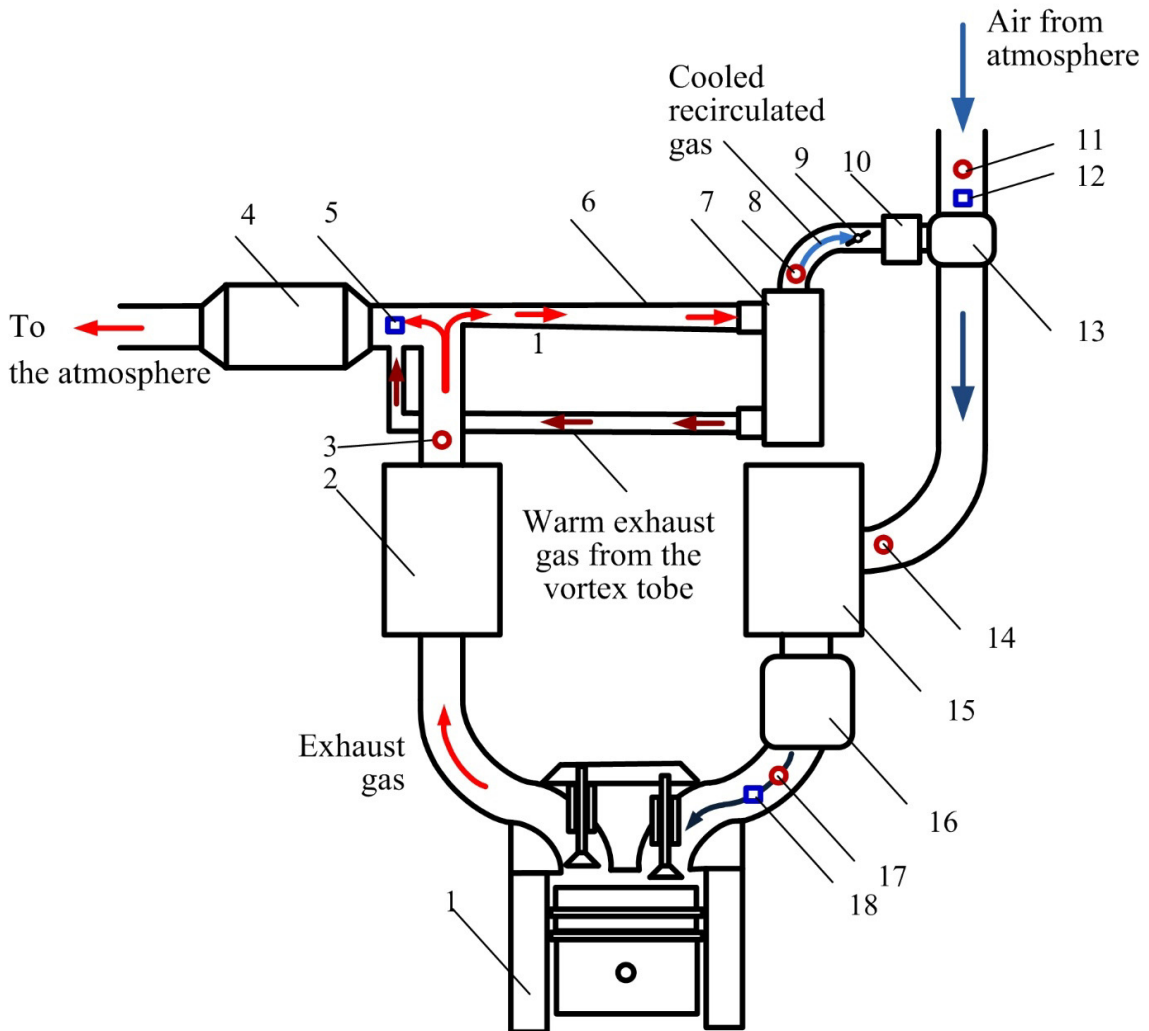


Fig. 1. System diagram of exhaust gases recirculation and after treatment:

1 – diesel; 2 – gas turbine; 3, 8, 11, 17 – temperature sensing points; 4 – oxidation catalyst, 5, 12, 18 – pressure sensing point; 6 – exhaust gases feeder to vortex tube; 7 – vortex tube; 9 – clapper, controlling the volume of recirculated gas; 10 – consumption indicator; 13 – gas converter; 15 – compressor, 16 – charge air cooler.

General engineering characteristics of vortex tube, optimized for operating conditions in exhaust gas recirculation system diesel 4CH13/15, as follows in Table 1, Fig. 2 displays its circuit diagram and physical form.

Table 1. General engineering characteristics of vortex tube

Engineering characteristics	Unit of measurement	Parameters
Body length of vortex tube	m	0,5
Body bore of expiratory fitting of cooled exhaust gas flow	m	0,037
Overall opening diameter of port for air flow of warmed exhaust gas	m	0,1
Port bore for air flow of warmed exhaust gases, in case of temperature drop up to 60 K	m	0,097
Area of exhaust gas inlet fitting in vortex	m ²	0,11·10 ⁻²
Restriction of body bore diameter	degree	7

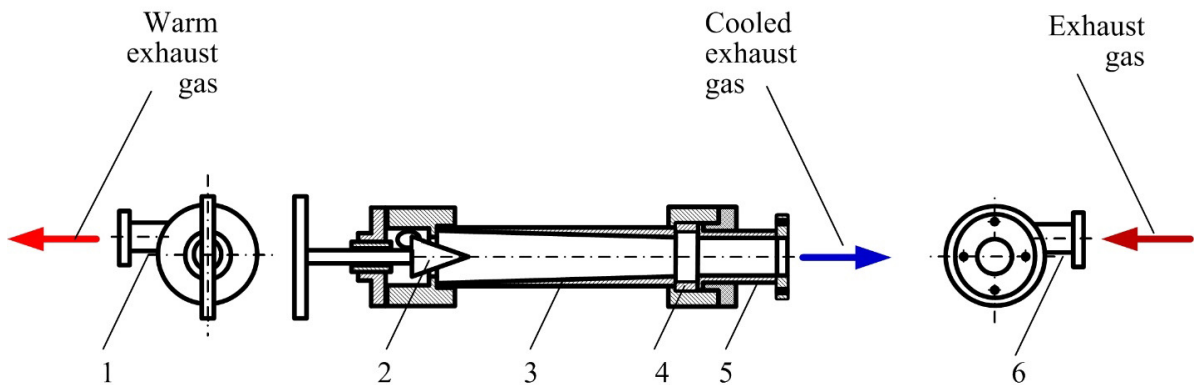


Fig. 2. Vortex tube,

a – circuit diagram of the vortex tube: (1 – expiratory fitting of air flow of warmed exhaust gas; 2 – throttle flap; 3 – body; 4 – vortex; 5 – expiratory fitting of cooled exhaust gas flow; 6 – inlet fitting of exhaust gas in vortex); b – physical form.

Exhaust gas recirculation system with the vortex tube provides the ability to control the volume flow of recirculated gases within the range not less than 0-20% from the volume flow of inlet charge and maximum temperature fall of recirculated gas at 60K relatively the temperature of exhaust gas, penetrating into the vortex tube.

2. Experimental results of the implementation of cooling of recirculated gas.

During the experimental research of emissions release of diesel 4CH13/15 with their recirculation and cooling, we started out from toxicity index of particulate matter being twice higher than nitrogen oxide, 10 times higher than carbon hydride, and 20 times than carbon oxide [5], aggressivity coefficient of nitrogen oxide (49) and particulate matter (41,5) surmount greatly the aggressivity indexes of carbon hydride (1,26 and 1,0 relatively) [6]. Taking into account the above mentioned data and the circumstance that the pilot experiments proved that carbon oxide and carbon hydride content in diesel 4CH13/15 exhaust gases is much lower of the standardized values, in further research works we restricted to the estimation of particulate matter and nitrogen oxide exhaust.

In determining of the influence of exhaust gas recirculation system functioning on the content in exhaust gas diesel 4CH 13/15 of particulate matter and nitrogen oxide, we also estimated the quantity contribution and temperature of recirculated gas during its general modes operation, corresponding to the Rule of Economic Commission for Europe Organization of United Nations #96

Implementation of cooling of recirculated gas naturally leads to certain temperature fall of incoming charge on the input to cylinder barrels, resulting in content fall in exhaust gases of nitrogen oxide (by means of temperature fall of working body in cylinder), and particulate matter (taking into account density of incoming charge, penetrated into the cylinder, consequently boosting coefficient of excess air). (Table 2)

Table 2. The content of nitrogen oxide and particulate matters in exhaust gases of diesel 4QH13/15 during its general modes operation, corresponding to the Rule of Economic Commission for Europe Organization of United Nations #96 (share of recirculated gases is 18%; cooling of recirculated gas up to 60 °C).

Mode	Content NO _x [ppm]			Content PM [g/m]			
	Original	Recirculation added	Recirculation and cooling added	Original	Recirculation added	Recirculation and cooling added	
n = 1850, min ⁻¹	Load 100 [%]	250,2	75,5	71,7	39,1	51,9	51,5
	Load 75 [%]	149,8	50,1	44,3	17,5	32,3	31,1
	Load 50 [%]	121,1	18,0	14,6	5,6	13,8	10,5
n = 1250, min ⁻¹	Load 100 [%]	712,4	190,1	173,8	139,4	142,4	139,1
	Load 75 [%]	370,8	100,7	88,8	111,0	119,1	114,8
	Load 50 [%]	38,2	10,4	8,7	40,3	49,5	45,3

The data from the table depict, that the organization of exhaust gas recirculation appeared to influence positively on reduction of content in exhaust gas of nitrogen oxide, however it led to some growth of the general flow of particulate matter. Implementation of recirculated gas cooling provided NO_x abatement and some decrease of particulate matter emissions, quantitative concept is illustrated in the Table 3.

Table 3. The content of nitrogen oxide and particulate matters in exhaust gas of diesel 4QH13/15 by means of cooling of recirculated gas at 60 °C during its general modes operation, corresponding to the Rule of Economic Commission for Europe Organization of United Nations #96 [%]

Mode					
n = 1850 min ⁻¹			n = 1250 min ⁻¹		
Load 100 [%]	Load 75 [%]	Load 50 [%]	Load 100 [%]	Load 75 [%]	Load 50 [%]
<i>Nitrogen Oxide</i>					
5,1	11,6	18	8,5	11,8	16,3
<i>Particulate matter</i>					
0,08	3,7	16,3	2,3	3,6	8,5

Results of the conducted work witness of the possibility and reasonability of using heat pipes in exhaust gas recirculation system. Thus appliance of the vortex tube in this system in diesel 4QH13/15 in case of temperature reduction of recirculated gas at 60 °C with their share in incoming charge 18 % allowed to low nitrogen oxide and particulate matter emissions on the modes, typical for road building machines (75 % load) at 11.6 and 3.7 % relatively.

Going further, authors aim to estimate the positive influence of incoming charge cooling by using vortex tube with exhaust gas recirculation at effective fuel rate and possibility to provide an optimal temperature of exhaust gas on the input to oxidation catalyst for its effective functioning during different operation modes of an engine.

References.

- [1] V.S. Kukis, Sistemno-termodynamicheskie osnovy primeniya dvigatelya, Stirlinga dlya povysheniya effektivnosti silovykh i teploispolzuiuuschikh ustanovok mobilnoi tekhniki, Thesis, D.Sc. of engineering, Chelyabinsk, 1989.
- [2] V.A. Romanov, V.S. Kukis, Povyshenie moshchnostnykh, ekonomicheskikh i ekologicheskikh pokazatelei porshnevukh DVS putem ispolzovaniya sistem akumulirovaniya energii, Dvigately vnutrennego sgoraniya, kharkiv: University of Science and technology. 1 (2007) 53–56
- [3] V.A. Kozminykh, Issledovanie ellemenov sistemy utilizatsii teploty na baze dvigatelya Stirlinga dlya avtomobilnoy tekhniki, Thesis, Cand. Tech. Sc., Chelyabinsk, 1994.
- [4] V.D. Levenberg, Akkumulirovanie tepla, Nauka, Moscow, 1991.
- [5] G. Bekman, P. Gilli, Teplovoe akumulirovanie jenerгии, Mir, Moscow, 1987.
- [6] M.M. Kenisarin, High-temperature phase change materials for energy storade, Renew Sustain Energy Rev. (2009). DOI: 10.1016/j.rser.
- [7] S.V. Slastilova, Razrabotka materialov dlya teplovykh akumulirovateley s ispolzovaniem teploty phasovogo perekhoda: ThesisCand.Tech.Sc., Moscow, 2000.
- [8] A.M. Gorshkov, Z.N. Nestratova, A.G. Podolskiy, Processy v otkrytykh termodynamicheskikh sistemakh, Mashinosroeniie. 9 (1987) 45–51.

- [9] A.V. Raznoshinskaia, Povyshenie effektivnosti utilizatsii teploty I neitralizatsii otrabotavshikh gazov porshnevykh DVS putem demphirovaniya kolebaniy ikh temperatury: thesis, Cand.Tech.Sc., Chelyabinsk, 2005.
- [10] V.A. Kozminykh, A.V. Raznoshinskaia, V.A. Shibanova, Programma rascheta termodinamicheskikh processov v teplovom akkumuliatore, ustanovlennom v sisteme utilizatsii teploty otrabotavshykh gazov DVS, Nauchnyi vestnik, Chelyabinsk: CHVAI. 16 (2003) 16–20.



International Conference on Industrial Engineering

Forces of friction at the wheel-to-ground contact in a turning vehicle

Troyanovskaya I.P.^{a,b*}, Pozin B.M.

^aSouth Ural State University, 76, Lenin Avenue, Chelyabinsk, Russia

^bSouth Ural State Agrarian University, 75, Lenin Avenue, Chelyabinsk, Russia

Abstract

Forces of friction appear when the wheel of a moving vehicle contacts the ground during. Curvilinear movement of a vehicle is of special interest. The moment of friction appears during the turn in addition to the force of friction. In a turning vehicle the values of friction force and moment of friction depend on each other. The force increases when the moment decreases and vice versa. They are calculated in movement of instant rotation. The force of friction and moment of friction are functions of the coordinates of the instant center of the sliding. It allows to connect forces with the kinematics of movement.

Published by Elsevier Ltd. This is an open access article under the CC BY-NC-ND license (<http://creativecommons.org/licenses/by-nc-nd/4.0/>).

Peer-review under responsibility of the organizing committee of the International Conference on Industrial Engineering (ICIE-2015)

Keywords: forces of friction, the moment of friction, turn of the machine, sliding, the instant center of rotation, reaction of a ground.

1. Introduction

The main complexity of model of movement of the machine in turn consists in the correct description of reactions from the basis. The reality consists in aggregate forces and the moment of friction in contact of a wheel to a ground. Many authors consider total force of friction on turn of the machine maximal and enclosed in the center of contact [1, 2, 3]:

$$f_{\max} N = \sqrt{P_x^2 + P_y^2} . \quad (1)$$

In formula 1: P_x, P_y – a longitudinal and cross-section component of force of friction; N – normal reaction to a

* Corresponding author. Tel.: +7-951-113-76-30.

E-mail address: tripav@rambler.ru

wheel; f_{\max} – the maximal factor of friction.

Such approach contradicts laws of mechanics. We shall consider in detail process of summation of elementary forces of friction.

The full moment M equal to the sum of elementary forces dP_{mi} , various in a management. The total moment M is equal to the sum of the elementary moments which are equal to multiplication of elementary forces dP_{mi} and shoulders r_i : $M = \sum r_i dP_{mi}$ (figure 1,a).

Total force of friction P is the sum of other elementary forces of friction $P = \sum dP_{pi}$ (figure 1,b). All elementary forces dP_{pi} are identical on the module and a direction. If total force of friction is equal to the maximum $P = f_{\max} N$ then all elementary forces of friction making it too are equal to the maximum $dP_{pi} = f_{\max} dN_i$.

The resultant elemental force is the vector sum $d\vec{P}_i = d\vec{P}_{pi} + d\vec{P}_{mi}$ (figure 1,c). The sum of elementary forces cannot be more maximum $dP_i \leq f_{\max} N_i$ in each point [4]. If one elementary force dP_{pi} is equal to a maximum other elementary force dP_{mi} is equal to zero. Excess of the maximal force of friction in a point is not dependent on a way of calculation of the moment [5, 6, 7].

Force of friction can reach a maximum only in absence of the moment. That takes place at rectilinear movement. Force of friction less than the maximum on turn of the machine. Its value depends on size of the moment of friction. The situation takes place, that force of friction and the moment of friction [8, 9] in contact of a wheel to a ground] are connected with each other on turn of the machine.

Let's consider it more in detail.

2. Methodology

Each elementary force of friction dP is opposite to a direction of relative sliding. Each point of contact has its direction of speed sliding. It allows to reduce a problem in formation of forces in contact to kinematics of relative sliding.

How are forces of friction in contact of a wheel and road on turn formed? We shall consider it on the basis of the mathematical theory of friction [10]. The local system of coordinates OXY is connected with the center of contact (figure 2).

The axis OX is directed along movement of a wheel, but the axis OY is perpendicular. The elementary point with the area dF has in local system of coordinate ξ, η . Its speed of sliding V is directed perpendicularly to distance r up to the instant center of speeds (point C with coordinates x, y).

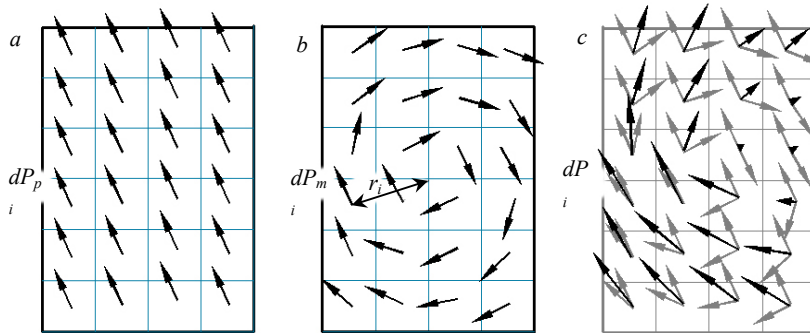


Fig. 1. Sum elementary forces of friction in contact:
(a) elementary forces dP_{pi} ; (b) elementary forces dP_{mi} ; (c) elementary forces dP_i .

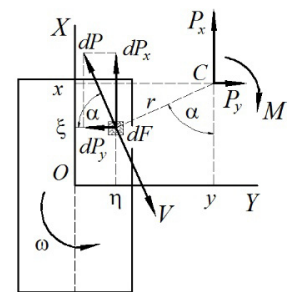


Fig. 2. Power factors of friction in contact of a wheel to a ground.

Projections of elementary force of friction dP to the axes OXY are equal:

$$dP_x = dP \sin \alpha \quad \text{and} \quad dP_y = -dP \cos \alpha . \tag{2}$$

We shall consider

$$r = \sqrt{(x-\xi)^2 + (y-\eta)^2}, \tag{3}$$

$$\sin \alpha = \frac{y-\eta}{r} \quad \text{and} \quad \cos \alpha = \frac{x-\xi}{r}, \tag{4}$$

The projection of elementary force of friction dP became equal:

$$\left. \begin{aligned} dP_x &= fq \frac{y-\eta}{\sqrt{(x-\xi)^2 + (y-\eta)^2}} dF, \\ dP_y &= -fq \frac{x-\xi}{\sqrt{(x-\xi)^2 + (y-\eta)^2}} dF. \end{aligned} \right\} \tag{5}$$

where $q = dN / dF$ is normal pressure in a point with coordinates ξ, η .

We have combined all elementary forces on the area of contact and led to their instant center of speeds [10]:

$$\left. \begin{aligned} P_x &= \iint_{\eta\xi} fq \frac{y-\eta}{\sqrt{(x-\xi)^2 + (y-\eta)^2}} d\xi d\eta, \\ P_y &= -\iint_{\eta\xi} fq \frac{x-\xi}{\sqrt{(x-\xi)^2 + (y-\eta)^2}} d\xi d\eta, \\ M &= \iint_{\xi\eta} fq \sqrt{(x-\xi)^2 + (y-\eta)^2} d\xi d\eta. \end{aligned} \right\} \tag{6}$$

The total force and the total moment in the center of contact resulted in the following:

$$P = \sqrt{P_x^2 + P_y^2} \quad \text{and} \quad M_o = M - yP_x + xP_y, \tag{7}$$

Force of friction P and the moment of friction of M_o are functions of coordinates (x,y) of the instant center of sliding. They depend on each other. Force increases, and the moment decreases and vice versa (figure 3).

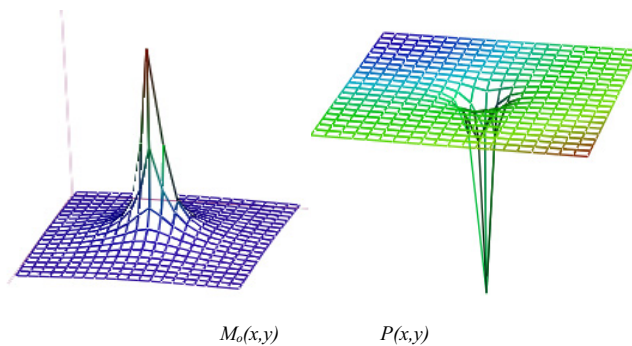


Fig. 3. Dependence of force of friction and the moment of friction.

Special cases take place [11]:

- rectilinear sliding (the instant center of speeds is in infinity) $x \rightarrow \infty$, и $y \rightarrow \infty$ $M_o \rightarrow 0$, $\sqrt{P_x^2 + P_y^2} \rightarrow \max$;
- turn sliding (the instant center of speeds coincides with the center of a spot of contact $x = y = 0$)
 $P_x = P_y = 0$, $M = \max$.

The factor of friction $f \leq f_{\max}$ is taken under integral and it makes it variable. This factor considers elastic properties of a ground and the trunk. Experimental dependence with elastic properties of the trunk and a ground is presented in figure 4 [12].

Dependence in figure 4 is described by different formulas at different authors [1, 6, 12, 13]. The best formula is the equation of Katsygin [12]. Advantages of this function are:

- it has smaller number of empirical factors;
- it describes both of a kind of a ground (a plastic ground and a friable ground).

The transformed kind of the formula is equal [14]:

$$f = f_{\delta} \left(1 + \frac{\chi}{\text{ch}(k_{\delta} / \lambda)} \right) \text{th} \left(\frac{k_{\delta}}{\lambda} \right), \tag{8}$$

where k_{δ} is relative sliding (slipping), λ, χ are experimental factors, f_{δ} is factor of friction at full slipping.

3. Results.

Power factors of friction in contact of a wheel with elastic properties of the trunk and a ground is equal:

$$\left. \begin{aligned} P_x &= \iint_{\eta\xi} f_{\delta} q \left(1 + \frac{\chi}{\text{ch}(k_{\delta} / \lambda)} \right) \text{th} \left(\frac{k_{\delta}}{\lambda} \right) \frac{y - \eta}{\sqrt{(x - \xi)^2 + (y - \eta)^2}} d\xi d\eta, \\ P_y &= - \iint_{\eta\xi} f_{\delta} q \left(1 + \frac{\chi}{\text{ch}(k_{\delta} / \lambda)} \right) \text{th} \left(\frac{k_{\delta}}{\lambda} \right) \frac{x - \xi}{\sqrt{(x - \xi)^2 + (y - \eta)^2}} d\xi d\eta, \\ M &= \iint_{\xi\eta} f_{\delta} q \left(1 + \frac{\chi}{\text{ch}(k_{\delta} / \lambda)} \right) \text{th} \left(\frac{k_{\delta}}{\lambda} \right) \sqrt{(x - \xi)^2 + (y - \eta)^2} d\xi d\eta. \end{aligned} \right\} \tag{9}$$

Friction factor changes the form of the dependence of the friction force P and the moment of friction Mo from each other (figure 5) [15].

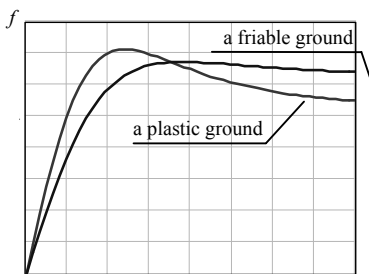


Figure 4. Experimental dependence of factor of friction

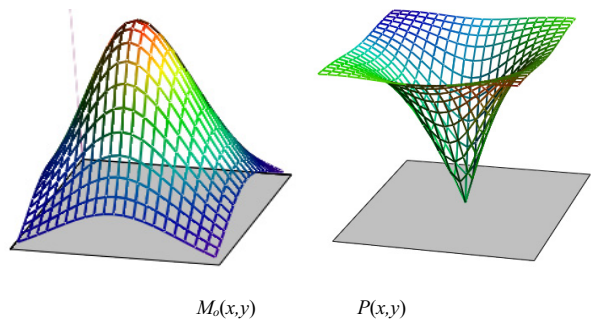


Figure 5. Dependence of force of friction and the moment of friction with elastic properties of the trunk and a ground

4. Conclusions

This approach is based on laws of mechanics and the mathematical theory of friction. It has some advantages:

- it allows to replace a problem by definition of forces in contact to a kinematic of movement by definition of coordinates of the instant center of sliding and it solves these problems in common;
- it describes each wheel individually in view of its sizes and the form of a spot of contact by limits of integration;
- it considers any law of normal pressure on a spot of contact;
- introduction of variable factor of friction considers elastic properties of a ground and the pneumatic wheel.

References

- [1] V.V. Larin, Methods of forecasting and increasing of basic passableness of the wheel machine with several leading axes on district, Dissertation of the doctor of technical sciences (Engineering), Moscow, 2007.
- [2] G.I. Gladov, Bases of the theory of curvilinear movement and designing of control systems by turn of supersize transport-technological units, Dissertation of the doctor of technical sciences (Engineering), Moscow, 1998.
- [3] G.A. Smirnov, The theory of movement of wheel machines, Mechanical engineering, Moscow, 1990.
- [4] S.M. Targ, A brief rate of theoretical mechanics, Graduate School, Moscow, 1986.
- [5] A.V. Shymilin, Method of definition of characteristics of turn of a wheel vehicle on not deformable basis, Journal: Tractors and agricultural machines. 8 (1993) 17–19.
- [6] V.A. Gorelov, Scientific methods improve safety and energy movement multiaxial wheeled transport system, Dissertation of the doctor of technical sciences (Engineering), Moscow, 2012.
- [7] U.L. Rojdestvenskiy, K.U. Mashkov, About formation of reactions an elastic wheel on not deformable basis in modes of onboard turn, Proceedings of the Moscow Higher Technical School. 390 (1982) 56–63.
- [8] N.N. Schiller, The text about balance of a steady body at action of friction on some flat part of its surface, Works of branch of physical sciences of a society of fans of natural sciences, 5(1) (1892) 17–19.
- [9] N.E. Zhukovsky, Conditions of balance of a firm body leaning a motionless plane some platform and moving along this plane with friction, Journal: Works of branch of physical sciences, Societies of fans of natural sciences. 9(1) (1897) 339–354.
- [10] F.A. Apeika, The mathematical theory of friction, Academy Agricultural Sciences of the Belarus Soviet Socialist Republic, Minsk, 1971.
- [11] I.P. Troyanovskaya, Errors at the description of interaction of a wheel with a basic surface on turn, Journal: Automotive industry. 8 (2009) 17–19.
- [12] V.V. Katsygin, About the law of resistance of ground to compression, Journal: Mechanization and electrification of a socialist agriculture. 4 (1962) 28–31.
- [13] V.A. Umnyashkin, N.M. Fil'kin, V.U. Salnikov, D.U. Noskov, Modelling of process of interaction of a wheel of the machine with a basic surface, The collection of proceedings of the Moscow road institute (Technical University). (2000) 40–44.
- [14] I.P. Troyanovskaya, About formation of reactions in contact of a wheel to a ground on turn, Materials of the international scientific-technical conference of Association of automobile engineers, Moscow. (2010) 490–503.
- [15] I.P. Troyanovskaya, Methodology of modelling of curvilinear movement of tractor units, Dissertation of the doctor of technical sciences (Engineering), Chelyabinsk, 2011.

International Conference on Industrial Engineering

Differentiation of the seasonal loading of combine harvester depending on its technical readiness

Shepelev S.^{a*}, Shepelev V.^a, Cherkasov Yu.^a

^aSouth Ural state agrarian university, 75, Lenin Avenue, Chelyabinsk, 454080, Russia

Abstract

Development of the worn machinery market on the former USSR and availability of the commercial farm units with varying areas of cereal cropping causes the necessity in grounding the economically viable correlation between the combine harvester season load and its technical readiness. It is determined that on the increasing the combine harvester season load from 150 to 350 hectares the rational operational readiness must be raised from 0,4 to 0.85, the repair time must be decreased from six hours to half an hour and the mean time between failures must be raised from six hours to twenty hours. It is possible to ensure these activities by means of repair-servicing correlations, increasing the number of participants in eliminating the consequences of failure and forming the fund of the changeable spare parts, their timely delivery to the mobile units, using the aggregate repair method.

© 2015 The Authors. Published by Elsevier Ltd. This is an open access article under the CC BY-NC-ND license (<http://creativecommons.org/licenses/by-nc-nd/4.0/>).

Peer-review under responsibility of the organizing committee of the International Conference on Industrial Engineering (ICIE-2015)

Keywords: reliability, combine harvester, productivity, production loss, mean time between failures, season load.

1. Introduction

Under conditions of the workforce and physical resources deficit in the agricultural production, it is necessary to decrease the production loss and lower the costs on attraction of the technical means [1]. On a high reliability of the grain harvesters and the low season load, the costs on its attraction are increased.

Charges disparity for the agricultural and industrial production, decreasing the amount of harvesting technical equipment requires the grounding of the rational level combine harvesters technical readiness and differentiating their

* Corresponding author. Tel.: +7-351-266-65-30; fax: +7- 351- 266-65-30.
E-mail address: shepelev2@yandex.ru

season load [4, 5, 6]. It is necessary to ground the expediency of investments into repair-servicing impacts to determine the rational grain harvesters technical readiness. The combine harvesters working efficiency analysis in the different business activities factories shows that the existing machinery usage theory does not fully consider the correlation of their reliability, season and daily productivity, costs on the technical services, repair, storage and fuel consumption. The modern productivity situation causes the necessity in grounding the expedient combine harvester technical readiness considering its season load and resource costs for the repair-restoring services.

The situation complexity is that on the one hand to decrease the harvest losses costs the repair-servicing impacts for increasing combine harvesters reliability and rising efficiency are necessary. On the other hand, their exploitation on small harvesting areas will not be always effective. The stated contradictions require the additional researches for getting the brand new knowledge about correlation between the reliability and charges for attraction and repairing the machinery with different operation state. This fact has determined the research objectives. Ascertain the season load range for combine harvesters depending on the level of their technical readiness; reveal the laws of technical readiness changes depending on the repair-servicing impacts volume on the combine harvesters after the standard operation time; ascertain the costs dependency for the combine harvesters attraction, technical servicing, repair, storage and fuel consumption on the technical readiness and give the technical-economical appraisal of the agreement between combine harvesters season load and their technical readiness efficiency. In order to fulfill these objectives the following research aim has been set – increasing the efficiency of using the combine harvesters with differentiate load on the basis of provisioning the expedient level of their technical readiness.

2. Theory research

To ground the rational reliability level of the combine harvesters with the differentiate season load considering the authors [7, 8] methods, the following criterion function based on the costs minimum has been developed [7, 8, 9]:

$$U(K_{og}) = Z(K_{og}(Q_n)) + P(K_{og}) + Z_{zap}(K_{og}) + R_t(K_{og}) \rightarrow \min \quad (1)$$

here: $Z(K_{og}(Q_n))$ – combine harvester market cost, rub/ha; $P(K_{og})$ – damage by production loss, rub/ha [2, 18]; $Z_{zap}(K_{og})$ – costs for the spare parts, rub/ha; $R_t(K_{og})$ – fuel costs, rub/ha; K_{og} – combine harvester operational readiness coefficient [12, 13].

In the general terms the criterion function can be presented in the following way:

$$U(K_{og}) = \frac{Z(B(K_{og}(Q_n)))}{Q_f} + 0,5 \cdot \frac{K_c \cdot K_p \cdot Y \cdot C_p \cdot Q_f}{Q_{sm} \cdot K_{sm} \cdot K_{og} \cdot K_m} + \frac{Z_{zp}(K_{og})}{Q_f} + R_{ass}(K_{og}) \cdot C_t \rightarrow \min \quad (2)$$

here $Z(B(K_{og}(Q_n)))$ – costs for combine harvesters attraction depending on the reliability level, rub; Q_n – general run, ha; K_p – loss coefficient; K_c – coefficient for loss decrease because of variety, culture combination on early ripening [15]; Q_{sm} – combine harvester turn productivity; Q_f – season load, ha; $Z_{zp}(K_{og})$ – costs for technical services, repair and storage depending on the operational readiness coefficient [16]; $R_{ass}(K_{og})$ – fuel consumption depending on the operational readiness coefficient, kg/ga [17]; C_p – fuel costs, rub/kg; Y – yield, cwt/ha; K_{sm} – shifting coefficient; K_m – technical reliability coefficient.

The dependence between the combine harvester (CH) rational reliability level and the season load has become possible by means of modeling (Figure 1). The rational activities of the average time to eliminate a technical failure and mean time between failures are determined as a relation of the restoring object total run to the expected value of

its failures during this run were revealed (Figure 2).

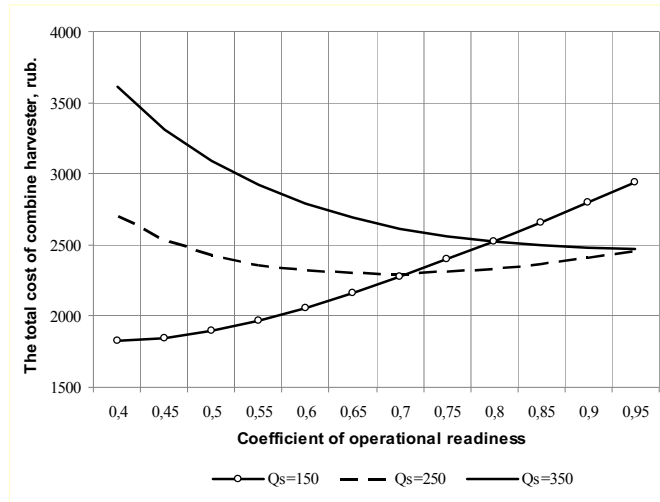


Fig. 1. Dependence of total costs on the CH operational readiness coefficient (Enisej -1200).

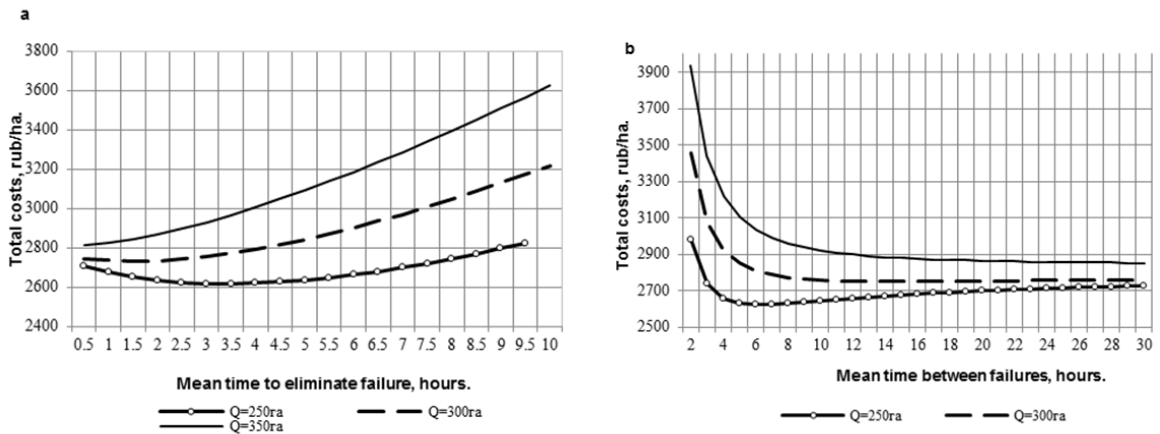


Fig. 2. (a) dependence of total costs on the average failure elimination time; (b) mean time between failures

It has been ascertained that on increasing the season load on the combine harvester from 150 to 350 hectares the operational readiness rational coefficient must be increased from 0,4 to 0,85. When the season load on the combine harvester is increased the average technical failure elimination rational time is decreased. Therefore, when the combine harvester season load increases from 250 to 350 hectares the failure elimination rational time decreases from four hours to half an hour. By means of modeling it is determined that for the combine harvester season load of 250 hectares the rational mean time between failures is equal to 6 hours. With the season load growing up to 350 hectares the rational mean time between failures is approximately 20 hours.

To ground the expediency of costs for repair-servicing impacts in order to improve their reliability the following expression has been derived based on the total costs minimum criterion [11]:

$$U(K_{og}) = K(K_{og}) + P(K_{og}) + Z_{zap}(K_{og}) + R_t(K_{og}) \rightarrow \min \quad (3)$$

here $K(K_{og})$ – dependence between investments in the combine harvester repair and its reliability, rub.

The developed criterion function is presented in the general terms:

$$U(K_{og}) = \frac{K(K_{og})}{Q_f} + 0,5 \cdot \frac{K_c \cdot K_p \cdot Y \cdot C_p \cdot Q_f}{Q_{sm} \cdot K_{sm} \cdot K_{og} \cdot K_m} + \frac{Z_{zp}^{cp}(K_{og})}{Q_f} + R_{ass}(K_{og}) \cdot C_t \rightarrow \min \quad (4)$$

The graphical interpretation of the criterion function is presented on the Figure 3.

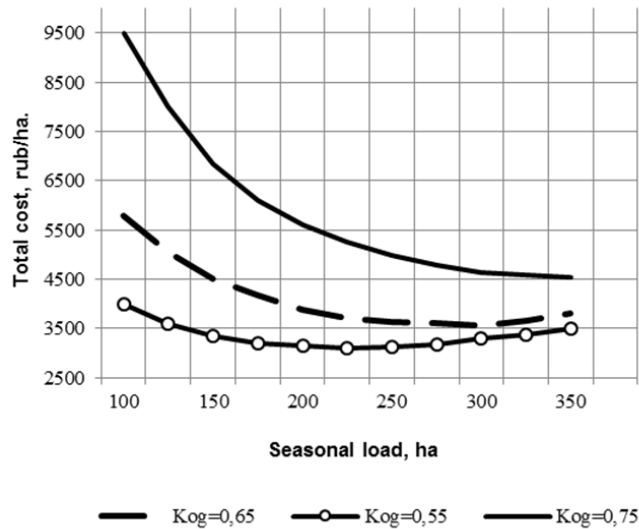


Fig. 3. Dependence between the total costs and combine harvester season load.

The research has disclosed that spare parts and fuel costs, as well as losses of production and investments in the combine harvester repair influence the season load. It has been determined that on increasing the operational readiness coefficient the total costs are increased because of increasing costs on repair-servicing impacts, but on the other hand the rational harvesting area is increased as well. Therefore, when the operational readiness coefficient increases from 0,55 to 0,75 the CH rational season load is increased from 150 to 350 hectares.

The elimination failure time and mean time between failures influence considerably on the complex reliability activity. The average restoring from failure time is composed of the search time and the elimination failure time (0,6 hours), as well as spare parts delivery time (1,9 hours). The correlation between the decreasing the CH mean time between failures and operational term is determined by the following formula: $t_0(T) = 23,561T^{-0,36T}$.

In the Table 1 regression equations for determining costs for the technological machinery attraction, technical servicing and storage (TSRS), fuel consumption on the harvesting machinery operational readiness are presented based on the statistical data. It is disclosed, that the costs for spare parts up to the service life ending are increased from 0,007 to 0,014% of the combine harvester cost as per hectare, and the fuel consumption to the service life end is increased by 1,3 times.

Table 1. Equations showing costs for CH attraction, TSRS, fuel consumption depending on operational readiness activity.

№	Activities	Regression equation
1	Costs for TSRS, rub.	$Z_{zap}(K_{og}) = 76547,426 - 42042,947 \cdot K_{og}$
2	Costs for combine harvesters attraction, rub. α - amortization coefficient.	$Z_{zap}(K_{og}) = (4953082 \cdot K_{og} - 2244223) \cdot \alpha$

3 Fuel consumption, l/ha.

$$R_t(K_{og}) = 9,6 - 5,5 \cdot K_{og}$$

3. Conclusion

Therefore, the productivity situation causes the necessity in grounding the expedient combine harvester technical readiness considering its season load and costs for repair-restoring services. The research results show that in farms with a small harvesting area it is expedient to use technological machinery with a low reliability level, whereas in large farming enterprises the technics renewal is necessary. On increasing the season load on the combine harvester such as Enisej-1200 from 150 to 350 hectares the operational readiness rational coefficient must be increased from 0,4 to 0,85 due to the repair-servicing impacts [19, 20]. The rational elimination failure time must be decreased from six hours to half an hour and the mean time between failures must be increased from six hours to twenty hours due to the increasing number of participants in the technical failure consequences elimination and forming the fund of changeable spare parts, their timely delivery to the mobile units, using the aggregate repair method.

References

- [1] A.M. Plaksin, Correlation between resource agriculture potential and the human village capital, *Vestnik CSAA*. 62 (2012).
- [2] V.D. Saklakov, M.P. Sergeev, Technical-economical grounds of mechanization means selection, *Kolos Publ.*, Moscow, 1973.
- [3] G.V. Korenev, Biological grounds of terms and means of harvesting, *Kolos Publ.*, Moscow, 1971.
- [4] M.R. Mihajlov, Combine harvesters utilization optimization by reliability parameters. Ph.D. Diss, Moscow, 2013.
- [5] A.I. Rjadnov, Combine harvesters reliability activities optimization (detailed for their carrying system) based on the results of exploitation examinations in Volgograd region. Ph.D. Diss., Volgograd, 1984.
- [6] V.D. Shepeljov, Grounds of technic-technological compliance between harvesting and afterwards grain processing. Ph.D. Diss., Cheljabinsk, 2007.
- [7] V.V. Blednyh, Introduction to the theory of technological processes in plant growing design, *Vestnik CSAU*. 23 (1998) 10–14.
- [8] Ju.E. Mihajlov, N.N. Churkin, Technical-economical grounds of the combine harvesters fleet, *Sbornik nauch. tr., ChIMJeSH Collection of studies*. 124 (1997) 78–84.
- [9] S.D. Shepeljov, Grounds of the efficiency limits in using the reservoir-diver, *Vestnik KGAU*. 12 (2013) 199–203.
- [10] S.D. Shepeljov, G.A. Okunev, Ju.B. Cherkasov, Combine harvesters service life influence on the technological lines structure, *Izvestija OrenSAU*. 1(45) (2014) 43–46.
- [11] S.D. Shepeljov, Ju.B. Cherkasov, Grounds of the rational reliability level of the technological machinery in the harvesting process, *Vestnik KGAU*. 5 (2015) 58–63.
- [12] V.V. Belov, Reliability and efficiency in technical equipment: reference book, *Mashinostroenie Publ.*, Moscow, 1986.
- [13] P.F. Pribytkov, V.F. Skrobach, Faultlessness of the harvesting outfits and complexes, *Agropromizdat Publ.*, Leningrad, 1987.
- [14] S.D. Shepeljov, V.D. Shepeljov, Ju.B. Cherkasov, Statistic activities of combine harvesters productivity depending on their run, *Agroprodovol'stvennaja politika Rossii*. 1 (2015) 36–40.
- [15] S.D. Shepeljov, I.N. Kravchenko, Technical means parameters on harvesting co-ordination, *Sibirskij vestnik sel'skohozjajstvennoj nauki*. 7(8) (2011) 71–76.
- [16] S.A. Kamsha, Rational harvesting process parameters (on the example of the Altai Kray) Ph.D. Diss, Barnaul, 2009.
- [17] S.D. Shepeljov, Ju.B. Cherkasov, Grounds of the combine harvesters differentiate reliability with regard to their season load, *Files of the LIV International sci-tech conference "Science achievements – to the agriculture production"*. 2 (2015).
- [18] S.D. Shepeljov, G.A. Okunev, Design of the flow lines on harvesting text: monograph, Cheljabinsk, 2006.
- [19] V.A. Lipp, Research of the aggregate method of failure elimination for combine harvesters SK-4 with the aim to increase their efficiency Text. Ph.D. Diss., Cheljabinsk, 1972.
- [20] E.V. Solonicyyn, Decreasing the duration of technological processes in the plant growing based on the aggregate method of restoring tractors working capacity. Ph.D. Diss., Cheljabinsk, 2003.



International Conference on Industrial Engineering

Refinement of hybrid motor-transmission set using micro turbine generator

Arav B.L.^a, Shulman R.^a, Kozminykh V.A.^{b*}

^aTurboGEN technology Ltd., Dolinsky 1, Rehovot, 76569, Israel

^bSouth Ural State University, 76 Lenina Avenue, Chelyabinsk 454080, Russian Federation

Abstract

The paper summarizes the results of the research, performed in 2010-2015, on topic vehicles based on hybrid propulsion system, using the “plug-in hybrid electric vehicle” scheme. The main technological improvement achieved is the vehicle weight reduction, in particular through the use of range extender generators based on micro-turbine technology. The requirements for generator were defined and a system design analysis was held. The concept of the company TurboGEN Technology is briefly discussed.

© 2015 The Authors. Published by Elsevier Ltd. This is an open access article under the CC BY-NC-ND license (<http://creativecommons.org/licenses/by-nc-nd/4.0/>).

Peer-review under responsibility of the organizing committee of the International Conference on Industrial Engineering (ICIE-2015)

Keywords: vehicle; hybrid propulsion system; range extender generator; micro-turbine generators.

1. Introduction to the research refinement of hybrid motor-transmission set

The current technological state of electric vehicles shown the ability to create electric vehicles (EV) with a large electric range and high-end dynamic performances [1,2]. However, even promising energy capacity of batteries is several times lower than that of fossil fuels. Therefore, the mass of the battery reaches 200-400 kg, and the EV weight by 30-50% higher than the weight of Conventional Vehicles (CV) that leads to an increase in energy consumption for propulsion and decreasing a total efficiency of vehicles. When comparing CV and EV at equal

* Corresponding author. Tel.: +7-904-309-02-60;
E-mail address: vladimir5@ya.ru

gross weight and cruising range, economic criteria are converted to a simple criterion - the vehicle total weight M_v . [1 – 4].

Rational solution corresponds to a minimum M_v weight. This condition is satisfied by a hybrid propulsion system (HPS) circuit (Fig. 1) - «plug-in hybrid electric vehicle» - PHEV [1 – 4]. Their feature - charging the battery from an external source and a power reserve of electric drive mode at least 50-100 km. The range extender generator - REG used a heat engine. It operates in a stationary mode and provides battery charging. However, the REG requirements need to be clarified. It is necessary to solve two problems:

- to establish reserves to reduce weight M_{reg} , for weight reduction of M_v and improvement of the vehicle efficiency;
- to define the rational type of heat engine and its parameters.

2. The object of the study (Model, Process, Device, Sample preparation etc.)

To solve the first problem, used modern simulation approved method - «The Parametric Analytical Model of Vehicle Energy Consumption» (PAMVEC) [4]. It is based on the use of the well-known equation of the vehicle power driving balance in the driving cycle, in our case, Urban Driving Cycle (UDC), Fig. 2. It is most relevant to the conditions of PHEV operation [1, 2].

When using HPS PHEV vehicle efficiency depends mainly on two factors. The first - the degree of perfection of the electric parts. They already has a high efficiency (battery - up to 0.95, the electric traction - to 0.9-0.95) and increase its reserves are exhausted.

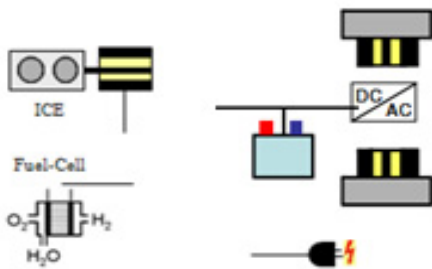


Fig.1. The scheme HPS PHEV.

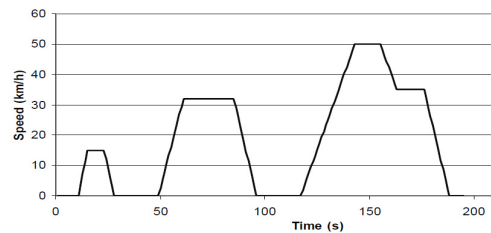


Fig.2. Urban Driving Cycle (UDC).

The second - the motion energy consumption N_m , related to the vehicle weight at a constant desired payload. Therefore, the main factor in increasing the vehicle efficiency becomes a weight reduction M_v . In modeling were determined energy consumption of N_m as a function of total mass M_v , with the initial value of 1200 kg. The power vehicle model has been correcting for achieving the set of dynamic parameters (speed and acceleration). Other parameters and indicators (aerodynamics, thermal characteristics of the engines, battery, motors etc.) were set in the initial data.

It was found that the vehicle weight decrease ΔM_v leads to lower motion energy consumption ΔN_m of the following relationships (Fig. 3): a) - close to the linear and increase a reserve range for the same power consumption of the battery; b) - growing while maintaining the range and reducing the required HPS power and the masses, including battery energy consumption and weight.

For the required payload weight, the reserves to reduce the vehicle mass is limited [1, 2, 4]. The main is unused reserve is to reduce the REG weight and size. Analyze vehicle designs showed that these REG indicators are not independent objects of optimization. Their influence should be read in conjunction with elements of the engine compartment. Decreasing weight M_v at reducing REG weight M_{reg} depends on the design of the vehicle. It is: for cars $\Delta M_v = (1,15-1,2) \Delta M_{reg}$; for the special vehicles $\Delta M_v = (1,4-1,6) \Delta M_{reg}$. For special vehicles, the role of REG dimensions in shaping the mass M_v , increases.

Decreasing weight, ΔM_{reg} , leads to lower motion energy consumption ΔN_M of the following relationships (Fig. 4): a) - close to the proportional (cars); b) - by increasing (special vehicles). The impact of fuel efficiency REG heat engine at the required power reserve vehicle to electric slightly, depending on the time of its operation. Therefore, reducing the REG weight and size becomes a priority, and increase the efficiency of its engine - secondary.

3. Methods of the research

Generalization of data of HPS PHEV concepts shows, that the REG mass does not exceed the 80-100 kg, electric power is 5-30 kW depending on the weight of the vehicle and the required reserve. The structure REG includes a heat engine with the fuel tank, generator and power electronics.

The following basic requirements for REG: weight and size parameters (specific power at least 0.3-0.5 kW / kg, the volume power at least 140-160 kW / m³); value in mass production of not more than 100-150 \$ / kW; service life up to 4000 hours; the need for environmental safety; multifuel and etc. [3, 5]. All current REG, do not meet the requirements for overall dimensions and cost (Table 1). This points to the need to analyze the possibilities of application in the REG alternative engines. The comparison shows (Table 1) that meet the requirements of most micro-turbine generator (MTG) [5, 6, and 7]. Their advantages and disadvantages are due to design features, the operating cycle, materials and technologies.

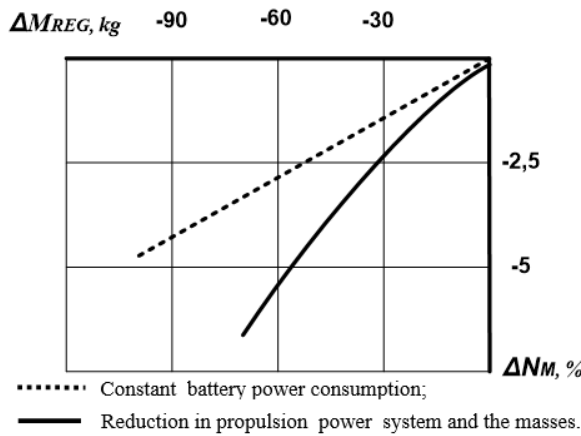


Fig. 3. Effect of reducing the vehicle mass to reduce motion energy.

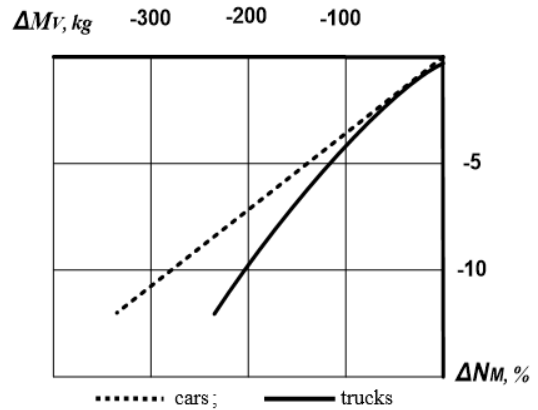


Fig. 4. Effect of reducing the REG mass to reduce motion energy consumption.

3.1. Structure of micro-turbine generator

MTG provides maximum design simplicity by integrating into a single unit (the rotor) compressor, turbine and high-speed electrical generator (Fig. 5). Other benefits MTG: multifuel; required environmental security; high reliability and low operating costs; unification; modular design and others. The duty cycle MTG studied, its efficiency largely depends on the gas temperature before the turbine, pressure ratio in the compressor, the degree of regeneration of exhaust heat. Modern technical capabilities can significantly increase the gas temperature before the turbine and to bring efficiency to the level of MTG REG based on diesel [6,7,8].

A wealth of experience in design, production and use MTG as mini power stations, in particular by «Capstone Turbine Corporation», the United States [6,7,10]. She also has experience with REG based on mini power stations (power 30-60 kW) for heavy vehicle. However, the REG does not meet the requirements of the application considered in light-duty vehicle.

3.2. Compressor characteristics and the gas generator

There are reserves to reduce the cost of the MTG and fast implementation into production on the basis of gas generator unification with a small-sized turbochargers. Turbochargers have small dimensions and weight, high

reliability and minimum operating costs [5, 8]. Turbochargers are at the stage of mass production (more than 50 million per year) at a cost of about \$300. One of the tendencies of their improvement is to create a hybrid turbocharger that is MTG with reversible electric [9].

During 2014-2015 «TurboGEN Technology» developed the concept MTG power up to 2.1 kW at a speed to 120,000 min⁻¹ with external combustion chamber operating on gas. We used a gas generator based on turbocharger GT2052 produced by company «Garrett» (Fig. 5) and experienced a synchronous AC generator on permanent magnets. Achieved meet the requirements for overall dimensions (specific power - 0.4 kW / kg, volume power - 145 kW / m³) at a moderate cost of the prototype. Currently, a concept MTG power up to 5 kW at a speed to 200,000 min⁻¹ higher calculated specific indicators (specific power to 0.8 kW / kg, volume power up to 165 kW / m³).

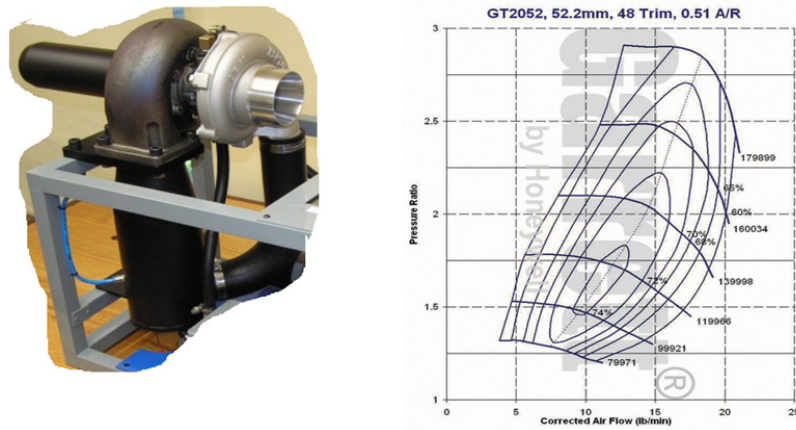


Fig. 5. Compressor characteristics and the gas generator general appearance with a combustion chamber (alternator removed).

Table 1. Comparative REG characteristics

Engine and generator types	Spec. power, kW/kg	Vol. power, kW/ m ³	Engine speed, min ⁻¹	Electr. Effic.	Product. Price, \$ / kW	Note
Spark-ignition; AC, sonhronny	0,1-0,12	80-90	4000-6000	0,26-0,29	<300	Small-sc production
Diesel; AC, sonhronny	0,04-0,06	20-30	1500-4500	0,3-0,34	<500	Concept
Rotary; AC, sonhronny, permanent magnet	0,12-0,15	100-120	6000-7000	0,25-0,28	<600	Concept
MTG based on the turbocharger; AC, sonhronny, permanent magnet	0,35-0,4	More 140	To 200000 and more	0,27-0,29	180- 200	Concept

Thus in this case we can conclude that:

1. The main factor in increasing the efficiency of vehicles with HPS PHEV is to reduce their weight. Prioritized reducing REG weight and size and influenced on the vehicle efficiency depending on the engine compartment design.
2. The basic requirements for the REG have been figured out and defined that the greatest degree corresponds to these requirements is MTG. The possibility of implementation of the requirements in the concept MTG based on a small-sized turbocharger.

References

- [1] Energy Technology Perspectives - Scenarios & Strategies to 2050, OECD/IEA, Paris, 2010.
- [2] M. Ehsani, Y. Gao, *Modern Electric, Hybrid Electric and Fuel Cell Vehicles: Fundamentals, Theory, and Design*, CRC PRESS, New York, 2010.
- [3] B.L. Arav, Analysis of the concepts of hybrid transmission systems vehicles, *Journal AAI*. 5 (2011) 35–39.
- [4] A.G. Simpson, *Parametric Modelling Of Energy Consumption In Road Vehicles*, Ph.D. Thesis, The University of Queensland, Brisbane, 2005.
- [5] B.L. Arav, N.E. Alexandrov, Prospects of application micro-turbine generators in hybrid propulsion system of mobile equipment, *Acad. Military Science*. 1 (2010) 10–17.
- [6] M.J. Moore, *Micro-turbine Generators*, Publisher Wiley, New York, 2002.
- [7] C. Soares, *Microturbines: Applications for Distributed Energy Systems*, Elsevier, New York, 2007.
- [8] A.E Simpson, V.N. Kaminsky, *Turbocharging high-speed diesel engines*, Engineering, Moscow, 1976.
- [9] S. Ibaraki, K. Yamashita, Y. Sumida, Development of the "hybrid turbo," an electrically assisted turbocharger , *Technical Review Mitsubishi Heavy Industries*. 3 (2006) 5–7.
- [10] Information on <http://www.microturbine.com/>



International Conference on Industrial Engineering

Improving the efficiency of led lighting by switching to low-voltage technology

Zhaparova A.T.^{a*}, Baklanov A.E.^b, Titov D.N.^c

^a D. Serikbayev East Kazakhstan State Technical University ITPED, Instrument Engineering and Technology Automation A.K. Protozanov Str. 69, 070004 Ust-Kamenogorsk, Kazakhstan e-mail: atj-43@mail.ru

^b Candidate of Physics - Mathematical Sciences, D. Serikbayev East Kazakhstan State Technical University ITPED, Instrument Engineering and Technology Automation A.K. Protozanov Str. 69, 070004 Ust-Kamenogorsk, Kazakhstan e-mail: ABaklanov@ektu.kz

^c Candidat of Technical Sciences, D. Serikbayev East Kazakhstan State Technical University ITPED, Instrument Engineering and Technology Automation A.K. Protozanov Str. 69, 070004 Ust-Kamenogorsk, Kazakhstan e-mail: D.Titov@ektu.kz

Abstract

This article is devoted to the use of low – voltage supply in the “Smart house” lighting system. This paper considers the low-voltage system of lighting power supply with a possibility of integration with alternative energy sources without additional devices, such as voltage converters and generators.

© 2015 The Authors. Published by Elsevier Ltd. This is an open access article under the CC BY-NC-ND license (<http://creativecommons.org/licenses/by-nc-nd/4.0/>).

Peer-review under responsibility of the organizing committee of the International Conference on Industrial Engineering (ICIE-2015)

Keywords: low-voltage technology, energy source, renewable energy sources, solar battery, energy-saving, energy-efficient technologies

Introduction

At the moment most countries use lighting systems with high-voltage power supply - 220, 110 volts. At the same time, development of new technologies in the field of alternative energy and production of highly-efficient reliable LED crystals with increased capacity gives the possibility of changing the old approach of organizing the lighting of the building.

* Corresponding author. Tel.: +7-705-531-82-35;
E-mail address: atj-43@mail.ru

In Kazakhstan, production and sale of 100W and above electric incandescent lamps are under a ban introduced from the 1st of July, 2012; 75W and above - from the 1st of January, 2013 and 25W light bulbs are recycled from the 1st of January 2014. The forecast of McKinsey consulting company - in 2015 LEDs will replace the traditional incandescent and luminescent lamps, occupying 50% of the market in money terms and in 2020 - 90% of the market in money terms and 75-80% in real terms.

Low-voltage power supply systems are mainly used for lighting and illumination of mirrors, bookshelves, portraits, photographs, as well as for landscape lighting, buildings and gardens. The proposed low-voltage power supply of 24 volts allows switching to LED lighting with the integration of renewable energy renewable energy sources (RES) [1-12].

The use of low-voltage power supplies is first of all due to the high reliability of performance that can significantly increase the life of the energy supply devices. Also the use of low-voltage power supply system increases electrical safety and fire safety of premises.

1. Justification of The use of double-conversion of CURRENT

Classic circuit for switching on LED in lighting device is shown in Fig. 1.

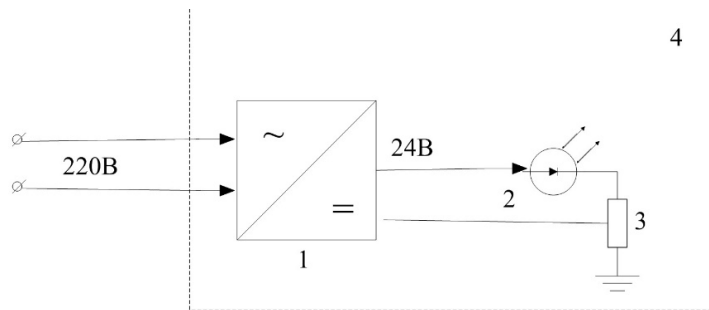


Fig. 1. Typical circuit of an illumination device device: 1 – ac/dc converter (driver), 2 – LED, 3 – equivalent resistance of LED, 4 – circuit of an illumination.

One of the elements of an illumination device is electric power supply 1 (ac/dc converter). Thus, in lighting the room with a LED lamp connected to the circuit with ac voltage 220V, there is the loss of power when converting voltage by the driver as its efficiency factor is not equal to 100%.

With wide integration of alternative energy sources, particularly solar batteries or solar cells for the use in standard illumination devices it is necessary to convert the received direct current into alternating, Fig. 3.

Typically, applying alternative energy sources, already available illumination devices are used, schematically presented in circuit form 4 in Figure 1. And for supplying alternating voltage 220V, converter 24-220V is installed. Thus, the general scheme of implementation of LED lighting system connection might be presented in the form of Fig. 2.

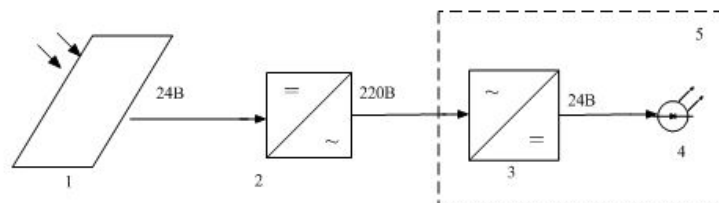


Fig. 2. General scheme of implementation of LED lighting system connection: 1 – solar battery, 2 – converter, 3 – ac/dc converter, 4 – LED, 5 – illumination device.

Despite the insignificant efficiency factor of solar batteries, their application is effective due to the use of renewable energy source. However, in this scheme (see Fig. 2) there are two converters 2 and 3 position which introduce losses and electrical leak in the lighting system. The first converter 2 converts the direct current produced by the solar panels of 24V into operating voltage of 220V AC, and the second converter (ac/dc converter) 3 converts AC to DC from 220V voltage to 24V.

To determine the efficiency of implementing double conversion of current we need to calculate efficiency factor of the system.

2. Calculation of efficiency of double conversion of current

Conversion ratio (efficiency factor) of the converter is characterized by the ratio of active power, supplied to the load, to the total power consumed by the conversion device.

2.1 Calculating of efficiency factor

Efficiency factor characterizes system efficiency of any device with respect to power conversion or transmission. It is determined by the ratio of effective energy used to the total amount of energy received by the system. Efficiency factor is a dimensionless quantity and is often measured in percentage and denoted by η . The mathematical definition of efficiency factor can be written as:

$$\eta = (A/Q) \times 100\% \quad (1)$$

where A – effective power; Q – expended work.

By energy conservation law, efficiency factor is always less than one or equal to it. Let's consider the general scheme of measuring the efficiency factor of the converter 2 and the converter 3 (ac/dc converter) in Figure 4. Supposing that up converter of the voltage is taken for the base. To the circuit disconnect of power supply we switch in the amperemeter A_1 , and in parallel of the input of power supply - voltage converter voltmeter V_1 , indicated values of which are necessary for the calculation of power consumption P_1 of the device and their load from the power supply. To the output of the voltage converter into the disconnect of load power supply we also switch in the amperemeter A_2 and voltmeter V_2 which are necessary for the calculation of load power consumption P_2 from the voltage converter. Then we switch on the device, measure the indicated values and calculate power P_1 and P_2 by the following formulae (2) and (3) correspondingly, [13-14]:

$$P_1 = I_1 \times U_1 \quad (2)$$

$$P_2 = I_2 \times U_2 \quad (3)$$

Efficiency factor of the converter η_1 we determine by the formula (4):

$$\eta_1 = (P_2/P_1) \times 100\% \quad (4)$$

This formula (4) defines the actual efficiency factor of the voltage converter.

The power of the converter 3 (ac/dc converter) Figure 3, is determined by the following formulae (5), (6) correspondingly:

$$P_2 = I_2 \times U_2 \quad (5)$$

$$P_3 = I_3 \times U_3 \quad (6)$$

Efficiency factor of the ac/dc converter η_2 is determined by the formula (7):

$$\eta_2 = (P_3/P_2) \times 100\% \quad (7)$$

Summarized total efficiency factor $\Sigma\eta$ of the converters can be defined by the formula:

$$\Sigma\eta = \eta_1 \times \eta_2 \tag{8}$$

To study the effectiveness of a low-voltage power supply circuit based on the use of solar batteries, we carried out measuring operations for determining the efficiency factor of the converter 2 and the converter 3 (ac/dc converter) Figure 3. General scheme for measuring the efficiency factor of the system is shown in Fig. 3.

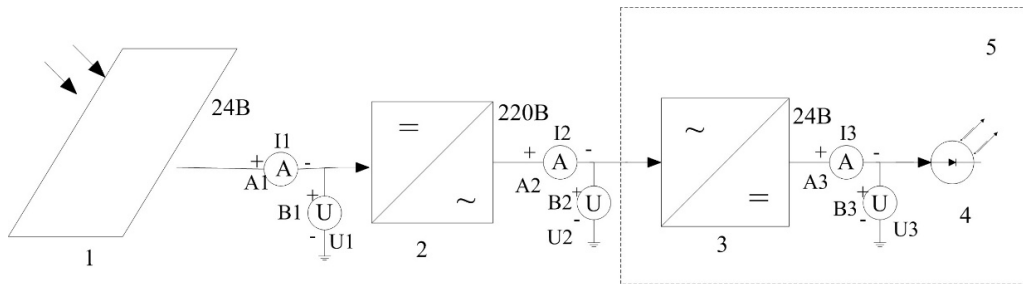


Fig. 3. General scheme for measuring the efficiency factor of the system: 1 – solar battery, 2 – converter, 3 – ac/dc converter, 4 – LED, 5 – illumination device.

The values of currents and voltage measured according to the scheme 4 are listed in the table 1.

Table 1. Experimental values of currents and voltage

$I_1,$ [A]	$U_1,$ [V]	$P_1,$ [W]	$I_2,$ [A]	$U_2,$ [V]	$P_2,$ [W]	$I_3,$ [A]	$U_3,$ [V]	$P_3,$ [W]
2,2	12,6	27,7	0,06	207	11,1	0,14	37,6	5,3

Calculation data on the received experimental values are listed in the table 2.

Table 2. Calculation data on the received experimental values

$P_1,$ [W]	$P_2,$ [W]	$P_3,$ [W]	$\eta_1,$ [%]	$\eta_2,$ [%]	$\Sigma\eta,$ [%]
27,7	11,1	5,3	40	47,8	20

As a result of carried out study and calculations, the efficiency factor of the converter 2 Figure 4 is 40,1%, the efficiency factor of the converter 3 Figure 4 is 48%. Summarized efficiency factor is 20%. This shows a very low efficiency of application of this scheme.

2.2 The usage of solar batteries

The usage of solar batteries and system without current converters (Fig. 4) has a great perspective.

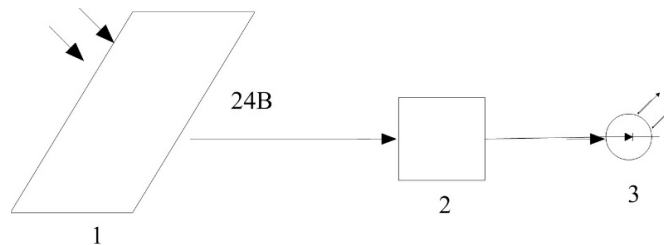


Fig. 4. LED illuminator connection scheme without using current converters: 1 – solar battery, 2 – current stabilizer, 3 – LED.

Figure 5 shows the scheme of low voltage lighting connection on the basis of LEDs without voltage converters. This scheme is relevant in that the voltage of energies worked out with the solar battery allows using LEDs of high power without conversion of energy, which in turn increases the efficiency factor of the system.

For stabilizing direct current a self-made driver on the basis of microcircuit PT4115 was used, its typical scheme is presented in Fig. 5, and the photo of this model is shown in Fig. 6.

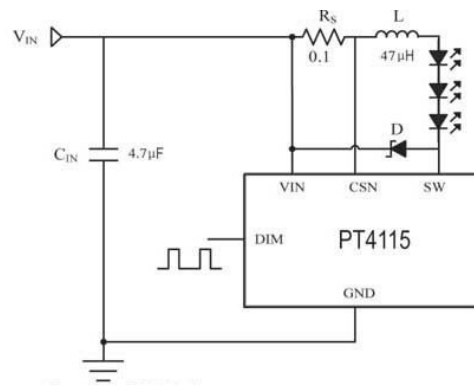


Fig. 5. Scheme of current stabilization.

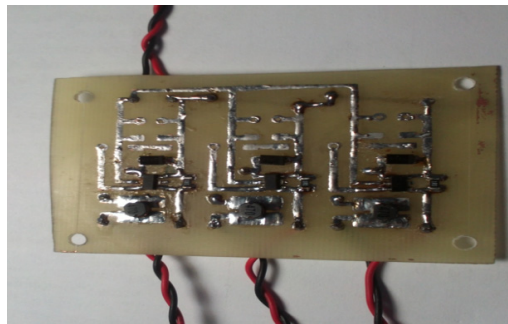


Fig. 6. Self-made current stabilizer.

For energy-storage and provision of stable operation of the scheme in Figure 8 there installed an additional accumulator 4 and controller 2, providing optimal charge of the energy and desired voltage for the work of low voltage system of lighting, Fig. 7.

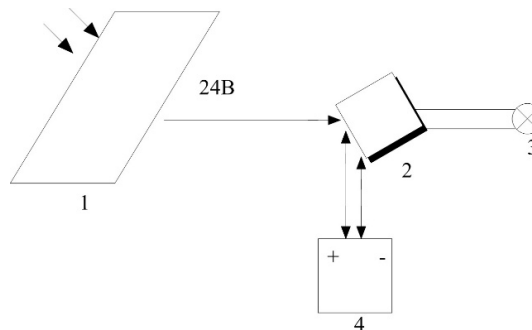


Fig. 7. Scheme of low voltage system of lighting using energy storage unit: 1 – solar battery, 2 – controller, 3 – low voltage illumination device, 4 – accumulator.

Direct current is supplied from the solar battery 1 in Figure 7 to the controller 2, which provides an uninterrupted supply of electrical power to the low-voltage lighting system simultaneously charging the accumulator 4.

Testing of the system showed its full working efficiency. The system operated autonomously within seven days, while its energy consumption for lighting was only 10% of the generated by solar panels energy, that is, you can still add a load equivalent to 100 watts of electrical energy.

One of the problems of integrating low voltage system is adapting of available electrical wires interconnection used for the voltage of 220V to the voltage of 24V. The problem is related to the increase in electric current intensity that results the increase in lighting cable heating up (raise of temperature).

For integration of low voltage system we calculated the necessary wire section while using low voltage LED lamps.

2.3 Calculation cross-section area

For calculations there were used copper wires, with electrical resistivity $0,0175 \text{ Ohm} \times \text{mm}^2/\text{m}$, [13-14].

Wire resistance, Ohm, is defined by the formula:

$$R = \rho \times (l/S), \quad (9)$$

where ρ – electrical resistivity of a wire, $\text{Ohm} \times \text{mm}^2/\text{m}$; l – length of a conductor, m; S – its cross-section area, mm^2 .

Cross-section area is determined by the formula:

$$S = \rho \times (l/R). \quad (10)$$

Current line in the cable is determined by the formula:

$$I = P/U, \quad (11)$$

where P – power consumed by the load, W; U – line voltage in the cable, V.

To determine the coincidence of existing copper wires with the new low-voltage system we determine the cross section of the existing wire (results are shown in the table 3).

Table 3. Calculation data of existing wire cross-section

P, W	U, V	I, A	S, mm^2
1000	220	4,54	2,5

Required wire section for low voltage system is shown in the table 4.

Table 4. Calculation data of wire section for low voltage system

P, W	U, V	I, A	S, mm^2
400	24	16,7	2,5

Conclusions

Thus, using low voltage system due to higher energy efficiency and higher efficiency factor of the system and the absence of two converters (Fig. 6) with available wire section of high lighting system with voltage 220V, we can use wires in the system which size is not less than 2.5 mm^2 . At the same time changing incandescent light bulbs for LED lamps does not require rewiring the entire system.

With integration of low voltage system due to the results presented in the tables 3 and 4 there is no need in changing existing wires.

The considered variants of using alternative energy sources for lighting system show that tradition ways of their

application are not effective. Double conversion of current makes the system inviable, its efficiency factor do not to exceed 20%. It was demonstrated that application of non-traditional lighting system with the voltage 24V without conversion of electrical energy is more effective and less traumatic. It was also shown that at the expense of application energy-efficient lighting system it is allowed to use existing electrical wiring with no risk of overheating problem.

Acknowledgment

This research is funded for 2015-2017 years by the Scientific Committee of the Ministry of Education and Science of the Republic of Kazakhstan within the project No. 29-417-15 "The innovative technology of ultrasonic flow measurement of liquids density and the development of a densitometer prototype".

References

- [1] Energy Savings Estimates of Light Emitting Diodes in Niche Lighting Applications. Navigant Consulting, Washington, D.C., 2008.
- [2] Key World Energy Statistics 2009. International Energy Agency, Paris, France, 2009.
- [3] C. DiLouie, Daylighting is the use of daylight as a primary source of general illumination in a space, Automated Building. 1 (2007). www.automatedbuildings.com
- [4] R. Sampath, Green Lighting: Solar-based HBLED Lighting Solutions, Beyond Bits. 3 2008 10–12. (www.freescale.com)
- [5] P.J.J. Welfens, B. Meyer, Energy Policies in the European Union Germanys Ecological Tax Reform, New York Springer, Berlin, 2001.
- [6] Technology Partnership. Enhancing the Competitiveness, Efficiency, and Environmental Quality of American Industry, U.S. Department of Energy. Washington, 1995. DOE/60-100095-170.DE 95004086
- [7] Using a PIC Microcontroller for DMX512 Communication. Application Note AN 1076. Microchip Technology, Inc., 2007. (www.freescale.com)
- [8] G. Gyorok, S. Grigoryeva, Search of optimal parameters for work of LED lighting system, International scientific-practical conference Green Economy - the future of humanity. 2 (2014) 62–71.
- [9] Adding Intelligence to Lighting Applications. LED Lighting Design Guide. Microchip Technology. Inc., 2008. (www.microchip.com)
- [10] Györök Györqy. Számítógép perifeák I. Budapest, 2013.
- [11] A. Zhaparova, G. Gyorok, A. Kvasov, Autonomous light-emitting-diode (LED) low voltage systems of lighting integrated into smart home, 9th International Symposium on Applied Informatics and Related Areas New Faculty, New Ability. (2012).
- [12] A. Zhaparova, A. Baklanov, D. Titov A. Kvasov, Systems low-voltage "Smart House" with the use renewable energy sources. Scope Academic House, B&M PUBLISHING, 2 International Conference "Technical sciences: modern issues and development prospects". (2014).
- [13] S.A. Eranocyan, Cetevye bloki pitaniy s vysokochactotnye preobrasovateli, Vysshaya shkola, Moscow, 2010.



International Conference on Industrial Engineering

An automated control system by probe signal generator in radar

Zhiganov S.N.^a, Smirnov M.S.^{b*}

^a23, Radiozavodkoe highway, Murom 602264, Russian Federation

^b23, Radiozavodkoe highway, Murom 602264, Russian Federation

Abstract

The article discusses the creation an automated system by probe signal generator in radar. This system was created by means of National Instruments measurement equipment and LabVIEW software environment. The paper shows a block diagram of test system and describes its components. For this test system a test method, software and typical signals were developed. This system is used for the production monitoring of the probe signal generators.

© 2015 The Authors. Published by Elsevier Ltd. This is an open access article under the CC BY-NC-ND license (<http://creativecommons.org/licenses/by-nc-nd/4.0/>).

Peer-review under responsibility of the organizing committee of the International Conference on Industrial Engineering (ICIE-2015)

Keywords: PXIe-1085, PXI-5105, radar, chirp pulses, radar receiver signal compress, heterodyne.

1. Introduction

Modern radar – is a complex system comprising mechanical, hydraulic, electrical and other elements. But the main importance is the radio equipment. Radio equipment is used for control of the radar, for generating and receiving radar signals, for transmit, receive, processing and storage of information [1-6]. In the production of radio is very important to monitor its performance. Currently, control is carried out by conventional methods which are based on measuring the values of input and output signals and reception waveforms at the control points. Unfortunately, these methods do not allow finding a failure and operational error, especially when verifying digital signal processing systems [7-9].

One example is the evaluation of the main characteristics of the chirped pulse for probing signals that are generated by radar heterodyne. Radar heterodyne consist of frequency synthesizer for producing carrier, modulator, amplifiers, and balanced circuit. The efficiency of radar depends on quality of heterodyne signal. Therefore, parameter monitoring of chirp pulses is important part of the control system by radar. Due to the large number of measurements, parameter monitoring must be automatized.

* Corresponding author. Tel.: +7-905-140-52-51

E-mail address: smirnov.murom@gmail.com

One of the most effective ways to solve this problem is the using modular instruments from National Instruments. The redefined instrumentation approach provided by National Instruments uses open software and modular hardware with key elements (multicore CPUs, user-programmable FPGAs, PCI Express, data converters, and LabVIEW system design software) to address such demanding challenge. Using NI LabVIEW software with PXI modular instrumentation to create a test system that can be used in both characterization and production testing and delivers 11X reduction in capital equipment costs, 15X reduction in footprint, 66X reduction in weight, and 16X reduction in power consumption over the previous automated test equipment used in production. With this approach, we can build test systems based on flexible hardware and scalable software resulting in savings in capital equipment, system development, and maintenance costs while realizing faster test execution. [10].

The aim of the presented paper is the development of an automated system for control of parameters of probing chirp signal.

2. Methods of solving the problem

A number of methods to creation of automated systems is referred in works [11-16]. Similar systems are described in works [17-19]. As we can see from that works, the optimum way is use modular measurement equipment with integrated software development environment. Modular measurement equipment from National Instruments is used for generating test signals, digitizing measured signals and measuring parameters. Software development environment LabVIEW is used for processing received information and display of results.

3. Description of the system

Block diagram of the measurement system is shown in Fig. 1.

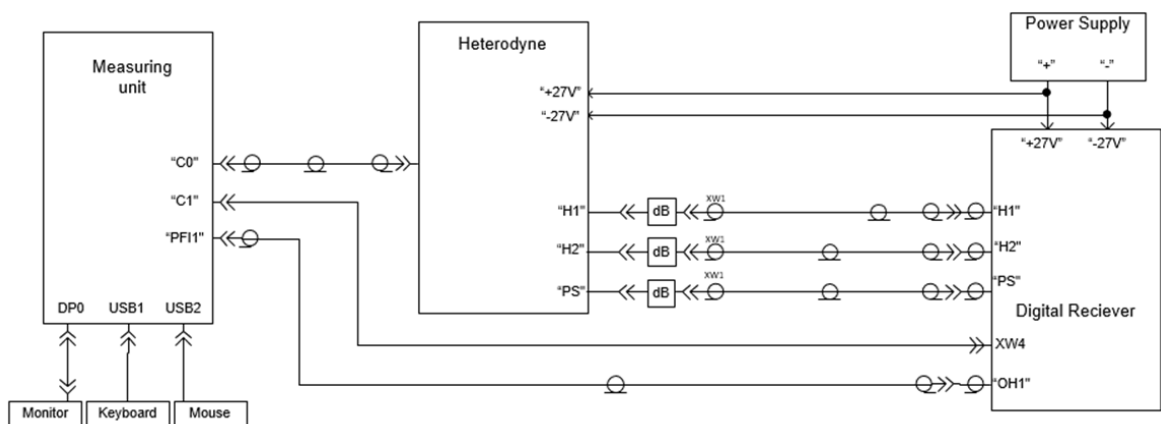


Fig. 1 Block diagram of the measurement system

The system comprises: a heterodyne, a receiver and a measuring unit. To supply the heterodyne and the receiver uses an external power supply ± 27 V.

Heterodyne generates the following signals:

- pilot signal (PS), which is chirped pulse with a duration of 67 μ s and frequency deviation of 1.2 MHz in most measurement modes;
- start trigger (H1);
- coherent wave signal with frequency 24 MHz (H2).

The signals from the heterodyne through attenuators are fed to the regular radar receiver. Signals H1 and H2 are directly fed to the measuring unit. PS signal is supplied to the measuring unit only after transferring it to an intermediate frequency of 30 MHz.

In the measuring unit is coherent digitizing of signal PS with the signal H2. Process of digitizing is triggered by signal H1. Measuring unit is used to detect and measure the parameters of chirped pulses generated by radar heterodyne. The main functions of this unit:

- visual display of digitized packets chirped pulses;
- calculation of the phase values in each pulse in degrees and determining the range of the phase change in the chirp pulses;
- calculation of the range of variation of maximum values of the amplitude chirp pulse;
- convolution chirped pulses;
- estimate of the range of variation of the maximum convolute chirp pulses;
- calculation of the range of variation of the maximum levels of side lobes in a pack of convolute chirp pulses.

Measuring unit (fig. 2) is based on PXI chassis (PXIe-1085), composed of digitizer (PXI-5105) and controlled by a PXIe-8135.

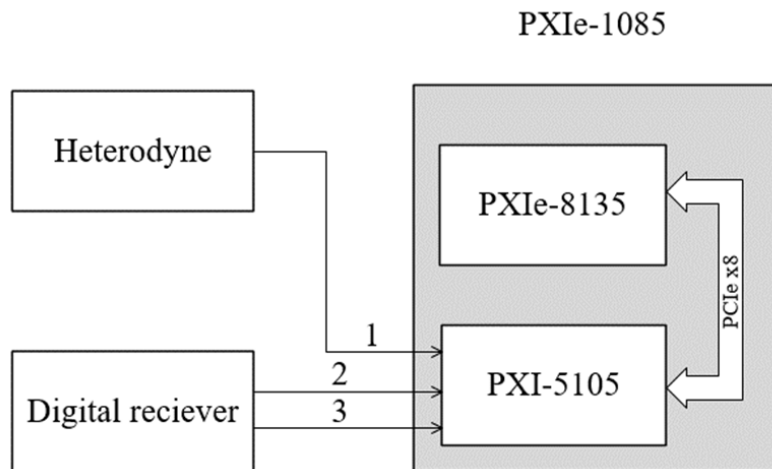


Fig. 2. A block diagram of a measuring unit

Front panel of measuring unit is shown in Fig. 3. VI created in LabVIEW 2013 allows measurements in sequential mode and batch mode (from 2 to 12 pulses in batch). Before start measurements must be set frequency deviation and the base of signal. In batch mode we must set the number of pulses in the pack and each pulse repetition period.

During the measurements, the front panel displays the digitized packs of chirped pulses before and after convolution. At each pulse in the packet is determined the amplitude and phase of the peak. Then we calculate the maximum, minimum, median value among the pulses of one pack.

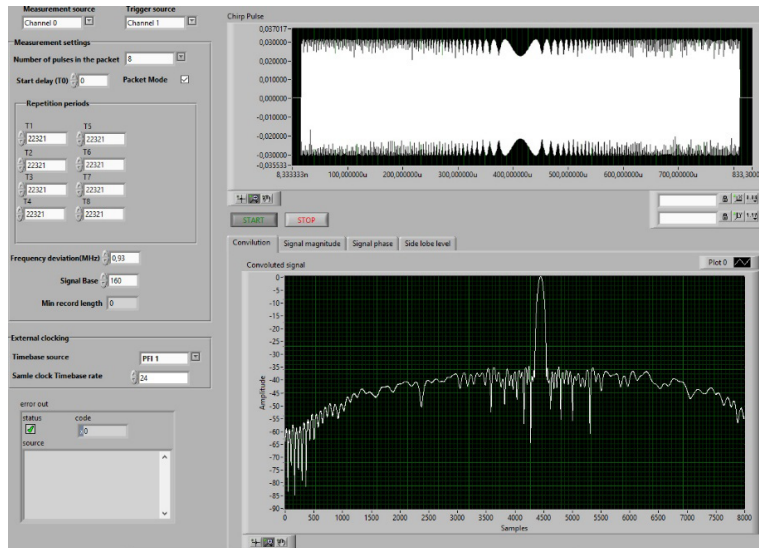


Fig. 3. Original and convolute chirp pulse

In each pulse calculated value of the phase of even and odd discrete.

$$\varphi_i = a \tan\left(\frac{S_i}{S_{i+1}}\right) \quad (1)$$

Convolution chirped pulses works based on two algorithms: discrete convolution and fast convolution. For discrete convolution we used expression:

$$Sg_i = 20 \cdot \lg \left(\sqrt{\left(\sum_{k=0}^{N-1} S_{i+k} \cdot \sin(\phi_{i+k}) \right)^2 + \left(\sum_{k=0}^{N-1} S_{i+k} \cdot \cos(\phi_{i+k}) \right)^2} \right) \quad (2)$$

$$\phi_{i+k} = \frac{5\pi}{2} \cdot \left(i+k - \frac{N}{2} \right) + \frac{\pi B}{N^2} \cdot \left(i+k - \frac{N}{2} \right)^2 \quad (3)$$

N – number of discrete in one chirp pulse;

B – base of chirp pulse.

Fast convolution algorithm consists from six steps:

1. Forming of the reference chirp signal samples with Hamming (fig. 4).

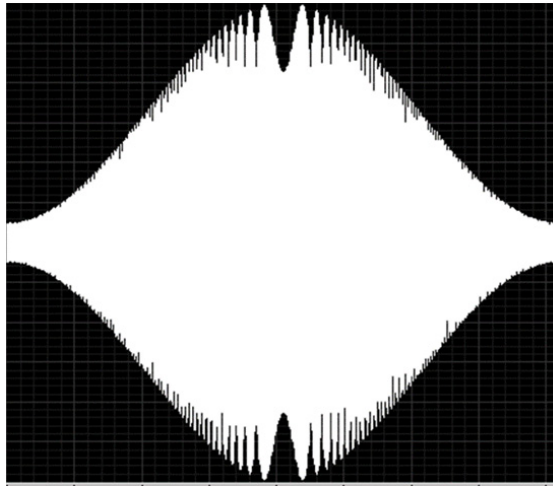


Fig. 4 Reference chirp signal samples with Hamming

2. Calculating FFT from reference signal.
3. Calculating FFT from input chirp pulse (fig. 5).

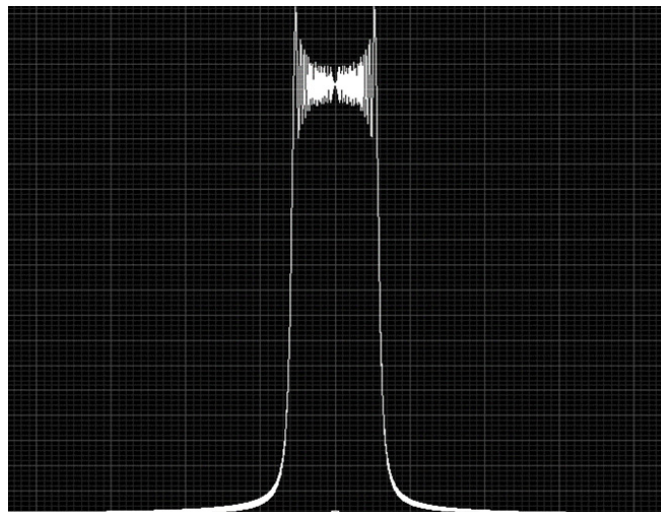


Fig 5. FFT from chirp pulse

4. FFT samples from chirp pulse multiply on complex conjugate FFT samples from reference signal.
5. By using inverse FFT we calculate cross correlation.
6. For calculation of the range of variation of the maximum levels of side lobes we define envelope from cross correlation.

In separate windows in front panel of VI shows a graph of relations of maximum and minimum peak convolute chirp pulses in the packet, difference between maximum and minimum of convolute chirp pulses in the packet, and the mean value of the phase, minimum and maximum side lobe level of the convolute chirp pulses.

New automated system has successfully replaced the existing system based on desktop devices and expanded the possibilities measuring system. This allowed significantly speeding up the process of testing and improving the

quality of measurements.

4. Summary

New automated system is successfully replacing traditional test system based on desktop devices and expand its capabilities. New automated system accelerates all measurements and improves measurement quality.

Acknowledgements

This work was supported by grants RFBR #14-07-00293 and RFBR #14-02-97510 r_center_a.

References

- [1] V.A. Vasin, I.B. Vlasov, Y.M. Egorov, Information technologies in radio systems, Moscow State Technical University, Moscow, 2004.
- [2] S.Z. Kuzmin, Digital radar. Introduction, KVITS, Kiev 2000.
- [3] Y.D. Shirman, Radioelectronic systems: Fundamentals and theory, Radiotec, Moscow, 2007.
- [4] G. Richard, Curry Radar System Performance Modeling, Artech house, inc., 2005.
- [5] B.A. Bakulev, Radar systems, Radiotec, Moscow, 2004.
- [6] Y.P. Grishin, V.P. Ipatov, Y.M. Kazarinov, Radio system, Vishaya shkola, Moscow, 2004.
- [7] V.I. Nefedov, A.S. Sigov, V.K. Bityukov, V.I. Khakhin, Metrology and radiomeasurement, Vishaya shkola, Moscow, 2006.
- [8] G.G. Raneev, Information-measurement technology, Vishaya shkola, Moscow, 2002.
- [9] V.I. Nefedov, A.S. Sigov, Metrology and electric and radio measurements in telecommunication systems, Vishaya shkola, Moscow, 2005.
- [10] Information on <http://www.ni.com/pxi/>
- [11] S.N. Danilin, M.V. Makarov, S.A. Shchanikov, S.V. Pantelev, Algorithm of choice the parameters of artificial neural network in the evaluation of the amplitude of the harmonic signal with respect to the destabilizing influences, Methods and devices of transmission and processing of information. 16 (2014) 70–73.
- [12] S.N. Danilin, M.V. Makarov, Shchanikov, Algorithm of designing neural networks with minimum capacity. 1 (2013) 245–251.
- [13] S.N. Danilin, Study of fault tolerance device transform coordinates with neural network architecture, Methods and devices of transmission and processing of signals in radio and radars. 5 (2009) 31–33.
- [14] S.N. Danilin, M.V. Makarov, The method for determining the minimum capacity of artificial neural networks, Radio- and telecommunication systems. 2 (2013) 71–75.
- [15] S.N. Danilin, Research of work quality index choice influence on result of devices faulttolerance estimation with neuro architecture, Radio- and telecommunication systems. 4 (2011) 15–19.
- [16] S.N. Zhiganov, Crimean Conference “Microwave & Telecommunication Technology”. (2014) 334–335. DOI: 10.1109/CRMICO.2014.6959419
- [17] S.N. Zhiganov, M.S. Smirnov, D.N. Romanov, Stand for assessing the quality decimated signal to a digital receiver NI – NIDays. (2014) 46–47.
- [18] S.N. Zhiganov, M.S. Smirnov, D.N. Romanov, Signal measurement system of intermediate frequency radar receiver, NIDays. (2014) 48–50.
- [19] Correlation and frequency properties of nonequidistant pulse sequence obtained by means of Frank codes CriMiCo. (2014) 334–335.
- [20] K.K. Khramov, S.N. Zhiganov, Investigation of the characteristics of digital filters in the software-hardware device for evaluation of modulation parameters of chirp waveform, Radio- and Telecommunication Systems. 3 (2011) 30–34.
- [21] N. Levanon, Eli Mozeson Radar Signals, Wiley-Interscience, 2004.



International Conference on Industrial Engineering

Information-measuring system for the flow process hydraulic machines testing stand

Dubrov V.I.^a, Shaykhtudinov D.V.^a, Shirokov K.M.^a *

^a *Platov South-Russian State Polytechnic University (NPI), 132, St. Prosvescheniya, Rostov region, Novocherkassk, 346428, Russian Federation*

Abstract

The article describes the materials on the development of intelligent algorithms, hardware and software configuration of information-measuring system that automates the stand for the operational life testing of hydraulic machines - oil sediment and motors. The cRIO was selected as a basic hardware platform with a set of input-output modules interacting with a personal computer via Ethernet interface to start the test and display the results. The intelligence of the system is provided by the implementation of artificial neural networks that analyze the stand values and make decisions on its operation.

© 2015 The Authors. Published by Elsevier Ltd. This is an open access article under the CC BY-NC-ND license (<http://creativecommons.org/licenses/by-nc-nd/4.0/>).

Peer-review under responsibility of the organizing committee of the International Conference on Industrial Engineering (ICIE-2015)

Keywords: cRIO, hydraulic motors, hydraulic pumps, hydraulic test stand, operational life testing, flow process, neural networks

1. Introduction

In order to technological process automation of the product operational life testing of the factories producing hydraulic machines, reducing the proportion of defects, increasing the objectivity and observability of the testing process is required to develop information-measuring system for collecting, primary processing and transmitting to a personal computer information of the temperature, pressure, and flow levels in test stand nodes, as well as to develop and implement diagnosis algorithms of the condition of the test hydraulic machine using parameters on the PC.

* Corresponding author. Tel.: +7-863-525-5240; fax: +7-683-525-5240.

E-mail address: iimt-srstu@mail.ru

2. Equipment And Software Used

Creating software to solve the problem carried out in the programming environment NI LabVIEW 2013 using the module NI LabVIEW FPGA. For the implementation of the system has been used platform NI cRIO-9075 [1] with the connected modules: NI 9205 [2], NI 9403 [3], NI 9263 [4]. To supply information-measuring system (IMS) has been used module NI PS-15 [5]. Stand contain preset flow sensors (4 pieces), Pressure (4 pieces), temperature sensor, speed sensor motor stand. To power the sensors used power supply type BP15B-D2-12 [6].

3. Solution Description

Technological scheme of hydraulic pumps and motors in general can be represented as a flowchart shown in Fig. 1.

Presented in Figure 1 is a block diagram of the production of hydraulic technology has some significant shortcomings, which appear in the final stages of testing and motor control. According to the requirements hydraulic motor should work a certain number of hours on test stands. To monitor the testing process human resources are engaged that not only increases the cost of the test phase and slows them. Process slowing of testing due to the limited staff time - 8 hours. The eight-hour working day leads to the fact that the pump test, requiring 720 hours of trouble-free operation is not reduced to one month of continuous testing, and by 3 months of tests during working hours. Automating this process will lead to significant economic and timing benefits.

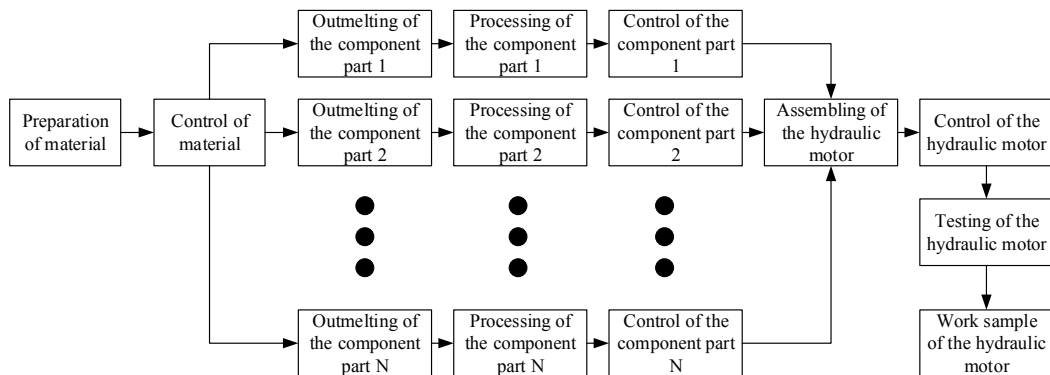


Fig. 1. Flow diagram of the flow process of motors

To solve the problem of automation of the scheme of electrical block data acquisition module of measurement/control unit information-measuring system shown in Fig. 2.

In Fig. 2 following notation is used: PC - personal computer, providing information processing of information-measuring system and process control tests, NI cRIO-9075 - control module of data collection process, NI 9205 - ADC module recording signals from the output of sensors, PS1 - power supply sensors BP15B-D2-12, PS2 - power supply for data collection manage module NI PS-15, FFS1- FFS3 - fluid flow sensors, PS - pressure sensor, TS - temperature sensor.

The electrical block scheme of the control module of the measure/control unit of information-measuring system is shown in Figure 3.

In Fig. 3 the following notation is used: NI 9403 [6] - module digital lines, NI 9263 - DAC module, PS1 - power supply unit BP60B-D4-24 for the control module for safety valve (CMSV) EDM-M112 / 20E0 , SV - safety valve PRE10-350 / 10N-D24K1 [7-9], YA1-YA4 ON/OFF - electromagnets involved in the process of testing, PK1-PK2 - starters AC.

The unit of measurement/control transmits the values of the measured parameters in the process of hydraulic tests on a personal computer connected via Ethernet interface with a frequency of at least sample per second. The

measurement/control unit sends the digital control signals to a control unit (7 keys): the keys ON (4 pieces) and OFF (3 pieces) of electromagnets installed in the hydraulic system, the keys ON (2 pieces) and OFF (1 key) of starter motors AC current.

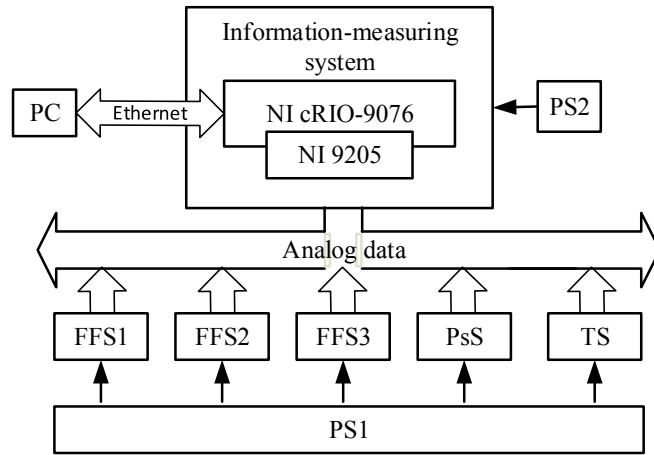


Fig. 2. Block diagram of data acquisition module of measurement/control unit

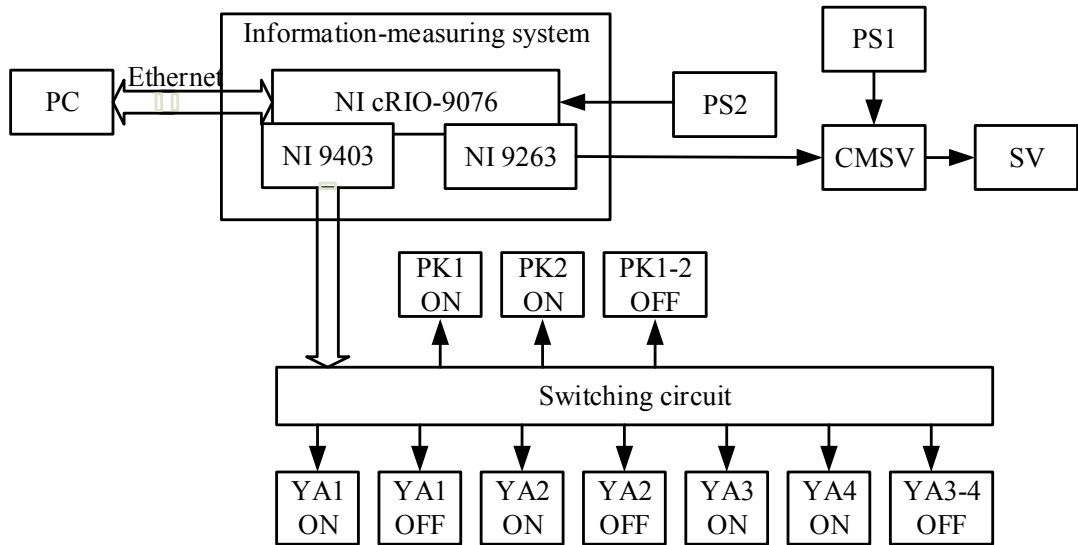


Fig. 3. Block diagram of the control module of measurement/control unit

Control signals correspond to the next parameters: voltage 0-0.2 V - off; 4-4.5 V - on, current to 2mA, the switching frequency - less than 1 Hz. The measurement/control unit provides the ability to supply the analog control signal to the control module of pressure control valve in the hydraulic system of the stand-type PRE10-350 / 10N-D24K1.

The structure of the software of control system of test stand is shown in Fig. 4.

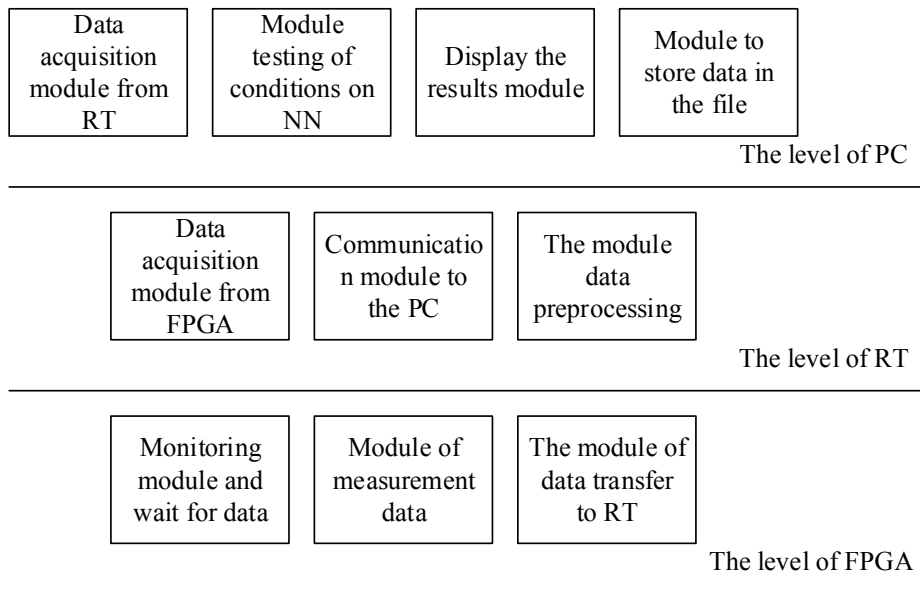


Fig. 4. The modular structure of embedded software control system for test stand

The structure of Figure 4 shows that the software (SW) has three levels: the software on a personal computer (PC) - the level of PC software on the real-time system (RTS) - the level of RT, the software on the field-programmable gate array (FPGA) - level FPGA. Each of these levels are associated with each other, the FPGA with RT - via the RS232 interface inside the module cRIO, RT with a PC - via an Ethernet interface. At levels of FPGA and RT the collecting and primary processing of information is implemented and data is being transferred to the PC. At the top level (PC) in system intelligent control algorithms of the conditions of work with the use of artificial neural networks was integrated [10, 11]. All the results of the algorithms used directly displayed on the screen in real time and saved to a file for further investigation and possible treatment.

Role of artificial neural network (ANN) [12] in this system is shown in Figure 5.

Neural networks have been applied in various fields of science and technology [13-19]. Application of neural networks in control was to meet quite often in various publications [20].

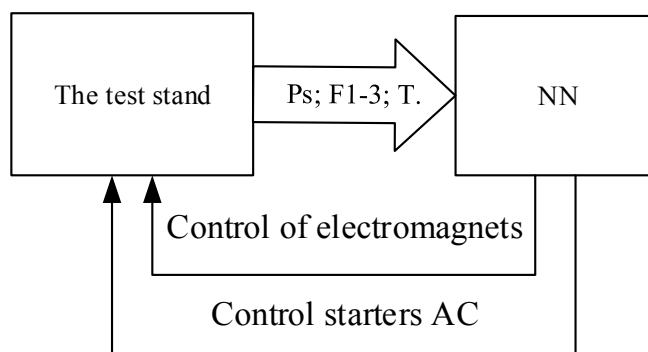


Fig. 5. The block diagram of the interaction of ANN and the test stand

Figure 5 shows the following symbols: Ps - signal from the pressure sensor, F1-3 - signal flow sensors, T - signal from the temperature sensor.

Multilayer perceptron with one hidden layer is used as ANN [21]. Based on the scheme in Figure 5 the input vector X and output vector Y of the neural network is equal to:

$$X = \begin{bmatrix} x_0 \\ D \\ F_1 \\ F_2 \\ F_3 \\ T \end{bmatrix} = \begin{bmatrix} x_0 \\ x_1 \\ x_2 \\ x_3 \\ x_4 \\ x_5 \end{bmatrix}, \quad Y = \begin{bmatrix} PK1ON \\ PK2ON \\ PK1-2OFF \\ YA1ON \\ YA2ON \\ YA3ON \\ YA4ON \\ YA1OFF \\ YA2OFF \\ YA3-4OFF \end{bmatrix} = \begin{bmatrix} y_1 \\ y_2 \\ y_3 \\ y_4 \\ y_5 \\ y_6 \\ y_7 \\ y_8 \\ y_9 \\ y_{10} \end{bmatrix}, \quad (1)$$

where x_0 - bias unit.

And input vector X compose of numerical values with a range of measured values from 0 to 1 and increments of 0.01. Output vector consists of the Boolean variables that can take values of either 0 or 1.

The number of neurons in the hidden layer is equal to the number of neurons in the output layer. The output vector A of the hidden layer and respectively output vector Y of the output layer of the neural network is:

$$A = \begin{bmatrix} a_1 = g \left(\sum_{i=0}^5 \omega_{1i}^1 \cdot x_i \right) \\ a_2 = g \left(\sum_{i=0}^5 \omega_{2i}^1 \cdot x_i \right) \\ \bullet \\ \bullet \\ \bullet \\ a_{10} = g \left(\sum_{i=0}^5 \omega_{10i}^1 \cdot x_i \right) \end{bmatrix}, \quad Y = \begin{bmatrix} y_1 = g \left(\sum_{i=0}^{10} \omega_{1i}^2 \cdot a_i \right) \\ y_2 = g \left(\sum_{i=0}^{10} \omega_{2i}^2 \cdot a_i \right) \\ \bullet \\ \bullet \\ \bullet \\ y_{10} = g \left(\sum_{i=0}^{10} \omega_{10i}^2 \cdot a_i \right) \end{bmatrix}, \quad (2)$$

where ω_{ji}^1 – transfer coefficient values from the i -th neuron of the input layer to the j -th neuron of the hidden layer, $g(f)$ - the transfer function of the neuron, ω_{ji}^2 – transfer coefficient values from the i -th neuron of the hidden layer to the j -th neuron of the output layer.. At the current task sigmoid function is used: $g(f) = \frac{1}{1 + \exp(-f)}$.

The structure of the neural network used is shown in Figure 6.

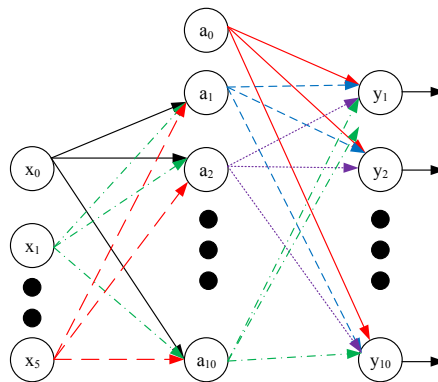


Fig. 6 - The structure of the neural network used

The main feature shown in Figure 5 scheme is its simplicity and efficiency simultaneously. The output of the neural network derived vectors are binary vectors control the test stand. Due to the small amount of data and a simple structure of ANN at a satisfactory rate responds to changes in the measured parameters.

4. Implementation

The device is embedded at OJSC "Shakhtinskiy zavod Gidroprivod" and is currently in trial operation.

Acknowledgements

The results obtained with the support of the grant RFBR № 15-38-20652 "Development of the theory of predictive methods for sensorless control and diagnosis of electric drives".

References

- [1] Information on <http://www.labviewportal.eu/viewtopic.php?f=618&t=5948/>
- [2] Information on ftp://ftp.ni.com/pub/branches/russia/c_series_modules/ni_9205.pdf.
- [3] Information on www.ni.com/pdf/manuals/372617a.pdf.
- [4] Information on ftp://ftp.ni.com/pub/branches/russia/c_series_modules/ni_9263.pdf.
- [5] Information on <http://www.ni.com/pdf/manuals/372911b.pdf>.
- [6] Information on <http://www.owen.ru/catalog/57736788>.
- [7] D.V. Shaykhutdinov, N.I. Gorbatenko, Sh.V. Akhmedov, M.V. Shaykhutdinova, K.M. Shirokov, Experimental and Simulation Tests of Magnetic Characteristics of Electrical Sheet Steel, Life Science Journal. 10(4) (2013). http://www.lifesciencesite.com/ljs/life1004/361_22173life1004_2698_2702.pdf.
- [8] D.V. Shaykhutdinov, S.G. Yanvarev, K.M. Shirokov, R.I. Leukhin, The method of technical diagnostics interturn faults in electromagnetic devices on the basis of the flux-current curves // Sovremennye naukoemkie tehnologii. 8 (2014) 69–71.
- [9] D.V. Shaykhutdinov, S.G. Yanvarev, K.M. Shirokov, Sh.V. Ahmedov, The method of technical diagnostics of the geometric parameters of the magnetic system of electromagnetic devices on the basis of the flux-current curves, Mezhdunarodnyj zhurnal jeksperimental'nogo obrazovanija. 8(1) (2014) 84–86.
- [10] S. Haykin, Neural Networks: A Comprehensive Foundation, second ed., Prentice Hall, Inc. 1999.
- [11] M. Mohri, Murphy, Foundations of Machine Learning, The MIT Press, 2012.
- [12] Hugh Cartwright, Artificial Neural Networks, Springer-Verlag New York, 2015.
- [13] G.A. Rovithakis PhD, A. Manolis, Christodoulou. Adaptive Control with Recurrent High-order Neural Networks: Theory and Industrial Applications, Springer-Verlag London, 2000.
- [14] K. Patan, Artificial neural networks for the modelling and fault diagnosis of technical processes, Springer-Verlag Berlin Heidelberg, 2008.
- [15] R.S. Govindaraju, A. Ramachandra Rao, R.S. Govindaraju, Artificial Neural Networks in Hydrology, Springer Netherlands, 2000.
- [16] S. Behnke, Hierarchical Neural Networks for Image Interpretation, Springer-Verlag Berlin Heidelberg, 2003.
- [17] J. R. Rabunal, J. Dorrado, Artificial Neural Networks in Real-life Applications, Idea Group Publishing, 2005.
- [18] T.W.B. Kibble, F.H. Berkshire, Artificial Neural Networks in Vehicular Pollution Modelling, Springer. 2006.

- [19] P.T. Quinlan, *Connectionist Models of Development: Developmental Processes in Real and Artificial Neural Networks*, Psychology Press. 2003.
- [20] N.A. Markov, Prognozirujushhee inversnoe nejroupravlenie jeksperimental'noj ajerodinamicheskoy ustanovkoj (Predictive inverse neurocontrol by experimental aerodynamic plant, *Vestnik inzhenernoj shkoly dvfu*. 4(13) (2012).
- [21] J.G. Taylor, *Concepts for Neural Networks*, Springer-Verlag London. 1998.



International Conference on Industrial Engineering

Application of brushless machines with combine excitation for a small and medium power windmills

Kiessh I.E., Gandzha S.A.*

South Ural State University, 76, Lenin Avenue, Chelyabinsk, 454080, Russian Federation

Abstract

This article shows the advantages in application of the brushless machines with combine excitation (excitation from permanent magnets and excitation coil) for small and medium power windmills. This type of electric machine is compared with a typical brushless motor and an induction motor. The main advantage is the decreasing of the outline sizes of electric machine and the reduction of price for an electronic control system. The design and the principle of operation of the electric machine are provided. This machine was modeled using Solisworks program to create the design and Maxwell program to analyze the magnetic field. The results of testing are shown too.

© 2015 The Authors. Published by Elsevier Ltd. This is an open access article under the CC BY-NC-ND license (<http://creativecommons.org/licenses/by-nc-nd/4.0/>).

Peer-review under responsibility of the organizing committee of the International Conference on Industrial Engineering (ICIE-2015)

Keywords: brushless electric machine, combine excitation, permanent magnet, excitation coil, regulation of magnet flow.

1. Introduction.

Alternative power source systems are being developed rapidly. The main reason for that is the energy collapse appearing from the limitations of coal, gas, oil.

Among all other renewables the wind turbine is one of the most developing machines due to several advantages:

- wind is the endless power source;
- it's an ecologically clean machine.

* Corresponding author. Tel.: +7-908-812-5819.

E-mail address: gandja_sa@mail.ru

One of the main aggregates of the wind turbine is alternator. High reliability requirements do not allow the use of brush electric machines in turbines. So only brushless machines can be discussed so far:

- asynchronous alternators with capacitor batteries as a excitation source;
- synchronous alternators with excitation from permanent magnets;
- synchronous induction alternators with excitation from winding;
- synchronous alternators with combined excitation with excitation from permanent magnets and winding.

Practice shows that asynchronous alternators with capacitor batteries on more than 1 kW power are not competitive by a price comparing to other electric machines due to the high price of battery [2].

Recently synchronous alternators of the above mentioned types are dominating in wind power industry.

Below there is a try to analyze these alternators.

The distinctive feature of wind turbine operation is variable frequency of rotor rotation, which in turn depends on the wind speed.

EMF of alternator changes with the changing of rotation frequency. The voltage on the output terminals changes as well.

However though the frequency and loading are changing, the constant voltage on the terminals is the critical issue for the customer as the most appliances are made for the constant nominal voltage.

- The stabilizing of the voltage on the terminals of alternator is possible by 2 ways: Use of pulse-duration modulation for power circuit.
- Change of the excitation flux due to the change of rotation frequency.

Alternator with permanent magnets is acceptable for the 1st approach.

Alternator with excitation winding or combined excitation are acceptable for the 2nd approach.

All these approaches are used in industry. But the main factor while making a choice for any specific power module will be:

The price of alternator + control electronics + power electronics.

The research shows that the total cost of combined excitation alternator could be less than others [3]. So let's discuss this design in details.

2. Design and operation principle of alternator with combined excitation

Alternator with combine excitation has permanent magnet and excitation coil [1]. It gives the following advantage if compare alternator with electric machine another kind. The using powerful permanent magnet such as Neodymium-Iron-Bore or Samarium-Cobalt allows decrease the outline sizes. The using of excitation coil allows to control voltage in circuit with low current and electronic control system will has low cost in this case.

The design of AC alternator with combined excitation is illustrated by fig. 1, where the cross-section of alternator is shown.

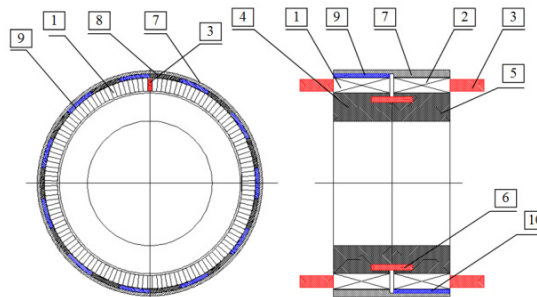


Fig.1. The cross-section of alternator

Alternator consists of stator and rotor. Stator consists of laminated packages 1 and 2 with slots. The slots have the same direction along the axis. Multi-phase winding 3 is located in the slots of packages. Laminated packages are pressed on the big parts of laminated core 4 and 5. Motionless excitation winding 6 is located between packages of laminated core. Rotor 7 of alternator is located outside stator. It has big poles 8 and permanent magnets 8 and 10. Permanent magnets and poles are alternated one after another along the circle. They form two rings which cover laminated packages 1 and 2. The rings are located so that the permanent magnet 9 is located opposite the pole 8 along the axis direction. Magnets 9 and 10 have radial magnetization. In one ring the magnets have “south” magnetization 9 on the surface directed to the package, in another ring the “north” magnetization 10.

Alternator operates as follows:

Under the DC the excitation winding 6 generates magnetic flux which is looped by the following way: laminated package 1, air gap, big pole 8 of the first ring, back of rotor, big pole 8 of the second ring, air gap, laminated package 2, part of laminated core 5, part of laminated core 4.

Magnetic flux generated by magnets, is looped by the following way: laminated package 1, air gap, “south” magnet 9, back of rotor, “north” magnet 10, air gap, laminated package 2, part of laminated core 5, part of laminated core 4.

Magnetic fluxes have the same areas in the bush and in the back of rotor. In the other areas magnetic fluxes are not crossing. Direction of magnetic flux generated by magnets, is constant, is not changing. Direction of flux from excitation winding depends on polarity of power source. Then flux either must be added to the flux of permanent magnets, or subtracted.

During rotation of rotor the total flux induces EMF in stator winding 3. The value and direction of the current in excitation winding 6 during frequency changing is chosen so that the multiplication of rotation frequency on the flux value should be constant.

Amplitude of output voltage of alternator is constant during changing of frequency in wide range. This result for alternator 8 kW,28V is shown in diagram below (fig.2).

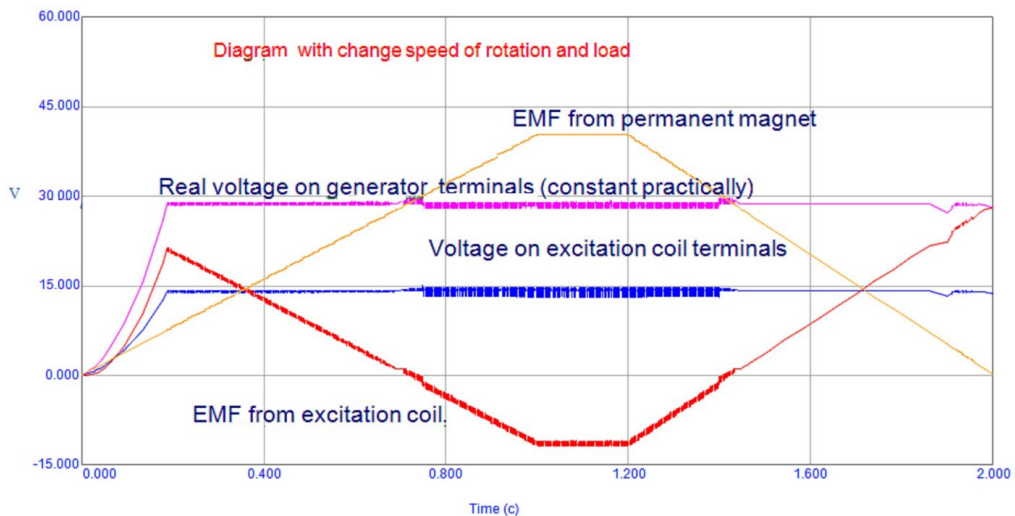


Fig.2. Diagram for generator 8 kW,28 V

The electromagnetic processes and heating condition in equipment is very complex. To be sure in quality of engineering design it is necessary to use the exact engineering technologies for modeling these processes. In this case only the choice of engineering design would be correct.

This modeling has been executing in South Urals State University with using super computer and necessary software. In the fig. 3 is showed the fragments of electromagnetics analysis for this generator.

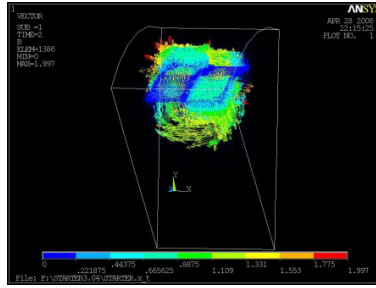


Fig.3. The result of magnet field analysis

The authors hold the method of design such generators for different capacities and sizes and this method is based on the exact engineering technologies.

This idea was used for alternator for windmill 3 kW.

Bellow the prototype of windmill is shown fig.4 .



Fig.4. Project for windmill 3 kw.

The advantages of generator with combine excitation can be used for another autonomous power source operating from drives with variable frequency of rotation (cars, diesel generator, hydro-stations, wind turbines).

A patent has been issued on this concept;

The project has received some funding for development at the University. Inquiries for Collaboration partners are invited.

3. Conclusion

The concept of generator with combine excitation is proposed for different application. Its allow decrease the sizes and cost for autonomous electric sources.

The validity of the proposed concept is confirmed by complex engineering calculations using the finite element method and the results of the testing of prototypes.

Power engineering faculty of the SUSU owns the methods of analysis and synthesis of the proposed drive and has the ability to conduct research and development on the proposed topics. It is possible to do design and manufacture necessary equipment with using skills and opportunities the authors have.

References

- [1] GOST 27471, Rotating electric motors. Terms and definition, Mashini electriccheskie vrashaushiesy. Terminy i opredeleniy. (In Russian)
- [2] I.P. Kopilov, Electric machine, fifth ed., Visshay shkola, Moscow, 2006.
- [3] S.A. Gandzha, A.V. Erlisheva, Starter-generator for autonomous source of energy supply, Vestnik uzhno-uralskogo gosudarstvennogo universiteta. Seria "Energetika". 6(9) (2005) 84-86.

International Conference on Industrial Engineering

Using solar optical fibers for public buildings illumination in the South Urals

Kirpichnikova I.M., Volkova O.S., Maliugina A.A.*

South Ural State University, 76, Lenin Avenue, Chelyabinsk, 454080, Russian Federation

Abstract

The article shows the problem of energy shortage and justifies the necessity of energy-saving activities to be applied in the lighting of buildings. The analysis of solar radiation throughout the year and the length of daylight availability in Chelyabinsk region is made. Based on the analysis of designs and technical characteristics of solar optical fibers their use in newly constructed buildings and social facilities is justified, disclosing the terms of using solar optical fibers in the Urals conditions. The data on the changes of the natural lighting in the room, depending on the time of the day, cloudiness, and the location of the buildings to the cardinal points is produced, the expediency of the combined lighting systems "solar optical fiber+ light-emitting diode" application, which will significantly reduce the lighting costs, is illustrated.

© 2015 The Authors. Published by Elsevier Ltd. This is an open access article under the CC BY-NC-ND license (<http://creativecommons.org/licenses/by-nc-nd/4.0/>).

Peer-review under responsibility of the organizing committee of the International Conference on Industrial Engineering (ICIE-2015)

Keywords: energy efficiency, solar optical fibers, illumination (lighting), solar radiation, light-emitting diodes.

1. Introduction

The priority trend of social and economic development of the Chelyabinsk region is the development of medicine, education, sports, culture and arts, which leads to the construction of major sports complexes, swimming pools, schools, kindergartens, medical centers, clinics, exhibition centers, museums and other public buildings.

Modern buildings have not only an interesting design, but also provide maximum comfort for guests: well-chosen lighting, ventilation and air conditioning, heating systems - resulting in an overall increase in electricity consumption in the region. But Chelyabinsk region already experiencing energy shortages (South Ural power plants

* Corresponding author. Tel.: +79226366140; fax: +7 351-2679894.

E-mail address: ionkim@mail.ru

can provide electricity demand is only 80%). [1]. In addition, the annual growth of tariffs for energy in the region is about 4%. [2]. All of the above makes think seriously about energy efficiency. Since the share of energy consumption for lighting in public buildings is 30-50%, the introduction of energy-saving-measures in these systems is especially important.

2. Rationale for the use of solar optical fibers

2.1. Traditional light sources

The traditional methods of energy efficiency increasing of lighting systems include:

- Replacement of artificial light sources others with greater light output and lower power consumption (for example, replacing incandescent lamps with fluorescent and fluorescent with light-emitting diode);
- Light flow of artificial light sources control using a variety of dimmers, light sensors, motion sensors and etc.

Energy-saving light sources, in addition to high luminous efficiency, low power consumption, long life time, has a number of disadvantages:

- Pulsing the light flux;
- Ultraviolet radiation;
- The presence of mercury in gas discharge lamps;
- The poor quality of some of the manufacturers of lamps.

All this leads to deterioration in health and limitation of the use of these light sources in public buildings, especially in children and medical institutions.

An alternative source is the use of natural light by using the solar optical fibers.

2.2. Solar optical fibers

Solar optical fiber is the light conducting device transmitting light at a distance by multiple reflections within the hollow structure having a reflective surface.

Advantage of solar fibers is that they can:

- To replace the source of artificial lighting during daylight hours;
- To reduce the heat inflow from the artificial lighting and thus the cost and power of conditioning equipment and operating costs;
- To receive the full spectrum of lighting (for the transmission of the completeness of colors of the interior space, as well as increasing operability and reduce fatigability, which causes the artificial light sources);
- To increase the level of comfort in the buildings;
- To include in the system a source of artificial lighting (for the dark time of day), adjust the brightness of the transmitted light or turn it off completely [3,4,5].

Thus, the installation of solar optical fibers in public buildings will not only reduce energy costs but also reduce the harmful effects of artificial lighting sources on human health.

2.3. Goals and objectives of the study

Objective: to investigate the possibility of using solar optical fibers in public buildings in the South Urals.

The research problem:

Evaluate the effectiveness of the use of solar optical fibers with regard to:

- Climatic features of South Urals;
- The amount of solar radiation reaching the surface, for different areas of the Chelyabinsk region;
- Lighting of buildings;
- Design features of optical fibers.

3. The climatic characteristics of the Chelyabinsk region

The climate in Chelyabinsk region is continental, which is determined by the position of the territory on the mainland. The main features of the climate are the long cold winter with frequent snowstorms, dry and hot summers with droughty periods.

The average value of total solar radiation over the region is $1150 \text{ kW} \cdot \text{h} / \text{m}^2$ per year. By the magnitude total annual solar energy arriving on a horizontal surface, the region is divided into five areas [6]. Average annual duration of sunshine in the region is 12 hours. The duration of sunshine varies in the region around 2000 hours per year. Thus, only 50% of the days in a year are sunny, other days are cloudy (Table. 1).

The length of daylight varies throughout the year and ranges from 7 hours in January to 17 hours in June (Figure 1). Moreover sunrise starts at 10:30 in January and at 5:30 in July, and sunset at 17:30 takes place in January and at 22:30 in July [9].

Table 1. An example of a table. Table 1. Zoning of the Chelyabinsk region [7, 8].

Magnitude	V. Ufaley, Kyshtym	Chelyabinsk, Chebarkul	Plast, Chesma	Troitsk, Varna	Bredy, Kartaly
The mean values of total solar radiation H, $\text{kW} \cdot \text{h} / \text{m}^2$	1050	1100	1150	1200	1250
The average duration of sunshine S, h	70.2	67.9	71.4	72.5	79.1
The percentage of sunny days per year, %	48.7	47.1	49.5	50.3	54.9

A special feature of winter in the region is the presence of stable snow cover, on average, from November to April. The duration of snow cover from 160-170 days in mountainous areas up to 140-150 days in the south. The average height of snow cover in the region is 30-40 cm [10].

4. The research of the premises illumination

One of the main factors of a comfortable stay of people indoors is to maintain standardized illumination in it, which is achieved by natural and artificial lighting. The construction of most buildings in the Chelyabinsk region has natural side lighting, an area which does not exceed 30% of the area of the outer wall.

We conducted a research - the lighting dependence inside the buildings of the following factors:

- The location of the outer wall of the room from the cardinal point;
- The distance to the wall with windows;
- Cloudiness.

Measurements were taken directly from the window aperture.

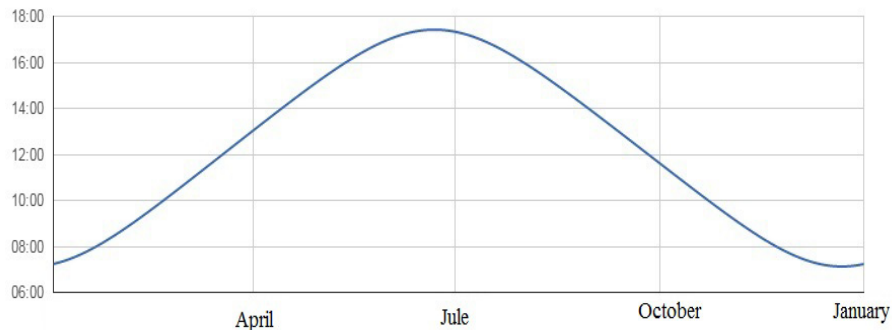


Fig. 1- The duration of the daylight in Chelyabinsk during the year

Research time: in July 2015, the average duration of daylight for the Chelyabinsk city is 16 hours, sunrise at 6:00, sunset at 22:00. Comparison of illumination changes from the location of the outer walls of buildings with windows, showed that the average illumination of the southern side is 3.73 times higher than the northern (Figure 2).

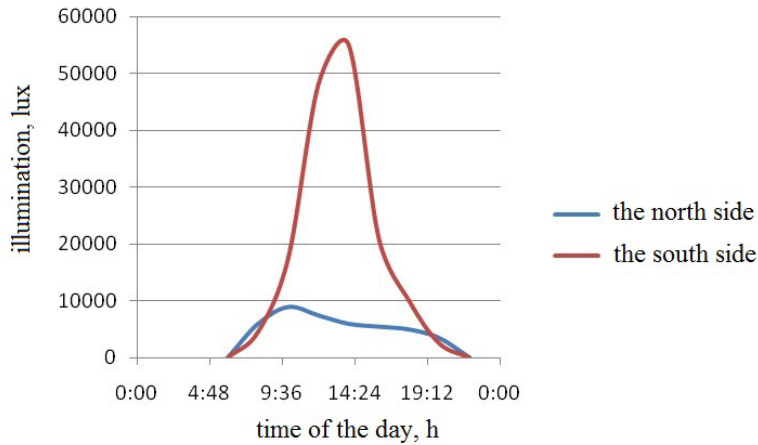


Fig. 2- Changing the lighting in the room, depending on the time of the day and buildings location by cardinal points

Dependence the research of indoor illumination from the distance from the source of natural light (see Fig. 3) shows that the luminance decreases, and a distance of 5 m from the window, this value is an average of 13.3 times. In addition, the standardized lighting 200 lux for public buildings at a distance from the windows of 4 m or more can not be achieved at any time of the day, and at a distance of 3 m is achieved only until 12:00. Research of the effect of clouds showed that illumination indoors is reduced by 3.9 times in comparison with the clear day. Considering that in the Chelyabinsk region less than half the days in a year are clear, this fact is necessary to include in the design of lighting buildings systems. Thus, our studies indicate that in buildings with natural side lighting, it is not enough light during the day and artificial lighting is required.

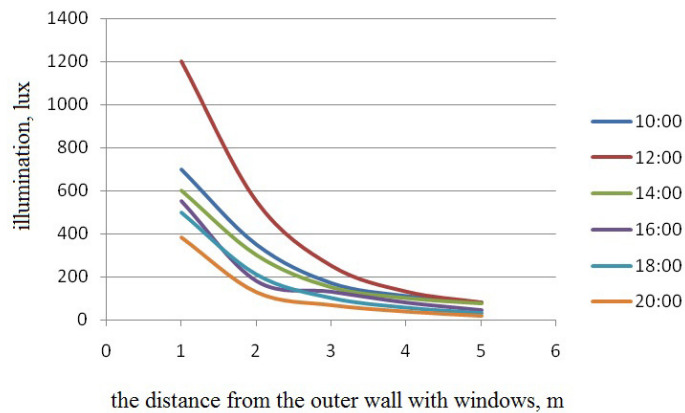


Fig. 3. - The dependence of the illumination indoors from the distance from the outer wall with windows

We propose to increase the number of sources of natural light by installing solar optical fibers.

Analysis of Chelyabinsk region climate and our studies have shown that the use of optical fibers will increase the solar illumination indoors to standardized, subject to the following conditions:

- The location of the optical fibers domes on the south side of the building or on the roof;
- The dome has to collect not only the direct rays, but also scattered since more than the half of the days in a year are cloud;
- The dome should be placed above the height of the snow cover, i.e, higher than 40 cm.

5. Choosing the design of solar optical fibers for the premises illumination

Today, solar optical fibers produce dozens of foreign companies. In Russia, widely spread only two: Solatube (USA) and Allux (Czech Republic).

After studying design features of fibers of these firms, we chose the European company as more appropriate to the conditions of the South Urals. The Allux fiber dome is made of polycarbonate, which allows it to remain transparent to ultraviolet rays over the lifetime. The dome shape is a hexahedral prism, which allows absorbing the maximum amount of light even on a cloudy day. Special “winter” design of optical fibers is not subject to condensation inside the fiber and prevents its freezing in the winter period of operation. The hollow Allux optical fiber inside has a mirror coating, consisting of a number of optical and protective layers coated on the base sheet of aluminum by chemical vacuum spraying that allows it not to burn up under the action of ultraviolet light and does not crack when the temperature drops.

Modern structures of solar lighting systems have additional accessories, such as daylight regulator, which shuts off the light in the room, or reduces its amount or kit for night-time, containing an artificial light source, thereby reducing the number of lamps. Most often incorporated energy-saving lamps in them. The reflecting fiber length depends on the diameter of the cylinder. Thus, the manufacturer offers optical fibers with a diameter up to 400 mm length of the cylinder up to 10 m and with a diameter of 600 mm and more - up to 25 m [11].

Given that the average duration of daylight for the year in the South Urals is 12 hours, the use of combined lighting systems: "optical fiber + light-emitting diode" will significantly reduce energy costs, while allowing a person to feel comfortable in the dark time of the day. Figure 4 shows the duration of light-emitting diodes switching-on in the system "optical fiber + light-emitting diode" during the year for the 12-hour working day from 10:00 to 22:00.

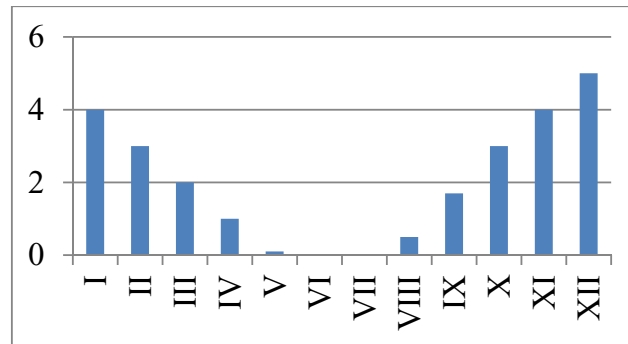


Fig. 4- The duration of the light-emitting diode bulbs operation incorporated in solar optical fibers, h

Thus, making natural illumination of public buildings with solar optical fibers with the set of light-emitting diodes for working in the dark time of the day, will reduce the time of energy consumption to an average of two hours a day, therefore, save energy up to six times.

6. Conclusions

- The increasing energy consumption for newly constructed public buildings lighting requires a search for new energy-saving technologies and devices.
- Research of the changes of the natural lighting in the room, depending on the time of the day, cloudiness, and the location of the buildings to the cardinal points revealed that the lighting does not correspond to standardized, therefore, the installation is required for additional artificial lighting.
- If the average total solar radiation in the South Urals is $1150 \text{ kW} \cdot \text{h} / \text{m}^2$ and the duration of the daylight in average is 12 hours per year, the most expediency is the use of the dome solar optical fibers installed on the south side of the roof or buildings.
- The use of combined lighting systems "solar optical fiber+ light-emitting diode", significantly reduce energy costs, while allowing a person to feel comfortable in the dark period of the day.

References

- [1] L.A. Saplin, Jekonomicheskoe obosnovanie ispol'zovanija netradicionnyh vozobnovljaemyh istochnikov jenergii v Cheljabinskoj oblasti, Polzunovskij al'manah. 1 (1999) 88–101.
- [2] Information on <http://www.tarif74.ru/htmlpages/Show/Tarifypotrebitelyam/Tarifynaelektricheskuyenergiy>
- [3] A.V. Salomatin, Ju.N. Kazakov, Nauchnoe obosnovanie novyh tehnologij ustrojstva solnechnogo osveshhenija v zdaniyah, Jenergosovet. 6(31) (2013).
- [4] Information on <http://www.solatube.su/o-tehnologii-solatube/preimushhestva-sistemyi-osveshheniya-solatube/>
- [5] Information on <http://www.solarway.su/index.php>
- [6] L.A. Saplin, S.K. Sher'jazov, O.S. Ptashkina-Girina, Ju.P.Il'in, Jenergosnabzhenie sel'skohozejstvennyh potrebitelej s ispol'zovaniem vozobnovljaemyh istochnikov, Cheljabinsk, ChGAU, 2000.
- [7] Information on <http://voshod-solnca.ru.html>
- [8] I.M. Kirpichnikova, O vozmozhnosti ispol'zovanija vozobnovljaemyh istochnikov jenergii v Cheljabinskoj oblasti, Vestnik Jenergosberezhenija Juzhnogo Urala. 2 (2007) 58–68.
- [9] L.A. Saplin, Utochnennaja metodika rascheta solnechnoj jenergii na primere Cheljabinskoj oblasti, Vestnik Cheljabinskogo agroinzhenerenogo universiteta. 26 (1998) 121–125.
- [10] Agroklimaticheskie resursy Cheljabinskoj oblasti, Gidrometeoizdat, Leningrad, 1977.
- [11] Information on <http://www.allux.cz/cz>.



International Conference on Industrial Engineering

Simulation of lithium battery operation under severe temperature conditions

Andreev A.A.^{a*}, Vozmilov A.G.^a, Kalmakov V.A.^a

^a South Ural State University, 76, Lenin Avenue, Chelyabinsk, 454080, Russian Federation

Abstract

The use of lithium batteries in the conditions associated with the operation at low temperatures requires studying the effect of temperature factor on battery performance. Using the simulation, and particularly equivalent circuit models method, may be useful at the initial stages of the study. The paper describes the use of lithium battery model with one voltage source, one series resistor, and a single RC block for simulating the LiFePO₄ battery operation at low temperatures. The model was validated using experimental data obtained by LiFePO₄ battery discharge at different temperatures and showed good accuracy. The simulation results allow estimating the negative effect of low operating temperature on battery parameters and making a conclusion about the need for systems creating optimum operating conditions for batteries working under severe temperature conditions.

© 2015 The Authors. Published by Elsevier Ltd. This is an open access article under the CC BY-NC-ND license (<http://creativecommons.org/licenses/by-nc-nd/4.0/>).

Peer-review under responsibility of the organizing committee of the International Conference on Industrial Engineering (ICIE-2015)

Keywords: lithium cell; lithium cell simulation; electrical equivalent lithium cell model

1. Introduction

Batteries (chemical sources of electricity) are now widely used in various technical systems – from mobile phones and power systems to backup power. One of the most perspective and promising application include electric and hybrid vehicles, as well as energy storage systems for stand-alone power systems. [1,2,3] Distributed and autonomous energetics is particularly relevant for Russia, since according to various estimates from 60 to 70% of the territory is not covered by centralized power. About 20 millions of people and up to 15% of natural resources of the Russian Federation are concentrated in this area. [4] The use of autonomous energy systems based on renewable

* Corresponding author.

E-mail address: toxin711@rambler.ru

energy sources is the most appropriate in these areas. Application of autonomous power covers all aspects of human life, which requires a source of power: power supply of remote settlements, equipment for the protection of borders and critical facilities, oil and gas pipelines, temporary parking camps, engineering constructions, mobile operators equipment. The battery is an essential part of the autonomous power supply system, smoothing the curve of electricity generated by the renewable sources and ensuring the load operation

2. Task formulation

Battery performance and lifetime are affected by a number of factors (charge and discharge dynamics, depth of discharge, operating temperature, storage temperature, etc.). [1,5] It is especially important to emphasize the factor of temperature, which become critical in the severe temperature conditions of Russia, where the average annual temperature is $-23\text{ }^{\circ}\text{C}$ in some regions. [6] Battery's available discharge capacity and lifetime can dramatically decrease under such conditions.

Studies of severe temperature conditions influence on the batteries characteristics can be performed both by full-scale tests [7], and simulation. Conducting full-scale research requires significant financial and time costs. Therefore, at the initial stage it is rationally to use computer simulation, which allows to simulate the battery operation, analyze obtained characteristics and dependences, as well as predict the behavior of batteries under various environmental conditions.

There are a number of batteries models developed [8,9,10], but the most common approach is the equivalent circuit model (ECM) method, which provides acceptable accuracy and low computational cost. The lithium battery ECM with a single RC-block developed by Robin Jackey at Mathworks [11] was used in this work. This model (Fig. 1) includes voltage source E_m , RC-branch of the capacitor C_1 and resistor R_1 , and the series resistor R_0 . The parameters of all elements of the equivalent circuit are changed depending on the battery temperature (T) and the state of charge (SOC). This change is realized by means of two-dimensional tables of values of each element, where the rows represent the values of the SOC and temperature columns. The model is able to predict changes in the battery voltage during operation and estimate an SOC in real time based on changes in ambient temperature [12], but it needs to be validated – the model parameters must be estimated so the behavior of the model adequately represents battery operation.

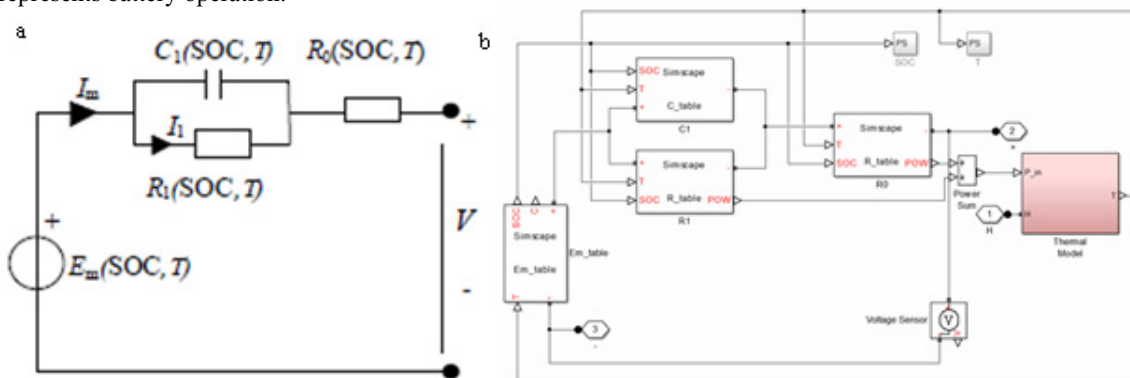


Fig. 1. (a) Electrical scheme of cell ECM; (b) Matlab Simulink ECM.

3. Experimental testing and simulation

LiFePo4 (Lithium iron phosphate) battery Zippy Flightmax was used for experimental testing. Some characteristics of the selected cell that are necessary for further simulation are given in Table 1.

The values of 955.4 J/kg·K as specific heat capacity of the cell (as a standard value for LiFePo4 batteries [13]) and 10 W/m² as the heat transfer coefficient between the cell and the environment (which corresponds the natural cooling) were selected for simulation.

Table 1 Cell characteristics.

Parameter	Value
Nominal capacity	2100 mAh
Weight	0,063 kg
Height	0,121 m
Width	0,044 m
Thickness	0,006 m

The experimental setup for the investigation of temperature influence on the battery performance consisted of the Imax B6 AC Charger, the cell with the attached temperature sensor, a laptop connected to the charger via RS-485 for data collection using Logview software.

The cell was discharged with 0,5 A and 1 A current at a 25 °C temperature, and with 1 A current at –15 °C temperature in a climatic chamber. Received dependencies of discharge voltage from SOC at different temperature and discharge current, approximated in Matlab, are shown in Fig. 2.

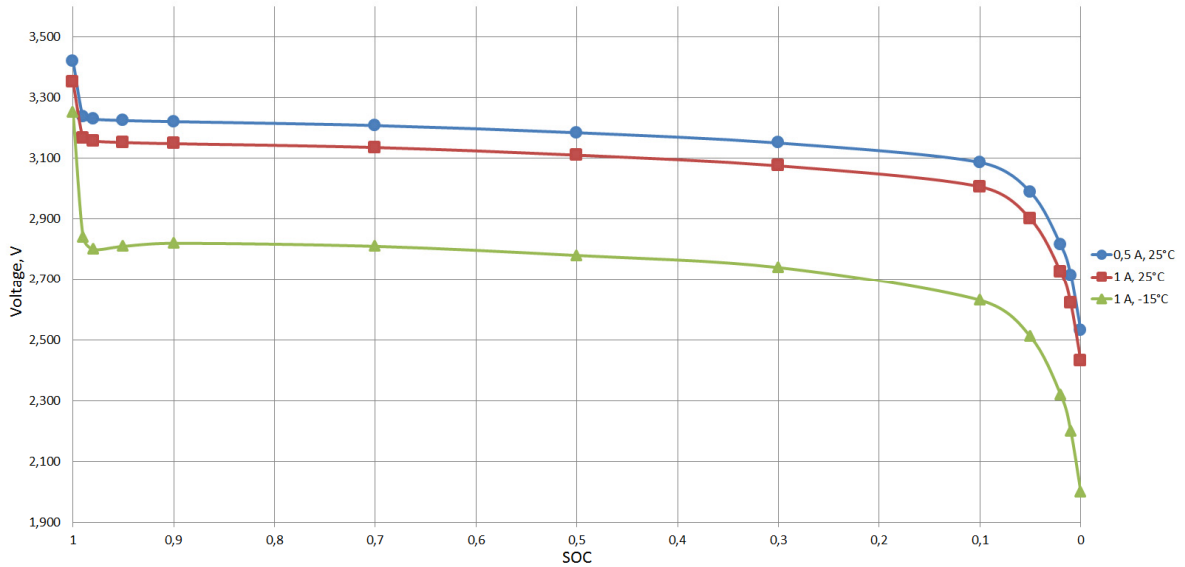


Fig. 2. Dependencies of discharge voltage from SOC at different temperature and discharge current.

The lookup tables for each circuit element were chosen to be based on 13 different points of SOC (0; 0,01; 0,02; 0,5; 0,1; 0,3; 0,5; 0,7; 0,9; 0,95; 0,98; 0,99; 1). SOC breakpoints spaced with a bias toward low and high SOC in order to more accurately reflect the change of the cell voltage at the beginning and end of the discharge.

The discharge curves $U_{I_1}(SOC, 25^\circ C)$ and $U_{I_2}(SOC, 25^\circ C)$ where $I_1 = 0,5$ A, $I_2 = 1$ A (Fig. 2) were used to determine the internal resistance of the cell at 25 °C temperature using the following equation:

$$R(SOC, 25^\circ C) = \frac{U_{I_1}(SOC, 25^\circ C) - U_{I_2}(SOC, 25^\circ C)}{I_2 - I_1} \quad (1)$$

The calculated values of the cell internal resistance and their approximation curve are shown in Fig. 3. The cell EMF was calculated knowing cell internal resistance and discharge voltage in the breakpoints using the equation:

$$E(SOC, 25^{\circ}C) = U_{I_1}(SOC, 25^{\circ}C) + I_1 \cdot R(SOC, 25^{\circ}C) = U_{I_2}(SOC, 25^{\circ}C) + I_2 \cdot R(SOC, 25^{\circ}C) \quad (2)$$

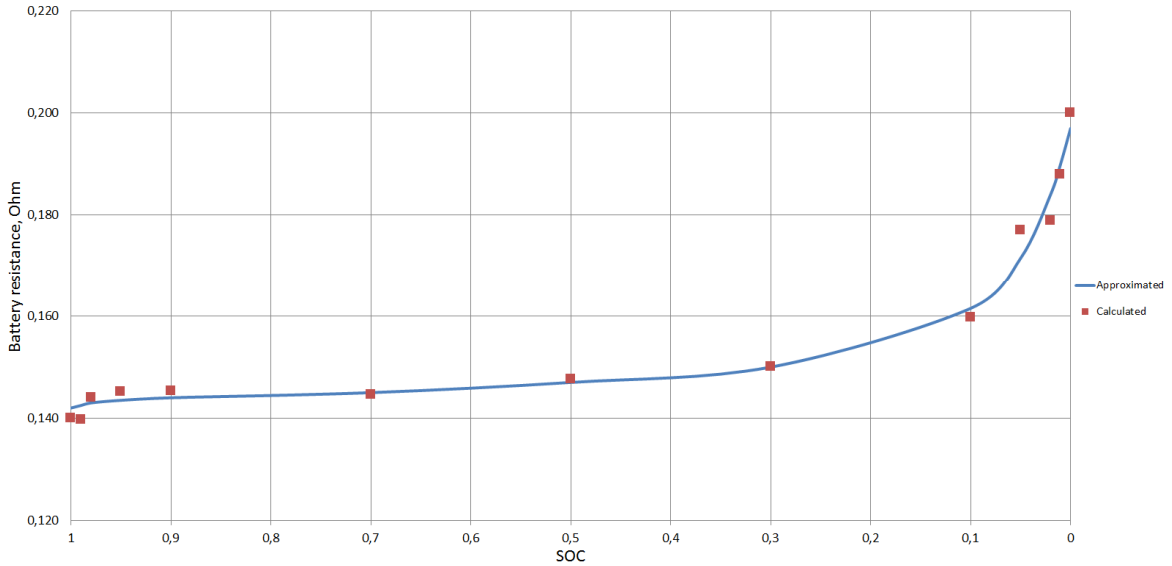


Fig. 3. Calculated and approximated cell internal resistance at 25 °C.

EMF of the battery is weakly dependent from temperature, the resistance, on the contrary, significantly increases with decreasing temperature. [13,14,15]. Cell internal resistance at -15 °C temperature was calculated using parameter estimation to make the simulation curve match the experimental data with the maximum accuracy. The dependence of the cell internal resistance from the SOC and the temperature is shown in Fig. 4. As can be seen from the Fig. 4, the cell internal resistance at -15 °C temperature is 3,5 times greater than at 25 °C.

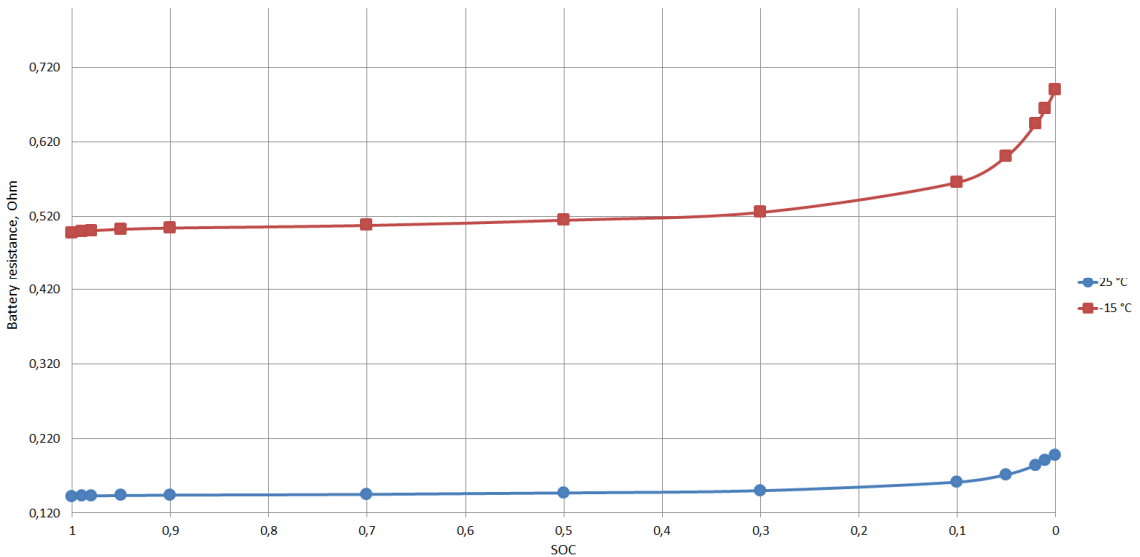


Fig. 4. Cell internal resistance at different temperatures.

The simulation of the cell discharge with 1A current at 25 °C and –15 °C was conducted and the results were compared to the experimental data to test the accuracy of the model. Simulated and experimentally obtained discharge curves are shown at Fig. 5.

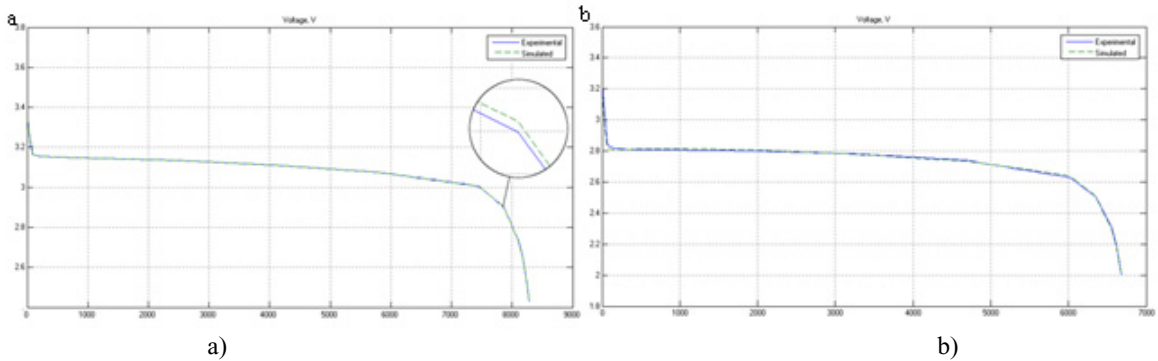


Fig. 5. (a) Simulated and experimentally obtained discharge curves at 25 °C; (b) simulated and experimentally obtained discharge curves at –15 °C

Analysis of the results (see. Fig. 5) shows good alignment of simulation results with experimental data. The validated model can be used to predict the battery performance under a variety of operating conditions. To estimate the effect of low temperatures the discharge with 1 A current at different temperatures was simulated and the results are shown on Fig. 6.

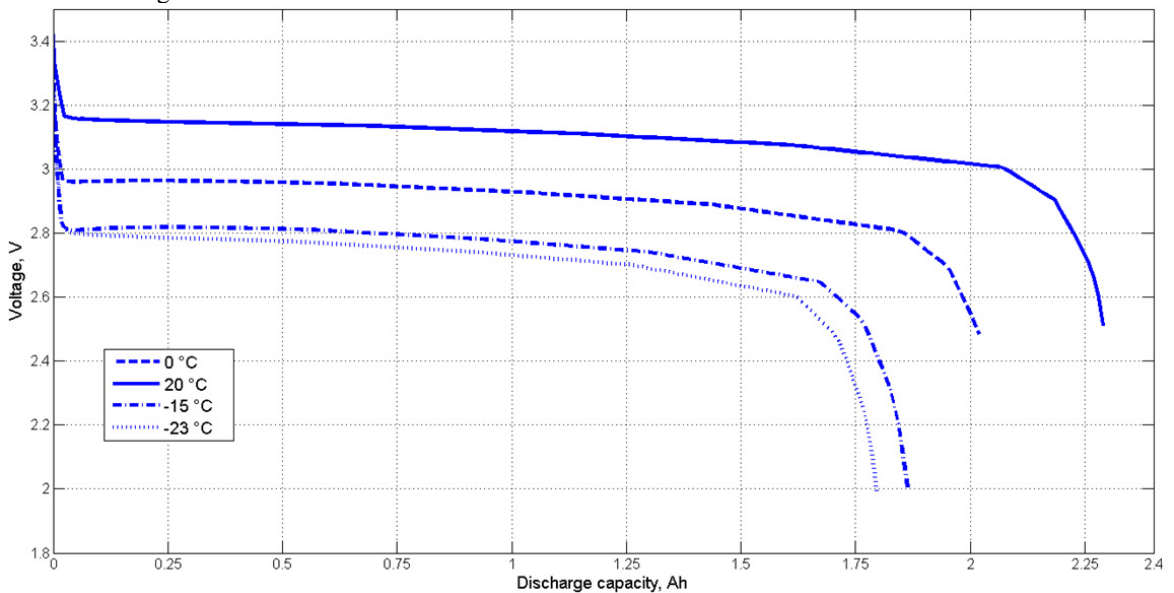


Fig.6. Simulated discharge curves at different temperatures.

The simulation showed the cell discharge capacity of 1800 mAh at –23 °C temperature, which is more than 20% less than discharge capacity at 25 °C temperature (2300 mAh). These simulation results provide an estimation of the

negative effect of low operating temperature on battery parameters and help to make a conclusion about the need for systems creating optimal operating conditions for batteries working under severe temperature conditions.

4. Conclusions

- The use of equivalent circuit models method in the applied battery allows to obtain the results which are align with the experimental data.
- The simulation results of the LiFePO₄ battery operation showed the increase of internal resistance with the factor of 3.5 and the decrease in available discharge capacity more than 20% with the decrease of ambient temperature from 25 °C to –23 °C.
- One of the methods of increasing the performance of the batteries, working under severe temperature conditions, is the application of the systems creating optimal operating conditions for batteries.
- The verified battery model can serve as the basis for its further development by taking in the account changes in the battery characteristics caused by aging, widening the temperature range of the model by adding more temperature breakpoints, as well as adding of the devices creating optimal operating conditions for batteries.

References

- [1] T.B. Reddy, Linden's handbook of batteries, McGraw Hill Companies, New York, 2011.
- [2] Portable equipment moves to lithium ion cells, *Purchasing*. 128(2) (2000) 92–93.
- [3] Information on https://en.wikipedia.org/wiki/Lithium-ion_battery.
- [4] E.V. Solomin, Renewable energy sources, *New opportunities International scientific journal for alternative energy and ecology*. 10 (2013) 38–40.
- [5] Information on <http://www.mpoweruk.com/life.htm>.
- [6] Information on <http://stroy-svoimi-rukami.ru/fundament/temperatura/43>.
- [7] R.Yu. Ilmbetov, V.A. Kalmakov, A.A. Andreev, N.P. Tychenok, Development of the experimental assembly for research of energy storage for wind turbine *Scientific Journal of CSAA*. 70 (2014) 67–70.
- [8] M.A. Roscher, J. Assfalg, O.S. Bohlen, Detection of Utilizable Capacity Deterioration in Battery Systems, *Vehicular Technology, IEEE Transactions on*. 60(1) 98–103.
- [9] M. Chen, G.A. Rin-con-Mora, Accurate electrical battery model capable of predicting runtime and I-V performance, *Energy Conversion, IEEE Transactions on*. 21(2) (2006) 504–511.
- [10] M. Ceraolo, G. Lutzemberger, T. Huria, Experimentally Determined Models for High-Power Lithium batteries, *SAE Technical Paper*. 1 (2011) 1365.
- [11] Information on <http://www.mathworks.com/matlabcentral/fileexchange/36019-lithium-battery-model--simscape-language-and-simulink-design-optimization>.
- [12] T. Huria, M. Ceraolo, J. Gazzarri, R. Jackey, High Fidelity Electrical Model with Thermal Dependence for Characterization and Simulation of High Power Lithium Battery Cells, *IEEE Electric Vehicle Conference*. (2012).
- [13] Information on <http://www.cse.anl.gov/us-china-workshop-2011/pdfs/batteries/LiFePO4%20battery%20performances%20testing%20for%20BMS.pdf>.
- [14] A.H. Zobaa, *Energy Storage, Technologies and Applications*, 2013.
- [15] Y. Li, B. Zhang, M. Chen, D. Yang, J. Liu, Investigation of the internal resistance in LiFePO₄ cells for battery energy storage system, *Industrial Electronics and Applications (ICIEA), IEEE 9th Conference on*. (2014) 1596–1600.



International Conference on Industrial Engineering

Arrangement of Data Exchange between Adaptive Digital Current and Voltage Transformer and SCADA-system under IEC 61850 Standard

Solomin E.V. *, Topolsky D.V., Topolsky N.D.

South Ural State University, 76, Lenin Avenue, Chelyabinsk, 454080, Russian Federation

Abstract

The paper presents the approach for solving the task of development of technology of high accuracy measurement digital information transmission via communication system from remote terminal unit on the base of adaptive digital combined current and voltage transformer (ADCCVT) to SCADA-system. We showed the design and technical characteristics of the said transformer, ADCCVT–SCADA communication system structure and also the programming model of data exchange between ADCCVT and SCADA-system. We analysed transformer design features determining the technology and means of data transmission. Discussed an opportunity of using the universal SCADA-systems and OPC-servers for control digital substations under IEC 61850 standard. Presented the modelling results.

© 2015 The Authors. Published by Elsevier Ltd. This is an open access article under the CC BY-NC-ND license (<http://creativecommons.org/licenses/by-nc-nd/4.0/>).

Peer-review under responsibility of the organizing committee of the International Conference on Industrial Engineering (ICIE-2015)

Keywords: digital measuring transformers; Smart Grid, SCADA; digital substation; remote terminal unit, communication system

1. Introduction

One of the actual modern scientific and technical areas is the Smart Grid concept development. This area of scientific-technical progress characterizes by rapid development of a new intellectual electronic devices (IED). The IEDs are the physical devices which partly contain the system of automation of substation. They should be connected with SCADA-systems on the software level and should exchange data with control devices via digital

* Corresponding author. Tel.: +7 912 317 1805; fax: +7 912 3171 1805
E-mail address: nii-uralmet@mail.ru

communication system on each section of grid in real time. Integration of IED into electric grids together with active components changing its parameters along with the parameters of grid depending on the grid operation mode, arranged the conditions of building the electric grids of new technological structure, characterized by higher efficiency, reliability and controllability.

Due to the said demands we have started the applied scientific-technical research and experimental development with the goal of construction the scientific base for building the automation, control and protection devices for smart electric grids with algorithms of automatic adaptation to topology and electric grid mode parameters change using the modeling of electric grid operation on the base of usage of modern technologies of control on the base of ADCCVT prototype connected with the alternating current electric power transmission line (EPTL) on 220 kV voltage class, with current measuring range 300–2000 A, accuracy current rating 0.2S, voltage rating 0.2.

2. ADCCVT design features determining the technology and means of data transmission

Basic document regulating the architecture of digital substation (DSS), is the Federal Standard [1]. The development of ADCCVT should be implemented in accordance with its requirements. Technical solutions for digital electrical substation automated control systems are presented in [2]. Standardization points in the development of digital substation concept could be found in [3]. Experience of the development of digital substations is shown in [4, 5]. The outlook of development of digital software-hardware combined digital substations described in [6]. General approaches of automation of digital substations are presented in [7].

The group of important parameters of electric grid are currents and voltages in EPTL, incoming to the substations. Currents are measured recently by high voltage electromagnetic measuring current transformers with oil or gas-insulated high voltage insulation, converting big currents of high voltage into small currents of low voltage, which in turn could be converted into digital codes with the help of analog-digital converters (ADC) [8]. These devices have such disadvantages as a large mass and dimensions, complicating their montage at substations. In addition to that the oil transformers have high explosion and fire hazard, and gas-insulated require regular pressure control of insulation. During recent years a Faraday effect based optoelectronic measuring current transformers measuring the currents of high voltages, became one of a basic research areas [9, 10]. Such devices are fabricated by lots of foreign (NxtPhase T&D Corporation, ABB, etc.) and domestic (NPP OptoLink, Profotech, etc.) companies. These converters have a substantially less mass, measure both alternating and DC current, and transfer optical signals about current on a significant distance. The main disadvantage of optical converters is their high price [11, 12].

At the same time the traditional structure of current converters output into digital code on the base of the system «electromagnetic current transformer – ADC – fiber-optic communication line (FOCL)» is still actual and didn't exhausted all its opportunities. Application of amorphous alloys for magnetic conductors [13] and compensation feedback communications [14] allow significantly decreasing device accuracy. Moreover, the price of one combined current and voltage transformer is less than of two current and voltage transformer made in two devices separately, and the reliability is higher.

In accordance with the above mentioned requirements to the modern trends and the level of engineering development, we developed the experimental prototype of ADCCVT. The structure and technical characteristics of the device are shown in [15]. It contains the high voltage part (HVP) and low voltage part (LVP) divided between each other by the high voltage support. We presented the high voltage components of ADCCVT in Fig. 1.

HVP includes primary current and voltage converters, primary converter and primary power source. HVP and LVP are connected between each other with the FOCL located inside the high voltage support.

Secondary converter operates with digital signals only and converts the received from HVP data into standard format output package, and transfers it to the final receiver. The package contains data about measured current and voltage, transformer status and several other parameters. The transformer status informs about its operation modes adapting in accordance with the value of voltage at EPTL. Final receiver for secondary converter is the terminating unit of ADCCVT, which presents the process bus merging unit (MU). MU is assigned to collect data from measuring current and voltage transformers and transfer this data by IEC 61850-9-2LE protocol to equipment of relay protection and automation (RPA), and other IEDs on digital substation.

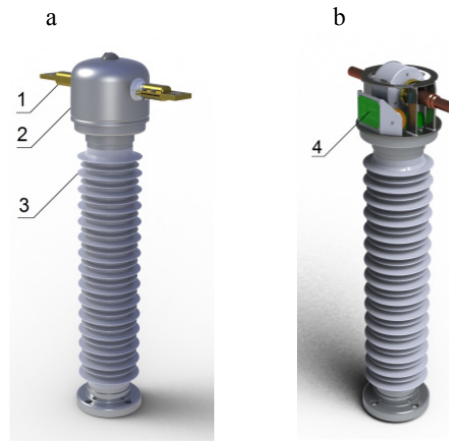


Fig. 1. Components of ADCCVT: a – ADCCVT with protecting cover, b – ADCCVT without protecting cover; 1 – current-carrying high voltage conductor, 2 – protecting cover, 3 – high voltage insulation support, 4 – HVP equipment.

3. Development of communication system structure

According to IEC61850 the DSS has three-level architecture. The lower level represents the local devices of communication with the object and digital RPA devices [16]. Medium level represents the basic system servers, time synchronizing devices and computer-gateway. Upper level is presented by workstations (WS) of operators and off-site SCADA-systems. One or several servers in such a system perform the functions of centralized collection, storage and transmission of signals. The number of servers determines the degree of system reliability. The number of WS determines degree of convenience of system usage. Algorithms of «hot» reservation are used in power object SCADA-systems. In case of emergency they allow automatic changing of basic components of the system by reserved ones (without personnel action), providing the permanent operability of the system in general.

The said structure of complex is not a hard one. There are many variants of its variations. For instance the usage of server combined with the gateway, or one operating station including the server, gateway and WS. Different variants provide a different degree of reservation and reliability. We propose the following communication system structure to provide the information exchange between ADCCVT and SCADA-system (Fig. 2).

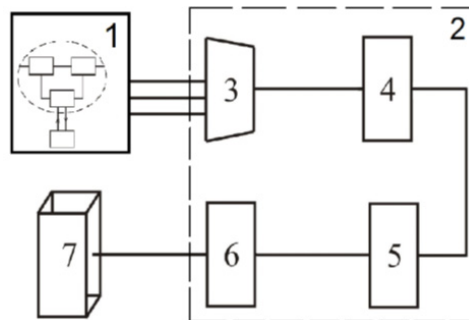


Fig. 2. Structure of ADCCVT-SCADA communication system: 1 – combined current and voltage sensor on ADCCVT base, 2 – communication system, 3 – merging unit, 4 – process bus, 5 – RPA, 6 – station bus, 7 – SCADA server.

Algorithm of communication system operation is as follows: after MU received the data from ADCCVT by proprietary protocol, it should convert this data into SV message described in IEC 61850-9-2LE. This is hardly structured frame containing 4 phase currents and 4 phase voltages data. Measuring signal sampling frequencies are also to be recorded. They present 4000 Hz (80 samplings over a period) for relay protection and commercial

accounting goals, and 12800 Hz (256 samplings over a period) for control of energy quality. Standardized Ethernet frame then should be formed to transmit the SV message. Frame format is shown in Fig. 3a.

The structure of APDU is shown in frame format. This structure contains a group of current and voltage measures. It is shown in Fig. 3b for the frame transmitting 80 samplings over a period (SV80).

Difference between SV80 and SV256 frames is in the number of APDU, presented in message. When the sampling frequency is 80 samplings, there is 1 ASDU in message, when the sampling frequency is 256 samplings, then there are 8 ASDU in message. The RPA devices receiving these messages should be subscribed on SV80 delivery in process bus.

Further so-called reports would be adjusted on the RPA devices received the SV80 messages. The reports will store a data about substation status and will be transmitted by MMS protocol to SCADA-system via station bus.

Whilst developing a communication system it's required to take into account that the development of MU needs such a special technical characteristics for Ethernet of DSS to operate normally in accordance with the requirements of IEC 61850 standard [17].

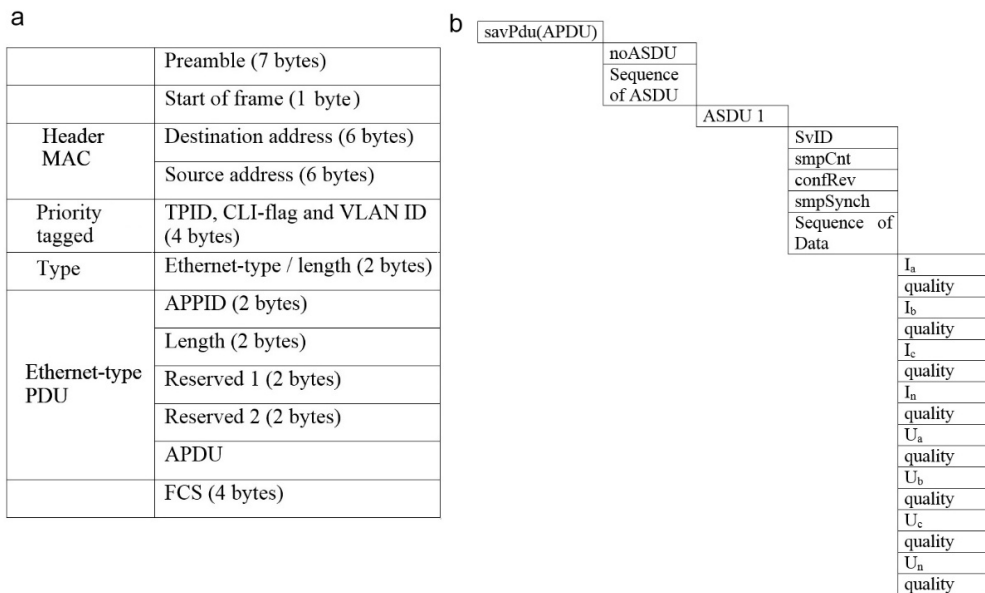


Fig. 3. Features of Sampled Value (SV) under IEC61850: a) SV frame format; b) structure of APDU for SV80.

4. Programming model of data exchange between ADCCVT and SCADA-system

The scientific aspect of modelling of data exchange between ADCCVT and SCADA-system is not only the analysis of ADCCVT–SCADA information network operation efficiency and the development of recommendations for IED speed performance made on the preliminary development stage [18], but the problems of DSS equipment compatibility with IEC-61850 standard and upper level software. Also there is a need of study the opportunity of usage the universal SCADA-systems for new IEDs.

For modelling the interaction of ADCCVT with SCADA-system we used software products from SCADA-system MasterSCADA and OPC-server MasterOPC_DI_61850, presented by InSAT company [19]. Software part of MasterScada system is the complex of software means based on the technology of object linking and embedding (OLE) for industrial automation for Process Control (OPC). The used MasterOPC_DI_61850 in modelling (Fig.4a) was tested with configurations of the most equipment distributed on Russian substations (SIEMENS, ABB,

AREVA, GE, SATEC, etc.) and showed the full compatibility with it. Loading testing of server has shown its high speed performance [20].

As we showed above, when ADCCVT communicates with SCADA-system, the data from ADCCVT are transmitted to SCADA via RPA. The chart of data transmission is presented in Fig. 4b.

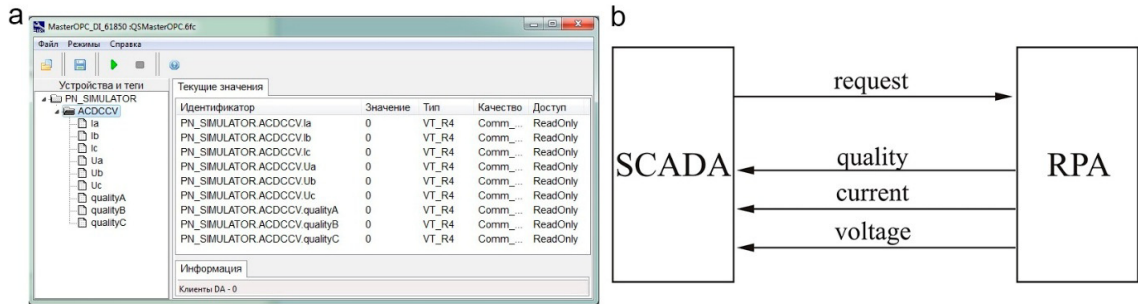


Fig. 4. Data transmission to SCADA-system: a) Window of control of MasterOPC_DI_61850 server; b) Chart of data transmission to SCADA-system.

5. Results

We arranged generation, request and transmission of MMS-reports in IEC 61850-8-1 standard for SCADA-system in modeling software complex developed on the base of interaction of MasterSCADA and OPC-server MasterOPC_DI_61850. The reports contain metrological information about high accurate current and voltage measurements, as well as the status of ADCCVT. The results of modeling of ADCCVT with SCADA-system are presented in Fig.5.

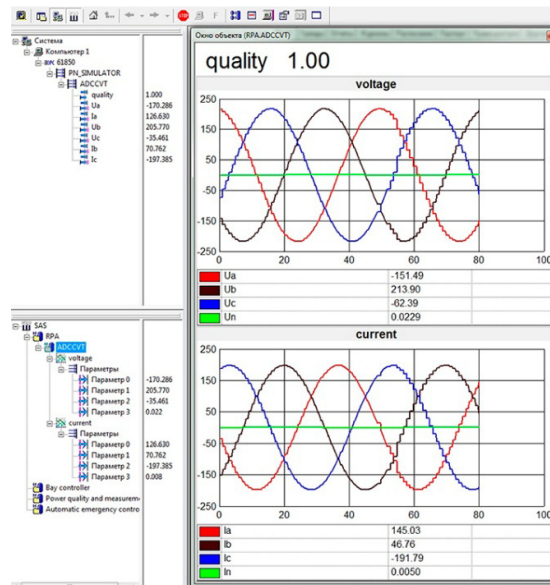


Fig. 5. Window of view/setting the values of variables and trends of corresponded current values of current and voltage

The above presented screenshots identify the evidence of correct mutual operation of ADCCVT, MasterSCADA and OPC-server MasterOPC_DI_61850. Integration of these software and devices became possible as a result of mutual work with the developers of software.

6. Conclusions

The research results allow making the following conclusions:

- The developed models of IDE are adequate.
- The developed technology of ADCCVT-SCADA data exchange allows transmitting metrological information data in real time according to IEC 61850 standard.
- It is reasonable to make a final device of ADCCVT in the form of separate module.
- Usage of universal SCADA-systems in the development of adaptive devices of automation, control and protection for smart electric grids is technically justified and reduces the development cost.

To summarize the research results we consider that the usage of standardized international protocols allows increasing the reliability and accuracy of information transmission, standardize the corresponding technical means and increase the efficiency of IED interaction in general. The most complete solution of the IED integration problem will be developed with wider usage of IEC 61850 communication protocol.

Acknowledgement

This work was supported in part by the R.F. Ministry of Education under Grant 14.576.21.0047 of 22 August 2014 (ID: RFMEFI57614X0047).

References

- [1] GOST R MEK 61850-3-2005. Networks and systems in substations. Architecture of digital substation, Moscow, 2006.
- [2] S.Yu. Kalinkin, Technical solutions in the field of process control system for digital substation 110/35 kV. Energy turnkey. <http://forca.ru/stati/rzia/resheniya-v-oblasti-asutp-dlya-cifrovyyh-podstanciy.html>.
- [3] A.M. Maslov, P.L. Lobanov, Questions of standardization in the implementation of the concept of digital substation, Proc. of the 2nd Inter. Exhibition and Conference on innovative projects in the electric grid complex IPNES 2011. (2011).
- [4] Yu.I. Morzhin, S.G. Popov, P.A. Gorozhankin, V.G. Norovlyanskiy, M.A. Vlasov, A.A. Serdchev, Digital substation UNEG, *EnergoEkspert*. 4 (2011) 27–32.
- [5] S.I. Chichev, V.F. Kalinin, E.I. Glinkin, Systems for monitoring and control of electrical substation equipment, *Spektr*, 2011.
- [6] A.M. Gelfand, P.A. Gorozhankin, V.G. Norovlyanskiy, L.I. Fridman, Prospects for the creation of digital software and hardware systems UNEG substations, *Elektricheskie stantsii*. 5 (2012) 55–58.
- [7] V.O. Tazin, A.V. Golovin, A.O. Anoshin, Engineering automation of Digital Substations, *Releyshchik*. 1 (2012).
- [8] G.I. Volovich, The circuitry of analog and analog-to-digital electronic ustroyst, third ed., Dodeka, Moscow, 2011.
- [9] A. Enokihara, M. Izutsu, T. Sueta, Optical fiber sensors using the method of polarization-rotated reflection, *J. Lightw. Technol.* 5 (1987) 1584–1590.
- [10] S.I. Chichev, E.I. Glinkin, Optical high-current transformers and voltage, *Electrics*. 4 (2011) 28–31.
- [11] V. Gurevich, Optical current transformer: it is necessary to be realistic, *Electrical networks and systems*. 4 (2010).
- [12] T.W. Cease, P. Johnston, A magneto-optic current transducer, *IEEE Trans. on Power Delivery*. 5 (1990) 548–555.
- [13] V.F. Matyuk, A.A. Osipov, Mathematical models of the magnetization curve and magnetic hysteresis loops. Part 1. Analysis of models: Nondestructive testing and diagnostics. 2 (2011) 3–35.
- [14] G.I. Volovich, Simulation of current transformer in the package VisSim, *Power Electronics*. 3 (2014) 66–69.
- [15] G.I. Volovich, D.V. Topolskiy, I.G. Topolskaya, Development of adaptive digital combined current and voltage transformers for Smart Grids: Devices and systems. 11 (2014) 44–49.
- [16] D.Yu. Apukhtin, A.A. Savinov, SCADA-system for power «Atlant»: Computerization and control system in the industry. <http://www.isup.ru/articles/2/242/>.
- [17] IEC 61850: Communication networks and systems in substations, Part 3, 5, 7, 8-1, 9-2.
- [18] E.V. Solomin, D.V. Topolskiy, N.D. Topolskiy, Integration of Adaptive Digital Combined Current and Voltage Transformer into Digital Substation Ethernet Grid, Control and Communications (SIBCON), 2015 International Siberian Conference on. <http://ieeexplore.ieee.org/xpl/login.jsp?tp=&number=7147242&url=http%3A%2F%2Fieeexplore.ieee.org%2Fiel7%2F7133660%2F7146959%2F07147242.pdf%3Fnumber%3D7147242>, 2015.
- [19] Information on <http://www.insat.ru/>.
- [20] Information on <http://www.masterope.ru/products/?category=1143>.



International Conference on Industrial Engineering

Algorithms of LiFePO₄ batteries automatic charge

Solomin E.V.^{a*}, Topolsky D.V.^a, Toposkaya I.G.^a

^a South Ural State University, 76, Lenin Avenue, Chelyabinsk, 454080, Russian Federation

Abstract

A wide variety of rapidly evolving algorithms of lithium-ion battery charge leads to the lack of statistics on the differential coefficient of a specific battery degradation, or in other words, a misunderstanding of the difference in the state of charge after several charge-discharge cycles as compared to a single one. As a solution of the problem the authors propose the usage of a universal integrated algorithm of LiFePO₄ batteries charging with initial and final trickle charge, which will both train the battery and reduce the differential coefficient of degradation, as well as allow testing of local grid power which the battery is charging from. This approach, if distributed widely, may give rich statistic information to be used for further improvement of charge algorithms.

© 2015 The Authors. Published by Elsevier Ltd. This is an open access article under the CC BY-NC-ND license (<http://creativecommons.org/licenses/by-nc-nd/4.0/>).

Peer-review under responsibility of the organizing committee of the International Conference on Industrial Engineering (ICIE-2015)

Keywords: lithium-ion battery, accumulating battery, charge-discharge, differential coefficient of battery degradation, LiFePO₄, state of charge

1. Application of Trickle Charge in LiFePO₄ batteries

Our earlier published materials on the development of charging algorithms for lithium-ion batteries intended for the heavy load electric vehicles and city transportation, had caused a living feedback in the part of optional trickle charge [1]. The reason of variances is the proposed universality of charging algorithm.

In particular a lot of lithium-ion batteries used earlier, were dangerously explosive [2]. This type of batteries is the electrochemical device using chemical reactions, leading in some cases to the internal short circuits caused by overheating. That was actually the main reason of their failure. During a few milliseconds the chain reaction of

* Corresponding author. Tel.: +7 912 317 1805; fax: +7 912 3171 1805.
E-mail address: nii-uralmet@mail.ru

“dominoes” type leads in specific conditions to the explosive effect. One of the ways of reliable defense was the use of copper jumpers between electrodes in battery, melting when the temperature exceeds 1000°C , which leads to the chain breakup.

We carefully studied this type of batteries for the application of trickle charge. In the algorithms proposed in [1], there was no any data about the type of battery or temperature control and thermal chain/charge disconnection. Nevertheless this research was actually in mind during the scientific experiments planned step by step in the iterative sequence “problem study – analysis and generalization – heuristic approaches and hypotheses – experiment verification”.

2. Advantages and Disadvantages of Trickle Charge

Trickle charge proposed in some cases for charging the Li-ion battery after it is fully charged (i.e. 95-99% from the initial state of charge), in most cases can be dangerous because in accordance with manuals, the batteries of this type cannot consume energy when overcharged, and can be damaged. And vice versa, the lack of trickle charge leads first to the progressive steadfast aging (degradation) of battery because of partly not full charged, and second to the non-efficient usage of the battery. Thus the “golden mean” is required, and the problem could be solved by adding the temperature feedback into the charging algorithm. This entry would help to avoid the overheating, switching to the trickle charge in time, and even during the trickle charge stage would help to control the battery state of charge, and therefore to prolong its life from charge to charge. Today a lot of equipment for batteries trickle charge, is available on the market. However there is no available accurate data about the time of charge and thermal features for specific batteries and in particular about the impulses duty factors, excluding the only [14].

It is necessary to note that as a rule there is no any information about trickle charge even in manual documentation on the batteries, which causes some apprehensions in the usage of trickle charge in general, moreover in automatic duties. However due to the research of lithium-ion batteries’ structure and the results of long term testing [4,5], we can make a conclusion that the main charge could be applied without trickle charge [15-21]. But in this case every charge will slowly be aging the battery as the memory effect is also presented in this type of batteries according to the research of [5], in analog with nickel-cadmium and nickel-metal-hydride batteries. Thus lithium-ion batteries are liable for degradation and the charging processes require exclusively important attention.

Degradation of LiFePO_4 batteries is caused by the fact that the electrode material consists of multitude minute micrometer size particles which charge and discharge individually one after another. This model of charge-discharge is known as a “multi-element model” [6]. During the charging process the lithium ions are being released. Fully charged particle becomes free of lithium presenting the phosphate ion FePO_4 . Discharge is vice versa returns lithium ions back and phosphate ion becomes a lithium-phosphate ion LiFePO_4 . The difference between the number of lithium ions repeatedly interacting with phosphate ions, reflects the battery voltage reduction. In this case this difference represents the specific battery differential coefficient of degradation which has a non-linear aging characteristic known as a dependence of SOC (state of charge) on different charging currents varying from 0.1C to 10C. Thus the difference in the number of ions leads to some critical results which in turn lead to the reduction of chemical potential [22].

3. Individuality of Battery Differential Coefficient

In accordance with the above mentioned arguments each charge-discharge cycle of lithium-ion battery leads to some its degradation, the differential coefficient of which is individual not only for different types of batteries, but for the products of the same type because of different structure of materials [23,24]. So the only instrument for “pulling” the weak battery with the big differential coefficient to the strong one, is charging with low currents taking into account all applicable cautions for keeping the original battery chemical structure.

In the proposed algorithm [1] the trickle charge was optional (or secondary). We assumed that the most important was the initial trickle training charge included the series of charge-discharge impulses for the determination of SOC and charging current value. However due to the recent research results [5] the trickle charge on the final stage of charge starts dominating to prevent the early aging of batteries.

4. Algorithms of Charge with Adding Temperature Control and Trickle Charges

In accordance to these data we found one serious disadvantage in algorithm [1] – the lack of the temperature control. It is being obvious that each battery type would require specifically determined individual boundary conditions. In our case we researched LiFePO₄ batteries as the most explosively safe and having high electrochemical potential.

Adding the temperature control feedback into the algorithm taking into account the initial and final trickle charge, will represent the following chart of charging algorithm for the said batteries [7,9]:

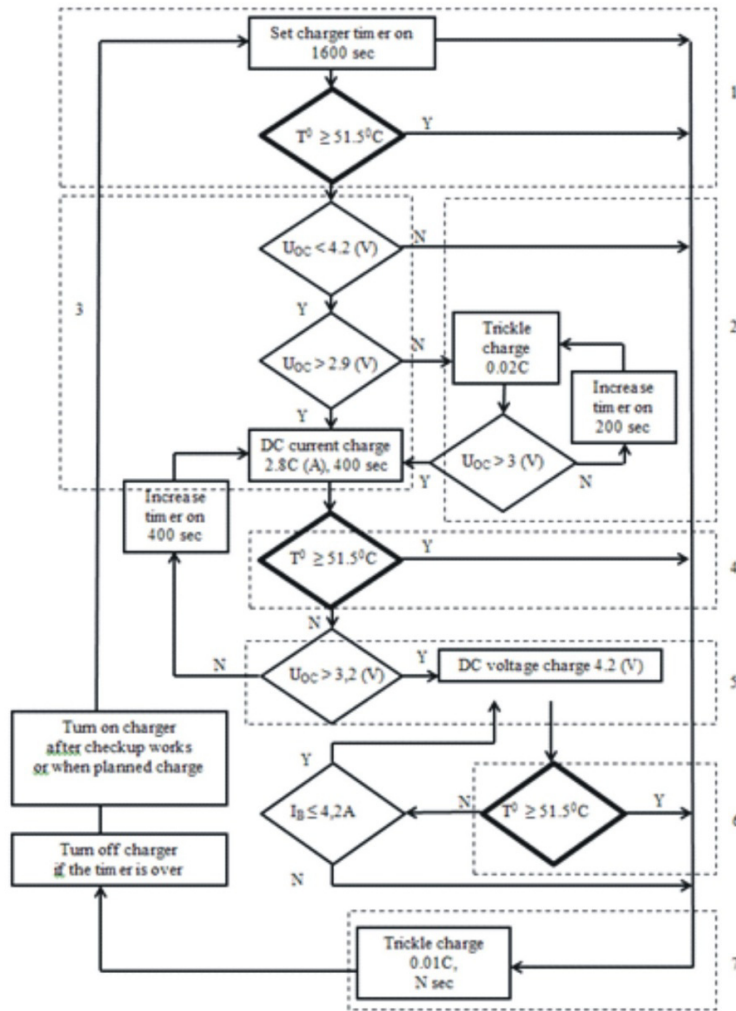


Fig. 1. Algorithm of charge for LiFePO₄ battery with trickle charge and temperature feedback.

In Fig. 1:

U_{OC} – open circuit voltage of battery, I_B – charging current, T^0 – temperature of battery, C – battery capacity. The bold elements represent the temperature testing.

In accordance with the proposed chart we then may form the stages of battery charge (discharge) algorithm which contains the following number of algorithms as it is marked in Fig. 1:

- 1 – algorithm of initial temperature testing;
- 2 – algorithm of initial (test and/or training) trickle charge;
- 3 – algorithm of the main charge by DC current;
- 4 – algorithm of permanent temperature testing;
- 5 – algorithm of the main charge by DC voltage;
- 6 – algorithm of permanent temperature testing;
- 7 – algorithm of final (finalizing) trickle charge.

The time of the trickle charge N depends on the battery type and developer or manufacturer [25]. Therefore the duration has to be determined in accordance with the operation manual, recommendations of developer and/or experimental data. Fig.1 shows that the processes of initial and final trickle charge are relatively long. For shortening the time of charge the trickle charge could be eliminated. In this case the end-user should make the appropriate economic calculations taking the following conditions into consideration:

- Eliminating the trickle charge the charger cannot detect the unbalance in battery, therefore the charge would be finalized by the timer, but the battery wouldn't be charged in full. In this case it's necessary to make a calculation of the probability of this event appearance, then form (determine) a mathematic expectation value of the event on the base of statistic approaches, evaluate the harm and make a decision about elimination or usage of the said charging stage.
- In case of eliminating the final trickle charge the battery is the subject of irreversible aging. The characteristic of degradation is not linear. In this case it's necessary to evaluate statistically the curve of degradation of batteries being charged, without trickle charge comparing with the batteries charged up to 100%. The gradient of differential coefficient will give the information for making a decision on the base of economic analysis about the usage of the entire trickle charge, taking into account the expenses on energy delivery, idling time on the charging station and small but unavoidable degradation.

When applying the algorithm to the other, different from [7] batteries, it's required to use another charge parameters in accordance with [1,8] and nominal parameters according to the product operation manual(s).

We have to note that the algorithm is a universal tool, and following the above mentioned conditions it cannot accelerate the battery degradation.

Thus using the proposed algorithm, the positive effect is absolutely predictable but differential coefficient of degradation must be numerically determined for each type of batteries in the process of the appropriate experimental research.

5. Temperature Sensor

Special topic of applied research is the determination of location of temperature sensor. As a rule the material of lithium-ion battery housing is a polymer and it would bring a hysteresis effect and/or data displacement into the curve of temperature registration recorded by thermal control system on external wall of the battery cell. Moreover the influence of the next cells may lead to the high differential error in calculation of the cell internal temperature. Therefore to increase the reliability, the manufacturer of the batteries should be recommended to place temperature sensors inside each cell. The cost of this arrangement would be significantly less than placing the components of balancing system into the battery which is widely used now in the production of modern lithium-ion batteries [26].

6. Grid Power Determination

The automatic determination of grid power is required for the evaluation of charging availability for specific accumulating battery from the given local source. The power source may be in the form of either main or local grid on the base of low power generators, and therefore the proposed condition should be obligatory for the charger. To meet these conditions the vehicle should be equipped by the appropriate control apparatus. In some cases, especially when charging at the stations on the base of renewable energy sources, the grid power determination is required because in case when the grid charging parameters are insufficient for qualitative charge, the differential coefficient of degradation will be increased considerably.

Algorithm of grid power determination is worth the process of determination of available power, in measuring the voltage drop on terminals of the battery. In general the algorithm of charger control could be proposed in the following succession:

- Charger should be connected galvanically separately to the grid and battery in accordance with the electric device connection circuit operation manual. The charger after turning on, measures the voltage both on terminals of the battery and grid voltage in open circuit duty (the grid and the battery are galvanically disconnected).
- Control system of the charger generates a short impulse(s), 3-5 seconds duration to charge a battery.
- Charger voltage sensor generates a voltage value on the terminals of the battery and the grid, after that the control system compares the recorded data and those earlier measured on the open circuit duty. If the charger detects the voltage drop as acceptable value then it shows the appropriate information on display and starts the charge. If the voltage was sank more than acceptable, in accordance with the optional commands the charger either disconnects the batteries using the internal contacts, or turns to the duty of charging by small (but available in local grid) currents, notifying the operator.
- To turn on the small current charge it is necessary to use the following extra algorithm of diagnostics: when the voltage drops on significantly higher value than available, the charger reduces the voltage on 30% or 70%, acting by Fibonacci search by coordinate-wise descent with bringing the penalty functions for the most rapid detection of available voltage.
- After the available voltage is determined, the charger computes the available charge current and turns on the charge, using the main algorithm but with the applicable corrections.

7. Summary

From the point of view of the general scientific research approaches, the proposed method is a compilation of the wide spectrum of approaches described in the World literature. Nevertheless the proposed algorithm is the new instrument in the applied research, proposed as a result of studying the specific batteries [7,9]. Taking into account that it combines the methods, approaches and algorithms, using in the operation of lithium-ion batteries, with generating the mass statistics of degradation differential coefficients, the proposed algorithm is important for improvement of quality and increase of efficiency of charge for newest modern Li-FePO₄ batteries and can be applied for any type of lithium-ion batteries, using the appropriate re-counting of charge-discharge parameters.

Acknowledgements

This study was awarded by RF Ministry of Education and Science under Subsidy Agreement # 14.577.21.0154 of 28.11.2014 (Unique Identifier of Agreement RFMEFI57714X0154). The software patent applications were accomplished for 3 variants of controller programming.

References

- [1] A.V. Keller, D.V. Korobov, E.V. Solomin, D.V. Topolskiy, I.G. Topolskaya, Development of Algorithms of Rapid Charging for Batteries of Hybrid and Electric Drives of City Freight and Passenger Automobile Transportation Vehicles, XI Mezhdunarodnaya IEEE Sibirskaia konferentsiya po upravleniyu i svyazi SIBCON-2015. (2015). <http://iee.tpu.ru/musor/sbornik/papers/176em.pdf>.
- [2] T. Ghose, Why Some Lithium-Ion Batteries Explode, LiveScience. (2015). <http://www.livescience.com/50643-watch-lithium-battery-explode.html>.
- [3] H. Grewal, Li-ion Nattery Charger solution using the MSP430, Application report. Texas Insyuments. (2015). <http://www.ti.com/lit/an/slaa287/slaa287.pdf>.
- [4] A. Paryan, US Patent 2011/0012563 A1. (2011).
- [5] L. Cai, R.E. White, Mathematical modeling of a lithium ion battery with thermal effects in COMSOL Inc. Multiphysics (MP) software, Journal of Power Sources. 196 (2011) 5985–5989.
- [6] L. Leiva, Memory effect now also found in lithium-ion batteries, Paul Scherrer Institute. (2013). <http://www.psi.ch/media/memory-effect-now-also-found-in-lithium-ion-batteries>.
- [7] Batteries Li-ion LT-LFP 300, Manual. LT-LFP.300.11.01.000 RE, 2014.
- [8] D. Linden, T.B. Reddy, Handbook of Batteries, third ed., McGrawHill, New York, 2002.

- [9] Batteries Li-ion LT-LYP200AH, LT-LYP240AH, LT-LYP300AH, LT-LYP380AH, LT-LYP700AH i LT-LYP770AH. LT.64366939.3482.001-2013 RE, Manual, 2013.
- [10] F.-C. Yang, C.-C. Chen, J.-J. Chen, Y.-S. Hwang, W.-T. Lee, Hysteresis-Current-Controlled Buck Converter Suitable for Li-Ion Battery Charger, IEEE. (2006) 2723–2726.
- [11] Y.-S. Hwang, S.-C. Wang, Fong-Cheng-Yang, J.-J. Chen, W.-T. Lee, New Li-Ion Battery Charger Based on Charge-Pump Techniques, IEEE. (2006) 2259–2262.
- [12] Y.-S. Hwang, S.-C. Wang, Fong-Cheng-Yang, J.-J. Chen, W.-T. Lee, Built-in Resistance Compensation (BRC) Technique for Fast Charging Li-Ion Battery Charger, IEEE. (2008) 2259–2262.
- [13] C.-H. Lin, C.-L. Chen, Y.-H. Lee, S.-J. Wang, C.-Y. Hsieh, H.-W. Huang, Fast Charging Technique for Li-Ion Battery Charger. (2008) 618–621.
- [14] L.-R. Chen, S.-L. Wu, T.-R. Chen, W.-R. Yang, C.-S. Wang, P.-C. Chen, Detecting of Optimal Liion Battery Charging Frequency by Using AC Impedance Technique. (2009) 3378–3381.
- [15] J.-J. Chen, F.-C. Yang, C.-C. Lai, Y.-S. Hwang, R.-G. Lee, A High-Efficiency Multimode Li-Ion Battery Charger With Variable Current Source and Controlling Previous-Stage Supply Voltage”, IEEE Trans. 56(7) (2009).
- [16] M. Chen, G. A. Rincón-Mora, Accurate, compact, and power-efficient Li-Ion battery charger circuit, IEEE Trans., Exp. Briefs. 53(11) (2006) 1180–1184.
- [17] Y.-L. Ke, Y.-C. Chuang, A novel high-efficiency battery charger with a buck zero-voltage-switching resonant converter, IEEE Trans. 22(4) (2007) 848–854.
- [18] Y.S. Hwang, C.C. Wang, F.C. Yang, J.J. Chen, New compact CMOS Li-Ion battery charger using charge-pump technique for portable applications, IEEE Trans. Circuits Syst. I, Reg. Papers. 54(4) (2007) 705–712.
- [19] N.A. Rahim, E.L. Chan, S. Mekhilef, DSP-Based Fuzzy Logic Controller for a Battery Charger , TENCON 02 Proceedings IEEE Region 10 Conference on Computers, Communications, Control and Power Engineering. (2002) 1512–1515.
- [20] L.R. Chen, A design of optimal pulse charge system by variable frequency technique, IEEE Trans. Ind. Electron. 54(1) (2007) 398–405.
- [21] L.R. Chen, J.Y. Han, J.L. Jaw, C.P. Chou, C.S. Liu, A Resistance-compensated phase-locked battery charger, Proc. IEEE. (2006) 1087–1092.
- [22] C.C. Tsai, C.Y. Lin, Y.S. Hwang, W.T. Lee, T.Y. Lee, A multi-mode LDO-based Li-ion battery charger in 0.35 μ m CMOS technology, in Proc. IEEE Asia-Pacific Conf. Circuits and Systems. (2004) 49–52.
- [23] S. Mekhilef, M.N. A. Kadir, Novel Vector Control Method for Three-Stage Hybrid Cascaded Multilevel Inverter, IEEE Transactions on Industrial Electronics. 58(4) (2011) 1339–1349.
- [24] A. Safari, S. Mekhilef, Simulation and Hardware Implementation of Incremental Conductance MPPT with Direct Control Method Using Cuk Converter, IEEE Transactions on Industrial Electronics.58(4) (2011) 1154–1161.
- [25] T.S. Ustun, S. Mekhilef, Design and Implementation of Static Synchronous Series Compensator with a soft- switching H-bridge Inverter with DSP-Based Synchronization Control, International Review of Electrical Engineering (IREEE). 5(4) (2010) 1347–1353.
- [26] N. Mohamad, A. Kadir, S. Mekhilef, Dual Vector Control Strategy for a Three-Stage Hybrid Cascaded Multilevel Inverter, Journal of Power Electronics. 10(2) (2010) 155–164.



International Conference on Industrial Engineering

Intelligent diagnosis of the electrical equipment technical condition

Kruglova T.N.^{a*}

^aPlatov South-Russian State Polytechnic University (NPI), 132, St. Prosvescheniya, Rostov region, Novocherkassk, 346428, Russian Federation

Abstract

An intelligent method of diagnosing the technical condition of electrical equipment and mechanical devices connected with it is described. The method is based on the combined use of fuzzy logic and neural networks. Fuzzy submodel determines the degree of development of each fault. The neural network determines the state of the object as a whole. The experimental study of the method for the diagnosis of a brushless DC motor and associated equipment at different speeds is presented. It was found that this method allows troubleshooting at any speed. The most informative rate equals half of the maximum. The fault detected in the experiment was confirmed during the inspection of electrical equipment.

© 2015 The Authors. Published by Elsevier Ltd. This is an open access article under the CC BY-NC-ND license (<http://creativecommons.org/licenses/by-nc-nd/4.0/>).

Peer-review under responsibility of the organizing committee of the International Conference on Industrial Engineering (ICIE-2015)

Keywords: electrical equipment, diagnostics, fuzzy logic, neural networks, neuro-fuzzy based diagnosis model, supply current

1. Introduction

Electrical equipment is very important link in the country's energy supply and demand, which places special demands on reliability and performance. Operation in poor technical condition of generators, motors, transformers and cable lines leads both to direct financial losses related to unpredictable failure of equipment and a consequent violation of the technological process, and significant indirect unproductive expenses of electricity, due to increased power consumption at the same useful power. Therefore, the actual problem is to ensure reliable and efficient operation of high-voltage electrical equipment. One way to solve this is to control the current condition of the application of methods and means of diagnosis. The main problem of the development of such methods is the large amount of non-

* Corresponding author. Tel.: +7(918)557-59-35
E-mail address: tatyana.kruglova.02@mail.ru

formalized qualitative information that can't be used with conventional modeling methods. To solve this problem allows the use of artificial intelligence methods.

2. Intelligent method for diagnosis of electrical equipment

Long operation activity of the electrical equipment at the large reversed loads can produce faults. Therefore it is necessary to supervise periodically the high-voltage electrical equipment inspection done by means of a systematic diagnosing.

One of the most simple and accessible methods of diagnosing is the method of the spectral analysis of stator current signals, as it does not require additional material and time expenses and can be made directly on the working equipment.

The spectral analysis of the stator current signals allows to carry out diagnostics of the electric motor and the mechanical devices connected with it at which during the set time interval the steady-state currents consumed by the motor are recorded as exemplarily shown in Fig 1,a

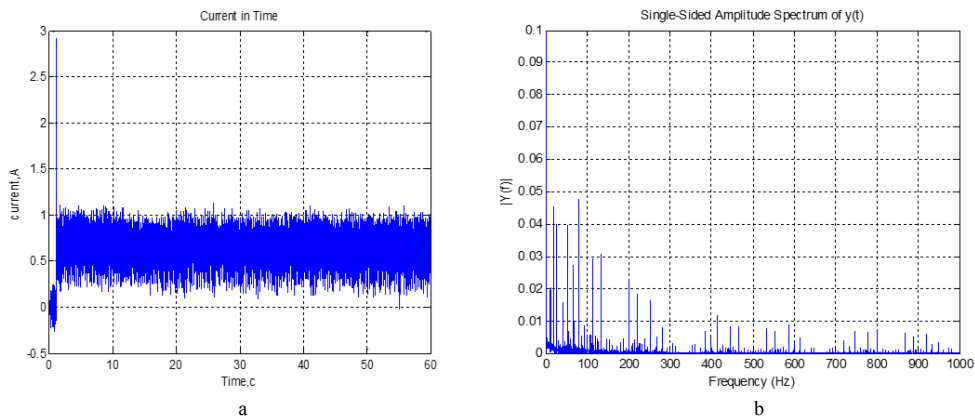


Fig. 1. (a) Steady state time series of the current consumed by electrical equipment; (b) frequency spectrum of the electrical equipment

The received data are converted into the frequency domain using the Fourier transformation (refer with: Fig 1,b).

3. The neuro-fuzzy based diagnosis model

Characteristic frequency peaks contain the electrical equipment faults and can be extracted from spectral analysis of the stator current. For the analysis the current signal of a new serviceable motor, which is accepted to be the basic reference standard, is measured once before the long-time exploitation. When faults advance there is a change in the common level and single amplitudes on the characteristic frequencies. The search of faults is carried out by comparison of a currently spectrum with the basic reference spectrum done by means of computational intelligence. Midrange current signal (refer with: Eq. 1), which can be considered as a bias arising from process noise is obtained from all amplitudes of a current spectrum without characteristic frequencies/
where a_i - current signal amplitude ; i, j - frequency indices; g - frequencies of a spectrum interval; h - characteristic frequencies of diagnosing.

The spectrum analysts is restricted to the normalized characteristic frequencies under consideration (refer with: Eq. 2).

$$k_i = \frac{A_i - A_i^0 + \Delta a_{mid}}{a_{mid 0} + A_i^0}$$

where A_i - amplitude of the analyzed spectrum on the i -th characteristic frequency; A_i^0 - amplitude of a reference spectrum on the i -th characteristic frequency; $a_{mid 0}$ - midrange current signal of the reference spectrum;

$\Delta a_{mid} = a_{mid i} - a_{mid 0}$ - absolute deviation of the midrange current signal; $a_{mid i}$ - midrange current signal of the analyzed spectrum.

If the analyzed spectrum is equal with the reference one then the normalized factor $k_i = 0$. If a fault occurred then the change of the midrange current signal and amplitude on characteristic frequencies lead to a change of normalized factor [1].

If all normalizing factors are «nearby 0» the object is serviceable. If all normalizing factors are «nearby 1» that the object is corrupt. These data is written down in the form of predicate rules:

IF k_i is B_1 and k_m is B_1 , then $x_i = f_1$

IF k_i is B_2 and k_m is B_2 , then $x_i = f_2$

where $k_i \dots k_m$ – current amplitude on characteristic frequencies; B_1, B_2 – S and Z shaped functions of sigmoid type (Fig. 2,a); x_i –predicted output fault; f_1 – conclusion «object is supposed to operation»; f_2 – conclusion «object is not supposed to operation».

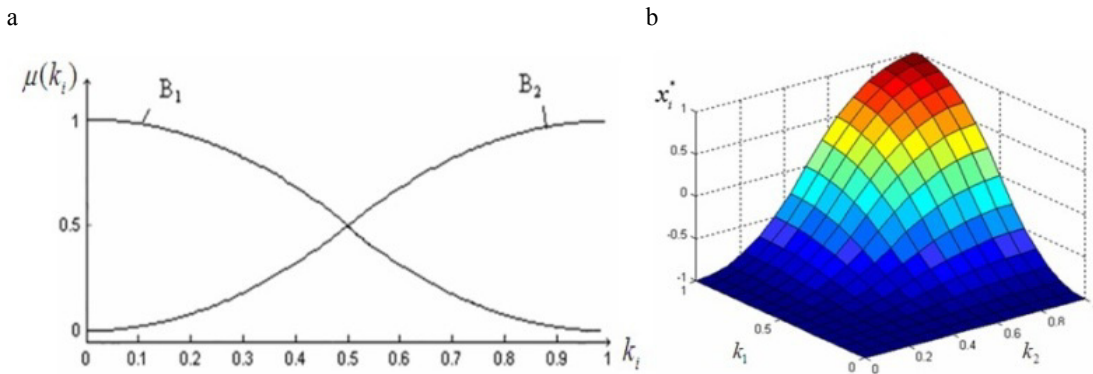


Fig. 2. (a) membership functions of the fuzzy sub model of diagnosing; (b) surface of the fuzzy sub model of diagnosing

The output is defined by means of an algorithm of the fuzzy logic *Takagi-Sugeno*[2].

- It is supposed, that the input variables offer some determined values $k_1^0 \dots k_m^0$ and there are α - levels of precondition for each of the rules:

$$\alpha_1 = \min[B_1(k_1^0) \dots B_1(k_m^0)]$$

$$\alpha_2 = \max[B_2(k_1^0) \dots B_{12}(k_m^0)]$$

- For each individual rule the outputs are computed $x_1^* = f_1$ and $x_2^* = f_2$.
- The output of the fuzzy logic system is determined by

$$x^* = \frac{\alpha_1 \cdot x_1^* + \alpha_2 \cdot x_2^*}{\alpha_1 + \alpha_2}$$

The simulated results of an exemplarily two-dimensional output surface are referred with: Fig. 2,b.

Similar sub models are involved for making each fault decision, having received a set of current factors of faults progress $X = \{x_i^*\}, i \in [1, n]$. As a progress of any faults leads to the object refusal an approximating minimum function is chosen. The approximation is carried out by a radial basic network with Gauss functions of activation [3], with displayed target layer linear neuron (refer with: Fig. 3).

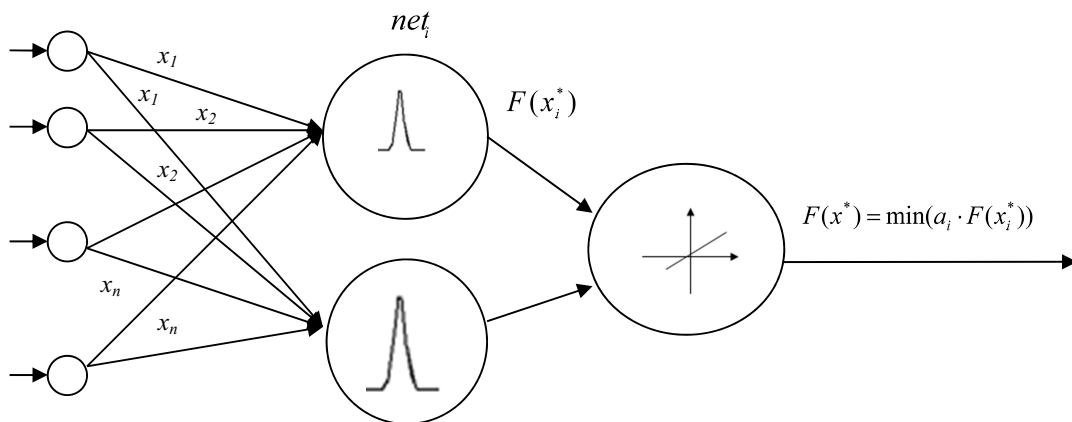


Fig. 3: Structure of a neural network of the used approximation

Output of the radial neuron (refer with: Eq. 3):

$$F(x_i^*) = \sum_{i=1}^N \rho(\|x_i^* - c_i\|)$$

where N - the number of neurons in the hidden layer; c_i - the center vector for neuron i ; ρ - Gaussian; $\|x_i^* - c_i\|$ - the Euclidean distance.

Outputs of the radial neuron are multiplied by weights vectors of the linear neuron. Weights vectors of the linear neuron are set on an interval $[-1, 1]$ such that maximum $F(x_i^*)$ corresponded the minimum weight. As training function is the minimum then the output of the linear neuron:

$$F(x^*) = \min(a_i \cdot F(x_i^*))$$

where a_i - are the weights of the linear output neuron.

The received output value allows to estimate a current condition of the object, having carried it to one of the following classes: $F(x^*) = 1$ - serviceable; $0 < F(x^*) < 1$ - operative; $-1 \ll F(x^*) \ll 0$ - corrupt.

4. Experimental results

The proposed method of diagnosing has been evaluated on the BLDC actuator having the principal structure as depicted in Fig. 4.

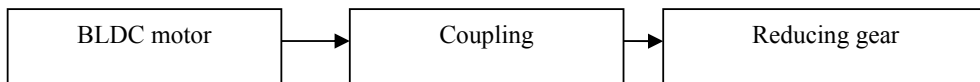
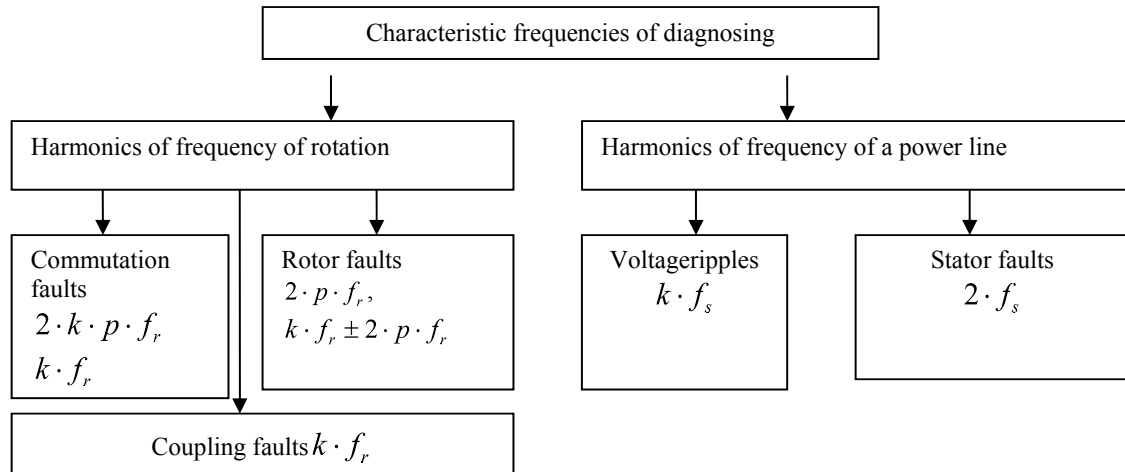


Fig.4: Block diagram of a BLDC drive

Rotary motion of the BLDC motor is transferred through the coupling of the reducing gear connected to an actuation mechanism. Current measurement is carried out within a low level BLDC control, therefore using a spectrum current it is possible to determine only the technical condition for BLDC with the full load which is directly connected with it. Reducing gear is a constant passive load and there is no variable influence on a frequency spectrum of the current consumed by the motor. In Fig. 5, the basic typical faults of the BLDC motor and their characteristic frequencies are summarized.



where f_s - frequency of power supply for the rectifier, Hz;

f_r - rotation frequency of the motor, Hz;

$k = 1, 2, 3$ - current harmonic number;

p - number of poles.

Fig 5. Classification of characteristic frequencies of diagnosing

Time series of the consumed current of the motor are recorded at frequencies of rotation 1, 10, 15, 20, 25 and 30 Hz. Two types of equivalent measurement were performed, once with a priori faultless coupling, and once with a damaged coupling that exhibits a side crack. The collected data is converted by fast Fourier transformation to the frequency domain and scanned by the aforementioned method. Results of diagnosing at various frequencies of rotation of the BLDC motor are referred with Table 1.

Table 1. Value of diagnosing function at various frequencies of rotation of the motor

Fault type	Rotation frequency, Hz					
	1	10	15	20	25	30
Commutation faults	0.5	0.6324	0.9398	0.5	0.5	0.9470
Rotor faults	0.5	1	1	0.5	1	1
Voltage ripples	0.0011	0.7964	1	0.5	0.4984	0.5154
Coupling faults	-1	-1	-1	-0.1354	-1	-1
Stator faults	1	1	1	1	0.9753	0.7871

Results of the diagnosing testifies the coupling fault. From the Tab. 4 it is visible, that to the same faults on various frequencies of rotation there are corresponding various values of diagnosis function. For an establishment of the reasons of these divergences it is necessary to carry out the analysis of amplitudes on characteristic frequencies of diagnosing. The characteristic frequencies given allows to make the following classification (Figure 7). From the listed classification follows, that all characteristic frequencies are the natural either of the rotation frequency or of the power line frequency. The commutation and coupling faults have identical characteristic frequencies. Therefore the values of dividing functions for commutation fault are decreased.

The reason for decrease of the dividing functions at 1 Hz frequency is a noise by the switching of the windings of the motor [1].

Voltage ripples are shown on 1., 2., and 3. harmonics of a power line (50, 100, 150 Hz). Low stator faults variations defect are shown on the second harmonic of the frequency of a power line (100 Hz). Characteristic frequencies of diagnosing of other faults are harmonics of the frequency motor rotation. Commutation faults are

shown on 1 - 4, 8 and 12, rotor defect - on 4, 5, 6 and 7, coupling defects - on 1, 2 and 3 harmonics of frequency of rotation (refer with: table 2).

Table 2. Value of characteristic frequencies of diagnosing

Number of a harmonic of frequency of rotation	Frequency of rotation of the motor, Hz/ <i>frequency of a power line, Hz</i>					
	1	10	15	20	25	30
1	1	10	15	20	25	30
2	2	20	30	40	50/50	60
3	3	30	45	60	75	90
4	4	40	60	80	100/100	120
5	5	50/50	75	100/100	125	150/150
6	6	60	90	120	150/150	180
7	7	70	105	140	175	210
8	8	80	120	160	200	240
12	12	120	180	240	300	360

From the Tab. 2 it is visible, that at the fifth harmonics of frequencies of rotation 10, 20 and 30 Hz are equivalents with the first, second or third harmonics of frequency of the power line. It is a reason by decrease in value of dividing function for voltage ripples and rotor faults on the frequency 20 Hz.

The fact, that the values of dividing function for «coupling fault» are larger than -1 can be explained by the oscillation damping of the second and third harmonics rotation, which be balanced out by increase on the 4 and 6 harmonics of rotation.

The imposing of three harmonics of a power line on 2, 4 and 6 harmonics of rotation on the frequency 25 Hz are decreased of the second and sixth and increase of the fourth and eighth harmonics of frequency of rotation. Decrease in the values of dividing function «stator faults» at 30 Hz is characterized by increase on the second harmonic of the power line which compensates at the fifth harmonic of rotation and at the second harmonic of the power line.

5. Conclusions

The neuro-fuzzy method of diagnosing BLDC motor on a current spectrum is described.

The analysis of initial data has shown, that the spectrum of the current which has been removed on low frequencies of rotation (1 Hz), has a large noise contribution which hinder to analyses properly the characteristic fault frequencies. In the current spectrum which has been obtained on frequencies 10, 20, 25 and 30 Hz there is an impose of harmonics of a power line and rotation that can give an uncertain information about a currently technical condition of the motor. The most informative spectrum is obtained on the frequency of rotation of 15 Hz at which there are marginal imposing harmonics.

The described neuro-fuzzy method of diagnosing allows to determine the technical drive condition, using the current spectrum of the steady-state drive, from which the normalized characteristic values are determined. The latest ones constitute an adequate input for the applied neuro-fuzzy method.

References

- [1] T.N. Kruglova, The neural-fuzzy method of operation effectivization for mechatronic motion modules of mining equipment, Proceedings of Institutions. North Caucasian region. Technical science, Spec.edition. Problems of mechatronic. (2008)71–75
- [2] Applikation of artificial intelligence: expert systems, fuzzy logic and neural networks. Edited by Mamede, Nuno J. Pinto-Ferreira Trans Tech Publications, 1996.
- [3] V.S. Petuchov, V.A. Sokolov, Diagnosis of a condition of electric motors on the basis of the spectral analysis of a consumed current. Magazine, News Electrical engineers. 1(31) (2005) 23.



International Conference on Industrial Engineering

Selective isolation continuous monitoring system in the networks of 6, 10 kV

Sidorov A.I., Medvedeva Yu.V.*

South Ural State University, 76, Lenin Avenue, Chelyabinsk, 454080, Russian Federation

Abstract

The need for the isolation selective monitoring for networks with the isolated neutral of 6, 10 kV is shown. The lack of monitoring systems possessing selectivity of action is presently noted. A possibility of isolation selective control on the basis of regime parameters measurement in networks of 6, 10 kV, such as voltage and currents at the beginning and the end of the line, and also angles between them is proved. According to the regime parameters measurement for the most difficult case, the line with tap, the analytical dependences for determination of isolation conductivity concerning the earth is given. Errors of the network conductivity determination concerning the earth in case of lines with tap in it are analyzed. It is shown that at isolation conductivity determination of a network concerning the earth by the formulas offered the error won't exceed 10%. The increase of measurement accuracy can be provided with measurement of regime parameters at the beginning of the tap line.

© 2015 The Authors. Published by Elsevier Ltd. This is an open access article under the CC BY-NC-ND license (<http://creativecommons.org/licenses/by-nc-nd/4.0/>).

Peer-review under responsibility of the organizing committee of the International Conference on Industrial Engineering (ICIE-2015)

Keywords: selective monitoring system of isolation; electric networks with the isolated neutral; regime parameters

1. Introduction

It is difficult to overestimate the role of isolation in power industry: in both reliability of power supply, and electrical safety, and fire and explosion safety. In spite of the fact that the first monitoring systems of isolation appeared on coal mines of England in 1912, this problem isn't solved yet.

The analysis of the existing schemes of continuous control of isolation [1-14] showed that common fault for each of known schemes of isolation monitoring is the lack of action selectivity. Sites or accessions where there was a decrease in level of isolation concerning the earth, don't come to light, and, at best, the condition of a network

* Corresponding author.

E-mail address: author@institute.xxx

isolation in general is estimated. It results in emergence of electro dangerous situations or to failure of power supply [15].

The idea about the use of regime parameters of an electric network (currents and voltage at the beginning and the end of the line, and also shift angle between them) for continuous monitoring of isolation concerning the earth in networks with the isolated neutral was offered for the first time in [15].

Further this idea was developed and received official confirmation by the patent for the invention [16].

In radial electric networks with the isolated neutral realization of this idea doesn't cause any technical difficulties. However in practice the number of pure radial networks is considerably small among the networks of 6, 10 kV.

The more difficult case is the existence of tap on the line. We will show the possibility of isolation conductivity determining of a network concerning the earth in this case.

In fig. 1 the P-shaped equivalent circuit of one phase of the tap line is presented.

Initial phase of voltage at the beginning of the line \dot{U}_1 we accept equal to zero, therefore, $\dot{U}_1 = U_1$ voltage at the end of the main line, $\dot{U}_2 = U_2 \cdot e^{j\psi_2}$ tension at the end of the tap line, $\dot{U}_3 = U_3 \cdot e^{j\psi_3}$ where ψ_2 and ψ_3 – shift angles between voltage at the beginning of the main line and respectively in the ends of the main and tap lines. Angles ψ_2 and ψ_3 are necessary to be defined.

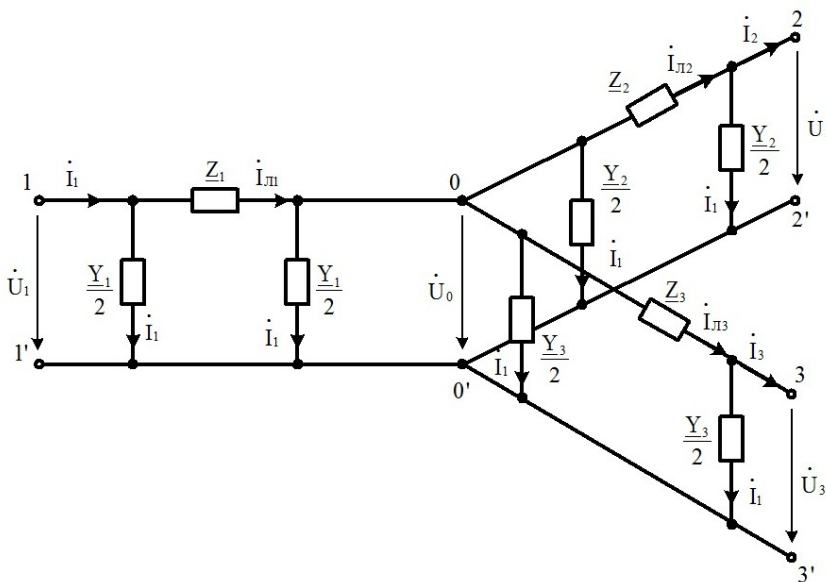


Fig. 1. P-shaped equivalent circuit of a tap network section for one phase.

Using the method of nodal potentials, we write the equations for a circuit in fig. 1:

$$\begin{cases} 0 = \underline{Y}_{00} \cdot \dot{U}_0 - \underline{Y}_{01} \cdot \dot{U}_1 - \underline{Y}_{02} \cdot \dot{U}_2 - \underline{Y}_{03} \cdot \dot{U}_3; \\ \dot{I}_1 = -\underline{Y}_{10} \cdot \dot{U}_0 + \underline{Y}_{11} \cdot \dot{U}_1; \\ -\dot{I}_2 = -\underline{Y}_{20} \cdot \dot{U}_0 + \underline{Y}_{22} \cdot \dot{U}_2; \\ -\dot{I}_3 = -\underline{Y}_{30} \cdot \dot{U}_0 + \underline{Y}_{33} \cdot \dot{U}_3, \end{cases} \tag{1}$$

where the conductivity of branches wiring in knots are defined as follows:

$$\underline{Y}_{11} = \frac{\underline{Y}_1}{2} + \frac{1}{\underline{Z}_1} = \frac{k \cdot \underline{Y}}{2} + \frac{1}{\underline{Z}_1}; \quad (2)$$

$$\underline{Y}_{22} = \frac{\underline{Y}_2}{2} + \frac{1}{\underline{Z}_2} = \frac{(1-k) \cdot \underline{Y}}{2} + \frac{1}{\underline{Z}_2}; \quad (3)$$

$$\underline{Y}_{33} = \frac{\underline{Y}_3}{2} + \frac{1}{\underline{Z}_3}; \quad (4)$$

$$\underline{Y}_{00} = \underline{Y}_{11} + \underline{Y}_{22} + \underline{Y}_{33} = \frac{\underline{Y}}{2} + \frac{\underline{Y}_3}{2} + \underline{Y}_s; \quad (5)$$

$$\underline{Y}_s = \frac{1}{\underline{Z}_1} + \frac{1}{\underline{Z}_2} + \frac{1}{\underline{Z}_3}; \quad (6)$$

and the general conductivities between knots are equal:

$$\underline{Y}_{10} = \underline{Y}_{01} = \frac{1}{\underline{Z}_1}; \quad (7)$$

$$\underline{Y}_{20} = \underline{Y}_{02} = \frac{1}{\underline{Z}_2}; \quad (8)$$

$$\underline{Y}_{30} = \underline{Y}_{03} = \frac{1}{\underline{Z}_3}. \quad (9)$$

Solving the system of equations given above, we get dependences for defining required conductivities \underline{Y} and \underline{Y}_3 :

$$\underline{Y} = 2 \cdot \frac{(\underline{Z}_1 \cdot \dot{I}_1 + \underline{Z}_2 \cdot \dot{I}_2 - \dot{U}_1 + \dot{U}_2)}{k \cdot \underline{Z}_1 \cdot \dot{U}_1 - (1-k) \cdot \underline{Z}_2 \cdot \dot{U}_2}; \quad (10)$$

$$\underline{Y}_3 = 2 \cdot \frac{\left(\dot{U}_1 - \dot{U}_3 + \frac{k \cdot \underline{Z}_1 \cdot \dot{U}_1 \cdot \underline{Y}}{2} - \underline{Z}_1 \cdot \dot{I}_1 - \underline{Z}_3 \cdot \dot{I}_3 \right)}{\underline{Z}_3 \cdot \dot{U}_3}. \quad (11)$$

For simplification of expressions we will introduce the following symbols:

$$\dot{V}_1 = U_1 - \underline{Z}_1 \cdot \dot{I}_1; \quad (12)$$

$$\dot{V}_2 = U_2 + \underline{Z}_2 \cdot \dot{I}_2^*; \quad (13)$$

$$\dot{V}_3 = U_3 + \underline{Z}_3 \cdot \dot{I}_3^*, \quad (14)$$

where $I_2^* = I_2 \cdot e^{-j\varphi_2}$, $I_3^* = I_3 \cdot e^{-j\varphi_3}$;

$$\dot{W}_1 = k \cdot \underline{Z}_1 \cdot U_1; \quad (15)$$

$$\dot{W}_2 = (1-k) \cdot \underline{Z}_2 \cdot U_2; \quad (16)$$

$$\dot{W}_3 = \underline{Z}_3 \cdot U_3. \quad (17)$$

As a result we obtain the following:

$$\underline{Y} = 2 \cdot \frac{\dot{V}_1 - \dot{V}_2 \cdot e^{j\psi_2}}{\dot{W}_2 \cdot e^{j\psi_2} - \dot{W}_1}; \quad (18)$$

$$\underline{Y}_3 = 2 \cdot \frac{\dot{W}_1 \cdot (\dot{V}_1 - \dot{V}_2 \cdot e^{j\psi_2})}{\dot{W}_3 \cdot e^{j\psi_3} \cdot (\dot{W}_2 \cdot e^{j\psi_2} - \dot{W}_1)} + 2 \cdot \frac{(\dot{V}_1 - \dot{V}_3 \cdot e^{j\psi_3})}{\dot{W}_3 \cdot e^{j\psi_3}}. \quad (19)$$

From the equation (1) we state (express) \dot{U}_0 :

$$\dot{U}_0 = \dot{W}_1 \cdot \frac{Y}{2} + \dot{V}_1. \quad (20)$$

Replacing the voltage \dot{U}_0 according to the expression (20) in the equation (1), and conductivity according to expressions (2-9) we will transform it to the following:

$$\left(\frac{Y}{2} + \frac{Y_3}{2} + Y_{\Sigma} \right) \cdot \left(\dot{W}_1 \cdot \frac{Y}{2} + \dot{V}_1 \right) - \frac{\dot{U}_1}{\underline{Z}_1} - \frac{\dot{U}_2}{\underline{Z}_2} - \frac{\dot{U}_3}{\underline{Z}_3} = 0. \quad (21)$$

In the equation obtained we replace conductivities \underline{Y} and \underline{Y}_3 with expressions (18, 19) and we consider that $\dot{U}_1 = U_1$, $\dot{U}_2 = U_2 \cdot e^{j\psi_2}$, $\dot{U}_3 = U_3 \cdot e^{j\psi_3}$. After a regrouping with association of members containing identical degrees at "e" and divisions on $e^{j(\psi_2+\psi_3)}$ we receive the following equation:

$$\underline{M}_1 \cdot e^{j(2\psi_2)} + \underline{M}_2 \cdot e^{j(\psi_2+\psi_3)} + \underline{M}_3 \cdot e^{j\psi_2} + \underline{M}_4 \cdot e^{j\psi_3} + \underline{M}_5 \cdot e^{j(\psi_2-\psi_3)} + \underline{M}_6 + \underline{M}_7 \cdot e^{j(\psi_3-\psi_2)} + \underline{M}_8 \cdot e^{-j\psi_2} = 0. \quad (22)$$

The received equality (22) has to be true for the actual and imaginary parts. As a result we obtain the system of two equations concerning two unknowns – $/_2$ and $/_3$:

$$\text{Re}[\underline{M}_1 \cdot e^{j(2\psi_2)} + \underline{M}_2 \cdot e^{j(\psi_2+\psi_3)} + \underline{M}_3 \cdot e^{j\psi_2} + \underline{M}_4 \cdot e^{j\psi_3} + \underline{M}_5 \cdot e^{j(\psi_2-\psi_3)} + \underline{M}_6 + \underline{M}_7 \cdot e^{j(\psi_3-\psi_2)} + \underline{M}_8 \cdot e^{-j\psi_2}] = 0; \quad (23)$$

$$\text{Im}[\underline{M}_1 \cdot e^{j(2\psi_2)} + \underline{M}_2 \cdot e^{j(\psi_2+\psi_3)} + \underline{M}_3 \cdot e^{j\psi_2} + \underline{M}_4 \cdot e^{j\psi_3} + \underline{M}_5 \cdot e^{j(\psi_2-\psi_3)} + \underline{M}_6 + \underline{M}_7 \cdot e^{j(\psi_3-\psi_2)} + \underline{M}_8 \cdot e^{-j\psi_2}] = 0. \quad (24)$$

To find α_2 and α_3 angles it is necessary to solve this system (for example, in Mathcad package by minimization of a mean square error method) [17-19].

For defining of formulas errors, numerical experiments on digital model of the analyzed network section were executed in a Mathcad Professional package [18, 20, 21].

The analysis of errors allows us to draw the following conclusions:

- It is possible to determine precisely the total conductivity of isolation of the line concerning the earth by the offered formulas, thus the error won't exceed 10%.
- The most significant errors are observed when determining tap line conductivity by means of the offered formulas, thus errors can be more than 10%. This results from the fact that the offered formulas don't contain information on regime parameters in a tap accession place (i.e. at the beginning of the tap line), and only data on mode parameters at the end of the tap line are used.

However the last shortcoming can be almost completely excluded by installation of the recloser in a tap place. It has the opportunity to provide information on regime parameters at the beginning of tap (at the end of tap such opportunity is available).

Thus, we received and investigated the analytical dependences allowing to define isolation conductivity concerning the earth according to the results of regime parameters measurement in distributive electric networks of 6, 10 kV with taps. It provides possibility of selective continuous isolation monitoring in networks of 6, 10 kV.

References

- [1] Yu.V. Kosorotova, Development of the system of continuous control of isolation in distributive electric networks of 6-35 kV, Competition of grants of students, graduate students and young scientific higher education institutions of Chelyabinsk region: Collection of papers of research works of students, Publishing house of SUSU, Chelyabinsk. (2002) 67–68.
- [2] A.S. Kudryavtsev, Operation of the device of continuous control of resistance of isolation in networks of 6 kV, Safety of work in the industry. 7 (1985) 43–44.
- [3] K.B. Mousse, S.P. Shuletskaya, The device of the preventive directed control of isolation in the distributive networks of 6 kV with the isolated neutral, Industrial power. 1 (1982) 35–38.
- [4] A.A. Selnitsyn, Classification of ways of continuous control of resistance of isolation in three-phase electric networks with the isolated neutral, Health and safety: Collection of scientific works, ChSTU, Chelyabinsk. (1992) 16–24.
- [5] A.I. Sidorov, The theory and practice of system approach to ensuring of electrical safety on open mining operations: dissertation of the doctor of technical sciences, Chelyabinsk, 1993.
- [6] A.I. Sidorov, V.I. Peturov, Yu.V. Kosorotova, Continuous control of isolation in distributive electric networks, Science – Production – Technologies – Ecology: Collection of materials of the All-Russian scientific and technical conference, Publishing house of VyatSU, Kirov, 2002.
- [7] E.F. Tsapenko, A.S. Kudryavtsev, The valve scheme of control of resistance of isolation in networks 6, 10 of kV with the isolated neutral, Industrial power. 8 (1984) 46–48.
- [8] E.F. Tsapenko, I.A. Oryol, I.F. Goryachov, The device of continuous measurement of resistance of isolation in networks 6, 10 of kV with the isolated neutral, Industrial power. 10 (1988) 27–29.
- [9] A.N. Shatkin, Continuous control of resistance of isolation of a flexible cable of 6 kV and equipment of the excavator, Industrial power. 8 (1985) 48–50.
- [10] A.N. Shatkin, The device of continuous control of a condition of isolation in factory electrical installations of 6 kV, Industrial power. 2 (1981) 18–20.
- [11] N.V. Shipunov, Protective shutdown, Energy, Moscow, 1968.
- [12] V.I. Shchutsky, A.M. Mavritsyn, A.I. Sidorov, Yu.V. Sitchikhin, Electrical safety at open mountain works, Subsoil, Moscow, 1983.
- [13] High Impedance Fault Detection Technology, Report of PSRC Working Group D15, IEEE Power Engineering Society, IEEE, 1996.
- [14] B.M. Aucoin, R.H. Jones, High Impedance Fault Implementation Issues, IEEE Transactions on Power Delivery. 11(1) (1996) 139–148.
- [15] A.I. Sidorov, The theory and practice of system approach to ensuring electrical safety on open mining operations, Dissertation on competition of a doctor of technical sciences academic degree, ChSTU, Chelyabinsk, 1993.
- [16] A.I. Sidorov, N.A. Khusainova, RF Patent. 2242015. (2004).
- [17] Yu.V. Kosorotova, N.A. Khusainova, A.I. Sidorov, Determination of parameters of isolation in extensive distributive electric networks on the basis of measurement of regime parameters, the Collection of reports of the Eighth Russian scientific and technical conference on electromagnetic compatibility and electromagnetic safety of EMS-2004, Publishing house of WITU. (2004) 108–111.
- [18] E.G. Makarov, Engineering calculations in Mathcad, Training course, Piter, St. Petersburg, 2005.
- [19] N.A. Khusainova, Yu.V. Kosorotova, A.I. Sidorov, Determination of parameters of isolation of a power line with tap in distributive networks in regime parameters, Electrical safety. 2-3 (2001) 9–13.
- [20] Yu.V. Kosorotova, N.A. Khusainova, The analysis of dependences for determination of conductivity of isolation concerning the earth in distributive networks 6, 10 kV containing lines with tap by results of measurement of regime parameters, Electrical safety. 3 (2004) 6–15.

- [21] Yu.V. Kosorotova, Research of a way of control of isolation in extensive electric networks by means of digital modeling, Competition of grants of students, graduate students and young scientific higher education institutions of Chelyabinsk region: Collection of papers of research works of graduate students. (2004) 128–129.



International Conference on Industrial Engineering

The study of continuous rolling mill inter-stand tension inferential control systems

Shokhin V.V., Permyakova O.V.*

Nosov Magnitogorsk State Technical University Magnitogorsk, Russia

Abstract

The inter-stand tension inferential control systems are used to stabilize the rolling motor torque. To stabilize the motor torque the electric drive system with the properties of the rolling motor torque supply may also be used. An alternate option may include torque stabilization by to the effect on speed of the previous, further or controlled mill stand. The tension control accuracy depends on how exact the unhindered rolling torque is determined. Nevertheless, a change in tension due to this factor may result in improving gauge accuracy in some systems. Using the model of the continuous rolling mill, the paper considers the force interaction between the stand electric drives for different technological conditions of rolling. It analyses the operation of the rolling mill using different system for tension inferential control. The finished studies prove that size alignment is provided with the tension control system affecting speed of the further stands. The paper verifies that the characteristics of the rolling mill including aligning ability depend on the rolling speed. It is a good practice to apply those results during the selection and calculation of the inferential tension controllers.

© 2015 The Authors. Published by Elsevier Ltd. This is an open access article under the CC BY-NC-ND license (<http://creativecommons.org/licenses/by-nc-nd/4.0/>).

Peer-review under responsibility of the organizing committee of the International Conference on Industrial Engineering (ICIE-2015)

Keywords: electric drive, rolling mill, tension control, simulation, stand force interaction, size alignment.

1. Introduction

On the modern bar and wire mills inter-stand tension is controlled at rolling [1, 2]. For a variety of reasons, it is impossible to use tension direct control systems that is why tension value is inferred by the rolling motor torque. The rolling motor torque is defined with the torque of unhindered rolling that at a first approximation can be specified as

* Corresponding author. Tel.: +7-919-113-81-27.
E-mail address: shww@mgn.ru

constant during rolling and torques affected by the front and back tensions. If there is no back tension for the first stand, so after the torque of unhindered rolling of the stands has been estimated with one of the possible methods, we can evaluate torque components from tension effect for each stand of the rolling mill. With these values, we can develop the systems for inter-stand tension control while stabilizing the torque of the rolling motor.

2. Relevance

To stabilize the motor torque the electric drive system with properties of the rolling motor torque supply may be used. An alternative variant may include torque stabilization due to the effect on speed of the previous, further or controlled mill stand. A disadvantage of such systems is sensitivity of the unhindered rolling torque to fluctuating technological conditions of rolling. It ultimately affects accuracy of the tension control. In some cases, however, resulting tension deviations at rolling with such systems may have a beneficial effect on size alignment. Because of the need to increase gauge accuracy and provide stability of continuous rolling it is relevant to study and compare different tension control systems.

3. Problem statement

According to the studies [4–7], when the rolling motor torque is controlled by effecting the roll speed of the further stand this system can adjust tension as well as align sizes at measuring technological conditions of rolling. It is associated with elastic expansion of the stand at changing rolling conditions. Specifically, when increasing the original size of rolled products, yield stress and friction coefficient in the deformation zone that should result in gain of the motor torque; rolling product size in the reduction direction due to the stand elastic expansion the front tension for the stand will also grow. It will influence size reduction as at raising tension the roll pressure and stand elastic expansion are decreased. As a result, changing roll product size occurs to a lesser extent, that is, gauge alignment is enabled [8].

The study aims to determine effect of the fluctuating technological conditions of rolling on distribution of inter-stand tensions and loads of rolling motors for three variants of the continuous rolling mill: with the speed control system only, for electric drive of the rolling mill with properties of the torque supply as well as for the system stabilizing the torque due to the effect on speed of the following stand of the inter-stand gap.

4. Theory

We consider the wire mill with four-roll passes that uses a variable frequency electric drive with the asynchronous vector speed control motor [9-12].

The rolling mill is simulated by means of MATLAB environment and SIMULINK application [13, 14]. Structural diagrams of the asynchronous motor with frequency converter and vector speed control have been developed, the structural diagram of strip within the inter-stand gap is also provided.

Equations describing operation of the asynchronous motor in the rotating coordinates are offered in [9]. According to these equations, the structural diagram of the asynchronous electric motor at alignment of the rotating α - β coordinates due to the vector of rotor's flux linkage (Fig. 1) is provided. Inputs of this model are $U_{1\alpha}$ and $U_{1\beta}$ projections of the voltage space vector, the M_s value of static torque of the electric drive. Output variables are the ω rotor speed of the asynchronous motor and value of the flux linkage of ψ_2 rotor. The model relies on saturation of the motor magnetic system [15, 16].

The structure of the automatic speed and motor torque control system accounts for the principle of the subordinate coordinate adjustment (Fig. 2). Flux linkage is controlled with double-circuit; speed is controlled with two-circuits for control of the current component in β -direction, motor torque and speed [8, 9]. Inputs of this model are signals setting motor speed and rotor flux linkage, feedback signals of the $i_{1\beta}$ and $i_{1\alpha}$ current components, rotor flux linkage and motor speed. Outputs are $U_{1\alpha}$ and $U_{1\beta}$ projections of the voltage space vector.

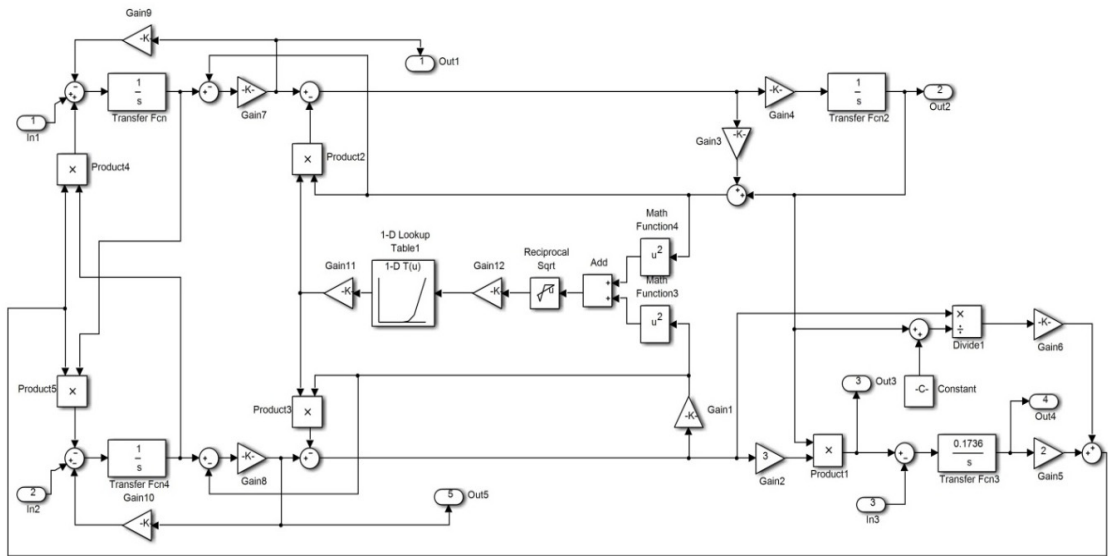


Fig. 1. Structural diagram of the asynchronous motor model

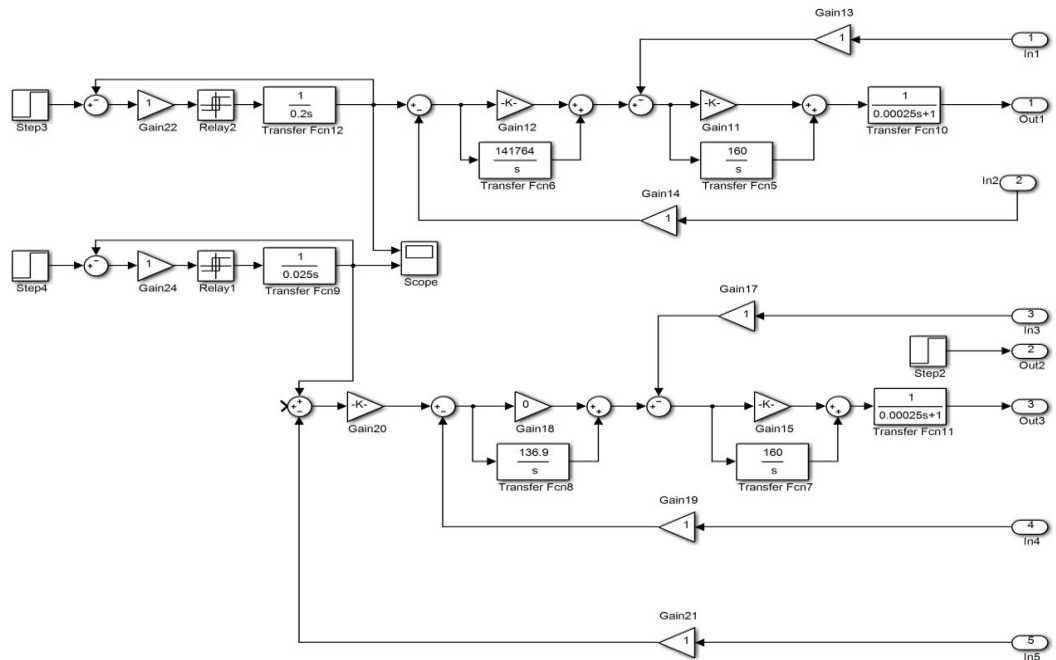


Fig. 2. Structural diagram of the speed control system model

For simulation of strip behavior within the inter-stand gap the known tension expression in the integral form, proposed first by D.P. Morozov [17, 18], is used. Speed calculation considers the values of leads and lags of the metal speed related to the roll speed in the deformation zones. Strip behavior model is shown in Fig. 3. Input variables of this model are rotation speed of rolls of the adjacent stands; an output variable is the value of tension within the inter-stand gap.

$$T_{i,i+1} = \frac{EQ_i}{l_{i,i+1}} \int_0^t (v_{i+1} - v_i) dt + T_{(i,i+1)0}$$

where E – elasticity modulus of the rolled material; Q_i – cross-section of strip between i and $i+1$ stands; $l_{i,i+1}$ – length of the inter-stand gap; v_i, v_{i+1} – speed of metal output from rolls of the stand with i order number and metal entry to the stand with $i+1$ order number.

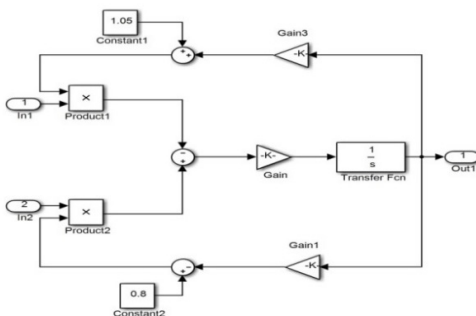


Fig.3. Structural diagram of the strip model in the inter-stand gap.

At simulation, each model has the form of subsystem with input and output parameters. It enables a relatively easy simulating the multi-stand mill with stand electric drives correlated through the rolled strip.

The established model of the continuous three-stand rolling mill is shown in Fig. 4.

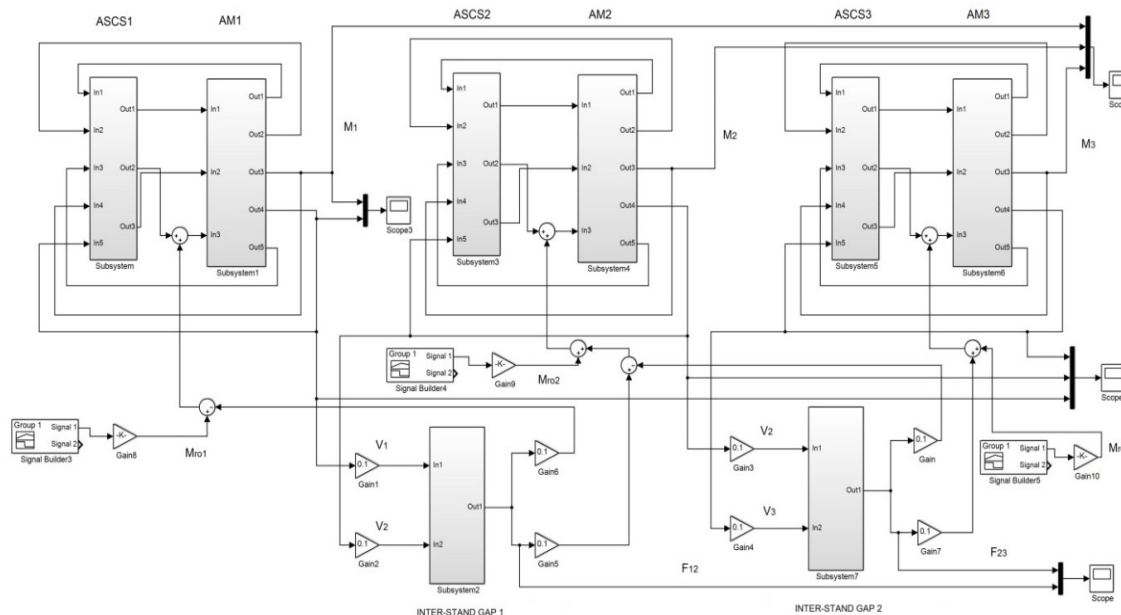


Fig.4. Model of the continuous three-stand mill

(ASCS– automatic speed control systems of the 1st, 2nd and 3rd stands; AM– models of asynchronous motors of the 1st, 2nd and 3rd stands; M – torques of motors of the 1st, 2nd and 3rd stands, Mro1 – torques of rolling of the 1st, 2nd and 3rd stands; v – peripheral speed of rollers of the 1st, 2nd and 3rd stands; F12 , F23 – tensions in the first and second inter-stand gaps).

Torques of the stand motors change due to the variations of the rolling technological conditions. So, the torques at rolling are effected by the origin size of the rolled products, friction coefficient in the deformation zone and yield stress of the rolled strip. During investigations, such changes were simulated by setting a deviation of the rolling torque to 10% in one of the stands and changing values of the inter-stand tensions and motor torques of every stand was calculated. Investigation results are provided in Table 1 and 2.

Table 1 Tension Alterations at Rolling Torque Fluctuation in the Stand

Specified Conditions		Change of T_{rol} in the stand by 10%	Inter-stand Tension Alteration, T	
			Stand 1 – 2	Stand 2 – 3
ASCS	Rate of the output stand 178 1/s	in the 1.	117.7	10.7
		in the 2.	-79	80
		in the 3.	-67.3	-69.3
	Rate of the output stand 17.8 1/s	in the 1.	472	181
		in the 2.	-219	297.7
		in the 3.	-102	-328
Tm3=const Tm2=const (ED-torque source)	Rate of the output stand 178 1/s	in the 1.	0	0
		in the 2.	-1000	0
		in the 3.	-1000	-1000
	Rate of the output stand 17.8 1/s	in the 1.	0	0
		in the 2.	-1000	0
		in the 3.	-1000	-1000
Torque stabilization Tm1, Tm2 due to the front tension	Rate of the output stand 178 1/s	in the 1.	464	-58.1
		in the 2.	-32.8	373
		in the 3.	-3	-48.1
	Rate of the output stand 17.8 1/s	in the 1.	870	600
		in the 2.	-30	765
		in the 3.	-10	-110

Table 2 Motor Torque Alterations at Rolling Torque Fluctuation in the Stand

Specified Conditions		Change of T_{rol} in the stand by 10%	Motor torque alteration, Tm		
			1	2	3
ASCS	Rate of the output stand 178 1/s	in the 1.	88.8	10.8	1.5
		in the 2.	8.5	82.6	7
		in the 3.	0.4	6.3	93.5
	Rate of the output stand 17.8 1/s	in the 1.	52.6	29.2	18.3
		in the 2.	21.9	48.3	30.5
		in the 3.	10.4	21.9	67.3
Tm3=const Tm2=const (ED-torque source)	Rate of the output stand 178 1/s	in the 1.	100	0	0
		in the 2.	99.8	0	0
		in the 3.	99.9	0	0
	Rate of the output stand 17.8 1/s	in the 1.	100	0	0
		in the 2.	100	0	0
		in the 3.	99.9	0	0
Torque stabilization Tm1, Tm2 due to teh front tension	Rate of the output stand 178 1/s	in the 1.	53.6	52.2	-5.5
		in the 2.	3.3	59.3	37.5
		in the 3.	0.3	4.5	95.5
	Rate of the output stand 17.8 1/s	in the 1.	10	30	60
		in the 2.	2	20	80
		in the 3.	2	10	90

At low speeds and the same deviation of the rolling torque, that is, similar changes of rolling conditions, variations of inter-stand tensions and motor torques are established to increase significantly.

For instance, when rolling conditions in the first stand are changed at high speed the deviation of tension in the first inter-stand gap is 117.7 N, at low speed– 472 N; here, tension variations in the second gap amount 10.7 N and 181 N, correspondingly. At this, the most essential motor torque changes take place in those stands where rolling conditions vary while motor torques of other stands alter due to the changing inter-stand tensions.

For electric drive with properties of the torque supply [19] all alternations of rolling conditions in the second and third stand are proven to result in changing motor torque of the first stand. As we can see, changes of the rolling conditions in the mill stands of such system spread against rolling direction and may significantly load motors of the first mill stands. Furthermore, the value of the rolling speed with the use of the system considered does not effect on the value of variations of inter-stand tension and rolling motor torques.

In the systems stabilizing motor torque due to the front tension alterations of the rolling torques in the stands lead to substantial changing front tension enabling alignment of the rolled product sizes. In this case changes of the rolling conditions in the mill stands spread in the rolling direction increasing loads of the further motors. Here, when rolling conditions undergo changes in the third stand only the motor torque of this stand will essentially raise.

It should be noted that the system stabilizing inter-stand tensions cannot promote alignment of the rolled product size as at constant tension elastic expansion of the stand does not depend on this factor.

The results provided prove that properties of the mill depend on rolling speed. To estimate dynamic characteristics of the continuous mill with different speeds the frequency response characteristics of the three-stand mill (Fig.5) were determined that associate tension alternations in the inter-stand gaps and changes of the signal setting speed for the first stand at different rolling speed.

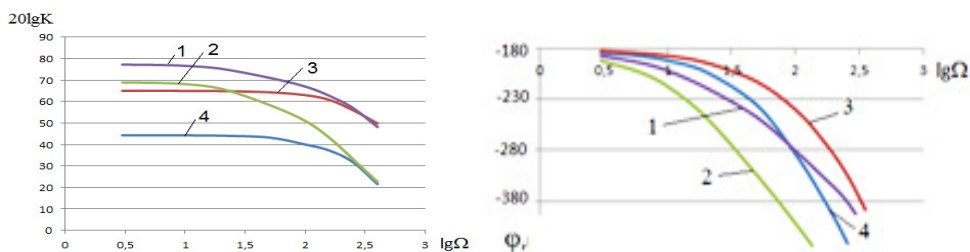


Fig.5. Frequency response characteristics of the rolling mill at change of the speed setting for the first stand (1,2- for rolling speed 1.78 m/s, 3,4- for rolling speed 17.8 m/s; 1,3- for the first inter-stand gap, 2,4- for the second inter-stand gap).

The analyses of characteristics show that dynamic properties of the strip have the main influence on the frequency bandwidth in the case under consideration. At the change of rolling speed, the strip speed ratio and its time constant will significantly vary in the inter-stand gap. Coefficients connecting speed alterations in the first stand and inter-stand tensions have the highest values at low speeds. Speed alterations in the first stand have more pronounced influence on the tension change in the first inter-stand gap when compared to the second. This is due to the impact of the second (intermediate) stand acting here as a kind of damper. At low rates, the phase delay is shifted towards the lower side under influence of the strip properties.

The frequency response characteristics obtained testify that at the use of the system stabilizing motor torque with change of the further stand speed the rolling mill will have the best alignment capacity at lower speeds; at raising speed the size alignment will be less efficient. However, even in that case when technological rolling conditions are changed at higher speeds it will have less effect on the tension alteration, so improve the operation of the rolling mill, too [20-24].

To maintain dynamic properties of the control system at change of the rolling speed one should consider a significant alteration of speed ratios connecting the stand speed setting and values of the inter-stand tensions [25-28].

5. Conclusion

1. It is a good practice to use the principle of the three-stand mill modeling developed at investigation of rolling mills with different number of the continuous stands.
2. The actual rolling mill has been quantitatively evaluated with regard to the force interaction of the electric drives at fluctuations of the rolling conditions.
3. The finished studies prove that gauge alignment is provided with the tension control system effecting on speed of the following stands. It verifies that the characteristics of the rolling mill including aligning ability depend on the rolling speed.
4. At higher speeds the alignment property is reduced but at the same time the inter-stand tensions undergo less alterations at fluctuations of the rolling conditions, that is, rolling operation is improved.
5. It is advisable to apply modeling methods and obtained findings to selection and calculation of the tensions regulators for continuous rolling mills.

References

- [1] A.A. Radionov, Automated Electric Drive for Mills Producing Steel Wire, Federal State Budgetary Educational Institution of Higher Professional Education G.I. Nosov Magnitogorsk State Technical University, Magnitogorsk, 2007.
- [2] Kh.N. Belalov, B.A. Nikiforov, G.S. Gun, Production of Steel Wire: monograph, Federal State Budgetary Educational Institution of Higher Professional Education G.I. Nosov Magnitogorsk State Technical University, Magnitogorsk, 2006.
- [3] V.V. Shokhin, A.S. Karandaev, A.V. Kosenkov, USSR Inventor's Certificate 1519806. (1989).
- [4] M.G. Polyakov, I.A. Selivanov, V.V. Shokhin, USSR Inventor's Certificate 555928. (1977).
- [5] I.A. Selivanov, V.V. Shokhin, Yu. I. Kuznetsov, USSR Inventor's Certificate 900901. (1982).
- [6] V.P. Bychkov, I.A. Selivanov, V.V. Shokhin, USSR Inventor's Certificate 942839. (1982).
- [7] M.G. Polyakov, I.A. Selivanov, V.V. Shokhin, USSR Inventor's Certificate 555929. (1977).
- [8] M.G. Polykov, I.A. Selivanov, V.A. Tkachenko, Efficiency of Methods for Wire Size Control at Continuous Rolling Mills with Multi-Roll Gauges, in: Theory and Practice of Metalware Production, UFU, Sverdlovsk. (1985) 33–43.
- [9] G.G. Sokolovski, AC Frequency Control Electric Drives: textbook for higher schools, Academia publishing center, Moscow, 2007.
- [10] V.M. Terekhov, O.I. Osipov, Control System of Electric Drives: textbook for higher schools, Academia publishing center, Moscow, 2006.
- [11] V.A. Dartau, V.V. Rudakov, A.E. Kozyaruk, Fundamentals of Construction of Variable Frequency Electric Drives with Vector Speed Control, in: Automated Electric Drive, Energy, Moscow. (1980) 93–101.
- [12] L.Kh. Datskovsky, V.I. Rogovoy, State-of-the-Art and Trends in Asynchronous Frequency Control Electric Drive (Brief Analytical Survey), in: Electrical Engineering. 7 (1997) 18–28
- [13] R.T. Schreiner, Mathematical Modeling AC Electric Drives with Semiconductor Frequency Converters, Ural Department of Russian Academy of Sciences, Ekaterinburg, 2000.
- [14] I.V. Chernykh, Modeling electric devices in MATLAB, SimPowerSystem and Simulink, DMK Press, Moscow, 2008.
- [15] A.B. Vinogradov, Consideration of Steel Losses, Saturation and Skin Effect at Modeling Dynamical Processes of Frequency Control Electric Drive, in: Electrical Engineering. 5 (2005) 57–61.
- [16] A.B. Vinogradov, Vector Speed Control of AC Electric Drives, State Educational Institution of Higher Professional Training V.I. Lenin Ivanovo State Power Engineering University, Ivanovo, 2008.
- [17] D.P. Morozov, On Theory of Electric and Mechanical Process of Cold-Rolling Mills, in: Bulletin of Electrotechnical Industry. 3 (1944) 16–19.
- [18] N.N. Druzhinin, Continuous Stands as an Automation Object, Metallurgy, Moscow, 1975.
- [19] K.D. Gutermann, N.F. Ilinsky, V.V. Mikhaylov, V.K. Tsatsepnik, Electric Drive with Properties of Torque Source, in: Atomated Electric Drive in National Economy, Energy, Moscow. 1 (1971) 190–192.
- [20] I.A. Selivanov, V.V. Shokhin, Calculating Parameters of Indirect Size Controller for Continuous Bar and Wire Mills, in: Electric Equipment of Industrial Enterprises, Chuvash State University, Cheboksary. (1982) 92–97.
- [21] P.V. Shilyaev, I.Yu. Andryushin, V.V. Golovin, A.A. Radionov, A.S. Karandaev, V.R. Khrumshin, Algorithms of a digital automatic system for tension and loop control in a widestriphotrolling mill, Russian Electrical Engineering. 84(10) (2013) 533–541. DOI 10.3103/S106837121310009X.
- [22] A.A. Radionov, A.S. Karandaev, V.R. Khrumshin, I.Yu. Andryushin, A.N. Gostev, Speed and Load Modes of Rolling Hollow Billet at the Wide-Strip Rolling Mill. Proceedings of 2014 International Conference on Mechanical Engineering, Automation and Control Systems (MEACS). (2014) 5. DOI 10.1109/MEACS.2014.6986841.
- [23] Khrumshin V.R. Ways to Compensate for Static Deviations in Speed in Electric Drives of Broad Strip Hot Rolling Mill Stand. Russian Electrical Engineering. 2013. Vol. 84, No. 4. Pp. 221–227. DOI 10.3103/S1068371213040032.
- [24] Karandaev A. S., Khrumshin V.R. Andryushin I.Yu., Khrumshin R.R., Petryakov S.A. Method for Correction of Gauge Interference of the Head Strip Section in a System for Automated Controlling of the Thickness of a Broad Strip Hot Rolling Mill. Russian Electrical Engineering. 2013. Vol. 84, No. 8. Pp. 441–445. DOI 10.3103/S1068371213080087.

- [25] Karandaev A.S., Radionov A.A., Khramshin V.R., Andryushin I.Yu., Shubin A.G. Automatic Gauge Control System with Combined Control of the Screw-Down Arrangement Position. 12th International Conference on Actual Problems of Electronic Instrument Engineering (APEIE-2014). – Novosibirsk. 2014. Vol. 1. Pp. 88-94. DOI 10.1109/APEIE.2014.7040794.
- [26] Khramshin V.R., Evdokimov A.S., Kornilov G.P., Radionov A.A., Karandaev A.S. System for Speed Mode Control of the Electric Drives of the Continuous Train of the Hot-Rolling Mill. Proceedings of the 2015 International Siberian Conference on Control and Communications (SIBCON-2015). – Omsk: Omsk State Technical University. May 21-23, 2015. DOI 10.1109/SIBCON.2015.7147264.
- [27] Khramshin V.R., Evdokimov S.A., Karandaev A.S. Andryushin I.Yu., Shubin A.G. Algorithm of No-Pull Control in the Continuous Mill Train. Proceedings of the 2015 International Siberian Conference on Control and Communications (SIBCON-2015). – Omsk: Omsk State Technical University. May 21-23, 2015. DOI 10.1109/SIBCON.2015.7147263.
- [28] W. Strunk Jr., E.B. White, *The Elements of Style*, third ed., Macmillan, New York, 1979.



International Conference on Industrial Engineering

Automated information-measurement system used to test the immunity of the medical equipment protective elements to the discharges of the defibrillator

Stetsenko I.A., Leuhin R.I., Shirokov K.M.*

Platov South-Russian State Polytechnic University (NPI), 132, St. Prosvescheniya, Rostov region, Novocherkassk, 346428, Russian Federation

Abstract

The article discusses the information-measurement system used for testing of protective elements medical equipment for their resistance to the discharge of a defibrillator, which is designed to test medical products, which may be exposed to high voltage defibrillator pulses, up to 5000 V while in operation. The Information-measurement system should provide a fully automated testing process in accordance with the international standard IEC 60601-1, as well as analyze the result and diagnose the parameters of elements the of a defibrillator block simulating the pulses.

© 2015 The Authors. Published by Elsevier Ltd. This is an open access article under the CC BY-NC-ND license (<http://creativecommons.org/licenses/by-nc-nd/4.0/>).

Peer-review under responsibility of the organizing committee of the International Conference on Industrial Engineering (ICIE-2015)

Keywords: test medical devices for resistance to the pulse of defibrillator, the system of diagnostics of parameters of high voltage source.

1. Information-measuring system

To ensure the automation of the testing process of the developed information-measuring system that fully automates the testing process and allows [1][2][3] for self-diagnosis storage capacitor C3 of the high voltage [4] source [5][6][7]. The General scheme of application of the test voltage to the medical device [8] shown in figure 1.

* Corresponding author. Tel.: +7-863-525-5240; fax: +7-683-525-5240.
E-mail address: iimt-srstu@mail.ru

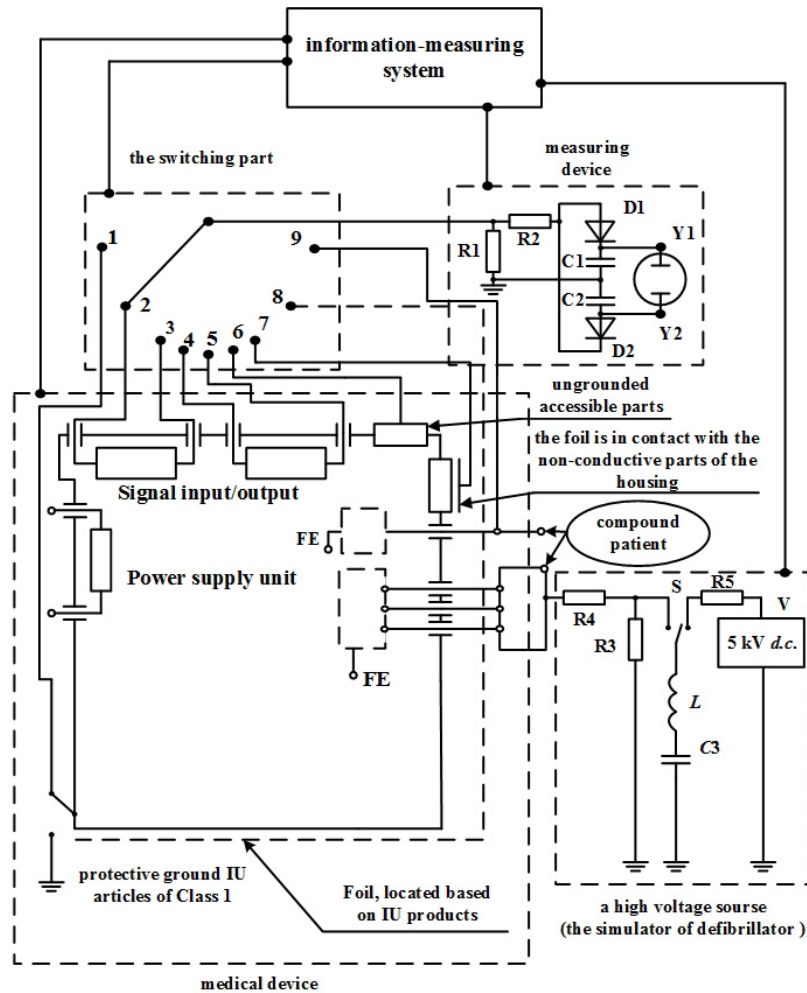


Fig. 1. The General scheme of application of test voltage to medical device

VT – test voltage, S – switch test voltage, R1, R2 - resistors with a tolerance of $\pm 2\%$ for voltage less than 2 kV, R3, R4 - resistors with a tolerance of $\pm 2\%$ for voltage less than 5 kV, R5 - limiting resistor, D1, D2 - miniature silicon small signal diodes (remaining components have a tolerance of $\pm 5\%$), 1 - the output of the switching control part, 2 – output of conclusion control the high voltage source, 3 - the sync output from the measuring.

2. Functions of IMS

The basic functions of the design information-measuring systems is the provision of a process of testing medical devices and self-diagnosis function of the parameters of the high voltage source such as the voltage on high voltage plates of capacitor C3 and its capacity[9][10][11]. In operation, the high voltage capacitor can change its settings and deviate from the values of the normalized standard[12][13].

The control voltage is produced by connecting the microprocessor control system to the terminals of the capacitor[14][15]. The program converts the analog signal into the voltage value on the capacitor plates. Resistors

R1, R2 form a voltage divider 5000/5 Volts. The scheme of connection of capacitor for the microprocessor shown in figure 2.

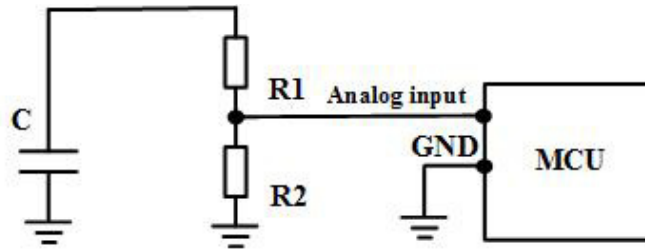


Fig. 2. The scheme of connection of the capacitor to the microprocessor
C - high voltage capacitor, R1, R2 – ladder, MCU – microprocessor.

A general algorithm for read voltage shown in the figure.3

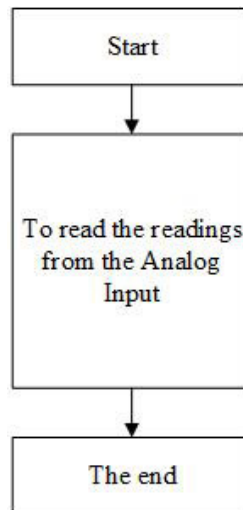


Fig.3. The general algorithm for read voltage.

The capacity control is performed by determining the time constant [16][17][18] of the capacitor charge, which is 63.2% of voltage a full charge, and is calculated by the formula (1)

$$\tau = R * C . \quad (1)$$

The scheme of connection of the capacitor to measure the capacitance shown in figure 4.

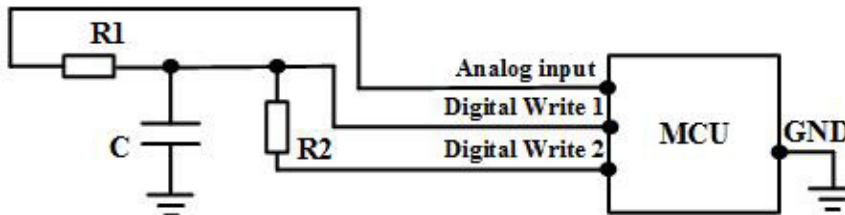


Fig. 4. The scheme of connection of the capacitor to measure the capacitance
 C - high voltage capacitor, R1- limiting resistor, R2 - resistor capacitor discharge, MCU – microprocessor.

A general algorithm for measuring the capacitance of the capacitor [19][20] shown in the figure.5

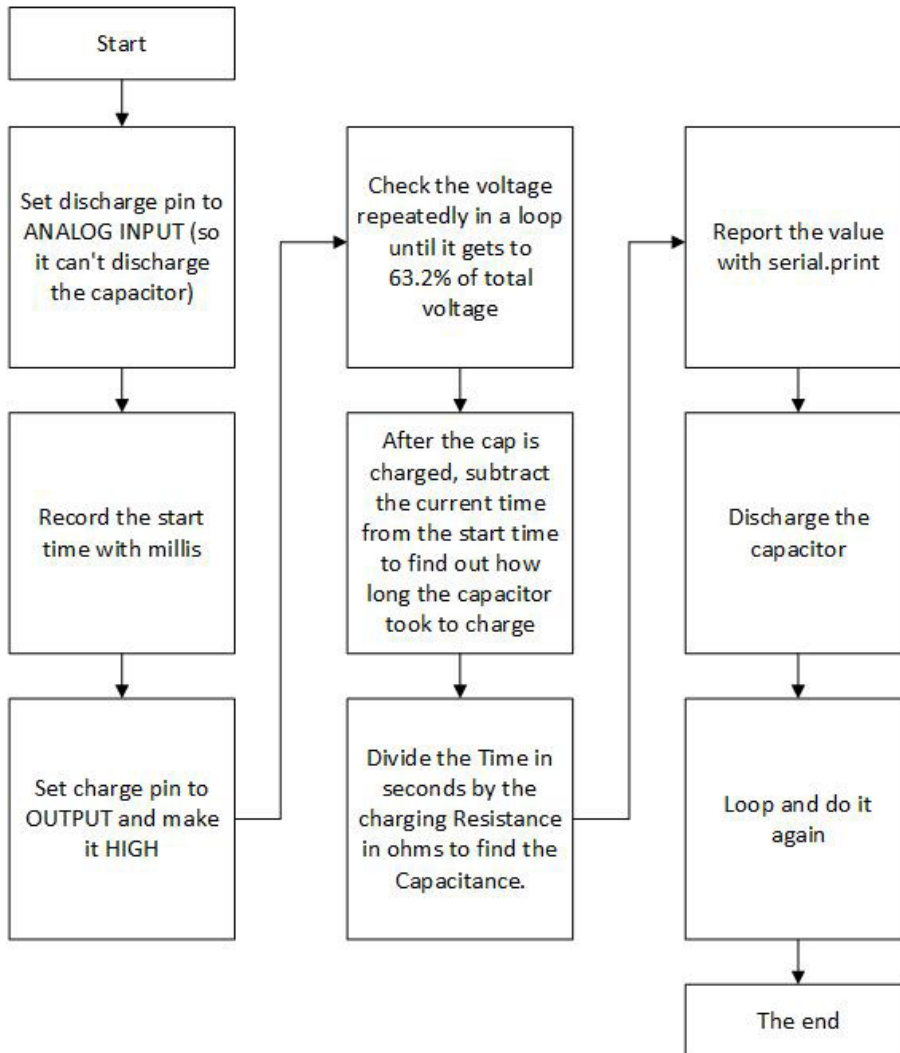


Fig.5. The algorithm for capacitance measurement.

3. Conclusion

Thus, the design of information-measuring system will ensure a process of testing medical equipment, but also possess the self-diagnosis function of the parameters of the high voltage source.

Acknowledgements

The project became the winner of the youth program Participant research scientific-innovation competition "P.R.S.I.C.". Project #4475GU1/214.

References

- [1] GOST R IEC 60601-1-2010 "Medical electrical equipment. Part 1: General requirements for safety on the major functional characteristics."
- [2] M.V. Lankin¹, N.I. Gorbatenko¹, I.A. Stetsenko¹, D.V. Shaikhutdinov¹, V.I. Dubrov¹, K.M. Shirokov, Automated test bench for security elements of medical equipment for resistance to defibrillator. SIBCON-2015, International Siberian Conference on Control and Communications, Omsk. (2015).
- [3] V.A. Vostrikov, B.B. Gorbunov, S.V. Selishchev, Construction of energy-optimal smooth monophasic defibrillation pulse waveforms using cardiomyocyte membrane model, *J Biomed Sci Eng.* 8(9) (2015) 625–631.
- [4] V.A. Vostrikov, B.B. Gorbunov, A.N. Gusev, I.V. Nesterenko, S.V. Selishchev, Determination of threshold energy level of monopolar defibrillation pulses using the Luo–Rudy cardiomyocyte model, *Biomedical Engineering.* (47)2 (2013) 61–64. DOI 10.1007/s10527-013-9335-8.
- [5] V.A. Vostrikov, B.B. Gorbunov, S.V. Selishchev, I.V. Venin Founder of biphasic waveform defibrillators, *J Biomed Sci Eng.* 8(5) (2015) 345–349.
- [6] V.A. Vostrikov, B.B. Gorbunov, I.V. Venin i ego vklad v razrabotku otechestvennykh defibrilljatorov, *Obshhaja reanimatologija.* 9(5) (2013) 68–73.
- [7] S. Zabodaev, I. Nesterenko, D. Telyshev, CPR artifact removal for providing continuous heart rate recovery procedure, *Proceedings of 1st Russian German Conference on Biomedical Engineering RGC, Germany.* (2013) 72.
- [8] V.A. Vostrikov, B.B. Gorbunov, A. Gusev, Comparison of the influence of the first phase of some biphasic defibrillation pulses on the cardiomyocyte model, *Proceedings of 1st Russian German Conference on Biomedical Engineering RGC 2013.* October, 23rd — 26th, 2013 Hannover, Germany. B. Cichkov, E. Fadeeva, L.A. Kahrs, T. Ortmaier, PZH Verlag, Germany. (2013) 14.
- [9] N.A. Bazaev, A.A. Danilov, A.Yu. Gerasimenko, B.B. Gorbunov, Yu.P. Masloboev, D.A. Potapov, D.V. Telyshev, S.A. Tereshchenko, S.V. Selishchev, Research and education complex for personnel training and basic and applied science research at the Biomedical Systems Department of the National Research University of Electronic Technology (MIET), *Biomedical Engineering.* (47)3 (2013) 111–115.
- [10] I.A. Stetsenko, Sh.V. Ahmedov, D.V. Shajhutdinov, R.I. Leuhin, Razrabotka algoritmov raboty stenda dlja ispytanij zashhitnykh jelementov medicinskoj apparatury na ustojchivost' k razrjadam defibriljatora, *Teorija, metody i sredstva izmerenij, kontrolja i diagnostiki : materialy 15-oj Mezhdunar. nauch.-prakt. konf. Juzh.-Ros. gos. politehn. un-t (NPI) im. M.I. Platova, Novochoerkassk : JuRGPU.* (2014) 45–48.
- [11] D.V. Shajhutdinov, V.I. Dubrov, I.A. Stetsenko, Stend dlja ispytanij zashhitnykh jelementov medicinskoj apparatury na ustojchivost' k razrjadam defibriljatora na baze tehnologij National instruments pech, *Nauka tret'ego tysjacheletija: sb. st. Mezhdunar. nauch.-prakt. konf., 5 sent, Ufa, Ajeterna.* (2014) 48–50.
- [12] I.A. Stetsenko, Stend dlja ispytanij zashhitnykh jelementov medicinskoj apparatury na ustojchivost' k razrjadam defibriljatora na baze tehnologij National instruments, *Nauchno-tehnicheskaja konferencija i vystavka innovacionnykh proektov, vypolnennykh vuzami i nauchnymi organizacijami JuFO v ramkah uchastija v realizacii federal'nykh celevykh programm i vneprogrammykh meroprijatij, zakazchikom kotorykh javljaetsja Minobrnauki Rossii: sb. materialov konf., Juzh.-Ros. gos. politehn. un-t im. M.I. Platova, Novochoerkassk: Lik.* (2014) 112–114.
- [13] I.A. Stetsenko, Postroenie i analiz perehodnykh processov avarijnogo rezhima izmeritel'noj chasti stenda dlja ispytanija zashhitnykh chastej medicinskoj apparatury na ustojchivost' k razrjadam defibriljatora v srede razrabotki NI MULTISIM, *Nauka: proshloe, nastojashhee, budushhee: sb. st. Mezhdunar. nauch.-prakt. konf., Nauch.-izdat. centr Ajeterna, Ufa.* 1 (2015) 65–68.
- [14] I.A. Stetsenko, Postroenie matematicheskoi modeli specializirovannogo istochnika pitaniya v sostave zarjada vysokovol'tnykh kondensatorov. *Sovremennij vzgljad na budushhee nauki: sb. st. Mezhdunar. nauch.-prakt. konf., Nauch.-izdat. centr "Ajeterna", Ufa.* 1 (2015) 44–49.
- [15] I.A. Stetsenko, Razrabotka specializirovannogo istochnika pitaniya i issledovanie ego raboty v sostave shemy zarjada vysokovol'tnykh kondensatorov, *Problemy i perspektivy tehniceskikh nauk: sb. st. Mezhdunar. nauch.-prakt. konf., NC Ajeterna, Ufa.* (2015) 39–43.
- [16] I.A. Stetsenko, Samodiagnostiruemyj istochnik pitaniya dlja stenda ispytanija medicinskoj apparatury, *Fundamental'nye problemy nauki: sb. st. Mezhdunar. nauch.-prakt. konf., Nauch.-izdat. centr "Ajeterna", Ufa.* 2 (2015) 57–58.
- [17] I.V. Venin, A.I. Red'ko, S.V. Serikov, V.Ja. Bersenev, Defibrilljatory: otechestvennaja istorija i priorityty, *Ekstrena medicina: vid nauki do praktiki.* 4(5) (2013) 125–131.
- [18] V.A. Vostrikov, B.B. Gorbunov, A.N. Gusev, S.V. Selishchev, Opredelenie porogovoj jenerгии monopoljarnykh defibrillirujushchih impul'sov s ispol'zovaniem modeli kardiomiocita Luo-Rudy, *Medicinskaja tehnika.* 2 (2013) 6–8.
- [19] S.S. Luksha, Portativnyj defibrilljator-monitor s funkciej kontrolja parametrov serdečno-sosudistoj sistemy, *Materialy XXIV Vserossijskoj nauchno-tehnicheskaja konferencija studentov, molodykh uchenykh i specialistov «BIOMEDSISTEMY – 2011».* (2012) 169–171

- [20] A.V. Il'ich, I.N. Bokarev, Resinhronizirujushhie ustrojstva s funkciej kardiostimuljatora /defibrilljatora, Klinicheskij opyt Dvadcatki. 4 (2012) 57–58.



International Conference on Industrial Engineering

Robotic Laser Inspection of Airplane Wings Using Quadrotor

Tatyana Kruglova^a, Daher Sayfeddine^a, Kovalenko Vitaliy^{a*}

^a *Platov South-Russian State Polytechnic University (NPI), 132, St. Prosvescheniya, Rostov region, Novocherkassk, 346428, Russian Federation*

Abstract

In course of the new development in construction materials, micro and nanoelectromechanical systems, a new sophisticated class of machinery are rising. This has created the need of diagnostic and inspection algorithm matching with the level of artificial intelligence implemented in the end product. In this paper, we present a case study, a simulation on inspecting airplane wings using unmanned quadrotor. The aim is to automate the inspection process, maximize the efficient allocation of resources and minimize possible risks caused by human errors. In order to achieve wing inspection, a laser setup is mounted on the quadrotor, which trajectory and flight stabilization is controlled by optimized fuzzy logic position controllers using particle swarm optimization.

© 2015 The Authors. Published by Elsevier Ltd. This is an open access article under the CC BY-NC-ND license (<http://creativecommons.org/licenses/by-nc-nd/4.0/>).

Peer-review under responsibility of the organizing committee of the International Conference on Industrial Engineering (ICIE-2015)

Keywords: robotic inspection, quadrotor, fuzzy logic, swarm optimization, aircraft diagnostic.

1. Introduction

Laser inspection has been used to identify cracks on a smooth surface. In particular, such technology is implemented in car assembly lines [1,2] and glass, metal and plastic manufacturing [3]. In parallel, inspection methods were developed based on machine vision algorithms or X-ray scanning [4,5]. The monitoring results are satisfactory. On the other hand, such solutions are immobile, need preparation and activation time and are dependent on site conditions. Per instance, setups used to scan granite-building facades cannot reach difficult corners, require additional manpower, smooth working ground and perfect climatic conditions. In Order to achieve the aim of automating any process, it is necessary to use resources efficiently. Here, multitasking is an essential pillar to consider. It allows reducing time consumption to achieve a project milestone and maximize the technical and financial earned value.

* Corresponding author. Tel.: +7(918)557-59-35

E-mail address: tatyana.kruglova.02@mail.ru, daher@live.ru, vitaliy_kovalenko_1994@mail.ru

Particularly speaking about aerospace industry, statistics shows that aircraft crashes are increasing. The reasons seem to be hidden. This number of accidents cannot be allowed in parallel with the advances in information technology, communication and artificial intelligence. Human errors and operating inappropriate interventions are being pinpointed to be the reason behind 17% of the accidents [6].

Underlining these facts and limitations, we suggest in this paper a solution based on miniature unmanned aerial vehicle (UAV). A quadrotor, basically a vertical take off and landing rotorcraft (VTOL), equipped with laser, can perform aircraft wing inspection for cracks. In order to achieve reliable results, sensors readings have to be recovered from noises caused by rotors' vibration and external disturbance. In addition, the quadrotor flight has to be stabilized. Optimized fuzzy logic controllers using particle swarm optimization achieve precise positioning of the UAV.

2. Related Works

With the new development in technology, robots became cheaper and they are implemented more frequently in civil field. Researchers launched a variety of special inspecting robots. Typically, these robots are inspired by the nature creatures and their type of movement: sliding, swinging, extending, flying and jumping. A new-sophisticated field has born: the Bionics. As end product, we got new generation robots. For instance, The StickyBot has a hierarchical adhesive structure to hold itself on any kind of surfaces [7], the climbing RiSE V3 robot is designed for high-speed climbing of a uniformly convex cylindrical structure, such as a telephone or electricity pole [8]. The efficiency of these robots was satisfactory but still their acquisition is not justifiable financially. The success achieved by using the UAV in military tasks has expedite the migration of such technology to the civil market. Nowadays, UAV is being used to perform several diagnostic tasks such as inspection of building facades [9], high-rise structure [10], municipality lights [11], bridges and performing indoor radiation safety tests [12]. Quadrotors are a good alternative for the climbing robots; they are cheaper and more service friendly. An autonomous quadrotor is not Wi-Fi dependent and can fly for longer range. Also, it can carry several sensors due to the new development in nanotechnology. Nowadays, quadrotors can be equipped with double or multiple high definition cameras, digital and auto calibrated, enough internal storage to capture long videos and necessary position sensors that assist in achieving better flight control.

Regarding the topic, X-ray setups and 3D laser immobile machines are used to scan airplane wings. Firstly, human-inspector carries out the diagnostic process, searches for viewable cracks. The second step consists of passing manually laser waves on the wing surface (fig.1). Readings on crack depth are acquired and filtered out according to safety norms and conditions. Hereafter, a decision is taken to send for maintenance team or to allow using. This process is made also for helicopter blades and others rotorcrafts. As it can be seen, the workflow requires high precision diagnostic, time and repeated steps. Automating the inspection process using quadrotor can be adequate solution. Moreover, quadrotors can scan multiple airplanes at the same time.



Fig. 1. Manual laser wing scanner.

3. Quadrotor Model

3.1. Quadrotor dynamics

As its name underlines, a quadrotor has four rotors working in two sets to achieve six degrees of freedom. The quadrotor changes its positioning by modifying the rotation speed of the rotors. This allows a change in positioning according to one of the following flight regimes: roll, pitch, yaw and hover. The first three regimes are rotational movements and correspond to variation in position along axis X, Y and Z respectively. A change in a value of one of the three angles causes horizontal linear movement of the quadrotor. The hovering is the fact of vertically standing over an assigned area. Hence the quadrotor dynamics can be described using the following equations:

$$\ddot{X} = (\sin\psi \sin\varphi + \cos\psi \sin\theta \cos\varphi) \frac{U_1}{m}; \quad (1)$$

$$\ddot{Y} = (-\cos\psi \sin\varphi + \sin\psi \sin\theta \cos\varphi) \frac{U_1}{m}; \quad (2)$$

$$\ddot{Z} = -g + (\cos\theta \cos\varphi) \frac{U_1}{m}; \quad (3)$$

$$\dot{p} = \frac{I_{YY} - I_{ZZ}}{I_{XX}} qr - \frac{J_{TP}}{I_{XX}} q\Omega + \frac{U_2}{I_{XX}}; \quad (4)$$

$$\dot{q} = \frac{I_{ZZ} - I_{XX}}{I_{YY}} pr - \frac{J_{TP}}{I_{XX}} p\Omega + \frac{U_3}{I_{YY}}; \quad (5)$$

$$\dot{r} = \frac{I_{XX} - I_{YY}}{I_{ZZ}} pq + \frac{U_4}{I_{ZZ}}; \quad (6)$$

where, \ddot{X}, \ddot{Y} and \ddot{Z} are the projection of the linear acceleration of the quadrotor in the Earth fixed axis, \dot{p}, \dot{q} and \dot{r} are projection rotational acceleration of the quadrotor in the body fixed axis, g is the gravitational acceleration, the torque generated from the rotors, m is the mass of the quadrotor, I_{XX}, I_{YY} and I_{ZZ} are the projection of the Inertia of the quadrotor, Ω is the rotational speed of the propellers, φ, θ and ψ are the roll, pitch and yaw angle consequently, U_1, U_2, U_3 and U_4 are the torques requirement for the hover, roll, pitch and yaw flight regimes respectively.

3.2. Observer

Observers are used to recover the vectors of the controlled object. In accordance with this paper, an adaptive observer shall identify sensors noise and regenerate recovered noise-free signals. To identify the observer, we will be using the system of equations (1-6) and reshape it into differential equation for each state. Hence system (7) can be written as follows:

$$\begin{bmatrix} \dot{v}_x \\ \dot{x} \\ \dot{v}_y \\ \dot{y} \\ \dot{v}_z \\ \dot{z} \\ \dot{\omega}_\phi \\ \dot{\phi} \\ \dot{\omega}_\theta \\ \dot{\theta} \\ \dot{\omega}_\psi \\ \dot{\psi} \end{bmatrix} = \begin{bmatrix} \frac{1}{m} C_t a U(1) \cdot \theta \\ v_x \\ -\frac{1}{m} C_t a U(1) \cdot \phi \\ v_y \\ -\frac{1}{m} C_t a U(1) \\ v_z \\ \frac{1}{I_{xx}} C_t l a U(3) \\ \omega_\phi \\ \frac{1}{I_{yy}} C_t l a U(4) \\ \omega_\theta \\ \frac{1}{I_{zz}} C_q a R U(2) + J_r \dot{U}(5) \\ \omega_\psi \end{bmatrix}, \quad (7)$$

where $C_t a$ is the thrust coefficient of the propeller, l – is the distance between the center of the quadrotor to each motor, C_q is the coefficient of the peripheral thrust, R – propeller radius, J_r – is the moment of inertia of the drive, \dot{v}_x, \dot{v}_y and \dot{v}_z are the projection of the linear velocity, $\dot{\omega}_\phi, \dot{\omega}_\theta$ and $\dot{\omega}_\psi$ are the projection of the rotational velocity.

The differential equation that describes the six states of degree of freedom of the quadrotor and their derivatives is illustrated in (8)

$$\dot{\hat{x}} = A\hat{x} + Bu + K(y - C\hat{x}) + K_{-1}J, \quad (8)$$

where x is the state vector, y – is the a scalar output signal, u – control vector, K – matrix size of $n \times 1$, K_{-1} matrix size of $(n \times n)$, J – matrix size of $(n \times 1)$.

The completion condition of coincidence between the observer equation and the quadrotor equation can be identified using the following equation

$$K_{-1}J \int_0^\infty (y - C\hat{x}) dt = w = const. \quad (9)$$

Thus the output of the integrator in equation (8) provides an estimate of the unknown external influence w . The simulation results illustrated in figure 5 show the effectiveness of the observer to recover the original signal from the applied noises.

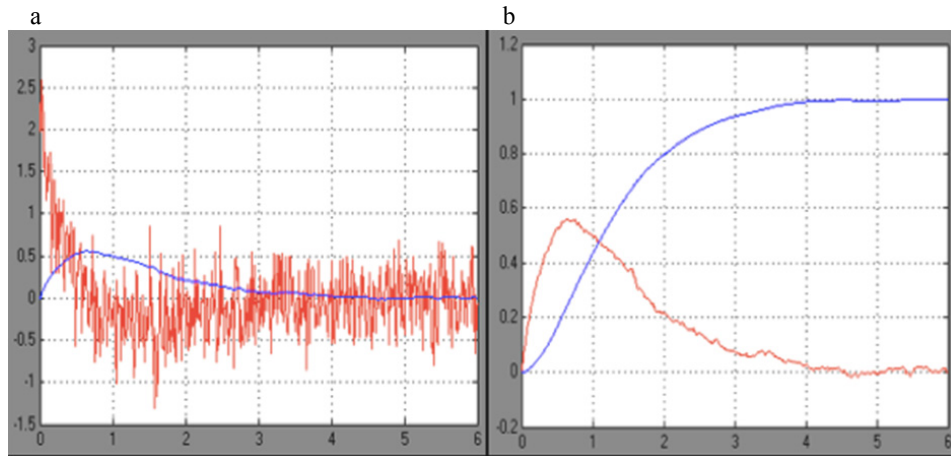


Fig. 2. Adaptation of the observer with reference to the applied external noises w

(a) The gyroscope signal to left (red curve), the integrated filtered signal to the right (red curve); (b) the roll angle (blue curve).

From fig.2, it can be clearly seen that the observer has successfully recover the sensor signals from the disturbance. It assures better stabilization of the roll angles as shown by the purple curve.

3.3. Optimized Fuzzy logic controllers

As it is important to know the value of the error, it is similarly critical to understand how it is changing over time. The error and its derivative in time are one of the possibilities to configure a Fuzzy logic controller. It is an artificial intelligence approach that computes mathematical operations based on degree of truth rather than the conventional True-False Boolean logic. The Fuzzy logic allows having more adaptable controller specially when dealing with nonlinearities (i.e. nonlinear aerodynamic model of the quadrotor as described in equations 1-6) and uncertainties (i.e. permanent changes in the flight circumstances, wind, temperature, obstacles positions etc.). Although in many cases, heuristic algorithms were ruled out, due to the time consumption, we saw a need to include this algorithm in our survey to cover most of the techniques used. We would like to clarify that the term heuristic is used to describe the estimation ability in artificial intelligence. Moreover, the linguistic power of the fuzzy logic may be extremely useful while navigating in totally unknown areas.

We assign the following labels for the numeric values: Negative big (NB) = -1, Negative Small (NS) = -0.5, Zero (Z)=0, Positive Small (PS)= 0.5 and Positive Big (PB) =1. As a result we obtain the linguistic rules listed in table (1). A linguistic rule defines the output of the fuzzy controller based on discrete logic (i.e. if $e(t) = \mathbf{NB}$ and $d(e(t)) = \mathbf{PB}$, then the output is \mathbf{Z}). The inputs of the fuzzy controller $de(t)$ and $e(t)$ are represented using triangular membership functions. The output of the fuzzy control is also 5 triangular membership functions.

The optimization method is a Runge -Kutta solver of differential equations. In particular, it uses six functions to estimate and calculate the fourth and fifth tolerance order. The difference between these solutions is taken as an error. This error estimate is very convenient to design adaptive algorithms, such as the use of fuzzy logic to control the process. The optimization algorithm works as follows: each particle in the swarm has a position. PSO determines the next best position the particle should migrate to, with reference to optimum criteria. The cycle continues until the particle reaches the most optimal position. Consequently, the system moves to the global best value updating the swarm positions to the target. Equation (10) describes mathematically used PSO model

$$V_{011}^{k+1} = wV_i^k + c_1(k+1)(pbest_i - S_i^k) + c_2(k+1)(gbest - S_i^k), \quad (10)$$

where, V_{011}^{k+1} is next value speed, w -weight function, V_i^k -current moving speed, c_1, c_2 are weights, $pbest_i$ is the personal best value for the particle, S_i^k is the current position of the i -th particle and $gbest$ is the global best position or the target. The optimization diagram is illustrated in figure 3.

Table 1. Fuzzy rules

<i>de</i>	NB	NS	Z	PS	PB
<i>e</i>					
NB	NB	NS	NB	NB	Z
NS	NS	NS	NS	Z	NS
Z	NB	NS	Z	PS	PB
PS	NS	Z	PS	PS	PS
PB	Z	PB	PB	PB	PB

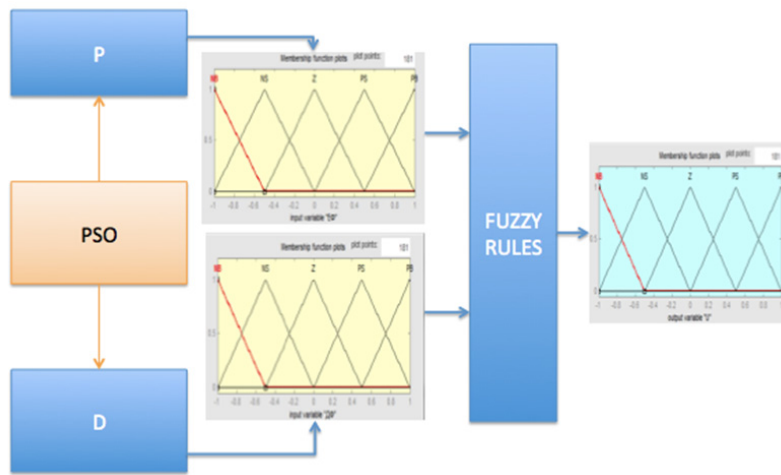


Fig. 3. Optimization of FLC using PSO.

The results of controlling the quadrotor using fuzzy logic regulators are shown in fig. 4.

The results shown in fig. 5 gives a fair idea about the reliability of the fuzzy controller. For instance, figure it illustrates the fact of stabilizing the linear movement of the quadrotor (described in equations 1-3, X (red curve), Y (blue curve), Z (green curve)) without overshooting. This allows the quadrotor to move along Earth-axis OXYZ smoothly. The other advantage of avoiding overshooting is contributing to better energy-efficient control systems (i.e. overshooting in altitude control means flying higher and consuming more power). Taking into consideration the nonlinearity of the aerodynamic model of the quadrotor, linear movement cannot be achieved unless stabilizing Euler angles (roll (red curve), pitch (blue curve) and yaw angles (green curve)). Control signals are generated in order to increase or decrease Euler angles (equation 4-6) with reference to linear position control task (equations 1-3).

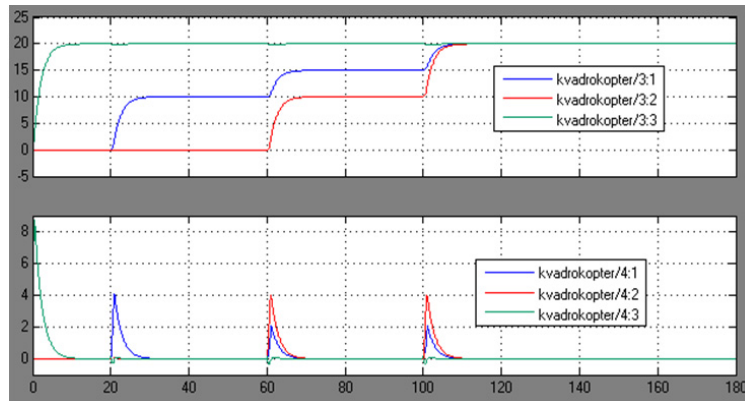


Fig. 4. Quadrotor position control with reference to waypoints.
Horizontal axis – time [s], vertical axis- position [m]

3.4. The Verdict

In this paper, a simulation of controlling quadrotor flight performing aircraft wing inspection is presented. The quadrotor dynamics were illustrated mathematically, based on which a control algorithm was suggested. The optimized fuzzy logic controllers using particle swarm method was implemented. The stability of the quadrotor was achieved based on the reliability of the control approach. In addition the observer has played an important role by filtering out the noises acquired from external disturbance and rotors vibration. The feedback signal from the gyroscope in particular was recovered, which reduced the overshooting in roll, pitch and yaw angles.

This paper contributes with the simulation results obtained to form a platform for further modeling and physical experience.

4. References

- [1] K. Johnston, Automotive applications of 3D laser scanning. Metron systems incorporated, 2002.
- [2] Moon Hong Baeng, Seung-Ho Baeg, Chanwoo Moon, Gu-Min Jeong, Hyun-SikAhn, Do-Hyun Kim, A New Robotic 3D Inspection System of Automotive Screw Hole, *International Journal of Control, Automation, and Systems*. 6(5) (2008) 740–745.
- [3] C. Teutsch, D. Berndt, J. Schnee, M. Hübner, N. Bachfischer, Optical Inspection of Laser Markings in the Production Process. *International Journal of Advanced Science and Technology*. 21 (2010) 31–40.
- [4] W. Wu, M. Wang, C. Liu, Automated inspection of printed circuit boards through machine vision, *Computers in Industry*. 28 (1996) 103–111.
- [5] H Golnabi, A. Asadpour, Design and application of industrial machine vision systems, *Robotics and Computer- Integrated Manufacturing*. 23 (2007) 630–637.
- [6] T. Tyler, International Air Transport Association. Annual report 2012. Statistical summary of commercial jets airplane accident. Worldwide operations 1959-2011.
- [7] K. Sangbae, M. Spenko, S. Trujillo, B. Heyneman, D. Santos, M.R. Cutkosky, Smooth Vertical Surface Climbing With Directional Adhesion, *Robotics, IEEE Transactions*. 24 (2008) 65–74.
- [8] G.C. Haynes, K. Alex, L. Goran, A. Jon, S. Aaron, A. R. Alfred, Rapid Pole Climbing with a Quadrupedal Robot, *IEEE International Conference on Robotics and Automation (ICRA)*. (2009) 2767–2772.
- [9] S. Emelianov, A. Bulgakow, D. Sayfeddine, Aerial laser inspection of buildings facades using quadrotor. *Proceedings of creative construction conference*. (2014) 24–30. ISBN 978-963-269-434-4.
- [10] A. Bulgakow, S. Emelianov, T. Bock, D. Sayfeddine, Control of hovering altitude of a quadrotor with shifted center of gravity for inspection of high-rise structures, *ISARC 2014 proceedings*. (2014) 762–768.
- [11] A. Bulgakow, T. Bock, D. Sayfeddine, Inspection of municipality lights on express ways using quad-rotor. *Construction technology and management CTM*. (2014) 53–62.
- [12] A. Bulgakow, D. Sayfeddine, Performing indoor radiation leakage test using quadrotor, *58th Ilmenau scientific colloquium*. (2014) 1–12.



International Conference on Industrial Engineering

Set-valued estimation of linear dynamical system state when disturbance is decomposed as a system of functions

Shiryaev V.I., Podivilova E.O.*

^a South Ural State University, 76, Lenin Avenue, Chelyabinsk, 454080, Russian Federation

Abstract

The article deals with set-valued estimation of dynamical system state when there is no statistical information about the initial state, disturbances and noises but the sets of their possible values are available. In some cases we can have additional information about disturbance dynamics that can improve the accuracy of the estimates. The article describes set-valued estimation algorithm when disturbance is decomposed as a system of functions with unknown coefficients. The comparison of estimates for the case when the kind of decomposition is known and the case when only a set of possible values is available is performed.

© 2015 The Authors. Published by Elsevier Ltd. This is an open access article under the CC BY-NC-ND license (<http://creativecommons.org/licenses/by-nc-nd/4.0/>).

Peer-review under responsibility of the organizing committee of the International Conference on Industrial Engineering (ICIE-2015)

Keywords: dynamical system; set-valued estimation; decomposition of disturbance as system of functions.

1. Introduction

The problem of dynamical system state estimation appears in different technical areas like aircraft control systems, tracking systems, target detection systems, automatic control systems for manufacturing processes and companies[3,13,15].

The processes in the control system are described with equations:

$$x_{k+1} = Ax_k + \Gamma w_k, \quad (1)$$

* Corresponding author. Tel.: +7-904-301-91-95; fax: +7-351-267-9848.
E-mail address: podivilovaeo@susu.ac.ru

$$y_{k+1} = Gx_{k+1} + Hv_{k+1}, \quad k = 0, 1, \dots, N, \quad (2)$$

where $x_k \in R^n$, w_k , $y_k \in R^m$, v_k are state, disturbance, measurement, noise vectors at a sample time k correspondingly; A , Γ , G , H are known matrices.

Different estimation algorithms can be applied depending on suggestions about the behavior of initial state, disturbances and noises. When disturbances, noises and initial state are assumed to be stochastic values with known distribution functions, Kalman filter has widespread application [3,4,15]. However in real applications there is usually no prior statistical information, for example, when only one realization of the process can be performed, but the sets of possible values of initial state, disturbances and noises are available. It involves set-valued estimation that is construction of feasible set at each sample time k that contains real state [5,6,9,10,12,14]. It is supposed that initial state x_0 , uncertain disturbances w_k and noises v_k at a sample time k are bounded with some convex polyhedras which are described with linear inequalities systems:

$$\begin{aligned} x_0 &\in X_0 : A_{x_0} x_0 \leq b_{x_0}, \\ w_k &\in W : A_w w_k \leq b_w, \\ v_k &\in V : A_v v_k \leq b_v. \end{aligned} \quad (3)$$

In this case set-valued estimation is performed. It consists of a construction of feasible sets \overline{X}_{k+1} , which are guaranteed to contain all state vectors at the sample time k [5]:

$$\begin{aligned} \overline{X}_{k+1} &= X_{k+1/k} \cap X[y_{k+1}], \quad k = 0, 1, \dots, N-1, \\ X_{k+1/k} &= A\overline{X}_k + \Gamma W, \quad X[y_{k+1}] = \{x \in R^n \mid Gx + v = y_{k+1}, v \in V\}. \end{aligned} \quad (4)$$

Feasible set construction (4) involves performing set operations like Minkowski sum, set intersection, linear transformation. But when the system state vector dimension increases troubles in performing set operations real-time occur. Then feasible set outer approximations with some canonical forms, like ellipsoids [2,7,16], parallelotopes [8], and zonotopes [1] can be applied. These methods rely on computing set-valued estimates through Minkowski sum and set intersection; but the results of these operations are upper approximated with the corresponding canonical form. This approach allows to reduce computational complexity but it can cause loss of accuracy, i.e., the approximating set can be much more larger than the real feasible set.

Additional information about uncertain system parameters can also be used to reduce computational complexity and to increase estimates accuracy [6,11]. For example, in some operating conditions disturbance w_k can be defined not only with some convex set W , but with some dynamical model. Let us suppose that there is some prior information about disturbances w_k , $k = 0, 1, \dots, N$ and it has decomposition as a system of functions $\varphi_{ik} \in R^m$:

$$w_k = \sum_{i=1}^m \alpha_i \varphi_{ik}, \quad k = 0, 1, \dots, N, \quad (5)$$

where α_i , $i = 1, 2, \dots, m$ are constant coefficients, which are computed real-time after getting measurement y_k , $k = 1, 2, \dots, N$. In matrix form the disturbance can be represented as

$$w_k = \Phi_k \alpha,$$

where $\Phi_k = [\varphi_{1k} \quad \varphi_{2k} \quad \dots \quad \varphi_{mk}]$, $\alpha = [\alpha_1 \quad \alpha_2 \quad \dots \quad \alpha_m]^T$. Then the dynamical system model can be represented as

$$x_{k+1} = Ax_k + \Gamma \Phi_k \alpha.$$

Consider next algorithm of set-valued estimation of dynamical system state and coefficients in disturbance decomposition. The paper describes feasible set polyhedral approximation that allows to construct set-valued estimate as a polyhedra of any shape. The algorithm consists of solving a row of linear programming problems and can be easily programmed.

2. Algorithm of set-valued estimation

Step 1. Set the iterations counter at $k = 0$.

Step 2. Let us present dynamical system state model using extended state vector

$$\begin{aligned} z_{k+1} &= \tilde{A}_k z_k, \\ y_{k+1} &= \tilde{G} z_{k+1} + H v_{k+1}, \end{aligned}$$

where $z_k = \begin{pmatrix} x_k \\ \alpha \end{pmatrix}$, $\tilde{A}_k = \begin{bmatrix} A & \Gamma \Phi_k \\ 0 & I \end{bmatrix}$, $\tilde{G} = [G \ 0]$.

Step 3. At a sample time k the system dynamics starting from initial state is described with the linear equations system:

$$\begin{aligned} z_1 &= \tilde{A}_1 z_0, & y_1 &= \tilde{G} z_1 + H v_1, \\ z_2 &= \tilde{A}_2 z_1, & y_2 &= \tilde{G} z_2 + H v_2, \\ \dots & & \dots & \\ z_k &= \tilde{A}_{k-1} z_{k-1}, & y_k &= \tilde{G} z_k + H v_k \end{aligned} \tag{6}$$

Step 4. At a sample time k the bounds for initial state, disturbances and noises are described with linear inequalities system:

$$\begin{aligned} A_{x_0} x_0 &\leq b_{x_0} \\ A_w \Phi_1 \alpha &\leq b_w, & A_v v_1 &\leq b_v, \\ A_w \Phi_2 \alpha &\leq b_w, & A_v v_2 &\leq b_v, \\ \dots & & \dots & \\ A_w \Phi_k \alpha &\leq b_w, & A_v v_k &\leq b_v. \end{aligned} \tag{7}$$

Step 5. The systems (6) and (7) implicitly describe the dynamical system state at a sample time k . It is necessary to solve these systems for variable z_k , i.e., we need to get approximating polyhedra $Z_k : A_z z_k \leq b_z$ such that $z_k \in Z_k$. Matrix A_z prescribes the shape of the required polyhedral and it is defined in advance. In a simple case when we need to determine the bounds of parameters the polyhedra is presented as parallelepiped $A_z = [I \ -I]^T$, where I is identity matrix of size $n \times n$. To compute the vector b_z for each direction a_i (i -th row of matrix A_z) the following linear programming problem is solved:

$$z_k^* = \arg \max_{z_k} \langle a_i, z_k \rangle \text{ subject to (6) and (7),} \tag{8}$$

where $\langle a_i, z_k \rangle$ is a scalar product of vectors a_i and z_k , then i -th coordinate of vector b_z is equal to $b_z(i) = \langle a_i, z_k^* \rangle$.

Step 6. If $k = N$, then the algorithm stops; otherwise set $k = k + 1$ and go to Step 2.

3. Numerical Example

Suppose matrices in the system (1), (2) equal:

$$A = \begin{bmatrix} 0.9976 & 0.0464 \\ -0.0928 & 0.8584 \end{bmatrix}, \Gamma = \begin{bmatrix} 0.1189 \\ 4.639 \end{bmatrix} \cdot 10^{-3}, G = I_{2 \times 2}, H = I_{2 \times 2}.$$

Set of possible values of initial state, disturbance and noise are:

$$X_0: \begin{pmatrix} 1 & 0 \\ 0 & 1 \\ -1 & 0 \\ 0 & -1 \end{pmatrix} x_0 \leq \begin{pmatrix} 0.00075 \\ 0.03 \\ 0.00075 \\ 0.03 \end{pmatrix}, \quad W: \begin{pmatrix} 1 \\ -1 \end{pmatrix} w_k \leq \begin{pmatrix} 1.5 \\ 1.5 \end{pmatrix}, \quad V: \begin{pmatrix} 1 & 0 \\ 0 & 1 \\ -1 & 0 \\ 0 & -1 \end{pmatrix} v_k \leq \begin{pmatrix} 0.000145 \\ 0.0228 \\ 0.000145 \\ 0.0228 \end{pmatrix}.$$

The disturbance is composed as system of functions (Fig.1):

$$w_k = \alpha_1 \sin\left(\frac{\pi k}{6}\right) + \alpha_2 \cos\left(\frac{\pi k}{6}\right), \quad (9)$$

where α_1, α_2 are unknown constant coefficients. When modelling the process the coefficients were equal to 1, measurement noises v_k were generated randomly within set V .

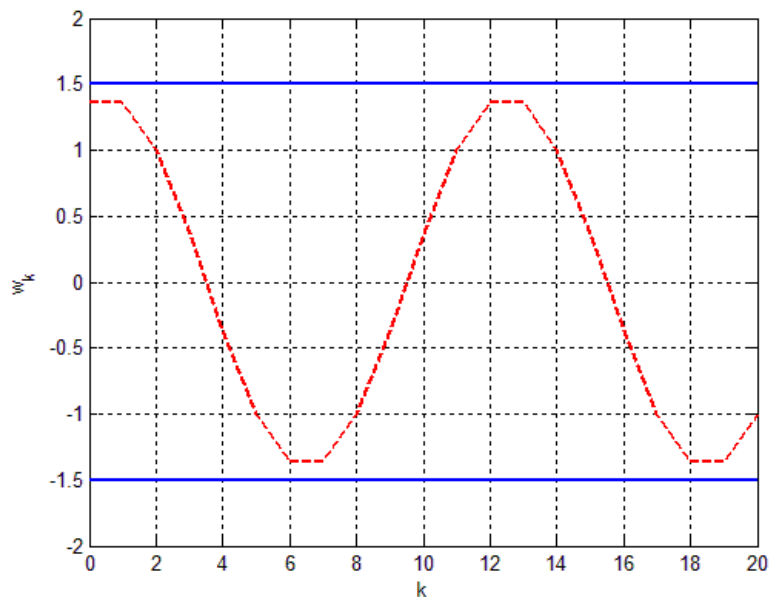


Fig. 1. Disturbance realization (dotted line shows the real value of disturbance, solid line shows the border of set of possible values of disturbance).

Set-valued estimates were constructed in two cases:

- when only the set of possible values of disturbance is available (Fig.2);

- when the kind of disturbance decomposition (9) is known (Fig.3).

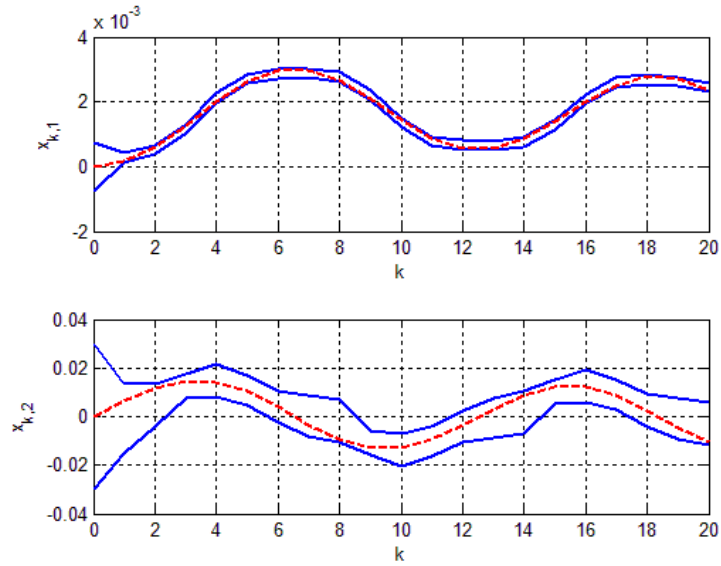


Fig. 2. Set-valued estimates in case when only the set of possible values of disturbance is available (dotted line shows the real system state, the solid line shows the border of set-valued estimates, $x_{k,1}$ and $x_{k,2}$ denote the first and the second coordinates of state vector x_k).

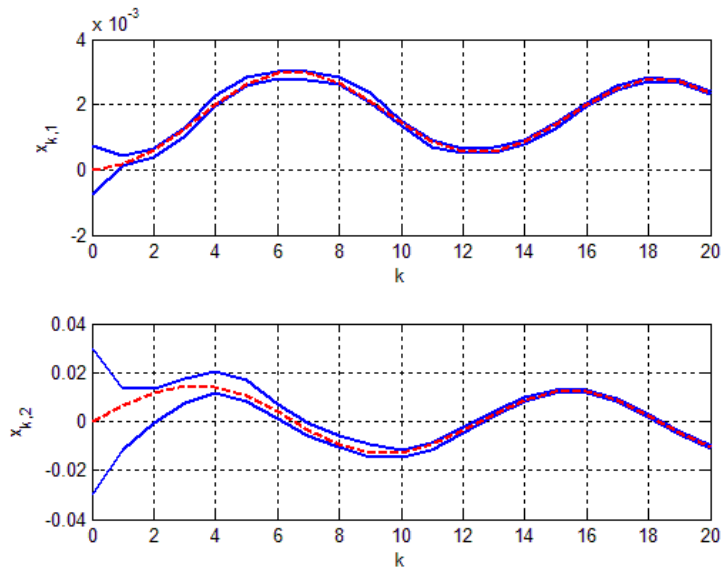


Fig. 3. Set-valued estimates in case when the kind of disturbance decomposition is known (dotted line shows the real system state, the solid line shows the border of set-valued estimates $x_{k,1}$ and $x_{k,2}$ denote the first and the second coordinates of state vector x_k).

In the second case, when the kind of disturbance decomposition (9) is known, the set-valued estimates are more accurate than in the first case. For example, when the kind of disturbance decomposition is known at a sample time

$k = 20$ the range of possible values of the first coordinate of the state vector x_k is 2.8 times tighter, and the range of possible values of the second coordinate is 15.8 times tighter than corresponding ranges in the case when only the set of possible values of disturbance is available.

The presented algorithm also allows compute set-valued estimates for decomposition coefficients. Longer we collect measurement data more accurate estimate of the coefficients we have (Fig.4). For the parameter α_1 after step $k = 14$ the bounds are $0.94 \leq \alpha_1 \leq 1.07$, for the parameter α_2 after step $k = 17$ the bounds are $0.95 \leq \alpha_2 \leq 1.07$, that is 11 times more accurate than the prior bounds of α_1 and α_2 .

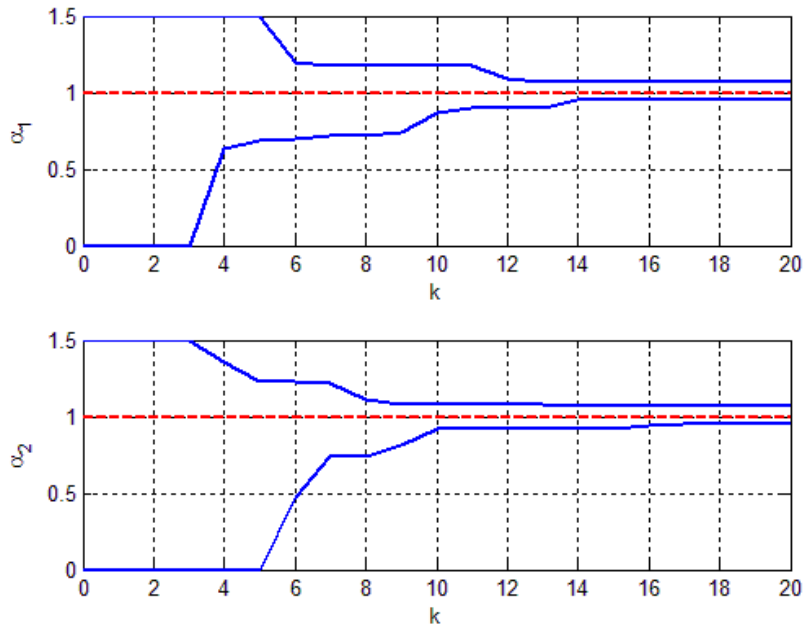


Fig. 4. Set-valued estimates of disturbance decomposition coefficients (dotted line shows the real value of system state vector, the solid line shows the border of set-valued estimates).

4. Conclusion

We have presented the algorithm for set-valued estimation of dynamical system state and coefficients in the decomposition of disturbance as the system of functions. The numerical example for set-valued estimation when the disturbance has harmonic decomposition was performed. The example showed that the information about the kind of decomposition allows to improve set-valued estimates of dynamical system state by several times in comparison with the case when only set of possible values of disturbance is available.

References

- [1] T.Alamo, J.M. Bravo, E.F. Camacho, Guaranteed state estimation by zonotopes, *Automatica*. 41 (2005) 1035–1043.
- [2] F.L. Chernousko, Minimax control for a class of linear systems subject to disturbances, *Journal of Optimization Theory and Applications*. 127(3) (2005) 535–548.
- [3] L.A. Fokin, V.I. Shiryayev, Preliminary Comparison of Kalman and Minimax Approaches to Error Estimation of Integrated Navigation System. *IEEE International Siberian Conference on Control and Communications (SIBCON-2013) Proceedings*. (2013) 212–214.
- [4] R.E. Kalman, A new approach to linear filtering and prediction problems, *Journal of Basic Engineering*. 82(1) (1960) 35–45.
- [5] I.Ya Kats, A.B. Kurzhaniski, On Some Observation and Control Problems for Uncertain Systems, *Automat. Telemekh.* 12 (1970) 15–25.
- [6] V.M. Kuntsevich, Set-Valued Estimation of State and Parameter Vectors within Adaptive Control Systems. *Bounding Approaches to System Identification*. (1996) 239–259.

- [7] A.B. Kurzhanski, P. Varaiya, On ellipsoidal techniques for reachability analysis, *Optimization Methods and Software*. 17 (2000) 177–237.
- [8] E.K. Kostousova, State estimation for dynamic systems via parallelotopes: optimization and parallel computations, *Optimization Methods & Software*. 9(4) (1998) 269–306.
- [9] A. I. Matasov, *Estimators for uncertain dynamic systems*, Kluwer Academic Publishers, Dordrecht, 1998.
- [10] E. O. Podivilova, V. I. Shiryayev, Comparison of Minimax Filter and Kalman Filter Estimations, *South Ural State University Bulletin, Series Mathematical Modelling, Programming & Computer Software*. 14 (2012) 182–186.
- [11] V.S. Pugachev, Estimation of variables and parameters in discrete time non-linear systems, *Automation and Remote Control*. 4 (1979) 39–50.
- [12] F.C. Schweppe, Recursive state estimation: Unknown but bounded errors and system inputs, *IEEE Transactions on Automatic Control*. 13(1) (1968) 22–28.
- [13] V. I. Shiryayev, Synthesis of control of linear systems in incomplete information, *Journal of Computer and Systems Sciences International*. 3 (1994) 229–237.
- [14] V. I. Shiryayev, E.O. Podivilova, Feasible Set Approximation in Dynamic System State Guaranteed Estimation Problem under Condition of Uncertainty. *Mechatronics, automation, control*. 7 (2014) 10–16.
- [15] B.L. Stevens, F.L. Lewis, *Aircraft Control and Simulation*, Wiley, New York, 1992.
- [16] Bo Zhou, Kun Qian, Xu-Dong Ma, Xian-Zhong Dai, New Nonlinear Set Membership Filter Based on Guaranteed Bounding Ellipsoid Algorithm, *Acta Automatica Sinica*. 39(2) (2013) 146–154.



International Conference on Industrial Engineering

Roller seismic impact oscillation neutralization system for high-rise buildings

Burtseva O.A.*, Tkachev A.N., Chipko S.A.

Platov South-Russian State Polytechnic University (NPI), 132, St. Prosvescheniya, Rostov region, Novocherkassk, 346428, Russian Federation

Abstract

The passive neutralization oscillations systems for high-rise construction are under consideration. Their advantages and disadvantages have been revealed. A roller oscillation neutralization system for high-rise constructions subject to seismic affecting is offered. The principle of its work is described and its advantages are estimated. A mathematical movement model for carrying and carried bodies is made. Low-frequency oscillation vibration protection systems under the influence of external harmonious impact are considered. Optimum adjustment parameters for a roller damper in the structure of the compensation system are defined.

© 2015 The Authors. Published by Elsevier Ltd. This is an open access article under the CC BY-NC-ND license (<http://creativecommons.org/licenses/by-nc-nd/4.0/>).

Peer-review under responsibility of the organizing committee of the International Conference on Industrial Engineering (ICIE-2015)

Keywords: high-rise building, damping oscillations, passive systems, neutralization roller system, vibration insulation.

1. Introduction

The urgency of seismic protection of buildings and constructions is explained by constant presence of seismic activity in various areas of the Earth. For only the last decade there have been registered more than 4 thousand acts of nature. The passive and active systems of oscillation damping are applied for solving vibration protection problem. They are classified by the activity principle as: damping, adaptive, inertial (with oscillations damper), constructions regulating rigidity, and isolating ones. The last three groups can be referred to as the most effective and less cost price. Systems of active vibration protection are aimed to suppression of residual undesirable

* Corresponding author. Tel.: +7-951-511-33-59;
E-mail address: kuzinaolga@yandex.ru

oscillations of a building after working off the passive system. Therefore to form an active compensation system is possible only after studying the efficiency of the passive one

This paper considers the isolating system of compensating oscillations of a high-rise building with kinematic relations. Similar systems have been offered by M. Viskordini and V.V.Nazin [1-4]. However application of systems with kinematic support is studied insufficiently, especially if the horizontal effect with prepotent phase is more than 1 s. In this case the building with kinematic support receives considerable displacement, at which there occurs a stability loss of the entire construction and its full collapse.

Some investigations of dynamic behaviour of mechanical systems constrained by kinematic relations, are presented in works [5-9].

2. Setting the problem

The dynamic behavior of a three-mass system of absolutely solid bodies is considered: bearing body in mass m_1 ; The spherical rotating joint with roller mass m_2 ; working body with mass m_3 under the influence of external kinematic excitation $F(t)$.

The carried body models a construction installed on column piles, each of which built in the form of a "glass". The bottom part of a pile is equipped by concave cycloidal concavities of radius r (see, fig. 1). Quantity of gettings is symmetrical by horizontal coordinates in order to save the pile's stability. The pile's weight and its loading is the mass of the carried body. The pile leans against spherical homogeneous hinges with the roller's mass m_2 and radius r .

As the pile glass is located in the soil layer so the stiffness and dissipative soil characteristics are presented in parametres $C_{x1}(C_{y1})$ and $k_{x1}(k_{y1})$ accordingly.

In addition impulse neutralizers with dissipation $k_{x3}(k_{y3})$ are installed between the pile and the glass. Any number of impulse neutralizers can be applied, but not less than two from each side of a pile.

The carried body movement represents the dynamics of the upper structure of a building which leans against the basement through the system of spherical balls. It models a construction or a building design oscillations of which we will be considered only according to the first form of the basic tone frequency.

It models a construction or a building design, oscillations which we will consider only under the first form with frequency of the basic tone. The movement of the bearing body reflects the dynamic behavior of the base.

The offered system of Oscillation Neutralization compensating oscillations realises the principle of seismoisolation of a building from the base, with its being able to return to a starting position after a seismopush under the influence of the building's body weight.

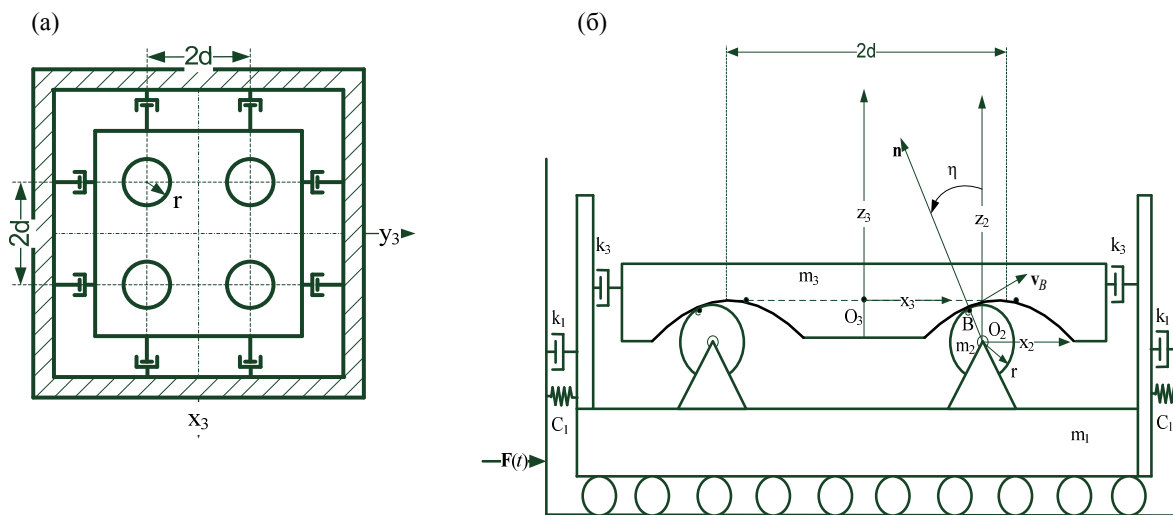


Fig. 1. The basic scheme of seismoprotective system: a) the top view; b) a side view.

Besides, the piles slippage concerning the base in two directions is provided. Restriction of relative displacement is carried out with the help of cycloidal concavities.

The given system is well entered in a design of the pile base, it does not demand additional space, it is noiseless. Moisture, ice, and dust are not accumulated in cycloidal dredgings due to their upwards convex construction

This factor is essential as the system is established in a hard-to-reach place of a construction.

The purpose of the present work is a construction of dynamic model of Neutralization system with roller dampers and definition of optimum tuning parameters.

3. Geometrical and kinematic relations

Let's consider the plane OXZ. On fig. 2 arch KBN - a cycloid representing a working curve roller damper. Points A and B are points of tangenting of a roller and working curve KBN.

Let's enter two generalised coordinates: x_1 is moving of the centre of the carried body mass; η is an angle of a deviation of a roller at changing the position of point B of the cotact of the roller and the bearing body getting.

Co-ordinates of a vector of a normal are equal in the contact point of surfaces:

$$\vec{n} = (\sin \eta; 0; \cos \eta).$$

The condition of a roller's movement on a working getting without slippage is the equality of linear speeds of the carried body surfaces and the roller in the contact point B:

$$\vec{v}_B = \dot{x}_1 \vec{i} + \dot{\eta} \vec{j} \times r \vec{n},$$

where $\dot{\eta}$ - angular speed of a roller concerning the centre of its weight C_2 ; \dot{x}_1 - the speed of a bearing body gained owing to a seismopush; r - roller radius; \vec{i}, \vec{j} - unit vectors of co-ordinate axes.

Projections of speed of a point B on the axis of coordinates at bearing weight movement to the right the following (fig. 2)

$$v_{Bx} = \dot{x}_1 - \dot{\eta} r \cos \eta, \quad v_{Bz} = \dot{\eta} \sin \eta;$$

or at movement of the bearing weight to the left (fig. 3)

$$v_{Bx} = -\dot{x}_1 + \dot{\eta} r \cos \eta, \quad v_{Bz} = \dot{\eta} \sin \eta.$$

As working body makes a translational motion, that a square of a point B speed, consequently and the centre of weights C_3 , is equal

$$v_B^2 = v_{C_3}^2 = v_{Bx}^2 + v_{Bz}^2 = \dot{x}_1^2 + \dot{\eta}^2 r^2 - 2\dot{x}_1 \dot{\eta} r \cos \eta.$$

General form of Lagrang's equation is the following:

$$\frac{d}{dt} \left(\frac{\partial T}{\partial \dot{x}_1} \right) - \frac{\partial T}{\partial x_1} = Q_{x_1}; \quad \frac{d}{dt} \left(\frac{\partial T}{\partial \dot{\eta}} \right) - \frac{\partial T}{\partial \eta} = Q_{\eta},$$

where Q_{x_1}, Q_{η} - the generalised forces corresponding to generalised coordinates x_1, η . They include external influence, potential and dissipative components.

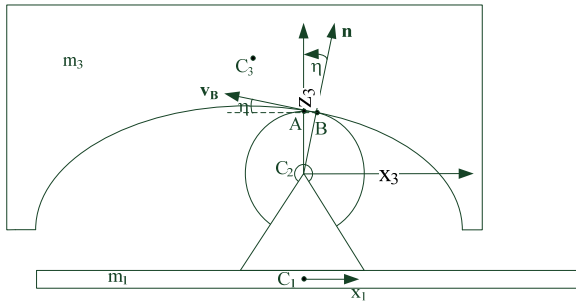


Fig.2.

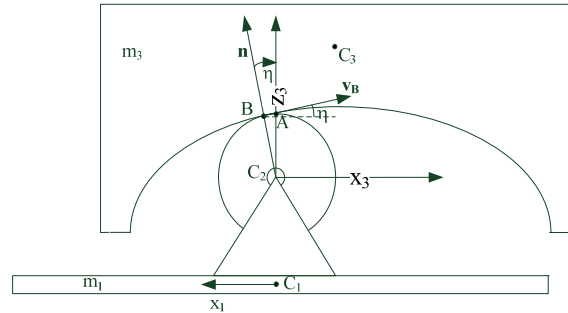


Fig.3.

As for a carried body the work is performed by: a gravity $P_3 = m_3g$; force of viscous resistance in the in a damper $k_3(\dot{x}_3 - \dot{x}_1)$; for the spherical hinge - work of a frictional force in a roller $(m_2 + m_3)g\mu \text{sign}\dot{\eta}$, where μ - coefficient of friction; in a bearing body - elastic work C_1x_1 ; forces of viscous resistance in the a damper $k_1\dot{x}_1$ and force of external harmonious excitation $F(t)$.

Entering designations $\rho = \frac{m_3}{m_1}$, $2n_x = \frac{k_1}{m_1}$, $2n_\eta = \frac{k_3}{m_3}$, $\omega_k^2 = \frac{C_1}{m_1}$ and expecting $\frac{m_2}{m_3} \rightarrow 0$, we will transform the received equations to a form

$$(1 + \rho)\ddot{x}_1 + 2n_x\dot{x}_1 + \omega_k^2x_1 - \rho r(\ddot{\eta} \cos \eta - \dot{\eta}^2 \sin \eta) = \frac{F(t)}{m_1};$$

$$r\ddot{\eta} - \ddot{x}_1 \cos \eta + 2n_\eta r\dot{\eta} \cos \eta \sin \eta = -\left(g \cos \eta + \frac{g\mu}{r} \text{sign}\dot{\eta}\right). \tag{1}$$

Let's establish frequency ω_r and period T_r of own fluctuations a roller damper. For this purpose we will fix the bearing body ($x_1 = 0$) and, having put $n_\eta = 0$, $\mu = 0$, from the second equation (1) it is received

$$\ddot{\eta} + \omega_r^2 \cos \eta = 0, \quad \omega_r^2 = \frac{g}{r}, \quad \omega_r = 2\pi\sqrt{\frac{r}{g}}. \tag{2}$$

Thus, frequency of fluctuations damper inversely is proportional to roller radius.

4. Linearized model of object with roller system of the seismoisolation

The equations (1) represent the system of nonlinear differential equations the study of which is inconvenient. Research of dynamic behavior of compensating system will be carried out with the help of linearized mathematical model.

Let's consider plane OXZ . On fig. 4 arch KBN - a cycloid representing a working curve of the roller's damper. Arch of cycloid AB is divided into rectilinear sites with angle of inclination α . Then the angle turn of a roller η is equal to the relation of arch AB to roller radius r . We consider, that the angle α is constant on a corresponding site of a cycloid. Vector S approximately equal to cycloid arch AB on the module defines the change of weights center position of a working body.

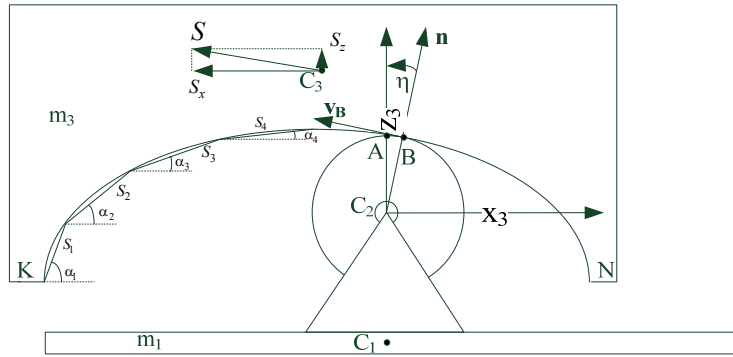


Fig. 4. Kinematics of the compensating system.

Let's enter two generalized coordinates: \$x_1\$ - moving of the weights center of a bearing body; \$S\$- moving of the weights center of a working body, and its projections on axis of coordinates and speeds are equal:

$$S_x = x_1 - S \cos \alpha, \quad S_z = S \sin \alpha, \quad \dot{S}_x = \dot{x}_1 - \dot{S} \cos \alpha, \quad \dot{S}_z = \dot{S} \sin \alpha.$$

Kinetic energy of three-mass system:

$$2T = 2(T_1 + T_2 + T_3) = m_1 \dot{x}_1^2 + 2J_y \frac{\dot{S}^2}{r^2} + m_3 v_B^2 = m_1 \dot{x}_1^2 + m_2 r^2 \frac{\dot{S}^2}{r^2} + m_3 (\dot{S}_x^2 + \dot{S}_z^2),$$

where \$T_1\$ and \$T_3\$ - kinetic energy of translational movement of a bearing and working bodies; \$T_2\$ - kinetic energy of rotary movement of a roller; \$J_y\$ - the moment of roller inertia accepted in the form of a homogeneous body of radius \$r\$. As \$m_2 \ll m_1\$ and \$m_3\$ by kinetic energy of a roller it is neglected \$r\$.

Expression for the generalized work looks like:

$$\begin{aligned} \delta A &= (F(t) - C_1 x_1 - k_1 \dot{x}_1) \delta x_1 - P_3 \delta S \sin \alpha - k_3 (\dot{S}_x - \dot{x}_1) (\delta S_x - \delta x_1) - m_3 g \mu \operatorname{sign} \frac{\dot{S}}{r} \delta S = \\ &= (F(t) - C_1 x_1 - k_1 \dot{x}_1) \delta x_1 + \left(-P_3 \sin \alpha - k_3 \dot{S} \cos^2 \alpha - m_3 g \mu \operatorname{sign} \frac{\dot{S}}{r} \right) \delta S. \end{aligned}$$

By Lagrange's equating of the movement we obtain:

$$\begin{aligned} \ddot{x}_1 + 2n_x \dot{x}_1 + \omega_k^2 x_1 &= \frac{F(t)}{m_1} + \frac{k_3}{m_1} \dot{x}_3; \\ \ddot{x}_3 + 2n_{x3} \dot{x}_3 &= 2n_{x1} \dot{x}_1, \end{aligned} \tag{3}$$

where mark out: \$2n_{x1} = \frac{k_1}{m_1}\$; \$2n_{x3} = \frac{k_3}{m_3}\$; \$\omega_k^2 = \frac{C_1}{m_1}\$.

System (3) will be subjected to Laplas's transformation and transfer functions will be fulfilled:

- without compensating \$W(p) = \frac{1}{m_1(p^2 + 2n_x p + \omega_k^2)}\$;

- with oscillations damper the roller's $WG(p) = \frac{1}{m_1(p^2 + 2n_x p + \omega_k^2)(p + 2n_{x3}) - 2n_{x3}k_3 p}$.

The varied damper parametre is the damping factor n_{x3} . For the numerical analysis we use parameters vibroprotection systems: frequency of the basic tone of oscillation of the working body $\omega_k = 1$ Hz, frequency of seismoexcitation is close to frequency of the basic tone $\omega_v = 0.9$ Hz, $n_{x1} = 0.1 \div 0.3$ (for a flexible construction and a construction raised in the sliding casing); $F_0 = 0.3 \div 0.5$ g (seismic impact by intensity 7÷9 balls). Maximum AFC (Amplitude-Frequency the Characteristic) constructions without damper $A(\omega) = 5.025$.

The technique of defining parameters of damper adjustment is based on the fact that AFC vibroprotection system with optimum adjusted parameters looks symmetric to frequency $\varpi = (\omega_1 + \omega_2)/2$ [10].

We find the fixed frequencies ω_1 and ω_2 , at which the maximum AFC with damper is to obtain. From fig. 5 we define $\omega_1 = 0.5$ Hz and $\omega_2 = 1.2$ Hz.

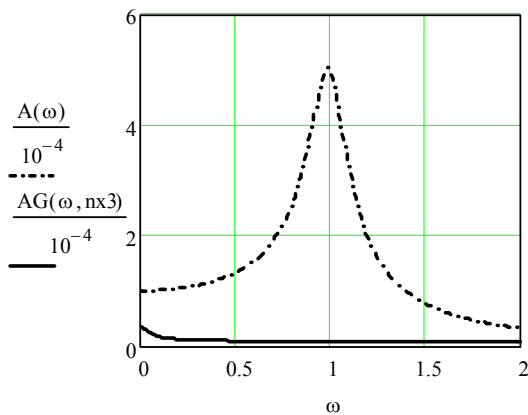


Fig. 5. AFC of construction without damper $A(\omega)$ and with optimum parameters of roller's damper $AG(\omega, n_{x3})$.

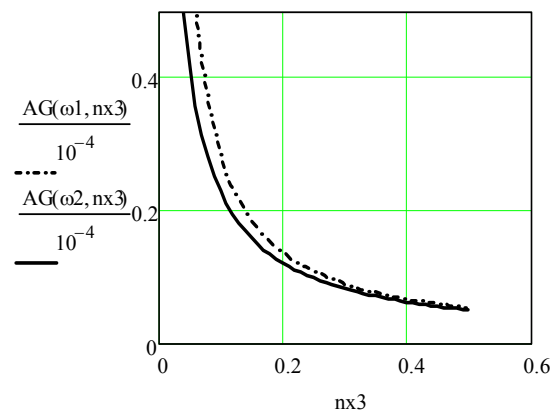


Fig. 6. Definition of factor damping optimum.

Further we define graphically a point of crossing of two graphs $AG(\omega_1, n_{x3})$ and $AG(\omega_2, n_{x3})$, constructed at change n_{x3} . Value n_{x3} , at which this crossing takes place and defines optimum value of damping factor $n_{x3} = 0.2$, see. fig. 6.

The amplitude-frequency characteristic of a construction without damper $A(\omega)$ and with optimum adjusted damper is showed on fig. 5.

Amplitude-Frequency the Characteristic of construction without damper $A(\omega)$ and with optimum parameters damper is resulted on fig. 5. The maximum amplitude of construction oscillations with roller damper $AG(\omega, n_{x3}) = 0.35$, that testifies the high effectiveness of compensation system.

5. Conclusions

The dynamic model of a roller compensation system develops a new method of vibroprotection of flexible constructions operating on basic oscillation frequency in the low-frequency range.

The offered system is compact and effectively reduces the level of the maximum amplitudes of high-rise constructions compelled fluctuations in the specified frequency range.

The received equations of compensation system movement have allowed to define equations AFC. On their basis the graphic method of roller vibrodamper optimum parameters definition is offered, which allows to adjust it on frequency and amplitude.

The results of research obtained in this paper represent scientific and practical interest for experts in the field of fluctuations theory. They also can be used by developers of roller vibrodamper for decreasing compelled fluctuation level of various objects in a low-frequency range.

References

- [1] Seismoisolation and adaptive systems of seismoprotection, Science, Moscow, 1983.
- [2] S.V. Polyakova, Seystoystoykie zdaniya i razvitiye teorii seystoystoykosti, On materials 6 International conferences on aseismic building, Stroyizdat, Moscow, 1984.
- [3] R.G. White, Vibration control, Noise and Vibr., Chester etc. (1989) 685–712.
- [4] YU.D. Cherepinskiy, K seystoystoykosti zdaniy na kinematicheskikh oporakh, Osnovaniya, fundamenti i mekhanika gruntov. 3 (1972) 13–15.
- [5] YU.I. Neymark, N.A. Fufaev, Dinamika negolonomnykh system, Science, Moscow, 1967.
- [6] L.G. Lobas, On rolling system, Int. Appl. Mech. 36(5) (2000) 691–696.
- [7] V.P. Legeza, Dynamics of vibroprotection systems with the damper's roller of the low-frequency fluctuations, Fastnessproblems. 2 (2004) 106–118.
- [8] V.P. Legeza, YU.G. Akhmetov, Efficiency of vibroprotection systems with cycloidal, roller seismodamper, News of the Russian Academy of Sciences. Mechanics of a rigid body. 4 (2006) 56–68.
- [9] V.P. Legeza, Effektivnost vibrozashchitnoy systemy s izokhronym rolikovym gasitelem, Izvestiya RAN. Mekhanika tverdogo tela. 2 (2013) 65–76.
- [10] B.G. Korenev, L.M. Reznikov, Dymamicheskie gasiteli kolebaniy: teoriy i tekhnicheskie prilozheniya, Science, Moscow, 1988.



International Conference on Industrial Engineering

The design of safety control systems for unattended points of technological communication on oil and gas pipelines

Minatsevich S.P., Sharonov A.A.* , Borisov S.S.

Perm National Research Polytechnic University, Komsomolskiy prospect, 29, Perm City 614000, Russia

Abstract

The article covers the methodology used to design safety control systems for unattended points of technological communication on oil and gas pipelines; it gives the review of safety control system design, the relevance of the researched area and research methods; it describes the structure of an unattended point of technological communication, specific hazardous factors, affecting factors; the article focuses on the possible safety system structures, suggests the ways to select the necessary safety system structure, the design of its central block and qualitative content of information sources on hazardous factors; it describes the mathematical model for quantitative safety assessment, and shows the results of the research outcome implementation in the safety systems in operation.

© 2015 The Authors. Published by Elsevier Ltd. This is an open access article under the CC BY-NC-ND license (<http://creativecommons.org/licenses/by-nc-nd/4.0/>).

Peer-review under responsibility of the organizing committee of the International Conference on Industrial Engineering (ICIE-2015)

Keywords: methodology, design, safety, safety system, technological communication, unattended communication point, pipeline

1. Introduction

Currently oil and gas branches are deemed as significant industry areas for Russia. One of the crucial factors in these branches is the most effective and safe transportation of oil and gas from the fields up to the consumer. This activity is generally performed via oil and gas pipelines. The control of pipeline conditions requires diverse systems of Telemechanics; the connection with these systems is provided by the lines of specialized technological communication set along the pipeline. Technological communication efficiency directly affects the efficiency of

* Corresponding author. Tel.: +7-964-194-6734; fax: +7-342-219-8173.

E-mail address: stepper88@inbox.ru

transportation – communication break, and namely the lack of data about real-time pipeline condition, is taken as a kick and has to be removed immediately.

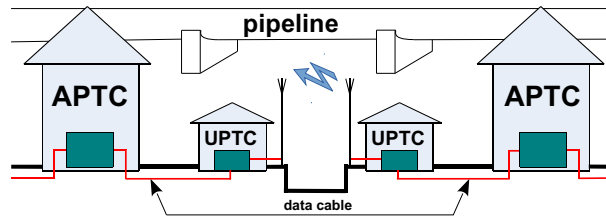


Fig. 1. Simplified scheme of a standard technological communication point.

Simplified scheme of a standard technological communication unit is given in Figure 1.

APTC (attended point of technological communication) is defined as communication construction where data transmission system equipment is installed. The operation personnel are working 24 hours.

UPTC (unattended point of technological communication) is defined as communication construction where data transmission system equipment is installed. In this case no personnel is required; the point either operates automatically (not typical on oil and gas pipelines) or is fully distantly operated (also in most cases not typical on oil and gas pipelines), or operates in an automated mode, when the operator is required only in specific non-nominal cases.

Data transmission channel is a physical environment where data transmission is performed (copper cable, optical cable, radio channel).

If we consider the technological communication as a consecutive system when the break of any component leads to the breakdown of the whole system in general, we can say that the efficiency of technological communication is determined by the efficiency of the weakest element.

The weakest point of technological communication is unattended communication points as there are no personnel at these points who can react in non-nominal situations.

Hence we face the problem of controlling the efficiency and safety of the operation of unattended technological communication points. Safety control systems are to be applied in order to tackle this issue; these systems should be specially designed for the technological communication of oil and gas pipelines.

2. Survey

The issue of the methodology of safety systems' design is generally covered in a big number of scientific and practice oriented works.

Tikhonova V.A. and Vorona V.A. thoroughly focus in their papers on the methodology of design and different elements of safety control systems [1, 2, 3, 4, 5, 6, 7].

Ryzhova V.A. develops certain methodology aspects [8].

Petrov S.V. [9] gives in his paper the set of recommendations how to provide the safety of production units.

The issues of efficiency assessment are covered in the works of Ryabinin I.A. [10].

You can read more about the elements of alarm system in the works of Vinogradov Yu.A. [11] and Magaenov R.G. [12, 13].

One of the most significant components of almost any safety control system and namely video surveillance is taken up in the works of Gedsberg Yu.M., [14], Peskin A.E. [15] and Gvozdeka M. [16].

Fire protection tools are considered in the paper of Lepeshkin O.M., Kopytov V.V. and Zhuk A.P. [17].

Certain methodology elements are given in the government regulations [18, 19].

3. Research relevance

Despite the considerable research of the issue that has been done in the general context, the issue of the methodology of safety control systems applied to the unattended points of technical communication hasn't been taken up in any of the works given above as unattended points of technological communication on oil and gas

pipelines started to be massively used quite recently.

It should also be stressed out that currently there is a steady trend towards the growth of the amount of unattended points of technological communication on oil and gas pipelines. This growth is explained by the construction of new communication lines, initially designed as automated lines; the re-equipment of existing technological communication lines also contributes to this growth. Automation is triggered by the steady current trend of minimizing the impact of a human factor on communication efficiency; it can also be explained by economic reasons, and namely the decrease of overhead expenses and the increase of profitability.

Hence it can be concluded that the development of the methodology for the design of safety control systems and the efficiency of unattended points of technological communication on oil and gas pipelines is a crucial and relevant task nowadays; currently this issue hasn't been fully solved yet.

4. Research methods

Based on the experience of theoretical and practical activities in the sphere of providing and assessing the safety the authors suggest the following research program:

- Define object structure (“What are we protecting?”);
- Determine typical hazardous factors and their affecting factors (“What are we protecting from?”);
- Determine the structure of the safety system (“How do we protect?”);
- Determine safety methods (“What do we use for protection?”);
- Define quantitative safety parameter (“How to assess the protection?”).

5. UPTC structure

Refer to the works of the following authors [20] to study this issue in the context of the facilities set on the point. The structure is given in the Figure 2.

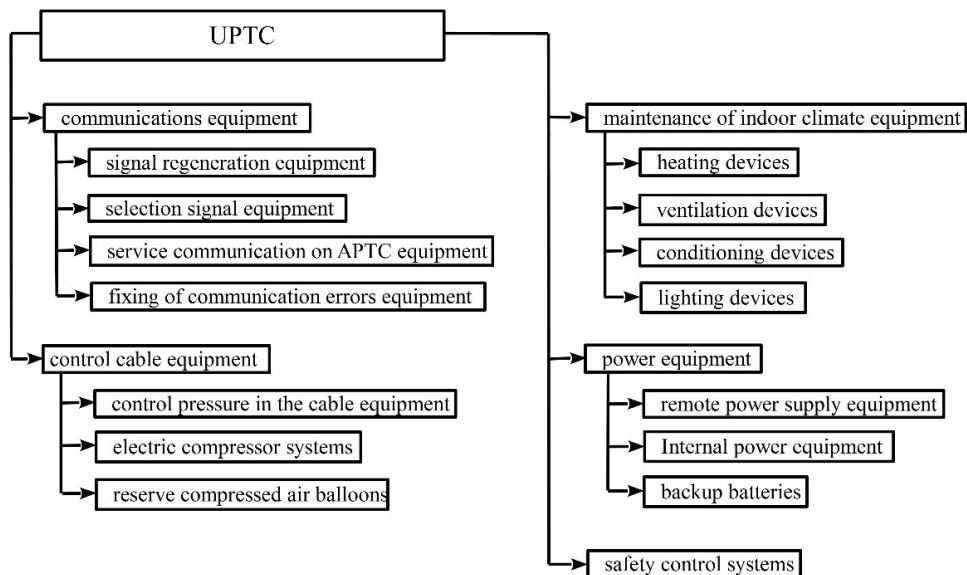


Fig. 2. UPTC Structure in the context of the facilities set on the point.

6. Typical danger for UPTC and their affecting factors

That issue was studied in the works of the following authors [20].

The typical UPTC hazardous factors are as follows:

- The factors of a natural character: icing of premises, high humidity in premises, flooding of premises;
- Technogene factors: fire in the premises, compressed air cylinder explosion, significant decrease of communication quality, power supply interruption;
- Social factors: vagrancy, thefts.

Find below the list of affecting factors that are to be controlled by UPTC safety system (set by decreasing the priority):

- Communication quality;
- Electric current;
- Electric voltage;
- Air temperature;
- Air moisture;
- Unauthorized access;
- Pressure in compressed air cylinders.

7. The structure of safety control system

Generalized structure of safety control system is given in the Figure 3.

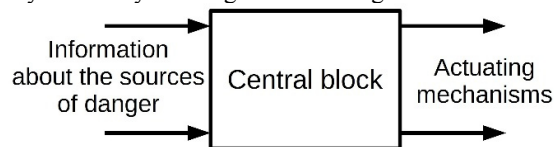


Fig. 3. Generalized structure of safety control system.

UPTC safety control system necessarily should connect with the remote operator in order to run manual monitoring of unit safety and take solutions in complicated non-nominal cases.

As already mentioned in the papers [21], there are different kinds (concepts) of the structure (architecture) of safety control systems described below.

7.1. Module architecture concept

Module architecture concept is shown on Figure 4.

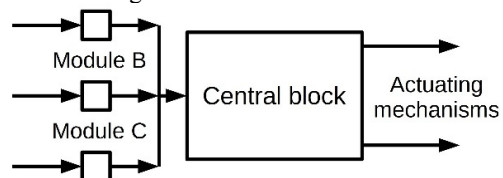


Fig. 4. Module architecture.

The central block that is responsible for taking safety control solutions includes the minimum number of functions, but can connect with a big number of additional divergent modules. This approach makes system architecture more complicated via additional communications and reduces the efficiency via a big number of connections; at the same time the space of system application significantly increases and labor input is decreasing.

7.2. Monolithic architecture structure

Monolithic architecture structure is shown on Figure 5.

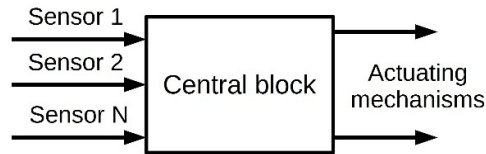


Fig. 5. Monolithic architecture.

The central block includes all the functions and gives no possibility to extend them. Such approach simplifies system architecture and increases the efficiency, but in this case application space is constricting and labor input expenses are elevating.

7.3. Mixed architecture concept

Mixed architecture concept is shown on Figure 6.

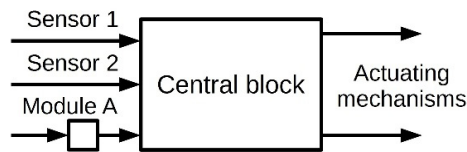


Fig. 6. Mixed architecture.

The central block contains a number of functions set as main functions; all minor functions are connected via extension modules. By such approach there is a combination of flexible application, slight increase of system complexity and labor input as well as slight reduction of efficiency.

We suggest taking mixed architecture concept for UPTC safety control system; the validation of this idea is given below:

- The place of system application is determined, which means that the factor of wide application is not relevant; hence module architecture is irrelevant either;
- Despite the fact that all main affecting factors are defined some typical UPTC hazardous factors might occur which means that the possibility should be considered to expand the system; hence monolithic architecture is irrelevant.

Therefore UPTC safety control system should contain in the central block sensors' supports to control all the typical affecting danger factors (described above) and have interface to connect extension modules.

8. The control of hazardous factors

The control of hazardous factors is performed with help of the information that comes from the tool that measures hazardous factors into the central block (Figure 3).

According to the paragraph "Typical UPTC dangers and their affecting factors" UPTC safety control systems require the following tools:

- Temperature sensor;
- Smoke sensor;
- Air moisture sensor;
- Sensor of water in the premises;
- Measuring indicator of current value in the network;

- Measuring indicator of voltage value in the network;
- Measuring indicator of communication quality;
- Video cameras.

We cannot generally define specific characteristics and measurement permission of each sensor or indicator that measures an affecting factor, as by different UPTC we can deal with different conditions, therefore we need a wide range of sensors or differently configured sensors.

It should be noted that if possible hazardous factor measurement tools should have a unified interface to connect with the central block in order to reduce the number of mechanical connectors and consequently increase general system efficiency.

9. Protection methods

The follow protection methods are offered:

- From natural character’s danger factors: frosting of the room – setup of heater, high humidity of air into the room – setup of air driers or automatic ventilation systems, flooding of the room – setup of exhaust pumps;
- From industrial character’s danger factors: fire in the room – setup of fire-prevention systems, power supply termination – setup of reserve power supply sources, explosion of cylinders with compressed air – maximum removal of cylinders with compressed air from communication equipment (into the territory of UPTC) in special room;
- From social character’s danger factors: plunder – setup of closed-circuit television systems.

More than, at any object’s protection-reduce situation UPTC must send signal to the similar APTC.

10. Quantitative safety assessment

Based on the following works [22, 23, 24] we worked out a simplified mathematical model (1) for quantitative safety assessment.

$$B_{pm} = \frac{1}{12} \left(\begin{aligned} & \left(\frac{P_{lim} - P_i(t) \left(1 + \frac{C_p}{\sigma_p \sqrt{2\pi}} \exp \left(\frac{-(P_i(t) - M(P_i(t)))^2}{2\sigma_p^2} \right) \exp(-l_p t) \right)}{P_{lim}} \right) + \left(\frac{V_{lim} - V_i(t) \left(1 + \frac{C_v}{\sigma_v \sqrt{2\pi}} \exp \left(\frac{-(V_i(t) - M(V_i(t)))^2}{2\sigma_v^2} \right) \exp(-l_v t) \right)}{V_{lim}} \right) + \\ & + \left(\frac{U_{lim} - U_i(t) \left(1 + \frac{C_U}{\sigma_U \sqrt{2\pi}} \exp \left(\frac{-(U_i(t) - M(U_i(t)))^2}{2\sigma_U^2} \right) \exp(-l_U t) \right)}{U_{lim}} \right) + \left(\frac{I_{lim} - I_i(t) \left(1 + \frac{C_I}{\sigma_I \sqrt{2\pi}} \exp \left(\frac{-(I_i(t) - M(I_i(t)))^2}{2\sigma_I^2} \right) \exp(-l_I t) \right)}{I_{lim}} \right) + \\ & + 3 \left(\frac{\left(\delta + a e^{-b t} \right) \left(\delta + a e^{-b t} \right) \frac{C_\rho}{\sigma_\rho \sqrt{2\pi}} \exp \left(\frac{-(\rho_i(t) - M(\rho_i(t)))^2}{2\sigma_\rho^2} \right) \exp(-l_\rho t) - \rho_{ext}}{\rho_{ext}} \right) + \left(\frac{\rho_i(t) - \rho_i(t) \frac{C_\rho}{\sigma_\rho \sqrt{2\pi}} \exp \left(\frac{-(\rho_i(t) - M(\rho_i(t)))^2}{2\sigma_\rho^2} \right) \exp(-l_\rho t) - \rho_{ext}}{\rho_{ext}} \right) + \\ & + 3 \left(\frac{\left(\tau_{ext} - \tau_i(t) \left(1 + \frac{C_\tau}{\sigma_\tau \sqrt{2\pi}} \exp \left(\frac{-(\tau_i(t) - M(\tau_i(t)))^2}{2\sigma_\tau^2} \right) \exp(-l_\tau t) \right) \right)}{\tau_{ext}} \right) + \left(\frac{\tau_{ext} - \tau_i(t) \left(1 + \frac{C_\tau}{\sigma_\tau \sqrt{2\pi}} \exp \left(\frac{-(\tau_i(t) - M(\tau_i(t)))^2}{2\sigma_\tau^2} \right) \exp(-l_\tau t) \right)}{\tau_{ext}} \right) \end{aligned} \right) \quad (1)$$

where T – temperature, V – moisture, U – electric voltage, I – electric current, T_{lim} - maximum temperature limit, V_{lim} - maximum moisture limit, U_{lim} - maximum electric voltage limit, I_{lim} - maximum electric current limit, τ_{lim} - maximum time limit of exposure duration, ρ_{lim} - maximum distance limit of exposure, $T_i(t)$, $V_i(t)$, $U_i(t)$, $I_i(t)$, $\tau_i(t)$, $\rho_i(t)$ – respectively the current values of temperature, moisture, electrical voltage and current, exposure time, exposure distance. C_T , C_V , C_U , C_I , C_τ , C_ρ - the truncation coefficients of the truncated normal law of temperature, moisture, electrical voltage and current, exposure time, exposure distance. $M(T_i(t))$, $M(V_i(t))$, $M(U_i(t))$, $M(I_i(t))$, $M(\tau_i(t))$, $M(\rho_i(t))$ – mathematical expectation of a random variable of temperature, moisture, electrical voltage and current, exposure time, exposure distance. l_T , l_V , l_U , l_I , l_τ , l_ρ – manifestations' intensity of random changes of temperature, moisture, electrical voltage and current, exposure time, exposure distance. t – current time.

In this model we don't consider the hazardous factor of unauthorized access and a number of other specific moments; but many authors believe that in most cases received values are relevant enough and by the determination of legitimate values of safety parameter the algorithm can be used in safety control system.

11. Implementation results

Theoretical data that were received in the research were used by running the updating works for safety control systems of the production organization Science & Technology Center “SIMOS” JSC, city Perm, Russia. The following results were received (extract from implementation act):

«The recommendations <...> were used at the Science & Technology Center “SIMOS” JSC, city Perm for the further development and improvement of safety control systems and the efficiency of unattended points of technological communication on oil and gas pipelines which were developed and produced by the enterprise. Particularly the implementation was performed in the system of video surveillance. These recommendations extend the functionality of the system and increase its efficiency. The Chief Constructor Tchumakov O.B., Science & Technology Center “SIMOS” JSC”.

12. Conclusion

The article describes the methodology of safety control systems' design for unattended points of technological communication on oil and gas pipelines; it shows the results of implementing research outcome in real-time operating safety systems.

References

- [1] V.A. Vorona, V.A. Tihonov, Kompleksnye (integrirovannye) sistemy obespechenija bezopasnosti, Gorjachaja linija-Telekom, Moscow, 2013.
- [2] V.A. Vorona, V.A. Tihonov, Ohrannye podrazdelenija, Gorjachaja linija-Telekom, Moscow, 2012.
- [3] V.A. Vorona, V.A. Tihonov, Konceptual'nye osnovy sozdaniya i primeneniya sistemy zashhity ob'ektov, Gorjachaja linija-Telekom, Moscow, 2012.
- [4] V.A. Vorona, V.A. Tihonov, Inzhenerno-tehnicheskaja i pozhnarnaja zashhita ob'ektov, Gorjachaja linija-Telekom, Moscow, 2012.
- [5] V.A. Vorona, V.A. Tihonov, Tehnicheskie sistemy ohrannoj i pozhnarnoj signalizacii, Gorjachaja linija-Telekom, Moscow, 2012.
- [6] V.A. Vorona, V.A. Tihonov, Tehnicheskie sredstva nabljudeniya v ohrane ob'ektov, Gorjachaja linija-Telekom, Moscow, 2011.
- [7] V.A. Vorona, V.A. Tihonov, Sistemy kontrolja i upravlenija dostupom, Gorjachaja linija-Telekom, Moscow, 2011.
- [8] V.A. Ryzhova, Proektirovanie i issledovanie kompleksnyh sistem bezopasnosti, NIU ITMO, SPb., 2013.
- [9] S.V. Petrov, Obespechenie bezopasnosti organizacij i proizvodstvennyh ob'ektov, NC JeNAS, Moscow, 2007.
- [10] I.A. Rjabinin, Nadezhnost' i bezopasnost' strukturno-slozhnyh sistem, Izdatel'stvo Sankt-Peterburgskogo universiteta, SPb., 2007.
- [11] Ju.A. Vinogradov, Ohrannaja tehnika, Solon-Press, Moscow, 2008.
- [12] R.G. Magaunov, Ohrannaja signalizacija i drugie jelementy sistem fizicheskoj zashhity: kratkij tolkovyj slovar', Gorjachaja linija-Telekom, Moscow, 2007.
- [13] R.G. Magaunov, Sistemy ohrannoj signalizacii. Osnovy teorii i principy postroeniya, Gorjachaja linija-Telekom, Moscow, 2008.
- [14] Ju.M. Gedzberg, Ohrannoe televidenie, Gorjachaja linija-Telekom, Moscow, 2005.
- [15] A.E. Peskin, Sistemy videonabljudeniya. Osnovy postroeniya, proektirovaniya i jekspluatacii, Gorjachaja linija-Telekom, Moscow, 2013.
- [16] M. Gvozdek, Spravochnik po tehnike dlja videonabljudeniya. Planirovanie, proektirovanie, montazh, Tehnosfera, Moscow, 2010.
- [17] O.M. Lepeshkin, V.V. Kopytov, A.P. Zhuk, Kompleksnye sredstva bezopasnosti i tehniceskije sredstva ohranno-pozhnarnoj signalizacii, Gelios ARV, Moscow, 2009.

- [18] Tehnicheskie rekomendacii po proektirovaniju sistem antiterroristicheskoj zashhishhennosti i kompleksnoj bezopasnosti vysotnyh i unikal'nyh zdaniy - TR 205-09, Moskva, 2009.
- [19] Sistemy pozharnoj signalizacii adresnye. Obshhie tehicheskie trebovanija. Metody ispytaniy, NPB 58-97, 1997.
- [20] Minacevich S.F., Borisov S.S. Opredelenie rjada opasnostej, harakternyh dlja neobsluzhivaemyh punktov tehnologicheskoy svjazi nefte- i gazoprovodov. Fundamental'nye issledovanija. – 2015. - №5-1. – pp.109-113.
- [21] Minacevich S.F., Borisov S.S. Analiz sushhestvujushhijh sistem kontrolja bezopasnoj i nadezhnoj raboty neobsluzhivaemyh uzlov tehnologicheskoy svjazi nefte- i gazoprovodov Rossii. Prikladnaja fotonika. – 2013. - t. 7 - №1-4. – pp.157-162.
- [22] Trefilov V.A. Teoreticheskie osnovy bezopasnosti proizvodstvennoj dejatel'nosti: ucheb. posobie. – Perm': Izd-vo Perm. gos. tehn. un-ta, 2009. – 84 p.
- [23] Ventcel' E.S. Teorija verojatnostej: ucheb. dlja vuzov. – M.: Vysshaja shkola, 2002. – 575 p.
- [24] Kalugin M.N. Opredelenie zon bezopasnosti v avtomatizirovannoj sisteme upravlenija bezopasnost'ju kotel'noj. Prikladnaja fotonika. – 2013. - t. 7 - №1-4. – pp.101-106.



International Conference on Industrial Engineering

Automatic control of supplying the uninterrupted action loading machine at casual outside influence

Khazanovich G.S.^a, Otrokov A. V.^{a,*}, Breusov A.N.^a

^a *Shakhty institute (branch) of Platov South-Russian state polytechnic university (NPI), 1, Lenin Square, Shakhty, Rostov region, Russia*

Abstract

The condition of the loading process research, working out the principles and installations of automatic control of supplying the loading machines with grabbing claws is considered. The experience of application of discrete control system with regulated upper and lower levels of turning in the adjusters of loading the grabbing part engines is based. The task of automatic control providing, with the consideration of occasional character of forming the load with the grabbing claws, the achievement of maximum productivity at keeping power and energy limits, is formulated. The necessary mathematical models and control algorithms, the peculiarity of which is preliminary modeling of the process, putting the results into the system of microprocessing control and consideration of deviations from the standard variant, are worked out. Using the offered system provides with the productivity increase up to 15 %, increasing the reliability and reducing labour capacity in the machine control.

© 2015 The Authors. Published by Elsevier Ltd. This is an open access article under the CC BY-NC-ND license (<http://creativecommons.org/licenses/by-nc-nd/4.0/>).

Peer-review under responsibility of the organizing committee of the International Conference on Industrial Engineering (ICIE-2015)

Keywords: loading machine of uninterrupted action; productivity of the machine; automatic supply to the pile; mechatronic system of control; occasional character of loading to the drive; maximum frequency of the drive switching on; sensors of the main parameters; defence from overloading; turning in the adjuster of current level; control algorithm.

1. Introduction

Loading machine with grabbing claws was patented for the first time by Joseph Joy in 1916. The unique trajectory of the claws movement became the standard in the branch and is used at underground loading machines, and cutting combines all over the world. The machines of 2PNB-2 type produced in Russia are the greatest part of the loading machines parks at the Eastern Donetsk Basin mines. They are equipped with twin grabbing claws and, in

* Corresponding author. Tel.: +7-918-509-03-07; fax: +7-8636-22-30-88.
E-mail address: oav711@gmail.com

spite of their having been industrially produced, are hand-operated. Casual character of forming loads to the drive of grabbing claws mechanism owing to non-homogeneous characteristics of the pile material and changing conditions of forming the volumes of grabbing the material with the claws makes impossible to use the machine resources completely even at the considerable experiences of the operator. In consequence of it the problem of creating an automatic equipment which would give the possibility to increase the reliability and efficiency of the machine in the whole and decrease the labour capacity of the loading process for the operator is quite actual.

2. Short history of working out the system of controlling supply

The collective bodies of scientists of the Novocherkassk polytechnical institute (now Platov South-Russian state polytechnic university (NPI)) [1, 2], the Communarsk mining metallurgical institute (the town of Alchevsk, Ukrainian SSR) [3], the institute of geotechnical mechanics of the Academy of Science of the Ukrainian SSR (the city of Dnepropetrovsk) [4], as well as the Copeisk and Yasnogorsk plants producing the machines of this type had been going in for working out the systems of the automatic control of the loading machines of the PNB type during the last 50 years.

The main problem is the principle of the supply control which is determined with physics of the process of interaction of grabbing claws with the pile. The two conceptions are based: 1) the velocity of automatic supply should change smoothly into the functions of loading in the drive of the grabbing part [1]; 2) interrupted supply of the machine the beginning and ending of the cycle of which depend on the level of load in the drive [2]. Among the realized in the experimental and tested models there were machines with a regulated drive of direct current [3], double-differential hydrodrive [1], asynchronous drive with relay-controlled and impulsive regulators [2, 5]. Produced by the Copeisk machine building plant the machine 1PNB-2D with relay-controlled regulator of supplying passed industrial test successfully [2, 5], other models were tested in stand conditions.

3. Peculiarities of the loading machine interaction with the mining mass pile

Working out the system of automatic control of supplying the loading machine should be based on the results of the analysis of interactions in the system of “the pile – loading organ – travelling part – drive – control system”.

The conclusions about the interaction of the pile and the loading organ of the machine with grabbing claws are based both on the materials of the preceding research [6-8] including the loading organs with grabbing spiders having the similar regularities [9, 10], and on the results of computer and physical modeling conducted in the mechatronic system of automatic control [1-4, 11, 12]. The interaction of the control system and the loading machines is reflected in the works [13-15], the influence of casual processes at loading large lumps material is reflected in the works [16, 17].

As the preceding investigations showed, at loading the pile of large lumps rock of more than 0.5 m high, discrete supplying control (i.e. the cycle of supplying should include 2-4 scooping) is the most effective. However, unlike the previously created relay regulator [3], for the concrete conditions automatic choice of regulating parameters should be realized, i.e. the upper J_u and lower J_l levels of turning in the adjusters of loading in dependence on the current load to the drive of the aggregate of limitations. When the loading reaches the meaning J_u , the supplying stops, when the loading reaches the meaning J_l , the supplying renews. Besides, on the previous investigations casual character of forming loads is not considered, but it is especially essential at loading large lump material.

Load M to the claws, and therefore the current of engines of the grabbing part in the period of every disc rotation is the separate realization of the casual function M from corner of turning the driving crank φ . Moreover, the considered casual function $M = f(\varphi)$ has a number of peculiarities:

- mathematical expectation and correlative function at changing the corner of turning $0 \leq \varphi \leq 2\pi$ do not stay constant but consist conditionally of four parts – inculcation of the claw into the pile, scooping the portion of the material, pushing the portion of the material into the conveyer and idle running;
- in the process of loading the machine and the loading organ installed on it are in two conditions:
 - immovable – with working some quantity of scooping;
 - supplying – moving the machine to the pile. In each of these conditions some conditional depth of inculcation and the volume of the material in the active zone is realized, that is why the characteristics of the

5. The main task of controlling

The purpose of creating mechatronic system of automatic control of supply is reaching the maximum possible value of average productivity of the loading machine at loading out the volume of a pile between two next in turn cycles of maneuverings considering the maximum power, energy possibilities of the machine, fulfilling the demands of reliability and safety, considering the following limitation:

- equivalent power of drives of grabbing and running parts should not exceed the permissible meaning;
- frequency of turning on the supplying mechanism should not exceed the maximum permissible meaning;
- pressure effort of the running part should be in permissible limits with consideration of the factors of adhesion of caterpillar with the ground and the power of running drive.

These limitations should be kept in the concrete conditions of work of the loading machine: the angle of inclination of the underground working, hardness, coarseness and humidity of the mining mass being loaded, the pile high.

An addition the demands of adaptivity are made to the system of automatic control, i.e. self-turning for the optimal meaning of lower and upper levels of turning in the adjusters of loading in the adjusters of loading in dependence on the conditions of work of the loading machine.

6. Mathematical model and algorithm

Mathematical model of control is the combination of mathematical correlations and algorithm of microcontroller actions with the help of which, after finishing every complete revolving of the leading disks, the forming of controlling signal of “turning on / turning off electrohydrovalve of the running mechanism” with the purpose of reaching the maximum meaning of the average productivity of the loading organ takes place.

Analytical function for the purpose can be written as [16]:

$$q_{cp} = \frac{q_0}{T_1 + T_2} \cdot \int_0^{T_1+T_2} \chi dt \Rightarrow \max \quad (1)$$

where q_0 – normative productivity;

T_1 – time of giving the machine to the mining mass pile;

T_2 – time of loading of the rock mass during stationary feeder;

χ – coefficient of productivity ($\chi = q_{min} / q_{max}$).

With the consideration of the peculiarities of physical phenomena of mining mass loading by twins grabbing claws it is established that the automatic system of controlling the supply of the loading machine of uninterrupted action is mainly reduced to discrete acts of comparison and correcting the meanings of the levels of turning in the adjusters of upper J_u and lower J_l after each next in turn scooping. Comparison is fulfilled by confronting “standard” and actual processes of forming the loading organ productivity and loading the engines of grabbing part with the consideration of fulfilling the combination of limitations.

For modeling on a computer the standard coming of the working process of loading mathematical models received as a result of complex experimental investigations on physical models and natural samples are used:

- of a grab volume in a single scooping;
- the volume of the material on the active zone;
- calculated depth of penetrating after finishing next in turn scooping;
- maximum depth of penetration of the nose of the plate restricted by the pressure effort on linking the caterpillar with the ground;
- resistance to penetration of the inclined plate into the pile;
- mathematical expectations of a casual function of the moment on the shaft of the leading disk (on phases of the claw movement, from the depth of penetration and other factors);
- forming the frequency-response component of casual function of the moment on the shaft of the leading disk — spectrum density;

- electromechanical characteristic of the grabbing part drive;
- mathematical models of limitation:
 - on power of drive of the loading process and breaking for the maneuvering;
 - on maximum loading with consideration of casual character of the process and the velocity of increasing the signal;
 - on the frequency of turning on the frictional clutch and electrohydrovalve with the considerable of heating the construction.

Using the results of preliminary modeling gives the possibility to prognose with the necessary the character of changing the load, its value for scooping. The analysis of changing the main coefficients — productivity, the level and character of loading the drive of the grabbing part (according to the value of mathematical expectation, spectral density of the load, availability of throwing out behind the upper level of forming in the adjuster), active volume of the pile and others — give the possibility to choose optimal algorithm of control, i.e. to turn in the adjusters of upper and lower levels and to choose the algorithm of their changing in such a way to provide the maximum meaning of the function in purpose with keeping all the restrictions.

The system offered for correcting and turning in the adjusters of loading levels is used the measurement of deviation of the four main indexes: productivity, the engine temperature, the engine current frequency of turning on the mechanism of supplying. As for every measured index there are two possible variants of correlations demanded and real indexes: productivity, the engine temperature, the engine current, frequency of turning on the mechanism of supplying. As for the every measured index there are two possible variants of correlations demanded and real indexes: the first one – derivation is in the normal limits, the second one – the derivation increases the adopted value, we receive 16 possible variants of the system state, the program action of microprocessor controlling system on changing the level of turning in the adjusters in the next in turn cycle of scooping corresponds to each of them.

7. Short conclusions

- The task of automatic controlling the process of loading by the machine with grabbing claws is formulated.
- Mathematical models and algorithms of searching maximum productivity of the loading machine with consideration of casual character of the process of loading.
- Computer modeling has demonstrated the possibility of automatic controlling the process of loading and shown the possibility of increasing the productivity for 5 - 15 %, the reserve on the frequency of supplying being 5 - 10 %, in heating the engines of the grabbing part being 10 - 20 % in comparison with manual control of loading.

References

- [1] G.M. Vodyanik, A.N. Drovnikov, Yu.A. Vasil'ev, Pogruzochnaya mashina bokovogo zahvata s avtomaticheskim reguliruemym rezhimom raboty, Izvestiya Sev.-Kavk. Nauch. centra vyssh. shk. Seriya: Tekhnicheskie nauki. 1 (1973) 29–33.
- [2] G.Sh. Hazanovich, S.E. Lohovinin, P.F. Nozdrin, A.V. Urosov, Pogruzochnaya mashina 1PNB-2, osnashchennaya regulyatorom podachi. Gornyj zhurnal. 11 (1979) 73–76.
- [3] B.A. Verklov, A.I. Rovenok, B.A. Zhukov, Sistema avtomaticheskogo regulirovaniya nagruzki pogruzochnyh mashin nepreryvnogo dejstviya, Gornyj zhurnal. 10 (1970).
- [4] V.K. Kozlo, N.N. Kazachkovskij, V.V. Zvorykin, Pogruzochnaya mashina nepreryvnogo dejstviya kak ob"ekt upravleniya, Izvestiya vuzov. Gornyj zhurnal. 6 (1980) 85–88.
- [5] S.E. Lohovinin, Povyshenie ehffektivnosti pogruzochnyh mashin tipa PNB primeneniem ustrojstv preryvistoj podachi. Avtoref. dis. ... kand. tekhn. nauk, Dnepropetrovsk. 1988.
- [6] S.E. Lohovinin, Povyshenie e'ffektivnosti pogruzochnyh mashin tipa PNB primeneniem ustrojstv preryvistoj podachi [Text]. – Avtoref. diss... kand. texn. nauk Zashhishhena, 1988.
- [7] G.Sh. Hazanovich, Optimizaciya rabochih processov i parametrov shahtnyx pogruzochnyh mashin [Text] .– Avtoref. diss. ... d-ra texn. nauk. Zashhishhena, 1990.
- [8] LI Xiaohuo, Simulation and Analysis of a Two-raking Pawl Loading Mechanism, Journal of Heilongjiang Institute of Science. (2002).
- [9] LI Jun, Analysis and Research of How to Raise Loading Efficiency that Stalled Loader Owns, Coal Mine Machinery. 3 (2011).
- [10] LIANG Xiao-dong, LI Xiao-huo, Determination of star wheel loading mechanism's lowest rotating speed of road-headers which don't jam, Journal of Liaoning Technical University. (2006).

- [11] G.Sh. Hazanovich, K voprosu ob avtomatizacii podachi pogruzochnyh mashin nepreryvnogo dejstviya, Rezul'taty issledovanij – 2012: materialy 61-j nauchnoj konferencii professorsko-prepodavatel'skogo sostava, nauchnyh rabotnikov, aspirantov i studentov. (2012) 70–73.
- [12] A.V. Otrokov, G.S. Khazanovich, Problem designing of loading machines with grasping claws, 3 International Symposium ENERGY MINING 2010, Energy mining, new technologies, sustainable development : proceedings. (2010) 343–352.
- [13] G.Sh. Hazanovich, A.N. Breusov, E.A. Shemshura, Ya.G. Shemshura, Imitacionnaya model' pogruzochnoj mashiny nepreryvnogo dejstviya s avtomaticheskim upravleniem. Perspektivy razvitiya Vostochnogo Donbassa: materialy 61-j Vseros. nauch.-prakt. konf. Shahty. (2012) 114–121.
- [14] G.Sh. Hazanovich, Ya.G. Shemshura, A.N. Breusov, Modelirovanie processa pogruzki mashinoy 2PNB-2 pri avtomaticheskom upravlenii rezhimom podachi, Sbornik rabot pobeditelej otborochnogo tura Vserossijskogo smotra-konkursa nauchno-tekhničeskogo tvorčestva studentov "Evrika". (2012) 122–124.
- [15] A.N. Breusov, V.V. Vitkovskij, Ya.G. Shemshura, N.B. Afonina, Proekt ehksperimental'noj model'noj ustanovki s avtomaticheskim upravleniem processa podachi. Perspektivy razvitiya Vostochnogo Donbassa: materialy IV Mezhdunar. i 62-j Vseros. nauch.-prakt. konf. Shahty. (2013) 62–67.
- [16] G.Sh. Hazanovich, G.V. Lukyanova, A.V. Otrokov, Imitacionnoe modelirovanie raboty klinovogo peregruzhatelya pri sluchajnom haraktere vneshnih vozdejstvij, Issledovaniya v oblasti konstruirovaniya rabochih processov i ehkspluatacii tehničeskikh mashin sb. nauch. tr. (2006) 8–11.
- [17] G.Sh. Hazanovich, G.V. Lukyanova, E.A. Revyakina, A.V. Otrokov, Modelirovanie prohodkačeskikh pogruzočno-transportnyh podsystem s ciklovymi ispolnitelnymi organami dlya vzryvonavaločnyh tehničeskij: monograph, Shahtinskij in-t (filial) YURGTU (NPI), Shakhty, 2010.



International Conference on Industrial Engineering

Modeling truck driveline dynamic loads at differential locking unit engagement

Keller A.V.^a, Gorelov V.A.^b, Anchukov V.V.^{a*}

^aSouth Ural State University, 76, Lenin Avenue, Chelyabinsk, 454080, Russian Federation

^bBauman Moscow State Technical University, 5, 2-ya Baumanskaya, Moscow, 105005 Russian Federation

Abstract

The paper shows the results of the truck driveline dynamic loading processes made with an imitation modeling approach. The developed mathematical model of a vehicle motion includes the functioning features of all principal automotive mechanical systems and units. We considered one of the most difficult driving conditions, when the potential necessity of interaxial differential locking arises. The loads acting in transmission at the differential locking unit engagement were estimated.

© 2015 The Authors. Published by Elsevier Ltd. This is an open access article under the CC BY-NC-ND license (<http://creativecommons.org/licenses/by-nc-nd/4.0/>).

Peer-review under responsibility of the organizing committee of the International Conference on Industrial Engineering (ICIE-2015)

Keywords: Vehicle dynamics; mathematical model; driveline loads; power dividing units

1. Introduction

Trucks are one of the most widely spread kind of vehicles used in different road conditions. The off-road movability is a very important property of the trucks that determines the general vehicle efficiency.

Vehicle movability and other principal exploitation characteristics are widely studied in the world. To make the functioning of trucks in difficult and extremely difficult conditions more effective the development of the power distribution system is required [1, 8, 10, 11]. The application of lockable power dividing units is one of the most effective and popular methods of vehicle off-road movability enhancement.

* Corresponding author. Tel.: +7-982-304-14-40.
E-mail address: vv.anchoukov@gmail.com

The lockable differentials are extensively used in many kinds of vehicles: road cars, military and ground trucks etc. [9]. Active differentials are the most effective type of lockable power dividing unit as they enable to improve fuel efficiency, vehicle maneuverability and stability [4, 5, 6]. It should be noted, that active differentials have been successfully applied in car transmission. Further research in the sphere of automotive industry lies in the active differentials' application for heavy-duty trucks.

The development and implementation of a new technical item require significant financial expenses with an experimental part being the most expensive stage of a design process. However, nowadays simulation modeling methods are increasingly developing [2, 3, 7]. Mathematical models allow to get the necessary features of a developed vehicle without any experiments at a design stage. It enhances the quality of the launched products and decreases their costs. Carmakers have successfully used simulation and PLM modeling over the years.

2. Methods

2.1. Research tasks and problem formulation

The tasks of this research are all-terrain threeaxial truck "KAMAZ-65222" (Fig. 1), the layout scheme and the typology of differential mechanisms [9] shown in Fig. 2.



Fig. 1. All-terrain truck "KAMAZ-65222".

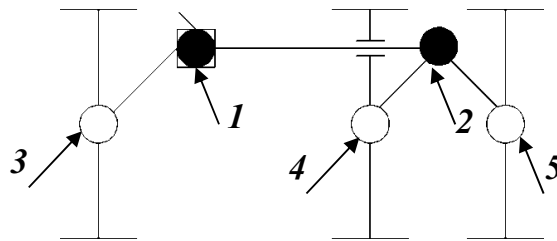


Fig. 2. Driveline layout of all-terrain truck "KAMAZ-65222"
(1, 2 – interaxial lockable differentials;
3, 4, 5 – interwheel differentials)

2.2. Mathematical model description

To obtain the valid results of vehicle dynamics' processes a mathematical model must include the description of all principal vehicle systems with real parameters of the research subject. The truck scheme with forces acting in a straight line motion mode is shown in Fig. 3.

To model the vehicle dynamics we use CAE LMS AMESim. The created mathematical model represents a vehicle motion process for all the required driving modes taking into account the dynamics of principal vehicle units and subsystems.

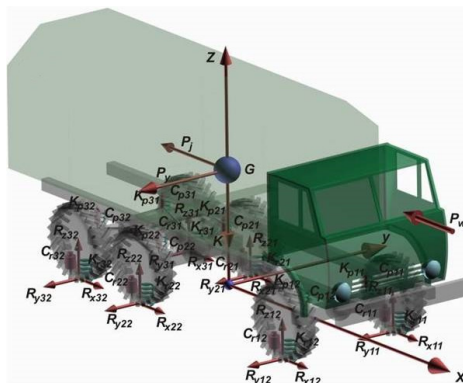


Fig. 3. Truck scheme in a straight line motion

(G – truck center of gravity (COG); XYZ – axes of global coordinate system; P_x, P_y, P_z – axes of local coordinate system with origin in vehicle COG; R_x – wheel longitudinal force; R_y – wheel lateral force; R_z – wheel normal force; c_p – wheel damping; k_s – wheel stiffness; c_p – suspension damping; k_p – suspension stiffness; P_w – aerodynamic resistance force).

The common view of model is shown in Fig. 4. This model includes all the most important subsystems: engine, driveline, suspension, and car body. It describes all the necessary physical characteristics of a vehicle and environment: masses and inertias, tire/road interaction, road adhesion, aerodynamic resistance etc.

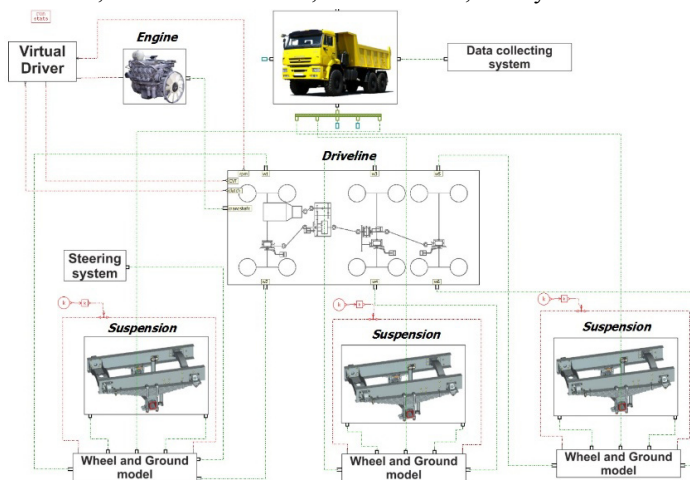


Fig. 4. The mathematical model made in LMS Imagine.Lab AMESim

Powertrain units, environment and driving conditions influence the truck body. Vehicle body equations of motion in Lagrange II kind formulation in steady fixed coordinate system are presented below:

$$\begin{cases} \dot{\omega} = T_1 - G_s h_{COG} \lambda (\dot{V}_x - \dot{V}_y \omega) / J_z \\ \dot{V}_x = V_y \omega + T_2 \\ \dot{V}_y = V_x \omega + T_3 \end{cases}, \tag{1}$$

$$T_1 = \frac{\left[\sum_{i=1}^2 R_{y12}^i a + \sum_{i=1}^2 R_{y22}^i b_2 + \sum_{i=1}^2 R_{y32}^i b_3 + 0,5(R_{x1}^{right} + R_{x1}^{left}) B_1 + 0,5 \left(\sum_{j=2}^3 R_{xj}^{right} + \sum_{j=2}^3 R_{xj}^{left} \right) B_2 \right]}{J_z}, \tag{2}$$

$$T_2 = \sum_{j=1}^3 \sum_{i=1}^2 R_{xy}^i / G, \quad (3)$$

$$T_3 = \sum_{j=1}^3 \sum_{i=1}^2 R_{xy}^i / G, \quad (4)$$

here

ω - Vehicle body rotational velocity;

G_s - Total sprung mass;

G - Vehicle mass;

h_{COG} - Center of gravity height;

λ - Roll angle;

V_x - Velocity in longitudinal direction;

V_y - Velocity in lateral direction;

J_z - Vehicle body moment of inertia;

R_x - Longitudinal wheel reaction;

R_y - Lateral wheel reaction;

a - Distance between vehicle front axle and center of gravity;

b_2 - Distance between vehicle center of gravity and middle axle;

b_3 - Distance between vehicle center of gravity and rear axle;

B_1 - Front track width;

B_2 - Rear track width.

The powertrain unit comprises an engine, functioning according to a throttle position. A detailed driveline model includes a clutch, a gearbox, a transfer case, compliant driving shafts with cardan joints, five differentials (two interaxial and three interwheel) and bevel gears on each axle.

The suspension takes into account drive connection, the dynamics working process of the solid axle distributing force and vibrations to the truck body. A built-in tire model of Rocard/Brossard [12, 13] provides the wheel/road interaction with the following assumptions made:

- The deformation of the tread centerline is the result of two independent orthogonal components: side and longitudinal slip.
- The modeling does not include the longitudinal and lateral coupling of the tire.
- The vertical load is evenly distributed over the contact patch.
- After the point at which the sliding between tread and road begins, tread deformation remains uniform (application of the Coulomb's friction theory).
- The friction coefficient is independent of normal pressure and independent of the relative sliding velocity.

The “virtual driver” system maintains the driving mode. It comprises the set of probing vehicle technologies and logic elements. The “virtual driver” solves the following tasks: to throttle position, to provide clutch control, to control vehicle speed, to monitor breaking and driving trajectory.

The model created enabled us to get a loading process of interaxial differential locking unit engagement. So, we consider the following controlling case. The vehicle starts driving on the first gear along the sloped road and continues driving without gear shifting and full throttle position. The full description of controlling case is shown in Table 1.

Table 1. Initial conditions of controlling case parameters

Driving process	
Initial vehicle state	State of rest with the further start
Slope angle, grad	35
Road friction coefficient	0,8
Driveline mode	

Differential conditions	All are open
Gear number	1 (i = 13,8)
Throttle position	Full supply

3. Results

During the straight line motion on the sloped road the vehicle COG moves back. This leads to the reduction of normal forces on front wheels. As a result, the truck front wheels slip and resist to further motion. The change of the efficiency criteria for vehicle motion is shown in Figures 5-8.

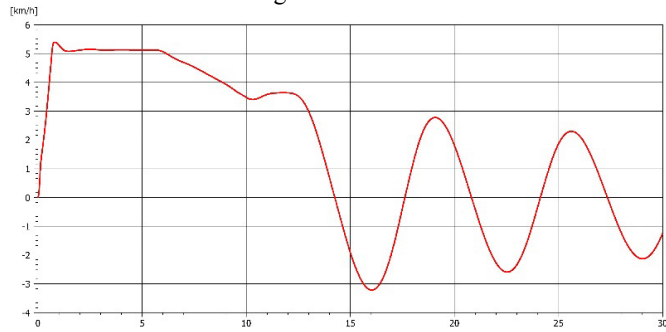


Fig. 5. Change of vehicle speed, km/h

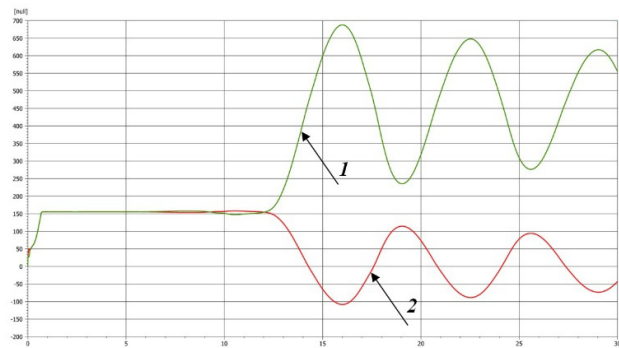


Fig. 6. Change of rotational velocities in the driving process, rpm
 (1 – change of rotational velocity of transfer case output shaft to the front axle;
 2 – change of rotational velocity of transfer case output shaft to the rear axles)

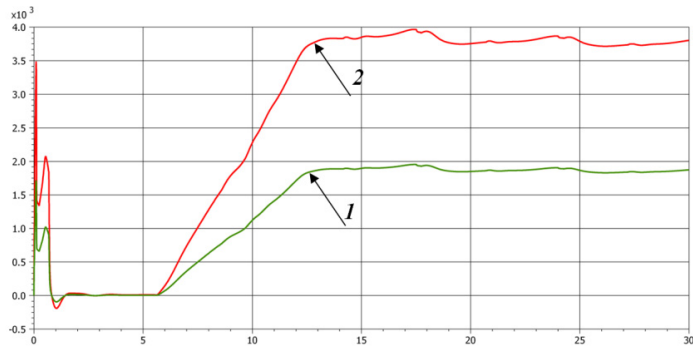


Fig. 7. Change of torques in the driving process, Nm
 (1 – transfer case output shaft torque to the front axle;
 2 – transfer case output shaft torque to the rear axles)

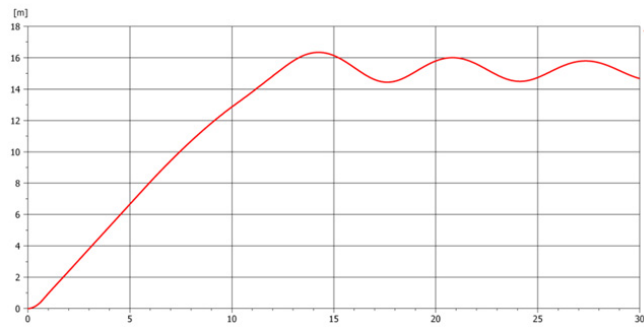


Fig. 8. Vehicle centre of gravity displacement in longitudinal direction, m

The figures 5-8 show that the vehicle motion on the road with the slope angle equal to 35 degrees is not feasible. Front wheels slippage is the main reason. To solve this problem the mathematical model of active interaxial differential with simple control algorithm was developed. During the vehicle movement the active differential control system evaluates the difference between transfer case output shafts rotational velocities. When the difference is 50 rpm the differential locks. The obtained results for the same controlling case are shown in Figures 9-11.

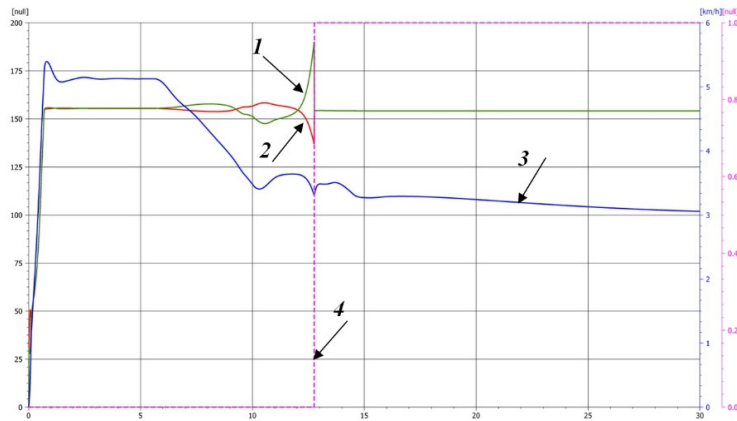


Fig. 9. Change of rotational velocity and vehicle speed

- (1 – transfer case output shaft rotational velocity to the front axle, rpm;
- 2 – transfer case output shaft rotational velocity to the rear axles, rpm;
- 3 – vehicle longitudinal speed, km/h;
- 4 – control signal for differential locking)

The results prove the efficiency of active lockable differentials applied to all-terrain truck to improve truck movability on the sloped road. The values of obtained loads at differential locking are given in Table 2.

Table 2. The values of obtained loads at differential locking unit engagement

Front axle driveshaft rotational velocity, rpm	189,2
Rear axles driveshaft rotational velocity, rpm	137,4
Torque value on front axle driveshaft at differential locking unit engagement, Nm	1848,5
Torque value on rear axles driveshaft at differential locking unit engagement, Nm	3753,0
Torque maximum value on front axle driveshaft after differential locking unit engagement, Nm	1848,5
Torque maximum value on rear axles driveshaft after differential locking unit engagement, Nm	6140,0

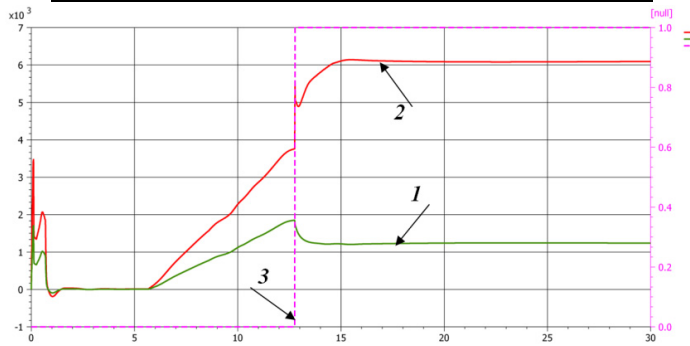


Fig. 10. Change of torques in the driving process, Nm
 (1 – transfer case output shaft torque to the front axle;
 2 – transfer case output shaft torque to the rear axles;
 3 – control signal for differential locking)

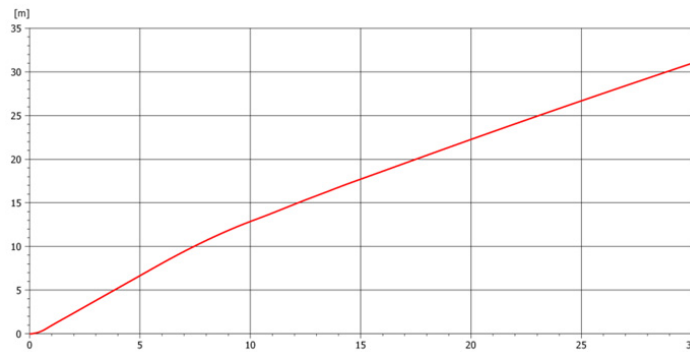


Fig. 11. Vehicle centre of gravity displacement in longitudinal direction, m

According to received torque changes shown in Fig. 10, the differential locking unit engagement leads to the fast increase of rear axle driveshaft torque. Hence, the stress in coupling unit and other differential joint connections increases. So, the dynamic loads values obtained can be used in the future for the design of transfer case interaxial differential locking coupling unit and actuating mechanism.

4. Conclusions

The created mathematical model of all-terrain truck motion can be applied for researching vehicle dynamics of different exploitation modes. The model includes the “external” car body dynamics and dynamic processes in all principal vehicle subsystems and powertrain units. With the help of an imitation of a typical driving mode driveline dynamic loads at differential locking unit engagement was estimated. The received results allow evaluating transmission dynamic loads and stresses’ values that are necessary for future coupling unit design.

Using the mathematical model developed the control algorithm of transfer case active differential depending of different environment condition was made.

Acknowledgement

The work was performed under the financial support of the Ministry of Education and Science of Russian Federation in the frames of the project «The development of scientific-and-technical solutions for controlling power distribution in the cargo trucks transmission trains to increase their power and fuel efficiency» according to the agreement № 14.574.21.0106 DATED 09.08.2014.

Unique identifier of the applied scientific research (project) RFMEFI57414X0106.

References

- [1] V.V. Vantsevich, AWD vehicle dynamics and energy efficiency improvement by means of interaxle driveline and steering active fusion, 2013 International Design Engineering Technical Conferences and Computers and Information in Engineering Conference. 1 (2013) 9.
- [2] V.V. Vantsevich, A.D. Zakrevskij, S.V. Kharytonchyk, Heavy-duty truck: inverse dynamics and performance control, 2007 International Mechanical Engineering Congress and Exposition. 9 (2007) 345–354.
- [3] F.Cheli, M. Pedrinelli, A. Zorzutti, Integrated modeling of vehicle and driveline dynamics, ASME 8th Biennial Conference on Engineering Systems Design and Analysis. 2 (2006) 235–244.
- [4] F.Cheli, M. Pedrinelli, S. Campo, A. Fortina, P. Martella, Vehicle dynamics control system actuating an active differential, ASME 8th Biennial Conference on Engineering Systems Design and Analysis.2 (2006) 251–260.
- [5] V.V. Vantsevich, B.N. Shyrokau, Autonomously Operated Power-Dividing Unit for Driveline Modeling and AWD Vehicle Dynamics Control, ASME 2008 Dynamic Systems and Control Conference. (2008) 891–898.
- [6] J. Deur, M. Hancock, F.Assadian, Modeling of Active Differential Dynamics, ASME 2008 International Mechanical Engineering Congress and Ex-position. 17 (2008) 427–436.
- [7] V.A. Gorelov, The prediction of all wheel drive vehicle with steering 1-0-3 formula curvilinear motion characteristics under various steering principles of rear axle wheels, Ph. D thesis, Moscow, 2008.
- [8] A.V. Keller, I.A. Murog, D.V. Shafikov, V.YU. Usikov, S.V. Ushnurtsev, Complex estimation of power distribution methods in mechanical transmissions, *Avtomobilnaya promyshlennost*. 4 (2013) 14–17.
- [9] A.F. Andreev, V.I. Kabanau, V.V. Vantsevich, *Driveline systems of ground vehicles. Theory and design*, CRC Press, Boca Raton, 2010.
- [10] A. Keller, I. Murog, S. Aliukov, Comparative Analysis of Methods of Power Distribution in Mechanical Transmissions and Evaluation of their Effectiveness, SAE 2015 World Congress & Exhibition, 2015.
- [11] A.V. Keller, G.D. Dragunov, Algorithms of controlling the distribution of power between drive wheels of motor transport facility, *Avtomobil'naya Promyshlennost, Mashinostroenie*, Moscow. 1 (2004) 10–13.
- [12] J.P.Brossard, *Dynamique du Vehicule, Modelisation des systemes complexes*, PPUR, Lyon, 2006.
- [13] Information on LMS Amehelp

International Conference on Industrial Engineering

Application of block elements method to calculate the electromechanical systems magnetic field and force characteristics

Tkachev A.N.^{a*}, Pashkovskiy A.V.^b, Burtceva O.A.^a

^aPlatov South-Russian State Polytechnic University (NPI), Prosveshenia St., 132, Novocherkassk, 346428, Russian Federation

^bNorth-Caucasus Federal University, Pushkin St. 1, Stavropol, 355009, Russian Federation

Abstract

The problem of two-dimensional magnetic field during the calculation in electromechanical systems comprising a ferromagnetic body with nonlinear magnetic characteristics is described. New geometric patterns in the form of block finite and infinite elements of arbitrary shape are proposed to be used in the simulation of magnetic field in a piecewise homogeneous medium electromechanical systems, in which an error can be controlled to perform the linearization of the material characteristics of ferromagnets. Two scalar potentials are used to find the field. Potentials form a complex magnetic potential, which is defined on the boundaries of block elements. Cauchy's integral formula is used for the purpose. The system of algebraic equations for the nodal values of the potentials on the boundaries is solved using the software developed by minimizing the functional errors. The results of the simulation of the magnetic field of the induction motor with a complicated geometry of magnetic systems are shown. The proposed method allows simplifying and improving the accuracy of calculation of the magnetic field in the design of electromechanical systems containing moving ferromagnetic elements.

© 2015 Published by Elsevier Ltd. This is an open access article under the CC BY-NC-ND license

(<http://creativecommons.org/licenses/by-nc-nd/4.0/>).

Peer-review under responsibility of the organizing committee of the International Conference on Industrial Engineering (ICIE-2015)

Keywords: electromechanical system, the ferromagnetic body, block elements, the complex potential

1. Introduction

The calculating problem of the magnetic field in a non-linear ferromagnetic environment occurs at the design stage of electromechanical system development. It connected with a mathematical model which have the aim to select design parameters, providing required technical and economic indicators [1]. The main issue here is that the systems contains movable elements. The movement leads to dynamic changes in the geometry of the computational

* Corresponding author. Tel.: +7-928-901-7070; fax: +7-863-525-5394.

E-mail address: npi-pm@mail.ru

area as well as the spatial distribution of the field in the ferromagnetic domains and modes of local magnetization reversal. The usage of the finite element method for magnetic field calculation requires to specify initial data for the triangulation of a calculation with each change of design parameters, but also with every position change of the magnetic systems [2]. Such a process considered to be extremely time consuming. It motivates us to develop new methods for the calculation of a physical field in a technical system with dynamically changing geometry and modify existing ones [3]. The article is dedicated to the solution of this problem.

2. Formulation of the calculating problem

Let calculation of the magnetic field in the plane xOy must be done in a piecewise-homogeneous bounded or unbounded area Ω , which contains ferromagnetic bodies Ω_k boundaries Γ_k , as well as an area Ω_0 not filled with a steel (Fig. 1). Let the contour Γ_0 be its outer boundary when an area Ω_0 is limited. The properties of a material in an area Ω_0 bounded by contour Γ_i are defined by the equation $\bar{H} = \bar{F}(\bar{B}) = \nu(\bar{B})\bar{B}$.

We suppose that the calculation of the field is performed with an iterative algorithm based on time layers $t = t_0, t_1, t_2, \dots$, and the field distribution is known at the primary level t_0 : $\bar{B}(M, t_0) = \bar{B}^0(M)$.

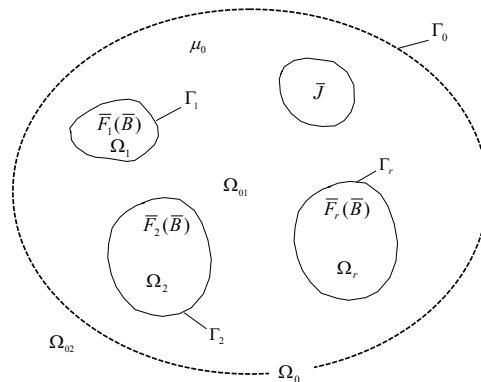


Fig. 1. Ferromagnetic bodies in an external magnetic field.

The field is described by the system of following equations at each fixed layer $t = t_k$ in the area $\Omega = \bigcup_{i=0}^r \Omega_i$:

$$\text{div } \bar{B} = 0 \text{ in } \Omega \cup \Omega_0; \text{rot } \bar{H} = 0; \bar{H} = \bar{F}(\bar{B}) \text{ in } \Omega; \text{rot } \bar{H} = \bar{J}; \bar{B} = \mu_0 \bar{H} \text{ in } \Omega_0. \tag{1}$$

The following conditions are met at the separating boundary $\Gamma = \bigcup_{i=1}^r \Gamma_i$

$$B_n^+|_{\Gamma} = B_n^-|_{\Gamma}; H_{\tau}^+|_{\Gamma} = H_{\tau}^-|_{\Gamma}. \tag{2}$$

Let us assume a distribution of induction and (or) intensity vectors are defined on the outer boundary $\Gamma_0 = \Gamma_{01} \cup \Gamma_{02}$ if the area Ω_0 is limited:

$$B_n|_{M \in \Gamma_{01}} = \varphi(M, t); H_{\tau}|_{M \in \Gamma_{02}} = \psi(M, t), \tag{3}$$

The field $\bar{B}(M, t)$, $\bar{H}(M, t)$, $M \in \Omega$ is supposed to be determined at the previous layer $t = t_k$. So it needs to be calculated at the next layer $t = t_{k+1} = t_k + \Delta t$, where Δt is a sufficiently small value. Vector fields $\bar{B}(M, t_k)$,

$\bar{H}(M, t_k)$, $\bar{B}(M, t_{k+1})$, $\bar{H}(M, t_{k+1})$ are the solutions of the equations (1) and (2). Increment vectors $\Delta\bar{B} = \bar{B}(M, t_{k+1}) - \bar{B}(M, t_k)$ and $\Delta\bar{H} = \bar{H}(M, t_{k+1}) - \bar{H}(M, t_k)$ are small while so is Δt . They satisfy the following system of equations:

$$\text{rot } \Delta\bar{H} = \Delta\bar{J}; \text{div } \Delta\bar{B} = 0; \Delta\bar{B} = \mu_0 \Delta\bar{H} \text{ in } \Omega_0; \tag{4}$$

$$\text{rot } \Delta\bar{H} = 0; \text{div } \Delta\bar{B} = 0; \Delta\bar{H} = \hat{v} \Delta\bar{B} \text{ in } \Omega_k, k = \overline{1, r}, \tag{5}$$

where \hat{v} is determined as a result function $\bar{H} = \bar{F}(\bar{B})$ linearization $\Delta\bar{J} = \bar{J}(M, t_{k+1}) - \bar{J}(M, t_k)$.

3. Numerical problem solution

A solution of the system (4) is sought in the the form

$$\Delta\bar{B} = \Delta\bar{B}_0 + \Delta\bar{B}_J; \Delta\bar{H} = \Delta\bar{H}_0 + \Delta\bar{H}_J. \tag{6}$$

In the equation (6): $\Delta\bar{B}_J$, $\Delta\bar{H}_J$ – increment fields generated by currents which are distributed in the area Ω with predetermined density in the absence of ferromagnetic bodies $\bar{J} = \bar{J}(M, t)$ – considers the influence of the ferromagnetic bodies Ω_k .

Vectors $\Delta\bar{B}_J$, $\Delta\bar{H}_J$ satisfy the equation (6). Therefore, we have following in the field Ω_0 :

$$\text{rot } \Delta\bar{H}_0 = 0; \text{div } \Delta\bar{B}_0 = 0; \Delta\bar{B}_0 = \mu_0 \Delta\bar{H}_0. \tag{7}$$

Vectors $\Delta\bar{B}_0$, $\Delta\bar{H}_0$ and $\Delta\bar{B}$, $\Delta\bar{H}$ can be set using two potentials $u^{(k)}(x, y)$, $v^{(k)}(x, y)$, $k = \overline{0, 1}$ as it follows from (6) and (7):

$$\Delta\bar{H}_0 = \text{grad } u^{(0)}; \Delta\bar{B}^0 = \text{rot} [v^{(0)} \bar{e}_z] \text{ in } \Omega_0; \tag{8}$$

$$\Delta\bar{H} = \text{grad } u^{(1)}; \Delta\bar{B} = \text{rot} [v^{(1)} \bar{e}_z] \text{ in } \Omega. \tag{9}$$

The area Ω_k , $k = \overline{1, r}$ can be split into p simply connected small sets (block elements) with any geometric shape and boundaries γ_k . It can be selected so that magnetic induction $\bar{B}(M, t)$ and intensity $\bar{H}(M, t)$ vary within the limits of allowable at points M that belong to the sets s_q , $q = \overline{1, p}$. Then value \hat{v} is assumed to be constant with an error, which can be estimated through accuracy linearization function $\bar{H} = \bar{F}(\bar{B})$, in the area s_q . We define it by the average value of the induction $\langle \bar{B}_q \rangle$ in the area s_q considering that $v = v_q = v(\langle \bar{B}_q \rangle)$.

Taking into account (9) we obtain:

$$\Delta H_x = \frac{\partial u^{(1)}}{\partial x} = \hat{v} \frac{\partial v^{(1)}}{\partial y}; \Delta H_y = \frac{\partial u^{(1)}}{\partial y} = -\hat{v} \frac{\partial v^{(1)}}{\partial x}. \tag{10}$$

Functions $u^{(1)}(x, y)$, $\hat{v} v^{(1)}(x, y)$ satisfy the Cauchy-Riemann equations in each element of the partition as it follows from (10). Potentials $u^{(0)}(x, y)$; $v_0 v^{(0)}(x, y)$; $v_0 = 1/\mu_0$ have similar property in the area Ω_0 as it can be seen from (8). Therefore, these potentials can be regarded as the real and imaginary parts of the complex potentials $\omega^{(k)}(z) = u^{(k)}(z) + \hat{v} v^{(k)}(z)$, $k = 0, 1$; $z = x + iy$ in Ω_0 . The functions $\omega^{(0)}(z)$ и $\omega^{(1)}(z)$ are analytic, respectively in the areas Ω_0 and S_q . So they are expressed in terms of their values on the boundary with Cauchy's integral formula [4]:

$$\omega^{(0)}(z) = \frac{\beta}{2\pi i} \oint_{l_0} \frac{\omega^{(0)}(\zeta)}{\zeta - z} d\zeta, \tag{11}$$

where l_0 is the boundary of the area Ω_0 : $l_0 = \bigcup_{k=j_0}^r \Gamma_k$; $\beta = 1$, $j_0 = 0$ if the area Ω_0 is bounded and $\beta = -1$, $j_0 = 1$ otherwise.

Similarly, we obtain for the area s_q with boundary l_q :

$$\omega^{(1)}(z) = \frac{\beta}{2\pi i} \oint_{l_q} \frac{\omega^{(1)}(\zeta)}{\zeta - z} d\zeta; \beta = 1; q = \overline{1, p}. \tag{12}$$

Let us introduce the node system $\{z_{mj}\}_{j=1}^{n_m}$ on each circuit l_m , $m = \overline{0, p}$, where n_m – the number of nodes on the boundary l_m and the approximate boundaries with broken lines \tilde{l}_m . Segments of these lines are connected with selected nodes. Complex potentials $\omega^{(k)}(z)$, $k = 0;1$ can be approximated with piecewise linear functions at the boundary ℓ

$$G^{(k)} = \sum_{m=0}^r \sum_{j=1}^{n_m} \omega_{ij}^{(k)} e_{ij}(z); k = 0;1, \tag{13}$$

where $\omega_{mj}^{(k)}$ – the value of the function $\omega^{(k)}(z)$ at the node z_{mj} ; $e_{mj}(z)$ – function that varies linearly on the segments adjoining to the node z_{mj} , and is equal to zero outside of these segments and satisfying $e_{mj}(z_{mj}) = 1$.

Let us substitute functions (13) in the equations (12). So we obtain a representation of the potentials $\omega^{(k)}(z)$ in the areas Ω_0 ($k = 0$) and S_q ($k = 1$) through the nodal values $\omega_{mj}^{(k)}$ on the boundaries. Let the inner point z tends the node z_{mf} . We obtain the following system of equations for nodal potential values by calculating the limit:

$$\omega_{mf}^{(k)} = \frac{\beta}{2\pi i} \sum_{j=1}^{n_m} \frac{(z_{mf} - z_{mj})\omega_{mj+1}^{(k)} - (z_{mf} - z_{mj+1})\omega_{mj}^{(k)}}{z_{qj+1} - z_{qj}} \ln \frac{z_{mj+1} - z_{mf}}{z_{mj} - z_{mf}} + \omega_{mf}^{(k)} \ln \frac{z_{mf+1} - z_{mf}}{z_{mf-1} - z_{mf}}, \tag{14}$$

$$k = 0,1; m = \overline{0, r}; f = \overline{1, n_m},$$

where the terms that appropriate $j = f$ and $j = f - 1$ are not taken into account, and $z_{mn_m+1} = z_{m1}$ by definition.

We get in view of the of (6) that the condition of field continuity (2) are satisfied if the following equations are valid on the ferromagnetic bodies boundaries Γ_k :

$$u^{(0)}|_{\Gamma_k} + u_J|_{\Gamma_k} = u^{(1)}|_{\Gamma_k}; v^{(0)}|_{\Gamma_k} + v_J|_{\Gamma_k} = v^{(1)}|_{\Gamma_k}; k = \overline{1, r}, \tag{15}$$

where: v_J – the module of the vector potential field: $\vec{B}_J = rot[v_J \vec{e}_z]$; $u_J(z_{kj}) = \int_{L_{kj}} H_{J\tau} dl$.

Conditions (3) can be written in finite difference form for the nodes that lie on a boundary Γ_0 .

The number of the equations exceeds the number of variables in the system. Special software is developed for this purpose. The linearization of the material equation has to be done at the next layer $t = t_{k+2} = t_{k+1} + \Delta t$, when solution for the previous layer is known and average values of induction $\langle \bar{B}_q \rangle$ are set in the each area S_q , $q = \overline{1, p}$.

The average value of induction $\bar{B}(x, y)$ on the boundary γ_k of element s_q is taken as $\langle \bar{B}_q \rangle$.

4. The example of the method of block elements application

The described method was used to calculate the magnetic field of electric traction motor (Fig. 2). The calculation was performed in the idle mode when the current in the rotor winding can be considered as zero. The field distribution was based on the nonlinear characteristics of the magnetic system of the rotor and stator at the time when the current in the phase winding C is maximal ($i_C = 712 A$), and the currents of the phases A and B are equal: $i_A = i_B = 356 A$. Following conditions were set on the boundary of the computational area (Fig. 2)

$$B_n|_{AB} = B_n|_{CD} = B_n|_{BC} = 0; H_\tau|_{AD} = 0.$$

The results of the calculations is shown on Fig. 3. It shows the lines of the field induction for the moment when the distribution of the currents in the windings are $i_C = 712 A$; $i_A = i_B = 356 A$.

The calculation of the magnetic field of the engine was performed by finite element method with the number of elements of equal to 9545 for comparison. The results of the two methods of calculation coincided with an accuracy of 2%.

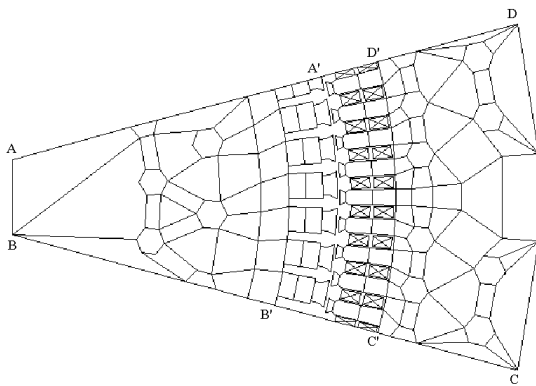


Fig. 2. Geometry of the computational area and its partition into block elements.

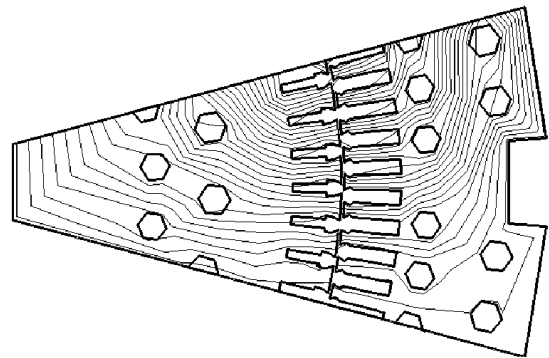


Fig. 3. Lines of magnetic field induction in the pole pitch of motor.

5. Conclusion

This method of block elements is particularly effective when multiple calculations of the magnetic field of electromechanical systems have to be performed at the stage of their design. The block elements, covering an area filled with ferromagnetic bodies, retain their configuration. The movement is taken into account by simply changing the coordinates of the nodes lying on the boundaries of the block elements in a vacuum.

The application of two potentials simplifies the solution and increases the accuracy of finding the integral characteristics of electromechanical systems: magnetic fluxes, inductances, forces. The latter is achieved due to the fact that these characteristics are the result of a differentiation potential in the direction tangent to the boundaries of the ferromagnetic bodies.

The described method can be developed in the three-dimensional case if canonical shapes (ball, a box, etc.) is

used the block elements. These shapes has to have an analytic representation of the solution for a given change in the potential on the boundary. The solution of the problem is reduced to solving the system of equations in this case. It follows from the boundary conditions, written in an approximate or weak forms.

Acknowledgement

This work is in part funded the Ministry of Education and Science of the Russian Federation within the public task for Research and Development, application code number 2819.

References

- [1] U. Pahner, R. Meztens, R. Belmans, K. Hameyez, A parametrica finite element environment tuned for numerical optimization, *IEEE Transaction on Magnetics*. 34(5) (1998) 2936–2939.
- [2] W. Rachowicz, L. Demkowiez, An hp-adaptive finite element method for electromagnetic, Part: A3-D implementation, *Int. T. Numer, Methods Eng*. 53(1) (2002) 147–180.
- [3] E. Vassent, G. Meunier, A. Foggia, Simulation of induction machines-using complex magnetodynamic finite element method coupled with the circuit equations, *IEEE Transactions on Magnetics*. 27(5) (1991) 4246–4249.
- [4] T. Hromadko, C. Lai, *The Complex variable boundary element method in engineering analysis*, Springer Vergas, New York, 1987.



International Conference on Industrial Engineering

Modern aspects of technological processes modeling to meet the challenges of increasing energy and resource efficiency of food production

Kretova Y.I.^{a*}

^aSouth Ural State University, 76, Lenin Avenue, Chelyabinsk, 454080, Russian Federation

Abstract

Improving energy and resource efficiency of food production technological processes, particularly the processing of raw agricultural materials, based on the use of modern physical methods, is presently one of the directions of food and processing industry development in Russia. Successful implementation of knowledge-based approaches and innovative solutions in this field is a guarantee of sustainable development of food and processing industry. Simulation is a key tool in solving this problem. The construction of adequate mathematical models of technological processes based on fundamental principles for developing a set of qualitative and functional characteristics of plant origin raw materials allows you to create differentiated technologies of processing and storage to ensure consistent quality, storage capacity and minimize losses of the target product. Using mathematical models we defined the next task as to organize the production of food grain-based target quality when using grain raw materials with predictable consumer characteristics at a certain level. We have investigated the processing of barley grain brewing by electrophysical effects and optimum parameters of this impact: the heating rate of 0.4 °C/s and the exposure processing 90 C; the heating rate from 0.4 to 0.8 °C/s and the exposure processing from 30 to 60 C; heating rate of 0.6 to 0.8 °C/s and the exposure processing from 30 to 45 s; heating rate of 0.6 to 0.8 °C/s and the exposure processing from 60 to 90 s. The values of these parameters allowed us to obtain stable disinfecting effect of saving, and for some indicators – improving malting grain quality of barley. Overall, it can be noted that electrical effects can reduce energy consumption, along with efficient contributes to the destruction of the grain pathogenic microflora of various etiologies, to ensure the safety of the protein complex, the quantity and quality of starch in barley, as well as improve the whole complex of physical and chemical parameters that determine malting quality of barley, and, most importantly, allows obtaining environmentally safe products.

© 2015 The Authors. Published by Elsevier Ltd. This is an open access article under the CC BY-NC-ND license (<http://creativecommons.org/licenses/by-nc-nd/4.0/>).

Peer-review under responsibility of the organizing committee of the International Conference on Industrial Engineering (ICIE-2015)

* Corresponding author.

E-mail address: kretova555@mail.ru

Keywords: optimization of technological processes; mathematical model; quality and safety of grain raw materials; energy and resource saving technologies, environmental safety.

1. Introduction

The decision of the majority of scientific and engineering tasks associated with the design and optimization of technological processes of production, forecasting of development of processes in time, based on mathematical modeling [1,2,3].

Mathematical modeling in solving the problem of increasing energy and resource efficiency of food production primarily involves obtaining mathematical models of the studied processes accurately and adequately describe them [4,5,6].

The construction of such models enables further research of the process of food production on the basis of his analysis of mathematical models, which greatly reduces material and human resources to address specific tasks – food manufacturing grain-based target quality when using grain raw materials with predictable consumer characteristics a certain level.

Thus, to solve the problem of increasing energy and resource efficiency of food production, using methods of mathematical modeling, we have investigated the processing of barley grain brewing by electrophysical effects and optimum parameters of this impact, which yielded grain a given level of quality.

2. Relevance, the scientific importance of the question with a brief review of the literature

Today sharply there is a question about the environmental safety of the grain food commodity. Every year increasingly deteriorating health of the population and the process of depopulation due to high mortality rates [7,8].

In this regard, a priority in the food industry is providing the population of Russia high quality and ecologically safe food products. Food security of the population and the sustainability of food products are one of the most important criteria of their socio-economic well-being [9].

Considering that food security is a critical component of national security of the population; recognizing that Russia's dependence on foreign producers of food products and agricultural raw materials makes it vulnerable because of the possibility of penetration into the domestic market of low-quality products, we note that at present this problem is very actual, especially in adverse environmental conditions of the human environment [10].

Grain resources are the basis of food security of Russia. Grain of various crops used in milling, bakery, confectionery, pasta, cereal industry, in addition, grain is the raw material for starch, beer and soft drinks, alcohol, oil and other industries [11].

The main task in the production of food grain-based is the most complete preservation of the useful natural properties of the grain, therefore, timely monitoring of its quality at the stages of reception, storage and processing are crucial. The quality of grain and products of its processing are characterized by a set of technological, biological, physical, chemical and consumer properties that contribute to its suitability for intended use. Maintaining a certain level of grain quality continues to remain a challenge: the crops are affected by microorganisms in the process of vegetation and maturation; during harvesting, transportation, storage of grain germs remain, only their quantitative and qualitative composition gradually changes [12,13].

Microorganisms are the most physiologically active part of such geo-ecological system, as the grain mass. Years of studies have shown that the leading role in the deterioration and spoilage of grain, even at short-term storage, is played by microorganisms, primarily filamentous fungi. Exactly filamentous fungi, which has a powerful enzyme aid, contribute to the loss of dry matter, the deterioration of the nutritional and technological qualities of the grain during storage. For this reason, grain party may become unsuitable for food production, which may entail large losses [12].

The products of vital activity of microorganisms not only reduce palatability of products, but also can give people food poisoning, goiter, allergic reactions, aseptic angina and other serious diseases. Many species of filamentous

fungi may develop in the product during its storage even at low temperatures, forming toxic products of metabolism [12].

It is therefore necessary to carry out activities aimed at the reduction of microbial contamination. This can be achieved through the use of highly effective and ecologically safe methods.

3. Statement of the problem

To optimize the technological process of production of food grain-based certain level of quality based on the formation of the fundamental principles of developing a set of qualitative and functional characteristics of vegetable raw materials for the creation of differentiated technologies for its processing and storage to ensure consistent quality, storage capacity and minimize losses of the target product, using innovative technological methods and modern methods of mathematical modeling.

4. The theoretical part

Traditional methods such as grain cleaning from impurities; heat treatment at a temperature of 40-50 °C; storage in a refrigerated state with the moisture content of the grain to 15.5 %; dielectric fractionation; sound processing; chemical preservation; the use of enzyme preparations, antibiotics; exposure to ultrasound, infrared radiation, α -, β -, γ -rays, etc., with varying degrees of satisfaction were adequate, but not always able to provide environmentally friendly products [14,15,16,17].

Today effective is environmentally safe decontamination of grain energy of the electromagnetic field of ultrahigh frequency. The novelty of this method is confirmed by the patent of the Russian Federation [18].

5. Practical significance

Two patents of the Russian Federation: No. 2283861 (2005) and No. 2292164 (2005) [18,22]. The results of researches of influence of modes of electrophysical effects on fungal microflora of grain produce an environmentally friendly product, improve quality and improve technological properties of grain and products of its processing. The results of experiments and research methodology used in the educational process of the Department of equipment and technologies for food production, South Ural state University, and also at the course and degree designing.

6. The results of experimental studies

With the aim of creating effective technologies that improve the quality of food is grain-based, was conducted a complex of studies on the question of the degree of influence of electrophysical influence on the number of fungus infection on grain quality indicators, defined and effective modes of this impact.

During the experiment, the methodology of active planning, according to which was chosen as the experiment plan Kono-2, which allows to study the influence of two factors: the exposure treatment and heating rate on microbiological and technological characteristics of grain of barley. The experimental setup consisted of 10 options, including one control, for control (option 10) was taken as a sample of barley grain, which is not subjected electrophysical effects.

Table 1 presents the experimental data of the research of the degree of influence of electrophysical effects on phytopathogenic complex and technological parameters of grain quality of malting barley.

The adequacy of the obtained equations was assessed by the Fisher test. Two-factor design of experiments allowed to establish the optimal range of temperature of heating of the product – 58–60 °C, which gives the effect of disinfection and bacterial filamentous microorganisms, while maintaining the viability of the grain.

Mathematical modeling of processes allowed to establish laws associated with purposeful management of the studied process by changing input parameters, and to examine the degree of influence of these parameters on the technological properties of the object, thereby to obtain a finished product of the required quality level.

So defined two modes of electrophysical influence in which there is a maximum disinfecting effect and maintained the viability of barley grain: option 1 – the heating rate of 0.4 °C/s and the exposure processing with 90; option 2 – the heating rate of 0.6–0.8 °C/s and the exposure processing, 30–45 s.

The effectiveness of disinfection was compared with indicators of the biochemical composition of barley grain [14].

Table 1. These studies of the influence of the energy field of ultrahigh frequency on phytopathogenic complex and indicators of quality of grain of malting barley.

Number options	The heating temperature, [°C]	The infestation of fungal infection [%]					The energy of germination [%]	The protein content, [%]	The starch content, [%]	Extract, [%]
		p. Aspergillus	p. Alternaria	p. Penicillium	p. Fusarium	p. Mucor				
1	78	0	0	0	0	18	0	7.15	38.8	74.0
2	35	0	14	7	3	20	88	8.15	44.8	73.9
3	52	0	19	10	2	30	71	7.65	42.4	73.0
4	30	93	37	8	5	35	89	7.8	52.0	72.3
5	63	0	2	0	0	23	13	7.4	35.2	75.8
6	33	13	41	10	1	26	86	7.8	45.4	72.6
7	62	0	0	0	0	12	38	7.15	25.6	73.8
8	48	37	44	8	3	25	72	8.4	49.6	72.6
9	55	0	14	5	1	14	67	7.4	44.8	75.8
10	23	100	31	21	6	49	80	8.4	52.0	72.4

Statistical processing of experimental data, regression and ANOVA allowed us to obtain an adequate mathematical model in the form of regression equations of the second order (1) – (10) [19,20]:

$$\hat{y}_1 = 54,9 + 16,2 \cdot x_1 + 7,5 \cdot x_2 - 6,6 \cdot x_1^2 + 5,4 \cdot x_1 \cdot x_2, \quad (1)$$

$$\hat{y}_2 = 55,2 - 5,2x_1 - 4,8x_2 - 1,3x_1x_2 - 45,2x_2^2; \quad (2)$$

$$\hat{y}_3 = 8,7 - 7,4x_1 - 13,1x_2 + 1,1x_1x_2 + 2,9x_1^2 + 3,8x_2^2; \quad (3)$$

$$\hat{y}_4 = 4,4 - 2x_1 - 1,6x_2 + 0,8x_1x_2 - x_1^2 - 1,5x_2^2; \quad (4)$$

$$\hat{y}_5 = 2,9 - 1,1x_1 - 1,2x_2 - 1,6x_2^2; \quad (5)$$

$$\hat{y}_6 = 15 - 1,6x_1 - 6,7x_2 + 8,6x_1^2 + 2,3x_2^2; \quad (6)$$

$$\hat{y}_7 = 56,3 - 29,8x_1 - 18,1x_2 - 17,5x_1x_2 - 1,5x_1^2 + 4,5x_2^2; \quad (7)$$

$$\hat{y}_8 = 7,5 - 0,3x_1 - 0,2x_2 - 0,2x_1x_2 + 0,03x_1^2 + 0,2x_2^2; \quad (8)$$

$$\hat{y}_9 = 39,7 - 4,3x_1 - 5,8x_2 + 0,9x_1x_2 + 3,3x_1^2 + 0,4x_2^2; \quad (9)$$

$$\hat{y}_{10} = 75,0 + 0,69x_1 + 0,62x_2 - 0,14x_1x_2 - 0,45x_1^2 - 1,45x_2^2 \tag{10}$$

where \hat{y}_1 – the heating temperature, [°C]; $\hat{y}_2 - \hat{y}_6$ – infestation by fungi p. *Alternaria*, p. *Fusarium*, p. *Penicillium*, p. *Aspergillus*, p. *Mucor*, [%], accordingly; \hat{y}_7 – the energy of germination, [%]; \hat{y}_8 – the protein content, [%]; \hat{y}_9 – the starch content, [%]; \hat{y}_{10} – extract, [%].

In the course of the investigation it was determined that the content of total nitrogen (Fig. 1) slightly decreases with consideration of temperature effects (1.29±0,4) %, which determines the subsequent decrease of the mass fraction of protein in the grain to (8.12±0,4) %.

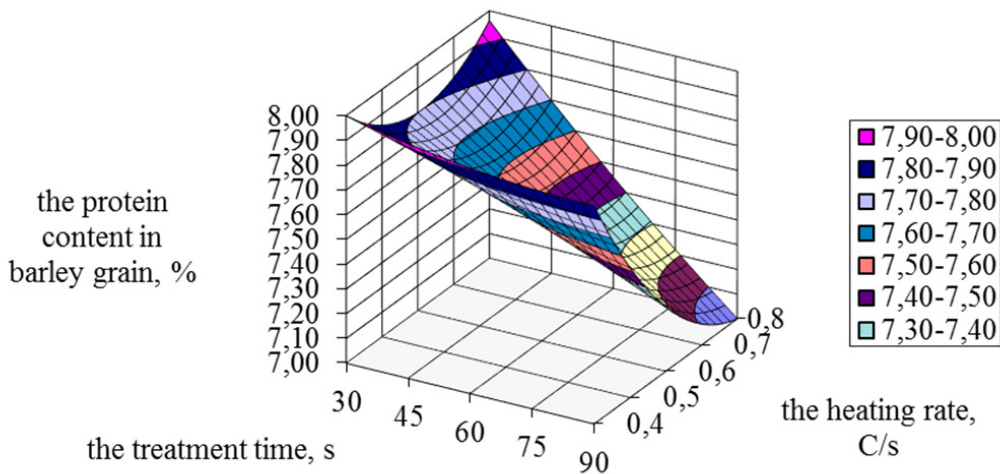


Fig. 1. Mathematical model of the proces of electrophysical effects on grain protein content of malting barley, [%].

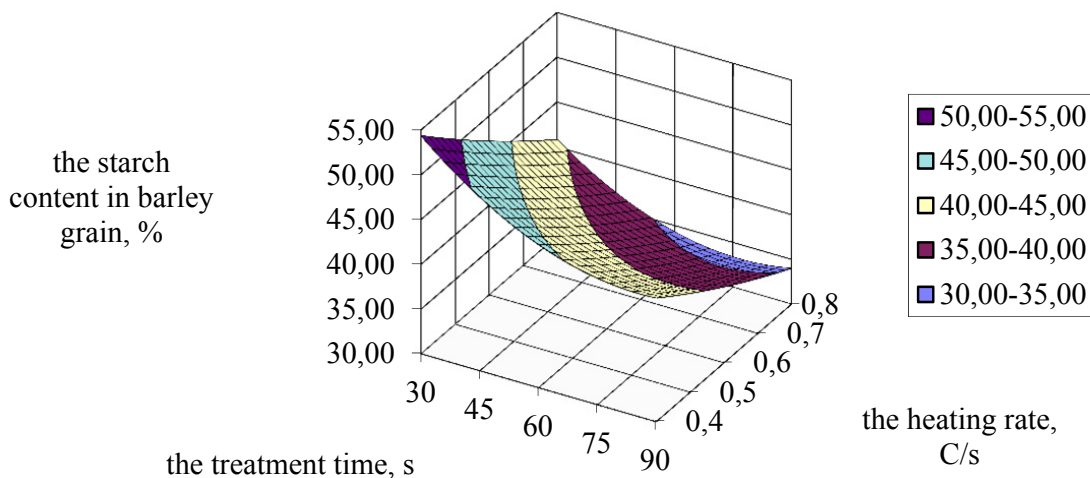


Fig. 2. Mathematical model of the process of electrophysical influence on the content of starch in barley grain brewing, [%].

A slight decrease in protein content provides the ability to get beer, more resistant to the formation of turbidity. The most effective will be the next mode of action: heating rate from 0.4 to 0.8 °C/s and the exposure processing

from 30 to 60 s.

The brewing properties of barley are defined in the same amount of starch and structure, the ratio of large and small starch grains. Usually, the more barley contains starch, the higher the yield of the extract, the difference between the content of starch in barley and its extract is in the range of 10–20 % [15].

Under the influence of microwave field is observed some changes in the carbohydrate fraction by raising the temperature. The change of starch under the influence of microwave field is presented in Figure 2.

Processing of experimental data has allowed to establish effective exposure field of ultrahigh frequency, which is heated to 55 grain 63 °C and simultaneously stimulated the hydrolysis of starch, increases the amount of extractives, namely: the heating rate of 0.6 to 0.8 °C/s and the exposure processing from 60 to 90 s.

7. Conclusions

Treatment of the grain field of ultrahigh frequency heating rate of 0.6 to 0.8 °C/s and the exposure processing from 60 to 90 C causes the disinfectant effect for almost all types of fungus infection, the heating temperature of grain in this case is from 60 to 70 °C.

As a result of electrophysical influence changes the biochemical composition of barley grain. Effective you should consider modes with a heating rate of 0.4 to 0.8 °C/s, the exposure processing from 30 to 60 sec and a temperature of from 30 to 64 °C, and the modes at a heating rate of 0.6 to 0.8 °C/s, the exposure processing from 60 to 90 C, a temperature of 32 to 77 °C, at which stored the technological parameters of grain, namely, increases the vigour 1.1 times; reduced content of proteins 1.1–1.2 times; decreases the starch content of 1.1–1.2 times; increases the extract of barley grains brewing in 1,02–1.1 times.

Thus, a detailed analysis of the technological process of processing of grain raw materials by means of mathematical modeling allowed us to determine the optimal parameters of the flow of the process and to obtain products with desired characteristics, thereby the products of a certain level of quality.

References

- [1] N.V. Golubev, *Mathematical modeling of systems and processes*, Saint-Petersburg, 2013.
- [2] V.I. Dudorin, *Modeling in problems of production management*, Moscow, 1980.
- [3] R.V. Pan, *Statistical methods for modeling and optimization of processes pulp and paper production*, Krasnoyarsk, 1982.
- [4] I.T. Kretov, A.A. Shevtsov, *Optimization of the process of drying malt by methods of mathematical modeling*, *Izvestiya vuzov, food technology*. 1–2 (1994) 39–42.
- [5] S.A. Shevtsov, S.V. Kutsov, E.A. Ostrikov, *Mathematical modeling of the process of roasting oats superheated steam*, *Bulletin of the Russian Academy of agricultural Sciences*. 3 (2008) 10–12.
- [6] G.V. Alekseev, B.A. Voronenko, N. Lukin, *Mathematical methods in food engineering*, St. Petersburg, 2012.
- [7] A.A. Kudryasheva, *Physical and food security: criteria, categories*, *Bioregulation facilities, Food processing*. 10 (2004) 10–14.
- [8] H.P. Lviv, O.N. Kislenco, *The problems of ecological safety of grain*, *Cereals*. 5 (2004) 38–41.
- [9] *Strategy of development of food and processing industry of Russia for the period up to 2020*, the Government decree of the Russian Federation. 559–R (2012).
- [10] *Fundamentals of state policy of the Russian Federation in the field of healthy nutrition of the population for the period till 2020*, the Government decree of the Russian Federation. 1873–p (2010).
- [11] T.V. Meledina, *Raw and auxiliary materials in brewing*, St. Petersburg, 2003.
- [12] V. Kartsev, L.V. Belov, V.P. Ivanov, *Sanitary Microbiology of food*, St. Petersburg, 2000.
- [13] M.K. Koishibaev, *Cereal crop Diseases*, Almaty, 2002.
- [14] T.P. Kulebakina, K.A. Kalwant, A.I. Garden, *Microflora of barley and its impact on the quality of malt and beer, brewing and soft drinks industry*. 10 (1982).
- [15] V. Kunze, G. Mit, *Technology of brewing and malting*, Tr., St. Petersburg, 2008.
- [16] E.P. Zarubin, S.F. Danko, T.N. Danilchuk, *The Influence of frequency of alternating current on solidarista barley*, *Beer and drinks*. 4 (2003) 14–15.
- [17] K.V. Puchkov, *Application elettromagnetico field of ultrahigh frequency in food processing industry*, *Bulletin of the Council*. (2002) 40–41.
- [18] Y.I. Kretova, G.I. Cuglenok, N.In. Cuglenok, RF Patent 2,283,861. (2005)
- [19] Y.V. Vasil'kov, N.N. Vasilkov, *Computer technology computing in mathematical modeling*, Moscow, 2002.
- [20] A.N. Tikhonov, M.V. Ufimtsev, *Statistical processing of results of experiments*, Moscow, 1988.
- [21] V.P. Taras, *Mathematical modeling of technical systems*, Minsk, 2013.
- [22] E.I. Cherkasova, Yu.I. Kretova, G.I. Cuglenok, N.In. Cuglenok, G.G. Usenova, RF Patent 2,292,164. (2005)



International Conference on Industrial Engineering

8×8 wheeled vehicle modeling in a multibody dynamics simulation software

Gorelov V.A.^{a*}, Komissarov A.I.^a, Miroshnichenko A.V.^c

^a *Bauman Moscow State Technical University, ul. 2-ya Baumanskaya 5, Moscow, 105005 Russian Federation*

^b *OKB "Tekhnika", ul. Novaya Zarya.6, Moscow, 115191 Russian Federation*

Abstract

The article describes a three-dimensional non-linear dynamic model of a 8×8 wheeled vehicle. The authors used the "Universal Mechanism" MBS software to build the model. The article also presents a tire – rigid terrain interaction model built in Matlab/Simulink. The authors tested the process of linking a Matlab/Simulink DLL to the vehicle MBS model. The authors used the developed model to analyze the wheeled vehicle dynamic behavior at different operation conditions. The article contains the results of the lane change test simulation. The simulation results confirmed the validity of the model. The developed model allows the estimation of the wheeled vehicle dynamic behavior at various operation conditions at the design stage.

© 2015 The Authors. Published by Elsevier Ltd. This is an open access article under the CC BY-NC-ND license (<http://creativecommons.org/licenses/by-nc-nd/4.0/>).

Peer-review under responsibility of the organizing committee of the International Conference on Industrial Engineering (ICIE-2015)

Keywords: vehicle dynamics; simulation; tire model; multibody dynamics simulation software.

Introduction

Reliable estimation of the wheeled vehicles main operation characteristics at the design stage needs development of three-dimensional dynamical models describing suspension and steering gear kinematics. The number of bodies in the models of multi-axle wheeled vehicles can amount to several dozen which makes the analytical deriving of equations of motions extremely complicated. The multibody dynamics simulation (MBS) software is an effective tool for solution of this sort of problems [1, 2, 3, 4, 5]. In the MBS software, the user describes the mechanical system as a set of rigid bodies, joints, and force interactions from the library of standard elements, and the software generates the equations of motion automatically and provides built-in means for their numerical solution. Besides, most of the MBS software packages allow linking user models of the force interactions as DLLs.

*Corresponding author.

E-mail address: gvas@mail.ru

This article deals with the problem of building the dynamical model for calculation of the main operation characteristics of a multi-axle wheeled vehicle in the MBS software package “Universal Mechanism” and linking the Matlab/Simulink tire – rigid terrain interaction model developed for this purpose to the MBS model.

1. Wheeled Vehicle Model

The subject of the research is a 8x8 wheeled vehicle having mass 36 t, two steerable axles and a hydropneumatic double wishbone independent suspension for all wheels. The vehicle model consists of the subsystems shown in Fig. 1. Models of the braking system and power train system are included into the model of the assembled vehicle.

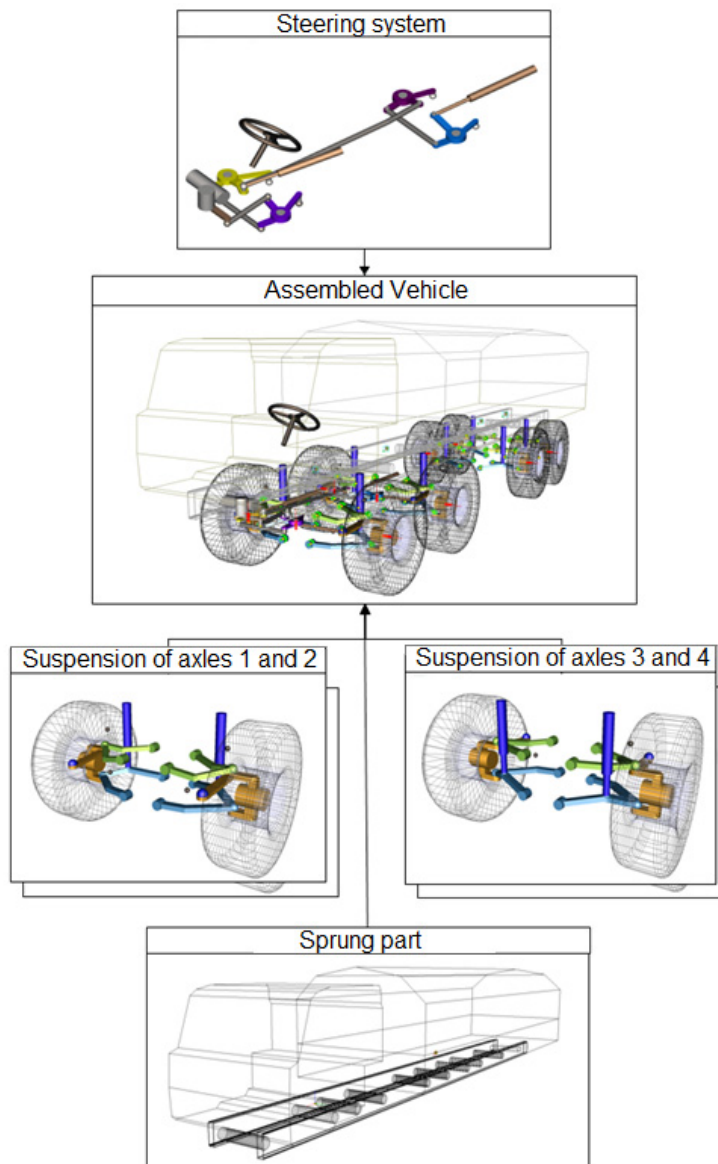


Fig. 1. Structure of the 8x8 wheeled vehicle model.

The sprung mass model consists of a massless geometry model and a mass-inertial model presented by the point mass and tensor of inertia.

Suspension and steering linkages are modeled as a set of rigid bodies connected by ideal joints and force elements. Masses of the suspension and steering system bodies are input as the model parameters and inertia are calculated from the geometry models.

The hydropneumatic spring is modeled as a system of spring and damper coupled in parallel and having tabular characteristics. There are no hydraulic connections between the hydraulic cylinders of the suspension.

The braking system model distributes the total braking torque generated according to the control signal of the braking system between the wheels of the vehicle by the selected scheme. The power train model distributes the engine output torque generated according to the control signal of the power train system equally between the wheels of the vehicle, which corresponds to the drive train with open differentials for all axles. For simulations of different tests we used two different power train models. For the tests which require maintaining constant vehicle velocity we created the variant with the engine having a constant output power and a constant gear ratio of the transmission. For analysis of the dynamics of the vehicle acceleration we built the powertrain model with analytical description of the external characteristic of the internal combustion engine and a variable gear ratio of the power train.

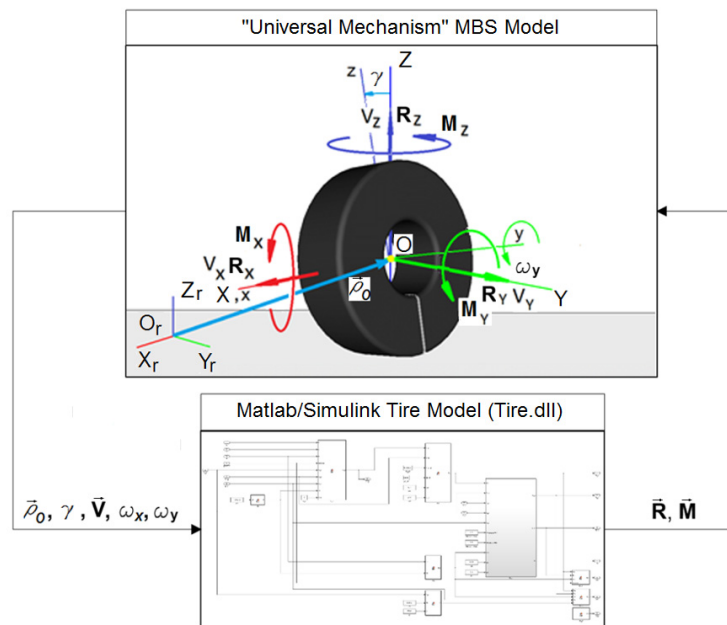


Fig. 2. Interaction of the "Universal Mechanism" MBS model and the Matlab/Simulink tire model.

2. Tire-Road Interaction Model

Road reaction forces and moments acting on the wheel are calculated by the tire model created in Matlab/Simulink and compiled as the DLL module Tire.dll. The schematic diagram of the interaction between the tire model and the "Universal Mechanism" model of the wheel dynamics is shown in Fig. 2.

The MBS model of the wheel dynamics transmits kinematic parameters of the wheel to the tire model. On the base of these parameters the tire model calculates the forces and moments acting on wheel and send them to the wheel dynamics model. The models use the following coordinate systems (see Fig. 2):

wheel stability coordinate system (SCS) $OXYZ$ – a movable coordinate system whose origin is at the wheel center, Z axis is perpendicular to the road plane, X axis is perpendicular to the wheel rotation axis;

road fixed coordinate system (FCS) $O_r X_r Y_r Z_r$ – an orthogonal coordinate system fixed on the road.

The transmitted parameters include the following: projections of the wheel center radius vector \vec{r}_O onto the axes of the FCS, projections V_X, V_Y, V_Z of the wheel center velocity onto the wheel SCS axes, projections ω_x, ω_y of the wheel rotation velocity onto the wheel coordinate system axes, and wheel camber angle γ .

Schematic diagram of the tire – rigid terrain interaction model is shown in Fig. 3.

The vertical reaction is calculated by the visco-elastic model:

$$R_z = P_{z_st} \cdot \left(\frac{h_z}{h_{z_st}} \right)^{1.5} - b_z \cdot V_z, \tag{1}$$

here P_{z_st} – static wheel load, h_{z_st} – tire static deflection; b_z – vertical visco-elastic resistance force coefficient ; h_z – tire normal deflection:

$$h_z = \min(0, r_0 \cdot \cos(\gamma) - r_l), \tag{2}$$

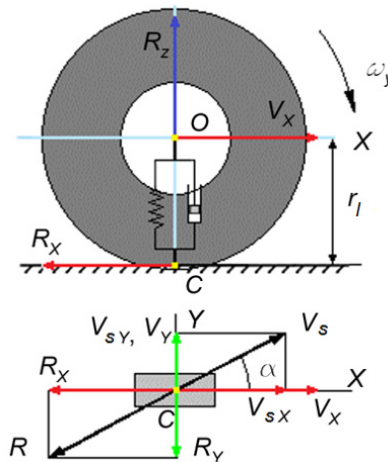


Fig. 3. Tire – road interaction model.

here r_0 – unloaded tire radius; r_l – loaded tire radius which is the projection of the wheel center radius vector onto the vertical axis of the road FCS.

The reaction in the road plane can be calculated by the following equation [6, 7]:

$$R = \mu_s(S_k) \cdot R_z, \tag{3}$$

here S_k – tire slip; $\mu_s(S_k)$ – tire – terrain interaction coefficient.

For the cohesive soils the following equation for $\mu_s(S_k)$ can be applied [8, 9]:

$$\mu_s(S_k) = \mu_{s\alpha \max} \cdot \left(1 - e^{-\frac{S_k}{S_0}} \right) \cdot \left(1 + e^{-\frac{S_k}{S_1}} \right), \tag{4}$$

here S_0, S_1 – constant parameters of the curve shape; $\mu_{s\alpha \max}$ – coefficient of the tire – terrain interaction at complete slip:

$$\mu_{s\alpha \max} = \frac{\mu_{sx \max} \cdot \mu_{sy \max}}{\sqrt{\mu_{sx \max}^2 \cdot \sin^2 \alpha + \mu_{sy \max}^2 \cdot \cos^2 \alpha}}, \quad (5)$$

here $\mu_{sx \max}$, $\mu_{sy \max}$ – friction ellipse parameters (see Fig. 4).

Coefficient S_k is calculated as:

$$S_k = \frac{V_s}{\omega_y \cdot r_e}, \quad (6)$$

here r_e – free rolling tire radius which can be approximately calculated by the following equation [10]:

$$r_e = \frac{3 \cdot r_l}{1 + \frac{2 \cdot r_l}{r_e}}; \quad (7)$$

V_s – sliding velocity defined as:

$$\begin{aligned} V_s &= \sqrt{V_{sX}^2 + V_{sY}^2} \\ V_{sY} &= V_Y - \omega_x \cdot r_l; \\ V_{sX} &= V_X - \omega_y \cdot r_e. \end{aligned} \quad (8)$$

The tire – terrain interaction force vector \vec{R} is opposite to the slip velocity vector \vec{V}_{ck} . Angle α between the slide velocity vector and the wheel SSC X axis can be found from the following equations:

$$\begin{aligned} \sin \alpha &= \frac{V_{ckY}}{V_{ck}}; \\ \cos \alpha &= \frac{V_{ckX}}{V_{ck}}; \end{aligned} \quad (9)$$

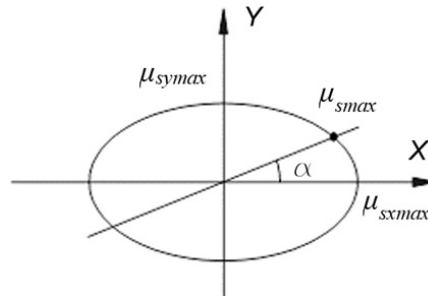


Fig. 4. Friction ellipse.

The projections of the tire – terrain interaction force in the road plane are calculated in the following way:

$$R_X = -R \cdot \cos \alpha; \quad R_Y = -R \cdot \sin \alpha. \quad (10)$$

The moments acting on the wheel:

$$\begin{aligned} M_X &= R_Y \cdot r_l - R_Z \cdot r_l \cdot \frac{\sin(\gamma)}{\cos(\gamma)}; \\ M_Y &= -R_X \cdot r_e + M_f; \\ M_Z &= 0; \end{aligned} \quad (11)$$

here M_f – tire rolling resistance torque:

$$M_f = -R_z \cdot r_e \cdot f \cdot \text{sign}(\omega_y), \quad (12)$$

here f – tire rolling resistance coefficient:

$$f = f_0 + k_f \cdot (V_x)^2, \quad (13)$$

here f_0 – tire rolling resistance at low speed (about 5 km/h), k_f – tire rolling resistance growth factor describing increase in the rolling resistance with the growth of the forward velocity.

3. Vehicle model testing

The authors tested the model by performing simulations of the vehicle motion at different operation conditions.

Figures 5a –5b show the time histories of the vehicle motion parameters obtained during simulation of the lane change test performed within 20 m interval according to the standard [11] at the speed 40 km/h, the maximum attainable speed at which there is no wheel lift-off. Fig. 5 shows snap shots of the characteristic positions of the vehicle.

The maximum velocity is rather low for a vehicle of this class. This can be explained by the fact that the vehicle is not equipped with antiroll bars and there are no hydraulic links between the cylinders of the hydropneumatic suspension. Considerable roll of the sprung mass during the maneuver (see Fig. 6a) implicitly confirms this conclusion.

The obtained results of the lane change test simulation confirm validity of the model.

Conclusion

The “Universal mechanism” MBS software allowed to build a spatial non-linear dynamical model of the multi-axle wheeled vehicle and to link it to the Matlab/Simulink tire – terrain interaction model compiled into a DLL module.

The developed model can provide estimation of the vehicle handling and stability as well as the vehicle dynamics at acceleration and braking at the early design stage before the production of the first prototypes.

The research was funded by the Russian Ministry of Education as a part of the contract between KAMAZ and Bauman Moscow State Technical University.

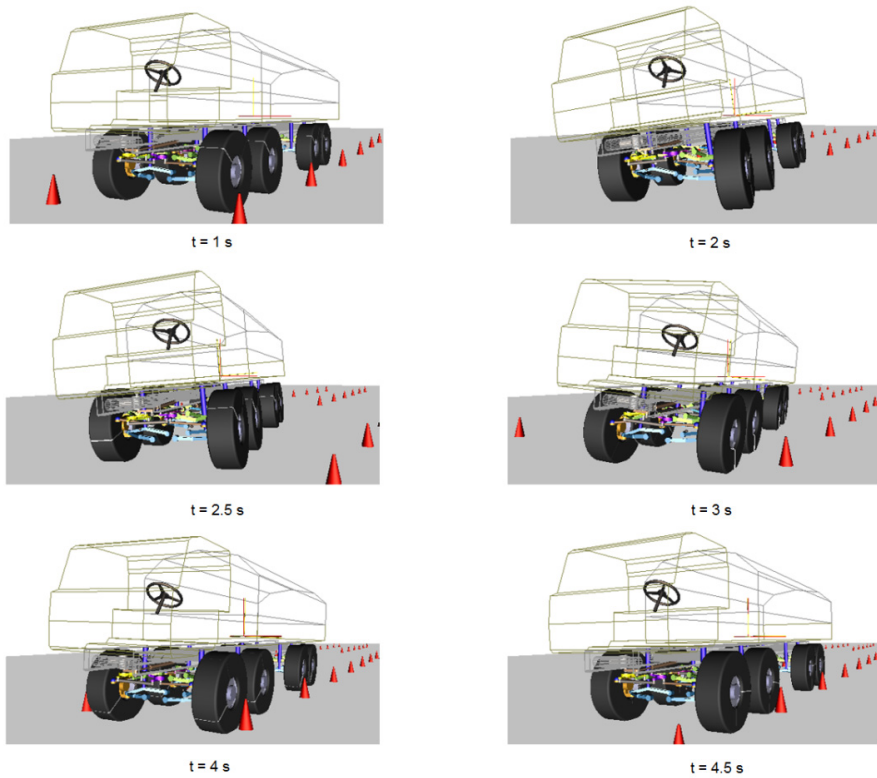


Fig. 5. Snap shots of the vehicle motion obtained during simulation of the lane change within the 20 m interval at speed 40 km/h.

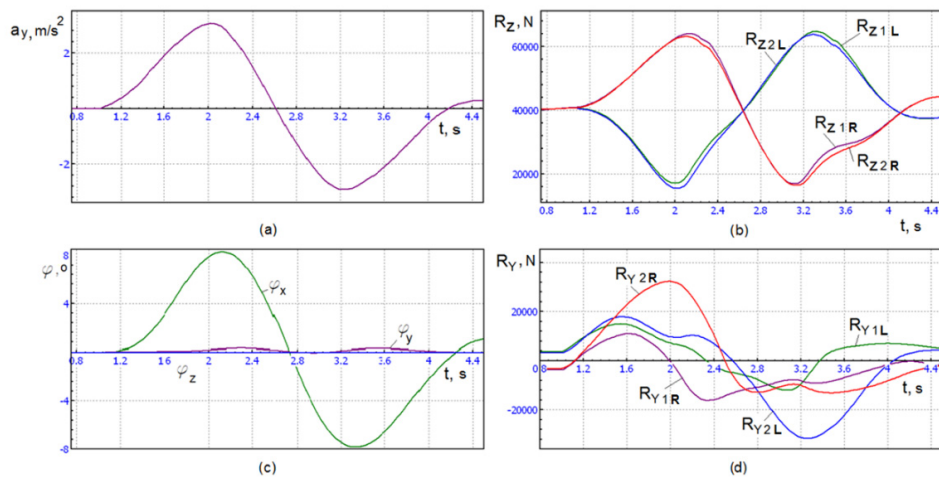


Fig. 6. Time histories of the parameters of the vehicle motion obtained during simulation of the lane change within the 20 m interval at speed 40 km/h:

(a) lateral acceleration of the sprung mass center of gravity; (b) vertical reactions of the tires of the steerable wheels (L –left side wheels; R –right side wheels);(c) roll, yaw and pitch angles of the sprung mass; (d) lateral reactions of the tires of the steerable wheels (L –left side wheels; R –right side wheels).

References

- [1] M. Blundell, D. Harty, *The Multibody Systems Approach to Vehicle Dynamics*. Oxford: Elsevier Butterworth-Heinemann, 2004.
- [2] Information on <http://www.umlub.ru>
- [3] Information on <http://www.euler.ru>
- [4] Information on <http://www.simpack.com>
- [5] Information on <http://www.mscsoftware.com/product/adams>
- [6] Yu.L. Rozhdestvenskiy, K.Yu. Mashkov, Generation of the reaction forces in a flexible wheel rolling on the rigid road [O formirovani reaktiv pri kachenii uprugogo koleasa po nedeformiruemomu osnovaniyu], *BMSTU proceedings*. 390 (1982) 56–64.
- [7] A.B. Dik, *Raschet statsionarnykh i nestatsionarnykh kharakteristik tormozyashchego koleasa pri dvizhenii s uvodom*, Ph.D. thesis. Omsk, 1988.
- [8] S.M. Marokhin, G.O. Kotiev, A.A. Ergin, Predicting characteristics of the curvilinear motion of a special-purpose vehicle performing standard maneuvers which correspond to the real-life handling and stability tests, *Izvestiya Akademii inzhenernykh nauk RF im. akad. A.M. Prokhorova, Transportno-tehnologicheskie mashiny i komplekсы*. 5 (2003) 26–35.
- [9] S.M. Marokhin, Predicting mobility characteristics of a special-purpose vehicle equipped with active safety systems. [Prognozirovanie kharakteristik podvizhnosti spetsavtomobilya, osnashchennogo sistemami aktivnoy bezopasnosti: avtoref. diss. kand. tekhn. nauk], Ph.D. thesis abstract. Moscow, 2005.
- [10] G.A. Smirnov, *Teoriya dvizheniya kolesnykh mashin: ucheb. dlya vuzov. – 2-e izd., pererab. i dop*, Mashinostroenie, Moscow, 1990.
- [11] Russian State Standard 31507-2012. Road vehicles. Handling and stability. Technical requirements. Test methods.



International Conference on Industrial Engineering

Simulation of electrical circuits using conjugate gradient algorithm

Burtsev Y.A.*

Platov South-Russian State Polytechnic University (NPI), 132, St. Prosvescheniya, Rostov region, Novocherkassk, 346428, Russian Federation

Abstract

Problems of electrical circuits' simulation are known for a long time. However, the simulation quality and speed are far from perfect, especially when it comes to non-linear circuits. The method offered is based on table form of electrical circuits' equations. Differential-algebraic equations of electrical circuits are converted to the systems of linear algebraic equations (SLAE) with finite differences method. It is important that SLAE are solved with Conjugate Gradient Algorithm (CGA) that is well adapted to systems with sparse matrixes. The solution of the SLAE at previous time step is a good initial approximation of the solution at present time step. That is why CGA reduces calculations to 20-40% of the full algorithm typically. The possibility of using CGA for solving SLAE with matrixes that have no specific sign is proved by numerical experiments. A method for acceleration of solving electrical circuits' SLAE is proposed. It differs from the Nodal Voltages Method as no apparent avatar of circuit SLAE is formed. A comparison of program "Electroscope" based on proposed method with programs "PSIM" and "Fastmean" is presented. "Electroscope" is leading in terms of quality and speed of test circuits' simulations.

© 2015 The Authors. Published by Elsevier Ltd. This is an open access article under the CC BY-NC-ND license (<http://creativecommons.org/licenses/by-nc-nd/4.0/>).

Peer-review under responsibility of the organizing committee of the International Conference on Industrial Engineering (ICIE-2015)

Keywords: Electrical circuits; simulation; table form of equations; Conjugate Gradient Algorithm; matrixes with no specific sign; simulation speed; reliability; comparing.

1. Introduction

Problems of electrical circuits simulation and methods for their solving are known for long time. However, quality and speed of existing computer programs are far from perfect, especially for nonlinear circuits. For example, it is shown in article [1] that well known programs Micro-Cap 10.8.0, Multisim 10.0.144 and PSpice 9.1 produce solutions with rough defects, and by the way work much slower than programs Electroscope, Fastmean 5.2 and

* Corresponding author. Tel.: +7-908-505-30-39.

E-mail address: proton36@yandex.ru

PSIM 9.0. That also can be said about program TINA Version 10.1.30.22 DT-DS build date 22 January 2015. As it is shown below, programs Fastmean 5.2 and PSIM 9.0 also generate solutions with defects and have not best simulation speeds. Program Micro-Cap does not allow contours of "voltage controlled elements" – ideal voltage sources or inductances, and their combinations. Programs Multisim, PSpice and Micro-Cap do not allow nodes that have no DC connection to grounded base node.

Existing programs for electrical circuit simulation cannot cover all needs of engineer calculations, because new devices often contain original components that are not provided by authors of programs. Circuits with switching and nonlinear elements and semiconductor devices which resistances vary by several orders are common in digital and power electronics. Nonlinear inductances of electrical machines that furthermore depend of the rotor rotation are also complicated circuit elements. Existing methods of circuit simulation are complicated and bulky, or they have considerable restrictions and are not universal. That is why development of new algorithms and programs that can effectively simulate electrical circuits for designing of new devices is an actual problem.

2. Simulation of Resistive Circuits

Popular practical electrical circuits' simulation methods usually are variants of the Nodal Voltages Method. However, for this method simulation of circuits with magnet coupling may have problems. Equation systems for circuits with big difference of resistances are poor conditioned.

So called table form of electrical circuits equations has some advantages [2, 3], main of them are simplicity and universality. Both voltages and potentials usually are present in the table form of equations. But voltages can be easily expressed via potentials and then they can be removed from the system. In this case an equation system of resistive circuit can be written in the form:

$$\begin{bmatrix} -\mathbf{R} & \mathbf{K}^T \\ \mathbf{K} & \mathbf{0} \end{bmatrix} \begin{bmatrix} \mathbf{i} \\ \boldsymbol{\phi} \end{bmatrix} = \begin{bmatrix} \mathbf{e} \\ \mathbf{j} \end{bmatrix}, \tag{1}$$

where \mathbf{R} is diagonal matrix of branch resistances; \mathbf{K} is incidence matrix without string and column that correspond to basic node with zero potential; $\mathbf{0}$ is zero submatrix, \mathbf{i} is vector of branch currents, $\boldsymbol{\phi}$ is vector of node potentials; \mathbf{e} is vector of EMF (electromotive force) sources; \mathbf{j} is vector of current sources. Let us denote \mathbf{A} matrix of the system (1).

For example, for the circuit shown at Fig. 1, the system (1) will have such appearance:

$$\begin{bmatrix} 0 & 0 & 0 & 0 & 0 & 0 & 1 & 0 & -1 & 0 \\ 0 & 0 & 0 & 0 & 0 & 0 & 0 & 1 & 0 & -1 \\ 0 & 0 & -R_1 & 0 & 0 & 0 & 0 & 0 & 1 & 0 \\ 0 & 0 & 0 & -R_2 & 0 & 0 & 1 & 0 & 0 & -1 \\ 0 & 0 & 0 & 0 & -R_3 & 0 & 1 & -1 & 0 & 0 \\ 0 & 0 & 0 & 0 & 0 & -R_4 & 0 & 1 & 0 & 0 \\ 1 & 0 & 0 & 1 & 1 & 0 & 0 & 0 & 0 & 0 \\ 0 & 1 & 0 & 0 & -1 & 1 & 0 & 0 & 0 & 0 \\ -1 & 0 & 1 & 0 & 0 & 0 & 0 & 0 & 0 & 0 \\ 0 & -1 & 0 & -1 & 0 & 0 & 0 & 0 & 0 & 0 \end{bmatrix} \begin{bmatrix} i_1 \\ i_2 \\ i_3 \\ i_4 \\ i_5 \\ i_6 \\ \phi_1 \\ \phi_2 \\ \phi_3 \\ \phi_4 \end{bmatrix} = \begin{bmatrix} e_1 \\ e_2 \\ 0 \\ 0 \\ 0 \\ 0 \\ 0 \\ j_1 \\ 0 \\ 0 \end{bmatrix}.$$

Matrix \mathbf{A} is several times larger compared with the matrix of the Node Voltage Method, but it is very sparse and does not require any calculations for its forming. Its structure is so simple that it is no need to form it in any apparent avatar in the computer memory. It is sufficient only to know for each circuit element numbers of nodes to which it is connected.

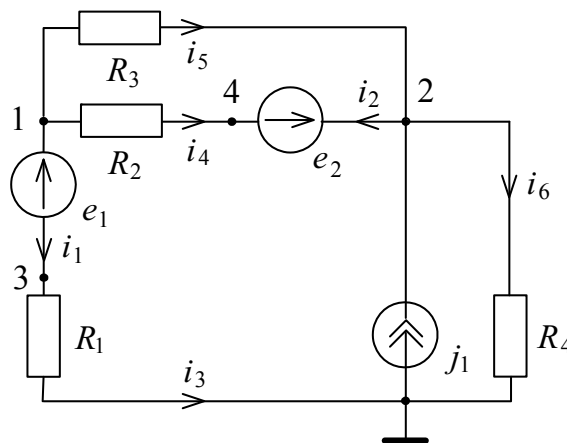


Fig. 1. Scheme of the electrical circuit.

It is principally important that structure of the matrix \mathbf{A} is suitable for use Conjugate Gradient Algorithm (CGA) [4-12], that is very effective for solving of systems of linear algebraic equations (SLAE) with sparse matrices. This algorithm does not change matrix of the SLAE, and thus it makes possible to use the sparsity completely. CGA uses multiple multiplication of vectors by matrix \mathbf{A} , and also scalar multiplications of the vectors. Multiplication of vector by matrix \mathbf{A} requires only N arithmetical multiplications and less than $4N$ additions, where N is number of circuit branches.

CGA is useful also by another reason. Voltages and currents of the electrical circuit are continuous or piecewise-continuous functions. That is why state of the circuit at previous time step usually is a good initial approximation for its state at present time step, and CGA requires little number of iterations – typically 20-40% of the matrix \mathbf{A} dimension. In addition, CGA can be easily combined with parallel calculations.

Researches [13] have shown that probability of CGA fail during solving SLAE with symmetrical matrix with no specific sign is vanishingly small, though it is not zero. Practically, only special constructing of particular case can lead CGA to fail due to critically little value of denominator ($\mathbf{A}\mathbf{s}_k, \mathbf{s}_k$) in one of the CGA formulas, here \mathbf{s}_k is "direction vector" of the CGA. But even if CGA fails, the fail can be easily and quickly detected in the computer program, for its correction it is sufficient to take another initial approximation.

Singularity of the matrix \mathbf{A} also does not prevent using CGA. This fact is proven by simulations of electrical circuits in which submatrix \mathbf{K} was full incidence matrix of the circuit graph (including all nodes), and also by simulations of the circuits that were sectioned into insulated parts (with "floating" potentials). Circuits consisting of separate parts, present one of two variants of topological degeneration. It is important that circuits at the edge of such degeneration often appear in practical computations. For example, a diode rectifier working in parallel with load and capacitor, periodically closes all of the diodes and thus separates source from the load.

Let us describe using of proposed method for simulation nonlinear circuits. Let us suppose that we have some initial approximation of branch currents and nodal potentials of the circuit. Using these values, we can calculate static resistances of nonlinear branches and insert them into the system (1). Having solved it, we get the next approximation of the currents and potentials. Then we shall continue the process until desired accuracy will be reached. This practical method of nonlinear circuit calculation is known in electrical engineering and is briefly presented, for example, in the book [14]. This method is called in mathematical literature as "method of false position", "method of linear interpolation", or "regula falsi". All currents and potentials are known at each time step. It makes possible easy using of volt-ampere characteristics of the elements either if they are presented as voltages depending on current, or as currents depending on the voltages.

This method always converged after few number of iterations, usually 1, 2 or 3, for huge number of simulations of different circuits with diodes, transistors and nonlinear inductances.

3. Simulation of Circuits with Reactive Elements

Equation systems of the electrical circuits with reactive elements are systems of differential-algebraic equations (DAE). Finite-difference method [6] makes possible to convert DAE systems into SLAE. Three-point backward differentiation formula (BDF) generally gives solutions with quite satisfactory accuracy if we do not consider such cases as long transient processes in the circuits with high reactance factor. For example, tree-point BDF of the inductance current calculated at the time moment t looks like this:

$$i'_L(t) \approx \frac{i_L(t-2\Delta t) - 4i_L(t-\Delta t) + 3i_L(t)}{2\Delta t}, \quad (2)$$

where i_L is current of the inductance, t is time, Δt is time step.

Derivation of the capacitor voltage can be obtained like formula (2). Taking into account that

$$u_C(t) = \phi_{C1}(t) - \phi_{C2}(t),$$

where u_C is voltage of the capacitor, ϕ_{C1} and ϕ_{C2} are potentials of the nodes to which the capacitor is connected, we gain:

$$\begin{aligned} u'_C(t) &\approx \frac{u_C(t-2\Delta t) - 4u_C(t-\Delta t) + 3u_C(t)}{2\Delta t} = \\ &= \frac{\phi_{C1}(t-2\Delta t) - \phi_{C2}(t-2\Delta t) - 4(\phi_{C1}(t-\Delta t) - \phi_{C2}(t-\Delta t)) + 3(\phi_{C1}(t) - \phi_{C2}(t))}{2\Delta t}. \end{aligned} \quad (3)$$

After substitution of expressions (2) and (3) into equations of inductance and capacitor respectively, we gain equations similar to the equations of resistive branches:

$$-\frac{3L}{2\Delta t}i_L(t) + \phi_{L1}(t) - \phi_{L2}(t) = \frac{L}{2\Delta t} [i_L(t-2\Delta t) - 4i_L(t-\Delta t)], \quad (4)$$

$$\begin{aligned} -\frac{2\Delta t}{3C}i_C(t) + \phi_{C1}(t) - \phi_{C2}(t) &= \\ = -\frac{1}{3} [\phi_{C1}(t-2\Delta t) - \phi_{C2}(t-2\Delta t)] + \frac{4}{3} [\phi_{C1}(t-\Delta t) - \phi_{C2}(t-\Delta t)], \end{aligned} \quad (5)$$

where L is inductance, C is capacitance, i_C is current of the capacitor, ϕ_{L1} , ϕ_{L2} are potentials of the nodes to which the inductance is connected.

Equations (4, 5) make possible to write an equation system of electrical circuit with reactive elements in form (1) for an equivalent resistive circuit, and then solve it by the CGA at each time step. The coefficients of the currents in the equations (4, 5) play role of quasi-resistances. Adding magnet couplings to the circuit inductances only makes submatrix \mathbf{R} non diagonal, but does not change something essentially.

In equations of the circuits with time-dependent (including nonlinear) reactive elements there is necessary to consider capacitances and inductances as differential parameters, calculated in some point of the charge-voltage or flux-current characteristic:

$$C = \frac{dq}{dt}, L = \frac{d\Psi}{dt}.$$

In this case there are no derivations of the parameters C and L present in the differential equations of the capacitors and inductances, the equations preserve their common form:

$$i = \frac{dq}{dt} = C \frac{du}{dt}, \quad u = \frac{d\Psi}{dt} = L \frac{di}{dt}.$$

If capacitance and inductance are considered as static parameters

$$C = \frac{q}{u}, \quad L = \frac{\Psi}{i},$$

then their derivations also must be taken into account in the equations. That makes equations too complicated with no need.

4. Acceleration of Simulation by Substitutions

If matrix \mathbf{R} is diagonal and does not contain little resistances, it can be easily inverted. In this case multiplication by the matrix \mathbf{A} that is necessary in CGA, can be done in two steps. First, we calculate fictive currents that are caused by branch voltages without sources:

$$\mathbf{i}_0 = \mathbf{R}^{-1} \mathbf{K}^T \boldsymbol{\phi}.$$

Then we substitute these currents into equations of the first Kirchhoff law and find vector

$$\boldsymbol{\phi}_0 = \mathbf{K} \mathbf{R}^{-1} \mathbf{K}^T \boldsymbol{\phi}.$$

Right part of the system (1) must be previously converted to the form

$$\left[\mathbf{0} \quad \mathbf{j} + \mathbf{K} \mathbf{R}^{-1} \mathbf{e} \right]^T.$$

That corresponds to converting EMF sources to the current sources and temporarily replacing real currents \mathbf{i} with fictive currents \mathbf{i}_0 . As a result of all these transformations, only vector of potentials $\boldsymbol{\phi}$ will be found as a solution of the SALE, and thus the number of unknown variables and the number of the SLAE equations will be reduced compared to immediately solving the system (1). Real branch currents are calculated after solving SLAE as

$$\mathbf{i} = \mathbf{R}^{-1} (\mathbf{K}^T \boldsymbol{\phi} + \mathbf{e}).$$

Described procedure gives a method of multiplication of vector $\boldsymbol{\phi}$ by matrix of the Node Voltages Method equation system that looks like

$$\mathbf{K} \mathbf{R}^{-1} \mathbf{K}^T \boldsymbol{\phi} = \mathbf{j} + \mathbf{K} \mathbf{R}^{-1} \mathbf{e}.$$

Such multiplication is useful for solving this system by the CGA. The difference between the proposed procedure and the Node Voltages Method is not calculating the SLAE matrix in any apparent form. That considerably reduces

calculations and simulation time. A variant of such substitutions for circuits with very little and zero resistances, and also with magnet coupling is developed and successfully tested.

Besides that, simulation time can be reduced by eliminating of branches that consist only of ideal EMF sources. It can be done by transferring of the sources via the nodes (reduction of the EMF sources).

5. Comparing of the Programs

Fig. 2 and Fig 3 show test circuits for comparing program "Electroscope" based on proposed method, with two most qualitative and fast programs of considered in article [1] – with American program PSIM Professional Version 9.0.3.400 and Russian program Fastmean ver. 5.2 (issued Oct 30 2012/08:38:55). EMF sources of first test circuit give square pulse voltage with minimum -10 V and maximum 10 V, duty cycle 50%, frequencies are 50 Hz and 111 Hz. All EMF sources of the second test circuit give square pulse voltage with minimum -400 V and maximum 400 V, duty cycle 50%, frequencies are 10,1; 10,3; 10,7; 10,9; 11,3; 12,7 and 13,1 kHz.

Program "Electroscope" has only nonlinear diode models. Programs PSIM and Fastmean can use either simple linear diode models or nonlinear models. Tables 1 and 2 show simulation time for different time steps (all of the programs use fixed time step).

There are used such notifications for variants of the "Electroscope" program: "Cur+EMF" – for program with acceleration by substitution of fictive currents and EMF reduction; "Cur" - for program with acceleration by substitution of fictive currents without EMF reduction; "Sys (1)" – program with immediate solving of the SLAE (1).

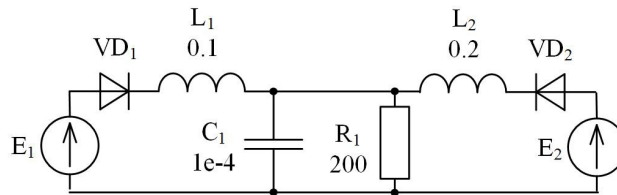


Fig. 2. Test circuit # 1.

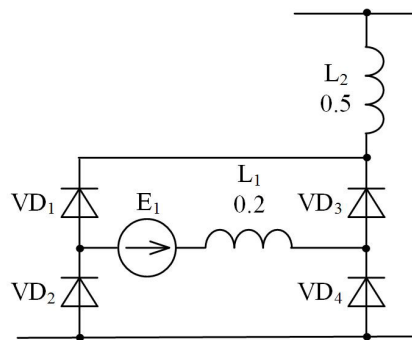


Fig. 3. A part of the test circuit # 2. The whole circuit consists of 7 such parts connected in parallel to resistor 10 Ohm.

Table 1. Comparing of simulation time (in seconds) for test circuits. Modeling time 0.2 s, time step 1 us.

Circuit #	Electroscope			Fastmean		PSIM	
	Cur + EMF	Cur	Sys (1)	Linear model	Nonlin. model	Linear model	Nonlin. model
1	1,031	1,531	5,484	1,750	3,312	2,3	57
2	5,719	12,391	31,265	12,89	13,94	10,3	111

Table 2. Comparing of simulation time (in seconds) for test circuits. Modeling time 2 s, time step 10 us.

Circuit #	Electroscope			Fastmean		PSIM	
	Cur + EMF	Cur	Sys (1)	Linear model	Nonlin. model	Linear model	Nonlin. model

1	1,141	1,547	6,344	1,828	3,094	2,0	50
2	13,297	16,734	93,125	34,36	33,218	17,8	112

It is critically important that program "Electroscope" produces solutions without rough defects. Programs PSIM and Fastmean show significant (double and more) false peak overvoltages of the diodes. Program PSIM apparently uses Newton-Raphson method for solving nonlinear equations. During simulation of both test circuits it gives numerous warnings "The program fails to converge after 10 iterations when determining switch positions". Quality of simulation results you can evaluate from Fig. 4 – Fig. 6.

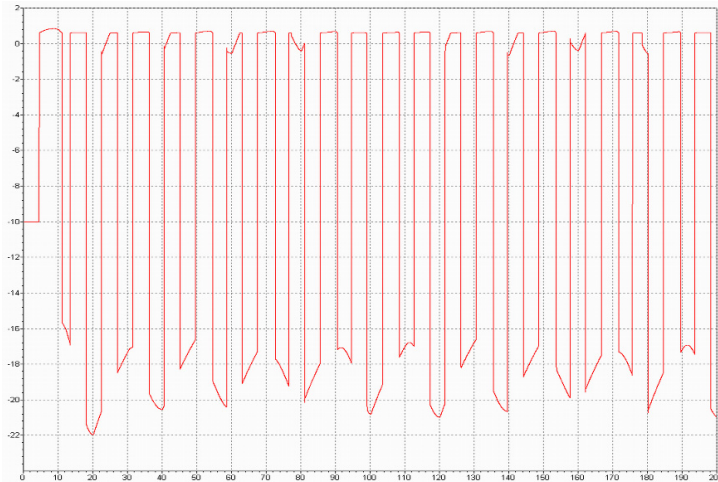


Fig. 4. Program "Electroscope". Circuit # 1, voltage of diode VD_2 [V] vs time [ms], time step 1 us.

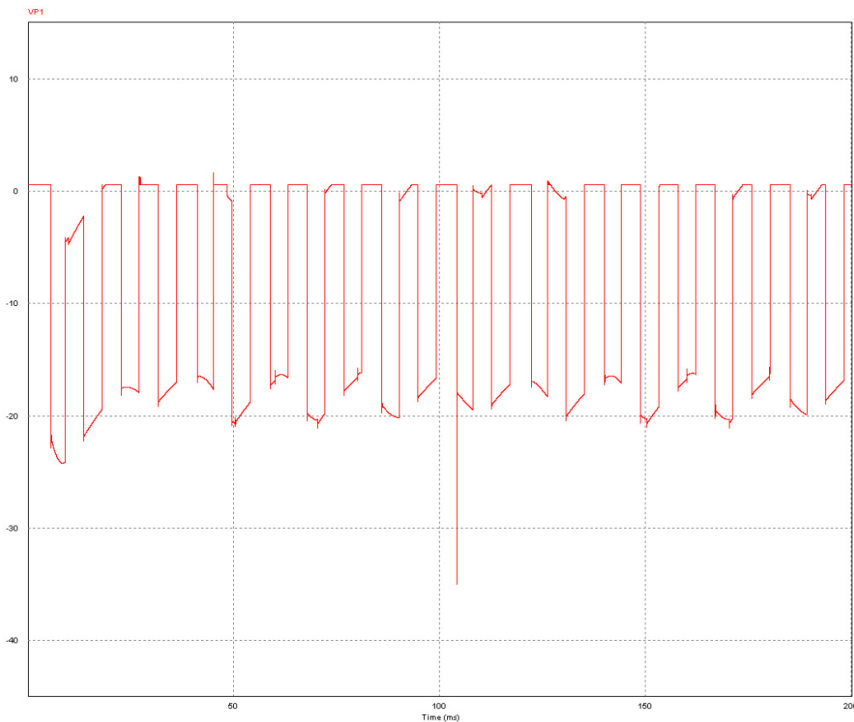


Fig. 5. Program PSIM. Circuit # 1, voltage of diode VD_2 [V] vs time [s], time step 1 us. Linear model of the diodes.

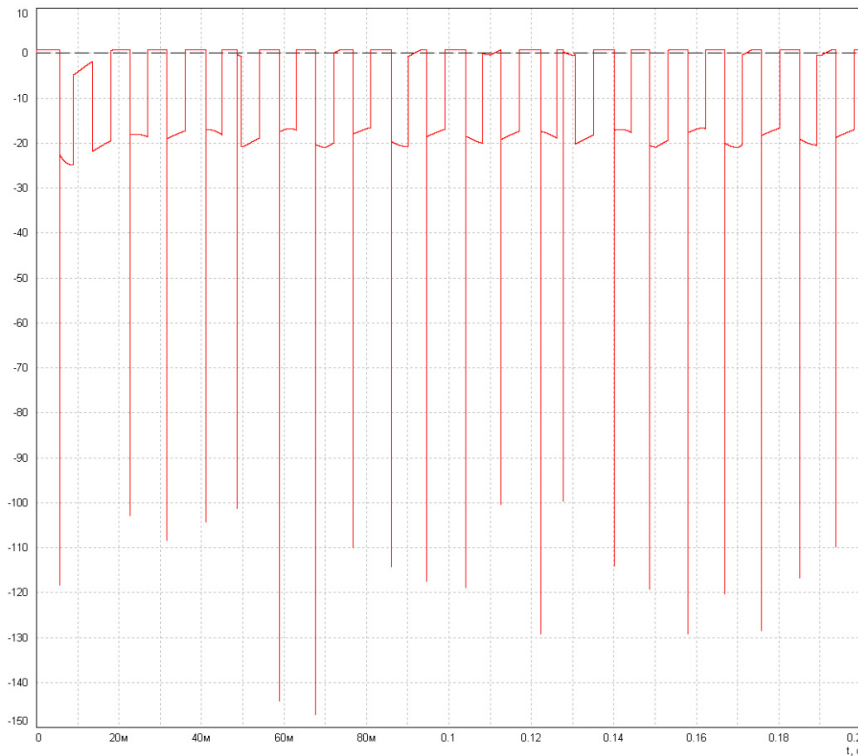


Fig. 6. Program Fastmean. Circuit # 1, voltage of diode V_{D_2} [V] vs time [s], time step 1 us. Linear model of the diodes.

6. Summary

Proposed method of electrical circuit simulation is universal and makes possible simulation of any processes in any electrical circuits consisting of two-terminals. It makes simulation simply, fast and with little computational work. Resistances of the two-terminals can vary by some orders, that situation is typical for circuits with nonlinear and switching elements. Circuits divided into several insulated parts or circuits at the edge of such condition also can be simulated. Multi-terminal elements of the electrical circuits can be presented as equivalent connections of two-terminals.

Possibility of simulation of electrical circuits with arbitrary magnet couplings is one of important advantages of the proposed method comparing with widely used Nodal Voltages Method. Apparently, limitations of the last are the main reason of absence possibility of arbitrary magnet coupling in many electrical circuit simulation programs. Meanwhile, presence of complicated magnet couplings is typical for example, for transformers and electrical machines.

Proposed method has high simulation speed and reliability that can be seen from comparing of program "Electroscope" with other programs. Defects in their simulation are caused probably by incorrect using of finite-difference formulas, by lack of accuracy in calculations of the time moments of diode switching, and also by failings of convergence in processes of solving the nonlinear equations.

Let us notice that developed mathematical apparatus may be useful not only for electrical circuits simulation, but also with help of the well known analogies it can be used for simulation of hydraulical, pneumatical and mechanical systems, and also for simulation of heat spreading in solid state constructions. To this purpose the corresponding objects must be presented as equivalent electrical circuits. In addition, there are methods for converting various problems of physical field computations into problems of electrical circuits' computations that can be solved by proposed method.

References

- [1] Y.A. Burtsev. Comparing of program for simulation of electrical circuits at the base of modified table method with known analogs, *Izvestiya vyshih uchebnyh zavedenij. Elektromehanika*. 4 (2013) 8–13.
- [2] A.I. Petrenko, A.I. Vlasov, A.P. Timchenko, *Table Methods of Electronic Schemes Computer Modelling*, Visha shkola, Kiev, 1977.
- [3] J. Vlach, K. Singhal, *Computer Methods for Circuit Analysis and Design*, Radio i Svyaz, Moscow, 1988.
- [4] L. Hageman, D. Yong, *Applied Iterative Methods*, Mir, Moscow, 1986.
- [5] N.S. Bakhvalov, N.P. Zhidkov, G.M. Kobelkov, *Numerical Methods*, Science, Moscow, 1987.
- [6] G. Korn, T. Korn, *Mathematical Handbook for Scientists and Engineers*, fourth ed., Science, Moscow, 1978.
- [7] I.M. Vinogradov, *Mathematical Encyclopedy*, vol. 5, *Sovetskaya Encyclopediya*, Moscow, 1984.
- [8] G.I. Marchuk, *Methods of Calculus Mathematics*, third ed., Nauka, Moscow, 1989.
- [9] I.S. Berezin, N.P. Zhidkov, *Methods of calculation*, State Publishing of Physical and Mathematical Literature, Moscow, 1962.
- [10] D.K. Faddeyev, V.N. Faddeyeva, *Calculus Methods of Linear Algebra*, State Publishing of Physical and Mathematical Literature, Moscow, Leningrad, 1963.
- [11] V.V. Voevodin, *Numerical Methods of Algebra (theory and algorithms)*, Nauka, Moscow, 1966.
- [12] R. Hockney, J. Eastwood, *Computer Simulation Using Particles*, Mir, Moscow, 1987.
- [13] Y.A. Burtsev, Numerical-experimental Research of Use Conjugate Gradient Algorithm for Solving Electrical Circuit Equations in Table Form, *Izvestiya vyshih uchebnyh zavedenij. Elektromehanika*. 3 (2013) 8–15.
- [14] A.E. Kaplyansky, *Fundamental Theory of Electrical Engineering*, second ed., Vysshaya shkola, Moscow, 1972.



International Conference on Industrial Engineering

Modeling a rotating circle thermal field with a thermal source on the edge

Herreinstein A.V.^a, Herreinstein E.A.^b, Mashrabov N.^{a,b*}

^aSouth Ural State University, 76, Lenin Avenue, Chelyabinsk, 454080, Russian Federation

^{ab}South Ural State Agricultural University, Institute of Agricultural Engineers, Chelyabinsk, Russia, 454080

Abstract

The task of circle heating by a thermal source moving along the circle edge with a constant angular velocity is considered. The circle is a cylinder in which the temperature is the same on each straight line parallel to a cylinder axis, i.e. at each point the temperature is a function of time, distances from a cylinder axis and a polar angle. The computing schemes based on numerical methods are usually used for the similar tasks solution. Explicit schemes solve one equation for each time step of each spatial knot. Implicit schemes solve a system of linear algebraic equations for each time step. The number of equations is connected with the number of spatial knots. In the first case the process is rather simple, but the scheme is not absolutely steady. For this scheme the step order by time should not exceed the square of step order by coordinate. In the second case the scheme is absolutely steady, but it is necessary to solve a complex system of equations, especially for a multidimensional case. The purpose of this work is to use absolutely steady differential-difference explicit scheme based on linear equation application with partial derivatives of the first order which analytical solution (an explicit formula) is known.

© 2015 Published by Elsevier Ltd. This is an open access article under the CC BY-NC-ND license (<http://creativecommons.org/licenses/by-nc-nd/4.0/>).

Peer-review under responsibility of the organizing committee of the International Conference on Industrial Engineering (ICIE-2015)

Keywords: heat conductivity; heat conductivity equation; differential-difference scheme; polar coordinate system; the equation of the first order partial derivatives.

* Corresponding author. Tel.: +7-9517856571.
E-mail address: Ark239@yandex.ru

1. Research foundation

The differential schemes of the heat conductivity equation approximate solution are divided into explicit and implicit ones [1,2,3]. Implicit schemes are absolutely steady, but they require solution of complex equation system, storing of big data array. Moreover, it results in rounding errors accumulation. Explicit schemes don't demand storing of big arrays, but these schemes are relatively steady (the step size maximum of time is determined by the step of coordinate; violation of this condition results in instability) [3]. This explicit scheme drawback can be eliminated by application of the explicit differential-difference scheme [4,5,6,7,8,9].

2. Materials and methods

We will use the following designations: t' - time, r' - distance from this point to the center of a circle, Q - heat source power density on the circle edge, ω' - the angular speed of circle rotation, μ' - heat-transfer coefficient on the circle edge, R - circle radius, q - heat conductivity coefficient, c - thermal capacity per the unit of volume, T - ambient temperature, ϕ - polar angle. Let's introduce nondimensional variables and parameters [10,11] r, t, Q, ω, μ using the formulas:

$$r' = rR, t' = tR^2 c / q, \omega' = \omega q / cR^2, Q' = Qq / R, \mu' = \mu q / R. \quad (1)$$

Dimensionless radius of a circle in this case will be equal to 1. The heat source affects the part of the circle edge (for example, heat emitted when polishing a circle surface). Other part of the edge is cooled according to the Newton law. The equation of heat conductivity has the form [12,13]:

$$\frac{\partial u}{\partial t} - \omega \frac{\partial u}{\partial \phi} = \frac{1}{r} \frac{\partial u}{\partial r} + \frac{\partial^2 u}{\partial r^2} + \frac{1}{r^2} \frac{\partial^2 u}{\partial \phi^2}. \quad (2)$$

Instead of the variable r we will introduce the variable s by the formula:

$$s = r^2. \quad (3)$$

The equation of heat conductivity will take the form:

$$\frac{\partial u}{\partial t} - \omega \frac{\partial u}{\partial \phi} = 4 \frac{\partial u}{\partial s} + 4s \frac{\partial^2 u}{\partial s^2} + \frac{1}{s} \frac{\partial^2 u}{\partial \phi^2}. \quad (4)$$

Condition on the edge ($S = 1$):

$$\frac{\partial u}{\partial s} = 0.5(Q - \mu(u - T)). \quad (5)$$

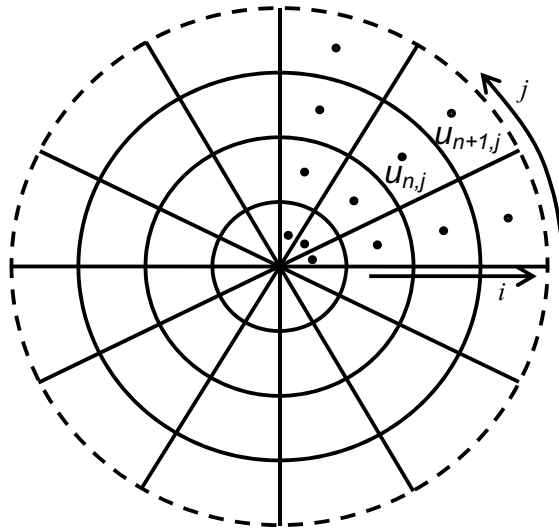


Fig. 1. The grid used

We break the radius (length 1) into n identical elementary parts of $h = 1/n$ length, a circle – on m identical sectors of $\alpha = 2\pi / m$ length. When replaced (1) elementary segments turn into rectangles of the same (radius independent) sizes. To provide edge conditions we will add the so-called fictitious layer [14,15,16] to the external part of the circle, i.e. we will increase the radius for the value h . We place knots of a grid in the center (i, j) of an elementary rectangle, where i – the number of radius part, j – the number of sector by angle.

Throughout each time interval of the dt length we will designate temperature as u_{ij} at the beginning of this time interval and as U_{ij} – the current temperature. We will designate also:

$$p_i = \frac{8i}{h} + \frac{2i}{\alpha^2 ih}, \tag{6}$$

$$f_{ij} = 4i \frac{u_{i+1,j} + u_{i-1,j}}{h} + 2 \frac{u_{i+1,j} - u_{i-1,j}}{h} + \frac{u_{i,j-1} + u_{i,j+1}}{ih\alpha^2}. \tag{7}$$

As a result we will obtain the differential-difference scheme with partial derivatives of the 1st order:

$$\frac{\partial U_{ij}}{\partial t} - \omega \frac{\partial U_{ij}}{\partial \phi} + p_i U_{ij} = f_{ij}. \tag{8}$$

We will choose a dt time step so that the circle turns on α angle for this time. Then at the end of a time interval $[0, dt]$, solving the equation (8), we will obtain [17]:

$$U_{ij} = e^{-p_i dt} u_{i,j+1} + \frac{f_{ij} - e^{-p_i dt} f_{i,j+1}}{p_i} + \frac{f_{i,j+1} - f_{ij}}{p_i^2 dt} (1 - e^{-p_i dt}). \tag{9}$$

On the elementary part containing the center of a circle, the formula (9) for temperature U_0 in the center of the circle will be the following:

$$U_0 = e^{-p_0 dt} u_0 + \frac{1 - e^{-p_0 dt}}{m} \sum_{j=0}^{m-1} u_{1,j}. \tag{10}$$

Having obtained values of temperature U_{ij} in the circle (where $i = 0, 1, \dots, n-1$), on a fictitious layer for edge conditions satisfaction we determine U_{nj} temperatures from the equation:

$$\left(\frac{1}{h} + \frac{\mu}{4}\right)U_{nj} = \left(\frac{1}{h} - \frac{\mu}{4}\right)U_{n-1,j} + \frac{Q + \mu T}{2}. \tag{11}$$

Obtaining such scheme is due to the results of research work [4,6,7]. Stability substantiation of the scheme offered is similar to the one given in the following works [18,19].

The numerical method was considered under the initial condition (23) and with the radius step of $1/10$ and with the $\pi/5$ angle and was compared to the exact solution (with the first term of Fourier's method solution). The relative error didn't exceed 6%. The schemes obtained were used for a blank temperature field modeling in the process of flute grinding of spiral drills [20,21].

3. Conclusions

The explicit differential-difference scheme offered is absolutely steady in comparison with purely differential scheme and allows calculating the thermal field of a circle (cylinder) beyond the differential scheme stability.

References

- [1] V.M. Verzhbitsky, Fundamentals of numerical methods, Higher school, Moscow, 2002..
- [2] A.A. Samarskiy, Theory of differential schemes, Science, Moscow, 1989.
- [3] N.S. Bakhvalov, N.P. Zhidkov, G.M. Kobelkov, Numerical methods, Science, Moscow, 1987.
- [4] A.V. Herreinstein, N. Mashrabov, E.A. Herreinstein, Steady explicit schemes for the heat conductivity equation, Bulletin of SUSU, a "Mathematical modeling and programming" series. 1-15(115) (2008) 9–11.
- [5] A.V. Herreinstein, N. Mashrabov, Heating of a circle by moving heat source. - Applied and industrial mathematics review. 15(5) (2008) 870–871.
- [6] A.V. Herreinstein, E.A. Herreinstein, N. Mashrabov, Steady explicit schemes of the heat conductivity equation for an axially symmetric problem. SUSU Bulletin, "Mathematics, mechanics, physics» Series. 2,9(185) (2010) 4–8.
- [7] A.V. Herreinstein, E.A. Herreinstein, Steady explicit schemes of the heat conductivity equation SUSU Science: materials of the 62nd scientific conference. Sections of natural sciences, Chelyabinsk: SUSU Publishing center. (2010) 22–26.
- [8] A.V. Herreinstein, N. Mashrabov, E.A. Herreinstein, The state registration certificate of the computer program 2008612210. (2008).
- [9] A.V. Herreinstein, A.A. Dyakonov, A.A. Koshin, The state registration Certificate of the computer program 2010610052.
- [10] L.I. Sedov, Methods of similarity and dimension in mechanics. eighth ed., Science, Moscow, 1977.
- [11] M.G. Ivanov, Dimensions and similarity, Dolgoprudny, 2013.
- [12] A.N. Tikhonov, A.A. Samarskiy, Equations of mathematical physics, Science, Moscow, 1972.
- [13] I.G. Aramanovich, V.I. Levin, Equations of mathematical physics, Science, Moscow, 1969.
- [14] N. Mashrabov, A.V. Herreinstein, E.A. Herreinstein, Steady explicit schemes of the heat conductivity equation for a one-dimensional problem. CSAA Bulletin. 67(1) (2014) 50–54.
- [15] A.V. Herreinstein, N. Mashrabov, E.A. Herreinstein, Modeling of thermal fields with variable heat physical properties of a detail, Materials of the LIII international scientific and technical conference Part III, CSAA, Chelyabinsk. (2014) 31–38.
- [16] M.Z. Hayrislamov, A.V. Herreinstein, The explicit scheme of the third mixed problem solution for the quasilinear equation of heat conductivity, SUSU bulletin "Mathematics, mechanics, physics" series. 5(2) (2013) 174–177.
- [17] V.V. Stepanov, The differential equations course, Fizmatgiz, Moscow, 1959.
- [18] A.V. Herreinstein, M.Z. Hayrislamov, Explicit differential scheme of the one-dimensional quasilinear heat conductivity equation solution. SUSU bulletin, "Mathematics, mechanics, physics" series. 5(1) (2013) 12–17.
- [19] A.V. Herreinstein, N. Mashrabov, E.A. Herreinstein, Certificate on registration of an electronic resource 19347
- [20] A.V. Herreinstein, A.A. Koshin, Yu.S. Khudyakova, D.V. Vostroknutov, Mathematical problem definition of blank temperature field modeling in the process of flute grinding of spiral drills, Progressive technologies in mechanical engineering : collected articles, Chelyabinsk: SUSU Publishing house. (2008) 206–211.
- [21] A.V. Herreinstein, A.A. Koshin, Yu.S. Khudyakova, D.V. Vostroknutov, The numerical problem solution of a blank temperature field modeling in the process of flute grinding of spiral drills, collected articles, Chelyabinsk: SUSU Publishing house. (2008) 211–215.



International Conference on Industrial Engineering

Analysis of production line with finite buffers and a general service term

Korolkova L.I.^a, Mashrabov N.^{b*}

^aSouth Ural State University, 76, Lenin Avenue, Chelyabinsk, 454080, Russian Federation

^bSouth Ural State Agricultural University, Institute of Agricultural Engineers, Lenin Avenue 75, Chelyabinsk, 454080, Russia

Abstract

This paper considers a production line with continuous loading at the first automation service station or machine and buffers placed forward the queuers. Each machine operates within an indefinite service time. There is much data available on modeling and analysis of the transfer lines. However, most of the results are for the steady-state operation. The system under consideration operates within the finite time interval. A method is suggested to study the production line. According to the method, we chart the system operation process; calculate of distribution formula for the remaining durations of time period of the system being in the states marked at the chart. Then we calculate the state indexes. A detailed description of the states allows calculating, for example, blocking machine indexes and machine down time probabilities and durations.

© 2015 The Authors. Published by Elsevier Ltd. This is an open access article under the CC BY-NC-ND license (<http://creativecommons.org/licenses/by-nc-nd/4.0/>).

Peer-review under responsibility of the organizing committee of the International Conference on Industrial Engineering (ICIE-2015)

Keywords: production line, finite time interval, chart of the system operation process, remaining durations, blocking machine indexes, machine down time probabilities and durations

* Corresponding author. Tel.: +7-351-267-99-00; fax: +7-351-267-99-00.
E-mail address: korolkovali@rambler.ru

1. Introduction

Functioning of a real production line is a complicated process and falls a long way short of any simplified description. Real system service time as a rule does not obey the exponential distribution as the process runs during a real shift rather than infinite time. Therefore, it is clearly an important task to investigate production line characteristics.

Tandem queueing systems modulate the line manufacture flow. Manufacturing line is a linear network of machines separated by buffer storages. The majority of studies investigate two-stage tandem queue within exponentially distributed processing times. These systems are observed under general conditions, reliability of devices (reliable – unreliable) and types of buffers (finite - infinite), for example [1 – 7]. In [8, 9] the Markov systems capacity was assessed. The systems consisted of five or more machines within unequal service periods. The Markov systems transient results were discussed in [10].

A multiphase system research suggests a method aimed at continuous and discrete random processes [16]. In [17] the method was applied to obtain machines blocking characteristics of a four-phase unbuffered tandem queueing systems with continuous loadings.

2. Method description

The following assumptions are made:

- the system consists of three successive reliable machines which perform single-line service;
- the first machine receives demands continuously. The second and the third machines have two objects capacity buffers;
- if the buffer placed forward the machine is filled up the served object blocks the service station;
- service time T_i for i -machine has a random value and is characterized by general distribution function formula $F(t_i)$;
- the system operates within the t_0 period.

According to the method, we chart the system operation process including its states and states transitions. We define state as a set of durations of simultaneous service processes. Finite time interval represents a state as any other duration. However when the duration ends up all other processes are suspended. Each state is assigned with a number. A state ends up when the machine service time or finite time interval is over. So the general process enters another state. At the chart it is represented by an arrow. The machine (phase) that completed the service is a point when an adjoint state transits to the next state. The machine gets a number at the chart marked at the arrow in brackets.

The first application served by the first machine and the finite time interval make up the system initial state. At the Figure 1 both are marked as 1_1 and O accordingly. T is omitted. The figure critical distinction from the chart is represented particularly in [18], are *one-side* transitions. It helps to explore system indexes during the target periods.

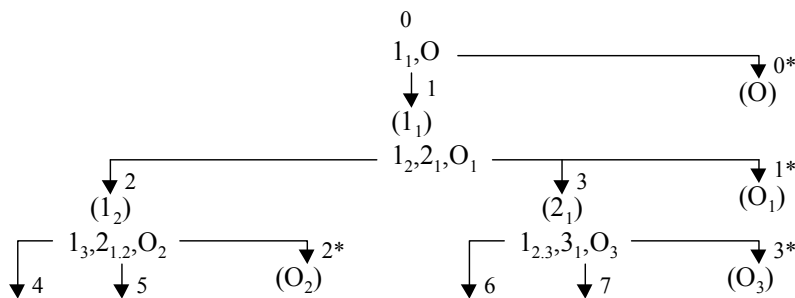


Fig. 1. First part of tandem queue system operation scheme.

Initial state is over either due to the end of finite time interval so the process proceeds to state 0^* , or due to service end. In this case the process proceeds to state 1 (number, right to the arrow) characterized by the first object serviced at the second machine (1_2), the second one at the first machine (2_1) and the remaining time interval (O_1). Therefore, there are three alternatives of general service process implementation. The service of the first object at the second machine may be completed first so the general process enters state 2 as well as the second object service at the first machine may be completed first so the general process enters state 3. Moreover, there is a third option. The finite time interval may be over (it is a state transition 1^*).

State 3, for example, is characterized by the first object service in operation at the second machine, the third object service in operation at the first machine and the remaining time interval while the second object is at the standby mode at the buffer preceding the second device. i - machine blocking state is characterized by object service completion at the machine, filled up buffer preceding the $(i+1)$ - machine and object service in operation at $(i+1)$ - machine.

The next step is calculations of distribution formula for the remaining durations of time period of the system being in the states marked at the chart and probabilistic jockeying.

Calculation algorithm for service period distribution formula.

- Single an i_k process performed at the machine with completed service out of the multitude of service processes representing the k -state. The i_k process is characterized by service period distribution formula $F_{ik}(t) = P\{T_{ik} \leq t\}$. We need to find distribution formula $F_{jk}^{(x)}(t)$ for the j machine with service in operation. The formula deals with the service period remained in transition from the k -state to the x -state. $F_{jk}(t)$ is a service period distribution formula for application by j machine which is in k - state.
- Calculate a time distribution formula for z machines service equal to k -state not taking into account i_k - and j_k - machines:

$$R_{kx}(t) = P\{Y_{kx} \leq t\} = P\{\min(T_{zk}) \leq t\} = 1 - \prod_z [1 - F_{zk}(t)]$$

- Calculate a conditional service period distribution formula for i_k machines. The service period in this case is less than for a group of machines which make up k -state not taking into account i_k and j_k machines:

$$Q_{kx}^+(t) = P\{X_{kx} \leq t\} = P\{T_{ik} \leq t \mid T_{ik} < Y_{kx}\} = Q_{kx}^+(t) / Q_{kx}^+(\infty),$$

where $Q_{kx}^+(t) = \int_0^t [1 - R_{kx}(z)] dF_{ik}(z)$.

- Use the formula for remaining service period from the k -state for j_k - machine which is already in x -state

$$F_{jk}^{(x)}(t) = P\{T_{jk}^{(x)} \leq t\} = P\{T_{jk} - X_{kx} \leq t \mid T_{jk} > X_{kx}\} = [F_{jk}^{(x)+}(0) - F_{jk}^{(x)+}(t)] / F_{jk}^{(x)+}(0),$$

where $F_{jk}^{(x)+}(t) = \int_t^\infty Q_{kx}(z-t) dF_{jk}(z)$

Further calculations of indexes for x -state require rewriting $F_{jk}^{(x)}(t)$ into $F_{jx}(t)$ as well as for k -state.

V_{kx} -durations of the system transited in the state characterizes unrestricted k -state. Only under condition that each i_k - machine is accomplished individually in a due time from the whole number of services performed in this state [19]. If the conditions are met the state transits into x -state. The distribution formula for V_{kx} duration is calculated as the following:

$$S_{kx}(t) = P\{V_{kx} \leq t\} = P\{T_{ik} \leq t \mid T_{ik} < U_{kx}\},$$

where $U_{kx} = \min\{T_{jk}\}$.

3. Numerical example

We investigate the indexes connected with system blocking and device standbys for three-unite service systems. Finite time interval is t_0 equals to 10 time units. The first part of tandem queue system operation is charted at Fig. 1.

We took the service period distribution subordinated by the Weibull distribution and the distribution formula.

$F_i(t) = 1 - \exp(-\lambda_i \cdot t^{\alpha_i})$. We counted machines service period as equal which means $F_1(t) = F_2(t) = F_3(t)$.

The following indexes were calculated (see Table 1):

- probability s_1 that at least one machine may be blocked out once within a finite time period;
- average duration b_1 for the first blocking of at least at one work position within a finite time period;
- probability s_2 for the second blocking within a finite time period where b_2 is a blocking duration.

Table 1. Blocking time probabilities and durations.

	$F(t) = 1 - \exp(-2,303t^{1,05})$ $\bar{t} = 0,45, \nu = 0,94$	$F(t) = 1 - \exp(-0,46t^2)$ $\bar{t} = 1,31, \nu = 0,52$	$F(t) = 1 - \exp(-3,68 e^{-3}t^5)$ $\bar{t} = 2,83, \nu = 0,23$
s_1	0,204	0,068	0,002
b_1	0,60	0,49	$4 \cdot 10^{-5}$
s_2	0,069	0,014	$1 \cdot 10^{-6}$
b_2	0,32	0,57	0,50

According to the Table 1 there is a direct proportion between variability index ν and blocking probability and duration despite that the average service duration \bar{t} rises if $\alpha = 5$ rather than $\alpha = 1,05$. Therefore, it is recommended to reduce the spread of service period in comparison to the average index.

Detailed description of the states allows to calculate machine down time probabilities and durations (see Table 2).

Table 2. Machine down time probabilities and durations.

	$F(t) = 1 - \exp(-2,303t^{1,05})$ $\bar{t} = 0,45, \nu = 0,94$		$F(t) = 1 - \exp(-0,46t^2)$ $\bar{t} = 1,31, \nu = 0,52$		$F(t) = 1 - \exp(-3,68 e^{-3}t^5)$ $\bar{t} = 2,83, \nu = 0,23$	
	probability	duration	probability	duration	probability	duration
Device 2, first down time	0,585	0,24	0,590	0,82	0,590	1,72
Device 2, second down time	0,339	0,44	0,339	0,59	0,337	0,38
Device 3, first down time	0,582	0,32	0,580	0,55	0,636	0,57
Device 3, second down time	0,353	0,37	0,356	0,58	0,381	0,50

4. Conclusion

- The method allows to examine the system during the finite deterministic time interval in detail. It will be helpful for the system analysts and engineers in order to provide quantitative and qualitative insight and to improve their systems.
- The method extends to more complicated queueing systems. In the case of tandem system with arbitrary distributed arrival time this time is added to the initial state 0. In addition, systems with more complicated configuration can be studied
- Service system research is applied by a single performance summary and further changes of time distribution and finite time intervals.
- The generic method (whatever the process is, it can be described by identical structures) provides computer task programming comfort.

References

- [1] Y. Perlman, A. Elalouf, E. Bodinger, Dynamic repair priority for a transfer line with a finite buffer, *J. of Manufacturing Systems*. 33 (2014) 16–26.
- [2] S.A. Matveev, A.N. Moiseev, A.A. Nazarov, Investigation of the multi-stage queueing system $GI/(M/\infty)K$ by means of the raw moment method, *Reports TUSUR*. 3 (2014) 129–133.
- [3] E.V. Viskova, Two-stage queue with Markov arrivals and discrete service time, *J. Information processes*. 5 (2005) 247–253.
- [4] H.T. Papadopoulos, M.E.J. O’Kelly, Exact analysis of production lines with no intermediate buffers, *Eur. J. Opnl. Res.* 65 (1993) 118–137.
- [5] Y. Xiajun, L. Ronggui, On properties of a serial service system of two service counters with finite waiting space, *Acta Mathematica Science*. 15 (1995) 31–38.
- [6] M.N. Gopalan, N. Anantharaman, Stochastic modelling of a two-stage transfer-line production system with end buffer and random demand, *J. Microel. and Reliab.* 33 (1992) 11–15.
- [7] V.I. Klimenok, Two-phase systems of service with the group Markov flow and recall, *J. Automation and Remote Control*. 1 (2010) 3–17.
- [8] H.T. Papadopoulos, C. Heavey, M.E.J. O’Kelly, Throuput rate of multistation reliable production lines with interstation buffers: (I) Exponential case, *J. Computers in Industry*. 13 (1989) 229–244.
- [9] Yi Cheng Su, J.M Chandra, An approximation analysis for multistage production lines, *J. Comp. and Operations Research*. 22 (1995) 779–791.
- [10] C. Dinçer, B. Deler, On the distribution of throughput of transfer lines, *J. of the Opnl. Res. Society*. 51 (2000) 1170–1178.
- [11] B. Chandrasekar, P. Chandrasekhar, N.R. Kumar, A tandem queue with dependent structure for interarrival and service times: an estimation study. In: *Proceedings of the 41st Int. Conf. Comp. and Industrial Engineering (CIE41)*, Los Angeles. (2011) 145–150.
- [12] T. Nishida, Optimal allocation of service rate for interchangeable parallel two-stage tandem queue. *J. Math. Japonica*. 41 (1995) 211–215.
- [13] K. Yoneyama, H. Ishii, The throughput rate of interchangeable parallel two-stage tandem queue with correlated service times. *J. Computers Math. Applic.* 33 (1997) 29–37.
- [14] K. Jongyoon, B.S. Gershwin, Integrated quality and quantity modeling of a production line, *J. OR spectrum*. 27 (2005) 287–314.
- [15] V.V. Grachev, A.N. Moiseev, A.A. Nazarov, V.Z. Yampolsky, Multistage queueing model of the distributed data processing system, *Reports TUSUR*. 26 (2012) 248–250.
- [16] I.V. Korolkov, L.I. Korolkova, Digital composition and continuous time stochastic processes, *Review of Applied and Industrial Mathematics*. 8 (2001) 614–615.
- [17] L.I. Korolkova, P.P. Pereverzev, Optimization of the company based on a new methodology for calculating the characteristics of multiphase queueing system with continuous loading without intermediate storage, *J. Modern problems of science and education*. 3 (2012). <http://www.science-education.ru/103-6424>.
- [18] M.N. Gopalan, U.K. Dinesh, Analysis of an n-unit cold-standby system with general failure and repair time distributions, *Int. J. of Quality & Reliability Management*. 12 (1995) 77–85.
- [19] R. Gupta, S.Z. Mumtaz, N. Rastogi, Profit analysis of a system with mutual changeover of units and correlated failures and repairs, *J. of Quality in Maintenance Engineering*. 5 (1999) 51–55.
- [20] D. Stoyan, *Qualitative properties and evaluation of stochastic models*, Mir, Moscow, 1979.



International Conference on Industrial Engineering

Probabilistic model parameter optimization for the problem solving algorithm

Mikhaylov A.A., Bazuyeva S.A.*

Platov South-Russian State Polytechnic University (NPI), 132, St. Prosvescheniya, Rostov region, Novocherkassk, 346428, Russian Federation

Abstract

The variety of problem solving algorithms models over set of the alternative solutions determines the application of the principle of equivocation logical reduction by narrowing of the solutions set. The choice of an optimum decision comes to the logical conversion of alternative solutions set to the feasible solutions set and to the effective solutions set. The alternative solution set is transformed to the feasible solution on the constraints set. The article explains the application of Hidden Markov Model (HMM) for the choice of optimum problem solving algorithm concerning the observable consistency. In this case we use the maximum likelihood criterion with the constraints in the form of normalizing conditions and semantic measure of the information expedience of A.A. Harkevich for the optimization of unknown parameters of the problem solving algorithm. The “committee” constructions are used for the “integration” of some algorithms for collective decision. We receive the optimal parameters for the algorithm of the collective decision using estimation of the posterior probabilities of algorithm appliance.

© 2015 Published by Elsevier Ltd. This is an open access article under the CC BY-NC-ND license (<http://creativecommons.org/licenses/by-nc-nd/4.0/>).

Peer-review under responsibility of the organizing committee of the International Conference on Industrial Engineering (ICIE-2015)

Keywords: Hidden Markov Model, alternative solution set, feasible solution set, effective solution set, optimal solution.

1. Introduction

In the real-world problems concerning decision-making the great information uncertainty is remained during the choice of optimal solution algorithm. This uncertainty is governed by the great initial variety of the problem solving algorithms models on alternative solutions set Y . It is difficult to make choice of the problem solving algorithm from the given set. In this connection we use the principle of the logical reduction of uncertainty. It comes to the narrowing of the problem solving set.

* Corresponding author. Tel.: 8-928-195-7381; fax: 8-863-525-5240.
E-mail address: mih01@mail.ru

As is known there are three stages of this procedure. During the first stage the initial set of the alternative solutions Y is narrowed down to the feasible solution set $Y_g \subseteq Y$. During the second stage the feasible solution set is narrowed down to the effective solution set $Y_0 \subseteq Y_g$. During the third stage we realize the choice of the optimal solution. That is the choice of the optimal solution comes to the sequence of the set transformations $Y \supseteq Y_g \supseteq Y_0 \supseteq Y^*$.

The alternative solution set is transformed down to the feasible solution set (we take into account constraints set). Performing constraints is the pre-requisite for the solution algorithm choice. That's why the singular finish making decision Y^* is in the good-enough solution set. Narrowing of the solution set down to the feasible solution set begins at the stage of the initial set forming. Narrowing of the feasible solution set down to the effective solution set raises the definiteness of optimal solution choice on the effective solution set. All initial information is completely used for the extraction of the effective solutions from the feasible solution set. That's why the optimal solution choice is possible when we receive new information, method of its introduction.

The optimal solution choice concerning observable consistency O comes to the characterization using Hidden Markov Model Θ^* . They maximize probability of the observable sequence appearance $O = o_1 o_2 \dots o_T$, [1-5]

$$\Theta^* = \max_{\Theta} (P(O|\Theta)). \quad (1)$$

The aim of this article is the characterization Θ of the problem solving algorithms using HMM. Parameters must satisfy the optimality criterion of maximum likelihood.

2. Constraint qualification for criterion

The important element of the algorithm model is the constraint of the performance criterion of the problem solving. These problems are determined by the information features used in the algorithm. We can be limited by the minimum constraint group during the algorithm parameter optimization. We allocate two constraints required for algorithm synthesis.

1. The constraints in the form of the normalizing conditions which are applied on the density of distribution of the random variables. Thus for probability P_k of the model belonging k is non-negative and the sum of the probabilities equal to one

$$\sum_{k=1}^l P_k = 1, P_k \geq 0 \quad \forall k = \overline{1, l}.$$

2. The second constraints type for the criterion of the problem solving algorithm optimization is determined by the feature of the algorithm function which comes to the purposeful logical transformation of the A.A. Harkevich information semantic measure [6]. We appreciate amount of information taking into account the change of the action expediency degree, the goal attainment of the algorithm function which is controlled by the information influence in the form of the some message. Using this constraint we have alternative solution set. Feasible solution set is formed from these alternative solutions in accordance with the aim of the algorithm function. Given constraint decreases the limitations of Bayesian approach because it is determined by the posterior information on the goal attainment of the algorithm function. Numerical measure of the conditionality of the information value introduced by Bongard and Harkevich [7, 8] is determined by the goal attainment probability during the information pull and equal

$$I = \log_2(P_1 / P_0),$$

where P_0 —the goal attainment probability before the information pull; P_1 — the goal attainment probability after the information pull and its using. This expression is transformed into (2) when the control action influences the algorithm:

$$I_i^v = \log_2(P_{ij}^v / P_j), \quad (2)$$

where I_i^v — numerical measure of the controlling factor force in the form of the machine instruction v_i to the algorithm transition from i state to j state.

Given constraint in the condition of the synthesis of the problem solving algorithm determines the condition of the problem solving goal attainment in the form of: $P_{V-1,V}^v = 1$, i.e.

$$\sum_{i=0}^V \log(P_{i,i+1}^v / P_i) = \sum_{i=0}^V I_i^v = \log(1 / P_0),$$

where $P_{i,i+1}^v$ – probability of the transitions from i state to $j=i+1$ state. It's given by the value of the machine instruction v_i ; V – sequence of transitions forming Viterbi method which receives the most probable sequence of the states [9] and gives the problem solving algorithm.

Other constraints can be used besides given constraints. Thus the constraints of the variance of the distribution law are required for the algorithm of signal extraction from the signal-noise mixture. The constraints of the signal swing are required for the algorithm of the signal determination.

3. General approach to the models parameter estimation

Conceptual model of the deterministic algorithm is represented as the sequence of the machine instructions v_i determined on the machine instructions set $V = \{v_i\}$, $i = \overline{1, n_{mk}}$, where n_{mk} – number of the machine instructions which are in the algorithm class fetch. They are represented as the system of the instructions of used processor class.

The stochastic algorithm is represented as the doubly stochastic problem which consists of the set of the known discrete observed variables $O = \{o_1, \dots, o_N\}$, which describe the appearance of the machine instructions $o_n \in R^d$ and hidden variables $Q = \{q_1, \dots, q_N\}$. Hidden variables Q determine the changes N of the model states (state variables). Values of the observed vector o_i taken in the instant i depend on the i state

$$P(o_i | o_1, o_2, \dots, o_{i-1}) = P(o_i | o_i), \quad (3)$$

i. e. it doesn't depend on the time and hidden state q_i , in previous instant q_{i-1} , that is the transition function

$$P(q_i | q_{i-1}, \dots, q_1, o_1) = P(q_i | q_{i-1}), \quad (4)$$

we don't know how many states and how much connection there are between them.

Given axioms determine the algorithm in the form of the hidden Markov process. It is represented as bicomponent random process with hidden component and observed component of the observation symbol appearance (handles of the assembler language machine instructions).

Hidden Markov Model HMM [2, 4] has the form

$$\Theta = (N, M, A, B, \Pi),$$

where N – number of the model states. Model states set is represented as $S = \{s_i\}$, $i = \overline{1, N}$, model state-of-the-art in the instant t – as q_t from the sequence Q , which is the implementation of the hidden process; M – number of the possible symbols in the observed sequence.

These symbols are appeared from the model and form the alphabet $V = \{v_k\}$, $k = \overline{1, M}$; $A = \{a_{ij}\}$ – transition probability matrix, where $a_{ij} = P_A[q_t = s_j | q_{t-1} = s_i]$, $1 \leq j, i \leq N$ – probability of the model transition from the state $q_{t-1} = s_i$ in instant $t-1$ into the state $q_t = s_j$ next moment t , q_t – the state in the instant $t=2, T$, T – length of sequence; $B = \{b_j(k)\}$ – probability distribution of the symbols appearance in the state j , ($1 \leq j \leq N$), where $b_j(k) = P_B[o_k = v_k | q_t = s_j]$ – reference probability distribution that in the instant t system in j state (state s_j) gives k symbol (v_k) into observed sequence O , $k=1, M$ – number of the different observation symbols ok. They can be given by the model (dimension of the discrete alphabet) $V = \{v_k\}$; $\Pi = \{\pi_i\}$ – probability distribution of the initial state $\pi_i = P[q_1 = s_i]$, $1 \leq i \leq N$, where q_1 – the state

in the instant $t=1$ from the sequence Q , which is the implementation of the hidden process i.e. the probability that s_i – initial state of the model.

HMM realizes cybernetic model “black box” which generates observed sequence after performing of the given steps number $O=o_1o_2\dots o_T$.

This observed sequence is formed by the symbols of discrete alphabet V , which consists of the machine instructions handles $v_k=o_b$, where $o_t \in R$ – observation fixed in the instant $t=1, T$, T – number of the symbols in the observed sequence.

4. Parameter optimization of hidden Markov model problem formalization

Problem statement: observed sequence in the form of the machine instruction chains is the initial data. HMM is determined for every machine instruction chain. Three problems connected with HMM are underlined [2].

The first problem comes to the estimated probability $P(O|\Theta)$ that given observed sequence $O=o_1, o_2, \dots, o_T$ was created only for model $\Theta=(A, B, \Pi)$

$$P(O|\Theta) = \sum_Q P(O|Q, \Theta).$$

In the second problem for the sequence of observations $O=o_1, o_2, \dots, o_T$ and HMM we must choose the states sequence $Q=q_1, q_2, \dots, q_T$, which determines the sequence of observations $P[Q|O, \Theta]$ and has maximum probability $P[Q|O, \Theta]$. In the third problem we must select model parameters $\Theta=(A, B, \Pi)$ maximizing $P(O|\Theta)$.

Required: for three problems solving connected with the determination of structure and parameters Θ of the problem solving algorithms (1) we must choose correct criterion of the maximum likelihood optimization.

Task solution: we introduce hidden variables Q of HMM model for problem solving given by incomplete function of likelihood (1) with the observed variables O and parameters Θ . We estimate the vector of parameters Θ of complete function of likelihood $\log p(O, Q|\Theta)$, for which

$$\log p(O|\Theta) = \log \left\{ \sum_Z p(O, Q|\Theta) \right\}.$$

We determine the joint distribution of HMM variables. From the conditions of independence (3, 4) in the determination of HMM we realize that the generation probability by the sequence $Q=\{q_1, q_2, \dots, q_T\}$ of the hidden states the observation sequence $O=\{o_1, o_2, \dots, o_T\}$ is calculated as:

$$P(O|Q, \Theta) = P(o_1, o_2, \dots, o_T | q_1, q_2, \dots, q_T, \Theta) = \prod_{t=1}^T P_B(o_t | q_t).$$

The probability of sequence appearance $Q=\{q_1, q_2, \dots, q_T\}$ equal

$$P(Q|\Theta) = P(q_1, q_2, \dots, q_T | \Theta) = \pi_{q_1} \prod_{t=1}^{T-1} P_A(q_t | q_{t+1}),$$

i.e. probability of observation of some symbol depends on the model state in the given instant.

Because of the appearance of the concrete sequence of the states and the appearance of the sequence of observation for HMM is autonomous, probability of the sequence observations O which was formed from the sequence Q in the form of the joint distribution is given by the formula

$$P(O, Q|\Theta) = P(O|Q, \Theta),$$

and

$$P(O|\Theta) = p_{\pi}(q_1) \prod_{n=1}^N P_B(o_n | q_n) \prod_{n=2}^N P_A(q_n | q_{n-1}),$$

where $O=\{o_1, o_2, \dots, o_N\}$ – observed states of the model with the hidden variables; $Q=\{q_1, q_2, \dots, q_N\}$ – hidden states of the model which describe its inner state; Θ – model parameters with hidden variables.

Apart from the probability of transition between the hidden states q_n of the model algorithm which describes magnitude of connection between the states we'll introduce Viterbi variable in the form of k -measure binary random vector $z_{ij}, j \in \{0, 1\} K$ its component equal to one, i.e. $\sum_{j=1}^K z_{nj} = 1$. This vector determines the hidden states choice and their sequence. Given sequence in the form of the Viterbi approach V gives the conversion direction of the dataflow in the algorithm

$$P(O, Q|\Theta) = \prod_{j=1}^K \pi_j^{z_{1j}} \left(\prod_{n=2}^N \prod_{i=1}^K \prod_{j=1}^K [P(q_n|q_{n-1})]^{z_{n-1,j} z_{nj}} \right) \left(\prod_{n=1}^N \prod_{k=1}^K (p(o_n|q_n))^{z_{nk}} \right).$$

For the parameters estimation Θ we use the method of maximum likelihood

$$\Theta_{ML} = \arg \max p(O, Q|\Theta) = \arg \max \log p(O, Q|\Theta),$$

for the logarithmic likelihood function

$$\log p(O, Q|\Theta) = \left(\sum_{j=1}^K z_{1j} \log \pi_j \right) + \left(\sum_{n=2}^N \sum_{i=1}^K \sum_{j=1}^K z_{n-1,i} z_{nj} \log P\{q_n|q_{n-1}\} \right) + \sum_{n=1}^N \sum_{k=1}^K z_{nk} \log P(o_n|q_n).$$

Parameters which enter Θ cannot have arbitrary values. Hence the optimization takes place in the conditions of the constraints

$$\sum_{j=1}^K \pi_j = 1, \quad \sum_{j=1}^{N_V} P_{ij} = 1, \quad \forall i = \overline{1, K},$$

where N_V – number of the transitions forming algorithm Viterbi approach.

We use the rule of Lagrange multiplier [10] and we have

$$L(\Theta, \lambda, \mu, \eta) = \log p(O, Q|\Theta) + \lambda \left(\sum_{j=1}^K \pi_j - 1 \right) + \sum_{i=1}^K \mu_i \left(\sum_{j=1}^K P_{ij} - 1 \right) + \sum_{i=1}^K \mu_i \left(\sum_{j=1}^V \log \frac{P_{ij}}{P_0} + \log P_0 \right) + \sum_{k=1}^K \eta_k \left(\sum_{n=1}^K P(q_n|o_n) - 1 \right) \rightarrow \text{extr.} \quad (5)$$

5. Characterization of hidden Markov model

Lagrangian (5) allows determining HMM structure and parameters.

1. For the distribution of the probability of the initial states we determine Lagrangian derivative using the element π_j of the matrix of the initial states probability Π

$$\frac{\partial L(\Theta, \lambda, \mu, \eta)}{\partial \pi_j} = \frac{z_{1j}}{\pi_j} + \lambda = 0, \quad \text{hence, } \pi_j = -\frac{z_{1j}}{\lambda}.$$

We sum this expression using the Viterbi variable taking in account that $\sum_{j=1}^K \pi_j = -1$, we have $\lambda = -\sum_{j=1}^K z_{1j} = -1$,

i.e. the element π_j estimation of the matrix Π has form

$$\pi_j = z_{1j}. \tag{6}$$

2. For the distribution of the probability of the model transition from the state i into the state j we determine Lagrangian derivative using the element P_{ij} of the matrix of transitional probabilities A

$$\sum_{n=2}^N \frac{z_{n-1,i} z_{nj}}{P_{ij}} + \mu_i \frac{1}{P_{ij}} = -\mu_i, \text{ hence, } P_{ij} = \frac{\sum_{n=2}^N z_{n-1,i} z_{nj} + \mu_i}{-\mu_i}.$$

Sum this expression taking into account that $\sum_{j=1}^K P_{ij} = 1$ и $\sum_{j=1}^K z_{nj} = 1$ and receive

$$\sum_{j=1}^K P_{ij} = 1 = \frac{\mu_i + \sum_{j=ln=2}^K \sum_{n=2}^N z_{n-1,i} z_{1j}}{-\mu_i} = \frac{\mu_i + \sum_{n=2}^N z_{n-1,i}}{-\mu_i}, \text{ i.e. } \mu_i = -\frac{\sum_{n=2}^N z_{n-1,i}}{2}.$$

As a result the estimation of the elements P_{ij} of the matrix A

$$P_{ij} = 2 \frac{\sum_{n=2}^N z_{n-1,i} z_{nj}}{\sum_{n=2}^N z_{n-1,i}} - 1. \tag{7}$$

Sum the expression (7) on the set K

$$\sum_{i=1}^K \mu_i = -\frac{\sum_{n=2}^N \sum_{i=1}^K z_{n-1,i}}{2},$$

and receive the expression for the average value of the coefficient μ

$$\frac{\sum_{i=1}^K \mu_i}{N-1} = -\frac{1}{2}.$$

3. For the distribution of the probabilities of the symbol appearance in j state we determine Lagrange derivative using the element $P(o_k|q_n)$ of the matrix of the conditional probabilities B

$$\frac{\partial L(\Theta, \lambda, \mu, \eta)}{\partial P(o_n|q_n)} = \frac{\sum_{k=1}^K z_{nk}}{P(o_n|q_n)} + \sum_{k=1}^K \eta_k \frac{P(q_n)}{P(o_n)} = 0 \text{ i.e. } 1 = -P(q_n|o_n) \sum_{k=1}^K \eta_k.$$

Sum this expression and have $K = -\sum_{k=1}^K \eta_k$. Taking into account this result we receive the element $P(o_n|q_n)$ of the matrix B

$$P(q_n|o_n) = \frac{1}{K} \text{ or } P(o_n|q_n) = \frac{P(o_n)}{KP(q_n)}. \tag{8}$$

6. Parameter optimization of the algorithm (committee) model

For the collective decision we use some algorithms mix “integration” into the “committee” instructions which use the estimation of the posterior probabilities of the belonging to the initial algorithm class.

At the “committee” model of the algorithm in the form of the mixture 1 of algorithm the initial dependence $p(y|x)$ is expressed as the models composition $p(y|x, \Theta_k)$:

$$p(y|x) = \sum_{k=1}^l G(\Theta_k|x) p(y|x, \Theta_k) = \sum_{k=1}^l g_k p(y|x, \Theta_k), \tag{9}$$

where $g_k = G(\Theta_k|x)$ – the gate of mixture in the form of the belonging to the model Θ_k with the normalizing condition

$$\sum_{k=1}^l g_k = 1, g_k \geq 0 \quad \forall k. \tag{10}$$

As the objects in the sampling are autonomous, the density of the joint distribution (9) is transformed into the product of the distribution densities of every object

$$p(y|x) = \sum_{k=1}^l g_k \prod_{i=1}^n p(y_i|x_i, \Theta_k) = \prod_{i=1}^n \sum_{k=1}^l g_k p(y_i|x_i, \Theta_k). \tag{11}$$

For the characterization of the mixture parameters we maximize $p(y|x)$. We change the order of summation and multiplication and use the principle of maximum likelihood. We form Lagrange’s function [10] from (10), (11) in the form of:

$$L = \sum_{i=1}^m \ln \left[\sum_{k=1}^l g_k p(y_i|x_i, \Theta_k) \right] - \gamma \left(\sum_{k=1}^l g_k - 1 \right). \tag{12}$$

For the determination of the models gates we equate Lagrange’s function derivative (12) on g_k to zero:

$$\frac{\partial L(\Theta_k, \gamma)}{\partial g_k} = \sum_{i=1}^m \frac{p(y_i|x_i, \Theta_k)}{\sum_{s=1}^l g_s p(y_i|x_i, \Theta_s)} - \gamma = 0. \tag{13}$$

For next transformation of this equation we denote the probability $P(y, \Theta_k|x)$ that the object (x, y) is determined by the component Θ_k , $P(\Theta_k|y_i, x_i)$ – the probability that k component of the model is determined by i -object. Every object was created by some model with the formula of the complete probability

$$\sum_{k=1}^l P(\Theta_k|y_i, x_i) = 1, \quad \forall i. \tag{14}$$

For the object (x, y) the probability of its determination by the model Θ_k with the formula of conditional probability equal:

$$P(y, \Theta_k|x) = P(\Theta_k|x) p(y|x, \Theta_k) \equiv g_k p(y|x, \Theta_k). \tag{15}$$

We substitute the equality (15) in the Bayes’ formula for $P(\Theta_k|y_i, x_i)$ and receive

$$P(\Theta_k|y_i, x_i) = \frac{g_k p(y_i|x_i, \Theta_k)}{\sum_{s=1}^l g_s p(y_i|x_i, \Theta_s)}. \tag{16}$$

We multiply both parts of the equality by g_k and sum on $k=1...l$. Taking into account the equality (16) we receive

$$m = \sum_{k=1}^l \sum_{s=1}^m \frac{g_k p(y_i | x_i, \Theta_k)}{\sum_{s=1}^m g_s p(y_i | x_i, \Theta_s)} = \gamma \sum_{k=1}^l g_k = \gamma. \tag{17}$$

Using received result we have from 13

$$g_k = \frac{1}{m} \sum_{s=1}^m \frac{g_k p(y_i | x_i, \Theta_k)}{\sum_{s=1}^m g_s p(y_i | x_i, \Theta_s)} = \frac{1}{m} \sum_{i=1}^m P(\Theta_k | y_i, x_i). \tag{18}$$

The equality 18 allows determining the gate g_k of the committee model.

2. For the characterizing of the committee model components we calculate Lagrange’s function derivative using the parameters k of model Θ_k :

$$\frac{\partial L(\Theta_k, \gamma)}{\partial \Theta_k} = \sum_{i=1}^m \frac{g_k p(y_i | x_i, \Theta_k)}{\sum_{s=1}^m g_s p(y_i | x_i, \Theta_s)} \frac{\partial \ln p(y_i | x_i, \Theta_k)}{\partial \Theta_k} = \frac{\partial}{\partial \Theta_k} \sum_{i=1}^m P(\Theta_k | y_i, x_i) \ln p(y_i | x_i, \Theta_k) = 0. \tag{19}$$

Received equality determines necessary conditions of the maximum of the committee model likelihood function. These conditions match the conditions of the maximum of the likelihood function of the committee model components.

7. Problem solving algorithms of the algorithm parameter optimization

The choice of the problem solving algorithm of the algorithm parameter optimization is performed for the given select (O, Q) in the form of one or several sequences with known values of the hidden components. Matrices of the probability distributions A, B, Π of the model are filled by the equiprobable values (stage of the initialization).

1. For the probability of the generation $P(O | \Theta)$ of the sequence of observations $O = o_1, o_2, \dots, o_T$ for the model $\Theta = (A, B, \Pi)$ in the first task [2] we use the algorithm of forward-backward procedure [2,3,11-13].

Forward procedure. We calculate logically the intervening forward variable $\alpha_t(i)$ as

$$\alpha_t(i) = P(o_1, o_2, \dots, o_t, q_t = s_i | \Theta),$$

i.e. the probability that for given model Θ till the instant t we observed the sequence o_1, o_2, \dots, o_t . In this instant it is situated in the state s_i . Required probability $P(O | \Theta)$ is represented as $P(O | \Theta) = \sum_{i=1}^n \alpha_T(i)$.

We calculate the value $\alpha_t(i)$ by the method of induction using next algorithm:

1. At the stage of initialization we calculate the probability of the state s_j and the first observation o_1 overlap $\alpha_1(i) = \pi_i b_i(o_1), 1 \leq i \leq N$.

2. At the stage of induction we find the method which shows how the system in the instant comes into the state s_j from N possible states of previous instant. As $\alpha_t(i)$ – joint probability of observation display $o_1 o_2 \dots o_t$ and system location in the state s_i in the instant t

$$\alpha_{t+1}(j) = \left[\sum_{i=1}^N \alpha_t(i) a_{ij} \right] b_j(o_{t+1}), \quad 1 \leq t \leq T-1, \quad 1 \leq j \leq N.$$

3. Finish at the step T :

$$P(O | \Theta) = \sum_{i=1}^N \alpha_T(i).$$

Backward procedure. We introduce backward variable $\beta_t(i)$ – conditional probability that system will be situated in the state i by the instant t . The sequence of its observations $o_{t+1}, o_{t+2}, \dots, o_{T-1}, o_T$

$$\beta_t(i) = P(o_{t+1} \dots o_T | q_t = s_i, \Theta).$$

1. For all i from 1 to N we take $\beta_T(i) = 1$, then using induction.
2. For all t in the reverse direction from $T-1$ to 1 and for all i from 1 to N

$$\beta_t(i) = \sum_{j=1}^N a_{ij} b_j(o_{t+1}) \beta_{t+1}(j).$$

3. At the completion phase we determine $P(O|\Theta) = \sum_{i=1}^N \pi_i b_i(o_1) \beta_1(i)$.

II. For the solving of the second class problems we denote Viterbi algorithm [14-17] which uses dynamic programming for finding the calculation of the best chain of the states (fig.1) with the maximum probability $P[Q|O, \Theta]$.

We introduce the auxiliary variables in the form of the maximum probability to reach the state s_i at the stage t among all methods with observed variables

$$\delta_t(i) = \max_{q_1, \dots, q_{t-1}} P(q_1, q_2, \dots, q_t = x_i, o_1, o_2, \dots, o_t | \Theta).$$

1. At the stage of the initialization we determine $\delta_1(i) = \pi_i b_i(o_1)$ and $\Psi_1(i)$ – the most probable states sequence, reliable for the appearance of the first observed symbols. It finishes in the state i .
2. At the stage of induction the most probable states sequence q_1, \dots, q_T is given by the recurrent relations

$$\delta_t(j) = \max_{1 \leq i \leq n} [\delta_{t-1}(i) a_{ij}] b_j(o_t), \Psi_t(j) = \arg \max_{1 \leq i \leq n} [\delta_{t-1}(i) a_{ij}].$$

3. At the final stage T we calculate

$$P^* = \max_{1 \leq i \leq n} \delta_T(i), q_T^* = \arg \max_{1 \leq i \leq n} \delta_T(i)$$

the most probable sequence of the hidden states q_T^* , reliable for the appearance of the first t observed symbols. It finishes in the state n

$$q_T^* = \Psi_{T+1}(q_{T+1}^*).$$

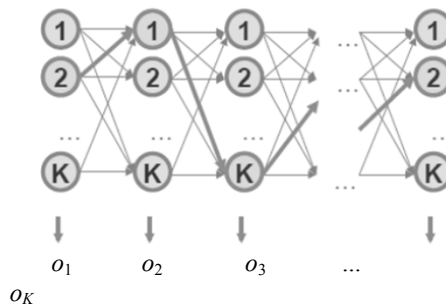


Fig. 1 Viterbi path $\Psi_1(i)$ of algorithm

III. In the third task we use the iteration Baum-Welch algorithm. It's the modification of the Estimation Maximization algorithm (EM). It allows determining the parameters A, B, Π which maximize the likelihood function

of the given model $\Theta=(A, B, \Pi)$ [2]. It performs this action for the appropriate sequence of the observed values O iteratively with given accuracy threshold ε [2].

At the E-step we calculate expectation model parameters values a_{ij} , $b_n(n)$, π_i in the condition of the given data. We introduce the third auxiliary variable as the probability that with the given sequence of observations in instant t – in the state s_i , in instant $t+1$ – in the state s_j

$$\xi_t(i, j) = P(q_t = s_i, q_{t+1} = s_j | O, \Theta),$$

which have the form through the first and the second auxiliary variables

$$\xi_t(i, j) = \frac{\alpha_t(i) a_{ij} b_j(o_{t+1}) \beta_{t+1}(j)}{P(O | \Theta)} = \frac{\alpha_t(i) a_{ij} b_j(o_{t+1}) \beta_{t+1}(j)}{\sum_i \sum_j \alpha_t(i) a_{ij} b_j(o_{t+1}) \beta_{t+1}(j)},$$

and the forth variable

$$\zeta_t(i) = P(q_t = s_i | O, \Theta) = \frac{\alpha_t(i) \beta_t(i)}{\sum_{t=1}^N \alpha_t(i) \beta_t(i)} = \sum_{j=1}^N \xi_t(i, j),$$

which is represented as containment probability in the instant t in the state s_i with the given sequence of observations O and the model Θ .

At the M-step (maximization) we have next probability approaching:

- expected rate of the i state in the instant t_1 $\bar{\pi}_i = \zeta_1(i)$;
- expected rate according to the expression (7) as the doubled ratio of the number of the transitions from the i state to the j state to the number of the output appearance in the i hidden state without 1

$$\bar{a}_{ij} = \frac{2 \sum_{t=1}^{T-1} \xi_t(i, j)}{\sum_{t=1}^{T-1} \zeta_t(i)} - 1;$$

- expected rate according to the expression (8) as the ratio of the couples number (q_n, o_n) , m_q –number of the hidden states, m_o –number of the observed states (symbol v_n) to number of the appearances n hidden states q_n

$$\bar{b}_n(n) = P(o_n | q_n) = \frac{P(o_n) P(q_n | o_n)}{P(q_n)} = \frac{P(q_n, o_n)}{P(q_n)} = \frac{1}{K} \frac{m_o}{m_q} = \frac{1}{K} \frac{m_o}{m_q},$$

when $P(q_n | o_n) = \frac{1}{K}$.

In the iterative repetition of two steps EM-algorithm beginning from $\Theta=(A, B, \Pi)$, we determine $\bar{\Theta} = (\bar{A}, \bar{B}, \bar{\Pi})$, then we calculate the parameters again and so on.

Given algorithm was offered by M.I. Schlesinger [18]. It was covered all over again as the EM-algorithm (expectation – maximization) [19]. Application of the auxiliary hidden variables Q into EM-algorithm provides algorithm convergence [20, 21] and its conditioning with HMM. It simplifies the calculation of the likelihood maximum for the determination of the values of the parameters vector $\Theta=(A, B, \Pi)$.

8. Summary

1. Great information ambiguity typical during the choice of optimal problem solving algorithm and caused by the great initial variety of algorithms models on the alternative solution set determines necessity of the logical transformation of initial set of the alternative solution to the feasible solutions and to the set of the effective solutions which is narrowed down to the set of the optimal solution.

2. We take into account many constraints during the transformation of the alternative solution set to the feasible solution set. These constraints must conform to the informal specificities of the problem solving. We must take into consideration the specificities of the operation formalization of the synthesizable algorithm during the algorithm synthesis. Constraint satisfaction is the necessary condition for the choice of the solution algorithm that's why the final solution is situated in the set of the feasible solutions.

3. The likelihood function in the form of the Lagrange equation is formed for the parameter optimization. The constraints in the least compound are formed by way of the normalizing conditions for each model variable and in the form of the Harkevich information.

4. The common approach to the estimation of the HMM algorithm optimal parameters determines the probability distribution of the initial states by the expression (6), model transition probability from the state i to the state j (7), probabilities of the symbol appearance in the j state (8).

5. We use Mixture of Experts in the form of the "committee" constructions during making collective decision. They use the gates estimation (a posteriori probability of the algorithm belonging to the class).

6. During the optimization of the algorithm committee model:

- the optimal values of the gates parameters are determined by the expression (18);
- the optimal parameters of the algorithm committee model are given by the necessary conditions of the likelihood function maximum of the algorithm committee model. They match the conditions of the likelihood function maximum of the committee model components.

References

- [1] L.E. Baum, An inequality and associated maximization technique in statistical estimation for probabilistic functions of a Markov process, *Inequalities*. 3 (1972) 1–8.
- [2] L.R. Lawrence, A tutorial on hidden Markov models and selected applications in speech recognition, *Proceedings of the IEEE*. 77 (1989) 257–286.
- [3] L.R. Rabiner, B.H. Juang, An introduction to hidden Markov models, *IEEE ASSP Magazine*. (1986) 4–15.
- [4] A.A. Mikhaylov, S.A. Bazuyeva, Probabilistic Approach to the Synthesis of Algorithm for Solving Problems, *Modern Applied Science. Canadian Center of Science and Education*. 9(5) (2015) 125–132
- [5] L.R. Rabiner, Skriptivnye markovskiyeh modeli i ih primeneniye v izbrannih prilozheniyah pri raspoznavanii rechi, *Obzor/TIER*. 77(2) (1989) 86–102.
- [6] V.P. Zabolotskiy, A.A. Ovodenko, A.G. Stepanov, *Matematicheskiye modeli v upravlenii*, Saint-Petersburg, 2001.
- [7] A.A. Harkevich, O sennosti informatsii, *Problemi kibernetiki*. 4 (1960) 53–72.
- [8] M.M. Bongard, *Problemi uznvaniya*, Nauka, Moskva, 1967.
- [9] G.D. JR. Fomey, The Viterbi Algorithm, *Proceedings of the IEEE*. (3) (1973) 268–277.
- [10] V.A. Zorich, *Matematicheskiy analiz*, FAZIS, Moskva, 1997.
- [11] J.P. Haton, Automatic speech recognition: Past, Present and Future, *Proceeding of SPECOM*, St. Petersburg "Anatoliya". (2004) 3–7.
- [12] X. Huang, *Hidden Markov Models for speech Recognition*, Edinburg: Edinburg University Press, 1990.
- [13] J. Binder, K. Murphy, S. Russell, Space-Efficient Inference in Dynamic Probabilistic Networks, *Int'l, Joint Conf. on Artificial Intelligence*. 1(5) (1997) 1292–1296.
- [14] A.J. Viterbi. Error bounds for convolutional codes and an asymmetrically optimum decoding algorithm, *IEEE Transactions on Information Theory*. 13 (1967) 260–267
- [15] A.D. Viterbi, J.K. Omura, *Printsipi tsifrovoy svyazi i kodirovaniya*, Radio i svyaz, Moskva, 1982.
- [16] V.V. Zolotarev, G.V. Ovechkin, *Pomehoustoichivoye kodirovaniye. Metodi i algoritmi*, Goriachaya liniya. Telekom, Moskva, 2004.
- [17] R. Morelos-Karagosa, *Iskusstvo pomehoustoichivogo kodirovaniya. Metodi, algoritmi, primeneniye*, Tehnosfera, Moskva, 2006.
- [18] M.I. Shlezinger, *O samoproizvolnom razlichenii obrazov*, Chitajushhie avtomaty, Naukova dumka, Kiev, 1965.
- [19] A.P. Dempster, N.M. Laird, D.B. Rubin, Maximum likelihood from incomplete data via the EM algorithm, *J. of the Royal Statistical Society, Series B*. 34 (1977) 1–38.
- [20] C.F.G. Wu, On the convergence properties of the EM algorithm, *The Annals of Statistics*. 11 (1983) 95–103.
- [21] M.I. Jordan, L. Xu, Convergence results for the EM algorithm to mixtures of experts architectures, *Tech. Rep. A.I. Memo №1458*: MIT, Cambridge, MA, 1993.



International Conference on Industrial Engineering

Evaporator system of water desalination based on Ranque-Hilsch vortex effect

Terekhin A. A.^{ab}, Zolotykh I.K.^{ab*}

^aSouth Ural State University, 76, Lenin Avenue, Chelyabinsk, 454080, Russian Federation

^bControl Systems, Russian Instrument-Making Corporation, Closed Joint Stock Company, Chelyabinsk, Russia, 454008

Abstract

The vortex tube of the water desalination evaporator system is studied based on the Ranque-Hilsch vortex effect. Vortex effects mathematical model is based on Reynolds Equations which is completed by k-w SST turbulence differential model. One of the goals of the research is to define the geometry of the vortex tube scaled model. Another goal of the research is to define the input parameters for Reynolds Stress Turbulence Model. The results of the research are the defined optimal geometry parameters of the vortex tube prototype and input parameters required for Reynolds Stress Turbulence Model analysis.

© 2015 The Authors. Published by Elsevier Ltd. This is an open access article under the CC BY-NC-ND license (<http://creativecommons.org/licenses/by-nc-nd/4.0/>).

Peer-review under responsibility of the organizing committee of the International Conference on Industrial Engineering (ICIE-2015)

Keywords: Computational Fluid Dynamics, Ranque-Hilsch effect, vortex tube.

1. Introduction

Nowadays in Russia the desalted water is mainly produced using chemical demineralization. This technology is expensive, harmful for ecology and obsolete. The introduced design of the evaporator system allows the water desalination employing the intensified heat and mass processes in the centrifugal force field.

An effectiveness of the vortex tube operation depends on its design and operating parameters. Therefore, the key term of the vortex tube implementation is determination of its optimal design and operating parameters.

* Corresponding author. Tel.: +7-908-578-6854.

E-mail address: Aleksandr.Terekhin@gmail.com

For the numerical simulation of viscous turbulent flow of gas a mathematical model based on the system of Reynolds equations [1, 2] completed by $k-\omega$ SST turbulence differential model [3, 4].

2. Formulation of a problem

The main goal of the numerical simulation is to determine the geometric and technical parameters of the vortex tube evaporator water desalination, which are necessary for the design and further produce the prototype model of of evaporator system. The second goal is to determine the input parameters for numerical simulation with use mathematical model based on Reynolds Stress Turbulence Model.

Schematic drawing of the vortex tube is showed in Fig. 1. Vortex tube dimensions choosing according recommendations of [5] and summarized in tab. 1.

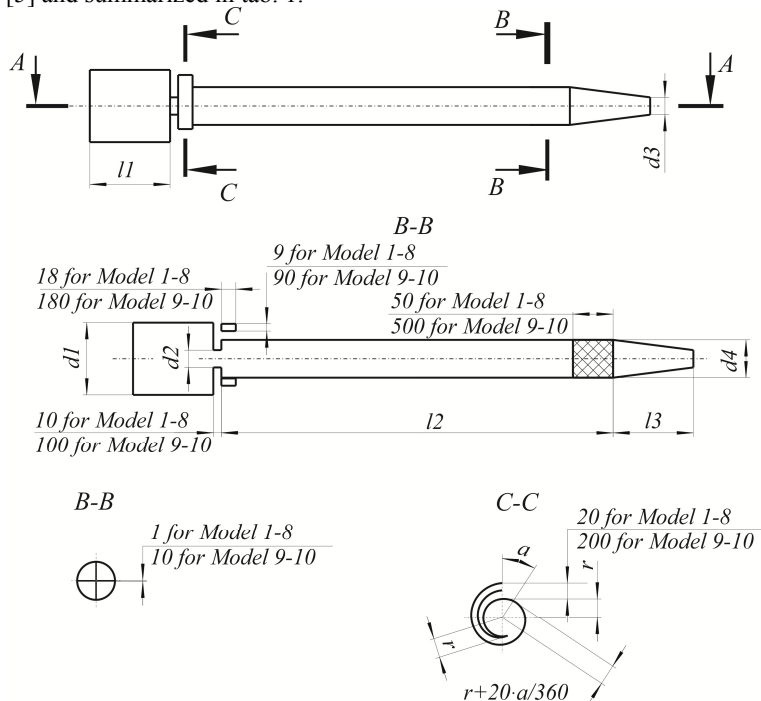


Fig. 1. Schematic drawing of the vortex tube.

Table 1. Dimensions of models.

Model name	L, mm	l3, mm	d1, mm	d2, mm	d3, mm	d4, mm
Model №1	488	50	60	13.5	6.75	21.6
Model №2	488	50	60	13.5	10.125	21.6
Model №3	488	50	60	13.5	13.5	21.6
Model №4	418	50	60	13.5	6.75	21.6
Model №5	488	50	60	21.6	21.6	47.1
Model №6	488	50	60	21.6	10.8	47.1
Model №7	418	50	60	13.5	6.75	21.6
Model №8	303	50	60	13.5	3	21.6
Model №9	3030	500	600	135	30	216
Model №10	3030	500	600	135	30	216

Models from 1 to 7 are prototype model which will be used in full-scale experiment for correction mathematic model of vortex tube of evaporator system of water desalination. Models 8, 9 and 10 are full-scale industrial models. Boundary conditions of mathematical model and their names is showed in Fig. 2. The numerical values of the physical parameters which set up at the boundaries conditions summarized in tab. 2 and 3. Thermophysical properties of vapor chosen in accordance with the recommendations [6, 7].

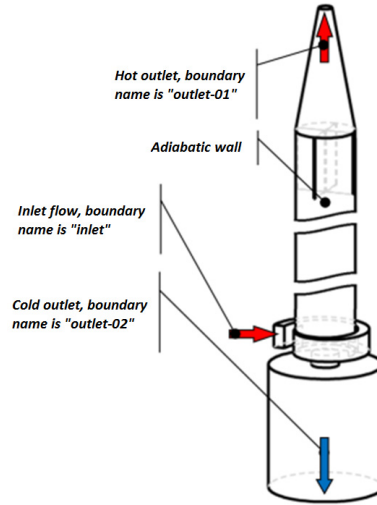


Fig. 2. Scheme of boundary conditions.

Table 2. Grid value and material of fluid.

Model name	Number of Elements in computing model	Fluid material
Model №1	640 742	Air
Model №2	653 580	Air
Model №3	657 833	Air
Model №4	604 087	Air
Model №5	826 909	Air
Model №6	817 558	Air
Model №7	4 852 368	Air
Model №8	4 212 802	Air
Model №9	4 212 802	Air
Model №10	4 212 802	Vapor

Table 3. Material properties.

Fluid material	T_{inlet} , K	$P_{outlet-01}$, $P_{outlet-02}$, Pa	μ , Pa·s	c_p , J/(kg·K)	λ , W/(m·K)	R , J/(kg·K)
Air	373.15	-9700	$1.83 \cdot 10^{-5}$	1004.4	0.0261	287
Vapor	373.15	-9700	$1.85 \cdot 10^{-4}$	2042.0	1.4000	461

- T_{inlet} – fluid temperature in inlet;
- $P_{outlet-01}$ – reference pressure of fluid in outlet-01;
- $P_{outlet-02}$ – reference pressure of fluid in outlet-02;
- R – gas constant for state equation;
- c_p – specific heat capacity for constant pressure;
- λ – thermal conductivity;
- μ – dynamic viscosity.

3. Mathematical model

For the numerical simulation of vortex flow used Reynolds Averaged Navier-Stokes equations (RANS) [1, 4, 8] closed by two-equation $k-\omega$ SST turbulence energy model [3, 4, 8].

The solution of the Reynolds Averaged Navier-Stokes equations (RANS) closed by two-equation $k-\omega$ SST turbulence energy model was using program DinamLGTM [10] which based on control volume approach [9].

4. Results of numerical simulation

Schematic eddy generation in vortex tube for models 6, 7 and 9 is shown in Fig. 3. These eddy generation is typical for all considered flows. Fig. 3 is shown separated on cold flow and hot flow according Ranque-Hilsch effect.

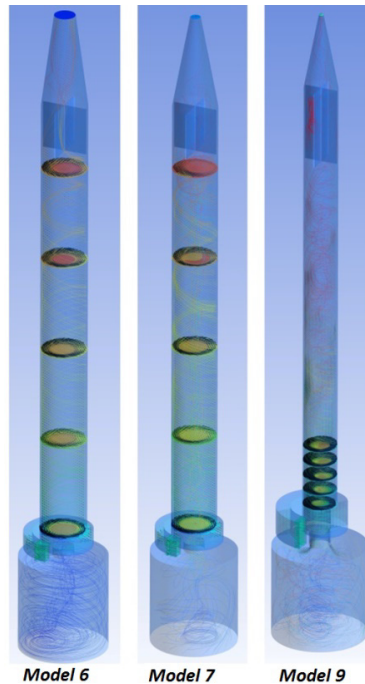


Fig. 3. Scheme of eddy generation in vortex tube.

The main goal of the calculations is the choice of optimal geometric parameters of the prototype. The results of the calculations for all cases are summarized in table 4.

The main characteristic of the quality of the process of desalination is ratio of mass flow of hot gas to mass flow of cold gas, which advises boundary condition “outlet-01” and “outlet-02”, Fig. 2. The model 1 to 4 has the same structure partitioning the computational domain into control volumes. The difference between models was only in geometry. As shown by calculations, the most successful geometric dimensions model is model 4, Fig. 4-a.

Models 5 and 6 differ from models 1 to 4 the increased volume inner section of tube where reduce (generate) vortex flow. The model 6 has productivity by 4 times less than the model 4, Tab 4, Fig. 4.

Model 4 and 7 differ in the quality of approximation of the computational domain. The number of control volumes of the computational domain differs by 6 times (tab. 2). The summarized time of the calculation for the model 4 is 10 hours and for model 7 is 0.8 hours. On structurally stable grid (coarse mesh) more comfortable to make a preliminary calculation and the next step is use of fine mesh for refinement parameters of calculation model. Comparison results of calculation showed that the grinding significantly affects the final results and for similar vortex flow necessary to carry out the analysis grid independence for all models, Fig. 4-b. The influence of the

length of inner section of tube where reduce (generate) vortex flow is showed comparing model 7 and model 8 (model 8 shorter on 30% then model 7). Results of calculation between model 7 and model 8 the similar (tab. 4, fig. 5-a), but length of inner section of tube model 8 shorter on 30%. Model 8 is more compact and is preferable for manufacture of the prototype model.

Model 8 and model 9 different by scale, model 9 is 10 times more model 8. Scale vortex structures formed in the volume inner section of tube are substantially different, as the transition from air to vapor (Fig. 5-b).

Table 4. Results of numerical simulation.

Model name	Inlet Velocity, m/s	Inlet Pressure, bar	Ratio of the mass hot flow and cold flow	Difference between hot flow temperature and cold flow temperature, K	Average reference pressure in domain, bar	Mass flow of gas (vapor), kg/s	Volume-flow rate of gas (vapor), l/min
1	100	0.09	6.9	7.1	-0.05	0.01644	818.5
1	150	0.53	7.7	31.9	0.09	0.03468	1727.0
1	200	1.52	8.0	63.5	0.37	0.07610	3789.2
1	250	3.65	9.2	104.1	0.96	0.17549	8738.1
2	100	0.09	11.1	7.1	-0.05	0.01645	818.9
2	150	0.54	9.8	28.5	0.07	0.03497	1741.5
2	200	1.77	7.4	65.0	0.40	0.08370	4167.4
2	250	6.06	7.5	109.3	1.51	0.26651	13270.2
3	100	0.001	30.0	1.1	-0.14	0.01513	753.4
3	150	0.41	20.3	11.7	0.00	0.03191	1588.7
3	200	1.70	12.0	49.7	0.32	0.08153	4059.6
3	250	8.07	10.0	122.0	1.85	0.34243	17050.5
4	100	0.09	6.8	7.1	-0.05	0.01642	817.5
4	150	0.56	6.2	32.7	0.09	0.03536	1760.4
4	200	1.73	6.1	69.1	0.41	0.08249	4107.2
4	250	4.46	5.1	110.3	1.11	0.20614	10264.2
5	100	-0.04	1500	-0.8	-0.09	0.01443	718.6
5	150	0.02	316.4	0.6	-0.08	0.02312	1151.2
5	200	0.16	192.2	3.4	-0.07	0.03504	1744.8
5	250	0.43	111.2	1.5	-0.05	0.05418	2697.8
6	100	-0.04	22.9	0.4	-0.09	0.01453	723.7
6	150	0.05	21.3	3.0	-0.08	0.02375	1182.8
6	200	0.20	18.4	8.4	-0.05	0.03614	1799.5
6	250	0.56	22.6	21.6	0.01	0.05903	2939.3
7	100	-0.04	22.9	0.4	-0.09	0.01453	723.7
7	150	0.05	21.3	3.0	-0.08	0.02375	1182.8
7	200	0.20	18.4	8.4	-0.05	0.03614	1799.5
7	250	0.56	22.6	21.6	0.01	0.05903	2939.3
8	100	0.06	13.3	5.1	-0.07	0.01601	797.1
8	110	0.14	16.2	10.3	-0.04	0.01896	944.3
8	120	0.26	28.0	15.4	-0.01	0.02283	1136.5
8	130	0.33	27.0	17.8	0.00	0.02605	1297.3
8	140	0.40	26.4	20.7	0.02	0.02952	1469.8
8	150	0.47	27.1	24.5	0.04	0.03331	1658.6
9	100	0.06	12.8	4.1	-0.07	1.59833	79585.0
9	120	0.24	47.1	10.1	-0.03	2.24131	111600.7
9	150	0.46	48.2	21.1	0.02	3.29885	164258.0
10	100	0.34	26.5	3.1	0.00	1.27337	63404.4
10	120	0.79	17.2	11.5	0.14	2.03187	101171.7
10	150	1.42	17.1	17.2	0.29	3.43358	170966.5

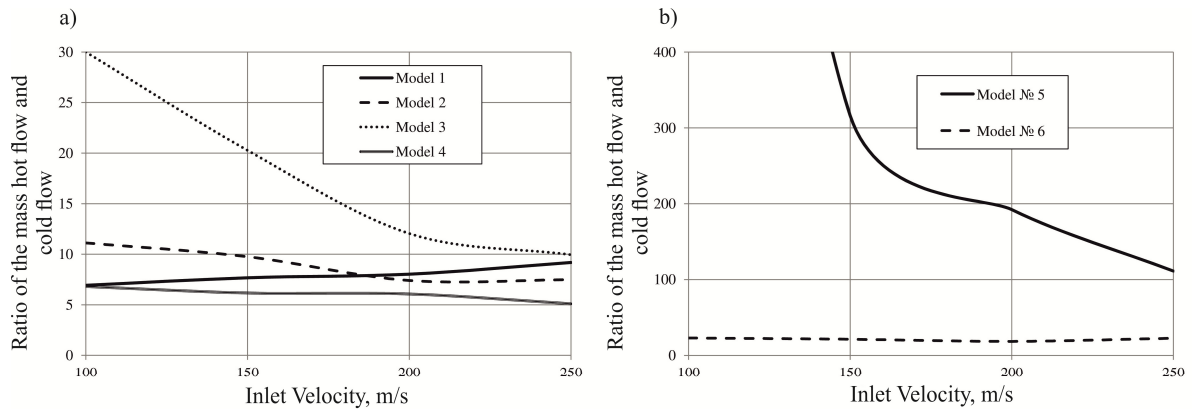


Fig. 4. Ratio of the mass hot flow and cold flow (a) for models 1 to 4; (b) for models 5 and 6.

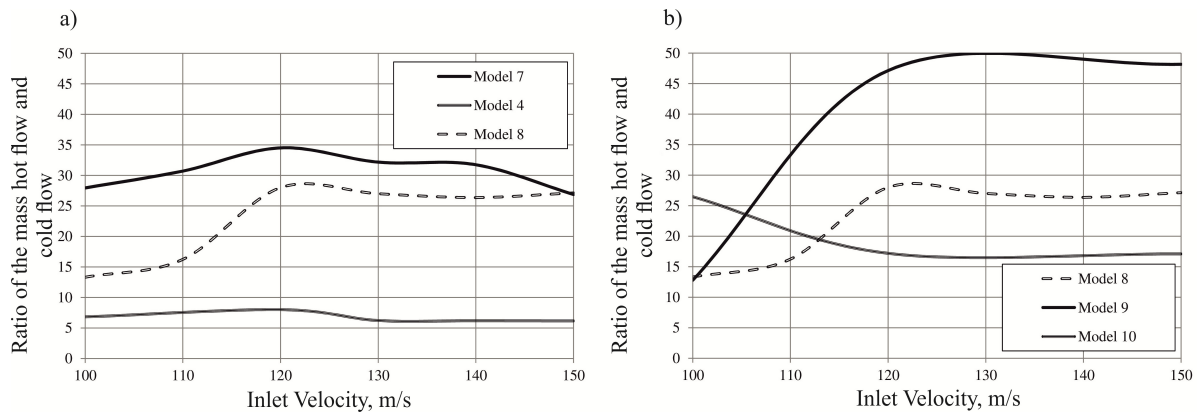


Fig. 5. Ratio of the mass hot flow and cold flow (a) for models 4, 7 and 8; (b) for models 8 to 10.

5. Conclusion

For manufacture prototype according calculations more reasonable is model 8, which is scaled-down industrial model 10. Manufacture of prototype and running of physical experiment for air make more precise setup calculation with use Reynolds Stress Turbulence Model.

Analyzing of vortex in the tube of evaporator water desalination with appear separation flow according Ranque-Hilsch effect for Reynolds Stress Turbulence Model necessary make calculation with fine grid where minimal controls volume of domain will be 4.5 million. The next necessary condition for get reliable data is achieved grid independence. This work is planned to be performed at the next step of calculations.

Acknowledgements

The work was conducted with the financial support of the Ministry of Education and Science of the Russian Federation in the framework of the project “Applied research and development of the method of preparation of the boiler and heating water by phase transitions in the vortex under high vacuum” according to the contract no. 14.579.21.0063 d.d. 20.10.2014, identifier RFMEFI57914X0063 between the Ministry of Education and Science of the Russian Federation and Federal State Educational Institution of Higher Professional Education “South Ural State University” (National Research University).

References

- [1] D.C. Wilcox, *Turbulence Modeling for CFD*, DCW Industries, 1994.
- [2] H. Schlichting, *Boundary-layer theory*, McGraw-Hill, New York, 1968.
- [3] F.R. Menter, Two-equation eddy viscosity turbulence models for engineering applications, *AIAA J.* 32(1) (1994) 1299–1310.
- [4] T.J. Chung, *Computational Fluid Dynamics*, Cambridge University Press, 2002.
- [5] A.P. Merkulov, *Vortex effect and its application in engineering*, Mashinostroenie, Moscow, 1969.
- [6] M.P. Vukasovich, *Thermodynamic Properties of water and steam*, Mashinostroenie, Moscow, 1955.
- [7] A.A. Aleksandrov, B.A. Grigoriev, *Tables of thermophysical properties of water and steam*, MPEI, Moscow, 1999.
- [8] H.K. Versteeg, *An introduction to computational fluid dynamics the finite volume method*, Longman Group Ltd, 1995.
- [9] S. Patankar, *Numerical heat transfer and fluid flow*, Hemisphere Publishing Corporation, New York, 1980.
- [10] A.A. Terekhin, T.V. Terekhina, V.A. Shcheglov, R.V. Sidelnikov, A.L. Kartashev, Certificate of state registration the computer program 2009613165. (2009).

International Conference on Industrial Engineering

Mathematical modeling of the process of perforation with a hydraulic drilling perforator during oil and gas field development

Mesropyan A.V., Mityagina M.O.*

Ufa State Aviation Technical University, 12, K. Marksa, Ufa, 450008, Russia

Abstract

This paper presents a mathematical model of a hydraulic drilling perforator, which takes into account the effect of the reciprocating movement of the drill mounted on a flexible shaft, as well as the effect of the physical and mechanical properties of reservoirs, on the operation processes. The transition process during channel perforation by a hydraulic drilling perforator is modeled. The calculation results for the mathematical model of a hydraulic drilling perforator demonstrate that due to the concurrent use of both rotational and reciprocating movement of the drill mounted on a flexible shaft, it is possible to reduce the time spent for the perforation of a single channel in a productive formation by a drilling perforator by up to 90 %

© 2015 Published by Elsevier Ltd. This is an open access article under the CC BY-NC-ND license

(<http://creativecommons.org/licenses/by-nc-nd/4.0/>).

Peer-review under responsibility of the organizing committee of the International Conference on Industrial Engineering (ICIE-2015)

Keywords: Drilling perforator; mathematical model; reservoir; layout diagram

1. Introduction

The problem of the fullest extraction of hydrocarbons from the earth sets important tasks for the oil producing companies, related to the development and adoption of new technologies and technical means aimed at increasing the efficiency of oil field development. Experts estimate that a wide application of new oil recovery methods and modern technical facilities during oil field development will enable a 30 – 50 % increase in the recoverable oil reserves [1].

A promising area for the enhancement of oil recovery of productive formations is the improvement of oil recovery technologies through the application of modern resource-saving field development systems, using low-impact methods for opening of productive formations.

From the point of view of getting the maximum possible oil recovery of a formation, the most promising method appears to be drilling perforation. The use of drilling perforation enables the operation of facilities under complex geological and technical conditions: high-viscosity oil pool with a low productivity and small thickness, oil pools with formations contacting closely with bottom water, facilities with poor-quality cement sheath where productive

formations are divided from the water-bearing part of the pool by a thin unstable bridge, as well as facilities with alternating permeable and compacted interlayers.

2. Topicality and task definition

At the present time, drilling perforation is not widely used due to a relatively low productivity of reservoir perforation and a small depth of perforation channels which is, in some cases, insufficient for passing through clogging zones (table 1) [2 – 6].

Table 1. Time and depth of perforation of a single channel by drilling perforators.

Drilling perforator name	Manufacturer	Time of channel perforation, (min)	Depth of perforation channel, (mm)
PS-112	OJSC NPP «VNIIGIS»	5	50
PS-112/70	OJSC NPP «VNIIGIS»	5	70
PS-112/18/500	«PITC «Geofizika» LLC, NPF «ERGIS»	at least 30	500
Electrical drill for side-tracking	OJSC «OSKBP»	about 45	up to 850

The borehole operation conditions of drilling perforators, associated with a wide variation range of pressure and temperature characteristics combined with different geological features of a perforated rock, determine the complex and ambiguous nature of the physical and hydrodynamic processes running in the flow section of a drilling perforator. Currently, the mathematical modeling of perforation of productive formations by borehole drilling perforators has a rather experimental character. The absence of any mathematical models of the process of perforation by drilling perforators, corresponding to real borehole facilities, creates certain difficulties during the development of new advanced technical means for perforation of productive formations. This determines the need for works dealing with design of drilling perforators and modeling of the process of perforation of oil-and-gas-bearing formations by drilling perforators.

At the present time, there is a topical task to develop and design drilling perforators ensuring an enhanced productivity of formation perforation, as well as the perforation of channels with the required length in complex-structure reservoirs that contain alternating productive and impermeable interlayers, thin oil-filled formations located near water-bearing formations, oil rims.

3. Mathematical model of a hydraulic drilling perforator

On the basis of the technical conditions of opening of oil-bearing formations and analysis of scientific and technical literature, the main technical specifications of hydraulic drilling perforators have been defined (table 2) [7, 8, 9].

Table 2. Main technical specifications of a hydraulic drilling perforator.

Technical specifications	Values of the characteristics
Time for perforation of a single channel, (min)	not more than 2.5
Perforation channel depth, (m)	at least 0.2
Perforation channel diameter, (m)	0.2
Maximum number of drilling operations per one run in the hole	up to 40*
Time for channel perforation, (s)	not more than 120
Energy-independent system of perforator release in a borehole	available

* determined by the drilling tool life, as well as the geological and technical conditions of a borehole

Figure 1 shows the layout diagram of a hydraulic drilling perforator [10, 11].

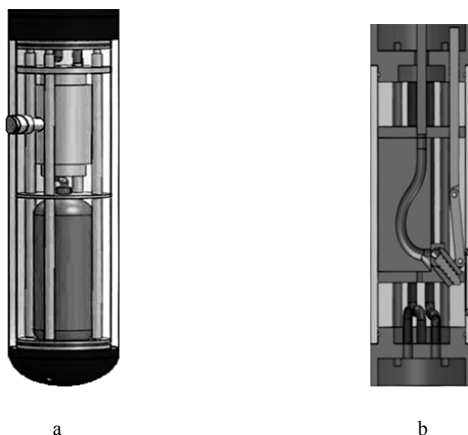


Fig. 1. Fragment of a layout diagram of a hydraulic drilling perforator: (a) fixation circuit; (b) perforation circuit.

Channel perforation by a hydraulic drilling perforator is ensured by a coordinated operation of three circuits: a fixation circuit, a drill feeding circuit and a perforation circuit.

The fixation circuit ensures the fixation of the drilling perforator’s body in a casing with the help of the stems of two hydraulic cylinders for fixation, which extend uniformly, taking up the clearance between the perforator’s body and the casing (normally, to a length not more than 0.02 – 0.1 m within 2 – 10 s). The drill feeding circuit ensures the feeding of a drill head mounted on a flexible shaft to the target perforation depth (0.2 – 0.5 m). The perforation circuit ensures, if necessary, a concurrent rotational and reciprocating movement of a drill mounted on a flexible shaft (the rotation speed is from 200 to 800 rev/min, the percussion frequency of the drilling perforator is 1800 min⁻¹), thereby increasing the productivity of perforation of productive formations by a hydraulic drilling perforator. It is rational to use the concurrent rotational and reciprocating movement of the drill when perforating a rock, and to conduct perforation of a casing and a cement sheath using the working tool’s rotation.

$$\left\{ \begin{aligned}
 &U_D = R_D \cdot i_D(t) + L_D \cdot \frac{di_D(t)}{dt} + K_{CE_D} \cdot \frac{dx_D(t)}{dt}, \\
 &m_{S_D} \cdot \frac{d^2x_D(t)}{dt^2} + b_{S_D} \cdot \frac{dx_D(t)}{dt} + c_{SPR_D} \cdot x_D(t) = K_{FID} \cdot i_D(t), \\
 &\mu \cdot f_D \cdot \sqrt{\frac{2 \cdot |p_{SUP} - p_{1D}(t)|}{\rho}} \cdot \text{sign}(p_{SUP} - p_{1D}(t)) = \\
 &= A_{p_D} \cdot \frac{dy_D(t)}{dt} + \frac{W_{HC_D}}{2 \cdot E} \cdot \frac{dp_{1D}(t)}{dt}, \\
 &\mu \cdot f_D \cdot \sqrt{\frac{2 \cdot |p_{2D}(t) - p_{DR}|}{\rho}} \cdot \text{sign}(p_{2D}(t) - p_{DR}) = \\
 &= A_{EF_D} \cdot \frac{dy_D(t)}{dt} - \frac{W_{HC_D}}{2 \cdot E} \cdot \frac{dp_{2D}(t)}{dt}, \\
 &m_{HC_D} \cdot \frac{d^2y_D(t)}{dt^2} + R_{STAT_D} \cdot \text{sign}\left(\frac{dy_D(t)}{dt}\right) + b_{HC_D} \cdot \frac{dy_D(t)}{dt} + R_p \cdot \chi = \\
 &= A_{EF_D} \cdot |p_{1D}(t) - p_{2D}(t)|,
 \end{aligned} \right. \tag{1}$$

$$\left\{ \begin{array}{l}
 U_p \cdot \sin(\omega \cdot t) = R_p \cdot i_p(t) + L_p \cdot \frac{di_p(t)}{dt} K_{CEP} \cdot \frac{dx_p(t)}{dt}, \\
 m_{SP} \cdot \frac{d^2 x_p(t)}{dt^2} + b_{SP} \cdot \frac{dx_p(t)}{dt} + c_{SRPP} \cdot x_p(t) = K_{FIP} \cdot i_p(t), \\
 \mu \cdot B_p \cdot x_p(t) \cdot \sqrt{\frac{2 \cdot |p_{SUP} - p_{1P}(t)|}{\rho}} \cdot \text{sign}(p_{SUP} - p_{1P}(t)) = \\
 = A_{EFP} \cdot \frac{dy_p(t)}{dt} + \frac{W_{HCP}}{2 \cdot E} \cdot \frac{dp_{1P}(t)}{dt}, \\
 \mu \cdot B_p \cdot x_p(t) \cdot \sqrt{\frac{2 \cdot |p_{2P}(t) - p_{DR}|}{\rho}} \cdot \text{sign}(p_{2P}(t) - p_{DR}) = \\
 = A_{EFP} \cdot \frac{dy_p(t)}{dt} - \frac{W_{HCP}}{2 \cdot E} \cdot \frac{dp_{2P}(t)}{dt}, \\
 m_{HCP} \cdot \frac{d^2 y_p(t)}{dt^2} + R_{STATP} \cdot \text{sign}\left(\frac{dy_p(t)}{dt}\right) + b_{HCP} \cdot \frac{dy_p(t)}{dt} = \\
 = A_{EFP} \cdot (p_{1P}(t) - p_{2P}(t)),
 \end{array} \right. \quad (2)$$

where U_D , U_P is the voltage of the electrical direct-current network in the drill feeding circuit and the perforation circuit, respectively; R_D , R_P is the resistance of the electromagnet's control winding in the drill feeding circuit and the perforation circuit; $i_D(t)$, $i_P(t)$ is the function of electric current in the electrical network of the drill feeding circuit and the perforation circuit; L_D , L_P is the inductance of the electromagnet's control winding in the drill feeding circuit and the perforation circuit; K_{CED} , K_{CEP} is the coefficient of the counter-electromotive force in the electrical network for the hydraulic distributor (HD) controlling the drill feeding hydraulic cylinder (HC) and the perforation HC; $x_D(t)$, $x_P(t)$ is the displacement of the spool of the HD controlling the drill feeding HC and the perforation HC; m_{SD} , m_{SP} , m_{HCD} , m_{HCP} is the mass of the spool of the HD controlling the drill feeding HC and the perforation HC, as well as the mass of the drill feeding HC and the perforation HC, respectively; b_{SD} , b_{SP} is the coefficient taking into account the friction in the plunger – liner friction couple in the drill feeding circuit and the perforation circuit; c_{SPRD} , c_{SRPP} is the stiffness of the spring of the HD controlling the drill feeding HC and the perforation HC; K_{FID} , K_{FIP} is the coefficient of current in the electrical network for the HD controlling the drill feeding HC and the perforation HC; μ is the coefficient of fluid flow through the spool in the HD controlling the fixation HC; f_D is the area of the spool in the HD controlling the drill feeding HC; B_p is the slit width of the spool in the HD controlling the perforation HC; $p_{1D}(t)$, $p_{1P}(t)$, $p_{2D}(t)$, $p_{2P}(t)$ is the pressure of the hydraulic fluid in the cavities of the drill feeding HC and the perforation HC, respectively; p_{SUP} , p_{DR} is the supply pressure and the drain pressure of the hydraulic system; ρ the density of hydraulic fluid; A_{PD} , A_{EFD} , A_{EFP} is the effective area of the piston of the drill feeding HC and the perforation HC on the side of the piston and the stem, respectively; $y_D(t)$, $y_P(t)$ is the displacement of the piston of the HC; W_{HCD} , W_{HCP} is the volume of the hydraulic fluid in the chamber of the drill feeding HC and the perforation HC; E is the reduced elastic modulus of the hydraulic fluid; R_{STATD} , R_{STATP} is the static load on the drill feeding HC and the perforation HC; b_{HCD} , b_{HCP} is the coefficient taking into account the force of viscous damping in the drill feeding HC and the perforation HC; R_p is the force required to fracture a rock; χ is the coefficient taking into account the rotation speed of the drill head and the hardness of a rock.

4. Results

Figure 2 displays the results of mathematical modeling of the hydraulic drilling perforator.

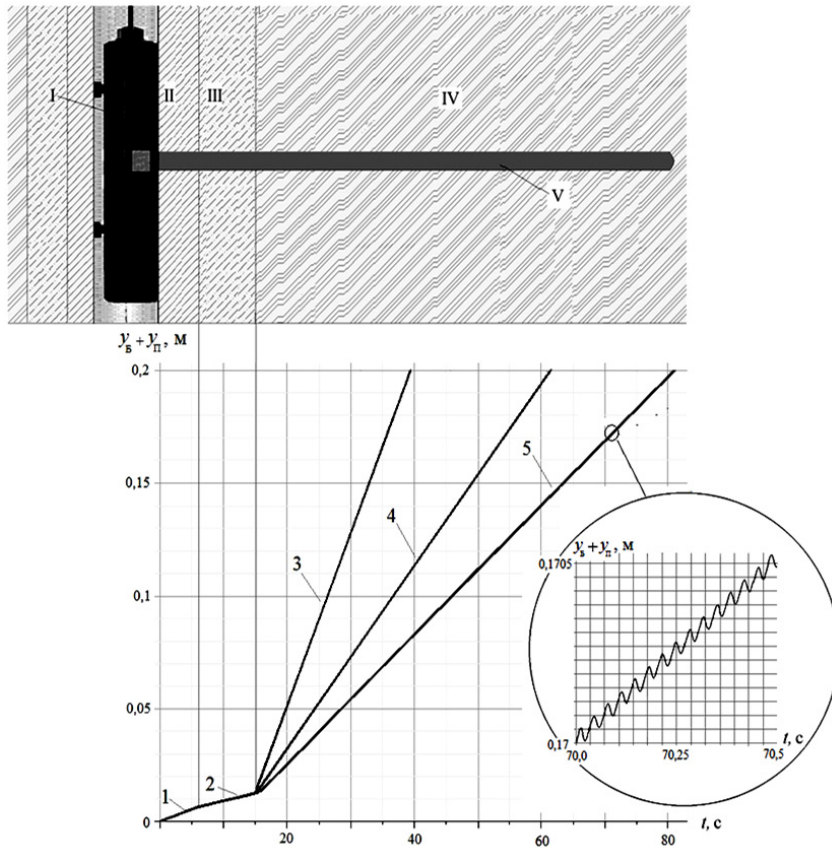


Fig. 2. The results of modeling of channel perforation by a hydraulic drilling perforator:

I – hydraulic drilling perforator; II – cement sheath; III – casing; IV – productive formation; V – perforation channel;
 1 – perforation of a casing; 2 – perforation of a cement sheath; 3, 4, 5 – perforation of sandstone, limestone and dolomite, respectively

The results of modeling of channel perforation by a flexible drill of the drilling perforator, taking into account the physical and mechanical properties of reservoirs (1) and the reciprocating movement of the perforation hydraulic cylinder (2), demonstrate that, when perforating a channel with a depth of 0.2 m in dolomite, the perforation time has decreased 15-fold and 8-fold in comparison with the perforation time for the drilling perforator PS-112 and the electrical drill for side-tracking, respectively (fig. 2) [12, 13].

5. Conclusion

The developed mathematical model of the hydraulic drilling perforator enables, on the basis of the numerical method for solving a formed system of differential equations, to model the process of perforation of productive formations by borehole equipment, taking into account the geological features of the perforated rocks. The results of the mathematical modeling show that the main time during channel perforation (up to 80%) is spent for the perforation of a rock. It is possible to increase the efficiency of perforation of productive formations by drilling perforators by way of using concurrently the rotational and reciprocating movement when perforating rocks. It has been established that when perforating dolomite, one of the hardest hydrocarbon-bearing rocks, the time spent for the perforation of a single channel with a length of 0.2 m is less than 1.5 min. Thus, the productivity of perforation

of productive formations by low-impact methods increases (by up to 90%). This approach ensures the perforation of a productive formation without any deformation and fracture of casings and cement sheath, which cumulatively increases the oil recovery of a formation and promotes a more rational development of well stock.

References

- [1] D.Yu. Kryanev, S.A. Zhdanov, Scientific providing of new development technologies of oil fields with hardly extractable reserves // *Bureniye i Nef*. 2012. No. 08. P. 29–34 (in Russian).
- [2] Drilling perforator PS-112/70. [Electronic resource]. URL: <http://vniigis.com/pdf/pmks/6.pdf> (access date: 30.06.2015) (in Russian).
- [3] P.N. Gulyaev, M.I. Zhulanova, Yu.B. Frolov, Drilling perforation of deep penetration // *Neftegaz INTERNATIONAL*. 2008. No. 2. p. 33 (in Russian).
- [4] A.V. Lyagov, E.L. Malikov, N.Yu. Kuznetsova, et al. Improving the technology of the secondary opening and development of wells // *Neftegazovoye Delo*. 2011. No. 6. pp. 160–175 (in Russian).
- [5] OJSC «Omsk Special Design Bureau of Instruments - OSKBP». Electrical drill for side-tracking in a productive oil (gas) formation. [Electronic resource]. URL: <http://www.oskbp.ru/index.php?id=20> (access date: 30.06.2015) (in Russian).
- [6] Russian Federation patent # 2244104, IPC7 E 21 B 43/11. Method for opening productive bed from well and device for realization of said method / M.P. Sergienko, A.A. Sharov, Ju.G. Metel'; patent owner OJSC «Omsk Special Design Bureau of Instruments - OSKBP». Application number 2003112934/03; application date 30.04.2003; publication date 10.01.2005.
- [7] A.I. Bulatov, Yu.M. Proselkov, S.A. Shamanov, *Technique and Technology of Drilling of Oil and Gas Wells: a textbook for higher educational institutions*. Moscow: Nedra-Biznestsentr, 2003. 1007 p. (in Russian).
- [8] S.S. Sulakshin, *Drilling of Exploration Wells: a reference guide*. Moscow: Nedra, 1991. 334 p. (in Russian).
- [9] *Physical Properties of Rocks and Minerals (Petrophysics): a geophysicist's reference book/* edited by N.B. Dortman. Moscow: Nedra, 1984. 455 p. (in Russian).
- [10] T.G. Kazakova, A.V. Mesropyan, M.O. Mitaygina, Development of boring perforator with electric-hydraulic system // *Automation, Teleautomation and Communication in Oil Industry*. 2012. No. 1. pp. 25–31 (in Russian).
- [11] Russian Federation patent 2465443, IPC7 E 21 B 43/11. Drilling perforator with hydroelectric system for re-exposure of beds / Sh.R. Galljamov, A.V. Mesropjan, M.O. Mitjagina; patent owners Sh.R. Galljamov, A.V. Mesropjan, M.O. Mitjagina. Application number 2011108780/03; application date 09.03.2011; publication date 27.10.2012.
- [12] Russian Federation patent 2466269, IPC7 E 21 B 43/11. Drilling perforator with electric hydraulic system and adjustment of drill inclination angle / L.U. Davletova, A.V. Mesropjan, M.O. Mitjagina; patent owner Ufa State Aviation Technical University. Application number 2011122153/03; application date 31.05.2011; publication date 10.11.2012.
- [13] Yu.V. Vadetskiy, *Drilling of Oil and Gas Wells*. Moscow: Akademiya, 2013. 352 p. (in Russian).
- [14] Hardness of rocks. [Electronic resource]. URL: <http://www.drillings.ru/tverdost> (access date: 30.06.2015) (in Russian).



International Conference on Industrial Engineering

Synthesis of control system for actuators based on shape memory ferromagnetic alloy using inverse problem solution

Bakhvalov Y.A., Grechikhin V.V.* , Kraevskiy I.S.

Platov South-Russian State Polytechnic University (NPI), 132, St. Prosvescheniya, Rostov region, Novocheerkassk, 346428, Russian Federation

Abstract

A control system of actuators based on ferromagnetic shape memory alloy is considered. The distinctive feature of the devices is the usage of the distributed magnetizing system and the pulse mode of magnetic reversal. A definition algorithm of ampere-winding of magnetizing system coils with application of the methodology based on the inverse problem solution is developed. A mathematical model of the actuator considering influence of eddy currents and losses of energy on a hysteresis on dynamic processes in active elements is developed. The results of experimental studies are given. The values of ampere-winding in coils and delay time of a magnetic field in pulse control mode of the actuator with active elements from Ni_2MnGa alloy are defined. The offered approaches allow raising the efficiency of the control system of actuators based on ferromagnetic shape memory alloy.

© 2015 The Authors. Published by Elsevier Ltd. This is an open access article under the CC BY-NC-ND license (<http://creativecommons.org/licenses/by-nc-nd/4.0/>).

Peer-review under responsibility of the organizing committee of the International Conference on Industrial Engineering (ICIE-2015)

Keywords: actuator, ferromagnetic shape memory alloy, impulse magnetic reversal, inverse problem;

1. Introduction

Development of industrial control systems using intellectual materials in measuring and actuation mechanisms is on the front burner nowadays. Such intellectual material is ferromagnetic shape memory Ni_2MnGa alloys (FSMA), which generate stress and change their geometrical shape in the magnetic field. This distinctive feature allows increasing conversion accuracy, simplifying design of devices, reducing quantity of the components subject to breakage or wear and, as a consequence, increasing efficiency of industrial control systems [1, 2]. Therefore,

* Corresponding author. Tel.: +7-928-600-2864.
E-mail address: vgrech@mail.ru

development of the theory and the principles of creation of the control systems containing actuation and measuring mechanisms on the basis of FSMA is an actual task.

2. Statement of the Problem

The strict requirements are set up in the industrial control systems to actuation mechanisms (actuators). They are to have fast response time, small dimensions and weight. In familiar devices [3-8] the magnetizing system containing coils with the ferromagnetic core is used, that increases their inductance, the reaction time and mass of the device. In the paper [8] the actuator design is offered with two active (subject to deformation) elements from FSMA allowing providing stable position of the drive without continuous consumption of energy. We developed the design which uses positive properties of the specified actuator, but it has the distributed magnetizing system containing n pairs of coils without ferromagnetic cores, with pulse magnetic reversal of active elements being applied (Fig. 1) [9]. All the above allows increasing high-speed response, reducing weight and dimensions of the device. Usage of the distributed magnetizing system increases sensitivity and flexibility of control as this provides opportunity to realize the demanded laws of movement of the executive mechanism due to deformation of an active element in the magnetic field, created by separated coils. While in-feeding one couple of coils the length of active element increases by value Δ_m/n , where Δ_m – the maximum increment of the element length at in-feeding of all n pairs of coils.

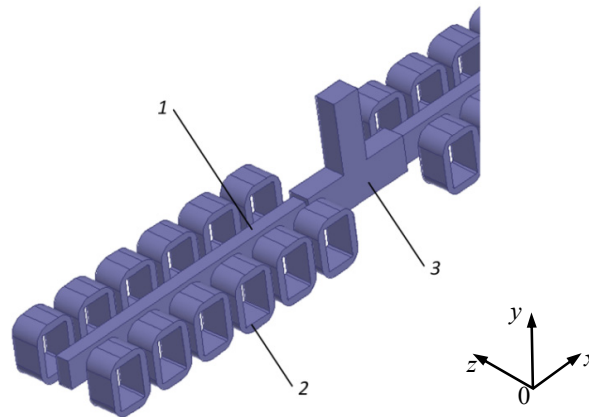


Fig. 1. General view of an actuator with two active elements (1), distributed magnetizing coil (2) and actuating mechanism (3).

The purpose of the present article is to develop a control system of the considered actuator, to define active elements for ampere-windings of coils required for deformation control, and to assess delay time of a magnetic flux in active elements due to eddy currents, magnetic viscosity and hysteresis applying the methodology based on the inverse problem solution. [10]. Devices for program setting for implementation of the demanded law of movement of the executive mechanism and formation of impulses do not differ from the known ones, therefore are not considered in the article [11].

3. Computational algorithm

The algorithm of the inverse problem solution for definition of coils' ampere-windings i_w consists in performing the following stages for every $k = 0, 1, 2, \dots$:

- A. at $i_w = i_w^{(k)}$ direct problem to be solved: calculation of three-dimensional stationary magnetic field by method of final elements. Internal cycle of specification of magnetic permeability of active element with the use of dependence $B(H)$ is applied. As a result, $H_{z_{\min}}^{(k)}$ in active element is defined;
- B. the value of target function $J^{(k)}(i_w^{(k)})$ to be calculated and fulfillment of the condition to be checked;

$$J^{(k)}(iW^{(k)}) = (H_{z\min}^{(k)} - H_z^*)^2 \leq (\varepsilon H_z^*)^2 \quad (1)$$

where ε – set fractional error, H_z^* – z-component of intensity of magnetic field, at which lengthening of active element along axis Oy is maximum (Δ_m).

If the condition (1) is satisfied, the external cycle of calculations is completed, the target value of ampere-windings $iW = iW^{(k)}$. If the condition (1) is not satisfied, we pass to the following stage.

C. We minimize the target function by gradient method and define the following approximation

$$iW^{(k+1)} = iW^{(k)} - t^{(k)} \frac{\partial J^{(k)}}{\partial iW} iW^{(k)} \quad (2)$$

where $t^{(k)}$ – step. The derivative in (2) to be defined in number.

D. Coming back to point 1.

For assessment of magnetic flux delay time influencing high-speed response of the device, we transform the Maxwell's system of equations which describes three-dimensional quasistationary electromagnetic field using vector magnetic \vec{A} and scalar electric ϕ potentials to the view

$$\text{rot} \left(\frac{1}{\mu} \text{rot} \vec{A} \right) + \gamma \left(\frac{\partial \vec{A}}{\partial t} + \text{grad} \phi \right) = 0 \quad (3)$$

$$\text{div} \text{grad} \phi = 0 \quad (4)$$

$$\text{rot} \text{rot} \vec{A} = \mu_0 \vec{j} \quad (5)$$

$$\text{rot} \text{rot} \vec{A} = 0 \quad (6)$$

where \vec{j} – current density in coils; γ – electric conductivity, μ – magnetic permeability of ferromagnetic elements; μ_0 – magnetic constant. Equations (3), (4) are valid for ferromagnetics, (5) – for coils, (6) – for other space. The solution of the given equations system with the corresponding boundary and entry conditions is carried out by method of final elements [10].

Not only eddy currents, but also magnetic viscosity and losses of energy on FMSA hysteresis have impact on the dynamic parameters of actuators.

To consider magnetic viscosity the Georgie's equation is added to the system of the equations (3) – (6)

$$T \frac{d\vec{H}}{dt} + \vec{H} = \vec{H}_{st} + \frac{T}{\mu_0} \frac{\partial \vec{B}}{\partial t}, \quad T = \frac{T_0}{1 - \left(\frac{\vec{B} - \mu_0 \vec{H}}{B_s} \right)^2} \quad (7)$$

where B_s – saturation magnetic induction; T_0 – magnetic viscosity constant; \vec{H}_{st} – coercitive force of hysteresis static loop.

To consider losses of energy on a hysteresis Jiles-Atherton model is used. [13, 14]

$$\frac{dM}{dH} = \frac{c}{c+1} \frac{dM_{an}}{dH} + \frac{\tilde{\delta}}{c+1} \frac{M_{an} - M}{k\delta - \alpha(M_{an} - M)} \quad (8)$$

where M_{an} – unhyeresis magnetization, that is magnetization that would be in case of absence of closing domains wall process; c –elastic displacement constant of ferromagnetic domain borders; k – positive constant of ferromagnetic properties; α – positive constant of magnetic domain coupling,

$$\delta = \text{sign}(dH/dt); \quad \tilde{\delta} = \begin{cases} 1, \{dH > 0 \cup M < M_{an}\} \cap \{dH < 0 \cup M > M_{an}\} \\ 0, \{\text{other case}\} \end{cases}$$

The equations (3) – (8) form mathematical model for dynamic parameters study in the devices containing active elements from FMSA.

4. Results and discussion

Experimental studies of the actuator with two active elements (Fig. 1) were carried out to check the offered algorithm and the model developed for control system of the actuator on the basis of active elements. The active elements made from Ni_2MnGa alloy in the form of parallelepipeds with $1 \times 2 \times 20$ mm sizes produced by Adaptamat Inc. were used. [15].

Dependence of $B(H)$ and specific electric conductivity $\gamma = 1.65 \cdot 10^8$ Cm/m of FSMA is considered to be known. It is required to provide $n = 6$ discrete conditions of active elements. Fig. 2 shows the sizes of the magnetizing coils: $A = 3$ mm; $B = 2$ mm; $C = 0,5$ mm; $H = 2$ mm; $L_S = 0,5$ mm; $R = 0,2$ mm.

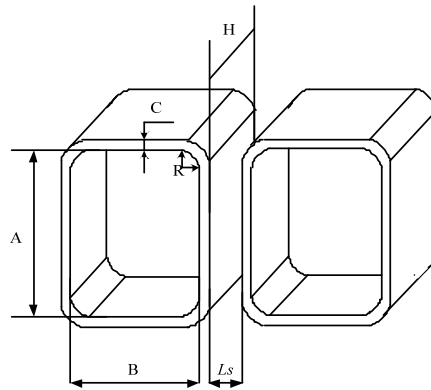


Fig. 2. Form and dimension of a magnetizing coil segment.

It is necessary to define ampere-windings of each coil with which the minimum intensity of a magnetic field in active element meets $H_{z \min} \geq H_z^*$ condition. For the material chosen $H_z^* = 370$ kA/m.

On the basis of scoping calculations $i_w^{(0)} = 4000$ A. On the iteration $k = 5$ $i_w^{(5)} = 10000$ A is obtained by using algorithm of inverse problem solving for determination of necessary ampere-windings of coils. In this case magnetic field pattern in active element from FSMA takes the following form (Fig. 3). Fig. 4 shows distribution of magnetic field along active element.

Application of model (3) – (9) for determination of dynamic parameters of active elements from FSMA in some cases is complicated due to the lack of data in literature on values of constants (T_0 , c , k , etc.) at calculation of influence of viscosity and losses of energy on hysteresis on these parameters. Experimental definition of constants for active elements from alloy Ni_2MnGa is planned in future work [16]. At this stage of the research delay time of magnetic field may be estimated approximately, considering that the energy losses caused by eddy currents make one third of total losses. Then, the total delay of magnetic field is defined by ratio $\tau_\Sigma = 3\tau_{ec}$, where τ_{ec} – the delay caused by action of eddy currents. As shown in [17], for active elements from FSMA $\tau_{ec} = 0.2$ ms. Hence, duration of control impulses is to be more than 0.6 ms.

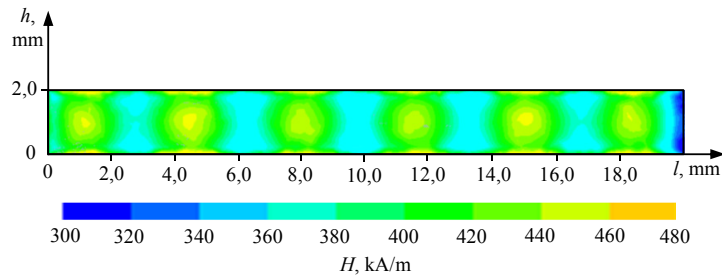


Fig. 3. Pattern of magnetic field in active element from FSMA

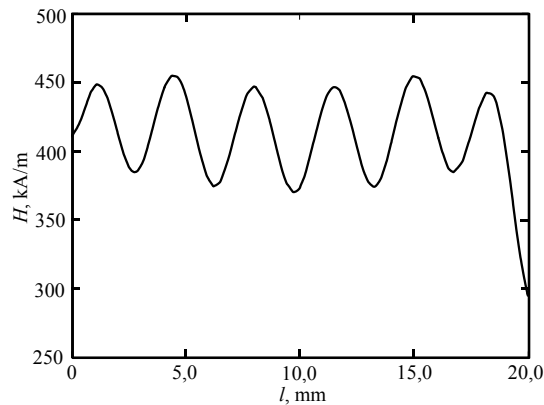


Fig. 4. Distribution of magnetic field along active element

5. Conclusions

Application of active elements from FSMA in actuators of pulse magnetic reversal allows increasing high-speed response, reducing the weight and dimensions of the device. Usage of the distributed magnetizing system increases sensitivity and flexibility of control due to realization of discrete control mode. To choose optimum parameters for control impulses it is rational to use the developed algorithm for coils ampere-windings definition of the magnetizing system with application of the inverse problem solution methodology and the developed mathematical model of the device considering influence of eddy currents, magnetic viscosity and losses of energy on a hysteresis on dynamic processes in active elements. The approaches offered allow solving a problem of efficiency enhancing of synthesis of actuators control on the basis of FSMA.

Acknowledgements

The study results are obtained with the support of the project #1.2690.2014/K "Methods to solve inverse problems of complex system diagnostics (in engineering and healthcare industry) based on full-scale and modeling testing", implemented within the scope of a designing stage for the state-given job.

References

- [1] A.N. Vasilev, Ferromagnetics with shape memory effect, *Advances in physics*. 173 (2003) 577–608.
- [2] S.A. Wilson, New materials for micro-scale sensors and actuators: an engineering review, *Materials Science & Engineering R-Reports*. 56 (2007) 1–129.

- [3] I. Suorsa, E. Pagounis, K. Ullakko, Magnetic shape memory actuator performance, *Journal of Magnetism and Magnetic Materials*. 272 (2004) 2029–2030.
- [4] F.-X. Wang, W.-J. Li, Q.-X. Zhang, X.-J. Wu, C. Ge, Design and control of linear actuators made by magnetically controlled shape memory alloy, *Proceedings IEEE International Conference on Mechatronics*. (2005) 583–586.
- [5] E. Asua, J. Feuchtwanger, A. Garcia-Arribas, V. Etxebarria, I. Orue, J.M. Barandiaran, Ferromagnetic shape memory alloy actuator for micro- and nanopositioning, *Sensor Letters*. 7 (2009) 348–350.
- [6] R. Techapiesanchaoenkij, J. Simon, D. Bono, S.M. Allen, and R.C. O'Handley, Frequency response of acoustic-assisted Ni–Mn–Ga ferromagnetic-shape-memory-alloy actuator, *J.Appl. Phys.* 105 (2009) 093923.
- [7] L. Riccardi, D. Naso, B. Turchiano, H. Janocha. A precise positioning actuator based on feedback-controlled Magnetic Shape Memory Alloys, *Mechatronics*. 22 (2012) 568–576.
- [8] J. Gauthier, A. Hubert, J. Abadie, C. Lexcellent, Multistable actuator based on magnetic shape memory alloy, *Actuator 2006*, 10th International Conference on New Actuators, Bremen, Germany. (2006) 787–790.
- [9] N.I. Gorbatenko, V.V. Grechikhin, D.V. Shaikhutdinov, Measuring and Actuating Devices Based on Shape Memory Ferromagnets, *Metal Science and Heat Treatment*. 56 (2015) 609–613.
- [10] Yu.A. Bakhvalov, N.I. Gorbatenko, V.V. Grechikhin, Inverse problems in electrical engineering, *News of Higher Educational Institutions. Electrical engineering*, Novocherkassk, 2014.
- [11] Ya.Z. Tsypkin, *Foundations of the automatic systems theory*, Science, Moscow, 1977.
- [12] E.M. Gyorgy, Rotational Model of Flux Reversal in Square Loop Ferrites, *J. Appl. Phys.* 28 (1957) 1011.
- [13] D.C. Jiles, D.L. Atherton, Theory of Ferromagnetic Hysteresis, *Journal of Magnetism and Magnetic Materials*. 61 (1986) 48–60.
- [14] D.C. Jiles, J.B.Thoelke, Theory of ferromagnetic hysteresis: determination of Model parameters from Experimental hysteresis loops, *IEEE Transactions on Magnetism*. 25 (1989) 3928–3930.
- [15] Information on <http://www.adaptamat.com>.
- [16] N.I. Gorbatenko, Full-scale and model experiments of pieces made from ferromagnetic materials, SKNZ VSH, Rostov on Don, 2001.
- [17] V.V. Grechikhin, A.V. Kudrya, N.A. Kudrya. Estimation of eddy current influence on high-speed response of actuators on the basis of shape memory material, *News of Higher Educational Institutions. North Caucasian region. Engineering sciences*. 6 (2014) 33–35.



International Conference on Industrial Engineering

Object-oriented approach to design of the complex mechanical system dynamics mathematical models

Grinchenkov D.V., Mokhov V.A., Spiridonova I.A.*

Platov South-Russian State Polytechnic University (NPI), 132, St. Prosvescheniya, Rostov region, Novocherkassk, 346428, Russian Federation

Abstract

The article presents the results of an object-oriented approach applied to modeling the dynamics of complex mechanical systems when it is used in the educational process. The results of formalization the mathematical model design in the form of the second kind (conventional) Lagrange equations and the resulting Cauchy problem are considered. The article contains the authors' presentation of the corresponding information flows diagram. The ways to use of object-oriented approach discussed in this article are proposed to be used in the educational process to establish interdisciplinary connections, as well as to create e-learning resources for students of applied mathematics, information technology and engineering profiles. The examples of the display forms for designed software used in the simulation of a transport vehicle mechanical system are presented.

© 2015 The Authors. Published by Elsevier Ltd. This is an open access article under the CC BY-NC-ND license (<http://creativecommons.org/licenses/by-nc-nd/4.0/>).

Peer-review under responsibility of the organizing committee of the International Conference on Industrial Engineering (ICIE-2015)

Keywords: Modeling; computer simulation; object-oriented approach; complex mechanical system; formal method; e-learning

1. Introduction

Computer simulation of the dynamics of complex mechanical systems is an essential task in many practical applications. A task to teach students of technical and informational training areas is very relevant to create new CAD/CAM systems, including specialized software with support the functions of modeling and simulation to design of mechanical systems. The basis of student training to construct of mathematical models of mechanical systems is the study of the basic principles and methods for solving classical problems of theoretical mechanics [1-4]. It should

* Corresponding author. Tel.: +7-928-121-61-77.
E-mail address: sia1706@yandex.ru

be noted that at present there are a number of software systems designed for computer simulation of the kinematics and dynamics of certain types of mechanical systems such as russian software systems "Euler" [5], "Universal Mechanism" [6], as well as a specialized module "Simulink" [7] of software system "Matlab", and also software tools [8] for implementing simulation technology using the international standard VHDL-AMS. Mathematical modeling units of these software systems are based on classical methods of theoretical mechanics [1-4], and is used also methods, algorithms, find mathematical models [9-13], which are based on the principles of graph theory, affine transformations, tensor analysis and the existence of electromechanical analogy with the use of elements of the circuitry.

The main shortcoming for application of above-mentioned software of educational process is fact that the demanded mathematical model, which is a basis of the analysis of characteristics of mechanical system, is usually not available to the user to direct adjustment of parameters. Software mathematics is hidden in internal representation of a program complex in most cases.

2. Design of mathematical model

The aim of teaching to the principles of mathematical and computer modeling of mechanical systems is: a student should understand the impact of the type of motion of each system element, its inertial and geometric characteristics, the way of interaction of solids in the system to the contributions of the solids and relationships in the system of differential equations describing the system dynamics.

As mathematical tools to describe the dynamics of the classical problems [1-4] to modeling of mechanical systems it is convenient to use the method of conventional Lagrange equations (Lagrange equations of the second kind), the algorithm of which is described in [1, 3]. The mathematical tools and method for forming the conventional Lagrange equations are tools, original intended to describe dynamics of complex mechanical systems with many degrees of freedom, what is clear considered in article [15].

The relationship of data sources and stages of constructing a mathematical model that allows implement adequately a solution of standard educational tasks within a model of a solids system are identified in proposed in figure 1 scheme of generalized information flows.

In the shown scheme q_i denotes a generalized coordinate, \dot{q}_i denotes the generalized velocity, T denotes the kinetic energy, \dot{I} represents the potential energy, \dot{O} represents the Rayleigh dissipation function. Generalized force Q_i describes the effect of forces that are outside \dot{I} or \dot{O} . The scheme can be a basis for the implementation of the object-oriented approach for modeling of complex mechanical systems.

For planar mechanical system corresponding to the standard tasks of the study discipline "Theoretical (classical) mechanics" [4], there are three possible types of motion, namely: translational, rotational and plane-parallel, which in turn is decomposed into translational motion together with the center of mass and rotation around its center of mass. The type of movement and type of solid body (set of its parameters) allow only one way to determine the expression of the kinetic energy of each body and of the complete mechanical system. The number and type of generalized coordinates are determined by the type of the relationship and interaction between bodies. Within the system (subsystem) with one degree of freedom the number of ways of connection between bodies is limited and definitely sets the speed ratio expressed through a generalized speed. The use of these ratios in the expression of the total kinetic energy of the complete system allow to find the the expressions of "reduced mass" of the system to each particular generalized coordinate. The presence of the elastic connection between the bodies defines an additional degree of freedom and its associated generalized coordinate and generalized velocity. An additional degree of freedom and generalized coordinate, of course, is also determined in the case of independent motion of one body relative to another moving body in one system.

The type of external constraints in a flat system, first, determines the type of motion of the solid and, second, the external force reactions including external forces of elasticity or friction (which can be considered as "dry" or "viscous"). The right side of the conventional Lagrange equations describes the impact of potential forces, with the power function, dissipative forces, depending on speed, and also forces which aren't entering the described categories. Each expression in the right part corresponds to the some generalized coordinate. The expression should be constructed in depending on external forces that are reaction forces and active forces.

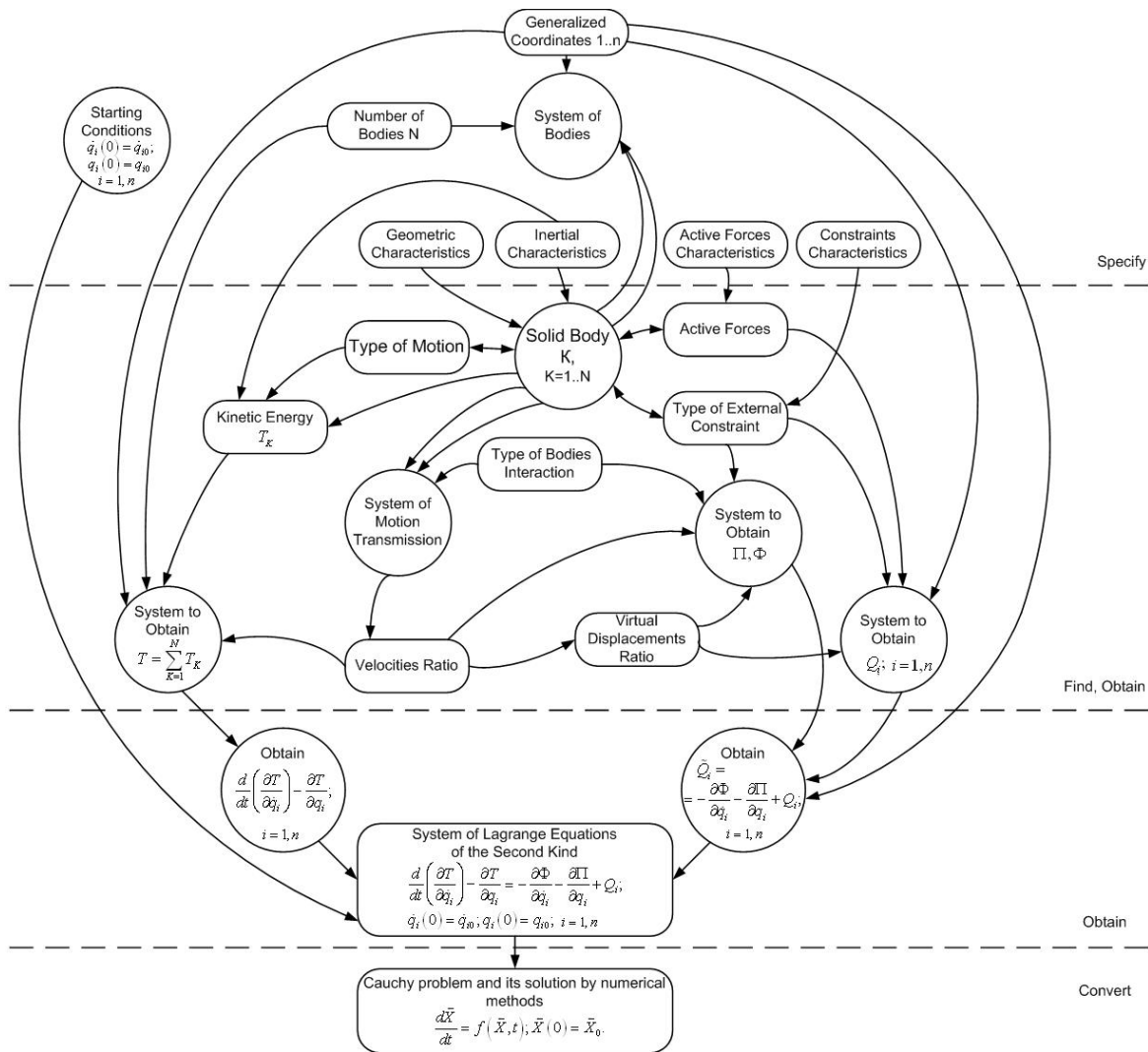


Fig.1 Generalized scheme of information flows.

Formalization of data flows and interrelation of objects easily leads to object-oriented [14] modeling and program realization: to encapsulation of data, formal definition of classes and establishment of communications between them. Similar methods of application of object-oriented technology are currently widely used to solve mathematical and specialized tasks [16, 17], including by multi-agent approach as a development of object-oriented programming technology [18, 19].

Design of equations of dynamics of mechanical systems with many degrees of freedom can be a complicated procedure as it discussed in [15]. This is due to the growing complexity of the expressions for the kinematic variables that determine the position, velocity and acceleration of solids included in the system, by increasing the length of kinematic chains. Object-oriented approach is very convenient to two-step mathematical dynamics macro-modeling of mechanical systems [20] with many degrees of freedom, similar to the "transport type" system (railway or automotive vehicle), presented in figure 2. From the point of view of theoretical mechanics separation of macro-elements means splitting system into the interconnected subsystems for such task, each of which has one degree of

freedom and is characterized by own generalized coordinate. The complete system of macro-elements can be considered as translational moving system.

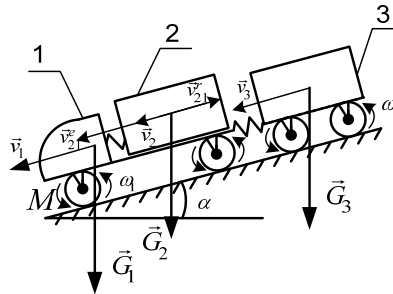


Fig. 2. System with display of sampling, active forces and velocities.

In figure 2 are denoted the gravity forces G_1 , force moment M applied to the axis of the driving wheel pair, the angular velocity ω_i of the wheelsets and velocities v_1, v_2, v_3 of centers-of-mass of macro-elements, where total (absolute) velocity

$$v_2 = v_2^c + v_{21}^r \tag{1}$$

is the sum of velocity of transporting body and the relative velocity.

As a result of preparing [15] the conventional Lagrange equations the mathematical model is obtained in the form of a system of strongly coupled differential equations of the second order, as:

$$\begin{cases} \ddot{q}_1 = \frac{1}{m_1} \cdot \left(F - \left((b_{10} \cdot \dot{q}_1)^* - b_{21} \cdot (\dot{q}_1 - \dot{q}_2) \right) - (c_{12} \cdot (q_1 - q_2) + c_{13} \cdot (q_1 - q_3)) \right); \\ \ddot{q}_2 = \frac{1}{m_2} \cdot (b_{21} \cdot (\dot{q}_1 - \dot{q}_2) + c_{12} \cdot (q_1 - q_2)); \\ \ddot{q}_3 = \frac{1}{m_3} \cdot \left(-(b_{30} \cdot \dot{q}_3)^* + c_{13} \cdot (q_1 - q_3) \right). \end{cases} \tag{2}$$

The force in (2) have [15] expression

$$F = m_c \cdot g \cdot \sin \alpha + F_d, \tag{3}$$

where m_c is the total mass of all system elements, and the driving force F_d generated by the traction of the supporting surface and depends on the moments acting on the axis of the driving wheelsets. The mathematical model [15, 20] can be easily transformed into a representation of the standard form Cauchy problem to further solving by numerical methods. The quality is not quite evident at first glance of the results of mathematical modeling in [15], it is possible to note the fact that when driving on an inclined plane in the equations for bodies 2 and 3 connected elements of elasticity with the first body, the resulting removal of the force of gravity due to the initial elastic deformation of compounds that persist in the law of motion of these bodies relative to the first body during the whole time of motion of a system. Significantly, the sliding friction "on ground" present only at the stage of braking and it is only for items with driving wheel pairs, which is reflected in the inheritance of the options classes in the software implementation. The relevant components of the equations (2) are marked by asterisks.

Rational way consists in the complex [20] application of methods that use an object-oriented approach to define the inertial characteristics of the macro-elements and to describe the relationship between subsystems. To do this

should first identify the subsystems (macro-elements) with one degree of freedom and then to do some stage of simplified modeling by method of the conventional Lagrange equations for each subsystem. Only those actions which will allow obtain correctly parameters of system for application of a method of the generalized energy phase variables (GEPV) have to be executed [20].

Described in [9] method GEPV is based on the principles of the existence of analogies mathematical description of the energy processes occurring in the systems of different physical nature. This method uses the equations in the form of dependences of the energy variables of type "I"–"stream" and type "U"–"potential" corresponding to the standard VHDL-AMS [8, 12] "global" variables "through quantity" and "quantity across".

Further formal modeling of the translational motion of a system of macro-elements sufficient to carry out the GEPV method as discussed in [15, 20]. A mathematical model (2) of the method of conventional Lagrange equations can easily be brought to an absolute coincidence [15] GEPV constructed mathematical model by adding the equations the equations arising from the mathematical representation of the law of elastic interaction.

The formal method GEPV is useful in educational process. In the algorithm of this method not only the principles of Electromechanical analogies and circuitry are used clearly, but also representation of mechanical systems in form of oriented graphs is used with the further constructing the topological equations by formalism of discrete mathematics. Formalization of the description of the basic "energy elements" by types of energy storage (C and L) and by energy dissipation type R is an independent source to use the principles of object-oriented approach to designing a mathematical model of the mechanical system and its computer realization.

3. Computer simulation

With the help of the described approaches in laboratory practical course on "Computer Modeling" by languages object-oriented programming designed a number of software products, performing simulation of mechanical systems as composed vehicle with different layout of macro-elements. Computer simulation using the created software allows the student to get a clear understanding of the impact of system parameters on the consistency of the laws of motion subsystems and the nature of the changing force of the elastic interaction between the subsystems.

As an example figure 3 shows the concerted velocity graphs of five macro-elements at the stages of "speed up", "inertia" and "braking". The figure 3 presents the results of computer simulation "vehicle" system, which is represented in figure 4. For clarity, the use of the software product in the interface (fig. 4) also includes a display of the simulated phase of the "movement" of the system using the display "traffic light" (the token "green-yellow-red").

The software product also enables to get graphics accelerations, displacements and forces changes in the elastic elements of the connection of subsystems and make changes to the system parameters for the analysis of the motion coherence of its elements. Thus, in Fig. 3 clearly displayed a gradual damping of the velocities of subordinate elements of the kinematic chain.

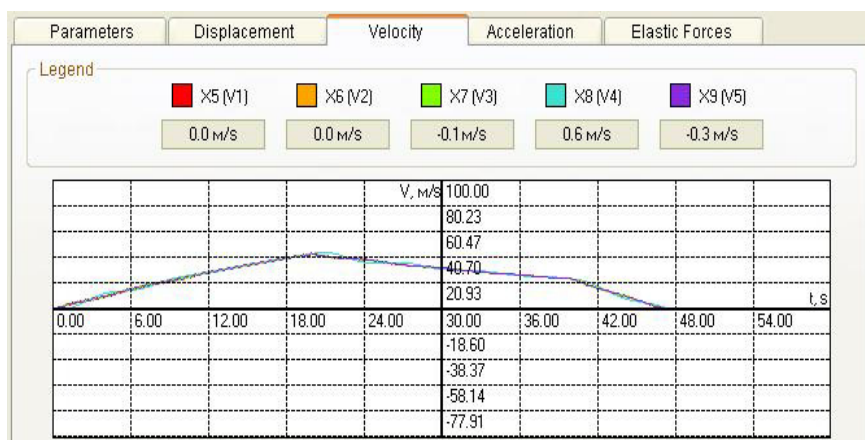


Fig. 3. Graphs of velocity of macro-elements.

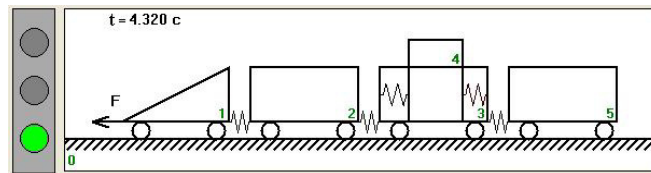


Fig. 4. The simulated system.

4. Conclusions

Discussed in this article ways to use object-oriented approach to construction of mathematical models of mechanical systems from the point of view of the authors are useful for use in the educational process to establish interdisciplinary connections, as well as when creating e-learning resources [21] for students applied mathematics, information technology and engineering directions, in-depth learning of mathematical and computer modeling of mechanical systems. In other works of authors of this article the various approaches [20, 21] to the organization of the corresponding material and opportunities of use of interactive multimedia tutorials at realization of the similar electronic training resources are considered in more detail.

References

- [1] S.T. Thornton, J.B. Marion, *Classical Dynamics of Particles and Systems*, fifth ed., Belmont CA: Brooks/Cole, Learning, 2004.
- [2] D.C. Karnopp, D.L. Margolis, R.C. Rosenberg, *System Dynamics: Modeling, Simulation, and Control of Mechatronic Systems*, fifth ed., Hoboken, New Jersey, 2012.
- [3] M.I. Bat, G.Yu. Dzhanelidze, A.S. Kelzon, *Theoretical Mechanics at Examples and Problems*, tenth ed., Lan, St. Petersburg, 2013.
- [4] A.A. Yablonsky, *Collection of Tasks for Term Papers on Theoretical Mechanics : study guide*, fifteenth ed., Integral-Press, Moscow, 2006.
- [5] Information on <http://www.euler.ru>
- [6] Information on <http://www.umlub.ru>
- [7] Information on <http://matlab.ru/products/simulink>
- [8] Information on <http://vhdl.ams.mechdir.com>
- [9] I.P. Norenkov, *CAD Basics*, fourth ed., BMSTU Publ., Moscow, 2009.
- [10] D.Y. Pogorelov, On numerical methods of modeling large multibody systems, *J. Mechanism and Machine Theory*. 34(5) (1999) 791–800.
- [11] D.Y. Pogorelov, Contemporary algorithms for computer synthesis of equations of motion of multibody systems, *J. Computer and Systems Sciences International*. 44(4) (2005) 503–551.
- [12] M. Graziano, M. Ruo Roch, Automotive VHDL-AMS electro-mechanics simulations, *New Trends and Developments in Automotive System Engineering*. (2011) 541–566.
- [13] L.M. Vosskamper, R. Schmid, G. Pelz, Combining models of physical effects for describing complex electromechanical devices behavioral modeling and simulation, *Proc. IEEE/ACM*. (2000) 42–45.
- [14] G. Booch, R.A. Maksimchuk, M.W. Engle, B.J. Young, J. Conallen, K.A. Houston, *Object-Oriented Analysis and Design with Applications*, third ed., Pearson Education, Boston, 2007.
- [15] I.A. Spiridonova, D.V. Grinchenkov, On a mathematical modeling of a complex mechanical system by formal and by classical methods, *J. Russian Electromechanics*. 5 (2013) 75–79.
- [16] A.N. Ivanchenko, A.A. Dorofeev, An object-oriented approach to computation of higher derivatives, *J. University News. North-Caucasian Region. Technical Sciences Series*. 1 (2014) 9–15.
- [17] A.N. Ivanchenko, A.A. Dorofeev, An object-oriented approach to construction of spline functions defined on linear spans, *J. University News. North-Caucasian Region. Technical Sciences Series*. 1 (2015) 11–18.
- [18] I.V. Georgitca, S.S. Goncharov, V.A. Mokhov, Multiagent simulation of network attacks DDoS-type, *E-J. Engineering Journal of Don*. 26(3) (2013) 75–85. available at: http://ivdon.ru/uploads/article/pdf/IVD_79_georgitca.pdf_1852.pdf.
- [19] A.V. Kuznetsova, V.A. Mokhov, E.V. Turovskaya, Simulation of the process of optimal placement of goods in stock self-service by evolutionary search algorithms, *E-J. Engineering Journal of Don*. 28(1) (2014) 56–66.
- [20] I.A. Spiridonova, D.V. Grinchenkov, On a formalization of a construction by two-stage of a mathematical macromodel to complex mechanical system, *J. University News. North-Caucasian Region. Technical Sciences Series*. 6 (2013) 47–51.
- [21] D.V. Grinchenkov, D.N. Kushchiiy, The methodological, technological and legal aspects of using the e-learning resources, *J. University News. North-Caucasian Region. Technical Sciences Series*. 2 (2013) 118–123.



International Conference on Industrial Engineering

Formal method to design a macro-model of a transport vehicle mechanical system translational motion

Grinchenkov D.V., Mokhov V.A., Spiridonova I.A.*

Platov South-Russian State Polytechnic University (NPI), 132, St. Prosvescheniya, Rostov region, Novocherkassk, 346428, Russian Federation

Abstract

The article is devoted to the formalization [1] of the design of mathematical model for the computer simulation of complex mechanical systems. The simulation object is the mechanical system of the transport vehicle (railway or automotive). The complete system is split into subsystems (macro-elements), each of macro-element has one degree of freedom. The whole system of macro-elements can be considered as a translational moving system. A two-stage algorithm to construct a mathematical macro-model of the transport vehicle mechanical system - is presented. The results of the computer simulation are presented. This modeling method is beneficial to be used in the educational process to establish interdisciplinary connections, as well as to create e-learning resources for students of applied mathematics, information technology and engineering profiles.

© 2015 The Authors. Published by Elsevier Ltd. This is an open access article under the CC BY-NC-ND license (<http://creativecommons.org/licenses/by-nc-nd/4.0/>).

Peer-review under responsibility of the organizing committee of the International Conference on Industrial Engineering (ICIE-2015)

Keywords: Computer simulation; complex mechanical system; vehicle; formal method; object-oriented approach; e-learning.

1. Introduction

One of the significant areas of research in the field of solving the problems of modeling through the use of modern computer technologies is a computer simulation of complex mechanical systems.

It should be noted that at present, particular significance is the formalization of mathematical models of systems and processes in the context of solving specific practical problems, due in no small measure to solving of the urgent problem of import substitution in the field of software systems CAD/CAM/CAE. A very important problem is the

* Corresponding author. Tel.: +7-928-121-61-77.
E-mail address: sia1706@yandex.ru

problem of teaching students to create new, including specialized software systems that support the functions of mathematical modeling complex mechanical systems [2-11].

The problem of modeling the dynamics of mechanical systems of vehicles [1,4-9] is a good example of the object of research in teaching students the principles of computer simulation [10, 11]. This task allows student to have the intuitive interpretation of system parameters. Intuitive interpretation also corresponds to results, which are presented in the form of dependency graphs from the time the motion. From a practical point of view, to the area of the considered mechanical systems are included trains and railway crews, and it includes means of road (automotive) transport, including vehicles of auto truck transport.

2. The ways to modeling of mechanical systems

Due to the practical importance of a problem, currently the considerable number of works is devoted to creation of adequate mathematical model of mechanical systems of transport vehicles and their computer realization. In particular, for several years the design of the relevant modules of software system "Universal Mechanism" (UM) is developing under the supervising of prof. Pogorelov D.Y. [5, 6, 12, 13]. However, it should be noted that the study of models and methods [5-9, 12, 13] for implementation of mathematical software of software complex UM [14] is a separate task that requires a good mathematical training and deep knowledge in the subject area. This task is beyond the base curriculum for computer simulation training course for the bachelor studying, for which mechanical transport systems are not the main and only object to study.

As a different approach to the construction of mathematical models of complex mechanical systems process can be used formal methods based on the principles of the existence of the Electro-mechanical analogy and on the using of "global" variables, objects, and elements of circuitry [15, 16]. An example of such approach is the use of simulation technology of mechanical systems by means of a formal language and a graphical representation of the modeled mechanical system using similar electronic circuits in accordance with international standard VHDL-AMS.

However, in order to establish interdisciplinary connections in the learning process more rational approach may be the use of the method of generalized energy phase variables (GEPV) proposed in [10] for the design of mathematical models within CAD systems. The topology of the system in this method can be represented as in the form of the electrical circuit analog electronic devices and as in the classic form of a directed graph. The implementation steps of this method are based on mathematical and formal tools of the disciplines of applied mathematics. Objects for modeling by method GEPV can be discrete dynamical systems and sub-systems of different physical nature. It is worth noting that the GEPV analogy of phase variables, of topological and of component equations for different physical systems are consistent with the standard VHDL-AMS in which the corresponding phase variables appear with the names "across quantity" and "through quantity". The construction of mathematical models of complex mechanical systems can be carried out using classical methods of theoretical mechanics [2-4] with the use of modern technology implementation in an object-oriented approach also. Object-oriented approach is widely used now to solve different mathematical and specialized problems [17-20] by means of simulation by tools of object-oriented programming technology.

Method GEPV and object-oriented approach at the correct introduction of the parameters of the system elements allows to construct a mathematical model which fully corresponds [1, 4] to the model obtained by mathematical tools of theoretical mechanics. It should be noted that when modeling systems consisting of the solids that perform various types of mechanical motion, the basic method GEPV [10] require to design of a complex system of circuits and the imposition of laws of interrelation variables based from the subject area.

3. Two-stage method to modeling of mechanical systems of transport vehicle

As discussed in [1], for use in the educational process rationally [20] integrated application of methods of classical mechanics with GEPV method. When using the proposed technology the resulting system to describe the in relation to each other of movement of macro-elements in the direction of the main (target) movement can be seen as performing translational mechanical movement that corresponds to one of five basic types of physical subsystems, adequately simulated by the method GEPV [4]. Under the proposed approach, the macro system, shown in left part of figure 1, means to split the system into interconnected subsystems, each of which is characterized by separate

generalized coordinate. In right part of figure 1 shows a directed graph of the relationship of macro-elements, constructed to apply the method GEPV.

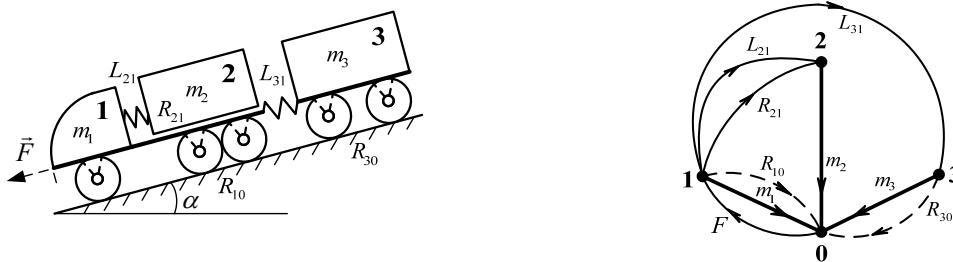


Fig.1. Left: sampling of the system and the interaction effects to method GEPV; Right: directed graph.

Directed graphs in a method GEPV allow to present conveniently and visually the topology of the system with different types of layout and interaction of the elements, as its are shown in figures 2, 3.

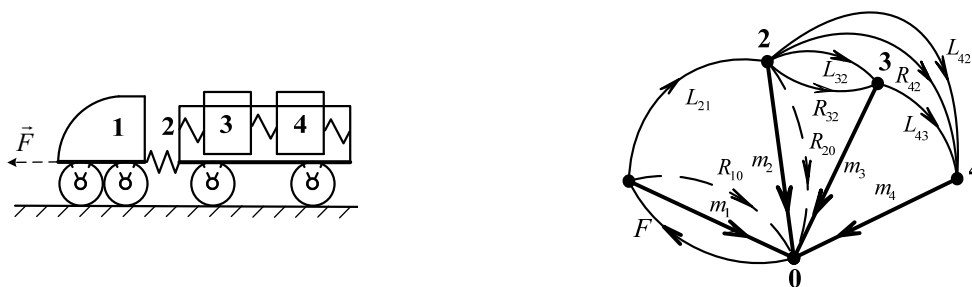


Fig. 2. Left: second system; Right: directed graph to second system.

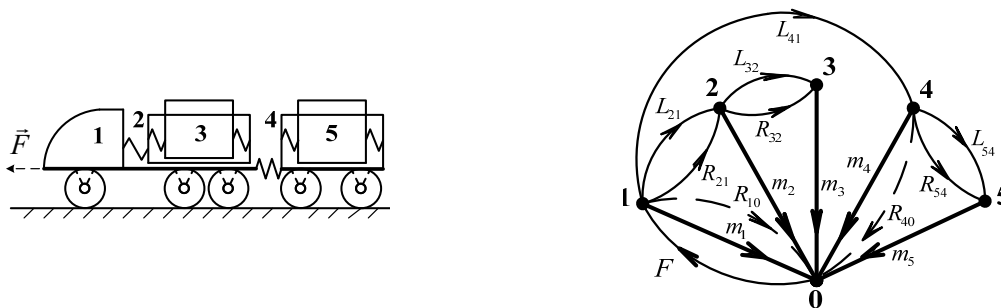


Fig. 3. Left: third system; Right: directed graph to third system.

Proposed by the authors in [1] for use in the educational process the two-stage algorithm to construct mathematical macro-model of the mechanical system of the transport vehicle in the general form is presented below.

Stage 1. First, it should make splitting (left parts of figures 1, 2, 3) of the system into subsystems (macro-elements). Using the principles of the second kind Lagrange equations it should determine the inertial characteristics (reduced mass) of each object and the external action on the system.

Stage 2. It should identify interaction effects of macro elements (subsystems) between themselves and with the external environment (constrains). It should build equivalent circuit and a directed graph (rights parts of figures 1, 2,

3) in accordance with the principles and algorithm of method application GEPV for the mechanical translational system. By formal tools should construct the mathematical model in the Cauchy problem form.

Generalized information flow diagrams to implementation of the formalized steps of the proposed algorithm are showed in figure 4.

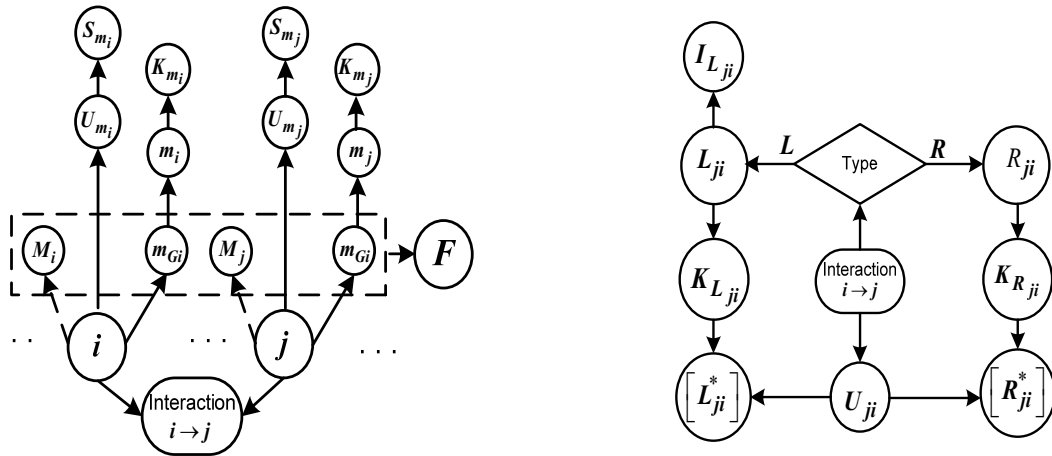


Fig. 4. Left: scheme of information flows of stage 1; Right: scheme of information flows of stage 2.

The most important aspect of drawing up of mathematical model by proposed methodology [1] is the correct description of the topology of the system: correct numbering of macro elements (subsystems) and indexation of the parameters of the energy elements in accordance with the following elements in the kinematic chain, i.e. a sequence of "transfer" to move from item to item.

The reduced mass for the subsystem (*k*) that contains ‘*n*’ wheels pairs:

$$m_k = m_{rm}^{(k)} = \left(m_1^{(k)} + 2n \cdot m_2^{(k)} \cdot \left(1 + \left(\frac{i_2^{(k)}}{R_k} \right)^2 \right) \right), \tag{1}$$

where the notation means: *m*₁ – mass of main element; *m*₂ – mass of each wheel; *R* – radius of wheel; *i* – inertia radius of wheel.

The force of external actions on the system causing its translational moving on the inclined surface consists of two parts:

$$F = \pm F_d \pm m_C \cdot g \cdot \sin \alpha = \pm \sum_j \frac{M_j}{R_j} \pm m_C \cdot g \cdot \sin \alpha. \tag{2}$$

This force [4] is directly applied to a driving macro-element, at the movement on an inclined surface it depends on the mass of whole system *m*_C representing the total mass of all elements of system, but not their reduced mass analogs. At the movement up the inclined plane the component of influence of gravity has, naturally, the negative sign, and at the movement on a horizontal surface in general is absent.

The traction force *F*_d is generated by the adhesion of the wheels with the support surface and depends on the moments acting on the axis of the driving wheels pairs with index ‘*j*’. At the stage of the braking system, the driving force is absent. It should be noted that only at this stage, the mathematical model must have components of friction

about "the earth" that are shown in graphs of right parts of figures 1, 2, 3 by dashed lines for subsystems (macro-elements) that are including driving wheels pair.

The resulting mathematical model [1, 4] when it presented in the form of the classical Cauchy problem contains the basis phase variables as absolute velocities U_m for all macro-elements and as forces I_L of elastic interaction.

The interaction of subsystems « $i \rightarrow j$ » of any type (elastic L_{ji} or friction R_{ji}) introduced in the mathematical model by dependence on the difference of velocities

$$U_{ji} = U_{m_i} - U_{m_j}, U_{j0} = U_{m_j} - 0 = U_{m_j}. \tag{3}$$

To automate the construction of a mathematical model by means of object-oriented programming is convenient to introduce a generalized representation of the components of the right side of the equations:

$$K_{m_i} = \frac{1}{m_i}; [L_{ji}^*] = K_{L_{ji}} \cdot U_{ji}; [R_{ji}^*] = K_{R_{ji}} \cdot U_{ji}, \tag{4}$$

where $K_{L_{ji}} = \frac{1}{L_{ji}}; K_{R_{ji}} = \frac{1}{R_{ji}}.$

4. Resulting mathematical model

So, for the system presented in figure 1 the resulted mathematical macro-model beyond the stage of "braking" has the form:

$$\begin{aligned} \frac{dI_{L_{21}}}{dt} &= [L_{21}^*]; \frac{dI_{L_{31}}}{dt} = [L_{31}^*]; \frac{dU_{m_1}}{dt} = K_{m_1} \cdot ((-1) \cdot [R_{21}^*] + (-1) \cdot I_{L_{21}} + (-1) \cdot I_{L_{31}} + (+1) \cdot F); \\ \frac{dU_{m_2}}{dt} &= K_{m_2} \cdot ((+1) \cdot [R_{21}^*] + (+1) \cdot I_{L_{21}}); \frac{dU_{m_3}}{dt} = K_{m_3} \cdot ((+1) \cdot I_{L_{31}}); \frac{dS_{m_i}}{dt} = U_{m_i}, i = 1, \dots, 3. \end{aligned} \tag{5}$$

The resulting system of equations must be complemented by an unambiguous definition of the initial conditions of each stage of the movement.

5. Results of computer simulation

In figures 5, 6 are presented the results of computer simulation of the dynamics of the five macro elements with the help of a software product that is implemented using object-oriented programming based on the described algorithm for the construction of mathematical software.

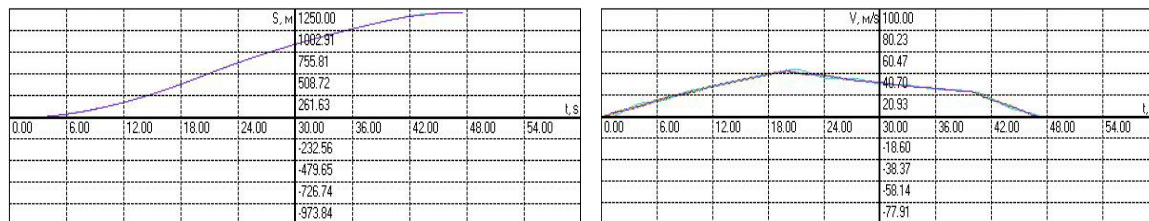


Fig. 5. Left: graphs of displacements; Right: graphs of velocities.

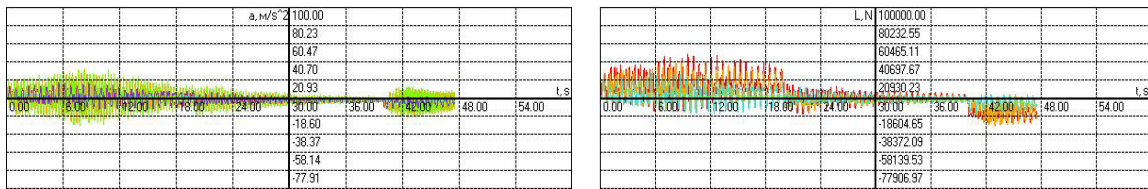


Fig. 6. Left: graphs of accelerations; Right: graphs of elastic forces.

Object-oriented approach to the implementation of the technologies of constructing mathematical software allows simulate the behavior of the system in different modes: controlled motion, inertia and braking, which is clearly reflected in right part of figure 5. The definition and treatment of "exceptions" in the software product also allows you to track the permissible limits of relative movement of macro-elements. When reaching these values the characteristics of the elastic connecting elements change automatically.

6. Conclusions

Presented in this article, the technology of constructing mathematical models of complex mechanical systems is useful for use in the educational process in order to establish interdisciplinary links at example that is clear and intuitively understandable to the student. Development of electronic educational resources in this area allows you to combine educational material relating to the principles and foundations of mathematical and computer modeling, classical problems and methods of the subject area, use the principles of object-oriented approach to modeling, the characteristics and limitations of formal methods computer-aided design. When you set out the way to solve the described problem presents material [20] relating to such sections applied mathematics like graph theory, theory of algorithms, numerical methods of solution of problems of mathematical analysis and other sections of educational material related to the problem of modeling specific tasks programmatically. Additional elements which increase the quality of e-learning resources is also developing expert systems for selection of model parameters and their adjustment in accordance with the formal characteristics and analysis of the obtained results in order to improve the adequacy of the model.

References

- [1] I.A. Spiridonova, D.V. Grinchenkov, On a formalization of a construction by two-stage of a mathematical macromodel to complex mechanical system, *J University News. North-Caucasian Region. Technical Sciences Series*. 6 (2013) 47–51.
- [2] D.C. Karnopp, D.L. Margolis, R.C. Rosenberg, *System Dynamics: Modeling, Simulation, and Control of Mechatronic Systems*, fifth ed., Hoboken, New Jersey, 2012.
- [3] M.I. Bat, G.Yu. Dzhanelidze, A.S. Kelzon, *Theoretical Mechanics at Examples and Problems*, tenth ed., Lan, St. Petersburg, 2013.
- [4] I.A. Spiridonova, D.V. Grinchenkov, On a mathematical modeling of a complex mechanical system by formal and by classical methods, *J. Russian Electromechanics*. 5 (2013) 75–79.
- [5] D.Y. Pogorelov, Contemporary algorithms for computer synthesis of equations of motion of multibody systems, *J. Computer and Systems Sciences International*. 44(4) (2005) 503–51.
- [6] D.Y. Pogorelov, On numerical methods of modeling large multibody systems, *J. Mechanism and Machine Theory*. 34(5) (1999) 791–800.
- [7] R. Sinha, C.J.J. Paredis, P.K. Khosla, Integration of mechanical CAD and behavioral modeling, *Proc. IEEE/ACM*. (2000) 31–36.
- [8] A.A. Zarifian, P.G. Kolpachyan, Computer Modeling of Electric Locomotive as Controlled Electromechanical System, *J Multibody System Dynamics*. 22(4) (2009) 425–436.
- [9] R. Kovalev, N. Lysikov, G. Mikheev, D.Pogorelov, V. Simonov, V. Yazykov, S. Zakharov, I. Zharov, I. Goryacheva, S. Soshnikov, E. Torskaya, Freight Car Models and Their Computer-Aided Dynamic Analysis, *J Multibody System Dynamics*. 22(4) (2009) 399–423.
- [10] I.P. Norenkov, *CAD Basics*, fourth ed., BMSTU Publ., Moscow, 2009.
- [11] M.A. Bauer, M. Sarrafzadeh, F. Somezi, Fundamental CAD algorithms, *IEEE Transaction on Computer-Aided Design of Integrated Circuits and Systems*. 19(12) (2000) 1449–1475.
- [12] D.Y. Pogorelov, Jacobian Matrices Of the Motion Equations of a System of Bodies, *J Computer and Systems Sciences International*. 46(4) (2007) 563–577.
- [13] D.Y. Pogorelov, Simulation of Constraints by Compliant Joints, *J Computer and Systems Sciences International*. 50(1) (2011) 158–173.
- [14] Information on <http://www.umlub.ru>

- [15] M. Graziano, M. Ruo Roch, Automotive VHDL-AMS electro-mechanics simulations, *New Trends and Developments in Automotive System Engineering*. (2011) 541–566.
- [16] A.C.R. Silva, I.A. Grout, A methodology and a tool to design of mixed-signal technology, *Proc. Electronic, Robotics and Automotive Mechanics Conference*. (2007) 164–169.
- [17] A.N. Ivanchenko, A.A. Dorofeev, An object-oriented approach to computation of higher derivatives, *J. University News. North-Caucasian Region. Technical Sciences Series*. 1 (2014) 9–15.
- [18] A.N. Ivanchenko, A.A. Dorofeev, An object-oriented approach to construction of spline functions defined on linear spans, *J University News. North-Caucasian Region. Technical Sciences Series*. 1 (2015) 11–18.
- [19] I.V. Georgitca, S.S. Goncharov, V.A. Mokhov, Multiagent simulation of network attacks DDoS-type, *E-J. Engineering Journal of Don*. 26(3) (2013) 75–85. available at: http://ivdon.ru/uploads/article/pdf/IVD_79_georgitsa.pdf_1852.pdf.
- [20] D.V. Grinchenkov, D.N. Kushchiy, The methodological, technological and legal aspects of using the e-learning resources, *J University News. North-Caucasian Region. Technical Sciences Series*. 2 (2013) 118–123.



International Conference on Industrial Engineering

Development of solid-state models for the gears of different geometry

Bruzhas V.V.* , Lopatin B.A.

South Ural State University, 76, Lenin Avenue, Chelyabinsk, 454080, Russian Federation

Abstract

This article describes the preparation methods for solid models of gears of different geometries using emulation cutting tooth profile generating circuit rack and further processing in Autodesk Inventor. The parameters of the rack contour can be set at a designer's request.

© 2015 The Authors. Published by Elsevier Ltd. This is an open access article under the CC BY-NC-ND license (<http://creativecommons.org/licenses/by-nc-nd/4.0/>).

Peer-review under responsibility of the organizing committee of the International Conference on Industrial Engineering (ICIE-2015)

Keywords: solid model, spur gear, helical gear, conical involute gear, bevel wheel non-involute tooth profile.

1. Introduction

In assessing the stress-strain state of gears it is necessary to obtain solid models that accurately reflect the geometry of the tooth profiles, depending on the parameters of the tool and the trajectory of its movement.

The analysis of existing software products has shown that at present there are no universal developments, allowing the generation of gears produces complex shapes of working surfaces of teeth. These software products represent only a graphical representation of the gear, and the libraries of CAD systems are a simplified representation, usually a standard profile.

The aim of the study was to develop solid models that accurately reflect the shape of the surfaces of the teeth obtained when profiling tool rack with different parameters of the original circuit.

2. Production models of gears

The basis of the working surfaces of the teeth getting laid emulation software package cutting gear rack

* Corresponding author. Tel.: +7-919-324-19-86.
E-mail address: brugaz@mail.ru

generating circuit [1]. The developed program allows for the processing of cylindrical gears with different parameters of the original contour (α , h_a^* , h_f^* , c^* , ρ^*) and different coefficients of x bias generating circuit rack (Fig. 1). For the further construction of three-dimensional model using a program Autodesk Inventor, with which obtained on the basis of the profile, you can create models of various gears.

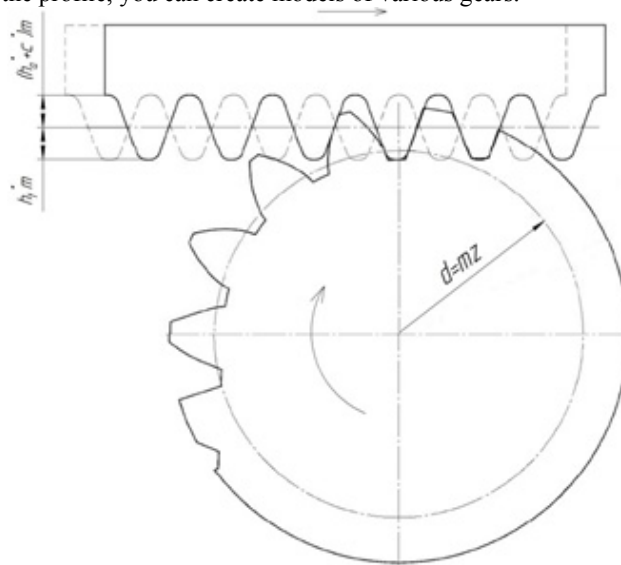


Fig. 1. The scheme forming the tooth profile in the face section wheels.

3. Spur and helical gear

To create the model spur gear (Fig. 2) is sufficient to use the extrusion operation. In contrast to the spur gear created by standard means of Autodesk Inventor (via the Design Wizard gears) profile tooth surfaces completely fit the profile, really get at run-rack instrument to the settings of the original path. In the case of a helical gear (Fig. 3) extrusion is not a straight line, and the spiral. You can use the application spring. In this application, given shape in the form of a sketch prepared tooth profile and its position relative to the axis of the wheel. The angle of the tooth wheel β is given through a step helix and the length of the pitch circle.



Fig. 2. Spur gear.



Fig. 3. Helical gear.

4. Involute-bevel gear

Solid models of gears with more complex geometry surfaces of the teeth, you can create a combination of the two above-described software systems. For example, involute bevel wheel (Fig. 4). Involute-bevel gear (IBG) - the wheel, sliced tool rack type (Gear comb, hob, grinding wheel) with variable displacement along the axis of the wheel tool [2]. A feature of such wheels is that in each face section profile is obtained with a certain offset coefficient which is changed in each section by the amount

$$\Delta x = s \cdot \operatorname{tg} \delta / m, \quad (1)$$

where s – move; Δx – increment of bias; δ – taper angle IBG; m – module.

Coefficient of radial clearance:

$$c_i^* = c^* \cdot \frac{\cos \beta}{\cos \delta}. \quad (2)$$

The coefficient of the tooth head height tool:

$$h_{at}^* = h_a^* \cdot \frac{\cos \beta}{\cos \delta}, \quad (3)$$

Socket module:

$$m_t = \frac{m}{\cos \beta}. \quad (4)$$



Fig. 4. Involute-bevel gear

With the help of emulation tooth profile rack-type tool to create a number of profiles with a certain step s along the axis of the wheel. In Autodesk Inventor, create work planes at a distance from each other at a pitch s , and copy to the appropriate profiles. IBG get a solid model using the Loft applications.

5. Bevel gears with teeth profile non-involute

These wheels are formed on the basis of the wheel and producing involute gear is used for special purposes [3].

To construct a model using the software package: "The calculation and analysis of the geometry of the links cylinder-conical gears", created at the Department of technical mechanics, a branch of South Ural State University. [4]

The complex consists of several modules:

- a) a module for calculating the coordinates of points of the lateral surface of the conical wheels non-involute tooth profile, is an executable file exe MS-DOS (KOORD.exe);
- b) a module for calculating the coefficients of the displacement of various sections non-involute bevel gear, is an executable file exe MS-DOS (KOSM.exe);
- c) a module for preparing data for profile modification non-involute bevel gear, which is a file-aided calculation and data storage applications Microsoft Excel (MOD.xls);
- d) a module for calculating the trajectory of the cutters, is an executable file exe MS-DOS (FREZ.exe);
- e) detailed operating instructions of «calculation and analysis of the geometry of the links cylinder-conical gears», including a step by step description of the actions of the operator workstation (a solid copy and electronic version in format PDF).

The procedure for constructing a solid model of the conical wheels non-involute tooth profile with the parameters ($z = 38$, $m = 2$ mm., $\beta = 0^\circ$, $b = 5$ mm.), As follows:

1. With the help of the module software package [4] calculated the parameters of face sections of the wheels through a step along the axis of the wheel (Table 1);
2. Using a complex emulation gear cutting rack generating circuit formed end section of the tooth. The parameters of initial contour are selected from the table for each value of w .

Table 1. The parameters of the mechanical section of the conical wheels

Applicate section w	Coefficient bias x_t	The average radius of the tooth r_l	Thickness tooth s	α_t	h_{ta}^*	h_{te}^*	c_t^*
0.0	2.584	42.517	2.815	19,887	1,006	2,012	0,252
0.5	2.556	42.447	2.853	19,865	1,007	2,015	0,252
1.0	2.525	42.377	2.886	19,841	1,009	2,017	0,252
1.5	2.491	42.307	2.912	19,815	1,010	2,020	0,253
2.0	2.453	42.236	2.934	19,788	1,012	2,023	0,253
2.5	2.414	42.166	2.951	19,759	1,013	2,027	0,253
3.0	2.371	42.096	2.964	19,728	1,015	2,030	0,254
3.5	2.325	42.026	2.972	19,695	1,017	2,034	0,254
4.0	2.278	41.955	2.977	19,660	1,019	2,038	0,255
4.5	2.229	41.885	2.978	19,624	1,021	2,042	0,255
5.0	2.178	41.815	2.976	19,586	1,023	2,046	0,256

Before the formation of the toothed wheel in the program Autodesk Inventor, you must in each profile format AutoCAD allocate segments with one tooth as in the construction of helical wheel. In Autodesk Inventor, create sketches of the mechanical section of teeth at a certain distance from each other along the axis of the wheel and insert in each of its segments. With the application "Loft" form a solid-tooth, which were formed by applying an array of bevel gear (Fig. 5).

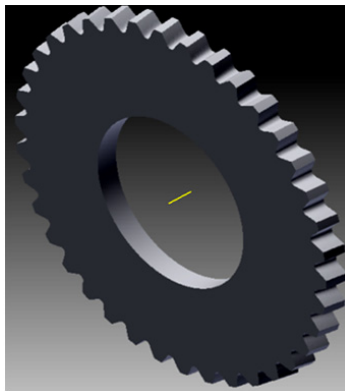


Fig. 5. The conical wheel non-involute tooth profile.

6. Summary

Thus, using the software "Simulation cutting involute spur gear generating rack contour" software "Calculation and analysis of the geometry of gearing helical bevel gears" and of Autodesk Inventor, you can get a solid model of involute bevel and bevel gears with non-involute profile teeth, which further allows to produce a study of stress-strain state of the transmission data composed of gears.

References

- [1] B.A. Lopatin, S.A. Khaustov, RU patent №6853. (2006).
- [2] B.A. Lopatin, O.N. Tsukanov, Helical-bevel gears: monograph, SUSU, Chelyabinsk, 2005.
- [3] B.A. Lopatin, O.N. Tsukanov, E.A. Poluektov, Angular adjustment electromechanical drive in aerospace industry, Vestnik mashinostroeniya. 2 (2009) 14–16.
- [4] B.A. Lopatin, S.A. Khaustov, E.A. Polouektov, RU certificate of state registration of the computer software package 200961002, № 2009614819. (2009).



International Conference on Industrial Engineering

The review of spatial objects recognition models and algorithms

Andrianov D.E., Ereemeev S.V., Kuptsov K.V.*

Department of Information Systems, Murom Institute (branch) of Vladimir State University, 602264 Murom, Russia

Abstract

The article considers the problem of spatial objects recognition in geographic information systems. The solutions for this problem are given, a classification of the methods and algorithms already available is executed and the ways of development in search of the optimum decision on the matter are offered. Firstly, it is the improvement in the quality of recognition. Secondly, it is the creation of general rules of sufficient accuracy rating to prevent erratic classification of objects of a certain type. Thirdly, it is the establishment of rules defining correlations of spatial objects of different classes.

Models and algorithms of spatially distributed objects recognition can be classified based on the following directions: with using external and internal topological relations, with application of neural network approach and mixed methods. Not only the issue of object recognition importance, but also the importance of accounting of their relative positioning and determination of spatial characteristics in relation to each other is considered.

© 2015 The Authors. Published by Elsevier Ltd. This is an open access article under the CC BY-NC-ND license (<http://creativecommons.org/licenses/by-nc-nd/4.0/>).

Peer-review under responsibility of the organizing committee of the International Conference on Industrial Engineering (ICIE-2015)

Keywords: algorithms of recognition ; allocation of spatial objects; processing of images; separation of contours; spatial distributed objects; topology;

1. Introduction

The person can perceive information visually therefore he studies considerable part of information by means of sight, considering pictures, drawings, maps and diagrams [6]. Recognition of spatial objects is one of the most complex and interesting challenges in digital image processing. Therefore separation of required objects in pictures of the district remains the actual task which requires the optimum decision.

* Corresponding author. Tel.: 8-960-727-8910.
E-mail address: kirill-kuptsov@rambler.ru

Recognition of spatial objects in a topographical or space picture is a task of separation significant for the user of part of the image from a background, that is classification of copies of some type (class). There is a set of algorithms of separation of objects on the image. The number of the proposed solutions for recognition of objects is also great, but, as a rule, the decision is applicable to the separate task. Purpose of this article is to make the review of the existing methods and algorithms for recognition of objects on raster maps.

2. Recognitions of objects on the topology basis

One of fundamental tasks in topological data analysis consists in that to treat information on the spatial distributed objects in topological space. In operation [3] some sets are represented and reviews of the discrete theory of the Morse and its generalization are given. The sets of closeness considered in a method have the equivalent double determination which are used in this operation. Delaunay set is often used in case of topological data analysis. The algorithm is generalized by the following methods: settings of parameter; settings of scales which influence “importance” of points, and also operation in the Euclidean space of any fixed dimensionality.

In work [10] the task of automated recognition on images of topographical plans of contours of buildings is considered. In this method signs of spatial object like “building” are specified. The algorithm includes the following stages. These are creation of “skeleton” of the source binary or halftone image and creation on it linear and nodal structure in the form of a graph, and also preliminary processing of “skeleton”. Also the method includes such operations as creation on the basis of a skeleton of closed polygons, finding in potential contours of buildings of texts and receiving a final set of contours of buildings and creation of vectorial objects in geographic information systems with record of semantic data from the recognized text. Results of recognition shall possess the following signs. These are isolation, saving right angles, absence of excess points of “fracture” of a contour, false contours, coincidence of boundaries of adjacent objects, and also requirement for the maximum error of a rejection of rather initial raster original.

In work [1] approach to application of the topological relations is considered in the group spatial analysis of cartographical objects. The task of algorithm of topological selection - fast execution of spatial request of the user. It is possible on the basis of determination of the spatial relations prior to processing of request, besides information on them shall be placed in a random access memory for fast processing. The concept of an array from matrixes of the topological relations storing correlations between objects that allows to make their selection according to the given rules is entered. Three classes of the topological relations are selected. These are intraobject, conceptual and interobject. The interobject relations can be such types as isolation, intersection, an enclosure, the neighbourhood, closeness, remoteness. This method is based on preliminary formation of matrixes on number of the basic interobject topological relations. Binary matrix elements show existence or absence of the topological relation. The method allows to organize fast data sampling by topological rules and simplifies operation of the user in case of object search which advantages of use are especially visible in case of execution of a set of procedures of selection of data on different rules.

In operation [2] algorithms of separation of such objects as buildings, the land plots and reservoirs are offered. Spatial characteristics for these classes of objects are set. This technology assumes existence of the input image with which preliminary processing is made. It includes such operations as binarization and a skeletization. The technology assumes the minimum set of settings in which the object type and color of separation for visual display of search results are set. This algorithm includes the following stages. These are search algorithm of closed objects; algorithm of separation of the object containing other object; the search algorithm of distinctions in closed objects. These algorithms assume operation with a bit image matrix. The search algorithm of closed objects consists in finding of offset of originating point to adjacent, applying a mask 3x3. Thus, if the contour is shorted, there is a resetting in originating point. If the contour isn't shorted, at some point it is found out that adjacent points aren't present at all. The algorithm of separation of the object containing other object consists in the following. A certain contour undertakes and in it the point is considered. From this point the straight line to an opposite point is drawn. If this straight line crosses any contour, so the object contains in itself other object or objects. If the straight line doesn't cross a contour, the following point undertakes and so to the middle of this contour. In case the object doesn't contain other objects in itself, it is classified either as the building, or as a reservoir.

The algorithm of search of distinctions in the closed objects assumes classification of objects on two types: “buildings” and “reservoirs”. The algorithm consists in consideration of all points of the classified object. Calculation of quantity of points of turn is made (such points that in them the contour starts appearing in other direction). On the drawn interest of such points the conclusion about object belonging to this or that class is drawn. It is supposed that the objects having required percent higher than 30, possess more roundish form, that is are reservoirs.

Shortcoming of this algorithm is reference of object to a certain type on the sign revealed in the empirical way. For an exception of errors in recognition it is required to support experiment with new signs or provision of the mathematical description of this phenomenon.

Shortcomings of this group of methods are need of creation of more exact signs of spatial objects to exclude their erratic classification [10], large volume for data storage [1], need of confirmation of experiment by mathematical rules [2].

3. Neural networks using

In this group of methods the database of images is applied to training of a neural network. So, for example, in [4] the problem of the automatic analysis of satellite pictures for determination of level of marshiness of terrain is solved. The algorithm of segmentation of satellite images of the territory, on covered and uncovered by water area is developed. It consists of the following stages: formation of collections of satellite pictures on which there can be a water space; compilation of learning selection; implementation of methods of processing and the analysis of images for computation of local and global signs; machine training; implementation of results of training in system together with other methods of computation of signs.

Signs of images which are used in this method are defined, and also the description of the neural network qualifier of points which is its cornerstone is provided. Results of the automatic analysis of real satellite images are given.

Shortcomings of this group of methods is need of training of a neural network which can take the long time for obtaining the acceptable accuracy of recognition of objects. And only the limited circle of tasks can be solved.

4. Mixed methods

The methods considered in this group assume using of several algorithms of image processing for receiving better results.

4.1. Analysis of images of moving objects

One of the principal problems of synthesis of the color image of certain RGB canals is the impossibility of automatic combination of moving objects. As a result, on the image, synthesized in the color, there are three RGB copies of each moving object (red, blue and green) which correspond to different timepoints.

In case of detection of RGB copies of objects there can be following difficulties: the small size of objects concerning permission of space pictures, imposing of RGB copies of the friend on the friend, non-uniformity of brightness of objects in one color copy, distinction in the linear size of objects of one type.

The offered algorithm of normalization of images of the moving objects [9] received as a result of sequential registration of RGB channels allows to integrate multi-colored copies of moving objects and to calculate their characteristics. The method is based on use of correlation of coordinates, sizes and orientation of multi-colored copies of objects. High quality of work of this method can be seen at normalization of red and blue copies of objects.

4.2. The search algorithm of objects in high-precision pictures

In operation [5] the analysis of the existing methods on separation of spatial objects on the bitmap image is made. The search algorithm of vehicles in high-precision pictures in tasks of the analysis of emergency situations is offered. The transformed high-precision picture with the spatial objects selected on it like “vehicles” is given as result of implementation of a method. Images' recognition happens automatically then layout of spatial object of the interesting user of type is defined.

The algorithm includes such steps as binarization of the image, application of the Canny method, sifting of contours, using the removed mathematical formulas.

4.3. Methods of the unified processing procedure of images

The idea of this method [7] consists that the author offers practical implementation of the unified processing procedure of images which will allow to replace application of a set of methods for receiving the same results.

It is supposed that there is some hypothetical “reference” conversion of the ideal image to the required day off. By reviewing enough the coordinated couples of input and output images as learning selection it is possible to make procedure of training of the qualifier which puts in compliance to a vector of the signs calculated according to the input image, the output image. In operation use of some limited two-dimensional areas is offered. After the recursive computation of the generalized moments is considered. The main task in case of this approach is algorithm elaboration and methods of formation of local signs of images in the sliding window. As signs local “the generalized moments” - the linear signs which are calculated by means of the discrete convolutions of the image are offered. Classification of counting of the image is given. In operation the qualifier which is realized in the treelike (hierarchical) form in case of the simplest piecewise constant approximation of function of decisions is used. Also process of synthesis of such qualifier is given. This unified processing procedure showed qualitative results in such tasks as separation of contours, recovery of the binary (two-graded) image like the printing text, filtering the halftone (fuul-gray-scale) image, detection of local two-dimensional objects, recognition of spatial objects on raster maps.

In [8] the correlation method of detection of objects on the image is considered. It is based on computation of values of cross correlation between analysable function of brightness and a standard. Shortcoming of a method is that required coordinates of objects not always manage to be determined with the set accuracy. Therefore for elimination of this shortcoming two modifications of algorithm of correlation which increase the accuracy of calculation of coordinates of objects at recognition are offered.

One of the offered modifications: “A peak filtration of a correlation field”. It allows to simplify procedure of detection of objects and to increase the accuracy of determination of coordinates. The peak filter belongs to the class the rank methods of processing of images. In them each output value is calculated on the basis of the analysis of the variation row constructed of counting of some vicinity which corresponds to a point of an entrance field. If entrance counting has the highest rank in set, he is sent on an exit without change, otherwise receives zero value.

After such processing on a correlation field nonzero points are only local maxima the distance between which exceeds window “radius”. For reduction of number of false detection the area of a window has to be as much as possible.

One more modification of a correlation method consists in transition to the adaptive indication of the purposes. At it for each provision of a window the calculated value of correlation can be referred to any point of the screen. Receiving narrower correlation peak that leads to improvement of a standard method is result of this modification. The given experiments show good operability of the offered modifications of algorithm of correlation. For practical tasks modification with the adaptive indication of the purposes provides higher quality of detection of objects with big noise level and smoothness that can be used at detection and allocation of spatial objects on raster images.

4.4. Methods of recognition of objects in space pictures

In a method [11] the question of recognition of objects of a road network is considered. This task is complicated by that the road network belongs to difficult spatial objects with various extent, geometrical and brightness

characteristics. Besides, complicates detection overlapping of a road network various objects of other classes. In work signs of a road network, in particular, the considerable extent of straight sections, identical width on an extent area, uniform distribution of brightness within object, accurate contours of a roadbed are created.

Mathematical formulas which are applied at selection of objects are given. The filter with the final pulse characteristic which applications to the initial image are result of using: the map of average quadratic deviations for points with a nonzero response of function and the map of the directions of angles of rotation of a window of the filter.

In a method [12] information technology for recognition of pictures of buildings in topographic maps of the cities is considered. It is based on combinatory and geometrical approaches.

Shortcomings of this group are false detection of green component of RGB channels and lack of automatic calculation of characteristics of moving objects [9]; need of improvement of quality of recognition of objects [5]; lack of special selection of signs with which efficiency of this group of algorithms would be higher [7]; loss of part of points of spatial objects therefore additional data processing is made [11]. It consists in use of the map of angles of rotation of a window of the filter containing information on the direction of a road network concerning image abscissa axis.

5. Conclusion

In work the question of detection and allocation of spatial objects on raster maps in geographic information systems is considered. Versions of solutions of this problem are given, classification of already available methods is executed. Algorithms and methods of such groups as are presented: based on topology and various topological rules, on the basis of a neural network, the combined methods in which solutions of questions on the basis of using of several methods and algorithms are proposed. Most often the combined methods are directed on the solution of certain practical tasks. For example, methods and algorithms of this group are used at the solution of such tasks as recognition of spatial objects, in particular, of buildings [10], vehicles [5, 9], an assessment of marshiness of territories [4], recovery of the binary (two-graded) image [7]. Ways of development in search of the optimum decision on the matter are offered. Firstly, this improvement of quality of recognition. Secondly, creation of the general rules possessing sufficient accuracy rating for an exception of erratic classification of objects of a certain type. Thirdly, creation of the rules defining correlations of spatial objects of different classes. In particular, without reducing importance of process of improvement of recognition of spatial objects, it is worth paying attention to a question of the accounting of interposition of these objects and other spatial characteristics. The partial solution is proposed in the form of algorithm [5], but this technology, firstly, demands improvement of quality of recognition; secondly, it is directed on a certain type of spatial objects that, certainly, doesn't resolve an issue in general. Therefore in parallel with a question of recognition of spatial objects it is necessary to pay attention to generalization of topological regularities and creation of mathematical rules. The topology will give the chance to leave from comparing of standards, and to determine an object type by a set of its characteristics.

References

- [1] D.E. Andrianov, M.S. Sokolov, Use of topological rules in the spatial analysis of cartographical objects, *Izvestiya vysshikh uchebnykh zavedeniy, Priborostroenie*. 53(9) (2010) 14–19
- [2] S.V. Ereemeev, D.E. Andrianov, A.E. Barinov, D.V. Titov, Algorithms for searching objects according to spatial characteristics in problems of municipal geoinformation system, *Izv. Yugo Zap. Federal. Univ.* 2 (2012) 37–41.
- [3] U. Bauer, H. Edelsbrunner, The Morse theory of Cech and Delaunay filtrations, In *Proc. 30th Ann. Sympos. Comput. Geom.* 2014.
- [4] A.D. Varlamov, R.V. Sharapov, Use of neural networks for an assessment of level of marshiness of the territory on the basis of data of remote sensing, *Neurocomputers: development, application*. 3 (2015) 29–33.
- [5] K.V. Kuptsov, The search algorithm of vehicles in high-precision pictures in tasks of the analysis of emergency situations, *Algorithms, methods and data handling systems*. 2 (2015) 50–58.
- [6] K.V. Kuptsov, Yu.A. Bulanova, Research of algorithms of separation of objects on the image, the Scientific potential of youth – the future of Russia, VI All-Russian scientific Zvorykinsky readings: All-Russian interuniversity scientific conference. (2014) 635–636.
- [7] V.V. Sergeyev, Application of methodology of image identification in tasks of digital image processing, *Autometria*. 2 (1998) 63–76.
- [8] V.V. Sergeyev, M.A. Chicheva, Some modifications of the digital correlator for detection of objects on the image, *Computer optics*. 5 (1989) 78–84.

- [9] A.V. Chernov, M.V. Gashnikov, N.V. Chupshev, Normalization of images of moving objects in case of sequential registration of RGB channels, *Computer optics*. 32(1) (2008) 93–95.
- [10] A.V. Chernov , O.A. Titova, N.V. Chupshev, Automatic recognition of circuits of buildings on cartographical images, *Mathematical methods of image identification, 13th All-Russian conference, Zelenogorsk, collection of reports. (2007)* 424–427.
- [11] A.A. Yashchenko, S.Yu. Miroshnichenko, Method of recognition of objects of a road network in space pictures, *Izv. Yugo Zap. Federal. Univ.* 2-1 (2012) 158–163.
- [12] O.A. Bashkurov, Yu.G. Vasin, N.V. Khoroshenkov, Detecting buildings on topographic maps of cities, *Pattern Recognition and Image Analysis (Advances in Mathematical Theory and Applications)*. 11(2) (2001) 284.



International Conference on Industrial Engineering

About the use of interactive electronic technical manuals for the machine builder

Tuktamyshev V.R.^a, Glukhov D.A.^a, Kataev Ya.A.^{a*}

^a Perm National Research Polytechnic University, 29 Komsomolsky prospekt, Perm 614600, Russian Federation

Abstract

The support of complete product life cycle (PLC) of mechanical facilities is very important. The consumer is a full participant in the PLC stages of the operation, so the producer is obliged to ensure his exploitative documents. The problems of ensuring PLC support of the operation stage - the complexity of perception, development and support of exploitative documents in a paper form is represented. The experience of domestic enterprises to develop interactive electronic technical manuals (IETM) is given. The tool for creating and managing IETM and the way of solving problems that arise in the creation and use of interactive electronic documents is proposed.

© 2015 The Authors. Published by Elsevier Ltd. This is an open access article under the CC BY-NC-ND license (<http://creativecommons.org/licenses/by-nc-nd/4.0/>).

Peer-review under responsibility of the organizing committee of the International Conference on Industrial Engineering (ICIE-2015)

Keywords: interactive electronic technical manuals; product life cycle

1. Introduction

By now the complete support of the product lifecycle (PLC) is an important component of the competitiveness and efficiency of any industrial enterprise.

Information technologies significantly increases the efficiency of the complete support PLC due to extensive use of 3D computer aided design (CAD) system, computer aided engineering (CAE) system, computer aided production planning (CAPP) system, computer-aided manufacturing (CAM) system, product data management (PDM) system

* Corresponding author. Tel.: +7-922-3000-215.

E-mail address: kataev.yakov@mail.ru

and others. All work should be carried out within the framework of the common information space (CIS) for the most efficient operation of enterprise services.

The approach to design and manufacture of high-tech and science-intensive products, which is the use of information technology at all stages of the PLC, called the continuous acquisition and lifecycle support (CALS) or information support product lifecycle (ISP) [1].

On account of continuous information support to provide the uniform methods of process management and interaction of all participants in PLC: customers, suppliers, producers, exploitative and repair personnel.

Current requirements for almost all design, technological, exploitative and repair documents gradually develop from the release of paper documents to the release of electronic documents and even interactive documents. This tendency is explained by the general development of technologies and is not confined to machine-building industry. Every company has to think about the development and support of such documents to ensure effective development. The process of development and support of such documents requires special approaches and techniques.

One of these approaches is the integrated logistics support (ILP). ILP is a set of engineering activities types, which are implemented by the management, engineering and information technologies, aimed at ensuring a high level of products availability, while reducing the costs that are associated with their exploitative and repair. The development and support of exploitative and repair documentation is one of the major activities, which is included in the ILP concept [2].

The aim of this activity is to provide the customers the technical documentation (mostly in electronic form), which regulates the implementation of exploitation and repair of products, as well as information logistics support.

The consumer is a full participant PLC during the operational phase, so the manufacturer shall provide the consumer with complete informational support. The exploitative document (ED) is used as a means of information support at this stage.

Now one of the major problems of support process PLC on the exploitation stage is the difficulty of develops, support and perception the ED, which is being developed in the traditional paper form. So there is a tendency in the industry to create electronic ED, which is an order of magnitude more easily perceived by consumers and which is easier to support up to date.

The ED includes text, graphic and multimedia design documents, that individually or collectively enable familiarization with the product and determination with the rules of product's exploitation. ED may be formed of paper design documentation and/or digital design documentation [3]. The electronic ED may be in the form of interactive electronic documents (IED). IED is a document, which a substantial part of the information is available in an interactive form [4]. Interactive electronic technical manuals (IETM) is generic name for a coherent set of exploitative documents, executed in the form of IED and is usually contained in a single database [3].

When develop IETM, problem of maintain the relevance arises, because the development of the interactive documentation is more difficult than the traditional. So there is a aim of creating a complex automation and multimedia content filling of the IETM, as well as the aim of full transition to the developing of ED immediately as IETM and receiving data to develop and support directly from the information and associative 3D-models, that are stored in the enterprise's CIS.

At the same time it is necessary to determine the area of rational use of IETM. IETM use is not always justified.

2. Theory

For the most accurate identification of the area of the rational use of the developed technology is necessary to analyze the basic components of the cost of the process of development and support of operational documentation of various kinds.

ED consists of data modules. Data module (DM) is a set of interrelated technical information on the operation of the product relating to specific topics and not allows their further split into its component parts, which contains text and multimedia content. [3]

$$\sum_{i=1}^N DM_i = ED \quad (1)$$

where N is the total number of data modules.

Let us consider:

- E_1 is the development costs the traditional paper ED;
- E_2 is the IETM development costs by using a common database (DB);
- E_1^{3D} is the development costs the traditional ED by using 3D models;
- E_2^{3D} is the IETM development costs by using a common DB and 3D models;
- E_3 is the IETM development costs by using CIS and associative 3D models.

The cost of developing a similar IETM using a common DB assumes the form [5, 6]:

$$E_1 = \overline{S_{DM}} \times \sum_{i=0}^K n_i \quad (2)$$

where $\overline{S_{DM}}$ is the average cost of developing a data module; $n_i \in \mathbb{N}$ is the total number of DM ED in the i -th modification of the product; K is the amount of modifications.

The development IETM costs by using a common DB have a view [5, 6]:

$$E_2 = \overline{S_{DM}} \times n_0 + \overline{S_{DM}} \times \sum_{i=1}^K n_i - \overline{S_{DM}} \times \sum_{i=1}^K (n_i \times L_i) \quad (3)$$

where n_0 is the amount DM of in the basic modification of the product; $L_i \in \mathbb{R}$ is the DM share of i -th modification products which are borrowed from the basic product (the unification degree):

$$L_i = \frac{m_i}{n_0} \quad (4)$$

where m_i is the amount of borrowed DM from the basic product in the i -th product modification.

Let us assume that:

- The average number of DM n is not changed for all product modification.
- The unification degree L is the same on the average for all models.

We obtain:

$$E_1 = \overline{S_{DM}} \times n \times (1 + K) \quad (5)$$

$$E_2 = \overline{S_{DM}} \times n \times (1 + K - K \times L) \quad (6)$$

where $n \in \mathbb{N}$ is the average number of MD in the ED of all product modifications within the same product type; $L \in \mathbb{R}$ is the average share of borrowing DM from the basic modification ED.

Let us consider development costs ED using 3D models.

Let us decompose the average cost of developing the DM on the components:

$$\overline{S_{DM}} = \overline{S_{DM}^P} + \overline{S_{DM}^{3D}} \quad (7)$$

where $\overline{S_{DM}^P}$ is the cost of DM component containing text and other data, that are not associated with the 3D model; $\overline{S_{DM}^{3D}}$ is the cost of DM component containing multimedia and other data, that are associated with the 3D model.

Because the multimedia content is created automated, costs should not be taken into account in the cost of ED developing. But we should not neglect it because it makes a significant contribution. We obtain:

$$E_1^{3D} = (1 - \mu) \times \overline{S_{DM}} \times n \times (1 + K) \quad (8)$$

$$E_2^{3D} = (1 - \mu) \times \overline{S_{DM}} \times n \times (1 + K - K \times L) \quad (9)$$

where $\mu \in \mathbb{R}$ is the average share of costs in the DM for multimedia data, that created on the basis of 3D models:

$$\mu = \frac{\overline{S_{DM}^{3D}}}{\overline{S_{DM}}} \quad (10)$$

Let us consider development costs of IETM with using associative 3D models and CIS.

$$E_3 = (1 - \mu) \times \overline{S_{DM}} \times n \times (1 + K - K \times L) \quad (11)$$

3. Conclusion

So development costs of IETM with using CIS and associative 3D models (11) are equal development costs of IETM with using common DB and 3D models (9). However, it should be noted that there are benefits of using associative 3D models:

- simplification the development of multimedia content for MD filling;
- improving the quality of ED;
- automatic/automated updating of multimedia data, which are based on associative 3D models.

Consequently, one of the advantages of using associative 3D-models is to reduce the costs of change documents.

Should be noted that enterprises began developing ED at once in IED form using 3D models [8].

Currently, PSC "Motovilikhinskiye zavody" and the Perm National Research Polytechnic University are developing complex of technologies for the design, production, production management and exploitation of innovative hi-tech products [9]. The complex includes the development technology of interactive documents, which is intended to form the company policy in this area, and development and support of methods of IED creation and support up to date. The interactive documents include both IETM, as well as the interactive design documents, technological processes, repair documents and etc.

The development technology of interactive documents includes the following subsystems:

- The subsystem of control the process of creating interactive documents, which is designed to regulate the process of develop or selecting software to develop various types of interactive documents, and which is designed to regulate the process of development the interactive documents;
- The interactive document management subsystem for managing electronic archives of approved interactive documents in the CIS.

So in the future there is task to realize the modern system of development of interactive documents and support documents during the PLC. At the same time ensuring the preservation of the level of development costs and improves the quality of IED.

Acknowledgements

The work was supported by the Ministry of Education and Science of the Russian Federation (the contract from 05.23.2013 № 02.G25.31.0068, in the framework of the Russian Federation Government Resolution № 218)

References

- [1] I.P. Norenkov, *Osnovy avtomatizirovannogo proektirovaniia* [Basics of computer-aided design], Bauman MSTU Publ., Moscow, 2009.
- [2] State standard specification R 53393-2009. Integrated logistic support. General principles, Standartinform, Moscow, 2010.
- [3] State standard specification 2.601-2013. Unified system for design documentation. Exploitative documents, Standartinform, Moscow, 2014.
- [4] State standard specification 2.051-2013. Unified system for design documentation. Digital documents. General principles, Standartinform, Moscow, 2014.
- [5] I.Yu. Galin, *Avtomatizacija sozdaniia interaktivnykh jelektronnykh tehniceskikh rukovodstv (IJeTR)* [Automating the interactive electronic technical manuals (IETM) creation]: Ph.D. author's abstract in Engineering Science: 05.13.06, National Research Nuclear University (NRNU), Moscow, 2011.
- [6] S.V. Veretkhina, *Metodika razrabotki interaktivnoj jelektronnoj jekspluacionnoj dokumentacii dlja naukojomihih izdelij otrasli svjazi i informatizacii* [The methodology of development the interactive electronic exploitative documents for high-tech products of communications and informatization branch]: Ph.D. author's abstract in Economics: 08.00.05, 08.00.13, All Russia Scientific Research Institute of Computer Technology and Informatization Problems (ARSRICITP), Moscow, 2008.
- [7] State standard specification 2.503-2013. Unified system of design documentation. Rules of making modifications, Standartinform, Moscow, 2014.
- [8] V.A. Devyatkin, V.R. Tuktamyshev, Ya.A. Kataev, *O tehnologii razrabotki interaktivnoj jekspluacionnoj dokumentacii* [About technology of interactive exploitative documents development], *Modern materials, apparatus and technologies*. 1(1) (2015) 65–67.
- [9] V.F. Makarov, *The development of approaches to defense and industrial complex specialists education within the framework of product lifecycle management system* [Razrabotka podhodov k podgotovke specialistov oboronno-promyshlennogo kompleksa v ramkah sistemy upravleniya zhiznennym ciklom izdeliya], *Thermalphysic and technological aspects of increase of efficiency of engineering production: IV International Scientific and Engineering Conference (4 Reznikovskii reading)*. (2015) 389–392.



International Conference on Industrial Engineering

A study of the identification method for the test flat objects based on dimensionless signs of their contours

Sadykov S.S.^a, Kulkov Y.Y.^{a*}

^a*The Murom institute of Vladimir state university, Orlovskaya st., 23, Russia*

Abstract

The article is devoted to the experimental study of the possibility to use dimensionless signs of an object binary image contour. The basis for the attribute vectors formation is the characteristics of the image contour. The experiments on the identification of the objects are based on the calculation of standard deviation.

© 2015 The Authors. Published by Elsevier Ltd. This is an open access article under the CC BY-NC-ND license (<http://creativecommons.org/licenses/by-nc-nd/4.0/>).

Peer-review under responsibility of the organizing committee of the International Conference on Industrial Engineering (ICIE-2015)

Keywords: Image recognition; vision system;

1. Introduction

The paper presents the results of experimental studies on the identification of test flat objects (TFO) based on using dimensionless signs derived from the characteristics of the binary image contour of these objects, developed in [1].

Detection and identification of objects is an integral part of human activity. An object is defined not only as a digital representation of a fragment of the local two-dimensional scene, but its approximate description, as a set of specific properties or signs. The main purpose of their description - is their use in the process of establishing of object compability, carried out by comparison. The objective is to identify the recognition of any object to a particular class by analyzing the vector of values of calculated signs. The information about the relationship between the values of the object signs and its belonging to a certain class a recognition algorithm has to learn from the training set of objects for which the signs of attributes and classes are known [2-13].

* Corresponding author. Tel.: +7-910-7777386
E-mail address: y_mail@mail.ru

2. Methodology

For the study proposed in [1] algorithm a set of binary images of individual test flat objects was chosen. It is shown in figure 1.

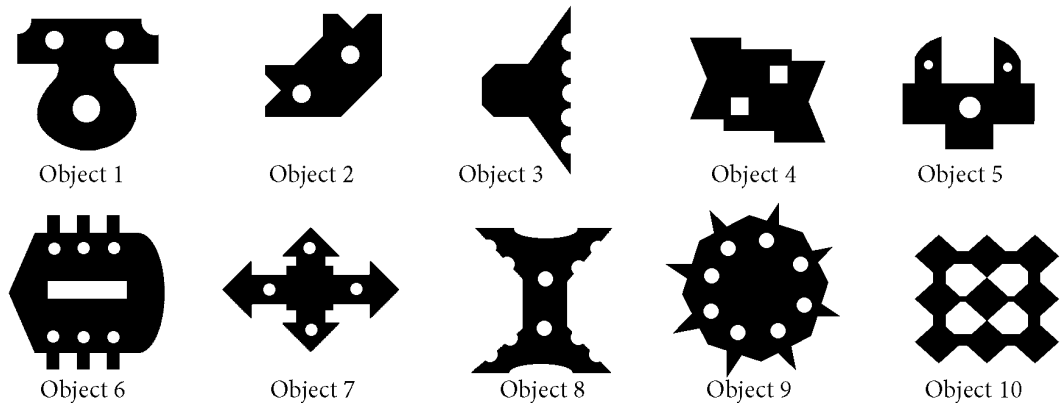


Fig.1 Test images

The experiment was conducted on a presentable display access of each of the 10 TFO. To do this, initially generating of a set of rotated images is performed. For each of the images centroids of objects are calculated and an array of rotated images of each of the 10 TFO in a step of 1 degree is formed. On the whole, we get 3600 images.

Then we make simulation of accidental occurrence of an object in the field of recognition pattern.

With the help of random number generators (RNG) with a normal distribution 10 sets of 2,000 images are formed from 360 rotated images of each of the 10 TFO.

With the second RNG we get a number in the range of 0.364 to 0.720. This limitation is necessary to minimize the layout of images out of the operating field. 4000 numbers are generated for 2000 implementations of each object. We will assume the first number RNG the coordinate of the center of gravity on the axis X X_n of an object, the second number - Y_n . Thus, the coordinates of the center of gravity of each of 2000 of the implementations of each of the 10 TFO can be defined. According to these coordinates 2000 of the implementations of each of the 10 TFO are placed on the display space.

Then we calculate the number of dots in each of 2000 of the implementation of each of the 10 TFO, that is calculate the area of object S_0 . The example of calculation result of 2000 of the implementations of each of the 10 TFO is shown in table 1.

Table 1. Parameter S_0

implementation №	1	2	...	846	...	1999	2000
Parameter S_0	34041	22039		47925		44865	36684

For each of the obtained object implementation single-point contours are formed according to the algorithm in [4].

For each of them the number of dots forming the contour of each of the 2000 of the implementations of each of the 10 TFO is calculated. The example of such a calculation is shown for implementations of the 1st TFO in table 2.

Table 2. Parameter P_0

implementation №	1	2	...	356	...	1999	2000
Parameter P_0	843	600		960		1054	778

Next we define the metric length of the contour of each of the 2000 of the implementations of each of the 10 TFO. The example of such a calculation is shown for the implementations of the 1st TFO in table 3.

Table 3. Parameter L_{cont}

implementation №	1	2	...	1875	...	1999	2000
Parametr P_0	927.91	690.29		1138.70		1236.25	1018.66

For each implementation the value of the curvature at the points of each contour of the 2000 of the implementations of each of the 10 TFO is determined. According to the obtained points the reference point of convex and concave sections of the contour are determined.

We determine the number of reference points of convex, concave and linear plots of contours. The example of calculation of the reference points 1st TFO implementations is given in table 4.

Table 4. Parameters M_1 - M_4 and K, T

implementation №	1	2	...	956	...	1999	2000
M_1	4	0		5		7	10
M_2	3	1		5		0	0
M_3	111	12		158		43	68
M_4	109	4		150		49	84
K	528	374		716		526	120
T	88	209		26		335	495

where:

M_1 - the number of contour points with a value of 90;

M_2 - the number of contour points with a value of -90;

M_3 - the number of contour points with a value of 135;

M_4 - the number of contour points with a value of -135;

K - the number of 4 connected contour points;

T - the number of D connected points of the contour.

With formulas (1), (2) and (3) we calculate the total length of the convex, concave and basic blocks of the entire contour of each object:

$$L_{tot.conv.} = \frac{1}{2}[M_1 2b + M_3(a+b)] \quad (1)$$

$$L_{tot.conc.} = \frac{1}{2}[M_2 2b + M_4(a+b)] \quad (2)$$

$$L_{tot.lin.} = \frac{1}{2}(K 2a + T 2b) \quad (3)$$

where:

a - distance between 4th connected points;

b - distance between D's connected points.

Example calculation results of the of parameters based on the formulas (3), (4) and (5) is shown in table 5

Table 5. Parameters L_{cont} .

implementation №	1	2	...	1233	...	1999	2000
$L_{tot.conv.}$	139.64	14.485		197.79		143.26	96.23
$L_{tot.conc.}$	135.81	6.2426		188.13		139.64	101.39
$L_{tot.lin.}$	652.45	669.57		752.77		542.48	820.03

Using calculated parameters, calculates the vectors of dimensionless signs of the 2000 of the implementations of each of the 10 TFO with formulas (4) - (19).

$$KI = P_0 / S_0 \quad (4);$$

$$K2 = M_1 / S_0 \quad (5);$$

$$K3 = M_2 / S_0 \quad (6);$$

$$K4 = M_3 / S_0 \quad (7);$$

$$K5 = M_4 / S_0 \quad (8);$$

$$K6 = K / S_0 \quad (9);$$

$$K7 = T / S_0 \quad (10);$$

$$K8 = M_1 / P_0 \quad (11);$$

$$K9 = M_2 / P_0 \quad (12);$$

$$K10 = M_3 / P_0 \quad (13);$$

$$K11 = M_4 / P_0 \quad (14);$$

$$K12 = K / P_0 \quad (15);$$

$$K13 = T / P_0 \quad (16);$$

$$K14 = L_{tot.lin.} / L_{cont} \quad (17);$$

$$K15 = L_{tot.conc.} / L_{cont} \quad (18);$$

$$K16 = L_{tot.conv.} / L_{cont} \quad (19);$$

The example of final signs for the 2000 of the implementations of the 1st TFO is in table 6.

Table 6. Parametrs $K_1 - K_{16}$

implementation №	1	2	...	2000
K_1	0.0247	0.02252		0.02193
K_2	0.00011	0.00038		0.00032
K_3	8.812e-5	0.00044		0.00020
K_4	0.00326	0.0045		0.00358
K_5	0.0032	0.00428		0.00358
K_6	0.0155	0.00443		0.00449
K_7	0.0025	0.00840		0.00977
K_8	0.0047	0.0169		0.0147
K_9	0.0035	0.01955		0.00937
K_{10}	0.1316	0.2033		0.16332
K_{11}	0.1293	0.1903		0.16332
K_{12}	0.6263	0.1968		0.20481
K_{13}	0.0247	0.0225		0.02193
K_{14}	0.7031	0.5788		0.66199

K ₁₅	0.1463	0.2057	0.16675
K ₁₆	0.1504	0.2153	0.17275

3. Recognition

After receiving vector signs for all generated realizations the standards for recognizing each of the 2000 implementations of each of the 10 TFO is carried out in the dialog mode. In the histogram obtained while generating we choose a vector sign of the most frequently used

options from 360 rotated variants, for example, the 1st TFO, while the formation of 2000 implementations. For this vector of coefficients of the standard deviation (20) we calculate Z_i from 2000 implementations.

$$Z_i = \frac{1}{n+1} \sum_{j=1}^n (K_j - K_{ji})^2 \quad (20)$$

where:

n - number of signs;

l – number of recognizable object ($l = 1, 2, \dots, 2000$);

K_j - the value of the j- feature vector of coefficients K of the selected standard;

K_{ji} - the value of the j-feature vector of coefficients K of the selected implementation.

2000 implementaions are calculated Z_i . Among them are Z_{\min} sought

$$Z_{\min} = \min\{Z_i\} \quad (21)$$

Found values Z_{\min} indicate the number of implementations among 2000 images which vector signs coincide with the vector-sign selected as a reference implementation. Obviously, with one standard it is impossible to recognize all 2000 implementations of the 1st TFO.

Secondly, based on the histogram we select as a standard the reference vector of the next most frequently used options from 360 rotated, for example, the 1st TFO, while formation of 2000 implementations. We calculate 2000 standart deviation Z_i . Among them Z_{\min} are searched by the formula (21).

Found values Z_{\min} indicate the numbers of implementations among 2000 images which vector signs coincide with the vector sign of a standard implementation, etc. Selecting of standards for the realization of the 1st TFO continues till until all 2000 implementations are recognized.

Similarly, the choice of standards is carried out for all implementations of all other 9 TFO. The results of standard selection for 2000 implementations of each of the 10 TFO are shown in table 7.

Table 7. Numbers of etalons of all TFO

N _o TFO	1	2	3	4	5	6	7	8	9	10
Number of etalons	28	35	17	25	43	27	34	28	8	33

Thus, this training of the recognition system is completed.

To check the operation of the system of recognition, an examination of 20000 trained implementations of all 10 TFO on the basis of formulas (20) and (21) is carried out. The exam consists of comparing the vector signs of all 20000 implementations of all 10 TFO with the selected standards.

A random object is selected. It features all the above procedures of producing dimensionless signs of contours. The resultant vector of the unknown ITFO is compared to all standard vectors in table. 7. The type of TFO is determined according to $\min\{Z_{\min}\}$.

The exam procedure is repeated for the 2nd unknown object, and so on for all of 20 000 realizations of all 10 TFO.

4. Conclusion

Object 9 has a simple symmetrical contour. Its rotated images do not differ substantially among themselves. Therefore, it took only 8 standards for the detection of the object. The object 5 has a complex shape. This led to the need to use 43 standards for the full recognition of all implementations of the object. On average, it takes about 30 standards.

During the research the experimental studies have been conducted on the recognition of individual testing of flat objects on the basis of non-dimensional signs of their contours. Experiments were carried out on the basis of presentable selection in 2000 images for selected 10 objects.

The results showed high efficiency of the proposed non-dimensional signs. The amount of standards required for the recognition depends on the complexity and symmetry of the contour of the object.

With this set of standard vectors of coefficients the detection of unknown objects was 100%.

Recognition time indicators are obtained for algorithms for test selection circuit and for determination of the coefficients. The method of guided search was used as an algorithm for contour detection. This method and algorithm of marking reference points are the most time-consuming in this system and they can be optimized for use in a real system in order to reduce the recognition time.

References

- [1] S.S. Sadykov, Formation of the dimensionless coefficients form a closed loop digital, Algorithms, methods and computing. 4(29) (2014) 91–98.
- [2] S.S. Sadykov, The algorithm is a logical definition of the curvature of the discrete points of the line, Algorithms, methods and computing. 1(30) (2015) 52–59.
- [3] S.S. Sadykov, A. Belyakov, Regression models of stenocardia and the dependence of their information on the number of parameters of the heart, Control systems and information technologies. 45(3.1) (2011) 190–194.
- [4] S.S. Sadykov, S.V. Savicheva, Identifying real flat objects on the basis of a single characteristic points of their external contours, Information technologies. 8 (2011) 13–16.
- [5] S.S. Sadykov, E.A. Zakharova, Yu. Bulanov, Technology selection brush area on a mammogram, Reporter of the Ryazan state radio university. 1(43) (2013) 7–12.
- [6] S.S. Sadykov, Y. Bulanov, E.A. Zakharov, V.S. Yashkov, A study of the watershed marker to highlight Breast Cancer, Algorithms, methods and computing. 1 (23) (2013) 56–64.
- [7] S.S. Sadykov, An algorithm for constructing the convex hull of a binary image, and the formation of its dimensionless signs, algorithms, methods and computing Number. 2(23) (2015) 77–85.
- [8] S.S. Sadykov, N.N. Stulov, Methods and algorithms for feature extraction of objects in vision systems, Hotline Telecom, Moscow, 2005.
- [9] D.E. Andrianov, S.S. Sadykov, R.A. Simakov, Development of municipal geographic information systems, Mir, Moscow, 2006.
- [10] A.L. Zhiznyakov, S.S. Sadykov, Theoretical Foundations of multiscale processing sequences of digital images, Vladimir State University Publishing House, Vladimir, 2008.
- [11] O.I. Evstigneeva, S.S. Sadykov, E.E. Suslov, A.S. Belyakov, Criteria allocation of risk groups of people of working age in the medical research on the system AFS, algorithms, methods and computing. 19 (2012) 33–39.
- [12] S.S. Sadykov, Y. Bulanov, E.A. Zakharova, An interactive system for analyzing mammography images, Algorithms, methods and computing. 19 (2012) 155–167.
- [13] A.A. Ermakov, A.A. Orlov, S.S. Sadykov, D.N. Starodubov, Methods and algorithms for processing and analysis of flaw and metallographic images, Vladimir State University Publishing House, Vladimir, 2008.



International Conference on Industrial Engineering

Finding correspondences between images using descriptors and graphs

Zakharov A.A.^{a*}, Tuzhilkin A.Yu.^a, Zhiznyakov A.L.^a

^a*Murom Institut, Vladimir State University, Orlovskaya 23, Murom, 602264, Russian Federation*

Abstract

The problem of finding correspondences is considered in the article. The main objective of this method is to reduce the number of false matches by using structural performance. The relevance of the problem is proven. The review of existing methods of finding correspondences is provided. The method presented is finding correspondences based on combined use of graphs and descriptors. Scott and Longuet-Higgins algorithm is used in the first stage. We construct a graph the vertices of which are the features on the two images. Singular value decomposition of the graph matrix is performed. The correspondences based on the descriptor are used. An example of the algorithm is shown. Test images are researched. A comparison of the algorithm with the RANSAC is carried out. The proposed approach allows excluding a significant portion of false correspondences found using the existing descriptors. The algorithm has high speed.

© 2015 The Authors. Published by Elsevier Ltd. This is an open access article under the CC BY-NC-ND license (<http://creativecommons.org/licenses/by-nc-nd/4.0/>).

Peer-review under responsibility of the organizing committee of the International Conference on Industrial Engineering (ICIE-2015)

Keywords: Image recognition, inexact graph matching, finding correspondences, descriptors, graphs.

1. Introduction

The problem of finding correspondences in images is the most important in computer vision. Finding correspondences is used in pattern recognition [1], tracking the movement of objects [2], reconstruction of three-dimensional scenes[3-5]. The success of finding and comparing features depends on timing differences of shooting, shooting angles, the characteristics of a sensor. In addition, significant restrictions are imposed not only by shooting

* Corresponding author. Tel.: 8(49234) 77236;
E-mail address: aa-zaharov@ya.ru

parameters, but geometric and physical characteristics of the scene: the location of a light source and the elements of the scene, reflecting and diffusing capacities of surfaces. In the development of methods of finding correspondences the following indexes should be obtained: full automation process; resistance to noise, overlaps, optical effects; high speed processing, the invariance to affine transformations; the possibility of processing of images with different photometric characteristics, scale, etc.

The proposed approach suggests using the information on relative location of points on stereo images with the help of graphs to improve the accuracy of comparisons. Thus, there is no comparison of separate points, and structures represented in the form of graphs.

2. The review of the existing methods used to find correspondences

To find correspondences in images, detectors and descriptors are used. The detector is a method of finding the characteristics of an image. Feature detectors used in computer vision can be divided into three main categories [5, 6]:

- edge detectors: Roberts [7], Prewitt [8], Sobel [9], Hough Transform [10], Canny [11];
- corner detectors: Harris [12], SUSAN [13], FAST [14], AGAST [15], STAR [16];
- blob detectors: MSER [17], SIFT [18], SURF [19].

The descriptor is a method that identifies and compares the characteristics of image features. The most famous descriptors are: SIFT [18], SURF [19], DAISY [20], ORB [21], BRIEF [22], BRISK [23], HoG [24]. The drawback of the existing approaches is that it is necessary to compare some separate features in two images, which leads to errors when finding correspondences.

The use of computer vision is limited by sound and optical effects, the textured background, mutual overlapping of objects. An important objective when using descriptors is to reduce the number of false correspondences. One approach to reduce the error of the first type is to use RANSAC method (RANDOM SAMPLE CONSENSUS) [5]. In this case, based on the detected features, there is a transformation in which the number of superposed points reaches its maximum. It should be noted that RANSAC method results often depend on particular implementation features.

To increase the reliability it is proposed to use structured information in the form of graphs. The advantage of structural methods is that they give an opportunity to analyze a big set of elements on the basis of a small quantity of simple components and rules of forming the graphic model. Also structural methods allow to describe the characteristics of the object excluding its reference to another class that increases the reliability of the recognition. Scott and Longuet-Higgins used graphs to find the corresponding [25]. Our method of finding correspondences based on the combined use of graphs and descriptors.

3. The algorithm for finding correspondences based on approximate comparison graphs

To avoid false correspondences a singular matrix layout is used [25]. Suppose there are two sets of correspondences $S_1 = \{f_{1i} | i = 1, \dots, m\}$ and $S_2 = \{f_{2j} | j = 1, \dots, m\}$ derived from images I_1 and I_2 . To represent the graph based on the characteristics, matrix of distances G is constructed (1):

$$G_{ij} = e^{-\frac{r_{ij}^2}{2\sigma^2}}, \quad (1)$$

where, $r_{ij} = \|f_{1i} - f_{2j}\|$ – the distance between features f_{1i} and f_{2j} ; σ – coefficient, regulating the degree of interaction between the features.

The values of the matrix elements are in the range from 0 to 1.

It is proposed to describe the degree of correspondence by using coefficient K . If a correspondence, based on a descriptor, is found, in this case $K = 1$, otherwise $K = 0$.

In this case the algorithm for finding correspondences takes a look.

Step 1. The construction of matrix of distances G .

Step 2. The performance of a singular matrix decomposition: $G = TDU$, where, D – an eigenvalues matrix; T , U – eigenvector matrix.

Step 3: The calculation of the correspondence matrix by replacing matrix D with identity matrix E : $P = TEU$.

Step 4. The calculation of matrix $M_{ij} = K_{ij}P_{ij}$, where K - a coefficient matrix, determining the correspondence between i and j features of the first and the second images. For matrix M values the threshold $0 < z < 1$ is set. If value $M_{ij} < z$, then the correspondence, found on the basis of the descriptor used, is excluded from consideration. In this case, matrix L value of 0 is recorded.

Step 5. A binary matrix formation. The idea is to get matrix L through matrix M in which the values equal to 1 indicate the presence of correlations between features f_{1i} and f_{2j} . If a current matrix M element is the maximum element in the line and the column, value 1 is written into binary matrix L , otherwise value 0 is written. If the value of the element of matrix L is equal to zero, the correspondence between the features do not exist. If the value of the element of matrix L is equal to one, there is a correspondence between features with the index equal to the number of lines and columns.

4. An example of the algorithm

An example of finding false matches is shown below. The correspondence between the images found using an algorithm SURF (Fig. 1).

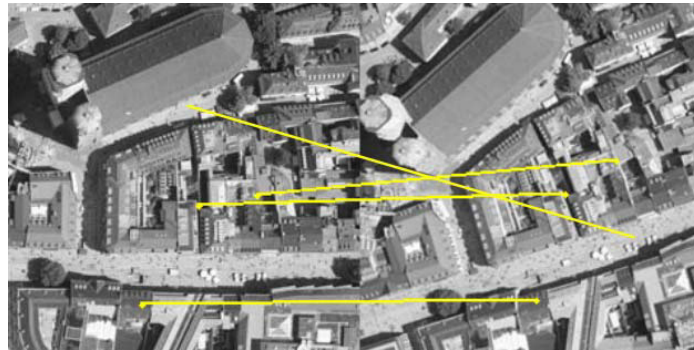


Fig. 1. An example of finding of false matches is shown.

The marking of the vertices as follows (Fig. 2): $f_{11} = (256, 196)$, $f_{12} = (292, 151)$, $f_{13} = (264, 147)$, $f_{14} = (235, 98)$, $f_{21} = (469, 169)$, $f_{22} = (444, 152)$, $f_{23} = (477, 131)$, $f_{24} = (431, 99)$.

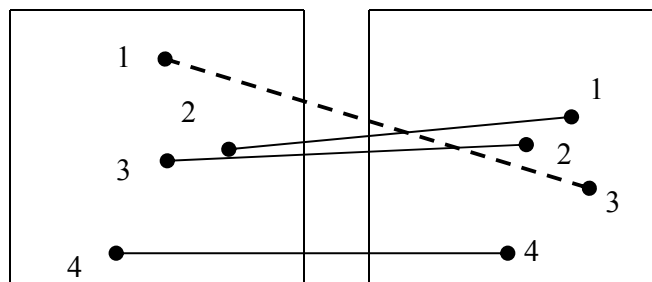


Fig. 2. The marking of the vertices.

The coefficient matrix is of the form (2). The line number indicates the number of features of the first image and the column number - is the number features of the second image.

$$K = \begin{bmatrix} 0 & 0 & 1 & 0 \\ 1 & 0 & 0 & 0 \\ 0 & 1 & 0 & 0 \\ 0 & 0 & 0 & 1 \end{bmatrix} \quad (2)$$

The coefficient is approximately equal to half the distance between the most distant features d in images. For σ values which are few times smaller than distance, the elements of matrix G_{ij} tend to zero, which makes the comparison difficult. At σ values which are a few times greater than distance d , the elements of the matrix tend to unity, which also leads to erroneous results. The coefficient σ in the example is equal to 100.

The matrix correspondence has the form (3):

$$P = \begin{bmatrix} 0.533 & 0.625 & -0.564 & -0.079 \\ 0.62 & 0.131 & 0.679 & 0.371 \\ -0.576 & 0.726 & 0.216 & 0.31 \\ -0.011 & -0.257 & -0.417 & 0.872 \end{bmatrix} \quad (3)$$

We obtain the matrix $M_{ij} = K_{ij}P_{ij}$ (4):

$$M = \begin{bmatrix} 0 & 0 & -0.564 & 0 \\ 0.62 & 0 & 0 & 0 \\ 0 & 0.726 & 0 & 0 \\ 0 & 0 & 0 & 0.872 \end{bmatrix} \quad (4)$$

All the entries that are less than 0.6 is considered equal to 0. Thus, we obtain the following correspondences: 2-1, 3-2, 4-4. This is true. The binary matrix has the form (3):

$$L = \begin{bmatrix} 0 & 0 & 0 & 0 \\ 1 & 0 & 0 & 0 \\ 0 & 1 & 0 & 0 \\ 0 & 0 & 0 & 1 \end{bmatrix} \quad (5)$$

5. The study of the developed algorithm

Studies were conducted on 30 stereo pairs of satellite images. At the initial stage correspondences were found on the basis of SURF method (Fig. 3).

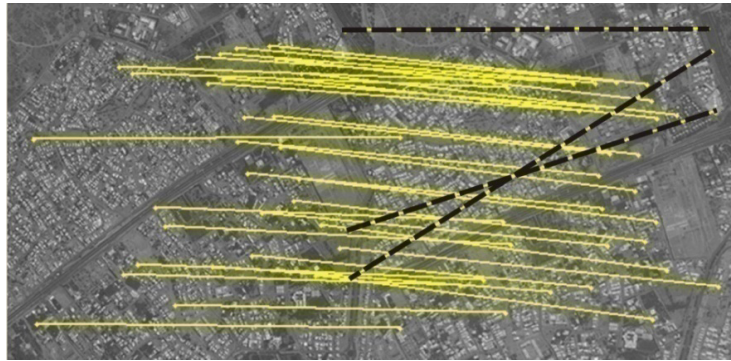


Fig.3. Finding false correspondences by using the developed algorithm (false correspondences are highlighted by dark dashed lines)

When choosing a threshold it was established that with z decrease, the number of false correspondences increases, and vice versa. During the experiments it was found that at a threshold of 0.6, almost 90% of false correspondences are eliminated (Fig. 4).

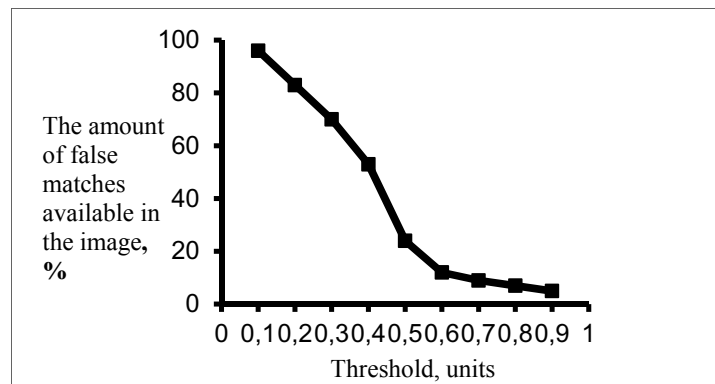


Fig.4. Graph representing the dependence of the number of false correspondences on selected threshold z .

A comparison of the algorithm with the RANSAC was carried out. The complexity of RANSAC $O((\log(p) / \log(1 - 1/k^2))n^2)$, p – the probability of error, n – the number of features found, k – the number of possible correspondences for each feature. The developed algorithm has complexity $O(m)$, m – the number of matches.

6. Conclusion

We developed the algorithm for finding correspondences using the approximate comparison graphs. We suggested the model of an image description using the features incorporated into the graph. The proposed approach allows us to exclude a significant portion of false correspondences, found using the existing descriptors. The algorithm has high speed. It may be used any descriptors in the implementation of the algorithm. The algorithm can be used in three-dimensional reconstruction tasks, determining the position and orientation of objects, image recognition, etc.

Acknowledgements

This work was supported by the RFBR grant 15-07-01612, project number 2918 in the framework of the basic tasks of the state of the Russian Ministry of Education.

References

- [1] A.A. Zakharov, A.E. Barinov, A.L. Zhiznyakov, Recognition of human pose from images based on graph spectra, *The International Archives of the Photogrammetry, Remote Sensing and Spatial Information Sciences*. XL-5/W6 (2015) 9–12.
- [2] A.E. Barinov, A.A. Zakharov, Graph matching algorithm in position and orientation estimation tasks, *Crimean Conference “Microwave & Telecommunication Technology”*, IEEE. CFP14788 (2014) 411–412.
- [3] A.A. Zakharov, A.E. Barinov, An Algorithm for 3D-Object Reconstruction from Video Using Stereo Correspondences, *Pattern recognition and image analysis*. 25(10) (2015) 117–121.
- [4] A.A. Zakharov, A.L. Zhiznyakov, Recognition and 3d-reconstruction of objects from images using a priori information, *Crimean Conference “Microwave & Telecommunication Technology”*, IEEE. CFP14788 (2014) 368–369.
- [5] R. Szeliski, *Computer Vision: Algorithms and Applications*, Springer-Verlag, New York Inc, 2010.
- [6] J.Le Moigne, N.S. Netanyahu, R.D. Eastman, *Image Registration for Remote Sensing*, Cambridge university press, 2011.
- [7] L.G. Roberts, *Machine Perception of Three-Dimensional Solids*, MIT Lincoln Laboratory Technical Report, 1963.
- [8] J.M.S. Prewitt, *Object Enhancement and Extraction, Picture Processing and Psychopictorics*. (1970) 75–149.
- [9] R.C. Gonzalez, R.E. Woods, *Digital Image Processing*, Prentice-Hal, 2002.
- [10] R.O. Duda, P.E. Hart, Use of the Hough Transformation to Detect Lines and Curves in Pictures, *Comm. ACM*. 15 (1972) 11–15.
- [11] J. Canny, A Computational Approach to Edge Detection, *IEEE Trans, Pattern Analysis and Machine Intelligence*. 8 (1986) 679–714.
- [12] C. Harris, M. Stephens, A Combined Corner and Edge Detector, *Alvey Vision Conference*. (1988) 147–151.
- [13] S.M. Smith, J.M. Brady, SUSAN - A New Approach to Low Level Image Processing, *International Journal of Computer Vision*. 23(1) (1997) 45–78.
- [14] E. Rosten, T. Drummond, Machine learning for high-speed corner detection, *ECCV 2006*. (2006) 430–443.
- [15] E. Mair, G.D. Hager, D. Burschka, M. Suppa, G. Hirzinger, Adaptive and generic corner detection based on the accelerated segment test, *Proceedings of the European Conference on Computer Vision*. 2 (2010) 183–196.
- [16] M. Agrawal, K. Konolige, M. R. Blas, CenSurE: Center Surround Extremas for Realtime Feature Detection and Matching, *European Conference on Computer Vision*. 4 (2008) 102–115.
- [17] J. Matas, O. Chum, M. Urban, T. Pajdla, Robust widebaseline stereo from maximally stable extremal regions, *BMVC*. (2002) 384–393.
- [18] D.G. Lowe, Distinctive Image Features from Scale-Invariant Keypoints, *International Journal of Computer Vision*. 60(2) 91–110.
- [19] H. Bay, A. Ess, T. Tuytelaars, L. Van, Gool, SURF: Speeded Up Robust Features, *Computer Vision and Image Understanding*. 110(3) (2008) 346–359.
- [20] E. Tola, V. Lepetit, P. Fua, DAISY: An Efficient Dense Descriptor Applied to Wide-Baseline Stereo, *IEEE Transactions on Pattern Analysis and Machine Intelligence*. 32(5) (2010) 815–830.
- [21] E. Rublee, V. Rabaud, K. Konolige, G. Bradski, ORB: an efficient alternative to SIFT or SURF, *ICCV*. (2011) 2564–2571.
- [22] M. Calonder, V. Lepetit, C. Strecha, P. Fua, BRIEF-Binary Robust Independent Elementary Features, *ECCV*. 4 (2010) 778–792.
- [23] S. Leutenegger, M. Chli, R. Siegwart, BRISK: Binary Robust Invariant Scalable Keypoints, *International Conference on Computer Vision (ICCV’11)*. (2011) 2548–2555.
- [24] N. Dalal, B. Triggs, Histograms of Oriented Gradients for Human Detection, *Computer Vision and Pattern Recognition*, San Diego, CA. 1 (2005) 886–893.
- [25] G. Scott, H. Longuet-Higgins, An algorithm for associating the features of two images, *Proceedings of Royal Society, London*. 244 (1991) 21–26.



International Conference on Industrial Engineering

Process modelling vertical screw transport of bulk material flow

Evstratov V.A., Rud A.V., Belousov K.Y.*

Shakhty Institute of Platov South-Russian state polytechnic University, Lenin square 1, Shakhty, 346500, Russian Federation

Abstract

Vertical screw conveying bulk and powdered materials are an integral part of many production processes in various industries and agriculture. With a wide range of applications in various industries, vertical screw conveyors, along with such qualities as the ease of construction, the continuity of transportation, integrity, the ability to transport and dusty badly smelling goods, have a significant drawback - the material, in addition to the translational motion in the direction of the axis of the conveyor, makes a rotary movement towards the peripheral speed of the screw, which reduces the productivity and increases the power consumption of the conveyor. The use of a simplified model of the movement of the material leads to the creation of inefficient machines, the structure and parameters of working bodies of which differ significantly from optimal. Adequate mathematical description of this process should allow the designers to significantly improve the efficiency of the vertical screw conveyors by means of calculation and selection of optimum values for the geometrical, kinematic and dynamic parameters of working bodies.

© 2015 The Authors. Published by Elsevier Ltd. This is an open access article under the CC BY-NC-ND license (<http://creativecommons.org/licenses/by-nc-nd/4.0/>).

Peer-review under responsibility of the organizing committee of the International Conference on Industrial Engineering (ICIE-2015)

Keywords: conveyor, bulk materials, auger, pitch, particle, screw blade, tube.

1. Introduction

Generally, conveying is accomplished by a combination of mechanical, inertial, pneumatic, and gravity forces. Conveyors utilizing primarily mechanical forces are screw, belt, and mass conveyors [1]. Screw conveyors are widely used for transporting and/or elevating particulates at controlled and steady rates. They are used in many bulk materials applications in industries ranging from industrial minerals, agriculture (grains), pharmaceuticals, chemicals, pigments, plastics, cement, sand, salt and food processing. They are also used for metering (measuring

* Corresponding author. Tel.: +7-863-622-5860; fax: +7-863-622-5860.
E-mail address: aaaikb@mail.ru

the flow rate) from storage bins and adding small controlled amounts of trace materials (dosing) such as pigments to granular materials or powders. If not designed properly for the transported material, problems experienced include: surging and unsteady flow rates, inaccurate metering and dosing, inhomogeneity of the product, product degradation, excessive power draw, high start-up torques, high equipment wear and variable residence time and segregation [2]. In a variety of industries meet screw conveyors: horizontal; vertical; in the form of combinations of the horizontal and vertical; inclined and combinations inclined conveyors and other [7].

2. The apparatus, operating principles and basic parameters of screw conveyors

The screw conveyor consists of a shaft that carries helicoidal flightings on its outer surface. These flightings are enclosed either in a trough for horizontal augers or in a tube for elevating augers. The tube or the trough is held stationary while the rotation of the flightings causes the material to move longitudinally. Figure 1 shows the essential components of a screw conveyor. At the inlet side, the auger flightings extend beyond the tube. Generally, a hopper is provided to hold the material while it is conveyed into the tube. Augers can be permanently installed in a machine, or at a site, or they can be portable. The augers are driven either at the intake side or the discharge side.

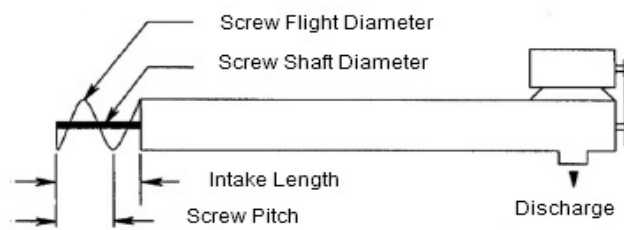


Fig. 1. A schematic diagram of a screw conveyor.

The auger length is defined as the length of the tube assembly including any intake but not including the intake hopper and/or the head drive. The intake length is the visible flighting at the intake of the auger. The intake shall be guarded or otherwise designed to provide a deterrent from accidental contact with the rotating flighting. The outside diameter of the tube is referred to as the auger size. A standard pitch auger is the one whose pitch is approximately equal to the outside diameter of the helicoidal flighting. Generally, the pitch is not less than 0.9 and not more than 1.5 times the outside diameter. Standard pitch augers are used for horizontal and up to 20° inclination angles. For inclination angles greater than 20°, half - standard pitch screws are used. Double - and triple - flight, variable - pitch, and stepped - diameter screws are available for moving difficult materials and controlling feed rates [8].

Screw conveyors are very effective conveying devices for free flowing or relatively free flowing bulk solids, giving good throughput control and providing environmentally clean solutions to process handling problems because of their simple structure, high efficiency, low cost and maintenance requirement. Screw conveyors vary in size from 75 to 400 mm in diameter and from less than 1 m to more than 30 m in length (Athanasiov et. al., 2006). The performance of a screw conveyor, as characterized by its capacity, volumetric efficiency, and power requirements, is affected by the conveyor geometry and size, the properties of the material being conveyed, and the conveyor operating parameters such as the screw rotational speed, screw clearance and conveying angle (Srivastava et al., 2006) [9].

Application of engineering principles for reducing energy requirement in the form of mechanical and electrical power is necessary to reduce cost of production. Factors affecting capacity include auger dimensions (diameter, auger geometry), shear-plane flighting orientation, auger speed, angle of inclination, commodity being conveyed, and entrance-opening configuration. For economical installation and dependable performance, the capacity and power requirement of each component of a system must be accurately predicted [9].

3. Disadvantages of screw conveyors and work to improve them

At the present time the most of investigations are based on the estimated scheme which substitutes the flow conveying with the conveying of a particle leaning against the screw blade and pushed to the tube. The particle's

moving for an upright screw conveyer in stationary condition can be described by following differential equations:

$$\left. \begin{aligned} N_s \cos \alpha_R - f_s N_s \sin \alpha_R - f_t N_t \cos \beta - mg &= 0; \\ f_t N_t \sin \beta - f_s N_s \cos \alpha_R - N_s \sin \alpha_R &= 0 \\ -N_s + mR\omega_0^2 \left[\frac{\sin \alpha_R \sin \beta}{\cos(\beta - \alpha_R)} \right]^2 &= 0 \end{aligned} \right\} \quad (1)$$

where f_s = friction coefficient of material against the screw blade, f_t = friction coefficient against the tube, m = mass of the material particle, N_s = normal reaction of the screw blade, N_t = normal reaction of the tube, R = screw blade radius, $\alpha_R = \arctg \frac{t}{2\pi R}$ = the helix angle on outer radius, $t = 2\pi R t g \alpha_R$ = lead of the screw, β = the angle contained by absolute velocity vector v of the material particle and the screw axis, ω_0 = screw angular velocity, $g = 9,81 M/c^2$ = free fall acceleration.

The equation for determination of angle β :

$$\frac{R\omega_0^2 f_t \left[\frac{\sin \alpha_R \sin \beta}{\cos(\beta - \alpha_R)} \right]^2}{g} - \frac{f_s + t g \alpha_R}{\sin \beta (1 - f_s t g \alpha_R) - \cos \beta (f_s + t g \alpha_R)} = 0. \quad (2)$$

Analysis of amount results of handling process taken from solution of the relation (2) with using a computer shows that functioning efficiency of upright screw conveyers is considerably influenced by geometrical and kinematical parameters of the conveyer tools (the radius and the helix angle of the screw blade and rotational speed of the shaft). Indeed, material flow moving will be simulate with a particle moving, but the amount will be differ (2).

The equilibrium of material volume element engaging sector of a blade with the central angle $d\varphi$ is plotted in Fig. 2. In order to proceed from particle moving it's necessary to ascertain flow cross section shape. If consider moving granular material flow as moving liquid flow, as the pressure is the free surface, the flow free surface equation is the following:

$$z = z_0 + \frac{\omega^2 x^2}{2g} \text{ or } z = ax^2 + b, \quad (3)$$

where ω = material angular velocity.

To determinate coordinates for the intersection point of the flow free surface and the screw blade r it's necessary to study particle equilibrium at this point. Suppose, the particle is on flow free surface, leans against the screw blade at the distance r from the axis, pushed to material flow and gyrating by concentric rotational speed ω_0

There are equations of particle moving:

$$\left. \begin{aligned} N_s \cos \alpha_r + f_s N_s \sin \alpha_r + f_t N_t \sin \alpha_r - mg &= 0 \\ f_m N_m \cos \alpha_r + f_s N_s \cos \alpha_r - N_s \sin \alpha_r &= 0 \end{aligned} \right\} ,$$

$$-N_m + mr\omega_0^2 = 0$$

where f_m = internal friction coefficient of the material, N_m = normal reaction of flowing material, $\alpha_r = \arctg(\frac{R}{r} \text{tg}\alpha_R)$ - the helix angle at the distance r from the axis.

Solving this set of equations and relation (3) simultaneously yields the following relation for coordinate of the intersection point of flow free surface and the screw blade:

$$f_m \omega_0^2 r^2 - f_s (f_m R \omega_0^2 \text{tg}\alpha_R + g)r - gR \text{tg}\alpha_R = 0. \tag{4}$$

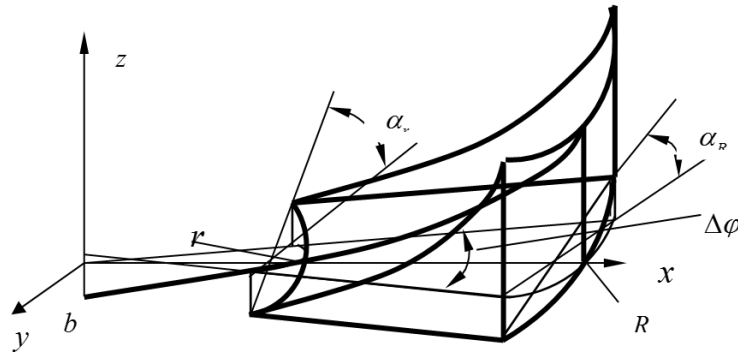


Fig. 2. The equilibrium of material volume engaging sector of a blade.

As the helix angle changes from the axis to periphery, in order to describe material flow moving it's necessary to substitute in relation (1):

$$N_s \sin \alpha_\rho = P_s S_v; N_s \cos \alpha_\rho = P_s S_h. \tag{5}$$

Taking into account (5) the set of equations (1) yields:

$$\left. \begin{aligned} P_s S_h - f_s P_s S_v - f_t P_t S_t \cos \beta - \gamma V &= 0; \\ f_t P_t S_t \sin \beta - f_s P_s S_h - P_s S_v &= 0; \\ -P_t S_t + \frac{\gamma}{g} V \rho_c \omega_0^2 \left(\frac{\sin \alpha_R \sin \beta}{\cos(\beta - \alpha_R)} \right)^2 &= 0, \end{aligned} \right\} \tag{6}$$

where P_s - pressure of the material volume engaging sector of the blade with the central angle $d\varphi$ on the screw blade, S_h - horizontal projection of the sector of the blade with the central angle, S_v - vertical projection of the sector of the blade with the central angle $d\varphi$, V - material volume engaging the sector of the blade $d\varphi$, ρ_c - the distance from the screw axis to the material volume element centre of mass, γ - bulk weight of the material.

Horizontal projection area of the sector of the blade $d\varphi$ between the limits r and R (Fig. 3)

$$S_h = \int_r^R x \Delta\phi dx = \frac{R^2 - r^2}{2} \Delta\phi \tag{7}$$

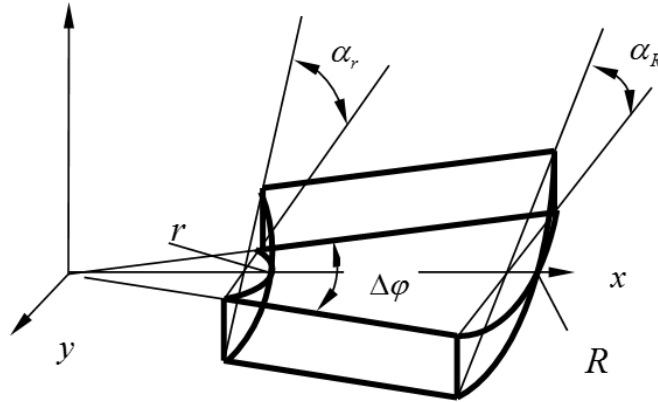


Fig. 3. The sector of the blade and its horizontal and vertical projections.

Vertical projection area of the sector of the blade $d\phi$:

$$S_v = \int_r^R x \operatorname{tg} \alpha_x \Delta\phi dx .$$

As $x \operatorname{tg} \alpha_x = t = \text{const}$, so that

$$S_v = \int_r^R t \Delta\phi dx = t(R-r)\Delta\phi = R(R-r) \operatorname{tg} \alpha_R \Delta\phi . \tag{8}$$

Material volume engaging the sector of the blade $d\phi$ (Fig. 2) is equal to material volume which is a part of body of revolution formed by plane xOy , cylinder surface formed by rotation (around axis z) of vertical elements passing through points of plane xOy of plot $y^2 + x^2 = R^2$ and curve surface formed as plot $z = f(x)$ or $z = a(x^2 + y^2) + b$ rotates around axis z . The equation for the material volume can be determined by relation (3).

$$V = \int_S \int f(\rho) d\rho d\theta = \int_0^{\Delta\phi} d\theta \int_r^R f(\rho) \rho d\rho = \left[(R^2 + r^2)a + 2b \right] \frac{R^2 - r^2}{4} \Delta\phi , \tag{9}$$

where $\rho = \sqrt{x^2 + y^2}$, $x = \rho \cos \theta$, $y = \rho \sin \theta$.

Coordinate for the centre of mass of material element, taking into account (9), can be determined by relation:

$$\rho_c = \frac{\int_0^R x dv}{V} = \frac{\int_0^R \int_r^R f(\rho) \rho^2 \cos \theta d\rho d\theta}{\int_0^R \int_r^R f(\rho) \rho d\rho d\theta} = \frac{\sin \Delta\phi \int_0^R (a\rho^2 + b) \rho^2 d\rho}{\frac{\Delta\phi R}{r} \int_0^R (a\rho^2 + b) \rho d\rho},$$

where $\Delta\phi$ is infinitesimal so that $\frac{\sin \Delta\phi}{\Delta\phi} \approx 1$, so that after integrating.

$$\rho_c = \frac{\frac{a}{5}(R^5 - r^5) + \frac{b}{3}(R^3 - r^3)}{\frac{R^2 - r^2}{4} [a(R^2 + r^2) + 2b]}. \quad (10)$$

Introducing relations (7-10) in set of equations (6) yields the following relation for angle beta

$$\frac{f_t \rho_c \omega_0^2}{g} \left[\frac{\sin \alpha_R \sin \beta}{\cos(\beta - \alpha_R)} \right]^2 - \frac{f_s S_h + S_v}{(S_h - f_s S_v) \sin \beta - (S_v + f_s S_h) \cos \beta} = 0. \quad (11)$$

4. Summary

Establishment of laws of flow of material transported in the vertical screw conveyor is of practical importance because it allows the design of screw conveyors more reasonable to choose their design and operating parameters, creating the preconditions for the production of high-performance conveying machines.

References

- [1] H.Zareiforoush, M.H.Komarizadeh, M.R.Alizadeh, Performance Evaluation of a 15.5 cm Screw Conveyor during Handling Process of Rough Rice (Oriza Sativa L.)Grains. *Nature and Science*.8(6)(2010).
- [2]P.J. Owen, P.W. Cleary, Screw conveyor performance: comparison of discrete element modelling with laboratory experiments, In the Proceedings of the Seventh International Conference on CFD in the Minerals and Process Industries. (2009) 1–7.
- [3] S.G.Silenok, A.A.Borshevskiy, M.N.Gorbovec, Mechanical equipment of enterprises of building materials, products and structures, Mechanical engineering, 1990.
- [4] M.I.Zhuravlev,A.A.Folomeev, Mechanical equipment companies astrigent materials and products based on them, Graduate School,1983.
- [5] M.Y.Sapozhnikov, Mechanical equipment for the production of building materials and products,Mashgiz, 1962.
- [6] L.G.Grabchik, V.I.Nesmotryaev, Mining equipment and systems, Nedra, 1990.
- [7] A.M.Grigorev, Screw conveyors, Mechanical engineering, 1972.
- [8] H.Zareiforoush, M.H.Komarizadeh, M.R.Alizadeh, AReviewonScrewConveyors Performance Evaluation During Handling Process, *Journal of Scientific Review*, 2010.
- [9] EzzatollahAskariAsli-Ardeh, Ahmad Mohsenimanesh,Determination of Effective Factors on Power Requirement and Conveying Capacity of a Screw Conveyor under Three Paddy Grain Varieties, *ScientificWorldJournal*.(2012).
- [10] A.V.Evstratova, The Mathematical description of Granular material handling with an upright screw conveyer, *Scientific papers of Donetsk National Technical University, Avg. Mining and electromechanical*. 127 (2007) 122–127.



International Conference on Industrial Engineering

Perspective construction of hydraulic impact device

Lazutkin S.L.^a, Lazutkina N.A.^{a*}

^aMurom Institute of Vladimir State University, Orlovskaya Street 23, Murom, 602264, Russia

Abstract

Article describes a design and the principle of operation of the hydraulic impact device, with automatic control for a new operating mode, depending on loading on the working tool. The idea is based on the analysis of various schemes of management of hydraulic hammers taking into account requirements for their control and regulation for various industries. Article contains the general description of structural and hydro- kinematical schemes of a hydraulic hammer with automatic control of frequency of influences depending on loading on the working tool. The objectives have to be achieved by introduction of the regulator of a stream of working liquid in the control unit. The main element of such regulator has to be connected with the shock block on the special channel. It will provide rotation of the internal valve with various speed depending on loading on the working tool of the shock block.

© 2015 Published by Elsevier Ltd. This is an open access article under the CC BY-NC-ND license (<http://creativecommons.org/licenses/by-nc-nd/4.0/>).

Peer-review under responsibility of the organizing committee of the International Conference on Industrial Engineering (ICIE-2015)

Keywords: Breaking of rocks, mine workings, hydraulic actuator of mining machines, hydro- kinematical scheme, principal scheme of hydraulic hammer, automatic regulation of impacts frequency depending on the load on work tool.

Introduction

Breaking of rocks of increased rock hardness ($\sigma \geq 60$ MPa) with mechanical impact was recognized as one of the most promising directions when developing machinery, providing given performance at the lowest energy consumption during mine workings in complicated mining and geological conditions.

In present-day hydraulic actuator of mining machines the mechanical impacts is implemented, using hydraulic devices of impact action (hydraulic hammers and hydraulic air hammers). At present time such devices are sufficiently mastered, including the issues of identifying of structural dimensions and output parameters that allows

* Corresponding author. Tel.: +7-910-777-05-17; fax:.
E-mail address: lsmurom62@yandex.ru

inferring about the prospectivity of their applications in the mining machines and in particular in narrow mine workings. To do this, compact hydraulic hammers with under metal consumption and high impact capability. The last condition allows usage of them in operating devices of tunneling machines, for the purpose to extend the scope of their application according to the rock hardness. However, we know that the load on the work tool of operating devices of tunneling machines varies in wide range. This is stipulated by the flow chart of bottom hole processing with operating device, the variation of the thickness of the separated layer of rock (strip) in the course of one revolution of the work disk, frequency of contact of work tool with solid mass, anisotropic structure of the rock, the alternation of the tool operation in the mode of fine crushing of rock and fracture of chunks [1-3].

So, the specificity of hydraulic hammer operation as a part of group of hammers, with which the operating device of the tunneling machine equipped, is that its impact capability shall vary in wide range, depending on the load on the work tool, in what connection this process shall occur in automatic mode. However, the existing basic diagrams of hydraulic hammers do not allow varying the impact frequency in wide range and consequently impact capability, and the main thing changing the one depending on the load on work tool.

As a result of operating experience of production machines with impact-shearing operating device the following wide field of their application was determined: mining one (construction, expansion and scalling of mine workings, crushing of boulders, access ways in open-cut mining); metallurgical one (slag cleaning, moving of old lining of converters in hot state); construction one (destruction of the coatings at reconstruction of highways, airfields, as well as brick and concrete at demolition of buildings), and other industries.

Domestic and foreign specialists have developed dozens of models of production machines of impact action. The result is that the nomenclature of special-purpose and multiple-function machines that corresponds to a wide range of their applications was formed.

On the basis of carried out analysis and comparison of parameters of hydraulic hammers, developed by foreign and domestic companies and organizations it was established the following:

1. The defining trend in both design and construction of impulse mining technique is the development of parametric series of hydraulic hammers on the basis of energy-saving hydro-kinematical schemes.

2. The overwhelming number of hammers was created on the basis of hydro- kinematical scheme with controllable chamber of operational stroke with differential actuation of anvil block and the switching of the power distributor according to position of anvil block.

3. Output parameters of hydraulic hammers, agreed with technological application, therefore they are distributed in wide range according to energy from 120 J (manual air hammers and rock drilling machines) to 10,000 J and impacts frequency from 8 to 3000, per minute.

4. Parametric series hydraulic hammers of number of foreign companies cover the range of the energy of one impact from 140 to 9000 J.

5. Specific Gravity (metal consumption), of the most of the reviewed models is from 0.3 to 0.45 kg/J.

6. The performance factor of present-day hydraulic hammers is 0.6 ... 0.7, and at the presence of a stabilizing system - is up to 0.8.

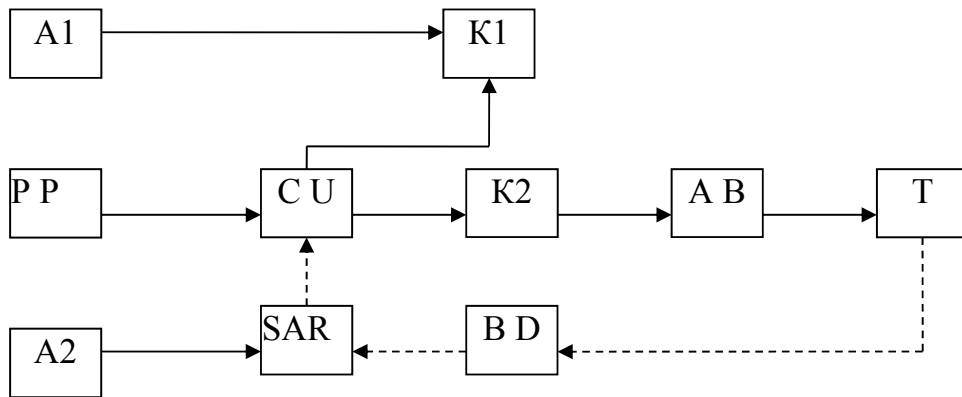
7. Power of 40% of hydraulic hammers is less than 10 kW, thus at the individual models reaches up to 40 kW.

8. Energy density in work tool mainly is kept in the range of 0.12 ... 0.3 J/mm²;

Purpose of Research

The issues of varying of both frequency and impact energy are solved in the construction of various manufacturers. It is achieved due to changing of parameters of the power-plant. However, the possibility of automatic regulation of impact frequency, depending on the load on work tool as a result of internal processes that occur at hydraulic impulse system, has not been implemented in known constructions of hydraulic hammers [4-10].

On the basis of analysis of various control schemes of hydraulic hammers the requirements for systems with their control and regulation for various fields of application were formulated; structural (fig. 1) and principal (fig. 2) scheme of hydraulic hammer with automatic regulation of impacts frequency depending on the load on work tool was developed.



P P – power-plant; C U - control unit; K1 and K2 - reversal and working stroke actuator (chamber); A1 and A2 - accumulators of actuating medium; B D – brake device; A B – anvil block; T – tool; SAR – system of automatic regulation of impacts frequency depending on the load on work tool

Fig. 1 Structure of hydraulic device of impact action with system of automatic regulation of impacts frequency depending on the load on work tool

It was suggested principal solution of system of automatic regulation of impacts frequency of hydraulic hammer, depending on the load on work tool. The objective shall be achieved by implementation of flow regulator in the device design, the head end of which is connected to actuating chamber of anvil block, using special channel, while choke groove - with pressure mains and distributor chamber, in which the turbine is located that provides the rotation of the inner valve.

Results and Discussion

In fig.2 the scheme of hydraulic device of impact action is shown. Device contains body 2, where differential four-stage anvil block 3 with brake step 6 with end planes, tool 1, distributor 8, flow regulator 16, pressure tanks 11 and 21, safety valve 12 in pressure main, pressure valve 23, adjustable throttle valve 13 and orifice 22 are installed. Enclosure 2 and anvil block 3, having ability of axial reciprocal movement, form the chambers: braking 4 reverse 5 and working 7 strokes. At that braking chamber 4 is connected to reversal stroke chamber 5, which is separated from the working stroke chamber 7 by anvil block 3. Braking chamber 4 has diameter that by the value of calculated gap clearance is more than diameter of brake step 6 of anvil block 3. Reversal stroke chamber 5 has continuous connection with pressure mains and pressure tank 11 through adjustable throttle 13. At entrance of anvil block 3 into braking chamber 4, the one separates it from chamber 5 of reversal stroke. Distributor 8 has fixed sleeve 10 with row of slots that are connected to pressure and drain mains, as well as to chamber of working stroke 5, and revolving valve 9, on cylindrical surface of which along generatrix are made grooves. The grooves are located circumferentially in such a way that when revolving of valve the sequential connection of work stroke chamber 7 with pressure or drain mains occur. Revolving valve 9, equipped with turbine 14, located in turbine chamber 15 of the distributor that connects to rod side of flow regulator 16 and drain mains. Flow control valve 16 includes piston 18 with throttle needle, adjusting screw 20 и springs 24. Piston 18 forms with enclosure 16 the cavities: piston one 19 and throttle one 17, where the spring 24 is located. Throttle cavity 17 is connected to pressure mains and turbine chamber 15 of the distributor, while piston one - with brake chamber, using regulated orifice 22 and pressure control valve 23, installed in parallel. In the same line pressure tank 21 is installed. Adjusting screw 20 is used for setting of consumption of operating fluid that reaches the turbine 14. Whereby the range of device impacts frequency in special cases of its application (processing of materials with pressure, driving of grounding pivots, impact compression of soils, concrete and etc.) is determined by limiting of stroke of piston 18 with throttle needle, blocking the channel, by which the operating fluid reaches the turbine 14. The device works as follows. On fluid supply by pressure main, accumulator 11 charging is performed, filling with fluid of reversal chamber 5, as well as turbine 14 revolving with valve 9, on which, using the flow regulator 16 the specified amount of operating fluid that enters the device is delivered.

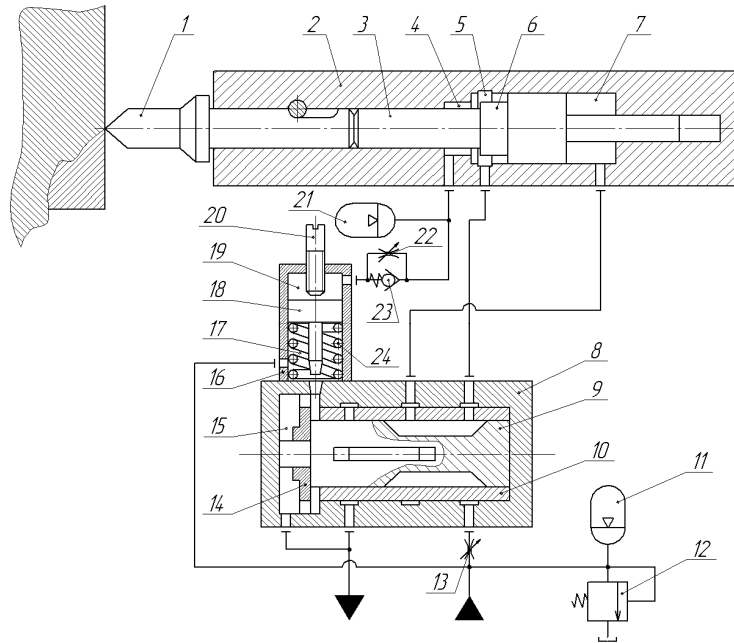


Fig. 2 Scheme of hydraulic device of impact action

If anvil block end 3 is located in chamber of reversal stroke 5, then upon connection, using the grooves on the valve 9 of chamber of working stroke 5 with drainage mains, reversal stroke of anvil block 3 occurs (according to figure to the right). If anvil block 3 is located in brake chamber 4 and blocks access of fluid from reversal stroke chamber 5 to end plate, then the reversal stroke of anvil block 4 doesn't occur, until enclosure 2 of the device won't be displaced by steady-state force (according to figure to the left). After certain displacement of enclosure 2 under action of static force in direction of processed object, work tool 1 that rests on object, sliding into enclosure 2, displace anvil block 3 to the right and its end shall be come out from brake chamber 4 to the chamber of reversal stroke 5. Further displacement of anvil block 3 to the right is carried out by pressure force of fluid that flows to the chamber of reversal stroke 5 from pressure mains, while chamber of working stroke 7 is connected with the grooves on valve 9 to drainage mains and its pressure is decreased.

Reversal stroke is carried out, during which the driving-out of liquid, which filled the chamber of working stroke 5, during previous working cycle is performed into drainage mains. Simultaneously pressure tank charges 11.

At revolution of valve 9 on given angle, the next groove on its surface connects the chamber of work stroke 7 to pressure mains. Now the chambers of reversal stroke 5 and working stroke 7 are connected simultaneously to pressure mains, however the area of work stroke chamber is greater, so the equivalent force, acting from its side, displays the anvil block 3 in direction of tool 1. The working stroke is performed, during which the anvil block 3 shall be displaced with acceleration in direction of tool 1 and upon completion of working stroke the one make impact on tool with given energy. During the work stroke the fluid from reversal stroke chamber 5 overflows through throttle 13 and distributor 9 into the chamber of working stroke. Pressure tank 11 is being charged.

There are three possible scenarios of development of physical process of implementation of tool into rock mass:

- all energy, accumulated by anvil block shall be transferred fully to mine working at set displacement of anvil block together with tool before entrance of anvil block into the brake chamber 4;
- energy, accumulated by anvil block isn't sufficient for design implementation (displacement) of tool and anvil block stops;
- energy, accumulated by anvil block, exceeds required one for tool implementation into mine working by specified value. Anvil block, following the tool doesn't stop, but enter brake chamber 4. Such mode is called as "chambering".

The first two variants are standard working modes of hydraulic device of impact action.

In case of “chambering” for protection of construction from damage, anvil block 3 enters brake chamber 4, where the high pressure is formed, impact of which on the anvil block causes its slowdown and stopping down.

Liquid from brake chamber 4 is displaced into line with pressure tank 21, and the portion of liquid through the pressure valve 23, which set the value of excessive pressure, enters head end 19 of flow regulator 16, so piston 18 with needle valve is displaced (per fig. down) and the one decreases the channel flow passage, by which the liquid from the pressure mains enters turbine 14 of the valve 9. As a result the rotation speed of the valve 9 is decreased and it leads to decrease of device impacts frequency.

In the absence of repeated “chamberings”, piston 18 with throttle needle is displaced under action of spring 24, displacing the liquid from the head end 19 through the orifice 22, and opens the feed channel of the working fluid to the turbine 14 before the inlet section. Whereupon the rated rotation frequency of the valve 9 and frequency of anvil block impacts 3 against tool 1 are renewed. Pressure tank 21 smoothes pressure ripples in head end of the flow regulator 16, stabilizing the turbine rotation velocity 14 with valve 9.

On the next “chamberings” that occur one after another that is upon decrease of material resistance under work tool, as well as at absence of tool contact with the mass that is being demolished in case of chipping of large pieces of rock, from brake chamber 4 to head end 19 of flow regulator 16 the successive portions of liquid are entered. The further displacement of piston 18 with throttle needle, which decreases the channel flow passage into turbine pocket 15 is occurred. At numerous “chamberings” the throttle needle blocks the working liquid input channel from the pressure mains to turbine 14 of the rotating valve, 9, which stops and as a result the work of hydraulic device of impact action is terminated.

At increase of material resistance under the work tool, “chamberings” stop, excessive pressure in head end of flow regulator 16 is decreased to working pressure due to overflow of the working fluid through the orifice 22. Piston 18 with throttle needle under the impact of pressure of working liquid that enters throttling flap 17 of flow regulator 16, and return spring force 24 is moved upward, forcing out the working liquid from throttling cavity 19 through orifice 22. At that the flow passage of the channel is increased, as a result, consumption of working liquid, which enters turbine 14, valve rotation velocity 9, and anvil block impacts frequency 3 on tool 1 are increased. Frequency of impacts is increased up to rated value if there are not new “chamberings”.

Conclusion

Usage of flow regulator 16 allows automatic regulation of impacts frequency of hydraulic device of impact action, depending on the load on work tool 1. Such structural scheme extends the technological capabilities, the one will allow using more efficiently the input power and lead to increase of efficiency factor of system: actuating motor - hydraulic pump - device of impact action.

References

- [1] A.A. Griffith, The phenomenon of rupture and flow in solids, *Phil. Trans. Roy. Soc.*A221 (1920) 220.
- [2] G.R. Irwin, *Fracture dynamis in fracture of metals*, ASM Cleveland, 1948.
- [3] E.O. Orowan, *Fundamentals of brittle behaviour of metals. Fracture of metals*, Willey. 4 (1952) 32–50.
- [4] A. Hermann, *Schlaqkopf-Maschinen, Bergbau*. 4 (1981) 169–174.
- [5] *Hammer new system MEC*, Jndeco, Italy, 1990.
- [6] I. Howkes, *High-Energy Impact Hammers. Underground Mining Methods, Handbook*, New-York. (1982) 1404–1408.
- [7] *Reducing dust and increasing capacity in a primary crusher*, World Mining. 1981.
- [8] *Schaqkopf-Nachreibmaschine HNM-4*, Rudolf Hausherr & Sohne GmbH & Co. KG, Germany, 1980.
- [9] *Hydraulic Breakers*, Fukurawa Rock Drill Sales Co. Ltd., Jahan, 1982.
- [10] *Hydraulic Hammers*, Caterpillar, USA, 1993.



International Conference on Industrial Engineering

The Comparative Analysis of Permanent Magnet Electric Machines with Integer and Fractional Number of Slots per Pole and Phase

Gandzha S.A.^a, Sogrin A.I.^{a*}, Kiessh I.E.^a

^aState South Ural State University, 76, Lenin Avenue, Chelyabinsk, 454080, Russian Federation

Abstract

The comparison of permanent magnet motors with integer and fractional number of slots per pole and phase was made. The torque developed by the motor and the torque ripples level were chosen as the major criterions. The comparison was made according to the results of equations of numerical calculation of magnetic field in active motors volumes using the finite element analysis. The recommendations on the choice of the most suitable option are given.

© 2015 The Authors. Published by Elsevier Ltd. This is an open access article under the CC BY-NC-ND license (<http://creativecommons.org/licenses/by-nc-nd/4.0/>).

Peer-review under responsibility of the organizing committee of the International Conference on Industrial Engineering (ICIE-2015)

Keywords: Permanent magnet motor; Torque ripples; Cogging torque; Fractional-slot winding; Finite element analysis

1. Introduction

The brushless permanent magnet DC motors are being developed fast over the years. Nowadays we can see a new intensive turn of their development. It is connected with the appearance and commercial exploitation of powerful and comparatively cheap high-coercive magnets, the development of power electronics.

By nature an electric machine is a quite conservative drive part which is upgrading slower than electronic components and program control logic. Nevertheless, optimization of this unit is very important as it is the motor which determines to a great extent energetic data and weight-size parameters of the drive on the whole.

* Corresponding author. Tel.: +7-351-267-9057; fax: +7-351-267-9172.
E-mail address: sogrinai@susu.ac.ru

One of the last tendencies is application of the electric machines with fractional numbers of slots per pole and phase [1]. If a few decades ago such solutions were used for low power devices then now quite powerful motor electric drives appear with similar machines [2,3,4,5].

It should be noted that analysis and synthesis theory of conversion devices to be observed is behind of practice requirements that is connected with complication of electromagnetic processes in the machines with fractional numbers of slots per pole and phase. In the academic circles we can observe active disputes concerning effectiveness of such machines. This article is directed to partial settlement of these disputes. The analysis was carried out with the help of modern program means of finite element analysis of electromechanic and electromagnetic devices ANSYS Maxwell.

2. Task description

The primary objective of this work is research of winding distribution influence on the value and ripples of electromagnetic torque of the permanent magnet motor.

The electric motor DB-72 (variant 1) was chosen as a subject of research which is designed for usage in the respiratory medical device. The passport specifications are given in table 1. The number of motor stator slots is 18, the number of poles of the inductor is 20. Then, the motor is made with fractional number of slots per pole and phase $q=3/10$. The motor has a converse construction: the armature is located inside, the rotating induction coil — outside.

Table 1. Nominal data of the motor DB-72

Parameter	Value
nominal power, (W)	25
DC nominal voltage, (V)	24
nominal speed, (rpm)	1000
nominal current, (A)	2.5
nominal torque, (Nm)	0.25
number of phases	3
phase connection scheme	Y

The specially designed motor with integer number of slots per pole and phase having the equal dimensions with the base motor was accepted as an alternative variant (variant 2). The inductor of the alternative motor is the same as the base model. The stator has the number of slots per pole and phase $q=1$. At that the number of machine slots turned out to be equal:

$$z = 2p \cdot m \cdot q = 20 \cdot 3 \cdot 1 = 60,$$

where p — poles pair number, m — phase number of the armature winding. Note that value $q=1$ turned out to be the most possible on design considerations for given sizes and polarity of the machine: slots number increase crushes the stator teeth dimensions unacceptably.

For comparison accuracy the number of phases ampere-turns of motors to be observed was accepted equal (180 turns in the phase, phases currents — nominal, according to the nominal data of the base motor). The total areas of slots and teeth of motors to be observed are equal accordingly.

3. Design models

The designing of magnetic field in active motors volumes was carried out according to the finite element analysis in 3D task description. It allowed to take into account a possible stator slot skewing while analysis. The developed models of the motors consider the properties nonlinearity of ferromagnetic materials, alternation of electromagnetic

quantity over time, machine members moving relative to one another. The magnets were made of alloy NdFeB (coercive force by induction $H_c = 890$ kA/m, residual flux density $B_r = 1,23$ T).

The motors phases power was carried out by current supply, it allowed to exclude the resistance of armature circuit from the number of factors affecting the electromagnetic torque. The direct currents (nominal specified current) for the phase A and the phase C with corresponding marks and zero current for the phase B were set in accordance with 120-degree commutation algorithm.

The models designed due to axial and radial symmetry of the electric machines are presented in fig. 1.

In the course of experimental testing the nominal speed was imposed to the rotor, the torque on the motor shaft was measured, the torque average value was calculated in the closed interval corresponding to the intercommutating interval.

The measurement of cogging torque caused by variability of the magnetic permeability of the air gap was carried out for the electromagnetic torque estimation. While the experiment the rotor was brought to rotation with nominal rate, the phases currents were accepted as equal to zero. The electromagnetic torque of the motors was calculated according to the results of conducted experiments by means of coordinatewise diminution of the cogging torque curve from the full torque curve:

$$M_{em}(t) = M(t) - M_c(t). \quad (1)$$

4. The results of experiments

The total torque tracings obtained while the experiment are shown in fig. 2. The cogging torque tracings captured in the process of the rotor turning are shown in fig. 3. The electromagnetic torque curves obtained by the (1) are shown in figure 4.

The average torques values for each motor in intercommutating interval were calculated by the equation:

$$M_a = \int_0^T M(t) dt, \quad (2)$$

where T — intercommutating interval size, $M(t)$ — torque dependence on instant.

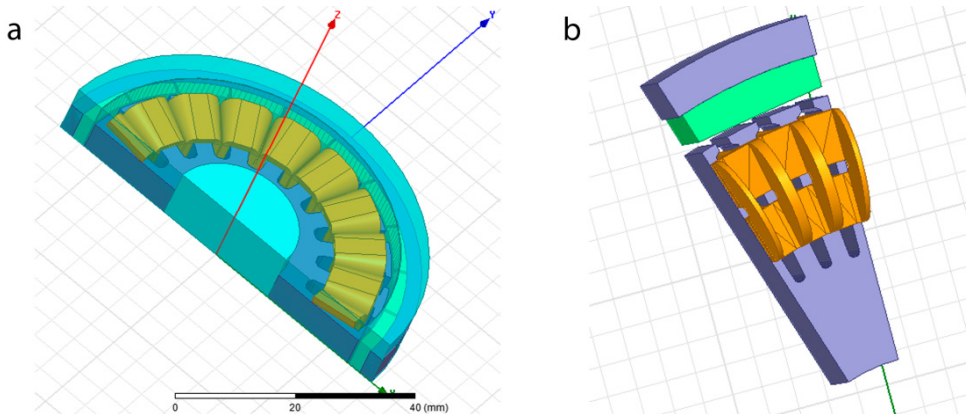


Fig. 1. Three-dimensional designed models of the motors to be observed:
(a) with fractional number of slots per pole and phase; (b) with integer number of slots per pole and phase.

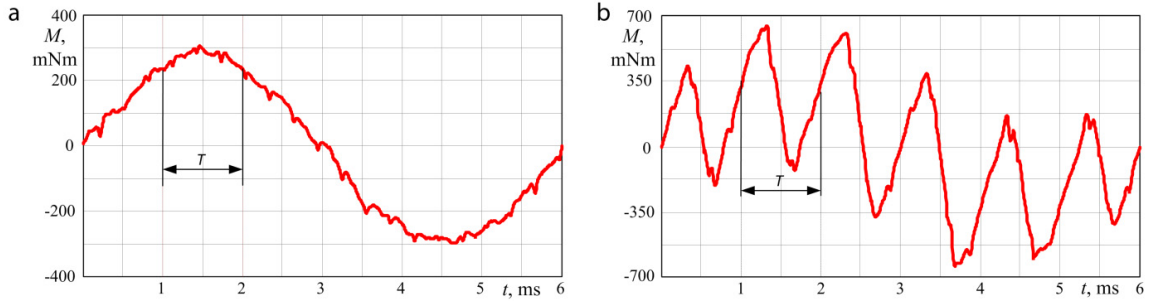


Fig. 2. The total torque tracing in the process of the rotor turn: (a) for variant 1; (b) for variant 2.

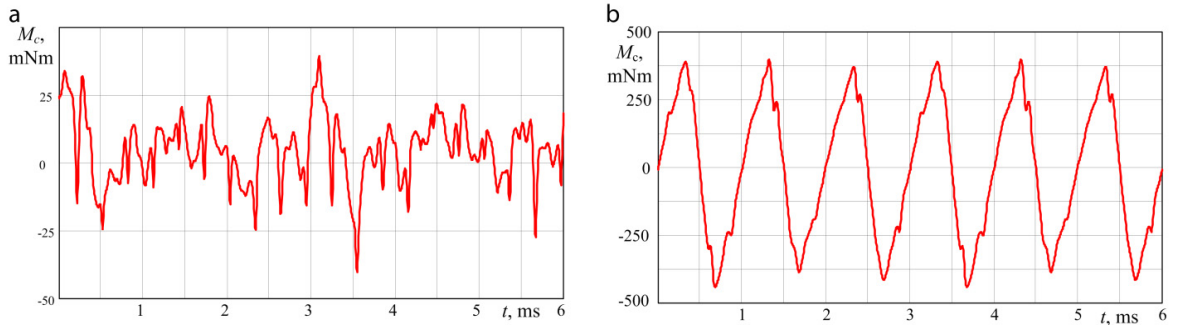


Fig. 3. The cogging torque tracing in the process of the rotor turn: (a) for variant 1; (b) for variant 2.

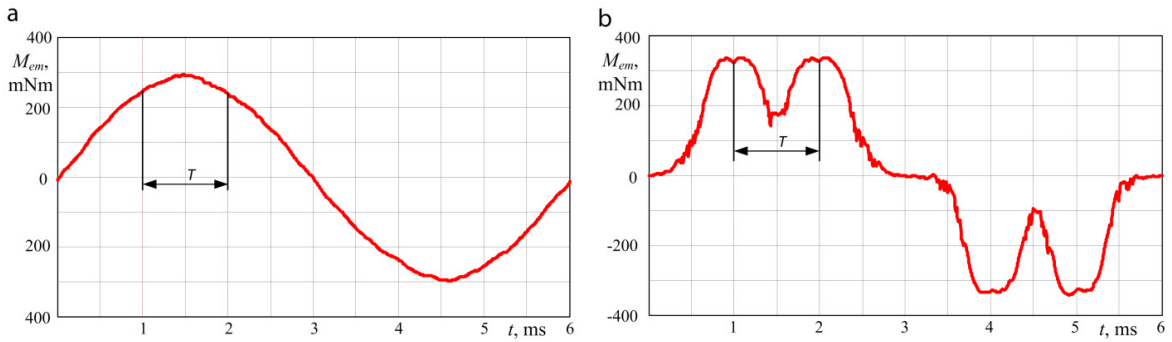


Fig. 4. The electromagnetic torque tracing in the process of the rotor turn:(a) for variant 1; (b) for variant 2

The ripple factor in the intercommutating interval was calculated for full and electromagnetic torques [6]:

$$k_r = \frac{(M_{max} - M_{min})/2}{M_a}, \tag{3}$$

where M_{max} and M_{min} — maximal and minimal torque value in the intercommutating interval respectively.

The cogging torque was estimated due to its maximum value. The calculations data were summarized in tab. 2, where: M_a — average torque on the motor shaft, M_a^{em} — motor average electromagnetic torque, k_r — torque ripple factor on the motor shaft, k_r^{em} — motor electromagnetic torque ripple factor, M_m^c — maximum value of motor cogging torque.

Table 2. Experimental data

	M_a , Nm	M_a^{em} , Nm	k_r	k_r^{em}	M_m^c , Nm
<i>Variant 1</i>	0.271	0.272	0.129	0.101	0.040
<i>Variant 2</i>	0.272	0.274	1.415	0.292	0.400

5. Discussion of the results

As the experiment showed both motors are approximately equivalent by the electromagnetic torque value but relating to torque ripples level variant 1 is ahead of variant 2 without doubt. It should be noted that torque ripples are common for all permanent magnet motors and connected with discrete behavior of position in vector space of armature magneto-motive force, however in this case the ripples have unacceptably high values.

According to the obtained data the essential cogging torque and, to a lesser extent, torques from the interaction of non-fundamental harmonics of the armature and induction coil fields are the primary reasons of high motor ripples torque with integer q . Actually in cogging torque generation in this case all stator teeth take part which are located equal on each polar pitch relative to poles.

In the motor with fractional q these factors are expressed weaker. Moreover, the cogging torque is lower due to the smaller number of teeth which are the reason of air gap variation and thanks to the fact that teeth are located on different polar pitches asymmetrically relative to the poles.

In the electric machine of variant 2 the winding has a full pitch, distribution is absent. In consequence of the specified characteristics of the motor winding in armature field curve except fundamental harmonic there are quite strong non-fundamental harmonics which are able to generate the electromagnetic torque ripples interacting with field harmonics of inductor.

Non-fundamental harmonics of the armature field in the machines with fractional q are significantly weakened due to teeth shift belonging to one phase in relation to one another in the limits of polar pitch and it affects like a pitch reduction and winding distribution by the slots in the windings with integer q [7].

For confirmation of these facts calculated dependencies of the time electromagnetic torques were expanded to harmonic series.

The electromagnetic torque of the motor with fractional number of slots per pole and phase is given as fundamental harmonic which has amplitude 0.287 Nm. The torque non-fundamental harmonics amplitudes do not exceed 1% of the fundamental harmonic amplitude.

The electromagnetic torque curve of the motor with integer q except the fundamental harmonic (0.290 Nm) contains a series of ultra ones, the strongest of them are the fifth (34% of the fundamental one) and the seventh (9.85% of the fundamental one). It should be noted that fundamental harmonics of the motors torques of both variants are approximately equal.

It is possible to decay torques ripples of the motor of variant 2 having weakened the non-fundamental harmonics of the armature field and having reduced the cogging torque. The reduction of non-fundamental harmonics amplitudes of the armature field which in this case are tooth harmonics is possible by increasing the number of slots per pole and phase and that does not seem possible with the specified dimensions without reducing the number of the machine poles. The increase of machine air gap that is connected with its increase in dimensions gives the other opportunity for reducing the torques from tooth harmonics.

The effective way of tooth harmonics influence reduction on the electromagnetic torque is a stator slot skewing [8,9]. At that the harmonics skewing of the armature field happens along the machine axis relative to similar harmonics of the induction coil field that weakens the torques to be generated by them. The slot skewing introduction affects favorably to the cogging torque reduction.

Let us estimate the slot skewing influence on the total and cogging torques of the machine of variant 2.

The research was conducted on the same model in the process of slot skewing alteration from 0 to 1 of the tooth pitch. Higher skewing values are not used as that increases leakage significantly [10]. The current loading in the process of the total torque determination remained also constant.

The best results were obtained in the process of the skewing to one tooth pitch. At that, the torque average value in the intercommutating interval was 0.279 Nm. The total and electromagnetic torques of the motor with integer q in the process of skewing to one tooth pitch are shown in fig. 5. The calculation results of the cogging torque maximal values and the results of the strongest harmonics amplitudes of the electromagnetic torque are given in Table 3.

The experiments revealed that in the process of slot skewing to one tooth pitch the cogging torque reduces significantly, being still slightly higher than the cogging torque of the motor with fractional q .

Table 3. The effect of the skew of slots on the torque of the motor with the integer q .

	M_{em}^1 , Nm	M_{em}^5 , Nm	M_{em}^7 , Nm	M_c , Nm
Without skewing	0.290	0.098	0.029	0.400
Skewing to one tooth pitch	0.286	0.043	0.001	0.045

The non-fundamental harmonics of the motor electromagnetic torque are weakened quite effectively also. It should be noted that in spite of ripples decay by more than 50% their values remained still unacceptably high ($k_r = 0,37$).

Consequently taking into account all factors (value of total and cogging torques, ripples torque level) variant 1 is ahead of variant 2.

Moreover, the following advantages of variant 1 over variant 2 should be pointed out:

- shorter half-turn length as the end parts of different coils do not cross over each other but entail only one tooth; consequently the armature coil has a lesser active resistance that affects the electric losses favorably;
- better usage of machine volume due to a lesser area of slot insulation;
- more simplified manufacturing technique: a lesser number of slots simplifies the punches and mounting for the winding works.

6. Conclusions

The permanent magnet motors with fractional number of slots per pole and phase can compete successfully with equivalent motors with integer number of slots per pole and phase having acceptable value of the electromagnetic torque, lesser values of the cogging torque, lesser torque ripples, copper losses in simplified manufacturing technique.

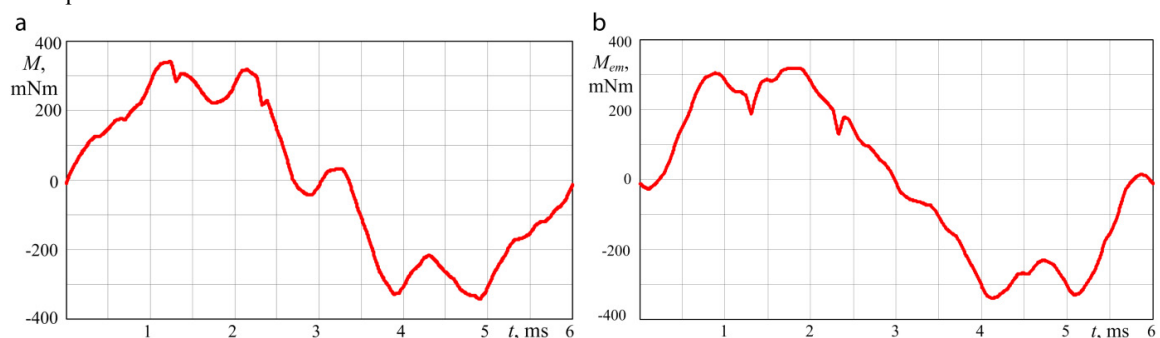


Fig.5. The tracings of full (a) and electromagnetic (b) torques in the process of the rotor turn for the motor variant with integer number of slots per pole and phase and slot skewing to one tooth pitch

In particular the distinct advantages of the machines with fractional number of slots per pole and phase should occur in extensively used electrical machines when the severe space restrictions are imposed on the requirements of high energy data of the motor.

References

- [1] S.A. Gandzha, Modelling of Permanent Magnet Direct Current Motor with Electromagnetic Reduction, Collection of papers of Software Users Sixth Conference CAD_FEMGmbH. (2006) 358–360.
- [2] I.-A. Viorel, L. Szabó, L. Löwenstein, C. Stet, Integrated Starter-Generators For Automotive Applications, *Acta Electrotehnica*. 45(3) (2004) 255–260.
- [3] S. Jurkovic, E.G. Strangas, Comparison of PMAC Machines for Starter-Generator Application in a Series Hybrid-Electric Bus, *International Journal of Vehicular Technology* Volume. (2011) 11. DOI:10.1155/2011/275785
- [4] A.F. Shevchenko, A.S. Medvedko, Yu.G. Bukhgo'ls, Sh.R. Singatulin, D.N. Skorobogatov, A.I. Erokhin, Starter-generator device for VAZ-2110 type passenger cars, *Russian electrical engineering*. 74(9) (2003) 17–21.
- [5] S.G. Voronin, A.I. Sogrin, P.O. Shaburov, B.D. Shumakov, A starter-generator for a diesel power plant, *Russian Electrical Engineering*. 84(10) 556–559.
- [6] G.H. Lee, W.C. Choi, S.I. Kim, S.O. Kwon, J.P. Hong, Torque ripple minimization control of permanent magnet synchronous motors for EPS applications, *International Journal of Automotive Technology*. 12(2) (2013) 291–297.
- [7] A.F. Shevchenko, Multipole synchronous machines with fractional $q < 1$ tooth windings and excitation with permanent magnets, *Russian electrical engineering*. 78(9) (2007) 451–455.
- [8] L. Dosiek, P. Pillay, Cogging torque reduction in permanent magnet machines, *IEEE Trans. Industry Application*. 43(6) (2007) 1656–1657.
- [9] R. Islam, I. Husain, A. Fardoun, K. McLaughlin, Permanent magnet synchronous motor magnet designs with skewing for torque ripple and cogging torque reduction, *IEEE Trans. Industry Applications*. 45(1) (2009) 152–160.
- [10] D. Hanselman, *Brushless permanent magnet motor design*, second ed., Magna Physics Publishing, 2006.



International Conference on Industrial Engineering

Higher harmonic components of rectifiers magnetic fields and their adverse health effects

Kuznetsov K.B.^a, Zakirova A.R.^{a*}

^a *Technospheric Safety Department (Research and Education Center), Ural State University of Railway Transport, Ekaterinburg, Russian Federation*

Abstract

The adverse health effects of magnetic fields affecting electrical personnel are studied; the magnetic field at converter stations is generated by the rectifiers. Harmonic composition of the rectified current is analyzed. The article shows that a rectifier converter is a source of AC harmonic components and has a variety of magnetic forces, whose harmful effects on the staff have not yet been studied. The basic analytical relationships are given, allowing to estimate the levels of harmonic components and induced magnetic field parameters by calculation current. The calculation of magnetic fields based on harmonic components of the rectified current allows comparing the theoretical values against the experimental studies. Following the comparison of theoretical calculations and experimental magnetic field measurements, a conclusion is made about the harmful effects of the magnetic field of certain rectified current harmonics.

© 2015 The Authors. Published by Elsevier Ltd. This is an open access article under the CC BY-NC-ND license (<http://creativecommons.org/licenses/by-nc-nd/4.0/>).

Peer-review under responsibility of the organizing committee of the International Conference on Industrial Engineering (ICIE-2015)

Keywords: magnetic field, electrical installation, rectified current.

1. Introduction

A number of studies [1-6] shows that rectified voltage of a rectifier (RV) has a higher harmonics spectrum of the order (equation 1).

* Corresponding author. Tel.: +7-922-189-77-19.
E-mail address: AZakirova@usurt.ru

$$k = m \cdot l, \quad (1)$$

where m – number of pulsations of the rectified voltage curve; $l = 0, 1, 2, 3 \dots$ positive integer.

To account for health effects of the magnetic field of rectifier currents, we consider primary current of a 6-pulse rectifier.

With perfectly smoothed rectified current ($X_d = \infty$) and instant valve switching ($X_a = 0$), the rectified primary current curve has rectangular or stepped shape. For the above conditions, the amplitude of the k -th harmonic of the primary current at 6-pulse converters is [2]:

$$I_k = \frac{2\sqrt{3} \cdot I_d}{\pi \cdot k_T \cdot k}, \quad (2)$$

The value of the specified maximum rectified current of I_{dIII} substation is determined by the formula

$$I_{dIII} = \frac{P_T}{U_{du}}, \quad (3)$$

where U_{du} – nominal rectified voltage on substation bus bars (3.3 kV); P_T – train traction power set point (12700 kW).

2. Experimental

2.1 Theoretical procedure

For infinitely long wires with opposite currents, the magnetic field voltage can be determined from the expression for vector potential A of this field in accordance with Fig. 1.

In addition to harmonics with ratio (1), harmonics having lower frequencies occur in the rectified current due to non-sinusoidal nature of the primary rectifier AC voltage [2].

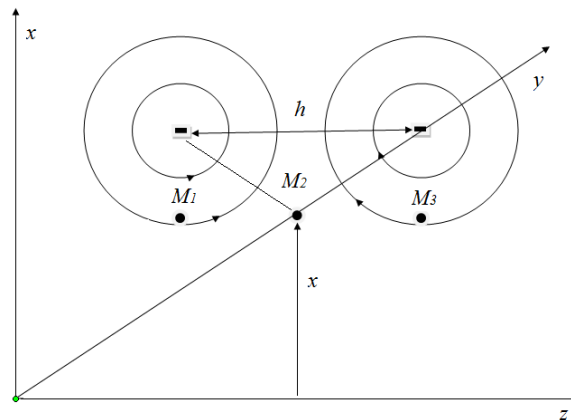


Fig. 1. Diagram showing EMF generated by a source with two parallel wires with opposite currents ($L \rightarrow \infty$).

All wire elements in the presented EMF source model [7] are directed along Y-axis, so the vector A has a changing component along Y-axis only. In this case, vector potential of the magnetic field can be determined from the relationship

$$A_y = \mu_0 \frac{I_k + L}{4\pi} \int_{-L}^L \frac{dy}{\sqrt{y^2 + r_2^2}} - \mu_0 \frac{I_p + L}{4\pi} \int_{-L}^L \frac{dy}{\sqrt{y^2 + r_1^2}} \tag{4}$$

Assuming equality of currents in the "+" and "-" bus: $I_k = I_p = I$ and infinite length of wires in the network $L \rightarrow \infty$ we obtain

$$A_y = \mu_0 \frac{I}{2\pi} \ln \frac{r_1}{r_2} \tag{5}$$

By differentiating the expression (4), we can derive the terms of the magnetic field intensity along Z and X axes

$$H_z = \frac{1}{\mu_0} \frac{\partial A_y}{\partial x}, \quad H_x = -\frac{1}{\mu_0} \frac{\partial A_y}{\partial Z} \tag{6}$$

and total magnetic field intensity at the point M (M_1, M_2, M_3) as a vector sum of intensity along Z and X axes

$$H_M = H_Z + H_X \tag{7}$$

Substituting the expression from (6) to (5), we find

$$H_x = \frac{I}{2\pi} \left[\frac{-z}{x^2 + z^2} + \frac{z-h}{x^2 + (h-z)^2} \right] \tag{8}$$

$$H_z = \frac{Ix}{2\pi} \left[\frac{1}{x^2 + z^2} - \frac{1}{x^2 + (h-z)^2} \right] \tag{9}$$

The module of the absolute value of magnetic field intensity vector from harmonic components at the point M can be found from the vector sum of the modules H_z and H_x from the expression [7]:

$$H_M = \sqrt{H_z^2 + H_x^2} \tag{10}$$

2.2 Materials

The calculated values of alternating currents of higher harmonic components, with a 6-pulse rectifier ($k_T=3,16$) are given in Table 1.

Table 1. Calculated values of alternating currents of higher harmonic components of the maximum rectified current (3849 A).

k	f_k , Hz	I_{k3} , A	H , at $z=0$	H , at $z=1$	H , at $z=2$	MPL N (EU), A/m
Traction substation machine room						
1*	50	-	-	-	-	400
2*	100	-	-	-	-	200
4*	200	-	-	-	-	100
6	300	224	14,73	16,82	14,73	67
12	600	112	7,36	8,41	7,36	33,3
18	900	75	4,93	5,63	4,93	24,4
24	1200	56	3,68	4,21	3,68	24,4
30	1500	45	2,95	3,38	2,95	24,4
36	1800	37	2,43	2,78	2,43	24,4

* Harmonics, calculated values of (1) are not available, but recorded the experiments

Maximum permissible limits of magnetic field intensity (MF) with frequency up to 10 kHz are regulated in Russia for 50 Hz and 10 kHz.

To date, regulation of MF up to 10 kHz is carried out in the European Union. When comparing the obtained MF levels (Table. 1) with the EU limits [8], the MF values stay within maximum permissible limits.

2.3 Experimental method

Experimental studies of the magnetic field have been carried out at traction substation [9-10] at the points No. 1-9 under the bus bridge at RU-3.3 kV switchgear (Figure 2).

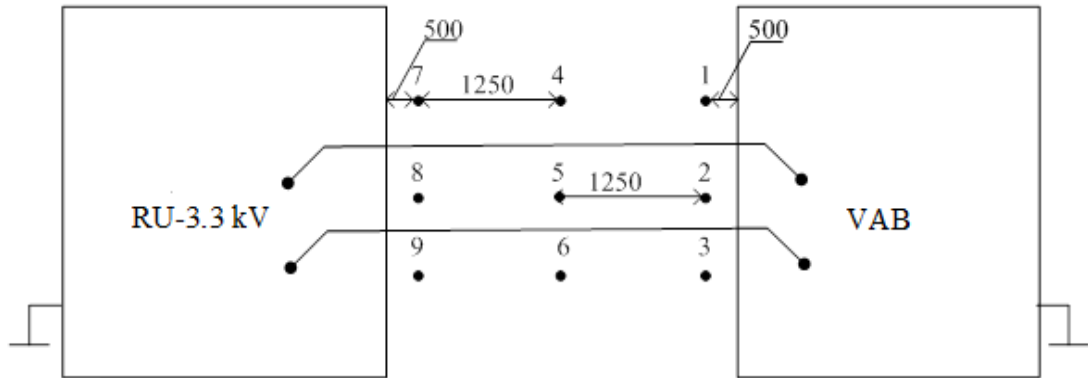


Fig. 2. Layout of bus bars from RU-3.3 kV unit from 3.3 kV rectifier circuit to VAB high-speed switches - top view.

Table 2 shows the measurements [9, 10] of magnetic field intensity at points No. 1-9 under the bus bridge at RU-3.3 kV switchgear of the traction substation.

Table 2. Measurement of magnetic field intensity (A/m) under the bus bridge at RU-3.3 kV switchgear.

No.	1	2	3	4	5	6	7	8	9	H_{norm} , A/m
f_k , Hz										
50	8	6	12	125	125	125	15	8,5	6,5	80
100	6	5	5	8	10	9	6	5	4	Not regulated.
200	2	1	1	5	7	7	3	2	2	Not regulated.
300	3	2	2	10	10	5	11	3	3	Not regulated.
I_{dk} , A	400	300	600	1000	1000	1000	750	420	350	

Table 2 shows that a certain MF intensity values correspond to individual current and frequency values. For points No.4-6, MF intensity is 125 A/m, which exceeds maximum MF values according to [11] by 1.56 times. There is a need to develop means of protection to reduce the duration of magnetic field exposure [12-20].

Table 3 shows MF values recalculated for maximum operating current in accordance with regulation method [11].

Table 3. MF intensity values reduced to the maximum current (3849 A).

No.	1	2	3	4	5	6	7	8	9	H_{regul} , A/m	MPL N (EU), A/m
f_k , Hz											
50	76,98	76,98	76,99	481	481	481	76,9	77,86	71,48	80	400
100	57,73	64,15	32,08	30,79	38,49	34,64	30,79	45,8	43,99	Not regulated.	200
200	19,24	12,83	6,416	19,24	26,94	26,94	15,39	18,32	21,99	Not regulated.	100
300	28,87	25,66	12,83	38,49	38,49	19,24	56,45	27,48	32,99	Not regulated.	67

Based on Table 3, it can be concluded that the obtained MF values do not exceed the maximum permissible limits applicable in the EU [8]. For points No. 4-6, MF intensity recalculated for maximum rated current is 481.12 A/m for MF 50 Hz, which exceeds MF MPL according to [11] by 6.0 times, and EU MPL by 1.2 times.

The negative inductive impact of higher harmonic components of AC current so far has been assessed in terms of its effect on operation of automatic equipment, remote control and communication systems. The above shows that harmonic components of rectified AC current can have detrimental health effects on rectifier substation personnel.

3. Conclusion

On the basis of the material presented, the following conclusions can be made:

- Rectified current of a rectifier converter has a spectrum of sinusoidal electric currents, and their magnetic field intensities may have a detrimental health effect on staff, which has not been considered so far as a scientific problem in Russia and abroad;
- For example, it is shown that in railway traction electric grid, in particular, when 6-pulse rectifier transformers are used (Kuebler scheme), realizable power of electric locomotives generates magnetic field intensities in the vicinity, which may exceed the regulated levels for individual harmonic component frequencies.

References

- [1] B.A. Arzhannikov, DC traction power supply for high-speed and heavy trains: a monograph, USURT Publishing, Ekaterinburg, 2012.
- [2] M.P. Bader, Electromagnetic compatibility / a textbook for railway universities, UMK MPS, Moscow, 2002.
- [3] A.T. Burkov, Electronics and converters: a textbook for railway universities, Transport, Moscow, 1999.
- [4] S.D. Sokolov, Semiconductor converters of traction substations, Transport, Moscow, 1979.
- [5] V.A. Chetvergov, G.P. Maslov, O.I. Pozdnyakov, M.G. Shalimov, R&D Report No. 960: experimental development, research and operation of 12-pulse traction substation rectifiers, 1980.
- [6] A.B. Kosarev, Fundamentals of electromagnetic safety of railway power supply systems, Inteks, Moscow, 2008.
- [7] K.B. Kuznetsov, A.S. Misharin, Electrical safety in electrical installations on railway transport, Izd-vo UrGAPS, Ekaterinburg, 1999.
- [8] Directive 2004/40/EC on the minimum health and safety requirements regarding the exposure of workers to the risks arising from physical agents, official Journal of the Europe Union, L 159, 30.4. 2004.
- [9] A.R. Zakirova, Protection of electrical personnel working on traction substations from harmful effects of electromagnetic fields: PhD in Engineering thesis, Ekaterinburg, 2013.
- [10] A.R. Zakirova, Assessment of harmful impacts of electromagnetic field on traction substation personnel, USURT Publishing, Ekaterinburg, 2010.
- [11] SanPiN 2.2.4.1191-03. Electromagnetic fields in working conditions [Text], Federalnyy tsentr Gossanepidnadzora Minzdrava Rossii, Moscow, 2003.
- [12] K.B. Kuznetsov, A.R. Zakirova, Health risks of EMF generated by electric installations, Vestnik Yuzhno-Uralskogo gosudarstvennogo universiteta. Seriya «Elektroenergetika». 16 (2012) 56–61.
- [13] A.R. Zakirova, K.B. Kuznetsov, RU Patent № 2436111. (2011).
- [14] A.R. Zakirova, K.B. Kuznetsov, RU Patent № 2441248. (2012).
- [15] A.R. Zakirova, K.B. Kuznetsov, RU Patent №. 2457500. (2012).
- [16] A.R. Zakirova, Devices and methods for measurements, quality control and diagnostics in industry and transport, Proceedings of the All-Russian Scientific and Technical Conference with international participation: collection of scientific works. (2013) 398–401.
- [17] A.R. Zakirova, Evaluation of electromagnetic fields in workplaces of traction substation personnel as a technospheric safety problem. Proceedings of International scientific-practical conference "Actual problems of environmental protection and technospheric safety in changing anthropogenic environment. (2014) 61–71.
- [18] A.R. Zakirova, K.B. Kuznetsov, The probability of occurrence of occupational disease of workers, Elektrobezopasnost. 2 (2015) 26–33.
- [19] K.B. Kuznetsov, A.R. Zakirova, Zh.M. Bukanov, Methods for personnel protection from magnetic fields, Elektrobezopasnost. 4. (2014) 37–44.
- [20] K.B. Kuznetsov, Using electric characteristics of the electromagnetic field to regulate its detrimental health effects, Health and Safety: a collection of scientific works. 79 (2009) 76–80.



International Conference on Industrial Engineering

Assessment of harmful health effects of AC rectifier converters harmonic components

Kuznetsov K.B., Zakirova A.R. *

Technospheric Safety Department (Research and Education Center), Ural State University of Railway Transport, Ekaterinburg, Russian Federation.

Abstract

The article examines the main sources of EMF harmful effects affecting the electrical personnel. Harmonic composition of the rectified voltage at traction substations is analyzed. The article presents rectified voltage timing diagrams. Canonical and harmonic components of rectified voltage at the output of 6-pulse rectifier are shown. The article shows that a rectifier converter is a source of AC harmonic components and has a variety of electric and magnetic forces, the harmful effects of which on the staff have not yet been studied. It is shown that particularly in the railway transport traction networks during the use of 6-pulse VP (Kubler circuit), the operating voltages and the electric traction currents result in the creation of electric field forces caused by harmonic components, which in some cases significantly exceed the maximum permissible forces regulated in foreign practice.

© 2015 The Authors. Published by Elsevier Ltd. This is an open access article under the CC BY-NC-ND license (<http://creativecommons.org/licenses/by-nc-nd/4.0/>).

Peer-review under responsibility of the organizing committee of the International Conference on Industrial Engineering (ICIE-2015)

Keywords: electromagnetic field, magnetic field, traction substations.

1. Introduction

Generation and consumption of electrical energy involves its conversion in order to transmit electricity over a distance, as well as change of the current type, frequency of AC consumed and other parameters for a variety of purposes [1].

* Corresponding author. Tel.: +7-922-189-77-19.
E-mail address: AZakirova@usurt.ru

Power supply systems (PSS) of energy-intensive DC consumers in ferrous and non-ferrous metal industries (aluminum, zinc, magnesium, iron and steel production), electrode and chemical industries, urban and mainline electric transport are built using high-power rectifiers. The quality of electrical energy at the output of rectifiers and efficiency of its conversion into DC power or other types of energy is determined by high harmonic spectrum of rectified voltage [2].

Typically, high harmonic spectrum of AC rectifier converter may be different, as it depends not only on the asymmetry and sinusoid laity of supply network current, but also on rectifier schemes, efficiency of smoothing devices and other technical features of the converter.

Electrical personnel involved in maintenance of the above power supply systems may be exposed to harmful effects of electric and magnetic fields of various kinds of current and frequency [3-6] for a long time.

Operating conditions of traction substation (TS) converters in electrical transport are very specific [7].

2. Experimental

2.1 Theoretical procedure

In accordance with the European standard EN 50163, adopted on 06.03.1995, the nominal voltage of the contact network on electric stock pantograph is 3.0 kV, maximum stable operating voltage is 3.6 kV and in terms of acceptable insulation standards (unstable) - 3.9 kV. The maximum voltage deviation on traction substation bus at nominal supply network voltage may reach 550 V, i.e., 14.3%, or within 3.85 ÷ 3.3 kV. At power system supply voltage tolerances (GOST 13109-67) of ± 5%, the upper level of 3.85 kV can reach up to 4.04 kW, and the lower level of 3.3 kW – 3.135 kW. Thus, the possible (normalized) maximum deviations of substation bus voltages are in the range from 3.135 to 4.04 kW (18.6%) [8].

The 6-pulse converters ($m = 3, q = 6$) with zero rectification circuit (Kuebler scheme) and bridge circuit (Larionov scheme) are currently used on traction substations, as well as serial and parallel 12-pulse converters ($m = 3, q = 12$) [9]. Rectifiers with a larger number of pulsations may be used.

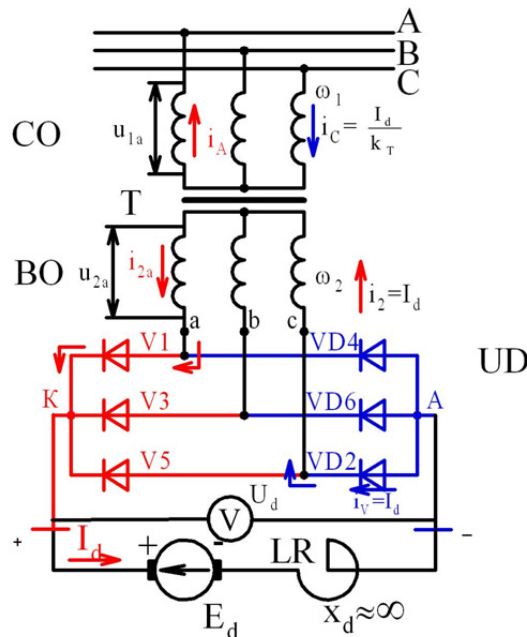


Fig. 1. 6-pulse bridge circuit.

A rectifier built according to the scheme shown in Fig.1 consists of a three-phase two-winding converter transformer, with wye- or delta-connection secondary winding, and two groups of diodes (UD).

In three-phase bridge rectifier circuit the load current passes through valves and valve side winding of two phases, and with commutations - three phases. Anode and cathode group valves are involved in operation, including valve groups VD2, VD 4, VD 6 and VD 1, VD 3, VD 5 respectively.

We assume that voltage in power supply network, and, hence in the secondary winding of converter transformer is sinusoidal.

The rectified voltage is generated as the sum of phase voltages (Fig. 2).

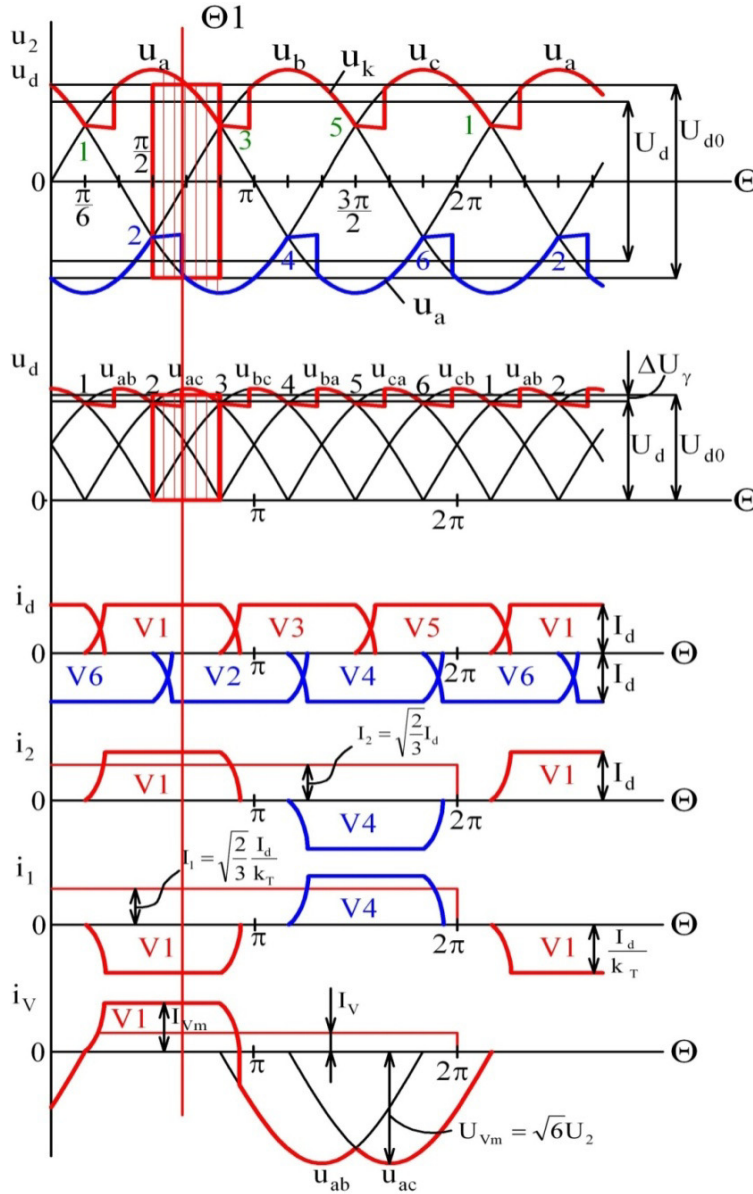


Fig. 2. Timing diagrams of voltages u_2 , rectified voltage u_d , diode arm u_a , load currents i_d, i_2, i_1 and diode arm i_v .

The voltage curve at the rectifier output is pulsating. The instantaneous value of the rectified voltage is the sum of the constant component U_d and a variable component consisting of an infinite number of harmonics [10]:

$$U_m = U_d + \sum_{n=1}^{\infty} U_{do} \sin(n\Theta + \phi_n) \quad (1)$$

where U_d - constant component; U_{do} - voltage amplitude of n-th harmonic; n - rectified voltage harmonics order; ϕ_n - initial phase of n-harmonic.

Let us consider the relationship between the voltages and currents of 6-pulse rectification circuit; when studying electromagnetic processes in the rectifier circuit, let us assume the following:

- Inductance in the rectified current circuit $X_d = \infty$;
- Valve current switching is instantaneous, i.e. valve current switching angle is $\gamma = 0$.

The calculated average rectified voltage when idle [10]:

$$U_{d0} = K_{cx} \cdot A \cdot U_{2\phi} \quad (2)$$

where K_{cx} - circuit coefficient for a 6-pulse bridge 1,73; A - rectification coefficient; $U_{2\phi}$ - effective phase voltage.

$$A = \sqrt{2} \frac{m}{\pi} \cdot \sin \frac{\pi}{m} \quad (3)$$

where m - number of pulsations of the rectified voltage curve.

For a 6-pulse bridge $A=1,352$. According to [7], the average rectified voltage is:

$$U_{d0} = \frac{1}{\pi/3} \int_{\pi/3}^{2\pi/3} U_m \cdot \sin \Theta d\Theta = \frac{3\sqrt{6} \cdot U_{2\phi}}{\pi} \approx 2,34 U_{2\phi} \quad (4)$$

where $\Theta = \omega t$.

During operation of the converter, the current passes from one converter arm to the other. This process is called current switching, and switching time expressed in angular units is called switching angle γ .

The switching process changes current and voltage curve shapes in the circuits, average value of the rectified voltage, high harmonics of the rectified voltage and network current, as well as power factor and efficiency.

The value of the switching angle γ depends on the converter circuit, its operation mode and inductive resistance of the switching circuit.

Switching angle γ is a function of load currents $I_{dH}=I_d$, per single converter and is determined by the formula, deg.:

$$\gamma_m = \arccos \left[1 - 2 \cdot U_{K3} \cdot \sin \frac{\pi}{m} \frac{I_d}{I_{dH}} \right] \quad (5)$$

It follows from the equation that the use of complex bridge circuits with an increased number of rectified voltage pulsations reduces the switching angle.

The effective value of harmonics voltage for a symmetrical supply voltage is determined by the formula, B

$$U_{dk} = \frac{U_{d0} \sqrt{2}}{3(k^2 - 1)} \cdot k \gamma \quad (6)$$

2.2 Materials

The results of analysis of variable high harmonic voltages, using a 6-pulse rectifier without smoothing filters on the traction substation are shown in Figure 3 [11].

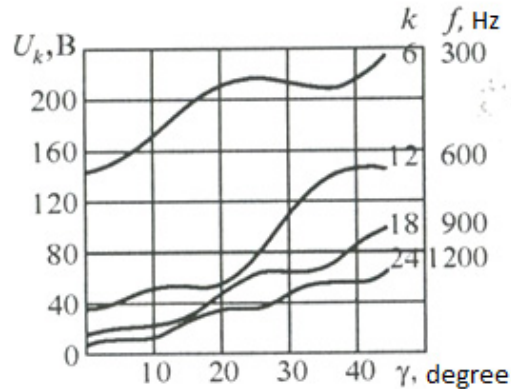


Fig. 3. Canonical harmonic components of the rectified voltage at the output of 6-pulse rectifier.

It can be seen from Fig. 3 that amplitude of rectified voltage harmonics increases with the switching angle. The presence of powerful single-phase loads leads to a phase voltage unbalance in three-phase voltage systems. The effective voltage of harmonic components at asymmetric supply voltage [11] is defined by the formula

$$U_{dk} = \frac{U_{d0} \sqrt{2}}{3(k^2 - 1)} \left[1 + 2 \sqrt{b_H^2 - b_H + 1} \cdot [\cos(k \cdot \alpha_H)] \cdot (-1)^{\frac{k}{2}} \right] \cdot k \gamma, \quad (7)$$

where U_{d0} – idle voltage of the rectifier (3300V); k – number of harmonic component of the rectified voltage; b_H – phase voltage unbalance factor of the supply line, determined by the ratio of the maximum phase voltage value on the secondary winding of traction transformer to its minimum value (1 and 1,03).

The angle α_H , is a function of unbalance factor, deg,

$$\alpha_H = \arctg \frac{2 \cdot b_H - 1}{\sqrt{3}} \quad (8)$$

where k_γ – coefficient, which depends on the switching angle, can be found [11] using the expression:

$$K_\gamma = 0,5 \cdot \sqrt{(-k \cdot \sin k \gamma - \cos k \gamma \cdot \cos \gamma - 1)^2 + (k \cdot \cos k \gamma \cdot \sin \gamma - \sin k \gamma \cdot \cos \gamma)^2} \quad (9)$$

Voltage of harmonic components of the rectified current at the rectifier output depending on the switching angle at supply voltage unbalance $b_n=1,03$ can be determined using the graph in Figure 4 [11].

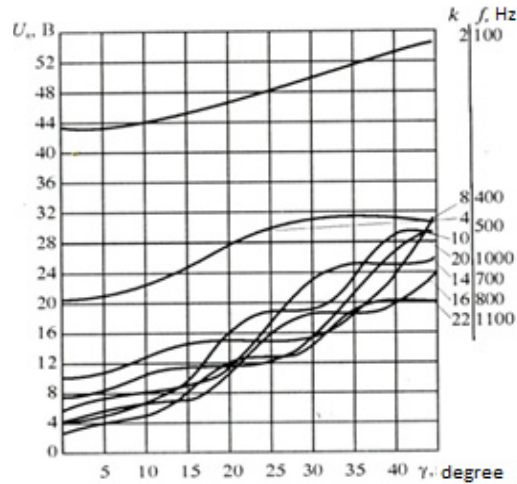


Fig. 4. Harmonic components of the rectified voltage at the output of 6-pulse rectifier.

The results of calculation of variable voltages of high harmonic components, with a 6-pulse rectifier, without smoothing filters on the traction substation are given in Table 1.

Table 1. High harmonic components of rectified voltage.

k	f_k, Hz	U_{dk}, B at $b_n=1,03, \gamma=40$ deg	L, connection area height, m	$E, \text{W/m}$	Threshold limit E (EC), B/m
2	100	54	1,8	30	5000
12	600	150	1,8	83	833
24	1200	60	1,8	33	0,61

Threshold limits of electric field (EF) intensity are regulated in the European Union. When comparing the EF values obtained (Table. 1) with the EU thresholds, a 54-fold increase of the maximum EF intensity is observed ($f=1200 \text{ Hz}, \gamma=40$). There is a need to develop means of protection to reduce the duration of magnetic field exposure [12-20].

3. Conclusion

Based on the above analysis, the following conclusions can be made:

- A. Rectified EF voltage has a variety of electric and magnetic impacts, whose harmful effects on the staff have not yet been studied.
- B. It is shown that in railway transport traction networks, in particular, when using 6-pulse VP (Kubler circuit), operating voltages and electric traction currents result in the creation of electric field forces caused by harmonic components, which in some cases significantly exceed the maximum permissible forces regulated in foreign practice.

References

- [1] Yu.I. Khokhlov, Energy-saving technologies for electrical energy conversion. Modern knowledge-intensive technologies. 2 (2004) 90–92.
- [2] Yu.I. Khokhlov, D.V. Gizzatullin, A.G. Osipov, Simulation of electromagnetic processes in a compensated rectifier with voltage feedback

- based on autonomous inverter with PWM, *Vestnik Yuzhno-Uralskogo gosudarstvennogo universiteta. Seriya: Energetika*. 11 (2008) 32–38.
- [3] K.B. Kuznetsov, Using electric characteristics of the electromagnetic field to regulate its harmful effects on humans, *Health and Safety: a collection of scientific works*. 79(162) (2009) 76–80.
- [4] A.R. Zakirova, Assessment of harmful impacts of electromagnetic field on traction substation personnel, USURT Publishing, Ekaterinburg, 2010.
- [5] A.R. Zakirova, K.B. Kuznetsov, S.O. Belinskiy, Regulation of permissible energy load of EMF in the frequency range of up to 10 kHz, *Nauchno - prakticheskiy i uchebno - metodicheskiy zhurnal «Bezopasnost zhiznedeyatelnosti»*. 7 (2012) 21–24.
- [6] A.R. Zakirova, K.B. Kuznetsov, The risk of harmful effects of EMF generated by electric systems on humans, *Vestnik Yuzhno-Uralskogo gosudarstvennogo universiteta. Seriya «Elektroenergetika»*. 16 (2012) 56–61.
- [7] S.D. Sokolov, Yu.M. Bey, Ya.D. Guralnik, O.G. Chausov, *Semiconductor converters of traction substations*, Transport, Moscow, 1979.
- [8] B.A. Arzhannikov, *DC traction power supply for high-speed and heavy trains: a monograph*, USURT Publishing, Ekaterinburg, 2012.
- [9] A.T. Burkov, *Electronics and converters: a textbook for railway universities*, Transport, Moscow, 1999.
- [10] V.A. Chetvergov, G.P. Maslov, O.I. Pozdnyakov, M.G. Shalimov, R&D Report No. 960: experimental development, research and operation of 12-pulse traction substation rectifiers, 1980.
- [11] M.P. Bader, *Electromagnetic compatibility: a textbook for railway universities*, UMK MPS, Moscow, 2002.
- [12] K.B. Kuznetsov, A.R. Zakirova, Health risks of EMF generated by electric installations, *Vestnik Yuzhno-Uralskogo gosudarstvennogo universiteta. Seriya «Elektroenergetika»*. 16 (2012) 56–61.
- [13] A.R. Zakirova, K.B. Kuznetsov, RU Patent № 2436111. (2011).
- [14] A.R. Zakirova, K.B. Kuznetsov, RU Patent № 2441248. (2012).
- [15] A.R. Zakirova, K.B. Kuznetsov, RU Patent №. 2457500. (2012).
- [16] A.R. Zakirova, Devices and methods for measurements, quality control and diagnostics in industry and transport, *Proceedings of the All-Russian Scientific and Technical Conference with international participation: collection of scientific works*. (2013) 398–401.
- [17] A.R. Zakirova, Evaluation of electromagnetic fields in workplaces of traction substation personnel as a technospheric safety problem. *Proceedings of International scientific-practical conference "Actual problems of environmental protection and technospheric safety in changing anthropogenic environment*. (2014) 61–71.
- [18] A.R. Zakirova, K.B. Kuznetsov, The probability of occurrence of occupational disease of workers, *Elektrobezopasnost*. 2 (2015) 26–33.
- [19] K.B. Kuznetsov, A.R. Zakirova, Zh.M. Bukanov, Methods for personnel protection from magnetic fields, *Elektrobezopasnost*. 4. (2014) 37–44.
- [20] K.B. Kuznetsov, Using electric characteristics of the electromagnetic field to regulate its detrimental health effects, *Health and Safety: a collection of scientific works*. 79 (2009) 76–80.



International Conference on Industrial Engineering

Evaluation of the permitted number of reduced-current starts of the powerful induction motor drives on the basis of the oscillatory component of electromagnetic torque

Vecherkin M.V.^{a*}, Sarvarov A.S.^a, Makarov A.V.^a

^a*Nosov Magnitogorsk Technical University, Magnitogorsk, 455000, Russia*

Abstract

Transient processes arising in direct on line (DOL) start of powerful induction motor drives have a negative effect on the motor technical condition and the drive mechanism, reducing their operating life. One of the reasons of this effect is the electromagnetic torque oscillations of the motor when starting. Various non-equipollent in the limitation extent of the torque oscillatory component methods are used to facilitate the start conditions. In this paper integral quantitative criteria resulting from the analysis of the calculation oscillograph traces, making possible to estimate the oscillation degree of the electromagnetic torque and make a comparative analysis of the different start methods are introduced. A method of calculation the permissible number of starts per year, based on the estimation criteria of the torque oscillation degree was developed. The method allows to estimate the number of starts as for the chosen method, so for the combination of different methods.

© 2015 The Authors. Published by Elsevier Ltd. This is an open access article under the CC BY-NC-ND license (<http://creativecommons.org/licenses/by-nc-nd/4.0/>).

Peer-review under responsibility of the organizing committee of the International Conference on Industrial Engineering (ICIE-2015)

Keywords: induction motor ; direct-on-line start ; soft start; reactor start ; electromagnetic torque ; thyristor voltage regulator ;

* Corresponding author. Tel.: +7-964-245-5681;
E-mail address: vecherkin@inbox.ru

Relevance of the topic

It is known that squirrel cage induction motors are widely used and consume the half of the all the world's energy output. Accordingly, there is a significant reserve of energy conservation in the operation of electric motor drives. One of the most effective energy saving measures is the shift of the unregulated electric motor drives from the continuous operation mode into a intermittent periodic, where technology conditions need it. High voltage electric motor drives can obtain the greatest economic effect. Such implementation is prevented by DOL start severe conditions of high-power induction motors. For the high inertia induction motor drives DOL start should be considered as dangerous emergency mode. The number of powerful high-voltage motor DOL starts is specified by the manufacturer and it varies from 250 to 500 DOLs per year.

For total or partial neutralization of the negative influence of transient processes different starting methods are used: reactor start, auto-transformer start, star-delta start, start using thyristor voltage regulator (TVR) or frequency converter. When implementing one of these methods, the number of DOL starts can be increased without compromising the technical condition and engine service life.

The negative impact of starting processes, as far as it is known, is determined by two main factors: large starting current and electromagnetic torque fluctuations of wide amplitude arising in process of starting [1]. All these factors have a negative influence on the mechanical and electromagnetic systems of electric motor drives, as well as on their thermal state.

Existing methods of calculation the frequency of starts focused on compliance with the permissible heating conditions and based on the assessment of thermal losses in the motor. The negative impact of the oscillatory component of torque is not taken into account. At the same time, the oscillation energy of electrical and mechanical quantities in motor does not perform any useful work, and is converted into heat or in deformation and destruction work of the electromagnetic and mechanical part of the electric motor drive. Simultaneously energy oscillations are definitely determined by the electromagnetic torque oscillations.

Different starting methods are not-equipollent as in expenses so in the restriction degree of the electromagnetic torque oscillatory component.

Formulation of the problem

1. To analyze the influence of different ways of starting on the oscillation degree of the starting electromagnetic torque of powerful induction motor drive.
2. To develop a methodology which will make possible to evaluate the impact of different starting methods on the permitted number of starts.

Research

As the object of study was chosen an electric motor drive of the centrifugal fan equipped with high-voltage squirrel cage induction motor. The main technical characteristics of the analyzed motor are given in the Table. 1.

Table 1. Basic technical data of the studied motor.

Characteristics	Value
Power (kW)	800
Supply voltage (W)	6000
Rotation frequency (rots per min.)	1480
Nominal torque of the motor (N·m)	5140
Efficiency factor (%)	95,1
Rotor moment of inertia (Kg·m ²)	26
Interval between starts, not less (hour)	3
Starts quantity per year, not more	500

The fan has an impeller with a moment of inertia $J = 250 \text{ kg} \cdot \text{m}^2$. For such an inertial operating device the number of the sizable surges of the striking electromagnetic torque of the motor can reach ten times when starting [2].

In modern conditions, it is reasonable to conduct the analysis of starting modes by means of computer simulation. Fig. 1 a, described in relative units the calculated time-dependent oscillograph trace of the electromagnetic torque of the motor, achieved while investigating the prototype of the described electric motor drive, developed in the Matlab environment. Fig. 1 b, shows the emphasized torque oscillatory component obtained with the help of the Butterworth's digital filter of the eighth order with a cutoff frequency of 10 Hz.

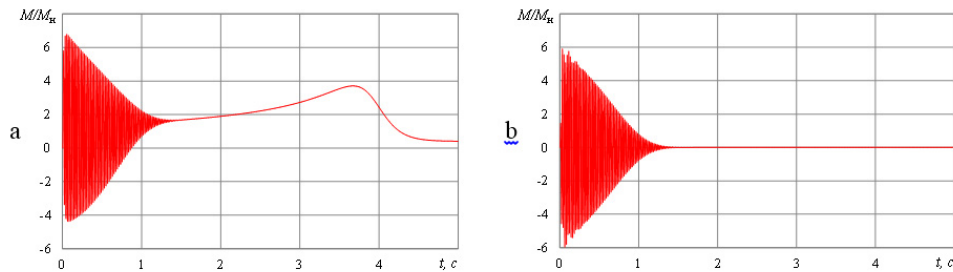


Fig. 1. The time-dependence of electromagnetic torque in DOL start:
(a) the calculating oscillograph trace; (b) emphasized oscillatory component.

Using different methods of the softened start, the striking torque start-amplitude takes smaller values than if using DOL start. As an example, Fig. 2 shows the calculating oscillograph trace generated as a result of reactor start simulation (fig. 2 a) and the two start modes using TVR (fig. 2 b).

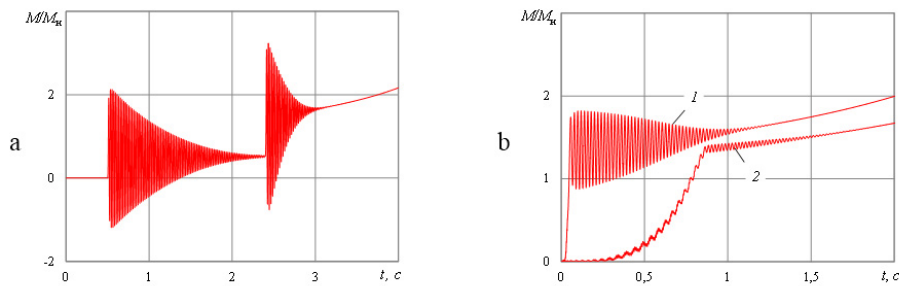


Fig. 2. The calculation oscillograph trace of the electromagnetic torque:
(a) reactor start; (b) soft start;
(1) high rate of voltage rise; (2) low rate of voltage rise.

The comparison of oscillograph traces shows that the problem of oscillatory component limiting can be the most efficiently solved by using thyristor voltage regulator and a choice of the rational starting mode. However, the high-voltage starting systems based on TVR are expensive, that is why relatively cheap ways remain popular: reactor start, auto-transformer start, star-delta start. These methods often provide satisfactory results in reducing dynamic loads which may arise in the electric drive when starting.

Under actual operating conditions, when using one of the ways of the softened start there can be the problem of determining the permissible number of the reduced-current starts under the chosen start method. This requires the using of quantitative criteria, reflecting the oscillation degree of the starting torque.

Oscillatory component can be estimated differently. For example, it can be based on the peak amplitude, or the multiplicity of initial oscillation amplitude. However, as it is shown in the work [3], these values are not sufficiently informative, since the change of the starting conditions has little influence on them. In addition, these characteristics do not take into account the number of the torque surges and cannot be applied to any of the known starting methods.

Development of the calculation method of the permissible starts quantity

For estimation of the torque oscillatory component when using different methods and modes of the start it is suggested to use an integral argument - the root-mean-square value (RMS) of the electromagnetic torque oscillatory component during startup moment of induction motor [3]:

$$T_{rms} = \sqrt{\frac{1}{t_{start}} \int_0^{t_{start}} (T(t))^2 dt}; \quad (1)$$

Where $T(t)$ – time-dependence of the electromagnetic torque oscillatory component; t_{start} - motor start time.

This argument is calculated from the electromagnetic torque oscillatory component, obtained from the calculation oscillograph traces (Fig. 1 b). Argument T_{rms} is universal and can be applied to any of the methods and modes of start [3]. Computer startup model research indicates that the argument T_{rms} is very sensitive to changes in the DOL start conditions.

Table 2. The values of integral criteria in different start conditions.

Start conditions	T_{rms} , (N·m)
DOL start in idle mode: $J_{\Sigma} = 26 \text{ kg}\cdot\text{m}^2$; $T_{static} = 0$	2340
Fan's DOL start on the closed damper: $J_{\Sigma} = 276 \text{ kg}\cdot\text{m}^2$	4310
Fan's DOL start on the closed damper : $J_{\Sigma} = 376 \text{ kg}\cdot\text{m}^2$	4600
DOL start with reactive torque on the shaft: $J_{\Sigma} = 276 \text{ kg}\cdot\text{m}^2$, $T_{static} = 0,4T_{nominal}$	4710
DOL start with reactive torque on the shaft : $J_{\Sigma} = 376 \text{ kg}\cdot\text{m}^2$, $T_{static} = 0,4T_{nominal}$	4990
DOL start with reactive torque on the shaft : $J_{\Sigma} = 276 \text{ kg}\cdot\text{m}^2$, $T_{static} = T_{nominal}$	5680
DOL start with reactive torque on the shaft: $J_{\Sigma} = 376 \text{ kg}\cdot\text{m}^2$, $T_{static} = T_{nominal}$	5860

Then, the non-dimensional integral argument should be introduced - RMS oscillatory component multiplicity with respect to RMS oscillatory component in DOL start:

$$k_{T_0} = \frac{T_{rms}}{T_{rms0}}; \quad (2)$$

where T_{rms} is RMS of the oscillatory component in the studied start method; T_{rms0} is RMS of the oscillatory component in DOL start.

This argument determines the quantity of the oscillatory component in the chosen method and start mode with respect to the oscillatory component in DOL start. It is obvious that: $k_{T_0} = 1$ corresponds to the conditions of the DOL start; $k_{T_0} > 1$ corresponds to better conditions than in DOL start; $k_{T_0} < 1$ - the worst conditions than in DOL start. The latter is possible in the reverse, self-starting, reverse-current braking.

Table 3. The arguments values T_{rms} and k_{T_0} for the starting processes shown in Fig. 1 and Fig. 2.

Start method	T_{rms} , (N·m)	k_{T_0}
DOL start (fig. 1 a)	4310	1,0
Reactor start (fig. 2 a)	1424	0,33
Soft start (fig. 2 b, curve 1)	391	0,091
Soft start (fig. 2 b, curve 2)	44,3	0,01

Clearly, in these cases the reactor start allows to reduce RMS of the torque oscillatory component in 3 times in comparison with the DOL start and the soft start– in 10-100 times, depending on the chosen TVR operating mode.

On this basis, the use of the soft start devices based on TVR allows to drop the start quantity limits per year completely, that are determined by the torque oscillatory component, and keep only limitations related to the permissible heating terms.

When implementing other ways of starting the oscillatory component is limited to the less extent, and it is unacceptable to ignore its negative impact. To calculate the permitted starts quantity in these cases, it is suggested to use the following method.

Initial data for calculation are the calculated criteria k_{T_0} and installed by the manufacturer the allowable DOL starts quantity per year $N_{permitted}$.

Consider the situation where the induction motor with the permissible number of DOL start $N_{permitted}$ is operated with opportunity to implement a DOL start and induction start. Let the torque oscillatory component be defined by the argument $k_{T_0} = k_r$. In situations where DOL is needed, argument $k_{T_0} = k_{DOL}$, is by definition.

Obviously, the number of DOL starts N_{DOL} must come up to the inequality:

$$N_{DOL} \leq N_{permitted}; \quad (3)$$

where N_{DOL} is the number of DOL starts made per year.

Given that $k_{DOL} = 1$ this inequality can be rewritten as:

$$N_{DOL} k_{DOL} \leq N_{permitted}; \quad (4)$$

In implementing of reactor start, negative impact of transients is reduced, and the argument (2) takes smaller value in comparison with the DOL start. For the reactor start can be written by the inequality:

$$N_r k_r \leq N_{permitted}. \quad (5)$$

Then, the permissible number of the reactor starts is:

$$N_r \leq \frac{N_{permitted}}{k_r}; \quad (6)$$

Thus, in reactor engine start with the arguments given in the Table. 1 when $k_i = 0,333$ the permissible number of the reactor starts per year will be $N_r \leq 1500$. So, 4 starts are permitted per day.

A similar calculation for the TVR start when $k_{TVR} = 0.091$ gives the permissible number of starts per year $N_{TVR} = 5494$ or 15 starts per day. The result allows to run the engine every 1.5 hours. However, this is less than the permitted interval between starts $\Delta t = 3$ hours specified by the manufacturer. Thus, whatever the start method is, the number of starts should not exceed the value:

$$N' = \frac{24}{\Delta t}; \quad (7)$$

where Δt is an interval between the starts, an hour according to the motor certificate.

In this case there are 8 starts per day.

When operating the electric motor drive it is possible to carry out the start of the motor in different ways. Usually, it is a combination of the DOL and one of the methods of softened start. In this case, the permitted number of starts for the combination of DOL and reactor start is defined by the inequality:

$$N_r k_r + N_{DOL} \leq N_{permitted}; \quad (8)$$

Generally, if different methods are used:

$$N_{DOL} + \sum_{i=1}^n N_i k_i \leq N_{permitted} ; \quad (9)$$

where n is a number of the used methods of softened start; N_i is a number of starts of this method; k_i is multiplicity of RMS of the oscillatory component of this start method in respect to RMS of the oscillatory component in DOL start.

Conclusions

1. On the basis of the research, it was found that the root-mean-square value (RMS) of the electromagnetic torque oscillatory component during the start time of induction motor, obtained from the calculation oscillograph traces is the most sensitive to the changes in the DOL start conditions.

2. On the basis of the introduction of the non-dimensional integral argument - multiplicity of RMS of the oscillatory component in respect to RMS of the oscillatory component in DOL start was obtained the opportunity to quantify the impact of the different start methods to the improvement of performance for increasing the number of starts per year.

3. Method of calculating of the permissible number of starts per year was developed, using the calculating oscillograph traces obtained on the basis of the powerful induction motor model during the researching of DOL start and when implementing the startup system into the operation.

References

- [1] L.P. Petrov, Control of start-up and braking asynchronous electric motor, JenergoizdatPubl, Moscow, 1981.
- [2] M.M. Sokolov, L.P. Petrov, L.B. Masandilov, V.A. Ladenzon, Electromagnetic transient processes in an asynchronous motor drive, Energiya, Moscow, 1967.
- [3] M.V. Vecherkin, A.S. Sarvarov, E.V. Makarcheva, A.V. Makarov, Comparative assessment of starting methods of induction motors, according to oscillatory component of electromagnetic torque, proceedings of the VIII international (XIX all-Russian) conference on the automatic electric drive, Tom 1 Mordovian University Publisher, Saransk. (2014) 197-202.



International Conference on Industrial Engineering

Short-circuit failures simulation for evaluation of structural reliability of power supply systems

Malafeev A., Iuldasheva A.*

Nosov Magnitogorsk State Technical University, 38, Lenin ave., Magnitogorsk, 455000, Russia

Abstract

The work is dedicated to the application of the sequential reduction method use to evaluate structural reliability of the industrial enterprises power supply systems. The review of publications has shown the lack of attention to these issues. Most researchers are focused on the reliability of electric power systems; probabilistic-statistical approach and the approach from the standpoint of financial and credit policy dominate here. The algorithm of scheme reduction is considered in terms of the most common type of failure - the short-circuit failure. The algorithm includes the following main steps –the identification of scheme elements, which allow selecting a group of elements, the failure of which leads to the failure of the entire group; the grouping of selected elements for which the equivalent reliability indices will be calculated; the convolving of resulting calculation scheme to the selected user and the definition of equivalent values the failure intensity, restoration time, and other reliability indices of interest. The algorithm is illustrated by an example of calculation scheme of the power supply system fragment containing a branch line. The calculations are carried out for the existing industrial enterprise.

© 2015 The Authors. Published by Elsevier Ltd. This is an open access article under the CC BY-NC-ND license (<http://creativecommons.org/licenses/by-nc-nd/4.0/>).

Peer-review under responsibility of the organizing committee of the International Conference on Industrial Engineering (ICIE-2015)

Keywords: Power supply, structural reliability, failure, recursive function, scheme bypass, sequential reduction, equivalent reliability indices.

1. Introduction

The evaluation of power supply reliability is the problem solved, as a rule, at the stage of design and reconstruction of power grids; for complex electrical systems of large energy-intensive enterprises having closed

* Corresponding author. Tel.: +7-951-128-05-90.
E-mail address: alinayuldasheva1@gmail.com

networks from the junction to the grid, their own power plants. This problem should be solved also in the process of operation, for example, when considering the dispatching applications for withdrawal of equipment in repair or reserve. The substantial margin of overload capacity of elements is laid at designing of power systems, in particular for 35-110 kV levels; if this fact is considered the structural reliability should be first evaluated. The structural reliability consider only the connection layout of the network elements, but deviations of the regime parameters from allowable values are not taken into account, which is greatly simplifies the solution.

The selection of a failure model is one of the component of the task of assessment of the consumers power supply reliability. In addition to the statistical characteristics it is necessary to determine the necessity of considering the such failures types as the "disconnection" or "short-circuit". Short-circuits in comparison with disconnections occur more often in circuits of power stations and substations, as well as in electrical networks. Disconnections occur on overhead transmission lines and flexible busbar switchgear and often lead to complex damages, such as open-phase fault of conductors with the closure of each other or to the ground. Thus, in networks 110-220 kV of Magnitogorsk energy hub the disconnections observed at the average rate of 2 times per year, while the short-circuits approximately 50-60 times.

It should also be noted that the short circuit, regardless of whether they are symmetrical or not, lead to shutdown of the damaged area, while asymmetric disconnections are partial failures. It is also resulted to change of the functional reliability parameters, which is difficult to evaluate.

2. Review of publications

Significant part of publications devoted to the issues of reliability of the electric power systems. For example, in [1] the characteristics of software, which is developed by the authors, for assessing the adequacy indices, is given. The article [2] devoted to assessing the sensitivity of the reliability indices (primarily LOLP, loss of load probability), taking into account the regime restrictions of systems, which combine power transmission with direct and alternating current. Some of the work is focused on increasement of the reliability by improving the station power grid and equipment, in particular, due to the active implementation of devices FACTS [3]. Serious attention is paid to assessing the reliability primarily to the regime positions. In a number of works the reliability assessment is considered in the context of the larger task of planning the development of generation, supply and distribution networks, taking into account the costs of reconstruction [4], on the basis of a multi-purpose non-linear control model, in particular in [5] an approach based on a set of Pareto is used. Variety of mathematical apparatus is used, for example in [6] Bayesian networks was applied to account the impact of relay protection failures on the reliability of power systems; the adaptation of fuzzy Petri networks to the assessment of the reliability of power supply is proposed in [7]; in [8] the integer nonlinear programming in conjunction with the medium-dispersion method is used to assess the effectiveness of investments in improving the reliability. In the work [9] two different regime situation in relation to the microgrid networks is considered: when the power flow direction through the network element (UPF and BPF) unchanged or change; for these cases approaches to the reliability calculation is developed. The work [10] is dedicated to the questions of reliability centered maintenance (RCM) in the competitive market. The authors advocate the position of evaluating the reliability solely on cost criteria "... the most understandable to decision-makers." The impact of demand management programs, aimed to the alignment of the load curve and the reliability of the power system, are examined in [11]. Logical and probabilistic methods are also used, for example, in [12] the fault tree method in conjunction with the Monte Carlo method are used for reliability analysis in SmartGrids, this approach is applied to assess the criterion LOLP and to quantify the risks on its basis. The theoretical studies related to the development of the failure models is also observed. Proposed in [13] the probabilistic model of consumers outages, which is a distribution of consumers failure probability by hours of the day, is focused on the practice of dispatching management. Another important issue for the consumers - the reliability of cogeneration system - is considered in the article [14]; Markov chains are used for the failure flow simulation. A number of works devoted to assessing the impact of the "human factor" on the reliability of energy systems [15], [16], [17].

In general it can be concluded that investigations in the field of statistical research of reliability indices and in the field of evaluation of economic efficiency of procedures for reliability maintaining are prevailed. Most studies

examine the reliability issues on the part of generating, electric distribution and retail electricity companies, but reliability assessment on the part of the consumer is considered less often.

3. The algorithm for the scheme composition for the calculation of reliability in case of the "short-circuit" failure

The distinguishing characteristic of power supply reliability calculation for the "short-circuit" failure primarily is in the fact that the scheme for reliability calculation will not coincide with the real electric connection diagram. This is because in the circuit elements, which are not separated by the circuit-breakers [18], in the context of reliability calculation are considered as connected in series. This can be applied to the busbars with the busbar disconnectors; to the branch lines with taps attached tightly or through tap disconnectors; to cable lines of several parallel laid cables, which are connected through a common circuit-breakers, and others.

At the Industrial power supply department of Nosov Magnitogorsk State Technical University the algorithm for structural reliability calculation was developed. It allows to calculate of equivalent reliability indices relative to arbitrarily chosen consumer, taking into account only the circuit elements involved in the power transfer to that consumer [19]. The algorithm provides an opportunity to perform calculations for power systems, including open and closed networks, with nodes due to the regional power grid, its own power plants, and is based on the sequential reduction method [20]. The algorithm is implemented in the module "Reliability" of program complex (PC) KATRAN on in C++.

At the primary stage, the steady-state mode calculation is carried out. The power flow direction through the circuit elements is the main result of this operation. User selects an element-load, relative to which the equivalententing will be carried out.

The next step in the calculation is the marking of the scheme elements; it will provide the elements involved in the transfer of power to the selected element (hereinafter - Group I; these elements in the code corresponds to the flag InstRel), as well as elements with the opposite power flow direction, which is associated with the elements of Group I directly (Group II and the corresponding flag FailSC). The elements of the Group II, which adjacent to circuit-breakers and form the boundary of the group (Group II-a flag FailSCEnd), are highlighted.

The functions performing the marking of elements, primarily is called for the element, associated with the selected element, then its recursive call is made for the one of the element, associated with the current one, until all of the elements belonging to Groups I and II will not be passed.

The grouping of elements belonging to the Group II is carried out after their marking. The values of failure intensity λ_{gr} and restoration time $T_{R,gr}$ are passed as parameters to the grouping function. For the "i"-element of the Group II, and for the previous "i-1"-element this parameters are determined according to the rules of serial addition (1), (2):

$$\lambda_{gr,i} = \lambda_{gr,i-1} + \lambda_i, \quad (1)$$

$$T_{Rgr,i} = \frac{T_{Rgr,i-1} \lambda_{gr,i-1} + T_{R,i} \lambda_i}{\lambda_{gr,i-1} + \lambda_i}. \quad (2)$$

These values are assumed to be zero at the first function call.

Inside of the grouping function, it is determined whether the current element is the beginning of a chain with the opposite power flow, included in the Group II. The flag IsReduct is set for all of the group elements which are already accounted. For each element is detected, whether it is related to the chain, for which FailSC = true, but that has not yet passed when grouping (IsReduct = false). In this case, for the current flag is set IsFirstFailSC.

If the element associated with the current element has the flags values as InstRel = true, FailSC = true, IsReduct = false the recursive call of grouping function is carried out. In the opposite case, that element is the first for the concerned circuit and the final sums calculation (1), (2) is made for it. For the considered circuit elements the InstRel = false and they are excluded from the further equivalententing procedure.

The procedure of elements marking is shown in Fig. 1, 2 at the example of the fragment of power supply system comprising the branch line.

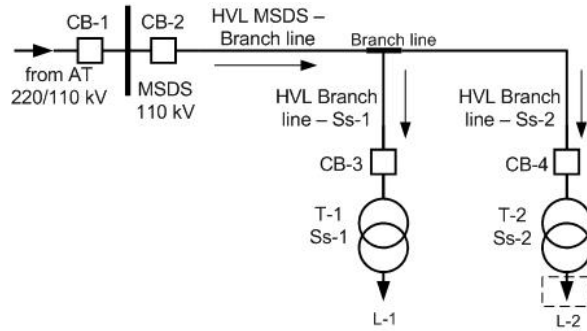


Fig. 1. Fragment of the power supply system: : CB – circuit-breaker, L – load, Ss – substation, MSDS - main step-down substation, T – transformer, AT – autotransformer, HVL – high-voltage line.

At the calculation scheme (Fig. 1) each of the elements of the power supply system is represented as a node, the number of bonds is equal to the number of actual connections with the other elements of the element (for the power transmission line, double-wound transformer, circuit-breaker - two bonds, for triple-wound transformer - three, etc.). HVL branch line is added to the scheme by fictitious node “2” with three bonds. The reliability indices of power supply are estimated with relatively to the consumer “L-2”. This consumer will fail supply in case of short-circuit on the line “HVL Branch line – Ss-2” and the line “HVL Branch line – Ss-1”. Thus, the circuit formed by the nodes 2 and 3 (elements “Branch line” and “HVL Branch line – Ss-1”) should be taken into account when analyzing the short-circuit failures. The circuit-breaker “CB-3” is its boundary, which is detected as a result of the marking function. The total failure intensity of this circuit will be equal $\lambda_{2-3} + \lambda_{3-2} + \lambda_{3-CB3}$. This value is assigned to λ_{2-4} in the result of call the grouping function as branches of 2-4 corresponds to the power flow $\dot{S}_{4,2}$, directed from the power source “MSDS”. Then node 2 participates in equivalenting only as λ_{2-4} .

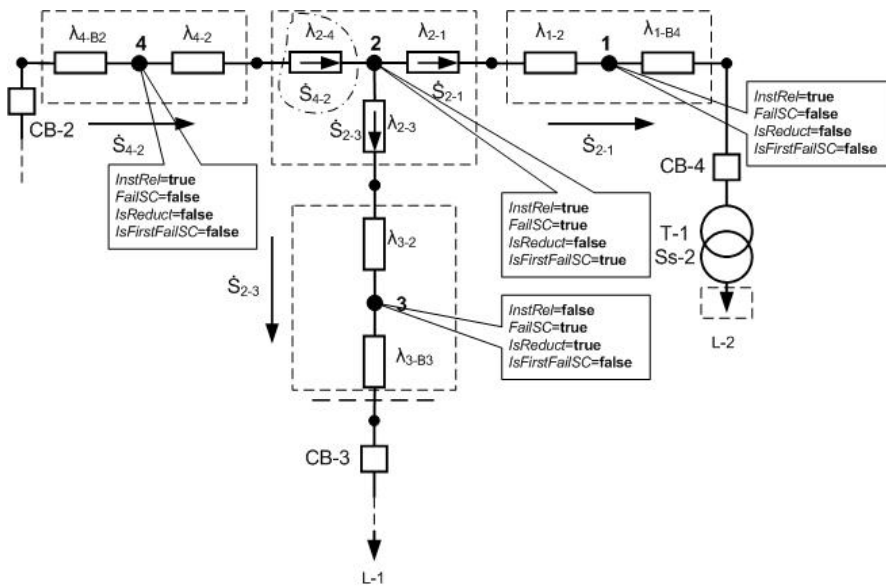


Fig. 2. The calculation scheme of the power supply system fragment after labeling and grouping of elements.

The algorithm discussed in [22] is used for further equivalenting procedure. The algorithm flowchart is shown at Fig. 3: λ_{ekv} , T_{Rekv} , p_{ekv} – equivalent failure intensity, recovery time and the probability of no-failure, respectively.

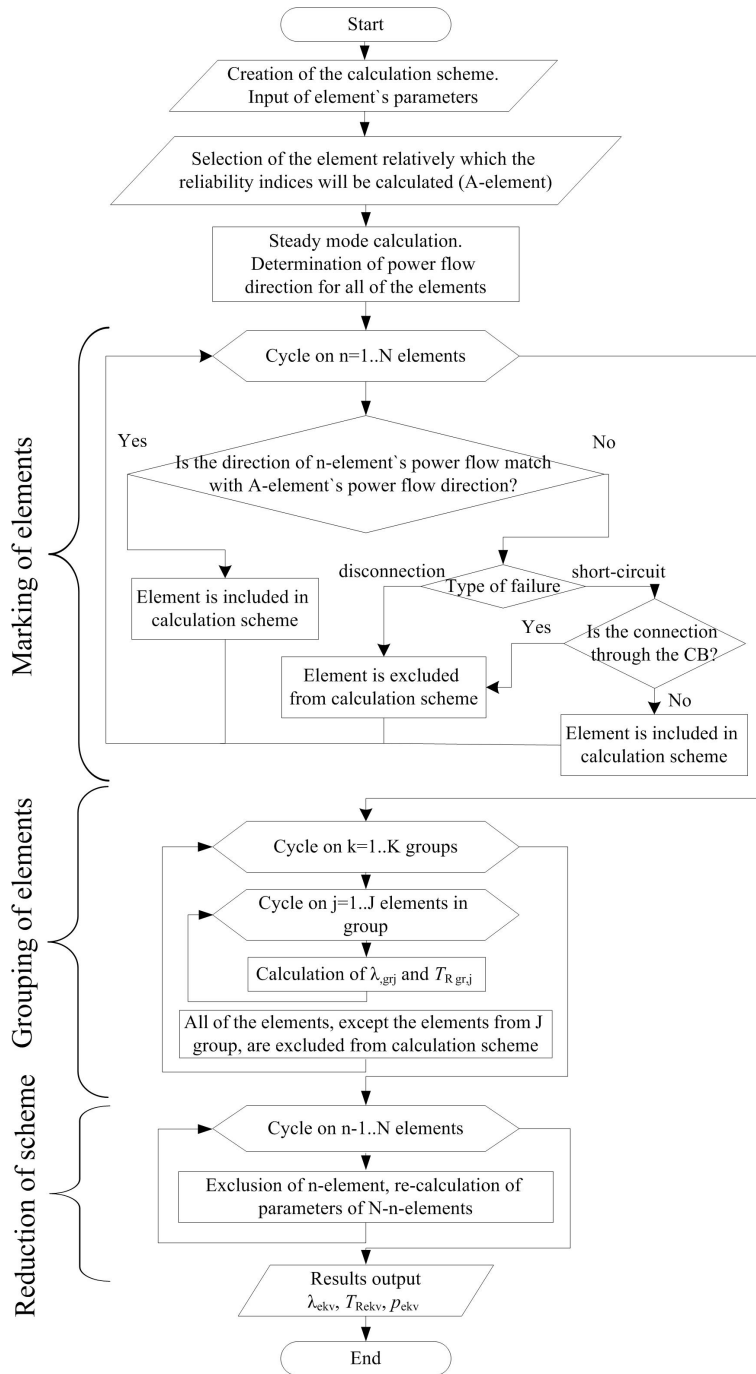


Fig. 3. The algorithm for calculating structural reliability.

4. Practical application

As an example the fragment of the power supply system of Iron and Steel Works is considered (Fig. 4). The basic reliability indices were calculated in case of failure of the "short-circuit" and "disconnection" relatively to the selected load. The results of calculation are shown in Table 1.

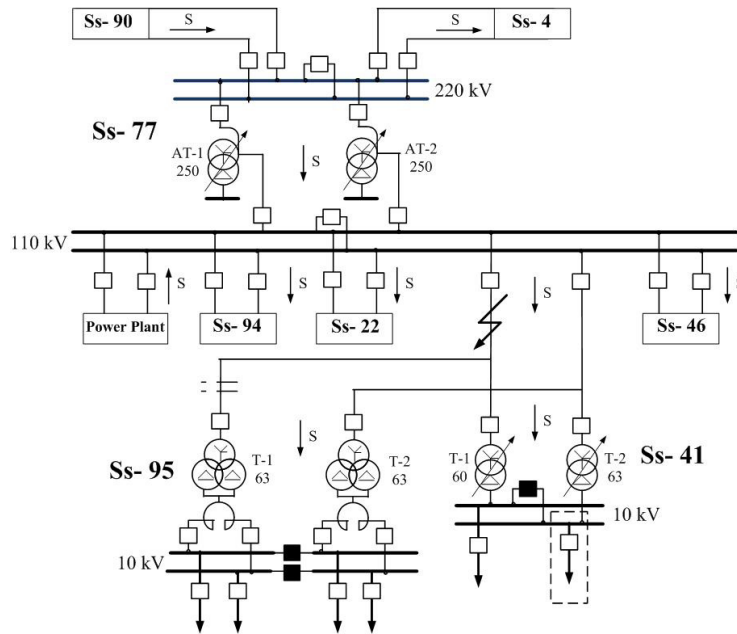


Fig. 4. The fragment of power supply system of OJSC "MMK".

Table 1. The results of calculation.

Operating mode	p_{ekv}	$\lambda_{ekv}, 1/\text{year}$	T_{Rekv}, year
Short-circuit	0,9995	0,1576	0,0032
Disconnection	0,9997	0,0607	0,00542

Thus, the probability of system failure in the event of "short-circuit" is higher than the "disconnection", but the recovery time below and that can lead to more significant damage.

5. Conclusion

The developed algorithm allows to compare different variants of normal maintenance and repair schemes on the basis of reliability indices in planning mode or network reconstruction. Accounting of the power flow direction allows to take into account in the calculation of equivalent reliability indices only those elements that affect to the reliable operation of the selected item. Accounting of the failure types as "disconnections" or "short-circuit" – makes it possible to take into account the failure of equipment are most typical for the analyzed part of the network, as well as a course of accident is most often observed. For example, the example of the fragment of power supply system it was shown that erroneous choice of the failure type could give an error in determining the reliability indices approximately 40%.

References

- [1] P. Anbalagan, V. Ramachandran, Service-oriented architectural model for generating system adequacy evaluation, *Electrical Engineering*. 94(1) (2012) 19–25.
- [2] M. Benidris, J. Mitra, Reliability and sensitivity analysis of composite power systems considering voltage and reactive power constraints, *IET Generation, Transmission & Distribution*. 9(12) (2015) 1245–1253.
- [3] B. Sadeghi, M. Rostami, H. Torabipour, A. Gholami, Y. Shahsavari, Reliability Enhancement of the Power System by the SVC Replacement, *Majlesi Journal of Electrical Engineering*. 7(4) (2013) 17–26.
- [4] A.M. Cossi, L.G.W. da Silva, R.A.R. Lázaro, J.R.S. Mantovani, Primary power distribution systems planning taking into account reliability, operation and expansion costs, *IET Generation, Transmission & Distribution*. 6(3) (2012) 274–284.
- [5] H. Mavalizadeh, A. Ahmadi, A. Heidari, Probabilistic multi-objective generation and transmission expansion planning problem using normal boundary intersection, *IET Generation, Transmission & Distribution*. 9(6) (2015) 560–570.
- [6] M. Eliassi, H. Seifi, M.-R. Haghifam, Incorporation of protection system failures into bulk power system reliability assessment by Bayesian networks, *IET Generation, Transmission & Distribution*. 9(11) (2015) 1226–1234.
- [7] Z. Hongzhan, H. Zhanjun, L. Fenfang, Research of power communication network system reliability based on cloud model and fuzzy petri nets, *Applied Mechanics & Materials*. 630-642 (2014) 1140–1146.
- [8] S. Yaakob, J. Watada, T. Takahashi, T. Okamoto, Reliability enhancement of power systems through a mean–variance approach, *Neural Computing & Applications*. 21(6) (2012) 1363–1373.
- [9] W. Feng, Q. Yanpeng, F. Zhengcai, Reliability evaluation of distribution system with microgrids considering power control mode, *Australian Journal of Electrical & Electronic Engineering*. 10(3) (2013) 389–396.
- [10] R. Ghorani, M. Fotuhi-Firuzabad, P. Dehghanian, L. Wenyuan, Identifying critical components for reliability centred maintenance management of deregulated power systems, *IET Generation, Transmission & Distribution*. 9(9) (2015) 828–837.
- [11] E. Saied, S. Soliman, Y. Rihan, S. Mahmoud, H. Gad-Alla, Impact of demand-side management on power system reliability, *Journal on Electrical Engineering*. 8(4) (2015) 26–33.
- [12] G. Song; H.Chen; B. Guo. A layered fault tree model for reliability evaluation of smart grids, *Energies* (19961073). 7(8) (2014) 4835–4857.
- [13] Ilie Irinel-Sorin, Hernando-Gil Ignacio, Djokic Sasa Z., Theoretical interruption model for reliability assessment of power supply systems, *IET Generation, Transmission & Distribution*. 8(4) (2014) 670–681.
- [14] E. Valakevicius, M. Snipas, V. Radziukynas, Markov Chain Reliability Model of Cogeneration Power Plant Substation, *Electronics & Electrical Engineering*. 19(5) (2013) 61–66.
- [15] J.X. Tang, Y.K. Bao, L.C. Wang, C.X. Guo, W.H. Liu, T.P. Wang, An application of CREAM for human reliability analysis in power system switching operation, *Applied Mechanics & Material*. 584-586 (2014) 2585–2588.
- [16] J.X. Tang, Y.K. Bao, P.J. Shi, W.H. Liu, T.P. Wang, C.X. Guo, Research on software implementation of human reliability analysis in power system, *Applied Mechanics & Materials*. 631-632 (2014) 1071–1074.
- [17] Y.K. Bao, J.X. Tang, G. Huang, C.X. Guo, J. Liu, B. Zhou, Impact analysis of human errors on operation reliability in power system, *Applied Mechanics & Materials*. 584-586 (2014) 2597–2603.
- [18] Yu. Fokin, V. Tufanov, Evaluation of reliability of power supply systems, *Energoizdat*, Moscow, 1981.
- [19] A. Malafeev, A. Iuldasheva, Accounting for power flow direction in the problem of structural reliability analysis of power systems, *Russian Electromechanics*. 2 (2015) 36–40.
- [20] V.A. Igumenshev, B.I. Zaslavets, A.V. Malafeev, O.V. Bulanova, Yu.N. Rotanova, The modified method of successive equivalenting for calculation of complex modes of power supply systems, *Industrial Power Engineering*. 6 (2008) 16–22.
- [21] V.A. Igumenshev, A.V. Malafeev, O.V. Bulanova, Y.N. Rotanova, E.A. Panova, A.V. Khlamova, V.M. Tarasov, E.B. Yagolnikova, N.A. Nikolaev, V.V. Zinoviev, Certificate 2012612069 Russia. Programme “The complex of automated modal analysis KATRAN 6.0”. – Publ. in the bulletin “Programme for the computer, database, TIMS”. 2 (2012) 500–501.
- [22] A. Iuldasheva, A. Malafeev, Electricity supply reliability of the industrial enterprises with local power plants and the outage cost evaluation, *Tagungsband zum Power and Energy Student Summit 2015, Dortmund*, 13. und 14. Januar 2015. P01.7.



International Conference on Industrial Engineering

Visual duplicates image search for a non-cooperative person recognition at a distance

Ilya Sochenkov, Aleksandr Vokhmintsev *

Chelyabinsk State University, Br. Kashirinkh 129, Chelyabinsk and 454001, Russia

Abstract

The project is aimed at developing new person recognition algorithm, which deals with the problems using matching of filtered histograms of oriented gradients computed in circular sliding windows and using inverted index of histograms for efficient image retrieval. The project results have various scientific, industry and social applications, which require automatic non-cooperative indoors and outdoors person recognition at a distance using multimodal biometrics extracted from multisensory noisy data. For instance, new security and surveillance systems working under in open weather could be developed based on the proposed methods. The performance of the proposed person recognition algorithm in the actual environment is presented and discussed. The results of computer simulation obtained with the proposed algorithm are compared to those of available algorithms in terms of matching accuracy and processing time.

© 2015 The Authors. Published by Elsevier Ltd. This is an open access article under the CC BY-NC-ND license (<http://creativecommons.org/licenses/by-nc-nd/4.0/>).

Peer-review under responsibility of the organizing committee of the International Conference on Industrial Engineering (ICIE-2015)

Keywords: face recognition, matching algorithm; local oriented gradient histogram; image search; inverted index; histogram analysis; vector-space metrics

1. Introduction

Research in biometric person recognition has recently received a notable attention due to a growing interest in development of new real-time automatic security and surveillance systems. Many of the biometric features that are highly distinctive and have permanence (such as fingerprints and iris) require a cooperative subject in close

* Corresponding author. Tel.: +7-351-799-7134; fax: +7-351-799-7134
E-mail address: sochenkov@gmail.com, vav@csu.ru

proximity to a biometric system. Existing reliable methods of active cooperative identification cannot be used for passive non-cooperative person recognition at a distance. Even under fully favorable conditions (controlled illumination, good image quality, sufficient resolution, frontal images, and neutral expression), the best algorithms of passive non-cooperative face recognition at a distance produce a high equal error rate, and thus, the performance is unlikely to be sufficient for most applications [1]. Therefore, it is extremely important to develop new non-cooperative methods for person recognition at a distance using multimodal biometrics extracted from multisensory noisy data that are robust to uncontrolled environment conditions. Methods of face recognition is one of the most rapidly developing area and they just might provide a basis for constructing a non-cooperative person authentication system. Face recognition systems use different methods for obtaining information: by a single image, by a video, by a three-dimensional image, by using infrared light. Many approaches have developed to allocate face at images or video streams. Once the face is localized, different techniques can be applied on the base of face appearance or face geometry [2]. Facial recognition technology can be global [3] and local [4], different processing methods based on 2D images and 3D face models. Face recognition systems based on 2D images possesses a drawback of sensitivity to light, effects of changing the face position. To compensate these effects, a 2D image is transformed to canonical position storage of facial images from different angles, and recognition uses generalized models of faces. The analysis of three dimensional data can help to overcome the drawbacks: using 3D image interpolation position can be reduced to turn restored 3D face model to a new position, and illumination affects only texture, while reconstruction of the surface retains its properties. Existing recognition methods can be classified as follows: global methods, statistical methods, parametric models. The most popular methods of face recognition are principal component analysis (PCA) [5] and linear discriminant analysis (LDA) [6], elastic graph models, local binary patterns, using 3D descriptors [7-8]. Recent methods of face recognition utilize 3D descriptors invariant to facial expressions, dynamic information, gait analysis and gestures. To achieve 3D face recognition, there are two parts devised: image matching and visual image search [9]. The most popular matching algorithms based on key points are SIFT (Scale Invariant Feature Transform) [10], SURF (Speeded-Up Robust Features) [11] and ORB (Oriented FAST and Rotated BRIEF) [12]. In the current research is considered image search method that uses features, which give an opportunity to detect near duplicates of given image examples by separation from the other images of the collection. The proposed method consists of the following stages: preprocessing, matching and image search. The paper is organized as follows. In Section 2, the proposed matching algorithm based on HOGs descriptor are presented. In Section 3, the visual duplicates image search is considered. In Section 4, using inverted index of histograms for effective image retrieval is considered. Computer simulation results are provided in Section 5. Section 6 summarizes our conclusions.

2. Matching algorithm based on HOGs Descriptor

In this topic a new fast matching algorithm based on recursive calculation of oriented gradient histograms over several circular sliding windows is presented [13]. Let us define a set of circular windows $\{W_i, i = 1, \dots, M\}$ in a target fragment as a set of closed disks:

$$W_i = \{(x, y) \in R^2: (x - x_i)^2 + (y - y_i)^2 \leq r_i^2\} \quad (1)$$

where (x_i, y_i) are the coordinates of the center and r_i — is the radius of the disks. Numerous experiments have shown that the number of circular windows may be chosen from 2 to 4 to yield good matching performance. Histograms of oriented gradients are good descriptors for matching because they possess a high discriminant capability and robust to small image deformations such as rotation and scaling. The histograms are calculated over the sliding geometric structure. At each position of the i -th circular window on a frame fragment we compute gradients inside the window with the help of the Sobel operator. Next, using the gradient magnitudes $\{Mag_i(x, y) : (x, y) \in W_i\}$ and orientation values $\{\varphi_i(x, y) : (x, y) \in W_i\}$, quantized for Q levels, the histogram of oriented gradients can be computed as follows:

$$HOG_i(\alpha) = \begin{cases} \sum_{(x,y) \in W_i} \delta(\alpha - \varphi_i(x,y)), & \text{if } Mag_i(x,y) \geq Med \\ 0, & \text{otherwise} \end{cases} \tag{2}$$

where $\alpha = \{0, \dots, Q - 1\}$ are histogram values (bins), Med is the median value inside of the circular window, and $\delta(z) = \{1, \text{ если } z = 0, 0, \text{ otherwise}\}$ is the Kronecker delta function. The correlation output for the i th circular window at position k can be computed with the help of the fast Inverse Fourier Transform as follows:

$$C_i^k(\alpha) = IFT \left[\frac{HS_i^k(\omega)HR_i^*(\omega)}{\sqrt{Q \sum_{q=0}^{Q-1} (HOG_i^k(q))^2 - (HS_i^k(0))^2}} \right] \tag{3}$$

where $HS_i^k(\omega)$ is the Fourier Transform of the histogram of oriented gradients inside of the i -th circular window over the frame fragment, and $HR_i(\omega)$ is the Fourier Transform of $HOG_i^R(\alpha)$ the asterisk denotes complex conjugate. The correlation peak is a measure of similarity of the two histograms, which can be obtained as follows: $P_i^k = \max_{\alpha} \{C_i^k(\alpha)\}$. The main advantages of the new fast matching algorithm are the following: the total decision is made using the results of combined comparison for all sliding windows; local threshold filtering of histograms is used instead of the classical pyramidal approach of low-pass filtering for speedup of the processing.

3. Visual Duplicates Image Search

Denote by $I = \{a_i | i = 1..K\}$ the image collection. It is necessary to match images from this collection using visual similarity estimation [14]. Each image $a \in I$ is described by vector of features $\Phi(a) = \langle \varphi_1^a, \dots, \varphi_N^a \rangle$. Two images $a \in I$ and $b \in I$ are visual similar, if holds the condition $\rho(a,b) = 1 - f(\Phi(a), \Phi(b)) \geq f_{min}$, where $f(\dots)$ – is any normalized distance (or pseudo distance) in the space R^N , and f_{min} – is boundary value of similarity. Proposing similarity estimation method is based on approach described in [15]. Consider the image as a set of points $P(a) = \{(x,y)\}$. Color value $C(x,y)$ is given for each point in chosen colorspace $\Omega: C(x,y): P(a) \rightarrow \Omega$. We have chosen RGB colorspace for our research. Histograms must provide adequate level of abstraction, therefore we transform the colorspace RGB (2^{24} colors) to lower dimensional colorspace: $\sigma = |\Omega|$ (4, 64, 128, 256 etc. colors). In this way histogram:

$$H_{\sigma}(a) = \langle v_1^a, \dots, v_N^a \rangle, \tag{4}$$

where $v_i^a = |\{(x,y) \in P(a) | C(x,y) = c_i\}| \cdot |P(a)|$, c_i – i -th color channel in the colorspace with dimension σ . In some cases histograms of the whole images with different content could be similar. To account color distribution in different areas of the image we take histograms of the individual segments of the image instead of the full image. Each image $a \in I$ divides into areas $S(a) = \{s_i(a) | i = 1..K\}$ intersection of image areas is allowed. Each segment $s_i(a)$ is square area of original image, $K = r \times r$, where r , is dissection parameter. It is necessary to transform images into square shape to provide possibility of this dissection. For each segment $s_i(a)$ we build histogram $H_{\sigma}(s_i(a))$. Further comparison goes segment-by-segment:

$$\varphi_i^a = v_{i-J\sigma}^{s_{J+1}(a)}, \tag{5}$$

where $i = 1..(r \cdot \sigma)$, $J = [i/r]$, and $[.]$ is the integer part of argument. In this way vector space of features is of dimension $r \cdot \sigma$.

4. Using Inverted Index of Histograms for Effective Image Retrieval

To provide fast search and information analysis on big data could be used special data structures – inverted indexes [16-17]. Each vector component φ_i^a contains information about the relative number of pixels, that has certain color channel from the colorspace Ω in one of the segments – Eq. (5). All components have to be associated

with "histogram words", that characterize original real values $\varphi_j^a, i=1..(r\cdot\sigma)$ [18]. To do this we take finite covering of the interval $[0;1]$ by intervals (they could partially overlap): $\Delta = \{[x; y] | 0 \leq x \leq y, \cup [x; y] = [0; 1]\}$. We associate each component φ_j^a of $\Phi(a)$ to the set of ordered pairs $\xi_j^a = \{ \langle j, i \rangle | \varphi_j^a \in [x_i; y_i], i = 1..|\Delta| \}$. That way we introduce the mapping: $E: R \rightarrow \Lambda$, where $\Lambda = \{ \langle j, i \rangle | j \leq N, i \leq \Delta \}$, that means $\xi_j^a \subseteq \Lambda$. Ordered pairs $\langle j, i \rangle$ we call "histogram words". Here i means natural index of $[x_i, y_i]$, that cover value φ_j^a . This value could be covered by several intervals of Δ . To index features without information loss it is necessary to use quantization with overlapping intervals. Consider mapping $\Sigma: R^N \rightarrow \Lambda$. By the construction of the sets ξ_j^a we have $\xi_j^a \cap \xi_{j'}^a = \emptyset, j \neq j'$, so we take $\Sigma(\Phi(a)) = \cup_{j=1}^N \xi_j^a$. It is a set of "histogram words", which characterize all segments of image. Introduce linear order relation R1 on the set Λ : pair $\langle j, i \rangle$ precedes pair $\langle j', i' \rangle$ if and only if: a) holds condition $j < j'$; b) hold equality $j = j'$ and condition $i < i'$. Equality $i = i'$ in condition b) is impossible because Λ is a set. Therefore using vector $\Phi(a)$ we build the direct index of the image $a \in I$: $DI(a) = \{ \langle j, i, \varphi_j^a \rangle | \langle j, i \rangle \in \Sigma(\Phi(a)) \}$. After that direct index has to be ordered according to order relation R1 by "histogram words" $\langle j, i \rangle$. Inverted index of the image collection associates each "histogram word" $\langle j, i \rangle$ with linearly ordered set: $\Pi(a) = \{ \langle id^a, \varphi_j^a \rangle | a \in I \}$, where id^a is a natural numeric identifier of the image $a \in I$, and the order on the set of pairs $\langle id^a, \varphi_j^a \rangle$ is introduced by id^a . Inverted index is built on image collection using merge of linear ordered direct indexes $DI(a)$. At the stage of visual duplicates search we build vector of features $\Phi(c)$ for reference image c , then we build direct index of the image $DI(c)$, which "histogram words" $\langle j, i \rangle \in \Sigma(\Phi(c))$ are the query to the inverted index. Received for each "histogram word" sets $\Pi(\langle j, i \rangle), \langle j, i \rangle \in \Sigma(\Phi(c))$ are transformed to sets of triplets: $S(\langle j, i \rangle) = \{ \langle id^a, j, \varphi_j^a \rangle | a \in I \}$, $\langle j, i \rangle \in \Sigma(\Phi(c))$ by adding j -th feature from $\Phi(a)$ to $\langle id^a, \varphi_j^a \rangle$. Introduce linear order relation R2 for using merge operation of linear ordered sets $S(\langle j, i \rangle)$: triplet $\langle id^a, j, \varphi_j^a \rangle$ precedes triplet $\langle id^b, j', \varphi_{j'}^b \rangle$ if and only if: a) holds condition $id^a < id^b$; b) hold equality $id^a = id^b$, and also condition $j < j'$. In this way, merge operation of the sets $S(\langle j, i \rangle)$, that are received from the inverted index for each $\langle j, i \rangle \in \Sigma(\Phi(c))$, produces linearly ordered set $S(c)$, which contains information about potentially similar images-candidates, that were detected in the inverted index.

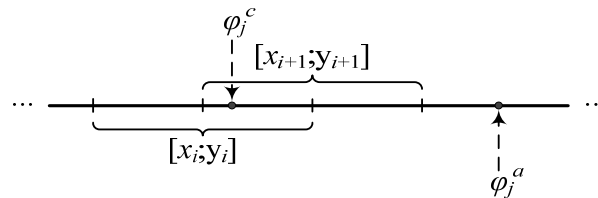


Fig. 1. Difference estimation $|\varphi_j^a - \varphi_j^c|$ based on the length of the intervals

Similarity estimation of reference image and found images-candidates could be performed with help of single-pass algorithm on set $S(c)$ using pseudometric (e.g. based on Manhattan, cosine, Euclidian distances). Pseudometric is not symmetric since we know values φ_j^a not for all j while using inverted index. In fact, we have information extracted from inverted index just about such "histogram words" and values j , for which φ_j^a and φ_j^c are covered by the same interval $[x_i, y_i]$. Otherwise we just estimate $|\varphi_j^a - \varphi_j^c| \geq \max\{y_{i+1} - \varphi_j^c, \varphi_j^c - x_i\}$ – Fig. 1.

5. Computer simulation

For testing we used the following databases: Labeled Faces in the Wild, 3D Mask Attack Dataset, Texas 3D Face Recognition Database. The proposed algorithm outperforms the common algorithms for in-plane rotation (Table 1), yields a similar performance with the SIFT for out-of-plane rotation and a slight scaling, and requires processing time close to the SURF. One variation of the visual duplicates image search method based on inverted index of color histograms was implemented and experimentally-verified. The inverted index of color histograms was performed using library MongoDB (Python). Tests were performed on two subsets of the whole collection each containing 1000 random images. All the images were transformed to the size 640*512 pixels using linear filter [19]. These

subsets were verified by experts to contain similar images. The first dataset was used to optimize the quality of search and find the parameters for indexing. The second dataset is used to test image search quality with these parameters. The optimal parameter set is presented in Table 2.

Table 1. Accuracy of image matching for in plane rotations

Matching algorithm	Accuracy of matching				
	0.8X	0.9X	1.0 X	1.1X	1.2 X
Scale Invariant Feature Transform	92	95	100	98	91
Speeded-Up Robust Features	79	90	99	97	92
Oriented FAST and Rotated BRIEF	78	79	90	83	89
Proposed algorithm	84	94	100	99	91

Table 2. Optimized parameters

Amount of segments	Overlay, %	Amount of color channels in histogram
16	7	24

We took $\alpha=0.05$ as a length of each interval of Δ with overlap $\beta=0.025$, and used pseudometric based on Manhattan distance. We compare the baseline (“Base”) method that uses «brute force» for similarity estimation (reference image is being compared with each image from the Dataset-X). Method «InvIndex» is associated to visual duplicates image search using inverted index for each Dataset-X. The quality of visual duplicates image search is shown in Table 3. Gain in time using inverted index is 80% in comparison with “Base” method. With rising size of collection advantage of inverted index became greater. Person recognition or tracking algorithms usually employ prediction methods for evaluation of the person position and trajectory in a sequence of frames and for reduction of the search region [20]. The proposed algorithm in terms of the processing time are the following characteristics: 0.64 s. Therefore, a real time tracking based on the proposed algorithm becomes possible.

Table 3. Quality of visual duplicates image search

Method	Dataset-1	Dataset-2
Precision of image search		
Base	92	80
InvIdx	88	78
Recall of image search, %		
Base	92	79
InvIdx	90	74
F1-Measure of image search, %		
Base	92	80
InvIdx	89	76

6. Conclusion

In this paper a matching algorithm based on recursive calculation of oriented gradient histograms over several circular sliding windows for face recognition at a distance was presented.. The simple method of color histogram comparison solves the task of near duplicates visual search with a good quality. The experimental results show that inverted index provides a good level of information abstraction. With correct setup of parameters it does not lead to significant information loss. The greater the size of an image collection is, the greater is the gain in time using

inverted index. Inverted index could be used to preselect a small set of similar images-candidates (in compare with the whole collection), and then similarity estimation for these candidates could be calculated on full sets of features. In such case recall of candidate retrieval is preferable than precision.

Acknowledgements

The work was supported by the Russian science foundation, grant № 15-19-10010.

References

- [1] S. Garduño-Massieu, V. Kober, Face recognition in real uncontrolled environment with correlation filters, Proc. SPIE's Annual Meeting: Applications of Digital Image Processing XXXV. 8499 (2012) 849928-1.
- [2] R. Brunelli, T. Poggio, Face recognition: Feature versus templates, IEEE Trans. on Pattern Analysis and Machine Intelligence. 15 (1993) 1042–1052.
- [3] T. Kim, J. Kittler, Locally Linear Discriminant Analysis for Multimodally Distributed Classes for Face Recognition, IEEE Trans. on Pattern Analysis and Machine Intelligence. 27 (2005) 318–327.
- [4] V. Blanz, P. Grother, J. Phillips, T. Vetter, Face Recognition Based on Frontal Views Generated from Non-frontal Images, In IEEE Conf. on Computer Vision and Pattern Recognition. (2005) 454–461.
- [5] T. Papatheodorou, D. Rueckert, Evaluation of 3D face recognition using registration and PCA, Conf. Audio- and Video-based Biometric Person Authentication. (2007) 997–1009.
- [6] P.M. Aguilar-Gonzalez, V. Kober, V.H. Diaz-Ramirez, Adaptive composite filters for pattern recognition in nonoverlapping scenes using noisy training images, Pattern Recognition Letters. 41 (2014) 83–92.
- [7] A. Moreno, A. Sanchez, J. Velez, F.Diaz, Face recognition using 3D surface extracted descriptors, In Irish Machine Vision and Image Processing Conference. (2003) 10.
- [8] Y. Lee, H. Song, U. Yang, H. Shin, K. Sohn, Local feature based 3D face recognition, Int. Conference on Audio- and Video-based Biometric Person Authentication. (2007) 909–918.
- [9] N. Dalal, B.Triggs, Histograms of oriented gradients for human detection, IEEE Computer Society Conference on Computer Vision and Pattern Recognition. 1 (2005) 886–893.
- [10] D.G. Lowe, Object recognition from local scale invariant features, IEEE Proc. 7th Int. Conf. on Computer Vision. 2 (1999) 1150–1157.
- [11] H. Bay, A. Ess, T. Tuytelaars, L. Van Gool, SURF: Speeded Up Robust Features, Comput. Vis. Image Underst. 110 (2008) 346–359.
- [12] E. Rublee, V. Rabaud, K. Konolige, G. Bradski, ORB: an efficient alternative to SIFT or SURF, Proc. IEEE Int. Conf. on Computer Vision. (2011) 2564–2571.
- [13] V. Kober, Robust and Efficient Algorithm of Image Enhancement, IEEE Transactions on Consumer Electronics. 52 (2006) 655–659.
- [14] S. Murala, A.B. Gonde, R.P. Maheshwari, Color and texture features for image indexing and retrieval, IEEE International Advance Computing Conference. (2009) 1411–1416.
- [15] D.M. Squire, W. Müller, H. Müller, J. Raki, Content-based query of image databases, inspirations from text retrieval: inverted files, frequency-based weights and relevance feedback, Pattern Recognition Letters. (1999) 143–149.
- [16] M. Stricker, A. Dimai, Color indexing with weak spatial constraints, SPIE Proceedings. 2670 (1996) 29–40.
- [17] D.M. Chen, Inverted Index Compression for Scalable Image Matching, DCC. (2010) 525.
- [18] A. Vokhmintsev, A. Makovetskii, V. Kober, I. Sochenkov, V. Kuznetsov, A fusion algorithm for building three-dimensional maps, Proceedings. SPIE's Annual Meeting: Applications of Digital Image Processing XXXVIII. 9599 (2015) 9599–81.
- [19] A. Makovetskii, A. Vokhmintsev, V. Kober, V. Kuznetsov, Frequency analysis of gradient descent method and accuracy of iterative image restoration, Analysis of Images, Social Networks and Texts, Springer International Publishing. (2015) 109–118.
- [20] V.H. Diaz-Ramirez, O.G. Campos-Trujillo, V. Kober, P.M. AguilarGonzález, Real-time tracking of multiple objects using adaptive correlation filters with complex constraints, Optics Communications. 309 (2013) 265–278.



International Conference on Industrial Engineering

Characteristics and Calculation of Cavitation Mixers

Spiridonov E.K *

South Ural State University, 76, Lenin Avenue, Chelyabinsk, 454080, Russian Federation

Abstract

It is shown that one of the most efficient ways to obtain emulsion is cavitation treatment of the mixed stream in the jet boundary layer. The authors offer a model for calculating the operational process in the hydrodynamic mixer with multiple-jet nozzle as agitator of cavitation, based on hydrodynamic equations and data of experimental research on jet pumps. There has been considered and analyzed the characteristic of the cavitation mixer, which shows how relative loss of total stream pressure depends on relative nozzle square, and hydraulic resistance coefficient of flow-part elements. It is shown that gradual reduction of hydraulic resistance coefficient allows to decrease considerably the loss of total stream pressure. Besides, there exists the range of optimal relative square values where losses of total pressure are minimized. If the elements of the mixer flow-part are made hydraulically proper then the optimal values of the nozzle relative square are 0,66...0,76, whereas minimum losses of relative pressure don't exceed 0,22.

© 2015 Published by Elsevier Ltd. This is an open access article under the CC BY-NC-ND license (<http://creativecommons.org/licenses/by-nc-nd/4.0/>).

Peer-review under responsibility of the organizing committee of the International Conference on Industrial Engineering (ICIE-2015)

Keywords:

1. Introduction

An urgent task of machine building, power engineering, chemical, oil and food manufacturing industries is to develop efficient and low-power mixer to prepare emulsions. For instance, in heat-power engineering burnout of diesel oil emulsion in steam boiler furnace units allows to reduce toxicity of stack gases, and if there is an optimum choice of parameters of fuel burnout and preparation of diesel oil emulsion, environmental and technical-and-economic indexes of boilers will be increased [1]. However, application of high capacity mixers helps to prevent disposal of wastewater contaminated by petroleum products into environment.

* Corresponding author.

E-mail address: spiridonovek@susu.ac.ru

The quality of emulsion is characterized by structure homogeneity and dispersion degree of components. Consequently, operational efficiency of mixers, i.e. devices for emulsion preparation, significantly depends on the preparation method. Creation of highly-dispersive emulsion by means of traditional mechanical stimulation of flow components is rather complicated. Cavitation treatment of mix elements, which generates local energy concentration (pulsations and cavitation bubble collapse) enough for diffusion of medium components on the micro level, allows to obtain highly-dispersive product resistant to breaking. [2]. Literature review devoted to cavitation in jet pumps has shown that one of the most efficient ways to create emulsion is cavitation in the jet boundary layer [3]. At the same time to increase emulsion dispersion degree it is necessary to equally distribute cavitation points along the standard cross-section of the flow, and to enlarge their number when possible. One of such devices – agitators of cavitation is a multiple-jet nozzle with equally spaced holes which form several high velocity jets in a flow-part of a mixer.

The goal of this research is to perform calculation and analysis of characteristics of the jet cavitation mixer.

2. The schematic diagram and calculation model, characteristics of the hydrodynamic mixer

The schematic diagram of the jet mixer is shown in Figure 1. The mixer consists of a nozzle (1), the mixing chamber (2), and diffuser (3). The acceleration of a mixed stream and its dispersion into high-speed jets takes place in a multi-jet nozzle, where further in the jets' boundary layers cavitation is initiated. Cavitation treatment of the flow results in the breakdown of jets and formation of highly dispersed medium. Due to equal distribution of cavitation points along the standard cross-section of the flow at a certain distance from the nozzle (1) vapor-liquid turbulent flow is formed in the mixing chamber (2) which further turns into low flow in the condensation shock. As a result emulsion is created near the outlet section of the mixing chamber. In a diffuser the part of kinetic energy of emulsion flow transforms into potential one. The pressure thus increases to the value smaller than before the mixer.

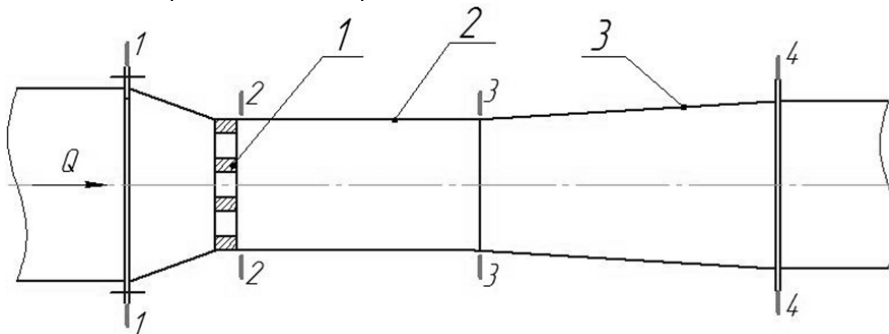


Fig.1. The schematic diagram of the hydrodynamic ejector.

Input equations which describe operational process in a mixer are the equations of balance of consumption:

$$Q = v_i A_i = const; \quad (1)$$

and specific energy of flow in the area between sections 1-1 and 4-4:

$$\bar{p}_1 = \bar{p}_4 + \zeta_C \frac{\rho v_2^2}{2} + \frac{\rho v_3^2}{2} (\zeta_K + \zeta_D) + \Delta \bar{p}_P \quad (2)$$

Bernoulli equations for the mixed stream in the area between sections 1-1 and 2-2:

$$\bar{p}_1 = \frac{\rho v_2^2}{2} (\alpha_C + \zeta_C) \quad (3)$$

expression of the Euler number Eu which characterizes cavitation phenomena in the jet boundary layer:

$$Eu = \frac{p_2 - p_{II}}{\frac{\rho v_2^2}{2}} \quad (4)$$

where ρ - density of the mixture; p_{II} - equilibrium *vapor pressure* of mixture component with minimum boiling point; Q - volume flow rate of the mixture; i - number of section on the schematic diagram; A_i, v_i, p_i - square of the normal cross section, average velocity and static pressure in « i »-th section, \bar{p}_1, \bar{p}_4 - total (static plus dynamic) pressure at the input ($i=1$) and output ($i=4$) mixer section; $\zeta_s, \zeta_k, \zeta_d$ - coefficients of hydraulic resistance of the nozzle, mixing chamber and diffuser; α_C - the coefficient of kinetic energy of the mixed stream at the nozzle exit ($i=2$); $\Delta \bar{p}_p$ - specific energy loss due to abrupt deceleration of the stream from the exhaust velocity v_2 of liquid mixture from nozzle holes to velocity v_3 of the emulsion in the mixing chamber upon its total filling.

According to the theory of Borda-Carnot [4]:

$$\Delta \bar{p}_p = \rho \frac{(v_2 - v_3)^2}{2} \quad (5)$$

Simultaneous solution of these equations (1)-(5) results in the formula:

$$\Delta h = \frac{\bar{p}_1 - \bar{p}_4}{p_1 - p_{II}} = \frac{\zeta_C + (\zeta_k + \zeta_d) \cdot \Omega^2 + (1 - \Omega)^2}{\alpha_C + \zeta_C + Eu} \quad (6)$$

which is an expression of the basic characteristic of the hydrodynamic mixer, which establishes the relationship of the relative head flow loss Δh of the relative square of the nozzle $\Omega = A_2 / A_3$, cavitation Euler number Eu , coefficient of hydraulic resistance of the flow-part elements.

In the following works [5] an empirical formula of the relationship of the Euler cavitation Eu , and the relative square of the nozzle is proposed.

$$Eu = 0.07 + 1.36(1 - \Omega) \quad (7)$$

With regard to the latter Figure 2 shows performance characteristics of the cavitation mixer with a kinetic energy coefficient $\alpha_C=1$ and several values of hydraulic resistance coefficients.

By comparing the lines, we can see that a steady decline in the hydraulic resistance coefficients of the flow-part elements allows to significantly reduce the losses of pressure in the mixer, and for each set of resistance coefficients there is a range of optimal values of the relative square of the nozzle, where the pressure losses are minimal.

For example, with a resistance coefficient of the nozzle $\zeta_s = 0.14$, the mixing chamber and diffuser $\zeta_k + \zeta_d = 0.4$ minimum relative pressure losses are $\Delta h_{min} = 0,255$ with relative square of the nozzle $\Omega_{opt} = 0.6$; and at $\zeta_s = 0.06$, $\zeta_k + \zeta_d = 0,2$ $\Delta h_{min} = 0,185$ when relative square of the nozzle is $\Omega_{opt} = 0.76$.

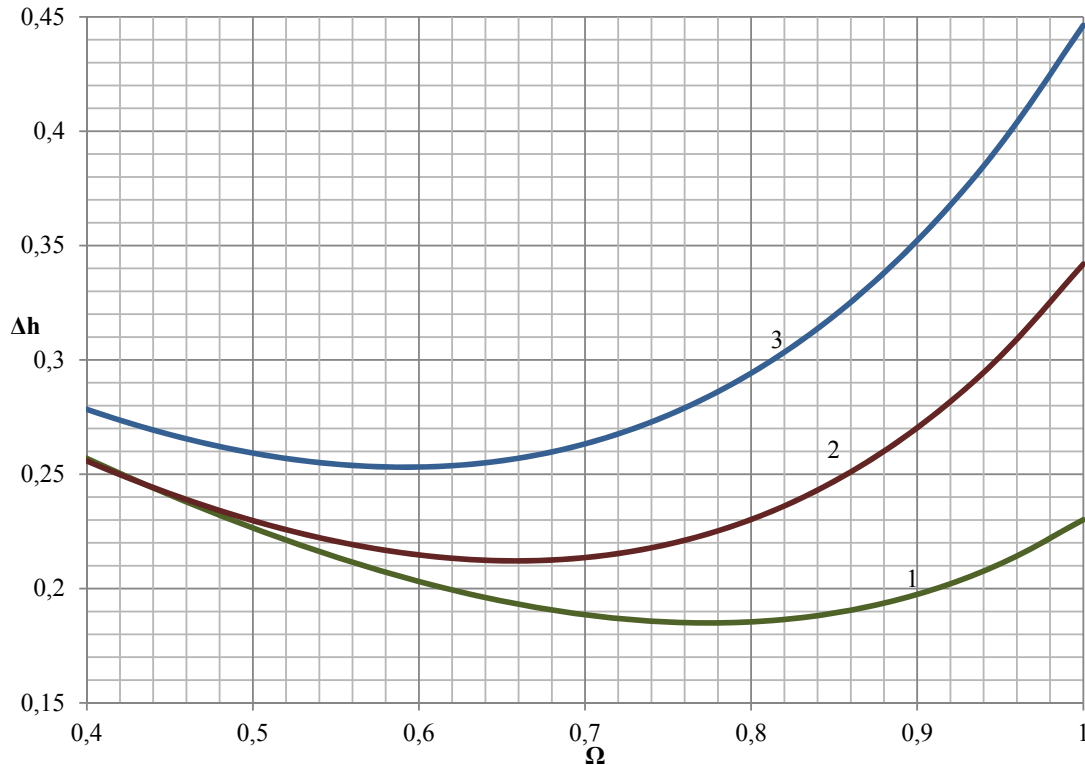


Fig. 2. Performance characteristics of the cavitation mixer when $\alpha_c=1$: 1 – $\zeta_c=0,06$; $\zeta_k+\zeta_{st}=0,2$; 2 – $\zeta_c=0,1$; $\zeta_k+\zeta_{st}=0,3$; 3 – $\zeta_c=0,14$; $\zeta_k+\zeta_{st}=0,4$.

3. Conclusion

Hydraulically perfect performance of the flow-part elements of the cavitation mixer and the optimum relationship between the nozzle square and the mixing chamber square are the basic requirements for the development of the cavitation mixer.

References

- [1] V. Tausher, Technology of Static Mixing, J. Chemical and Petroleum Engineering. 3 (1996) 26–32.
- [2] V.I. Kormilitsyn, M.G. Lyskov, A.A. Rymunskiy, Integrated Biocompatible Compression Technology of Water-Oil Emulsion and Natural Gas with the Addition of Waste Water. J. Teploenergetika. 9 (1996) 13-17.
- [3] N.V. Golub, Combustion Efficiency of Water-Oil Emulsion in Industrial CHP Plants, VTI, Moscow, 1985.
- [4] R.Y. Akchurin, Preparation of Fuel Oil for Burning in a Cavitation Reactor, J. Energetik. 9 (1986) 8–9.
- [5] A.I. Popov, N.V. Golub, V.I. Yerofeyev, Reducing Emissions from Water-Oil Emulsion Combustion, J. Energetik. 2 (1983) 11–14.
- [6] V.M. Ivanov, The Fuel Emulsion, Publishing House of the USSR Academy of Sciences, Moscow, 1962.
- [7] O.M. Yahno, N.N. Yaske, A.D. Koval, Features of Cavitation Technology of High Viscosity Fluids Mixing, J. Chemical and Petroleum Engineering. 3 (1996) 23–25.
- [8] M.A. Promtov, Prospects for Cavitation Technologies Use for Chemical-Engineering Processes Intensification, J. Vestnik TSTU. 4 (2008) 861–869.
- [9] R. Knapp, J. Daily, F. Hammit, Cavitation, Mir, Moscow, 1974.
- [10] I. Peirsol, Cavitation, Mir, Moscow, 1975.
- [11] L.G. Podvidz, Cavitation Properties of Jet Pumps, J. Vestnik mashinostroeniya. 3 (1978) 17–20.
- [12] N.L. Sanger, A Jet Pump Cavitation Prediction Parameter, ASME Fluids Engineering Meeting, 1968 Cavitation Forum, Pamphlet Publication. (1968) 10-18.
- [13] V.K. Temnov, Basic Theory of Fluid Ejectors, ChPI, Chelyabinsk, 1971.

- [14] V.K. Temnov, O.A. Perepletchik, Critical Cavitation Coefficient of Liquid Ejectors, *J. Dynamics of Hydro Pneumatic Systems*. 197 (1978) 82–87.
- [15] V.K. Temnov, E.K. Spiridonov, *Calculation and Design of Liquid Ejectors: textbook*, ChPI, Chelyabinsk, 1984.
- [16] E.K. Spiridonov, *Energy Analysis of Gas-Liquid Flows*, Winter School on Continuous Media Mechanics (12th): Abstracts. All-Russian conf., Ural Branch of Russian Academy of Sciences, Yekaterinburg, 1999.
- [17] E.K. Spiridonov, *Energy Analysis of Liquid Jet Gas Flows*, *J. Vestnik of SUSU. A series of "Mechanical Engineering"*. 1 (2003) 151–155.
- [18] A.D. Girgizov, *Fluid Mechanics (Hydraulics): textbook for Universities*, third ed., rev. and add., Publishing House of the Polytechnic University, St. Petersburg, 2007.
- [19] D.N. Popov, S.S. Panaiotti, M.V. Ryabinin, D.N. Popov, *Hydromechanics: textbook for Universities*, Publishing House of the MSTU, Bauman, Moscow, 2002.
- [20] I.E. Idelchik, M.O. Steinberg, *Handbook of Hydraulic Resistance*, third ed., rev. and add., Engineering, Moscow, 1992.
- [21] A.D. Altschul, *Hydraulic resistance*, second ed., rev. and add., Nedra, Moscow, 1982.



International Conference on Industrial Engineering

Investigation of the oil strength as a complex index of its condition

Barushev V.I., Laiko K.K.*

South Ural State University, 76, Lenin Avenue, Chelyabinsk, 454080, Russian Federation

Abstract

The laboratory studies on the strength of oil were carried out by stretching it in the bellows and identified the opportunity of the strength index usage as a complex and diagnostic factor. The burst pressure and tensile modulus are used as a measure of strength. The authors study the ratio of burst pressure and the physical properties (viscosity, density, mass fraction of solids, acidity, flash point, etc.) of engine oils. The correlation with high reliability for the viscosity and the flash point is detected. This fact expands the opportunities of modeling oil viscosity and hydrodynamic cavitation.

© 2015 The Authors. Published by Elsevier Ltd. This is an open access article under the CC BY-NC-ND license (<http://creativecommons.org/licenses/by-nc-nd/4.0/>).

Peer-review under responsibility of the organizing committee of the International Conference on Industrial Engineering (ICIE-2015)

Keywords: oils, indicators of quality, durability, cavitation processes, evaluation, monitoring, diagnostics.

1. Introduction

The usage of the high-quality oil, in other words the oil with required characteristics, continues to remain among the foundations and reserves of enhancement of machines' sustainability. The composition and the condition of oil determine cavitation mode. The principle of this occurrence in the hydraulic transmission is the insufficient strength that is connected with its aging treatment and impurity: the particles become the centers or cores of oil discontinuity in addition to gas ones, and it causes the strength loss. The cavitation can significantly impair the operation of the hydraulic transmission, destroy its construction units and devices. So the main objective of these investigations is to determine the methodic opportunity of oil's strength usage as a aggregated factor of its condition and the opportunity of oil's diagnose by its cavitating characteristics [1, 3, 4].

* Corresponding author. Tel.: +7-912-798-6-793;
E-mail address: ivnt_atya@mail.ru

2. Strength physical bodies

In science and engineering the comprehension of strength is broad. It is connected with the all types of materials and machineries disintegration as physical agents, with all types of actions of external forces, aggregative and limit states or deformations. Therefrom static and dynamic strength, or strength on compression, strain, fatigue, etc.

Up to the present moment there are two conceptions in the strength investigations:

- Purely physics – the science of objects and their surfaces defects' influence on theoretical;
- Purely engineering – the science of physicochemical influence of condition and circumstances on mechanical behavior of actual materials and machineries.

Fig. 1 demonstrates a universal scheme that shows strength's rules in science and technology. The curve is based on the basic law about the dependence of the potential energy and interacting force of the insulating particles from the distance between them. The molecular forces of attraction and repulsion or resistance to compression and tensile strain determine the strength of particles' interaction independent from the hypothesis about their physical nature.

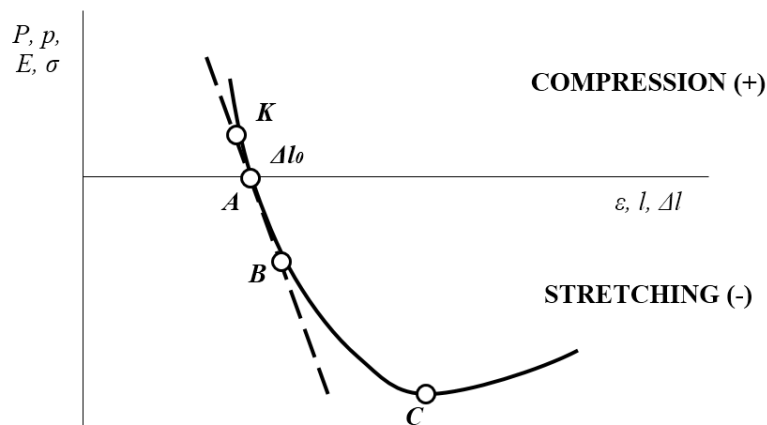


Fig. 1. The law (the resultant curve) of the physical agents' particles interaction.

The zero point A corresponds to the equilibrium state when attractive and repulsion forces counteract each other in the case of absence of outside forces, so their resultant force equals zero on the resultant curve. The dependence is approximated as a linear one at the initial section AB. Therefore the repulsion forces decrease faster than the attractive forces in the situation of stretching, in other words when the distance between the particles grows. However, at the point C the curve has its maximum that determines the outside force's magnitude which is sufficient for the beginning of the progressive system breakdown and the depth of so called "the potential hole" which corresponds to the energy E of the particles' dissociation in the process of the system breakdown. So it is reasonable to lay it down that the point B which indicates the getaway of the stretching from the linear law is the check point for the process evaluation.

This rule is among fundamental ones in engineering science as a technical reflection of physics. Consequently, in material science and in the theory of strength of materials this rule is illustrated as a diagram of stretching which fixes the dependence of materials' stretching ε from strain σ . At the diagram the section AB that is congruent with the theoretical straight line corresponds to the elastic deforming region, particularly the metals of polycrystal structure. In the region of the elastic deformations (the section BC and further) the values of stretching and strain are not connected identical but they depend on the defects of construction and composition. In the material the existence of the pollution's particles as the phases appears the essential factor of the materials' strength reduction. The point B is indicative and can be taken as valuating and check in this case.

In tribology such a regularity appears in the all types of friction. On condition of unlubricated friction – when direct proportionality between the shear force and the displacement in the primary stage of the process is seen. On condition of boundary friction such a curve (diagram) represents a dependence of oil boundary film's deformation on the solid bodies' (phase's) surface from the pressure [4].

In this case the diagram represents relevant modulus of elasticity and tensile strength of oil boundary films under the one-way compression (crush) and abruption. The last notion corresponds to the notion of adhesion as an adhesive-cohesive counterstand of oil boundary film to the abruption in the normal plane. In this case on the initial phase *AB* of the process or of the curve the dependence of the oil film's deformation from the pressure (strain) can be taken as linear, but with another modulus of elasticity than in the situation of compression. It is notable that the section of pressure and compression that are correspond to the linear motion of the curve seizes the values of this magnitude from null (point A) to the high-high ones that appear in practice (point K).

The limit of the asymptotic section of the curve with the point C and further corresponds to tensile strength under such a oil layer thickness when the value of disruptive force is indicated not by boundary but by volumetric characteristics of the layer.

The quantitative and qualitative changes stipulate each other; the rule determines an inverse dependence: the qualitative changes conduce to the quantitative changes. The transformation is discrete and continuous at the same time: discontinuity is represented as quantum leap and continuity – as quantitative changes. Thus the process of oil stretching is constituted from three stages or modes that are gas development, evaporation and boiling. And they also determine gas, gas-steam and steam cavitation in oil.

3. Destruction of oil

The petroleum oil contains relatively large quantity of air in view of its extremely porous structure that is determined by its specific molecular structure and composition that provide its low density as a measure of packing.

Gas content and gas development are extremely essential background factors that determine liquids' strength. In particular the investigations [2] show that the tension stress can measure up $\sigma=27$ MPa. In the case of vapor free oil and high purity of unit. In such conditions the strength of water reaches the value of $\sigma \leq 0.5$ MPa.

During the gas development (the first stage or mode) the growth of the air bubbles' quantity and sizes takes place in the oil, in other words, the free surface increases that leads to (the second stage or mode) the intensive evaporation of the oil with the enlargement of quantity and sizes of the gas-steam bubbles. Their growth and confluence lead to the cold boiling of the oil (the third stage or mode) [2–4].

Each of the three stretching process' stages must be represented by its own physics bubble model. But it's problematic to represent and to describe these models objectively even if it's practically possible. It is connected with the complexity of the cavitation processes where a huge amount of bubbles at the same time comes up, grows up, blows out and collapses momentary, so they influence on each other's and liquid's indexes in general [3].

In chemmotology, especially in chemmotology of hydraulic gear, the volumetric oil's strength is represented by cavitation characteristics that reflect a technical compatibility of oils with the speed, power and temperature operating modes of hydraulic gear [2, 5]. It is notable for example that from a practical standpoint the minimum permissible pressure on entering the pump is usually not limited to the prime steam pressure but to the pressure of the permissible amount of air separation from oil. This pressure is significantly higher and is determinative for the current rip and the pump output reduction. That's why the determination of the discharge pressure influence on the pump output is a technical substance of its cavitating characteristics.

For example, according to the investigations [2] the absolute pressure at the pump's absorption reached 220, 425, 500 and 585 millimeters of mercury in accordance with the temperature of 18, 40, 60 and 100 °C when operated at the oil I-20A which causes bubbling. It is worth noting that the heavy vapor pressure of this oil amounted to about 1 millimeter of mercury at the temperature of 60 °C. Today the most common recommendation for minimum allowed value of the pump's operational pressure input is 0.08 MPa

The essential factor of oils' strength reduction is the presence of the embedded particles, in other words – inclusions, because naturally the oil matures and becomes soiled in operation. That's why the oils are represented as the suspensions and emulsions that are the multiphase systems. All these impurities are the defects of a system that

decrease the oil's surface tension. Also they are the cores or centers of primordial seats of oil's destruction and decrease of its strength in particular.

4. Laboratory research

The investigations of different factors' influence on the oil's strength are conducted for a long time. The large variety of strength indexes and methods for their determination testify the complexity of the liquids' strength investigation as a characteristic, an effect or a process. Thus the equilibrium vapour pressure (All-Union state standard 1756), tensile stress, negative pressure, burst pressure, etc., are accepted as a strength index [5]. Centrifugal, bellows-sealed, piston and other methods are used as methods of the liquid's breaking strength investigation.

It must be taken as the most preferable the investigation of oils' strength by the method of their stretching in a bellow valve with the assessment of the toughness' change and the nature of the change. The fact is that a metallic bellow valve fits into totally leakproof and relatively easily deformable shell of the definite volume of the oil. The viscid, cohesive, adhesive forces resist better to oil's stretching in the volume of its adsorb boundary film of the vast space that are also exposed to the slide because of the goffer's deformation.

The following ideas were taken as a basis of our investigation.

1. The method of the investigation is bellows-sealed as the most simulative for the deformation up to oil's definite volume abruption which is caused by micro- and macromovement of the slide valves, pistons, etc. in the hydraulic drive.

2. The stretching as a deformation is opposite in sign to the compression and is characterized by the similar molecular mechanism: the molecules are under the effect of the stretching efforts that aspire to change the surface tension, molecular structure and density of the oil. In this behalf its strength together with the burst pressure or pulling stress can be estimated for the tensile modulus which is similar to the pressure modulus, as the production of the pressure p_p that causes a deformation, and ratio of the initial volume W_0 to its excess ΔW :

$$\beta_p = -\frac{p_p \cdot W_0}{\Delta W}.$$

The scientific and practical value of the tensile modulus' usage is that the tensile stress is relating to the unit of volume in this case, so, the complete model of oil as a three-dimensional solid is used. In particular, for this purpose the possibility exists for taking into account (leaving out) a dry bellow valve's amenability by analogy with the valuation of a coil's amenability which can be evaluated by the characteristic λ that is like a displacement of a goffer under the influence of a fixed load (equal to 10 N) or by the characteristic δ which represents the modulus to density of a bellow valve as a value that is opposite to the amenability.

3. The oils are the strictly dosed and well-balanced compositions of the range of the petroleum hydrocarbons' factions and groups. The oils are like the multiple-component or multiphase system (emulsion, suspension) that determines their relative strength as a display of variation of different materials' interparticle interaction's forces. The cavitation stages in the oil in such an order as gas development, evaporation and boiling can be designated as the external manifestations. It is naturally that a peculiar tensile modulus and a section of a curve of the law of stretching must correspond to each of these cavitation's stages or modes.

4. A comparison (overlapping) of the current curve of the oil's strength with the basic, prelusory or preliminary one can be a foundation of oils' quality diagnostic by the method of standard dependences, i.e. transient characteristics.

In this case the investigations were conducted on the multilayer bellow valves that are made from the corrosion-resistant steel (flexible high-pressure hoses) in 3 versions. The characteristics of the most utilizable bellow valve (№2) are described at the fig. 2.

The fig. 2 illustrates one of the boundary curves of the most oil rigidity in the bellow valve's composition during the investigation in normal conditions ($t=20$ °C, $p=1$ atm). In this case for the purpose of the rise of the

experiment’s objectivity the double scale of the bellow valve’s movement was used during the elaboration. It allows to register the bellow valve’s rigidity in graphic form in the process of testing of oil’s rigidity and strength. Thus for the targeted load through the relevant point B the movement (0.02 mm) of the bellow valve with oil can be defined on the curve of the bellow valve’s deformation. And after that its movement and the expended load (0.2 mm, 4 N) can be defined by the relevant point in the of the dry bellow valve’s characteristics.

The calculation demonstrates that the pressure in the oil will be about 10 kPa under the bellow valve’s load (about 10 N).

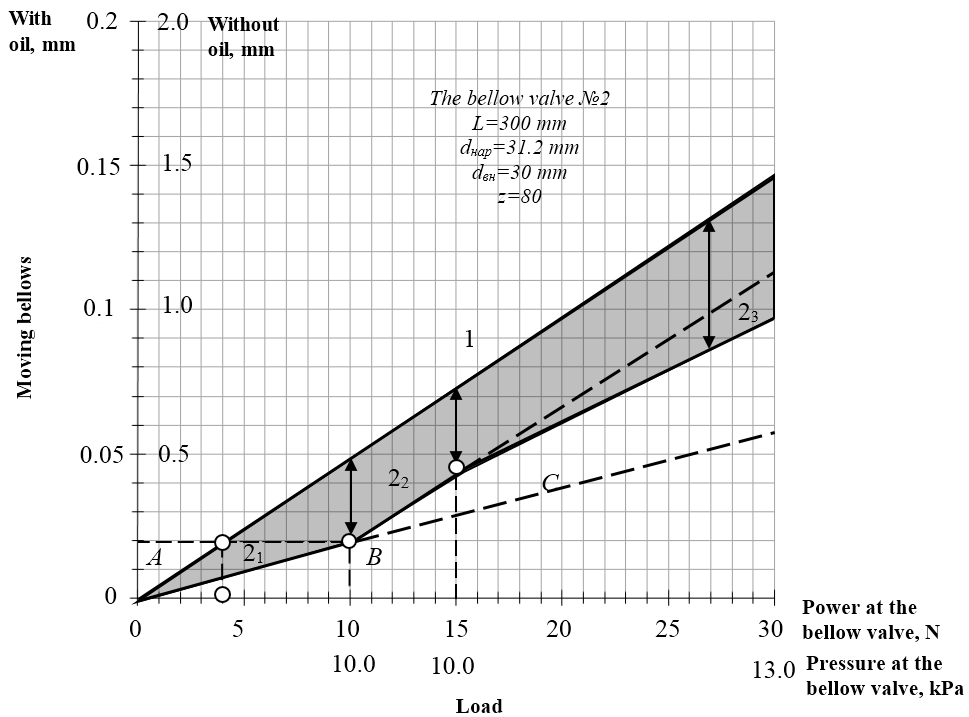


Fig. 2. The indicative trend of the oil deformation under the stretching in the bellow valve’s composition: 1 – dry bellow valve; 2 – bellow valve with compressor oil Kp-8S.

The regularities of the oil’s deformation that are described at the picture 2 correspond to the regularities that are distinctive for the processes of the materials’ abruption. For example, for this case the rigidity of the oil with the bellow valve is a lot higher than the rigidity of the bellow valve.

The beginning of the curve AB (2_1) is like an indicative linear dependence of the movement from the load for the stage of gas development in this case. The change of this dependence in the point B at the part BC (2_2) of the curve can be explained by the oil’s viscosity reduction which is caused by the intensive production of the bubbles because of the gas development and evaporation of the light fractions of the oil. Then there is a stage (higher than the point C) of the oil’s rigidity increase due to the resistance growth under the enlargement of the velocity of the oil’s flow with the froth balance increase.

Therefore, the method of the control of the bellow valve’s deformation with the oil in it is acceptable for the diagnostic of the oil’s condition for its strength index.

The investigations demonstrated that this method allows controlling the oil’s condition of viscosity with its strength. There are the examples of dependence of the burst pressure on the oil ranges’ viscosity at the fig. 3.

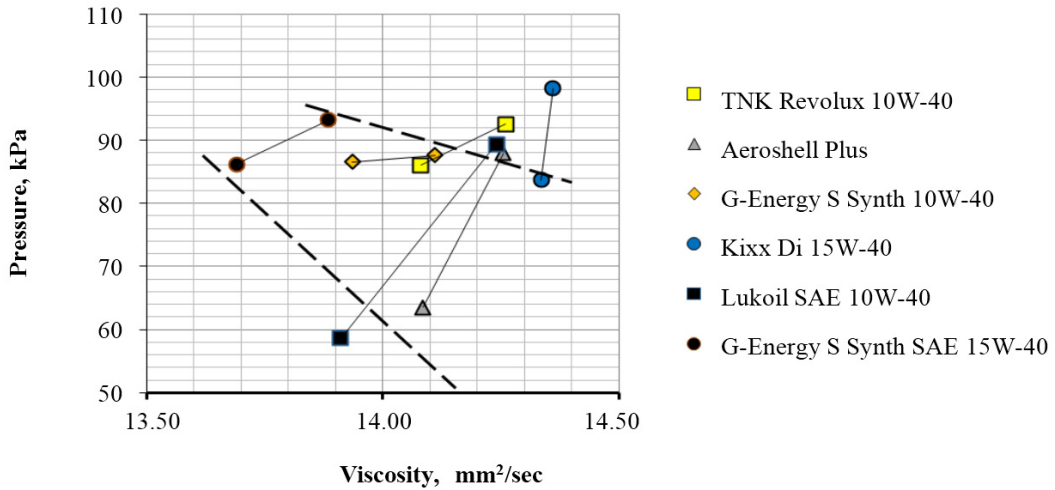


Fig.3. The influence of the oil (mark) viscosity on its strength.

Fig. 3 illustrates the oil viscosity that is indicated at the oil grade and corresponds to the temperature of 100 °C while the investigations were held under the normal temperature of 20°C. Naturally, the oil strength increase with the viscosity growth, as a rule. The results of the investigation of the oil-flash temperature influence on the oils' strength that are illustrated at the fig. 4 lend support to it.

The presented dependences are determined by the chemical and fractional composition of oil and by the quantity of volatile fractions of hydrocarbons, in particular, that is taken into account in the process of their classifications. Thus, the oils are classified by their composition into mineral, mineral with synthetic additives, semisynthetic and synthetic. It is must be taken into account during processing of the results of the researches similar to the held ones. The general conclusion over the investigations that were held is that the oil strength can be used as a complex index of its condition and can be measured indirectly by the bellows method.

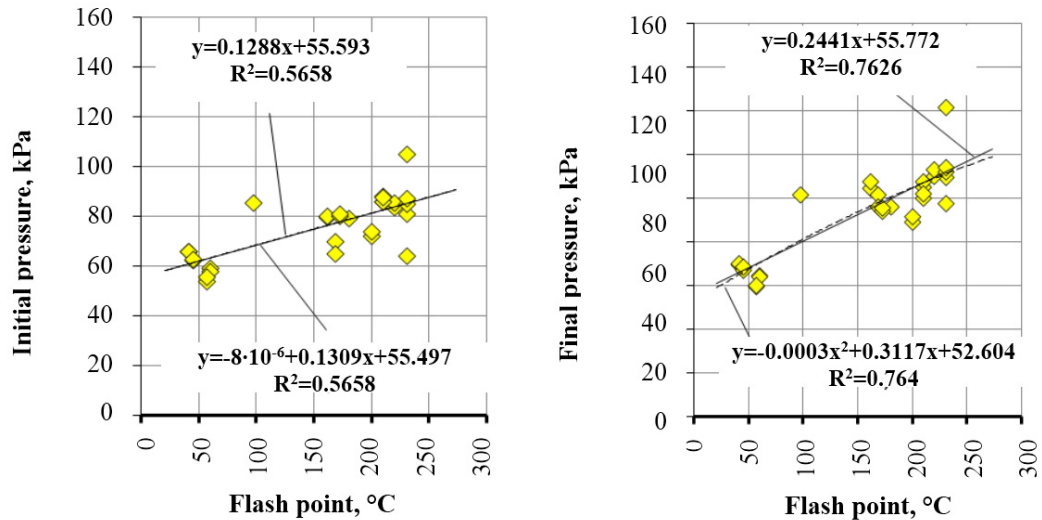


Fig. 4. The change of the oils' burst pressure depending on the oil-flash temperature.

Table. 1. Tensile modulus.

Oil	THK-Revolutux" SAE 10W-40	Aeroshell Plus	G-Energy S Synth SAE 10W-40	Kixx Di 15W-40	Lukoil SAE 10W-40	G-Energy S Synth SAE 15W-40
β_p	22.59	14.29	15.36	8.16	14.12	21.59

5. Conclusion

The introduction to engineering practice of the indexes of the oil strength that are deduced by the method of their stretching in the bellow valve, i.e. static cavitation, expand the opportunities of their viscosity modeling essentially and also the hydrodynamic cavitation that includes gas, gas-steam, steam and in the machines. In particular, a polyharmonic pressure pulsation takes place at the side of absorption of the volume hydraulic pump as well as at the pressure side [5]. The magnitude of the pressure pulsation at the side of absorption increase with the growth of the injection pressure. Wherein the growth of the magnitude caused by the increase of the maximum value and by the reduction of the minimum value of the oscillatory pressure. The decrease of the minimum pressure to the absolute zero is possible under the increase of the pressure. It is evidence of the dynamic cavitation at the side of the absorption of the hydro machine under the high enough value of the medium pressure.

The presence of the strength characteristics allows preventing or limiting this fact because it sets the optimal ranges of oils usage in a specific machine upon the viscosity, temperature and pressure.

References

- [1] V.I. Barushev, K.K. Laiko, Strength criteria of working fluids, Vestnik PNIPU. 35 (2013) 64–82.
- [2] V.I. Barushev, K.K. Laiko, Basics of experimental determination of the strength of the working fluids Vestnik YUUrGU. 2 (2013) 105–112.
- [3] V.I. Barushev, K.K. Laiko, Problems of experimental measurement of the strength of working fluids, Izvestiya samarskogo nauchnogo tsentra rossiyskoy akademii nauk. 14 1(2) (2012) 332–334.
- [4] T.M. Bashta, I.Z. Zaychenko, V.V. Ermakov, E.M. Khaitovici, Volumetric hydraulic actuators, Obemnye gidravlicheskie privody, Mashinostroenie, Moscow, 1969.
- [5] P. Knepp, D. Daily, F. Hammit, Cavitation, Mir, Moscow, 1974.
- [6] L.A. Kondakov, Working fluids and sealing hydraulic systems, Mashinostroenie, Moscow, 1982.
- [7] Y.M. Orlov, Fluid mechanics, hydraulic machines and hydraulic drive bases missile systems, Izdatelstvo permskogovoennoho instituta raketnyh voisk, Perm, 2001.
- [8] V.A. Hohlov, Electro-hydraulic servo drive, Nauka, Moscow, 1964.



International Conference on Industrial Engineering

Prediction of stress-life curve of a material under random or cyclic loading with asymmetry

Erpalov A.V.^{a*}, Shefer A.P.^a

^a South Ural State University, 76, Lenin Avenue, Chelyabinsk, 454080, Russian Federation

Abstract

Estimation of structures fatigue life under dynamic loading remains an unexplored area in the field of mechanical engineering. Accounting the asymmetry under operational loading is one of features of durability computation for a part of a structure. Common methods of asymmetry considerations result in significant errors in the lifetime of computed structures. This paper describes the methodology approach that allows to predict a fatigue curve for any asymmetry coefficients using the results of a limited number of tests with symmetry and asymmetry under random or cyclic loading. This approach is based on the experimental results of the herein presented research. The scattering signature of the material is necessary for fatigue probability calculations. The methodology also presents the recipes for prediction of fatigue curve and scattering signature with the given asymmetry coefficient and given probability of failure.

© 2015 The Authors. Published by Elsevier Ltd. This is an open access article under the CC BY-NC-ND license (<http://creativecommons.org/licenses/by-nc-nd/4.0/>).

Peer-review under responsibility of the organizing committee of the International Conference on Industrial Engineering (ICIE-2015)

Keywords: S-N curve; Asymmetry loading; Random loading; Cyclic loading; Scattering signature.

1. Introduction

Currently, coefficient ψ_σ is used for the estimation of fatigue life of a structure under asymmetric loading [1-4]. It is assumed that the Haigh diagram of stress is described by single straight line, and the value of the coefficient ψ_σ varies within a small range for various materials. According to [5], coefficient ψ_σ varies from 0.1 to 0.2 for carbon steels, and from 0.2 to 0.3 for alloyed steels. The selection of a value for a material is difficult and it does not

* Corresponding author. Tel.: +7-351-267-90-62
E-mail address: aerpalov@ya.ru

correlate well with the experimental results in most cases. It is worth noting that the majority of researches study the cyclic loading [6-9], while random loading with asymmetry remains poorly explored [10, 11].

The purpose of this study is to determine the influence of asymmetry loading on the fatigue curve of a material under cyclic or random loadings.

Nomenclature

ψ_σ	coefficient of Haigh diagram
σ_a	stress amplitude value
S	standard deviation of stress value
μ	asymmetry coefficient
σ_m	mathematical expectation value of stress
R_m	tensile strength of a material
G	loading process structure parameter
$\lg N$	logarithm of the lifetime
A	constant parameter of fatigue curve
B	constant parameter of fatigue curve
S_0	standard deviation of stress value corresponding to unbounded value fatigue strength
P	probability of failure
r	correlation coefficient
S_s	standard deviation of endurance strength
v_s	coefficient of variation
\bar{S}	expectation value of endurance strength
$S_{\lg N}$	standard deviation of lifetime logarithm
t_q	inverse normal distribution for the failure probability

2. Fatigue curve equation

Random asymmetrical loading process cannot be characterized by the standard parameters for the cyclic process without schematization of the original stress history. For example, the standard for the cyclic process stress amplitude σ_a is not a valid parameter for random process. In this case, the amplitude for the random process is replaced by the standard deviation (S) of stress value. For cyclic loading with amplitude σ_a , the standard deviation of stress value is calculated by

$$S = \frac{\sigma_a}{\sqrt{2}}. \quad (1)$$

In this paper, the asymmetry coefficient for cyclic and random loadings is defined as the ratio of the mathematical expectation value of stress σ_m to tensile strength R_m of the material:

$$\mu = \frac{\sigma_m}{R_m} \quad (2)$$

The processes of loading (cyclic and random) characterize the combination of the following parameters described in [12]: the mathematical expectation value of stress σ_m , the standard deviation of stress value S and the loading process structure parameter G . The number of the intersections by the process of the mean level of the mathematical expectation with the positive sign of the process derivative is taken as the lifetime of the random process. For the cyclic loading the value N_0 is the number of cycles. There are many methods to process the results of fatigue tests [13-17]. The algorithm described in [12] is used in this work. The expectation of logarithm of the lifetime $\langle \lg N \rangle$ is described by S-N curve equation:

$$\langle \lg N_{0i} \rangle = A - B \lg(S_i - S_0). \quad (3)$$

3. Fatigue tests

The research was performed using random and cyclic types of loading. Flat-shaped specimens made of light alloys AMg-61 and MA-15 were tested (see Fig. 1). Chemical compositions of the tested alloys are given in Tables 1 and Table 2. Fatigue properties of specimens were tested by the electrodynamic shaker *LDS V780* that allows cyclic or random loading of different bandwidths. Description of the equipment is given in [18].

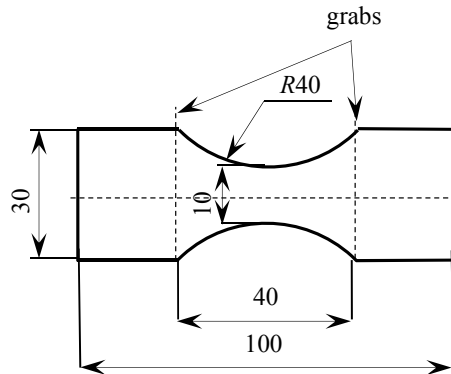


Fig.1. Geometry of specimen.

Table 1. Chemical composition of AMg-61 alloy (in %)

Mg	Al
5,70	94,30

Table 2. Chemical composition of MA-15 alloy (in %)

Mg	Al	Si	Ca	Fe	Zn	Cd
85,74	6,76	0,39	0,41	0,42	1,60	4,68

At each stress level at least six specimens were tested. The specimens were tested until complete failure.

4. Analysis of the results

From the test results of AMg-61 alloy, the fatigue curves under cyclic and random loadings for the symmetry and asymmetry with the probability of failure $P = 0.5$ were obtained using Eq. 3. (see. Fig. 2). Each point in these plots is the expectation of logarithm of the lifetime corresponding to the stress level. From the plots it is hard to assess if the curves are parallel to each other thus we have to use different variables: the standard deviation of stress value S and the asymmetry coefficient μ .

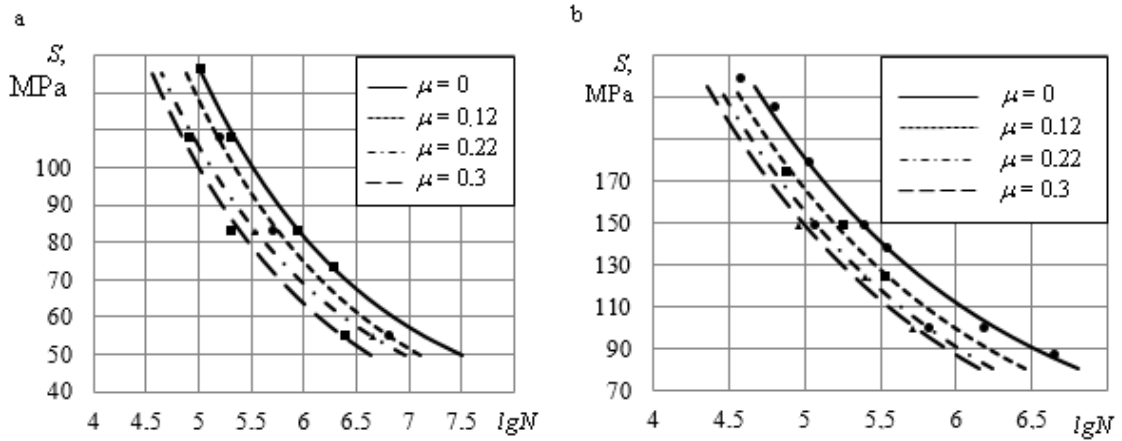


Fig. 2. (a) fatigue curves of AMg-61 alloy under random; (b) cyclic loadings with asymmetry.

According to [19], the range of interest for the high cycle fatigue life corresponds to $lgN = 4 \dots 7$ for calculating the lifetime of structures. Therefore, the set of lifetimes $lgN_i = \{4; 5; 6; 7\}$ in increments of $lgN = 1$ was selected. The values of standard deviation of stress for each lifetime lgN_i were found using the plots of fatigue curves (see Fig. 2) and Eq. 3, accounting for asymmetry. Points in Fig. 3 are well fitted with the linear function with correlation coefficients are $r > 0,993$. Each line corresponds to different value of lifetime logarithm.

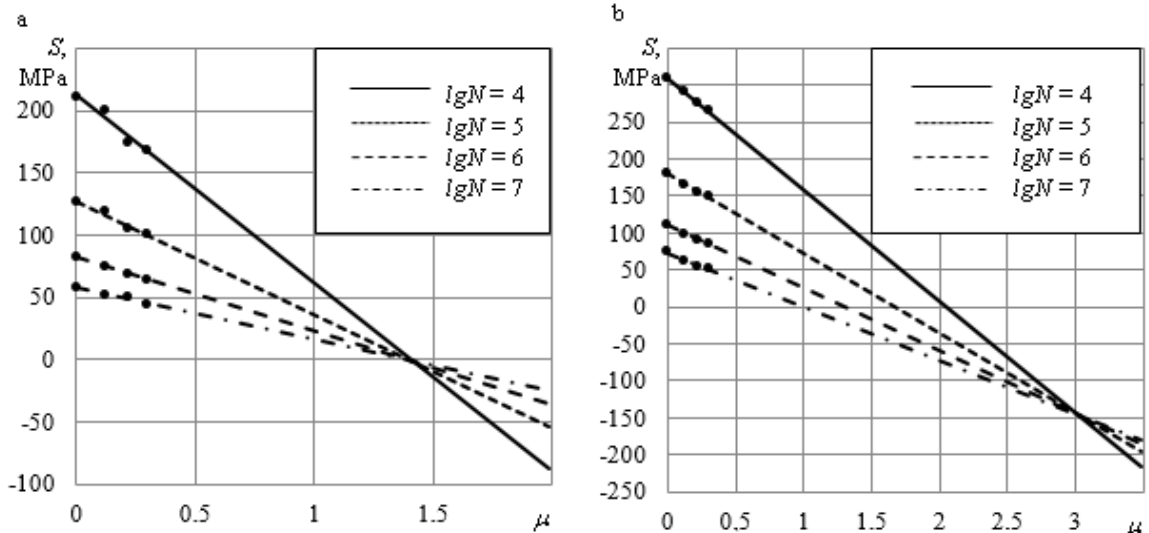


Fig. 3. (a) standard deviation of stress S vs. asymmetry coefficient μ for AMg-61 alloy under random; (b) cyclic loadings.

As can be seen from Fig. 3, all lines converge in one point. However, as tests have shown, coordinates of this point depend on the loading process structure parameter G and cannot be predicted due to limited number of tests. It should be noted that the point of convergence of all lines has no physical meaning because it lies outside the region of tensile strength of the material.

In order to verify the tests results, the vibration tests of MA-15 alloy under cyclic loading with asymmetry have been performed. The plots of fatigue curves and relations of standard deviation of stress value S to the asymmetry

coefficient μ are shown in Figure 4. As seen from the plots, the lines converge in a single point, same as in the case of AMg-61 alloy.

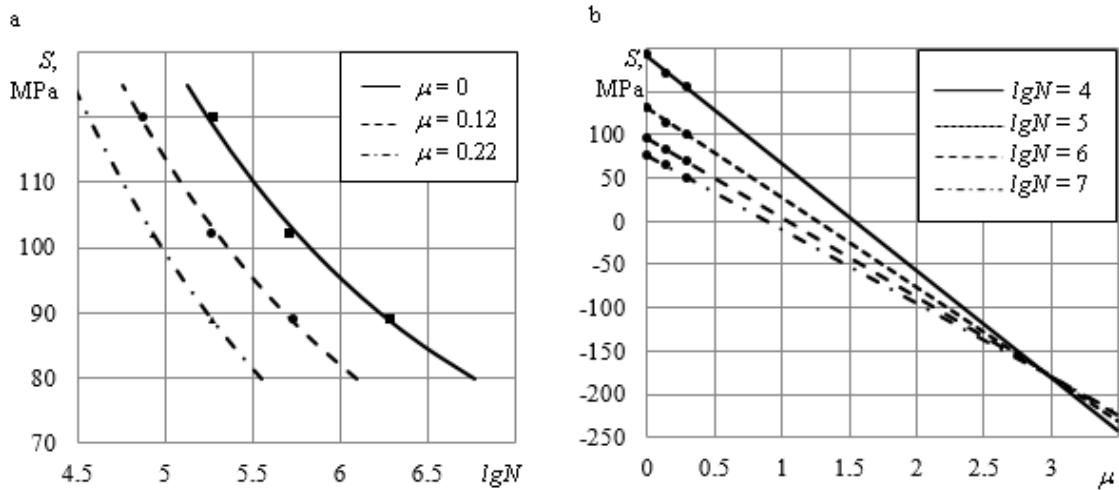


Fig. 4. (a) for cyclic loading, fatigue curves of MA-15 alloy with asymmetry; (b) standard deviation of stress S vs. asymmetry coefficient μ .

The analysis of the plots shows the possibility of predicting fatigue curves with asymmetry. It is sufficient to perform fatigue tests under symmetric loading and just one additional test with an arbitrary value of asymmetry. Then, one needs to plot linear graphs of standard deviation of stress value S vs. asymmetry coefficient μ . If the lines converge in single point, then test results are correct. Thus, for any value of the asymmetry coefficient μ one can find the corresponding standard deviation of stress value S for each line. The number of these lifetime lines can be increased by adding more values lgN . Thus, it is possible to obtain the points $(lgN; S)$ that are processed as in [12] and obtain the material fatigue curve for a given asymmetry with failure probability $P = 0.5$.

For the probability calculation of lifetime it is necessary to know the characteristics of scattering signature of a material under asymmetric loading. Dispersion of endurance strength obeys the normal distribution and may be estimated from the standard deviation – S_s . However, in practice it is convenient to use the relative value – a coefficient of variation v_s instead of S_s . According to [20], coefficient of variation v_s is a constant value and does not depend on number of cycles to fracture

$$v_s = \frac{S_s}{S} = const . \tag{4}$$

The coefficient of variation can be found from the standard deviation of lifetime logarithm S_{lgN} [20]:

$$v_{si} = \frac{2.3 S_{lgN_i} (S_i - S_0)}{B S_i} \tag{5}$$

Thus, the standard deviation of stress value S with a failure probability can be calculated as follows:

$$S = \bar{S} \pm t_q S_s \tag{6}$$

According to Eq. 4:

$$S = \bar{S} \pm t_q v_s \bar{S} , \tag{7}$$

Consider the relationship of the standard deviation of stress value S and the asymmetry coefficient μ for AMg-61 alloy under random loading from Fig. 5, where two solid lines for $lgN = 5$ and $lgN = 7$ lifetimes were plotted. For

each experimentally obtained point, the confidential interval with confidence level $t_q = 3$ was obtained using Eq. 7. The regression values through the points were plotted in Fig. 5 using dashed lines. The smallest correlation coefficient is $r = 0.995$. These lines show the scattering signature for the failure probability.

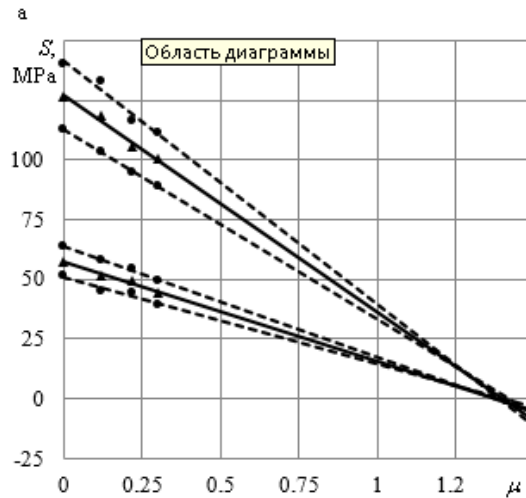


Fig. 5. Standard deviation of stress S vs. asymmetry coefficient μ for AMg-61 alloy under random loadings, and scattering signature.

5. Conclusions

The methodology has been developed and implemented. It has predicted fatigue curves of a material with different asymmetry under cyclic and random loadings using limited experimental tests. Furthermore, the methodology allows accounting for the scatter signature of a fatigue curve and plots this fatigue curve with given asymmetry and failure probability.

References

- [1] J. Schijve, *Fatigue of Structures and Materials*, CBS Publishers, New Delhi, 2009.
- [2] A.V. Zhelubovskiy, A.D. Pogrebnjak, M.N. Regulski, A.T. Sagitov, Y.V. Klyuchnikov, P.V. Kondrashev, Reserve estimate of strength of machine parts subject laden with asymmetrically, *Easter-European Journal of Enterprise Technologies*. 66 (2013) 8–12.
- [3] V.P. Golub, E.S. Kochetkova, A.D. Pogrebnjak, Metodika postroeniya diagrammy predel'nykh napryazheniy pri asimmetrichnom mnogotsiklovom nagruzhenii, *Industrial laboratory. Materials diagnostics*. 72 (2006) 42–48.
- [4] M. Nihei, P. Heuler, C. Boller, T. Seeger, Evaluation of mean stress effect on fatigue life by use of damage parameters, *International Journal of Fatigue*. 8 (1986) 119–26.
- [5] L.M. Shkol'nik, *Metodika ustalostnykh ispytaniy*. Spravochnik, Metallurgy, Moscow, 1978.
- [6] Ying Xiong, Yanyao Jiang, Fatigue of ZK60 magnesium alloy under uniaxial loading, *International Journal of Fatigue*. 64 (2014) 74–83.
- [7] Johannes Dallmeier, Otto Huber, Holger Saage, Klaus Eigenfeld, Uniaxial cyclic deformation and fatigue behavior of AM50 magnesium alloy sheet metals under symmetric and asymmetric loadings, *Materials and Design*. 70 (2015) 10–30.
- [8] Guozheng Kang, Yujie Liu, Zhao Li, Experimental study on ratchetting-fatigue interaction of SS304 stainless steel in uniaxial cyclic stressing, *Materials Science and Engineering*. 435–436 (2006) 396–404.
- [9] M. Liakat, M.M. Khonsari, An experimental approach to estimate damage and remaining life of metals under uniaxial fatigue loading, *Materials and Design*. 57 (2014) 289–297.
- [10] Tadeusz Lagoda, Ewald Macha, Roland Pawliczek, The influence of the mean stress on fatigue life of 10HNAP steel under random loading, *International Journal of Fatigue*. 23 (2001) 283–291.
- [11] Krzysztof Kluger, Tadeusz Lagoda, Fatigue lifetime under uniaxial random loading with different mean values according to some selected models, *Materials and Design*. 28 (2007) 2604–2610.
- [12] L.A. Shefer, A.V. Erpalov, D.Kh. Valeev, Obobshchennaya diagramma ustalosti materialov pri deystvii razlichnykh sluchaynykh, harmonicheskikh i poligarnicheskikh protsessov, *Industrial laboratory. Materials diagnostics*. 82 (2015) 58–62.

- [13] S.A. Faghidian, A. Jozie, M.J. Sheykhloo, A. Shamsi, A novel method for analysis of fatigue life measurements based on modified Shepard method, *International Journal of Fatigue*. 68 (2014) 144–149.
- [14] Yong Xiang Zhao, A fatigue reliability analysis method including super long life regime, *International Journal of Fatigue*. 35 (2012) 79-90.
- [15] Qin Sun, Hong-Na Dui, Xue-Ling Fan, A statistically consistent fatigue damage model based on Miner's rule, *International Journal of Fatigue*. 69 (2014) 16–21.
- [16] G. Zonfrillo, A. Rossi, A fuzzy approach for drawing S–N curves in the finite life region, *Fatigue & Fracture of Engineering Materials & Structures*. 34 (2011) 868–876.
- [17] Adam Niesłony, Khalid el Dsoki, Heinz Kaufmann, Peter Krug, New method for evaluation of the Manson–Coffin–Basquin and Ramberg–Osgood equations with respect to compatibility, *International Journal of Fatigue*. 30 (2008) 1967–1977.
- [18] A.V. Erpalov, L.A. Shefer, E.E. Rikhter, P.A. Taranenko, Ustalostnye ispytaniya materialov i konstruktsiy s ispol'zovaniem sovremennogo oborudovaniya, *Bulletin of the SUSU, Series "Mechanical engineering industry"*. 15 (2015) 70–80.
- [19] V.P. Kogaev, N.A. Makhutov, A.P. Gusenkov, *Raschety detaley mashin i konstruktsiy na prochnost' i dolgovechnost'*. Spravochnik, Mashinostroenie, Moscow, 1985.
- [20] L.A. Shefer, *Veroyatnostnye metody rascheta resursa i zapasov prochnosti nesushchikh elementov konstruktsiy transportnykh system*, SUSU Published, Chelyabinsk, 2000.



International Conference on Industrial Engineering

Research and testing complex for analysis of vehicle suspension units

Novikov V.V.^a, Pozdeev A.V.^{a,*}, Diakov A.S.^b

^aDepartment of Automatic Units, Volgograd State Technical University, Volgograd, Russia

^bDepartment of Wheeled Vehicles, Bauman Moscow State Technical University, Moscow, Russia

Abstract

Volgograd State Technical University (Russia) has collaborated with BISS-ITW (India) and Test Rigs (Russia) to develop a unique research and testing servo-hydraulic complex designed to study various vehicles suspension units to determine their elastic-damping characteristics and vibration isolation properties. Bench equipment allows to test individual suspension components (hydraulic and gas-filled shock absorbers, coil springs, leaf springs, shock absorber struts, pneumatic and hydro-pneumatic springs, wheels and tires, bushings) and the single support suspension unit as an assembly with sprung mass corresponding to the real load on the wheel. The test program set the operating modes of the suspension units at the kinematic and force excitation using servo-hydraulic equipment that is controlled by a special software suit. The capabilities of the test rig allow to obtain the real characteristics of the tested suspension system elements and a comprehensive assessment of their efficiency in the modes which are typical for operating conditions of the vehicle suspension.

© 2015 The Authors. Published by Elsevier Ltd. This is an open access article under the CC BY-NC-ND license (<http://creativecommons.org/licenses/by-nc-nd/4.0/>).

Peer-review under responsibility of the organizing committee of the International Conference on Industrial Engineering (ICIE-2015)

Keywords: test rig; dropulser; testing program; loading mode; suspension units; suspension characteristics; efficiency of vibration isolation.

1. Introduction

Testing of the vehicle suspension units and determination of their characteristics is performed on various types of special and universal test rigs. Industrial plants mainly use test rigs that have narrow functionality. They are usually

* Corresponding author. Tel.: +7-987-643-8514

E-mail address: avp24897@mail.ru

designed for endurance tests of a particular suspension element or suspension unit with the wheel. However, suspension systems development requires universal multifunctional test rigs that would allow to test various types of suspensions and wheels in conditions similar to operational modes of loading [1-25].

Volgograd State Technical University (Russia) with the companies BISS-ITW (India) and “Test rigs” (Russia) developed a unique research and testing servo-hydraulic complex intended for analysis of the characteristics and vibration isolation properties of the various vehicles suspension units. The versatility of the test rig equipment allows testing individual elastic and damping elements of the suspension system, and the single-support suspension unit as an assembly with sprung mass corresponding to the real load on the wheel. In 2015, research and testing servo-hydraulic system was installed at the Department of Automatic Units of the Volgograd State Technical University and included in the equipment of the Testing Laboratory of the university.

2. Structure and functionality of the rig

The main structural elements of the rig are horizontal support base 1, hydropulsers 2, vertical post guide 3 with moving frame 4 and loads 5 simulating the sprung mass, and winch 6 (Fig. 1).

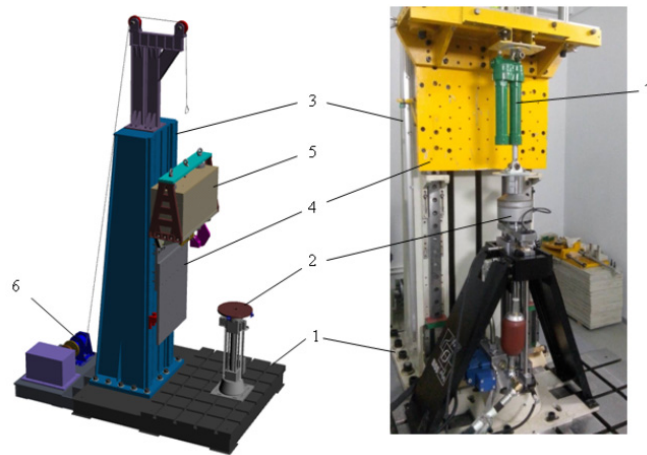


Fig. 1. Solid model and photographic image of the test rig:

1 – base frame stand, 2 – hydropulsers, 3 – vertical post guide, 4 – movable frame, 5 – loads, 6 – winch, 7 – the test element

In addition, the system comprises a pumping station with a radiator and servo-hydraulic valves, a box for electronic control of the test rig operation modes and for recording the registered parameters. The rig can test hydraulic and gas-filled shock absorbers, coil springs, leaf springs, shock absorbers struts, pneumatic and hydro-pneumatic springs, wheels and tires, bushings, single-support suspension units with the sprung mass corresponding to the real load on the wheel.

Main parameters of the research and testing servo-hydraulic complex are given in table 1.

Test program sets various operation modes of the suspension units at kinematic and force excitation using servo-hydraulic equipment controlled by a special software complex.

Dynamic modes of operation of the rig provide:

- force excitation of the test element with a given vibration spectrum to determine its performance (in a closed loop);
- kinematic excitation of the test element by vibration within a given spectrum with the free vertical movement of the moving loads simulating the sprung mass of a vehicle relatively to the frame of the rig to determine forced oscillations (in an open loop), including undulation road test simulation, road profile playback of different levels;

- definition of the free-damped oscillations of the sprung mass by the method of pull-up, drop or set a single hydropulsor of the kinematic momentum;
- determination of power characteristics of the test element when simulating free fall horizontal force on the basis of the definition of the contact force interaction.

Table 1. The main parameters of the rig

Parameter	Value	Dimension
Hydropulsor stroke range	10 ⁻⁶ –0,5	m
Hydropulsor stroke speed range	0,001–2,4	m/s
Hydropulsor rod oscillation frequency range	0,0001–50	Hz
Hydropulsor maximum force:		
- during compression (test element tension)	50	kN
- during tension (test element compression)	12	
Test element maximum vertical dimension	1,5	m
Main modes of the hydropulsor operation:	harmonic triangular rectangular random	
Sprung mass range	0,2–2	t
Movable loads vertical stroke range	± 0,25	m
Maximum force of the winch	30	kN
Winch cable speed range	0,01–0,1	m/s

Using the instrumentation and sensors it is possible to record absolute and relative vertical displacements (deformations), velocities and accelerations of the sprung and unsprung masses of the vehicle suspension and hydropulsor rod, vertical force in the test element attachment point on the stem of the hydropulsor, friction forces, pressure and temperature in the working cavity and on the surface of the test elements. Multifunctional system of fixtures, fasteners and holes provides versatility and modular design of the rig (Fig. 1), because it's mechanical part can be quickly adapted to various configurations and geometries of the test elements.

Fig. 2 shows a high-pressure hydro-pneumatic spring of a special-purpose vehicle, a suspension unit consisting of shock absorber strut, spring and pneumatic wheel, and a gas-filled shock absorber mounted on the rig.

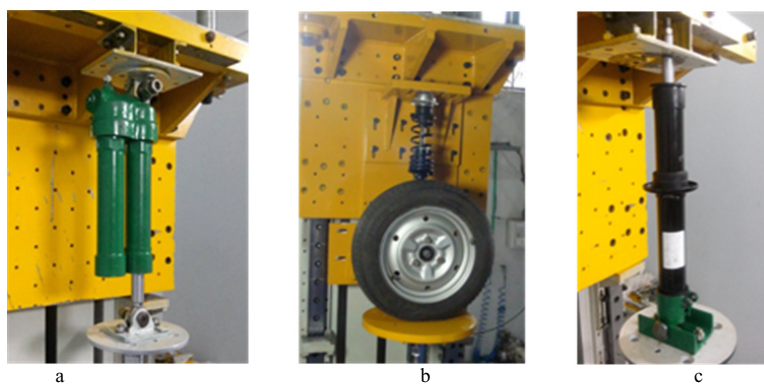


Fig. 2. (a) A high-pressure hydro-pneumatic spring of a special-purpose vehicle, (b) a suspension unit consisting of shock absorber struts, springs, and pneumatic wheels, and (c) a gas-filled shock absorber mounted on the rig

Examples of the recorded force curves while testing various suspension units in a closed loop are shown in Fig. 3.

Fig. 3 (a, b) presents a series of force curves of gas-filled shock absorbers for BMW X5 (Fig. 3,a) and Hyundai Sonata (Fig. 3,b) recorded when using a multi-stage program mode.

Fig. 3 (c, d) shows single force curves of the springs with linear and nonlinear elastic characteristics. The force curve in Fig. 3(c) relates to leaf springs, and Fig. 3(d) shows a force curve of a high-pressure hydro-pneumatic spring (in this case, the spring pressure is 2.0 MPa) at various amplitudes and frequencies of vibrations.

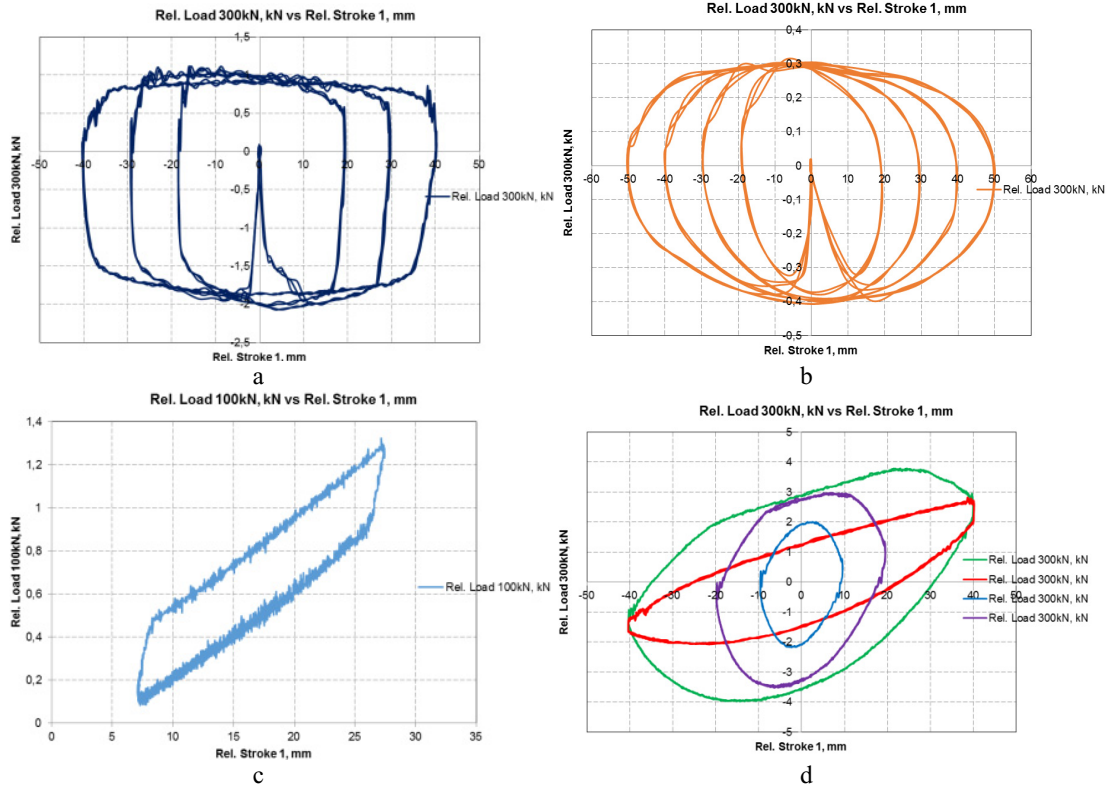


Fig. 3. Force curves for tested gas-filled shock absorbers (a, b), leaf springs (c) and a hydro-pneumatic spring (d).

The software as well as the hardware of the test complex has a number of features that differentiate a new rig from the previously known analogues. The first feature is the ability to control the operation of the hydropulsor through the channels of force and displacement. The second feature is automatic and manual fine-tuning PID-parameters of the high-speed servo valve. The third feature includes a mode of loading history and multistage programming of the test modes which can be generated standard forms of loading and operator input loading profiles.

3. Conclusion

Research and testing servo-hydraulic complex allows registering actual characteristics of the test elements of the suspension system and comprehensive assessment of their effectiveness in the typical operating conditions of the vehicles suspension. This results in the reduction of material and time costs, and improvement of the accuracy of the results when checking the technical condition of the elements of the suspension system, configuration management systems, its internal characteristics, the development of new types of suspension elements and algorithms for controlling their properties depending on the desired operating modes and specified test conditions.

References

- [1] Nosov N.A. Raschet i konstruirovaniye gusenichnykh mashin [Calculation and design of tracked vehicles], Leningrad, Engineering Publ., 1972, 560 p.
- [2] Derbaremdiker A.D. Gidravlicheskie amortizatory avtomobily [Hydraulic shock absorbers of vehicles], Moscow, Engineering Publ., 1979, 236 p.
- [3] Pevzner Ya.M. Kolebaniya avtomobilya. Ispytaniya i issledovaniya [The vibrations of the car. Testing and research], Moscow, Engineering Publ., 1979, 208 p.
- [4] Gubin V.V., Kulikov A.O., Shevchuk V.P. Methods and means of tractors suspension bench testing [Metody i sredstva stendovykh ispytaniy podveski traktorov], Dinamika kolesnykh i gusenichnykh mashin: mezhvuz. tem. sb. [Dynamics of wheeled and tracked vehicles: interuniversity thematic collection], Volgograd, 1980, pp. 89-96.
- [5] Ryabov I.M., Kotelnikov V.N., Kolmakov V.I. Stend dlya ispytaniya uprugikh elementov [Rig for testing of elastic elements], the Copyright certificate of the USSR No. 1041903, 1983, Bull. No. 34.
- [6] Ryabov I.M., Novikov V.V., Kolmakov V.I. Stend dlya ispytaniya uprugikh elementov [Rig for testing of elastic elements], the Copyright certificate of the USSR No. 1332176, 1987, Bull. No. 31.
- [7] Buryakova M.V., Ryabov I.M., Novikov V.V., Chernyshov K.V., Vasiliev A.V. Analysis and classification of the known test rigs for testing of wheels and suspensions of vehicles [Analiz i klassifikatsiya izvestnykh stendov dlya ispytaniy koles i podvesok ATS], Aktual'nye problemy ekspluatatsii transporta: Mezhvuz. nauch. sb. [Actual problems of transport operation: interuniversity scientific collection], Saratov, 1998, pp.78-83.
- [8] Novikov V.V., Ryabov I.M. Tekhnika eksperimenta (pri stendovykh ispytaniyakh podvesok i koles ATS): uchebnoye posobiye [Experimental techniques (for bench testing suspensions and wheels of vehicles): study guide], Volgograd, VSTU Publ., 1999, 80 p.
- [9] Ryabov I.M., Novikov V.V., Chernyshov K.V., Vasiliev A.V., Buryakova V.M. Stend dlya ispytaniya pnevmaticheskikh shin i uprugikh elementov transportnykh sredstv [Rig for testing of pneumatic tyres and elastic elements of the vehicles], Patent RF, No. 2133459, 1999.
- [10] Novikov V.V., Ryabov I.M. Pnevmo gidravlicheskie resory podvesok avtotransportnykh sredstv: monografiya [Hydro-pneumatic springs of motor vehicles suspensions], Volgograd, VSTU Publ., 2004, 311 p.
- [11] Orucov I.N., Smolyanov O.V., Novikov V.V. Modernization of the rig for testing car suspension [Modernizatsiya stenda dlya ispytaniya podveski avtomobilya], Tez. dokl. yubileynogo smotra-konkursa nauch., konstruktorskikh i tekhnol. rabot studentov VolgGTU (Volgograd, 11-13 maya 2005 g.) [Abstracts of anniversary of review-competition of scientific, engineering and technological works of students of VSTU (Volgograd, 11-13 may 2005)], Volgograd, VSTU Publ., 2005, pp. 137-138.
- [12] Novikov V.V., Ryabov I.M., Lihousov E.N. Unit for testing of the vehicle suspension kinematic and force excitations of harmonic oscillations [Ustanovka dlya ispytaniya podveski avtomobilya pri kinematicheskoy i silovom vozbuzhdenii garmonicheskikh kolebaniy], Progress transportnykh sredstv i sistem – 2005: mater. mezhdunar. nauch.-prakt. konf. (Volgograd, 20-23 sent. 2005 g.) [Progress of vehicles and transport systems – 2005: Proceedings of the international scientific-practical conference (Volgograd, September 20-23, 2005)], Volgograd, VSTU Publ., 2005, Part I, p. 117.
- [13] Novikov V.V. Povysheniye vibrozashchitnykh svoystv podvesok ATS za schet izmeneniya struktury i kharakteristik pnevmogidravlicheskikh resor i amortizatorov. Dokt. diss. [Increasing vibration protection properties of motor vehicles suspensions through changes in the structure and characteristics of pneumo-hydraulic springs and shock absorbers. Doct. diss.], Volgograd, VSTU, 2005. 448 p.
- [14] Novikov V.V. Bench testing of the air suspension of the bus “VZTM-32731” with hydraulic shock absorbers of different capacity [Stendovyye ispytaniya pnevmopodveski avtobusa “VZTM-32731” s gidroamortizatorami raznoy moshchnosti], Gruzovik & [Truck &], 2007, no. 6, pp. 41-44.
- [15] Novikov V.V. Bench testing the air suspension system with air damper in the form of a choke and check valve [Stendovyye ispytaniya pnevmopodveski s vozdushnym dempferom v vide drosselya i obratnogo klapana], Gruzovik & [Truck &], 2007, no. 7, pp. 43-46.
- [16] Novikov V.V., Ryabov I.M., Kolmakov V.I., Chernyshov K.V. Universal test bench for testing the suspensions and tires of vehicles [Universal'nyy stend dlya ispytaniya podvesok i shin avtotransportnykh sredstv], Sbornik v mashinostroenii, priborostroenii [Assembly in machine building, instrument making], 2008, no. 3, pp. 45-50.
- [17] Novikov V.V., Ryabov I.M., Chernyshov K.V. Vibrozashchitnye svoystva podvesok avtotransportnykh sredstv: monografiya [The vibration isolation properties of the motor vehicles suspensions], Volgograd, VSTU Publ., 2009, 338 p.
- [18] Diakov A.S. Povysheniye dempfirovushchikh svoystv podvesok ATS putem izmeneniya struktury i kharakteristik rezinokordnykh pnevmaticheskikh resor. Kand. diss. [Improving the damping properties of the motor vehicles suspensions by changing the structure and characteristics of rubber-cord pneumatic springs. Cand. diss.], Volgograd, VSTU, 2009. 162 p.
- [19] Pozdeev A.V. Povysheniye vibrozashchitnykh svoystv dvukhpолоstnykh pnevmaticheskikh resor na osnove sinteza optimal'nykh algoritmov kommutatsii polostey. Kand. diss. [Improving vibration isolation properties of the double-cavity air springs on the basis of a synthesis of cavities switching optimal algorithms. Cand. diss.], Volgograd, VSTU, 2012. 220 p.
- [20] Pozdeev A.V., Diakov A.S., Novikov V.V., Pohlebin A.V. Eksperimental'nye issledovaniya podvesok NTS (Chast' 1. Mnogofunktional'nyy stend dlya eksperimental'nykh issledovaniy elementov sistem podressorivaniya avtotransportnykh sredstv): metod. ukaz. k lab. rabote [Experimental studies of suspensions of ground transport systems (Part 1. Multifunctional rig for experimental studies of the elements of the suspension systems of vehicles): methodical instructions for laboratory work], Volgograd, VSTU Publ., 2012, 16 p.
- [21] Pozdeev A.V., Diakov A.S., Novikov V.V., Ryabov I.M. Studies of dual-chamber pneumatic spring with a switching cavities [Issledovaniya dvukhkamernoy pnevmaticheskoy resory s kommutatsiyei polostey], Gruzovik [Truck], 2013, no. 1, pp. 35-37.

- [22] Novikov V.V., Ryabov I.M., Diakov A.S., Pozdeev A.V., Pohlebin A.V. Stendy dlya ispytaniya podvesok nazemnykh transportnykh sredstv: uchebnoye posobiye (grif). Dop. UMO vuzov po universitetskemu politekhnicheskomu obrazovaniyu [Rigs for testing of suspensions of land vehicles: study guide], Volgograd, VSTU Publ., 2013, 114 p.
- [23] Pozdeev A.V., Novikov V.V., Diakov A.S., Pohlebin A.V., Ryabov I.M., Chernyshov K.V. Reguliruemye pnevmaticheskie i pnevmogidravlicheskie resory podvesok avtotransportnykh sredstv: monografiya [Adjustable pneumatic and hydro-pneumatic springs of motor vehicles suspensions], Volgograd, VSTU Publ., 2013, 244 p.
- [24] Gorobtsov A.S., Novikov V.V., Diakov A.S., Hetman V.V., Kanygina E.A., Makarov A.A. Investigation of the heating intensity of the hydraulic shock absorber [Issledovanie intensivnosti nagreva gidroamortizatora], Gruzovik [Truck], 2014, no. 1, pp. 31-32.
- [25] Diakov A.S., Novikov V.V. Experimental study of hydro-pneumatic spring characteristics for wheel chassis of special purpose [Eksperimental'noe issledovanie kharakteristik pnevmogidravlicheskoj resory dlya kolesnogo shassi spetsial'nogo naznacheniya], Gruzovik [Truck], 2015, no.7, pp.7-11.



International Conference on Industrial Engineering

Dynamic synthesis of pulse action vibration exciter on foundation

Tussupova A.E., Bidakhmet Zh., Rakhmatulina A.B.*

Kazakh national research technical university after K.I.Satpayev, Almaty 22a, Satpaev Street, 050013, Kazakhstan

Abstract

This paper considers the task of the dynamic synthesis of six-link lever motion with least vapor, where links provides the required overall action for strut because of optimal arrangement of masses and rational proportion of geometrical dimensions of the links. This task is formulated by the way of quadratic approximation and recovered analytical solution. The general solution for dynamic synthesis of non-harmonic vibration exciter has been derived. The analytical results allow defining the “generalized unbalances” directly from constraint equations. Below is given the essence of the proposed method. A number of alternative kinematic diagrams of mechanisms of non-harmonic vibration exciters of pulse action on the foundation is developed.

© 2015 Published by Elsevier Ltd. This is an open access article under the CC BY-NC-ND license (<http://creativecommons.org/licenses/by-nc-nd/4.0/>).

Peer-review under responsibility of the organizing committee of the International Conference on Industrial Engineering (ICIE-2015)

Keywords: dynamic, syntheses, vibration, six-link lever, motion, kinematic pair, mechanism, Nedler-Midd algorithm.

1. Introduction

The vibration technique uses various types of vibration exciters designed to excite the mechanical vibrations [1, 2, 3]. Planetary vibration exciters of non-harmonic action are the most widespread. The main failure of the existing mechanisms is the complexity of fabrication and increased wear of higher kinematic pair elements.

An alternative way of solution is the use of linkages with lower pairs, the links of which provide the required cumulative impact on the rack through the optimal placement of the masses and the rational aspect ratio of the links.

The technique of optimal dynamic synthesis of non-harmonic vibration exciters is developed on the basis of hinge linkages which allow generating the specified behavior of the force action on the frame in two orthogonal

* Corresponding author. Tel.: (87272)257-71-68.

E-mail address: Tussupov_d@mail.ru

directions [4, 5]. The most common of the known vibration exciters are harmonic with unbalances rotating in opposite directions [6, 7, 8]. The main difficulty in their operation is connected with the need to synchronize the drives for the provision of identical angular rotation velocities. The problem can be solved by mechanical means, for example, based on gearing, which is associated with the wear of profiles at considerable dynamic loads. In addition, the law of impact on foundation in both cases – is the harmonic. It is known that mechanisms with non-circular wheels [9, 10, 11] are used to obtain the non-harmonic (e.g., pulse) law of impact on foundation which is associated with the complexity of manufacturing, increased wear of higher pair elements. An alternative way of solution is the use of linkages with lower pairs, the links of which provide the required cumulative impact on the rack through the optimal placement of the masses and the rational aspect ratio of the links. "Generalized unbalances" are introduced which include the mass-inertial characteristics of the mechanisms that can be determined analytically. The nonlinear parameters are found by minimizing the Euclidean or Chebyshev norm of approximation error based on Nedler-Midd algorithm [5, 8, 12].

2. Research Methods. Derivation of analytical dependences

We propose a method of dynamic synthesis of vibration exciter mechanisms based on hinge linkages. Mass inertia parameters of the mechanism are found by minimization of the Euclidean or Chebyshev norm of approximation error. Numerical implementation of minimization procedure on the basis of Nedler-Midd algorithm.

The essence of the proposed method is as follows.

Let xOy – is some absolute system of coordinates. For convenience, we assume that Ox axis is directed along the line connecting the centers of two hinges on the rack. Components of total inertial force F , acting on the frame of the mechanism, are as follows:

$$\begin{cases} F_x = -\varepsilon \sum_{i=2}^n m_i x'_{Si} - \omega^2 \sum_{i=2}^n m_i x''_{Si} \\ F_y = -\varepsilon \sum_{i=2}^n m_i y'_{Si} - \omega^2 \sum_{i=2}^n m_i y''_{Si} \end{cases}, \quad (1)$$

where n - number of movable links of mechanism; ω and ε - angular velocity and angular acceleration of input link.

Let us divide both members of equation by $Mr\omega^2$ to obtain equations in non-dimensional form and denote by:

$$\begin{cases} f_x = \frac{F_x}{Mr\omega^2} \\ f_y = \frac{F_y}{Mr\omega^2} \end{cases}, \quad (2)$$

where

$$M = \sum_{i=2}^n m_i, \quad (3)$$

r – length of crank.

Let us assume that normalized laws of actions of mechanism on foundation in 2 orthogonal directions are specified.

Let's consider the six-link hinge and linkage mechanism shown on Fig. 1. Let us assume $A(x_A, y_A)=0$, $D=(1, 0)$.

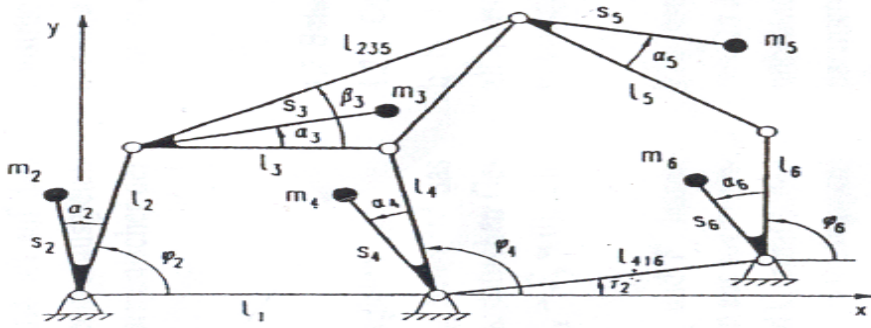


Fig.. 1. The six-link hinge and linkage mechanism

Then equations (1) in non-dimensional form will be as follows:

$$\begin{aligned}
 f_x = & \left[m_2 s_2 \cos \alpha_2 + m_3 l_2 \left(1 - \frac{s_3}{l_3} \cos \alpha_3 \right) + m_5 l_2 \left[1 - \frac{l_{235}}{l_3} \cos \beta_3 - \frac{s_5}{l_5} \left(\cos \alpha_5 - \frac{l_{235}}{l_3} \cos (\alpha_5 + \right. \right. \right. \\
 & \left. \left. \left. + \beta_3 \right) \right] \right] \left(\phi_2'^2 \cos \phi_2 + \phi_2'' \sin \phi_2 \right) + \left[m_2 s_2 \sin \alpha_2 - m_3 l_2 \frac{s_3}{l_3} \sin \alpha_3 + m_5 l_2 \left[\frac{l_{235}}{l_3} \sin \beta_3 + \right. \right. \\
 & \left. \left. + \frac{s_5}{l_5} \left(\sin \alpha_5 - \frac{l_{235}}{l_3} \sin (\alpha_5 + \beta_3) \right) \right] \right] \left(\phi_2'' \cos \phi_2 - \phi_2'^2 \sin \phi_2 \right) + \left[m_3 l_4 \frac{s_3}{l_3} \cos \alpha_3 + m_4 s_4 \cos \alpha_4 + \right. \\
 & \left. + m_5 l_4 \frac{l_{235}}{l_3} \left(\cos \beta_3 - \frac{s_5}{l_5} \cos (\alpha_5 + \beta_3) \right) \right] \left(\phi_4'^2 \cos \phi_4 + \phi_4'' \sin \phi_4 \right) + \left[m_3 l_4 \frac{s_3}{l_3} \sin \alpha_3 + \right. \\
 & \left. + m_4 s_4 \sin \alpha_4 + m_5 l_4 \frac{l_{235}}{l_3} \left(\sin \beta_3 - \frac{s_5}{l_5} \sin (\alpha_5 + \beta_3) \right) \right] \left(\phi_4'' \cos \phi_4 - \phi_4'^2 \sin \phi_4 \right) + \\
 & \left[m_5 l_6 \frac{s_5}{l_5} \cos \alpha_5 + m_6 s_6 \cos \alpha_6 \right] \left(\phi_6'^2 \cos \phi_6 + \phi_6'' \sin \phi_6 \right) + \\
 & \left[m_5 l_6 \frac{s_5}{l_5} \sin \alpha_5 + m_6 s_6 \sin \alpha_6 \right] \left(\phi_6'' \cos \phi_6 - \phi_6'^2 \sin \phi_6 \right)
 \end{aligned} \quad ; \quad (4)$$

$$\begin{aligned}
f_y = & \left[m_2 s_2 \sin \alpha_2 - m_3 l_2 \frac{s_3}{l_3} \sin \alpha_3 + m_5 l_2 \left[\frac{l_{235}}{l_3} \sin \beta_3 + \frac{s_5}{l_5} \left(\sin \alpha_5 - \frac{l_{235}}{l_3} \sin (\alpha_5 + \right. \right. \right. \\
& \left. \left. \left. + \beta_3 \right) \right) \right] \left(\phi_2'^2 \cos \phi_2 + \phi_2'' \sin \phi_2 \right) + \left[m_2 s_2 \cos \alpha_2 + m_3 l_2 \left(1 - \frac{s_3}{l_3} \cos \alpha_3 \right) + \right. \\
& \left. + m_5 l_2 \left[1 - \frac{l_{235}}{l_3} \cos \beta_3 - \frac{s_5}{l_5} \left(\cos \alpha_5 - \frac{l_{235}}{l_3} \cos (\alpha_5 + \beta_3) \right) \right] \right] \left(\phi_2'' \cos \phi_2 - \phi_2'^2 \sin \phi_2 \right) + \\
& + \left[m_3 l_4 \frac{s_3}{l_3} \sin \alpha_3 + m_4 s_4 \sin \alpha_4 + m_5 l_4 \frac{l_{235}}{l_3} \left(\sin \beta_3 - \frac{s_5}{l_5} \sin (\alpha_5 + \beta_3) \right) \right] \left(\phi_4'^2 \cos \phi_4 + \phi_4'' \sin \phi_4 \right) + ; \quad (5) \\
& + \left[m_3 l_4 \frac{s_3}{l_3} \cos \alpha_3 + m_4 s_4 \cos \alpha_4 + m_5 l_4 \frac{l_{235}}{l_3} \left(\cos \beta_3 - \frac{s_5}{l_5} \cos (\alpha_5 + \beta_3) \right) \right] \left(\phi_4'' \cos \phi_4 - \phi_4'^2 \sin \phi_4 \right) + \\
& + \left[m_5 l_6 \frac{s_5}{l_5} \sin \alpha_5 + m_6 s_6 \sin \alpha_6 \right] \left(\phi_6'^2 \cos \phi_6 + \phi_6'' \sin \phi_6 \right) + \\
& + \left[m_5 l_6 \frac{s_5}{l_5} \cos \alpha_5 + m_6 s_6 \cos \alpha_6 \right] \left(\phi_6'' \cos \phi_6 - \phi_6'^2 \sin \phi_6 \right)
\end{aligned}$$

Six-link mechanism on Fig. 1 has 15 inertia parameters: (m_i, s_i, α_i) , $i = 1, \dots, 5$.

Let us consider a specific task. Assume that all geometrical dimensions of mechanism are specified and all mass-inertia parameters of links are known except for link 5, i.e. let us define the variables m_5, s_5, α_5 . let us define mass m_5 and discrete mass point of the 5th link, i.e. parameters s_5, α_5 .

Let us introduce the following designations:

$$x_1 = m_5 ; \quad (6)$$

$$x_2 = m_5 s_5 \cos \alpha_5 ; \quad (7)$$

$$x_3 = m_5 s_5 \sin \alpha_5 . \quad (8)$$

Let us transfer the unknowns on the left member of equation, and knowns on the right member, and for each k ($k=1, N$) of mechanism position we obtain 2 linear equations in the following form (total $2N$ equations for N positions of mechanism).

Synthesis methodology and results testing.

Hereafter, let us consider first a special case, when $\beta_3 = 0$ to avoid bulky calculations and state the essence of methodology.

Then the expressions for components f_x, f_y of total force will be as follows:

$$\begin{aligned}
 & -x_1 l_4 \frac{l_{235}}{l_3} (\phi_{4k}'^2 \cos \phi_{4k} + \phi_{4k}'' \sin \phi_{4k}) + x_2 \left(l_4 \frac{l_{235}}{l_3 l_5} (\phi_{4k}'^2 \cos \phi_{4k} + \phi_{4k}'' \sin \phi_{4k}) - \right. \\
 & \left. - \frac{l_6}{l_5} (\phi_{6k}'^2 \cos \phi_{6k} + \phi_{6k}'' \sin \phi_{6k}) \right) + x_3 \left(l_4 \frac{l_{235}}{l_3 l_5} (\phi_{4k}'' \cos \phi_{4k} - \phi_{4k}'^2 \sin \phi_{4k}) + \right. \\
 & \left. + \frac{l_6}{l_5} (\phi_{4k}'' \cos \phi_{4k} - \phi_{4k}'^2 \sin \phi_{4k}) \right) = m_2 s_2 \cos \alpha_2 (\phi_{2k}'^2 \cos \phi_{2k} + \phi_{2k}'' \sin \phi_{2k}) - \\
 & + m_3 l_2 \left(1 - \frac{S_3}{l_3} \cos \alpha_3 \right) (\phi_{2k}'^2 \cos \phi_{2k} + \phi_{2k}'' \sin \phi_{2k}) + m_2 s_2 \cos \alpha_2 (\phi_{2k}'^2 \cos \phi_{2k} + \phi_{2k}'' \sin \phi_{2k}) + \\
 & + m_3 l_2 \left(1 - \frac{S_3}{l_3} \cos \alpha_3 \right) (\phi_{2k}'^2 \cos \phi_{2k} + \phi_{2k}'' \sin \phi_{2k}) - m_2 s_2 \sin \alpha_2 (\phi_{2k}'' \cos \phi_{2k} - \phi_{2k}'^2 \sin \phi_{2k}) - ; \tag{9} \\
 & - m_3 l_2 \frac{S_3}{l_3} \sin \alpha_3 (\phi_{2k}'' \cos \phi_{2k} - \phi_{2k}'^2 \sin \phi_{2k}) + m_3 l_4 \frac{S_3}{l_3} \cos \alpha_3 (\phi_{4k}'^2 \cos \phi_{4k} + \phi_{4k}'' \sin \phi_{4k}) + \\
 & + m_4 s_4 \cos \alpha_4 (\phi_{4k}'^2 \cos \phi_{4k} + \phi_{4k}'' \sin \phi_{4k}) - m_3 l_4 \frac{S_3}{l_3} \sin \alpha_3 (\phi_{4k}'' \cos \phi_{4k} - \phi_{4k}'^2 \sin \phi_{4k}) + \\
 & + m_4 s_4 \sin \alpha_4 (\phi_{4k}'' \cos \phi_{4k} - \phi_{4k}'^2 \sin \phi_{4k}) + m_6 s_6 \cos \alpha_6 (\phi_{6k}'^2 \cos \phi_{6k} + \phi_{6k}'' \sin \phi_{6k}) + \\
 & + m_6 s_6 \sin \alpha_6 (\phi_{6k}'' \cos \phi_{6k} - \phi_{6k}'^2 \sin \phi_{6k}) - f_{xk}
 \end{aligned}$$

$$\begin{aligned}
 & -x_1 l_4 \frac{l_{235}}{l_3} (\phi_{4k}'' \cos \phi_{4k} - \phi_{4k}'^2 \sin \phi_{4k}) + x_2 \left(l_4 \frac{l_{235}}{l_3 l_5} (\phi_{4k}'' \cos \phi_{4k} - \phi_{4k}'^2 \sin \phi_{4k}) - \right. \\
 & \left. - \frac{l_6}{l_5} (\phi_{6k}'' \cos \phi_{6k} - \phi_{6k}'^2 \sin \phi_{6k}) \right) + x_3 \left(l_4 \frac{l_{235}}{l_3 l_5} (\phi_{4k}'^2 \cos \phi_{4k} + \phi_{4k}'' \sin \phi_{4k}) - \right. \\
 & \left. - \frac{l_6}{l_5} (\phi_{6k}'^2 \cos \phi_{6k} + \phi_{6k}'' \sin \phi_{6k}) \right) = m_2 s_2 \sin \alpha_2 (\phi_{2k}'^2 \cos \phi_{2k} + \phi_{2k}'' \sin \phi_{2k}) - \\
 & - m_3 l_2 \frac{S_3}{l_3} \sin \alpha_3 (\phi_{2k}'^2 \cos \phi_{2k} + \phi_{2k}'' \sin \phi_{2k}) - m_2 s_2 \cos \alpha_2 (\phi_{2k}'^2 \cos \phi_{2k} + \phi_{2k}'' \sin \phi_{2k}) + \\
 & + m_3 l_2 \left(1 - \frac{S_3}{l_3} \cos \alpha_3 \right) (\phi_{2k}'^2 \cos \phi_{2k} + \phi_{2k}'' \sin \phi_{2k}) - m_2 s_2 \cos \alpha_2 (\phi_{2k}'' \cos \phi_{2k} - \phi_{2k}'^2 \sin \phi_{2k}) + . \tag{10} \\
 & + m_3 l_2 \left(1 - \frac{S_3}{l_3} \cos \alpha_3 \right) (\phi_{2k}'' \cos \phi_{2k} - \phi_{2k}'^2 \sin \phi_{2k}) + m_3 l_4 \frac{S_3}{l_3} \sin \alpha_3 (\phi_{4k}'^2 \cos \phi_{4k} + \phi_{4k}'' \sin \phi_{4k}) + \\
 & + m_4 s_4 \sin \alpha_4 (\phi_{4k}'^2 \cos \phi_{4k} + \phi_{4k}'' \sin \phi_{4k}) - m_3 l_4 \frac{S_3}{l_3} \cos \alpha_3 (\phi_{4k}'' \cos \phi_{4k} - \phi_{4k}'^2 \sin \phi_{4k}) + \\
 & + m_4 s_4 \cos \alpha_4 (\phi_{4k}'' \cos \phi_{4k} - \phi_{4k}'^2 \sin \phi_{4k}) + m_6 s_6 \sin \alpha_6 (\phi_{6k}'^2 \cos \phi_{6k} + \phi_{6k}'' \sin \phi_{6k}) + \\
 & + m_6 s_6 \cos \alpha_6 (\phi_{6k}'' \cos \phi_{6k} - \phi_{6k}'^2 \sin \phi_{6k}) - f_{yk}
 \end{aligned}$$

Let us write a system of equations (4) as follows:

$$\begin{cases} A_k^{(x)}x_1 + B_k^{(x)}x_2 + C_k^{(x)}x_3 = D_k^{(x)} \\ A_k^{(y)}x_1 + B_k^{(y)}x_2 + C_k^{(y)}x_3 = D_k^{(y)} \end{cases} \quad k = 1, N, \quad (11)$$

where

$$A_k^{(x)} = l_4 \frac{l_{235}}{l_3} (\phi_{4k}'^2 \cos \phi_{4k} + \phi_{4k}'' \sin \phi_{4k}). \quad (12)$$

As a result we obtain $2N$ linear algebraic equations with three unknowns:

$$a_{j1}x_1 + a_{j2}x_2 + a_{j3}x_3 = b_j, \quad j = 1, 2N, \quad (13)$$

where

$$a_{j1} = \begin{cases} A_k^{(x)}, & \text{at } j = 2k - 1 \\ A_k^{(y)}, & \text{at } j = 2k \end{cases}, \quad (14)$$

$$a_{j2} = \begin{cases} B_k^{(x)}, & \text{at } j = 2k - 1 \\ B_k^{(y)}, & \text{at } j = 2k \end{cases}, \quad (15)$$

$$a_{j3} = \begin{cases} C_k^{(x)}, & \text{at } j = 2k - 1 \\ C_k^{(y)}, & \text{at } j = 2k \end{cases}, \quad (16)$$

$$b_j = \begin{cases} D_k^{(x)}, & \text{at } j = 2k - 1 \\ D_k^{(y)}, & \text{at } j = 2k \end{cases}. \quad (17)$$

Let us designate approximation error as Δ_j

$$\Delta_j \equiv a_{j1}x_1 + a_{j2}x_2 + a_{j3}x_3 - b_j = 0, \quad j = 1, 2N. \quad (18)$$

We can write equations in a matrix form:

$$\Delta \equiv Ax - b = 0; \quad (19)$$

$$\Delta = [\Delta_1, \Delta_2, \Delta_3, \dots, \Delta_{2N}]^T; \quad (20)$$

$$b = [b_1, b_2, b_3, \dots, b_{2N}]^T \quad (21)$$

Matrix A has number of dimensions $2N \times 3$

Then let us use the method of square approximation to define the unknowns

$$x = [x_1, x_2, x_3]^T ; \tag{22}$$

$$S(x) = \frac{1}{2} \sum_{j=1}^{2N} A_j^2 \Rightarrow \min_x S(x) . \tag{23}$$

So far as

$$H = \frac{d^2 S}{dx^2} = A^T A ; \tag{24}$$

we obtain three equations with three unknowns multiplying both members of equation

$$Ax = b ; \tag{25}$$

by A^T

$$A^T Ax = A^T b \tag{26}$$

As a result we arrive at three equations with three unknowns:

$$\begin{cases} \left(\sum_{j=1}^{2N} a_{j1} a_{j1} \right) x_1 + \left(\sum_{j=1}^{2N} a_{j1} a_{j2} \right) x_2 + \left(\sum_{j=1}^{2N} a_{j1} a_{j3} \right) x_3 = \sum_{j=1}^{2N} a_{1j} b_j \\ \left(\sum_{j=1}^{2N} a_{j2} a_{j1} \right) x_1 + \left(\sum_{j=1}^{2N} a_{j2} a_{j2} \right) x_2 + \left(\sum_{j=1}^{2N} a_{j2} a_{j3} \right) x_3 = \sum_{j=1}^{2N} a_{2j} b_j . \\ \left(\sum_{j=1}^{2N} a_{j3} a_{j1} \right) x_1 + \left(\sum_{j=1}^{2N} a_{j3} a_{j2} \right) x_2 + \left(\sum_{j=1}^{2N} a_{j3} a_{j3} \right) x_3 = \sum_{j=1}^{2N} a_{3j} b_j \end{cases} \tag{27}$$

3. Numerical example

Let us assume that the law of action on foundation is preassigned by values given in Table 1.

Table 1. The law of action on foundation in 2 orthogonal directions

K	ϕ_k	$f_x(\phi_k)$	$f_y(\phi_k)$
1	0^0	-0,407	0,376
2	15^0	-0,512	0,555
3	30^0	-0,468	0,734
4	45^0	-0,196	0,820
5	60^0	0,214	0,675
6	80^0	0,420	0,165
7	100^0	0,027	-0,233
8	120^0	-0,002	-0,334

9	160 ⁰	0,199	-0,192
10	180 ⁰	0,110	-0,148
11	200 ⁰	0,022	-0,169
12	220 ⁰	-0,019	-0,243
13	240 ⁰	0,001	-0,328
14	260 ⁰	0,062	-0,365
15	280 ⁰	0,112	-0,317
16	300 ⁰	0,097	-0,189
17	320 ⁰	-0,008	-0,017
18	340 ⁰	-0,193	0,170

Let us define the parameters of this mechanism:
 length of links $l_1 = 1, l_2 = 0,28, l_3 = 0,93, l_4 = 0,73, l_5 = 0,6, l_6 = 0,7, l_{235} = 0,93, s_3 = 0,46$, mass of link - $m_3 = 0,93$,
 and angle values $s_3 = 0,46, \alpha_3 = 0, \beta_3 = 0$

We pre-assign a value $m_5 = 0,560$ and define s_5, α_5 to simplify the task.

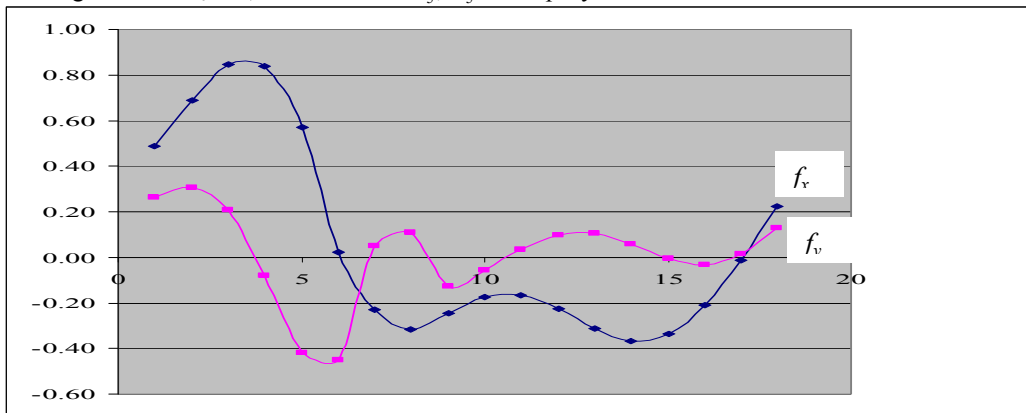


Fig. 2 - Cart results

After that according to equation (27) and multiplying the obtained matrixes by transpose of matrix A^T , we find a system of two equations:

$$\begin{cases} 1,4083s_5 \cos \alpha_5 + 1,8067s_5 \sin \alpha_5 = 0,4567 \\ 1,8067s_5 \cos \alpha_5 + 2,9294s_5 \sin \alpha_5 = 0,1634 \end{cases} \quad (28)$$

From where the unknowns α_5, S_5 can be found:

$$\alpha_5 = 0,017, \quad (29)$$

$$S_5 = 0,3, \quad (30)$$

4. Conclusion

The task of the dynamic synthesis of six-link lever motion with least vapor, where links provides the required overall action for strut because of optimal arrangement of masses and rational proportion of geometrical dimensions of the links was solved. This task is formulated by the way of quadratic approximation and recovered analytical solution. The general solution for dynamic synthesis of non-harmonic vibration exciter has been derived. The analytical results allow defining the “generalized unbalances” directly from constraint equations. Below is given the essence of the proposed method. A number of alternative kinematic diagrams of mechanisms of non-harmonic vibration exciters of pulse action on the foundation is developed.

References

- [1] A. Zholdasbekov, Theory of mechanisms and machines, Almaty Mektep, 1979.
- [2] I.I. Artobolevsky, Theory of mechanisms and machines, Nauka, Moscow, 1988.
- [3] V.I. Doronin, Y. Danshin, Dynamic synthesis of balanced flat linkages, DVG APS, Khabarovsk, 1993.
- [4] Y. Danshin, Analytical method for solving of the problem of dynamic balancing of flat linkages, Abstract of the thesis for the degree of Doctor of Technical Sciences, Omsk State Technical University, 1998.
- [5] S.M. Ibrayev, A.E. Tusupova, Analytical determination of mass and inertial parameters in a problem of dynamic synthesis of the lever mechanism, Theses of reports of the International scientific conference "Problems of Theoretical and Applied Mechanics". Almaty. (2006) 125.
- [6] H. Dresig, S. Ibrayev, Optimal Design of Non-harmonic Vibration Exciters Based on 6bar Linkages. Proceedings of the International Conference of Young Scientists, dedicated to the 10th anniversary of Kazakhstan's independence. Almaty, KazNTU. 2 (2001) 68–72.
- [7] L. Forsblad, Investigations of Soil Compaction by Vibration, Acta Politechnica Skandinavica, Civil Engineering an Building constructions, Stockholm. 34 (1965) 66–76.
- [8] A.E. Telibayeva, Analitiko-optimizatsionny synthesis of the executive mechanism of the vibroactivator of pulse action, Messenger of KAZNTU of K.I. Satpayev, Almaty. 2(46) (2004) 155–158.
- [9] H. Dresig, St. Naake, L. Rockhausen, Vollständiger und harmonischer Ausgleich ebener Mechanismen, VDI-Fortschrittbericht 18/155, VDI-Verlag, Düsseldorf, 1994.
- [10] H. Dresig, Schwingungen mechanischer Antriebssysteme: Modellbildung, Berechnung, Analyse, Synthese. Springer-Verlag, Berlin, Heidelberg, New York, 2001.
- [11] H. Dresig, Getriebedynamik: Starrkurper Mechanismen, VDI-Richtlinien, DVI 2149, 1998.
- [12] A.E. Tusupova, A.T. Nurmaganbetova, Zh.B. Koyshybayeva, D.M. Tusupov, Kinetostatik of the three-unit mechanism with the set relative movement of mobile links, the Messenger of KAZNTU of K.I. Satpayev, Almaty. 4(54) (2006) 142–146
- [13] R. Lohe, W. Lohr, Einfluss der Erregung auf das Schwingungsbild von Bodenverdichtern, Getriebetechnik: Tradition und Moderne, Wiss. Zeitschrift der TV, Dresden. 3 (2001) 89–94.
- [14] W. Schnell, Verfahrenstechnik der Baugrundverbesserung, Teubner, Stuttgart, 1997.
- [15] F. König, Verdichtung im Erd- und Strassenbau. Wiesbaden, Bauverlag, Berlin, 1995.
- [16] J. Berbuer, H. Greschnerr, Vorteile der Hydraulik bei Vibrationsplatten, VDBUM Seminarband, 1997.
- [17] U. Bathelt, Das Arbeitsverhalten des Rüttelverdichters auf plastisch - elastischem Untergrund, Bautechnik, Verlag Wilhelm Ernst & Sohn, Berlin, 1958.
- [18] C. Ephremidis, Die mathematische Erfassung der Vorgänge bei der Rüttelverdichtung von Boden, VDI, Zeitschnift, Bd. 101, 1969, H. 7.
- [19] W. Wittig, Untersuchungen über den Einflup der Frequenz auf die Bestimmung des Fuftreffimpulses von Vibrationsplatten unter Berücksichtigung der elasto-plastischen Eigenschaften der nichtbindigen Erdstoffe, Dissertation: Hochschule f.Bauwesen, Leipzig, 1965.
- [20] K. Hartman, Das Arbeitsverhalten des Einmassenrüttelverdichters, Dissertation, TH Hannover, 1963.
- [21] A. Hertwig, C. Friih, H. Lorenz, Die Ermittung der fur das Bauwesen wichtigsten Eigenschaften des Bodens durch erzwungene Schwingungen, Veröffentlichungen der Degebo, Springer Verlag, Berlin. 1 (1933) 44–52.
- [22] M. Novak, Über die Nichtlinearitat der Vertikalschwingungen von starren Körpern auf dem Baugrunde - Acta Technica, Rocnik Bd.2, Nakladatelstvi CSAV, Praha, 1957.



International Conference on Industrial Engineering

Comparative evaluation of the vibration isolation properties of a suspension with different flywheel dynamical absorbers of the car body oscillations

I.M. Ryabov^a, K.V. Chernyshov^b, Pozdeev^{c,*}

^aDepartment of Automobile Transportation, Volgograd State Technical University, Volgograd, Russia

^bDepartment of Operation and Maintenance of Automobiles, Volgograd State Technical University, Volgograd, Russia

^cDepartment of Automatic Units, Volgograd State Technical University, Volgograd, Russia

Abstract

The article is researching the vibration isolation properties of a flywheel dynamical absorber of the vehicle body oscillations. It is noted that the authors have previously proposed additional flywheel dynamical absorbers with mechanical drives and it is proved that they have improved the vibration isolation properties of the suspension system. However, such dynamical absorbers are heavy. That is why there is being developed a flywheel dynamical absorber with hydraulic drive containing a hydraulic cylinder and a hydraulic machine with a flywheel. The theoretical research identifies the parameters of the hydraulic drive, providing the minimum value of the sprung mass oscillation amplitude in the area of low-frequency resonance, and it is found out that the flywheel dynamical absorber with the hydraulic drive features a lower suspension mass and better vibration isolation properties than the flywheel dynamical absorber with a mechanical transmission.

© 2015 The Authors. Published by Elsevier Ltd. This is an open access article under the CC BY-NC-ND license (<http://creativecommons.org/licenses/by-nc-nd/4.0/>).

Peer-review under responsibility of the organizing committee of the International Conference on Industrial Engineering (ICIE-2015)

Keywords: dynamical vibration absorber; flywheel; hydraulic machine; hydraulic cylinder; vibration isolation properties; car.

1. Introduction

In the monograph [1] published in 1976, it's referred to the using appropriateness of the dynamical vibration absorbers of the car wheels in the form of additional spring-loaded weight. Conducted theoretical and experimental research of such absorbers [2-12] showed their effectiveness. However, for damping car body oscillations such the dynamical absorbers are not applicable due to their large mass.

* Corresponding author. Tel.: +7-987-643-8514 .

E-mail address: avp24897@mail.ru

The flywheel dynamical absorbers of the body oscillations in which the flywheel is driven in rotation by a mechanical transmission (Fig. 1, a) are proposed and studied in [12-24]. To avoid locking of the suspension at high frequencies in such a drive the clutch with optimal parameters is used [13-22]. In [23, 24] it is shown that to reduce the mass of the flywheel it's necessary to increase the gear ratio of the mechanical transmission. However, it's also increases the mass of the transmission, which limits the possibility of reducing the mass of the absorber as a whole. Finding ways to reduce the mass of the flywheel absorber of the body oscillations has led to the idea of using hydraulic machine, connected by pipelines with a hydraulic cylinder (Fig. 1, b) as a flywheel drive [16, 25-30].

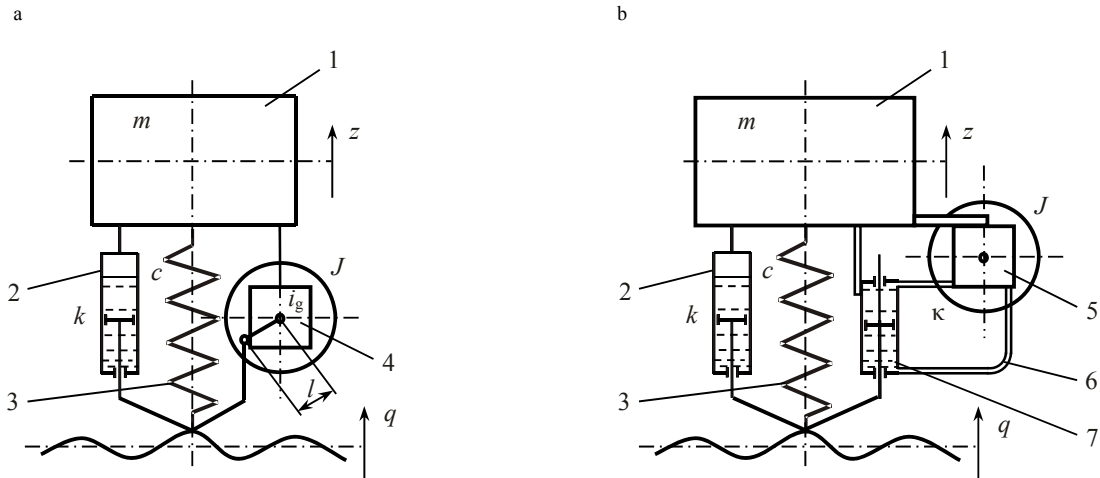


Fig. 1. (a) design schemes of suspensions containing flywheel dynamical vibration absorbers: with mechanical transmission of motion to the flywheel, (b) design schemes of suspensions containing flywheel dynamical vibration absorbers with hydraulic transmission of motion to the flywheel

This article is devoted to comparative evaluation of the vibration isolation properties of the considered flywheel dynamical absorbers.

2. Mathematical model

Any hydraulic machines have volumetric leakages. If we assume that the volumetric leakages of the working fluid in hydraulic motors and pumps are not available, so a constant volume (volume of fluid passing through the hydraulic machine during one revolution of the shaft) of the hydraulic machine is connected with the stroke of the piston in the cylinder by the dependence:

$$Q = F_a x_t \tag{1}$$

where F_a is the cross sectional area of the annular cavity in the hydraulic cylinder of the vibration absorber, x_t is the stroke of the piston for one revolution of the flywheel.

The dependence of the flywheel rotation angle ϕ from suspension deformation x can be determined by the formula

$$\phi = 2\pi \frac{x}{x_t} = 2\pi \cdot F_a \cdot \frac{z - q}{Q} \tag{2}$$

We denote a transfer coefficient from the suspension deformation to the flywheel rotation:

$$\frac{z-q}{\phi} = \frac{Q}{2\pi F_a} = b \quad (3)$$

Suspension dynamics with hydraulic flywheel vibration absorber without regard to leakages looks as follows:

$$\frac{J}{b}\ddot{\phi} + m\ddot{z} + k(\dot{z} - \dot{q}) + c(z - q) = 0 \quad (4)$$

either

$$m\ddot{z} + k(\dot{z} - \dot{q}) + c(z - q) + \frac{J}{b^2}(\ddot{z} - \ddot{q}) = 0 \quad (5)$$

Here J and ϕ are the inertia moment and the flywheel rotation angle; m and z are the sprung mass and its displacement; c – stiffness of the elastic element; k – coefficient of the shock absorber resistance (damping factor); q – kinematic perturbation.

We divide left and right part of (5) on m and get:

$$\ddot{z} + 2h(\dot{z} - \dot{q}) + \omega_0^2(z - q) + J_{rel}(\ddot{z} - \ddot{q}) = 0 \quad (6)$$

In this equation:

$$\omega_0^2 = \frac{c}{m} \quad (7)$$

$$2h = \frac{k}{m} \quad (8)$$

$$J_{rel} = \frac{J}{mb^2} = \frac{J}{m} \left(\frac{2\pi F_k}{Q} \right)^2 \quad (9)$$

Equations (4), (5) and (6) coincide in form with the corresponding equations of the suspension with the mechanical drive of the flywheel without the handing over link and have the same solution [16]. So the solution of equation (6) in the form of the dynamic factor represents the following expression

$$K_z = \frac{z_0}{q_0} = \sqrt{\frac{(1-t^2 J_{rel})^2 + 4\psi^2 t^2}{(1-t^2 - t^2 J_{rel})^2 + 4\psi^2 t^2}} \quad (10)$$

When accounting for the volumetric leakages in a hydraulic machine, a mathematical model describing the dynamics of the vibrating system, is complicated. When the flywheel is stopped during the movement of the rod-piston in the hydraulic shock absorber fluid flows through the gaps in hydraulic machine, forming hydraulic resistance, which in linear form is:

$$F_{d.h.}(\dot{x}_{st./fl.}) = \kappa \cdot \dot{x}_{st./fl.} \quad (11)$$

where $\dot{x}_{st./fl.}$ is a speed of the rod-piston movement in the hydraulic cylinder when the flywheel is stopped; κ is a damping coefficient of the hydraulic drive.

Locking the flywheel does not lead to the stillness of the oscillating system in the presence of the volumetric leakages. Thus, the presence of the volumetric leakages provides an additional freedom degree of vibrating system. As an additional generalized coordinate we can consider the flywheel rotation angle ϕ .

When the flywheel rotates, power of the hydraulic resistance to the rod-piston movement in the cylinder depends on the difference between the speed of the rod-piston movement and angular velocity of the flywheel rotation:

$$F_{d,h} = \kappa(\dot{z} - \dot{q} - b\dot{\phi}) \quad (12)$$

Then the equality condition of the forces acting on the center of the sprung mass, and the equality condition of the moments on the axis of a flywheel constitute a system of differential equations:

$$\begin{cases} m\ddot{z} + k(\dot{z} - \dot{q}) + c(z - q) + \kappa(\dot{z} - \dot{q} - b\dot{\phi}) = 0, \\ J\ddot{\phi} - \kappa \cdot b(\dot{z} - \dot{q} - b\dot{\phi}) = 0. \end{cases} \quad (13)$$

The second equation of the system admits a lower order. Considering this and the expressions (7), (8), (9), and as well as producing replacement

$$2\chi = \frac{\kappa}{m} \quad (14)$$

we get:

$$\begin{cases} \ddot{z} + 2h(\dot{z} - \dot{q}) + \omega_0^2(z - q) + 2\chi(\dot{z} - \dot{q}) - 2\chi b\dot{\phi} = 0, \\ \dot{\phi} + \frac{2\chi}{J_{rel}}\phi - \frac{2\chi}{J_{rel}b}(z - q) = 0. \end{cases} \quad (15)$$

The dynamic factor of the system relating to the sprung mass is equal to

$$K_z = \frac{z_0}{q_0} = \sqrt{\frac{\left[\frac{2\chi}{J_{rel}}\omega_0^2 - (2h + 2\chi)\omega^2 \right]^2 + \left[\omega_0^2\omega + 2h \cdot \frac{2\chi}{J_{rel}}\omega \right]^2}{\left[\frac{2\chi}{J_{rel}}\omega_0^2 - \left(2h + 2\chi + \frac{2\chi}{J_{rel}} \right)\omega^2 \right]^2 + \left[\omega_0^2\omega + 2h \cdot \frac{2\chi}{J_{rel}}\omega - \omega^3 \right]^2}} \quad (16)$$

In relative parameters it is equal to

$$K_z = \frac{z_0}{q_0} = \sqrt{\frac{\left(2\bar{\psi}_{fl} - (2\psi_d + 2\bar{\psi}_{fl}J_{rel})t^2 \right)^2 + \left(1 + 2\psi_d 2\bar{\psi}_{fl} \right)^2 t^2}{\left(2\bar{\psi}_{fl} - (2\psi_d + 2\bar{\psi}_{fl}J_{rel} + 2\bar{\psi}_{fl})t^2 \right)^2 + \left(1 - t^2 + 2\psi_d 2\bar{\psi}_{fl} \right)^2 t^2}} \quad (17)$$

where:

$$\psi_d = \frac{h}{\omega_0} \quad (18)$$

$$\bar{\psi}_{fl} = \frac{\chi}{J_{rel} \omega_0} \quad (19)$$

$$t = \frac{\omega}{\omega_0} \quad (20)$$

The analysis of oscillatory systems with the flywheel absorber having the hydraulic drive without leakages (analogue of the mechanical drive), shows that the amplitude-frequency characteristics of this oscillatory system have the frequency at which the vibration amplitude of the vibration protection object (sprung mass) is equal to zero. When deviation from this frequency is in the direction of increasing or decreasing the vibration amplitudes increase considerably. This circumstance leads to the necessity of application in mechanical drives gearboxes with variable gear ratio or the introduction in the drive to the dealer links, for example, a clutch.

We examine an oscillating system with a hydraulic drive of the flywheel for the existence of the invariant points at which all of the amplitude-frequency characteristics of the system with different values of the damping coefficient of the hydraulic drive intersect. In the absence of damping:

$$K_z = \sqrt{\frac{4\bar{\psi}_{fl}^2(1-t^2J_{rel})^2 + t^2}{4\bar{\psi}_{fl}^2(1-t^2 - J_{rel}t^2)^2 + (1-t^2)^2 t^2}} \quad (21)$$

The considered system has two invariant points:

$$t_{inv1} = \sqrt{\frac{J_{rel} + 1 - \sqrt{J_{rel}^2 + 1}}{J_{rel}}}, \quad t_{inv2} = \sqrt{\frac{J_{rel} + 1 + \sqrt{J_{rel}^2 + 1}}{J_{rel}}}. \quad (22)$$

The coefficients in the invariant points are equal, respectively:

$$K_{inv1} = \frac{J_{rel}}{\sqrt{J_{rel}^2 + 1} - 1} \quad \text{and} \quad K_{inv2} = \frac{J_{rel}}{\sqrt{J_{rel}^2 + 1} + 1}. \quad (23)$$

Invariant points break the whole range of relative frequencies into three intervals: $(0; i_{inv1})$, $(i_{inv1}; i_{inv2})$ and $(i_{inv2}; \infty)$. Oscillation amplitudes of the sprung mass are reduced with increasing damping in the hydraulic drive on the second interval, and are increased on the first and third intervals.

3. Simulation results

Fig. 2 presents the amplitude-frequency characteristics of the considered system in comparison with the amplitude-frequency characteristics of the system without flywheel absorber and the system with the flywheel absorber having the mechanical drive.

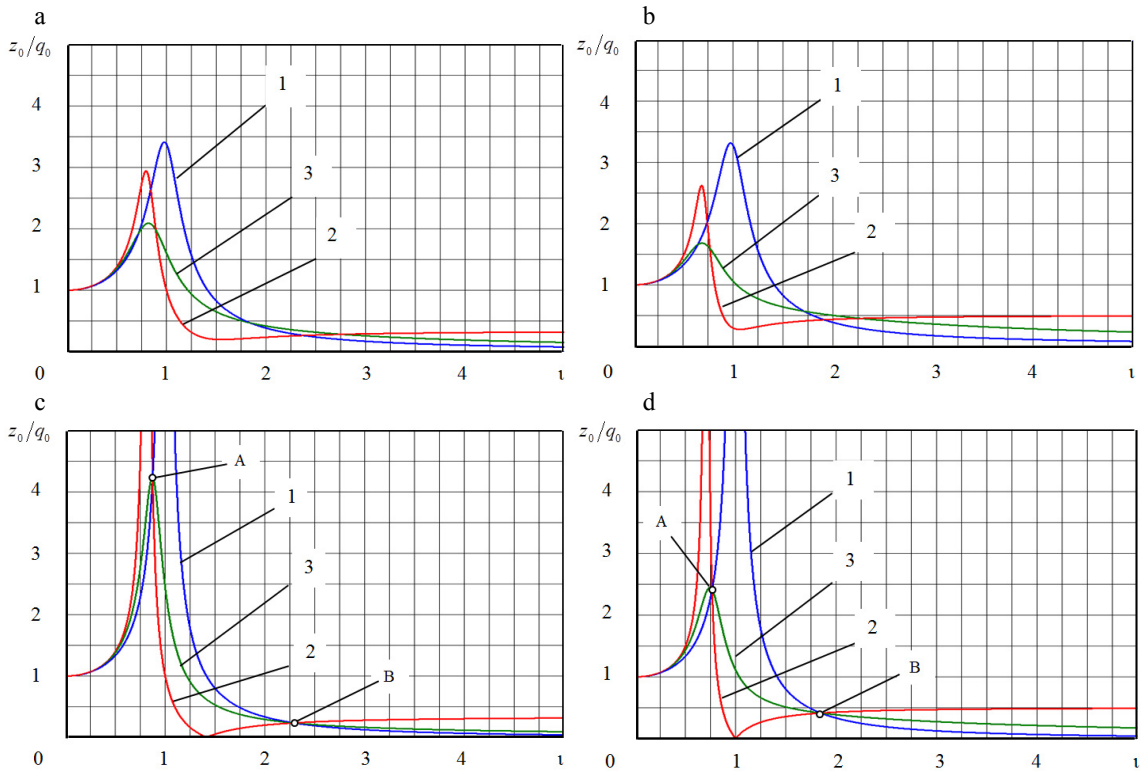


Fig. 2. (a) amplitude-frequency characteristics of oscillatory system at $\bar{\psi}_{fl} = 0,5$; $\psi_d = 0,15$; $J_{rel} = 0,5$; (b) amplitude-frequency characteristics of oscillatory system at $\bar{\psi}_{fl} = 0,5$; $\psi_d = 0,15$, $J_{rel} = 1$; (c) amplitude-frequency characteristics of oscillatory system at $\bar{\psi}_{fl} = 0,5$, $\psi_d = 0$, $J_{rel} = 0,5$; (d) amplitude-frequency characteristics of oscillatory system at $\bar{\psi}_{fl} = 0,5$, $\psi_d = 0$, $J_{rel} = 1$

Fig. 2 shows that the increasing a relative inertia moment lowers the natural (resonant) frequency of the system and reduces the oscillation amplitudes in the first two ranges (up to the second invariant point), and increases them in the third range. The existence of a standard shock absorber also reduces the oscillation amplitudes in the first two ranges, and increases them in the third range. The damping in the hydraulic drive also affects the oscillation amplitude of the sprung mass. The oscillation amplitudes of the sprung mass are reduced on the second range by increasing the damping in a hydraulic actuator, and are increased on the first and third ranges. The amplitude of the sprung mass at resonance depends on damping of the hydraulic drive. The minimum value of this amplitude is reached with the relative damping factor $\bar{\psi}_{fl} \approx 0,5$ for the parameters: $\psi_d = 0$ and $J_{rel} = 0,5$, and with the relative damping factor $\bar{\psi}_{fl} \approx 0,4$ for the parameters: $\psi_d = 0$, $J_{rel} = 1$.

4. Conclusion

Conducted research have shown that the dynamical flywheel absorber with hydraulic drive provides better vibration isolation properties of the suspension than the dynamical flywheel absorber with a mechanical transmission, because it provides smaller amplitude of the vehicle body oscillations in the area of low-frequency resonance and at high frequency perturbations in the area after resonance.

References

- [1] A.A. Khachaturov, V.L. Afanasiev, S.V. Vasiliev, The dynamics of the system road – tyre – vehicle – driver, Engineering Publ., Moscow, 1976.

- [2] D.A. Domnin, A Method for improving vibrocentric automotive suspension settings by choosing the rational parameters of the dynamical vibration absorber of the wheels. Cand. diss., MAMI, Moscow, 2005.
- [3] W.S. Yoo, Damping Models for Multibody Dynamic Simulation, Proceedings of the EUROMECH Colloquium 495 "Advances in simulation of multibody system dynamics", Bryansk, Bryansk State Technical University, 2008.
- [4] I.M. Ryabov, K.V. Chernyshov, A.M. Kovalev, Potential vibration isolation properties of the vehicle suspension with dynamical vibration absorber of the wheels, *Automotive industry*. 12 (2010) 13–16.
- [5] I.M. Ryabov, K.V. Chernyshov, A.M. Kovalev, Theoretical study of the vibration isolation properties of the suspension with dynamical vibration absorber of the wheels when the car is on a random profile, Proceedings of VSTU. A series of "Land transport systems". interuniversity collection of scientific articles. 3(10) (2010) 76–80.
- [6] K.V. Chernyshov, I.M. Ryabov, A.M. Kovalev, T.M. Rasulov, The impact of changes in damping in the dynamical vibration absorber of the wheels to the smoothness of the car, Proceedings of VSTU. A series of "Land transport systems", Interuniversity collection of scientific articles. 4(12) (2011) 57–60.
- [7] I.M. Ryabov, K.V. Chernyshov, A.M. Kovalev, The choice of parameters of dynamical vibration absorber of the wheels in view of the tire stiffness changing in operation, *The Truck*. 3 (2011) 2–5.
- [8] V.A. Gudkov, I.M. Ryabov, D.V. Gudkov, K.V. Chernyshov, A.M. Kovalev, Features of the suspension with a dynamical vibration absorber of the wheels, *Tyre Plus (Ukraine)*. 3 (2012) 8–9.
- [9] K.V. Chernyshov, I.M. Ryabov, A.M. Kovalev, T.M. Rasulov, Mathematical modeling of vibrating system with dynamical absorber, *The Truck*. 10 (2012) 14–21.
- [10] I.M. Ryabov, A.M. Kovalev, K.V. Chernyshov, T.M. Rasulov, The choice of a mass of dynamical vibration absorber of the wheel, *Automotive Industry*. 8 (2013) 15–17.
- [11] I.M. Ryabov, A.M. Kovalev, K.V. Chernyshov, T.M. Rasulov, Dynamical absorber of vertical oscillations of the a vehicle wheel integrated with design of the disk brake mechanism, *Automotive Industry*. 4 (2015) 17–19.
- [12] I.M. Ryabov, V.V. Novikov, RF Patent 2142585. (1999)
- [13] I.M. Ryabov, V.V. Novikov, RF Patent 2142586. (1999)
- [14] V.V. Novikov, I.M. Ryabov, K.V. Chernyshov, V.V. Vorobiev, A.V. Gallov, Shock absorbers with energy recovery in an oscillation loop, *Handbook. Engineering magazine*. 7 (2001) 31–34.
- [15] I.M. Ryabov, V.V. Novikov, V.V. Vorobiev, S.V. Danilov, O.V. Smolyanov, Inertial dampers with the handing over element for vehicle suspensions, *The Truck &*. 4 (2005) 9–10.
- [16] V.V. Novikov, I.M. Ryabov, K.V. Chernyshov, The vibration isolation properties of the motor vehicles suspensions, VSTU Publ., Volgograd, 2009.
- [17] I.M. Ryabov, K.V. Chernyshov, V.V. Vorobiev, I.N. Urukov, Mathematical model of the vehicle suspension with inertial-frictional shock absorber, *Modern technologies. System analysis. Modeling*. 1(21) (2009) 29–31.
- [18] I.M. Ryabov, K.V. Chernyshov, A.V. Pozdeev, Theoretical study and choice of rational parameters of the relaxation suspension of the vehicle with the inertial element, Proceedings of VSTU. A series of "Land transport systems", Interuniversity collection of scientific articles. 3(1) (2010) 83–86.
- [19] I.M. Ryabov, K.V. Chernyshov, A.V. Pozdeev, Mathematical modelling of the relaxation suspension of the vehicle with the inertial element, Proceedings of VSTU. A series of "Land transport systems", Interuniversity collection of scientific articles. 3(10) (2010) 80–82.
- [20] I.M. Ryabov, K.V. Chernyshov, A.V. Pozdeev, Types of designs of inertial-frictional shock absorbers, modeling and testing, *Tractors and farm machinery*. 4 (2013) 23–26.
- [21] D.A. Chumakov, A.V. Pozdeev, V.I. Karlov, Vibration isolation properties of the air spring with the inertial damping devices, Anniversary XXV international innovation-oriented conference of young scientists and students MICYS-2013: proceedings, Moscow, Institute of machine science of. A.A. Blagonravova of Russian Academy of Sciences Publ. (2013) 381–387.
- [22] A.V. Pozdeyev, I.M. Ryabov, A.Y. Sokolov, A.S. Mitrochenko, D.A. Chumakov, The vibration isolation properties of the relaxation suspension with the inertial damping device, Proceedings of VSTU. A series of "Land transport systems". Vol. 8: interuniversity collection of scientific articles. 3(130) (2014) 30–33.
- [23] I.M. Ryabov, K.V. Chernyshov, V.V. Vorobiev, A.Y. Sokolov, RF Patent 2313014. (2007).
- [24] K.V. Chernyshov, I.M. Ryabov, A.M. Kovalev, A.V. Pozdeyev, Conclusion and analysis of the optimal control law of the dynamical vibration absorber parameters in single-mass vibrating system with harmonic perturbation, Proceedings of VSTU. A series of "Land transport systems". Vol. 7: interuniversity collection of scientific articles. 21(124) (2013) 47–52.
- [25] V.V. Novikov, O.V. Smolyanov, Vibrational protection provided by automobile suspensions with both hydraulic and inertial-frictional shock absorbers, *The mechanical engineering Bulletin*. 1 (2009) 81–83.
- [26] V.V. Novikov, O.V. Smolyanov, Vibrational protection provided by automobile suspensions with both hydraulic and inertial-frictional shock absorbers, *Russian Engineering Research*. 1 (2009) 68–70.
- [27] V.V. Novikov, I.M. Ryabov, K.V. Chernyshov, A.S. Dyakov, A.V. Pozdeyev, I.A. Golyatkin, Inertial-hydraulic damper with hydraulic motor of roller-vane type, Progress of vehicles and transport systems – 2013: Proceedings of the international scientific-practical conference, Volgograd, VSTU Publ. (2013) 78–79.
- [28] I.A. Golyatkin, V.V. Novikov, A.V. Pozdeyev, Calculation of the inertial-hydraulic shock absorber with hydraulic motor of the roller-vane type, XVIII regional conference of young researchers-users of the Volgograd region: abstracts, Volgograd, VSTU Publ. (2014) 65–67.
- [29] I.A. Golyatkin, A.V. Pozdeyev, V.V. Novikov, Vibration isolation properties of inertial-hydraulic shock absorber of the roller-vane type, XIX regional conference of young researchers of the Volgograd region: abstracts, Volgograd, VSTU Publ. (2014) 65–67.

- [30] I.A. Golyatkin, A.V. Pozdeyev, V.V. Novikov, Investigation of the vibration isolation properties of the inertial-hydraulic shock absorber with roller-vane hydraulic motor, XXVI international innovation-oriented conference of young scientists and students. MICYS-2014 (Moscow, 17-19 Dec. 2014): conference proceedings, Moscow, Institute of machine science of. A.A. Blagonravova Russian Academy of Sciences, the Russian Foundation for basic research, Department of energetics, engineering, mechanics and control processes of Russian Academy of Sciences. (2015) 483–487.



International Conference on Industrial Engineering

Modeling the combustion process of a powerful diesel engine

Kamaltdinov V.G.^{a*}, Markov V.A.^b, Lysov I.O.^a

^aSouth Ural State University, 76, Lenin Avenue, Chelyabinsk, 454080, Russian Federation

^bBauman Moscow State Technical University, 5 2-ya Baumanskaya st., Moscow, 105005, Russian Federation

Abstract

The authors develop models of the combustion process and a program for calculating the operating cycle of a powerful diesel engine with the set law of mixture formation. They also calculate how the temperature of a fresh charge after a charge air cooler impacts the operating cycle indicators of such an engine. Based on the results of the calculation, herein are constructed charts of in-cylinder pressure and heat release laws that accord with known experimental data.

© 2015 The Authors. Published by Elsevier Ltd. This is an open access article under the CC BY-NC-ND license (<http://creativecommons.org/licenses/by-nc-nd/4.0/>).

Peer-review under responsibility of the organizing committee of the International Conference on Industrial Engineering (ICIE-2015)

Keywords: powerful diesel, calculations, operating cycle, indicator parameters, the maximum combustion pressure, modeling, combustion process, molecules of fuel, the law of mixture formation, the temperature of the fresh charge, charge air cooler;

1. The peculiarities of combustion process in the diesel engine and models for its description

It is admitted that at fuel combustion the reaction rate initially increases, but as the process unfolded under certain conditions, it decreases.

By the simulation, theoretical and experimental research of the fuel combustion in the diesel engine it is determined that in the compression volume the two areas, the higher temperature area and the lower temperature area, are distinguished [1]. And in some areas the temperature reaches 3000°K (with the average temperature 1700-1800°K) and changes insignificantly within 50-60 degrees of the crankshaft position [2]. It indicates that when the temperature reaches 3000°K, the processes of the carbon dioxide dissociation limit the further progress of the combustion, and in the expansion process the carbon monoxide afterburning sustain the higher temperature until it is

* Corresponding author. Tel.: +7-951-777-00-11; +7-967-863-40-18.

E-mail address: vkamaltdinov@yandex.ru

fully oxidized.

The known models, which are used for mathematical formulation of the fuel combustion process in the internal-combustion engine, either consider this characteristics incompletely, or consider them in the implicit form. Therefore, the development of the combustion theory and making new models for the description of the real in-cylinder processes still remain urgent.

All the known combustion process models may be divided into three principal groups:

- models in which the heat generation process is described by the preset function of time or the crankshaft position;
- models which describe in detail the kinetics of the combustion process;
- models which are based on the application of the general kinetic law (Arrhenius equation).

Simple and useful combustion process models among which I.I. Wiebe's model became widespread refer to the first group [3]. The real variation of the parameters of the actuating medium (pressure, temperature and concentration of the reactants) in the combustion process are not considered in the models of this group. The combustion products dissociation heat losses are taken into consideration in the implicit form, as a rule, with the other heat losses which are expressed in terms of the heat utilization factor or the combustion efficiency factor. And the value of the dissociation heat losses is considered proportional to the part of the burnt fuel, and in the expansion process this heat doesn't return to the actuating medium.

The second group includes models that treat the fuel oxidation process by atmospheric oxygen as the combination of chemical reactions with the intermediate products generation [4,5]. For each similar reaction there are constants of reaction rate, activation energy and reagents concentration. It is too difficult to realize the models of this group in engineering computations as it demands great computational power.

The third group includes models that describe the combustion process in general and consider such important physical parameters as the temperature of the actuating medium and the fuel and oxygen concentration [1]. Meanwhile, in the models of this group there is no direct accounting of inert components (nitrogen, combustion products, etc.) that, as it's well-known, inhibits the combustion process. The key parameter of the process in these models is the combustion rate depending of the temperature and the concentration of the mixture active components. The relative quantity of the reactive fuel is not frequently used.

The parameters that characterize the time factor of the combustion process are applied to determine integrated timing values: an ignition delay period estimation and combustion duration with the constant reaction rate or isothermal reaction [6]. However, to model a variable reaction rate with the constantly decreasing fuel and oxygen molecule concentration and considerable temperature rise, it is necessary to control the time dynamics of the combustion process variation. Therefore, it became necessary to introduce the fuel oxidation reaction time factor which allows to control the state of the actuating medium in the engine cylinder in any time (on any process stage).

The Internal-Combustion Engine department of South Ural State University developed a new single-area model of the combustion process based on kinetic equations which more accurately considers the features of in-chamber processes of internal-combustion engines.

2. New models for computation of the fuel combustion process in the diesel engine

2.1. The Combustion Process Model

The Combustion Process Model is based on the following points:

- The whole combustion process is considered as a combination of successive oxidation reactions of active fuel molecules groups to carbon dioxide and water. These reactions progress according to Arrhenius equation and possess the energy that is larger than the conditional activation energy by the present temperature.
- The quantity of reacting active fuel molecules in the group depends on the total quantity of fuel molecules, the current mixture temperature and the conditional activation energy that changes according to the burnt fuel ratio.
- The conditional oxidation duration of active molecules in this group is considered dependent not only on the total quantity of fuel molecules but also such important for the combustion process parameters as the volume of the

combustion chamber, the oxygen molecule quantity, the inert component molecule quantity (nitrogen, carbon dioxide, water, carbon monoxide, etc.) and the turbulence inside the combustion chamber.

- The heat generating at oxidizing each active fuel molecule group is determined by the low fuel heat capacity and is consumed for the mixture temperature and pressure increase in the combustion area.
- At each step of the computation the quantity of molecules of all the substances is corrected as a result of the fuel combustion, the oxygen consumption for combustion, carbon dioxide and water formation, formation of carbon monoxide and oxygen at dissociation and the further oxidation of carbon monoxide.

The feature of the model is an introduction of the new parameter, the conditional duration of the fuel molecule oxidation reaction, which considers the time factor on the molecular level. When studying any process which develops with time, the timing parameter is used to trace the alteration of the phenomenon under study. In the internal-combustion engine the timing parameter is a crank angle in degrees (under the assumption of the steady rotation of the engine crankshaft). But when studying the combustion process when the crank angle is dependent on time and the compression volume value, this substitution is not always proper. The variation of the compression volume definitely results in the temperature variation in the cylinder and the concentration variation of the reactants and, consequently, the oxidation reaction rate. In this case it is impossible to identify the cause of the combustion rate alteration uniquely: either it is the result of the temperature and concentration variations, or it takes place with time. The new parameter eliminates this disadvantage as it considers the quantity of molecules of all the actuating medium components and the compression volume value in explicit form.

The equation to obtain the relative duration of the reaction oxidation of the active fuel molecule group is as follows:

$$\tau_y = \frac{Z_F}{const \cdot K_1 \cdot K_2 \cdot V \cdot C_F^p \cdot C_{O_2}^q} = \frac{V}{const \cdot K_1 \cdot K_2 \cdot Z_F^{p-1} \cdot Z_{O_2}^q}, \quad (1)$$

where Z_F – the total quantity of fuel molecules in the volume under study V of the engine cylinder; $const$ – the constant which considers the amount of collisions of active molecule reactants in time unit in volume unit; K_1 – the coefficient which considers the influence of the inert components of the actuating medium and combustion products; K_2 – the coefficient which regards the turbulence inside the combustion chamber, $K_2 \geq 1$; $C_F = Z_F/V$ и $C_{O_2} = Z_{O_2}/V$ – the concentrations of all the molecules of the fuel Z_F and the oxygen Z_{O_2} in the volume V respectively; p, q – exponents of power, and $p+q=n$ – the kinetic index of the reaction, $n=2$.

Coefficient K_1 is taken from the equation which is derived from the dependence of the ignition delay period [7] from the oxygen concentration in the oxidant (Fig. 1):

$$K_1 = 1 - \left(1 - \frac{Z_{O_2}}{Z_{O_2} + Z_{N_2} + Z_{CO_2} + Z_{H_2O} + Z_{CO}} \right)^6, \quad (2)$$

where $Z_{N_2}, Z_{CO_2}, Z_{H_2O}$ и Z_{CO} – the quantities of the nitrogen, carbon dioxide, water and carbon monoxide molecules in the rated volume V respectively.

Coefficient K_2 is worked in to model the influence of the combustion mixture motion (if it's necessary).

The active fuel molecule quantity (according to Arrhenius equation) is defined by the following expression:

$$dZ_F = Z_F \cdot e^{-\frac{E_a}{RT}}, \quad (3)$$

where E_a – the activation energy of fuel molecule.

The quantity of the molecules which react at a computation step $\Delta\phi$, is obtained from the equation:

$$\Delta Z_i = \frac{dZ_F \cdot \Delta\varphi}{\tau_r \cdot 6 \cdot n} \quad (4)$$

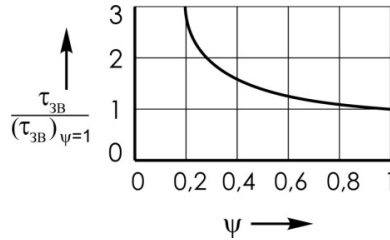


Fig. 1. Influence of concentration of oxygen in an oxidizer on relative size of an ignition delay time [7]

The mass of the fuel combusted at a computation step $\Delta\varphi$, is derived from the equation:

$$\Delta m_{comb} = \Delta Z_i \cdot \mu_F \cdot A_0, \quad (5)$$

where μ_F – the fuel molecule mass, A_0 – Avogadro constant.

The quantity of the heat generated by the fuel combustion at a computation step $\Delta\varphi$, is derived from the equation:

$$\Delta Q_{comb} = \Delta m_{comb} \cdot \xi \cdot H_u, \quad (6)$$

where ξ – combustion effectiveness ratio coefficient; H_u – low heat value of the fuel.

The more detailed description of the mathematical model is given in [8].

When the temperature in the fuel combustion area exceeds 1500-1700°K, the carbon dioxide dissociation process starts to influence on the law of pressure changing in the cylinder through energy consumption on this process. Therefore, to model the combustion process in the real engine the carbon dioxide dissociation process model is developed, and it allows to determine energy dissipation and instant quantities of oxygen, carbon monoxide and carbon dioxide molecules in the engine cylinder.

2.2. The model of the dissociation process of carbon dioxide

The model of the dissociation process of carbon dioxide generated at fuel combustion in the diesel engine cylinder under the conditions of non-stationary heat and mass exchange consists of equations for dissociation degree determination for quasi-equilibrium state according to V.V. Pomerantsev [9], the quantity of carbon dioxide molecules dissociated into carbon monoxide and oxygen molecules, and also energy consumptions on this process. It is considered that at temperature decreasing in the combustion area the dissociation process is going on in the opposite direction with heat generation by the carbon monoxide oxidation.

The carbon dioxide molecule quantity ΔZ_{CO_2} dissociated per the computation step is determined through the dissociation degree α at the current pressures, temperatures and the actuating medium composition.

The dissociation degree α is obtained as the solution of the cubic equation by the Viète-Cardan method:

$$\alpha^3 + \alpha^2 \frac{2\beta}{1 - K_p^2 p} + \alpha \frac{(-3 - 4\beta)}{1 - K_p^2 p} + \frac{2 + 2\beta}{1 - K_p^2 p} = 0, \quad (7)$$

where p – the in-cylinder pressure; K_p – reaction equilibrium constant, is obtained from the equation

$$\lg K_p^2 = \frac{29791}{T} + 0,169 \cdot 10^{-3} T - \frac{0,324 \cdot 10^5}{T^2} - 9,495 \quad [10]; \beta - \text{relation of the sum of the mole quantities of nitrogen}$$

N_{N_2} and water N_{H_2O} to the quantity of carbon dioxide moles N_{CO_2} in the actuating media at the beginning of the computation step: $\beta = \frac{N_{N_2} + N_{H_2O}}{N_{CO_2}}$.

The equation (4) is obtained for the reaction $N_2 + H_2O + 2CO + O_2 \Leftrightarrow N_2 + H_2O + 2CO_2$ after the equilibrium establishing [11].

The energy consumptions on the dissociation of these molecules are determined according to the equation

$$\Delta Q_d = \Delta Z_{CO_2} \cdot \mu_{CO_2} \cdot A_0 \cdot E_d \quad , \quad (8)$$

where μ_{CO_2} – the molecule mass of carbon dioxide; E_d – the energy consumed on the dissociation of one carbon dioxide molecule.

2.3. The model of a operating cycle of the diesel engine

The model of a operating cycle of the diesel engine assumes that the injected diesel fuel occupies only part of the current volume of the cylinder δ . Its value and changes in the law are set on the basis of experimental data on the results of the tests of mixture formation at motorless stand. In this part of δ is distributed evenly all the fuel Z_F , filed into the cylinder at the moment. For the calculation of step $\Delta\varphi$ active molecules fuel dZ_F , defined by the formula (1) is the mass of fuel burned Δm_{comb} by expression (2). Herewith heat release ΔQ_{comb} is determined by expression (3), which is consumed (goes) to heat the working fluid in the cylinder.

Calculations the operating cycle diesel engine is produced through the steps from point 1 (the beginning step) to point 2 (end of step) according to known method [3]. Herewith is used the following equation to determine the pressure in the cylinder of the diesel engine at each step of the calculation [11]:

$$p_2 = \frac{\frac{2(\Delta Q_{comb} - \Delta Q_{well} - \Delta Q_d)}{m} + p_1 \left(v_1 \frac{k+1}{k-1} - v_2 \right)}{v_2 \frac{k+1}{k-1} - v_1} \quad , \quad (9)$$

where ΔQ_{well} – the heat transfer through the walls of the cylinder head, the piston, and the liner; m – in-cylinder gas mass; p, v – the in-cylinder gas pressure and specific volume; $k = C_p/C_v$ – adiabatic index.

The heat transfer through the walls of the cylinder head, the piston, and the liner is calculated under law Newton-Rikhman

$$\Delta Q_{well} = \frac{\alpha_1 F_1 (T_1 - T_w) \Delta\varphi}{6n} \quad , \quad (10)$$

where α_1 – the in-cylinder heat transfer coefficient from gas to inner cylinder wall; F_1 и T_w – area and the surface temperature of cylinder volume at the beginning of the step of calculating; T_1 – temperature of gas in the beginning of the calculating step; n – engine speed, $\Delta\varphi$ – crank angle for a calculation step.

The models described above are assumed as a basis of the methodic and algorithm of the program for engineering calculation of the operating cycle diesel engine with a given law of of mixture formation. The possibilities of the program are shown in the example calculation research the influence of temperature of a fresh charge after charge air cooler on the indicators operating cycle of a powerful diesel engine.

Fig. 2 shows the results of calculation of the operating cycle of a diesel engine at different temperatures the actuating medium at the beginning of the compression T_a . The increase of this temperature from 360°K to 430°K at constant other parameters leads to a significant deterioration of indicated parameters and decrease of the maximum pressure of gases in the cylinder of a diesel engine. Best indicated parameters obtained at $T_a = 360$ K: mean

indicated pressure of cycle $p_i = 2,29$ MPa, the specific fuel consumption indicator $g_i = 180,6$ g/kWh, indicated efficiency $\eta_i = 0,469$. Maximum in-cylinder pressure p_{max} is 15.97 MPa. The deterioration of the indicated parameters and decreased of the maximum pressure in the cylinder occurs as a result of reduce the excess air ratio and changes of law heat release.

The given dependence on rice. 2 will well be agreed with the experimental data on the influence of the temperature of a fresh charge after charge air cooler on indicated parameters of a operating cycle of a diesel engine of increased power.

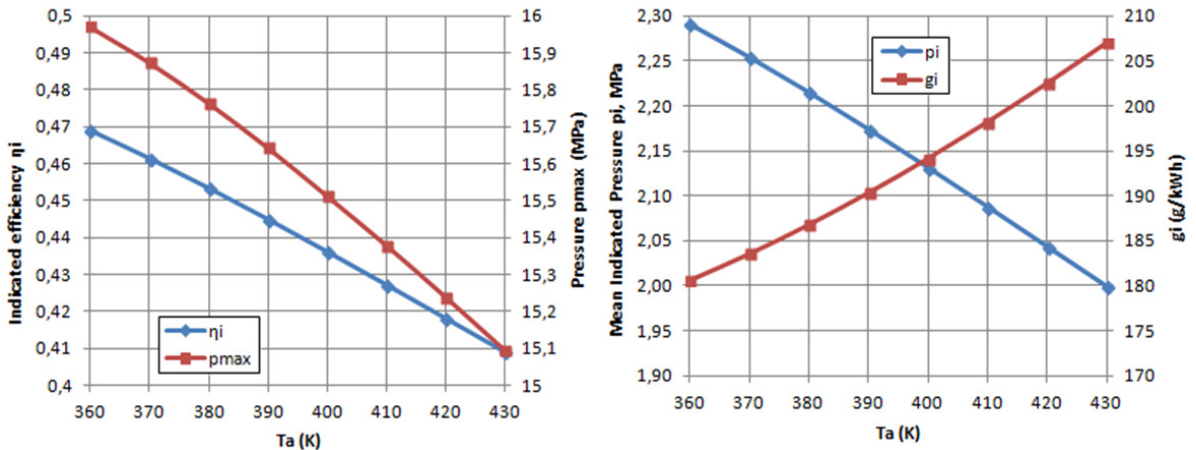


Fig. 2. The dependence of the parameters p_{max} , η_i , p_i , g_i from the temperature of the actuating medium at the beginning of compression

Fig. 3 shows curves of the calculated the in-cylinder pressure and the heat release rate at various temperatures of the actuating medium at the beginning of the compression T_a . Here it is seen that the higher the temperature T_a , the earlier the start of the combustion process and less the maximum heat release rate. When $T_a = 360^\circ\text{K}$ the largest ignition delay period during which a larger quantity of fuel being prepared. This results in to increased the rate of pressure increase, increasing the maximum pressure in the cylinder and improve the indicated parameters of the operating cycle diesel engine. The maximum heat release rate in the main period (the second maximum) is almost does not change.

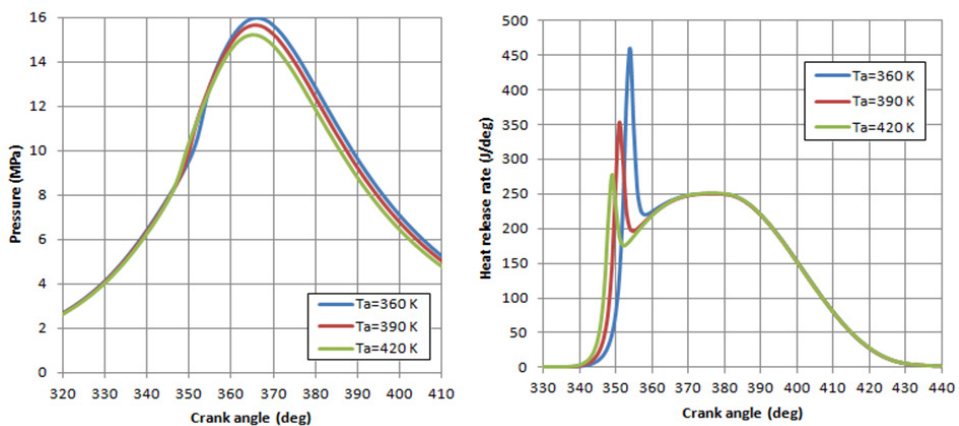


Fig. 3. Diagrams of variation of in-cylinder pressure and heat release rate at various temperatures T_a the actuating medium at the beginning of

the compression

Diagrams of pressure in the cylinder and the laws of heat release produced by the developed calculation models will well be agreed with the experimental data obtained in the analysis of the indicated parameters of diesel engines increased power. This proves the possibility of using the developed mathematical models for engineering calculation of the operating cycle of the powerful diesel.

Thus, the use of the developed program allows on the design stage to simulate and plan a rational law for of mixture formation for getting effective combustion process and the best indicated parameters of the operating cycle of the powerful diesel engine

3. Conclusion

We can make the following conclusions based on the results of the research.

- The models and program for calculating the operating cycle of diesel engine with a given law of of mixture formation is developed.
- The novelty of the combustion process model is the introduction of the new parameter considering the time factor in this process – the conventional duration of the fuel molecule oxidation reaction and the equation for its determination, in dependence on the oxygen, fuel, nitrogen and combustion products in the combustion chamber molecule quantity, the volume of the combustion chamber, the physicochemical property of the fuel.
- The best indicated parameters the operating cycle of the powerful diesel engine produced at a temperature the actuating medium at the beginning of compression $T_a = 360^\circ\text{K}$ and related to maximum cooling of the charge air cooler.
- Diagrams of pressure in the cylinder of the powerful diesel engine and laws of heat release produced calculation of the developed models will well be agreed with the experimental data.
- Using the developed program allows the design stage to simulate and plan a rational law for effective of mixture formation of the combustion process and the best indicators of the operating cycle of the powerful diesel engine.

Acknowledgements

This work is carried out under support of the federal goal-oriented program “Research and development on priority directions of scientific-technological complex of Russia, 2014-2020”.

References

- [1] R.Z. Kavtaradze, Lokalnyiy teploobmen v porshnevnykh dvigatelyakh, [Local heat exchange in piston engines]. Textbook for high schools, MSTU of N.E. Bauman Publ., Moscow, 2001.
- [2] A.K. Kostin, Teplonapryazhennost dvigateley vnutrennego sgoraniya, [Thermal stress of internal combustion engines]. Handbook, Mashinostroenie Publ., Leningrad, 1979.
- [3] I.I. Wiebe, Novoe o rabochem cikle dvigatelej, [New about the working cycle of the engines], Mashgiz Publ., Moscow, 1962.
- [4] Zhaolei Zheng, Mingfa Yao, Numerical study on the chemical reaction kinetics of n-heptane for HCCI combustion process. 85 (2006) 2605–2615.
- [5] A. Bhave, M. Balthasar, M. Kraft, F. Mauss, Analysis of a natural gas fuelled homogeneous charge compression ignition engine with exhaust gas recirculation using a stochastic reactor model, Int. J. Engine Res. 5(1) (2004) 93–103.
- [6] D.A. Frank-Kamenetskiy, Diffuziya i teploperedacha v himicheskoy kinetike, [Diffusion and heat transfer in chemical kinetics], Science Publ., Moscow, 1987.
- [7] Pahl, Beiträge zur Erforschung des Zündproblemens flüssiger Brennstoffe, München, 1927.
- [8] V.G. Kamaltdinov, Novaya model protsessa goreniya topliva v DVS, [New model of process of burning of fuel in an internal combustion engine], Dvigatelenstroenie. 233(3) (2008) 17–20.
- [9] V.V. Pomerantsev, Osnovyi prakticheskoy teorii goreniya, [Bases of the practical theory of burning], Manual, Energiya Publ., Leningrad, 1973.
- [10] A.A. Ravdel', A.M. Ponomareva, Kratkiy spravochnik fiziko-himicheskikh velichin, [Short reference book of physical and chemical sizes], Chemistry Publ., Leningrad, 1983.
- [11] V. Kamaltdinov, Combustion process modeling in HCCI engine. JSAE 201119118, SAE Technical Paper. 1(1789) (2011) 10.



International Conference on Industrial Engineering

Feed speed control to assure accuracy of complex profile surfaces processing

Guzeev V.I.*

South Ural State University, 76, Lenin ave., Chelyabinsk, 454080, Russian Federation

Abstract

This document describes how cutting force components influence the accuracy of processing complex profile surfaces of parts on CNC machines. It demonstrates how changing cutting zone geometrical parameters influences cutting force components. The article includes dependences for determining cutting force components. We propose a mathematical model to identify dynamic size-setting errors for 2D machining of complex profile surfaces. We suggest a processing method to reduce error occurrence rate by controlling feed speed. This document includes a method of setting feed motion speed depending on the geometrical parameters of the machined surface. We recommend changing feed motion speed depending on machined surface pitch against the feed motion vector. We demonstrate that feed motion speed control allows to increase machining efficiency while assuring the set accuracy of the shape and dimensions of the components' complex profile surfaces.

© 2015 The Authors. Published by Elsevier Ltd. This is an open access article under the CC BY-NC-ND license (<http://creativecommons.org/licenses/by-nc-nd/4.0/>).

Peer-review under responsibility of the organizing committee of the International Conference on Industrial Engineering (ICIE-2015)

Keywords: Processing accuracy, complex profile surfaces, cutting forces, feed speed control, cutting modes, CNC machines.

1. Introduction

Machine building industry has a task of increasing parts producing accuracy. We are talking about 10 times accuracy increasing and assuring roughness of up to $Rz = 0.001$ mm. Same time, approaches to designing technological processes of manufacturing parts on metal cutting machines mostly remain traditional. Process designing mainly uses reference data for evaluating processing accuracy per process steps. Cutting modes choosing reference books don't demonstrate full relation to all parameters of processing accuracy [1, 2, and 3]. Often cutting

* Corresponding author. Tel./fax: +7-351-267-92-73.

E-mail address: gvi174@yandex.ru

modes are determined by cutting tool strength and resistance. Lack of reference data on complex relation of all processing accuracy parameters with cutting modes, tool, fittings, and equipment parameters, leads to significant role of subjective decisions on designing technological processes. This leads to moving accuracy assuring tasks to technological process adjusting stage, leading to significant increase in its labor intense and cost. Taking into account small-scale of modern production with high concentrated process operations, accuracy becomes very critical. Processing of complex profile surfaces is the most difficult task if considering assuring accuracy.

2. Cutting forces influence on processing errors

Due to process non-stationary, main part of errors is due to dynamic setting size errors. In order to predict these errors it is necessary to evaluate cut forces and process system condition. Cutting forces can be determined with practical degree of accuracy on the basis of reviewing elementary components of cutting force, acting at infinitesimally small area of the tool cutting edge [4].

This approach allows creating universal mathematics model of the cutting force, invariant to different processing types.

According to forces and stresses on elementary area of the tool forward and rear surfaces, cutting forces components during sharpening are determined by:

$$\begin{aligned} dP_{xy} &= \frac{\sigma_i a_i db}{\sqrt{3} \sin\beta_1 \cos(\beta + \beta_1)} \sin\beta + 0,16\sigma_i l_w db; \\ dP_z &= \frac{\sigma_i a_i db}{\sqrt{3} \sin\beta_1 \cos(\beta + \beta_1)} \cos\beta + 0,16\mu\sigma_i l_w db, \end{aligned} \quad (1)$$

where: dP_{xy} – component of cutting force in main plain; dP_z – cutting force main component; a_i – cut-off layer thickness on tool cutting edge elementary area; db – cutting edge elementary area; β_1 – reference shear plane pitch. Most often it is determined by chip thickening coefficient; σ_i – intensity of stresses in shear area; β – angle between shear line and resultant force direction; l_w – worn face length; μ – friction coefficient.

When knowing the force, acting on elementary areas of the tool cutting edge active zones, we can determine (by integration) cutting force components for any processing conditions as for simple surfaces, with generator lines, parallel to machine coordinate axes, as for complex profile surfaces, randomly located in the machine coordinates system.

We shall discuss design accuracy prognosis on the example of 2D machining of complex profile surfaces in one stage [5].

We talk about 2D machining when performing contour turning, bore machining, and contour milling with core mills. This type of processing is characterized by the fact, that two cutting force components influence process system elastic displacements error and its changing. P_x, P_y for turning and P_z, P_y for contour milling.

Lets discuss analytical model of contour processing error forming $y = \phi(x)$ (Fig. 1). Resulting from joint acting of components P_x and P_y (for turning) and some extend of process system flexibility, point A , being a part of tool cutting edge with coordinates (x_i, y_i) , will move to point B with coordinates $(x_i + \Delta x, y_i + \Delta y)$. Where Δx and Δy are amounts of the tool elastic moving along appropriate coordinates. Part contour tangent line in point A is as follows:

$$y - y_i = \frac{\partial y}{\partial x}(x - x_i). \quad (2)$$

In order to find size error in point A along normal line in this point we'll modify coordinate axes XOY by relocating there beginning point to point A . In new coordinates system point B is determined by coordinates $(\Delta x, \Delta y)$, and equation (2) can be read as follows: $Ax + By = 0$, where $A = \frac{\partial y}{\partial x}$, $B = -1$.

Distance Δ_N from point B to tangent line in point A is determined according to known equation: $\Delta_N = \frac{A\Delta x + B\Delta y}{\sqrt{A^2 + B^2}}$ [6].

Taking previously determined designations into account, we'll have to following:

$$\Delta_N = \frac{\Delta y - \frac{\partial y}{\partial x} \Delta x}{\sqrt{1 + \left(\frac{\partial y}{\partial x}\right)^2}} \tag{3}$$

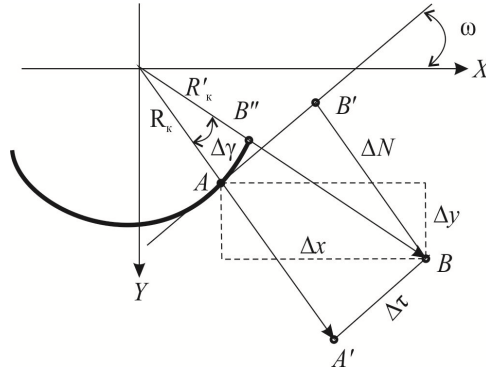


Fig. 1. Analytical model of determining errors for 2D machining.

Considering instrument displacement along X axis, actually this moment of machining forms part profile error in point B'' , where error Δ_f along normal line is equal to jog BB'' . Its size is determined from a triangle:

$$\Delta_f = \frac{R_k + \Delta_N}{\cos\left(\arctg \frac{\Delta_\tau}{R_k \pm \Delta_N}\right)} - R'_k \tag{4}$$

where R_k – machined contour curve radius in point A ; R'_k – machined contour curve radius in point B' ; Δ_τ – elastic relative tool movement to tangent line in point A .

Taking into account that $\Delta_\tau = \Delta y \sin\omega + \Delta x \cos\omega$, and using value Δ_N from relation (3), we'll obtain formula for determining dynamic setting size error for 2D contour machining:

$$\Delta_f = R_k + \frac{\Delta y - \frac{\partial y}{\partial x} \Delta x}{\sqrt{1 + \left(\frac{\partial y}{\partial x}\right)^2}} \cdot \cos\left[\arctg \frac{\frac{\partial y}{\partial x} \Delta y + \Delta x}{R_k \sqrt{1 + \left(\frac{\partial y}{\partial x}\right)^2} \pm \Delta y \mp \frac{\partial y}{\partial x} \Delta x}\right] - R'_k \tag{5}$$

In formulas (4) and (5) (+) signs are used for external turning and contour milling of contour convex areas, (–) signs – for bore machining and concave areas milling. Δ_x and Δ_y values are determined by dividing appropriate cutting force component by process system stiffness along machine coordinate axes directions. Stiffness can be determined by testing the process system [7].

Obtained relation demonstrates that kinematic angles changing in plan influence on machining error under all else being equal is as larger, as lower the machined part area curve radius is.

Calculations demonstrate that changing cutting forces, depending on part machined surface tangent line pitch, lead to errors of dynamic setting size, changing on different machined surface areas 4 and more times. This leads to machined part shape errors that, due to variability of their values within one surface, can't be compensated by introducing simple correction of static setting size.

Non-stationary machining parameters influence on accuracy can be decreased at technological process design stage by directed control over feed speed, set in control program.

3. Feed speed control

Having error value Δ_f as a target and solving equation (5) relative to feed S , we can determine law of feed control, assuring stabilization of pushing out the technological system elements. Graphs of feed changing for assuring dynamic setting size error constancy are presented in Fig. 2.

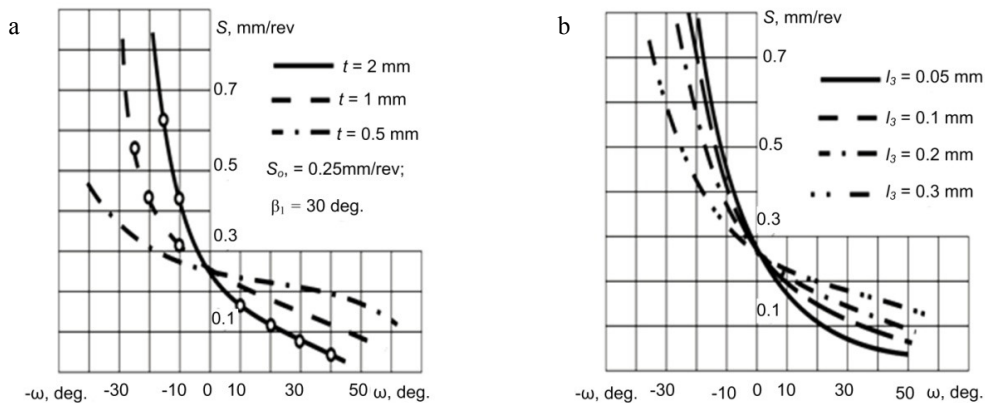


Fig. 2. Graphs of changing feed for assuring error constancy depending on (a) cutting depth (b) cutter wear.

Calculations and presented graphs demonstrate, that, when preparing control programs for complex profile surfaces machining, it is necessary to set different feed speeds for surface areas with different pitches of machined surface tangent line against machine spindle axis.

Practical experience in cylinder parts machining modes setting is quite enough. Usually parts, machined on CNC machines, have combinations of cylinder and profiled surfaces. Due to this fact it seems reasonable to determine law of setting feed change at profiled surface, taking into account feed speed for cylinder part. In this case speed change law should assure same machining error for all part sections, or different with regulating feed for each section. Method of determining such law is as follows:

- feed for cylinder surface is set on the basis of regulatory recommendations;
- based on set feed and implementing relation (5) dynamic setting error for cylinder surface is determined;
- values of cylinder part predicted error are introduced into formula for determining law of changing feed depending on shape of the machined profiled surface.

4. Conclusions

Software control over feed speed allows assuring necessary accuracy of machined surfaces shape and improves machining effectiveness.

In order to improve technological processes effectiveness on the stage of their implementation, it is reasonable to use machine computer for determining specific technological system status and to perform software customizing their parameters.

In this case it is reasonable to divide between designing and producing systems functions of assuring parts quality and assuring reliability of process operation performing.

Following can be taken as the basis for software-customizing designing of technological operations: analytical dependences, determining relations between main machining process parameters (cutting mode, tool geometry and its wear rate, physical-mechanical parameters of machined material, work pieces errors, and technological system stiffness) and assured parts sizes and shape accuracy, as well, as dependences, taking into account physical condition of the technological system. Testing of the technological system allows not only determining transfer factors for calculating designed operation accuracy balance, but also specifying technological process model according to calculated machining stages quantity and their content for each part surface. Necessary tests, allowing determining actual technological system status, are chosen for specified model. Transfer functions of dominant effects at each machining stage are also determined. Initial technological operation parameters are corrected by means of mathematical models, functionally linking produced component output parameters (accuracy and degree of roughness) with current operation parameters (5). Feed speed software control, taking into account actual technological system stiffness, allows decreasing machining cycle duration for complex profile surfaces 1.5 times by means of decreasing time period, spent for adjusting CNC machine control program.

Analyzed method allows controlling feed speed for 3D machining on CNC milling machines, taking into account three components of the cutting force influence on machining errors.

References

- [1] General Machine-Building Regulations on Time and Cutting Modes for Regulating Works, Performed on Multipurpose and Universal Machines with Numerical Control, Cutting Modes Rules, Ekonomika, Moscow, 1990.
- [2] A.D. Loktev, I.F. Gushchin, V.A. Batuev, General Machine Building Regulations on Cutting Time and Modes Guide Book, Mashinostroenie, Moscow, 1991.
- [3] V.I. Guzeev, V.A. Batuev, I.V. Surkov, Modes of Cutting for Turning and Drilling-milling-boring CNC Machines, Mashinostroenie, Moscow, 2005.
- [4] S.N. Korchak, Steel Details Grinding Process Effectiveness, Mashinostroenie, Moscow, 1974.
- [5] V.I. Gezeev, Particulars of Determining Cutting Modes for Multipass Machining, J. Bulletin of the South Urals State University. Series Mechanical Engineering Industry. 4 9(25) (2003) 112–120.
- [6] G. Korn, T. Korn, Reference Book on Mathematics for Scientific Workers and Engineers, Nauka, Moscow, 1973.
- [7] V.I. Guzeev, A.Kh. Nurkenov, A.V. Ignatova, Research Stiffness of CNC Plunge Grinding Machine Units, J. Russian Engineering Research. 35(1) (2015) 69–72.

International Conference on Industrial Engineering

Mathematic Model of the Blunting Area of an Abrasive Grain in Grinding Processes, with Account of Different Wear Mechanisms

Ardashev D.V.^{a*}

^a South Ural State University, 76, Lenin Avenue, Chelyabinsk, 454080, Russian Federation

Abstract

The intensity and the degree of blunting are the main factors which define the working capacity of a grinding wheel. When we consider the discrete contact of a grinding wheel with a work piece, the size of the blunting area can be such a factor. The article presents a mathematic model to calculate the blunting area of an abrasive grain whereby the main mechanisms of its wear such as mechanical and physicochemical phenomena are taken into account. The mechanical wear is studied from the standpoint of the kinetic theory of strength, a durability parameter for the abrasive grain is determined; the physicochemical wear is studied from the mass transfer theory, and coefficients of chemical affinity with the abrasive material are experimentally defined for the assortment of work piece materials. As mechanical and physicochemical wear of abrasive grain depend on the initial size of the blunting area, the suggested mathematic model is the first to consider nonlinear back-coupling, taking into account the size of the blunting area. The developed mathematic model is a multiple-factor one, which will allow to predict the worn area of the abrasive wheel for, and under different technological conditions.

© 2015 The Authors. Published by Elsevier Ltd. This is an open access article under the CC BY-NC-ND license (<http://creativecommons.org/licenses/by-nc-nd/4.0/>).

Peer-review under responsibility of the organizing committee of the International Conference on Industrial Engineering (ICIE-2015)

Keywords: grinding wheel, blunting area, wear of abrasive grain

1. Introduction

Different types of the abrasive grains' wear in grinding are described in detail in scientific literature in the works by T. N. Loladze and G. V. Bokuchava [1], L. N. Filimonov [2], L. L. Mishnaevskii [3], E. N. Maslov [4], V. A. Nosenko [5], S. Yossifon [6], S. J. Deutsch [7], R. Neugebauer [8], M. P. Hitchiner [9], O. I. Medvedeva [10] W. Graham, C.M. Voutsadopoulos [11] and others. All these works contain researches aimed at investigating this or

* Corresponding author. Tel.: +7-922-230-48-07;
E-mail address: dva79@inbox.ru

that wear mechanism of the abrasive grain in different technological conditions of grinding done by empiricism-theoretical methods. It is necessary to state that in the majority of technical literature mechanical and physicochemical wear of the abrasive grain in grinding processes are accepted as the main ones, which function while grinding the overwhelming majority of alloys and steels. However, nowadays there are no dependences which allow predicting the size of the blunting area of the abrasive grain in different technological conditions.

Nomenclature

$M_{a.g.}$	the weight of the abrasive grain abraded by the interaction with the workpiece
$M_{a.g.}^m$	the weight of the abrasive grain abraded by the mechanical interaction with the workpiece
$M_{a.g.}^{ph.-ch.}$	the weight of the abrasive grain abraded by the physicochemical interaction with the workpiece
τ_c	the durability of abrasive grain by cyclic load
v_w	the speed of the work piece rotation
V_{wh}	the speed of grinding wheel rotation
D_{wh}	the diameter of the grinding wheel
d_w	the diameter of the workpiece
n_w	the frequency of work piece rotation (the number of turns)
v_{Srad}	the speed of radial feed of the grinding wheel
I_0	the Bessel function of the imaginary argument
q	the coefficient of interatomic bonds overstrain
M_m	the atomic weight of Al_2O_3
ρ_a	the density of the abrasive material
σ	the tension in the abrasive grain
k	the Boltzmann constant
T_i	the absolute temperature of the abrasive grain (temperature in the interface)
$w_{a.g.}^m$	the elementary volume of the abrasive material
T	the period of the grain work
n_{wh}	the frequency of grinding wheel rotation (the number of turns)
ρ_w	the density of the workpiece material
m_a	the atomic weight of the Al_2O_3
m	the atomic weight of the workpiece material
C_0	the limiting solubility of fused alumina in the workpiece material
$l_{bl.}$	the size of the blunting area on the abrasive grain
D_{af}	the coefficient of the chemical affinity of the abrasive and work piece
L_c	the length of the contact arc of the abrasive grain with the work piece
V	the volume of the abrasive material outworn by the interaction with the workpiece
$l_{bl,i-1}$	the size of the blunting area on the abrasive grain at every previous time point

2. Research results

In general, the model of the wear of the abrasive grain in grinding processes which considers different mechanisms of its behavior is presented below:

$$M_{a.g.} = M_{a.g.}^m + M_{a.g.}^{ph.-ch.} \quad (1)$$

Examining the mechanical wear of the abrasive grain as the process which develops in time, the equation of durability by cyclic load for conditions of external cylindrical grinding with radial feed [12, 13] is:

$$\tau_c = \frac{n_{wh} \cdot \left(1 + \frac{v_w}{60V_{wh}}\right) \sqrt{\frac{D_{wh} \cdot d_w \cdot \frac{v_{Srad}}{n_w}}{D_{wh} + d_w}} \cdot I_0 \left(i, \frac{q \cdot M_m}{6\rho_a \cdot 10^{23} \cdot 2kT_t} \sigma \right)}{60V_{wh} \cdot \frac{q \cdot M_m}{6\rho_a \cdot 10^{23} \cdot 2kT_t} \sigma} \quad (2)$$

Then, having defined the elementary volume of the abrasive material $w_{a.g.}^m$, which experiences tension σ and separates from the grain in some period of time τ_c , it is possible to estimate the weight of the abrasive grain which is outworn as a result of its mechanical interaction with the work piece taking into account the action period of the work T :

$$M_{a.g.}^m = \frac{\rho_a \cdot w_{a.g.}^m \cdot T}{\tau_c} \quad (3)$$

If we put Eq. 2 in Eq. 3, we get the general formula to define the weight of the abrasive material which is outworn as a result of its mechanical interaction with the workpiece:

$$M_{a.g.}^m = \frac{60V_{wh} \cdot \rho_a \cdot w_{a.g.}^m \cdot T \cdot \exp\left(\frac{q \cdot M_m}{6\rho_a \cdot 10^{23} \cdot 2kT_t} \sigma\right)}{n_{wh} \cdot \left(1 + \frac{v_w}{60V_{wh}}\right) \sqrt{\frac{D_{wh} \cdot d_w \cdot \frac{v_{Srad}}{n_w}}{D_{wh} + d_w}} \cdot I_0 \left(i, \frac{q \cdot M_m}{6\rho_a \cdot 10^{23} \cdot 2kT_t} \sigma \right)} \quad (4)$$

Very detailed researches were carried out by T.N.Loladze and G.V.Bokuchava aimed at studying physicochemical processes which take place in the cutting area. These scientists worked out a formula (5), to calculate the size of the abrasive grain weight which is outworn as a result of its physicochemical interaction with the work piece [14]:

$$M_{a.g.}^{ph.-ch.} = 0,08\rho_w \frac{m_a}{m} C_0 l_{bl}^{3/2} D_{af}^{1/2} L_c V_{wh}^{1/2} \frac{T}{D_{wh}} \quad (5)$$

A complex of experiments was carried out to define the amount of the affinity coefficient D_{af} , the results of which allow to estimate the intensity of the physicochemical interaction of the abrasive and work piece [15].

Summarizing the research results of the mechanical and physicochemical wear of the abrasive grain in grinding processes and putting Eq. 4 and 5 into Eq. 1, we get a new formula to define the weight of the abrasive grain which is outworn as a result of the joint action of the mechanical and physicochemical wear:

$$M_{a.g.} = \frac{60V_{wh} \cdot \rho_a \cdot w_{a.g.}^m \cdot T \cdot \exp\left(\frac{q \cdot M_m}{6\rho_a \cdot 10^{23} \cdot 2kT_t} \sigma\right)}{n_{wh} \cdot \left(1 + \frac{v_w}{60V_{wh}}\right) \sqrt{\frac{D_{wh} \cdot d_w \cdot \frac{v_{Srad}}{n_w}}{D_{wh} + d_w}} \cdot I_0 \left(i, \frac{q \cdot M_m}{6\rho_a \cdot 10^{23} \cdot 2kT_t} \sigma \right)} + 0,08\rho_w \frac{m_a}{m} C_0 \cdot l_{bl}^{3/2} \cdot D_{af}^{1/2} \cdot L_c \cdot V_{wh}^{1/2} \frac{T}{D_{wh}} \quad (6)$$

In order to define the size of the blunting area depending on the volume of the outworn part of the abrasive grain we can present the abrasive grain in the form of a cone. As a result of geometrical transformations it is seen that the size of the grain blunting area at any period of time can be defined using Eq.7:

$$l_{bl,i} = 2\sqrt[3]{l_{bl,i-1} + \frac{3V}{\pi}} = 2\sqrt[3]{l_{bl,i-1} + \frac{3M_{a.g.}}{\pi\rho_a}} \tag{7}$$

Taking into account Eq. 6, we get an equation to define the size of the abrasive grain blunting area at any time of its interaction with the work piece:

$$l_{bl,i} = 2\sqrt[3]{l_{bl,i-1} + \frac{180V_{wh} \cdot w_{a.g.}^m \cdot T \cdot \exp\left(\frac{q \cdot M_m \cdot \sigma}{12kT_t \cdot \rho_a \cdot 10^{23}}\right)}{n_{wh} \cdot \left(1 + \frac{v_w}{60V_{wh}}\right) \sqrt{\frac{D_{wh} \cdot d_w \cdot v_{Srad}}{n_w (D_{wh} + d_w)}} \cdot I_0 \left(i, \frac{q \cdot M_m \cdot \sigma}{12kT_t \cdot \rho_a \cdot 10^{23}}\right) \pi} + \frac{0,24C_0 \cdot l_{bl,i-1}^{3/2} \cdot D_{af}^{1/2} \cdot L_c \cdot V_{wh}^{1/2} \cdot \rho_w \cdot m_a \cdot T}{D_{wh} \cdot m \cdot \pi \cdot \rho_a}} \tag{8}$$

Figure 1 shows dependencies of the size of the blunting area which were obtained using Eq. 8 and calculated for the initial period of the tool work, and also data of other researchers was used.

It is clearly seen from the figure that the model of calculation of the size of the blunting area considering different wear mechanisms is appropriate and can be used to predict the size of the wear of the abrasive instrument in general.

3. Conclusion

The developed mathematic model of defining the size of the blunting area of the abrasive grain in different technological conditions is:

- recursive, allows to take into consideration the inverse nonlinear coupling according to the size of the blunting area of the abrasive grain which is generated as a result of the previous contact with the workpiece at every time point of the abrasive grain work;
- multiple-factor, allows to take into account a lot of technological conditions of grinding operations and the time of the tool work;
- complex, allows to take into account different mechanisms of the abrasive grain’s wear.

The mathematical definition of the blunting area depending on the technological conditions, in which the abrasive tool is being operated, will allow predicting the amount of its operational performances [19–22].

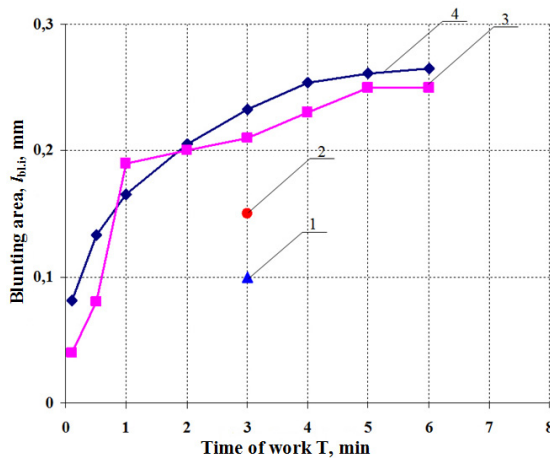


Fig. 1. The dependency of the size of the blunting ground on the time of the circle working:

1 – S. N. Korchak’s data – constant [16]; 2 – A. A. Matalin’s data – constant [17]; 3 – A. A. Dyakonov’s data (experiment) [18]; 4 – obtained by formula (8).

References

- [1] T.N. Loladze, The hardness and wear resistance of cutting tool, Mashinostroenie, Moscow, 1982.
- [2] L.N. Filimonov, The durability of grinding wheels, Mashinostroenie, Leningrad, 1973.
- [3] L.L. Mishnaevskii, The wear of grinding wheels, Naukova Dumka, Kiev, 1982.
- [4] E.N. Maslov, The Theory of Grinding, Mashinostroenie, Moscow, 1974.
- [5] V.A. Nosenko, M.V. Danilenko, The probabilities of types of the wear of wheel grains vertices and their dependence on the strength of the contact interaction and hardness of the abrasive tool, *Izvestiya of VolgGTU*. 5 (2009) 20–23.
- [6] S. Yossifon, Wheel wear when grinding workpieces exhibiting high adhesion, *International Journal of Machine Tool Design and Research*. 22 (1982) 159–176.
- [7] S.J. Deutsch, Analysis of mechanical wear during grinding by empirical-stochastic models, *Wear*. 29 (1974) 247–257.
- [8] R. Neugebauer, K.-U. Hess, S. Gleich, S. Pop, Reducing tool wear in abrasive cutting, *International Journal of Machine Tools & Manufacture*. 45 (2005) 1120–1123.
- [9] M.P. Hitchiner, J. Wilks, Some remarks on the chemical wear of diamond and cubic BN during turning and grinding, *Wear*. 114 (1987) 327–338.
- [10] O.I. Medvedeva, A.S. Yanushkin, V.Yu. Popov, The calculation of the adhesion energy of the contact surfaces in grinding instrumental materials by various methods, *Science Intensive Technologies*. 5 (2014) 14–19.
- [11] W. Graham, C.M. Voutsadopoulos, Fracture wear of grinding wheels, *International Journal of Machine Tool Design and Research*. 18 (1978) 95–103.
- [12] B.P. Regel, A.I. Slutsker, E.E. Tomashevsky, The kinetic theory of strength of solids, Science, Moscow, 1974.
- [13] D.V. Ardashev, Definition of Abrasive Grain Wear upon Grinding from the Standpoint of the Kinetic Theory of Strength, *Journal of Friction and Wear*. 3 (2015) 266–272.
- [14] T.N. Loladze, G.V. Bokuchava, About the theory of diffusion wear of diamond abrasive tools, *Trudy Vniish*. 1 (1965) 86–94.
- [15] D.V. Ardashev, Physicochemical wear of abrasive grains during grinding processes, *Journal of Friction and Wear*. 4 (2014) 284–289.
- [16] S.N. Korchak, The productivity of the grinding of steel parts, Mashinostroenie, Moscow, 1974.
- [17] E.N. Maslov, The mechanism of the working of abrasive grain in grinding, in: *The main questions of high-productivity grinding*. (1960) 5–30.
- [18] A.A. Dyakonov, Simulated stochastic thermo-physical model of grinding process, *Lecture Notes in Engineering and Computer Science*. 2 (2014) 914–917.
- [19] D.V. Ardashev, Two-parameter assessment of grinding wheel performance, *Russian Engineering Research*. 7 (2010) 705–707.
- [20] A.V. Popova, Design of optimal internal grinding cycles, *Russian Engineering Research*. 5 (2015) 378–380.
- [21] D.V. Ardashev, Group abrasive machining in flexible production, *Russian Engineering Research*. 4 (2015) 305–306.
- [22] D.V. Ardashev, Predicting the performance of abrasive tools in process design for diversified production, *Russian Engineering Research*. 3 (2015) 206–208.

International Conference on Industrial Engineering

Predicting the intensity of physicochemical interaction between the abrasive and workpiece material depending on the chemical composition of the material machined

Ardashev D.V.*

South Ural State University, 76, Lenin Avenue, Chelyabinsk, 454080, Russian Federation

Abstract

Physicochemical mechanism is one of the wear mechanisms of the abrasive grain in grinding. Existing scientific researches which deal with the wear of the abrasive grain show the presence of this wear mechanism but do not characterize it from the quantitative point of view. The article contains the results of the empirical studies on the physicochemical interaction between the abrasive grain and the workpiece material while grinding. The empirical studies allowed to determine the quantitative characteristics of physicochemical processes in grinding. The developed empirical models can predict the coefficient of chemical affinity for the workpiece materials with a variety of chemical compositions. The mathematical method used in this research makes it possible to define the size of the abrasive grain portion is worn as a result of such physicochemical interaction. In future, this circumstance will predict the extent of the abrasive tool wear under different technological conditions in order to define its operating capacity and apply the tool efficiently in multipart manufacturing.

© 2015 The Authors. Published by Elsevier Ltd. This is an open access article under the CC BY-NC-ND license (<http://creativecommons.org/licenses/by-nc-nd/4.0/>).

Peer-review under responsibility of the organizing committee of the International Conference on Industrial Engineering (ICIE-2015)

Keywords: physicochemical wear, abrasive grain, grinding.

1. Introduction

Grinding is the process of mutual fracture of two contacting solids: work and abrasive grains of the grinding wheel. It is supposed that the work material breaks more, and the cutting abrasive grains of the tool are worn during a long period of time – efficient tool life.

* Corresponding author. Tel.: +7-922-230-48-07;
E-mail address: dva79@inbox.ru

One of the main ways of the abrasive grain wear in grinding is physicochemical one [1-10], while there are no quantitative characteristics of this wear in scientific and technical literature. To define the quantitative parameter (coefficient of the chemical affinity of the abrasive and workpiece material) we used experimental researches with the electron scanning microscope JSM 6460LV (JEOL, USA) [11]. As a result, we got the bulk of experimental data which allow us to estimate quantitative and qualitative influence of chemical composition of the material being grinded on the density of physicochemical interaction with the abrasive material (fig. 1).

Nomenclature

T	the temperature of the abrasive grain (temperature in the interface)
D_{af}	the coefficient of the chemical affinity of the abrasive and work piece materials

2. Research results

Analyzing the influence of the temperature in the contact zone of the abrasive grain and workpiece it can be concluded that the rise of temperature in the contact zone of the abrasive grain and work leads to the rise of intensity of physicochemical interaction between materials. Therefore, in the cumulative volume of the worn spot abrasive the part of the wear increases as a result of this wear mechanism.

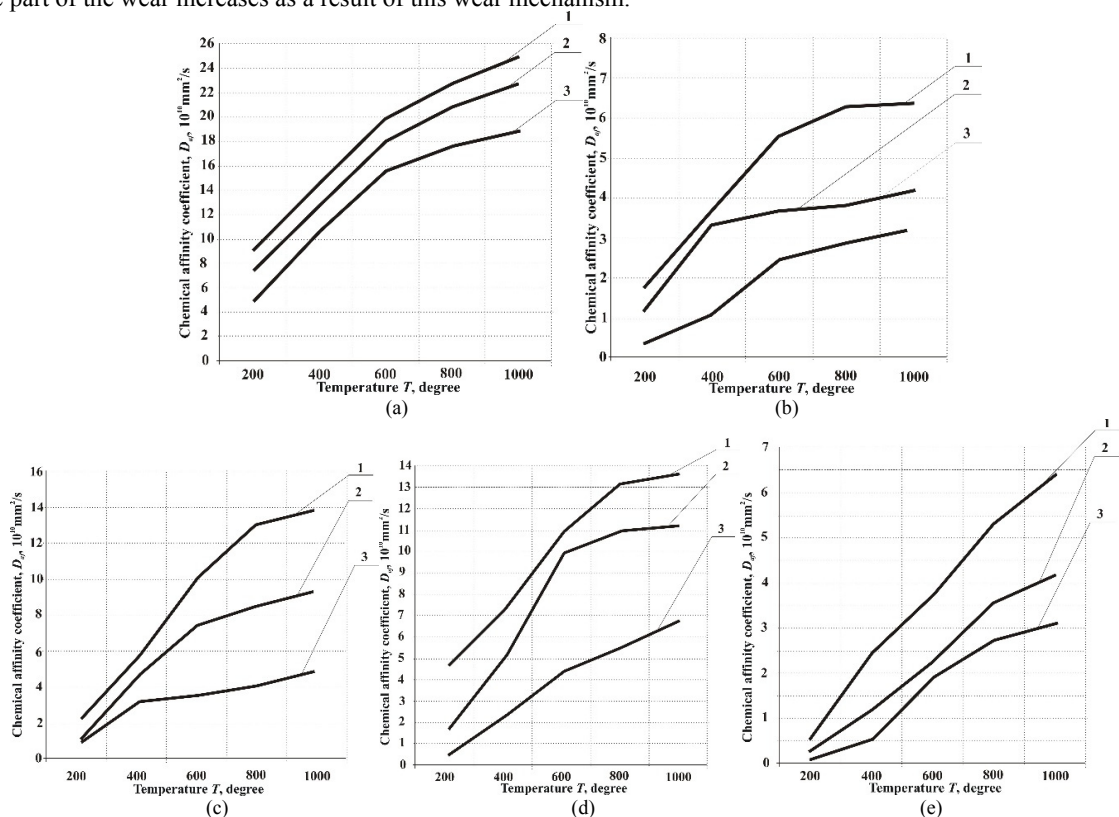


Fig.1. Dependence of the chemical affinity coefficient of different steels on temperature:
 (a) 1 – steel 20, 2 – 30, 3 – 40; (b) 1 – steel 20X, 2 – 30X, 3 – 40X;
 (c) 1 – steel 20X13, 2 – 30X13, 3 – 40X13; (d) 1 – steel 20XH, 2 – 30XH, 3 – 40XH;
 (e) 1 – steel 20XH3A, 2 – 30XH3A, 3 – 40XH3A.

The experimental data give opportunity to estimate the influence of specific chemical elements on the intensity of behavior of physicochemical interaction in the work area (fig. 2) with medium grinding temperature of 600 °C.

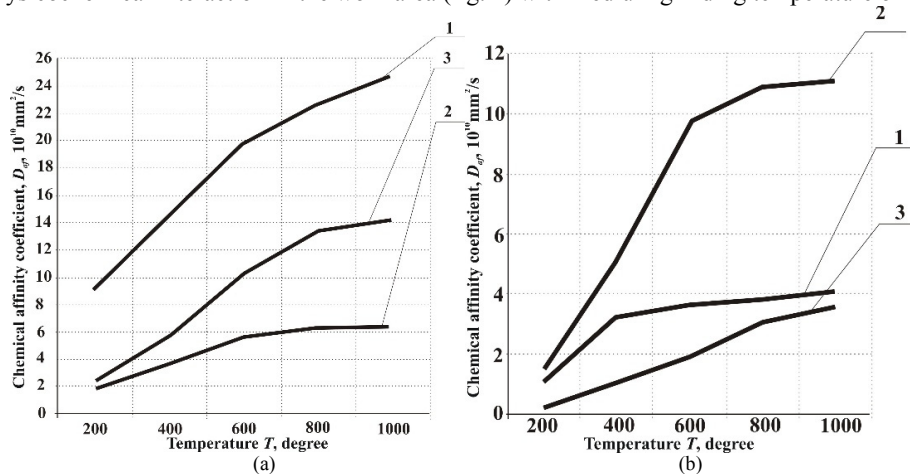


Fig. 2. Dependence of the chemical affinity coefficient of different steel on temperature: (a) 1 – steel 20, 2 – 20X, 3 – 20X13; (b) 1 – 30X, 2 – 30XH, 3 – 30XH3A.

Table 1 cites data for the temperature 600 °C. Figure 3 shows the dependences of influence of carbon (a), chrome (b), nickel (c) on the size of chemical affinity coefficient.

The finding allows us to estimate the influence of the main chemical elements on the intensity of behavior of physicochemical interaction of the workpiece and abrasive material. Thus, the increase of carbon concentration in the workpiece leads to the decrease of intensity of physicochemical processes in grinding: increasing the carbon concentration in the workpiece by 0,1% the chemical affinity coefficient reduces by 10%. While handling materials which contain less than 1% of chrome in its composition, the interaction intensity with the abrasive material greatly reduces (3 times more) due to the increase of chrome concentration in the composition of the work material. Then, the rise of chrome concentration (more than 1%) increases the chemical affinity coefficient: when rising chrome concentration tenfold the coefficient increases twice.

Nickel concentration in grinding material gives the reverse influence. When its concentration is less than 1% the twice increase of chemical affinity coefficient occurs. Further rise of nickel concentration leads to the decrease of the coefficient: every additional nickel percent reduces the coefficient twice.

The given influence of carbon on the chemical affinity coefficient in grinding steel is preserved while processing chrome-nickel steel: the rise of carbon concentration reduces the intensity of chemical interaction between the work and abrasive material.

Table 1. Chemical affinity coefficient for materials, which differ in concentration of different chemical elements (for the temperature of 600 °C)

Steel Make	Chemical element	Element composition, %, up to	Chemical affinity coefficient $D_{af} \cdot 10^{-10}, \text{ mm}^2/\text{s}$
20	Carbon	0,2	19,88
30		0,3	18,02
40		0,4	15,58
20	Chrome	0,25	19,88
20X		1,00	5,54
20X13		13,00	10,22
20X	Nickel	0,30	5,54
20XH		1,00	10,75
20XH3A		3,00	3,26

30	Chrome	0,25	18,02
30X		1,00	3,67
30X13		13,00	7,57
30X	Nickel	0,30	3,67
30XH		1,00	9,68
30XH3A		3,00	1,93
40	Chrome	0,25	15,58
40X		1,00	2,43
40X13		13,00	3,65
40X	Nickel	0,30	2,43
40XH		1,00	4,29
40XH3A		3,00	1,69

Further study of the influence of the concentration of chemical elements on the intensity of physicochemical interaction with the abrasive material while grinding will help to create a complex of mathematical models to predict the coefficient of chemical affinity while abrasive materials processing of different chemical composition. It will allow us to discover peculiarities of physicochemical wear of the abrasive material in different technological conditions.

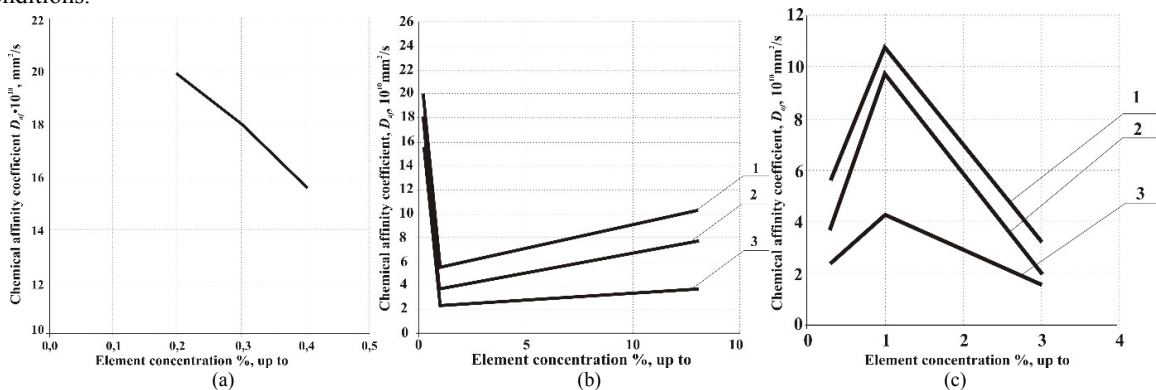


Fig.3. Dependence of the chemical affinity coefficient of different steel on concentration in steel:
 (a) carbon, (b) chrome, when carbon concentration is 1 – 0,2, 2 – 0,3 и 3 – 0,4 %
 (c) nickel, when carbon concentration is 1 – 0,2, 2 – 0,3 и 3 – 0,4 %

3. Conclusion

Prediction of intensity of physicochemical interaction of different grinding materials depending on their chemical composition will help to take into account physicochemical interaction of abrasive and work material to define the size of abrasive grain wear. This opens up possibilities to predict grinding performance criteria – components of cutting force [12, 13], roughness [14] and also to predict output factors of material processing by grinding [15–22].

References

- [1] L.L. Mishnaevskii, The wear of grinding wheels, Naukova Dumka, Kiev, 1982.
- [2] L.N. Filimonov, The durability of grinding wheels, Mashinostroenie, Leningrad, 1973.
- [3] E. Arriandiaga, A. Portillo, E. Sánchez, J.A. Cabanes, I. Pombo, Virtual sensors for on-line wheel wear and part roughness measurement in the grinding process / Sensors. 14(5) (2014) 8756–8778.

- [4] T. Moia, D.F.G. Thomazella, I.H. Aguiar, P.R. Bianchi, E.C. Martins, C.H.R. Marchi, Tool condition monitoring of aluminum oxide grinding wheel in dressing operation using acoustic emission and neural networks, *Journal of the Brazilian Society of Mechanical Sciences and Engineering*. 37(2) (2015) 627–640.
- [5] V.A. Nosenko, M.V. Danilenko, The probabilities of types of the wear of wheel grains vertices and their dependence on the strength of the contact interaction and hardness of the abrasive tool, *Izvestiya of VolgGTU*. 5 (2009) 20–23.
- [6] J. Čop, I. Lukovics, Research of grinding material tools by modern grinding wheels, *Key Engineering Materials*. 581 (2014) 211–216.
- [7] B.S. Linke, Review on Grinding Tool Wear with Regard to Sustainability. 6 (2015) 060801.
- [8] R. Neugebauer, K.-U. Hess, S. Gleich, S. Pop, Reducing tool wear in abrasive cutting, *International Journal of Machine Tools & Manufacture*. 45 (2005) 1120–1123.
- [9] K. Nadolny, Wear phenomena of grinding wheels with sol–gel alumina abrasive grains and glass–ceramic vitrified bond during internal cylindrical traverse grinding of 100Cr6 steel, *International Journal of Advanced Manufacturing Technology*. 77 (2015) 83–98.
- [10] O.I. Medvedeva, A.S. Yanushkin, V.Yu. Popov, The calculation of the adhesion energy of the contact surfaces in grinding instrumental materials by various methods, *Science Intensive Technologies*. 5 (2014) 14–19.
- [11] D.V. Ardashev, Physicochemical wear of abrasive grains during grinding processes, *Journal of Friction and Wear*. 4 (2014) 284–289.
- [12] A.A. Dyakonov, Simulated stochastic thermo-physical model of grinding process, *Lecture Notes in Engineering and Computer Science*. 2 (2014) 914–917.
- [13] U.S. Patnaik Durgumahanti, S. Vijayender, P. Venkateswara Rao, A new model for grinding force prediction and analysis, *International Journal of Machine Tools & Manufacture*. 50 (2010) 231–240.
- [14] L.V. Shipulin, Complex Model of Surface Grinding, *Lecture Notes in Engineering and Computer Science*. (2012) 1325–1327.
- [15] D.V. Ardashev, Predicting the Working Life of Abrasive Grains, *Russian Engineering Research*. 4 (2015) 302–304.
- [16] D.V. Ardashev, Two-parameter assessment of grinding wheel performance, *Russian Engineering Research*. 7 (2010) 705–707.
- [17] D.V. Ardashev, Standardization of grinding wheels, *Russian Engineering Research*. 9 (2011) 910–912.
- [18] D.V. Ardashev, Group abrasive machining in flexible production, *Russian Engineering Research*. 4 (2015) 305–306.
- [19] D.V. Ardashev, Predicting the performance of abrasive tools in process design for diversified production, *Russian Engineering Research*. 3 (2015) 206–208.
- [20] A.A. Dyakonov, L.V. Shipulin, Selecting the cutting conditions for plane grinding by the wheel periphery, *Russian Engineering Research*. 12 (2014) 814–816.
- [21] I.V. Schmidt, A.A. Dyakonov, Modeling of stressed state during the processing of laminated surfaces, *Lecture Notes in Engineering and Computer Science*. 2 (2014) 914–917.
- [22] A.A. Dyakonov, Capabilities of internal-grinding wheels, *Russian Engineering Research*. 12 (2014) 781–784.



International Conference on Industrial Engineering

Thermal vacuum deposition of transparent conductive layers on semiconductor electrode tools for electrochemical machining of engineering products

Glebov V.V.*

Don State Technical University, Rostov-on-Don 344000, Russia

Abstract

This paper proposes a novel process for electrochemical engraving of metals without a need for stencils and photolithography. It dwells upon the features of receptions of electrodeposition films on a semiconductor tool electrode for electrochemical machining. The analytical equations to calculate the necessary thickness of a film are obtained. The technique of drawing films by thermal transpiration on vacuum plant VUP-4 is observed. The authors study a technology of making and designing the photo-active electrode tool, based on Cu/Si structure. The electrical and optical properties of a semiconductor thin plate have been investigated. The paper analyses the results of electrochemical machining by electrode tools with various thickness of an electrodeposition film. The theory and method of making, experimental results and an application of the semiconductor tool electrode are presented in this paper.

© 2015 The Authors. Published by Elsevier Ltd. This is an open access article under the CC BY-NC-ND license (<http://creativecommons.org/licenses/by-nc-nd/4.0/>).

Peer-review under responsibility of the organizing committee of the International Conference on Industrial Engineering (ICIE-2015)

Keywords: electrochemical machining; vacuum thermal deposition; semiconductor; transparent film; electrode tool; electrochemical marking

* Corresponding author. Tel.: +7-928-154-31-81;
E-mail address: glebovdon@mail.ru

1. Introduction

Electrochemical machining (ECM) is one of the non-traditional machining techniques; it can achieve a wanted shape of a surface using metal dissolution by electrochemical reaction and can be applied to metals such as hardened, high-strength and heat-resistant steel. ECM is necessary to advance a wide variety of industries, such as mechanical engineering, aerospace, automotive, electronic etc. [1-5].

Except forming surface finish also plays a vital role on the functional properties of the components such as wear resistance, energy loss due to friction etc. Engraving processes have been continuously developed due to high demand in various fields [6-7]. Manufacturing processes can be categorized according to the type of energy used in the process itself, such as mechanical, chemical, electrochemical, electrical and laser processes. The electrodischarge machining (EDM) machine converts the electrical energy into thermal energy in the plasma discharge channel during the spark discharge. The thermal energy melts and vaporizes workpiece material during the process [1,8]. The high temperature also generates the thermal stress in the workpiece. Laser surface treatment results in the homogenization and refinement of microstructures, change in the chemical composition, and phase transformation [9-10].

At the ECM there is no mechanical contact, thus no thermal nor mechanical stress is brought into the material. The hardness of the metal does not influence the material removal rate and the process shows almost no toolwear.

One of effective marking methods on conductive surfaces is electrochemical marking (ECMr) [11-12]. ECMr is also a good way to evaluate sheet metal formability. Knowing the level and distribution of strain in the critical areas of the stamping is the key with this technique. ECMr grid patterns are ideally suited for this purpose [13-14].

Typical installations of ECMr use solid electrode tools (ET) and a stencil with hollows in the image of the picture being marked, there being no electrolytic flow canal; the process is carried out by means of electrolytic damping of a porous layer. It limits the marking depth. Besides, such stencils allow to apply a limited number of markings, require special materials and printers or using photolithographic methods for printing.

The installations having the minimized and equal inter-electrode gap (IEG) size, along the whole surface and providing the conditions for the uniform electrolytic flow allow actualizing the ECM advantages to the full extent [15].

In a photoelectrochemical cell for ECMr one of electrodes is executed from a semiconductor material on which the light image is projected. Depending on voltage direction, a material of electrodes, a design of an electrochemical cell and a used electrolyte, the image can be formed owing to electroplated coating, anodic dissolution of an electrode or in electrolyte volume (photoelectrochromic effect) [1,4,16-19]. The conductivity of semiconductor is several order of magnitude is less, than at metals and electrolytes, therefore for planar optoelectronic devices it is necessary to provide conditions for equipotential a current lead on all square light absorption surfaces.. For this purpose on a semiconductor surface superimpose a thin film metals or electroconductive oxides of metals. At sampling of a spending pellucid covering for contact to a semi-conductor material it is necessary to consider optical and electric parametres of this film, and also property of contact a film – the semiconductor [18-21].

The ultimate goal of the present research activities was to develop new technological processes leading to highly effective optical coatings of a semiconductor wafer for application in electrochemical engraving and marking.

2. The theoretical analysis

It is obvious that increasing the thickness of the deposited film, on the one hand, reduces the surface electric resistance of the film, but, on the other hand, leads to reduced transparency of the film. In [22] for definition of a necessary thickness of a film suggest to use the integrated factor of criterion Q , defined as the ratio of the normalized average transmittance to normalized resistivity. However, such optimisation, in our opinion, is justified for solar cells, light-emitting diodes, liquid crystal meshes of displays etc., where it is necessary to achieve integrated efficiency of photoelectric transformation of all element. In case of ET for ECMr, first of all, it is necessary to be aimed to equipotential surfaces, because the optical transmittance even if will decrease, all the same will be homogeneous for all surface. The decrease in transparency of the coating to actinic radiation, which accounts for the maximum of spectral photosensitivity of the semiconductor, can be compensated by increasing the light intensity. Besides, at correct sampling of a thickness of a covering it is possible to reduce light losses at reflexion from a semiconductor surface. The coefficient of reflexion A is defined by Fresnel's formula:

$$A = \left(\frac{n-1}{n+1} \right)^2, \tag{1}$$

where n is the refractive index.

For silicon over the range visible light a mean $n = 3.9$, calculation by formula (1) shows, that light losses on reflexion attain 35 %. If the waves reflected from an external and internal surface of a thin film are in phase opposition as a result of an interference these two waves are mutually relaxed. The greatest easing will occur at equality of amplitudes of these waves which occurs under a condition $n_0 = \sqrt{n}$, where n_0 - refractive index of a film.

Optical dispersion in semiconductors does not allow to solve a problem of elimination of reflexion completely. When choosing the thickness of the antireflection film on the premise, to reduce the reflection waves, which have maximum spectral photosensitivity. For tin dioxide, which is often used in optoelectronic devices [18,19,22], no in red light is approximately equal to 2, therefore, when the coating thickness d satisfying the condition $n_0 d = \lambda/4$ can achieve significant attenuation of reflection. The corresponding calculation for wave-length $\lambda = 0.9 \mu\text{m}$ gives a value of $d = 0.1 \mu\text{m}$. Thus, the SnO_2 coating thickness must be a multiple of the size of $0.1 \mu\text{m}$.

For metal films, the situation is more complicated because of strong absorption of light. For damped waves, the intensity of the transmitted light P at the depth d is determined according to Bouguer's law

$$P = P_0 \exp\left(-\frac{4\pi}{\lambda} n\chi d\right), \tag{2}$$

where P_0 is the intensity of the incident wave; χ is the absorption coefficient.

For example, at $n\chi = 1$ in metal on ways, numerically equal to wave length, intensity of an incident wave decreases approximately in 10^5 times. For copper $n = 0.62$, and magnitude $n\chi = 2.57$, for aluminium $n = 1.44$ and $n\chi = 5.23$. Let's define a depth of penetration in a copper film for wave length $\lambda = 0.9 \mu\text{m}$. Calculation by formula (2) gives value $d \approx 0.028 \mu\text{m}$. Therefore, transparent metal films for optoelectronic devices have a thickness of about 10 nm, and can perform the antireflective function. Moreover, as metal films are characterised by a considerable coefficient of reflexion of light, it is necessary to cover them with a clarifying dielectric film in addition. This clarifying antireflection coating simultaneously performs a protective anti-corrosion function.

Let's define dependence of electric parametres of a thin film on its thickness. For semi-conductor planar ET there is the specific lapse of machining connected with an anode drop in a film of a conductor at removal from a current lead. It is thus broken equipotentiality surfaces that leads to emersion of a density gradient of a current in places of equal light exposure. We will size up this lapse.

Let's observe a semi-conductor plate in the thickness d with surface radius r_i on which the thin film by thickness h is put (Fig. 1).

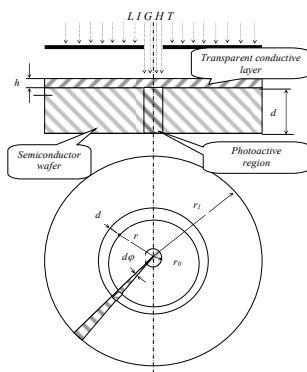


Fig. 1. Estimate drawing for determining the voltage drop in the conductive transparent film.

The current lead is carried out on film ambit not shown). On a plate the light stain with radius r_o is projected. From symmetry reasons it is obvious, that the maximum anode drop will be in case the light sonde gets to the plate centre.

For definition of resistance of a film we will gate out the part of sector restricted to an angle $d\varphi$ and rounds with radiuses r and $r+dr$. Resistance of this section of sector will be equal

$$dR(d\varphi, dr) = \frac{\rho dr}{r h d\varphi}, \quad (3)$$

where ρ is the resistivity of a film.

The resistance of all sector restricted $d\varphi$ is given by

$$dR(d\varphi) = \int_{r_0}^{r_1} \frac{\rho dr}{r h d\varphi} = \frac{\rho}{h d\varphi} \ln \frac{r_1}{r_0}. \quad (4)$$

Since the sector is connected "in parallel", the total resistance of the film on the site of the current supply to the light spot will receive

$$\frac{1}{R} = \int_0^{2\pi} \frac{h d\varphi}{\rho \ln \frac{r_1}{r_0}} = \frac{2\pi h}{\rho \ln \frac{r_1}{r_0}},$$

from here follows

$$R = \frac{\rho \ln \frac{r_1}{r_0}}{2\pi h}. \quad (5)$$

The general resistance of a thin film and the lighted section of the semiconductor is given by

$$R_{\Sigma} = \frac{\rho \ln \frac{r_1}{r_0}}{2\pi h} + \frac{\rho_{ph} d}{\pi r_0^2}, \quad (6)$$

where ρ_{ph} is the resistivity of the semiconductor at illumination (the light resistivity).

Drop of potential in a semi-conductor electrode ΔU is given by

$$\Delta U = j \pi r_0^2 R_{\Sigma} = j \left(\frac{\rho r_0^2 \ln \frac{r_1}{r_0}}{2h} + \rho_{ph} d \right). \quad (7)$$

From here follows, that the maximum drop of potential ΔU will be under a condition

$$r_0 = \frac{r_1}{\exp 0.5} \approx 0.607r_1, \quad (8)$$

at this size the light spot will be the maximum error processing caused by the voltage gradient on the film surface. The relative value of this error ε is defined by the expression

$$\varepsilon = 0.092 \frac{\rho r_1^2}{\rho_{ph} h d_1}, \quad (9)$$

and this should be considered when determining the thickness of the coating.

From the equation (2) follows, that ρ_{ph} depends on depth d . For practical estimated calculations it is necessary to define experimentally magnitude ρ_{ph} for the chosen magnitude of light exposure. With rather good accuracy it is equal

$$\rho_{ph} = \rho_0 \frac{I_d}{I_{ph}},$$

where ρ_0 is the specific dark resistance of the semiconductor; I_d / I_{ph} is the relation of a dark current to a photocurrent at used voltage (i.e. in the field of photocurrent saturation).

Let's define a thickness of a copper film for magnitude $\varepsilon=0.1$. Typical parametres of semi-conductor plates in our experiments were the following: $r_1=30$ mm; $d=0.38$ mm; $I_d / I_{ph}=180$. Matching calculation by equation (3) gives value $h=10$ nm.

Thus, with the account of estimated character of the spent calculations, it is possible to assume, that for reception of satisfactory results ECM the thickness of a metal film should not exceed 10 ... 20 nm.

3. Experimental technique

For film deposition we used a method of thermal spraying of metal in a vacuum installation VUP-4, which allows you to adjust the thickness of the sprayed layer with the indicator deposition, located on the remote control. The locations of the sensor indicator thickness in a vacuum chamber and its main elements is shown in Fig. 2. (a). Measurement method based on the proportional relationship between the film thickness control of the glass 6 and its coefficient of optical transmittance. The measuring circuit of the indicator are collected in a bridge circuit, one arm of which includes the photoresistor SF-1 (on the basis of cadmium sulfide). Before you start deposition a variable resistor of the bridge circuit established the necessary thickness. A measuring device included in the emitter circuit of the matching load balanced DC amplifier, which is the second diagonal of the bridge. In the coating process, the light flux through the check glass decreases, the resistance of the photoresistor increases, the bridge unbalance, and when the deflection of the measuring device by an amount proportional to the thickness of the deposition layer, the unlocking circuit of the evaporator and the process is terminated.

Calibration of the indicator deposition was carried out separately for each of the sprayed substance, the type of evaporator and the corresponding geometry of the deposition. In conditions of isotropic evaporation analytical calculation of the film thickness h was performed according to the formula

$$h = \frac{\Delta m \sin \Theta}{\gamma 4\pi R^2}, \quad (10)$$

where Δm is the total weight of evaporated substance; Θ is the angle of incidence of a stream of evaporating corpuscles on a surface; γ is the substance density; R is the distance from the evaporator to a surface.

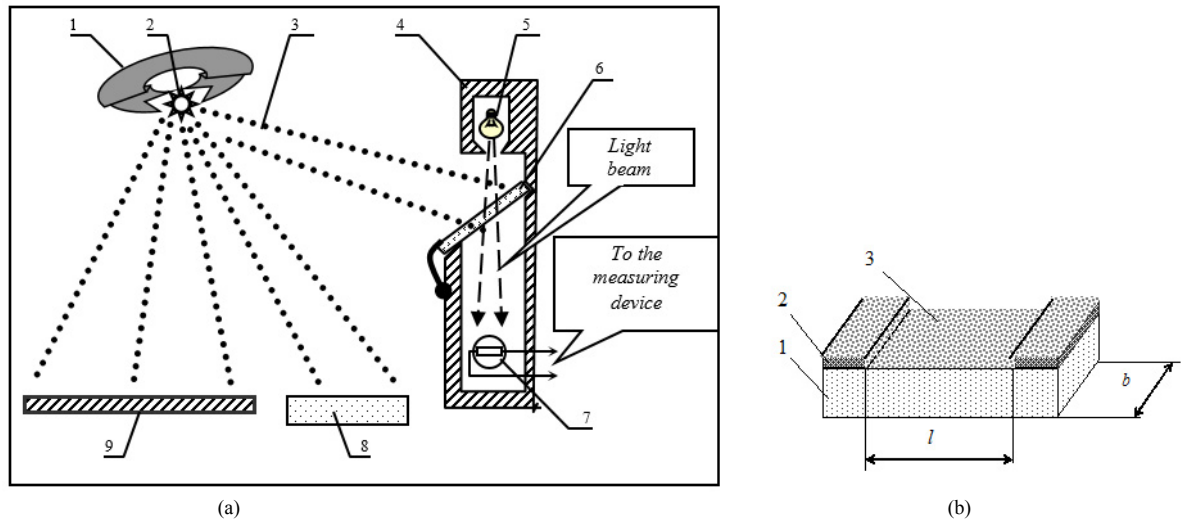


Fig. 2. (a) Location scheme of the indicator gauge thickness, semiconductor wafer, and "witness" in a vacuum chamber: 1 – heater; 2 – evaporable substance; 3 – the flow of evaporated particles; 4 – the capsule of the measuring sensor; 5 – light source; 6 – glass plate; 7 – photoresistor; 8 - "witness"; 9 - semiconductor wafer; (b) "Witness" for electrooptical measurements: 1 – a glass plate; 2 – the bonding pad; 3 – an deposition film.

It should be noted that the thickness of the deposition layer on the glass plate 6 (Fig. 2. (a)) is not equal to the thickness of the deposition layer on the semiconductor substrate 7. These thicknesses are proportional, and the proportionality factor depends on the geometry of irradiation, namely, the distance from respective surfaces to the evaporated material and the angles of inclination of the respective surfaces to the flow of evaporated particles. Even more complex relationship between optical transmission ratios of the respective layers.

With this in mind, for a more accurate measurement of optical transmittance and surface resistance of films on a semiconductor wafer in the coating process, next to it put "the witness" 8 (check glass substrate, Fig. 2. (b)). "Witness" (Fig. 2. (b)) consisted of a glass plate 1 positioned on contact pads 2. The width of the contact strips b equal to the distance between the contacts l . In this case, the resistance between contact pads R_p representation for equal specific surface resistance (or resistance per square). In this case, the resistance R_p of deposited thin film 3 depends on the film thickness:

$$R_p = \frac{\rho l}{bh} = \frac{\rho}{h},$$

where ρ is the resistivity of a film.

In general the resistivity is not equal to normal (reference) specific resistance of the material and depends on the conditions of film formation, therefore, the error in thickness measured by this method is small and is more than 10% [10]. The presence of a "witness" in our experiments allowed to determine the coefficient of optical transmittance of the film and its surface resistance. For a more accurate determination of the thickness of the deposited film laboratory balances LLDP-100g with a scale division of 0.05 mg were determined mass of the

substance Δm deposition on a wafer. Film thickness h was determined by the equation $h = \Delta m / S\gamma$, where S is the square of a surface of a plate.

This formula can be used in case the dimensions of the evaporation surface is much less than the distance from the heater to the surface. In our experiments, the radius r of the plate (excluding the site for current lead a width of 0.5 cm) was 3.3 cm, the distance R to the evaporator 30 cm (Fig. 2. (b)). Relative non-uniformity ε of the thickness of the deposited film in the center and on the edges of the plate, defined by the equation (4) is equal to

$$\varepsilon = 1 - \frac{R^3}{(R^2 + r^2)^{\frac{3}{2}}}$$

Calculation by this formula gives the relative non-uniformity of the film thickness is less than 2%, and this error is less than the error due to the voltage gradient on the surface of a semiconductor (10%, equation (3)).

The table presents calculated values of the film thickness by measuring the mass of copper precipitated on a silicon wafer with a diameter of 76 mm. In our calculations we used the density value of "solid" copper $\gamma = 8,93 \cdot 10^3 \text{ kg/m}^3$.

Table 1. Calculation of film thickness h measured mass Δm of copper precipitated on a silicon wafer with a diameter of 76 mm.

Δm , mg	0.25	0.40	0.75	1.05	1.55	2.55	3.05
h , nm	6	10	19	26	38	63	75

Graph to determine the thickness of the deposited film h on the testimony of indicating instrument N for this experiment is shown in Fig. 3. (a). Similar curves were constructed for each of the deposition substance separately. For deposition used the analytical grade metals from Al, Cu, Ag, Ni, Cr, and conductive oxides SnO_2 , CdO .

Scheme of electrochemical cell for the study of technological capabilities of ET on the basis of monocrystalline silicon with various conductive coatings are presented in Fig. 3. (b).

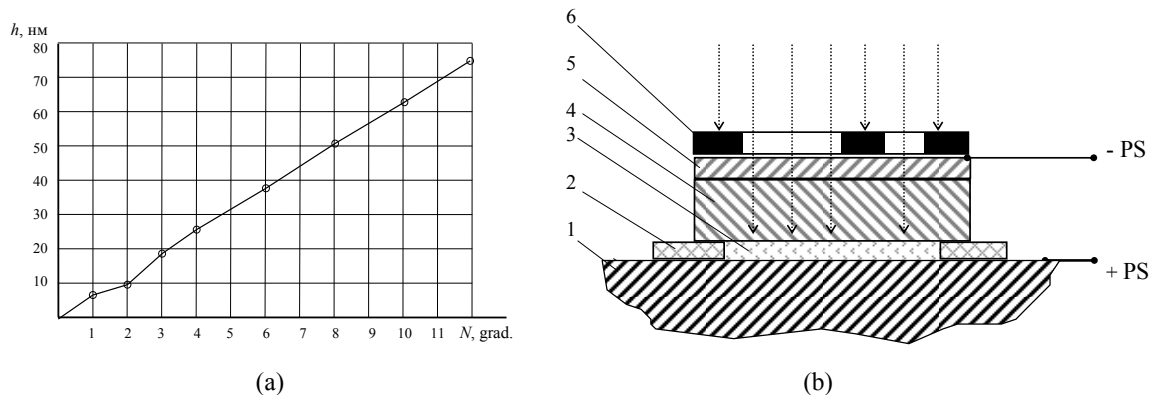


Fig. 3. (a) Graph to determine the thickness of the deposited film h on the testimony of N indicating instrument; (b) Scheme of the electrochemical cell to study a silicon ET: 1 – workpiece; 2 – dielectric strip; 3 – IEG filled with electrolyte; 4 – semiconductor wafer; 5 – transparent conductive layer; 6 – photostencil; the arrows indicate the direction of the light flux; PS – power source

For definition of technical characteristics of ECMr through the photomask 6 image projected on the transparent conductive layer 5 connected to the negative terminal IE. The positive terminal of the PS was connected to the workpiece 1. Through the gap formed by dielectric spacers 2, the electrolyte was passed. The current distribution on the working surface 3 of the semiconductor is determined by the illumination of the relevant parts of its outside surface. The required operating voltage between the electrodes was determined on the basis of current-voltage characteristics from the condition of saturation of the photocurrent.

4. The conclusion

Studies have shown that for electrochemical machining with semi-conductive transparent electrode tools for metal-coating for copper films better the results, you have the ET processing of single crystal cream nievoy plate thickness of 0.38 mm and a diameter of 76 mm (p -type KDB-10). On the surface of this wafer in a vacuum chamber VUP-4 was coated film thickness of 15 nm. The chamber pressure was 10^{-4} Pa, during evaporation plate was heated to 500°C. The transmittance of a copper film in the optical range was 45-55 % and surface electrical resistance was 2.1 Ω .

The present electrode tools is expected to be useful in various applications such as micro-texturing of surface, electrochemical marking, fabrication of microgrooves in an hydrodynamic bearing, etc.

References

- [1] K.P. Rajurkar, M.M. Sundaram, A.P. Malshe, Review of Electrochemical and Electrodischarge Machining, *Procedia CIRP*. 6 (2013) 13–26.
- [2] B.R. Acharya, Ch.P. Mohanty, S.S. Mahapatra, Multi-objective Optimization of Electrochemical Machining of Hardened Steel Using NSGAI, *Procedia Engineering*. 51 (2013) 554–560.
- [3] V.V. Glebov, Ju.V. Prisyazhnyuk, L.A. Kaplin, Features of electrochemical machining of details from magnetic alloys, *Nauchno-tehnicheskij Vestnik Povolzh'ja*. 5 (2012) 140–142.
- [4] M. Datta, D. Landolt, Fundamental aspects and applications of electrochemical microfabrication, *Electrochimica Acta*. 45 (2000) 2535–2558.
- [5] V.V. Glebov, About a problem etch factor at chemical and electrochemical engraving, *Fundamental'nye Issledovaniya*. 8 (2011) 623–626.
- [6] V.V. Glebov, Yu.V. Prisyazhnyuk, S.V. Kirsanov, Roughness and accuracy at electrochemical machining of details from magnetic, *Kazanskaya Nauka*. 2 (2011) 31–33.
- [7] F.I. Kukoz, V.V. Glebov, S.V. Kirsanov, V.V. Konovalenko, Method of electrochemical marking, *Surface Engineering and Applied Electrochemistry*. 5 (1995) 67–68.
- [8] P. Lijo, S.H. Somashekhar, Response Surface Modelling of Micro Holes in Electrochemical Discharge Machining Process, *Procedia Engineering*. 64 (2013) 1395–1404.
- [9] E.F. Pieretti, I. Costa, Surface characterisation of ASTM F139 stainless steel marked by laser and mechanical techniques, *Electrochimica Acta*. 114 (2013) 838–843.
- [10] H.S. Shin, M.S. Park, C.N. Chu, Electrochemical etching using laser masking for multilayered structures on stainless steel, *CIRP Annals - Manufacturing Technology*. 59 (2010) 585–588.
- [11] S.V. Kirsanov, V.V. Glebov, Application of electrochemical marking methods in machine building, *Surface Engineering and Applied Electrochemistry*. 5 (2004) 1–3.
- [12] V.V. Glebov, Research of regimes of high-speed anodic dissolution of magnetic alloys parts, *Inzhenernyj vestnik Dona (Rus)*. 2-2 (2015). URL: ivdon.ru/magazine/archive/n2p2y2015/2966.
- [13] J.Jr. Shippell, Electro-chemical marking of circular strain grids, *Experimental Techniques*. 5 (1978) 1–4.
- [14] E.-S. Lee, J.-W. Park, Y.-H. Moon, A Study on Electrochemical Micromachining for Fabrication of Microgrooves in an Air-Lubricated Hydrodynamic Bearing, *Int. J. Adv. Manuf. Technol.* 20 (2002) 720–726.
- [15] S.V. Kirsanov, V.V. Glebov, Using the methods of electrochemical labeling in machine building, *Elektronnaya Obrabotka Materialov*. 5 (2004) 4–6.
- [16] Ph.I. Kukoz, S.V. Kirsanov, V.V. Glebov, The possibility of amplifying the density of technological current in the photoactive electrode instrument, *Elektronnaya Obrabotka Materialov*. 4 (2000) 4–6.
- [17] F.I. Kukoz, V.V. Glebov, S.V. Kirsanov, V.V. Konovalenko, A method for producing a photographic image with the use of a semiconductor electrode, *Russian Journal of Electrochemistry*. 32 (1996) 1060–1061.
- [18] F.I. Kukoz, S.V. Kirsanov, V.V. Glebov, Feasibility of increasing process current density in photoactive electrode-tool, *Surface Engineering and Applied Electrochemistry*. 4 (2000) 1–2.
- [19] F.N. Crespilho, V. Zucolotto, O.N. Oliveira Jr., F.C. Nart, Electrochemistry of Layer-by-Layer Films: a review, *Int. J. of Electrochem. Sci.* 1 (2006) 194–214.
- [20] V.V. Glebov, Ju.V. Prisyazhnyuk, Manufacturing of printed-circuit boards serial-slot an electrochemical etching method, *Sovremennye Problemy Nauki i Obrazovaniya*. 4 (2011). URL: www.science-education.ru/98-4758
- [21] A.I. Dikumar, L.I. Bruk, E.V. Monaico, D.A. Sherban, A.V. Simashkevich, I.M. Tiginyanu, Photoelectric structures based on nanoporous p-InP, *Surface Engineering and Applied Electrochemistry*. 1 (2008) 1–5.
- [22] G. Kavei, A.M. Gheidari, The effects of surface roughness and nanostructure on the properties of indium tin oxide (ITO) designated for novel optoelectronic devices fabrication, *J. Mater. Process. Technol.* 208 (2008) 514–519.



International Conference on Industrial Engineering

A numerical model of mechanical interaction between rough surfaces of tribosystem of the high forced diesel engine

Goritskiy Y.^a, Gavrilov K.V.^{b*}, Rozhdestvenskii Y.V.^b, Doikin A.A.^b

^aNational Research University "MPEI", Krasnokazarmennaya 14, Moscow 111250, Russia

^bSouth Ural State University, 76, Lenin Avenue, Chelyabinsk, 454080, Russian Federation

Abstract

The paper analyzes the numerical model of interaction between the rough surfaces of a piston-cylinder liner tribosystem in the form of a Markov chain. It is based on a model that takes into account elastic and plastic deformation and fatigue failure under load. We have provided a system of equations for the distribution of time-varying heights of protrusions. We have also analyzed the evolution of distributions for the contact interface of the piston-cylinder liner tribosystem of the diesel engine.

© 2015 The Authors. Published by Elsevier Ltd. This is an open access article under the CC BY-NC-ND license (<http://creativecommons.org/licenses/by-nc-nd/4.0/>).

Peer-review under responsibility of the organizing committee of the International Conference on Industrial Engineering (ICIE-2015)

Keywords: piston-cylinder liner tribosystem; surface roughness; film thickness

1. Introduction

Existing methods for calculating of friction characteristics are approximate and often inadequate for the engineer. Friction characteristics determined by such factors as surface microgeometry, physical characteristics of materials, velocity and the applied load. There is an approach based on the representation of the relief function for the random arguments [1,2]. Such models can estimate the area of contact, the friction force, coefficient of friction, wear, etc. However, this approach ignores the surfaces change and, consequently, contact and friction characteristics over the time. In this paper model of random change of surfaces heights over the time for "piston-cylinder liner" tribosystem is developed.

* Corresponding author. Tel.: +7-950-742-0117; fax: +7-351-267-9214.

E-mail address: gavrilovkv1@rambler.ru

The "piston-cylinder liner" tribosystem is mostly in the hydrodynamic lubrication regime. At high loading levels, near the TDC, tribosystem is in the mixed or boundary lubrication regimes. The latter is important for the determination of the service life of the tribosystem as a whole.

2. Determination of the hydromechanical characteristics of the "piston - cylinder liner" tribosystem

The main hydromechanical characteristics (HMC) of the "piston - cylinder" tribosystem are: $h_{min}(\tau)$ – instantaneous values of the minimum oil film thickness; $p_{max}(\tau)$ – instantaneous values of the maximal hydrodynamic pressure; h_{min}^* – average value of $h_{min}(\tau)$; p_{max}^* – average value of $p_{max}(\tau)$; $N(\tau)$ and N^* – instantaneous and average power loss of friction; Q^* – the average flow rate of oil in the direction of the combustion chamber; T_{eff}^* – the average effective temperature of the lubricating layer.

Since the contact interaction of the elements is experimentally confirmed by the formation of "rubbing" on the piston skirt of diesel engine after certain hours (Fig. 1), the calculated characteristics of tribosystem complemented the areas, where minimal thickness of a lubricant film less than the permissible value $h_{lim} = \alpha_{h_{lim}}, \%$.

The reactions of the lubricating layer were determined based on the results of the numerical integration of the modified Elrod equation for pressure in the lubricating layer and the degree of filling of clearance [3,4]. The modified Elrod equation contains the function $\Omega(\varphi, \bar{z})$ and takes the form of:

$$\frac{\partial}{\partial \phi} \left[\frac{\bar{h}^3}{12 \bar{\mu}_{eff}^*} \frac{\partial}{\partial \phi} (g\Omega) \right] + \frac{1}{a^2} \frac{\partial}{\partial \bar{z}} \left[\frac{\bar{h}^3}{12 \bar{\mu}_{eff}^*} \frac{\partial}{\partial \bar{z}} (g\Omega) \right] = + \frac{\bar{w}}{2} \frac{\partial}{\partial \bar{z}} \{ \bar{h} [1 + (1-g)\Omega] \} + \frac{\partial}{\partial \tau} \{ \bar{h} [1 + (1-g)\Omega] \}, \quad (1)$$

where $\bar{h} = h/h_0$; $\bar{\mu}_{eff}^* = \mu_{eff}^*/\mu_0$; $-a \leq \bar{z} \leq a$; $\bar{z} = z/R$; $\varphi = xR$; $a = B/2R$; $\tau = \omega_0 t$; $\bar{w} = w/(\omega_0 R)$; \bar{h} , $\bar{\mu}_{eff}^*$ – dimensionless film thickness and the effective viscosity of the lubricant; B, R – the width and radius of the bearing; μ_{eff}^* – effective viscosity of the lubricant, the corresponding temperature to T_{eff}^* ; μ_0, h_0, ω_0 – respectively lubricant viscosity, typical film thickness at the center position of the piston in cylinder and rotation speed of crankshaft; \bar{w} – the dimensionless linear velocity of the piston; g – the switching function.

The function $\Omega(\varphi, \bar{z})$ is related to the degree of filling of the clearance $\theta(\varphi, \bar{z})$ and is characterized by a function that determines the mass content of the liquid phase (oil) in the volume of the clearance between the piston and cylinder using the relationship $\theta = 1 + (1-g) \cdot \Omega$.

For calculating the trajectory of the piston on the lubricating layer in the cylinder, the system of coordinates is fixed to a stationary cylinder. At the start, the origin of this moving coordinate system is at the center of mass (point C) of the moving piston (Fig. 2).

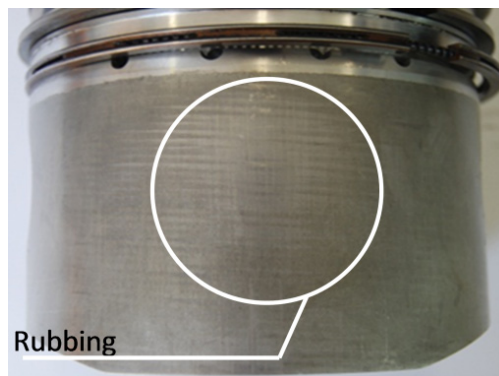


Fig. 1. The result of contact interaction of the piston-cylinder liner interface.

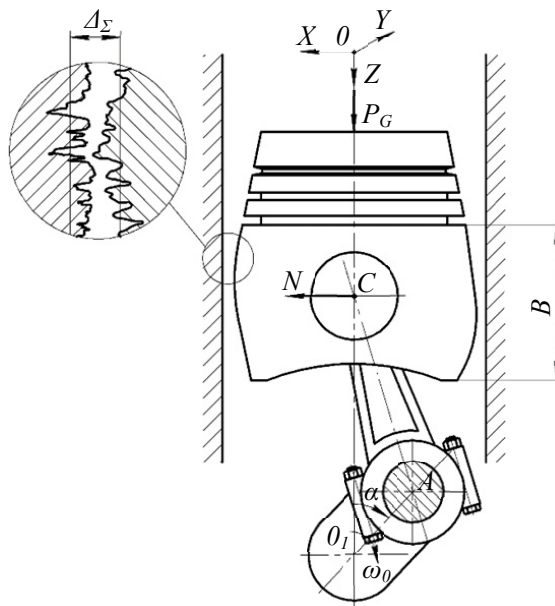


Fig. 2. The scheme of the piston-cylinder liner interface.

According to [5-7], it is assumed that movement of the piston in the cylinder is only in the plane perpendicular to the axis of the piston pin.

Given the initial data and the methodology for calculating the trajectory of piston's motion on the lubricating layer, as described in [8-10], we got the dependence of the minimum film thickness h_{min} in function of a crank angle α for a diesel engine (Fig. 3).

3. Markov chains

To analyze the process of friction in the contact area we used the discontinuous model where surfaces are represented by asperities of random height (Fig. 4). Pairs of contacting asperities are changed when the shift occurs. Asperities in contact deform and destruct each other, that is why heights of contacting asperities may change. Total height change of all surface asperities leads to roughness transformations and variation of friction characteristics (real contact area, friction coefficient, wear).

Let's consider K pairs of asperities positioned in one row. Time is discontinuous and is measured in shift counts. After n shifts heights of asperities of one surface are represented by vector $\xi_k(n)$, ($k = 1, \dots, K$), and heights of asperities of the other surface are represented by vector $\eta_k(n)$. The asperity height change of the k^{th} pair in one shift is described by general equations:

$$\xi_k(n+1) = \Psi(\xi_k(n), \eta_{k-1}(n)), \tag{2}$$

$$\eta_k(n+1) = \Phi(\xi_k(n), \eta_{k-1}(n)), \tag{3}$$

where $k = \overline{1, K}$, $\eta_0(n) = \eta_K(n)$, Φ and Ψ determine stochastic mechanism of asperity interaction as a sphere interaction, [11], with random radiuses. Presented model of asperity interaction takes into account elastic-plastic deformation and wear.

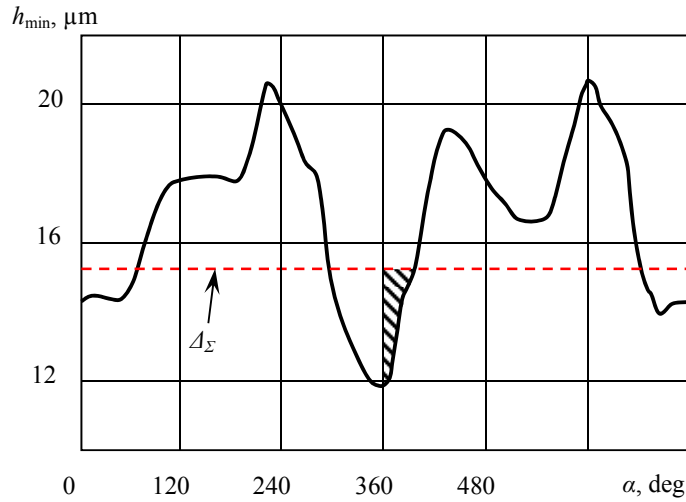


Fig. 3. The minimal lubricant film thickness in function of the crankangle.

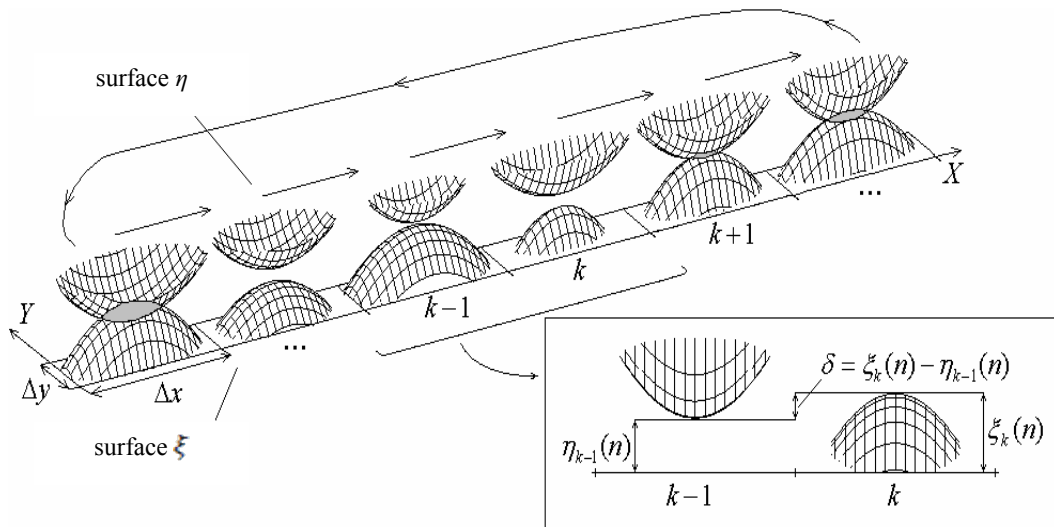


Fig. 4. Model of surfaces and sketch of cyclical shifts

Model is realized on a computer. After N shifts are performed, asperity height histogram is depicted, real contact area; friction force and wear are measured. Presented results agree to well known observations, such as independence of “equilibrium roughness” from initial surface roughness.

It is proposed to describe the trajectory of height changes of single asperity by means of Markov series, [12]. The height ξ of single asperity changes when it interacts with asperities of other surface, having heights $\eta(t)$ at the moment t . Time step Δt is selected in such a way, that values $\eta(t)$ and $\eta(t + \Delta t)$ are close to uncorrelated. It is supposed, that asperity with the height ξ interacts with the series of asperities of the other surfaces with heights $\eta_1, \dots, \eta_n, \dots$, distributed with density $q_\eta(y)$. Thus series of heights $\xi_1, \dots, \xi_n, \dots$ is obtained, height value ξ_{n+1} depends on

ξ_n and η_{n+1}

$$\xi_{n+1} = \Psi(\xi_n, \eta_{n+1}), \quad (4)$$

where Ψ determines accepted mechanism of asperity contact interaction.

Series $\xi_1, \dots, \xi_n, \dots$ is Markov series. Moreover, heights $\xi_1, \dots, \xi_n, \dots$ are discontinuous, series $\xi_1, \dots, \xi_n, \dots$ becomes Markov chain. Similarly, ξ is distributed with density $p_\xi(x)$ and next equation is obtained:

$$\eta_{n+1} = \Psi(\xi_n, \eta_{n+1}). \quad (5)$$

Once two functions Ψ and Φ are elaborated the system of equations for stationary distributions p^* and q^* is obtained:

$$\begin{cases} p^* = p^* \cdot P_\xi(q^*, \Psi), \\ q^* = q^* \cdot P_\eta(p^*, \Phi), \end{cases} \quad (6)$$

where $P_\xi(q^*, \Psi)$ and $P_\eta(p^*, \Phi)$ are matrices of transition probabilities for series of ξ_n and η_n . Elements of matrices are determined by distributions p^* and q^* – respondingly and by two functions Ψ and Φ . For example, elements of matrix $P_\xi(q^*, \Psi)$ is obtained:

$$\|P_\xi\|_{ij} = P\{\xi_{n+1} = j | \xi_n = i\} = \sum_{l: \Psi(i,l)=j} q^*(l). \quad (7)$$

Elements $P_\eta(p^*, \Phi)$ are determined similarly.

4. Results and discussion

Initial data were determined on base of recording profile traces of specimens of the piston skirt and cylinder liner [9]: the surface ξ is the surface of the cylinder liner, surface η - the surface of the piston skirt.

For period of time, where h_{min} less Δ_Σ we estimated next parameters: the distribution of the heights of roughness of surfaces (p_ξ, q_η); the root mean square deviations (rms) of surface roughness (σ_ξ, σ_η); the average contact area; the friction force F_{fr} and friction coefficient f ; the linear wear I_h .

Fig. 5 present the height distribution of surfaces in function of the friction distance. Changes of the surface (and consequently changes of the height distribution of the projections of the contact surfaces) due to fatigue failure is extremely slow, due to a low probability of this event. At the initial process of friction in contact come mostly high surface elements. The destruction of the high elements come into contact less high surface elements.

Under the influence of fatigue failure is a redistribution of the elements of heights, and in particular in the area of contact.

Fig. 6a, 6b confirm the existence of “equilibrium roughness”.

Fig. 7a, 7b shows the dependence of friction force and friction coefficient on friction distance. Friction force and friction coefficient remain about the same.

Fig. 8 shows the dependence of wear on friction distance. Wear increased slowly. The increase of wear is connected with change of the height of the surfaces roughness under the influence of fatigue failure, as well as with the convergence of the interacting surfaces.

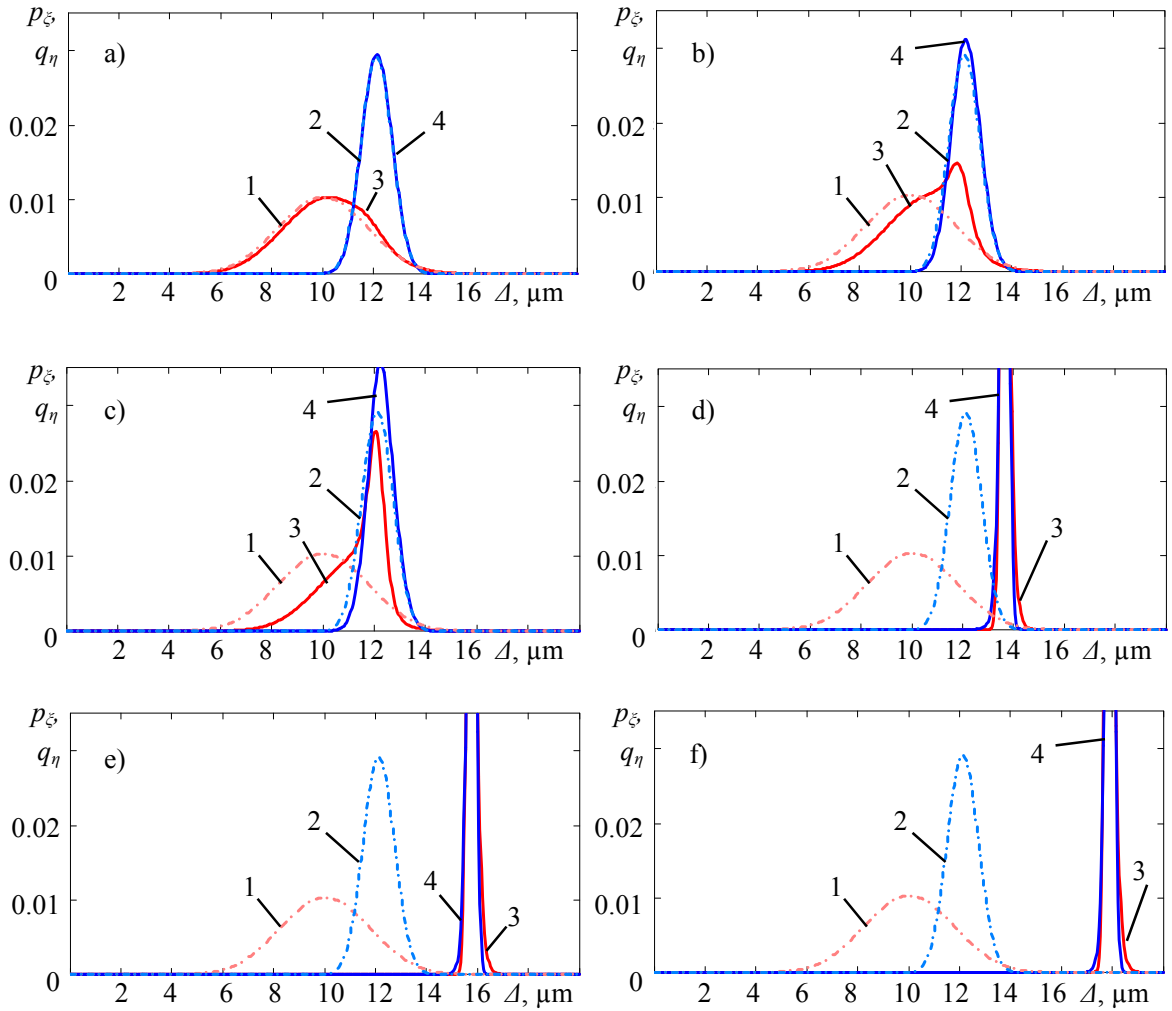


Fig. 5. The distribution of the heights of roughness of contact surfaces for friction distances 7 km (a), 35 km (b), 70 km (c), 350 km (d), 700 km (e) and 1050 km (f): 1, 2 – initial curves for cylinder liner and piston respectively; 3, 4 – curves after interaction.

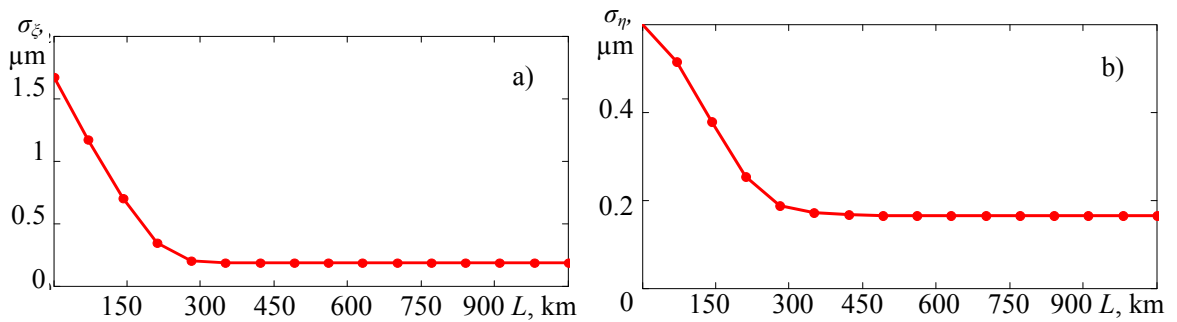


Fig. 6. The rms of the heights of surface roughness of cylinder liner(a) and piston (b) in function of friction distance.

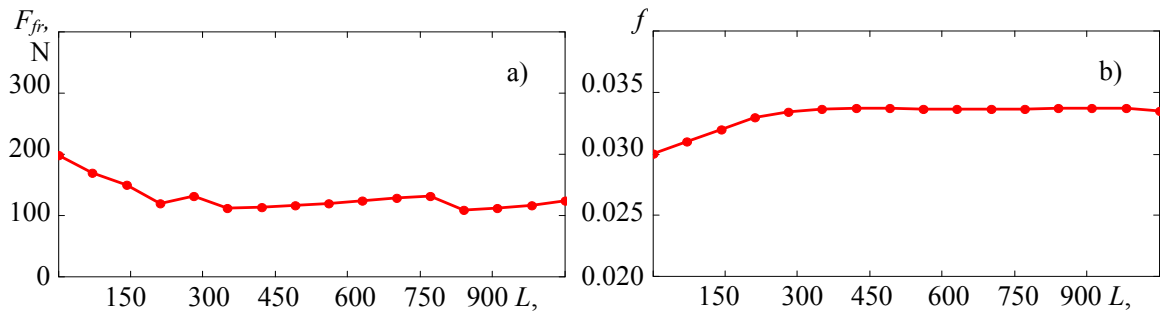


Fig. 7. The friction force (a) and friction coefficient (b) in function of friction distance.

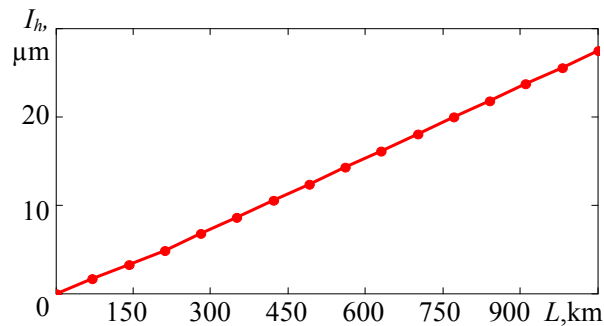


Fig. 8. The linear wear in function of friction distance.

5. Conclusion

1. The HMC of the "piston - cylinder liner" tribosystem were calculated for diesel engine, which allowed us to estimate the duration of the surfaces contact interaction.
2. We proposed a Markov model of the interaction of rough surfaces, which allows to estimate the friction characteristics over the time for contact area of "piston-cylinder liner" tribosystem.
3. Estimations agree with experimental observations.

Acknowledgements

This work was financially supported by a grant of the Ministry of Education and Science of Russian Federation for the implementation of applied research on the lot 2014-14-579-0109. Unique identifier for Applied Scientific Research (Project) RFMEFI57714X0102. This work has been carried out within the National Research South Ural State University - grantees, the agreement № 14.577.21.0102.

References

- [1] P.R. Nayak, Random Process Model of Rough Surfaces. Journal of Lubrication Technology, Elsevier. (1971) 398–407.
- [2] J.A. Greenwood, J.B.P. Williamson, Contact of Nominally Flat Surfaces, Proceedings of Royal Society, Series A, Elsevier. 295 (1966) 300–319.
- [3] V.N. Prokopiev, A.K. Boyarshinova, K.V. Gavrilov, Hydromechanical characteristics heavy-loaded bearings including non-round pins and bushings, Problems of mechanical engineering and reliability of the machines. Moscow: Science. 5 (2009) 98–104. (in Russian).
- [4] Y. Rozhdstvensky, E. Zadorozhnaya, A simulation of the thermal state of heavily loaded tribo-units and its evaluation. Bulletin of the South Ural State University, Series: Mathematical Modelling, Programming and Computer Software. 7(4) (2014) 51–64.

- [5] Y.V. Rojdestvensky, K.V. Gavrilov, A.A. Doikin, Solving of optimization task for tribological piston and rotor machines by using the mass conservation algorithm, *Friction and lubrication in machines and mechanisms*. 8 (2011) 38–43. (in Russian).
- [6] V.N. Prokopiev, Yu.V. Rozhdestvenskii, N.V. Shirobokov, Increasing of effectiveness of algorithms of outlet parameters of in a complicated manner loaded sliding supports of transport machines engines, *Vestnik Ural. Mezhrregion. Otd. Ross. Akad. Transporta*. 2 (1999) 28. (in Russian).
- [7] V. Lazarev, K. Gavrilov, A. Doikin, G. Vorlauffer, Sequad-Base J. Estimation of the tribotechnical parameters of the "piston skirt-cylinder liner" contact interface from an ic-engine for decreasing the mechanical losses, *WIT Transactions on Ecology and the Environment*. 190(1) (2014) 625–635.
- [8] V.N. Prokop'ev, E.A. Zadorozhnaya, V.G. Karavaev, I.G. Levanov, Improvement of the computation procedure for complex-loaded sleeve bearings lubricated with non-newtonian oils, *Source of the Document Journal of Machinery Manufacture and Reliability*. 39(1) (2010) 52–55.
- [9] I.G. Goryacheva, A.V. Morozov, Y.V. Rozhdestvensky, K.V. Gavrilov, A.A. Doikin, Development of method for calculating and experimentally evaluating tribological parameters of piston-cylinder tribosystem of diesel engine, *Journal of Friction and Wear*. 34(5) (2013) 339–348.
- [10] K.V. Gavrilov, A.A. Asaulyak, I.L. Kopyrkin, Method based on the application of backward differentiation formulas (bdf) and its modifications for calculating of dynamics for the tribosystem of piston engines, *Journal of Computational and Engineering Mathematics*. 2(1) (2015) 3–10.
- [11] K.L. Johnson, *Contact Mechanics*, Cambridge University Press, 1987.
- [12] J.L. Doob, *Stochastic Processes*, John Wiley & Sons, New York, 1953.



International Conference on Industrial Engineering

The mechanism of transforming the movements of a two-stroke-engine piston and the operational characteristics of its elements of strength

Boris Sharoglazov^{a,*}, Aleksandr Gofman^a

^aSouth Ural State University, 76, Lenin Avenue, Chelyabinsk, 454080, Russian Federation

Abstract

The article provides a new design of crankless piston heat car (engine), which runs a two-stroke cycle. It describes its operational principles and dwells upon the forces that affect the main elements of the mechanical transformation of the reciprocating piston motion (MTM) into the rotation of a freight roller. The authors analyse the transformation-related peculiarities of a crankless car piston in comparison with the transformation-related peculiarities of the motion in engines (heat cars), which are equipped with the crankgear. The paper contains a brief description of the method as well as the main equations to calculate forces involved in the transformation mechanism of the crankless car motion. Conformably to the specific example, herein are provided the numeral results of the calculation of the acting forces and voltage in reciprocating piston motion.

Based on the analysis of advantages the newly-designed crankless car can offer, the authors make conclusions on the expediency of engagement in research work on such type of cars.

© 2015 The Authors. Published by Elsevier Ltd. This is an open access article under the CC BY-NC-ND license (<http://creativecommons.org/licenses/by-nc-nd/4.0/>).

Peer-review under responsibility of the organizing committee of the International Conference on Industrial Engineering (ICIE-2015)

Keywords: crankless piston two-stroke car-engine; the mechanism for converting motion; piston; piston rod; a carriage mechanism for conversion of motion; treadmill; force of pressure of gases; inertial force; total force; torque (twisting) moment.

* Corresponding author. Tel.: +7-902-897-4557;
E-mail address: G389@mail.ru

1. Introduction

In the practice of the heat cars' (HM) creation, demands on limitation of their mass, size, and capacity (in litres) appear often. Today more and more attention is paid to the two-stroke work cycle (WC), see example [1], and engines with increased cyclic recurrence.

This circumstance is well written in constructing schemes of significant amount of cars: Revetec [2], Duke Engine [3], Dynacem engine (Axial Vector Engine) [4], Balandin engine [5, 6], Wankel rotary engine [7].

The instructors and staff of Internal-Combustion Engine "ICE" Department of South Ural State University (SUSU) have been occupying with the named task for a long period of time, see particularly [8,9,10,11]. Constructing scheme of crankless piston heat car-engine (CPM), see Figure 1, working on the two-stroke cycle, refers to one of the new results of work. As it follows from the name the engine doesn't contain crankgear: piston's reciprocal motion transforms into rotatory one without usage of usual crankshaft and connecting-rod.

Nomenclature

D	diameter of the cylinder
D_r	medium diameter of bush where the treadmill is implemented
dh	increment profile treadmill
da	increment shaft angle
F	squire of piston
h	profile treadmill
M	torsion torque
N	normal force
N	force acting along the normal line to the supporting treadmill surface
n	revolutions per minutes
P_c	force, operating along the connecting rod
P_g	pressure of gases
P_j	force of inertia of the reciprocal moving masses
P_Σ	algebraic sum of the forces
p	pressure of gases
r	crankshaft radius
S_h	full motion of the piston
S_{max}	maximum stroke
s	piston movement
T	tangential force
Z	force acting on the crank
α	current value of the shaft turn angle
β	limited angle tangent line to the treadmill and the horizontal
β	deflection angle of the connecting rod
ε	level of compression
π	ratio of the circumference to the diameter
ω	rotation frequency

2. Fundamental scheme and description of the CPM

Two-stroke crankless piston heat car-engine contains piston 1 set in cylinder 2 attached to the block-crankcase 3, mechanism of transfer and transformation of the motion. This mechanism contains two-horn Y-shaped outlet (freight) roller 4, which is connected to the carriage 5, the axis 6 of which has pins with the bush (roller) 7 set on them leaning against treadmill which has undulating (for example, sinusoidal) profile. The carriage 5 is connected with the piston 1 with the help of coupling rod 8, the lowest head of which is tied tough with the inner iron ring of the bearing 9 located in the socket of carriage, and the upper head is connected tough with the inner iron ring of the

piston 1. Underpiston cavity is separated from block-crankcase 3 with deflector fin 10 with the cuff compression 11 set in it. There is a hole for the coupling rod 8 held in the center of the deflector fin 10. Block-crankcase and deflector fin 10, which separates it from an underpiston cavity, make a cavity (bath) filled with oil where the most fraught elements of MTM are located.

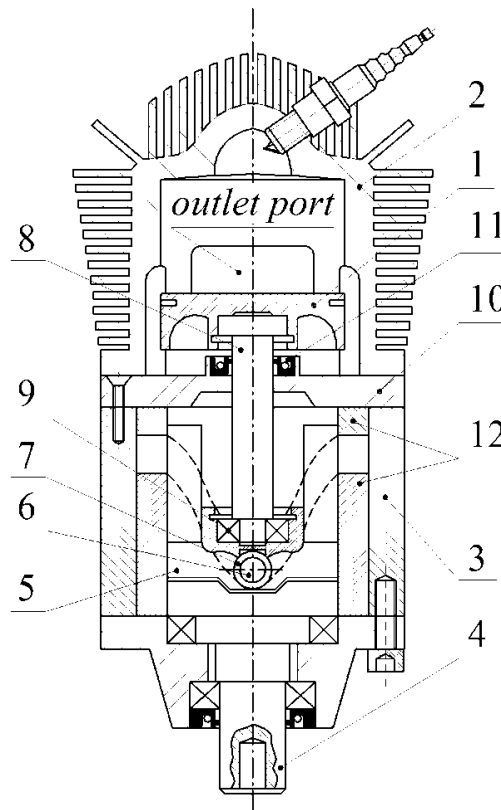


Fig.1. The scheme of crankless two-stroke engine with rotating freight roller: 1 – piston; 2 – cylinder; 3 – block-crankcase; 4 – outlet (freight) roller; 5 – carriage of the motion transformation mechanism; 6 – carriage axes; 7 – bush (roller) of the carriage axis bearing; 8 – coupling rod; 9 – bearing; 10 – deflector fin; 11 – cuff compression; 12 – bushes of the crankcase's body.

The described two-stroke crankless piston heat car-engine works on the two-stroke cycle with the loop friction system of gas exchange. Given scheme and short description allows noting an important peculiarity of the concerned CPM.

The piston is axisymmetric and connected, as it was marked before, with the carriage of the motions by coupling rod transformation mechanism, which implements only reciprocal motion. The axis 6 is located in the carriage, and on its pins the rolling bearings (bushes) are set. They lean against sinusoidal treadmill of the motion transformation mechanism formed by the butt cavity of the bushes of the crankcase's body 12. Stepped outlet (freight roller) roller is connected with the piston through the carriage 5 of the motion transformation mechanism. The upper part of the freight roller is implemented in the form of two-horn plug. The carriage 5 has the ability to move along groove made by the horns of the roller's plug.

Implementation of the piston of axisymmetric shape and its connection through the thrust bearing with the help of the coupling rod with the carriage of the piston's reciprocal motion transformation mechanism into the rotation of the freight roller in the period of WC provides the decrease of heat and mechanical deformations of the piston. The freight roller perceives and transfers only rotation. Except already mentioned advantages of the concerned constructing scheme, this heat car also possesses other advantages. For example, the piston of the car undergoes the

operation of so called normal force, which is typical for the engines with the crankgear. The vector of this force (in ICE with the crankgear, see Figure 2) is directed transversally to the surface of cylinder. As the line of the operation of this vector changes its mark during the cycle, in the engines with the crankgear the oscillations (piston transposition) between the walls of cylinder in triviality passing through the axis of the connecting rod and perpendicular to the axis of the crankshaft take place. This circumstance increases the expenses (in the engines with the crankgear) on the piston and cylinder walls friction overcoming.

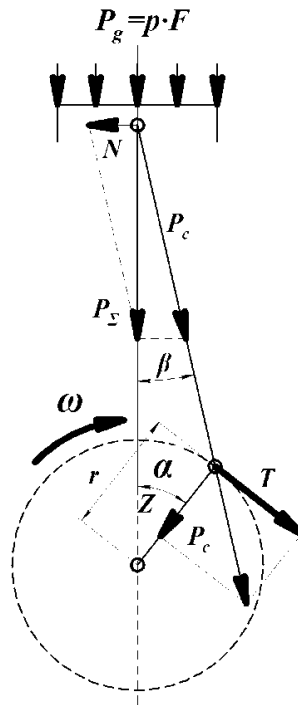


Fig. 2. The scheme of the crankgear and forces, loading its elements.

Axisymmetric construction of the CPM (cylindrical profile of the directing part, the absence of the boss for the crank pin setting) piston allows using more simple technology of its production. Symmetry of the construction, under the other equal conditions, leads to the decrease of the heat and mechanical loads level, the size and mass decrease.

3. Principle of operation of CPM

In order to give a comparative evaluation there is a typical scheme of the engine with the crankgear and forces loading its main elements shown on the Fig. 2.

In the engine with the crankgear reciprocal motion of the piston is converted into rotation of the crankshaft due to the force T on the crank (connecting rod) crankshaft journal. This in turn requires the presence of swinging (and reciprocal motion simultaneously) connecting rod.

In CPM the formation of a rotatory freight roller (carriage) motion is provided by the condition that the forces perceived by the carriage acting along the coupling rod axis transfer on the rollers (bearings) set on the pins of its axis which in turn encourages their rollers move (roll) on the undulating (for example, sinusoidal) surface of the running track formed by the curvilinear butt surfaces of the bushes 12 set in the body of CPM crankcase. And as the treadmill is closed, it provides the rotation of the carriage (and the freight roller accordingly).

Everything what was said before conformably to the CPM with two-periodical treadmill may be explained by the given scheme, see Figure 3. There is a profile (image dissection) of the treadmill (more precisely – the dissection of the lateral surface of one of the bushes 12 of the crankcase’s body on the butt of which the treadmill is located), the scheme of the carriage with rollers fixed on the carriage axis pins (the axis is not shown on the Figure), contacting with the track shown on the scheme. It (the scheme) corresponds in full to the constructing scheme of the CPM shown on the Figure 1: if you fold the scheme (combine the top dead center (TDC) responding for the position of $\alpha=360$ degrees with the line CPM appropriate to $\alpha=0$ degrees), you will get a cylinder where the rollers move on its frontal surface along the line of the treadmill. As the result, the carriage rotates and makes reciprocal motion simultaneously. The scheme refers to the period of the cycle corresponding to the initial phase combustion passing and the initial phase of the combustion stroke. Conformably to this period (the start of the named phase) the forces acting in the mechanism of the motion transformation are marked on the scheme.

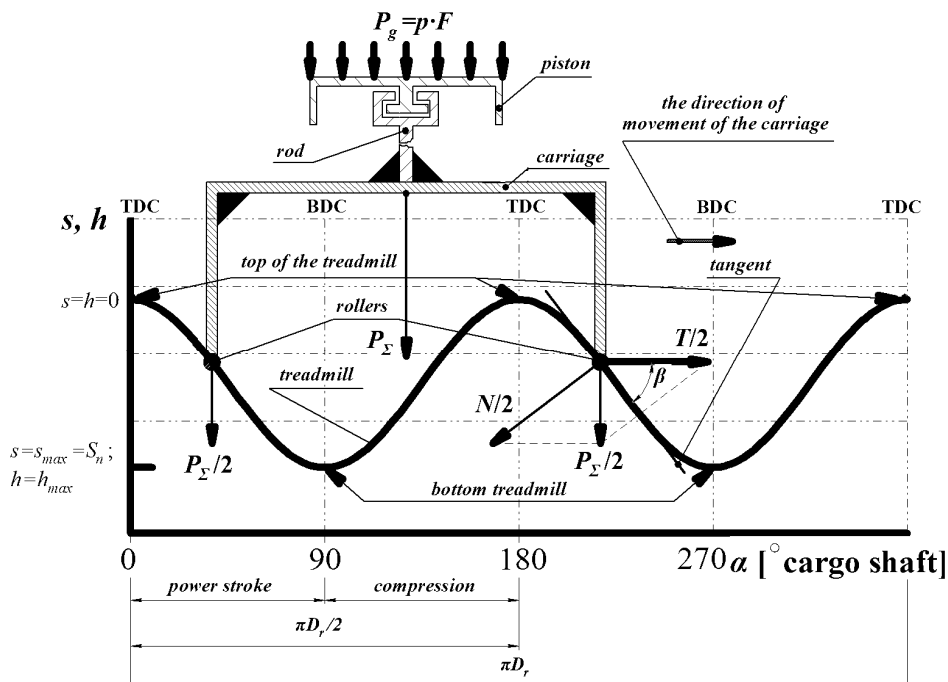


Fig. 3. The fundamental scheme CPM-engine (shown conformably to the constructing scheme given on the Fig. 1) and forces acting in the motion transformation mechanism.

The analysis of the given schemes on the figures (1, 2, 3) allows noting an important peculiarity of the considered CPM scheme. The peculiarity is that in such scheme of the piston car the piston and coupling rod are loaded with the forces acting only in the vertical cavity. It gives the grounds for its constructing schemes simplification: piston as a coupling rod may be implemented asymmetrically with the short-cut leading part. This, in its turn, creates conditions for the improvement of the heat mechanical characteristics of the motion transformation mechanism.

4. Torsion torque of the CPM

According to the analysis of engine with the crankgear scheme (Figure 2) the torsion torque transformation mechanism ($M=T \cdot r$) follows from it.

In the CPM the formation of the torsion torque is a little bit more difficult: the force P_{Σ} acting on the MTM carriage is distributed into two flows, each of them loads proper rollers of the motion transformation mechanism. It is possible to mark out two components from each $P_{\Sigma}/2$: $N/2$ – normal acting perpendicularly to the supporting treadmill surface, and $T/2$ (analogically to the force T acting in the crankgear, we will call it tangential), the motion line of which is perpendicular to the piston and coupling rod's axis of MTM, see Figure 3. These forces ($T/2$) provide the carriage and freight roller rotation: produce indicator torsion torque $M=(T/2)\cdot(D_r/2)\cdot 2=(T/2)\cdot D_r$.

Defining the named forces (P_{Σ} , T , N) and numeral values of proper moments M requires a detailed calculation of the machine's working cycle parameters. The methodology of calculating of this task (the calculation of the current parameters of the HM cycle) comfortably to the crankgear is enlightened in detail in the technical literature, see for example [12, 13, 14, 15, 16, 17]. There are some papers where the methods of crankless and conrod-free cars calculations are concerned. For example, [5, 18, 19, 20]. One of them is a recently published paper of authors, see [10]. There is a method of defining the working body current parameters and WC indicators of crankless piston heat car (engine) with two-periodical treadmill expounded in this paper.

The named condition allows not expounding the peculiarities of defining the working cycle current parameters in frames of this work but pay more reader's attention to the peculiarities of defining the parameters and loads acting in MTM of crankless car.

Thus, we will suppose that the character of movement (s) of the piston of crankless engine with two-periodical sinusoidal treadmill follows the dependence of

$$s = \frac{S_f}{2} \cdot (1 - \cos 2\alpha), \quad (1)$$

where S_f – full movement (motion) of the piston, α – current angle of the freight roller turn, articulated with the MTM carriage, see Fig. 1. The value α appropriate to the position of the piston in BDC takes as an initial point of change α ($\alpha = 90$ degrees of ISS; $s = s_{max} = S_f$), see Figure 3. The character of change of s is marked as a sinusoidal line on the figure.

As the value of $\alpha = 90$ degrees of ISS corresponds to the position of the piston in BDC ($s = S_f$), the MTM rollers (at this moment) are in the hollow of the treadmill. And the character of their vertical movement (h) defines the character of the piston's motion. In other words, it is also fair (1) for h . We can write down the following:

$$h = s = \frac{S_f}{2} \cdot (1 - \cos 2\alpha). \quad (2)$$

As it was noted before there can be defined current parameters of the working body condition in cylinder (particularly, the pressure as an a function) for any (arbitrary along a) moment of the cycle as the result of the heat calculation, then it turns out to be possible with the usage of (2) to define forces' numeral values acting in the MTM. Particularly, P_g , P_f , P_{Σ} , T , N forces.

The T and N forces ($T/2$ and $N/2$ marked in the Figure 3) can be defined with the graph-analytic approach which follows directly from the figure's scheme (and what is quite laborious) or analytically. And here the main task is to find the numeral value of β angle which is limited by the tangent to the h line which runs over the point of the P_{Σ} application and corresponded to the α , and by the horizontal line passing through this point.

This task is can be solved analytically, guided by $h = f(\alpha)$. From (2) it follows:

$$\frac{dh}{d\alpha} = \frac{S_f}{2} \cdot (2 \sin 2\alpha) d\alpha \quad (3)$$

In the marked (3), $d\alpha$ carries out the role of a scale factor connecting the dimension of the movement (S_f) and the angle of the freight roller (carriage) turn. It (this factor, scale parameter) can be defined. Full movement of the piston S_f is been making during the angle phase of the MTM carriage turn on $\pi/2$; the route projection passed by the MTM rollers to the horizontal surface which in the linear evaluation is equal $(\pi \cdot D_r)/4$. Is relative to this phase. Therefore, the numeral value of the scale factor in (3) is $(\pi/2)/(\pi \cdot D_r/4) = 2/D_r$. And then (3) will be rewritten:

$$\frac{dh}{d\alpha} = \text{tg} \beta = 2 \cdot \frac{S_f}{D_r} \cdot \sin 2\alpha \quad (4)$$

Thus we can find interesting for us β angle

$$\beta = \arctg \left[\frac{2 \cdot S_f}{D_r} \cdot \sin 2\alpha \right] \quad (5)$$

Thus, it turns out to be possible (with the usage of (5) and the forces parallelogram given on the Figure 3) to make an analytical definition of $T/2$, $N/2$ and total engine indicator torsion torque:

$$\frac{T}{2} = (P_\Sigma / 2) \cdot \tg \beta; N / 2 = \frac{P_\Sigma / 2}{\cos \beta}; M = T \cdot r. \quad (6)$$

5. The calculation of the loads acting in the CPM motion transformation mechanism

Let's view the example of the described means for the numeral evaluation of the parameters which characterize the loads of the crankless engine applicable to possible real conditions of its load. Let's imagine that main constructing parameters of the car defined by the heat calculation: the diameter of the cylinder D , full motion of the piston S_f , the level of compression ϵ , parameters characterizing the load conditions (the indicator of the air surplus a , the rotation frequency and so on). Numeral values of these parameters are (for our example): $D=58$ mm; $S_f=60$ mm; $\epsilon=7,5$; $\alpha=0,87$; $n=2250$ min⁻¹. There has been gotten cycle indicator diagram « p - a » on the basis of this heat calculation.

Named results of the heat calculation (particularly, numeral values D , S_f , current p and maximum p_{max} of the cycle pressure) allow making a preliminary evaluation of the loads (current and maximum) of the MTM (for example, $P_{g\ max}$, $P_{\Sigma\ max}$), making a selection of the materials (piston, coupling rod, the MTM carriage and its axis), carrying out a preliminary design of the main components (defining their size and mass). The results of these preliminary actions for the concerned example (taking into account WC data gotten by the heat calculation) are displayed in the Table 1, Figure 4, and Table 2.

Table 1. Masses numeral values of the MTM main elements.

Name and the mass of the element, gram					
Piston	Rod	Carriage	Carriage axis	rollers	Total mass
214,44	64,5	145,33	53,55	2*14,15	506,1

Table 2. Maximum value of the voltages acting on the main components of the MTM

Detail's name	Type of loading	Voltage value, MPa	Material	Limit of the material's fluidity, MPa
Piston	Bottom curve	25,9	AlMg10	170
Rod	Compression	71,4		
Carriage axis	Curve	259,2	37Cr4	1100 (heat-treatment with the cooling in oil, 48 HRC)
Treadmill	Contact compression	1080		

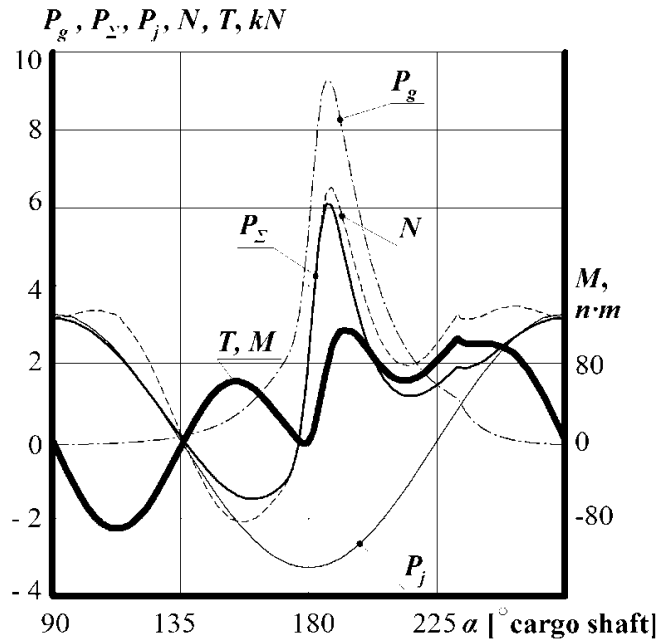


Fig. 4. The character of P_g , P_j , P_Σ , T , N forces' change and the M moment acting in MTM of the two-stroke of CPM-engine.

It is worth noting that the current and maximum values of the voltages acting on the elements of the CPM motion transformation mechanism was calculated with the usage of known methods [21, 22, 23] of such type of tasks.

6. Conclusions

The analysis of the principle of the realization of working cycle and forces, loading the force elements of the crankless piston car (engine) motion transformation mechanism working on two-stroke cycle allows concluding that there are more favorable conditions for loading the MTM main elements in the concerned constructing scheme of such car (engine). The MTM scheme itself allows to exclude such difficult and expensive in the production elements that are mass-applied in the engines of the crankgear as a crankshaft, a coupling rod, allows simplifying the construction of the piston: making it (the piston) axisymmetric and releasing (it and cylinder line) from the lateral (perpendicular to the mirror of the cylinder) loads.

The calculation materials given in the article (particularly, numeral values of forces and voltages loading the main elements of the MTM) give the grounds to make a conclusion that the research works on such type of cars are expedient.

References

- [1] Information on Innovations@renault 2014 behind-the-scenes of innovation at renault
- [2] Information on <http://www.revetec.com>
- [3] Information on <http://www.dukeengines.com>
- [4] Information on <http://www.engineeringtv.com/video/AVEC-Axial-Vector-Engine>
- [5] S.S. Balandin, Conrodless internal combustion engine, Mashinostroenie Publ., Moscow, 1982.
- [6] V.K. Chistyakov, Dynamics of piston and combined internal combustion engines, Mashinostroenie Publ., Moscow, 1989.
- [7] F. Wankel, Rotary piston machines, ILIFFE BOOKS LTD, 1965.
- [8] B.A. Sharoglazov, V.G. Vaganov, RF Patent 2156871. (2000)
- [9] B.A. Sharoglazov, S.Yu. Terekhov, I.I. Kolbin, RF Patent 2551717. (2014)
- [10] B.A. Sharoglazov, A.V. Gofman, Beskrivoshipnaya porshnevaya replovaya mashina- dvigatel: kinematika, rabochiy tsikl, pokazateli tsikla:

- monografiya, South Ural St. Univ. Publ., Chelyabinsk, 2014.
- [11] B.A. Sharoglazov, A.V. Gofman, Porshnevaya teplovaya mashina dlya preobrazovaniya energii i proizvodstva raboty na transporte [Piston heat engine for energy conversion and transport work performance], *Bulletin of the South Ural state university. Series mechanical engineering industry*. 14(1) (2014) 5–11.
- [12] I.I. Wiebe, *Brennverlauf und Kreisprozeß von Verbrennungsmotoren*, Vebverlagtechnik, Berlin, 1970.
- [13] R.Z. Kavtaradze, *The theory of piston engines. Special chapters: textbook for high schools*, Mashinostroenie Publ., Moscow, 2008.
- [14] N.K.H. Dyachenko, *Teoriya dvigateley vnutrennego sgoraniya*, Publ., Leningrad, 1974.
- [15] D.N. Vyubov, N.A. Ivashenko, V.I. Ivin, *Dvigateli vnutrennego sgoraniya. Teoriya porshnevnykh i kombinirovannykh dvigateley*, [Theory of Piston Engines and Combined], Mashinostroenie Publ., Moscow, 1983.
- [16] B.A. Sharoglazov, V.V. Shishkov, *Porshnevye dvigateli: teoriya, modelirovanie i raschet protsessov*, [Piston engine: theory, simulation and calculation process], South Ural St. Univ. Publ., Chelyabinsk, 2011.
- [17] B.A. Sharoglazov, O.G. Mashkov, P.B. Vakengut, *Avtomatizirovannaya otsenka chislennykh znacheniy iskhodnykh parametrov pri modelirovanii protsesov v porshnevnykh dvigatelyakh*, [The automated assessment of values of initial parameters at numerical modeling of processes in piston engines], *Bulletin of the South Ural state university. Series mechanical engineering industry*. 13(1) (2013) 80–85.
- [18] T.M. Bashta, *Obyemnye nasosy I gidravlicheskie dvigateli gidrosistem*, Mashinostroenie Publ., Moscow, 1974.
- [19] L.M. Logov, *Beskrivoshipnye mnogotsilindrovye nasosy*, Mashgiz Publ., Moscow, 1963.
- [20] R.A. Lang, *Basic principles and components of fluid technology*, Mannesmann Rexroth GmbH.
- [21] V.I. Feodosev, *Soprotivlenie materialov*, MSTU of N.E. Bauman Publ., Moscow, 1999.
- [22] D.Y. Reshetov, *Detali mashin*, Mashinostroenie Publ., Moscow, 1989.
- [23] G.S. Pisarenko, *Soprotivlenie materialov*, Graduate School. Publishing head. Publ., Kiev, 1979.



International Conference on Industrial Engineering

Study on Screw-Ball Differential Gear Operating Process

Keller A.V.^a, Shelepov A.A.^a, Istomin D.I.^{a*}

^a South Ural State University, 76, Lenin Avenue, Chelyabinsk, 454080, Russian Federation

Abstract

This article includes an analysis of structure, operating principle, main mathematical relation of the self-blocking screw-ball differential gear operation in different modes of the vehicle motion. Relations of the half-axes rotation speed, as well, as of the blocking factor to time are presented for each mode of motion. These relations were generated during testing on a dynamic operating test bench.

© 2015 The Authors. Published by Elsevier Ltd. This is an open access article under the CC BY-NC-ND license

(<http://creativecommons.org/licenses/by-nc-nd/4.0/>).

Peer-review under responsibility of the organizing committee of the International Conference on Industrial Engineering (ICIE-2015)

Keywords: screw-ball differential gear, self-blocking differential gear, differential gear testing, differential gear blocking factor, torques distribution in wheeled running gear

1. Introduction

At the present time we can see the tendency on using the screw-ball differential gear (SBDG) in automobiles transmission systems. SBDG is implemented in order to rationally use the automobile weight on driving axles and draft on adherence for improving dynamic parameters.

2. Design of SBDG

SBDG is one of the promising designs of the self-blocking differential gears. This differential gear design was patented in the middle of the XX century [3], but due to more strict requirements to materials and manufacturing accuracy the SBDG was not mass-produced until recent time. Upgraded design was patented by Russian engineer V.N. Krasikov, its production was already mastered [2].

* Corresponding author. Tel.: +7-951-775-7322 .

E-mail address: shelepov-aa@mail.ru

This differential gear has simple design and consists of the few components. The SBDG design is illustrated on Fig. 1.

The SBDG consists of a body 2 with two cylindrical half-axle elements (screws), located in central part and touching each other on butt ends. Half-axle elements surfaces have screw grooves of right-hand rotation on one screw, and of left-hand rotation on another screw. Pairs of parallel located close to each other holes 5 are penetrated in body 2. Holes diameter is equal to the used ball diameter. These holes ends join each other, forming closed channel, filled with balls 6.

In case half-axle elements are removed, closed chain of balls 6 can move freely in channel 5 without obstacles. Balls chain in the channel forms an oval pinion - satellite, balls being its teeth. One branch of the channel 5 (located closer to the half-axle elements rotating line) is opened in order to place balls into half-axle elements grooves. Closed balls chain connects both half-axle elements into united kinematic chain.

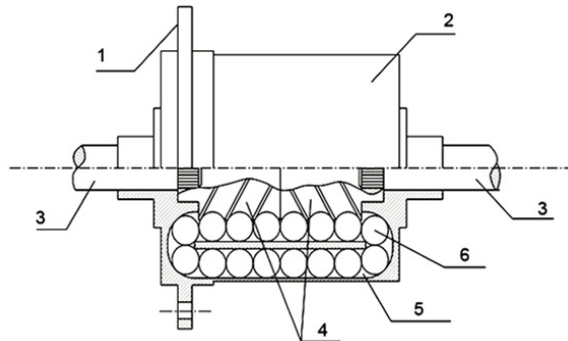


Fig. 1 - the SBDG design: 1) Final drive pinion flange, 2) Differential gear body, 3) Vehicle half-axes, 4) Half-axle elements, 5) Channel for balls passing, 6) Rolling bodies – balls.

Rotating of the body 2 through balls chain transfers power to screw grooves of the half-axle elements 4, which transfer power to the vehicle wheels through the half-axes 3. When the half-axle elements 4 are rotated in reverse direction through the half-axes, than balls 6 chain starts moving, allowing half-axle elements free and easy rotation. In this case the SBDG operates as a conventional differential gear [4].

Work was performed under financial support of the Ministry of Education and Science of Russian Federation in the frames of the project Generating Scientific-and-Technical Solutions on Controlling Power Distribution in the Cargo Trucks Transmission Trains in Order to Increase their Power Effectiveness and Fuel Effectiveness under agreement No. 14.574.21.0106 dated 09.08.2014.

Screw-ball differential gear operates as follows. Under uni-form moving, when the SBDG is characterized by the relative forces balance, balls chain freely moves over the channels and equally distributes power between wheels. The vehicle is maneuvering as if it was equipped with a conventional differential gear. Opposite to the limited-slip differential gear, in this mode the SBDG does not resist the turn. When forces balance is broken (different resistance coefficients on wheels, sharp speeding up or engine braking), the balls chain is loaded, and forces action balance in turning channel leads to locking the chain. The differential gear blocks. The higher is the driving wheels loads difference, the higher is the blocking factor. The SBDG reacts not on the wheels rotation speed difference, but on the difference between the driving wheels loads and engine power [2].

3. Screw-ball differential gears operating feature and mathematical relations.

Moment on the wheel with higher friction coefficient depends on the differential gear blocking factor (Eq. 1), which is determined by the ball transmission components effectiveness (Eq. 2).

$$M_{\max} = M_{\min} \cdot K_b \quad (1)$$

where: M_{\min} – moment on the wheel with lower friction coefficient, Nm ; M_{\max} – moment on the wheel with higher friction coefficient, Nm ; K_b – differential gear blocking facto.

$$K_b = \frac{1}{\eta_m} \quad (2)$$

where: η_m – mechanical effectiveness of the force flow by the balls in channel.

Total differential gear effectiveness is equal to (Eq. 3):

$$\eta_M = (1 - f \cdot \operatorname{tg} \alpha_n)^n \cdot \frac{(1 - 2f)^m \cdot \left(1 + \frac{2f}{3\operatorname{tg}q}\right) - \frac{4f}{3\operatorname{tg}q}}{1 + \frac{2f}{3\operatorname{tg}q}} \quad (3)$$

where α_n – ball angle of contact, *degrees*; n – quantity of balls, filling the toroid 360° ; f – friction coefficient; q – screw spiral line slope angle, *degrees*.

Screw-ball differential gear blocking factor is determined by the effectiveness of the force flow by the balls chain in turning and straight channel sections. Effectiveness is determined by the differential gear components geometrical parameters. [5]

4. Study gear operating process

Present work implementation included SBDG testing on the dynamic operating test bench [1].

Dynamic operating test bench (Fig. 2) includes mobile base with installed power electric motor, connected to the vehicle drive axle gear through the step down gear. Power distributing mechanism is installed into the vehicle drive axle gear. Drive axle gear output shafts through wheels interact with loading device, simulating different vehicle moving modes. Data collecting and processing is performed by an information collecting and processing module with a socket for linking to a PC.

Loading device simulates different moving modes (straight, turning with different radius, different wheels adhesion to surface). Test bench is controlled by the control panel by soft increasing of the power electric motor speed.

Information collecting and processing module registers results by means of torque sensors and rotation speed sensors.

Differential gears are tested as follows. Tested differential gear is installed into the drive axle final drive housing instead of the operational differential gear. Loading device generates necessary load separately for left and right wheels. Test bench is ready for operation after energizing power electric drive and information collecting and processing module. Drive axle output shaft rotation speed is regulated by a regulating device, located on the information collecting and processing module operating panel. Drive wheels loading parameters and input and output components rotation speed monitoring is performed by indicators, located on the information collecting and processing module operating panel. Measuring results are provided to the PC memory for further processing.

Lets analyze the differential gear operating under following simulated vehicle moving modes:

- straight moving under constant speed;
- straight accelerated moving;
- straight accelerated moving under different wheels loads;
- turning under constant speed;
- turning under acceleration;
- turning under acceleration and under different wheels loads.

Following parameters were analyzed during all bench tests: wheels rotation speed, and differential gear blocking factor (K_b).

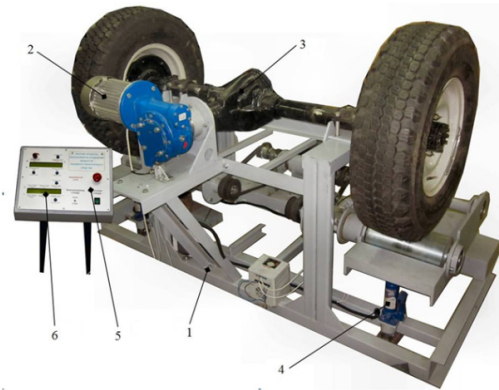


Fig. 2 - Dynamic operating test bench: 1) Power frame; 2) Driving electric motor; 3) Driving axle gear; 4) Loading device; 5) Control panel; 6) Information collecting and processing module

Lets analyze the automobile traction condition when straight moving under different drive wheels adhesion coefficient. Input shaft rotation speed changed from 0 to 500 min^{-1} , load on the right wheel was equal to 2,500 N, load on the left wheel was equal to 1,000 N. Obtained values are presented on Fig. 3 and 4.

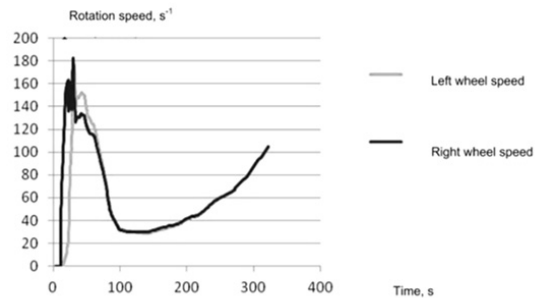


Fig. 3 - Rotation speeds

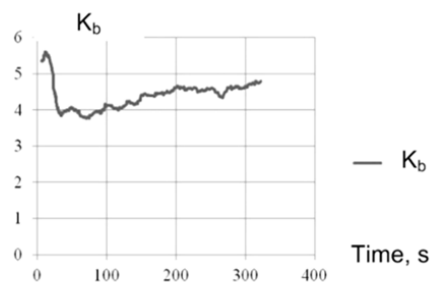


Fig. 4 - Blocking factor

When vehicle is moving under different load on the wheels, we can see a transition period, when K_b is growing. After wheels rotating speeds equalize, K_b value decreases and stays at a level, enough for even moving of the vehicle under these conditions.

Same investigation was performed for the differential gear operating under the vehicle turning and when maneuvering.

Discussed experiment simulates automobile moving when turning with constant speed and equal loads on wheels, turn radius - 8 m, input shaft rotation speed - 500 min⁻¹, driving wheels load 2,500 N. Obtained parameters for this mode are presented on Fig.s 5 and 6.

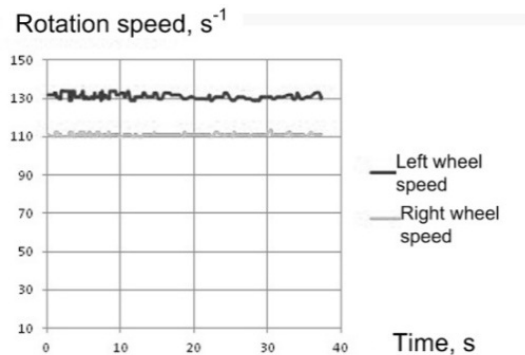


Fig. 5 - Rotation speeds

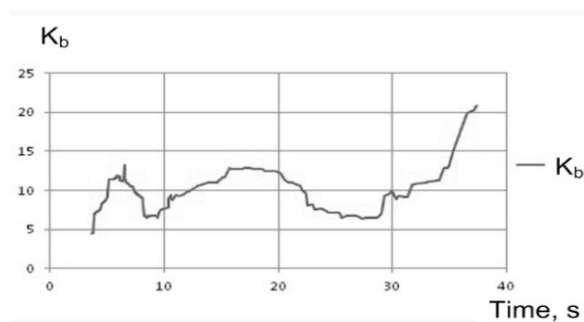


Fig. 6 - Blocking factor

Presented earlier relations indicate, that differential gear operating assures constant wheels rotating speed difference under turning with constant speed. Blocking factor K_b for the differential gear increases and distributes the torque on the behind wheel, increasing the vehicle stability, having negative effect on passing turns, maneuvering, and decreasing the dif-ferential gear and transmission components service life.

Next stage included the differential gear testing when sim-ulating passing the set radius turn under acceleration. Obtained in this experiment data on the differential gear parameters to a large extend determine its operating under all modes of vehicle moving, as uniformly accelerated or decelerated curvilinear motion is the most characteristic motion mode. Obtained parameters are presented on Fig.s 7 and 8. When performing the tests, load on driving wheels was equal to 2,000 N, and input shaft rotation speed increased from 0 to 500 min⁻¹.

One wheel slipping was noted in the beginning of the test, than speeds difference becomes constant. This moving mode leads to high K_b value, having negative effect on the automo-bile passing the turn.

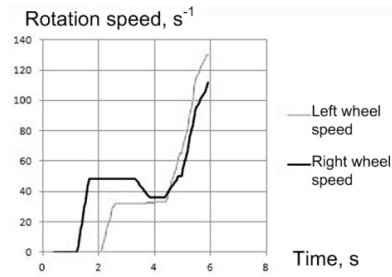


Fig. 7 - Rotation speeds

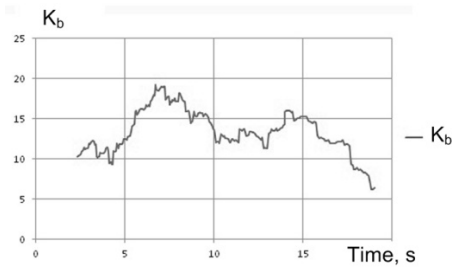


Fig. 8 - Blocking factor

Lets discuss turning under acceleration and under different wheels loads. Tests performing conditions: Input shaft rotation speed changed from 0 to 500 min^{-1} , load on the right wheel was equal to 1,700 N, load on the left wheel was equal to 1,500 N. Turn radius - 6.5 m. Obtained relations are presented on Fig.s 9 and 10. In this case running off wheel has higher set load, and the differential gear distributes higher torque to this wheel. Torque increases as input shaft speed increases. This leads to K_b increasing with moving speed increasing and to undesired transmission train loading.

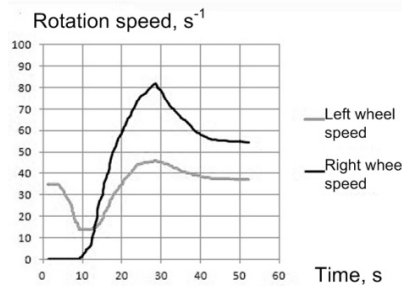


Fig. 9 - Rotation speeds

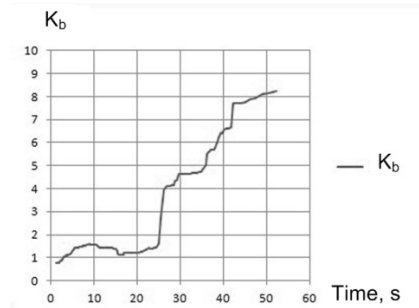


Fig. 10 - Blocking factor

Based on the above mentioned, we can conclude that by finding geometrical parameters on the designing stage we can establish necessary blocking factor and obtain optimal parameters of the differential gear operating for vehicles, operating under different road conditions. Tests results are quite repeatable with maximum error of about 15 percent. Calculated results differences are related to the fact that this equation does not take into account parameters of used lubrication oil.

Acknowledgements

Work was performed under financial support of the Ministry of Education and Science of Russian Federation in the frames of the project Generating Scientific-and-Technical Solutions on Controlling Power Distribution in the Cargo Trucks Transmission Trains in Order to Increase their Power Effectiveness and Fuel Effectiveness under agreement No. 14.574.21.0106 dated 09.08.2014.

References

- [1] A.D. Belokopytov, E.M. Kudryashov, V.N. Kravets, V.I. Shishkin, RF Patent 2178878. (2002).
- [2] V.N. Krasikov, RF Patent 2319875. (2008).
- [3] V.-O.A. Lucy, USSR Invention description to the inventor's certificate SU 1507603.
- [4] A.D.G. Krasikov's, Automatic Differential Gears: [Electronic source], Chelyabinsk, 2005-2014. URL: <http://www.dak4x4.com>.
- [5] A.A. Shelepov, D.I. Istomin, A.V. Keller, Screw-Ball Differential Gear Design and Main Parameters, Machine Engineering Future in Russia: Electronic Collected Works of the Seventh All-Russia Conference of the Young Scientists and Specialists. Moscow. (2014) 0321402784.
- [6] T. Bachmann, C. Bielaczek, B. Breuer, Der Reibwert zwischen Reifen und Fahrbahn und dessen Inanspruchnahme durch den Fahrer, Automobiltechnische Zeitschrift. 97(10) (1995) 658–667.
- [7] W. Bergmann, Considerations in determining vehicle handling requirements, SAE Technical paper series. 690234 (1969).
- [8] H. Bleckman, Traction control system with Teves ABS Mark II, SAE Technical Paper Series. 860506(78) (1995) 9.
- [9] J. Garnault, L'antiskid Bendix. La part de l'electronique digital, Ingenieurs de l'automobile. 9 (1987) 106–112.
- [10] O. Fersen, "Volks – ABV" von AP–Lockheed, Automobil Revue. 22,27 (1987) 27.
- [11] F. Jindra, Directional Stability and Control of four – wheeled Vehicle in a flat Turn, SAE "Preprint". 211A (1960).



International Conference on Industrial Engineering

Substantiation of parameters and operation modes of device for thermal comfort of a mobile machine operator

Glemba K.V.^{a,b,*}, Averianov Y.I.^{a,b}

^aSouth Ural State University, 76, Lenin Avenue, Chelyabinsk, 454080, Russian Federation

^bSouth Ural state agrarian University, Chelyabinsk 454080, Russia

Abstract

The effects of heat and cold on the human body lead to a reduction in its protective power and reserve capacity. The productivity of operators is reduced by 25~55% with ambient temperature increasing up to 28~31°C. It is proved that the temperature and human performance have a strong correlation. The process of forming the thermal state of the human operators in the cabs of mobile machines is still to be understood by automotive engineers. On the basis of theoretical research, we have identified the main factors influencing the thermal state of the human body, justified the blueprint and design parameters of the proposed device for thermal regulation. There is a power dependence of heat flux on the thickness of the operator's clothes, the power, and distance of their body from the local device. When experimenting with the relationships between the human operator's thermal state (thermal sensation) indicator and the parameters of microclimate in the mobile machine cabs, we considered the operating modes of the device. Experimental studies were carried out in a climatic chamber based on a unified cabin. The experiments determined the value of the power density of the heat flow. It amounted to 486 watts; this will be needed in the future to calculate the constructive and regime parameters of the proposed device.

© 2015 The Authors. Published by Elsevier Ltd. This is an open access article under the CC BY-NC-ND license (<http://creativecommons.org/licenses/by-nc-nd/4.0/>).

Peer-review under responsibility of the organizing committee of the International Conference on Industrial Engineering (ICIE-2015)

Keywords: The operator of the mobile machine; thermal comfort; conductance; thermoregulation; thermal sensation; the climate; the heat flux.

* Corresponding author. Tel.: +7-351-262-1347.

E-mail address: glemba77@mail.ru

1. Introduction

The level of conditions and safety in the workplace operators of automotive engineering determines its demand and the competitiveness of the market. High power equipment and complexity of control systems in modern mobile machines (MM) requires a search for new solutions to create comfortable conditions for the work of the human operator. The causes and the degree of reduction human performance are defined by the thermal condition of his body and its heat content. Scientists say that high efficiency is maintained for 6 hours at the heat content in the body 128 kJ/kg and decreases over time by 10~20%. But if you increase the value to the level of 129~131 kJ/kg return is reduced at the same time by 30~45%. In a cold climate an increase in the mass of clothes is the cause of poor performance. For example, the energy consumption of the body increases by 18% when performing the same job by increasing the mass of clothing from 4.3 to 6.5 kg. The effects of heat on the human body in conditions of heating microclimate leads to a reduction in its protective power and reserve capacity. The cold also affects the cardiovascular system and blood pressure. Observed dystonia and exacerbated chronic disease. The productivity of the human operator is reduced by 25~55% with increasing ambient temperature until the interval of 28~31°C, and reducing the skills of workers leads to a more intense decrease in performance [1 – 6].

2. Methods

2.1 Theoretical research

The influence of microclimate on the health of operators in the cabs MM devoted a significant amount of research. Human thermal comfort is one of the main factors that characterize the conditions of the production environment, the health and well-being, the degree of job satisfaction. It is proved that there is a high level of correlation between the temperature regime and the level of human activity. It was found that people performing work of moderate severity with the energy consumption of 313 watts (40 minutes work, 20 minutes rest) under conditions of heating microclimate occurs a pronounced decrease of efficiency, especially under thermal impact. Solution of tasks to ensure the comfortable state of the human operator in the cabins MM is a rather complex problem. The device of an artificial microclimate must meet the requirements of simplicity of design, low cost of fabrication, possibility of service personnel of low qualification, they must ensure that the design conditions with constantly changing modes of operation of the machines. Partial reduction of the air temperature in the cabin at the expense of natural ventilation leads to an increase in speed of air movement and dust accumulation in it. Currently numerous experimental studies have established a negative influence of adverse environmental conditions on productivity [7 – 25].

Many papers are devoted to the study of the formation of the thermal state of the human organism in the conditions of industrial premises. However, the process of forming the thermal state of the human operator in spaces of small closed volume, such as the cockpit MM remains poorly understood. This makes it difficult not only to control the thermal state (thermal comfort) of a person in the cockpit MM and evaluation of the effectiveness of normalization of the microclimate in their selection, testing and use, this hampers the development of new ways and means to ensure a comfortable state of the human operator [5, 6].

For the last time on the basis of the principles of control theory created a number of models of temperature regulation of man. In these models, represented the human body in the form of geometric segments, each subdivided into a number of layers and compartments. Passive thermoregulation system can be described using the heat balance equation for each compartment, taking into account the contact surface of the skin with the environment. On the basis of established reference temperature for each compartment in the system are formed by control signals, allowing you to modify physiological responses during exposure to various environmental factors, physical load and thermal resistance. Scientists recognized system *Stolwijk J. A. J.* in the field of thermoregulation, designed to study the thermoregulatory responses of the body in the field of positive temperatures. This model was the most appropriate for the interval of temperatures from 25~48°C and has a complex system of generation of control signals and their distribution, taking into account the deviation of the temperature values of each compartment and the reference level. The researchers obtained important information when using mathematical modeling to describe the thermal regime of the body. So, *Gagge A. R.* and co-authors have developed an index of effective temperature, which has been used in the practice of evaluation of physiological strain of an organism when exposed to a thermal

factor of the environment, using compartmental models. In the process of analysis of mathematical models describing the formation process of the thermal state of the human body, found that some authors do not take into account or neglected component of thermal balance – thermal conduction. Conducted targeted impact on certain portions of the surface of the human body will facilitate the process of heat exchange of the organism with the external environment under certain conditions, heating or cooling climate. To date remains unresolved question about the levels and modes of the thermal effects on the human body where there is no overstrain of thermoregulatory mechanisms of the body, where there is no local thermal discomfort. Conductive heat exchange of the human body contacting surfaces and means of ensuring thermal comfort of the human body deserves serious study [1 – 6, 12 – 14, 23 – 25].

2.2. Research methods

The methodology of the experimental studies included the measurement of microclimatic conditions in the external environment and in the interior of MM, a survey of the human operator on its thermal state, i.e. about the thermal sensation. In addition, the recorded date, time, and place of the research, the type of work performed, age and clothing of operator, weather conditions (cloud cover and solar radiat).

Objectives of the experimental studies was to obtain experimental dependencies between the indicator of the thermal state (thermal sensation) of the human operator and the parameters of the microclimate in the cabins MM, the justification of the thermal state of the body (heat content and thermal sensation) of the human operator based on the parameters and operating modes of local thermally regulating devices (LTRD) in the cockpit MM.

Field studies were conducted in weather conditions of the transition period, the regions of the southern Urals and Northern Kazakhstan. The outdoor temperature varied in the range of 10~31°C, relative humidity – 20~80%; standard deviation-wind speed – 0.5 to 6.0 m/s, cloudy – one or two points. Measurement of microclimate parameters in the cabins was carried out at performance of technological processes when you load the engines by 70% ($\pm 15\%$) from the nominal value. For research were selected groups of people from 5 to 10 people in the age 20~40 years old, not adapted to the specific working conditions of the operator MM. Performed work of moderate severity, the clothes were summer with a thermal resistance of 0.5~0.6 clo (1 clo = 0,155 (m² K)/W), the subjects familiarized with the modified scale of scores of thermal sensation, characterizing the thermal state of the operator. The studies were conducted during the working time. We measured microclimate parameters at the time of the evaluation in humans of one of established his thermal sensations in the cockpit MM. Measurements of microclimate parameters in the cockpit MM was carried out at three points: at the feet, at chest level and in the breathing zone. Repeated measurements were 25 times [3~6].

2.3. Experimental studies

As optimization criteria have been selected heat content and thermal sensation of the human operator. They reflect a comfortable thermal state of the body and can be evaluated by the criteria of comprehensive assessment of comfort conditions of microclimate. On the basis of theoretical research identified the main factors influencing the process of formation of the thermal state of the human body. Below is the diagram of the LTRD (Fig.1) and parameters of its design – the diameter and pitch of the tubes (Fig.2). Criteria for evaluation of the thermal state of the human operator are its q_h heat content and thermal sensation S_h . They are characterized by the parameters of the microclimate in the cockpit MM, are based on the characteristics and operating modes of the LTRD. For the purpose of characteristics of the comfort areas it is proposed to introduce the concept of criteria of comfort, a numeric value which can be determined from the following expressions in Eq. (1) and Eq. (2) [1, 2].

$$k_{ks} = k_s (S_{ha} - S_{hn}) / S_{hn} , \quad (1)$$

$$k_{kq} = k_q (q_{ha} - q_{hn}) / q_{hn} , \quad (2)$$

where k_{ks} , k_{kq} is the criteria comfort of microclimate due to the evaluation of thermal sensation and thermal content of man, conditional units; k_s , k_q is the normalizing coefficients of thermal sensation and thermal content of human

rights, taking into account the conversion into conventional units; S_{ha} , S_{hn} is the actual and normative values of thermal sensations, score; q_{ha} , q_{hn} is the actual and normative values of specific heat content, (kJ/kg).

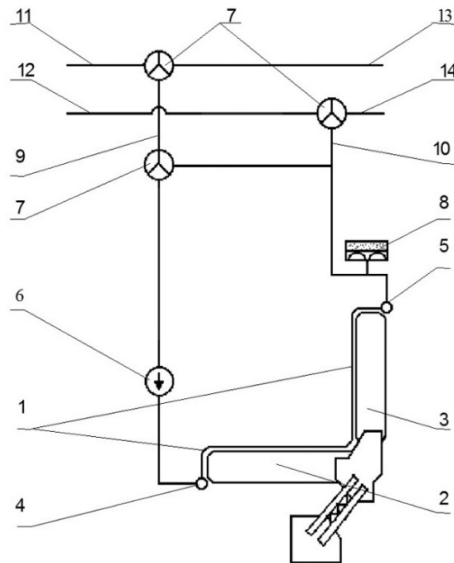


Fig. 1. Scheme of the experimental sample local thermally regulating devices, 1 removable cover, 2 airbag, 3 back, 4 and 5 respectively the collector inlet and outlet, 6 pump, 7 a liquid flow regulator, 8 accumulator, 9 and 10 flexible tubing, from 11 to 14 respectively, of the tube outlet and inlet of the thermal unit and cooling unit.

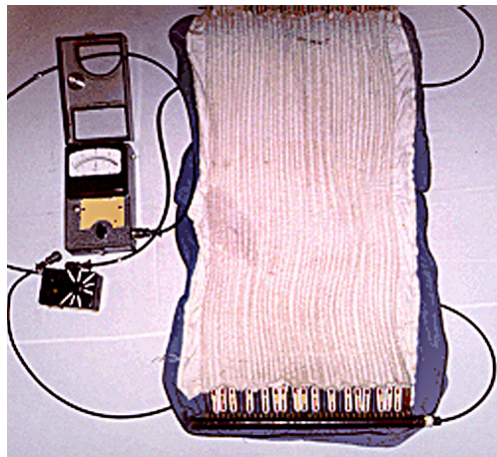


Fig. 2. The experimental sample of the device for the thermal comfort of the local action.

Experimental studies were carried out in a climatic chamber, which was established on the basis of a unified cockpit MM [3-6]. Parameters of microclimate in a climatic chamber maintained at a predetermined level when the doors and Windows closed during the whole time of the experiment, the indicators were: air temperature $32 \pm 0.5^\circ\text{C}$, relative humidity of 40~60% and air speed of 0.2~0.4 m/s. Periodically changed work LTRD by the method of experiment planning. The flow rate of fluid when the work has not changed and amounted to 120 liters/hour.

3. Results

Effective operation of the device according to the criterion of comfort with regard to reflecting thermal sensation depends on the subjective perception of the environment. There is a dependence of the power thermal flux from such quantities as the gap between the body of the human operator and LTRD, thickness of clothing of the operator, etc. It is therefore necessary experimental validation of microclimate parameters with minimum absolute values of the criteria categories, such as modes of operation is the temperature of the liquid (t_l , °C), and the design of the components is the total length of the tubes LTRD (L , m). The authors have built a graphic dependence (Fig.3), which links the parameters with the required power of the heat flux, fluid temperature, flow rate, etc. Thus, if the change in temperature of the fluid be in the range of 16~24°C, then the required total length of tubes will be in the range of 18~23 m.

Of greatest interest is the dependence of the power density of the heat flow from the speed of increasing the temperature of the human body (Fig. 4), since this speed determines the degree of comfort to the proposed LTRD. The power density of the heat flux significantly increases with increasing speed of increasing temperature of the human body and is 150 W/m² per 1°C. This is independent from the mass or growth. The required average power density of the heat flow is 268 W/m² at mean values of body mass and human growth (70 kg and 1.7 m) and the normative value of the speed of increase of body temperature (2°C per hour).

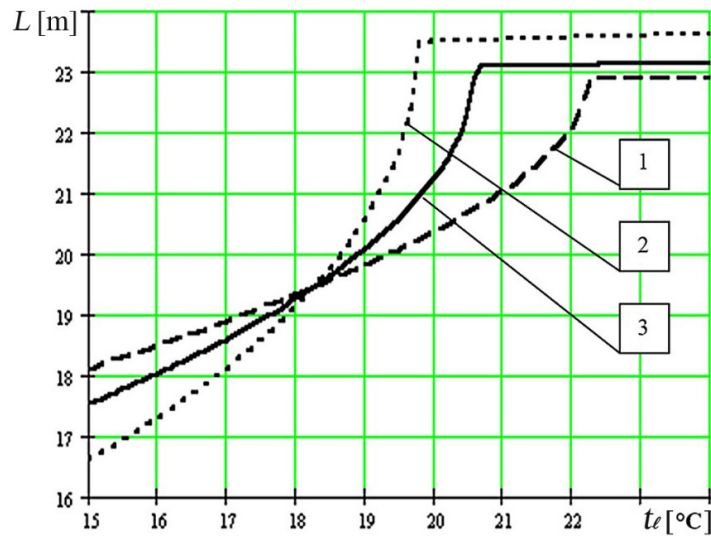


Fig. 3. Graphic dependence of the required total length of the tubes L [m] from the temperature of the liquid t_l [°C] according to the condition of minimality criteria of comfort, 1 the heat content of the body, 2 thermal sensation, 3 integral criterion.

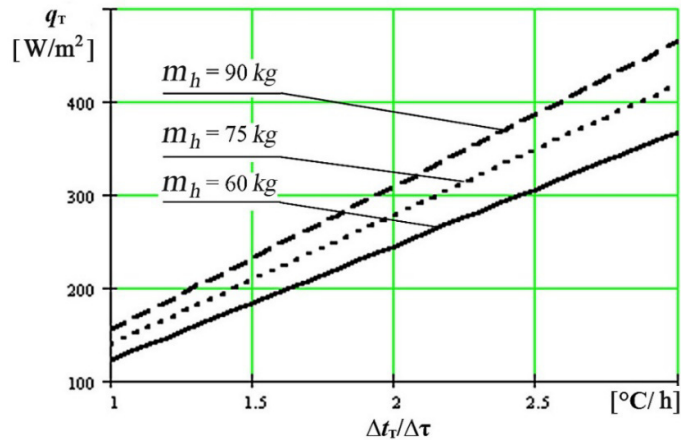


Fig. 4. The dependence of the power density of the heat flow q_r [W/m²] from the rate of rise of body temperature $\Delta t_r / \Delta \tau$ [°C/h] for an average growth of $H_h = 1.75$ m, at its mass m_h [kg].

The values of power density of the heat flow is easy to determine the full power of the heat flux on the entire surface of the human body, essential for maintenance of a desired (comfortable) speed temperature rise by multiplying the power density of the heat flux on the surface area of the human body. In this regard, graphical dependencies for full power heat flux are not shown. However, the value of the total power of the heat flux with standard parameter values were calculated and amounted to 486 watts. This value of power density of heat flow is necessary for further calculations of the design and operation of the LTRD.

4. Conclusion

Cabin equipment LTRD has the following advantages in comparison with a serial cabin, having a conventional air conditioning system or ventilation. Usage in the cabins LTRD is effective to reduce the excess heat content of the human operator. The use of liquid as the coolant provides maximum heat transfer from the surface of the human body (the heat transfer coefficient from the human body to the liquid is greater than air, the energy costs for the circulation of liquid is smaller than for air circulation). The improvement of working conditions through the use of a LTRD involves increasing production per unit of working time without excessive tension of functional systems of the human body. Is the time savings due to the reduction of losses due to temporary disability. Creates an increase in the volume of manufactured goods by reducing non-productive expenditure of energy to overcome the adverse conditions of a human operator.

It was established experimentally the relationship between comfort, climate and heat sensation and heat content of the body of the human operator. Becomes possible to make the best assessment of efficiency of functioning of the device, correcting the thermal state of the human operator.

Developed experimental design sample the LTRD to ensure a comfortable thermal state of the human operator in the cockpit MM. The experimentally determined value of the power density of the heat flow required for optimum calculations, both constructive and regime parameters of the LTRD.

References

- [1] K.V. Glemba, Yu.I. Averyanov, V.N. Kozhanov, An integral criterion for the evaluation of comfort conditions of microclimate in the cabins of mobile agricultural machines, Tractors and agricultural machinery. 4 (2005) 36–38.
- [2] K.V. Glemba, Yu.G. Gorshkov, Yu.I. Averyanov, I.N. Starunova, Indicators of working conditions and fatigue of operators of mobile agricultural machines, The journal Science, Kostanay. 2 (2003) 11–17.
- [3] K.V. Glemba, Improving working conditions and reducing injuries operators of mobile wheel cars of agricultural purpose: Cand. Sci. (Eng.) Dissertation, Chelyabinsk, 2004.
- [4] K.V. Glemba, Improving working conditions and reducing injuries operators of mobile wheel cars of agricultural purpose: abstract Cand. Sci. (Eng.) Dissertation, Orel, 2004.
- [5] Yu.I. Averyanov, The improvement of working conditions of operators of mobile agricultural machinery the application of local heat regulating device: Cand. Sci. (Eng.) Dissertation, Chelyabinsk, 2000.

- [6] Yu.I. Averyanov, Improving the safety of the process of harvesting grain crops on the basis of improving the system operator – machine – environment: Dr. Sci. (Eng.) Dissertation, Chelyabinsk, 2006.
- [7] K.V. Glemba, Yu.G. Gorshkov, Yu.I. Averyanov, I.N. Starunova, S.Yu. Popova, The hazards of mobile technological processes, *Mechanization and electrification of agriculture*. 7 (2003) 4–6.
- [8] K.V. Glemba, Yu.G. Gorshkov, Yu.I. Averyanov, O.F. Skornyakov, I.N. Starunova, Evaluation of potential process safety subsystems, *Tractors and agricultural machinery*. 12 (2003) 40–41.
- [9] K.V. Glemba, O.N. Larin, Yu.I. Averyanov, Aspects of increasing the security subsystem operator in transport on wheels, *Agro-industrial complex of Russia*. 70 (2014) 34–42.
- [10] K.V. Glemba, Yu.I. Averyanov, The results of the research of functional parameters of training of operators of mobile machines, *Proceedings of the conference Chelyabinsk state Agroengineering Academy, Chelyabinsk*. (2015) 134–140.
- [11] K.V. Glemba, O.N. Larin, Review of methods of determining the reliability of the operator in dynamic ergatic systems, *Transport in the Urals*. 32(1) (2012) 17–22.
- [12] K.V. Glemba, Yu.I. Averyanov, V.K. Glemba, Methods of evaluation of information overload for the operator in the machine control, *Bulletin Chelyabinsk state Agroengineering Academy, Chelyabinsk*. 56 (2010) 5–10.
- [13] K.V. Glemba, Yu.I. Averyanov, Identifying and improving problematic relationships of structural elements of the system safety movement of mobile machines, *Bulletin Chelyabinsk state Agroengineering Academy, Chelyabinsk*. 66 (2013) 25–34.
- [14] K.V. Glemba, Yu.G. Gorshkov, Yu.I. Averyanov, O.F. Skornyakov, N.V. Svetlakova, The indicator of the level of skill of the operator of a mobile agricultural machine, *Tractors and agricultural machinery*. 3 (2005) 32–35.
- [15] K.V. Glemba, Impact on road safety of pertinence of the information field, *Agro-industrial complex of Russia*. 68 (2014) 7–13.
- [16] K.V. Glemba, S.V. Gorbachev, Impact on traffic safety level information flow formalization in ergatic systems, *Bulletin of Orenburg state University, Orenburg*. 129(10) (2011) 88–93.
- [17] K.V. Glemba, O.N. Larin, V.I. Mayorov, The application of a systematic approach to improve road safety, *Monthly scientific journal Transport: science, technology, management, Moscow*. 11 (2013) 52–55.
- [18] K.V. Glemba, The influence of perceptual processes, spatial perception of road users on safety, *Bulletin Chelyabinsk state Agroengineering Academy, Chelyabinsk*. 62 (2012) 26–31.
- [19] K.V. Glemba, Yu.G. Gorshkov, Yu.I. Averyanov, I.N. Starunova, E.V. Shamanova, Security maintenance machines, *Mechanization and electrification of agriculture*. 11 (2003) 21–22.
- [20] K.V. Glemba, Yu.G. Gorshkov, Yu.I. Averyanov, I.N. Starunova, S.Yu. Popova, Automatic control of serviceability of brake system, *Tractors and agricultural machinery*. 5 (2003) 20–22.
- [21] K.V. Glemba, O.N. Larin, Influence of traffic organization on the process of perception of the driver information, *Monthly scientific journal Transport: science, technology, management, Moscow*. 11 (2012) 55–57.
- [22] K.V. Glemba, Yu.G. Gorshkov, Yu.I. Averyanov, E.Yu. Kulpin, I.N. Starunova, Rationale a safe speed wheeled vehicles, *Mechanization and electrification of agriculture*. 12 (2002) 27–30.
- [23] V.M. Mishurin, A.N. Romanov, The reliability and safety of the driver, *Transport Publishing House, Moscow*, 1990.
- [24] E.V. Gavrilov, *Ergonomics in road transport*, Publishing House Technika, Kiev, 1976.
- [25] A.S. Aruin, V.M. Zatsiorskiy, *Ergonomic biomechanics*, Moscow, 1988.



International Conference on Industrial Engineering

The evaluation of the stress-strain state for the cylinder heads of high-powered diesel engines using the multiphysics ANSYS technology

Romanov V.A.*, Lazarev E.A., Khozeniuk N.A.

South Ural State University, 76, Lenin Avenue, Chelyabinsk, 454080, Russian Federation

Abstract

The researchers have built a calculation model for comparative assessments of the heat balance, heat and stress-strain state for the head and cylinder liner of forced diesel engine, which model takes into account the redistribution of the quenching fluid between the cylinder head and crankcase. Computational experiments have been performed. The trade-off approach to the design of a diesel engine cooling system has been demonstrated to find out that improved cooling of the cylinder head is accompanied by deteriorating thermal state of the crankcase and the cylinder liner.

© 2015 The Authors. Published by Elsevier Ltd. This is an open access article under the CC BY-NC-ND license (<http://creativecommons.org/licenses/by-nc-nd/4.0/>).

Peer-review under responsibility of the organizing committee of the International Conference on Industrial Engineering (ICIE-2015)

Keywords: diesel engine, cylinder head; crankcase; cylinder liner; cooling system; redistribution of coolant; FEA; thermal stress

1. Introduction

Increasing load to cylinder head (thermal, mechanical, hydraulic and gas-dynamic) on the forcing diesel engine can lead to warping fire surface, cracks in intervalvular crosspieces, in the sealing valve timing, disclosure gas joint and other factors that are indicative of the loss of its efficiency. Difficulties of estimate of the thermal state and the stress-strain state of cylinder head at the design stage are closely connected with the need of modeling interdependent non-steady thermodynamic movement processes of working gas, quenching fluid, heat exchange

* Corresponding author. Tel.: +7-912-899-0926.
E-mail address: r.v@live.ru

with the environment, the contact interactions with the other elements diesel engine. Existing methods solve the problem of modeling the thermal state and the stress-strain state cylinder heads with different fullness and need to be improved.

2. Review

Modern approaches to the computational estimate of temperature fields, the strain and stress of the cylinder head is usually limited to a non-steady three-dimensional formulation of heat conduction problems and deformable solid mechanics based on numerical finite element method (FEM), embodied either by researchers independently or into one of the commercial software packages. The accuracy and adequacy of such a calculation model directly depends on representation and reliability of the boundary conditions (BC).

The boundary conditions of the heat conduction problem on the surfaces of the firing bottom, the inner surface of inlet and outlet ports include the time-averaged heat transfer coefficient α_{rez} and the resulting temperature of the gas $T_{g_{rez}}$ defined on the recommendations of [1]. The coefficient of heat transfer from the working gas is determined using [2] and its distribution across the hot surface of the cylinder head is determined using Z. Slivinski equation. Boundary conditions in the contact zone of valve seats are estimated taking into account the recommendations of [3]. Heat transfer boundary conditions in the cavities of the liquid cooling of the cylinder head are defined as the average time for the heat transfer coefficient and the average $\alpha_{L_{rez}}$ resulting coolant temperature $T_{L_{rez}}$ [4].

The boundary conditions of the problem of elasticity [5, 6] by the bottom surface of the combustion maximum pressure P_{max} include gas in the cylinder during combustion. The gas pressure on the inner walls of the inlet and outlet channels in the head, respectively, is determined taking into account the parameters of charge air and exhaust gases. The pressure of the quenching fluid on the inner surface of the cavities is estimated from the water pump parameters. Loads of tightening nuts power pins are applied in the form of distributed force to the shim contact area with the surface of the cylinder head.

There are also works based on the modeling of unsteady transfer processes of momentum, energy, mass, density and turbulent combustion in the cylinder of the engine [18, 19]. The simulation results are the values of velocity and temperature at all points of the combustion chamber and the local heat fluxes into the walls of the chamber, in such way is reached a clarification of the boundary conditions of the local heat transfer and heat transfer coefficients determination in determining the thermal state of the piston. However, these studies have not analyzed heat-stressed state of the cylinder head.

Reliability of calculated results increased when comparing the results of numerical simulation of the temperature state of the cylinder head with the results of thermometry and refinement of boundary conditions for solving test problems [7, 8]. Using this approach is useful when checking the particular design of the cylinder head. However, the use of such approaches in the design and the search for the most effective design solutions is not always possible and economically feasible.

3. Problem definition

The purpose of work is to construct a computational model of the cylinder head and crankcase for comparative assessments of the thermal state and the stress-strain state with relatively small changes in the object of research and is focused on support of the design process of new technology and reducing time to market.

A distinctive feature of the proposed calculation model is the quantitative estimation for parameters of heat exchange of the cylinder head by the solution of connected problem of motion of the gas flows and the flows of quenching fluid. After determination of the three-dimensional temperature field of the cylinder head and the cylinder crankcase of a diesel engine, the import of these results to the analysis of strain state is performed.

Similar staging task used in [9, 10, 15, 16, 17]. The authors of [9] used the method of numerical simulation of fluid flow and heat transfer only in cavities cooling of the cylinder head of the forced diesel engines. In [10] is suggested the technique of mathematical modeling of the agreed boundary conditions for the calculation of temperature fields, field strains and stresses only the elements of the cylinder-piston (cylinder head, valves) diesel. In [15, 16] focuses on the state of thermal stresses crankcase of diesel and its impact on the performance of main bearings. The authors of [17] calculated the thermal state of the cylinder head and engine valves and left unattended

the questions of the stress-strain state.

4. Model

A geometric model is represented by single-cylinder fragment (Fig. 1a) of six-cylinder V-type diesel dimension 15/16. As the main causes of stress in the component parts of the head housing unequal distribution of the volume of the head casing independent of the time component of the temperature (averaged over the cycle temperature) and the quasi-static force application of gas pressure in the cylinders are considered. Calculation model stress-strain state of head crankcase diesel engine considered in this paper focused on the selection of a preferred embodiment from the numbers involved compared to the limited number of distinctions. An analysis of the strengths and weaknesses of embodiment of the object of research is done by comparing the solutions of the stationary heat and power quasi-static problems.

Finite element method implemented in the application package Ansys v16.2 used for the settlement prediction of temperature distribution, thermal and mechanical stresses in the cylinder head. Numerical simulations were performed on workstation with six CPU and 64 GB of RAM.

Used interdisciplinary technology FSI (One-Way Fluid-Structure Interaction analysis), in which the actual constructional calculation of solid mechanics (Structural Analysis) precedes the solution to the problem of fluid dynamics CFD (Computational Fluid Dynamics). At the stage of solving CFD problems in geometric model of the object of the study was divided into four domains (Fig. 1a). There are two solid state domain (one of which includes a piston and connecting rod assembly, a fragment of the crankcase, the sleeve, the second - the cylinder head body fragments timing, intake and exhaust manifolds). There is gas domain representing the spatial region occupied by working gases while moving from the inlet manifold of the cylinder head into the cylinder and into the exhaust manifold (only used in CFD model). There is domain of quenching fluid communicating space formed of the regions occupied by the cooling fluid in the cylinder head, in the fragments of the crankcase, the outlet and inlet collectors (used only in the CFD model).

An algorithm for solving FSI tasks implemented in the package Ansys for the heat transfer problems and to determine the parameters of liquid and gas flow, involves the use of a non-deformable Eulerian grid finite element (FE) with the subsequent transfer of temperature fields in the Lagrangian deformable mesh to calculate the stress-strain state. Parameters FE models are shown in Table 1. Areas streaming domains in contact with the solid domains (parietal area) breaking-were five layers of prismatic elements, other areas broke tetrahedral with a typical size of 1 mm.

Power source of heat is determined by assessing the total irreversible heat loss of diesel. Flow of cooling fluid through a cylinder head performance was assessed by the power of a circulation pump. Airflow is determined by calculation of diesel engine working cycle.

For cylinder head domain used the properties of aluminum alloy AMX-605, and for the crankcase - ductile iron. For solid domains accepted model of continuous, homogeneous, isotropic material. When select a characteristic size of the finite element mesh for the structural calculation takes into account the heterogeneity of the structure-material-temperature case [13, 14]. For liquid-domain model used one- and two-phase medium (Homogeneous Binary Mixture), corresponding to the thermodynamic properties of water and steam. [20]

5. Results

Determination TNDS performed for two levels of heat dissipation from the diesel engine (see Table 2), and two variants of the cooling jacket (CJ). Differences between cooling jacket variants were reduced to open or closed the channels connecting the cavity cooling the head and intake manifold (Fig. 1b).

Heat flow Q in the domains of computational model (as a fraction of total heat loss) (Fig. 1c) for the examined cases are shown in Fig. 2a. Averaging of temperature for combined surface formed by the criterion of performance of similar thermal features reveals pronounced dependence of heating different parts of the model from the formation of the coolant flow the cooling jacket (Fig. 2b).

The differences in the formation of flow of coolant to CJ options under intense heat sink shown in Fig. 2c (the line intensity is proportional to the current flow rate of fluid through the corresponding spatial region of cooling jacket).

Table 1. FEA model data

Quantity	Computational Fluid Dynamics	Structural Analysis
Elements	8,78 mio	6,2 mio
Nodes	> 2 mio	> 9 mio

Table 2. Calculation options

Heat removal from the engine	Coolant flow, kg/s	Temperature, C °		
		coolant inlet	outside the crankcase	inside the crankcase
Intense	2	80	20	100
Hindered	0,2	95	120	220

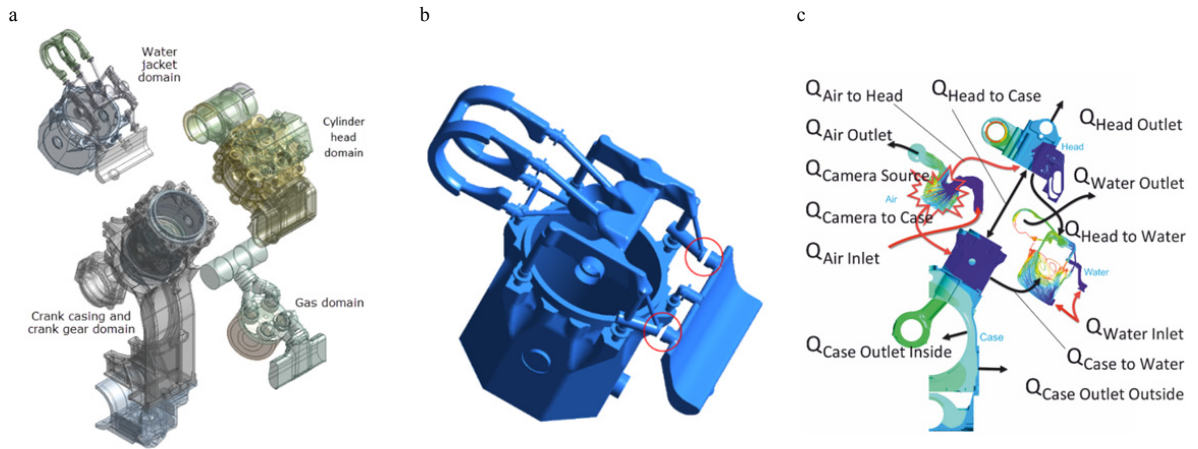


Fig. 1. (a) Components of the model, (b) Location connecting channels of cooling jacket, (c) Designation of heat flows between the components of the calculation model.

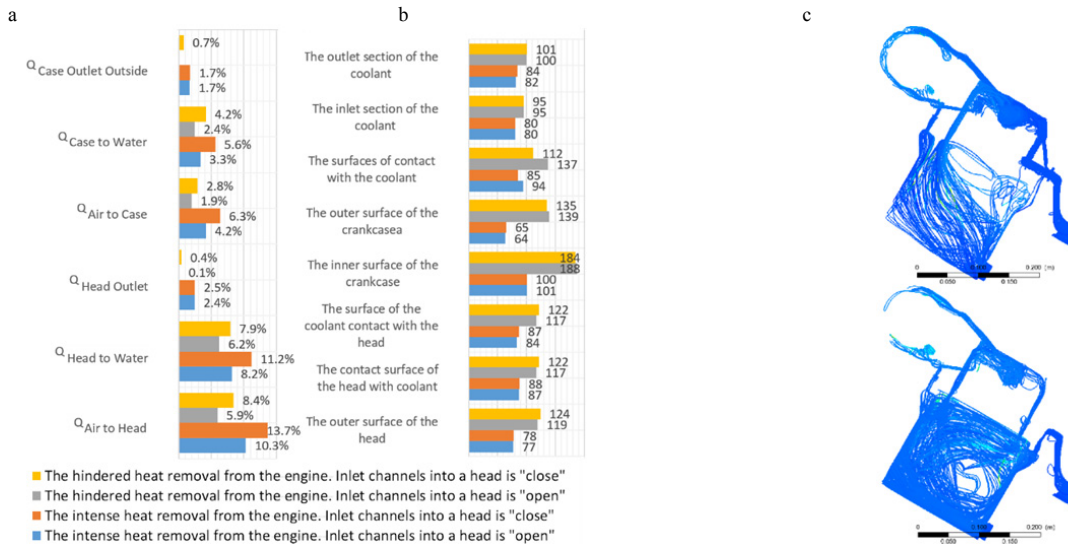


Fig. 2. (a) Thermal balance in the domains of the cylinder head and crankcase for different modes, (b) The average temperature (in C °) major surfaces CFD model, (c) Options for flow of coolant in the cooling jacket: at the top - the inlet manifold channels in the head is open;

Opening of the connecting channels between the intake manifold and the cylinder head intensify quenching fluid motion through a head. In the crankcase from the side of intake manifold is formed stagnation zone. There is boiling in the crankcase part of cooling jacket in case of the hindered heat removal from the engine and "open" channel between the intake manifold and the cylinder head (Fig. 3). Option "closed" channel in the head allows to intensify the movement of the coolant in the crankcase and to avoid virtually boiling coolant (Table 3).

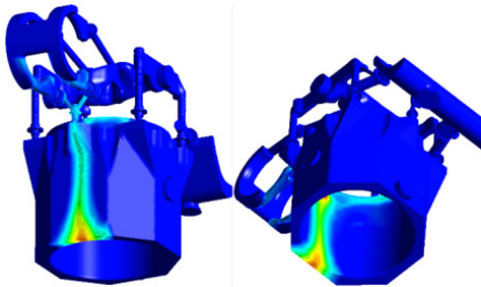


Fig. 3 Location zone boiling of coolant in the crankcase cooling jacket.

Table 3. Part of the boiling liquid in the volume of the cooling jacket

Heat removal from the engine	Open channels between the intake manifold and the cylinder head	Close channels between the intake manifold and the cylinder head
Intense	0	0
Hindered	0,134%	0,00102%

In Fig. 5b can be seen to what extent the movement of heat (the change of the inner surface of the cylindrical shape) of the sleeve connected with peculiarities of the cooling system. In the case of boiling coolant in the cooling jacket of crankcase the difference mutual displacements diametrically opposite points by the height of the cylinder liner is increased by 4.5 times.

a

b

c

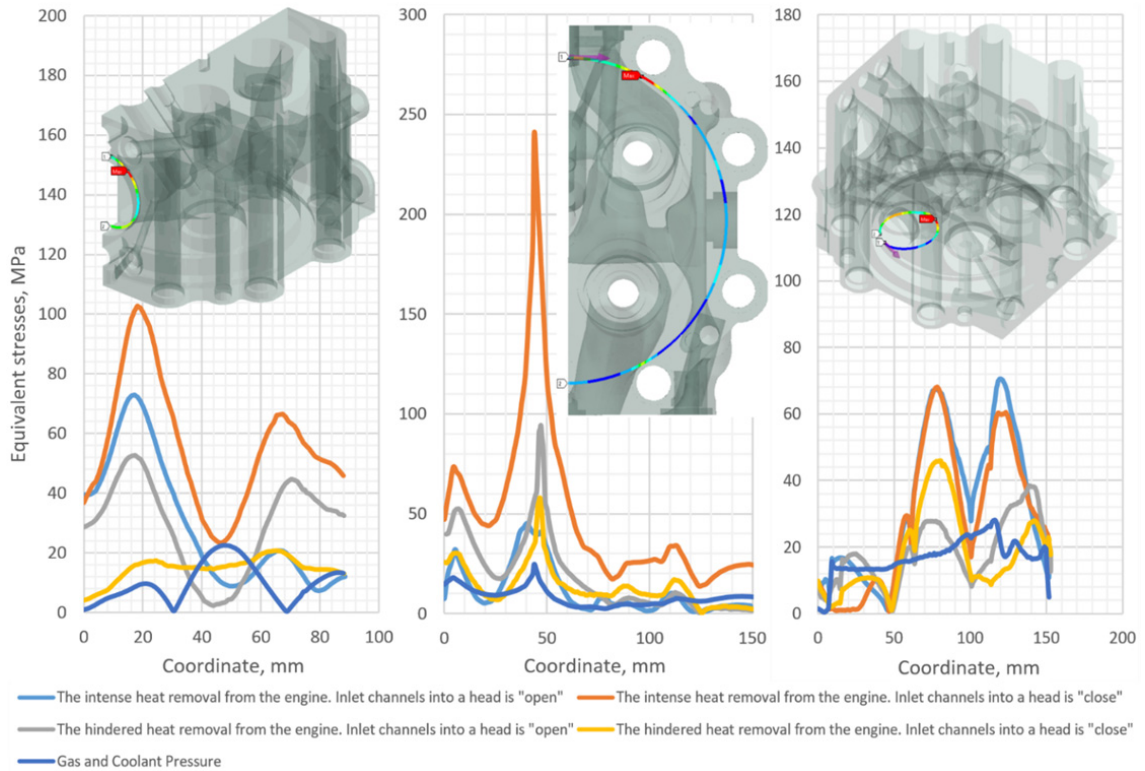


Fig. 4. The equivalent stresses in the elements of the cylinder head of a diesel engine: a) the edge of the window in the exhaust manifold; b) the edge of the cavity combustion chamber; c) the edge of the mounting surface of the exhaust valve seat.

The results of the calculations show the greatest stresses in cylinder head occur in the areas of the windows in the exhaust manifold, the rib groove in the head flange of the sleeve and the seat of the exhaust valve (Fig. 4 a, b, c).

Locking connecting channels between the intake manifold and the cylinder head intensifies the motion of the fluid in the crankcase reducing the temperature at the hottest points of the liner of more than 80 C° . The decrease in the flow of coolant through the cylinder head temperature rises is reflected in its local zones 50 C° .

The contribution thermal load to the total stresses for the analyzed areas of the head is the primary (Fig. 4). The maximum thermal stresses occur in the head at a low temperature in the engine compartment, maximum performance water pump and "closed" the input coolant channels in the cylinder head. Interestingly, this mode also corresponds to a maximum heat flow both from the combustor to the head and from the head to the coolant (Fig. 2a), but the average temperature of the outer surface of the head on the mode with the maximum heat stress is substantially (at 40 C°) below than with the hindered heat removal from the engine. But with the hindered heat removal from the engine (as seen from the graphs of Fig. 4), the highest values of thermal stresses in the analyzed fragments of the head are significantly lower: the most loaded by heat stress area of the window into the exhaust manifold - almost 5 times, to the edge of the combustion chamber - in 5.3 times, for the edge of the seat of the exhaust manifold - 1.7 times.

Qualitatively this result was predicted: the thermal stresses is higher than the above temperature gradient. However, the established calculation fact such a significant relationship between the levels of maximum values of thermal stresses in the head on the conditions of the heat sink once again confirms the need for very careful attention to detail design of the cooling system.

The redistribution of the coolant flow to the head at the open front into the head coolant channels allows to significantly reducing thermal stresses in it (Fig. 4a). However, the simultaneous reduction in the flow of coolant through the cooling jacket of the crankcase reduces the efficiency of the cooling sleeve. The result of reduced

cooling sleeve is to increase the danger of boiling coolant in the crankcase of the cooling jacket. One of considered calculation option leads to the boil (Fig. 3).

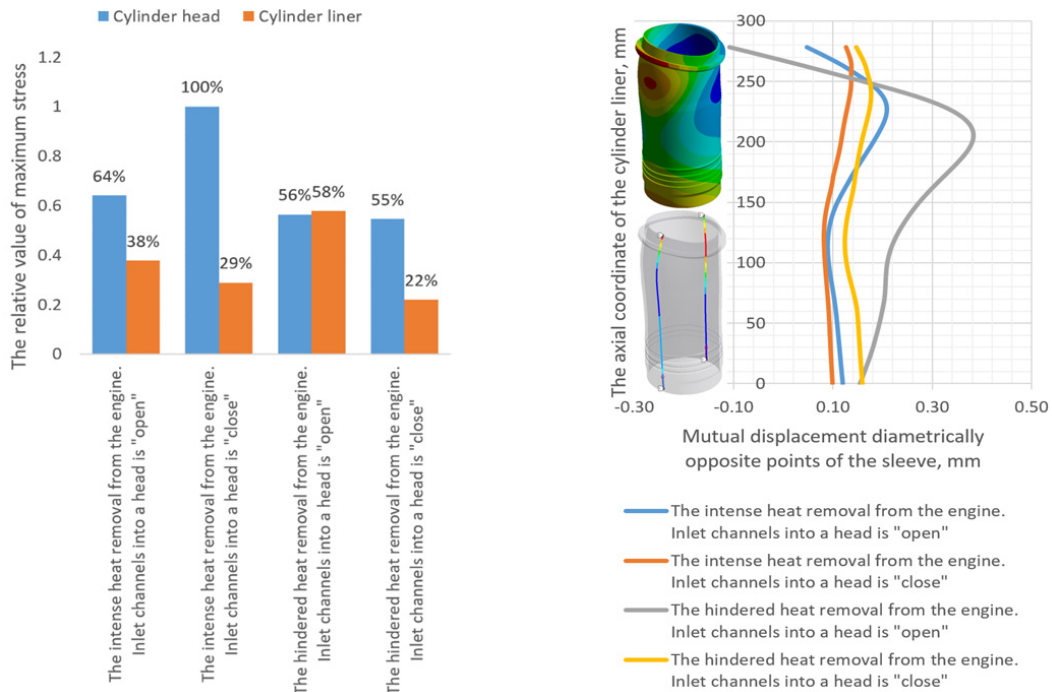


Fig. 5. (a) A comparison of thermal stresses in the cylinder head and cylinder liner, (b) Thermal displacement opposite points of the inner surface of the liner in a plane perpendicular to the axis of the crankshaft.

6. Conclusion

Using FSI technology for the computational analysis of the cooling system of a diesel engine has allowed estimating quantitatively the dependence of the stress state of the cylinder head and crankcase of a diesel engine on the operating conditions of the cooling system of the diesel engine.

It is shown that at the fixed level of power developed by the engine the maximum stresses in the cylinder head may vary up to 5 times depending on the cooling of the engine.

Showed compromise sense of the design of the cooling system of a diesel engine: improving the cooling of the cylinder head is accompanied by a deterioration of the thermal state of the crankcase and the cylinder liner until boiling coolant in the crankcase of the cooling jacket.

Boiling coolant in the cooling cavity crankcase is accompanied by the emergence of pronounced unevenness of the cylinder liner, resulting in take place a significant increasing (up to 4.5 times) of the distortion cylindricality inner surface of the cylinder liner with respect to the case of lack of boiling coolant.

Acknowledgements

This work was supported by a grant of the Ministry of Education and Science of the Russian Federation for applied research, code 2014-14-579-0109. The unique identifier for Applied Scientific Research (project) is RFMEFI57714X0102. Agreement No.14.577.21.0102.

References

- [1] A.K. Kostin, V.V. Larionov, L.I. Mikhaylov, Thermal stress of internal combustion engine, Leningrad, 1978.
- [2] G. Woschni, F. Anisitis, Eine Methode zur Vorausberechnung der Änderung des Brennverlaufsmittelschnellaufender Dieselmotoren bei geänderten Betriebsbedingungen, MTZ, 1973.
- [3] G.B. Rozenblit, Heat transfer process of diesel engines, 1977.
- [4] Yu.V. Galyshev, A.Yu. Shabanov, A.B. Zaitsev, M.N. Nemchikova, The boundary conditions of heat transfer in the working cavity of the cylinder head of the four-stroke internal combustion engine, Nauchno-tekhnicheskie vedomosti SPbGPU. 2(195) (2014) 58–64.
- [5] A.Yu. Shabanov, A.B. Zaitsev, M.A. Mashkur, New Method to Calculate Boundary Conditions for the Analysis of Thermal Load on Engine Cylinder Head, Dvigatlestroyeniye. 1 (2005) 5–9.
- [6] A.N. Avramenko, Mathematical model of the cylinder head thermal state. Internal combustion engine, Kharkiv, NTU KhPI, 2 (2006) 18–28.
- [7] A.F. Shekhovtsev, A.V. Trinev, A.N. Avramenko, Development of the finite element model of the thermal and state-strain states for cylinder head of the high speed Engine. Internal combustion engine, Kharkiv: NTU KhPI. 1 (2007) 20–30.
- [8] A.N. Gots, M.P. Prygunov, Modelling of a heat-stressed condition the head of the cylinder of a tractor diesel engine of air cooling. Tractors and agricultural cars. 10 (2014) 19–23.
- [9] O.V. Abizov, Yu.V. Galyshev, A.Yu. Shabanov, Mathematical Analysis of Hydrodynamic and Heat Exchange Processes in Diesel Engine Cylinder Head. Dvigatlestroyeniye. 2 (2014) 8–10.
- [10] N.D. Chainov, S.Yu. Roussinkovsky, Analysis of Stationary Thermal Fields in Cylinder Heads and Valves. Dvigatlestroyeniye. 2 (2014) 3–7.
- [11] N.D. Chainov, L.L. Myagkov, N.S. Malastovsky, Numerical modeling of the movement of liquid in a cavity of cooling of a cover of the cylinder of the sredneoborotny diesel. Gruzovik. 5 (2015) 4–8.
- [12] D.K. Grishin, P.R. Valyekho Maldonado, N.D. Chaynov, V.A. Lodnya, Mathematical modeling of heat state of head for the high-speed small-sized diesel with direct injection. Tractors and agricultural cars. 8 (2010) 28–30.
- [13] Romanov, V.A., 2011. The calculation of thermal stress state for the crankcase of the diesel engine of the industrial tractor. Science of SUSU: preceeding, pp.61–65.
- [14] V.A. Romanov, V.S. Murzin, S.B. Sapozhnikov, N.A. Khozeniuk, The loading calculation of the crankcase of the diesel engine of the industrial tractor, MGTU International conference DVIGATEL-2010. (2010) 71–75.
- [15] V.A. Romanov, N.A. Khozenjuk, Assessment of operability of main bearings of the internal combustion engine taking into account thermal deformations of case-shaped parts. Friction and greasing in machines and mechanisms. 3 (2013) 023–026.
- [16] Y. Rozhdestvensky, N. Khozeniuk, A. Mylnikov, I. Levanov, V. Romanov, Modeling of the main bearings of a multi-supporting crankshaft of the internal combustion engine, 5th world tribology congress, WTC 2013. (2013) 1825–1828.
- [17] D.O. Onishchenko, S.A. Pankratov, Simulation of thermal state of the diesel cylinder head and valves, Vestnik BMSTU: Machinostroenie. 4 (2013) 94–108.
- [18] R.Z. Kavtaradze, A.A. Zelentsov, D.O. Onishchenko, L.A. Finkelberg, A.N. Kostyuchenkov, Simulation of processes in the "inlet collector-cylinder" system of aviation reciprocating engine with distributed fuel injection, Vestnik BMSTU: Machinostroenie. 4 (2012) 3–15.
- [19] L.A. Finkelberg, Experiment-calculated research of the cylinder-piston and crank- connecting rod systems reliability of aviation reciprocating engine, Dvigatel. 6(96) (2014) 2–7.
- [20] W. Wagner, A. Kruse, The Industrial Standard IAPWS-IF97: Properties of Water and Steam, Springer, Berlin, 1998.



International Conference on Industrial Engineering

Particularities of Dispersed Materials Microcutting

Shmidt I.V.^{a*}, Gorodkova A.E.^a, Degtyareva A.S.^a

^aSouth Ural State University, 76, Lenin Avenue, Chelyabinsk, 454080, Russian Federation

Abstract

This article presents results of research on microcutting mechanics and dispersed structure of metallopolymers. It describes dispersed materials structure and composition. Article includes experimental identification of the particularities of metallopolymers microcutting. It determines where metallopolymers cutting physics mainly differs from physics of cutting conventional steels and alloys. It is demonstrated that under enhancing dispersion of the metallopolymers, plastic cutting is almost absent; in case of grain included into solid metallopolymer inclusion, inclusion particles can stick to this grain resulting in cutting, performed by this inclusion. This document includes results of the inclusions metric parameters calculation and data on average metallopolymer matrix grain size, based on the microscopic study of metallopolymers dispersed structure. The research the authors have performed demonstrates that classical cutting theory is not applicable to metallopolymers; it is necessary to develop new models, taking into account the dispersed structure of these materials.

© 2015 The Authors. Published by Elsevier Ltd. This is an open access article under the CC BY-NC-ND license (<http://creativecommons.org/licenses/by-nc-nd/4.0/>).

Peer-review under responsibility of the organizing committee of the International Conference on Industrial Engineering (ICIE-2015)

Keywords:

1. Introduction

Polymeric composite materials, namely – metallopolymers, are wider and wider used in modern machine building industry. As of now, metallopolymers are mainly used for surface repair of machines parts and structures. Metallopolymers are acting as repairing cover of worn-out surface. Different parts can be subject to repair: shafts, shafts bearing journals, cases bearing journals, covers, gear boxes covers, etc. Analysis of the metallopolymer repair

* Corresponding author. Tel.: +7-351-272-32-94, fax: +7-351-267-92-73.
E-mail address: shmidt174@mail.ru

technics, performed in dedicated repair organizations of the Urals region and Moscow, revealed, that in 75 % of cases, metallopolymeric cover is finally processed by grinding.

As of today, there are quite a lot of works, dedicated to issues, related to mechanical processing, namely by grinding, of metallopolymeric covers [1-5]. However, there are almost no any recommendations on processing modes for such covers, as almost all of present data are extremely empirical, resulting in their narrow applicability. In order to work out such recommendations it is necessary to reveal main mechanisms of the metallopolymer grinding processes - effects of grinding wheel and modes parameters on processed surface microprofile, assuring processing accuracy, assuring processing soundness, etc. All said processes are based on allowance removal mechanics, i.e. metallopolymer cutting.

Metallopolymer are classified as dispersed materials – metal or its carbides particles are randomly (with even distribution) located in polymer matrix. This allows supposing that chip formation mechanics under cutting these materials will differ from metals processing.

As no data on chip formation for metallopolymer cutting studies was found, first stage included qualitative analysis of such new materials cutting mechanics.

2. Experimental research of the fracture

Up-to-date interpretation of the grinding processes from the point of cutting model determines it as multiple stochastic micro cutting by abrasive grains [6]. Experiment on microcutting metallopolymer by a single abrasive grain under cutting speed of 35 m/s was performed in order to study metallopolymer cutting mechanics specifics under grinding conditions.

Qualitative evaluation of the metallopolymer microcutting specifics was performed by comparing microcutting notches for metals and covers from metallopolymer, used for repair works. Leo-Stea' and Chester Super Metal BR metallopolymer were used for tests. Steel 45 (HRC 42...45) was used as reference metal.

Experiments were performed on a special microcutting bench. Formocorund grains were used as cutting material. Cutting was performed in following modes: abrasive wheel speed $V_k=35$ m/s, sample temperature $T=20^\circ$, cutting depth $t=5$ μ m.

Fig. 1 shows pictures of the reference notches (microcuts) on steel 45 under magnification x12.5, x25, and x82.

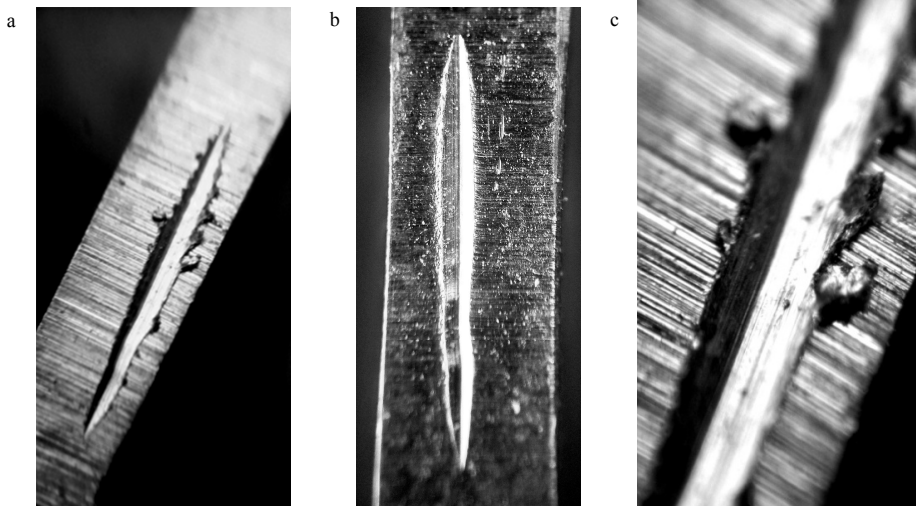


Fig. 1. Pictures of Notches on Steel 45: (a) under magnification x12.5; (b) under magnification x25; (c) under magnification x82

Fig. 2 and 3 show pictures of notches on metallopolymer Leo-Stel and Chester-Molecular Super Metal BR under same magnifications of x12.5, x25, and x82.

Metals cutting process is the process of cut-out layer plastic deformation. Following metal cutting specifics can be observed: plastic deformation of metal at notch edges - crowdings; sharp form of the notch (Fig. 1).

Metal filler particles size for Chester Super Metal BR metallopolymer is about 5 μm . This material can be considered as low dispersive against the deformation area. As it is demonstrated, under low dispersity, metallopolymers also demonstrate small crowdings at notch edges (Fig. 2).

Under increasing metallopolymers dispersity plastic cutting is almost absent (Fig. 3). Leo-Stal' metallopolymer has metal inclusions of about 200 μm , so its dispersity against cutting area is essential. In case of grain included into solid metallopolymer inclusion, inclusion particles can stick to this grain resulting in cutting, performed by this inclusion.

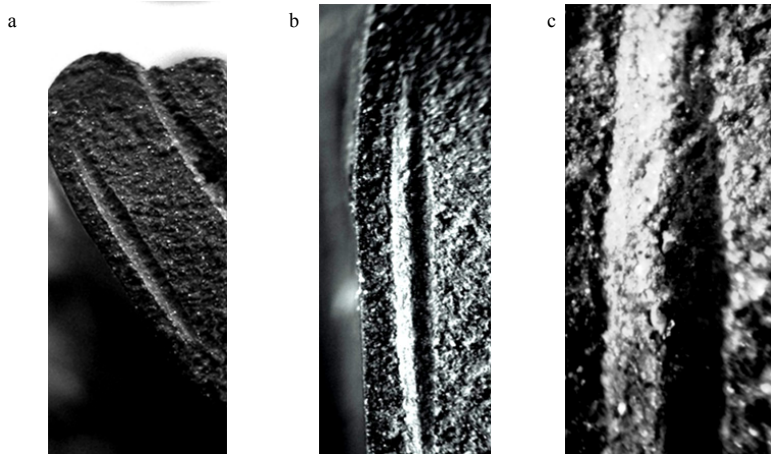


Fig. 2. (a) Pictures of Notches on Metallopolymer CHESTER Super Metal BR under magnification x12.5; (b) Pictures of Notches on Metallopolymer CHESTER Super Metal BR under magnification x25; (c) Pictures of Notches on Metallopolymer CHESTER Super Metal BR under magnification x82

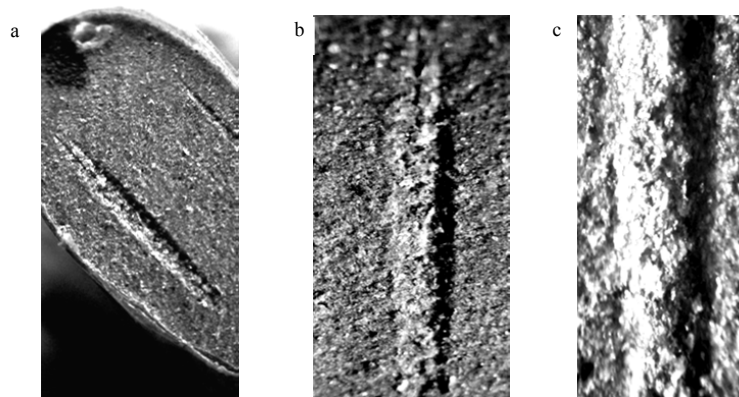


Fig. 3. (a) pictures of Notches on Metallopolymer Leo-Stal' under magnification x12.5; (b) pictures of Notches on Metallopolymer Leo-Stal' under magnification x25; (c) pictures of Notches on Metallopolymer Leo-Stal' under magnification x82

3. Study of the dispersive structure

Composites surface structure was studied on the electron microscope IM7200 MEIJI TECHNO. Following processing of the digital pictures was performed by the Thixomet *PRO* software, being analyzer of the pictures dedicated for solving tasks on quantitative metallography of steels and alloys, as well, as of other materials.

Problem of the terminal objects, located on the field of vision edge, is one of the unsolved tasks of the conventional quantitative metallography. As part of such objects area is located out of the field of vision, seen through oculars or camera, it is impossible to evaluate metric parameters of such objects. Excluding terminal objects out of analysis leads to essential problems of results repeatability from one field to another. Another problem of the conventional metallography is impossibility to observe large area in the field of vision under high resolution. Thixomet *PRO* solves both of these tasks by creating algorithm of splicing adjustment fields of vision. This algorithm allows forming a panorama of several dozens or hundreds of fields of vision and resolution of several dozen megapixels. Specific area of the terminal objects decreases a hundred times.

Software module Titan Alloys was used for calculating filler particles metric parameters. This module was worked out for evaluating two-phase titanium alloys but allows analyzing other two-phase alloys.

Discriminating ranges are used for recognition of different structure objects, differing in brightness or color. Range processing is performed in the color histograms window.

The simplest and most effective way of finding discriminating range, indicative for this type of the structure objects (nonmetallic inclusions, oxides, second phase, etc.) is implemented in automated mode. Thixomet *PRO* finds borders of the indicated object, as well as of all other objects, which color falls into found range. In case of inexact identification results it is possible to correct them by changing discriminating threshold.

Fig. 4 includes digital images of the studied metallopolymer surfaces, received on the electron microscope.

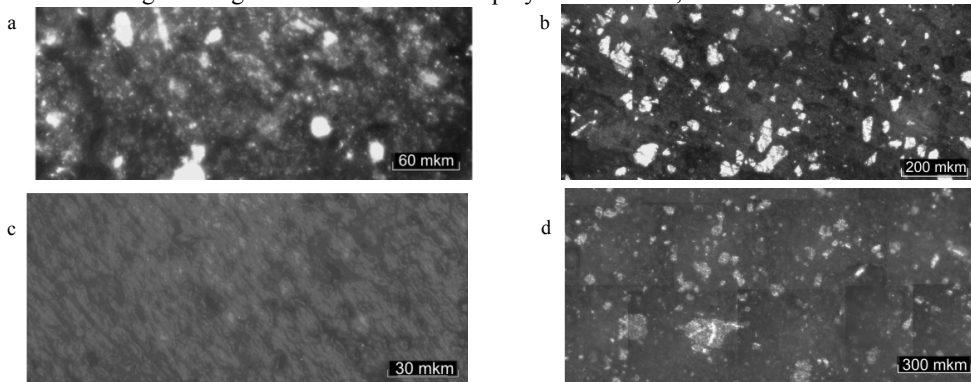


Fig. 4. (a) digital pictures of the metallopolymer surface Belzona 1321; (b) digital pictures of the metallopolymer surface Devcon Ceramic L; (c) digital pictures of the metallopolymer surface Diamant Ceramic FL; (d) digital pictures of the metallopolymer surface Leo-Ceramic

Metric parameters of inclusions calculation results are indicated in Table 1. For display purposes Fig. 5 shows diagram of grains numbers in the frames of the effective range, indicating mode value. Significance threshold is set on 85 % in order to exclude the smallest grains, having low effect on mechanical processing.

Table 1. Inclusions metric parameters calculation results.

Parameter	Belzona 1321	Devcon Ceramic L	Diamant Ceramic FL	Leo-Ceramic
Grains quantity	282	1,149	24	2,064
Grains quantity for 1 mm ²	31,869	4,800	152,012	8,902
Average grain area, [μm ²]	31	208	7	112
Minimum grain area [μm ²]	2.01	1.05	2.02	2.11
Maximum grain area [μm ²]	1,790.38	9,416.36	26.50	9,060
Average grain diameter [μm]	5.60	14.43	2.56	10.60
Grain number [G]	12	9	14	10
Grain number G mode	9	7	12	6
Grain number G and its frequency in the frames of the effective 85% range	6 (20.2%)	4 (15.4%)	12 (33.4%)	3 (11.4%)
	7 (10.3%)	5 (18.4%)	13 (11.1%)	5 (14.1%)

	8 (4.6%)	6 (19.2%)	14 (27.6%)	6 (21.5%)
	9 (23.2%)	7 (19.9%)	15 (19.8%)	7 (19.1%)
	10 (6.7%)	8 (12%)	16 (8.2%)	8 (13.8%)
	11 (10.4%)	9 (7.3%)		9 (8.7%)
	12 (10.5%)	10 (3.6%)		10 (4%)
	13 (5.0%)			
	14 (4.3%)			
	15 (3.6%)			
Coefficient of material volume filling with filler particles [%]	4.6	12.4	0.4	8.3

Mathematical expectation on grains size is indicated in Table 2.

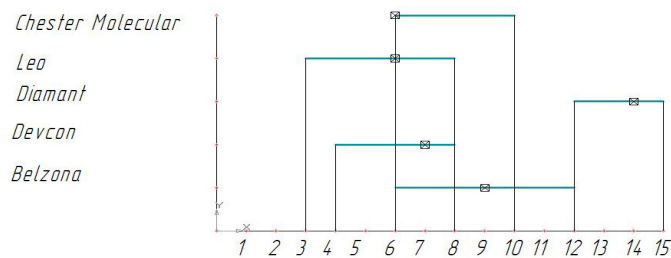


Fig. 5. Diagram of grains numbers distribution within effective range, indicating mode

Table 2. Inclusions metric parameters calculation results.

Metallopolymer type	Filler particles average size
Belzona 1321	9
Devcon Ceramic L	6
Diamant Ceramic FL	13.5
Leo-Ceramic	5.5

4. Conclusions

Microcutting mechanics and dispersed structure of metallopolymers analysis allows to conclude that metallopolymers microcutting mechanism differs from the one, typical for metals. The higher is the metallopolymer dispersity, the significantly is the difference between metal and metallopolymer microcutting mechanism. Therefore, classical cutting theory is not applicable to metallopolymers; it is necessary to work out new models, taking into account dispersed structure of these materials.

5. Acknowledgement

The reported study was supported by RFBR, research project No. 14-08-31064.

References

[1] S.D. El Wakil, 3–Grinding processes for polymer matrix composites, *Machining Technology for Composite Materials*. (2012) 65–74.

- [2] X. Cao , B. Lin , Y. Wang, S. Wang, Influence of diamond wheel grinding process on surface micro-topography and properties of SiO₂/SiO₂ composite, *Applied Surface Science*. 292 (2014) 181–189.
- [3] H.A. Kishawy, 1 Turning processes for metal matrix composites, *Machining Technology for Composite Materials Principles and Practice*. (2012) 3–16.
- [4] J. Sheikh-Ahmad, J.P. Davim, 5 Tool wear in machining processes for composites, *Machining Technology for Composite Materials Principles and Practice*. (2012) 116–153.
- [5] C.R. Dandekar, Y.C. Shin, Modeling of machining of composite materials: A review, *International Journal of Machine Tools and Manufacture*. 57 (2012) 102–121.
- [6] A.A. D'yakonov, Improvement of grinding speeds by assessing the machinability of materials, *Russian Engineering Research*. 32(7-8) (2012) 604–607.



International Conference on Industrial Engineering

Improved design of machine for cold cutting of oil pipes and gas pipelines

Lopatin B.A., Khaziev T.R.*

South Ural State University branch in Zlatoust, 16, Turgenev Str., Zlatoust 456209, Russia

Abstract

The article describes the methods and equipment for cold cutting of large diameter pipes and shows their main advantages. It presents the design of a new machine for cold cutting of pipes, with independent electromechanical drives. Study was carried out of this design, based on the mathematical model of the drive machinery. The research has obtained dependencies for calculating necessary drive capacities. Results of the study were used to design a test prototype of the new machine. This new design allows to speed up the process of pipe-cutting, eliminates overload-caused tool breakage, enables a remote control of the machine, and makes the operator's work safer.

© 2015 The Authors. Published by Elsevier Ltd. This is an open access article under the CC BY-NC-ND license (<http://creativecommons.org/licenses/by-nc-nd/4.0/>).

Peer-review under responsibility of the organizing committee of the International Conference on Industrial Engineering (ICIE-2015)

Keywords: cold cutting pipes, unbound drives machine, model of drive, optimum load machine.

1. Introduction

Currently, the oil and gas industry in the repair of the pipeline to remove the defective section used two methods of cutting pipes: using the energy of the explosion - cumulative cutting pipes (Fig. 1), cold method with the use of machines for cutting pipes (Fig. 2) [1].

* Corresponding author. Tel.: +7-904-305-64-70;
E-mail address: 89090692210@mail.ru

When using the cumulative method is difficult to ensure the safety of work in the field when cutting pipes. Damage to the pipes in the explosion, and possible structural changes of the pipe material are undesirable and unpredictable.

In this regard, the greatest application received a cold method. In this case, mechanical cutting is done with a special machine equipped with a cutter or cutters. Currently, the most common are the car, where the cutting tool is used disc Millings [2, 3]. In Russia has used machine for cold cutting of tubes like "Volzhanka 3M". The machine is mounted on the tube and secured with a chain (Fig. 2 not shown) covering the tube. Securing the machine by means of tensioning devices, including tensioners, shock absorbers 1, lever 2 with tensioning sprocket 3 [4, 5].

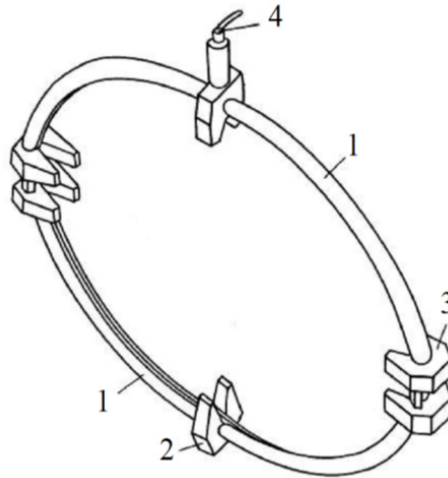


Fig. 1. Cutter cumulative ring:
1 – semicircle with high explosive; 2 – holder; 3 – castle; 4 – electric detonator.

Analysis of the MRI machine designs with mechanical drives showed that all machines have two major drawbacks:

- constant kinematic relationship;
- hand in cut tools (milling).

Permanent kinematic chain in a drive to move the machine, does not allow to adjust the cutting conditions, this leads to premature wear of the tool to increase the cutting forces. In the case of sudden tool breakage often occurs destruction of elements of the machine. Mechanical in feed tool is unsafe, because the operator carries out work in the cutting zone particularly dangerous is the first cut since in the pipeline may remain remnants of flammable oil. In view of the above, the aim is to develop and research the new machine design devoid of these shortcomings. The basis of the new machine design is the idea of exclusion tool breakage under overload and improve operator safety. Operating experience cutting machines such as MRI showed that the main problem in the process of cutting the pipe is insufficient tool life, which is often not enough for one cut pipes 1220 mm in diameter with a wall thickness of 30 mm. To increase tool life and elimination of breakage in construction proposed machine automatic adjustment of the cutting conditions, and in the case of a critical tool wear - light indication, signals the need for a tool change. The basis of the new machine design is the use of three independent electromechanical drives: the drive of rotation of the tool, the drive of movement of the machine and the drive of insertion tool in pipe. Kinematic scheme of the new machine design is shown in Fig. 3. the control system provides a consistent experience work drives machine.

In the analysis of the kinematic scheme machines of a new design have been adopted by the engines of drive tool and move the machine on the tube. To drive the cutting of tool and movement were taken valve engines with the frequency of rotation of the shaft 200 min-1 and a power of 40 watts. The drive of the instrument rotation remained

without significant changes. Output parameters drive insertion of tool and move the machines in specified the technical regulations [6], which contains the value of the tool feed no more than 30 mm / min. The total gear ratio actuator to move the machine on the tube is $i_1 = 1923$. From the experience of operation of machines is well known, that the filing the tool during plunging lower than when the moves along the pipe, and is about 15 mm / min.

An important step is to analyze the loading drive of cutting and drive of movement. The drive movement has an impact of the following factors: the load on the milling cutter, machine weight and friction losses in the elements and components machines. Drive tool of insertion accepts only the load on the milling cutter during insertion.

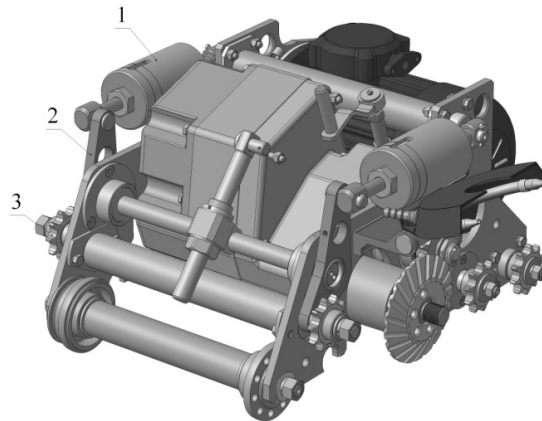


Fig. 2. Machine Cold cutting pipe "Volzhanka 3M".

2. An analysis of loading of drive insertion tool

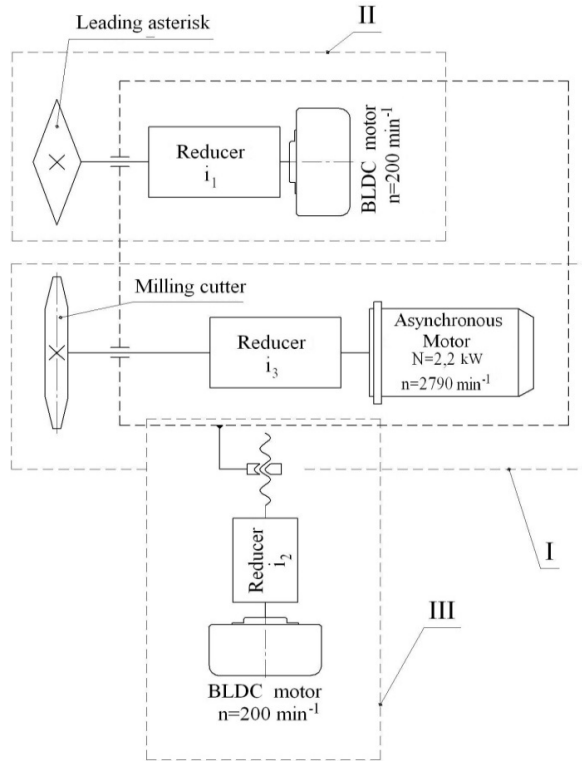


Fig. 3. Kinematic scheme of the new machine

Fig. 4 is a block diagram of a feed drive plunging tool.

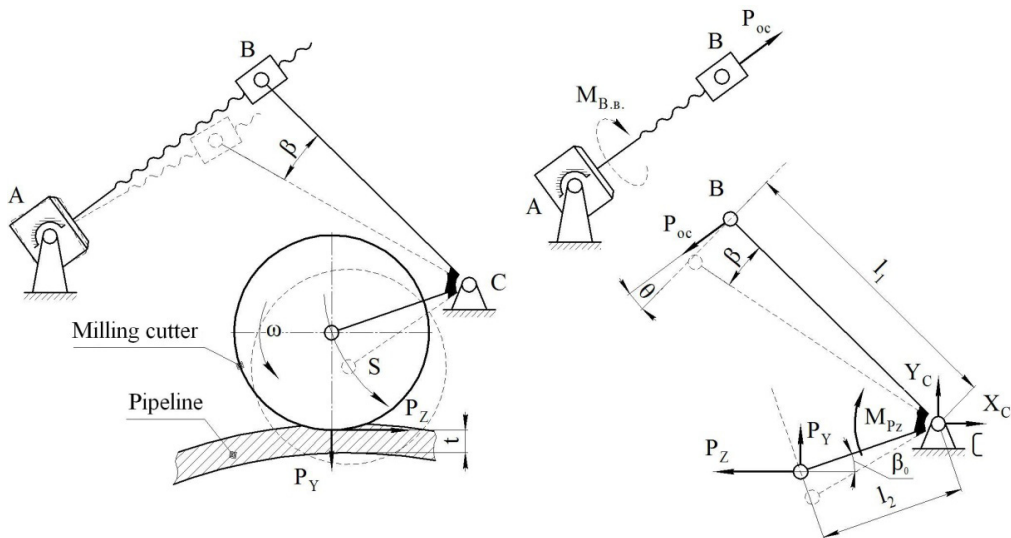


Fig. 4. Scheme drive filing plunging tool

The calculation of the load on the milling cutter with P_z carried out by the known formulas of the theory of

cutting. The main component of cutting force in milling - circumferential force, P_Z [7, 8]:

$$P_Z = \frac{10 C_p t^x S_Z^y B^u Z}{D^q n^w} K_{MP}, \quad (1)$$

where C_p – coefficient in formula of the circumferential force P_Z ; x, y, u, q, w – exponents in formula of the circumferential force P_Z ; K_{MP} – the correction factor for the quality of the processed material.

Radial force P_Y [4]:

$$P_Y = (0,4 \div 0,6)P_Z. \quad (2)$$

To determine the forces at the nodes of the machines of drive at point B is divided in two parts. To determine the power geared motor drive supply incision it was necessary to evaluate the axial force of the screw incision mechanism P_{oc} , which equals:

$$P_{in} = \frac{P_Z(0,5 l_2 \cos\beta - l_2 \cos(90^\circ - \beta) R_{fr})}{l_2 \cos\theta}. \quad (3)$$

Then torque $M_{B,B}$ on the screw plunging is:

$$M_{B,B} = P_{oc} \frac{d}{2} \operatorname{tg}(\delta + \gamma), \quad (4)$$

where d - nominal diameter of the thread, δ – lifting angle of the threads, γ – the resulted friction angle.

Required power motor - reductor is determined by the expression:

$$P_{M,p} = M_{B,B} \cdot \omega_{B,B}, \quad (5)$$

where $\omega_{B,B}$ – the angular velocity of rotation the screw of mechanism plunging.

To investigate the loading drive plunging using a mathematical editor VisSim were built graphics power demand (Fig. 5). The graphs show that when idling (the time interval from 0 to 30), the power consumption is constant, from the beginning of cutting to the end of cutting, the power consumption gradually increases (the time interval from 30 to 95 seconds) after which the actuator is stopped.

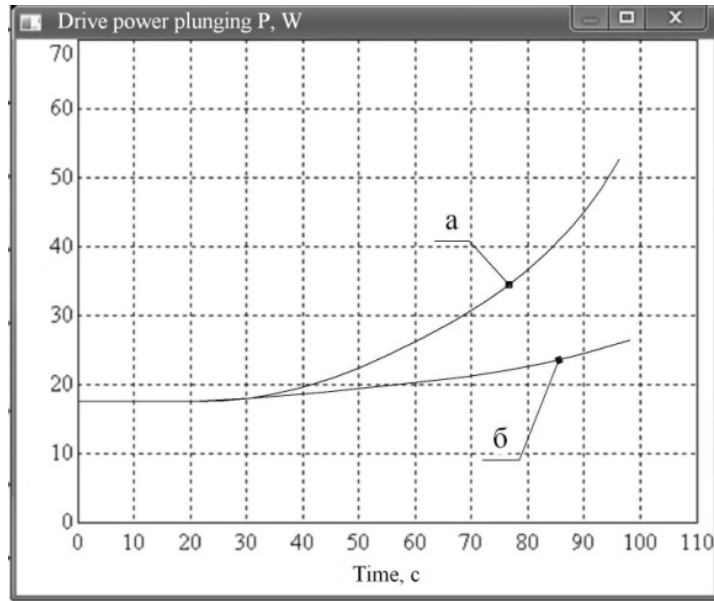


Fig. 5. Graphs drive power plunging tool:
a – when cutting shaped milling cutter $\varnothing 170 \times 32$; b – when cutting the milling cutter $\varnothing 170 \times 6$

Moving the machine by means of the actuator to move the machine along the pipe. The analysis of external factors [5], showed that the drive power is:

$$P_{p,p} = M_{ZV} \cdot \omega. \quad (6)$$

where M_{ZV} – aggregate torque an asterisk drive of movement, ω – the angular velocity of rotation an asterisk drive of movement .

3. Analysis of the load on the drive moving the machine along pipe

Aggregate torque an asterisk drive of movement M_{ZV} is the sum of the torques: M_{TR} – torque from the friction forces in the kinematic pairs of friction units, M_{Pyz} – torque from the cutting force P_{Yz} , M_G – torque from the weight of the machine G. Thus, torque is equal to:

$$M_{ZV} = M_{TR} + M_{Pz} + M_G. \quad (7)$$

Aggregate torque from the friction forces is calculated as the sum of the torque in friction sliding and rolling:

$$M_{TR} = \sum N_i \cdot r_i \cdot f + \sum R_i \cdot k, \quad (8)$$

where N_i – the normal force in a pair of sliding friction, r_i – the radius in a pair of sliding friction, f – coefficient of sliding friction, R_i – strength in support rollers machines, k – coefficient of rolling friction.

As an example of a graph (Fig. 4, a).

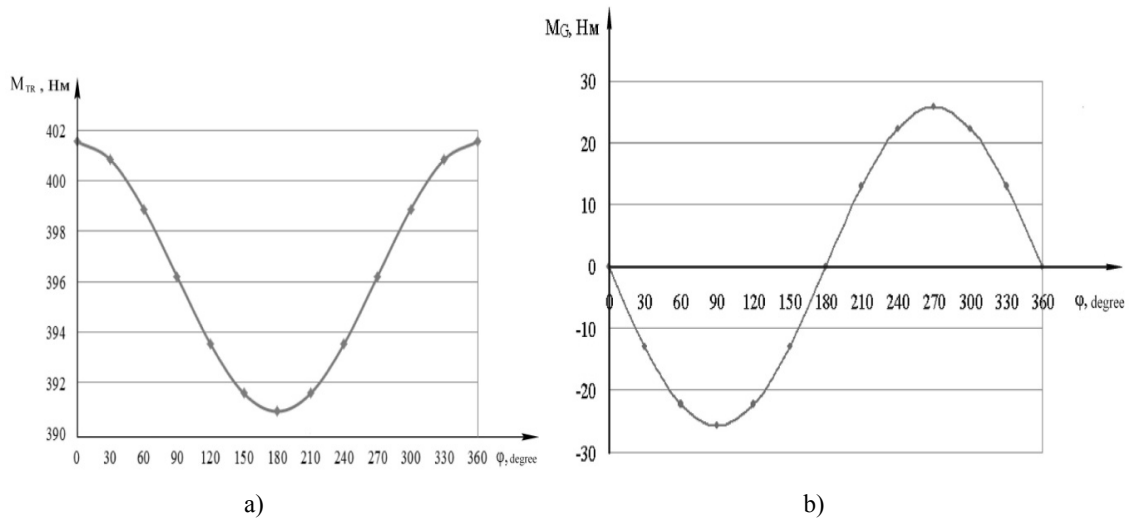


Fig. 6. Graphs of torques:
 a – friction torque $M_{TR}(\varphi)$; b – torque from the weight of the machine $M_G(\varphi)$

The lowest value of the friction torque corresponds to the position machines at the bottom of the pipe, when the weight of the machine unloads the friction bearings (position at an angle 180° in Fig. 6 a).

Torque to overcome the cutting forces is:

$$M_{Pz} = P_z \cdot r_\phi, \tag{9}$$

where P_z – tangential cutting force; r_f – cutter radius.

Significant impact on the movement of machines on the tube has its weight, the torque of the weight of machines changes sign depending on the angular position of the trumpet and is given by [9]:

$$M_G = G \cdot \sin \varphi \cdot r_{B3}, \tag{10}$$

where G – machine weight, r_{B3} – radius of the asterisk, φ – angle of the machines on the tube.

Torque by gravity machines Fig. 6, b. Such character generated due to the fact that the first half of the path weight of the machine facilitates movement machines, and the second half - interferes with.

The set of expressions (6) - (10) to determine the required drive power move.

On the basis of studies conducted in the work, it was manufactured laboratory prototype of a new design machines Fig. 7 [10]. Test sample confirmed the efficiency of the new construction of the machine.

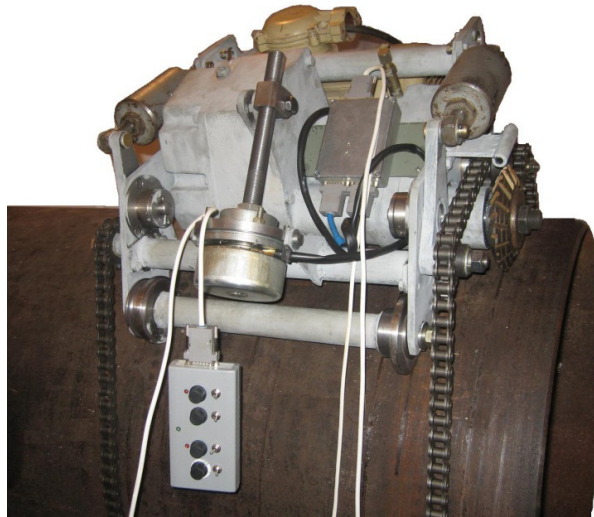


Fig. 7. Laboratory model machines of a new design.

4. Summary

The proposed design allows eliminate the MRI breakage tool and elements of machine during overloads, regulate the speed movement machine and the speed of plunging tool, and increase the safety of the operator.

Results of the study are used in the design of a prototype of the proposed construction of machine

References

- [1] A.G. Gumerov, A.G. Sabirov, M.G. Vekshteyn, R.S. Gumerov, H.A. Azmet, Overhaul of underground pipelines, Core-business centers, Moscow, 1999.
- [2] V.A. Greshnyaev, Cold cutting machine for pipes "Volzhanka - 3M", Journal "Pipeline transportation of oil". 8 (2009) 18–20.
- [3] V.A. Greshnyaev, Machine for cold cutting pipes MR 325 - 1420 "Volzhanka - 2", Supplement to the "crude oil pipeline". 6 (2001) 3–4.
- [4] Limited Liability Company "Trade - Industrial Company", RF Patent 2004106440. (2005).
- [5] B.A. Lopatin, D.B. Lopatin, E. Polouektov, T.R. Khaziev, RF Patent 2010104653/22. (2010).
- [6] RD 153-39.4-130-2002. Regulation on the tenderloin and the sidebar coil fittings, plugs, valves and control valves, and connecting sections of trunk pipelines, Oil & Gas, Moscow, 2002.
- [7] A.G. Kosilova, R.K. Meshcheryakov, Manual Machinist technologist, Engineering, Moscow, 1985.
- [8] G.I. Granovsky, V.G. Granovsky, Metal cutting, Higher School, Moscow, 1985.
- [9] T.R. Khaziev, D.G. Abuzyarov, Assessment of driving power movement cutting machine during the cutting of large diameter pipes, Science SUSU. Articles 63 conference. Section of Technical Sciences. 2 (2011) 322–326.
- [10] B.A. Lopatin, D.B. Lopatin, E. Polouektov, T.R. Khaziev, RF Patent 2012155841/02. (2013).

International Conference on Industrial Engineering

Adaptive control system of an electromagnetic actuator for the quickly moving flap of an air-impulse-charging internal combustion engine without using position, velocity, or acceleration sensors

Pavlenko A.V., Gummel A.A.* , Bolshenko I.A.

Budennovskaya st. 149/36, app. 20, Novocherkassk, Rostov region, 346411, Russia

Abstract

An adaptive control algorithm of a fast electromagnetic actuator has been developed without using position, velocity, or acceleration sensors. The algorithm is based on the fluctuation rate of the current in the electromagnet coil, which is measured during anchor movement. The proposed method and control algorithm compensate for external mechanical factors and are based on the interconnection of electric processes in the electromagnetic actuator coil, with mechanical processes relating to the movement of the movable element of the magnetic system. A structural diagram of a hardware device and an algorithm that implement the proposed control method are presented for a resonance type electromagnetic actuator, where there is a current change in the coil of the electromagnetic actuator. At each switching of the drive, parameters are controlled, and the length of pulse-width-modulated pulses is adjusted to ensure reliable switching and regulation of the anchor end. The control system responds to the disturbance in the current switching cycle. To test the adequacy of the proposed algorithm, an experimental model of an actuator with the proposed control system has been constructed, and its characteristics have been studied. It has been found out that the proposed algorithm ensures the required performance in terms of the operation speed and the lowest speed of the anchor landing without using position, velocity or acceleration sensors under external mechanical effects.

© 2015 Published by Elsevier Ltd. This is an open access article under the CC BY-NC-ND license (<http://creativecommons.org/licenses/by-nc-nd/4.0/>).

Peer-review under responsibility of the organizing committee of the International Conference on Industrial Engineering (ICIE-2015)

Keywords: electromagnetic actuator, adaptive control, control method, control of current, sensorless control, mechatronic drive, impulse charging.

* Gummel A.A. Tel.: +7-863-525-16-84.
E-mail address: gummel@rambler.ru

1. Introduction

The development of algorithms for the control system of an electromagnetic actuator (EMA) valve system air–gas exchange and fuel supply of combustion engines has been described in the literature [1–7]. Existing systems and methods of control that provide the required dynamic characteristics under the effects of external factors involve the use of specialized sensors (e.g., sensors of position, speed, and magnetic flux), which increases the system complexity, weight, size and cost and reduces the reliability of the system as a whole. A method of controlling a quickly moving actuator for air impulse charging, providing the minimum landing speed of the anchor at a predetermined switching time without the use of specialized position and velocity sensors, has been presented [8]. The drawback of this method is that the control system responds to a disturbance only in a subsequent switching cycle.

2. Problem definition

The present paper proposes an adaptive algorithm based on the rate measurement of current change in the coil EMA during anchor movement. This control method can be used to build control systems with electromagnetic actuators, allowing compensation of external factors [9]. These include the ambient temperature and external variable loads on the actuator and speed control of the anchor at the end of the armature stroke. A further advantage of the method is the compensation for slow switching, external effects (ambient temperature and the heating of the element of the electromagnetic actuator) and random mechanical action (e.g., vibration) affecting a movable element of the actuator during current switching. There is no need for specialized position, velocity or acceleration sensors of the movable actuator member, which would introduce additional load forces. Control is achieved with only current and voltage sensors, which greatly improves the durability and reliability of the electromagnetic actuator in general.

3. Main part

4. The proposed method is based on the relationship of electrical processes in the coil of the electromagnetic actuator with mechanical processes resulting from the movement of the movable element of the magnetic system (Fig. 1) [10]. Permeance of the air gap changes when there is an anchor movement and thus a change in the magnetic flux therein, resulting in a change in the magnitude of the current in the winding at constant voltage supplied to the coil U_1 given by:

$$U_1 = i \cdot R + \frac{d\Psi}{dt}, \quad (1)$$

where i is the current, R is the active resistance of the coil, and Ψ is the flux linkage of the coil.

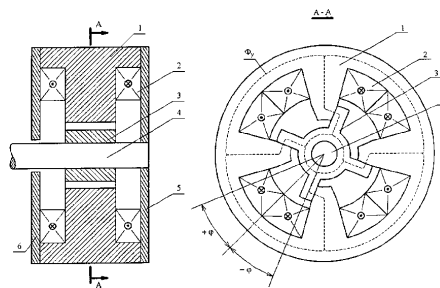


Fig.1. The electromagnetic actuator of resonance type with a symmetrical four-pole rotary anchor: 1 - a laminated magnetic core; 2 – coil of control; 3 - a laminated salient-pole anchor; 4 - a torsion spring

In accordance with Eq. 1 during the motion of the anchor in the electromagnet coil than EMF of the self-induction E_i , and occurs EMF of movement E_φ its value depends on the speed of the armature of the electromagnet:

$$U(t) = i(t) \cdot R + \frac{\partial \Psi}{\partial i} \frac{di}{dt} + \frac{\partial \Psi}{\partial \varphi} \frac{d\varphi}{dt}, \tag{2}$$

$$E_i = \frac{\partial \Psi}{\partial i} \frac{di}{dt},$$

$$E_\varphi = \frac{\partial \Psi}{\partial \varphi} \frac{d\varphi}{dt},$$

where E_i is the EMF of self-induction, E_φ is the EMF of movement, Ψ is the flux linkage of the coil EMA, and φ is the angular displacement of the movable part of the EMA.

Equation 2 reveals that the EMF of movement, as well as the EMF of self-induction, affects the current and hence the mechanical force generated by the electromagnet. The implementation of control algorithms thus requires the generation of current $i(t)$ in the coil of the electromagnet with the characteristic illustrated in Fig. 2. For a new cycle of switching in the holding coil in the time interval t_L , the holding current I_h is turned off and falls to zero. To reduce and stabilize the pick-up time t_a , a negative current pulse is generated in the holding coil (interval t_N). A pause in current for time t_A is needed to eliminate the possibility of counteracting the effect of the electromagnetic force acting on the anchor EMA generated by magnetic flux picked up by the coil. At each switch of the actuator, it is necessary to adjust the time interval t_A to account for changes in the parameters of the drive under the effects of temperature and slowly changing external mechanical factors.

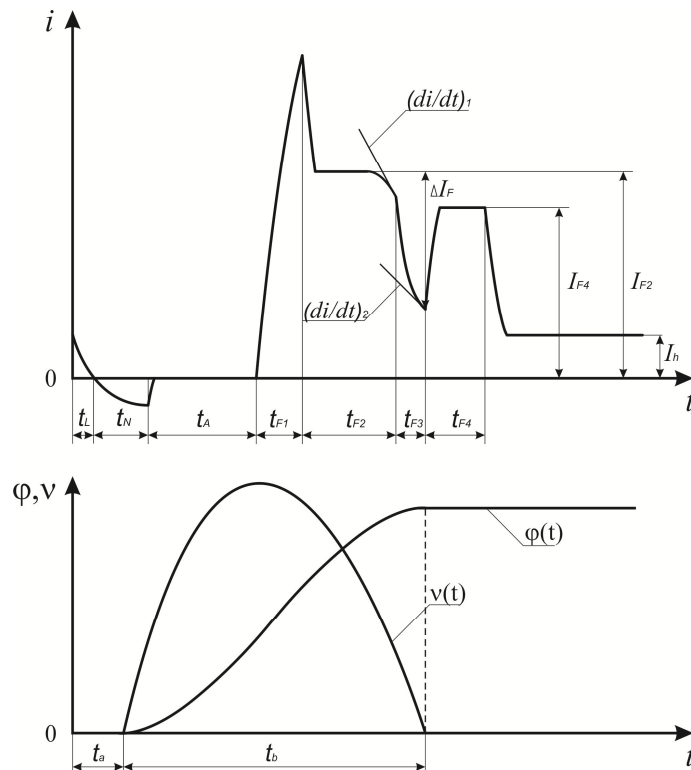


Fig. 2. The description of the control method

Because EMA valve systems used in the air impulse charging and fuel supply of internal combustion engines are required to have high performance (a response time of about 5 ms), a rapid increase in current (magnetic flux) in the time interval t_{F1} is required to force inclusion.

In the time interval t_{F2} , to pick up the coil, by pulse width modulation from the power supply generated value of the current pick-up I_{F2} . The end of the time interval t_{F2} is the time at which the first derivative of the current $(di/dt)_1$ in the coil is picked up. The value of the first derivative characterizes the position and speed of the anchor and is determined as

$$\frac{di}{dt} = \frac{i(t)R + \frac{\partial \Psi}{\partial \varphi} \frac{d\varphi}{dt}}{\frac{\partial \Psi}{\partial i}}.$$

At time interval t_{F3} , picks coil is put mode of circulating current (short-circuited coil terminals) and the value of the first derivative of the current with respect to time is determined by the moment that the anchor approaches the pole of the electromagnet in accordance with

$$\frac{di}{dt} = \frac{i(t)R}{\frac{\partial \Psi}{\partial i}},$$

at the maximum angle of rotation $\varphi = \varphi_{max}$.

For reliable pick-up and holding of an anchor at the pole, with the possible effects of external shock, an impulse of current I_{F2} is generated in the holding coil in the time interval t_{F4} , ensuring that the anchor is held.

During switching, the EMA controls the current derivatives $(di/dt)_1$ and $(di/dt)_2$, the moving time t_b and executed adaptation of the timing phase of uncontrolled movement t_A and the current pick-up I_{F2} at $I(t_{F3})$ and $(t_{F1} + t_{F2} + t_{F3}) = const$, in accordance with

$$\begin{cases} I_{F2} = I_{F2} + \Delta I_F, & \text{at } I'(t_{F3}) < I(t_{F3}), \\ I_{F2} = I_{F2} - \Delta I_F, & \text{at } I'(t_{F3}) > I(t_{F3}), \\ t_A = t_A + \Delta t, & \text{at } (t_{F1} + t_{F2} + t_{F3})' < (t_{F1} + t_{F2} + t_{F3}), \\ t_A = t_A - \Delta t, & \text{at } (t_{F1} + t_{F2} + t_{F3})' > (t_{F1} + t_{F2} + t_{F3}), \end{cases}$$

here $I'(t_{F3})$ is the holding current in the previous switching cycle and $(t_{F1} + t_{F2} + t_{F3})'$ is the duration of the phase controlled motion in the previous switching cycle.

Thus, at each switching monitored parameters of the electromagnetic actuator and corrects the parameters of the pulse width modulated (PWM) pulses to realize reliable switching and regulation of the end speed of the anchor. It should be noted that the control system responds to the disturbance in the current switching cycle.

The initial parameters of the adaptive control algorithm (Fig. 2) determined according a method based on the solution of differential equations of motion resonance EMA for the target values of t , ω , φ , which are determined by the desired characteristics of coil current [11].

Figure 3 is a block diagram of a device implementing the method of controlling the electromagnetic actuator resonance type using the characteristics of change in current in the coil for a one-wire EMA of resonance type [12].

The modes of operation of the device are as follows.

1. Generation of high-voltage U_2 for the forced switching of a short-term method of connecting the solenoid coil to the power source U_1 at U_2 less than the required value (T_1 —open, T_3 —briefly opens, T_2 and T_4 —closed).
2. The mode of fast transfer inductive power of the coil (interval t_1). Transistor switches T_2 – T_4 —closed, T_1 —open. There is charge capacitance C_2 , and the coil current decreases to zero.

3. The mode of formation of reverse current (interval t_N). Open switch T_4 provides resonant overcharge of capacitor C_2 .

4. The mode of uncontrolled movement of the anchor (interval t_A). Transistor switches T_1 – T_4 —closed. There is no coil current.

5. Forced power on (interval t_{F1}). Transistor switches T_2 – T_3 —open, T_1 and T_4 —closed. High voltage U_2 is applied to the coil of the EMA.

6. Time control closer to the pole of the anchor (interval t_{F2}). T_2 and T_4 - closed, T_1 - open, T_3 - controlled PWM pulses that achieve the desired current in the coil I_{F2} . The interval ends when $\frac{di}{dt} = \left(\frac{di}{dt}\right)_1$.

7. Control of the contact anchor at the pole (interval t_{F3}). Switches T_1 and T_3 - closed, T_2 and T_4 - open. Current is circulated in the coil. Conditions completion interval: $\frac{di}{dt} = \left(\frac{di}{dt}\right)_2$.

8. The mode of capturing and holding the anchor EMA (interval t_{F4}). Switches T_2 and T_3 —open, T_1 and T_4 —closed. The forced voltage U_2 is applied to the coil. When transistor switch T_2 closes and T_1 opens, T_3 controls the PWM pulses to achieve the desired current in the coil I_{F3} . Next, holding current I_h is generated. Switch T_4 closes if U_2 is greater than a predetermined value, and then T_2 opens and T_1 closes; otherwise, T_1 is open and T_2 is closed. Switch T_3 —controlled pulse width modulation for a given current I_h in the coil of the EMA.

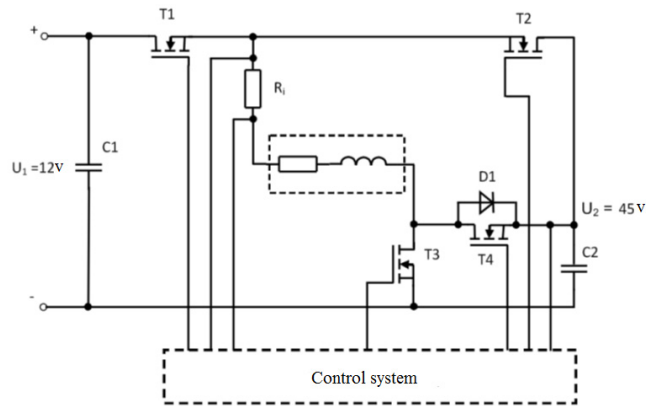


Fig 3. Block diagram of a power circuit for the control method, R_i - current sensor; T - power metal–oxide–semiconductor field-effect transistor switches; EMA - electromagnetic actuator

For the experimental investigation of the proposed method of management and determination of the dynamic characteristics of a mechatronic actuator, we designed and manufactured a hardware and software system for an internal combustion engine. Figure 4 is a structural and functional diagram of the hardware and software system.

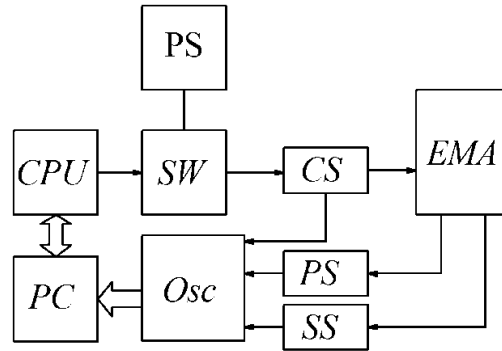


Fig. 4 - Structural and functional diagram of the hardware and software system: PS—power supply; CPU—control unit; SW—the power converter; CS—current sensor; EMA—electromagnetic actuator; PC—personal computer; PS—position sensor; SS—speed sensor; Osc—oscilloscope

5. Conclusion

The experimental investigation confirmed the adequacy of the developed control algorithm. Tests showed that the application of the proposed control algorithm realizes a final landing speed of the anchor lower than 0.4 m/s and a switching time of about 3.6 ms (Fig. 5) under the effect of external disturbances. The proposed control algorithm of the electromagnetic actuator for air impulse charging of an internal combustion engine thus achieved the required performance of the switching speed and the minimum landing velocity of the anchor without the use of position, velocity or acceleration sensors in the presence of external disturbances.

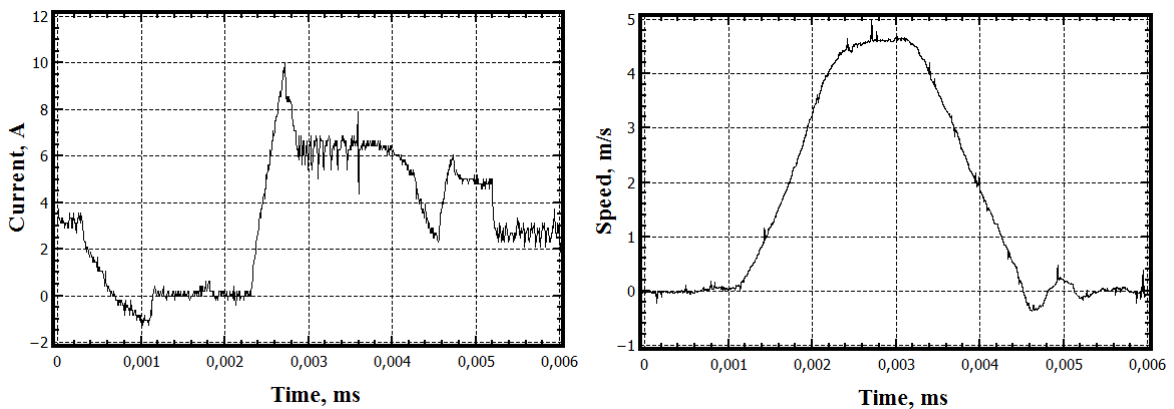


Fig. 5 - Experimental characteristics of the current and the speed of movement of the anchor EMA

The present study was supported by a Russian Federation President Research grant for young scholars and postgraduate students who implement advanced scientific research and developments in priority research areas of the modernization of the Russian economy (grant number SP-6838.2013.1).

References

- [1] Schatz O.: Lufttaktventil. Patent DE 4308931 1993.
- [2] Schatz O.: Gesteuertes Ruckschlagventil. Patent DE 3737828A1 (1987).

- [3] Porsche AG : Verfahren zur Laststeuerung einer Kolben-Brennkraftmaschine. Patent DE 102005033994 A1 (2007).
- [4] Elsasser A., Schilling W., Schmidt J., Brodesser K., Schatz O.: Impulsaufladung und Laststeuerung von Hubkolbenmotoren durch ein Lufttaktventil. MTZ 62 (2001), Nr. 12.
- [5] Schneider E., Scholten L., Wallrafen W., Zentgraf M.: Ein integriertes Saugmodul zur Anwendung der Impulsaufladung in der Großserie // 12. Aachener Kolloquium Fahrzeugund. — Aachen, 2003.
- [6] Gilmiyarov K.R. Metod i ustroystvo upravleniya mekhatronnym privodom klapana gazoraspredelitel'nogo mekhanizma dvigatelya vnutrennego sgoraniya: dissertatsiya kandidata tekhnicheskikh nauk [Method and control mechatronic drive valve timing internal combustion engine: diss. cand. tech. sciences]. Novocherkassk, 2012.
- [7] Pavlenko A.V., Gilmiyarov K.R., Bolshenko I.A. Upravleniye elektromagnitnym privodom klapana gazoraspredelitel'nogo mekhanizma dvigatelya vnutrennego sgoraniya [Management of the electromagnetic actuator valve of gas-distributing mechanism of internal combustion engine]. Elektrotehnika, 2014, no. 5, pp. 40-46.
- [8] Pavlenko A.V., Gilmiyarov K.R. Elektromagnitnyy privod dlya klapanov gazoraspredelitel'nogo mekhanizma dvigateley vnutrennego sgoraniya [The electromagnetic actuator valve of gas-distributing mechanism of internal combustion engine], Izvestiya vuzov Severo-Kavkazskiy region. Tekhnicheskiye nauki, 2009, Spets. Vyp. Mekhatronika. Sovremennoye sostoyaniye i tendentsii razvitiya 2009 :Vserossiyskaya nauch. Shkola dlya molodezhi, Novocherkassk, 2-15 November 2009, pp. 5-10.
- [9] Gummel A.A. Vliyaniye vneshnikh faktorov na dinamiku srbatyvaniya privoda vozdušno-taktovogo klapana dvigatelya vnutrennego sgoraniya [The influence of external factors on the dynamics of the operation of electromagnetic valve actuator for air impulse charging internal combustion engine], Izvestiya vuzov Severo-Kavkazskiy region. Tekhnicheskiye nauki, 2007, Spets. Vyp. Problemy Mekhatroniki, 2006, pp. 5-7.
- [10] Nikitenko A.G. Raschet elektromagnitnykh mekhanizmov na vychislitel'nykh mashinakh [Calculation of electromagnetic mechanisms on computers], Moscow, Energoatomizdat, 1985, 216 p.
- [11] Gummel A.A. Mekhatronnyy privod dlya vozdušno-taktovogo klapana dvigatelya vnutrennego sgoraniya: avtoreferat diss. kand. tekhn. nauk [Mechatronic actuator for valve of air impulse charging internal combustion engine: abstract diss. cand. tehn. sciences], Novocherkassk, 2015.
- [12] Pavlenko A.V., Gilmiyarov K.R., Gummel A.A.: Ustroystvo upravleniya mekhatronnym privodom [The control device for mechatronic actuator], RU Patent 2010140032/07. (2010)



International Conference on Industrial Engineering

Case study of a Conservation Power Plant concept in a metallurgical works

Kazarinov L.S.^a, Barbasova T.A.^{a*},

^a South Ural State University, 76, Lenin Avenue, Chelyabinsk, 454080, Russian Federation

Abstract

This paper considers application of the Conservation Power Plant concept to integrated resource planning and control in metallurgical works. A structure of local energy saving measures is proposed. The researchers have reviewed optimization issues of combined heat and power plants where secondary power resources of metal manufacturing are recovered to upgrade fuel usage efficiency. It serves as the terminal point where the effect of energy saving is realized in decreasing the total consumption of the natural gas as the primary resource. Similar approach can be used for energy saving organization in large-scale industrial complexes.

© 2015 The Authors. Published by Elsevier Ltd. This is an open access article under the CC BY-NC-ND license (<http://creativecommons.org/licenses/by-nc-nd/4.0/>).

Peer-review under responsibility of the organizing committee of the International Conference on Industrial Engineering (ICIE-2015)

Keywords: Conservation Power Plant, energy efficiency, integrated resource planning, negawatt.

1. Introduction

Energy saving is the RF policy's preference in all fields of business activities, including the heat and power facilities of iron and steel enterprises. To achieve the goals of energy saving in utilities the advanced nations' experience suggests that integrated resource planning and power control taken in whole, as Conservation Power Plant generating negawatts of power are preferred. Amory Lovins introduced term negawatt in 1989 for utilities [1-7].

However, the analogous approach may be used also for production plants.

* Corresponding author. Tel.: +7-912-474-0198
E-mail address: tatyana_barbasova@mail.ru

2. The Concept of the Conservation Power Plant for metallurgical works

Generally, energy generation, conversion and consumption are many-staged in complex industrial systems [8-22].

One of the approaches to comprehensive treatment of energy processes alongside energy efficiency is considering them in dual flows of energy – real energy flows and saved energy backflows.

The introduction of conditional flows of saved resources allows showing the structure of energy saving processes as the negawatt generating, converting and consuming structure. It enables us to consider the structure of energy efficiency process as a distributed energy saving plant and thus estimate its efficiency, plan and control its work in the whole. Such approach allows reaching energy efficiency effect in complex plants in a consistent manner.

Real resource consumers implementing energy efficient measures are the sources of saved resources. Converters of real resources are the saved resources converters considered in the context of the dual approach. Saved resources incoming is a dual interpretation of real resources converters' decreasing of the target volume. Obviously, this comes to decrease the real consumed resources at the inlet of the converter dually interpreted as output of the saved resources.

In the fig. 1, suppliers of real resources are consumers of saved resources. They are the final point where the economic effect of energy efficiency is made – this is the reduction of real primary resources consumption.

Below there is an example of a typical structure of the production power unit (fig. 1). The Central Power Plant (CPP) working under the controlling mode of operation is the main part here. This plant is made in accordance with the cross-connection structure where the power boiler (PB) unit, the turbine generator (TG) unit and the main steam collector (C_s) are its components. Power boilers consume natural gas B_{ng} and blast furnace gas B_{bfg} . If necessary, coke-oven gas and other secondary power resources (SPR) of coke and by-product process can also be used here. Plant's turbine generators produce electrical W_e and heat energy in heating water Q_h . Besides process steam U_s extraction is made through the pressure-reducing and desuperheating station (PRDS) from the steam collector C_s .

Blast-furnace gas B_{bfg} comes to the CPP's boilers from the blast furnace gas main M_{bfg} . The blast-furnace gas main is connected to the primary gas source, i.e. blast-furnace process. Here F_{bfg} is the flare for extra blast-furnace gas burning in the atmosphere, C_{bfg} – blast-furnace gas consumers.

Electric power W_e , heat power Q_h and process steam U_s produced by the CPP come to the electric N_e , district heating N_{dh} and steam N_s networks of the plant. C_e , C_{dh} , C_s – are consumers of electric, heat and steam power accordingly.

The main source of the process steam D_b is the base-load seam power plant (BSPP). Secondary steam sources B_s are additional. As secondary steam sources are variably loaded then steam accumulators (SA) are used for accumulating secondary steam. The flare F_s is used to discharge extra steam to the atmosphere. If necessary, additional steam ΔD_s is run to the steam network N_s to compensate sudden increase of consumers' steam load.

In the power structure presented here in order to save energy the secondary power resource, i.e. blast-furnace gas, is recovered at the CPP. Thereupon electric power cost price produced at the CPP considerably decreases in comparison with the electric power bought in the wholesale market. As the product cost price of such plants, e.g. rolling ones, highly depend on the electric power price therefore it is necessary to make the CPP produce electric power to the full.

However, such a direct conclusion is not system wide proved. The fact is that the blast-furnace gas consumption volume by the CPP boilers depends on the load. Besides nonlinear extreme dependence of the blast furnace gas consumption on the load is typical for many types of boilers. There is an example in fig. 2 containing power features of the CPP boilers depending on their load.

As a result, the relative blast-furnace gas consumption increases when the load is decreased, therefore relative natural gas consumption decreases and electric power cost price decreases. Thus to have system-based energy saving effect at the considered power facilities it is essential to deal with the totality of problems, including electric power production increase, electric power cost price decrease, natural gas consumption decrease and etc.

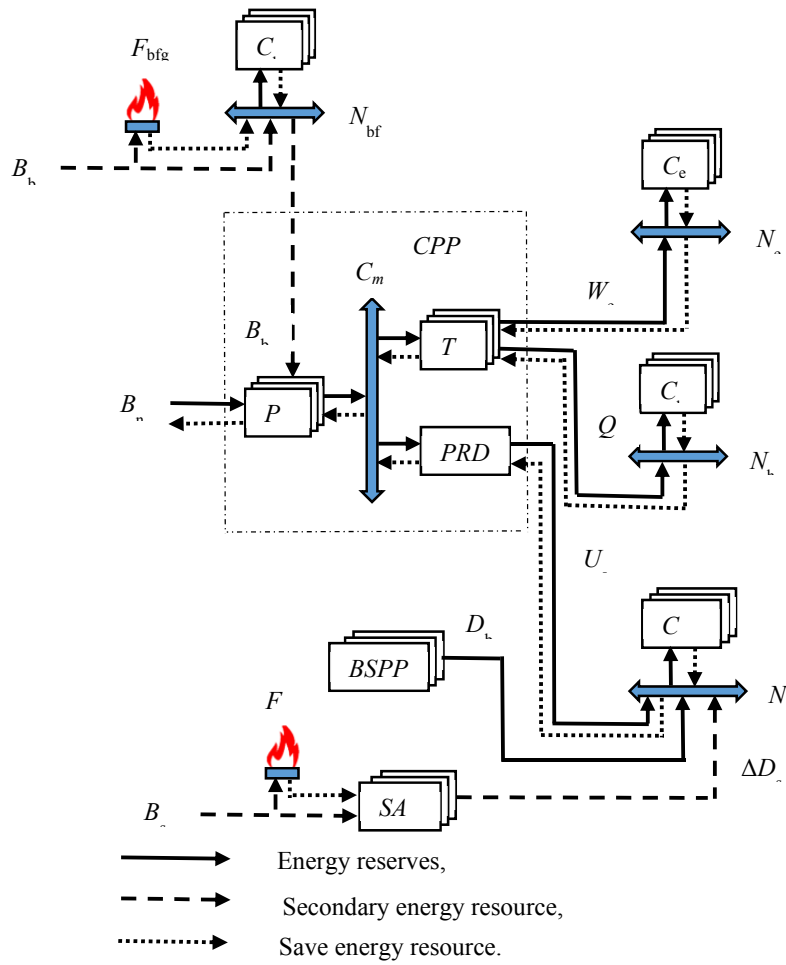


Fig. 1. Typical structure of iron and steel works power facility.

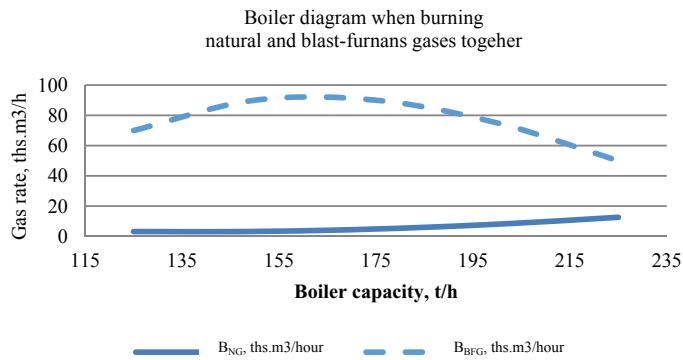
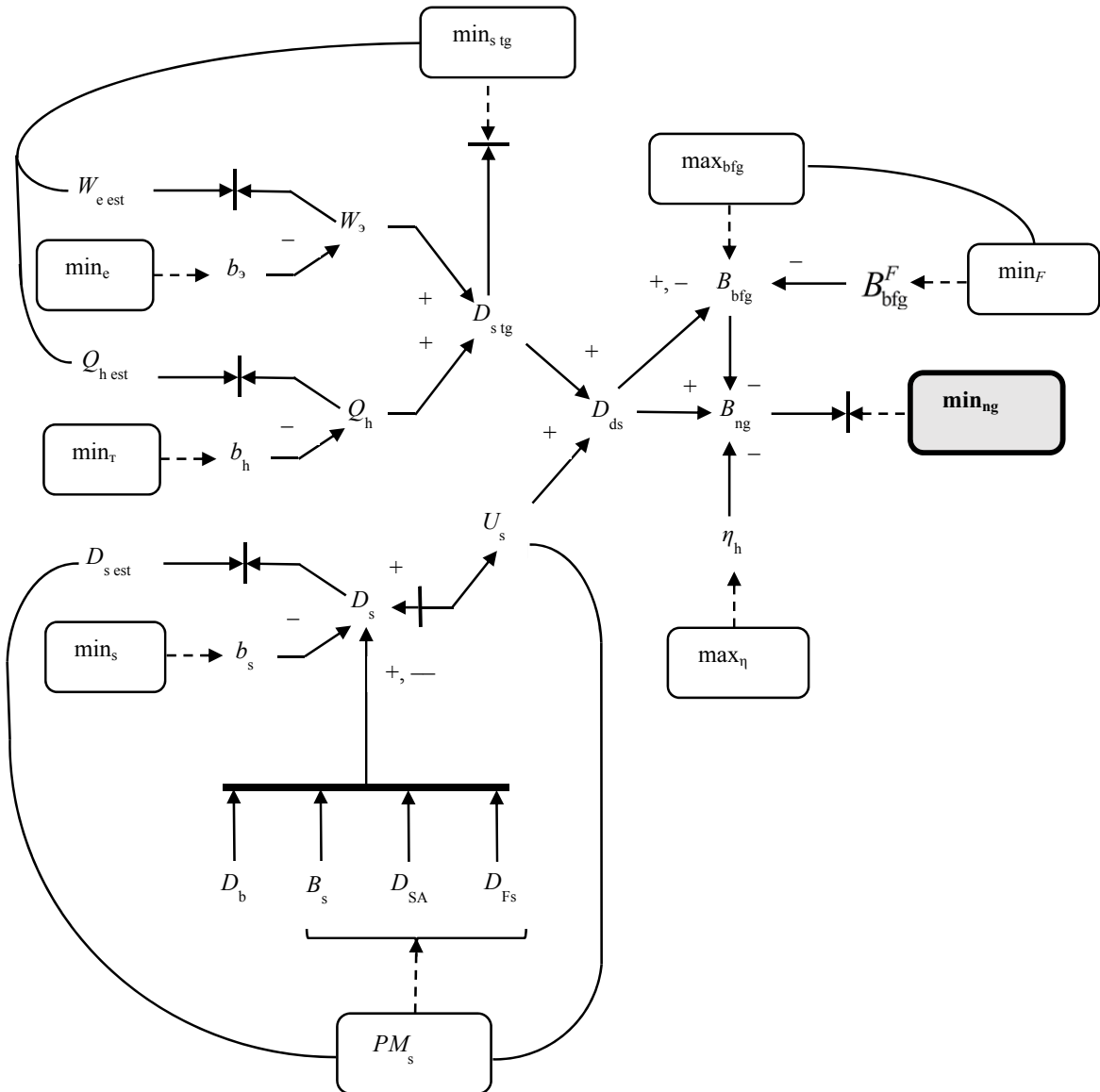


Fig. 2. Power features of iron and steel works power facility.

The chart showing connection between the efficiency increase tasks of the taken power facility is given in general in fig. 3.

Natural gas consumption minimization as a bought resource (\min_{ng}) for the taken power facility is the main energy saving task.

The natural gas consumption B_{ng} is determined by the total direct steam output of the CPP's boilers D_{ds} , by the consumed blast-furnace gas volume B_{bfg} and boilers' efficiency (η_h). Blast-furnace gas consumption increase leads to natural gas consumption decrease (-); therefore we have the task to consume blast-furnace gas to the maximum (\max_{bfg}).



‡ – equality sign of the right and the left arrows

Fig. 3. The chart showing connection between power facility efficiency upgrade tasks.

Total direct steam output increase leads to natural gas consumption increase (+); therefore there is a task to decrease direct steam output. But this task in the considered task chart is not the final one but an intermediate goal. Boiler efficiency increase leads to natural gas consumption decrease and thus there is a task to increase boiler efficiency (\max_{η}). In all the volume of the natural gas consumption B_{ng} is due to the influence of all the above factors B_{bfg} , D_{ds} , η_h . On the other part the variable B_{bfg} is due to the solution of the contrary problem (\min_{ng}). This duality is shown in the chart (fig. 3) by the equality sign.

Direct steam production D_{ds} chiefly influences on the volume of blast-furnace consumption B_{bfg} . But in accordance with the chart (fig. 3) this dependence is extreme and in relation to boilers' load may increase (+) as well as decrease (–) the blast-furnace consumption. Loss at the blast-furnace gas flare B_{bfg}^F is negative (–) and specifies the task to decrease flare loss (\min_F). This task is intimately related to the blast-furnace gas consumption maximization (\max_{bfg}).

The total direct steam output D_{ds} comes from the steam volume consumed by turbine generators D_{ds} (+), and the steam volume U_s (+) taken to control the total process steam D_s . Here the local task comes, i.e. to decrease steam consumed by turbine generators D_{stg} (\min_{ds}). This task closely relates to the tasks to provide the estimated volumes of electric $W_{e\ est}$ and heat energy $Q_{h\ est}$ output. The tasks of \min_e , \min_h , \min_s decrease of b_e , b_h , b_s power capacities of consumers of electric and heat energy, as well as the steam have great influence on the estimated volumes of electric $W_{e\ est}$ and heat $Q_{h\ est}$ energy, steam $D_{s\ est}$ output accordingly.

The total process steam volume D_s is determined by the primary steam source to the extent of D_b . Secondary source steam B_s is additionally provided to the steam network in order to save energy. Secondary source steam parameters are unstable over a wide range. Moreover steam consumption parameters are changing in a wide range. This is due to the fact that iron and steel works have significant process dynamics. In order to stabilize steam network parameters steam accumulators (SA) that produce stabilizing steam flow D_{SA} are used. Flares are used to discharge extra steam D_F to the atmosphere. The controlling steam flow U_s is provided for the CPP. All the mentioned tasks are closely connected and make a unified system of the steam network power management (PM_s).

Collectively these tasks provide integrated planning and resource management of the power facility (fig. 2) to make efficiency upgrading. Integrally this efficiency may be seen in decrease of primary resource consumption, i.e. natural gas. System connection of the saved resource flows is given in fig. 3.

3. Optimization of working Conditions of Combined Heat and Power Plants

As an example, consider the task of optimization of working conditions of combined heat and power plants, where secondary power resources (SPR) of iron and steel facilities are recovered to upgrade fuel utilization efficiency. Blast-furnace gas, coke-oven gas and other types of resources may be used as SPR. SPR recovering at iron and steel facilities gives great energy saving as it reduces natural gas consumption.

Fig. 4 shows a typical structure of the combined heat and power plant consisting of parallel energy boilers which provide steam to the general steam collector where turbine generators, the steam consumers, are connected.

Here PB_i – power boilers, TG_i – turbine generators; SC – steam collector. Natural (B_{NGi}) and blast-furnace (B_{BFGi}) gases are provided to power boilers (PB_i). Superheated steam (D_{OSi}) gained in the steam collector (SC) is generated at the boilers' output. Turbine generators (TG_i) consume overheated steam ($D_{TGOS,i}$) and produce electric ($W_{TG,i}$) and heat ($Q_{TG,i}$) energy.

The structure (fig. 4) is the fuel-mix fired power plant (FMFPP) with steam cross connections.

The general goal to upgrade energy efficiency of the considered FMFPP may be implemented based on the implementation of the following separate tasks:

- energy balance optimization;
- natural gas consumption minimization;
- power efficiency optimization.

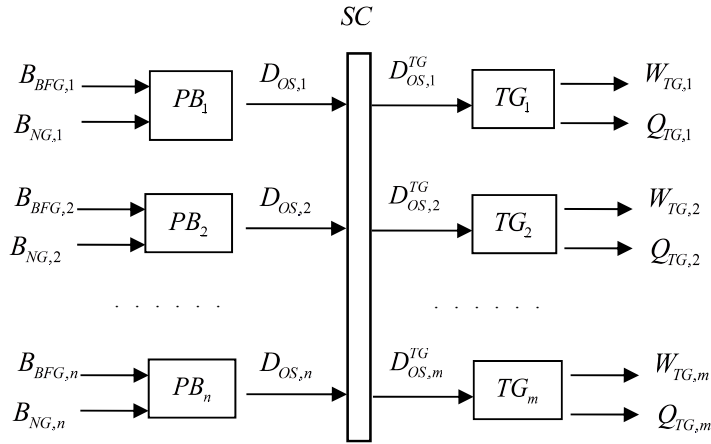


Fig. 4. Fuel-mix fired power plant.

Let’s consider the energy balance optimization task. It consists of two subtasks: optimization of load distribution of turbine generators and optimization of load distribution of boilers.

Let’s first consider the subtask of optimization of load distribution of turbine generators. The simplified pattern can be got by considering the typical power feature of the turbine generator (fig. 5).

Here W_E is electrical capacity produced, $Q_{H,i}$ – heating capacity, D_{OS} – overheated gas consumption. Electrical capacity and overheated gas consumption of the turbine generator are limited by the values W_E^{\max} and D_{OS}^{\max} accordingly.

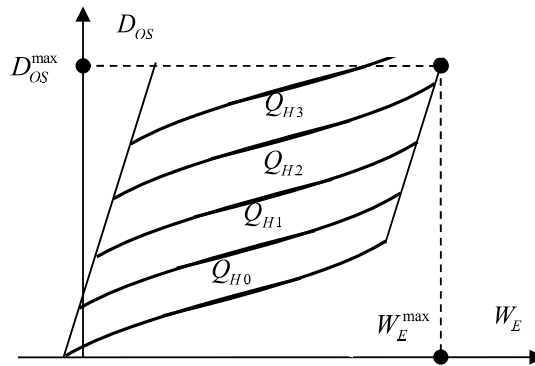


Fig. 5. Typical power feature of the turbine generator.

Analytically power features of turbine generators may be described by the formulas:

$$\left. \begin{aligned} D_{OS,i}^{TG} &= a_{0,i} + a_{1,i}W_{E,i} + a_{2,i}Q_{H,i} + \langle \text{corrections} \rangle; \\ D_{OS,i}^{TG} &\geq b_{0,i} + b_{1,i}W_{E,i} + b_{2,i}Q_{H,i} + \langle \text{corrections} \rangle; \\ W_{E,i} &\leq W_{E,i}^{\max}, \quad D_{OS,i}^{TG} \leq D_{OS,i}^{TG,\max}; \quad i=1, 2, \dots \end{aligned} \right\} \quad (1)$$

Here a_{ji} , b_{ji} - empirical coefficients of dependences. Corrections are determined for deviations of operating parameters of turbine generators from the nominal values. Typical operating parameters of turbine generators are:

temperature and pressure of overheated steam, steam pressure of heat extraction, temperature and condenser exhaust and etc. As a rule corrections are linear in relation to parameter deviations under nominal conditions.

Total turbine generator characteristic:

$$\left. \begin{aligned} W_{E,0} &= \sum_{i=1}^m W_{E,i}; \\ Q_{H,0} &= \sum_{i=1}^m Q_{H,i}; \\ D_{OS,0}^{TG} &= \sum_{i=1}^m D_{OS,i}^{TG}. \end{aligned} \right\} \quad (2)$$

The task is to find best values of electric $W^{E,i}$ and heat $Q^{H,i}$ loads of turbine generators in accordance with the minimum of the total steam consumption D under the set values of the total output of electric $W^{E,0}$ and heat $Q^{H,0}$ energy. This task is a typical one for linear programming.

Generally energy characteristics of turbine generators are nonlinear. In this case the task should be implemented based on the methods of experimental optimization, e.g. the steepest descent method. Related to the corrections for operating condition deviations it should be noted that depending on the sign of influence of condition deviation on the steam consumption decrease their values should be kept within the required tolerance limits of the process procedures. Because of the random nature of the process procedures the tasks to stabilize the operating conditions near to the said limits are separate tasks to make relative automated control systems.

Farther let's consider the following subtask of general optimization of the FMFPP energy balance, i.e. the task to optimize load distribution of boilers.

Fig. 6 shows the typical energy characteristic of the boiler during burning of the natural gas and blast-furnace gas mixture.

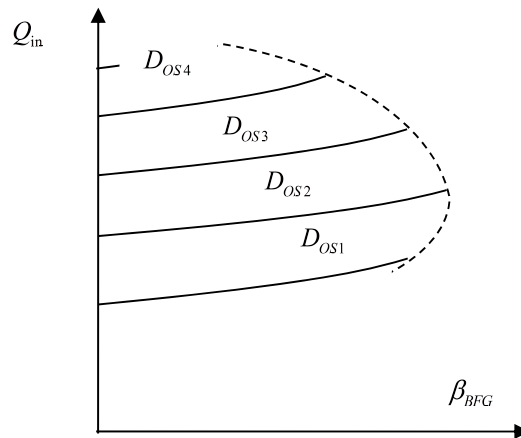


Fig. 6. Typical energy characteristic of the boiler during burning of natural gas and blast-furnace gas mixture.

Here Q_{in} - the amount of the heat energy coming into the boiler with the fuel; β_{BFG} - the share of the blast-furnace gas in the fuel mixture with natural gas: $\beta_{BFG} = B_{bfg} / B_{ng}$; D_{os} - the steam load of the boiler.

Analytic expression of the boiler energy characteristic is as follows

$$\left. \begin{aligned} Q_{in,i} &= a_{0,i} + a_{1,i} D_{OS,i} + a_{2,i} \beta_{BFG,i} + a_{3,i} D_{OS,i}^2 + a_{4,i} \beta_{BFG,i} D_{OS,i} + \langle \text{corrections} \rangle; \\ \beta_{BFG,i} &\leq \begin{cases} \beta_{BFG,i}^{\max} + b_{1,i} (Q_{in,i} - Q_{m,i})^2, & \text{if } Q_{in,i} - Q_{m,i} \geq 0, \\ \beta_{BFG,i}^{\max} + b_{2,i} (Q_{in,i} - Q_{m,i})^2, & \text{if } Q_{in,i} - Q_{m,i} < 0; \end{cases} \\ D_{OS,i} &\leq D_{OS,i}^{\max}; \quad i=1, 2, \dots \end{aligned} \right\} \quad (3)$$

Here $\beta_{BFG,i}$ - the maximum value of the parameter: β_{BFG} ; $Q_{m,i}$ - the value of $Q_{in,i}$ at the maximum value of the blast-furnace gas share consumption $\beta_{BFG,i}$, a_{ji} , b_{ji} - empirical coefficients.

Combined characteristic of the boiler unit:

$$\left. \begin{aligned} D_{OS,0} &= \sum_{i=1}^n D_{OS,i}; \\ Q_{in,0} &= \sum_{i=1}^m Q_{in,i}; \\ B_{NG,0} &= \sum_{i=1}^m B_{NG,i}. \end{aligned} \right\} \quad (4)$$

Taking into consideration the following formula

$$Q_{in,i} = B_{NG,i} Q_n^{NG} + B_{BFG,i} Q_n^{BFG} = B_{NG,i} (Q_n^{NG} + \beta_{BFG,i} Q_n^{BFG}) \quad (5)$$

where $B_{NG,i}$, $B_{BFG,i}$, Q_n^{NG} , Q_n^{BFG} - gas flow rates and caloric content accordingly, we can set the task to minimize the total natural gas consumption $B_{NG,0}$ by the values of the boiler load $D_{OS,i}$ and share consumption of blast furnace gas $\beta_{BFG,i}$ having restrictions as in constraint equation (3), (4).

4. Summary

The conception of Conservation Power Plant may serve as a systems principle for energy saving organization in metallurgical works. A structure of local energy saving measures in metallurgical works may be formulated based on this conception. The central link is here the Power Plant-regulator. It serves as the terminal point where the effect of energy saving is realized in summary lowering of the natural gas consumption as the primary resource.

Similar approach may be used for energy saving organization in large-scale industrial complexes.

References

- [1] N. Eyre, Energy saving in energy market reform – The feed-in tariffs option. *Energy Policy*. 52 (2013) 190–198.
- [2] P.L. Joskow, D.B. Marron, What does a negawatt really cost? Evidence from utility conservation programs. *Energy*, J. 13(4) (1992) 41–74.
- [3] A. Lovins, The Negawatt Revolution, The Conference Board Magazine “Across the Board”. XXVII(9) (1990) 18–23.
- [4] A. Lovins, W. Browning. *Negawatts for Buildings*. 1992. http://www.rmi.org/Knowledge-Center/Library/D92-22_NegawattsForBuildings
- [5] Fei Zhao, Godfried Augenbroe *Unlocking the Negawatt Lap* Lambert Academic Publishing GmbH KG, 2012.
- [6] F. Krause, D. Olivier, J. Koomey, *Negawatt Power: The Cost and Potential of Electrical Efficiency Resources in Western Europe: Executive Summary* International Project for Sustainable Energy Paths, 1995.
- [7] S. Doig, M. Bell, N. Mims, Rocky Mountain Institute. *Industrial Electric Productivity: Myths, Barriers & Solutions* Conference Proceedings. 2009 http://www.rmi.org/Knowledge-Center/Library/2009-18_IndustrialElectricProductivity
- [8] P. Joskow, D. Marron, What does a negawatt really cost? Further thoughts and evidence, *The Electricity Journal*. 6(6) (1993) 14–26.
- [9] S. Şevik, An analysis of the current and future use of natural gas-fired power plants in meeting electricity energy needs: The case of Turkey *Renewable and Sustainable Energy Reviews*. 52 (2015) 572–586.
- [10] J.K. Steinberger, J. van Niel, D.Bourg, Profiting from negawatts: Reducing absolute consumption and emissions through a performance-based energy economy, *Energy Policy*. 37(1) (2009) 361–370.
- [11] N. Adate, R.N. Awale, Energy conservation through energy efficient technologies at thermal power plant, *International Journal of Power System Operation and Energy Management*. 3(1) (2013).
- [12] L.S. Kazarinov, T.A. Barbasova, Energy efficiency anticipatory control of an enterprise *The Bulletin of the South-Ural State University. Series «Computer Technology, Control, Electronics»*. 35(294) (2012) 85–98.
- [13] L.S. Kazarinov, T.A. Barbasova, A.A. Zakharova, Automated Information Decision Support System on Control and Planning Energy Resources Usage *The Bulletin of the South-Ural State University. Series «Computer Technology, Control, Electronics»*. 23 (2012) 118–122.
- [14] L.S. Kazarinov, T.A. Barbasova, O.V. Kolesnikova, A.A. Zakharova, Method of Multilevel Rationing and Optimal Forecasting of Volumes of Electric-Energy Consumption by an Industrial Enterprise. *Automatic Control and Computer Sciences*. 48(6) (2014) 324–333.
- [15] J. Wood and B. F. Wollenberg, *Power Generation Operation and Control*. New York: Wiley. (1996) 37–45.

- [16] M. Shahidehpour, H. Yamin, Z. Li, *Market Operation in Electric Power Systems, Forecasting, Scheduling, and Risk Management*, New York: Wiley, (1996) (115–160).
- [17] Z. Li, M. Shahidehpour, Generation scheduling with thermal stress constraints, *IEEE Trans. Power Syst.* 18(4) (2003) 1402–1409.
- [18] R.A. Jabr, Optimal power flow using an extended conic quadratic formulation, *IEEE Trans. Power Syst.* 23(3) (2008) 1000–1008.
- [19] N. Sinha, R. Chakrabarti, P.K. Chattopadhyay, Evolutionary programming techniques for economic load dispatch, *IEEE Trans. Evol. Computat.* 7(1) (2003) 83–94.
- [20] I.A. Farhat, M.E. El-Hawary, Optimization methods applied for solving the short-term hydrothermal coordination problem, *Elect. Power Syst. Res.* 79(9) (2009) 1308–1320.
- [21] I.G. Damousis, A.G. Bakirtzis, P.S. Dokopoulos, Network-constrained economic dispatch using realcoded genetic algorithm, *IEEE Trans. Power Syst.* 18(1) (2003) 198–205.
- [22] D. Karaboga, B. Basturk, *Artificial Bee Colony (ABC) Optimization Algorithm for Solving Constrained Optimization Problems*, *Foundations of Fuzzy Logic and Soft Computing*, 2007.
- [23] K. Panigrahi, V. Ravikumar Pandi, S. Das, Adaptive particle swarm optimization approach for static and dynamic economic load disloaddispatch, *Energy Conversion and Management.* 49(6) (2008) 1407–1415.



International Conference on Industrial Engineering

Simulation study on supply temperature optimization of university campus heating system

Aleksandr A. Basalaev^{a*}, Tatyana A. Barbasova^a, Dmitry A. Shnayder^a

^aAutomatics and Control Department, South Ural State University, 76, Lenin Avenue, Chelyabinsk, 454080, Russian Federation

Abstract

The article deals with optimizing supply temperature at the district heating plant using simulations. It describes a new method of supply temperature optimization based on penalty functions considering indoor temperature and heat energy consumed. According to the method proposed the supply temperature is calculated and adjusted for maintaining the most comfortable indoor temperature in the buildings which lack an automated individual heating system. The article offers a scheme of the heating plant model predictive control making use of the optimization method developed.

© 2015 Published by Elsevier Ltd. This is an open access article under the CC BY-NC-ND license (<http://creativecommons.org/licenses/by-nc-nd/4.0/>).

Peer-review under responsibility of the organizing committee of the International Conference on Industrial Engineering (ICIE-2015)

Keywords: temperature optimization; district heating; heating system; supply temperature; simulation; university campus

1. Introduction

District heating systems are widely used in cities over the world [1]. Such systems are composed of one or several heating plants and plenty of consumers linked with the help of pipelines. Consumers of such systems are different purpose facilities [2]: manufacturing units, shopping complexes, educational institutions, office and apartment buildings, etc. Along with it heat energy consumers may be equipped with automated individual heating system (IHS) operated by local controller in order to distribute heat energy to domestic hot water and heating systems [3].

However, big district heating systems are characterized by consumers which often may not be equipped with an automated IHS. In this case there is applied central temperature control strategy which makes it possible to regulate

* Corresponding author. Tel.: +7-921-772-2514; fax: +8-351-257-9369.
E-mail address: alexander-basalaev@mail.ru

heat energy supply by changing the supply temperature [4]. This stipulated the task to maintain supply temperature which will be enough to provide all the users with heat energy they need.

The first problem solution was implementing control curves which reflect dependence between supply temperature and outdoor temperature. This solution, in fact, proved to be fairly good [5]. However, due to automated systems development it became possible to get access not only to current and statistic information on consumers' state and characteristics [6-9] but to methods and tools for simulating of consumption parameters and heat energy distribution [10-12].

Simulation brought in ample opportunities for heat energy supply management. In the abovementioned task context simulation allowed quick calculation of the supply temperature sufficient for maintaining required parameters in the nodes of the pipelines network, pointed out by a simulation tool user, taking into account the current parameters and configuration of the pipeline network and its consumers [13,14]. In particular, this function is performed using Termis Software produced by Schneider Electric [15].

Moreover, along with quick calculation of the heating system state, simulation permits to evaluate the microclimate parameters of the space heated [16]. This work will treat temperature control over heat energy supplied by a heating plant taking into account the indoor temperature of buildings.

2. Optimization problem

In order to increase heat energy consumption efficiency for a heating system, two tasks are solved:

- Minimization of heat energy consumption;
- Maximization of heat energy supply quality by maintaining comfortable microclimate.

In the district heating systems the main parameter regulated at heating plants is temperature of the heat energy T_{IS} , supplied to the heating system. The heat medium temperature at building inlets depends on T_{IS} , but it is lower than T_{IS} , due to heat losses when transferred through the pipeline system from heating plants to consumers.

Building heat energy consumption Q_D (Gcal) can be estimated according to [17] as follows:

$$Q_D = (T_1 - T_{OUT}) / (1/(k \cdot F) + 1/(2 \cdot G) + 1/q), \quad (1)$$

where T_1 is the heat medium temperature at the building inlet, T_{OUT} is the outdoor temperature, k is the heat transfer coefficient of radiators, F is the heating area of radiators, G is the heat medium flow rate, q is the heat transfer coefficient of the building.

Heat losses Q_L of the building can be estimated according to [17] as follows:

$$Q_L = q \cdot (T_{IND} - T_{OUT}), \quad (2)$$

where T_{IND} is the indoor temperature.

For heating systems the main indicator of the building microclimate quality is the mean indoor temperature T_{IND} which one can get using Eq. 1 after substituting Eq. 2 according to heat balance ($Q_D = Q_L$):

$$T_{IND} = T_{OUT} + (T_1 - T_{OUT}) / (q \cdot (1/(k \cdot F) + 1/(2 \cdot G)) + 1). \quad (3)$$

To calculate parameters of heating system consumers (T_1 и G) as a function of the supply temperature T_{IS} , a simulation macro-model was used. The design concept of the macro-model used is described in [18,19]. The macro-model allows calculating state variables of the heating system under the specified characteristics and configurations of the system facilities.

According to Eq. 1 and Eq. 3 the heating plant must produce heat energy Q sufficient for maintaining the most comfortable indoor temperature in each building. This task can be referred to minimax problems of optimization and described using the following system of objective functions:

$$\begin{cases} Q(T_{1S}) \rightarrow \min \\ M_{INDi}(T_{1S}) \rightarrow \max, i = 1..N, \end{cases} \tag{4}$$

where Q is the total heat energy produced, sufficient enough to provide all the buildings connected to the district heating system with heat energy; M_{INDi} is the assessment of the indoor microclimate quality of the i -building within the heating system; N is the number of buildings connected to the heating system.

To assess the indoor temperature quality R_{1i} of i -building let's employ penalty function R_1 of the indoor temperature which can be described using the following system:

$$R_{1i} = R_1(T_{INDi}(T_{1S})) = \begin{cases} 1 + p_i \cdot N \cdot (T_{INDi}^{\min} - T_{INDi}(T_{1S})), T_{INDi}(T_{1S}) < T_{INDi}^{\min} \\ \frac{T_{INDi}(T_{1S}) - T_{INDi}^{\text{comf}}}{T_{INDi}^{\min} - T_{INDi}^{\text{comf}}}, T_{INDi}^{\min} \leq T_{INDi}(T_{1S}) < T_{INDi}^{\text{comf}} \\ \frac{T_{INDi}(T_{1S}) - T_{INDi}^{\text{comf}}}{T_{INDi}^{\max} - T_{INDi}^{\text{comf}}}, T_{INDi}^{\text{comf}} \leq T_{INDi}(T_{1S}) \leq T_{INDi}^{\max} \\ 1 + p_i \cdot N \cdot (T_{INDi}(T_{1S}) - T_{INDi}^{\max}), T_{INDi}(T_{1S}) > T_{INDi}^{\max} \end{cases}, \tag{5}$$

where $T_{INDi}(T_{1S})$ is the mean indoor temperature of i -building depending on heating plant supply temperature T_{1S} and taking into consideration heat losses in the pipelines of the heating system. $T_{INDi}(T_{1S})$ is calculated with the help of the macro-model. T_{INDi}^{\min} , T_{INDi}^{comf} and T_{INDi}^{\max} are, respectively, correspond to minimum, comfortable and maximum indoor temperatures of i -building according to its sanitary regulations; p_i is the penalty coefficient for violating indoor temperature range required ($p_i > 1$).

Fig. 1 represents the penalty function curve of the mean indoor temperature of building.

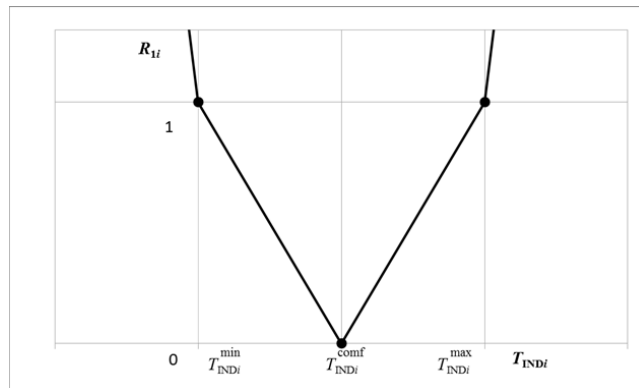


Fig. 1. The penalty function curve of indoor temperature.

To assess heat energy consumed while optimizing the heating plant supply temperature let's introduce penalty function R_2 which can be expressed by the following system:

$$R_2 = \begin{cases} 1 + p \cdot N \cdot (Q^{\min} - Q), Q < Q^{\min} \\ \frac{Q - Q^{\min}}{Q^{\max} - Q^{\min}}, Q^{\min} \leq Q \end{cases}, \tag{6}$$

where Q is the total heat energy produced; Q^{\min} and Q^{\max} are, respectively, total minimum and total maximum heat energy produced; p is the penalty coefficient for violating minimum heat energy produced ($p > 1$).

The total minimum heat energy produced is the one which is enough to maintain minimum mean indoor temperature for each i -building corresponded to its type (educational institutions, office or apartment buildings, etc.) according to the sanitary regulations. It is calculated while solving the optimization task which follows:

$$Q^{\min} = \begin{cases} Q(T_{1S}) \rightarrow \min \\ T_{\text{IND}i}(T_{1S}) \geq T_{\text{IND}i}^{\min} \end{cases} \quad (7)$$

where $Q(T_{1S})$ is the total heat energy produced by the heating plant and calculated using the macro-model.

The total maximum heat energy produced is the energy sufficient to maintain maximum mean indoor temperature for each i -building corresponded to its type according to the sanitary regulations. It can be found while solving the following optimization problem:

$$Q^{\max} = \begin{cases} Q(T_{1S}) \rightarrow \min \\ T_{\text{IND}i}(T_{1S}) \geq T_{\text{IND}i}^{\max} \end{cases} \quad (8)$$

Fig. 2 represents the penalty function curve of heat energy consumption R_2 .

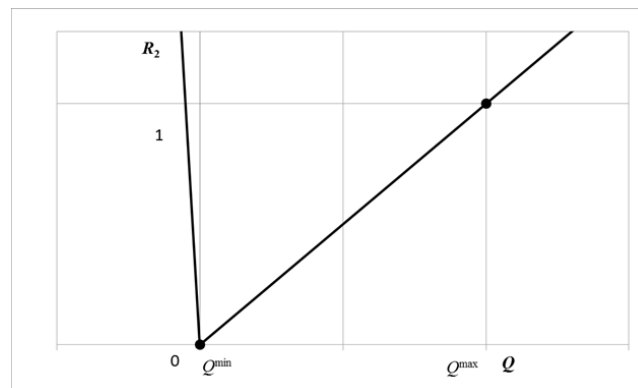


Fig. 2. The penalty function curve of heat energy consumption.

Using penalty functions of Eq. 5 and Eq. 6 the optimization problem of Eq. 4 can be reduced to the optimization problem described by the following cost function:

$$\alpha \cdot R_2(Q(T_{1S})) + (1 - \alpha) \cdot \frac{1}{N} \sum_{i=1}^N R_1(T_{\text{IND}i}(T_{1S})) \rightarrow \min, 0 \leq \alpha \leq 1, \quad (9)$$

where α is a coefficient identifying priority of optimization tasks. If α equals 1, heat energy economy optimization problem is solved according to Eq. 6. In this case optimization problem of Eq. 6 can be reduced to the optimization problem of Eq. 7. If α equals 0, comfortable indoor temperature optimization problem is solved according to Eq. 5.

3. Model predictive control

The approach proposed describes optimization of temperature supplied by one heat plant T_{1S} . So, the task of Eq. 9 is a one-dimensional optimization problem. Powell's method was employed to solve the optimization problem. Fig. 3 represents the block diagram for an iteration of optimization problem solution.

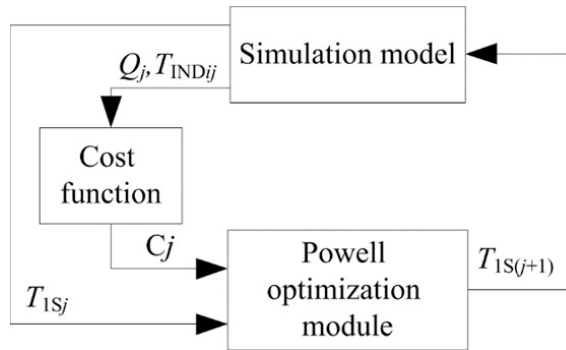


Fig. 3. The block diagram for an iteration of optimization problem solution.

In j -step of the block diagram the simulation model calculates the amount of heat energy Q_j produced by the heating plant and mean indoor temperatures of i -building T_{INDij} using Eq. 3. The values obtained by the simulations are substituted in cost function Eq. 9. The estimated cost function value is transferred to the optimization module which determines the power plant supply temperature for the next iteration of Powell's method. The initial value of heat plant supply temperature T_{1S0} is obtained using preset supply temperature curve depending on outdoor temperature.

Solution to the optimization problem will enable to put into effect model predictive control (MPC) under which the optimization block using simulation calculates temperature correction of supply temperature for the heating plant. Fig. 4 represents the block diagram of model predictive control. On the block diagram Q is the total heat energy consumed by the heating system. T_{INDi} corresponds to the mean indoor temperature of each consumer, T_1 is the optimized supply temperature, T_{1S0} is the initial supply temperature, T_{1C} is a supply temperature correction which is calculated by the optimization module using the proposed method with the help of the simulation model.

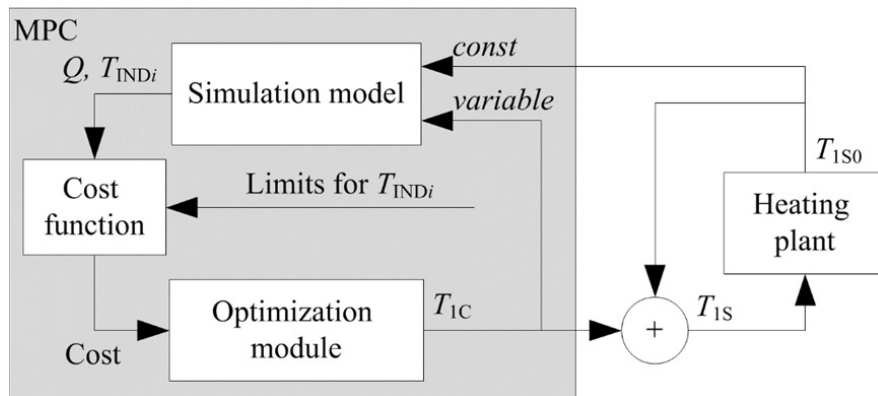


Fig. 4. The block diagram of model predictive control.

4. Simulation experiment

District heating model of the South Ural State University was used to validate the proposed optimization approach. Temperature optimization was performed for heating subsystem which includes 1 heating plant, 4 consumers with automated IHS and 3 consumers without automated IHS. Three outdoor temperature values were considered: $-10\text{ }^{\circ}\text{C}$, $-20\text{ }^{\circ}\text{C}$, $-30\text{ }^{\circ}\text{C}$. Three optimization scenarios were performed:

- Temperature optimization was not performed. Supply temperature was calculated using control curve of the heating plant depending on outdoor temperature.
- Temperature optimization was performed using Eq. 9 while priority coefficient α is equal 1. In this case the purpose of optimization performed is maximizing heat energy economy while maintaining the minimum indoor temperature requirements for each building.
- Temperature optimization was performed using Eq. 9 while priority coefficient α is equal 0.5. In this case the purposes of optimization performed are both maximizing heat energy economy and maintaining the most comfortable indoor temperature for each building.

Optimization and simulations are performed using block diagram language VisSim [20].

Table 1 represents the optimization results. It should be noticed that supply temperature optimization performed using the approach proposed affects consumers without automated IHS greater than consumers with automated IHS which have its own control curves. So, indoor temperature simulation results are under consideration in table 1 only for consumers without automated IHS.

Table 1. The optimization results.

Optimization scenario using simulations	Outdoor temperature, $^{\circ}\text{C}$	Without optimization according to heat plant control curve	Heat energy economy optimization ($\alpha=1$)	Heat energy economy and indoor temperature optimization ($\alpha=0.5$)	
Heating plant supply temperature T_{is} , $^{\circ}\text{C}$	-30	95.0	94.9	96.1	
	-20	85.0	80.0	81.0	
	-10	75.0	65.1	65.9	
Academic building 3-D (T_{IND} range is 20-24 $^{\circ}\text{C}$)	-30	20.2	20.2	20,7	
	-20	22.3	20.1	20,6	
	-10	24.3	20.0	20,4	
Indoor temperature for buildings without IHS, $^{\circ}\text{C}$	Hangars (T_{IND} range is 18-22 $^{\circ}\text{C}$)	-30	19.5	19.5	20,0
		-20	21.7	19.6	20,0
		-10	23.8	19.6	20,0
Valeology building (T_{IND} range is 20-24 $^{\circ}\text{C}$)	-30	20.1	20.0	20,5	
	-20	22.1	20.0	20,4	
	-10	24.1	20.0	20,4	
Total heat energy production Q , Gcal/h	-30	4.169	4.167	4.189	
	-20	3.454	3.367	3.384	
	-10	2.742	2.554	2.575	
Heat economy in the case of optimization, %	-30	-	0.06	-0.48	
	-20	-	2.54	2.02	
	-10	-	6.85	6.10	

The results show that more comfortable indoor temperature as a whole is reached using optimization which takes into account both indoor comfortable temperatures and heat energy economy requirements. But due to lower indoor temperature heat energy consumption is lower in the case of optimization which purpose is heat energy economy and maintaining of minimum comfort requirements.

5. Summary

The optimization method offered is of special interest for district heating systems where central temperature control strategy is applied and some facilities don't have their own automated IHS. The method allows calculating the heating plant supply temperature, which being maintained will result in the most comfortable indoor temperature of consumers in the heating system as a whole.

It is worth mentioning that the simulation model used to assess the heating system state variables can be designed and run in any simulation environment for physics and engineering involved in exchange of input data and results of heating plant and consumers simulation using a third party software.

Acknowledgements

This work was supported by the Federal Targeted Programme “Research and Development in Priority Areas of Development of the Russian Scientific and Technological Complex for 2014-2020” (14.577.21.0026, 05.06.2014) as a part of the project “Development of energy conservation real-time geographic information system for optimal controlling of thermal-hydraulic operating modes of municipal district heating systems” (2014-14-579-0003-035, RFMEFI57714X0026).

References

- [1] A. Nuorkivi, District heating and cooling policies worldwide, in: R. Wiltshire, *Advanced district heating and cooling (DHC) systems*, Woodhead Publishing, 2015, pp. 17–41.
- [2] H. Lund, S. Werner, R. Wiltshire, S. Svendsen, J.E. Thorsen, F. Hvelplund, B.V. Mathiesen, 4th Generation District Heating (4GDH) Integrating smart thermal grids into future sustainable energy systems, *Energy*. 68 (2014) 1–11.
- [3] M. Brand, A. Della Rosa, S. Svendsen, Energy-efficient and cost-effective in-house substations bypass for improving thermal and DHW (domestic hot water) comfort in bathrooms in low-energy buildings supplied by low-temperature district heating, *Energy*. 67 (2014) 256–267.
- [4] I. Olikar, Steam turbines for cogeneration power plants, *J. Eng. Power*. 102 (1980) 482–485.
- [5] H. Madsen, K. Sejling, H.T. Sogaard, O.P. Palsson, On flow and supply temperature control in district heating systems, *Heat Recovery Systems and CHP*. 14 (1994) 613–620.
- [6] B. Bohm, P.O. Danig, Monitoring the energy consumption in a district heated apartment building in Copenhagen, with specific interest in the thermodynamic performance, *Energy and Buildings*. 36 (2004) 229–236.
- [7] M. Iacob, G.D. Andreeanu, N. Muntean, SCADA system for a central heating and power plant, *Proceedings of the 5th International Symposium on Applied Computational Intelligence and Informatics*. Timisoara, 2009, pp. 159–164.
- [8] A. Zabasta, V. Sejmanovs, N. Kunicina, L. Ribickis, Wireless sensor networks for optimization of district heating, *Journal of Energy and Power Engineering*. 7 (2013) 1362–1369.
- [9] D. Shnayder, V. Abdullin, A WSN-based system for heat allocating in multi-flat buildings, 2013 36th International Conference on Telecommunications and Signal Processing. 2013, pp. 181–185.
- [10] G. Lukas, V. Swan, I. Ugursal, Modeling of end-use energy consumption in the residential sector: a review of modeling techniques, *Renewable and Sustainable Energy Reviews*. 13 (2009) 1819–1835.
- [11] J. Allegrinia, K. Orehounigb, G. Mavromatidisb, F. Rueschd, V. Dorerb, R. Evins, A review of modelling approaches and tools for the simulation of district-scale energy systems, *Renewable and Sustainable Energy Reviews*. 52 (2015) 1391–1404.
- [12] S. Lima, S. Parkb, H. Chungb, M. Kimc, Y. Baikd, S. Shin, Dynamic modeling of building heat network system using Simulink, *Applied Thermal Engineering*. 84 (2015) 375–389.
- [13] O.P. Palsson, H. Madsen, H.T. Sogaard, Predictor-based optimal control of supply temperature in district heating systems, *Proceedings of the International IFAC symposium on control of power plants and power systems*. Pergamon, Oxford, 1992, pp. 81–85.
- [14] G. Sandou, S. Oлару, Particle Swarm Optimization Based NMPC: An Application to District Heating Networks, *Nonlinear Model Predictive Control*. 384 (2009) 551–559.
- [15] T. Ostergaard, Return temperature optimization by use of smart meters and hydraulic calculations, *Proceedings from the 14th International Symposium on District Heating and Cooling*. Stockholm, 2014, pp. 549–552.
- [16] A. Gros, E. Bozonnet, C. Inard, M. Musy, Simulation tools to assess microclimate and building energy – A case study on the design of a new district, *Energy and Buildings*, *Energy and Buildings*, In Press.
- [17] D.A. Shnayder, V.V. Abdullin, A.A. Basalaev. Building heating feed-forward control method and its application in South Ural State University academic building , *Transactions on Engineering Technologies, World Congress on Engineering and Computer Science 2014*, Springer Netherlands, 2015, pp. 69–84.
- [18] M.V. Shishkin, D.A. Shnayder, Simulation of thermal-hydraulic systems in VisSim environment, *Bulletin of the South Ural State University, Series Computer Technologies, Automatic Control, Radio Electronics*, 9 (2004) 120–123.

- [19] A.A. Basalaev, Distributed simulation modeling of district heat supply system in VisSim, Bulletin of the South Ural State University, Series Computer Technologies, Automatic Control, Radio Electronics, 13 (2013) 82–87.
- [20] D. W.J. Pulle, P. Darnell, A. Veltman, Applied control of electrical drives, real time embedded and sensorless control using VisSim™ and PLECS™, Springer International Publishing, 2015.



International Conference on Industrial Engineering

Recognition of the fault regimes for the remote electrical objects

Nagay I.V., Nagay V.I., Kireev P.S.*

Platov South-Russian State Polytechnic University (NPI), 132, St. Prosvescheniya, Rostov region, Novocherkassk, 346428, Russian Federation

Abstract

This issue is urgent. Russian 6 to 110 kV electric networks are among the most widespread and extended and supply power to both industrial and municipal customers. It is a frequent case that networks of the voltage classes are based on the radial principle that simplifies the relay protection and automation (RPA), but at the same time the use of a simple technical solutions is problematic in terms of technical and informational performance as compared to solutions of higher voltage class networks. This is particularly evident in the backup protection design.

Herein are proposed solutions. Expanding the knowledge base of relay protection and the use of adaptive principles in design thereof can solve the abovementioned problems. The paper discusses the issues of improving the sensitivity of relay protection with the relative selectivity that ensures recognition of fault for the electrical "remote" objects. This approach is discussed as an example of relaying electrical networks, which include overhead lines and transformers. Increase in the number of monitored parameters in addition to the information signs in some cases can prevent damage and eliminate the "dead" zone with the fault recognizability effect.

© 2015 The Authors. Published by Elsevier Ltd. This is an open access article under the CC BY-NC-ND license (<http://creativecommons.org/licenses/by-nc-nd/4.0/>).

Peer-review under responsibility of the organizing committee of the International Conference on Industrial Engineering (ICIE-2015)

Keywords: "Relay protection; short circuit; selectivity; high-speed activity; transient resistance; electrical arcs."

1. Main text

Assessment of the informational signs, that characterize the reporting regime, such as the electrical distribution network shown in Fig. 1, is needed to solve the problem of recognition of phase fault with transient resistance of the electric arc (EA). Remote backup protection (RBP) are connects to current transformers TA1 and voltage

* Corresponding author. Tel.: +7-863-525-5291; fax: ..+7-863-525-5291.

E-mail address: nagayiv@mail.ru

transformers TV1 on the side of power supply substation and provides monitoring of the currents and voltages and their components (symmetric, orthogonal, emergency, etc.). Local backup protection (LBP) is installed on the branch or intermediate substation and provides monitoring of the currents, voltages from the higher and lower voltage sides, neutral current, as well as, for example, the luminous flux inside the compartments complete switchgear low voltage side. This allows to expand the information base of local backup protection compared with RBP.

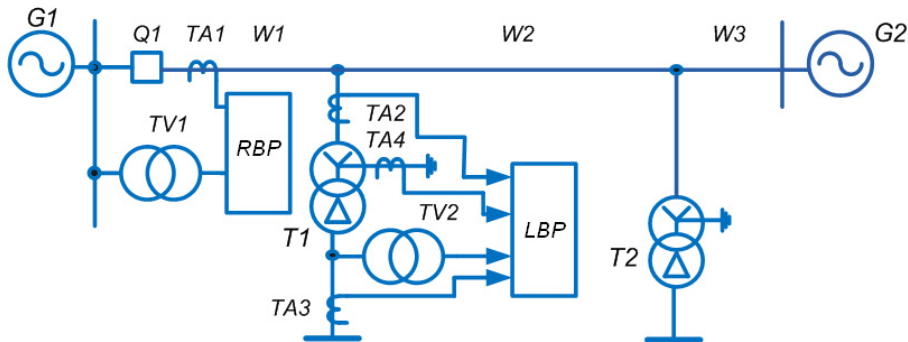


Fig. 1. Explanatory scheme of remote and local backup protection in the electrical network with branch substation.

It is necessary to specify ranges of parameters of informational signs of this type of fault on the base of the proposed classification for the minimization of the impact of the transient resistance on the functioning of the RBP and LBP: the increase in the active component and the stability of the reactive component of resistance of the short circuit chain, non-stationary EA processes, the presence of higher harmonics and symmetrical components in the current and voltage, the evolving nature of the fault, the presence of the luminous flux from the column of EA.

Transient resistance of electric arc is an active character and its presence leads to a reduction of current modules and current arguments [1-12]. This causes an increase in the total resistance of the short circuit. Modules of the current of the short circuit are reduced to 80% of the current level of the metal short circuit (SC), the value of the argument is reduced to a value $0,6\varphi_{MSC} = 55^\circ \div 60^\circ$, and transient resistance reaches values $0,6Z_T$, when the voltage on the electric arc changing $U_t = U_a = (0 \div 0,3)U_{nom}$.

Transient resistance of EA that representing the non-linear resistance for phase short circuit, causes the appearance of the higher harmonic components (HHC) in voltages and currents. Currently, the use of HHC is not widely used to recognize the arc fault, and it led to these studies.

Many factors affects the EA process [1,3-9]: airflow, electrodynamic effects, changes in the electrical conductivity of the medium, temperature changes, etc. There are as an extension of the arc column and its shortening by grafting individual sections with subsequent inflating by the air streams when electric arc is burning.

Non-stationary processes arc appears in one period of industrial frequency and from period to period. The voltage drop on the arc columns of the various phases are not the same, that causes the appearance of asymmetry. It marked hysteretic current-voltage characteristics of an electric arc "phase voltage - phase current". Changes in arc length results in a change of the voltage drop on it $U_a = E_a I_a$. It is reason of change of the short circuit resistance, modules and arguments of the current, as discussed in [13-16], i.e. signal parameters controlled by the RBP and LBP are changing because the process of high-voltage electrical arc is non-stationary, it is a sign of an arc fault.

Process EA may be associated with the movement of the arc column under the influence of air flow, electrodynamic forces on electrical parts and with changing of the type of fault. Single-phase ground fault can develop into a double-circuit to ground, and the next stage due to the small distances between under-voltage parts on the side of low voltage of 6-10 kV protected transformer develop in a phase to phase fault.

Two-phase short circuit is accompanied by the appearance of symmetrical components of negative sequence, that allows to effectively provide for the recognition of short-circuit for the protected transformer, especially when it designed coils' star - delta "[13]. If it SC switches to a three-phase short-circuit, asymmetry not disappears due to inequality of the lengths of arcs and possible their combustion between the outer and middle phases [13-16]. At the

same time negative sequence current reducing and can be about (10 ÷ 15)% of the current of the three-phase short-circuit for the transformer [13-16].

Authors of the article noted, when they had field tests on substations 110/10/6 kV, that zero sequence voltage $3U_0 \leq 500$ appeared when it was phase fault with an electrical arc in electrical cabinet design of 6-10 kV.

Solutions.

Authors offers some ways for recognition of the arc SC [11–20]:

- cooperative monitoring of the current modules and the current arguments, their fault components, resistance (fault component);
- monitoring of the presence of negative sequence current and it values;
- monitoring of the higher harmonic components of the voltage;
- monitoring of the change of the type of the fault (single-phase ground fault, two-phase short-circuit, three-phase short circuit), and non-stationary process of arc column ;
- monitoring of the luminous flux in conjunction with the current, especially in the electrical switchgear.

It should be noted that the proportion of higher harmonics in the current is not more than 5% of the first harmonic component of the current of the short-circuit. Calculation of the fault components of the current and voltage at the installation site protection, including the harmonic components of the signal, is possible, if transient resistance of the arc in the fault on the low voltage side of the transformer of the branch substation presents in the form of a non-linear resistance [3-7].

Authors developed a mathematical model of the electrical network by the software package Mathcad (Fig. 2) to determine the harmonic components in the presence of non-linear transient resistance, that depends on the instantaneous values of voltage and current.

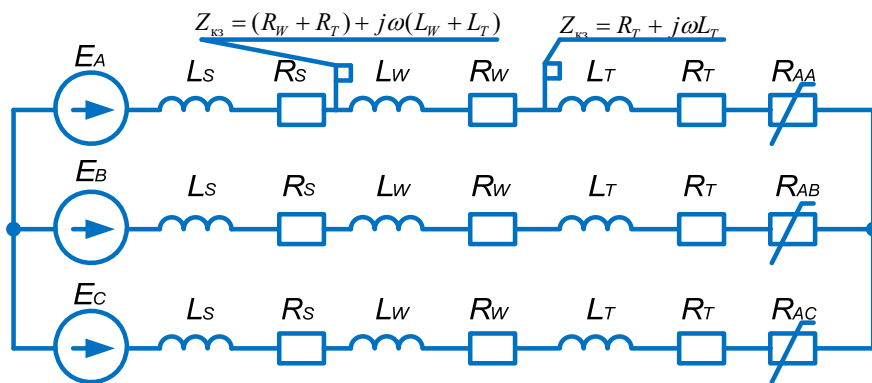


Fig. 2. The equivalent circuit scheme of 110 kV network "power supply - overhead line - transformer with resistance of electric arc".

The current-voltage characteristics (CVC) of the electric arc described by the ascending and descending branches in form of straight lines in the field of the non-self discharge [3-7,14-16].

$$u_{a,a} = i_a U_s / I_s \text{ и } u_{a,d} = i_a U_q / I_q, \tag{1}$$

It can be assumed in the area of self discharge that the change in voltage on the electric arc is exponential and is described by the following expressions:

$$u_{a,a} = U_{min} + (U_s - U_{min}) e^{-3(i_a - I_s)/(I_{max} - I_s)} \text{ at } i_a \geq 0, \tag{2}$$

$$u_{a,d} = U_{\min} + (U_q - U_{\min}) e^{-3(i_a - I_q) / (I_{\max} - I_q)} \text{ at } i_a \leq 0, \tag{3}$$

The simulation results were used to determine the optimal set of information signs of harmonic components and the sensitivity analysis of the measurement signals of different harmonics as the distance of the observer from the fault location to the power source. Values of the relative magnitude of voltage different harmonics (base quantities take the voltage fundamental harmonic of 50 Hz) are shown in Fig. 3. Relay protection device (conditional observer - the figure represented by the symbol Γ) could be in different locations of the equivalent circuit. Removes the observer from the point of fault have been assessed on the basis of the ratio $k = 1 - Z_{sc} / Z_{\Sigma eq}$, where $Z_{sc} = (R_W + R_T) + j\omega(L_W + L_T)$ – resistance of the branches that current flows from the observer to the place of fault.

Greatest amplitude signals have the first, third, fifth, sixth and seventh harmonics. Comparison algorithm of the sum of the quantities of harmonic voltage components in fault location with the value of the voltage fundamental can be implement for identifying transient resistance. Comparison of the sum of the quantities of harmonic voltage components in fault location with the magnitude of the voltage fundamental harmonic conducted for the frequency range from 100 Hz to 750 Hz at a distant observer from the source to the point of fault $k = 0.1 \div 0.995$.

Development of changes in the sum of voltage values of harmonic components in the short circuit site for the frequency range from 100 Hz to 750 Hz at a distant observer from the source to the point of fault $k = 0.1 \div 0.995$ is showed that the quadratic sum of a small deviation from the actual voltage value of the first harmonic $U_{\Sigma quad*} = 1.0 \div 1.08$, and the algebraic sum has advantages for detection transient resistance in the short circuit - $U_{\Sigma alg*} = 1.0 \div 1.71$. Using the algebraic sum of the harmonic components of the voltage in the monitoring location has the advantage compared with the parameter of the quadratic sum, because it varies considerably larger, for example, for values $k > 0,9$, that corresponds to an approaching of the observer to the fault site exceeds the maximum of the quadratic sum of the voltage harmonics of 1.7.

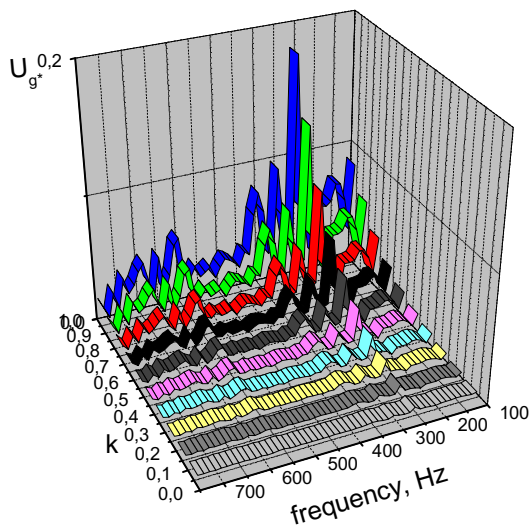


Fig. 3. The harmonic structure of a voltage at the protection installation site at a relative electrical distance from the protection installation to the fault.

Additional information sign of the three-phase asymmetric short circuit is change of the ratio of the frequency structure of the voltage at the point of observation (installation site protection) when type of short-circuit is

changing, for example, if one of the three arcs is shunting and burning of two arcs between the middle and edge phase wires after that. For example, there are changing the ratio between the third, fifth and seventh harmonics.

Ratio of the information sign of voltage harmonics are changing $|U_5|/|U_7|=1,27 \div 2,6$, $|U_6|/|U_3|=0,61 \div 2,31$, $|U_7|/|U_6|=1,47 \div 0,77$, $|U_5|/|U_3|=1,15 \div 4,66$ when arc resistance R_{AB}/R_{BC} are changing from 0,5 to 2 and R_{BC} is permanent resistance.

Conclusion

It defines the basic information signs of arc short-circuit: increase of the currents active component and their components; the presence of the higher harmonic components in the voltage; non-stationarity of the short circuit processes; the appearance of asymmetry at the three-phase faults with negative sequence current, that magnitude reaching 15% of the current of the metal short-circuit; appearance of the voltage zero sequence on the low voltage side of the protected transformer up to 500 V; the evolving nature of the fault "a single-phase circuit - a two-phase short circuit - three-phase short circuit", "two-phase short circuit - three-phase short circuit"; appearance of the light flux from the arc column, that represents the emitter.

There are founded most informative higher harmonic components of voltage for three-phase symmetrical and asymmetrical short circuit arc. The modules of the second, third, fifth, sixth and seventh harmonics are within the range (7,5÷18)% of the first harmonic component of the fault site.

This work was performed under the Agreement № 14.579.21.0083 with the Russian Ministry of Education.

Nomenclature

U_t	voltage on the transient resistance
U_a	voltage on the arc
U_{nom}	nominal network voltage
φ_{MSC}	current argument of the metal SC
Z_T	transformer resistance
E_a	electric field strength of the arc column
l_a	length of the arc column
$u_{a,a}$	voltage on the ascending branch
$u_{a,d}$	voltage on the descending branch
U_s	ignition voltage
U_q	voltage with quenching the arc
I_s	ignition current
I_q	current with quenching the arc
U_{min}	minimum value for the arc column
$Z_{\Sigma eq}$	equivalent resistance of the short circuit
R_w	resistance of the overhead line
L_w	inductance of the overhead line
R_T	resistance of the transformer
L_T	inductance of the transformer
R_S	resistance of the system
L_S	inductance of the system
E_A	voltage of the power sources phase A
E_B	voltage of the power sources phase B
E_C	voltage of the power sources phase C

References

- [1] G. Ziegler, Digital Distance Protection: Principles and applications, Translation from English. ed. Dyakova A.F., Energoatomizdat, Moscow, 2005.
- [2] E.M. Schneerson, Digital relay protection, Energoatomizdat, Moscow, 2007.
- [3] V.V. Bursdorf, Open electric arc high power, *Electricity*. 10 (1948) 15–23.
- [4] G.V. Butkevitch, Arc processes during switching circuits, Higher.sch., Moscow, 1967.
- [5] Y.M. Dolinskiy, V.P. Boiko, N.N. Sereda, Power arc fault in enclosed switchgear, *University news. Electromechanics*. 2 (1990) 102–108.
- [6] V.V. Zhukov, A. Dalla, Calculation of the electric arc resistance, *Electricity*. 1 (1990) 29–30.
- [7] V.V. Zhukov, Calculation of short-circuit currents, taking into account changes in the parameters of the short circuit, *Power Stations*. 6 (2000) 36–42.
- [8] V.V. Zhukov, Change of the parameters for overhead lines with short circuits, *Power Stations*. 5 (2000) 44–51.
- [9] A.S. Maykopar, Arc faults on overhead lines, *Energia*, Moscow, 1965.
- [10] S. Ulyanov, Electromagnetic transients in power systems, The textbook for higher educational institutions in the electric power industry, Energy, Moscow, 1970.
- [11] I.V. Nagay, Accounting for the influence of feeding on the transient resistance at the fault location after the transformer of the tapping substations, *University news. Electromechanics*. 2 (2012) 110–113.
- [12] I.V. Nagay, V.V. Nagay, Correction of the impact of the electric arc at the fault location site, *Modern power systems and complexes and management, Proceedings of the V international scientific-practical. conf., South. Rus. state. tehn. University (NPI), Novocherkassk, SRSTU (NPI)*. 2 (2005) 37–39.
- [13] V.V. Nagay, Analysis of the recognizability of asymmetric short circuits in the side of lower voltage of transformers of tapping and intermediate substations, *University news. Technical sciences, Special edition*. (2003) 46–49.
- [14] V.I. Nagay, Relay protection of the tapping substation in the electric networks, Energoatomizdat, Moscow, 2002.
- [15] I.V. Nagay, Providing Remote Backup Function of Relay Protection of Transformers in the Direct and Quadrature Axis Dissymmetry, *Proceedings of the 6th International Scientific Symposium on Electrical Power Engineering ELEKTROENERGETIKA 2011, Stara Lesna, Slovak Republic*. (2011) 266–269.
- [16] I.V. Nagay, V.I. Nagay, Problems and solutions for remote backup of the transformer on the tapping and intermediate substations, *Releyschik*. 4 (2009) 30–35.
- [17] E.P. Figurnov, Relay protection, Textbook in 2 parts. Part 2, SEI "Educational-methodical center on education on railway transport», Moscow, 2009.
- [18] A.V. Bogdan, M.J. Kletsel, K.I. Nikitin, Adaptive backup current protection of lines with branches, *Electricity*, Moscow. 2 (1991) 51–54.
- [19] Y.S. Kuznik, Possibilities for most remote backup transformer protections, *Power Station*, Moscow. 10 (1994) 49–53.
- [20] G.S. Hakopyan, Remote backup device for short circuit trip, *Power Station*, Moscow. 9 (2001) 51–52.



International Conference on Industrial Engineering

Methods of assessing information signs describing the regimes of electrical networks

Nagay V.I., Nagay I.V., Sarry S.V.*

Platov South-Russian State Polytechnic University (NPI), 132, St. Prosvescheniya, Rostov region, Novocherkassk, 346428, Russian Federation

Abstract

Creation of brand-new highly intelligent systematic and distribution electric grids in the Unified Energy System of Russia (intelligent grid - Smart Grid) is considered a priority of scientific and technical progress in the electricity industry according to the Energy Strategy of Russia for the period up to 2030. The concept of «Smart Grid» includes above all providing automated energy accounting; creation of intellectual protection and control; including alternative sources in the network of distributed power generation.

One of the most important elements of modern electrical network is relay protection that provides localization of the damaged equipment for all possible fault regimes and minimize the amount of damage while maintaining the stability of the rest of the grid. The power system as a source and consumers with varying power consumption renders recognizing the fault regimes problematic due to various interfering factors, i.e. startups and self-startups of powerful electric motors, transformers switching to idle mode, large power flows on the transit lines, and the transient resistance of the electric arc at the fault location.

Creation of state-of-the-art high-intelligence devices for relay protection at the stage of their development requires to verify functioning algorithms and to assess their ability to recognize the fault regime against the background of acceptable regimes. There has been developed a method for assessing information signs describing the regimes of electric networks with linear and polynomial decision functions. The article also proposes criteria for assessing information signs from the perspective of separating regime recognition areas. The authors discuss ways to build recognition systems in relation to relay protection of electric networks.

© 2015 The Authors. Published by Elsevier Ltd. This is an open access article under the CC BY-NC-ND license (<http://creativecommons.org/licenses/by-nc-nd/4.0/>).

Peer-review under responsibility of the organizing committee of the International Conference on Industrial Engineering (ICIE-2015)

Keywords: electrical networks; relay protection; information sign; normal and fault regime; short circuit; recognition.

* Corresponding author. Tel.: +7-863-525-5291; fax: +7-863-525-5291.
E-mail address: nagayiv@mail.ru

1. Introduction

The subject of this work is to develop a methodology for assessing the information signs describing the regimes of electrical networks, and testing its effectiveness for detecting fault and acceptable regimes by relay protection (RP). It can be used signals from the sensors of electric and non-electric quantities for modern relay protection. Signals of electrical quantities are current and voltage, that are proportional, respectively, to currents and voltage high-voltage electrical network. Signals non-electrical quantities are signals from optical sensors, temperature sensors, pressure sensors, position sensors switching devices and others.

Part information signs is characteristic of only one type of mode: normal, abnormal, fault, and the other part is typical of all types and have different or partially common value ranges of monitored parameters. Recognition of fault regimes against the background of confounding factors in acceptable conditions is one of the basic properties of relay protection – sensitivity. Use of traditional algorithms is not always possible to recognize an fault, so it needs to develop new multiparameter algorithms for operation of relay protection systems [1,2]. It needs to develop new algorithms that implement the principle of protection of multiparameter [3]. Authors suggest (developed) assessment methodology information signs describing the modes of electrical networks for the recognizability of alternative regimes and enhancing the effectiveness of the RP.

2. Main Part

The main stages of assessment information signs describing the regimes of electrical networks and their recognizability based on the proposed method in this paper, are presented in Fig. 1.

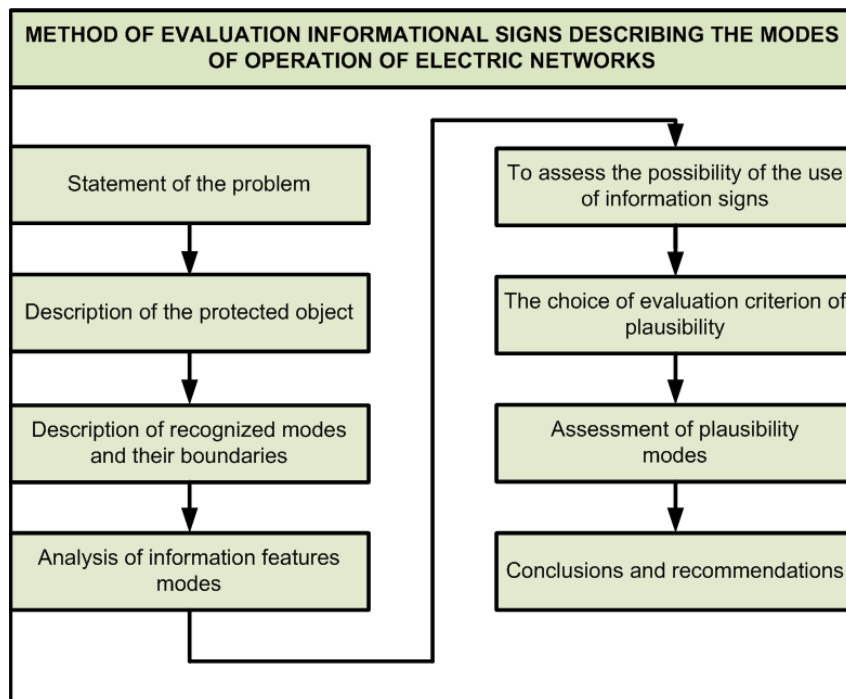


Fig. 1. Methods of assessing the information signs describing the regimes of electrical networks and their recognizability.

Stages, that are previous to assessment of recognizability of regimes: formulation of the problem and development of the system requirements of relay protection, the description of the protected object and its basic regimes of operation. Next, it needs to perform a preliminary assessment and analysis of information signs of

regimes, formation criterion of recognizability and final assessment of the sensitivity of the RP. At the final stage it formulates conclusions and recommendations on the establishment of a system of relay protection and the efficiency of its use at the object.

3. Selection criteria for assessment of the recognizability of regimes of electrical network

The use of the criterion of recognizability of fault and alternative regimes is provided to quantify the information signs describing the regimes of electric network. Application of the criterion allows us to formulate a conclusion about the effectiveness of a particular characteristic or group information signs. The conclusion is made after the investigation of areas of information signs on the basis of the results of calculation and simulation regimes for considered network [4-11].

The areas of the regime are displayed graphically on a plane or in any other way, and then it determines the smallest distance between the nearest points belonging to the area of fault and alternative regimes.

Monitored signals for backup protection in the multidimensional space of information signs can be formed, for example, [3, 12-18]:

$$\begin{aligned} \dot{F}_j(\dot{U}_i, \dot{I}_i, \dot{U}_{is}, \dot{I}_{is}, \Delta \dot{U}_i, \Delta \dot{I}_i, \Delta \dot{U}_{is}, \Delta \dot{I}_{is}) = & \dot{A}_j(\dot{U}_i, \dot{I}_i) + \dot{B}_j(\dot{U}_{is}, \dot{I}_{is}) + \\ & + \dot{C}_j(\Delta \dot{U}_i, \Delta \dot{I}_i, \Delta \dot{U}_{is}, \Delta \dot{I}_{is}) \end{aligned} \quad (1)$$

where $\dot{A}_j(\dot{U}_i, \dot{I}_i)$, $\dot{B}_j(\dot{U}_{is}, \dot{I}_{is})$, $\dot{C}_j(\Delta \dot{U}_i, \Delta \dot{I}_i, \Delta \dot{U}_{is}, \Delta \dot{I}_{is})$ – signals, depending on the arguments module voltages and currents applied to the protection, their orthogonal components $\dot{U}_{is}, \dot{I}_{is}$, and fault components $\Delta \dot{U}_i, \Delta \dot{I}_i, \Delta \dot{U}_{is}, \Delta \dot{I}_{is}$, $d(\dot{U}_i, \dot{I}_i, \dot{U}_{is}, \dot{I}_{is}, \Delta \dot{U}_i, \Delta \dot{I}_i, \Delta \dot{U}_{is}, \Delta \dot{I}_{is})$ – the distance between the recognizable regimes. This condition $F_{ja}(\dot{U}_i, \dot{I}_i, \dot{U}_{is}, \dot{I}_{is}, \Delta \dot{U}_i, \Delta \dot{I}_i, \Delta \dot{U}_{is}, \Delta \dot{I}_{is}) \rightarrow \max$ must hold in the field of fault regime and it condition $F_{jh}(\dot{U}_i, \dot{I}_i, \dot{U}_{is}, \dot{I}_{is}, \Delta \dot{U}_i, \Delta \dot{I}_i, \Delta \dot{U}_{is}, \Delta \dot{I}_{is}) \rightarrow \min$ must hold in the field of load regime [13,14], and

$$\begin{aligned} & \left| \dot{F}_{ja}(\dot{U}_i, \dot{I}_i, \dot{U}_{is}, \dot{I}_{is}, \Delta \dot{U}_i, \Delta \dot{I}_i, \Delta \dot{U}_{is}, \Delta \dot{I}_{is}) - \dot{F}_{jh}(\dot{U}_i, \dot{I}_i, \dot{U}_{is}, \dot{I}_{is}, \Delta \dot{U}_i, \Delta \dot{I}_i, \Delta \dot{U}_{is}, \Delta \dot{I}_{is}) \right| > \\ & > \Delta G_j(\dot{U}_i, \dot{I}_i, \dot{U}_{is}, \dot{I}_{is}, \Delta \dot{U}_i, \Delta \dot{I}_i, \Delta \dot{U}_{is}, \Delta \dot{I}_{is}), \end{aligned} \quad (2)$$

$$\Delta G_j(\dot{U}_i, \dot{I}_i, \dot{U}_{is}, \dot{I}_{is}, \Delta \dot{U}_i, \Delta \dot{I}_i, \Delta \dot{U}_{is}, \Delta \dot{I}_{is}) = \sqrt{N^{-1} \sum_{S=1}^N d^2(\dot{U}_i, \dot{I}_i, \dot{U}_{is}, \dot{I}_{is}, \Delta \dot{U}_i, \Delta \dot{I}_i, \Delta \dot{U}_{is}, \Delta \dot{I}_{is})}, \quad (3)$$

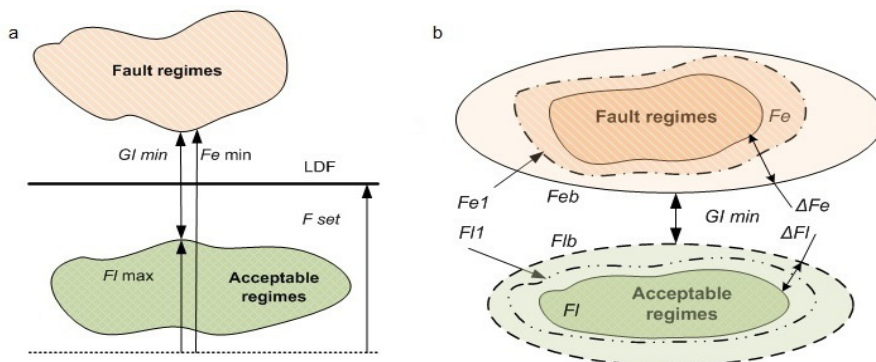


Fig. 2. The choice of the settings of relay protection and assessment of recognition of fault regimes using (a) linear decision functions; (b) polynomial decision functions.

Choice of criterion of the recognizability is illustrated at Fig. 2, which shows the acceptable and fault regimes.

The criterion of recognizability of fault regimes and acceptable regimes with using linear decision functions is the fulfillment of the conditions to achieve the required minimum distance between the regimes $GI_{\min} = F_{f \min} - F_{l \max} \geq (k_s k_{sa} - 1) F_{l \max}$, where $k_s = F_{l \min} / F_{set} \geq (1,2 \div 1,5)$ – the coefficient of sensitivity, k_{sa} – a safety factor, that taking into account the set of possible errors in the determination of areas of the sign and in the measurement of parameters of information sign by the relay protection.

It is intended to cover areas of the recognized regimes by some closed surface and assess the possibility of their separation on the criterion of minimum distance between the boundary regions (Feb and Flb) for using polynomial decision functions. The boundary region must absorb the acceptable and fault regimes Fe1 and Fl1, that is transformation of the initial areas Fe and Fl, taking into account possible errors in the simulation and measurement. The maximum margin of error (unbalance) can be $Fimb = \Delta Fe + Fl$ and minimum distance between the boundary regions modes must be at least $Gmin \geq ksa Fimb$.

It shown for example the starting regime and short-circuit for the transformer 6,3-16 MVA, that connected to radial overhead line with branches [19-21]. It monitors reactive components of the currents and their increments (fault components) (Fig. 3).

The minimum distance GI and $G\Delta I$ between areas of start-up regime (1, 2) and short-circuit (3, 4) is determined in the basis of the current of the metal short-circuit I_{k0} for the minimum power transformer on the branch substation:

$$GI = \frac{1}{Ik0} \sqrt{(|\dot{I}_{LITk}| \sin(\phi_{LITk}) - |\dot{I}_{LITkp}| \sin(\phi_{LITkp}))^2 + (|\dot{I}_{LITk}| \cos(\phi_{LITk}) - |\dot{I}_{LITkp}| \cos(\phi_{LITkp}))^2} \tag{4}$$

$$G\Delta I = \frac{1}{Ik0} \sqrt{(|\Delta I_{FTk}| \sin(\phi_{\Delta I_{FTk}}) - |\Delta I_{FTp}| \sin(\phi_{\Delta I_{FTp}}))^2 + (|\Delta I_{FTk}| \cos(\phi_{\Delta I_{FTk}}) - |\Delta I_{FTp}| \cos(\phi_{\Delta I_{FTp}}))^2} \tag{5}$$

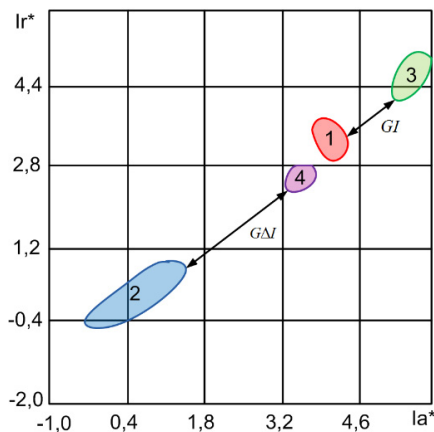


Fig. 3. Areas of the fault regime and the start-up regime for the electric transformer on the branch substations on the plane "reactive component I_r^* – active component of current I_a^* " for the measuring elements, that controlling components and full increment (fault component): 1- I_{LITkp} , 2- ΔI_{FTp} , 3- I_{LITk} , 4- ΔI_{FTk} .

It should be noted that in the above example, the distance between the start-up regime area and short-circuit regime area are almost twice the similar distance between the areas in the monitoring of the full component of the

currents (the base adopted for the nominal current of the protected transformer), if it is using the fault reactive current components.

A second example of the proposed method can be a problem of recognition of the fault regimes of two-phase short-circuit and a three-phase short-circuit with the transient resistance of electric arc with unequal lengths of [19-21].

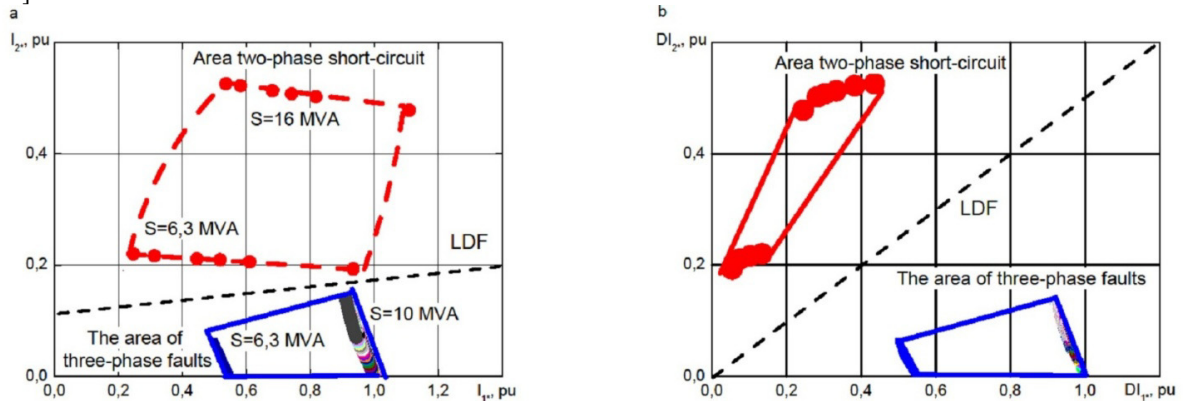


Fig. 4. The areas of two-phase and three-phase fault for transformer of the branch substation on the plane "negative sequence current – positive current sequence" for measuring elements that measures the (a) complete components; (b) increment (fault components).

The presence of asymmetry in the three-phase short-circuit for the transformers of different capacities (6.3, 10.0 and 16 MVA) does not permit a linear decision function between the areas of the two-phase and three-phase short-circuit (Fig. 4a) on the plane of the positive I_{1*} and negative sequences I_{2*} current in the base of current I_{k0} . The minimum distance between these regimes does not exceed 5% of the current I_{k0} . Using the fault components (Fig. 4b) DI_{1*} and DI_{2*} leads to a positive result and the possibility of the division of areas of recognized regimes. The minimum distance between the regime areas is not less than 38% of the current I_{k0} .

This work was performed under the Agreement № 14.579.21.0083 with the Russian Ministry of Education.

Conclusion

There is method for assessing the information signs, that are describing the regimes of electrical networks using linear and polynomial decision functions.

There is proposed criterion for assessment of information signs from the perspective of the separation of areas recognized regimes.

It are shown methods of designing of systems of pattern recognition applied to the relay protection of electric networks.

There is shown the effectiveness of the proposed methodology to determine the possibility of recognition of the regimes of motors start-up (self) and two-phase and three-phase short-circuit for the transformer on the branch substations.

A more effective division of acceptable and fault regimes is achieved by using increments of monitored signals, symmetrical components of the currents, it orthogonal components.

Nomenclature

ΔG_j	measure of proximity between recognizable regimes
N	number of regimes
$F_{l\max}$	maximum value of the information sign in a acceptable regime
$F_{f\min}$	minimum value of the information sign in the fault regime
F_{set}	value of the parameter of information sign for recognition of the regime
I_{LITkp}	motor starting current for the transformer
I_{LITk}	current of the short-circuit for the transformer
ΔI_{FTp}	increment of motor starting current for the transformer
ΔI_{FTk}	increment of current of the short-circuit for the transformer
φ_{LITk}	argument of the current of the short-circuit for the transformer
φ_{LITkp}	argument of the motor starting current for the transformer
$\varphi_{\Delta I_{\text{FTk}}}$	argument of the increment of current of the short-circuit for the transformer
$\varphi_{\Delta I_{\text{FTp}}}$	argument of the increment of motor starting current for the transformer

References

- [1] Actions to prevent the propagation of accidents involving insufficiently effective remote backuping, Collection of materials for operation of power systems, P.4.19, Electrical part, Energoatomizdat, Moscow. (1981) 91–94.
- [2] Department of Science and Technology of RAO UES Information letter IP 1-96 (e) of 30.09.96 y., About improvement of local and remote backup of the operating of the RPA devices in the electrical distribution networks 6-110kV, Energy, Moscow. 2 (2013) 18–21.
- [3] I.V. Nagay, V.I. Nagay, Designing of the multiparameter backup protection of electrical distribution networks 6-110kV, Energy, Moscow. 2 (2013) 18–21.
- [4] E.V. Podgorny, A.G. Ksyunin, V.I. Lyutkevich, Standard curves to calculate the inrush current of power transformers, University news. Electromechanics. 4 (1969) 376–379.
- [5] I.F. Maruda, A method for providing selective overcurrent protection zero sequence, Electricity, Moscow. 9 (2000).
- [6] V.A. Semenov, Assessment of the action of distance relay with the transient resistance in a short circuit, Power Stations, Moscow. 6 (1962) 81–83.
- [7] V.A. Semenov, About assessment of the resistance of an electric arc in the analysis of the action of the distance relay, Power Stations, Moscow. 8 (1961) 69–70.
- [8] M.A. Shabad, Protection of the transformers in the distribution networks, Energoatomizdat, Leningrad, 1981.
- [9] I.V. Nagay, Accounting for the influence of feeding on the transient resistance at the fault location after the transformer of the tapping substations, University news. Electromechanics. 2 (2012) 110–113.
- [10] I.V. Nagay, Adaptive backup protection in electric distribution grid, Elektroenergetika 2010, Proceedings of the 5th International Scientific Symposium on Electrical Power Engineering, Varna, Bulgaria. (2010) 367–371.
- [11] V.A. Rubinchik, Backup of short circuit trip in electrical network, Energoatomizdat, Moscow, 1985.
- [12] L. Devroye, L. Györfi, G. Lugosi, A Probabilistic Theory of Image Recognition, Springer-Verlag, New York, 1996.
- [13] A.L. Gorelik, V.A. Skripkin, Methods of recognition, Proc. allowance, Higher. HQ., Moscow, 1984.
- [14] A.E. Lepsky, A.G. Bronevich, Mathematical methods of image recognition, Lectures, Publishing house of the TTI SFU, Taganrog, 2009.
- [15] W. Grenander, Lectures on the theory of images, Mir, Moscow, 1979.
- [16] R. Duda, P. Hart, Image recognition and scene analysis, Mir, Moscow, 1976.
- [17] E. Patrick, Fundamentals of image recognition theory, Sov. Radio, Moscow, 1980.
- [18] J. Tu, R. Gonsales, Principles of image recognition, Mir, Moscow, 1978.
- [19] I.V. Nagay, Formation of the characteristics of operation of backup protection of overhead lines with branches, University news. Electromechanics. 2 (2011) 56–61.
- [20] I.V. Nagay, P.S. Kireev, Modeling of the load regimes of the branch substation, University news. Electromechanics. 2 (2012) 100–102.
- [21] V.I. Nagay, Relay protection of the tapping substation in the electric networks, Energoatomizdat, Moscow, 2002.



International Conference on Industrial Engineering

Comparative analysis of wind turbine control strategies

Martyanov A.S.^{*}, Martyanov N.A., Anikin A.S.

South Ural State University, 76, Lenin Avenue, Chelyabinsk, 454080, Russian Federation

Abstract

An article describes a comparative analysis of windmill control strategies based on computer modelling in Matlab/Simulink software. For the research purposes, the mathematical windmill model we developed consisted of a wind turbine, an electric generator, an electric power converter, and an accumulator battery. The main feature of the proposed model is the universal charge controller module operating under the control of different algorithms written in a high-level programming language. The model imitates three different control strategies. The main comparative criterion of windmill efficiency is the power coefficient, i.e. the ratio of the generated electric power to the aerodynamic wind power. The testing setup was equipped with a windmill controller developed for operation under the control program that supports different control strategies. Results showed the best control strategy is to maintain the optimal tip-speed ratio, and all the results can now be applied to other types of wind turbines.

© 2015 The Authors. Published by Elsevier Ltd. This is an open access article under the CC BY-NC-ND license (<http://creativecommons.org/licenses/by-nc-nd/4.0/>).

Peer-review under responsibility of the organizing committee of the International Conference on Industrial Engineering (ICIE-2015)

Keywords: renewable energy, wind turbines, wind generation systems, control strategies, variable speed control, power optimization.

1. Introduction

At the present time, because of ecological problems and due to limitation of natural energy sources the renewable energy becomes widespread and more popular competing with gas and oil energy extracting technologies. Concerning the renewable energy sources, the most developing technology is the wind energy. Modern wind turbine stations and windmill farms compile the complex system for electricity generation [21]. And research and investigation of such systems is not possible without modern mathematical theory operating on powerful computers and calculation clusters [5]. Usually this problem can be solved by numeric methods in mathematics [19] with the help of proper software operating on high-speed computers [11].

^{*} Corresponding author. Tel.: +7-902-600-2557;
E-mail address: martyanov_andrey@mail.ru

In wind energy industry during the developing of constructions, aerodynamic and mechanical properties there is a demand on improvement of operation control in a wide range of wind speed [1]. Many well-known researchers published their results about windmill speed control [1, 2, 3, 6, 7, 15, 16] in order to improve the efficiency of electric energy generation. Thus, the task of improvement of wind turbine efficiency by using the optimal control strategy is important part of scientific problem of renewable energy cost reduction [20].

Main reason to use the different wind turbines control strategies is the fact that the wind speed varies in time and the rotation speed of wind turbine should follow the wind speed in order to extract the maximum power [4]. Now there are several basic control strategies of windmill what are wide-spread:

- working at the constant rotation speed of wind turbine in a wide range of wind speed [17];
- working at step-fixed rotation speed of wind turbine in order to expand the wind speed range where the windmill operates with maximum efficiency [18];
- working at variable rotation speed of wind turbine in order to cover the whole wind speed range with maximum efficiency [1].

Main criteria for comparing of the strategies described above is a coefficient of power – ratio between generated electric power and aerodynamic power of wind [10]. Therefore, the task of research is to compare the coefficient of power obtained for different control strategies in wide range of wind speed.

2. Materials and Methods

The research was focused on measurement of wind turbine efficiency at different wind speed. Assumed that the mathematical model of wind turbine has power coefficient defined in advance as known [13]. The model contains the following equations. The main differential equation, describing the rotation of wind turbine [18]:

$$J \frac{d\omega}{dt} = M_a - M_e, \quad (1)$$

where J – inertia of wind turbine; ω – angular speed; M_a – aerodynamic torque; M_e – load torque.

Aerodynamic torque is:

$$M_a = C_p(Z) \frac{\rho \cdot S \cdot V^3}{2 \cdot \omega}, \quad (2)$$

where $C_p(Z)$ – power coefficient (depends on tip speed ratio Z); ρ – air density; V – wind speed; S – swept area.

Power coefficient $C_p(Z)$ is approximated by:

$$C_p(Z) = \left(\frac{c_1}{Z} - c_2\right) \cdot e^{\left(\frac{-c_3}{Z}\right)} + c_4, \quad (3)$$

where $c_1 \dots c_4$ – constants, tip speed ratio Z is:

$$Z = \frac{\omega \cdot r}{V} \quad (4)$$

where r – radius of turbine.

The mechanical power of wind turbine is:

$$P_a = C_p(Z) \frac{\rho \cdot S \cdot V^3}{2}, \quad (5)$$

where P_M – mechanical power of the alternator shaft.

Characteristic of $C_p(Z)$ is shown on figure 1(a). Based on $C_p(Z)$ dependence we found the dependence of aerodynamic power on wind speed and rotational speed. Diagram demonstrating aerodynamic power versus wind speed and rotational speed is shown on figure 2 (b). Based on this diagram we can declare that for each given wind speed value there is a rotational speed where mechanical power of wind turbine is maximal [7].

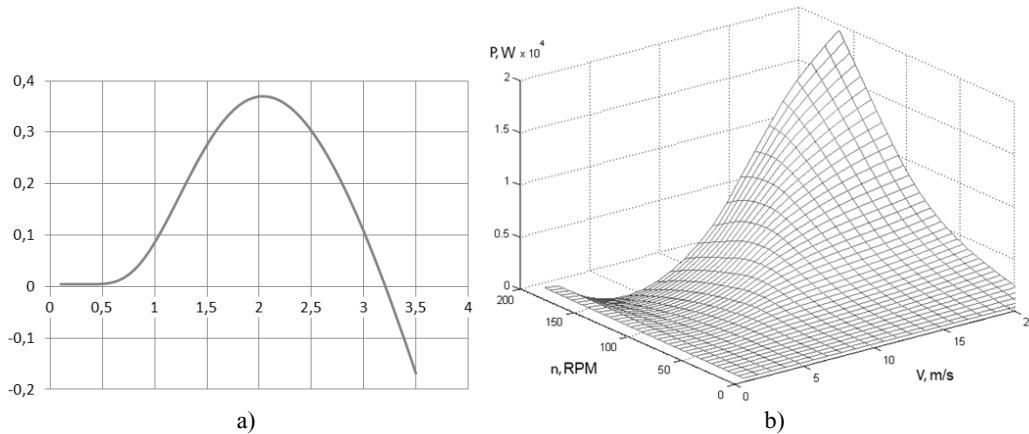


Fig. 1 Power coefficient versus tip speed ratio (a) and distribution of aerodynamic power according to wind speed and rotational speed (b).

Mathematical model of electric generator consists of the following equations. Voltage for one phase:

$$u = e - r \cdot i - L \frac{di}{dt}. \quad (6)$$

EMF in the phase is proportional to rotational speed:

$$\begin{cases} e_A = k \cdot \omega \cdot \sin(2p \cdot \omega \cdot t), \\ e_B = k \cdot \omega \cdot \sin(2p \cdot \omega \cdot t + \frac{2\pi}{3}), \\ e_C = k \cdot \omega \cdot \sin(2p \cdot \omega \cdot t - \frac{2\pi}{3}). \end{cases} \quad (7)$$

where k is a constant.

Output voltage after “star” connection is:

$$u_{AB} = u_A + u_B; u_{BC} = u_B + u_C; u_{CA} = u_C + u_A \quad (8)$$

Three phase rectifier bridge forms output voltage by:

$$u_{out} = \max(|u_{AB}|, |u_{BC}|, |u_{CA}|), \quad (9)$$

and electromagnetic torque of alternator is [9]:

$$M_e = \frac{u_{out} \cdot i_l}{\omega} \quad (10)$$

where i_l is the current of load.

Rectifier output is connected to power converter, which adjusts the current in alternator changing load impedance according to the modelling strategy [12]. For simulation the mathematical model of wind turbine was realized in Matlab/Simulink software. Diagram of wind turbine model and simulation setup is presented on figure 2.

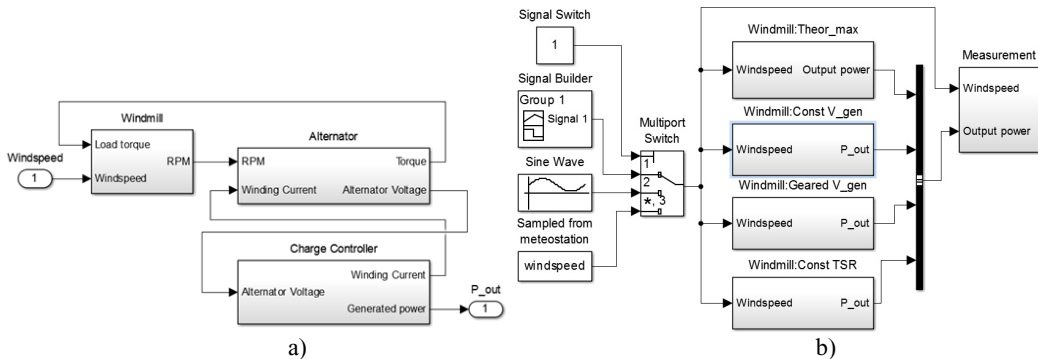


Fig. 2. Diagram of wind turbine model (a) and simulation setup (b) in Matlab/Simulink software.

Simulation setup consist of four modules of wind turbines named “Windmill:... ” where each module operates according to its own control strategy defined by algorithm described on high-level programming language in block “s-function” of Simulink. Module “Windmill:Theor_max” defines the maximum possible power at the given wind speed for the given wind turbine. Module “Windmill:Const V_gen” defines the operation of windmill with constant turbine speed where alternator shaft directly attached to the wind turbine. Module “Windmill:Geared V_gen” defines the operation of windmill with variable turbine speed and constant alternator speed provided by mechanical transmission with variable transfer ratio. Module “Windmill:Const TSR” defines the operation of windmill with variable turbine speed and constant tip speed ratio provided by alternator operating at variable speed. All the wind turbine models were affected by several wind speed influences [14]:

1. Linear increasing wind speed.
2. Periodic sine wave wind speed.
3. Sampled real wind speed recorded using anemometer in the field.

Each wind turbine module consist of three basic parts:

- «Windmill» – subsystem, providing conversion of driving torque from wind speed, its diagram presented on figure 3.
- «Alternator» – subsystem that converts the mechanical power to electric output, see figure 4(a).
- «Charge Controller» – subsystem for determining the wind turbine control strategy, figure 4(b).

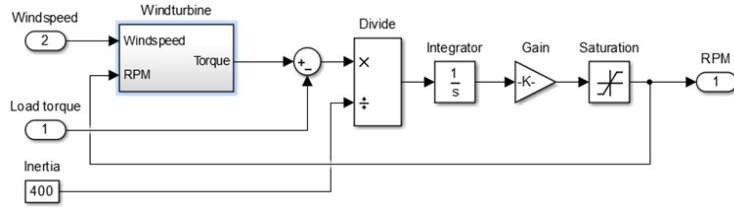


Fig. 3. Diagrams of «Windmill» subsystem for conversion of driving torque from wind speed.

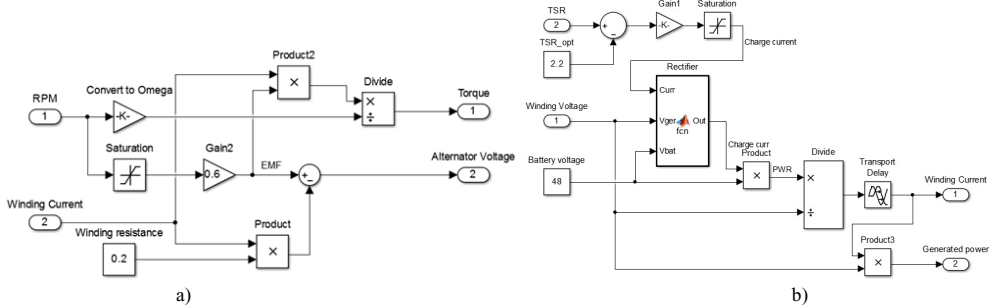


Fig. 4. Diagrams of subsystem for conversion of mechanical power to electric output (a) and subsystem for determining the wind turbine control strategy (b).

Wind turbine control strategy using mechanical transmission with variable ratio needs additional subsystem for imitation of gearbox [13]. This subsystem converts the rotation speed and transferred torque according to given transfer ratio and should be located between wind turbine and alternator subsystems. Diagram of gearbox subsystem is shown on figure 5.

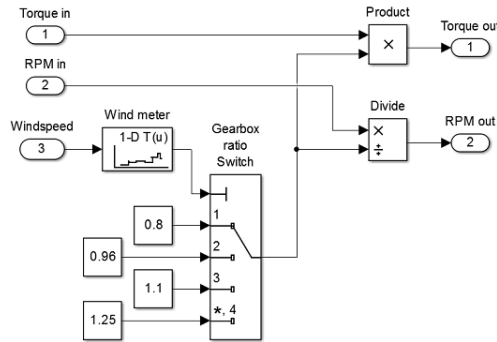


Figure 5 – Diagram of gearbox subsystem.

For measurement of the wind turbine efficiency at the variable wind speed the module “Measurement” was developed. Module provides the integrating of weighted values of C_p in time [8]. Contribution of C_p should be proportional to output power, and average value is as follows:

$$C_{p_{integr}} = \frac{\sum(Pe_i \cdot Cp_i)}{\sum Pa_i} \tag{11}$$

where Pe_i – current output power; Pa_i – current coefficient of power; n – number of samples.

3. Results

Simulation with linear increasing wind speed demonstrates the efficiency of each strategy in whole range of wind speed where wind speed is changing slowly (fig. 6).

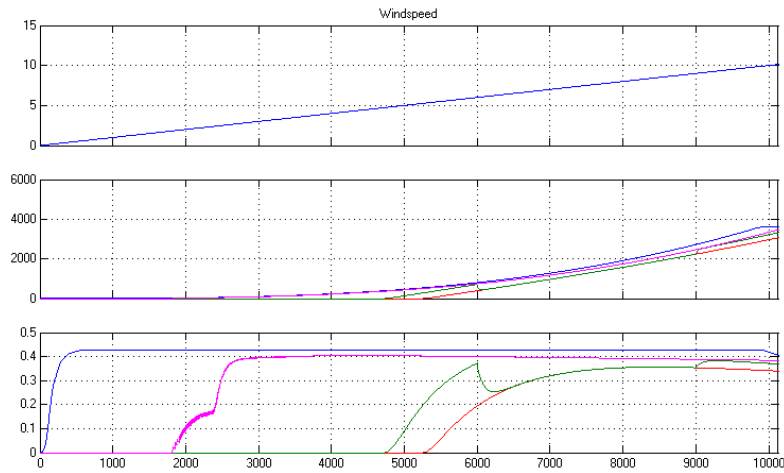


Fig. 6. Results of simulation with linear increasing wind speed.

Top diagram of figure 6 shows the wind speed in simulation time. Next one shows the generated electric power: blue line indicates the maximum possible power limited by defined coefficient of power in the turbine model. Red line shows the output power for constant speed wind turbine; green line demonstrates operation with gearbox. Purple line indicates the output power for variable speed wind turbine with variable speed alternator. Bottom diagram shows real coefficient of power calculated according to generated electric power at given wind speed. All line colors are similar to the lines described above. The testing shows that using gearbox can improve the efficiency of wind turbine that operates at wide range of wind speed comparing to operating with constant turbine speed. Moreover, the most effective strategy is the operation at variable speed of wind turbine with variable speed alternator.

Next test is the simulation of wind turbine models under sine wave wind speed influence, fig. 7. This testing demonstrate stability of operation for all control strategies. In addition, similar to previous testing the best operation strategy is for variable speed of wind turbine and electric generator.

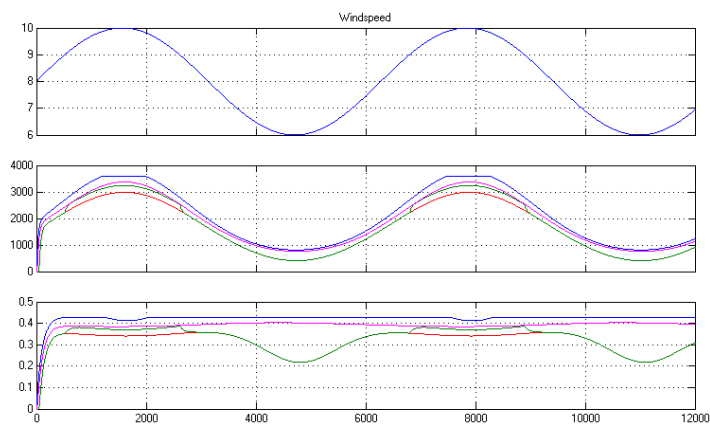


Fig. 7. Model response on periodic sine wave wind speed.

And final testing with sampled real wind speed shows the advantage of control strategy where wind turbine operates at variable speed and constant tip speed ratio, see figure 8.

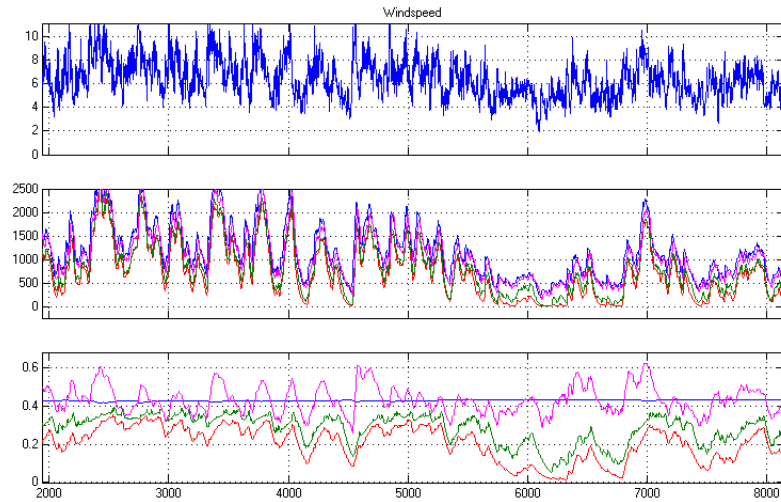


Fig. 8. Results of simulation with sampled real wind speed.

On the bottom diagram of figure 8 we can see that sometime the coefficient of power for constant TSR strategy is more than theoretical maximum. This fluctuation around mean value is normal because average value does not exceed the maximum limit. Fluctuation of coefficient of power occurs when the wind speed changes and control system tries to adjust the tip speed ratio. At that time the wind turbine starts to collect the wind energy in kinetic energy of rotation and later gives it back to alternator, so there is a time shift between wind energy extraction and generated energy utilization.

Conclusions

According to fulfilled research the results demonstrate the importance of choosing the proper strategy for given wind conditions. When the windmill location has a regular wind speed then the wind turbine can be designed for operations at constant wind turbine speed. This approach can reduce the cost of generated power because the constant speed windmills are cheaper. However, if there is a task to extract maximum energy from the wind in a wide range of wind speed, the best solution is to use the windmill operating with variable wind turbine speed at constant tip speed ratio.

Research was supported in part by R.F. Ministry of Education under Grant 14.577.21.0154 dated of 28.11.2014 (unique identifier is RFMEFI57714X0154).

References

- [1] B. Boukhezzer, H. Siguerdidjane, Maureen Hand M, Nonlinear control of variable-speed wind turbines for generator torque limiting and power optimization. *ASME Transactions, Journal of Solar Energy Engineering*. 128(4) (2006) 516–30.
- [2] E.F. Camacho, Bordons C, Model predictive control, Springer, UK, 1999.
- [3] P.W. Carlin, S. Laxson, E.B. Muljadi, The history and state of the art of variable-speed wind turbine technology, Report NREL/TP-500-28607, National Renewable Energy Laboratory, U.S.A, 2001.
- [4] R. Datta, V.T. Ranganathan, Method of tracking the peak power points for a variable speed wind energy conversion system, *IEEE Transactions on Energy Conversion*. 18(1) (2003) 163–168.
- [5] J. Espinosa, J. Vandewalle, V. Wertz, Fuzzy logic, identification and predictive control, Springer, UK, 2005.
- [6] Jianzhong Zhang, Ming Cheng, Zhe Chen, Xiaofan Fu, Pitch Angle Control for Variable Speed Wind Turbines, DRPT2008. (2008).
- [7] K.E. Johnson, L.Y. Pao, M.J. Balas, L.J. Fingersh, Control of variable-speed wind turbines: standard and adaptive techniques for maximizing energy capture, *IEEE Control Systems Magazine*. 26(3) (2006) 70–81.

- [8] A. Kusiak, Dynamic control of wind turbines, *Renewable Energy*. (2009). DOI:10.1016/j.renene.2009.05.022
- [9] A.S. Mart'yanov, Generator of Turbine Engine Power Station, *Eastern European Scientific Journal*. 5 (2014) 202–206.
- [10] A.S. Mart'yanov, E.V. Solomin, Modelling of Wind Turbine Performance Measurement, *Journal of Computational and Engineering Mathematics*. 2 (2014) 18–25.
- [11] N.V. Pronin, A.S. Mart'yanov, E.V. Solomin, Razrabotka matematicheskoy modeli vetroenergeticheskoy ustanovki moshchnost'yu 3 kVt proizvodstva OOO «GRTs-Vertikal' v pakete Matlab, *Alternativnaya energetika i ekologiya, NIIES*. 5 (2011) 41–44.
- [12] A.S. Mart'yanov, E.V. Solomin, Kontroller zaryada vetroenergeticheskoy ustanovki, *Mezhdunarodnyy nauchnyy zhurnal «Alternativnaya energetika i ekologiya»*. 1(81) (2010) 106–109.
- [13] A.S. Mart'yanov, Regulirovanie moshchnosti v vetroenergeticheskoy ustanovke, *Nauchnyy poisk: materialy tret'ey nauchnoy konferentsii aspirantov i doktorantov. Tekhnicheskie nauki, Chelyabinsk, Izdatel'skiy tsentr YuUrGU*. 2 (2011) 206–209.
- [14] I.M. Kirpichnikova, A.S. Mart'yanov, E.V. Solomin, Modelirovanie generatora vetroenergeticheskoy ustanovki, *Elektrotehnika*. 10 (2013) 46–49.
- [15] S. Morimoto, H. Nakayama, M. Sanada, Y. Takeda, Sensorless output maximization control for variable-speed wind generation system using IPMSG, *IEEE Transactions on Industry Applications*. 41(1) (2005) 60–7.
- [16] E.B. Muhando, T. Senjyu, N. Urasaki, A. Yona, T. Funabashi, Robust predictive control of variable-speed wind turbine generator by self-tuning regulator, In: *IEEE Power Engineering Society General Meeting*. (2007) 1–8.
- [17] N. Nanayakkara, M. Nakamura, H. Hatazaki, Predictive control of wind turbines in small power systems at high turbulent wind speeds, *Control Engineering Practice*. 5(8) (1997) 1063–9.
- [18] P. Novak, T. Ekelund, Modelling, identification and control of a variable speed HAWT, In *Proceedings of the European Wind Energy Conference*. (1994) 441–446.
- [19] Y.D. Song, B. Dhinakaran, X.Y. Bao, Variable speed control of wind turbines using nonlinear and adaptive algorithms, *Journal of Wind Engineering and Industrial Aerodynamics*. 5(3) (2000) 293–308.
- [20] E. Torres, M.Garcia-Sanz, Experimental results of the variable speed, direct drive multipole synchronous wind turbine, TWT1650, *Wind Energy*. 7 (2004) 109–118.
- [21] Y.C. Zhu, *Multivariable system identification for process control*, Pergamon Press, New York, 2001.

International Conference on Industrial Engineering

Multi-zone integrating regulator to control the electric drives with parallel regulation channels

Tsytovich L.I.^a, Brylina O.G.^{a*}, Shapkina E.V.^b, Chernysheva A.M.^b

^a *Electric drive and automation of industrial installations Department, South Ural State University, 76, Lenin Avenue, Chelyabinsk, 454080, Russian Federation*

^b *English Language Department, South Ural State University, 76, Lenin Avenue, Chelyabinsk, 454080, Russian Federation*

Abstract

This article dwells upon the principles of constructing the control system for a group of electric drives with parallel regulation channels (for example, water supply pump stations, air ventilation and fire extinction systems, etc.) on the basis of multizone integrating regulator with frequency-pulse-width modulation. It contains functional charts of discrete control systems and combined smoothly discrete regulation. It also considers a system able to self-diagnose catastrophic malfunctions of the circuit components and an automatic switch of reserve control channels. Herein is presented the case of a discrete control system for enterprise-level pumps used to supply recycling water. This system contains four electric drives with water pumps and is able to switch on the reserve control channels automatically. The article may be of interest to specialists in the field of power electronics and information electronics, electric drives and process automation.

© 2015 The Authors. Published by Elsevier Ltd. This is an open access article under the CC BY-NC-ND license (<http://creativecommons.org/licenses/by-nc-nd/4.0/>).

Peer-review under responsibility of the organizing committee of the International Conference on Industrial Engineering (ICIE-2015)

Keywords: Multizone regulator; Integrator; Relay element; Asynchronous electric drive; Pump stations; Electric drive with parallel regulation channels; Reservation; Diagnostic; Thyristor voltage regulator; Frequency converter; Pump; Filter

1. Introduction

The majority of electric drives of water supply pump stations for residential buildings and manufacturing plants, air ventilation and fire extinction systems are control systems with parallel regulation channels (hereafter SPRC)

* Corresponding author. Tel.: +7-351-267-9321; fax: +7-351-267-9385.
E-mail address: teolge@mail.ru

[1, 2], where some electric drives are operating ones, and others are reserve. The SPRC control using digital information regulators and power converters makes the entire set of electrical equipment unjustifiably complex, which leads to reducing its operational reliability. SPRC is often classified as a low accuracy system. It should be taken into account for its technical re-equipment. For this reason a compromise between the simplicity of technical feasibility of control system and its performance data should be struck. In this article we use the method of SPRC developing based on of multi-zone integrating regulators (hereafter MR) [3 – 8] combining high-accuracy control, interference immunity, the possibility of automatic reservation of control channels and technical simplicity. SPRC structures based on multi-zone integrating regulators are presented below.

2. Theoretical part

2.1. Discrete Control Systems

The structure of the simplest variant of the system controlled by the even number group of parallel-working MR electric drives (Fig. 1a) includes multi-zone integrating regulators, thyristor voltage regulators TVR1 – TVR_i for the “smooth” start of asynchronous electric motors, actuating motors M1 – M_i, water pumps P1 – P_i and feedback sensor FS (e.g. pressure sensor) in the output main M_{Σ} . FS can also be a discrete action sensor, which is typical of M_{Σ} as a detention tank.

MR includes adder units $\Sigma 1, \Sigma 2$, integrator I, and uneven number $n \geq 3, 5, 7, \dots$ of relay elements RE0 – RE_n with switching threshold symmetry relative to zero level $|\pm b_1| < |\pm b_2| < \dots < |\pm b_n|$, where «*b*» index corresponds to RE sequence number. RE output signals are changed discretely within $\pm A/n$. The number of MR modulation zones is equal to $k = (n+1)/2$ (Fig. 1 b). Self-oscillation mode in MR always takes place in the relay element path that has the least value of switching thresholds. The MR transition from one modulation zone to another is specified by the value of control signal in its data entry (Fig. 1 b). In this case frequency pulse-width modulation (FPWM) is realized when discretization intervals t_{i1}, t_{i2} and T_{0i} depend on the value of control signal X_{IN} (Fig. 1 c). Signal average value at the adder unit output $\Sigma 2 Y_{01} \dots Y_{0i}$ over the period T_{0i} is linear with respect to X_{IN} . The converter modes were considered in detail in work [3].

The system considered is classified as electric drives with discrete regulation. Their number corresponds to the value $n-1$. The control channels are switched on with thyristor voltage regulators (TVR), their control inputs being connected to corresponding outputs of relay elements RE2 – RE_n of MR.

The operating principle of the system is the following. Initially the MR moves into higher order modulation zone with input signal X_{IN} when TVR1 – TVR_i are turned on with the help of signal $+A/n$ from the outputs of RE2 – RE_n of MR. After the launch of M2 – M_i with increasing pressure in main M_{Σ} the level of signal at the feedback sensor output is increased while the value of error signal at MR integrator input is decreased. As a result, MR moves into the lower order modulation zone when the RE2 output signal equals to $-A/n$ and TVR1 is turned off. As the pressure M_{Σ} decreases and the unbalance signal increases at the input of the integrator I, multizone regulator is reverted to high order modulation zone and the process is repeated. The value of the maximum regulation error is proportional to $0,5X_{INi}$ where X_{INi} is the amplitude of the input signal for the *i*-th MR modulation zone. Thus, this type of control system is applicable in electric drives of low accuracy class where easy technical realization and maintenance of the equipment are preferable.

The regulation error can be reduced significantly by introducing the FPWM channel with its input connected to the output of RE1 (Fig. 1a). In this case the system will have an odd number of control channels according to the number of relay elements in the MR. However, this solution would require the infra-low-frequency self-oscillation mode in MR, which would prevent frequent on-off modes of the motor and the actuating mechanism. In terms of analogue electronics this task is rather complicated. So the implementation of MR based on microprocessor technology and programmable controllers will inevitably lead to the loss of one of such advantage of this system type as easy technical realization and maintainability.

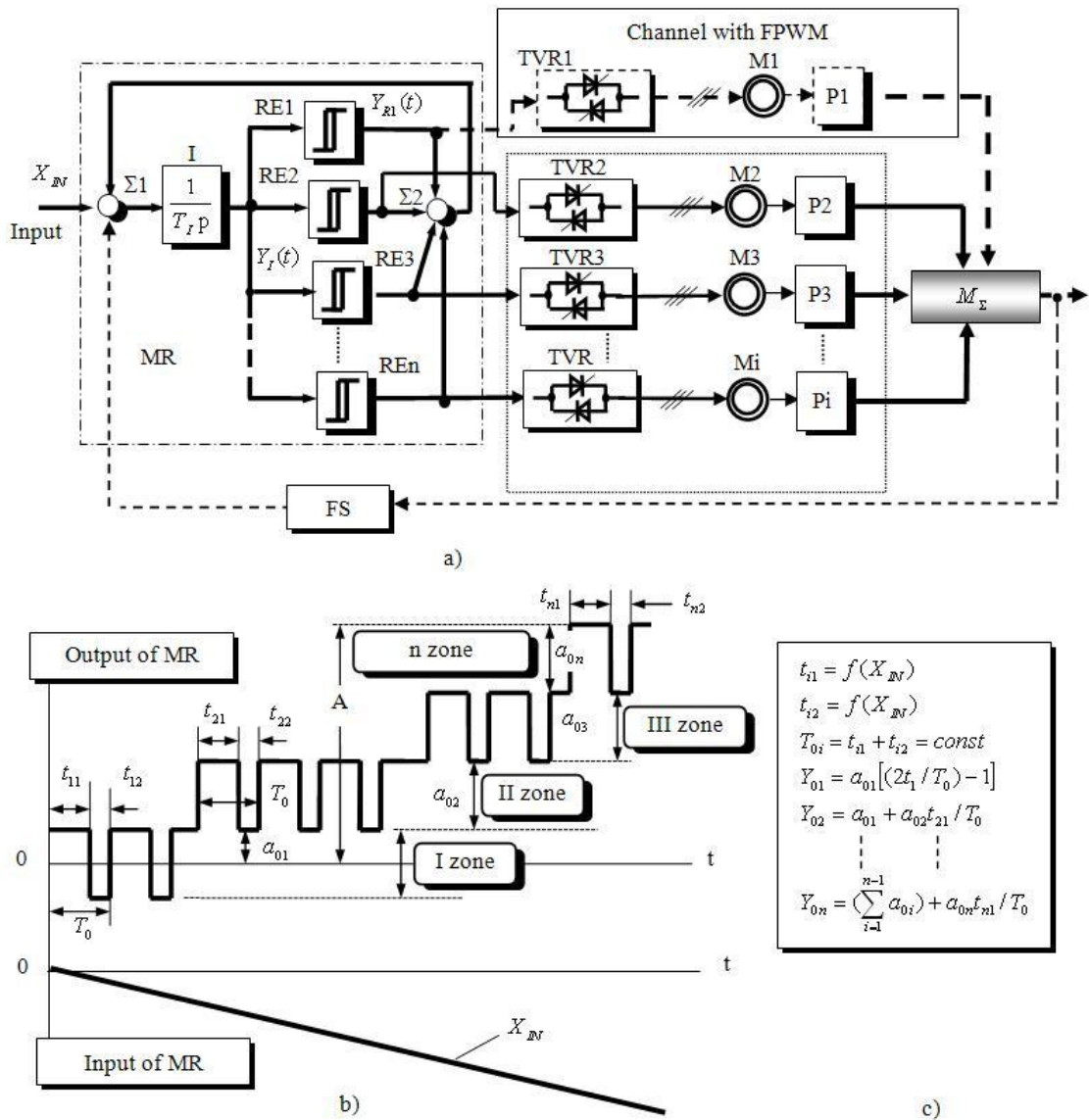


Fig. 1. Function chart (a) of discrete control system with even number of electric drives with parallel regulation channels on the basis of MR; time-diagrams of MR signals (b) and its characteristics (c).

The system in Fig. 2 is designed for discrete controlling the group of electric drives odd number and implemented on the basis of MR with even number of relay elements. Its specifics is the additional short-term switching of relay elements RE2 - RE n in its moving from one modulation zone to another [4], which is inadmissible for electric drive control system as it leads to false tripping of power electronics and actuating mechanisms.

In the structure (Fig. 2) this disadvantage of MR with an even number of relay elements is eliminated by the introduction of a memory register RG, a device of codes comparing DCC and a delay element DL [5].

In a steady mode the status of codes at the input and the output of RG are identical, so the output signals of DCC and DL correspond to a logic "0". During the moving of MR to another modulation zone and with the help of

unbalance signal when additional reorientation of relay elements is possible the output and input RG codes become different. DCC moves to the logic "1" condition.

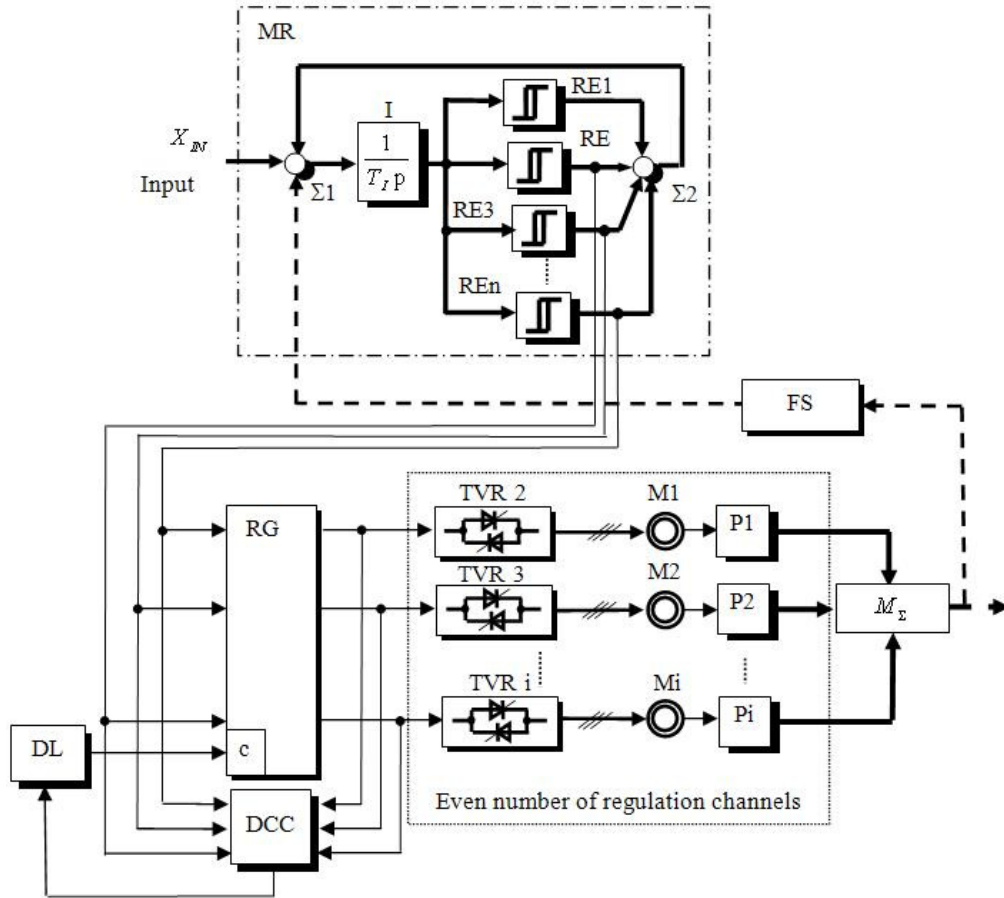


Fig. 2. Schematic structure of discrete control system with odd number of electric drives with parallel regulation channels on the basis of multi-zone integrating regulator.

But rewriting of a new code condition of RE in RG is delivered with a delay formed with DL. Time of the delay corresponds to the maximum value of the transient time in the MR with an even number of RE. In practice, this time value is 2 to 5 seconds, which, on the one hand, provides the work of the MR in a steady mode, and, on the other hand, this value is negligibly small for electric drives of water pumps or, for example, blower installations and fume exhausters.

After the end of time delay "1" is formed at the DL output, and the code conditions of MR relay elements are rewritten into the RG. As a result, the electric drives of regulating channels move to the ON (or OFF) position only after the end of the transition process in the MR.

2.2. Control system with combined smoothly discrete regulation

In AC drives with parallel channels the combined method of regulation is often applied, where one channel is controlled by the frequency converter and others - with the help of the TVR [9, 10]. The schematic structure of such system based on the MR is shown in Fig. 3.

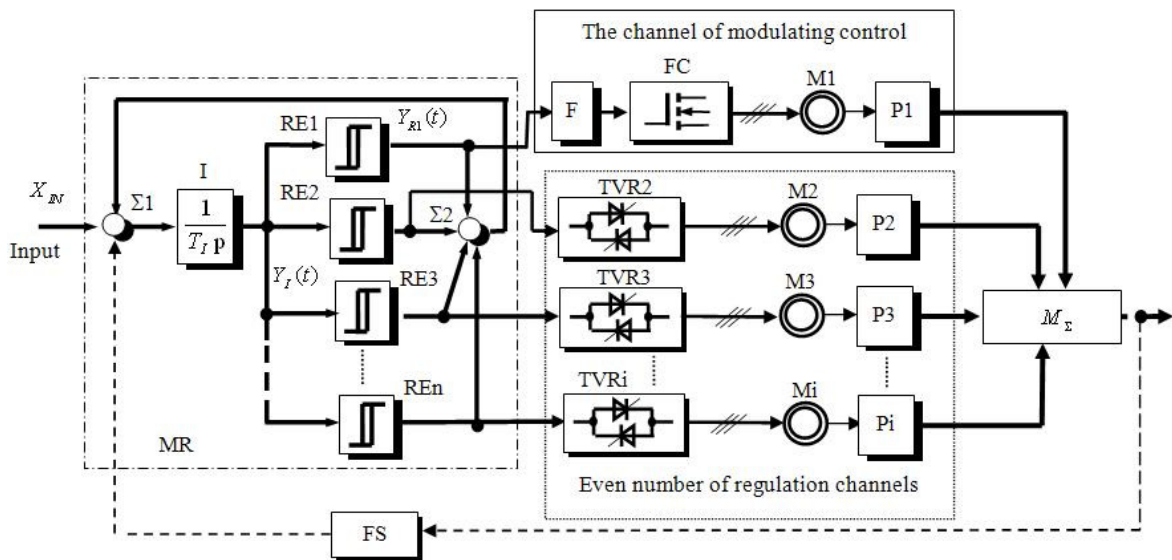


Fig. 3. Schematic structure of combined control system with odd number of electric drives with parallel regulation channels on the basis of multi-zone integrating regulator

Its difference from the system shown in Fig. 2 is that the RE1 is activated in the process of modulating control. The smoothing filter F, e.g. the aperiodic link of the first order, is connected at the RE1 output. Thus the average value of the RE1 output impulses for the sampling interval is determined. The value is proportional to the imbalance signal at the input of element I. Frequency converter FC performs the functions of the power converter. Its output voltage frequency and amplitude depend on the voltage at the data input. At the same time the channel of modulating control operates continuously, and discrete channels operate in the "on/off" mode depending on the number of the modulation zone and associated RE2 - RE_i output signals mark. It should also be mentioned that any control mode may be realized directly on the basis of MR: proportional, integral, proportional-integral, etc. [5].

2.3. Control system with automatic reservation of regulation channels

The structure of automatically reserved system with increased reservation multiple of (Fig. 4) [8] differs from systems discussed in [9 – 12] by the presence of smoothing filter F and the fixing element FE in each regulating channel (Fig. 4). It also allows to use the RE1 for controlling in "on/off" mode with additional regulating channels, which eventually increases the SPRC reservation multiple.

The introduction of logical variables from protection unit (PU) of TVC and actuating mechanisms (AM) into the closed loop of MR with blocking the work of the relevant relay element and placing it in the condition equal $-A/n$ (logical "0") will be similar to the system discussed in [13].

The start condition of the corresponding regulating channel of the system, for example, the channel controlled by the RE1 is the level of the imbalance signal at the input I when the average means of impulses $Y_{P1}(t)$ exceed the operating level of FE equal " c_2 " (Fig. 5b). At the same time the fixing element switches to the logical "1" and starts the required TVR. If the signal at the input of the FE is less than " c_1 ", it switches to "0", and the electric drive of the relevant regulating channel is stopped. Time constants of filters F should be selected so that the pulsation amplitude of signals $Y_{Fi}(t)$ would not exceed the switching level of the fixing element.

Let's consider the situation when the TVR1-AM1 and TVR2-AM2 channels are in operation, and TVR1 is controlled by RE1, which is under the self-oscillation mode (Fig. 5 a) and the average value of its output impulses exceeds " c_2 " and TVR2 is controlled by static signal equal " $+A/n$ " from RE2 output (Fig. 5 c).

Let's assume that at a time moment t_0 the RE1 moved to the uncontrollable state $-A/n$ (Fig. 5a). From this time moment t_{01} (Fig. 5b), AM1 moves to a braking mode. After that the self-oscillation mode arises in the RE channel. This mode has the lowest value of switching threshold that comes after RE1, i.e. in the RE2 (Fig. 5c). MR is a closed system, thus, relative duration γ_2 of the impulses $Y_{R2}(t)$ (Fig. 5c) is equal to the relative duration γ_1 of the previously operating RE1 (Fig. 5. a). As a result, the signal $Y_{F2}(t)$ at the output of the filter of the second channel will be equal in amplitude to $Y_{F1}(t)$ and the regulating channel TVR2-AM2 will stay in the ON position. The substitution of emergency OFF channel TVR1-AM1 will be done with the help of one of the reserve channels due to integrator I which seeks to minimize the control error by turning on the relevant relay element and the relevant actuating mechanisms TVR-AM.

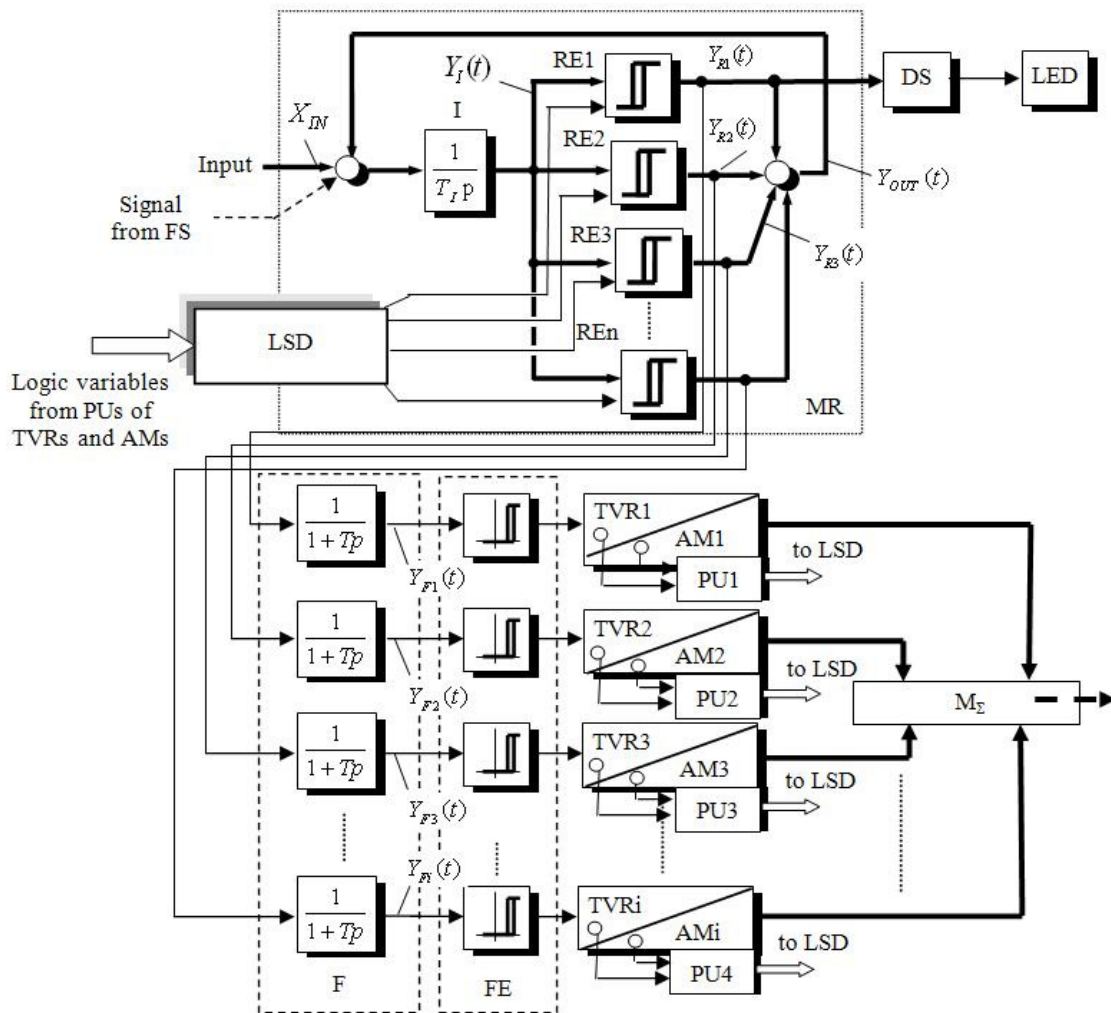


Fig. 4. Function chart of discrete control system with odd number of electric drives self-diagnosis and automatic reservation of regulation channels.

Taking into account the successive substitution of RE1 with other relay elements of MR, the frequency of self-oscillation falls, the time constants of filters F should be chosen so as to guarantee that even at the lowest frequency of self-oscillation the pulsation amplitude of F output signals will not exceed FE zone of ambiguity.

Diagnostic system (DS) (Fig. 5) controlling the operating condition of MR when RE1 is in self-oscillation mode [14 - 16]. Diagnostic system and LED indicator informs the maintenance staff about MR malfunction, but the system continues to operate as the self-oscillation mode is transferred to the next RE. This fact prevents the service personnel about the need to take measures to replace the failed element of control system during the stopping of technological process.

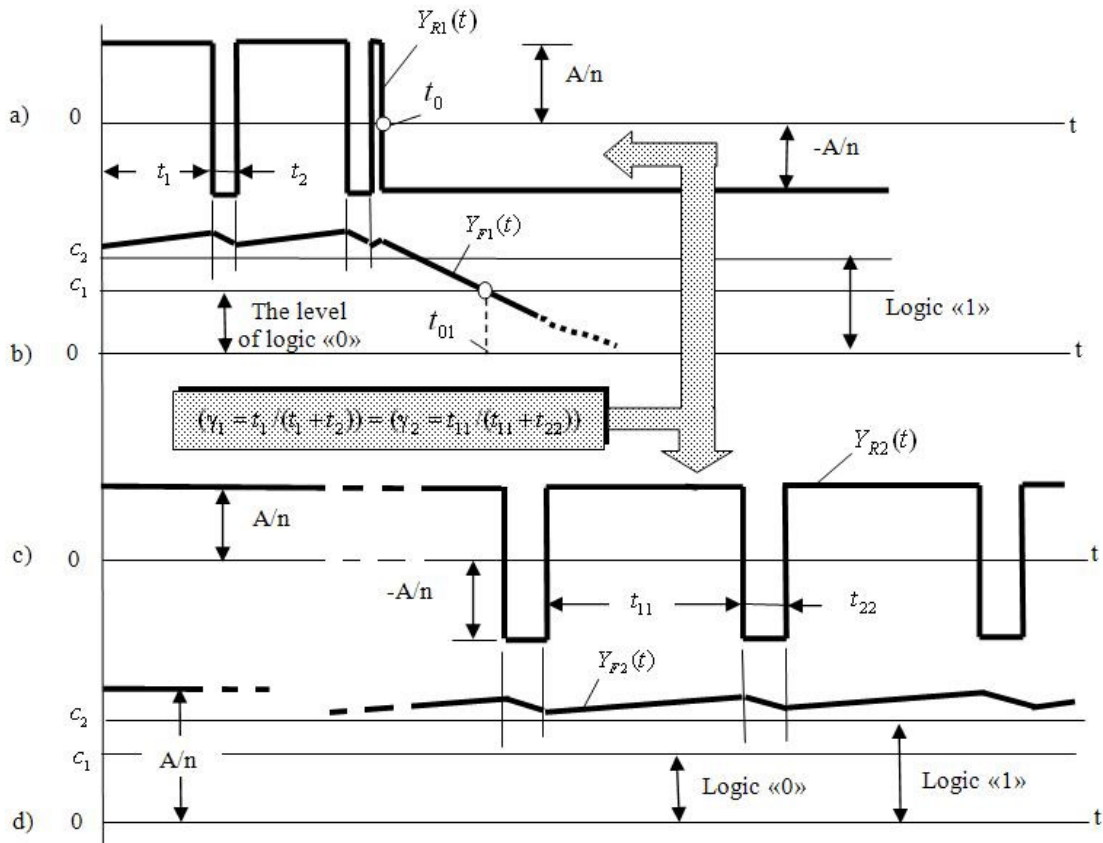


Fig. 5. Time diagrams of control system signals with increased multiple of reservation.

The structure shown in Fig. 5 can also be used for systems with modulating regulation of output signal, for example, with the usage of a frequency converter. For this purpose FE is excluded from the structural scheme, and data input of the frequency converter is connected directly to the output of the corresponding filter.

3. Application

Figure 6 shows the schematic structure of a multi-zone control system with asynchronous electro drives of recycling water supply pumps of industrial enterprise.

The system contains four water pumps P1 – P4; water pumps P3 and P4 are reserve ones. 50 kW electric motors are controlled with the help of TVR1-TV4 for smooth start. Each TVR is equipped with an individual availability block (AB) which forms deactivating signal of the corresponding relay element of MR with TVR-ON and the absence of any protection operation. An overheat protection signal of actuating mechanisms M and P is also used in the availability block (don't show on the fig. 6). A feedback is produced with low water level sensors (LLS), high

water level sensors (HLS) and the high critical level sensors (HCLS) operating in the self-oscillation mode [17 – 19]. The diagnostic system controls the MR, LLS, HLS and HCLS operability parametrically if there is a self-oscillation mode in them [20, 21]. MR contains five relay elements (Fig. 1 a), and RE2 - RE5 are connected to the control inputs of the TVR. The output signal of RE1 enters the diagnostic system. If any of the controlled elements breaks down, the diagnostic system generates a push installation signal of MR relay elements into the state $-A/n$ in which TVR switches off. The system is also deactivated if there is a fault in the diagnostic system or the water level is above the high critical level. When the water level exceeds the lower level, the M1 is in operation. If the low water level sensor actuates, the M2 is also put into operation. Both mechanisms M1-P1 and M2-P2 function until the water level drops below the lower critical level, then M1 and M2 are switched off. If any emergency signal actuates, the corresponding relay element of MR is forcibly converted to the position where the channel electric drive is switched off [14, 22 – 25]. After that the faulty electric drive is replaced by an efficient one. The cost of reconstruction is slightly more than 500 thousand RUB (2013).

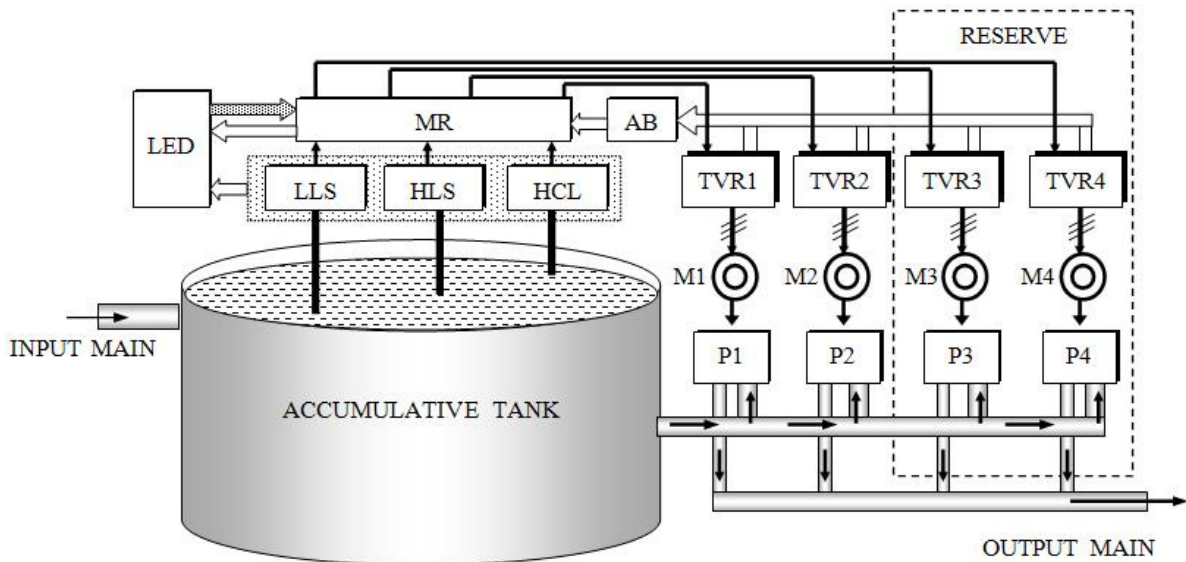


Fig. 6. Functional scheme of a multi-zone control system with asynchronous drives of the industrial circulating water supply system reservoir.

There have been two cases of switching to reserve mode because of the pumping equipment failure during the six years of system operation. As estimated the company averted the economic damage for the sum of 50 million RUB (1 million USD).

References

- [1] Tonghua Zou, Shu-yuan Ma, Analysis on Energy Saving of Pumps Movement Adjustment in a Closed Cycle, Power and Energy Engineering Conference (APPEEC). (2010) 1–4.
- [2] Pengfei Li, Yaoyu Li, Seem J.E., Extremum seeking control for efficient and reliable operation of air-side economizers, American Control Conference. (2009) 20–25.
- [3] L.I. Tsytoich, RF Patent 1336039. (1987).
- [4] L.I. Tsytoich, O.G. Tereshchina, Mnogozonnyie integriruyuschie razvertyivayuschie preobrazovateli s chetnyim chisлом releynykh elementov [Multizone integrating sweeping converters with an even number of relay elements], Bulletin of the South Ural State University. Series "Power Engineering". 5(4) (2004) 69–72.
- [5] L.I. Tsytoich, O.G. Tereshchina, RF Patent 2276449. (2006).
- [6] Yu.S. Usinin, M.A. Grigorjev, A.N. Shishkov, A. Bychkov, S.P. Gladyshev, The Losses in Control Electric Drives of Transport Mechanisms at Different Controlled Laws, SAE Paper 2011-01-0039, SAE 2011 World Congress and Exhibition; Detroit, MI; United States. (2011).

- [7] Yu.S. Usinin, M.A. Grigorjev, K.M. Vinogradov, Switching Losses in the Rotor of the Field Regulated Reluctance Machine, SAE Paper 2010-01-0485, SAE 2010 World Congress and Exhibition; Detroit, MI; United States. (2010).
- [8] L.I. Tsytoich, O.G. Brylina, A.I. Sidorov, U.S. Smirnov, Problemy ekspluatatsionnoy bezopasnosti v elektroprivodah s parallelnymi kanalami regulirovaniya i puti ih resheniya [Problems of operational safety in the electric drives with parallel channels of regulation and solutions], *Pribory i sistemy. Upravlenie, kontrol, diagnostika [Devise and System. Control, monitoring, diagnostics]*. 3 (2015) 5–17.
- [9] D. Yellamati, E. Arthur, S. James, G. Morris, T. Heydt, E. Graf, Predictive Reliability Models for variable frequency drives based on application profiles, Reliability and Maintainability Symposium (RAMS). (2013) 1–6.
- [10] G.K. Morris, B.W. Weiss, Driving energy efficiency with design optimization of a centrifugal fan housing system for variable frequency drives, Thermal and Thermomechanical Phenomena in Electronic Systems (ITherm), 13th IEEE Intersociety Conference. (2012) 1312–1319.
- [11] U.S. Usinin, M.A. Grigorjev, K.M. Vinogradov, Weight and dimensional parameters of a power drive for electrical vehicle, Powertrains, Fuels and Lubricants Meeting, Florence, ITALY. 09SFL-0251, Powertrains, Fuels and Lubricants Meeting, SFL 2009; Florence. (2009).
- [12] Yu.S. Usinin, M.A. Grigorjev, K.M. Vinogradov, The electric drive of a tram with a average floor, SAE International 2008, Powertrains, Fuels and Lubricants Congress, Shanghai, CHINA, 2008-01-1828, 2008 SAE International Powertrains, Fuels and Lubricants Congress; Shanghai. (2008).
- [13] L.I. Tsytoich, O.G. Tereshchina, M.M. Dudkin, RF Patent 2312452. (2007).
- [14] L.I. Tsytoich, O.G. Tereshchina, Mnogozonnaya sistema upravleniya gruppy elektroprivodov s avtomaticheskim perevodom silovogo elektrooborudovaniya v rejim holodnogo rezerva [Multizone control system a group of electric motors with automatic switch on reserve power cannels], *Bulletin of the South Ural State University. Series "Power Engineering"*. 6(9) (2005) 97–99.
- [15] L.I. Tsytoich, Mnogozonnyy razvertyivayuschiy preobrazovatel s adaptivnoy v funktsii neispravnosti aktivnykh komponentov strukturoy [Multizone sweeping converter with adaptive structure], *Pribory i tekhnika eksperimenta [Instruments and Experimental Techniques]*. 1 (1988) 81–85.
- [16] O.G. Brylina, L.I. Tsytoich, Chastotno-shirotno-impul'snyy regul'yator peremennogo napryazheniya s avtomaticheskim rezervirovaniem kanalov upravleniya [Frequency-width-pulse regulator of the alternating voltage with automatic reservation of control channel], *Bulletin of the South Ural State University. Series "Power Engineering"*. 16(34) (2011) 56–60.
- [17] L.I. Tsytoich, O.G. Brylina, RF Patent 2459249. (2012).
- [18] L.I. Tsytoich, O.G. Brylina, R.M. Rakhmatulin, M.M. Dudkin, RF Patent 2460134. (2012).
- [19] O.G. Brylina, Sistema upravleniya termonagrevatel'noy ustanovkoy s samodiagnostirovaniem i avtomaticheskim rezervirovaniem kanalov regulirovaniya [Control system of the heating device with self-diagnosis and automatic reservation of control channels], *Elektrotehnicheskie sistemy i kompleksy [Electro technical systems and complexes]*. 18(2010) 36–41.
- [20] L.I. Tsytoich, O.G. Tereshchina, M.M. Dudkin, Sistema upravleniya gruppy asinhronnykh elektroprivodov s samodiagnostirovaniem i avtomaticheskim rezervirovaniem kanalov regulirovaniya [Control system for a group of asynchronous motor with self-diagnosis and automatic reservation of actuating paths], *Electrotehnika [Russian Electrical Engineering]*. 11 (2006) 38–44.
- [21] L.I. Tsytoich, Razvertyivayuschie preobrazovateli s avtomaticheskim diagnostirovaniem i rezervirovaniem [Sweeping converters with automatic diagnosis and reservation], *Bulletin of the South Ural State University. Series "Power Engineering"*. 5(4) (2004) 55–61.
- [22] S.P. Lohov, L.I. Tsytoich, M.M. Dudkin, R.M. Rakhmatulin, O.G. Brylina, Zamknutyiy integriruyuschiy analogo-tsifrovoy preobrazovatel s bestaktovyim porazryadnyim uravnoveshivaniem [The closed integrating converter «Analog – Digit – Analog» with automatic bit-by-bit balance], *Pribory i sistemy. Upravlenie, kontrol, diagnostika. Razdel «Pribory i sredstva avtomatizatsii» [Devise and System. Control, monitoring, diagnostics]*. 11 (2012) 27–35.
- [23] L.I. Tsytoich, M.M. Dudkin, O.G. Brylina, A.V. Tugaev, The interval-code synchronizations for the power valve inverters control system, Science, Technology and Higher Education: materials of the international research and practice conference, Vol. II, Westwood, December 11th–12th, 2012 / publishing office Accent Graphics communications. (2012) 541–558.
- [24] L.I. Tsytoich, O.G. Brylina, M.M. Dudkin, A.V. Kachalov, R.M. Rakhmatulin, Adaptivnaya intervalo-kodovaya dvoichno-desyatchnaya integriruyushchaya sinhronizatsiya sistem upravleniya silovymi ventilnymi preobrazovatelyami [Adaptive interval-code integrating synchronization of control systems for power converters], *Electrotehnika [Russian Electrical Engineering]*. 3 (2013) 8–15.
- [25] L.I. Tsytoich, O.G. Brylina, M.M. Dudkin, R.M. Rakhmatulin, A.V. Tyugaev, Analogo-tsifrovoy preobrazovatel s integriruyushey sinfznoy amplitudno-chastotno-impul'snoy modulyatsiey dlya sistem ventilnogo elektroprivoda [Analog to digital converter with integrating amplitude-frequency-pulse modulation for systems of valve electric drive], *Electrotehnika [Russian Electrical Engineering]*. 5 (2013) 10–15.



International Conference on Industrial Engineering

Evaluation of reliability and technical conditions of tunneling machines

Nosenko A.C.^a, Domnitskiy A.A.^{b*}, Shemshura E.A.^c

^a *Ul. Lenina, 174-21, Shakhty, Rostov Oblast, 346500, Russia*

^b *Ul. Biriulevskaya, 58/2, 455, Moscow, 115547, Russia*

^c *Ul. Victory of the revolution, 99-64, Shakhty, Rostov Oblast, 346500, Russia*

Abstract

This article describes a way to increase operational reliability of selective heading machines by preventing sudden failures and adjusting the repair cycle based on the results of runtime diagnostics of executive unit drive in terms of technical conditions. Based on the statistical examination of heading machine reliability, the authors have worked out a range of parts and assembly units with limited failure-free lifetime and subject to operational control. There have been developed techniques for expeditious diagnostics of executive unit drive technical condition based on values of engine current with measured data presented in frequency domain, diagnostics being performed without interrupting the technological process of underground development. There have been found identification frequencies in current range corresponding to defects and failures of separate parts of the electro-mechanical drive of the executive unit. There has been developed a microprocessor diagnostic complex that analyses compliance of hardware-obtained amplitude-frequency characteristics with actual technical conditions of the examined heading machine unit.

© 2015 The Authors. Published by Elsevier Ltd. This is an open access article under the CC BY-NC-ND license (<http://creativecommons.org/licenses/by-nc-nd/4.0/>).

Peer-review under responsibility of the organizing committee of the International Conference on Industrial Engineering (ICIE-2015)

Keywords: reliability; diagnostics; technical condition; tunneling machines; heading machine with jib-type executive unit; spectral analysis; defect

1. Introduction

Increase in efficiency of building capital developments at mining enterprises, objects of underground city

* Corresponding author. Tel.: +7-918-527-32-27

E-mail address: aleshkastyle@gmail.com

infrastructure, road tunnels can't be carried out without tunneling cars, possessing high operational reliability.

Considerable decrease in level of reliability of the equipment after its long-term operation, long equipment downtimes due to imperfection of maintenance system cause unreasonably high maintenance costs [1].

One of the ways to increase operational reliability of tunneling cars by preventing sudden refusals and making their consequences less painful is the use of modern systems of monitoring and diagnostics of their technical condition [2-4].

The importance of diagnosis problem is determined not only by possibility of preventing failure, forecasting remaining lifetime and adjustment of repair cycle, but also by the possibility to manage without repair of faultless units, to reduce expenditures on their restoration. Application of expeditious diagnostics is the cornerstone of solution of the problem of optimizing the operation of tunneling cars.

2. Reliability of KP21 heading machine

For assessment of operational reliability of tunneling cars there are a number of widely approved techniques of collecting and processing statistical information, which can be applicable for driving combines [5, 6, 7]. Production monitoring of operability of selective action combines KP21 was held during the construction of horizontal and slightly sloping preparatory developments with section of 14.5 sq.m. in rock of maximum hardness at monoaxial compression of 100 MPas.

On the basis of statistical researches of reliability of KP21 combines the nomenclature of details and units limiting the period of trouble-free operation, their actual reliability index [8,9] have been defined. Mean mining volumes between refusals (V, m3) for details and units failing during the between-repairs period are presented in Fig. 1.

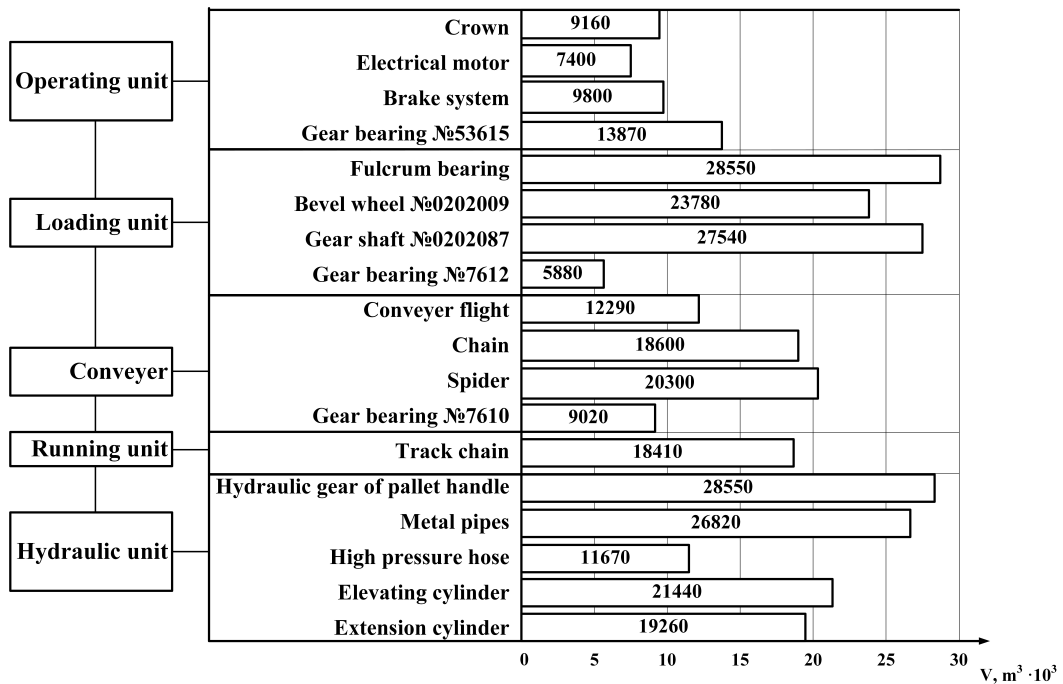


Fig. 1. Mean mining volume between failures for parts limiting heading machine reliability during time between repairs

It should be noted that the majority of characteristic failures of KP21 combines are related to malfunction of bearing units in drive electric motors and elements of transmission. Accordingly these elements have the smallest values of mean mining volume.

Obtained results are used to define which elements of the combine are subject to operating control for failure prevention, as well as for working out rational strategy of replacement of parts and adjustment of maintenance cycle.

3. Methods of diagnosing technical condition of mining machines

Vibration monitoring [10-12] is considered to be a modern method of expeditious diagnostics of technical condition of mountain cars, both stationary, and mobile, which proved as the most informative method reflecting a wide range of processes occurring in the working mechanisms. Along with vibration diagnostics methods of diagnostics of electric drives of technological machines based on monitoring of consumed current have been developed [13-16]. The subsequent spectral analysis of the received signals makes it possible to define technical condition of elements of the engine and transmission with high degree of reliability. Development of essentially new system of monitoring mining machines performance and their technical condition allows firstly, to keep exact account of operating time of the equipment and, secondly, having information on workload of units and structures, to predict their resource and to build system of operation with optimum parameters.

To monitor and evaluate technical condition of heading machines of selective action, in particular their boom executive units, without interrupting mining technological process the technique of expeditious diagnostics of the drive has been developed. It is different from popular techniques by the fact that measurement of change of current over the time is used as incoming information acquired directly from the power device of the car.

The identification frequencies in a current range corresponding to defects and malfunctions of separate elements of the electromechanical drive of executive body have been determined. Correlation dependences of values of rated amplitudes of a signal at the corresponding frequencies from the level of technical condition of the studied object have been established [17].

Hardware complex for diagnosing tunneling cars and acquisition of data necessary for the assessment of their technical condition in development workings has been developed. As a basis for the diagnostic device high-performance RISC microcontroller of AVR ATmega16-16AU family with the picoPower [18, 19] technology was chosen. It is established that for the research of the polynomial characteristic and frequencies located about cut point in retardation strip it is expedient to use Chebyshev's filter with frequency of cut of 1200 Hz.

4. Experimental results

Practical test using electromechanical drive of the executive unit of the KP21 combine with the asynchronous short-circuited engine 2EDKOFV250LB4 has been carried out. In the course of the experiment the developed and manufactured device for receiving and processing information was connected to stator winding of one of the electric motor phases. Measurements were taken for three different technical conditions of the studied object (Fig. 2): only put into operation (I – new engine), fulfilled 50% of a resource before capital repairs (II – engine that has been in operation) and with full working off of a resource (III – engine that wants repairing). After collecting all necessary data further analysis and data processing were carried out by means of applied computing MatLab 6.0 [20] package.

Changes of a range of current of the electric motor from 0 to 100 Hz at development of defects in the electric drive on a diagram characterizing condition of the whole drive of executive body of the KP21 combine (Fig. 2) may serve as an example. Representation of a signal in frequency area is evident and convenient, and significant amplitudes in a range confirm possibility of applying the method of spectral analysis of stator current of the engine for diagnostics of the drive of executive body of the combine.

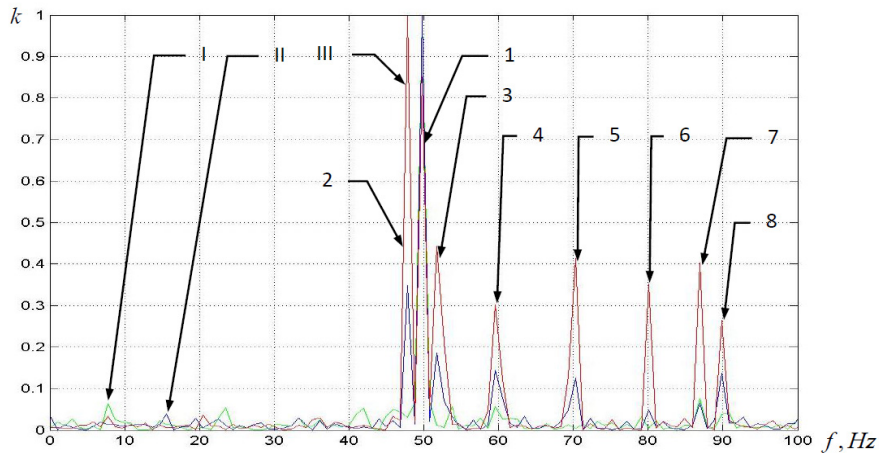


Fig. 2. Stator current spectrum of electric drive at emergence of defect in drive of executive unit

Fig. 2 shows the range of stator current acquired with clearly defined defects of electric drive rotor and stator of the electric motor and basic bearings of elements of transmission of executive body of the combine:

- Peak 1 at 50 Hz defines the frequency of supply voltage;
- Peaks 2 and 3 at 48 and 52 Hz respectively at such level of amplitude define the existing rotor defect;
- Variances 4, 5, 6 and 8 at 60, 70, 80, 90 Hz respectively confirm destruction of separators of basic bearings;
- Splash 7 at frequency of 87 Hz corresponds to calculated frequency in 86.9 Hz defining defect of the stator.

5. Conclusions

Comparative analysis of estimated data and experimental spectral amplitudes for different parts of electric drive and transmission of heading machine executive unit confirms their validity. Under 0.9 confidence level the divergence of calculated values and values received as a result of measurements doesn't exceed 12%, which is admissible [21].

On the basis of the contrastive analysis of the actual technical condition of the diagnosed units and values of rated amplitudes of signal at the corresponding frequencies in the measured range of current it may be concluded that defect needs to be fixed if amplitude of signal exceeds 10% of maximum, and defect is significant and demands eliminating if value of amplitude exceeds 30%.

The obtained results of research make it possible to perform scheduled preventive works according to actual state of executive unit of KP21 combines during their operation in the considered mining and geological conditions.

References

- [1] E.A. Shemshura, Optimization of ways of heading machines operation system, *Inzhenerniy vestnik Dona*. 4 (2013) <http://www.ivdon.ru/magazine/archive/n4y2013/2001>.
- [2] B.L. Gerike, P.B. Gerike, V.N. Shakhmanov, Fundamentals of mining machine assembly dynamic diagnostics, *Mining informational-analytical bulletin*. 12 (2011) 367-377.
- [3] A.A. Belikov, Application of principles of non-destructive testing and vibroacoustic diagnostics for estimation of mining machine condition, *Mining informational-analytical bulletin*. 9 (2006) 309-313.
- [4] B.L. Gerike, I. L. Abramov, P. B Gerike, Innovative ways of providing working efficiency of mining machines basing on their technical condition monitoring, *Mining informational-analytical bulletin*. 12 (2008) 228-240.
- [5] RD 50-204-87 Reliability in technics. Information collection and processing about reliability of parts in exploitation. Main conditions, Standards publishing, Moscow, 1987.
- [6] V.G. Chernykh. Statement of statistical data collection and processing about reliability of machine parts 2PNB-2, *News of Higher Educational*

- Institutions. North Caucasian Region. Technical science. Special edition, Problems of mining electro electromechanics. (2005) 189-196.
- [7] A.S. Nosenko, E.A. Shemshura, Reliability and operating effectiveness of tunneling machines, URGTU (NPI), Novochoerkassk, 2014.
- [8] V.G. Khazanovich, Reliability and operating effectiveness evaluation of selective heading machines, Mining equipment and electromechanics. 5 (2011) 2-6.
- [9] V.P. Tulupov, V.G. Chernykh, I.A. Nosenko. Experience of heading machine operation model KP21 in Russian Donbass field, Mining equipment and electromechanics. 6 (2007) 2-3.
- [10] B. L. Gerike, I. L. Abramov, P. B. Gerike, Vibrodiagnostic of mining machines and equipment, KuzGTU, Kemerovo, 2007.
- [11] S.G. Mukhortikov, Diagnostics of cutter gear of selective heading machine, Vestnik KuzGTU. 1 (2014) 19-20.
- [12] B. L. Gerike, Monitoring technical condition of mining equipment, Mining machines and automatics. 9 (2002) 30-34.
- [13] V. S. Petukhov, V.A. Sokolov, Electrical drive condition diagnostics. Consumption current spectral analysis method, News of electrotechnics, 1 (31) 2005 23-28 <http://www.news.elteh.ru/arh/2005/31/11.php>.
- [14] L. G. Sidelnikov, D.O. Afanasyev, Technical condition monitoring methodology review of induction motor operating. Review, Vestnik PNIPU. Geology. Oil and Gas Engineering and mining. 7 (2013) 127-137.
- [15] V. Thorsen, M. Dalva, Condition Monitoring Methods, Failure Identification and Analysis for High Voltage Motors in Petrochemical Industry, University of Cambridge. 444 (1997) 1–13.
- [16] William T.Thomson, Mark Fenger, Current Signature Analysis to Detect Induction Motor Faults, IEEE Industry Application Magazine. 7 (2001) 23-29.
- [17] I. A. Nosenko, Tunneling machines diagnostics methodology with frequency domain analysis explanation. Construction, working process and operation of technological machines researches, Collection of studies. (2003) 48-53.
- [18] I.A. Nosenko, Diagnostics device development. Main principles. Diagnostics of heading machine electrical drive condition. Heading machine model KP21, Future development of East Donbass, Collection of studies (2008) 331-333.
- [19] A.B. Sergienko, Digital signal processing, Saint-Petersburg, 2002.
- [20] I.A. Nosenko, IT diagnostics of electrical drive condition of heading machine KP21, Information-computer technology and their application, 9 (2008) 196-198.
- [21] I.A. Nosenko, Tunneling machines reliability improvement using operative diagnostics of execution unit drive, URGTU (NPI), Novochoerkassk, 2008.



International Conference on Industrial Engineering

Computer model of a synchronized asynchronous motor

Omelchenko E.Y.*, Telezhkin O.A., Enin S.S., Tanich V.O.

Nosov Magnitogorsk State Technical University, K.Marx av. 164/1 – 82, Magnitogorsk, 455038, Russia

Abstract

A computer model of a synchronized asynchronous motor has been designed and divided into blocks. The computer model consists of units calculating magnetizing currents, stator and rotor current, the main electromagnetic flux and EMF of windings, electromagnetic torque of the rotor, the angular velocity, and the angle of the motor shaft rotation. The paper presents the results of the synchronization process transients as well as the dependences of the motor torque on the synchronization phase.

© 2015 The Authors. Published by Elsevier Ltd. This is an open access article under the CC BY-NC-ND license (<http://creativecommons.org/licenses/by-nc-nd/4.0/>).

Peer-review under responsibility of the organizing committee of the International Conference on Industrial Engineering (ICIE-2015)

Keywords: Synchronized asynchronous motor; computer model

1. Introduction

1.1. Objectives

Computer model of a three-phase asynchronous motor with wound rotor (here is ADFNEW) is used as a universal, complete tool to research and study the following electric drive systems:

- «asynchronous motor with wound rotor with the resistor in the rotor winding»;
- «synchronized asynchronous motor» (rotor phase is energized by DC voltage);
- «double fed motor» (rotor is energized by three-phase AC voltage);
- «wound-rotor slip recovery system» (rotor winding is connected to diode rectifier).

* Corresponding author. Tel.: +7-3519-296-840.
E-mail address: momentum2@yandex.ru

1.2. Allowances

1. The windings of the stator and rotor are distributed on the grooves perfectly and they consist of several coil groups and create a spatial sinusoidal magnetizing force [1]. The sum of currents of the windings is zero while Y-connected. The phase resistance of the stator windings are equal. The rotor winding allows to connect any external resistors and voltages.
2. Slot ripples of magnetic flux during rotation of the rotor are not taken into account. It is considered that this problem is constructively solved through the bevel grooves on one tooth division and mutual selection of the number of grooves of the stator and rotor.
3. The inductance of the leakage flux of stator and rotor windings are assumed to be constant and independent on the saturation of main magnetic circuit.

2. What is new

- the model has combined form, the calculations of the variables are in 3-phase coordinate system stator and rotor windings [2] and in two-phase rotating system;
- the main equation for creating the model is based on the vector sum of the currents that are the components of the T-shaped equivalent circuit

$$\vec{I}_1 = \vec{I}_m + \vec{I}_2 + \vec{I}_C \quad (1)$$

To use equation (1), it is necessary to know the projection of all vectors on a rotating coordinate system.

3. Block scheme

Block scheme of the computer model ADFNEW (Fig. 1) is developed in MATLAB program and is divided on blocks. Each block of the program in accordance with the purpose of the model carries out the certain computational operations, has input and output variables. These variables at the level of the scheme links blocks of the program in one computer model, and if the blocks related by variables of the same type (vector variable), the relationship between the blocks is shown in bold line. Thin lines shows single (scalar) variables. Each unit can perform logic, non-linear operations, the solution of the differential equations system, etc for input variables.

3.1 Stator and rotor currents calculation

The magnitude of the phase current of the stator I_{li} depends on the magnitude of the stator voltage U_{li} , the magnitude of the back EMF E_{li} induced in the winding and the stator winding parameters. It is considered that the three parameters of the stator windings are the same and phase current in the operator form in three-phase fixed coordinate system ABC can be calculated by the formulas

$$\left. \begin{aligned} I_{li}(p) &= (U_{li}(p) - E_{li}(p) - U_{10}) \frac{1/R_1}{1 + T_1 p}, \\ I_{1A}(p) + I_{1B}(p) + I_{1C}(p) &= 0. \end{aligned} \right\} \quad (2)$$

where: I – the index of phases of the stator, takes the values A,B,C; $T_1=L_1/R_1$ – electromagnetic time constant of the stator winding, sec; L_1 – the inductance of the flux, H, U_{10} – offset voltage winding neutral to the network neutral, V.

Calculation of the three phase currents of the stator I_{Sj} in accordance with formula (2) is performed in the block 1/Z1. The unit input receives three-dimensional vector of the supply voltage U_S and a three-dimensional vector of the back EMF E_S .

The magnitude of the phase current of the rotor I_{2j} depends on the magnitude of the EMF E_{2j} induced in the coil, the magnitude of the rotor voltage U_{2j} and parameters of the rotor windings while rotor resistance R_{2j} can be different. Therefore, the phase current of the rotor in the operator form in the three-phase abc coordinate system, rotating with the slip speed can be calculated by the formulas

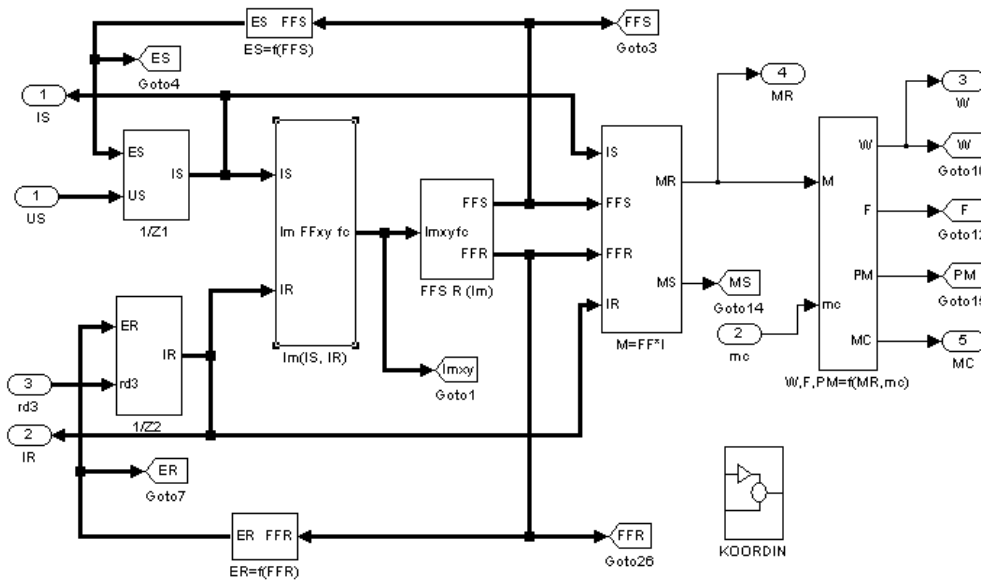


Fig. 1. Block scheme of the model ADFNEW.

$$\left. \begin{aligned} I_{2j}(p) &= (E_{2j}(p) - U_{2j}(p) - U_{20} - I_{2j}(p)R_{2j}) \frac{1}{L_2 p}, \\ I_{2a}(p) + I_{2b}(p) + I_{2c}(p) &= 0. \end{aligned} \right\} \quad (3)$$

where: j is the index of phases of the rotor takes the values a, b, c ; L_2 is the inductance of the rotor winding flux, H; U_{20} – offset voltage winding neutral to the external circuit neutral, V.

In the system with a resistor in rotor winding $U_{2j} = 0, R_{2j} = R_2 + R_{dj}$.

In double fed motor $R_{dj} = 0$ and voltage U_{2j} is set by three-phase vector of a given amplitude and frequency shifted on 120° between the vectors.

In the system of synchronized asynchronous motor additional resistance in the rotor $R_{dj} = 0$ and voltage U_{2j} while synchronization is: $U_{2a} = U_d; U_{2b} = U_{2c} = 0$.

Calculation of the three phase rotor currents I_{Rj} in accordance with the formula (3) is performed in the block 1/Z2. The unit input receives three-dimensional vectors ER, UR and three-dimensional resistance vector $rd3$.

3.2 The calculation of the two-dimensional magnetizing current vector

Equation (1) allows to calculate the two-dimensional components of the magnetizing current vector based on the components of the stator current vector, rotor current vector and current loss in steel. Three-dimensional vector components of stator current are converted by the known formulas from three-phase stationary coordinate system

ABC into two-phase stationary coordinate system $\alpha\beta$, and then converted into two-phase rotating coordinate system xy [2]. Three-dimensional vector components of the rotor current is to be converted from three-phase rotating coordinate system abc into two-phase rotating system dq , and then converted into two-phase rotating coordinate system xy .

These conversions are performed in the software unit $Im(IS, IR)$. Further, in accordance with equation (1) the two-dimensional projections of the vector of the magnetizing current and its module are calculating

$$\left. \begin{aligned} I_{mx} &= I_{sx} - I_{rx} - I_{cx}, \\ I_{my} &= I_{sy} - I_{ry} - I_{cy}, \\ I_m &= \sqrt{I_{mx}^2 + I_{my}^2}. \end{aligned} \right\} \quad (4)$$

Calculation of two-dimensional components of the vector of the main magnetic flux can be accomplished by the formulas

$$\left. \begin{aligned} \Psi_{mx} &= L_m \cdot I_{mx}, \\ \Psi_{my} &= L_m \cdot I_{my}. \end{aligned} \right\} \quad (5)$$

3.3 The calculation of three-dimensional vectors of the main magnetic flux and EMF of the windings

To calculate the EMF it is necessary to perform the following operations:

- for a stationary three phase system of the stator winding it is necessary to convert two-dimensional vector of the main magnetic flux from the rotating coordinate system xy in stationary coordinate system $\alpha\beta$, then convert into three-dimensional stationary system ABC and after that into components of three-dimensional flux to calculate the three-dimensional EMF of the stator winding;
- for rotating three-phase rotor system it is necessary to convert two-dimensional vector of the main magnetic flux from the rotating coordinate system xy in a rotating one dq , then convert into three-dimensional rotating system abc and then into components of three-dimensional flux to calculate the three-dimensional EMF rotor windings.

Software unit $FFS R(Im)$ converts a two-dimensional main flux vector from the rotating coordinate system into three-dimensional stator vector in the stationary coordinate system ABC and into a three-dimensional rotor vector in rotating coordinate system abc .

Calculation of three-dimensional EMF vector of the stator and rotor windings is performed in software units $ES=f(FFS)$ and $ER=f(FFR)$, respectively, by the equations

$$\left. \begin{aligned} E_{st}(p) &= K_{OB1} \Psi_{st}(p) \frac{p}{1+t_0 p}, \\ E_{rj}(p) &= K_{OB2} \Psi_{rj}(p) \frac{p}{1+t_0 p}. \end{aligned} \right\} \quad (6)$$

3.4 The calculation of the electromagnetic torque of the rotor

The calculations and transformations allow to operate with values of the multidimensional vector in stationary and rotating coordinate systems, either in three-phase or two-phase systems. According to the Ampere's law the force on the conductor with current in a magnetic field is proportional to current, induction in the gap and the length of the conductor in a magnetic field. Thus to calculate the electromagnetic torque of the rotor is enough information about the currents and fluxes of the rotor in three-phase rotating coordinate system abc [4]

$$M_r = p \Pi (I_{ra} (FF_{rb} - FF_{rc}) + I_{rb} (FF_{rc} - FF_{ra}) + I_{rc} (FF_{ra} - FF_{rb})) / \sqrt{3}. \tag{7}$$

The calculation of electromagnetic torque in the model is performed in block $M=FF*I$ by the formula (7) on the basis of information on three-dimensional vectors of the main magnetic flux and rotor winding current.

3.5 The calculation of angular speed and rotation angle of the motor shaft

The software block $W,F,PM=f(MR,mc)$ provides the calculation of the angular speed of rotation and the mechanical rotation angle of the rotor winding according to the equations

$$\left. \begin{aligned} \omega(p) &= (M_r(p) - M_c(\omega)) \frac{1}{J_{\Sigma} p} + \omega(0), \\ \Theta_r(p) &= \omega(p) \frac{1}{p} + \Theta_r(0). \end{aligned} \right\} \tag{8}$$

where: T is the integration time, sec; J_{Σ} is the total moment of inertia of the electric drive, $kg*m^2$; $M_c(\omega)$ is a resistance mechanism torque, Nm.

The transients on the laboratory bench confirm reliability of the model.

4. The results of the simulation

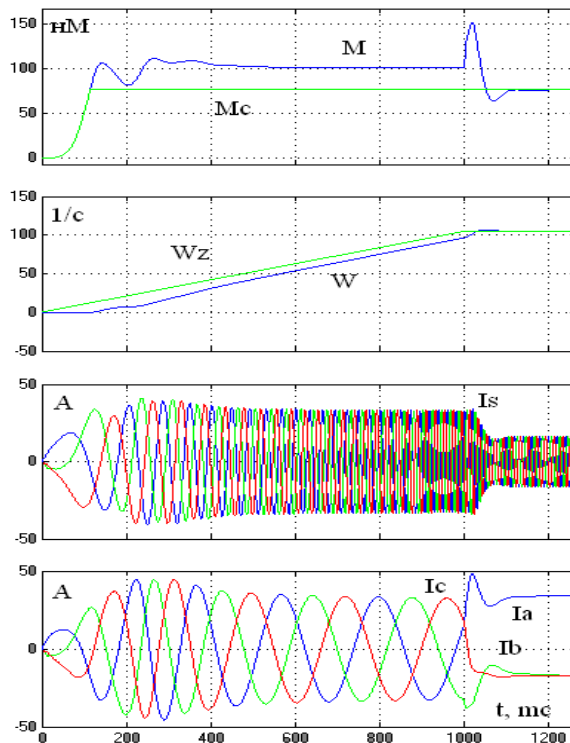


Fig. 2. Transients of start and synchronization processes.

Computer model ADFNEW is implemented in the software package MATLAB [5], on the basis of which is developed a model of the synchronized induction motor [6]. Fig.2 shows transient of synchronization of the asynchronous motor MTF211-6 (9 kW, 915 rpm). Asynchronous start occurs at 1.0 sec on the frequency converter with scalar control. The engine synchronization starts at $t = 1.0$ s with energizing the phase a of rotor windings by DC voltage. Phases b and c of rotor winding are connected in parallel. The synchronization process is accompanied by an oscillating transient of torque of the motor that depend on the time of the supply voltage and in phase a .

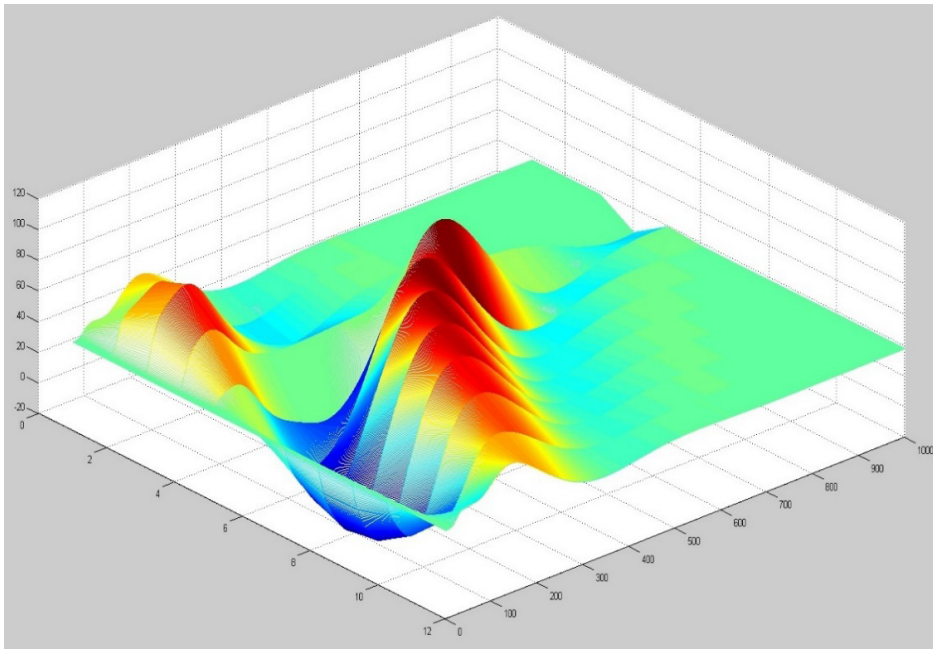


Fig. 3. Transient processes of the motor torque as a function of phase current of the rotor.

On the computer model has researched the impact of the moment of synchronization on quality of transient process of the engine torque. According to the results of computer simulation of asynchronous motor synchronization (Fig. 3) it can be concluded that the best moment of supplying a DC voltage is when rotor current of phase a increases from 0 to the maximum (phase current of the rotor from 0 to 90 deg.).

References

- [1] A.S.Sarvarov, E.Y Omelchenko, Magnetomotive forces of three-phase asynchronous motor windings, *Electrotechnika*. 1 (2013) 31–35.
- [2] I.A. Selivanov, E.Y. Omelchenko, Electromechanical properties of asynchronous motors, *Vestnik. Magnitogorsk: Nosov Magnitogorsk State Technical University*. 3(35) (2011) 35–38.
- [3] E.Y. Omelchenko, *Dynamic mathematic models of asynchronous motor: monograph*, Nosov Magnitogorsk State Technical University, Magnitogorsk, 2012.
- [4] R.T. Schreyner, *Mathematic modeling of AC electric drives with semiconductor frequency converter*, Ekaterinburg: Ural Dept. of the Russian Academy of Sciences, 2000.
- [5] E.Y. Omelchenko, O.A. Telezhkin, V.O. Tanich, A.B. Limar, State certificate of registration on the computer program 2014617619.
- [6] E.Y. Omelchenko, O.A. Telezhkin, S.A. Linkov, D.S. Tigarev, State certificate of registration on the computer program, 2014660570.



International Conference on Industrial Engineering

Evaluation assurance levels for human resource security of an information system

Astakhova L.V. *

South Ural State University, 76, Lenin Avenue, Chelyabinsk, 454080, Russian Federation

Abstract

Present methods for evaluating reliance on the information system security do not take into account the socio-technical nature of the information system and modern humanitarian approaches to the evaluation of reliance on them. The article defines the term "reliance to the personnel security of the information system" and substantiates a multi-criteria classification that categorizes evaluation levels of the reliance on the information system personnel security. The classification is the scientific novelty of this research. Seven stated evaluation levels of reliance on the personnel security are relevant to the seven evaluation levels of reliance on the information technologies embodied in the international standard ISO / IEC 15408-3: 2008 *Information Technology - Security Techniques - Evaluation Criteria For IT Security - Part 3. Security Assurance Components*.

© 2015 The Authors. Published by Elsevier Ltd. This is an open access article under the CC BY-NC-ND license (<http://creativecommons.org/licenses/by-nc-nd/4.0/>).

Peer-review under responsibility of the organizing committee of the International Conference on Industrial Engineering (ICIE-2015)

Keywords: reliance, personnel security, information security, assessment, level, user, information system.

1. Introduction

According to the report on security leakage for the 2014 year of InfoWatch Analytical Centre in comparison to 2013 year, the number of data leaks in the world increased by 22%, in Russia - by 73%. In the distribution of leaks in regions on the first position by the number of leaks traditionally are the United States (906), on the second position is Russia (167), on the third is the UK (85). Whereas 71% of cases the information leakage was caused by employees of companies - present or former (69.2% and 1.4%, respectively) [1]. These figures indicate that a user, an internal client as the most important link in the information system are greatly underestimated in the practice of

* Corresponding author. Tel.: +7-351-267-99-00; fax: +7-351-267-99-00.
E-mail address: lvastachova@mail.ru

information security. This conclusion is confirmed by the analytical results of the established approach to the achievement of reliance on in the security of information systems. The Standard ISO / IEC 15408-3: 2008 "Information technology - Security techniques - Evaluation criteria for IT security - Part 3. Security assurance components" [2] as well as an identical Russian National Standard ISO / IEC 15408-3-2013 "Information technology. Methods and tools of security protection. Information Technology Security Evaluation Criteria. Part 3: Components of reliance on security"[3] has a significant drawback. It attempts to solve the problem of reliance on security of the information system as a purely engineering system although nowadays any information system is a socio-technical. Therefore its safety can not be evaluated without taking into account trust to its users and, consequently, without the usage of scientific and humanitarian approaches. The problem of reliance on socio-technical systems has been actively studied today in economics, sociology, psychology. Thus, A.B. Kupreychenko includes a number of basic structural elements of the socio-technical system model trust into various types of people maintaining the system (the creators, providers, system moderators and other parties concerned) [4, P.435 - 436]. According to B. Uzzi, organizational trust is influenced by three groups of factors: organizational factors (characteristics of organizations) - the structure, the personnel organizational policy, organizational culture; relationship factors (situational characteristic) - the primary interaction, expectations, "cost of interchange"; individual factors (personal characteristics of the subject of trust) - the propensity to trust, self-efficacy, values [5]. However, the theory of information security pays insufficient attention to trust to the protected information system users although some personnel security issues are resolved up to standards [6] and even at the level of automation [7].

The contradiction between the increasing number of information leakage due to the fault of information systems users, on the one hand, and ignoring their users in the course of reliance on their security evaluation, on the other, determines the relevance of the problem of reliance on the information system user as its integral part, as well as the development of evaluation levels of the reliance on the personnel security of the information system.

2. The reliance on the personnel security of the information system and its evaluation criteria

"Reliance on the personnel security of the information system" we define as employers and employees subjective mutual expectation of constant observation of natural and moral laws, and commitment (personal component) as well as the competent actions in the field of information security (competence component) to ensure successful functioning and development of both entities. Subjective and objective ambivalence of a stated concept and analysis of modern approaches to the evaluation of reliance on the socio-technical systems made it possible to distinguish two groups of criteria for the reliance on the personnel security of the information system evaluation both for the employer and for the employee: competence and personal criteria.

2.1. Personal criteria. The level of transformation the cultural capital of employees into the cultural capital of the organization (ID_{pers})

It is stipulated by the modern needs of the person as a subject of economic life. According to the research, high-priority for people in modern culture and having the greatest positive impact on economic development are the values of self-actualization, spirituality and search for pleasure [8]. It requires the observation of the employees cultural capital and its implementation on the organization. The research on the problems of cultural capital evaluation is in progress in modern economics [9 and etc.]. However, our developed technique of "cultural capitals relationship" appears to be the most heuristic to evaluate the reliance on the personnel security of the information system. Based on the identification of the reliance index as the ratio of employees cultural capitals in the organization and outside, it makes possible to monitor these capitals and the gap between them, to evaluate necessary directions of the organization's structural capital development for information security derisking in respect of each employee at any time.

The index of reliance on each employee is calculated according to the formula as the ratio of two detected indicators for each employee:

$$D_{pers} = ICCIS_{pers}/corp : ICCIS_{pers} , \quad (1)$$

where: D_{pers} – the reliance index of an employee n ; $ICCIS_{pers/corp}$ – corporate cultural capital of the employee's information security in the organization; $ICCIS_{pers}$ – personal cultural capital of the employee's information security outside the organization.

The task of the organization in achieving the goal of its information security protection is to convert employee's personal cultural capital (User IS) into the corporate cultural capital [10, p.9].

The developed technique makes it possible to solve one of the most difficult problems related to employee motivation, his subjective views and ethical and moral qualities, and not to be restricted only to the level of professionalism and the kind of personnel [11]. It affords the opportunity to get closer to solving the dilemma "manager-employee" ("Principal-agent problem" or "agency dilemma"), which raises when an employee (agent) carries out any action (makes a decision) on behalf of the manager (principal) and is ruled by his own considerations, interests and motivation, but not the employer's ones [12]. To solve the problem scientists have developed the principles of employee's incentive payments: informativeness (the maximum of information about the responsibilities and compensation payments); motivation intensity (extra payments from extra efforts, employee's response to motivation); monitoring of motivation intensity; equivalent compensation to the motivation intensity of the employee [13]. These principles underline the need for achieving the employer and employee feedback in the process of stimulating the latter to implement his cultural capital.

2.2. Personal criteria. The level of mutual trust of employers and employees (LDD)

Foreign publications offer the following classification and characteristics of the bases of trust: the absence of trust - based on deterrence; low level of trust - based on the analysis; confidence level - based on knowledge; high level of trust - based on relationships; absolute trust - based on the identification; authentic trust [14, 15, 16, 17]. To avoid abovementioned "agency costs" [18], experts propose to use commissions; remuneration as percentage of profit; piecework payment; performance measurement; the list of all agent's obligations; threat of dismissal of the agent [19]. In consideration of this bases of trust classification, note that not all of these measures can help improve trust between an employer and an employee. For example, the threat of dismissal of the agent is deterrence, and therefore it is the basis of absence of trust. The most appropriate level of trust for the information security begins with trust-based relationship whereas the interaction is the ontological basis of security, including information one.

2.3. Competence criteria. The level of awareness in information security (LAP)

The most well-known standards and recommendations on awareness building process are: PCI Council Best Practices for Implementing a Security Awareness Program, NIST Special Publication 800-50, ENISA The new users' guide: How to raise information security awareness, Russian National Standard ISO / IEC TO13335-3—2007 Security techniques, ISO / IEC TR 13335-3: 1998 Part 10.3 Personnel training on information security, ISO 27001, COBIT 5, etc. Thus, ENISA recommendations include 71 awareness criteria, which can be divided into seven groups and brought in line with standard evaluation levels of the reliance on the personnel security of the information technologies.

2.4. Availability of monitoring the dynamics of the cultural capital of the organization procedures covering organizational measures to enhance reliance on personnel security of the information system (DP)

Personal and corporate cultural capitals in the organization should be objects of planning, accounting, monitoring, evaluation and improvement, and all these processes should be documented. This will indicate the level of management awareness of the importance of working with personnel on the usage of their knowledge, skills, experience and achievements for the economical growth of the organization and awareness of it.

The analysis of the indicators on the abovementioned criteria helps discern the level of the categorical personnel structure (LPR) and the level of labour risks. In any organization, there are four personnel categories which are selected depending on the performance of employees, on the set of their knowledge and skills, as well as psychophysiological peculiarities: personnel - capital, personnel - resource, personnel and staff.

The structural relationship of these categories influences the level of possible labour risk: high, medium and low[20]. The more procedures are carried out in the organization the more personnel of the category "personnel-capital" which can affect the economical growth it has and the lower is the level of labour risks.

3. The multi-criteria classification of evaluation levels of the reliance on the personnel security of the information system

The abovementioned criteria can be taken as the basis for the multi-criteria classification of evaluation levels of the reliance on the personnel security of the information system. Each level can be described by the model:

$$ELRPS = IDpers + LDD + LAP + DP + LPR \quad (2)$$

where: ELR PS – evaluation level of the reliance on the personnel security; IDpers – the reliance index of an employee on the organization (the level of transformation the cultural capital of employees into the cultural capital of the organization); LDD – the level of mutual trust; DP – monitoring the cultural capital of the organization procedures; LPR – the level of labour risks on the ratio of personnel categories; LAP – the level of staff awareness of information security.

Each of seven evaluation levels is characterized by indicators for each of the selected reliance criteria (Table 1). For example:

$$ELRPS7 = (IDpers = 0.8 - 1) + (LDD = Authentic\ trust) + (LAP = 7) + (DP = 6) + (LPR = Low). \quad (3)$$

Table 1. The multi-criteria classification of evaluation levels of the reliance on the personnel security of the information system.

ELR PS	IDpers	Personnel categories	LDD	LAP	DP	LPR
1	0,2	Staff	The absence of trust – based on deterrence	1	-	High
2	0,3	Staff	The absence of trust – based on deterrence	2	1	High
3	0,4	Personnel	Low level of trust – based on the analytics	3	2	High
4	0,5	Personnel	Confidence level of trust – based on knowledge	4	3	Medium
5	0,6	Personnel-resource	High level of trust – based on relationships	5	4	Medium
6	0,7	Personnel-capital	Absolute trust – based on the identification	6	5	Low
7	0,8-1	Personnel-capital	Authentic trust	7	6	Low

4. Conclusions

The growing number of information security incidents caused by corporate staff requires the development of methods of the reliance on the information security system evaluation by their personnel security enhancement. However, present methods of the reliance on the information system security evaluation do not take into account the socio-technical nature of the information system and modern humanitarian approaches to the evaluation of reliance on them. Determined on the basis of interdisciplinary research evaluation criteria of reliance for the first time allowed to justify theoretically the multi-criteria classification of evaluation levels of the reliance on the personnel

security of the information system. Seven stated evaluation levels of reliance on the personnel security are relevant to seven evaluation levels of reliance on the information technologies embodied in the international standard ISO / IEC 15408-3: 2008 "Information technology - Security techniques - Evaluation criteria for IT security - Part 3. Security assurance components". The practical relevance of the research involves the possibility of expanding the content of evaluation levels of reliance in the abovementioned standard to improve the information technologies security.

References

- [1] Information on http://www.infowatch.ru/report2014_half
- [2] Information on http://www.iso.org/iso/ru/home/store/catalogue_tc/catalogue_detail.htm?csnumber=46413
- [3] ISO / IEC 15408-3-2013 Information technology. Methods and means of ensuring safety. Criteria for Information Technology Security Evaluation. Security assurance components, Standartinform, Moscow, 2014.
- [4] A.B. Kupreychenko, I.V. Mersyanova, Trust and mistrust, Civil Society Development, HSE Publishing House, Moscow, 2013.
- [5] B. Uzzi, Social Structure and Competition in Interfirm Networks: The Paradox of Embeddedness, *Administrative Science Quarterly*. 42(1) (1997) 35–67.
- [6] N.L. Ulyanov, L.V. Astakhova, The problem of personnel security in the information security standards the Bank of Russia, *Bulletin of the Ural Federal District. Security in the information sphere*. 4(14) (2014) 66–70.
- [7] L.V. Astakhova, V.A. Efremov, A.I. Mitkin, Automation multifactorial assessment of human vulnerability information security, *Ural Federal District Bulletin. Security information sphere*. 4(14) (2014) 57–61.
- [8] N. Lebedev, A.N. Tatarko, Values and social capital as the basis of socio-economic development, *Journal of Institutional Studies (Journal of Institutional Research)*. 2(1) (2010) 17–34.
- [9] E.A. Kosmin, S.E. Metelev, A.D. Kosmin, The Cultural Capital of the Company in a Real Material Functioning Organization, *Economics, Moscow*, 2007.
- [10] L. Astakhova, Information security: risks associated with the cultural capital of staff, *Scientific and technical information. Series 1: Organization and methods of work of information*. 4 (2015) 1–13.
- [11] Information on http://www.intel.com/Assets/en_US/PDF/whitepaper/wp_IT_Security_RiskAssessment.pdf free.
- [12] M.C. Jensen, *Theory of the Firm: Managerial Behavior, Agency Costs and Ownership Structure*, Harvard University Press, 2000.
- [13] P.R. Milgrom, Jh. Roberts, *Economics, Organization and Management*, Prentice-Hall, 1992.
- [14] G. Durham, D. Hartog, Measuring trust inside organisations, *Personnel Review*. 5(35) 557–588
- [15] L. Coltri, *Conflict diagnosis and alternative dispute resolution*, Upper Saddle River, Prentice Hall, 2004.
- [16] Information on <http://www.citeman.com/3621-types-of-trust-in-organizational-relationships.html#ixzz3bpKE6nYX>
- [17] D.M. Rousseau, S. Sitkin, R.S. Burt, C. Farrell, Not So Different After All: A Cross-Discipline View of Trust, *The Academy of Management Review*. (1998).
- [18] P.R. Milgrom, Jh. Roberts, *Economics, Organization and Management*, Prentice-Hall, 1992.
- [19] R. Zhang, Y. Zhou, H. Zhuang, Study on the project supervision system based on the principal-agent theory, *Journal of Industrial Engineering and Management*. 8(2) (2015) 491–508.
- [20] A.G. Badalova, K.P. Moskvitin, Personnel risks: risk management of human enterprise, *Russian Entrepreneurship*. 7 (2005) 92–98.



International Conference on Industrial Engineering

Adaptive control over the permanent characteristics of a wind turbine

Solomin E.V.*, Sirotkin E.A., Martyanov A.S.

South Ural State University, 76, Lenin Avenue, Chelyabinsk, 454080, Russian Federation

Abstract

Herein is proposed a system for adaptive speed control of the permanent characteristics of a wind turbine to ensure safe operation thereof. The design of wind turbines is generally calculated with the nominal power generation at a wind speed of 11 m/s, and it should be controlled at higher wind flow velocities. Rotation speed is the main control parameter of wind turbine system. In addition, the control system can provide normalized thermal conditions for the alternator and prevents exceeding vibration level. Adaptive control system contains mechanical and electromechanical modules intended for braking rotor using friction components. There is also a structure diagram of control system and transfer functions of system components.

© 2015 The Authors. Published by Elsevier Ltd. This is an open access article under the CC BY-NC-ND license (<http://creativecommons.org/licenses/by-nc-nd/4.0/>).

Peer-review under responsibility of the organizing committee of the International Conference on Industrial Engineering (ICIE-2015)

Keywords: wind energy; control system; adaptive control; centrifugal brakes.

1. Introduction

Wind energy is well known and being utilized for a long time. During the last few centuries we saw a technology development in wind industry, as results we can find more and more wind turbines (WT) converting the kinetic energy of airflow into electric power (in some cases into mechanical one) [1]. Wind turbine companies are seeking for a different ways of the product cost reduction [2] including the wind turbines weight decrease. However, such lightweight constructions are not intended for a longtime operation in heavy duties and may fail [3]. Sometimes WTs are optimized to generate a maximum of energy in the most probable wind speeds (as a usual 11 m/s, but may vary

* Corresponding author. Tel.: +7-912-317-18-05;
E-mail address: e.solomin@bk.ru

up to 25 m/s) [4]. Showing the nominal wind speed higher is a trick of sales managers to show higher performance, because well known that the higher wind speed is more rarely observed in the continental areas [5]. Meanwhile, often there is a demand for control of WT on the high winds. Otherwise, the rotor of WT may be destroyed, mechanical transmission can be damaged, and alternator may overheat [6]. Also, one of the dangerous factors in WT operation is the vibration generating by a construction as a result of resonances on several frequencies, as a rule. The vibration effect leads to the increase of radial flapping, bearing failure, reduction of lifetime, basement concrete cracking. All these negative effects lead to the damage of WT and increase the danger during its usage [7].

2. Adaptive control system

We propose the adaptive control system as the way to provide the safe usage of wind turbine. The feature of this system is the control of wind turbine reaction. Since the control system is proposed initially to provide the safety operation, the main controlled parameters are the technical state of the wind turbine. In case of rotor failure caused over speed rotation, the turbine parts with high kinetic energy may damage the surroundings objects so the most important controlled parameter of wind turbine is rotation speed. The control of other characteristics (temperature of alternator [8]) can be taken into account as secondary or dependent on the primary values. There are many different modifications and variants of wind turbine design. Let's focus the discussion on centrifugal cam braking system for Vertical Axis Wind Turbine (VAWT), presented in Fig. 1. However, it is possible to spread this design for any WT type because almost each wind turbine contains such components as rotor shaft, mast, housing, etc. [9].

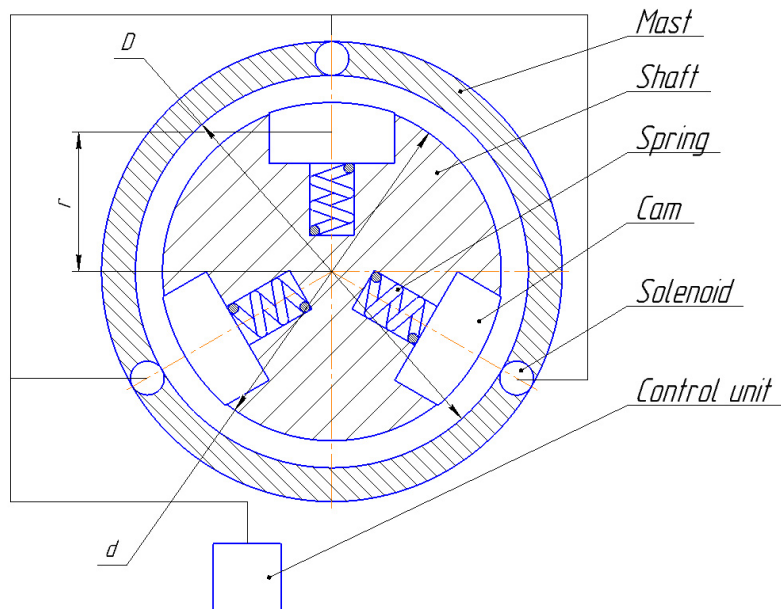


Fig. 1. Design of centrifugal cam device of mechanical action.

When the rotor rotation frequency is above zero ($\omega > 0$) the centrifugal force F_c all geometrical points of rotating rotor (excluding those on the rotation axis). Its value is in proportion with the square of rotation frequency:

$$F_c = mr\omega^2, \quad (1)$$

where m – mass of rotating element, r – distance from rotation axis to the center of mass of this section.

The cam moves in the slot along the radial direction, being connected with the shaft by a spring keeping cam moving from the slot. The spring stretching l can be calculated according to Hooke's law in relative form [10]:

$$l = \frac{F_{sp} L}{ES}, \quad (2)$$

where F_{sp} – stretching force of spring on the length l , L – length of spring, S – cross-section wire, E – Young modulus.

To move the cam from its initial position, the following condition is required:

$$F_{sp} < F_c. \quad (3)$$

In this case, the centrifugal force exceeds the elastic force and the cam gets moving from the center. However, this condition is not enough for the cam to contact a friction surface of the internal wall of mast starting the rotor braking. The determined value of angular velocity should correspond the determined value of centrifugal force acting on the cam. Thus the cam should cover the distance equal to the difference of outside radius of the cam and internal radius of the mast wall $l = D - d$. Reaching of distance l the cam touches the internal mast wall and start sliding along its surface.

Friction force in this case depends on support reaction force N_{normal} , and on the coefficient of friction for contacting surfaces in accordance with the following equation [11]:

$$|F_{fr}| \leq \mu N_{normal}. \quad (4)$$

Note that the friction coefficient depends also on the sliding speed. However, this dependence is quite small and the μ could be a constant when the high accuracy of measurement is not required [12].

Air flow affects the rotor of WT making a rotating torque. Applying a contrary acting torque by the brake reduces rotation speed [13]. Taking into account the inertia of rotor, the braking process can be considered as long in time that increases the failure probability. It is also known that the pressure on the blades has a wavy impact (as the wind gusts have a jumping type characteristic), and the system reaction speed should be relatively high to provide the safety operation in time [14]. Thus, it is necessary to generate a friction torque M_{fr} exceeding the torque generated by wind flow M_w to handle a braking process during a short time [13]:

$$M_{fr} = F_{fr} \frac{D}{2} > M_w. \quad (5)$$

Apparently, having high rotation speed the cams may transfer the whole rotating torque. The value of this rotating torque M_{fr} (friction torque), transferring by cams from the shaft to the mast, can be determined as follows [15]:

$$M_{fr} \leq 0,5(F_c - F_{sp})\mu z D = 0,5mrDz\mu(\omega_{lim}^2 - \omega_0^2), \quad (6)$$

where z – number of friction parts (cams).

Thus, the braking cams press the mast walls on nominal rotation speed with a force, when the rotating torque of wind rotor is not enough for driving the cams and rotor stops. It is important that the momentary stop or rotor may cause the high impact loading on all construction components, especially on the blades, and the aggregate may fail.

In this case, it is necessary to determine the optimal position between two boundary states of the system. I.e. we need a fast acting centrifugal system to reduce the risk of accidents to a minimum, but the time for response cannot be zero, as it lead to the destruction of the structure due to the critical loads. This means that the cams should have a soft braking characteristic, and braking process should start before rotation reaches the extreme speed. Therefore, it is necessary to operate in a vary ω_o with limitation of the maximum speed by ω_{lim} . In the speed range between ω_o and ω_{lim} the cam touches the mast wall, but keep sliding reducing the torque and rotation speed. By reducing the rotation speed of the rotor shaft, the centrifugal force gets less and the cams pressure on the wall reduces. Fig. 2 is a graph of torque transmitted by the cams and rotor speed. Up to ω_o the rotor rotates without activating a braking system, then in accordance with the shaft speed coming to the range between ω_o and ω_{lim} , the system will be automatically activated by moving cams.

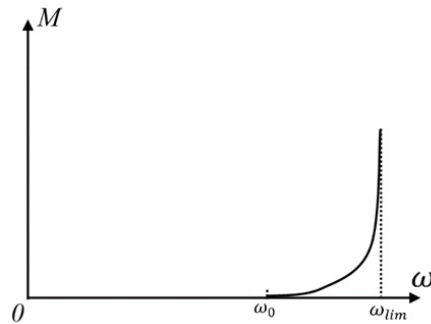


Fig. 2. A graph of the torque transmitted by the cam(s) and rotor speed of the wind rotor.

Such parameters as temperature of coils in the electric generator and the vibration depend on the rotation speed of the rotor [16]. One more feature of the adaptive control system is a possibility to monitor the abnormal temperature of the generator windings and vibration of the mast by respective sensors, and slow down or stop the turbine in the malfunction. In this case, some solenoids in the rotor shaft activate cams to stop rotation. The electric driven cam can touch the mast wall even in case when the rotation speed of rotor haven't reach ω_o value.

Solenoid should be activated by an electric signal from a smart control system, which will send control signals to solenoids. The cam touches the mast wall when magnetic field is strong enough to affect the cam and thereby stretch the spring, and the following condition should be true:

$$F_{act} > F_{sp}. \quad (7)$$

Process for getting a braking condition (5) requires the following:

$$F_{act} \geq 2 \frac{M_w}{D}. \quad (8)$$

Thus, controller system of adaptive wind turbine control gets the information from three different sensors: temperature, vibration and shaft speed. Last sensor seems redundant, since the rotation speed is controlled by spring stretching characteristic independently on the control signal. However, in case of failure of any component of centrifugal cam system, the rotor will accelerate to nominal speed and the sensor can send the signal to the controller, which could eventually prevent the accident.

3. The control scheme

For quantitative analysis of the processes during the signal exchange between the components of the control system, it is advisable to represent the system in the form of block diagram. The block diagram (Fig. 3) is a schematic representation of the control system as a set of functional blocks, each of which has a certain transfer function [17].

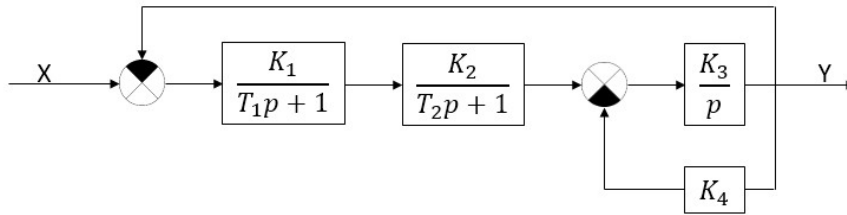


Fig. 3. Control system in a block diagram form.

The main regulating effect in the wind turbine control system (Fig. 4) is realized by pushing mechanism, which consists of solenoids and braking cams. The principle of control and adjustment is based on the control error compensation function. Control block diagram is shown in Fig. 5.

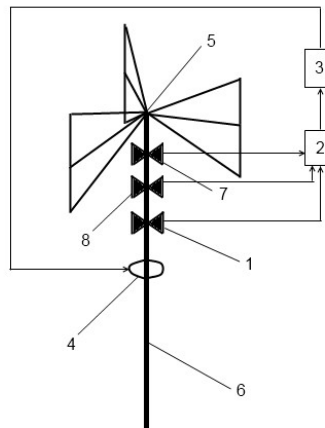


Fig. 4. adaptive control system of wind turbine: 1 – shaft ω speed sensor; 2 – comparing block; 3 – amplifier; 4 – pressing mechanism (solenoids) and moving cams; 5 – rotor; 6 – mast; 7 – alternator τ_g temperature sensor; 8 – vibration ψ sensor.

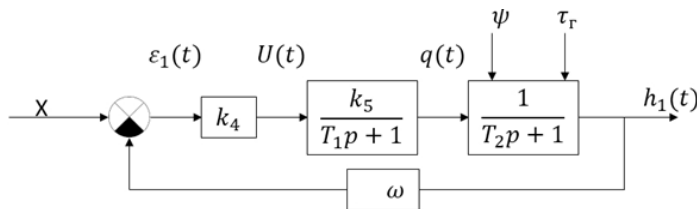


Fig. 5. Block diagram of wind turbine control system.

Since the temperature of the alternator windings τ_g and vibration levels ψ are determined by wind turbine rotor speed ω , the rotor rotation speed will be the major controlled parameter. The nominal value of the shaft speed h_1 is set up by sequential block as analog signal x_{task} . Information about current value of the controlled parameter $h_1(t)$ is obtained by the speed sensor and converted further into the signal $x(t)$, coordinated by referring to the signal x_{task} . Comparison of the set and the true values for the control parameter is in the comparator block. It generates the error signal $\varepsilon(t) = x_{task} - x(t)$. After the conversion required to obtain a signal suitable for testing by actuator, it implements the control action $U(t)$ on controlled object in the form of pressing the braking cams to the mast wall by solenoids in accordance with the magnitude and sign of the error $\varepsilon(t)$ [18].

Thus, the block diagram allows converting the quantitative dependences for cam motion estimation into the signal function to get a shaft speed distribution. Based on a spring rate and using formulas of elastic theory, the displacement of the cam is implemented into the contact with the mast wall to eliminate the deviation from the given value [19].

Transfer functions of system components:

- wind turbine speed sensor $W_1(p) = K_1$;
- converter (amplifier) $W_2(p) = K_2$;
- solenoids (actuators) $W_3(p) = K_3 / (T_1 p + 1)$;
- braking cams (controlled object) $W_4(p) = 1 / (T_2 p + 1)$.

Specific values of coefficients K_i and time constants T_i are defined by property of the equipment, and could be easily determined. If the controlled object and the control system are developing is at the same time, this allows getting the best combination of their characteristics. For instance, if the preliminary calculation indicates a lack of processing speed, then there is a number of possible solutions for this problem. Usage of high power solenoids is also possible. It will increase the dynamic response of the system and decrease the mass of braking cams, or reduce the spring stiffness. If characteristics of sensitivity or precision control are unsatisfactory, then these problems could be solved by increasing the gain in sensor blocks and converting the error signal, or interpose corrective links into the structure [20].

This work was supported in part by Ministry of Education and Science of Russian Federation under the project “Carrying out applied researches in the field of technology of high reliable energy saving systems for different purposes based on modern equipment of renewable and hybrid generation, accumulation, distribution and consuming of energy” according to the contract no. 14.577.21.0069 d.d. 05.06.2014, unique identifier RFMEFI57714X0069.

References

- [1] I.M. Kirpichnikova, A.S. Martyanov, E.V. Solomin, *Preobrazovanie energii v vetroenergeticheskikh ustanovkakh, Mezhdunarodnyy nauchnyy zhurnal «Alternativnaya energetika i ekologiya»*. 1 (2010) 93–97.
- [2] E.V. Solomin, *Vetroenergeticheskaya ekonomika, Mezhdunarodnyy nauchnyy zhurnal «Alternativnaya energetika i ekologiya»*. 2 (2010) 28–30.
- [3] E.V. Solomin, I.M. Kirpichnikova, A.S. Martyanov, *Iteratsionnyy podhod v razrabotke i optimizatsii vertikalno-osevyykh vetroenergeticheskikh ustanovok, «Elektrotehnika. Elektrotehnologiya. Energetika», Sbornik nauchnykh trudov VII mezhdunarodnoy nauchnoy konferentsii molodykh uchenykh, Novosibirskiy gosudarstvennyy tekhnicheskii universitet, Mezhdunarodnyy tsentr sodeystviya nauchnoy i innovatsionnoy deyatel'nosti studentov i molodykh uchenykh Novosibirskoy oblasti*. (2015) 92–95.
- [4] E.V. Solomin, *Vetroenergeticheskie ustanovki GRTs-Vertikal, Alternativnaya energetika i ekologiya -ISJAE*. 1 (2010) 10–15.
- [5] P.P. Bezrukih, *Ispolzovanie energii vetra. Tehnika, ekonomika, ekologiya, Kolos, Moscow*, 2008.
- [6] A.N. Kindryashov, A.S. Martyanov, E.V. Solomin, *Elektricheskie mashiny vetroenergeticheskikh ustanovok s vertikalnoy osyu vrascheniya, Mezhdunarodnyy nauchnyy zhurnal «Alternativnaya energetika i ekologiya»*. 1/2(118) (2013) 59–62.
- [7] I.M. Kirpichnikova, E.V. Solomin, *Vibrogasiteli macht sverhmalyykh vertikalno-osevyykh vetroenergeticheskikh ustanovok, Vestnik YuUrGU. Seriya «Energetika», Izd-vo YuUrGU*. 13-14(190) (2010) 78–81.
- [8] I.M. Kirpichnikova, A.S. Martyanov, E.V. Solomin, *Modelirovanie generatora vetroenergeticheskoy ustanovki, Elektrotehnika*. 10 (2013) 46–50.
- [9] P.P. Bezrukih, P.P. Bezrukih (mladshiy), *Vetroenergetika. Vyimysly i fakty. Otvety na 100 voprosov, Institut ustoychivogo razvitiya Obschestvennoy palaty Rossiyskoy Federatsii, Tsentr ekologicheskoy politiki Rossii, Moscow*, 2011.
- [10] Gorshkov, Troshin, Shalashilin, *Soprotivlenie materialov*, second ed., 2005.
- [11] F.P. Bowden, D. Tabor, *The Friction and Lubrication of Solids*, Oxford University Press, 2001.

- [12] Bo N.J. Persson, Sliding Friction, Physical Principles and Applications. Springer, 2002.
- [13] E.V. Solomin, I.M. Kirpichnikova, E.A. Sirotkin, RF Patent 142083 (2013).
- [14] V.M. Lyather, Razvitie vetroenergetiki, Malaya energetika. 1-2(4-5) (2006) 18–38.
- [15] G.P. Tarikov, A.T. Belskiy, V.V. Komrakov, Detali mashin : ucheb. posobie, M-vo obrazovaniya Resp. Belarus, Gomel. gos. tehn. un-t im. P. O. Suhogo, Gomel: GGTU im. P. O. Suhogo, 2010.
- [16] E.A. Sirotkin, A.S. Anikin, S.V. Kozlov, E.E. Solomin, Regulirovanie chastoty vrascheniya rotora vertikalno-osevoy vetroenergeticheskoy ustanovki, Mezhdunarodnyy nauchnyy zhurnal Alternativnaya energetika i ekologiya. 5(145) (2014) 32–36.
- [17] I.M. Makarov, I.M. Lohin, S.V. Manko, M.P. Romanov, Iskusstvennyy intellekt i intellektualnyie sistemy upravleniya, Nauka, Moscow, 2006.
- [18] V.G. Ilichev, Proektirovanie sistema avtomaticheskogo upravleniya, Izd-vo: YuUrGU, Chelyabinsk. 2001.
- [19] I.D. ZolotarYov, V.V. Valikov, RaschYot dinamicheskikh rezhimov kolebatelnyih sistem spetsialnogo vida: uchebnoe posobie, Izd-vo: OMGU, 2009.
- [20] Bianchi, D. Fernando, Wind turbine control systems: principles, modelling and gain scheduling design, 2007.



International Conference on Industrial Engineering

Feedback control based on neural networks

Yan Anisimov*

South Ural State University, 76, Lenin Avenue, Chelyabinsk, 454080, Russian Federation

Abstract

The paper describes an algorithm for the synthesis of neural networks to control gyrostabilizer. The neural network performs the role of a state vector observer. The role of such an observer is to provide feedback on gyrostabilizer, which is illustrated in the article. The paper details the issue of specific stage-related peculiarities of classic algorithms: choosing the network architecture, learning the neural network and verifying the results of feedback control. The article presents an optimal configuration of the neural network like memory depth, number of layers and neurons in these layers, and activation layer functions. It also provides data on dynamic systems to improve learning neural network learning. There is also provided an optimal training pattern.

© 2015 The Authors. Published by Elsevier Ltd. This is an open access article under the CC BY-NC-ND license (<http://creativecommons.org/licenses/by-nc-nd/4.0/>).

Peer-review under responsibility of the organizing committee of the International Conference on Industrial Engineering (ICIE-2015)

Keywords: "Neural network, feedback control, gyrostabilizer, observer, neural control"

1. Introduction

Currently, neural network technology is one of the fastest growing areas of artificial intelligence. It successfully applied in various branch of science, such as pattern recognition systems [2], nonlinear dynamic systems control [1], the signal processing application [9],[11] etc. This achievement by a some features of neural networks. One of these features is approximation any smooth function. The example of smooth function is the transient of state variables gyrostabilizer or control by time. But, general algorithm of the synthesis of neural network not formulated yet. Such of algorithms is the goal for scientists. This paper describes development of this algorithm for class of dynamic systems.

* Corresponding author. Tel.: +7-922-724-7089.
E-mail address: anisimovio@susu.ac.ru

2. Problem definition

Dynamic a channel of uniaxial gyrostabilizer can be described by the following system of linear differential equations [6],[18]:

$$\begin{aligned} A\ddot{\alpha} + H\dot{\beta} + h\alpha &= M^{ext} + M; \\ B\ddot{\beta} - H\dot{\alpha} &= 0, \end{aligned} \quad (1)$$

where H - Kinetic moment gyro unit, A - inertia gyro platform, B - of inertia of the power gyrostabilizer gyro unit, h - Damping factor, α - Angle pumping platform; β - Angle of rotation of gyro unit. We can measure only gyro precession angle β . The problem of generating a control torque for compensation of the external torque. Control is expected to form the law gyrostabilizer $M = g(\beta)$. Where $g(\beta)$, in generally, non-linear dynamic link that is in a feedback loop. There are some types of feedback controllers:

1. correcting unit [17];
2. observer with regulator[20],
3. neural network [4].

We consider case, when the feedback loop contains a neural network.

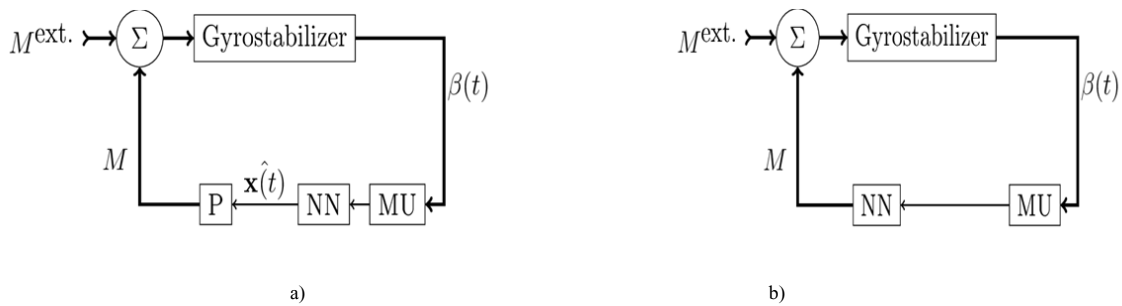


Fig. 1 The structure of the control system,

The NN - neural network; MU- memory unit; M^{ext} - external moment

y - gyroscope signal; u- control signal

Two schemas of control are proposed. In the first scheme the gyro signal put into the memory unit. Memory unit is generated a vector containing the current value and the previous several values of the vector. This vector is input for neural network.

The neural network connected to a motor. The motor creates a moment M , which balances external moment M^{ext} (case b at Figure 1). In the second case, neural network estimate of the state vector, which is connected to the regulator, the signal from the regulator is connect to the motors of stabilization (version "a" in Figure 1).

In the case when gyrostabilizer has a several channels of stabilization feedback loop consists of several of parallel neural networks. This allows reduce the load on each neural network.

3. Synthesis of a neural network

We consider the "classic" algorithm for the synthesis of neural networks, which consists of five stages. The formalization of the problem performed at the first stage. The unknown function is determined that the neural network during its work will be interpolated, the number of input and output variables. Next the step is selecting the

structure of the neural network: definition of topology and network settings, type activation functions. After, the creation of the training sample is following, which should reflect all the possible modes. Next step is a choice of algorithm training parameters and train neural network. And the final stage is the verification of the trained neural network on the test sample. When a result of checking is positive neural network is considered trained and may be used in the work.

Describe the algorithm for the synthesis of the control device consists of a neural network and regulator. So that the system (1) will be defined as [19]:

$$M = -P\hat{x}, \quad (2)$$

where $x = [\dot{\alpha}, \beta, \beta]^T$ - state vector, P - regulator.

3.1. The formalization of the problem

In article describe case when a neural network works as a observer. The input of the neural network is vector of the measured signal and several previous values of it, and the output of the neural network - estimation of the state vector .

3.2. Structure and parameters of neural network

Mathematical model of the neural network is described by the equation [7],[5],[13]:

$$\hat{x} = f^{(2)}\left(W^{(2)}\left(f^{(1)}\left(W^{(1)}[\beta(k), \beta(k-1) \dots \beta(k-n)] + b^{(1)}\right) + b^{(2)}\right)\right), \quad (3)$$

where W^j - weighting matrix j-th layer of the neural network, b^j - bias vector of j-th layer of the neural network, $f^{(j)}$ - activation function j-th layer of the neural network, $\beta(k)$ -current values of the measured signal, \hat{x} - An output vector of the neural network, n - depth of memory.

In articles [14],[3] describes a result of the numeric simulation. A large number of neural networks were synthesized during experiments for detecting the relationship between the parameters of the neural network and the features of the transients in the stabilization of the platform. The main idea of these article is neural networks with small memory are optimal. Also should be correct inequality:

$$n \leq \text{rank}(W^{(2)}). \quad (4)$$

Neural network with non-linear activation, like “tansig” or “logsig” function in hidden layer and linear in output layer are preferred. These features also work when the neural network is used for observing a linear dynamic system.

3.3. Selecting learning algorithm

The goal of training the neural network is changing the weight coefficients, which the minimization of the functional [8],[10]:

$$E = \frac{1}{N} \sum (x - \hat{x}(\beta))^2 \quad (5)$$

where x - the measurement state vector, $\hat{x}(\beta)$ - the output of the neural network, N - the number of the training samples.

As shown by mathematical modeling, the most efficient is the Levenberg-Marquardt algorithm [15],[16].

3.4. Creating a training sample

The training set is prepared with a special algorithm. The main aim is all system state variables are observable. Next, a closed system is formed by including a feedback loop controller by state. In some works are recommended use a harmonic signal with increasing frequency to the input of gyroscope stabilizer. But most prefer is use random normalized input signal or a harmonic signal at a fixed frequency. These results were obtained on the basis of numerical modeling.

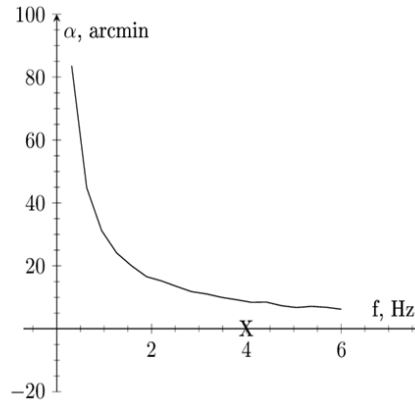


Fig. 2 The relationship between the number of iterations and the frequency of the disturbance

For determining the optimum frequency of the input harmonic signal numeric experiment was conducted. The input to the reference model supplied harmonic signal with a fixed frequency, after which the obtained sample was trained the neural network. The number of epochs required training the neural network, and maximum angle leveling platforms comprising a feedback loop neural network was measured in the experiments.

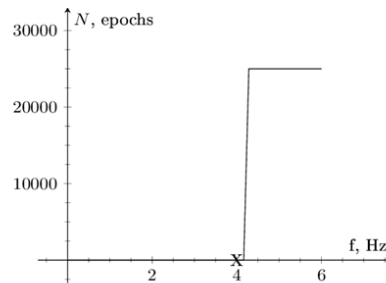


Fig. 3 of the maximum angle of the pumping frequency disturbance

The results of numeric experiments are shown in Figures 2 and 3. The figure shows that increasing the frequency of the input harmonic signal decreases the maximum angle pumping platform, but after a certain frequency is a sharp increase in the number of periods required for training and, therefore, the time required for training the neural network. The frequency, then a sharp increasing the number of periods, was close to the cutoff frequency of the reference model (at figures marked as X). Thus, the optimum in terms of the ratio of the time of training and the maximum angle of pumping is situated at the cutoff frequency.

3.5. Verification of a neural network

The neural network operates in a feedback loop of a dynamic system, so that traditional methods of verification of the neural network are not applicable. In this regard, the only method of verification is a simulation of a closed system. However, in some cases, simulations can take time comparable to the time of training, and even exceed it. In this regard, in addition to mathematical modelling, it is proposed to check the performance of neural network at the Prototyping stand [12].

4. Results

The article was considered a neural network algorithm for controlling a uniaxial gyro stabilizer. The optimal parameters of neural network based observer are determined. The optimum frequency of the harmonic signal input of ideal model for the formation of a training sample. The results can be used in the synthesis of control devices built using the device of neural networks for tracking systems.

REFERENCES

- [1] Kacai, D. Mathematical model of the unit to control the angular position of the cross-cutting drum, Bulletin of the South Ural State University. Series" Computer technology, management, electronics. ", Chelyabinsk Univ. Center SUSU, Volume 14, number 1., Chelyabinsk, 2014, p.39-49.
- [2] Egmont-Petersen M., de Ridder D., Handels H. Image processing with neural networks—a review, Pattern recognition. – 2002. – Volume . 35. – Number 10. – p. 2279-2301.
- [3] Anisimov Y, Kacai D Office triaxial indicator gyrostabilizer using neyrosetvogo approach // Navigation and Motion Control. Proceedings of XIII Conference of Young Scientists, St. Petersburg: SSC RF JSC "Central Research Institute" Electrical Appliance, St. –Peterburg, 2011, p. 217-222
- [4] Omatu S., Khalid M. B., Yusof R. Neuro-control and its applications. – Springer Science & Business Media, 2012.
- [5] Anisimov Y, Katz D Description of approaches to the synthesis of a three-axis control indicator stabilizer apparatus using neural networks, The world of scientific discoveries. Mathematics Series. Mechanics. Informatics, Number 8.1 (20), 2011, 439-448 p.
- [6] Lisov AN Lisova AA Theory gyroscopic stabilizer. Tutorial., South Ural State University Publishing Center, Chelyabinsk, 2009.
- [7] Ossowski Neural networks for information processing., IPRZHR, Moscow, 2000.
- [8] Haykin S., Network N. A comprehensive foundation //Neural Networks. Williams, Moscow, 2006.
- [9] Stepanov OA Neural network algorithms in the problem of nonlinear estimation. The relationship with the Bayesian approach, Navigation and Control movement. Proceedings XI conference of young scientists. RFJSC Concern CSRI Elektropribor, St-Peterburg, 2009., p. 39-65
- [10] Haykin S. Kalman filtering and neural networks. John Wiley & Sons, Inc., New York. 2001
- [11] Stepanov, O.A. and Amosov, O.S. Optimal Estimation Algorithms Based on the Monte Carlo Method and Neural Networks for Nonlinear Navigational Problems, Proc. of the CAC/CACD/ICC, Munich, Germany, 2006.
- [12] Anisimov, Ya.O. Prototyping system for the study of neural network control algorithm channel stabilization, In the world of science discoveries. Mathematics Series. Mechanics. Computer science., Volume 6.1 (54), 2014, Pp 314-323.
- [13] Bezmen GV Analysis of the possibility of using neural networks to solve the problems of filtration, Navigation and Motion Control. Proceedings of VIII Conference of Young Scientists, SSC RF JSC "Central Research Institute" Electrical Appliance", St. Petersburg: , 2002
- [14] Anisimov, Ya.O. Determination of the optimal parameters of the neural network to be used as an observer in uniaxial gyroscopic stabilizator , Natural and machine theme of science in the modern world / Coll. Art. Materials XVIII Intern. scientific and practical., "Seebach", Novosibirks, 2014, p. 14-20
- [15] Lera G., Pinzolas M. Neighborhood based Levenberg-Marquardt algorithm for neural network training, Neural Networks, IEEE Transactions on., Volume 13. Number 5., 2002 , p. 1200-1203.
- [16] Ngia L. S. H., Sjoberg J. Efficient training of neural nets for nonlinear adaptive filtering using a recursive Levenberg-Marquardt algorithm , Signal Processing IEEE Transactions on., Volume. 48 Number. 7., 2000. , p. 1915-1927.
- [17] D Pelpor, Y Kolosov, E Rahtenko .Calculation and design of gyroscopic stabilizers, Mechanical engineering, Moscow,1975.
- [18] V Besekersky, E Fabricant. Dynamic Synthesis of gyroscopic stabilization systems / Shipbuilding, Leningrad, 1968.
- [19] A Krasovsky. References control theory, The main edition of the physical and mathematical literature, Moscow,1987.
- [20] Bukov Attachment systems. an analytical approach to the analysis and synthesis of matrix systems., Izdatelstov scientific literature, Kazan, 2006



International Conference on Industrial Engineering

Simulation modeling of “Smart Home” operations using the data on a man’s position

Fomin S.P.^a, Orlov A.A.^{b*}

^a *Vladimirskaya oblast (region), RZSH street, 46-75, 602264 Murom, Russian Federation*

^b *Vladimirskaya oblast (region), ulitsa (street) Orlovskaya, 23, Murom Institute, Vladimir State University, 602264 Murom, Russian Federation*

Abstract

The paper describes the development of a Smart Home control system that employs data on the man’s position. It describes a basic model of this event and action based system, simulating a bedroom to exemplify Smart Home operations. The researchers have developed a simulated model for system tests, test results provided.

© 2015 The Authors. Published by Elsevier Ltd. This is an open access article under the CC BY-NC-ND license (<http://creativecommons.org/licenses/by-nc-nd/4.0/>).

Peer-review under responsibility of the organizing committee of the International Conference on Industrial Engineering (ICIE-2015)

Keywords: smart home, automation system, means, modeling, posture person, system mode, energy consumption

1. Introduction

Modern man uses a lot of devices that simplify the processes of life, making them more comfortable, as well as save time. According to research the person spends 1 hour per day on the average in the fulfilment of everyday operations, such as turning on lights, opening the curtains and so on. Home automation system will save time [9, 10].

One of the most promising directions of development of system "smart home" is the introduction of vision system [3, 8]. This technology has great potential for the development of cooperation of all possible systems with the person [5, 7]. One of the promising areas of automation system "smart home" is the recognition of human postures using vision systems.

* Corresponding author. Tel.: +7-904-957-24-27;
E-mail address: sergeyfomin@f5f5.ru

According to the definitions of Labunskaya [13] and Ushakov [13], "pose" is a static position of the human body, the basic unit of the spatial behaviour of the person, characterized by a certain position of the body, head and limbs toward each other [6, 11, 12]. So determining the spatial characteristics of the body and limbs of the body, you can interact with the system "smart house", as well as to conclude the findings of his needs and even the mental state of the person [2]. Extracting this information automatically and objective description of it in the form that is accessible to automation system "smart home" is an urgent research topic [1, 4]. The solution to this problem is to create an automated system for the registration and description of the person posing for the recognition of known positions and reactions of the necessary systems to them.

2. Functionality of the system "smart house"

Most systems "Smart House" are based on an event-efficient model, which includes things such as rules, events and actions.

In the given diagram the rule establishes the connection between the events and actions of the system. For example, the action of turning on the light in the room is caused by response of motion sensor. One event may be connected with several actions. Also there can be several events, if it's dark and cold outside, floor heating should be turned on and window-blinds should be drawn [8].

There is a need to determine the position of man in space, namely three states: sitting, standing, lying. This additional information will help the system to make decision. Even if the system is not an expert, the number of call options for action increased 3 times, allowing to control and make a decision and as a result to save energy. Table 1 shows a simple example of event processing logic. 5 buildings are reviewed with a focus on actions related to power consumption, the actions of turn-on are given, the actions of shutting down are not shown, but implied.

Table 1. An example of a table

	Bedroom			Sitting room			Hallway			
	Movement	Time 6:30	Presence			Time 6:15	Movement			
			lying	sitting	standing					
Switch on floor heating	+	-	-	+	+	-	+	+	+	n/a
Switch on lightening	+	+	-	-	+	-	-	+	-	+
Switch on soft lightening	-	-	+	+	-	+	+	-	+	-
Switch on multimedia	-	+	+	+	-	-	+	+	-	n/a
Switch on kitchen hood	n/a	n/a	n/a	n/a	n/a	n/a	n/a	n/a	n/a	n/a
Turn the water off	n/a	n/a	n/a	n/a	n/a	n/a	n/a	n/a	n/a	n/a
Switch on tea-kettle or coffeemaker	n/a	n/a	n/a	n/a	n/a	n/a	n/a	n/a	n/a	n/a
Water heating	n/a	n/a	n/a	n/a	n/a	n/a	n/a	n/a	n/a	n/a
Open window-blinds	-	+	-	-	-	-	-	-	+	n/a

3. Research

Simulation model, showing the operation of the home control system in real time, was developed to confirm the assumption that the energy efficiency of a system using human posture recognition.

The model allows doing research of the dependence of energy consumption (Watts), elapsed time (second) of the number of people in the system. The following entities were used: the switch, floor heating, lighting, man, checkpoint, room. Man moves between the control points arbitrarily. In the process of moving a man can take three possible postures: standing, sitting, lying, depending on these conditions in an automatic mode may turn on \ off the device. Testing was conducted in three possible modes:

- automation is shut down;
- automation detects the presence of a man;
- automation defines human's posture.

In the first mode the user has to approach the switch to enable\disable the devices, so it also takes time.

The second mode detects the presence of a person and turns on/off the devices in one mode of consumption.

The third mode turns on/off the devices in different modes of consumption.

Testing was conducted at 1500, 3000 and 4500 model minutes. The test results on the 4500 model minutes clearly shown in the charts below.

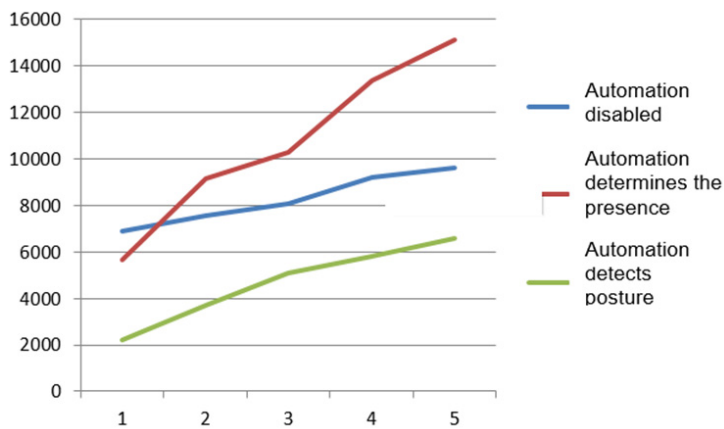


Fig. 1 The energy consumption depending on the number of people.

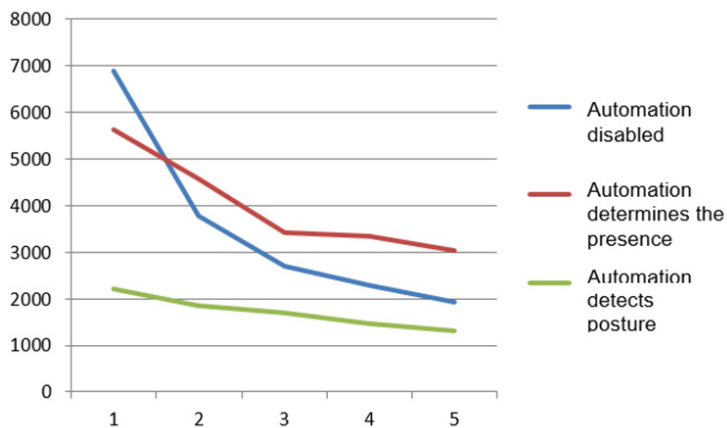


Fig. 2 The average power consumption per person.

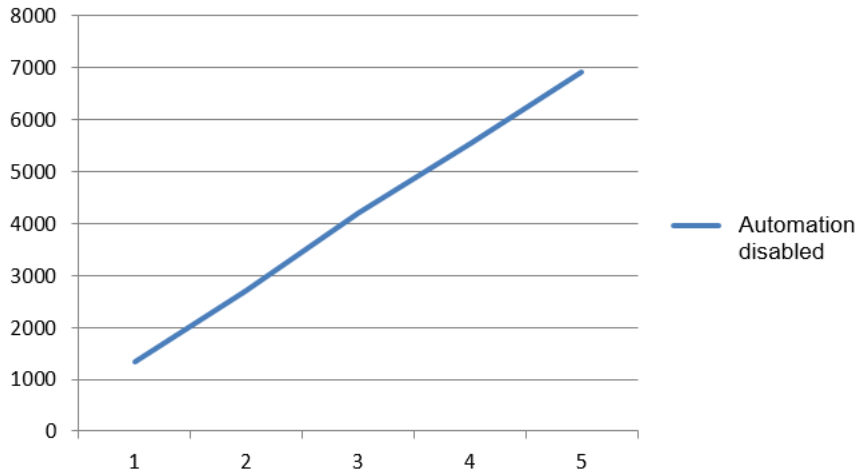


Fig. 3 Time spent in the system depending on the number of people in seconds.

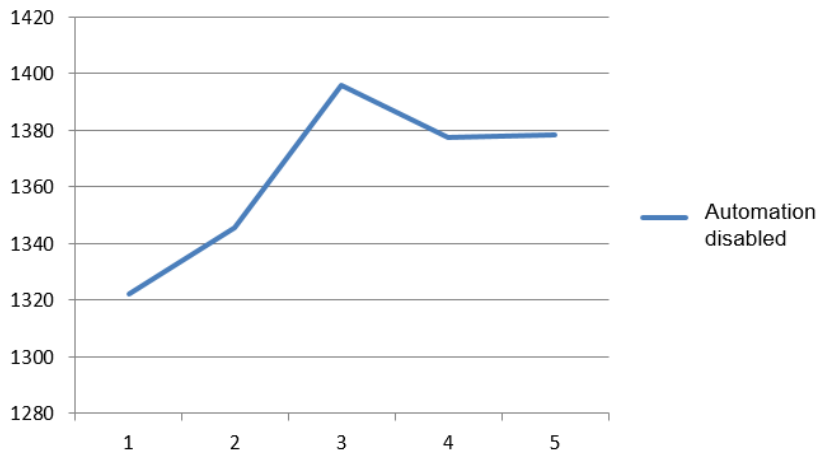


Fig. 4 Average time in seconds spent per person in the system.

Charts of economy are presented only for the mode with disabled automation, because only this mode implies the need for time-consuming for turning the devices on / off. Fig. 3, Fig 4 clearly show the superiority of the proposed mode.

4. Summary

The control system "smart house" on the basis of data on the position of man is the subject of this article. Simulation model was built for testing. The advantage of the mode with the definition of man postures was shown by such parameters as power consumption and flow of time. Mode with the definition of human posture showed results of more than 3 times superior to other modes of energy saving. It is also shown that the mode with the switched on automation saves time for turning on \ off the devices.

References

- [1] B.A. Knyazev, Research and development of multiagent hardware and software complex of man's posture recognition, FSBEI HPE. (2013) 523–538.
- [2] Information on <http://www.comvisionsys.ru/product/viziware/>
- [3] P. Turaga, R. Chellapa, V.S. Subrahmanian, O. Udrea, Machine recognition of human activities: A survey, *IEEE Transactions on Circuits and Systems for Video Technology*. 18(11) (2008) 1473–1488.
- [4] J.K. Aggarwal, M.S. Ryoo, Human activity analysis: A review, In *ACM Computing Surveys*, 2011.
- [5] V. Kellokumpu, M. Pietikainen, J. Heikkila, Human activity recognition using sequences of postures, In *Proc IAPR Conf. Machine Vision Applications*. (2005) 570–573.
- [6] J. Gales, Inside the race to hack the Kinect, *New Scientist*. 208(2789) (2010) 22.
- [7] Information on <http://www.xbox.com/en-GB/kinect/>
- [8] E.E. Kanunova, A.A. Orlov, *Methods and algorithms for image restoration of archival text documents*, World, Moscow, 2006.
- [9] A.A. Orlov, L.V. Antonov, Algorithms for image processing of industrial products, *Modern problems of science and education*. 6 (2012) 97.
- [10] A.A. Orlov, A.V. Astafiev, A.V. Provotorov, Multivariate analysis of the monitoring equipment in manufacturing plants, *The algorithms, methods and systems of manipulation of data*. 11 (2010) 131–135.
- [11] A.A. Orlov, Computed X-ray analysis of the quality of welded joints and the selection of line items on them, *Automation and modern technologies*. 6 (2009) 3–6.
- [12] A.A. Orlov, Implementation of processing systems of line facilities images, *Software and systems*. 4 (2007) 61.
- [13] A.A. Orlov, A.V. Provotorov, A.V. Astafiev, System analysis of labeling methods of industrial products, *The algorithms, methods and systems of manipulation of data*. 15 (2010) 136–140.
- [14] A.A. Orlov, A.A. Ermakov, Technology comparison and identification of raster lines, *Software and systems*. 1 (2007) 68.



International Conference on Industrial Engineering

Mathematical modelling and short-term forecasting of electricity consumption of the power system, with due account of air temperature and natural illumination, based on support vector machine and particle swarm

Nadtoka I.I.^{a*}, Al-Zihery Balasim M.^b

^a *Platov South-Russian State Polytechnic University (NPI), 132, St. Prosvescheniya, Rostov region, Novocherkassk, 346428, Russian Federation*

^b *University of Diyala, Addres: Diyala, Iraq*

Abstract

The goal of this paper is to describe a forecasting model for the hourly electricity load. The model takes into account the meteorological factors (temperature and natural illumination) in the area covered by the Rostov utility dispatcher. In this study, support vector machine (SVM) with particle swarm optimization (PSO) were used to forecast electricity consumption. To get more accurate evaluation of the results of SVM model, the standard measures for quantitative evaluation of statistical performance and mean absolute percentage error (MAPE) were employed to evaluate the performance of various models developed. The results also suggest that the SVM method can be successfully applied to the forecasting model for the hourly electricity consumption in the area covered by the Rostov utility dispatcher.

© 2015 Published by Elsevier Ltd. This is an open access article under the CC BY-NC-ND license

(<http://creativecommons.org/licenses/by-nc-nd/4.0/>).

Peer-review under responsibility of the organizing committee of the International Conference on Industrial Engineering (ICIE-2015)

Keywords: Short-term load forecasting, temperature, natural illumination, electricity consumption, adaptive neuro fuzzy inference system, support vector machine.

* Corresponding author. Tel.: +7-863-525-56-50;
E-mail address: pressa_npi@mail.ru

1. Introduction

Short term electric load forecasting is one of the important criterions in the operation and planning of electrical power production. It concerns the prediction of power system loads over standard periods. The basic quantity of interest is usually the hourly total system load. It also concerned with the prediction of the hourly (operation term), daily (short term), weekly and monthly values (medium term) of the system load and the maximum values occurred. However, much effort has been devoted over the past decades to develop and improve the short term electric load and its corresponding price forecasting models in order to make an appropriate market decision.

In figure 1 shows the hourly values of natural illumination (left ordinate axis) and the hourly temperature values (right ordinate axis) during one day.

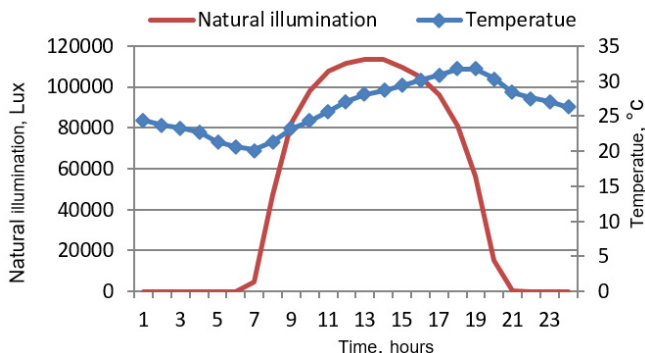


Fig. 1. The hourly natural illumination and the hourly temperature for 25.08.2010 in the operating area of the Rostov utility dispatcher.

The dependence of the power consumption on the temperature is shown in Fig. 2. The points of this dependence are characterized by the period from 1 September 2010 to 31 August 2011 in the territory of the Rostov utility dispatcher. They are approximated by linear and polynomial 5th degree:

$$P(T) = -20.253T + 2138; \tag{1}$$

$$P(T) = -1E - 07T^5 + 0.0024T^4 - 0.0423T^3 - 0.4905T^2 - 21.286T + 2183.2; \tag{2}$$

Coefficients of determination, which have a sufficiently high value for the polynomial $R^2 = 0.8465$, and the smaller the value of $R^2 = 0.6801$ for a linear dependency, indicating the presence of a non-linear relationship between the power consumption and the temperature.

Effect of temperature on power consumption is more definite than the Cloudiness and natural illumination. Power consumption depending on the natural illumination are much more vague. The fig. 3 is examples of dependences of the daily integrated power consumption on illumination for the operating zone of Rostov utility dispatcher during year. They are approximated by linear and polynomial 5th degree:

$$P(I) = -0.0093 I + 2052.1; \tag{3}$$

$$P(I) = -2E-24 I^6 + 2E-19 I^5 - 1E-14 I^4 + 2E-10 I^3 - 3E-07 I^2 - 0.0174 I + 2056.4. \tag{4}$$

Coefficient of determination for the linear $R^2 = 0.3894$, and nonlinear $R^2 = 0.3542$ models indicate a weak correlation.

Support Vector Machines (SVM) is a set of classification and regression techniques, which was invented by Vladimir N. Vapnik in 1995 [1–3]. As previously outlined, SVM can be used for either classification or regression, to which we restrict our attention for the remainder of this work. In the following, we briefly overview the theory behind the use of SVM for function estimation, introducing at the same time the most relevant notions

and parameters, with special attention to those parameters whose impact we investigate later on. In a sense, this overview is thus instrumental to the understanding of the performance evaluation section, but for a more thorough coverage of SVM we refer the reader to the excellent surveys [4–8].

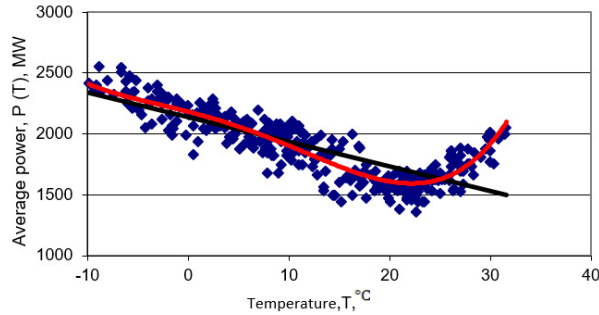


Fig. 2. The dependence of the daily power consumption on the average daily temperature during the year in the operating area of the Rostov utility dispatcher.

List square method of SVM (LS-SVM) was first proposed by J.Suykens [9, 10] et al, is an extension of the standard SVM. This method was applied for load forecasting of Rostov utility dispatcher [11, 12] and in [13] for region of England.

Minimization principle, structure, LS-SVM optimization objectives can be expressed as

$$\min J = \frac{1}{2} \|\omega\|^2 + \frac{1}{2} C \sum_{i=1}^l e_i^2 - \sum_{i=1}^l \alpha_i (\omega^T \phi(x_i) + b + e_i - y_i), \tag{5}$$

where, $e \in R^{l \times 1}$ - the error vector, C the regularization parameter, which control error punishment; α the Lagrange multipliers, $\alpha \in R^{l \times 1}$. Nonlinear predictive model expression:

$$P_{i+1} = \sum_{i=1}^m \alpha_i K(x_i, x) + b, \quad i = 1, \dots, m, \tag{6}$$

where x_i - input vector: power $P(t)$, temperature $T(t)$ and natural illumination $L(t)$; type of day; x – coordinates of the center of the scattering vector; α_i, b – linear coefficients; m : dimension of input vectors; $K(x_i, x)$ – kernel function, which performs a nonlinear mapping the input space of input data (electricity, meteorological factors) in the feature space of higher dimension.

The LS-SVM method applied to power system short-term load forecasting below support vector machine regression algorithm, summarized as follows:

- Let the training set is known $S = \{P_1(t), T_1(t), L_1(t), \dots, P_m(t), T_m(t), L_m(t)\}$;
- Select the appropriate positive number α and C , Select the appropriate kernel function $K(x_i, x)$;
- Construct and solve the optimization problem-optimal solution $\alpha = (\alpha_1, \alpha_1^*, \dots, \alpha_l, \alpha_l^*)^T$;
- Construct decision function(6), where b the value is calculated according to the formula :

$$b = P_i - \sum_{i=1}^m \alpha_i K(x_i, x) \quad \alpha_i \in (0, C) \tag{7}$$

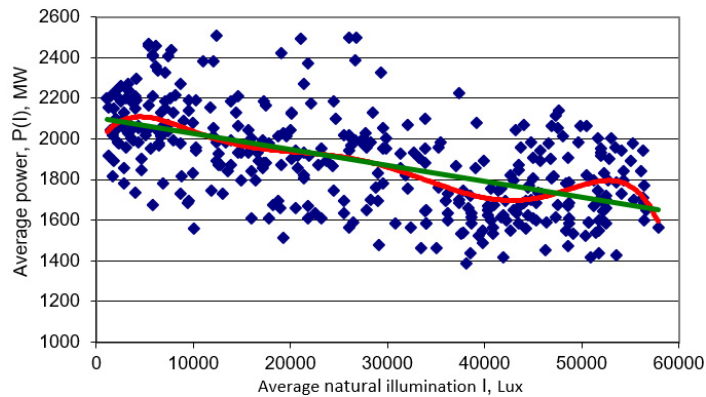


Fig. 3. The dependence of the daily power consumption on the average daily natural illumination during the year in the operating area of the Rostov utility dispatcher.

The radial basis function has the following advantages: (1) representation of simple, even for multi-variable input not add too much complexity; (2) radial symmetry, smoothness, arbitrary order derivatives are present; (3) Since the function of simple the parsing and good, and thus facilitate the theoretical analysis.

These features based on radial basis function, this article uses the radial basis function as a of kernel function in the regression model. Specific form is as follows:

$$K(x, x_i) = \exp(-\|x - x_i\|^2 / \sigma^2), \quad (8)$$

where: σ is the standardized parameter, determines the width of the function around the centre point, $\|x - x_i\|$ is the norm of the vector $x - x_i$, indicates the distance between x and x_i . Radial basis function non-linear transformation of the sample data to a high-dimensional space, Be able to handle the input and output of the nonlinear relationship. Selection of parameters SVM (σ , C) based on using algorithm particle swarm.

Particle swarm optimization is algorithm based on iterative optimization evolutionary computing technology, initialization for a group of random particles, and then search for the optimal solution by iteration [14–16]. In each iteration, the particles passing through the track of the two extremes to update the particle's position and speed, in order find the optimal solution.

Each particle is determined according to their own flight speed and distance. Suppose that d dimension in the search space, m particles form a population. The standard particle swarm optimization algorithm to update the particle velocity and position using the following formula:

$$v_{id} = wv_{id} + c_1 r_1 (p_{id} - x_{id}) + c_2 r_2 (p_{gd} - x_{id}); \quad (9)$$

$$x_{id} = x_{id} + v_{id}. \quad (10)$$

where, x_i the position of the i -th particle in d -dimensional search space, p_{id} the optimal location of the i -th particle, v_{id} the flying velocity of the i -th particle in a d -dimensional search space, w is the coefficient of inertia weight, c_1 and c_2 the two are non-negative constant called the acceleration constant, r_1 and r_2 random numbers between (0÷1).

The simulation environment MALAB2011a, Search range of setting Particle Swarm Optimization is: $C \in$

(0,1÷100) , $\sigma \in (0,1÷10)$. The number of particles m Choose 20, the more the number of particles, the more widely distributed, the greater the range of the search space, and thus easier to find the global optimum solution, but the longer running time. w inertia weight factor. Range of w selected as (0,4÷0,9). Acceleration constants c_1 and c_2 represent the weights of the stochastic acceleration terms that push a particle toward p_{ibest} and g_{best} respectively. Small values of c_1 and c_2 allow a particle to roam far from target regions. Conversely, large values result in the abrupt movement of particles toward target regions. In this work, constants c_1 and c_2 are both set at 2,0, following the typical practice in [17–20].

For the modeling of power consumption with the influence meteorological factors used procedures among MALAB2011a: (InitSwarm, BaseStepPso) for the implementation of the algorithm and particle swarm (AdaptFunc1, AdaptFunc) to create a predictive regression model of method SVM.

Initial data are taken from the statistics of the Rostov utility dispatcher for the period 2009 - 2012, at the output is the data load on the day forecasting. The results of prediction in different seasons of the year are shown in Fig. 4, 5, 6. Table 1 shows the prediction errors (mean absolute error percentage MAPE).

$$MAPE = \frac{1}{24 \cdot N} \cdot \sum_{i=1}^{24} \sum_{k=1}^N \frac{|P_{i,k}^{for} - P_{i,k}^{act}|}{P_{i,k}^{act}} \cdot 100\% . \tag{11}$$

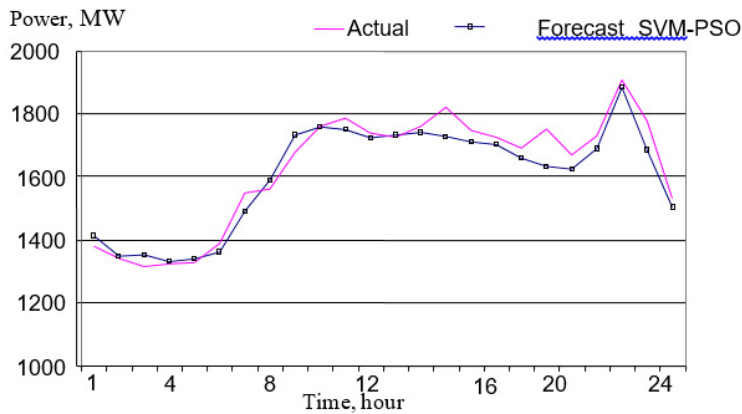


Fig. 4. Load forecasting for 31.05.2011 with account temperature and natural illumination (MAPE= 2,26%).

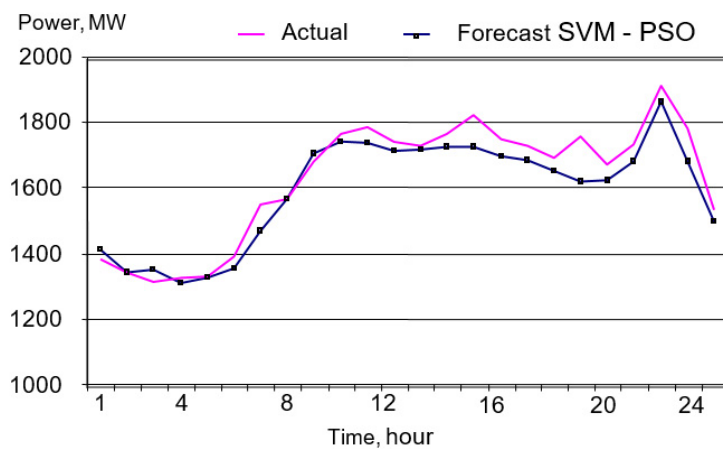


Fig. 5. Load forecasting for 31.05.2011 with account only temperature (MAPE= 2,60%).

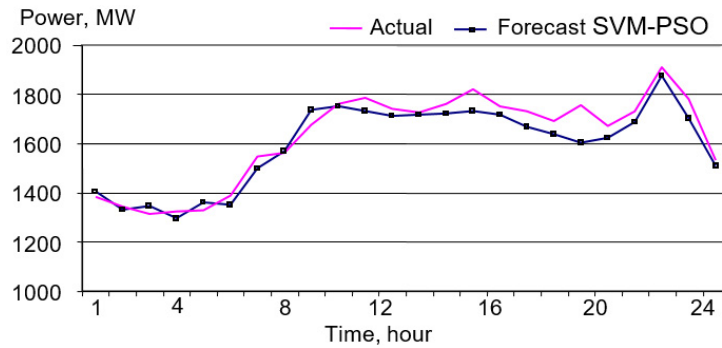


Fig. 6. Load forecasting for 31.05.2011 with account only natural illumination (MAPE= 2,65%).

Table 1. The result of error for each season.

Time of year	MAPE%		
	With account only natural illumination	With account only temperature	With account temperature and natural illumination
Spring 31.05.2011	2.65%	2.6%	2.26%
Summer 31.08.2011	1.23%	1.37%	1.41%
Autumn 30.11.2011	2.13%	1.94%	1.61%
Winter 26.1.2012	1.73%	1.9%	1.58%

2. Conclusion

In this study, SVM with PSO model was developed for forecasting the short term of electrical power consumption for Rostov region dispatcher utility. The results demonstrated that SVM with PSO can be applied successfully to establish accurate and reliable electrical power forecasting. Also results show that the account of temperature with natural illumination together improved the quality of forecasting by using SVM with algorithm PSO.

Forecasting results presented in Table 1 show that the prediction error of summer and winter is less than of spring and autumn. This is explained by the greater dynamics of length changing of daylight (light time of day) and the instability of the weather.

References

- [1] Information on <http://www.springerlink.com/content/k238jx04hm87j80g/>
- [2] A. Jain, B. Satish, Clustering Based Short Term Load Forecasting Using Support Vector Machines, Bucharest Power Tech Conference. (2009).
- [3] V. Vapnik, The Nature of Statistical Learning Theory, Springer-Verlag, New York, 1995.
- [4] J.A. Smola, S.A. Bernhard, Tutorial on Support Vector Regression, in Statistics and Computing, Kluwer Academic Pub. 14 (2004) 199–222.
- [5] J.C. Christopner, A Tutorial on Support Vector Machines for Pattern Recognition", Journal of Data Mining and Knowledge Discovery, Springer, Netherlands. 2 (1998)1–43.
- [6] R. Stefan, M. Katharina, Support Vector Machines and Learning About Time, Proc. of IEEE ICASSP - 03, Hong Kong. 4 (2003) 864–867.
- [7] S. Ruping, SVM Kernels for Time Series Analysis, Proceedings of the LLWA 01, Dortmund, 2001.
- [8] S.F. Crone, S. Pietsch, A Naïve Support Vector Regression Benchmark for the NN3 Forecasting Competition, International Joint Conference on Neural Networks, 2007.
- [9] A.K. Suykens, T.V. Gestel, J.D. Brabanter, B.D. Moor, J. Vandewalle, Least Squares Support Vector Machines, World Scientific, Singapore, 2002.
- [10] T. Falck, A.K. Suykens, B. De Moor M. Espinoza, Time Series Prediction using LS-SVMs, European Symposium on Time Series Prediction. (2008) 159–168.
- [11] I.I. Nadtoka, B.M. Al-Zihery, Short-term Load Forecasting Using Least Square Method for Support Vector Machine [Kratkosrochnoe Prognozirovanie Elektropotrebleniya s Pomoshchyu Metoda Naimenshikh Kvadratov Opornykh Vektorov (LS-SVM)], Sovremennyye

- Problemy Nauki i Obrazovaniya. 6 (2013). <http://www.science-education.ru/113-11213>.
- [12] I.I. Nadtoka, B.M. Al-Zihery, Short Term Load Forecasting Based on Support Vector Machine and Particle Swarm optimization algorithm methods, [Kratkosrochnoe Prognozirovanie Elektropotrebleniya Regiona s Uchetom Meteofaktorov na Osnove Metoda Opornykh Vektorov i Algoritma Roya Chastits], *Izvestiya Vysshikh Uchebnykh Zavedeniy [News of Higher Educational Institutions]*, Russian Electromechanics. 3 (2014) 44–47.
- [13] M. Božić, M. Stojanović, Z. Staji, Short-Term Electric Load Forecasting Using Least Square Support Vector Machines, *Automatic Control and Robotics*. 9(1) (2010) 141–150.
- [14] C. Sun, D. Gong, Support Vector Machines with PSO Algorithm for Short-term Load Forecasting, in *Proc. of IEEE Int. Conf. on Networking, Sensing and Control*. (2006) 676–680.
- [15] A.U. Asar, S.R. Hassnain, A. Khan, Short-term Load Forecasting Using Particle Swarm Optimization Based ANN Approach, *Proc. of IEEE Int. Joint Conf. on Neural Networks*, Orlando, Florida. (2007) 6.
- [16] L. Yunfei, Y. Jian, Improvements Based on Support Vector Machine Short-term Load Forecasting Method, *Xihua University*. 26(2) (2007).
- [17] J. Kennedy, The Behavior of Particle. In: *Proceedings of the 7th Annual Conference on Evolutionary Programming*; 1998.
- [18] J. Kennedy, Bare Bones Particle Swarms, In *Proc. of the Swarm Intelligence Symposium (SIS 2003)*, 2003.
- [19] R. Mendes, J. Kennedy, and J. Neves, The Fully Informed Particle Swarm: Simpler, Maybe Better, *IEEE Trans. Evol. Comput.* 8 (2004) 204–210.
- [20] P. Riccardo, J. Kennedy, T. Blackwell, Particle Swarm Optimization. *Swarm Intelligence*. 1(1) (2007) 33-57.



International Conference on Industrial Engineering

Development and experimental research on production data analysis algorithm in livestock enterprises

Antonov L.V., Makarov K.V., Orlov A.A.*

Department of Information System, Murom institute (branch) Vladimir State University, 602264 Murom, Russia

Abstract

Preliminary mathematical analysis of miscellaneous production data is presented in the paper. Research shows how strong is the impact of each parameter on the information picture of the enterprise. The article describes how critical deviations of production characteristics from the normal values can be timely identified. An algorithm based on least squares method, which allows to increase the efficiency and accuracy of identifying problematic situations in production is developed in the course of research. Experimental research of the developed algorithm is carried out by four metrics.

© 2015 The Authors. Published by Elsevier Ltd. This is an open access article under the CC BY-NC-ND license (<http://creativecommons.org/licenses/by-nc-nd/4.0/>).

Peer-review under responsibility of the organizing committee of the International Conference on Industrial Engineering (ICIE-2015)

Keywords: Information system; automation; livestock enterprise.

1. Introduction

Every company tries to increase its profits in the modern world of the market economy. Automation and modernization of the production process, minimization of costs and personnel are way to achieve the profitability of each enterprise. Mostly modernization requires serious private investments [1-3].

Implementation of automation on modern livestock enterprises is a difficult and lengthy process because there are a large number of intelligent information systems for production control. These systems are designed to improve the quality of milk, achieve full control of the herd, increase productivity and increase farm profitability in the future. The choice between intelligent systems is a difficult process because the market contains a large number of analogues. There is no one system with full functionality for solving all tasks of the enterprise. Therefore, farms

* Corresponding author. Tel.: +7 (919) 019-58-81.

E-mail address: levantonov@yandex.ru, umc@mivlgu.ru, alexeyalexorlov@gmail.com

have to purchase multiple systems, which together allow them to automate the processes of production. But they partially duplicate each other, have different mechanisms for managing, storing information, user interaction, and are incompatible with each other. It is necessary to integrate the information systems. This task is time consuming and expensive and in most cases fails or is not seen through to the end. Lactivator, NedapAgri BV, Groenlo, Alpro, DeLaval, Tumba are providers of this system. The existing system is fragmented and does not have a single intelligent mechanism, including cumulative analytical data processing [4]. Ultimately, the full automation of the livestock enterprise is impossible because there is no system that can simply utilize all of the enterprise components together.

There are many applied tasks that require solutions, using scientific methods and approaches in the enterprise. For instance, it is logical for farmers to aspire to select more productive animals to continue the herd. There is also the problem of determining the maximum activity of the animal in the postpartum period, because the probability of successful insemination is higher in this period [3,5]. All these problems can be solved by the intelligent analysis of miscellaneous data in the workplace. Thus, the preliminary task is the primary analysis of enterprise data using mathematical and statistical methods, and also methods of the probability theory.

2. Analysis of production factors

Large data volumes from each animal's sensor come into automated information management systems on a large livestock enterprise. Let us consider a set of factors traditionally used to diagnose the state of cows (Table. 1). Each of these factors is used to analyze the condition of the animal.

Table 1. The main parameters for monitoring cows' conditions.

Characteristic's name	Unit of measure
Daily milk yield	Liters
Average activity of the animal	Steps / hour
Milking time	Seconds
Conductivity	Millisiemens or Ohm
Weight of the animal	Kgs

Daily milk yield and milking time influence decision-making processes for the selection of animals. Fluctuations in daily milk yield may indirectly indicate problems with animal health or the equipment of the enterprise. If the index of the daily milk yield is 4-5 liters less than the previous value, the animal state is getting worse and the operator must know about it and react in time.

The average activity of the animal is a direct indicator of the health of the animal's activity. This parameter is important for determining estrous in the animal's post-natal period. The conductivity of the milk influences viscosity, i.e. the product quality. Deviation from the norm of this factor may indicate possible hidden diseases, such as mastitis. Additional results from the data are shown in Table 1. The hypothesis was made that the data conforms to the normal law of distribution. Pearson's chi-squared test (χ^2 -test) was used to test this hypothesis.

The null hypothesis shows that the sample and theoretical distribution are identical. The hypothesis is tested by comparing the calculated value of Pearson's chi-squared test and the value found using Pearson's table of critical points of distribution. Successful confirmation of the hypothesis that the numerical series conforms to the normal law of distribution allows us to carry out factor analysis.

These data need analytical research of the work systems to process the large data volume and allow a possible reduction of information redundancy (Table. 2).

Factor analysis is used in this study. If there is the possibility of a value determining the parameter from research of other factors, it eliminates that factor from further research. Factor analysis shows the most appropriate results of research when data conform to the normal law of distribution. The starting material for the procedure of factor analysis is a correlation matrix MxM ; its elements are Pearson correlation coefficients between the factors. Calculation of characteristic values shows the power of independence of the values of each factor from the rest.

The characteristic values of the matrix are sorted in descending order so that the most important factor is at the top (1 Column, Table 2). Normalized characteristic values show the overall contribution of each factor in the overall assessment of the state of the animal when the sum of the characteristic value equals 100%. The graph shows the power of information completeness when, descending step by step, we exclude factors from the study. Cumulative values show the percentage of the loss of useful information when we exclude one or more factors.

Table 2. Numeric data of mutual influence factors

Characteristic	Eigenvalues	% Variance	Cumulative variance	% Cumulative
Weight of the animal	1,538	30,77	1,5386	30,773
Conductivity	1,078	21,57	2,6171	52,343
Milking time	0,975	19,51	3,5931	71,863
Average activity of the animal	0,874	17,49	4,4681	89,362
Daily milk yield	0,531	10,63	5	100

3. Development of algorithm for determining critical parameter changes

Analysis of data from a large number of sensors and equipment allows us to monitor the status of animals in automated control systems in modern livestock enterprises. Well automation and robotized milking parlors allow farmers to make the right management decisions, improve the quality of production and reduce costs. Generally, automated milking systems and enterprise management systems include subsystems for monitoring animal welfare, such as automatically monitoring periods of insemination.

The purpose of the section is the development of an algorithm for the automatic monitoring of postpartum estrus periods based on the analysis of the cows' daily activity. There is also problem of investigating the algorithm on real production activity data. Testing of the algorithm to work with data from other sensors for early detection of critical deviations of vital signs in other production tasks is required. Time series of animal activity in one lactation cycle is shown in Figure 1.

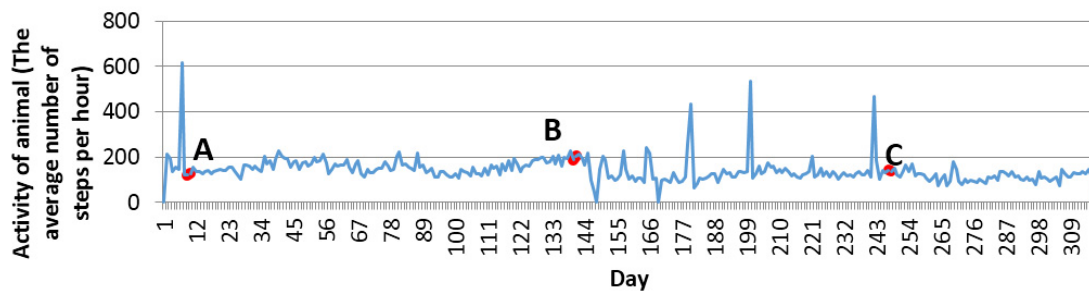


Fig. 1. Graph of the animal's daily activity

The graph is divided into several sections. There is a stable section (A-B) and sections with critical parameter changes (B-C), which show the changes in the behavior of the animal. The algorithm must identify spikes in the period B-C. The stable section of the chart values of daily activities can be divided into two parts: trend and deviation from the trend (Fig. 2). The interaction between a regular component is represented as an additive combination of:

$$Y(t) = T(t) + E(t) \quad (1)$$

where $Y(t)$ - value of activity in experimental day t ; $T(t)$ - the trend of activity in the day; $E(t)$ the deviation from the trend.

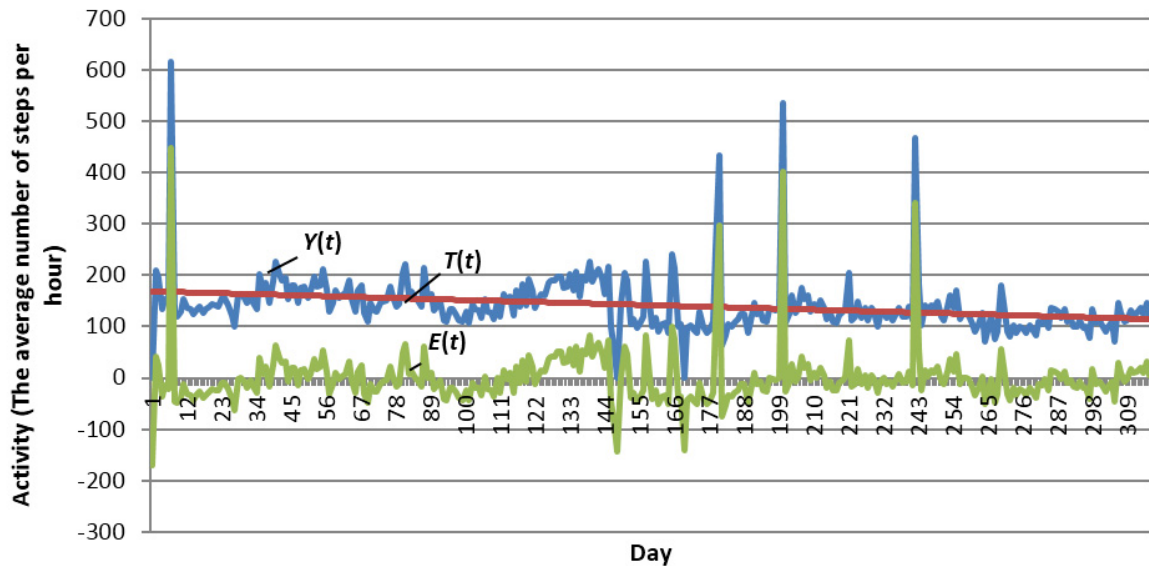


Fig 2. The decomposition of the time series of the production parameters on the trend and deviation from the trend

Trend $T(t)$ shows the basic tendency of change in daily activity of the animal over time. The straight line on the plane is defined by two parameters k and b . So the trend is described by the following mathematical formula taking into account the approach:

$$T(t) = kt + b, \quad (2)$$

where k and b - coefficients of direct the trend line in the retrospective period.

The most commonly encountered method of approximation of the time series function values is the method of least squares. k and b should be such that the trend line as much as possible approaches the point values of the time series. To solve this problem the least squares method is used. The mathematical condition for the method implementation is to minimize the sum of squared deviations daily distance from the trend line:

$$\sum (Y(t) - T(t))^2 \rightarrow \min \quad (3)$$

The most probable value of the next day's activity can be predicted if the parameters of the trend line are found. Predicted value is the future benchmark for the detection of extremely high or low activity. Some deviations in the graph are not right. The search for such deviations is performed using the three sigma rule.

We shall accept x as a current day observation of the animals. Let us assume D is the count of days in the retrospective period. The search algorithm for determining spikes and dips in animal data that indicate possible problems at the current time is designed according to a mathematical model. It consists of the following stages:

1. Method of least squares may determine coefficients of k and b the changes in the trend line of the investigated parameters on retrospective interval $[x-D, x-1]$ satisfying the equation (3).
2. Function values calculated by the formula $T(t) = k_x t + b_x$ to the retrospective period $[x - D, x - 1]$.
3. Function values $E(t)$ on a retrospective period is calculated using the formula (1).
4. Expected predictive value for the current day $T(x)$ is defined by the formula (2).
5. The standard deviation σ of function values $E(t)$ is evaluated on a retrospective period.
6. If $Y(x) - T(x) > 3\sigma$, it indicates a spike in the parameter.

7. If $T(x) - Y(x) > 3\sigma$, it shows a sharp decline in the value of the parameter.

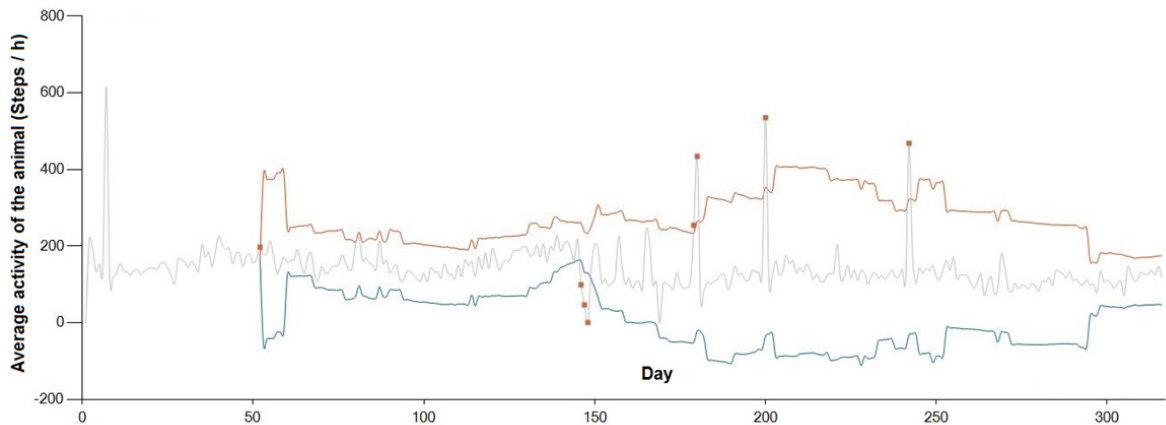


Fig. 3. The decomposition of the time series of production parameters on the trend and deviation from trend

Received thresholds using developed adaptive algorithm are visually shown in Fig. 3. Only the values of biggest bursts and dips that describe the changing state of the cows are outside the received boundaries.

Data for the research was received from 100 cows over the 330 days period from five sensors measuring parameters. The results of the algorithm were evaluated by four criteria. This is the most popular criteria when expert opinions are compared with the results of the algorithm work. These criteria are completeness, accuracy, F-measure and identification of the error deviation (Table 3).

Table 3. Experimental evaluation algorithm for detection of deviations.

Parameter	Recall	Precision	F-measure	Error
Average daily activity	92,8%	94,9%	93,8%	0,34%
Animal weight	98,9%	89,7%	94,1%	0,35%
Conductivity	98,0%	93,5%	95,7%	0,26%
Milking time	94,9%	97,9%	96,4%	0,23%
Daily milk yield	94,7%	98,2%	96,5%	0,23%

4. Conclusion

Analysis of the results shows that even if we exclude the most insignificant factor of the study, we lose more than 10% of useful information. This value is required for a finding of rational or optimal solutions to specific task management and execution of management activities.

A new algorithm for identifying unplanned peaks in parameter values based on the three sigma rule and least square method is received in the paper. The percentage of error detection periods of deviation from the norm is less than one; that is significantly lower than analog systems. Numerical evaluation of the completeness and accuracy of the algorithm is more than 90%. This result applies to all parameters of research and is the highest rate for potential use in the enterprise.

References

[1] D.C. Bulman, G.E. Lamming, Milk progesterone levels in relation to conception, repeat breeding and factors influencing acyclicity in dairy cows, *J. Reprod Fertil.* 54 (1978) 447–458.

- [2] A. Ismael, E. Strandberg, M. Kargo, A. Fogh, P. Lvendahl, Estrus traits derived from activity measurements are heritable and closely related to the time from calving to first insemination, *J. Dairy Sci.* 98 (2015) 3470–3477.
- [3] R. Firk, W. Stamer, W. Junge, Improving oestrus detection by combination of activity measurements with information about previous oestrus case, *Livestock Production Science.* 82 (2003) 97–103.
- [4] De Mol R., E. Woldt, Application of fuzzy logic in automated cow status monitoring, *J. Dairy Sci.* 84 (2001) 400–410.
- [5] J.B. Roelofs, F.J.C.M. Van Eerdenburg, N.M. Soede, B. Kemp, Pedometer readings for estrous detection and as predictor for time of ovulation in dairy cattle, *Source of the DocumentTheriogenology.* 68 (2005) 1690–1703.



International Conference on Industrial Engineering

Solving linear and bilinear problems with interval uncertainty

Latipova A.T.^{a*}

^a South Ural State University, 76, Lenin Avenue, Chelyabinsk, 454080, Russian Federation

Abstract

Two kinds of optimization problems, which can be used in production planning, have been considered: interval linear programming (ILP), finding equilibrium position interval for the Von Neumann model (bilinear problem). Initial data for these models commonly have interval uncertainty. The paper presents definitions of different solution types and methods for finding these solutions. These methods imply reducing interval optimization problems to exact ordinary linear programming problems.

© 2015 The Authors. Published by Elsevier Ltd. This is an open access article under the CC BY-NC-ND license (<http://creativecommons.org/licenses/by-nc-nd/4.0/>).

Peer-review under responsibility of the organizing committee of the International Conference on Industrial Engineering (ICIE-2015)

Keywords: Operational research; interval analysis; programming; bilinear problem.

1. Introduction

Methods for solving linear programming (LP) problems were greatly developed in the 20th century due to the development of mathematical theory together with hardware and software [1]. But in fact optimal plans obtained from LP were often ineffective, not applicable. There were different factors that could lead to this ineffectiveness. One of them was inexactness of initial data [2].

For real-world linear economic models, numerical values of input matrices items are obtained using statistical data and expert estimates, therefore there can be an uncertainty, which is commonly interval. Using of average values may cause ineffectiveness of optimal solution, because uncertainty wasn't taken into account properly. Another approach is stochastic linear programming. This method requires that probability distributions for initial data are known while in practice this requirement does not hold in most cases.

* Corresponding author. Tel.: +7-351-267-90-94; fax: +7-351-267-90-94.
E-mail address: latipovaat@susu.ru

2. Interval Linear Programming Problem

Let \mathbf{A} be interval matrix with size $n \times m$

$$\mathbf{A} = [\underline{\mathbf{A}}; \overline{\mathbf{A}}] = [\mathbf{A}_c - \Delta; \mathbf{A}_c + \Delta],$$

where

- $\underline{\mathbf{A}}$ and $\overline{\mathbf{A}}$ are point matrices of interval lower and upper bounds of matrix \mathbf{A} ;
- Δ is a point matrix, $\Delta = [\Delta_{i,j}]$, $\Delta_{ij} \geq 0$, $i = (1, n)$, $j = (1, m)$;
- \mathbf{A}_c – matrix of interval centers \mathbf{A} [3],
- $\mathbf{A}_c = (\overline{\mathbf{A}} + \underline{\mathbf{A}}) / 2$.

Let us introduce interval vectors $\mathbf{b} = [\underline{\mathbf{b}}; \overline{\mathbf{b}}] = [\mathbf{b}_c - \delta; \mathbf{b}_c + \delta]$ with size $n \times 1$ and $\mathbf{c} = [\underline{\mathbf{c}}; \overline{\mathbf{c}}] = [\mathbf{c}_c - \gamma; \mathbf{c}_c + \gamma]$ with size $m \times 1$.

Hereinafter, parameters of productivity are meant by equilibrium position if it is not defined exactly.

Vector $x \in \mathbf{R}^m$ is a *weak solution* of system of interval linear equations

$$\mathbf{A}x = \mathbf{b},$$

if it satisfies $Ax = b$ for some $A \in \mathbf{A}$ and $b \in \mathbf{b}$.

Oettli-Prager Theorem [2]. Vector $x \in \mathbf{R}^m$ is a weak solution of system $\mathbf{A}x = \mathbf{b}$ if and only if it satisfies

$$|\mathbf{A}_c x - \mathbf{b}_c| \leq \Delta |x| + \delta.$$

Checking weak solvability of linear interval equations system is NP-hard.

System of interval linear equations is *strongly solvable* if any system of point linear equations $Ax = b$ ($A \in \mathbf{A}$, $b \in \mathbf{b}$) is solvable. Checking strong solvability of linear interval equations system is NP-hard.

Vector $x \in \mathbf{R}^m$ is a *strong solution* of system of interval linear equations if x satisfies $Ax = b$ for any $A \in \mathbf{A}$ and $b \in \mathbf{b}$.

Theorem [2]. Vector $x \in \mathbf{R}^m$ is a strong solution of system $\mathbf{A}x = \mathbf{b}$ if and only if x satisfies both inequalities:

$$\mathbf{A}_c x = \mathbf{b}_c,$$

$$\Delta |x| = \delta = 0.$$

Existence of strong solution is a rare case.

Vector $x \in \mathbf{R}^m$ is a *weak solution* of interval linear inequalities system

$$\mathbf{A}x \leq \mathbf{b},$$

if x satisfies the system of point linear inequalities $Ax \leq b$ for some $A \in \mathbf{A}$ and $b \in \mathbf{b}$.

Gerlach Theorem [2]. Vector $x \in \mathbf{R}^m$ is a weak solution of system $\mathbf{A}x \leq \mathbf{b}$ if and only if x satisfies

$$\mathbf{A}_c x - \Delta |x| \leq \overline{\mathbf{b}}.$$

Vector $x \in \mathbf{R}^m$ is a *strong solution* of interval linear inequalities system if x satisfies the system of point linear inequalities $Ax \leq b$ for any $A \in \mathbf{A}$ and $b \in \mathbf{b}$.

System of interval linear equalities is strongly solvable if any system $Ax \leq b$ is solvable for any matrices $A \in \mathbf{A}$ and $b \in \mathbf{b}$.

It is proved [2] that if this system has feasible solution (x^1, x^2) then vector

$$x = x^1 - x^2$$

is a weak solution.

Checking strong solvability of linear interval inequalities system has polynomial complexity.

ILP problem is a family of point linear programming problems (LP problems)

$$\min\{c^T x \mid Ax = b, x \geq 0\}$$

for $A \in \mathbf{A}$, $b \in \mathbf{b}$ and $c \in \mathbf{c}$.

Let $f(A, b, c)$ be optimal solution of point LP problem with matrices (A, b, c) .

Let

$$\underline{f}(\mathbf{A}, \mathbf{b}, \mathbf{c}) = \inf\{f(A, b, c) \mid A \in \mathbf{A}, b \in \mathbf{b}, c \in \mathbf{c}\}$$

be lower bound of optimum for ILP problem.

Let

$$\underline{f}(\mathbf{A}, \mathbf{b}, \mathbf{c}) = \sup\{f(A, b, c) \mid A \in \mathbf{A}, b \in \mathbf{b}, c \in \mathbf{c}\}$$

be upper bound of optimum for ILP problem.

Note that these bounds for optimum can be infinite.

Let us consider supplementary problem for upper bound using duality.

$$\bar{\varphi}(\mathbf{A}, \mathbf{b}, \mathbf{c}) = \sup\{(\mathbf{b}_c^T p + \delta^T p \mid \mathbf{A}_c p - \Delta^T p \leq \bar{\mathbf{c}}\}.$$

Let $n \times 1$ vector y satisfy $y = \text{sgn } p$, i.e. $y_i = \{-1; 1\}$, $i = 1, 2, \dots, n$.

So there are 2^n combinations for vector y , the set of these combinations can be denoted Y^n . If vector y is fixed then we can solve LP subproblem for $\bar{\varphi}$

$$\varphi(y) = \max\{(\mathbf{b}_c^T p + \delta^T (y^T p) \mid \mathbf{A}_c p - \Delta^T (y^T p) \leq \bar{\mathbf{c}}\}.$$

Value $\varphi(y)$ can be infinite. After using all combinations for vector y , we can calculate upper bound

$$\bar{\varphi}(\mathbf{A}, \mathbf{b}, \mathbf{c}) = \sup\{\varphi(y) \mid y \in Y^n\}.$$

To find lower bound of optimum the following problem should be solved

$$\underline{f}(\mathbf{A}, \mathbf{b}, \mathbf{c}) = \min\{c^T x \mid \underline{\mathbf{A}}x \leq \bar{\mathbf{b}}, \bar{\mathbf{A}}x \geq \underline{\mathbf{b}}, x \geq 0\}.$$

This problem is a point LP problem which can be solved for polynomial time.

Problems for φ and \underline{f} can be split into series of subproblems, which can be solved using parallel computations with little exchange between processes.

Theorem [2]. For ILP problem the following statements are equivalent:

- for any matrices $A \in \mathbf{A}$, $b \in \mathbf{b}$, $c \in \mathbf{c}$ LP problem $\max\{c^T x \mid Ax = b, x \geq 0\}$ has optimal solution;
 - both lower bound and upper bound of optimum are finite;
 - both lower bound and supplementary problem for upper bound are finite;
- system

$$\{\bar{\mathbf{A}}^T p_1 - \underline{\mathbf{A}}^T p_2 \leq \underline{\mathbf{c}}, p_1, p_2 \geq 0; p_1, p_2 \in \mathbf{R}^n\}$$

is feasible and value $\overline{\varphi}(\mathbf{A}, \mathbf{b}, \mathbf{c})$ is finite.

The range of optimum is $[f(\mathbf{A}, \mathbf{b}, \mathbf{c}); \overline{\varphi}(\mathbf{A}, \mathbf{b}, \mathbf{c})]$ in every case.

The first step requires solving the only LP problem that is why it has polynomial complexity [2].

The second step requires solving of 2^n LP problems therefore it has exponential complexity (in the worst case).

Today LP problems can be effectively solved using parallel computations and exact rational-fractional calculations [4]. It is evident that each subproblem can be solved separately. So ILP problem has rather great potential for parallelism although coarse-grained parallelism is often used for each LP subproblem. CUDA C software engineering is suggested by author for parallel calculations.

Another approach to solve ILP problem is interval simplex-method [3]. The idea is to use rules of interval arithmetic to calculate elements of simplex-table. But this method has a lot of restrictions and disadvantages, so it is rather controversial.

3. Interval Linear Programming Problem

A *general equilibrium* position for von Neumann's model (A, B) , where A and B are given $n \times m$ input and output matrices with numerical nonnegative items,

$$a_{ij}, b_{ij} \geq 0, \quad i = \overline{(1, n)}, \quad j = \overline{(1, m)};$$

is defined as a solution (λ, x, w) of the system of bilinear inequalities and equations

$$(A - \lambda B)x \leq 0, \quad (x, e^m) = 1, \quad x \geq 0, \quad (1)$$

$$(A - \lambda B)^T w \geq 0, \quad (w, e^n) = 1, \quad w \geq 0, \quad (2)$$

where $e^l \in R^l$, $e^l = 1$, $i = \overline{(1, l)}$.

A *non-degenerate equilibrium* position in the model under examination is an equilibrium position (λ, x, w) satisfying the additional condition $w^T Ax > 0$.

The extreme feasible values of λ can be found by solving the bilinear optimization problems

$$\lambda_n = \min \{ \lambda \mid (A - \lambda B)x \leq 0, (x, e^m) = 1, x \geq 0 \}; \quad (3)$$

$$\lambda^* = \max \{ \lambda \mid (A - \lambda B)^T w \geq 0, (w, e^n) = 1, w \geq 0 \}. \quad (4)$$

The numbers λ_n and λ^* are called *von Neumann* and *Frobenius numbers* of the model (A, B) respectively. The von Neumann number λ_n determines the maximum possible balanced growth rate, while the Frobenius number λ^* determines the minimum possible balanced growth rate and the workability of the model [7].

Vectors x , w of equilibrium position (λ, x, w) are called *primal* and *dual von Neumann's rays* corresponding the value of λ .

An *isolated pair* for von Neumann's model is a pair of arbitrary subsets $S \subset \overline{1, 2, \dots, m}$ and $T \subset \overline{1, 2, \dots, n}$, for which if $j \in S$ and $i \notin T$ then $a_{ij} = b_{ij} = 0$.

If there is no isolated pair in von Neumann's model then the von Neumann's number and the Frobenius number coincide [7].

Thus finding parameters of productivity (the Frobenius number λ^*) and stable equilibrium position for von Neumann's model lies in solving the following bilinear programming problem

$$\begin{aligned}
 (\lambda^*, x^*, w^*) &= \arg \max_{(\lambda, x, w)^T \in D(A, B)} \lambda \\
 D(A, B) &= \left\{ \begin{pmatrix} \lambda \\ x \\ w \end{pmatrix} \mid \begin{cases} (A - \lambda B)x \leq 0, \\ (A - \lambda B)^T w \geq 0, \\ (x, e^m) = 1, (w, e^n) = 1, \\ \lambda \geq 0, x \geq 0, w \geq 0. \end{cases} \right\}
 \end{aligned} \tag{5}$$

Hereinafter, parameters of productivity are meant by equilibrium position if it is not defined exactly.

Numerical methods of solving this problem (5) are discussed in [5]. They are based on finding the roots of the monotone functions

$$u(\lambda) = \min_{x: (x, e^m) = 1, x \geq 0} \max_{j=1, 2, \dots, n} \sum_{j=1}^n (a_j - \lambda b_j) x_j \tag{6}$$

$$v(\lambda) = \max_{w: (w, e^n) = 1, w \geq 0} \min_{j=1, 2, \dots, m} \sum_{i=1}^n (a_{ij} - \lambda b_{ij}) w_i . \tag{7}$$

When λ is fixed then the values of functions $u(\lambda)$ and $v(\lambda)$ equal to optimal values of mutually dual linear programming problems

$$\min \{u : (A - \lambda B)x \leq u, (x, e^m) = 1, x \geq 0\}$$

and

$$\max \{v : (A - \lambda B)^T w \leq v, (w, e^n) = 1, w \geq 0\}.$$

When λ is close to the roots of $u(\lambda), v(\lambda) \rightarrow 0$, problems (6) and (7) become degenerate because of appearance of zero basic variables u and v in optimal basis solution of this problems. That is why problems (6) and (7) cannot be solved with conventional means based on floating-point arithmetic.

Let us introduce *interval von Neumann's model* by interval matrices of input $\mathbf{A} = \{\underline{a}_{ij}, \overline{a}_{ij}\}$ and output $\mathbf{B} = \{\underline{b}_{ij}, \overline{b}_{ij}\}$, $i = (1, n), j = (1, m)$ [6, 8], which have matrices of centers

$$\mathbf{A}_c = (\underline{\mathbf{A}} + \overline{\mathbf{A}}) / 2, \quad \mathbf{B}_c = (\underline{\mathbf{B}} + \overline{\mathbf{B}}) / 2.$$

The proofs of theorems presented below are given in [8].

Theorem 1. Let triplet $(\underline{\lambda}, \underline{x}, \underline{w})$ be equilibrium position for von Neumann's model $(\underline{\mathbf{A}}, \underline{\mathbf{B}})$, and triplet $(\overline{\lambda}, \overline{x}, \overline{w})$ be equilibrium position for von Neumann's model $(\overline{\mathbf{A}}, \overline{\mathbf{B}})$; then the Frobenius number $\tilde{\lambda}$ for any point von Neumann's model $(\tilde{A}, \tilde{B}) : (A \in \mathbf{A}, B \in \mathbf{B})$ belongs to $[\underline{\lambda}; \overline{\lambda}]$.

Strong solution (x_s, w_s) of interval model (\mathbf{A}, \mathbf{B}) provides equilibrium position $(\tilde{\lambda}, x_s, w_s)$ for any exact (point) von Neumann's model $(A, B) : (A \in \mathbf{A}, B \in \mathbf{B})$.

Weak solution for interval von Neumann's model (\mathbf{A}, \mathbf{B}) is a pair of vectors (x', w') , under which set of constraints

$$\begin{cases} (\tilde{A} - \tilde{\lambda} \tilde{B})x' \leq 0; \\ (\tilde{A} - \tilde{\lambda} \tilde{B})^T w' \geq 0; \\ (x', e^m) = 1; \\ (w', e^n) = 1; \\ x', w', \tilde{\lambda} \geq 0 \end{cases}$$

is feasible for any exact von Neumann's model $(\tilde{A}, \tilde{B}) : (\tilde{A} \in \mathbf{A}, \tilde{B} \in \mathbf{B})$.

Theorem 2. If set of constraints

$$\begin{cases} (\bar{\mathbf{A}} - \lambda \mathbf{B})x'' \leq 0; \\ (\underline{\mathbf{A}} - \lambda \mathbf{B})^T w'' \geq 0; \\ (x'', e^m) = 1; \\ (w'', e^n) = 1; \\ x'', w'' \geq 0 \end{cases}$$

is feasible under pair of vectors (x'', w'') then (x'', w'') is a weak solution of interval von Neumann's model (\mathbf{A}, \mathbf{B}) .

Theorem 3. Let (x', w') be a weak solution for interval von Neumann's model (\mathbf{A}, \mathbf{B}) . If exact von Neumann's model $(A, B) : (A \in \mathbf{A}, B \in \mathbf{B})$ has

$$\lambda' = \max\{\lambda \mid (\tilde{A} - \lambda \tilde{B})x' \leq 0; (\tilde{A} - \lambda \tilde{B})^T w' \geq 0\},$$

then $\lambda' \in [\lambda_n, \bar{\lambda}]$, where λ_n is the von Neumann's number for model $(\underline{\mathbf{A}}, \bar{\mathbf{B}})$.

Theorem 4. Let (x^*, w^*) be primal and dual Frobenius vectors for exact von Neumann's models (\tilde{A}, \tilde{B}) and (\hat{A}, \hat{B}) , where $\hat{a}_{ij} - \tilde{a}_{ij} = \Delta a_{ij} \geq 0$, $\hat{b}_{ij} - \tilde{b}_{ij} = \Delta b_{ij} \geq 0$. Let the Frobenius number for model (\tilde{A}, \tilde{B}) is equal to $\tilde{\lambda}$, and model (\hat{A}, \hat{B}) has the Frobenius number $\hat{\lambda}$, $\Delta \lambda = \hat{\lambda} - \tilde{\lambda}$. Let model (\tilde{A}, \tilde{B}) has non-degenerate equilibrium position $(\tilde{\lambda}, x^*, w^*)$. Then

$$\Delta \lambda = \frac{(w^*)^T (\Delta_A - \tilde{\lambda} \Delta_B) x^*}{(w^*)^T (\tilde{B} + \Delta_B) x^*}.$$

4. Conclusion

The main approach described is usage of lower and upper bounds to find different types of solutions. These solutions can be obtained from by solving series of exact LP problems by using parallel computations. It was shown that bilinear problem of finding equilibrium position for interval von Neumann's model can be treated similarly.

References

- [1] T.H. Cormen, C.E. Leiserson, Introduction to Algorithms, Massachusetts Institute of Technology, 2009.
- [2] M. Fiedler, J. Nedoma, J. Ramik, J. Rohn, K. Zimmermann, Linear Optimization Problems with Inexact Data, Springer Science+Business Media, 2006.
- [3] L. Jaulin, M. Kieffer, O. Didrit, E. Walter, Applied Interval Analysis, Springer-Verlag London Limited, London, 2001.
- [4] A.V. Panyukov, V.A. Golodov, Software engendering for algorithm of solving a linear equation set under interval uncertainty, Proc. Int. Conf. on Parallel Computations, vol. 2. Institute of Control Sciences V.A. Trapeznikov, Moscow. (2012) 155–166.
- [5] A.V. Panyukov, A.T. Latipova, Numerical Techniques or Finding Equilibrium in von Neumann's Model, Computational Mathematics and Mathematical Physics. 14(48) (2008) 1999–2006.
- [6] A.V. Panyukov, A.T. Latipova, Finding Equilibrium in von Neumann's Model in Case of Interval Uncertainty of Initial Data, Vestnik Ufmskogo Gosudarstvennogo Aviationsionnogo Tekhnicheskogo Univ., Ser. Control, Computer Engineering and Computer Science. 2(27) (2008) 150–153.
- [7] S.A. Ashmanov, Introduction to Mathematical Economics, Nauka, Moscow, 1984.
- [8] A.V. Panyukov, A.T. Latipova, Stability Analysis of Equilibrium Position of von Neumann's Model under Interval Uncertainty, Proc. of the 14th IFAC Symposium on Information Control Problems in Manufacturing (Bucharest, Romania, 2012). 14 (2012) 1470–1474.



International Conference on Industrial Engineering

Modeling the problem of transport network synthesis under conditions of uncertain initial information

Demchenko A.I.*

South Ural State University, 76, Lenin Avenue, Chelyabinsk, 454080, Russian Federation

Abstract

This paper dwells upon the problem of synthesising structures under indefiniteness. Herein is proposed a classification of initial information uncertainty types that influence the parameters of transport networks. It is shown that different types of uncertainties can be narrowed down to two types, internal and external. The article presents formal models of problems reflecting the said types of uncertainties and different ways of describing them by means of the interval analysis and fuzzy sets. Schemes for solving the problems posed are given based on the decomposition approach.

© 2015 The Authors. Published by Elsevier Ltd. This is an open access article under the CC BY-NC-ND license (<http://creativecommons.org/licenses/by-nc-nd/4.0/>).

Peer-review under responsibility of the organizing committee of the International Conference on Industrial Engineering (ICIE-2015)

Keywords: Transport networks, decomposition approach, uncertainty of information

1. Introduction

The article develops methods of synthesis of transport networks structures in view of uncertainty of initial information. The problems of designing transport networks arise at designing of different communications. Such communications can be exemplified by networks of highways and railways, power supply networks, product lines of different assignment, etc. In particular, such problem arises at designing of systems for infrastructure development of fields: oil, gas, coal, etc. Respective industries are most dynamic. Annually hundreds of fields are commissioned and developed in the country. Regions of mine field infrastructure development are characterized not only by commissioning of the fields themselves but also by establishment of their regional service systems.

* Corresponding author. Tel.: +7-919-115-55-20
E-mail address: aidchel@mail.ru

Initial information is generally uncertain for any types of transport networks, but the uncertainty degree and the number of uncertain factors are particularly high at synthesis of infrastructure development networks structures. Infrastructure development networks are defined here as transport networks created for development and operation of mine fields in regions with lacking infrastructure. These networks are characterized by the following uncertain factors: the power of source, time of network exploiting, information about geological conditions of building, directions of network development, modes of building, etc. A peculiar feature of building infrastructure development networks lies in existence of the only sink. Whereas there is no consumption inside the field region, all the produced products are exported to other regions from the single cargo-generating station, which constitutes the network's sink.

The network's cost consists of two components:

- capital, including the cost of construction of the network's communications and expenses on maintenance of their operability;
- operating, equal to the cost of expenses on product transportation through the network.

This type of networks is further considered, although the developed approach is universal and can be applied at designing of any transport networks structures.

At designing of transport networks a large volume of information is generally attracted for determination of parameters of the designed network. As a result, already at this stage many initial data cannot be defined unambiguously.

The basic factors taken into account in modern methods of automated designing include:

1. Natural factors formalized as engineering-geological and hydrogeological characteristics of territories. Processing of available information generally depends in many respects on the expert's experience and intuition and contains errors;
2. Different design and process solutions of building a specific transport and communication network. Selection of a solution is influenced by appearance of new materials and modes of building, etc.;
3. Operating characteristics of road structures determined by expenses on maintenance and current repair;
4. Expenses on cargo transportation calculated on the basis of scheduled volumes over a period of network functioning;
5. Expenses connected with the damage caused to the environment in the course of construction and operation of the network;
6. Situations when the influence of natural or artificial facilities on selection of an optimal solution are taken into account.

Formalization of the aforesaid factors generally contains errors, whereas it depends on completeness of available information and the designer's experience. This fact allows to make a conclusion that in real conditions there is uncertainty of information about parameters of the designed network. This circumstance requires an adequate formulation of the optimization problem, selection of a mathematical model including uncertainty of initial data and, generally speaking, does not allow to use algorithms meant for solution of deterministic problems. The analysis of causes that give rise to uncertainty of parameters allows to discriminate two types of factors:

1. factors that are external for the model and act equally to its parameters. They include: time of network using, power of source, modes of building, etc.;
2. factors that are the consequence of incompleteness of engineering-geological information about building and exploitation conditions and influencing internal model parameters.

The first group of factors defines the external uncertainty of the model, the second – the internal uncertainty of the model.

In order to describe the internal and external uncertainty methods of the interval analysis [1,2] and the fuzzy sets theory [3,4] are used in the work. The procedure of selecting optimal variants of networks structures is based on introduction of preference relations and the decomposition approach [5].

The second section is devoted to formulation of the problem of synthesis of an optimal network structure and formalization of two introduced types of uncertainty. Decomposition approach to the solving of a problem is presented in the third section. The fourth section introduces preference relations by a set of variants of the transport network structures and describes the scheme of problem decomposition. The fifth section describes models and algorithms of transport networks synthesis based on the decomposition approach.

2. Problem formulation

Usually the initial information for the transport network synthesis problem is set in the form of connected graph $G=(V,E)$, where V is the set of vertex, E is the set of edges corresponding to admissible communications.

The problem of transport network synthesis lies in minimization of objective function

$$F(T) = \sum_{(i,j) \in T} (\omega(i,j) + v(i,j) * y(i,j,T)) \rightarrow \min, T \in \Omega, \quad (1)$$

where T is the spanning tree of graph G , $w(i,j)$ is the edge (i,j) creation cost, $v(i,j)$ is the cost of transportation of a product item along the edge, $y(i,j,T)$ is the value of flow along the edge (i,j) determined unambiguously at the set sink, the set power of sources and the flow preservation condition. Ω – set of spanning trees of graph G .

In case of external uncertainty the problem of transport network synthesis can be presented as follows:

$$F(\tilde{\alpha}, \tilde{\beta}, T) = \sum_{(i,j) \in T} (\tilde{\alpha} * \omega(i,j) + \tilde{\beta} * v(i,j) * y(i,j,T)) \rightarrow \min, T \in \Omega, \quad (2)$$

where $\tilde{\alpha}$, $\tilde{\beta}$ – uncertain parameters.

In case of internal uncertainty the required objective function is presented as follows:

$$F(T) = \sum_{(i,j) \in T} (\tilde{\omega}(i,j) + \tilde{v}(i,j) * \tilde{y}(i,j,T)) \rightarrow \min, T \in \Omega, \quad (3)$$

where $\tilde{w}(i,j)$, $\tilde{v}(i,j)$, $\tilde{y}(i,j)$ – uncertain parameters set on edges of graph G .

For description of both external and internal uncertainty it is proposed to use methods of the interval analysis and fuzzy sets.

3. Decomposition approach to problem solution

The problem of transport network synthesis is characterized by such properties as discreteness, high dimension and non-linear nature. The aforesaid factors allow to refer the problem posed to problems of mathematical programming, which have no universal efficient solvation methods.

The considered problem is a synthesis of two problems: the first problem is designing of the network structure and its topology; the second is distribution of flows along the designed network. Such problem structure enables decomposition and organization of an efficient procedure for optimization of private problems.

The approach developed by Peltsverger B.V. and Khavronin O.V. [6] seems most expedient for solution of problems (2) and (3). The said approach is based on outlining of a class of NP-hard problems of combinatorial optimization, including problem (1), which are efficiently solved on the basis of the decomposition approach. As a result, solution of the initial NP-hard problem can be reduced to solution of a sequence of problems of polynomial complexity. Problem decomposition allows to increase significantly dimensionality of the solvable problem and is based on outlining of private criteria coordinated with the initial and further selection of a solution out of a Pareto set of solutions of a multi-criteria problem. Application of the decomposition approach is most expedient when a global problem and problems with private criteria have different complexity classes. The said scheme allows to reduce solution of the initial NP-hard problem (1) to solution of a sequence of private problems of polynomial complexity. The article proposes to apply the said scheme for solution of problems (2) and (3). The guaranteed estimation of complexity of such problems allows to modify the known algorithms in case of inaccurate initial information almost without prejudice to their efficiency.

4. Preference relations for a problem with interval and fuzzy estimations

Whereas estimation of an alternative in problems (2) and (3) is either an interval or a fuzzy set, for solution of such problems it is necessary to introduce non-vector and vector preference relations (PR) for a set of alternatives and to generalize the scheme of decomposition in case of these PRs. For problem (2) the introduced private criteria are deterministic. The description of the decomposition scheme for problem (1.2) with fuzzy estimations is set out in

paper [7]. It is evident that the above method is applicable for solution of problem (2) with interval estimations. As opposed to problem (2), in problem (3) private criteria are also nondeterministic and prescribed by some PRs. Consequently, for application of the decomposition approach it is necessary to formulate the condition of consistency of the global PR with private PRs. The PR consistency condition is a generalization of the condition of criteria monotonicity in the deterministic case [3], namely, PR η is consistent with relations v_1, \dots, v_m only when it follows from the fact that $\forall i$ x' dominates over x'' by PR v_i that x' dominates over x'' by PR η . It is easy to check that in case of consistent PRs the set of non-dominating solutions by PR η is contained in the set of non-dominating solutions by the vector PR (v_1, \dots, v_m) .

1.1. Preference relations for the case of interval estimations

In case of one criterion the PR is introduced naturally: two intervals $I_1=[a_1, b_1]$ and $I_2=[a_2, b_2]$ are incomparable only when $(b_1-a_2)(a_1-b_2)<0$, I_1 dominates I_2 ($I_1<I_2$) only when $a_2>b_1$. The solution of the problem is a set of non-dominating intervals (which are incomparable with each other). For multi-criteria problems with uncertainty several PRs are introduced in paper [8,9], but their application in problems with interval uncertainty is inexpedient, whereas in this case the problem becomes fully deterministic, which leads to a partial loss of information laid in the model and an unjustified narrowing of the selection area.

Let us introduce the vector PR for a multi-criteria problem with integral parameters

$$(U_1(x), U_2(x), \dots, U_m(x)) \rightarrow \min, x \in X$$

in such a way, so that each alternative x corresponds to m-dimensional parallelepiped in the space of criteria $D(x)=[a_1, b_1] \times [a_2, b_2] \times \dots \times [a_m, b_m]$, where $[a_i, b_i]$ – interval of values of criterion $U_i(x)$. Parallelepiped $D(x')$ dominates over parallelepiped $D(x'')$ only when $\forall i$ $b_i' < a_i''$.

1.2. Preference relations for a case of fuzzy estimations

Non-vector PR for fuzzy sets is defined in paper [4] as a PR induced by a natural order ($<$) on the number axis. The vector PR for this case is described in paper [7]. However, these PRs do not allow to consider the shapes of the curves described by the membership functions and depend only on mutual location of spheres with maximum values of the membership functions. In this work it is proposed to express these PRs through the PR for interval estimations.

Suppose a fuzzy set is prescribed by membership function $v: R^1 \rightarrow [0, 1]$. Subject to [4], a set of α -level of fuzzy set v is set $X_\alpha^v = \{x | x \in R^1, v(x) \geq \alpha\}$, $0 < \alpha \leq 1$.

It is evident that for convex fuzzy sets X_α^v is an interval. Fuzzy set v dominates over fuzzy set μ at level α only when X_α^v dominates over X_α^μ . Sets v and μ are incomparable only when respective intervals are incomparable. The vector PR is introduced analogously at level α . It should be noted that for normal convex fuzzy subsets the introduced PR in case $\alpha=1$ coincides with PR [4], and the set of alternatives, which are non-dominating by this PR, grows monotonously with reduction of α .

In case estimations are nonconvex (X_α^v is not continuous), instead of X_α^v we take an approximating interval, which lower border coincides with the minimum lower border, and the upper border coincides with the maximum upper border of intervals making up X_α^v . In this case, this set of non-dominating solutions can only increase.

5. Algorithm of transport network synthesis under uncertainty

The algorithm of solving problem (2) for the case of fuzzy estimation is described in [7]. Whereas the interval estimation is a private case of a fuzzy set, the described algorithm can be applied for solving problem (2) with interval estimations.

In order to solve problem (3) with interval estimations private cases of polynomial complexity are introduced:

$$U_1(T) = \sum_{(i,j) \in T} \tilde{\omega}(i, j) \rightarrow \min, T \in \Omega, \quad (4)$$

$$U_2(T) = \sum_{(i,j) \in T} (\tilde{v}(i,j) * \tilde{y}(i,j,T)) \rightarrow \min, T \in \Omega, \quad (5)$$

The problem can be solved in the course of building a set of efficient solutions P_u of problem

$$(U_1(x), U_2(x)) \rightarrow \min, x \in X$$

Field $D(T_i)$ corresponds to each solution T_i of problem (3) in the space of criteria.

$$D(T_i) = [a_1^i, b_1^i] \times [a_2^i, b_2^i], \text{ где } U_1(T_i) = [a_1^i, b_1^i], U_2(T_i) = [a_2^i, b_2^i].$$

By definition $T_i \in P_w$ if there is no such T_j that $U_1(T_j) \leq U_1(T_i)$ and $U_2(T_j) \leq U_2(T_i)$ besides, one of the inequalities is strict.

The algorithm of solving problem (3) with interval estimations is described in [10].

As it follows from cl. 3.2. problem (3) with fuzzy estimations of alternatives can be reduced to problem (3) with interval estimations.

As for selection of level α , at which fuzzy estimations are compared, it is generally difficult to give specific recommendations. It can be only noted that with decrease of α the number of non-dominating alternatives monotonously grows. In a specific problem α shall be selected empirically, based on the required power of the set of non-dominating alternatives.

6. Conclusion

The offered model of solving the problem of synthesis of the transport network structure is universal and allows to generate a set of non-dominating variants of networks in case of internal and external uncertainty. Implementation of the considered approach is used in software complexes at designing of oil field infrastructure development networks in West Siberia.

References

- [1] G. Alefeld, J. Herzberger, Introduction to interval computations, Academic Press, New York, 1983.
- [2] Yu.I. Shokin, Interval analysis, Nauka, Novosibirsk, 1981.
- [3] L.A. Zadeh, The concept of a linguistic variable and its application to approximate reasoning, American Elsevier Publishing Company, New York, 1973.
- [4] S.A. Orlovsky, Problems of decision making at uncertain initial information, Nauka, Moscow, 1981.
- [5] P.S. Krasnoschekov, V.V. Morozov, V.V. Fyodorov, Decomposition approach to designing problems, Izvestia AS USSR, *Technicheskaya kibernetica*. 2 (1979).
- [6] B.V. Peltserger, O.V. Khavronin, Application of decomposition approach for solution of complex problems of combinatorial optimization, Izvestia AS USSR, *Technicheskaya kibernetica*. 3 (1988).
- [7] B.V. Peltserger, O.V. Khavronin, Decomposition approach to network synthesis problem with fuzzy time of exploitation, Izvestia AS USSR, *Technicheskaya kibernetica*. 4 (1986).
- [8] V.I. Zhukovsky, V.S. Molostvov, Multi-criteria decision making under uncertainty conditions, IRIAS, Moscow, 1988.
- [9] E. Zhukovin, Fuzzy multi-criteria models of decision making, Metsniereba, Tbilisi. 1988.
- [10] A.I. Demchenko, B.V. Peltserger, O.V. Khavronin, Synthesis based on the decomposition approach of transportation network structures under conditions of indeterminacy of the initial information, Izvestia AS USSR, *Technicheskaya kibernetica*. 3 (1990).



International Conference on Industrial Engineering

Analysing the economic stability of an enterprise with the help of eigenstate method

Mokeyev V.V., Bunova E.V., Perevedentceva A.V.*

South Ural State University, 76, Lenin Avenue, Chelyabinsk, 454080, Russian Federation

Abstract

An analysis of enterprise performance is considered. The problem is solved based on the analysis of the base indicators of enterprise performance in terms of improving economic stability. An autoregulation mechanism of the economical stability of an enterprise is developed. An eigenstate method is proposed to analyse the basic indicators of the enterprise as it allows to construct an economical stability model of such enterprise. The article describe the methodology for analyzing the economic stability of an enterprise on the basis of eigenstate method. It provides formulas for calculating the complex indicator of economic stability. The efficiency of the methodology is demonstrated with evidence from the economic stability analysis of the trading company.

© 2015 The Authors. Published by Elsevier Ltd. This is an open access article under the CC BY-NC-ND license (<http://creativecommons.org/licenses/by-nc-nd/4.0/>).

Peer-review under responsibility of the organizing committee of the International Conference on Industrial Engineering (ICIE-2015)

Keywords: economic stability; enterprise, analysis; principal component; eigenstate method;

1. Introduction

In modern market conditions the basis for the stable operation of the enterprise is economic stability. When the enterprise is economically stable, it has several advantages over other companies in the same field for loans and investment, in the selection of suppliers and qualified staff. The higher economic stability of the enterprise makes the enterprise more autonomous from unexpected changes in market conditions and leads to decrease of bankruptcy risk. Lack of economic stability can lead to enterprises' insolvency, to lack of funds to finance current and investment activities, to bankruptcy at aggravation of a financial state. The excess of economic stability puts

* Corresponding author. Tel.: +7-912-779-9524

E-mail address: mokeyev@mail.ru, albv70@mail.ru

obstacles in the way of enterprise development, burdening them with unnecessary costs. There is no doubt that the effectiveness of the enterprise is caused by its financial capacity and efficiency of financial management. The low level of financial management leads to a crisis and deterioration of enterprise's financial condition, i.e. to the loss of its financial stability.

The issues of economic stability of enterprises are considered in a large number of scientific works [1-12]. Economic sustainability as the enterprise's ability to provide economic growth and efficiency by using accumulated economic potential is considered by researchers in Reference[13].

Nevertheless, the problem of economic stability companies demands further studying from the point of view of creation and using the tools that prove operating of the mechanism of autoregulation. Mechanism of economic stability autoregulation of companies includes a regular assessment and forecasting of the main indicators of functioning and also acceptance of reasonable administrative decisions on the basis of this analysis. In Reference [14] it is said that "main objective for many enterprises in Russian economy there is survival and such mechanisms are extremely necessary to provide their sustainable development".

Here introduce the paper, and put a nomenclature if necessary, in a box with the same font size as the rest of the paper. The paragraphs continue from here and are only separated by headings, subheadings, images and formulae. The section headings are arranged by numbers, bold and 10 pt. Here follows further instructions for authors.

Competent approach to administrative management is basis for stable existence in modern economic conditions. It's impossible to build the effective control system of enterprise based only on intuition. The effective control system has to provide fast and proper response to the changes of activity conditions of the enterprise. In paper we describe the overall control algorithm, which is based on the regular analysis of the deviations of the reference values from real values of indicators to identify the reasons of these deviations and making decisions for correction of negative influences. Each corrective action is tested for the possibility of increasing the economic stability of the enterprise, but it is possible only when forecasting indicators of the enterprise activity is used.

The principal component analysis effective approach allowing establishing and measuring the causal relationships between various processes within the socioeconomic systems [15-17]. One of the important advantages of the method of principal components is that it allows presenting the behavior of the system under investigation as a set of (statistically) independent components, each of which can be analyzed separately.

In paper the methodology of the analysis of economic stability of enterprise with the use of eigenstate method is described [18-20]. The analysis of economic stability of enterprise includes formation of model which uses only eigenstates satisfying the economic stability conditions. The use of analysis on the basis of eigenstate method allows to reflect the complex tendencies of development of enterprise in the simplified form (model) and to analyze their development in the real world with the help of the obtained model.

2. Mechanism of economic stability autoregulation

Mechanism of economic stability autoregulation of enterprise is based on an information system of the enterprise, for example, the IC: Enterprise. It allows to regularly provide to the management personnel the main indicators of business processes of enterprise and factors of stability with a list of signs of instability on the basis of the registration data obtained by information system. In Fig. 1, the diagram of mechanism of maintaining economic stability of enterprise is shown.

This diagram allows the leader of the enterprise to monitor the enterprise state real-time. Information system of enterprise can be used for data collection. The model of economic stability of the enterprise is formed using sample of data generated. The obtained model allows to compute the value of the indicator of economic stability of enterprises, to analyses the signs of instability and quickly take the corrective actions.

Thus the leader of enterprise analyse the indicators of the company in the terms of economic stability, but also to forecast the enterprise activity on the basis of a economic stability model and make competent administrative decisions to support the sustainability of the business. For example, resource reallocation, incoming cash flow increment and implementation activities can be such administrative decisions

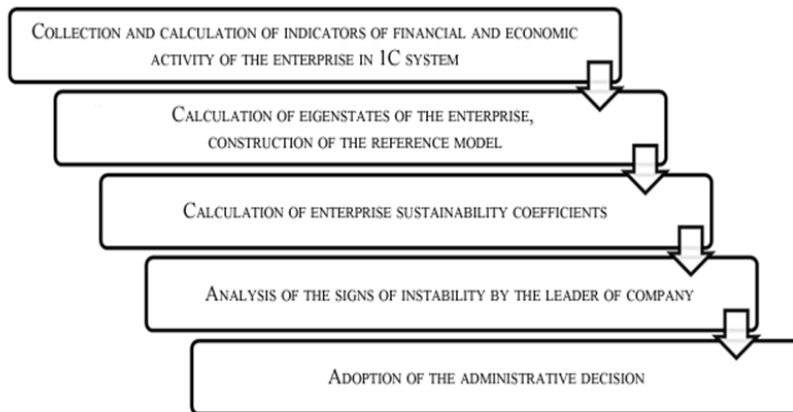


Fig. 1. Functional diagram of adoption of the administrative decision to maintain the economic stability of enterprise.

Effective way of analysis of enterprise economic stability is eigenstate method, which is the development of principal component analysis. In fact, when we use the principal component method, we implement transfer from the initial indicators to new indicators which are called principal components. The principal component is combination of initial indicators in which members of group (initial indicators) are connected among themselves, but group (principal component) as a whole is independent from other groups (principal components). The weighted coefficients of the principal components are determined by calculation of the eigenvectors of the covariance matrix. Each eigenvector corresponds to its eigenvalue. The eigenvectors are sorted in descending order of the eigenvalues. Thus, k -th eigenvector comprises weighted coefficients of k -th principal component, and the eigenvalue corresponding to the eigenvector is equal to the dispersion k -th principal component.

Each eigenvector has the same length as the state vector of the economic system, which makes it possible to interpret it as an eigenstate of the economic system. Thus, at any moment of time the state of the economic system can be described by weighted combination of eigenstates. Then the state of system is described not by a set of initial indicators, but by a set of principal components. But each principal component reflects not a separate initial indicator, but group of initial indicators which are called eigenstates. Eigenstates have two important properties [20]. Property 1: In describing the state of the economic system as a weighted sum of eigenstates, the principal components of the eigenstates are statistically independent.

Property 2: The change of the unit state associated with the change of the principal component of the j -th eigenstate can only be proportional to the coefficients of the j -th eigenstate.

These properties play an important role in the construction of economic systems models. To analyse the economic stability of enterprise the model of economic stability is proposed to build. The model represents a combination of eigenstates, satisfying the conditions of economic stability of enterprise. The economic stability conditions represent restriction on interrelation of a number of key indicators. For example, profit mark up of the enterprise must be accompanied by a decrease in production costs. The economic stability model is an idealization of a real business and serves as a model of the system in terms of its economic performance.

Any enterprise is sufficiently complex system with a large number of indicators that change over time. Management of economic stability is primarily a regular analysis of performance indicators of economic systems and planning strategies for their improvement, including the determination of the required funds and resources. Usually some indicators of the system are improved, others are deteriorating, which affects the economic stability of the enterprise. But it is very difficult to determine how the stability of the enterprise changes when the parameters change.

A set of indicators that characterize the behavior of the system forms the economic state of the enterprise. The state space of enterprise is a finite-dimensional space, which belongs to the state of the enterprise. Economic stability analysis of enterprise includes the formation of a model that uses only eigenstate satisfying the conditions of

stability. This condition is imposed on communication of volume and quality of the products sold with the volume and quality of the resources of the unit.

Economic stability of enterprise at any time interval is estimated by comparing the actual and reference values of the indicators. Reference values of indicators are calculated using economic stability model of enterprise. Large deviations from reference indicators are interpreted as signs of destabilization of the enterprise. Thus, the main objective of management enterprise is timely detection of the deviations destabilizing activity and definition of possible threats, research of sources and reasons of their causes and their elimination that provides economic stability of the enterprise as a system, in condition of the changing environment.

The complex economic stability indicator of the k-th moment of time can be obtained by the formula

$$R_k = 1 - \bar{f}_k \quad (1)$$

where \bar{f} is a mean square value of penalty functions which is determined as

$$\bar{f}_k = \sqrt{\frac{1}{r} \sum_{j=1}^r f_{kj}^2} \quad R_k = 1 - \bar{f}_k \quad (2)$$

In equation (2) f_{kj} is the value of penalty functions of j-th basic parameter of the k-th unit. The penalty function is defined as

$$f_{kj} = \begin{cases} 0 & \text{если } |(x_{kj} - x_{kj}^{et}) / x_{kj}| < \varepsilon_{don} \\ |(x_{kj} - x_{kj}^{et}) / x_{kj}| & \text{если } |(x_{kj} - x_{kj}^{et}) / x_{kj}| \geq \varepsilon_{don} \end{cases} \quad R_k = 1 - \bar{f}_k \quad (3)$$

where x_{kj} are actual values, x_{kj}^{et} are reference values, ε_{lim} ε_{don} – permissible variation. As we can see the penalty is assigned only if the deviation exceeds the allowable value.

3. Research of economic stability of trading company

The proposed methodology is demonstrated on the example of the analysis of stability of the large company trading in jewelry. The indicators of financial and economic activity were chosen as the initial data for the analysis. They are: x_1^0 – accounts payable (billion rubles), x_2^0 – revenue (billion rubles), x_3^0 – current assets (billion rubles), x_4^0 – accounts receivable (billion rubles), x_5^0 – profit on sales (billion rubles), x_6^0 – cost price sales (billion rubles), x_7^0 – accounts payable turnover ratio, x_8^0 – accounts receivable turnover ratio, x_9^0 – current assets turnover ratio, x_{10}^0 – return on sales, x_{11}^0 – margin costs, x_{12}^0 – the profitability of the organization, x_{13}^0 – price of gold (thousand rubles per gram), x_{14}^0 – price of silver (thousand rubles per gram).

The cost price is understood as the costs of trading activity, including administrative costs. The values are presented in Table. 1.

Eigenstates are used to build the economic stability model of company with the help of eigenstates, which are calculated from second initial moments matrix (the data not centered). The weighted coefficients of the eigenstates are represented in Table. 2.

Building the economic stability model of the company requires the formulation of requirements of economic stability of the considered company. Such condition is the following requirement: the growth of gold and silver prices leads to increased cost (rising price of purchased goods), but at the same time profit margins and sales should not be reduced. Restrictions on other parameters are not imposed, although it is possible to make claims to other indicators of financial and economic activity of the company, i.e. this requirement may be supplemented by other restrictions on indicators change.

Table 1. Financial and economic activity of the company.

	Feb	March	Apr	May	June	July	Aug	Sept	Oct	Nov	Dec	Jan
x_1	0.053	0.047	0.046	0.055	0.054	0.058	0.060	0.058	0.061	0.061	0.065	0.083
x_2	0.031	0.040	0.042	0.024	0.032	0.038	0.036	0.041	0.035	0.034	0.034	0.065
x_3	0.445	0.451	0.447	0.468	0.470	0.475	0.476	0.497	0.494	0.502	0.503	0.540
x_4	0.083	0.093	0.096	0.087	0.091	0.100	0.111	0.126	0.147	0.170	0.194	0.224
x_5	0.018	0.015	0.006	0.022	0.007	0.003	0.004	0.022	-0.005	0.006	0.002	0.022
x_6	0.013	0.025	0.035	0.002	0.025	0.034	0.032	0.019	0.040	0.028	0.032	0.043
x_7	0.588	0.837	0.896	0.443	0.594	0.650	0.598	0.699	0.571	0.564	0.527	0.779
x_8	0.376	0.427	0.433	0.278	0.354	0.376	0.323	0.324	0.235	0.203	0.178	0.289
x_9	0.070	0.088	0.093	0.052	0.068	0.079	0.075	0.082	0.070	0.069	0.069	0.120
x_{10}	0.570	0.380	0.150	0.920	0.220	0.080	0.120	0.530	-0.160	0.180	0.060	0.330
x_{11}	1.350	0.620	0.180	11.680	0.280	0.090	0.130	1.150	-0.140	0.220	0.070	0.500
x_{12}	0.560	0.370	0.220	0.920	0.210	0.070	0.130	0.550	-0.150	0.180	0.060	0.330
x_{13}	1.667	1.694	1.669	1.570	1.560	1.659	1.669	1.680	1.736	1.779	1.733	1.712
x_{14}	0.030	0.032	0.033	0.031	0.029	0.029	0.028	0.029	0.032	0.035	0.032	0.033

Within the first and second eigenstate increase in the prices of gold and silver leads to increased costs (increasing purchase prices for jewelry), profit and profitability of sales. Therefore, the first and second eigenstates are used in the formation of a sustainable development model of the trading company. The other eigenstates do not correspond to conditions of sustainable activities, as they describe the process by which the increase in the price of gold and silver results in a decrease in profitability.

Table 2. Coefficients of eigenstates.

Indicator	Number of eigenstate					
	1	2	3	4	5	6
x_1^0	0.008	0.029	-0.013	0.040	0.081	0.225
x_2^0	0.005	0.020	0.006	-0.013	0.103	0.156
x_3^0	0.069	0.239	-0.078	0.141	0.155	0.659
x_4^0	0.015	0.067	-0.063	0.181	0.551	0.263
x_5^0	0.003	0.004	0.027	0.007	0.040	0.053
x_6^0	0.002	0.016	-0.022	-0.020	0.063	0.103
x_7^0	0.081	0.338	0.169	-0.727	0.487	-0.182
x_8^0	0.045	0.159	0.155	-0.490	-0.593	0.435
x_9^0	0.010	0.041	0.015	-0.047	0.145	0.222
x_{10}^0	0.094	0.077	0.663	0.262	-0.036	0.181
x_{11}^0	0.955	-0.279	-0.090	-0.040	0.007	0.000
x_{12}^0	0.094	0.080	0.661	0.162	0.057	-0.216
x_{13}^0	0.237	0.840	-0.224	0.280	-0.185	-0.237
x_{14}^0	0.004	0.015	-0.005	0.001	0.011	-0.021

Fig. 2 shows the value of the "Revenue" indicator, and Fig. 3 demonstrates the value of the "Profit on sales" indicator. Actual values are shown by the solid line, and the values of parameters obtained using the economic stability model are represented by the dashed line. We assume that the deviation of actual values from their reference values by more than 20% is a sign of instability. Thus, the value of the penalty function is calculated by formula (3) where $\varepsilon_{dom} = 20\%$.

Values of penal functions for the indicators are presented in table 3. The table shows the values of the penalty functions for indicators "Profit on sales", "Return on sales", "The profitability of organization" reach their maximum values in September. The value of the penalty function in April is equal to zero.

The complex economic stability indicators of company are calculated according to the formula (1) and their values are shown in Fig. 4. The solid line represents change of complex economic stability indicator, calculated with using penalty functions of first 12 indicators, and the dashed line shows the change in stability indicator, obtained by the penalty functions of the first six indicators.

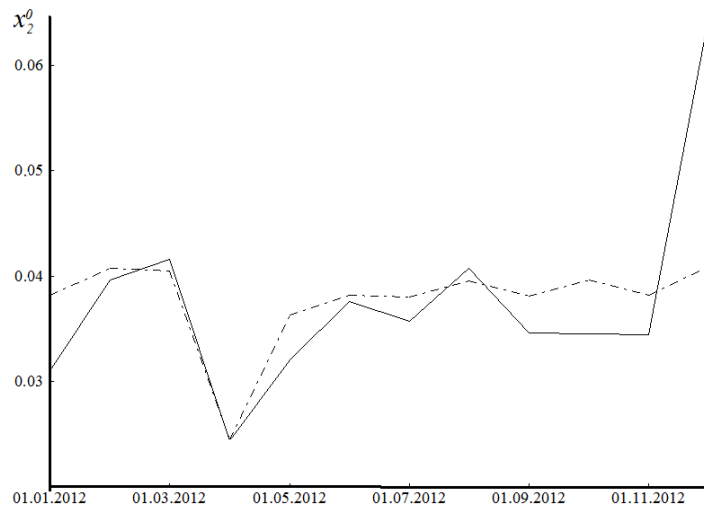


Fig. 2. Functional diagram of adoption of the administrative decision to maintain the economic stability of enterprise.

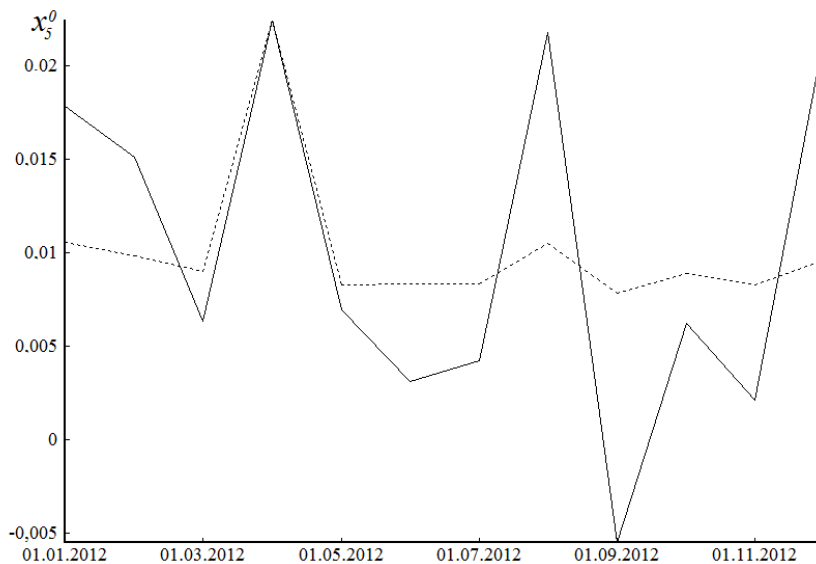


Fig. 3. Sales profit: solid line (actual values), dashed line (reference values).

Table 3. Penalty function values.

	x_1^0	x_2^0	x_3^0	x_4^0	x_5^0	x_6^0	x_7^0	x_8^0	x_9^0	x_{10}^0	x_{11}^0	x_{12}^0
Jan	-	-	-	0.36	0.41	0.52	-	-	-	0.49	-	0.47
Feb	0.24	-	-	0.32	0.35	0.21	-	0.21	-	0.35	-	0.31
Mar	0.24	-	-	0.30	0.29	-	0.23	0.24	-	0.29	-	-
Apr	-	-	-	-	-	-	-	-	-	-	-	-
May	-	-	-	0.26	-	-	-	-	-	-	-	-
June	-	-	-	0.22	0.63	-	-	-	-	0.59	-	0.65
July	-	-	-	-	0.50	-	-	-	-	0.39	-	0.36
Aug	-	-	-	-	0.52	0.35	-	-	-	0.47	-	0.47
Sept	-	-	-	-	1.00	0.25	-	0.24	-	1.00	-	1.00
Oct	-	-	-	0.22	0.30	-	-	0.37	-	-	-	-
Nov	-	-	-	0.34	0.74	-	-	0.43	-	0.69	0.24	0.70
Dec	0.26	0.37	-	0.39	0.55	0.28	-	-	0.29	0.28	-	0.26

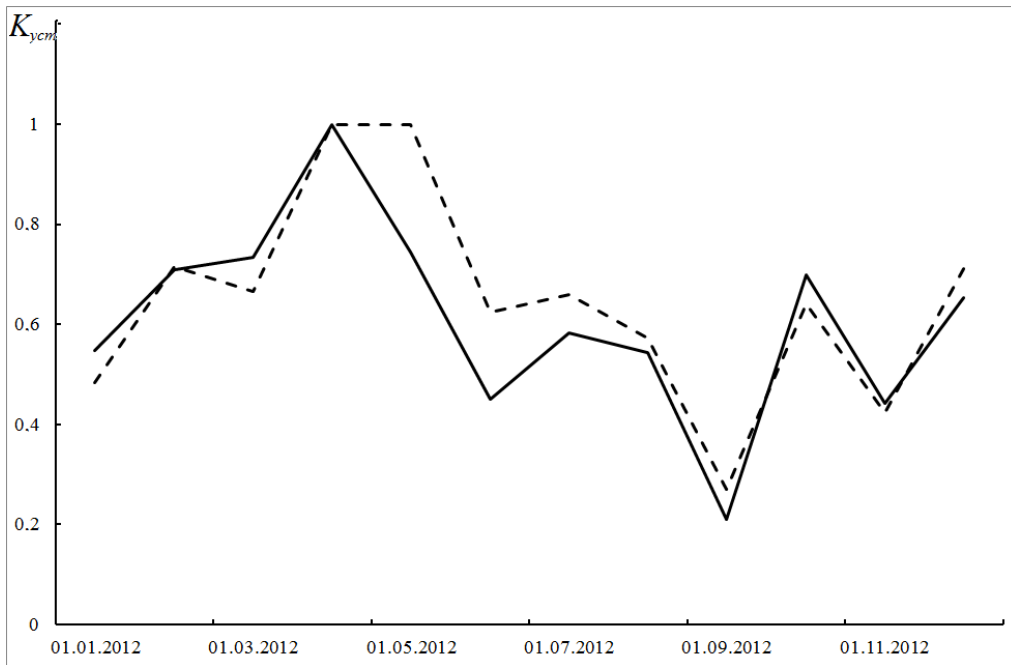


Fig. 4. Dependencies of complex economic stability indicator within a year.

4. Conclusions

In paper the solution of analysis of economic stability task of the company has been considered. Relevance of problem of economic stability analysis and development of the mechanism of enterprise management by criterion of economic stability led to that today in economic literature, along with works of foreign authors, there is enough the domestic works devoted to methodologies of the analysis of economic stability of the enterprise. The most of methodologies of the economic stability analysis of company are based on calculation of economic stability indicators and comparison with their standard values. When one of indicators goes beyond standard values, the enterprise is considered economically unstable. Such the result often incorrectly estimates economic stability of the enterprise. Thus, now there is no effective approach of the economic stability analysis of company. For the solution of task of company the economic stability methodology with use of eigenstate method is offered. The methodology allows to reveal structure of their interrelations at simultaneous reduction of number of the economic activity indicators of the enterprise and to build the complex indicator characterizing economic stability of the enterprise. The basis of this methodology is the development of economic stability model of enterprise (reference model), which is formed from their eigenstates satisfying the economic stability conditions. New indicator was proposed in order to assess the company development stability. It is named the economical stability indicator. The complex indicator of economic stability is defined by comparison of parameters of the actual and reference activity of the enterprise with the help of method of penal functions. The offered methodology includes formation of a set of indicators, the describing financial, production, ecological processes; the formulation of requirements of economic stability of the enterprise, the representing restrictions on changes of a number of indicators, calculation of eigenstate of the enterprise characterizing a certain tendency of development of the enterprise and check of compliance of own states to requirements of economic stability of the enterprise describes own state. Formulas for calculation of the complex indicator of economic stability of the enterprise are given in work. The eigenstate method can be used in the analysis of such complex systems, as the company (enterprise), the city, the region. The methodology of economic stability analysis of enterprise on the basis of eigenstate method represents the tool for effective control over assets of the enterprise and successful management of its expenses, and also reduction of time of adoption of administrative decisions is described. The developed methodology can be used for the companies of various fields of activity. The effectiveness of the methodology is demonstrated on the example of economic stability analysis of the large trading company.

As a result of research the model of economic stability of the company is constructed, also the complex economic stability indicator of the company is calculated. Results of researches can be used for development of the regulation mechanism of economic stability of the company.

This work was supported by the Russian Foundation Basic Research (project no. 14-01-00054).

References

- [1] M.S. Abryutina, *Enterprise Economy, Case and service*, Moscow, 2004.
- [2] D.G. Baur, N.N. Schulze, Financial market stability, A test. *Journal of International Financial Markets, Institutions and Money*. 19(3) (2009) 506–519.
- [3] C.T. Albuлесcu, Forecasting the Romanian financial system stability using a stochastic simulation model, *Romanian Journal of Economic Forecasting*. (2010) 81–98.
- [5] A.N. Zhilkina, *Financial Management. Financial analysis of a company*, INFRA-M, Moscow, 2005.
- [6] J. Creela, P. Huberta, F. Labondance, Financial stability and economic performance, *Economic Modelling*. 48 (2015) 25–40.
- [7] T.I. Okrainets, *Theory of management of financial stability of the company*, Bauman, Moscow, 2006.
- [8] C.T. Albuлесcu, Financial stability and monetary policy: A reduced form model for the euro area, *Romanian Journal of Economic Forecasting*. (2013) 62–81.
- [9] B.Gadanez, K. Jayaram, Measures of financial stability – a review, *Proceedings of the IFC Conference on "Measuring financial innovation and its impact"*. 31 (2009) 365–380.

- [10] Yu.M. Sulejmanova, Management of Economic Stability of an Enterprise in the Process of its Innovative Development, *Journal of Creative Economy*. (2013) 89–95.
- [11] A.D. Sheremet, A.F. Ionova, *Finance companies: management and analysis*, INFRA-M, Moscow, 2008.
- [12] Y. Krutín, Estimating of Financial Stability of Industrial Enterprise, *Practical Ideas in Economics and Finance*. (2014) 01–06.
- [13] R. Perciun, A. Stratan, A. Timush, The methodology of financial stability assessment of Republic of Moldova through macroeconomic indicators, *Procedia Economics and Finance*. (2014) 383–392.
- [14] E.V. Budumjan, Development of innovative and investment processes as objective need of modernization of industrial manufacture, *Scientific works of Free economic society of Russia*. (2011) 75–80.
- [15] E.V. Korchagina, Economic stability of enterprise: types and structures, *Problems of modern economics*. (2005) 23–27.
- [16] I.T. Jolliffe, *Principal Component Analysis*, Series: Springer Series in Statistics, second ed., Springer, NY, 2002.
- [17] V.V. Mokeev, The solution of the problem of eigenvalues in problems of multivariate analysis of economic systems, *Economics and Mathematical Methods*. 4 (2010) 82–90.
- [18] H. Abdi, L.J. Williams, *Principal component analysis*, Wiley Interdisciplinary Reviews: Computational Statistics. (2010) 433–459.
- [19] V.V. Mokeev, On enterprise performance evaluation based on the method of eigenstates, *Automatic Documentation and Mathematical Linguistics*. 48(5) (2014) 235–245.
- [20] V.V. Mokeyev, D.A. Vorobiev, Analysis of socio-economic system processes performance with the help of eigenstate models, *Bulletin of the South Ural State University, Series: Mathematical Modeling, Programming and Computer Software*. 8 (2015) 47–56.



International Conference on Industrial Engineering

A method of resonant series-parallel identification

Tkachenko G.I., Baklanov A.N.*

Platov South-Russian State Polytechnic University (NPI), 132, St. Prosvescheniya, Rostov region, Novocherkassk, 346428, Russian Federation

Abstract

This paper describes a method of resonant series-parallel identification of resistive-capacitive sensors parameters and the solution of the system object model that allows you to define its parameters, inaccessible to direct measurements. Computational experiments showed that the method of resonant series-parallel identification allows defining the parameters of RC-objects with distributed parameters. The proposed method has the following advantages: high speed while maintaining the desired accuracy of measurement and small error in calculations.

© 2015 The Authors. Published by Elsevier Ltd. This is an open access article under the CC BY-NC-ND license (<http://creativecommons.org/licenses/by-nc-nd/4.0/>).

Peer-review under responsibility of the organizing committee of the International Conference on Industrial Engineering (ICIE-2015)

Keywords: resistive-capacitive sensors, the solution of equations, the method of resonant series-parallel identification.

1. Introduction

Control of the main process parameters is carried out in order to obtain the information necessary for timely elimination of operating modes of the equipment [1]. In the measurement of process parameters are widely used potentiometers [2, 3]. With a large number of positive qualities such sensors they have a major drawback: a limited number of cycles due to wear the sliding contact portion of the sensor. The reason for this friction between the resistive layer and the collector movable element [4]. This lack deprived resistive-capacitive sensors with distributed parameters [5].

In currently prevalent resistive-capacitive sensors, which are a potentiometer with a movable electrode is moved by the measured value of the resistive element, without touching the latter. As a result, a circuit diagram of parametric resistive-capacitive sensor is a multi-element multi-pole circuit. The resistive-capacitive sensors with

* Corresponding author. Tel.: +7-951-527-9146.
E-mail address: baklanov-88@mail.ru

distributed parameters is not used galvanic and capacitive coupling of the movable element with the resistive layer. However, changes its average value with respect to the tank connection in an actual operation of a resistive-capacitive sensors distributed parameter, while moving the movable member to cause distortion of the transfer function of the sensor, and hence the output [6, 7]. To achieve permanence capacity communication is problematic without a significant appreciation of the sensor. Thus the control of the capacity of communication and information about its deviation is very important for accurate measurement, mathematical and circuit simulation of the measurement process in the design of a resistive-capacitive sensors and the development of transducers for them [8].

2. The method of resonant series-parallel identification

To determine the parameters of a resistive-capacitive sensors with distributed parameters is proposed to use the method of resonant series-parallel identification. It combines measurements on the physical object in three modes (normal, resonances, voltage and current), and the solution of equations of the model that allows you to define the parameters of the equivalent circuit, inaccessible to direct measurements [9].

Algorithm of a series-parallel resonant identification comprises the following steps:

- Measuring the physical object in three modes: normal, the resonance voltage and current;
- Preparation of the equivalent circuit of the object;
- The preparation and the solution of equations of the model parameters for the desired object.

The generalized scheme of measurements of currents in the above modes is shown in Fig. 1.

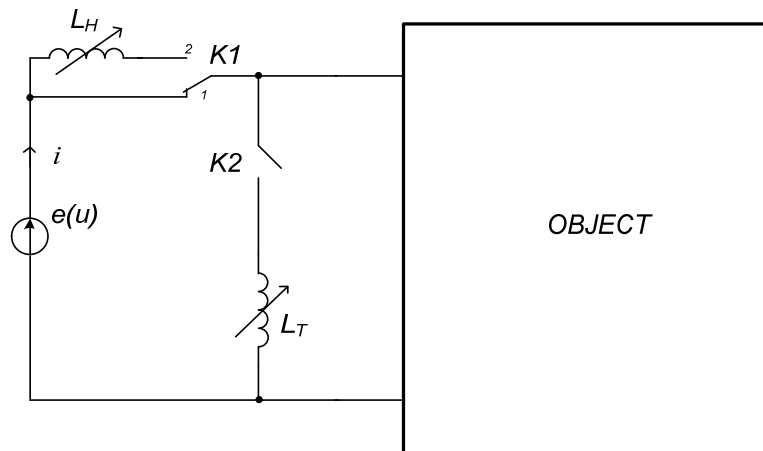


Fig.1. The generalized scheme of the experiment.

By measured object generator is connected sinusoidal voltage $e(u)$. You can connect using the keys $K1$ and $K2$ variable inductance L_H and L_T series in parallel with the object of study.

In the normal mode (the key $K1$ is in position 1, switch $K2$ open) produced by rms value of I , the voltage U and the phase difference φ therebetween. In a second experiment measuring mode (resonance voltage) key $K1$ is switched to position 2, the key $K2$ is open. By changing the inductance L_H are seeking to phase shift φ between the current i and voltage u is zero. In this mode, the measured current $I=I_H$ and the voltage U . In the third experiment, the measurement mode (mode resonance current) key $K1$ has been set to 1, and the key $K2$ is closed. By changing the inductance L_T to achieve a phase shift φ between the current i and voltage u is zero. In this mode, the measured current $I=I_T$ and voltage U .

RC-sensors distributed parameter corresponds to the equivalent circuit shown in Fig. 2 [8].

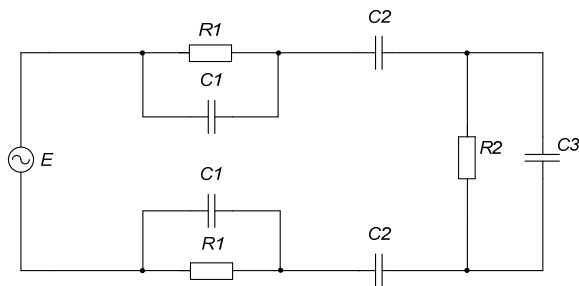


Fig. 2. Equivalent circuit.

For model describing the operation of the plant, set up a system of equations, and accept the capacity \$C1\$ and \$C2\$ are equal.

In the first (normal) measurement mode:

$$I = \frac{U}{\sqrt{\left(\frac{2R_1 X_{C1}^2}{R_1^2 + X_{C1}^2} + \frac{R_2 X_{C3}^2}{R_2^2 + X_{C3}^2}\right)^2 + \left(\frac{2R_1^2 X_{C1}}{R_1^2 + X_{C1}^2} + 2X_{C2} + \frac{R_2^2 X_{C3}}{R_2^2 + X_{C3}^2}\right)^2}}, \tag{1}$$

$$\varphi = \arctg \left(1 + \frac{2X_{C2}}{\frac{2R_1 X_{C1}^2}{R_1^2 + X_{C1}^2} + \frac{R_2 X_{C3}^2}{R_2^2 + X_{C3}^2}} \right). \tag{2}$$

Mode voltage resonance:

$$I_H = \frac{U}{\left(\frac{2R_1 X_{C1}^2}{R_1^2 + X_{C1}^2} + \frac{R_2 X_{C3}^2}{R_2^2 + X_{C3}^2}\right)}. \tag{3}$$

Mode resonance currents:

$$I_T = \frac{U \cdot \left(\frac{2R_1 X_{C1}^2}{R_1^2 + X_{C1}^2} + \frac{R_2 X_{C3}^2}{R_2^2 + X_{C3}^2}\right)}{\left(\frac{2R_1 X_{C1}^2}{R_1^2 + X_{C1}^2}\right)^2 + \left(\frac{2R_1^2 X_{C1}}{R_1^2 + X_{C1}^2} + 2X_{C2} + \frac{R_2^2 X_{C3}}{R_2^2 + X_{C3}^2}\right)^2}. \tag{4}$$

The solution of (1-4) gives the desired parameters of the circuit: \$C1\$, \$C3\$ and \$R1\$, \$R2\$.

3. Implementation of the method of resonant series-parallel identification

Experimental study of the method produced by performing a computational experiment. Measurements of currents, voltages and phase shifts made using the emulator Micro-CAP [10]. Driving computational experiment is shown in Fig. 3.

The output of the generator $V1$ sinusoidal voltage $U = 3$, the frequency $f = 50$ kHz. The values of equivalent circuit parameters $R1 = 100$ ohms, $C1 = C2 = 1$ nF, $R2 = 16$ ohm, $C3 = 0,1$ nF.

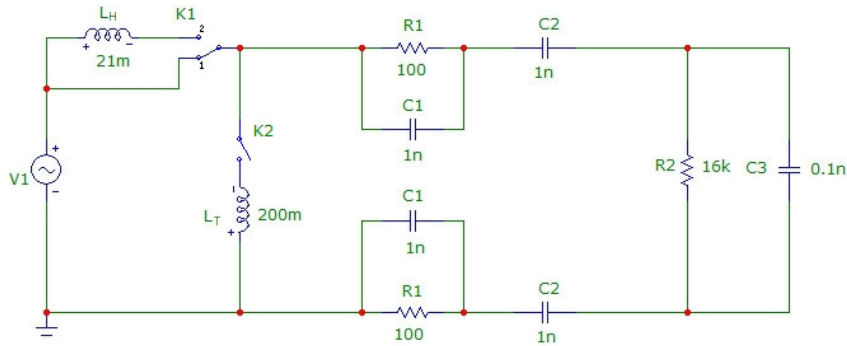


Fig. 3. The equivalent circuit in Micro-CAP 9.0.

In a first mode, measurement results are as follows: $I = 207,5$ microamps, $U = 3$, $\varphi = 0,98$ rad. In the second mode inductance $L_H = 21$ mH gives resonance current $I_H = 231,2$ mA, and the third – L_T inductance = 200 mH gives $I_H = 237,7$ mA.

The system of equations performed at Pomo-soup program Maple [11]. This package is widely employed, it forms an electrical engineering in solving problems, and medicine related to solving systems of equations [12-14]. Listing of the program is shown in Fig. 4.

$$\begin{aligned}
 f &:= 50000 ; U := 3 ; w := 2 \cdot 3.14 \cdot f \\
 Xc1 &:= \frac{1}{w \cdot C12} ; Xc2 := \frac{1}{w \cdot C12} ; Xc3 := \frac{1}{w \cdot C3} \\
 iu &:= \frac{U}{\left(\frac{(2 \cdot R1 \cdot Xc1^2)}{(R1^2 + Xc1^2)} + \frac{(R2 \cdot Xc3^2)}{(R2^2 + Xc3^2)} \right)} = 2.312 \cdot 10^{-4} \\
 im &:= \left(U \cdot \left(\frac{(2 \cdot R1 \cdot Xc1^2)}{(R1^2 + Xc1^2)} + \frac{(R2 \cdot Xc3^2)}{(R2^2 + Xc3^2)} \right) \right) / \left(\left(\frac{(2 \cdot R1 \cdot Xc1^2)}{(R1^2 + Xc1^2)} \right)^2 + \left(\frac{(2 \cdot R1^2 \cdot Xc1)}{(R1^2 + Xc1^2)} + 2 \cdot Xc2 + \frac{(2 \cdot R1^2 \cdot Xc3)}{(R1^2 + Xc3^2)} \right)^2 \right)^{1/2} \\
 &= 2.377 \cdot 10^{-4} \\
 ik &:= U / \left(\left(\left(\left(\frac{(2 \cdot R1 \cdot Xc1^2)}{(R1^2 + Xc1^2)} + \frac{(R2 \cdot Xc3^2)}{(R2^2 + Xc3^2)} \right)^2 + \left(\frac{(2 \cdot R1^2 \cdot Xc1)}{(R1^2 + Xc1^2)} + 2 \cdot Xc2 + \frac{(2 \cdot R1^2 \cdot Xc3)}{(R1^2 + Xc3^2)} \right)^2 \right) \right)^{1/2} \right) \\
 &= 0.002691430886 \\
 \varphi &:= \arctang \left(1 + \frac{2 \cdot Xc2}{\frac{(2 \cdot R1 \cdot Xc1^2)}{(R1^2 + Xc1^2)} + \frac{(R2 \cdot Xc3^2)}{(R2^2 + Xc3^2)}} \right) = 0.98 \\
 Z &:= \text{solve}(\{im, ik, iu, \varphi\}, \{R2, R1, C3, C12\}) \\
 &R2 = 16002.42546 \\
 &R1 = 99.70277655 \\
 &C3 = 9.999999999 \cdot 10^{-11} \\
 &C12 = 9.999999990 \cdot 10^{-10}
 \end{aligned}$$

Fig. 4. Listing of calculations in the program Maple.

In the course of solving the system of equations obtained the following results: $R_1 = 99,708$ ohms, $R_2 = 16,002$ ohms, $C_1 = C_2 = 0.999$ nF, $C_3 = 0.099$ nF

We find the error of the result obtained by the ratio of [15-17]

$$\gamma = \left| \frac{X - X_{CALC}}{X} \right| \cdot 100\%, \quad (5)$$

where X - the true value specified in the emulator Micro-CAP, X_{CALC} - value obtained from the system.

According to the formula (5) are calculated following error: $\gamma_{R1} = 0,3\%$; $\gamma_{R2} = 0,02\%$; $\gamma_{C1} = \gamma_{C2} = 0,3\%$; $\gamma_{C3} = 1\%$.

Of computational experiments showed that the method of resonant series-parallel identification allows you to define the parameters of RC-objects with distributed parameters. This can be identified four parameters of the equivalent circuit. If you want to define more parameters measuring experiment must be carried out at several frequencies, thus allowing a system containing a large number of equations.

4. Conclusion (Conclusion)

The proposed method allows to determine the parameters of the resistive-capacitive sensors with distributed parameters. If you want to define more parameters measuring experiment must be carried out at several frequencies, thus allowing a system containing a large number of equations. This experiment shows that with this method the calculation error does not exceed 1%.

References

- [1] D.V. Shaikhutdinov, N.I. Gorbatenko, K.M. Shirokov, V.V. Grechikhin, A.M. Lankin, Adaptive subsystem automatic production control intelligent electric, Modern problems of science and education. 1 (2015). URL: <http://www.science-education.ru/125-20095>
- [2] V.Y.Konchalovsky, YA.A. Kupersmidt, R.YA. Syropyta-tova, R.R. Kharchenko, Electrical transducers, Energy, Moscow-Leningrad, 1968.
- [3] V.M. Sharapov, E.S. Polishchuk, N.D. Mishka, G.G. Ishanin, I.G. Minaev, A.S. Sovlukov, Sensors: A Reference Guide, Technosphere, Moscow, 2012.
- [4] A.N. Andreev, A.I. Martyashin, B.L. Whistlers, V.I. Chernetsov, M.V. Chernetsov, Transducers displacement sensors, Sensors measuring systems, monitoring and control: Coll. Scien. tr., Penza: Publishing House of Perm State Technical University. (1995) 47–52.
- [5] A.N. Andreev, M.V. Chernetsov, V.I. Chernetsov, Design features a resistive-capacitive sensors, Complex support of precision automated production: abstracts of the international scientific research. tehn. Conf. (1995) 204–207.
- [6] I.V. Brovko, M.V. Chernetsov, V.I. Chernetsov, High sensitivity small displacements, sensor systems for measuring, monitoring and control: Hi. Sat. Scien. tr., Penza Univ Penz. state. tehn. University Press. (1996) 42–46.
- [7] A.H. Zyabirov, A.I. Martyashin, V.I. Chernetsov, A method of converting parameters of a resistive-capacitive sensors, Digital Information Measuring Technology: Hi. Sat. Scien. tr., Penza: Penz. poly-tehi, Inst. (1986) 24–28.
- [8] T.M. Aliev, A.A. Khachaturov, Measuring equipment, Higher School, Moscow, 1991.
- [9] D. Grop, V.A. Vassiliev, V.I. Lopatima, Methods of identification systems. Translated from English, World, Moscow, 1979.
- [10] M.A. Amelin, S.A. Ameline, Program chart-technical modeling Micro-Cap. Version 9, 10, Smolensk branch NIU MEI, Smolensk, 2012.
- [11] B.Z. Aladev, V.K. Boyko, E.A. Rovba, Programming and Application Development in Maple, Grodno: Int. Acad. Noosphere, 2007.
- [12] A.M. Lankin, M.V. Lankin, G.K. Aleksanyan, N.D. Narakidze, Development of principles of computer appliance functioning, determination of characteristics of the biological object, International Journal of Applied Engineering Research. 10(3) (2015) 6489–6498.
- [13] N.I. Gorbatenko, A.M. Lankin, M.V. Lankin, D.V. Shayhutdinov, Determination of weber-ampere characteristic for electrical devices based on the solution of harmonic balance inverse problem, International Journal of Applied Engineering Research. 10(3) (2015) 6509–6519.
- [14] A.M. Lankin, M.V. Lankin, N.I. Gorbatenko, D.V. Shayhutdinov, Determination of Weber-Ampere Characteristics of Electric Devices Using Solution of Inverse Problem of Harmonic Balance. Modern Applied Science. 9(8) (2015).
- [15] P.V. Novitsky, I.A. Zograph, Evaluation of errors of measurement results, Energoatomizdat, Leningrad, 1991.
- [16] M.V. Lankin, Methods of metrological certification of automatic control devices, News of higher educational institutions. Electromechanics. 1 (2003) 69–72.
- [17] M.V. Lankin, Metrological support processor means testing of permanent magnets, News of higher educational institutions. Electromechanics. 3 (2004) 69–73.



International Conference on Industrial Engineering

Investigation of dynamic characteristics of the hydraulic drive with proportional control

Forental V.I.*, Forental M.V., Nazarov F.M.

South Ural State University, 76, Lenin Avenue, Chelyabinsk, 454080, Russian Federation

Abstract

The dynamic characteristics of hydraulic drive with proportional control are investigated by experimental and modeling approaches. The article presents research on linear motion drive based on hydraulic cylinder with electrical position feedback. The mathematical drive model is developed taking into account the characteristics of pump station, hydraulic cylinder, inertial load, dynamic characteristic of proportional valve, and electrical position feedback. The proportional valve characteristic is determined based on experimental static flow characteristics and transfer function of spool displacement on input current. Bode diagram for displacement of cylinder is obtained experimentally and by modeling for frequencies of 0.05 to 5 Hz. It is shown that for frequencies of up to 3 Hz, the proposed model provides a 3% accuracy.

© 2015 The Authors. Published by Elsevier Ltd. This is an open access article under the CC BY-NC-ND license (<http://creativecommons.org/licenses/by-nc-nd/4.0/>).

Peer-review under responsibility of the organizing committee of the International Conference on Industrial Engineering (ICIE-2015)

Keywords: hydraulic drive, proportional directional valve, dynamic characteristic, transfer function, conductivity.

1. Introduction

Proportional hydraulic drives are used widely for the systems of processing equipment in various engineering industries [1...8]. Proportional hydraulic directional valves became widely used as control system in these systems. Proportional hydraulic directional valves have some disadvantages like wide deadband, low frequency bandwidth by contrast to servo valves but lower price, less sensitive to the purity of fluid are their advantages [8]. This is the reason of their wide use in proportional control systems.

* Corresponding author. Tel.: +7-351-267-96-29; fax: +7-351-267-96-29.
E-mail address: forental@mail.ru

Nomenclature

G	conductivity
I	current
k	ratio coefficient
p	pressure
Q	flow rate
y	displacement of spool

A quantity of published works are addressed to research of hydraulic drives with servo valves [1,3,4,6,7]. As a rule, servo valves have better characteristics in the view of drive control, allow to get a greater precision in tracking systems or regulation of characteristics as positioning, velocity, force. In general hydraulic characteristics of servo valves are described by linearized equations in drive researched. The essential values of deadband of proportional hydraulic valves reach the value to 20...25% of maximum spool travel, and the researches of drive characteristics should be carried out with regard to these values. Wide production tolerance of spool and sleeve sizes does not allow to use correctly the analytic description of hydraulic characteristics. Nevertheless it is a good idea to make some mathematical model of hydraulic drive with proportional control to reduce expenses for experimental development of this drive. The suggested model is based on the partial use of experimental characteristics of directional valve. Proposed model allows to reduce the experimental researches due to use only the experimental static hydraulic characteristic of directional valve.

In this work the model of drive are suggested based on the static experimental pressure-flow characteristics of directional valve. The determination of these characteristics is less difficult beside the testing of drive.

Mathematical model are developed for the drive that diagram is shown on figure 1.

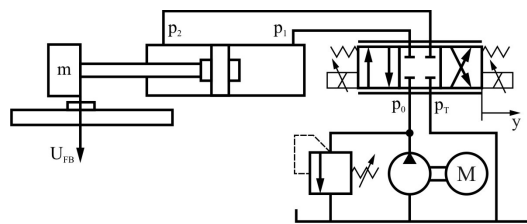


Fig. 1. The hydraulic diagram of drive.

2. The description of proportional directional valve

The experimental static flow-current characteristic of directional valve with proportional control are shown on figure 2 for some fixed values of pressure differential on orifice depending on current.

Flow rate Q throw orifice may be calculated in this way [1,3,4,6,7]:

$$Q = G\sqrt{\Delta p}, \quad G = \mu f \sqrt{\frac{2}{\rho}}, \quad (1)$$

where G – the conductivity of the orifice; μ – flow coefficient depend on Reynolds number, land form and etc.; f – orifice area depend on spool location y ; Δp – pressure drop on orifice; ρ – fluid density.

It is useful to take into account the non-dimensional parameter of conductivity:

$$\bar{G} = \frac{G}{G_{MAX}}, \quad (2)$$

current:

$$\bar{I} = \frac{I}{I_{MAX}}, \quad (3)$$

the displacement of spool:

$$\bar{y} = \frac{y}{y_{MAX}}, \tag{4}$$

and the ratio of conductivity to current:

$$k_{Gj} = \frac{\bar{G}}{\bar{I}}. \tag{5}$$

The maximal values of conductivity G_{MAX} and current I_{MAX} are defined experimentally.

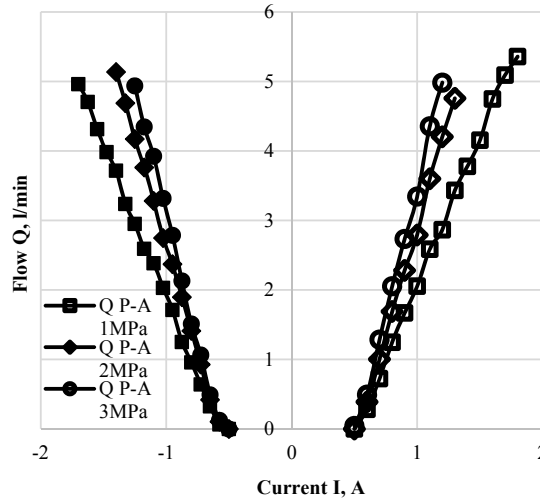


Fig. 2. The flow rate (lines P-A, P-B) of four-port hydraulic proportional directional valve vs current.

It is introduced the dimensionless current and spool displacement of deadband:

$$\bar{I}_{NS} = \frac{I_{NS}}{I_{MAX}}, \tag{6}$$

$$\bar{y}_{NS} = \frac{y_{NS}}{y_{MAX}}. \tag{7}$$

Then the dependence (1) taking into account the diagrams (fig. 2) may be presented in the form:

$$Q_j = \begin{cases} k_{Gj} \times (\bar{I} - \bar{I}_{NS}) \times G_{MAX} \times \sqrt{\Delta p_j}, & \text{при } \bar{I} > \bar{I}_{NS} \\ 0, & \text{при } \bar{I} \leq \bar{I}_{NS} \end{cases} \tag{8}$$

From experimental data the values of coefficient k_{Gj} was defined for each j combination from four combination of working orifice. The conductivity directly depends on spool position y that is the function of current. Dynamical characteristics of spool displacement usually give in datasheet of valve. The dependence of spool displacement $y(t)$ on current $I(t)$:

$$y(t) = W_v \times I(t), \tag{9}$$

where W_v – transfer function of proportional directional valve that close to second-order oscillatory link or two aperiodic link.

In dimensionless variable the equation (9) is of the form:

$$\bar{y}(t) = W_v \times \bar{I}(t). \tag{10}$$

Static spool displacement is proportional to current:

$$\bar{y} = k_v \times \bar{I}, \tag{11}$$

where k_v – the ratio of spool displacement to current. The equation (6) can be transformed to next:

$$Q_j = \begin{cases} k_{Gj} \times \frac{(\bar{y} - \bar{y}_{NS})}{k_V} \times G_{MAX} \times \sqrt{\Delta p_j}, & \text{при } \bar{y} > \bar{y}_{NS} \\ 0, & \text{при } \bar{y} \leq \bar{y}_{NS} \end{cases} \quad (12)$$

Using (10) the equations for flow throw each orifice of valve can be obtained:

$$Q_1 = \begin{cases} k_{GI_PA} \times \frac{(\bar{y} - \bar{y}_{NS})}{k_V} \times G_{MAX} \times \sqrt{p_0 - p_1}, & \text{при } \bar{y} > \bar{y}_{NS} \\ 0, & \text{при } -\bar{y}_{NS} < \bar{y} \leq \bar{y}_{NS} \\ k_{GI_AT} \times \frac{(\bar{y} + \bar{y}_{NS})}{k_V} \times G_{MAX} \times \sqrt{p_1 - p_T}, & \text{при } \bar{y} < -\bar{y}_{NS} \end{cases} \quad (13)$$

$$Q_2 = \begin{cases} k_{GI_BT} \times \frac{(\bar{y} - \bar{y}_{NS})}{k_V} \times G_{MAX} \times \sqrt{p_2 - p_T}, & \text{при } \bar{y} > \bar{y}_{NS} \\ 0, & \text{при } -\bar{y}_{NS} < \bar{y} \leq \bar{y}_{NS} \\ k_{GI_PB} \times \frac{(\bar{y} + \bar{y}_{NS})}{k_V} \times G_{MAX} \times \sqrt{p_0 - p_2}, & \text{при } \bar{y} < -\bar{y}_{NS} \end{cases}$$

where Q_1 – flow rate to cylinder piston side; Q_2 – flow rate to rod side of cylinder, p_1 and p_2 – pressure in piston and rod sides respectively.

The pressure in piston and rod sides of cylinder may be obtained from next equations:

$$\begin{cases} Q_1 = \frac{dx}{dt} A_1 + \frac{E_1}{V_1} \frac{dp_1}{dt} \\ Q_2 = \frac{dx}{dt} A_2 - \frac{E_2}{V_2} \frac{dp_2}{dt} \end{cases}, \quad (14)$$

where A_1 , A_2 – piston and rod side areas respectively; E_1 , E_2 – efficient elastic modulus for deformable system fluid-pipe [1, 2, 3].

The equation of cylinder dynamics:

$$\frac{d^2x}{dt^2} = \frac{1}{m} \left(p_1 \cdot A_1 - p_2 \cdot A_2 - b \cdot \frac{dx}{dt} - F_{CF} \cdot \text{sign} \left(\frac{dx}{dt} \right) \right), \quad (15)$$

where b – viscous friction coefficient; F_{CF} – Coulomb friction force.

3. The description of hydraulic power station

The characteristic of hydraulic power station was obtained experimentally and shown on figure 3.

This characteristic can be mathematically described by bilinear approximation:

$$\begin{cases} p_0 = k_{PQ1} \cdot Q + a_{PQ1}, & \text{при } Q \leq Q_{prv} \\ p_0 = k_{PQ2} \cdot Q + a_{PQ2}, & \text{при } Q > Q_{prv} \end{cases}, \quad (16)$$

where Q_{prv} – flow rate according to the relief valve opening; $k_{PQ1,2}$ and $a_{PQ1,2}$ – linearization coefficient.

The discharge pressure of directional valve can be defined by

$$p_T = Qk_{lam} + k_{turb} Q^2,$$

where k_{lam} and k_{turb} – coefficients that obtained experimentally.

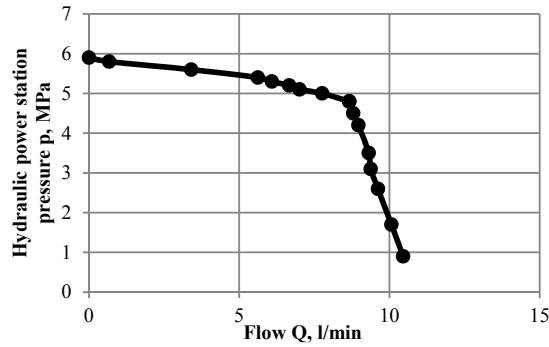


Fig. 3. The characteristic of hydraulic power station.

4. The description of electrical control system

The electrical feedback control system can be described using linear equation:

$$U_{ER} = U_{REF} - U_{FB}, \tag{17}$$

where U_{ER} – error signal that transfers to electronic amplifier of valve; U_{REF} –reference signal; U_{FB} – stroke displacement feedback signal.

Proportional hydraulic directional valves have large values of overlap up to 20% of spool travel. The electronic correction system are used for reducing of influence of this overlap for low input voltage signal. For this reason electronic amplifier has nonlinear characteristics with initial bias current. This characteristic is shown on figure 4. In consider system input signal to electronic amplifier gets from feedback system.

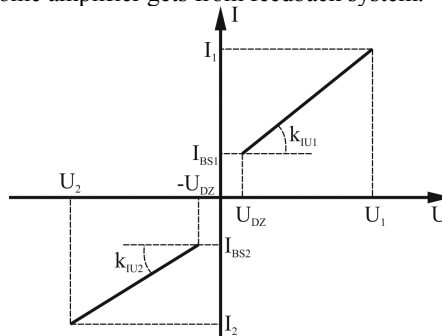


Fig. 4. Nonlinear transformation of input voltage signal to output current in electronic amplifier.

Output current signal of nonlinear electronic amplifier can be estimated by next equations:

$$I = \begin{cases} k_{IU1} \times U_{ER} + I_{BS1}, & \text{при } U_{ER} > U_{DZ} \\ 0, & \text{при } -U_{DZ} \leq U_{ER} \leq U_{DZ} \\ k_{IU2} \times U_{ER} - I_{BS2}, & \text{при } U_{ER} < -U_{DZ} \end{cases} ; \tag{18}$$

where k_{IU1} – the ratio of current to voltage of nonlinear amplifier that can be defined for positive and negative input voltage separately, I_{BS} – bias of current; U_{DZ} – deadband of amplifier to input voltage signal.

The equations presented above with the function of reference signal from time form closed equation system describing dynamic system. This equation system are solved numerical using computer.

5. Results

Investigated hydraulic drive includes hydraulic cylinder with one-side stroke, piston diameter 40 mm, stroke diameter 20 mm. Mass load is 40 kg. Control directional valve – proportional valve Atos DHZO-A-071-L1 with amplifier Atos E-BM-AC-05F/RR.

It is good to have the equal velocity of cylinder for equal by modulus input voltage signal but stroke and piston sides have different areas. This differ can be compensated by orifice areas of valve for straight and back action of cylinder. Orifice area depends on current so it can be adjusted by amplifier coefficient k_{IUi} .

The large values of positive overlap of spool (fig. 2) are compensated by adjustment of current bias I_{BS} .

Experiment and modeling are performed for next condition: input voltage signal amplitude 2 V, that corresponds displacement of stroke with amplitude 50 mm; Coulomb friction force was obtained experimentally and equal $F_{CF}=100\pm 16N$; adjustment pressure of relief valve 6 MPa. Bias current at an electronic amplifier of directional valve was $I_{BS}=0.5A$, that corresponds deadband current $I_{NS}=0.5A$, the ratio of current to voltage of nonlinear amplifier $k_{IU1}=1,8 A/V$, $k_{IU2}=1,4 A/V$. Different ratio provides different flow that result in approximately equals straight and back velocity of stroke for equal error signal U_{ER} (fig. 5).

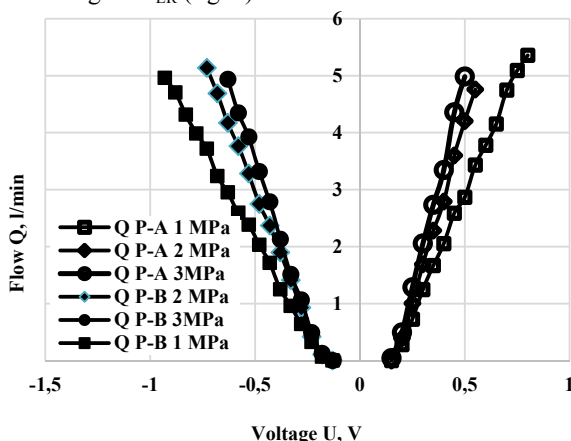


Fig. 5. The flow rate (lines P-A, P-B) of four-port hydraulic proportional directional valve vs input voltage signal U_{ER} .

Displacement of stroke that obtained experimentally and by modeling for input signal amplitude 2 V and frequency 0.5 Hz are presented on figure 6, Bode diagram for drive is presented on figure 7.

The estimated value of relative error between model and experimental displacement of stroke does not exceed 2% for frequency 0.5 Hz.

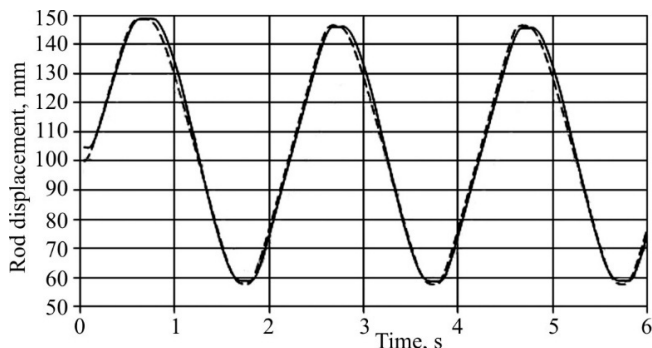


Fig. 6. The displacement of stroke vs time for harmonic reference signal 2V - 0,5 Hz (dash – model, line – experiment).

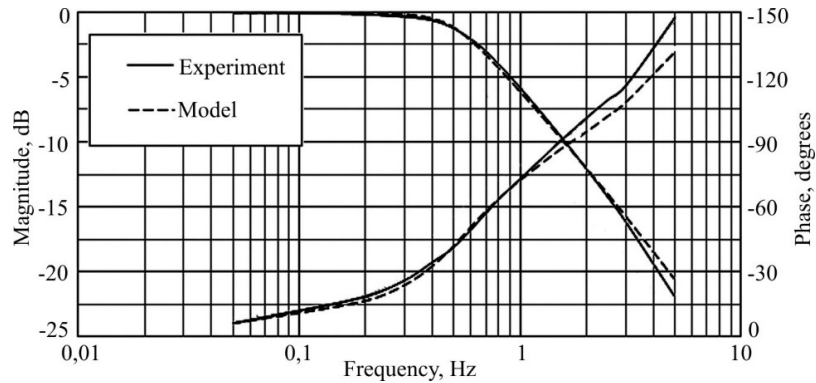


Fig.7. Bode diagram for drive.

The approximation of hydraulic characteristic of proportional directional valve allows to define the amplitude of displacement correct to 2–3%, for frequency 0.05–3 Hz, at that phase error does not exceed 10°. The amplitude error is less than 10% for frequency 3–5 Hz.

6. Conclusion

Hydraulic drive based on cylinder and proportional directional valve is nonlinear dynamic system with unknown parameters that depend on valve producing technology. Nevertheless, comparison between experimental researches and modeling results demonstrate that using experimental static flow characteristics allow to obtain the mathematical model of drive. This model describes the drive at frequency up to 5 Hz with enough accuracy for engineering design tasks. Modeling of drive at higher frequency requires taking into account elasticity and dissipative properties of system element such as high-pressure hose, pipe, connection socket, etc. and dynamic characteristic of hydraulic power station.

References

- [1] A.G. Burgvits, V.I. Forental, Characteristics of spool hydraulic directional valve with regard to microgeometry of control land, Journal "Vestnik mashinostroeniya". 3 (1993) 25–28. (in Russian).
- [2] V.A. Dubrovin, Modelling of hydraulic drive control system of cyclical movement of swing frame of tamping unit, Journl "Izvestiya TulGU". 2 (2008) 38–42. (in Russian).
- [3] T. Randall, Y.Li. Perry, Mathematical Modeling of a Two Spool Flow Control Servovalve Using a Pressure Control Pilot, Journal of Dynamic Systems, Measurement, and Control. 124 (2002) 420–427.
- [4] Juma Yousuf Alaydi, Modeling and Simulation of High-Performance Symmetrical Linear Actuator, International Journal of Scientific & Engineering Research. 3(8) (2012).
- [5] D. Shmid, A. Bauman, K. Kaufman, B. Zippel', Control system and automatic, Technosphere, Moscow, 2007. (in Russian).
- [6] V.F. Kazmirenko, Electrohydraulic mechatronical modulus of movement: Theoretical base and system design. Study guide, Radio and signal, Moscow, 2001. (in Russian).
- [7] S.V. Konstantinov, P.G. Red'ko, S.A. Ermakov, Electrohydraulic flight control actuator of maneuvering aircraft, Yanus-K, Moscow, 2006. (in Russian).
- [8] V.K. Sveshnikov, Machine-tool hydraulic drive: guide, Publishing "Mashinostroenie", Moscow, 2008. (in Russian).



International Conference on Industrial Engineering

Contemporary achievements in the field of acoustic ignition systems

Bogdanov V.V.*

South Ural State University, 76, Lenin Avenue, Chelyabinsk, 454080, Russian Federation

Abstract

This paper is to provide up-to-date information on the state of acoustic ignition system development, with such systems seen as one of the most promising alternative to the traditional electrical systems. The article summarizes the principles of the gas-dynamic (acoustic) ignition systems, describes the most commonly used igniter designs, and also describes some unusual and potentially promising igniter designs. It also contains a survey of contemporary domestic and foreign theoretical and experimental research in the field of gas-dynamic ignition. Descriptions of promising igniter designs are provided. The paper analyses identified strengths and weaknesses of the construction designs described. On the basis of accumulated and presented materials, recommendations are drawn for the future course of development, which comprise the need to address the thermal issues of such igniters, their lifetime and the need for more comprehensive studies on atypical designs, which can be more efficient than their currently used counterparts.

© 2015 The Authors. Published by Elsevier Ltd. This is an open access article under the CC BY-NC-ND license (<http://creativecommons.org/licenses/by-nc-nd/4.0/>).

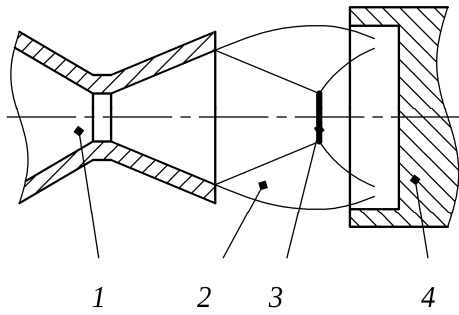
Peer-review under responsibility of the organizing committee of the International Conference on Industrial Engineering (ICIE-2015)

Keywords: ignition system, Hartmann generator, acoustic ignition, rocket engine, thruster, resonance system

1. Introduction

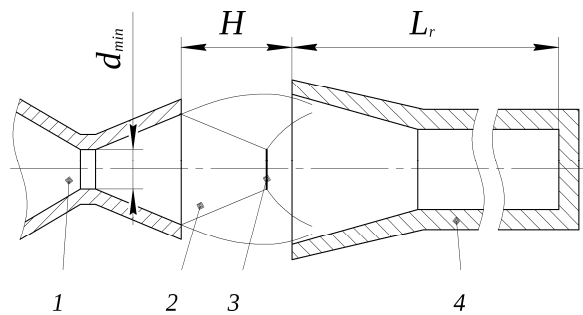
Traditionally, to launch rocket engines and thrusters using non-hypergolic propellants electrical or pyrotechnic ignition system are used. However, in some cases usage of such systems is not desirable, impossible (limited number of ignitions pyrotechnic system offers results in its inability to be used in pulse modes of an engine), or entail additional costs related to mass growth of the propulsion system and overall spacecraft mass. In this regard, attempts to develop alternative ignition systems not having aforementioned drawbacks and providing reliable ignition of various fuel compositions in the broad range of operating conditions are constantly taken.

* Corresponding author. Tel.: +7-351-267-92-65. E-mail address: alm888@mail.ru



1 – injector nozzle, 2 – working fluid stream, 3 – Mach disk, 4 – resonator

Fig. 1 – Hartmann generator



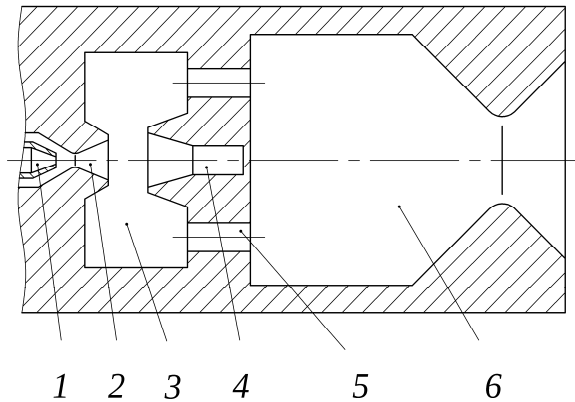
1 – injector nozzle, 2 – working fluid stream, 3 – Mach disk, 4 – resonance tube

Fig. 2 – Acoustic igniter design

Acoustic method of ignition using Hartmann generator is often proposed as one of such methods of non-electrical ignition [1, 2]. The scheme of Hartmann generator is shown in Fig. 1. The source of acoustic oscillations in sound generators of this type is a Mach disk moving (oscillating) along the axis as the time passes. The first and the main usage of Hartmann generators is to produce acoustic (sound) oscillations, but during this process some of initial energy of working fluid (compressed gas at high pressure) is dissipated into heat energy due to compression shock effects. Thermal energy formed in such way is accumulated in the stagnant zone of the resonator. The most common scheme, as shown in Fig. 2, consists of a nozzle performing injection of working fluid (sonic or supersonic) and a resonator (typically a blind hole in a wall) disposed co-axially and positioned in such a way that its outlet is directed towards the injection nozzle. In this scheme the resonator is a long tube in general case comprised of two parts: conical inlet part and cylindrical end point part. There are other implementations of the resonator design however. For example, work [3] describes a design in which a flat wall with adjustable position is used as the resonator.

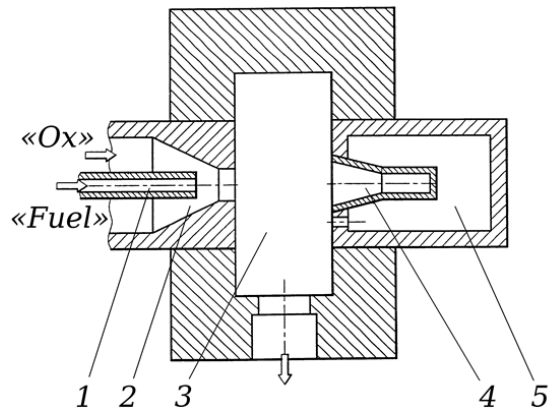
2. Research in the Field of Acoustic Ignition Being Conducted Abroad

Paper [4] describes the most common nowadays acoustic ignition workflow as shown in Fig. 3. According to the



1 – fuel injector, 2 – igniter injector, 3 – ignition chamber, 4 – resonator, 5 – apertures, 6 – main combustion chamber

Fig. 3 – Thruster scheme as proposed in [4] (oxidizer as working fluid variant)



1 – fuel injector, 2 – igniter injector, 3 – ignition chamber, 4 – resonator, 5 – protective cavity

Fig. 4 – Acoustic igniter scheme [6, 7]

source, this scheme consists of the working fluid (inert gas or oxidizer) injection nozzle, possibly devoid of the diffuser, injecting a jet of the working fluid into the resonator 4, which usually consists of two sections (the first section is a tapering cone and the second section is a cylinder with a wall on its end). The walls 3 span the volume around the system “nozzle – cavity” thus forming the ignition chamber separated from the main combustion chamber 6 by the wall having apertures 5 located “in suitable places” and made integral with the resonator. Fuel components injection is carried out by the means of disposed co-axially fuel and oxidizer nozzles. Additionally it is stated that in order to improve the uniformity of mixing the inert gas may be replaced with gaseous oxidizer and fuel injection (through the nozzle 1) can be implemented directly into the oxidizer injector confuser 2 as described in [5]. Thus the resonator is supplied with already pre-mixed fuel components and when under the influence of acoustic heating the mixture is ignited it ignites other portion of mixture (which was already there but did not ignite on its own) and the flame front propagates leaving the volume of the resonator and spreading into the whole ignition chamber. After that the flames leave the ignition chamber through the apertures spreading into the main combustion chamber.

The authors point out considerable disadvantages of existing nowadays acoustic resonator drafts associated with the fact that up until the ignition moment the igniter is in constant contact with cold fuel components which draws out part of available thermal energy and extends the time required for ignition.

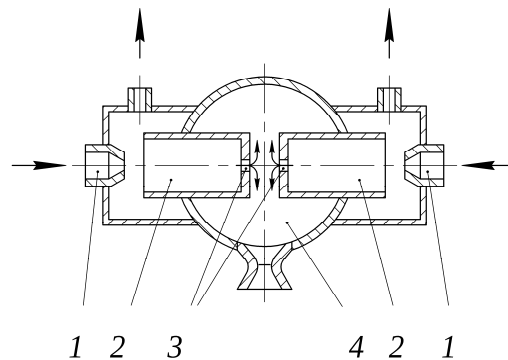
In order to mitigate the aforementioned drawback authors of [4] have chosen the design described in [6, 7] (as shown on Fig. 4). The core idea of this design is to eliminate the physical contact of the resonator and combustion chamber structure by means of inserting additional (as a variant – vacuumed) protective cavity around the resonator preventing the contact of the resonator wall material with the cold fuel components. The other idea is to choose a material with low heat conductivity (less than 25 W/m) as the resonator wall material which, under authors' expectations, should lower heat loss in the resonator and as a result accelerate the ignition process.

Another research team from “ORBITEC” company also achieved considerable success by designing their “SYREN” acoustic resonance igniter (or “Acoustic Resonance Reaction Control Thruster”). In 2008 (Phase I) [8] and 2010 (Phase II) [9] the research team successfully applied for participation in NASA SBIR (Small Business Innovation Research) program.

The research team's work resulted in development of the “ARCTIC” rocket engine validated during the P-15 rocket [11] test launch. A patent [12] describing the design used in this igniter was issued.

3. Research Being Conducted in Russia

One of the collectives working on the problem of creating acoustic ignition systems is the FSUE “R&D Institute of Mechanical Engineering” (“NIIMash”) research team. In particular, the researchers proposed igniter scheme (Fig. 5) incorporating two injection nozzles 1 with resonance cavities 2 opposing them with orifices 3 at their end



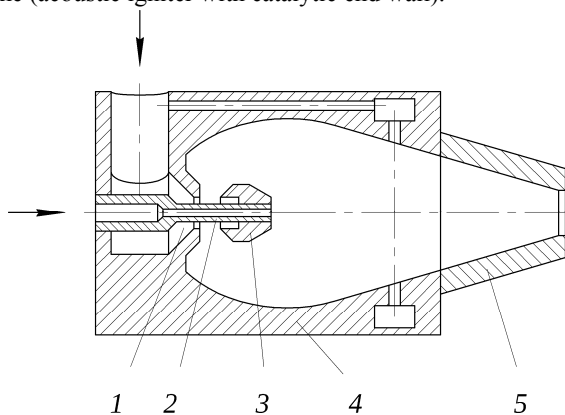
1 – injection nozzles, 2 – resonance cavities, 3 – orifices, 4 – ignition chamber

Fig. 5 – Conceptual igniter design using thermal separation in the resonance cavity [10]

walls, through which the most warmed-up propellant portions expire into the ignition chamber 4 while colder portions of propellant components leave the resonance cavities through the gaps between them and injection nozzle edges [10]. The hot and cold propellant component separation occurs as a result of heat accumulation in the region near the resonator end wall. The researchers also proposed rod-type [13] (Fig. 6) and disk-type (Fig. 7) acoustic resonance igniter schemes. In their work [14] authors describe the proposed design of the 100Э102 engine (with rod-type igniter) and its later modifications (100Э459 and 100Э560), as well as the 100Э168M engine (with disk-type igniter) operating on “oxygen – hydrogen” fuel composition. It is reported that the engines have passed a series of fire tests, proven their reliability of ignition (during the 24 starts of the 100Э168M engine no failures of the ignition system were observed), besides, the engine start-up time taking into account the time required for the valve to open did not exceed 25 ms. The authors noted the problem of the thermal state of the igniter: the wall of the ignition cavity of the 100Э168M engine (Fig. 7) collapsed after 24 start/stop cycles due to exposure to high temperatures. The collective has chosen to study the influence of the mixing and cooling systems parameters on combustion stability and the thermal state of the structure issue.

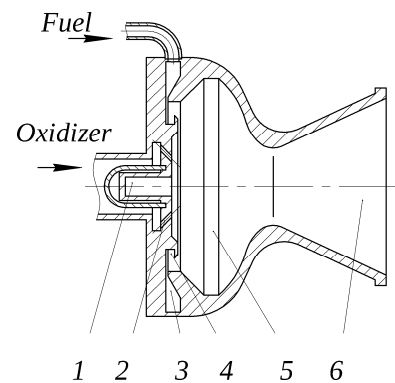
The authors' collective from Moscow Aviation Institute (National Research University) had conducted the work [15] of acoustic igniter design optimization. The scheme presented on Fig. 2 was taken as a basis. The work mostly focused on injector efficiency improvement by using supersonic nozzle and introduction of central body in order to create an annular flow. The researchers had conducted mathematical modeling of the igniter design and performed optimization of its geometrical parameters. For a number of schemes of interest a test study was performed. Considering acquired results for the proposed igniter designs [16, 17] the authors give recommendations on the choice of geometrical parameters: the angle of the supersonic nozzle diffuser should vary in range from eight to fifteen degrees; geometric expansion ratio of the nozzle should be in range from 2.56 to 4.41; resonator conical part outlet to inlet diameter ratio should be not more than 0.2; and the length of the resonator cylindrical part should be from 12 to 15 injection nozzle minimum cross-section diameters. It is noted that the usage of the nozzle with a central body provides igniter auto-tuning for any pressure drop up from the critical drop without sacrificing its performance.

The researchers from Bauman Moscow State Technical University have conducted their work in the field of application acoustic igniters to decomposition of nitrous oxide (used as a monopropellant). In their paper [18] the authors presented the results of carried out theoretical calculations of engine designs using combined ignition scheme (acoustic igniter with catalytic end wall).



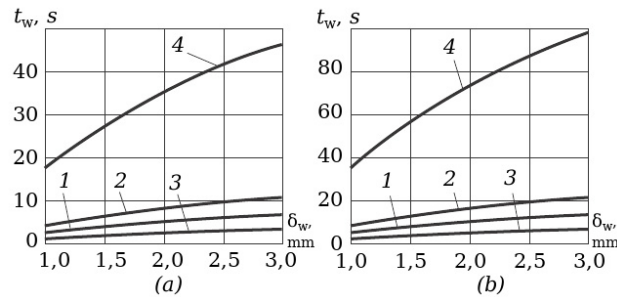
1 – injection nozzle, 2 – central rod (doubling as injection nozzle), 3 – resonator, 4 – chamber wall, 5 – main nozzle

Fig. 6 – The design of the 100Э102 experimental thruster [14], equipped with rod-type acoustic igniter



1 – ignition cavity, 2 – oxidizer injection orifices, 3 – annular slotted fuel injection nozzle, 4 – annular resonator, 5 – combustion chamber, 6 – engine nozzle

Fig. 7 – Principal scheme of the experimental 100Э168M thruster [14], equipped with disk-type igniter



1 – 12X18H10T stainless steel, 2 – XH60BT alloy, 3 – БрX08 bronze, 4 – niobium

Fig. 8 – Ignitor operation time graphs depending on wall thickness on (a) continuous and (b) pulse ($f = 1$ Hz) engine work modes [21]

In work [19] the authors described theoretical calculation research aimed at the acoustic igniter geometric parameters optimization relating to an engine using a single injector supplying the combustion chamber with “nitrous oxide – hydrogen” fuel composition as a working fluid. The selected scheme is the one depicted in Fig. 2. Calculations were carried out by means of numerical computer simulation. It is stated that for any size of the gap between the nozzle exit and the entrance into the resonance cavity ascribed to the minimum cross-section diameter of the nozzle (H/d_{\min}) an optimum value of the resonance (or tube) ascribed to the same minimum cross-section diameter of the nozzle (L_r/d_{\min}) exist and can be found. The authors suggest that this is due to concurrence between the natural frequency of the resonator and the frequency of pulsations of the straight shock wave in it. It is further noted that the temperature change in the igniter is cyclical and local changes in temperature may exceed the total inlet temperature more than 7 times, which is sufficient for self-ignition of fuel compositions, and the start-up time of the engine is not more than 15 ms. In paper [20] the authors describe dynamic characteristics obtained from the experiments for the selected igniter scheme and fuel compositions “ $N_2O - H_2$ ” and “ $H_2 - air$.” For “ $H_2 - air$.” fuel composition with excess oxidant ratio close to 1 the start-up time equals to 150 ms.

In paper [21] the authors present the results of the theoretical calculation research of thermal state of acoustic ignition system with cylindrical resonance cavity. Nitrous oxide was used as fuel and a working fluid. During the research several igniters made of several materials were simulated and tested with selected materials being: 12X18H10T stainless steel, XH60BT chrome-nickel alloy, БрX08 bronze, niobium and carbon-carbon composite material with a surface siliconizing. Based on the results obtained during the tests it is stated that a construction made of niobium has maximum operating time (46.5 s with a resonator wall thickness of 3 mm in the continuous mode, and up to 98.5 s for the same wall thickness at the pulse mode with a frequency of 1 Hz and a duty cycle of 50%). Other materials are significantly inferior to niobium: the best result for the pulse mode is approximately 20 s. It is further noted that at present time manufacturing of parts of complex shape made of carbon-carbon composite material with a surface siliconizing is technologically difficult. The authors point out that the test results show that initial destruction of the resonator wall originates from its outer surface.

In paper [22] the authors described experimental test of selected in [21] theoretical models of igniters and provide acquired amplitude-frequency characteristics; the authors deduced that the heat generation in the cavity is practically independent of the pressure drop in case of inlet pressure of the working fluid before the nozzle to the ambient pressure ratio exceeding 10 and the frequency of the pulsations does not depend on the distance between end faces of the nozzle and the resonator, as well as the pressure drop when the latter is greater than 5 times. The authors found a good correlation between theoretical model and experimental data.

4. Conclusions

On the basis of the domestic and foreign publications it is possible to conclude that the subject of acoustic ignition is one of the promising areas being intensively developed nowadays.

At the moment it is theoretically [15, 19] and experimentally [4, 11, 14] proven that gas-dynamic (acoustic) ignition systems are able to provide reliable ignition of a variety of both gas and gas-liquid [4, 20] fuel compositions, and current advances in resonator design improvement allow to achieve engine start-up time of less than 150 ms [20] and even 25 ms [14].

The main trends in acoustic ignition systems improvement are: works aimed at maximizing of thermal energy generation, for example, by introducing new structural elements [4, 6, 7, 10, 14] or geometry optimization of existing schemes [16, 17, 19] and developments aimed at the adaptation of existing schemes to work in real conditions [8, 9, 14] (such as tests in real engines and power plants during test launches). The authors of [14, 21] note that one of the main challenge impeding widespread adoption of acoustic ignition systems, is the task of ensuring acceptable thermal mode for achievement of durability of the construction during operation.

It should be noted that most of described design schemes are based on the use of resonance tube igniter (Fig. 2). Rod-type and especially disk-type igniters described in [14], are studied insufficiently and have the potential to be more efficient than traditional igniter schemes.

References

- [1] Hartmann Jul., On the production of acoustic waves by means of an air-jet of a velocity exceeding that of sound, Philosophical Magazine Series 7, Vol 11, № 72 (1931) 926–948.
- [2] Bergman L., Ul'trazvuk i ego primenenie v nauke i tekhnike [Der ultraschall und seine anwendung in wissenschaft und technik], Izdatel'stvo inostrannoj literatury, Moscow, 1957.
- [3] Gavrikov A. I., Russian Federation Patent 2175743. (2009)
- [4] Bhanu Swaroop Gaddam, Amar Subramanya, Preliminary Rocket Exhaust Plume Analysis and Compatible Acoustic Ignition Technology, International Conference on Mechanical, Automobile and Biodiesel Engineering (2012) 317–320.
- [5] Kesaev H. V., Demchenko V. V., Zinov'ev V. G., Soviet Union Patent 1657883. (1991)
- [6] E. Williaq Conrad, Albert J. Pavli, A Resonance-Tube Igniter for Hydrogen-Oxygen Rocket Engines, NASA, 1967.
- [7] Khoze Kessaev, Vassili Zinoviev, Vladimir Demtchenko, US Patent 6272845. (2001)
- [8] Information on <https://www.sbir.gov/sbirsearch/detail/259606>.
- [9] Information on <https://www.sbir.gov/sbirsearch/detail/8367>.
- [10] KHristenko YU. A., Evseev A. V., Lebedev I. N., Russian Federation Patent 2175743. (2001)
- [11] Information on <http://articles.sae.org/11560/>.
- [12] Scott M. Munson, US Patent 8966879. (2012)
- [13] Lebedev I. N., Sterzhnevye gazostrujnye izluchateli dlya intensivatsii smeseobrazovaniya, nagreva i samovosplamneniya topliv, Raketno-kosmicheskie dvigatel'nye ustanovki: Ma-terialy vsrossijs. nauch.-tekhn. Konf. (2008) c. 19.
- [14] Kutuev R. KH., Lebedev I. N., Salich V. L., Razrabotka perspektivnykh RDMT na ehkologicheski chistykh toplivnykh kompozitsiyakh, Vestnik Samarskogo gosudarstvennogo aehrokosmicheskogo universiteta imeni akademika S. P. Korolyova (natsional'nogo issledovatel'skogo universiteta). Spetsial'nyj vypusk : po materialam mezhdunarodnoj nauchno-tekhnicheskoy konferentsii «Problemy i perspektivy razvitiya dvigatelestroeniya», № 3-3 (19) (2009) 101–109.
- [15] Li CHzhun Min, Issledovanie termo-akusticheskogo nagreva gaza v gazostrujnykh generatorakh Gartmana, Moscow, 2004.
- [16] Semenov V. V., Li CH. M., Russian Federation Patent 2225574. (2004)
- [17] Li CH. M., Semenov V. V., Russian Federation Useful Model Patent 38899. (2004)
- [18] Aref'ev K. YU., Issledovanie metodov intensivatsii protsessa razlozheniya oksida azota v malogabaritnykh gazogeneratorakh s rezonansnoj gazodinamicheskoy sistemoy initsirovaniya rabocheho protsessa, Izvestiya vysshikh uchebnykh zavedenij. Mashinostroenie, № 6 (2013) 62–65.
- [19] Voronetskij A. V., Aref'ev K. YU., Zakharov V. S., Raschetno-teoreticheskoe issledovanie rezonansnoj sistemy gazodinamicheskogo vosplamneniya ZHRD maloj tyagi, Vestnik MGTU im. N. EH. Bauman, № 1 (86) (2012) 31–41.
- [20] Aref'ev K. Yu., Voronetskii A. V., Il'chenko M. A., Dynamic Characteristics of a Resonant Gas-Dynamic System for Ignition of a Fuel Mixture, Combustion, Explosion, and Shock Waves, Vol. 49, № 6 (2013) 657–661.
- [21] Vorozheeva O. A., Aref'ev K. YU., Issledovanie teplovogo sostoyaniya rezonatora gazodinamicheskoy sistemy initsirovaniya protsessa razlozheniya unitarnogo topliva, Izvestiya vysshikh uchebnykh zavedenij. Mashinostroenie, № 7 (652) (2014) 43-51.
- [22] Voronetskij A. V., Aref'ev K. YU., Il'chenko M. A., EHksperimental'noe issledovanie kharakteristik gazodinamicheskoy sistemy vosplamneniya toplivnoj smesi primenitel'no k ZHRD maloj tyagi, Vestnik MGTU im. N. EH. Bauman. Seriya «Mashinostroenie»Spets. vypusk № 7 (2012) 4–11.



International Conference on Industrial Engineering
Unsteady modes of moisture removal

Akhmedyanova E.N., Ptashkina-Girina O.S.*

Institute of Agricultural Engineering, South-Ural State Agrarian University, Chelyabinsk, Russia

Abstract

The article dwells upon the peculiarities of using granulated sawdust (pellets) and identifies the ways to improve the efficiency of plants by applying unsteady modes of drying granulated sawdust with thermal units (pumps).

© 2015 The Authors. Published by Elsevier Ltd. This is an open access article under the CC BY-NC-ND license (<http://creativecommons.org/licenses/by-nc-nd/4.0/>).

Peer-review under responsibility of the organizing committee of the International Conference on Industrial Engineering (ICIE-2015)

Keywords: pellets, pelleting, boiler unit, recycling, unsteady (oscillating) mode, heat pump

1. Introduction

The issues concerning low-cost fuels for heating low-rise constructions, administrative and industrial structures are highly urgent for the areas far enough from gas-supply systems. Thus, wood wastes (pellets) and their utilization as fuel are considered to be very promising.

The process of pellet production is rather energy-intensive. The production cycle includes the following steps: sorting, grinding, drying, pressing and packing, with the drying process being the most energy-intensive step. The other steps of the production cycle (sorting, grinding, pressing, packing) are less energy-consuming [7, 8].

2. Plants for unsteady moisture removal

In production the following plants for moisture removal are used most often: chamber dryers; belt dryers; vortex dryers; fluid-bed dryers [9].

The technical and economic performance of the most of the above mentioned drying plants (with one exception being batch-operating chamber dryers) can be improved when using recirculation systems and unsteady (oscillating)

* *E-mail:* girina2002@mail.ru

drying modes [2, 3, 6].

Despite the fact that the equipment used operates due to different physical principles but the drying process occurs uniformly and generally with a one-pass movement of the drying agent. This leads to pollution of the environment, as drying products containing not only moisture, but also volatile substances are emitted into the atmosphere, and moreover, it is not always economically effective.

In mobile plants the drying agent (fuel gases) is produced due to burning the feed stock up to 50%, but in our opinion it is very wasteful. Systems with partial or complete recirculation of the drying agent are used relatively seldom as described in the scientific literature.

To dry granular fuel it is necessary to use the so-called “soft” modes, with the temperature of the drying agent not being above 140°C and the moisture of the resulting product not exceeding 12%. From our point of view the most effective drying plants are the ones with partial recirculation and heat regeneration when heat pipes and heat-pump units are used.

To implement everything above stated the following scheme is proposed to be used in a dryer.

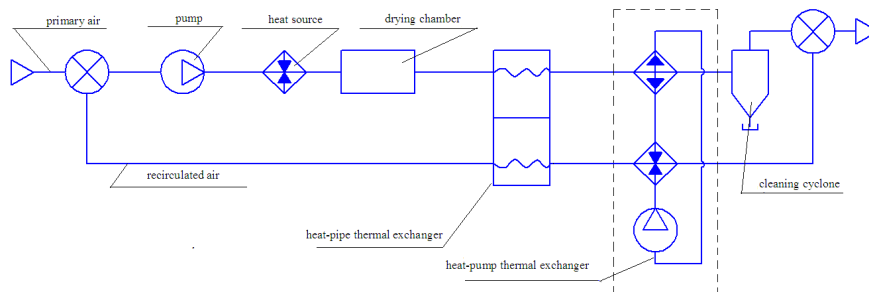


Fig. 1. A combination dryer diagram with partial recirculation.

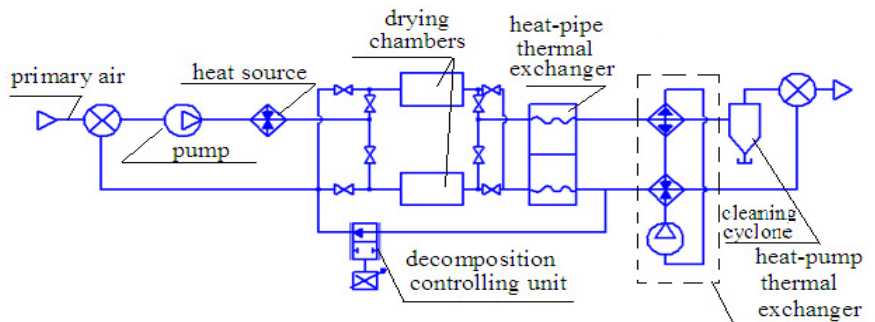


Fig. 2. A dryer diagram with partial recirculation, heat recovery and a unit to provide its unsteady (oscillating) operating mode.

A heat-pipe thermal exchanger allows transferring the heat from the removed drying agent (with a temperature about $120\text{-}135^{\circ}\text{C}$) partially to the circulating gas.

Such thermal exchangers are necessary to use Freon heat pumps, with a maximum temperature of the heated medium not exceeding 120°C . This is a peculiarity of the circulating gas.

Thus, a heat-pipe thermal exchanger can reduce the temperature of the drying agent up to $90\text{-}100^{\circ}\text{C}$ to ensure a more effective functioning of heat pumps.

The next and most important factor in improving the efficiency of drying plants is reducing the time of drying.

When drying wet materials, both the connection form of the moisture with the material and the drying mode are of great importance. Nowadays there exist three types of connections (bonds): chemical, physico-chemical and physico-mechanical ones [1, 2].

Chemical bonds occur due to ionic and molecular forces, they remain unchanged after drying and as they are very strong.

Physical-chemical bonds can be:

- adsorption-based when a thin water layer of a few hundreds of molecules is adsorbed on an active sawdust surface due to the adsorption force gravity;
- osmotic when the moisture penetrates into cells due to the osmotic pressure;
- structural (immobilized) when the moisture is slight with a very low binding energy, and it is captured by newly formed helium structures.

There are also two types of physical-mechanical bonds, with the main criterion of division being the size of the capillary radius. Thus, the first type is for the size greater than 10^{-5} cm and the second one is for capillary radii less than 10^{-5} cm [5].

3. Drying process with unsteady moisture removal

During the process of drying the moisture will move from the inner layers to the sawdust surface, and then evaporate into the atmosphere. To analyse drying processes the following notions are used: the intensity I and the drying rate N . The intensity of liquid evaporation from a free surface during a steady operating mode can be determined due to Dalton's formula [2, 6, 9]:

$$I = \frac{W}{F \cdot \tau} = \beta_p (p_n - p_c), \text{ kg}/(\text{m}^2 \cdot \text{sec}), \quad (1)$$

where W is the amount of the evaporated liquid, kg; F is the evaporation surface, m^2 ; τ is the time, sec; β_p is the mass-transfer coefficient, related to the difference of partial pressures, a moisture $\text{kg}/(\text{m}^2 \cdot \text{sec} \cdot \text{Pa})$; p_n is the partial pressure of the diffusing substance over the liquid (solid) surface, Pa; p_c is the partial pressure of the diffusing substance away from the interface, Pa.

For approximate calculations the following formula can be used

$$I = 5,7 \cdot \omega^{0,8} (p_n - p_c), \text{ kg}/(\text{m}^2 \cdot \text{sec}), \quad (2)$$

where ω is the air speed, m/sec.

To calculate the evaporated liquid we use the following formula

$$I = \beta_c (p_n - p_c), \text{ kg}/(\text{m}^2 \cdot \text{sec}), \quad (3)$$

where β_c is the mass-transfer coefficient related to the concentration difference of the diffusing substance, m/sec; p_n and p_c are the concentrations of the diffusing substance on the liquid (solid) interface and away from the interface, kg/m^3 .

The mass-transfer coefficients β_c and β_p are interrelated [10]

$$\beta_c = \frac{\beta_p}{R \cdot T}, \quad (4)$$

where $R \approx 287 \text{ J}/(\text{kg} \cdot \text{K})$ is the universal gas constant for dry air, m/sec; T is the temperature of the evaporated liquid, K.

The following relationship between the amounts of the evaporated liquid and the supplied heat becomes noticeable:

$$q = I \cdot r = \alpha(t_c - t_n), \text{ J/(m}^2 \cdot \text{sec} \cdot \text{C)}, \quad (5)$$

where r is the specific heat of evaporation, J/kg; α is the heat exchange coefficient, J/(m²·sec·°C); t_c , t_n are the ambient temperature and the evaporation surface temperature, °C.

The drying process can be divided into several periods: the warm period, the period of constant evaporation rate (as it is characterized by the highest rate of moisture evaporation), the period of the falling drying rate.

During the period of constant evaporation rate the temperature of the material is constant $dt/d\tau=0$, the rate of moisture diffusion to the surface is equal to the evaporation rate, and the heat necessary to evaporate the moisture is obtained from the ambient drying agent due to heat exchanges (convection and radiation in some cases). The evaporation intensity I , in this case, is directly proportional to the heat flux density on the body surface.

$$I_m = \frac{q}{r} = \frac{N}{100} \cdot R_V \frac{\rho}{r} = \left(\frac{d\omega}{d\tau}\right) \frac{R_V}{100} \cdot \frac{\rho}{r}, \quad (6)$$

where $N=(dw/dr)$ is the drying rate during the period of constant rate, $R_V=V/F$ is the ratio of the body volume to its surface, m; ρ is the density of the absolutely dry material, kg/m³.

According to the law of heat and moisture conductivity disclosed by A.V.Lykov the moisture in the material moves along the direction of the heat flux and the gas passes in the opposite direction [6]. Thus, during the drying period the moisture in the material can move to its surface due to the difference in its concentrations, the influence of heat and moisture conductivity and the gradient of the excess pressure (when the temperature of the material close to or greater than 100°C, there occurs a filtration transfer [2]).

In general the equation of the mass transfer when drying the material can be written as follows:

$$I_m = -a_m \rho_0 \frac{du}{dx} - \delta a_m \rho_0 \frac{dt}{dx} - a_p \rho_0 \frac{dp}{dx}, \quad (7)$$

where I_m is the amount of liquid moved inside the material per a time unit over an area unit, kg/(m²·h); a_m is the coefficient of potential conductivity (experimentally found for every particular material), m²/h; u is the moisture concentration, kg/kg; x is the coordinate, m; ρ_0 is the density of the absolutely dry material, kg/m³; δ is the thermal gradient coefficient, 1/°C (experimentally found for every particular material); a_p is the coefficient of the filtration transfer, m²/h, N/m² (experimentally found for every particular material); du/dx , dt/dx and dp/dx are partial derivatives that are proportional to the gradients of moisture, temperature and pressure.

A number of researchers [1, 4] consider the value and the direction of the temperature gradient to vary when cooling the material. This causes the moisture movement from the center towards the periphery due to the heat and moisture conductivity. In this regard, the results given in the papers [1, 3, 4] are of special interest. To intensify the drying process a mode with intermediate heating and cooling may be appropriate to be used.

When researching we used the method of mathematical modeling and the following system of equations

$$\frac{\partial u}{\partial \tau} = \alpha_m \cdot \rho \cdot \frac{\partial^2 u}{\partial x^2} + \alpha_m \cdot \rho \cdot \delta \cdot \frac{\partial^2 T}{\partial x^2}, \quad (8)$$

$$\frac{\partial T}{\partial \tau} = \alpha \frac{\partial^2 T}{\partial x^2} + \varepsilon \cdot \frac{r}{c} \cdot \frac{\partial u}{\partial \tau}. \quad (9)$$

We found the mass of the removed moisture according to

$$m_B = -D \cdot \rho \cdot \frac{\partial u}{\partial x} - D \cdot \delta \cdot \rho \cdot \frac{\partial T}{\partial x}, \quad (10)$$

where T is the temperature, u is the moisture content, x is the current coordinate, α is the heat diffusivity, a_m is the diffusion coefficient, r is the latent evaporation heat, ε is the evaporation criterion ($\varepsilon = 0$ for moisture diffusion and $\varepsilon = 1$ for vapour diffusion), τ is the time, δ is the coefficient of the thermal diffusion, c is the specific heat.

Conclusions

According to the mathematical modeling intensification of the drying process is proved to be possible due to periodically supplying of the drying agent with the invariant temperature. Thus, unsteady modes can increase the intensity of the drying process, and in some cases improve the quality of the resulting product.

References

- [1] N.I. Gamayunov, L.I. Ilchenko, *Khim. prom., Chem. Ind.* (1979) 344–348.
- [2] N.I. Gelperin, V.G. Aynshteyn, V.B. Kvasha, *Osnovy tekhniki psevdoozhizheniya*, Basic techniques of fluidization, Chemistry, Moscow, 1967.
- [3] A.S. Ginzburg, *Osnovy teorii i tekhniki sushki pishchevyykh produktov*, Basics of the theory and technique of drying food products, Food Industry, Moscow, 1973.
- [4] A.S. Ginzburg, *Khim. prom., Chem. Ind.* (1979) 328–330.
- [5] A.S. Ginzburg, V.A. Rezhnikov, *Sushka pishchevyykh produktov v kipjashhem sloe*, Drying food products in a fluidized bed, Moscow, 1966.
- [6] A.V. Lykov, *Teplo – massobmen v processah sushki*, Heat – mass transfer in drying processes, Gosenergoizdat, Moscow, 1956.
- [7] I.V. Krechetov, *Sushka drevesiny* [Wood drying], Moscow, 1987.
- [8] I.V. Krechetov, *Sushka drevesiny* [Wood drying], Moscow, 1992.
- [9] S.S. Kotaladze, *Osnovy teorii teploobmena* [Basics of the theory of heat transfer], Leningrad, 1968.
- [10] A.S. Slobodkin, An approximate method for calculating the kinetics of warming up a moist material in a fluidized bed with the oscillating mode [Priblizhennyi metod rascheta kinetiki progreva vlazhnogo materiala v kipiyashhem sloe pri oscilliruyushchem rezhime], IFK [IFC]. 3 (1964).



International Conference on Industrial Engineering

Optimal power distribution between the wheels of a mobile vehicle under different soil conditions

Pozin B.M.^a, Troyanovskaya I.P.^a, Yusupov A.A.^{a*}

^aSouth Ural State University, 76, Lenin Avenue, Chelyabinsk, 454080, Russian Federation

Abstract

This work is dedicated to minimizing power consumption for a vehicle propulsion, with power distributed non-uniformly between axles under different soil conditions for wheels on the right and on the left side of the vehicle. We present a method of calculating minimal total power required for the driving wheels of the mobile vehicle, for different transmission types. We've compared total required power for most common methods of controlling power flows in transmissions of the mobile vehicle, such as implementing unlocked differential gears, limited-slip differentials and their full locking, and systems of optimal power control. This document includes an efficiency assessment in case of alternating specific load on axles under different soil conditions for right and left wheels. We have formulated requirements to controlling differential gears locking based on road conditions.

© 2015 The Authors. Published by Elsevier Ltd. This is an open access article under the CC BY-NC-ND license (<http://creativecommons.org/licenses/by-nc-nd/4.0/>).

Peer-review under responsibility of the organizing committee of the International Conference on Industrial Engineering (ICIE-2015)

Keywords: control task, power distribution, wheels slipping, mobile wheeled vehicle, transmission.

1. Introduction

World science intensively deals with power distribution between mobile vehicle wheels in the frames of these vehicles theory [1–10]. Solving task of optimal power distribution between mobile vehicle wheels allows finding law of controlling power flows depending on vertical loads and traction resistance [11].

Let's discuss task of optimal distributing of power under different soil conditions.

* Corresponding author.

E-mail address:

2. Task solving method

Let's assume that two axial AWD wheeled vehicle at some point of time moves with one side wheels on high traction soil (solid soil; $\lambda_1=\lambda_3=0.55$; $\varphi_{d1}=\varphi_{d3}=0.8$; where φ_{di} , λ_i — parameters, characterizing traction forming properties of the soil areas, contacting with wheel number i), and with other side wheels — on low traction soil (soft soil, ice, etc.; $\lambda_2=\lambda_4=0.55$; $\varphi_{d2}=\varphi_{d4}=0.4$).

Wheels are numbered according to [8] (Fig. 1). Resistance to motion factor is equal to $f=0.3$. Each wheel is loaded with vertical load with weight component of γ_i . Vertical load is equally distributed among wheels.

Conditions of uniform linear movement, [11]:

$$\left. \begin{aligned} V_1 \cdot (1 - \delta_1) &= V_c & V_2 \cdot (1 - \delta_2) &= V_c \\ V_3 \cdot (1 - \delta_3) &= V_c & V_4 \cdot (1 - \delta_4) &= V_c \\ \gamma_1 \varphi_1(\delta_1) + \gamma_2 \varphi_2(\delta_2) + \gamma_3 \varphi_3(\delta_3) + \gamma_4 \varphi_4(\delta_4) - (\gamma_1 + \gamma_2 + \gamma_3 + \gamma_4) f &= 0 \end{aligned} \right\}, \tag{1}$$

where V_i — theoretical wheels speeds; V_c — actual vehicle centre of gravity speed; slipping coefficient δ_i and specific traction loads — φ_i , relate to soil parameters by equations

$$\varphi(\delta_i) = \varphi_{di} \cdot \tanh\left(\frac{\delta_i}{\lambda_i}\right). \tag{2}$$

Diagrams of slipping and specific traction loads dependences on these soils are presented on Figures 2 and 3.

Depending on transmission scheme, system of equations (1) is supplemented by equations of constraints. For the AWD vehicle with transmission with non-locked symmetrical interaxial and interwheel low friction differential gears we should add equations of equality of the traction loads at wheels of each axis and sums of traction loads between axes:

$$\left. \begin{aligned} \gamma_1 \varphi_1(\delta_1) - \gamma_2 \varphi_2(\delta_2) &= 0 \\ \gamma_3 \varphi_3(\delta_3) - \gamma_4 \varphi_4(\delta_4) &= 0 \\ \gamma_1 \varphi_1(\delta_1) + \gamma_2 \varphi_2(\delta_2) - \gamma_3 \varphi_3(\delta_3) - \gamma_4 \varphi_4(\delta_4) &= 0 \end{aligned} \right\}. \tag{3}$$

For the AWD vehicle with transmission with locked symmetrical interaxial and interwheel differentials we should add equations of equality of ideal velocities for all wheels:

$$\left. \begin{aligned} V_1 - V_2 &= 0 \\ V_3 - V_4 &= 0 \\ V_1 + V_2 - V_3 - V_4 &= 0 \end{aligned} \right\}. \tag{4}$$

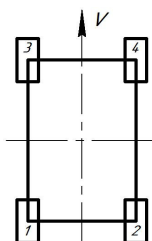


Fig. 1. Wheels numbering

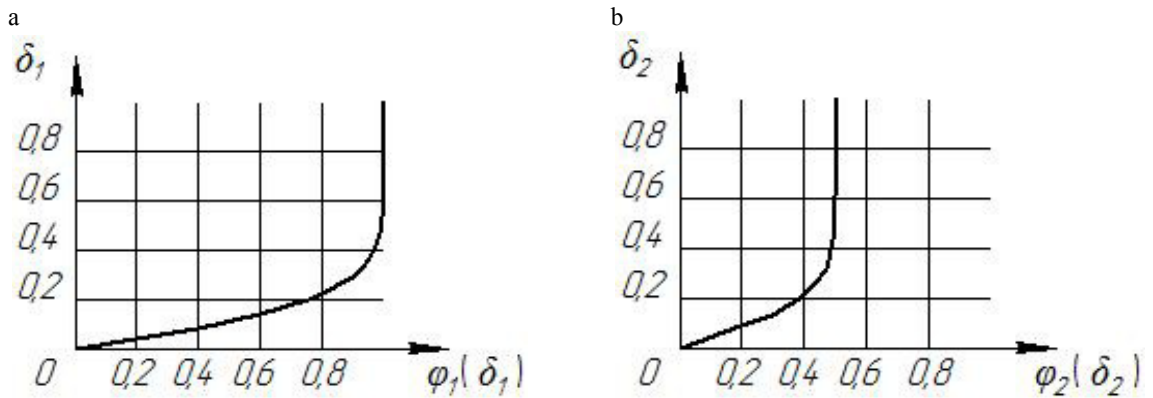


Fig. 2. (a) slipping dependence of specific traction force hard soil; (b) slipping dependence of specific traction force soft soil

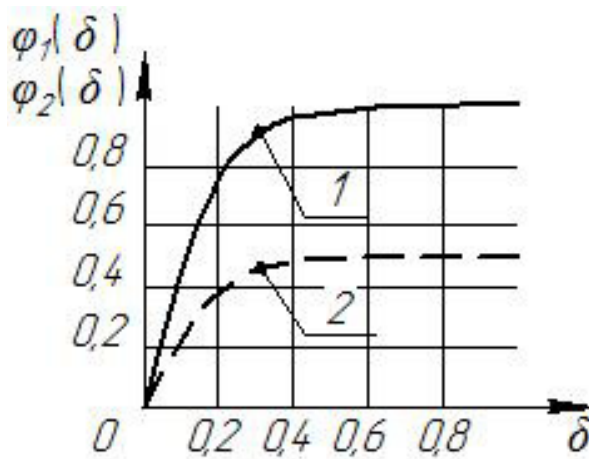


Fig. 3. Specific traction force dependence of slipping

For the AWD vehicle with transmission with non-locked symmetrical interaxial differentials and interwheel limited-slip differentials we should add equations of sums of traction loads at axles. Draw forces relations for each of the axles will be determined by differentials torque bias K_d :

$$\left. \begin{aligned} \gamma_1\varphi_1(\delta_1) + \gamma_2\varphi_2(\delta_2) - \gamma_3\varphi_3(\delta_3) - \gamma_4\varphi_4(\delta_4) &= 0 \\ K_d\gamma_1\varphi_1(\delta_1) - \gamma_2\varphi_2(\delta_2) &= 0 \\ K_d\gamma_3\varphi_3(\delta_3) - \gamma_4\varphi_4(\delta_4) &= 0 \end{aligned} \right\} \quad (5)$$

For AWD vehicle with transmission with interaxial low slipping differential we should add equations of equality of the traction forces at each of the axes. Relations between sums of the traction forces between axes are determined by interaxial differential torque bias K_d :

$$\left. \begin{aligned} \gamma_1 \phi_1(\delta_1) - \gamma_2 \phi_2(\delta_2) &= 0 \\ \gamma_3 \phi_3(\delta_3) - \gamma_4 \phi_4(\delta_4) &= 0 \\ K_d (\gamma_1 \phi_1(\delta_1) + \gamma_2 \phi_2(\delta_2)) - (\gamma_3 \phi_3(\delta_3) + \gamma_4 \phi_4(\delta_4)) &= 0 \end{aligned} \right\} \quad (6)$$

3. Calculations results

Following (Fig. 4 and 5) indicates calculations results for vehicles, equipped with transmissions with different power distributing units.

Curve (Fig. 4) demonstrates that total power on driving wheels essentially depends on scheme of its distribution. Full differential lock allows decreasing total power on driving wheels up to minimum, allowed by power distribution control system. Partial lock allows significant decreasing of power on driving wheels but does not allow its minimal value. Transmission without differential locking is less effective: while motion resistance factor f increases, relation between total power and minimal value increases and increases without limit under above conditions when $f = 0.46$.

The curve (Fig. 5) shows that implementing of the interaxial low slipping differential with constant torque bias instead of the low friction differential leads to decreasing total specific power on driving wheels under sufficiently great difference between loads on axles. For each constant torque bias there is a vertical axis load value, under which total specific power becomes lower than for non-locked differentials, so partial unlocking becomes reasonable (points of curve 1 crossings with curves 2, 3, and 4).

Each of the curves 2, 3 and 4 has a minimum upper than curve 5. So each torque bias value has specific vertical load on axles γ_{omn} under which total specific power on the wheels becomes maximum. Minimal values of the total specific power are the same for different constant values of the torque bias, and they are higher than value, assured by the power control system or by full differentials locking. In other words, for each value of the specific vertical load on axles there is a torque bias, assuring minimum specific power on driving wheels. So, we can decrease total specific power, spent for moving the vehicle, by controlling the torque bias.

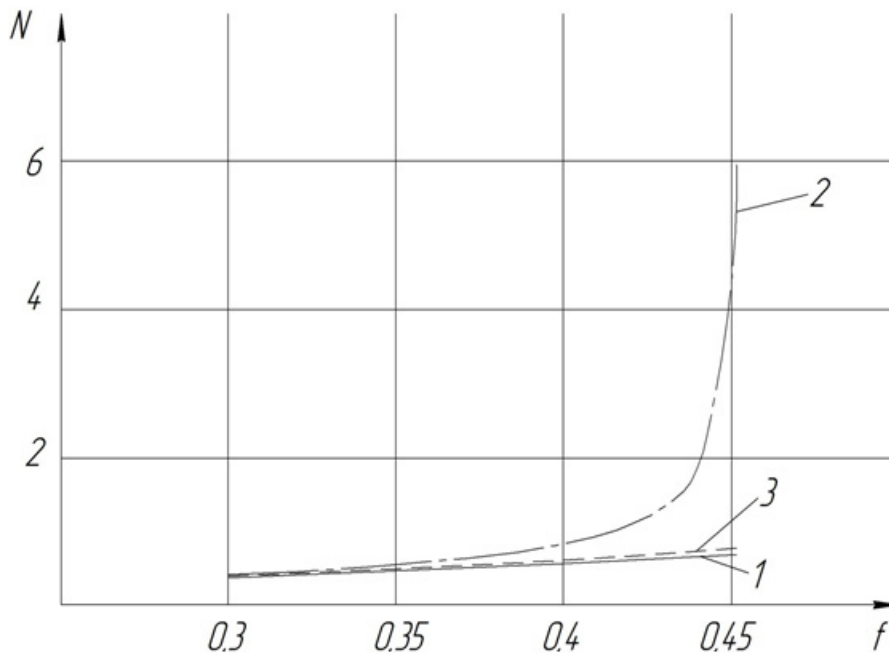


Figure 4. Dependences of total specific power on driving wheels on motion resistance coefficient: 1 — for vehicle with optimal distribution of power or with all differentials locked; 2 — for vehicle with non-locked differentials; 3 — for vehicle with inter wheels low slipping differentials.

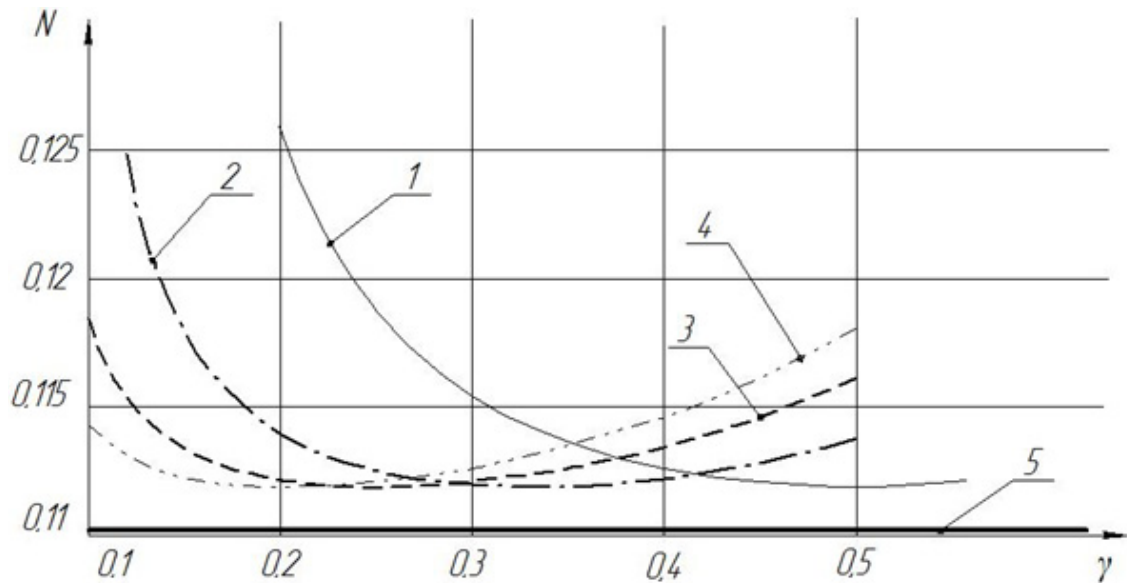


Figure 5. Dependences of the total specific power (N) on driving wheels from load on rear axle (γ): 1 — for vehicle with non-locked differentials; 2, 3, and 4 — for vehicles with interaxial low slipping differentials with constant torque bias 2, 3, and 4 accordingly; 5 — for vehicle with optimal power distribution or with all locked differentials.

4. Conclusion

In that way solving the task of external resistances power minimization allows not only evaluating effectiveness of implementing different kinematic schemes and transmission designs taking into account nonuniformity of load distribution between the vehicle wheels and different soil conditions, but also allows formulating requirements to controlling differential locking under different road conditions.

References

- [1] Abramov, V. N. Evaluating and Choosing Tires with Regulated Pressure for Army Vehicles / V. N. Abramov, M. P. Chistov, I. V. Veselov, A. A. Koltunov. — Bronnitsi: FSUE 21 R&D Institute of the MD of the RF, 2006 - 223 p.
- [2] Antonov, D. A. Theory of Battle Wheeled Vehicles Motion / D. A. Antonov, S. I. Bespalov. - M: Printing House of the Tank Forces Academy, Named after R. Ya. Malinovski, 1993 - 385 p.
- [3] Barakhtanov, L. B. Vehicle Floatation / L. B. Barakhtanov, V. V. Belyakov, V. N. Kravets - Nizhni Novgorod: NSTU printing house, 1996. - 200 p.
- [4] Keller A. V. Algorithms of Controlling Power Distribution Between Driving Wheels of the Motor Vehicle / A. V. Keller, G. D. Dragunov // Automobile Industry — 2004. — No. 1. - p. 10-12.
- [5] Keller A. V. Principles and Methods of Distributing Power Between Driving Wheels of Basic Automobile Chassis / A. V. Keller, I. A. Murog. — Chelyabinsk, 2009. - p. 224.
- [6] L'vov, E. D. Theory of Tractor/ E. D. L'vov. - M.: Mashgiz, 1960. — 252 p.
- [7] Murog, I., Keller, A., and Aliukov, S., "Comparative Analysis of Methods of Power Distribution in Mechanical Transmissions and Evaluation of their Effectiveness," SAE Technical Paper 2015-01-1097, 2015, doi:10.4271/2015-01-1097.
- [8] Troyanovskaya, I. P. Methodology of Modeling of Nonlinear Motion of the Tractor Units: dissertation doctor of technical science (05.05.03, 05.05.04) — Chelyabinsk, 2011. - page 296.
- [9] Vantsevich V.V. Driveline Configuration Effect on Longitudinal Vectoring of Power Flow Between Drive Wheels and Energy Efficiency in Transport Mode of a 6×6 Terrain Truck/ Vladimir V. Vantsevich; Dennis Murphy; Gianantonio Bortolin// ASME 45059 — 2012 P. 379-388.
- [10] Volskaya N. S. Working Out Methods of Calculating Supporting-and-Tractive Characteristics of the Wheeled Vehicles Based on Set Road-and-Soil Parameters of the Operating Area: author's abstract doctor of technical science (05.05.03) - M., 2008 — 36 p.
- [11] Keller A. V. For the Task of Distributing Power Between the Mobile Vehicle Wheels / A. V. Keller, B. M. Posin, I. P. Troyanovskaya, V. N. Bondar, A. A. Yusupov // Tractors and Agricultural Vehicles. — 2015. — No. 3. - p. 10-12.



International Conference on Industrial Engineering

Non-motorized study of supercharging piston engine compressor parameters

Sharoglazov B.A.*, Mashkov O., Martynov A.

South Ural State University, 76, Lenin Avenue, Chelyabinsk, 454080, Russian Federation

Abstract

This article is about the features and advantages of non-motorized estimates of the unit charge parameters (especially compressor) of a combined piston engine (engine). The scheme research facility equipped with measuring and control means to identify the numerical parametric values of the gas-dynamic flow moving along the flow of the supercharging compressor, with calculations made for different loading conditions of the power plant. Herein is also provided a brief description of the software-based collaborative modular system published and the PC. We present the results of non-motorized and systematized research on supercharging compressor different embodiment of the flow parts.

© 2015 The Authors. Published by Elsevier Ltd. This is an open access article under the CC BY-NC-ND license (<http://creativecommons.org/licenses/by-nc-nd/4.0/>).

Peer-review under responsibility of the organizing committee of the International Conference on Industrial Engineering (ICIE-2015)

Keywords: internal combustion engine, supercharging unit, compressor, motorless testing, modular data acquisition system, diffuser, vane diffuser

1. Introduction

One of the most important tasks of the present piston engine design (eg, diesel) is an increase in specific weight and size and economic indicators. At the present time combined power plants (based on diesel engines), ensuring the implementation of the mean effective cycle pressure p_e of 2.5 ... 3.0 MPa or more are created. And the use of machinery with p_e of 1.5 ... 2.5 MPa may be considered as already solved problem (see. Eg [1]).

* Corresponding author. Tel.: +7-902-897-4557;
E-mail address: G389@mail.ru

Implementation of such values of mean effective pressure cycle in aspirated engines is practically impossible: even p_c levels, equal to approximately 0.8 MPa, in naturally aspirated engines (with reference to the conditions of use of air as an oxidant) can not be ensured due to the impossibility of oxidant to be supplied in combustion chamber in amount sufficient for combustion. This objective (ensuring supply to the combustion chamber of the machine required amount of oxidant) is solved using the pre-compactation (compression) in the supercharging compressor device. Here, in most cases, preference is given to gas-turbine drives of such devices, ie, using of gas-turbine units of boost (GTUB) [2].

The task of matching and identify the numerical values of parameters of a combined power plant (ICPE - GTUB) is solved at the stage of pre-project, project, and after that, and during the pre-testing and debugging machines. At each of these stages, a lot of attention is paid to the identification of the individual characteristics of ICPE, GTUB and, in particular, an important component of these units - compressor supercharging.

In the experimental evaluation of the numerical values of the parameters of the charge unit (charge compressor) it is important to ensure conditions of his work (the numerical values of parameters such as mass flow rate, the temperature and the pressure, flow pattern) closer to the terms of use ICPE, for installation on which the unit is planned. The importance of this fact is confirmed by the fact that the beginning of the massive use of composite piston power plants (supercharged diesel engines), evaluation parameters and test GTUB (including compressors) are engaged in leading national organizations and researchers [3,4,5].

Nomenclature

α	temperature coefficient of thermal resistance conversion, SCI. GOST 6651
π_c^*	total pressure ratio
η_c^*	total-to-total efficiency of compressor
p_c^*	total pressure at the outlet of the compressor
T_c^*	total temperature at the outlet of the compressor
p_o^*	total pressure at the inlet of the compressor
T_o^*	total temperature at the inlet of the compressor
N_c	required to drive the compressor capacity
G_c	mass flow rate of air through the compressor
c_p	mass specific heat of the air
G_{cor}	corrected mass flow rate of air through the compressor
n_{cor}	corrected rotation speed of compressor wheel
\overline{G}_{cor}	depending on the relative corrected air mass flow

2. The circuit test rig and its features

Figure 1 shows a schematic layout of the charge compressor and turbine (as a source of energy for its drive) with appropriate devices for controlling the parameters of their work in the non-motorized research facility. Non-motorized installation is a device, which analyzed the boost unit (compressor) is represented as a separate object: it does not have the mechanical and gas connections with a piston machine (ICPE as an object of study is excluded from the scheme).

Moreover it is possible to play with the place of real gas dynamic relations corresponding to the specific combination GTUB-ICPE settings are saved. Parameters state working bodies of the turbine (as a source of mechanical energy), compressor (as a consumer of energy) recorded respective sensors, range and location of which is indicated in the diagram.

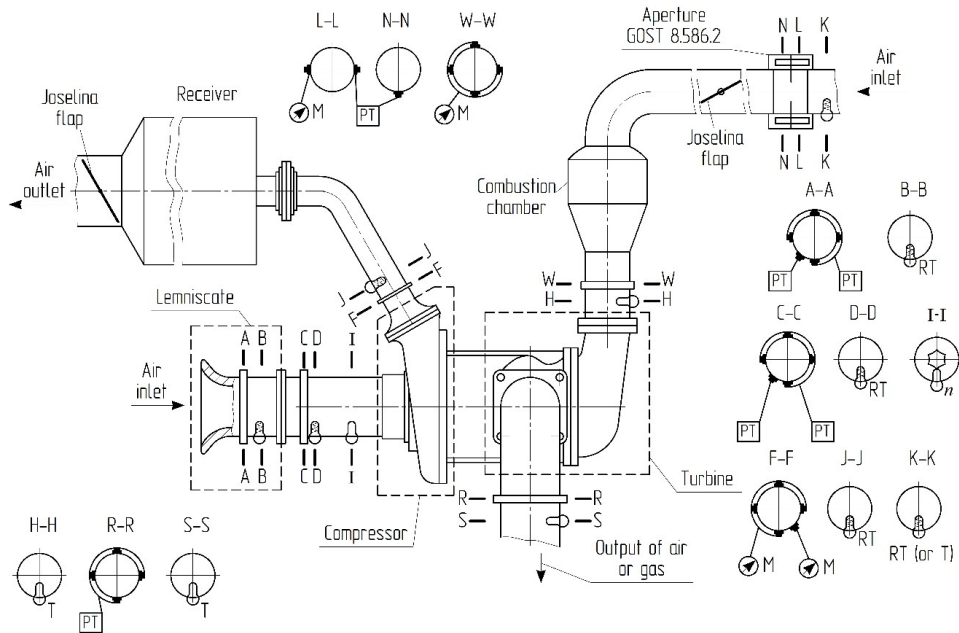


Fig.1. Schematic diagram of the experimental setup for the study of non-motorized units Charge: RT-resistance thermometer; T – thermoelectric converter; PT - pressure transducer; M - pressure gauge; ■ - Selection of static pressure; n - the wheel speed sensor of the compressor.

To measure the temperature of the working fluid at the compressor inlet is provided the use of resistance thermometers (sensor - copper) with a grading 50M ($\alpha = 0.00428 \text{ }^\circ\text{C}^{-1}$) and at the outlet of the compressor - resistance thermometers (sensor - platinum) with a grading 100P ($\alpha = 0.00391 \text{ }^\circ\text{C}^{-1}$) or Pt100 ($\alpha = 0.00385 \text{ }^\circ\text{C}^{-1}$). For the care of specialized connections, (4-wire or 3-wire) resistance thermometers to measure the secondary means (SI) used in the temperature normalizing converters (NTP-2.xx) 4 ... 20 mA. To determine the parameters of the gas, the temperature can reach 900 °C, it used a chromel-alumel thermocouple, also in conjunction with the temperature transducer. All temperature measurement specifically dissected with the recommendations contained in the special literature [4].

An important property of (and an essential requirement), the charge imposed on modern units are requirements governing their weight and dimensions [3]. This fact in the design of such units makes it necessary to use a relatively small sizes of the flow parts, which makes it difficult to complete the control parameters (braking parameters, in particular temperature and pressure) of gas streams flowing through the blower (compressor). This requires the use of special (a special kind of) the measuring instruments. The use of special measuring tips for determining the parameters of the braking flows in such cases, is inevitably linked to the changing nature of the motion of gas flows and changing conditions of the units and their parameters. In this connection (to avoid interference of the title) in the measuring circuit unit is provided with control static pressure gas streams, and characterizing the flow through the blower.

In determining, the static pressure as the primary measuring means (MM) used converters: AP (absolute pressure), GP (gauge pressure), DP (differential pressure). The output signal MM of temperatures and pressures under standardized 4 ... 20 mA, which greatly simplifies the selection of the secondary measuring means.

Total parameters are provided to be calculated on the basis of the results of measurements of mass flow rates of air flowing through the turbine and the compressor, on the results of control of static parameters and on using gas-dynamic functions of pressure and flow (appropriate algorithmic tools are developed and included in the software of processing of results of observations [6]).

In particular, total pressure ratio and total-to-total efficiency of compressor are defined by the formulas:

$$\pi_c^* = \frac{p_c^*}{p_o^*} \text{ и } \eta_c^* = \frac{T_0^* \left(\pi_c^{*\frac{k-1}{k}} - 1 \right)}{T_c^* - T_0^*}, \quad (1)$$

where p_c^* , T_c^* - total pressure and total temperature at the outlet of the compressor; p_o^* , T_o^* - total pressure and total temperature at the inlet of the compressor (often, when the speed of flow in the inlet device is slow, called parameters can be taken equal to the atmospheric).

Required to drive the compressor capacity is determined by the expression:

$$N_c = G_c \cdot c_p \cdot (T_c^* - T_o^*), \text{ kW} \quad (2)$$

where G_c – the mass flow rate of air through the compressor, kg/s; c_p – mass specific heat of the air, kJ/kg·K.

The control scheme of parameters (Fig.1) to determine the rotation speed of the compressor wheel, which may be in the range from 0 to 240000 min^{-1} (0 ... 4000 Hz), is provided by the use of proximity sensors are inductive type. This sensor is made in the form of a coil with a side of the magnetic core. It (the sensor) is installed in the housing compressor above the nut attaching the wheel to the shaft. When passing under the magnetic core faces of the nut duct, the sensor changes, the sensor's coil is induced electromotive force. A corresponding signal is transmitted to a registering apparatus.

As a secondary means of measurement modular collection station data LTR-EU-8-1 of company L-CARD is selected [7]. An important quality of this station is that its design allows configuration of measurement system by universal and specialized modules of LTR-series: analog to digital converters (ADC), digital analog converters (DAC) converters and discrete I/O signal. The station can be connected to the computer (PC) through a unified interface Fast Ethernet or USB.

The General scheme of primary measuring tools used for non-motorized installation with data acquisition system is shown in Fig.2.

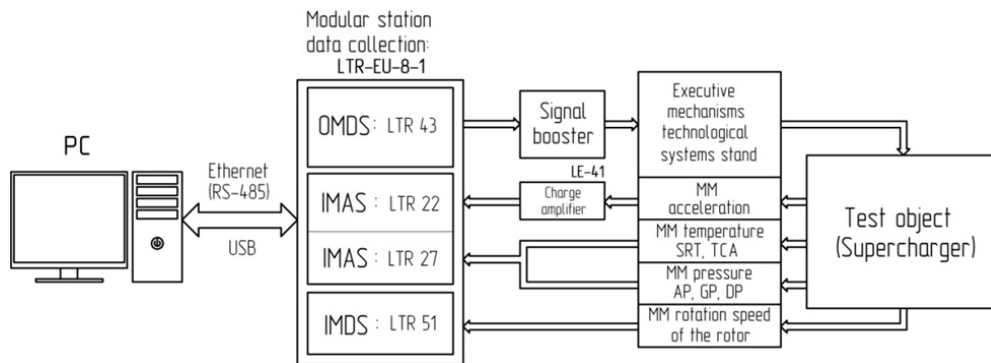


Fig.2. Schematic diagram of the connection used for installing sensors with a recording system and a computer: LTR 43 – module output of discrete signals; LTR 22, LTR 27 – input module of analog signals; LTR 51 – input module of digital signals.

To ensure joint work of computers (PCs) with modular data collection system LTR, as already mentioned, the specialized software is developed [6]. Software is written in Delphi and runs on the operating system Windows XP SP3 and above. During testing, the software automatically calculates the main parameters of compressor (and turbine, as an energy source for driving the compressor), the processing results are given to the computer display. It

should also be noted that the scheme of installation can be used for the purposes of non-motorized tests of a turbine of turbochargers. In this case, the compressor can function as a load device.

3. Non-motorized tests of compressor with different types of vaned diffusers

Investigations of compressors with different design schemes of vaned diffusers are provided on created non-motorized installation. In particular, two-row and two-cascade vaned diffusers are investigated [8-13]. Diagram of compressor stage with such diffusers is shown in figure 3.

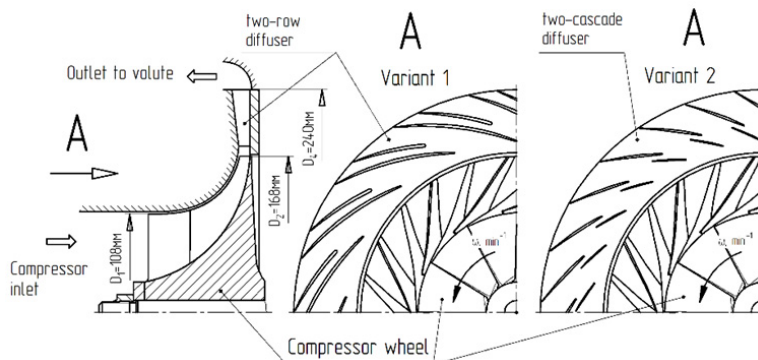


Fig.3. schematic Diagram of turbocharger compressor stage with different variants of vaned diffuser: variant 1: compressor stage with two-row vaned diffuser; variant 2: compressor stage with two-cascade vaned diffuser.

Figure 4 illustrates the results of these research. They are represented in the functions of corrected mass flow rate G_{cor} through compressor and corrected rotation speed n_{cor} of compressor wheel. Corrected parameters were defined with account of requirements of the Russian standard [3] that provided by the appropriate software [6] for registration and monitoring of parameters.

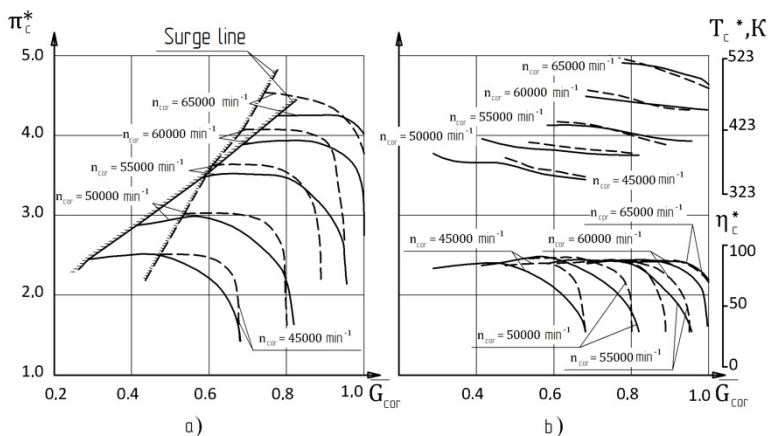


Fig.4. Parameters of the compressor, depending on the relative corrected air mass flow \bar{G}_{cor}^* : (a) General characteristics of the compressor with two-row and two-cascade vane diffuser; (b) Total temperature T_c^* and total-to-total compressor efficiency η_c^* related to different corrected rotation speeds n_{cor} of compressor wheel;

- compressor stage with two-row vaned diffuser;
- - - compressor stage with two-cascade vaned diffuser;

Note: * – the counting measure of the relative mass flow of compressor is the maximum mass flow corresponding to the rotation speed $n_{cor} = 60000 \text{ min}^{-1}$.

3. Analysis of the research results

The analysis of the results gives grounds to conclude that the compressor stage with two-row vaned diffuser (variant 1) allows a wider load range compared to a compressor provided with a two-cascade vane diffuser (variant 2). In particular, to such a compressor, the area of stable (free from surge effects) modes of operation is within the limits defined by the relative values of corrected air flow \bar{G}_{cor} , numerically equal to 0.35 ... 0.72 (for $n_{cor} = 45\ 000\ \text{min}^{-1}$) to 0.78 ... 1.0 ($n_{cor} = 65\ 000\ \text{min}^{-1}$). In the compressor stage with two-cascade vaned diffuser stable operation area is more narrow. It is determined by the values $\bar{G}_{cor} \approx 0.45 \dots 0.68$ ($n_{cor} = 45\ 000\ \text{min}^{-1}$) up to $\bar{G}_{cor} \approx 0.72 \dots 1.0$ ($n_{cor} = 65\ 000\ \text{min}^{-1}$) (Fig. 4a). In this compressor stage surge line is under a significantly larger inclination angle to x-axis than in the case where the compressor is provided with two-row vaned diffuser.

It is important to note the fact that in both cases (two-row and two-cascade vaned diffuser), compressor stage ensure high total pressure ratios π_c . The value of this parameter is at the level of 4.2 ... 4.5 (see fig. 4a). Thus, the efficiency of the compressor reaches values of 0.80 ... to 0.82, see Fig. 4b.

Thus, the analysis of the results of non-motorized tests of compressor stages, equipped with two-row or two-cascade diffusers, allows us to conclude that both compressors are of good parameters (by numerical values of π_c^* , η_c^* , T_c^* , \bar{G}_{cor}).

Conclusions

Preference to any of them is determined by the intended use of propulsion of specific destination. In the case where internal combustion engine is planned to be used on the transport unit, we choose a compressor stage equipped with two-row vaned diffuser. With regard to less loaded in dynamic relation machines (stationary units), compressor with two-cascade vaned diffuser may be preferred.

But in these two named cases should be taken into account heat characteristics of the internal combustion engine as a source of working fluid (turbine) and the consumer of compressed air.

References

- [1] B.A. Sharoglazov, V.V. Shishkov, V.V. Klement'ev, S.I. Kav'yarov, [Our vision of the main ways to improve the internal combustion engine] Aktualnye problemy teorii i praktiki sovremennogo dvigatelestroeniya: Trudy Mezhdunarodnoy nauchno-tekhnicheskoy konferentsii. (2006) 84–90. (in Russ.)
- [2] O. Varnier, Trends and limits of two-stage boosting systems for automotive diesel engines, Universidad politecnica de Valencia, 2012.
- [3] GOST R 53637-2009. State Standart Russia 53637-2009. Automotive turbochargers. General technical requirements and test methods, Standartinform, Moscow, 2010.
- [4] D.A. Portnov, S.M. Metallikov, Metodika polucheniya kharakteristik turbokompressora. Issledovanie gazoturbinnykh dvigateley i ikh elementov, [Technique for characterizing the turbocharger. Investigation of gas turbine engines and their components: Proceedings number 9], 1960.
- [5] A.B. Azbel', N.I. Verba, M.Ya. Rabinovich, K metodike ispytaniy turbokompressorov traktornykh i kombaynovykh dizeley [To test procedure turbochargers tractor and combine diesels.], Traktory i sel'khoz mashiny Publ. 9 (1981) 125.
- [6] O.G. Mashkov, A.A. Zholobov, RF Patent 2014618825. (2014)
- [7] Kreytovaya sistema LTR - sistema sbora dannykh i upravleniya, L-Card Razrabotka i proizvodstvo elektronnoy apparatury [System LTR - data acquisition and control, L-Card Design and manufacture of electronic equipment]. Information on: <http://195.91.155.90/products/ltr/>.
- [8] Turbocharger Test Stand with a Hot Gas Generator for High-Performance Supercharging Systems, MTZ 10I2008. 69
- [9] T. Noguchi, Y. Takata, Y. Yamashita, 220,000-r/min, 2-kW PM Motor Drive for Turbo-charger, Electrical Engineering in Japan. 161(3) (2007).
- [10] E.A. Lurie, P.R. Van Slooten, G. Medic, J.M. Mulugeta, B.M. Holley, J. Feng, O. Sharma, Design of a High Efficiency Compact Centrifugal Compressor for Rotorcraft Applications, United Technologies Research Center, 2011.
- [11] Pei-Yuan Li, Chu-Wei Gu, Yin Song, A New Optimization Method for Centrifugal Compressors Based on 1D Calculations and Analyses, Department of Thermal Engineering, Tsinghua University, Beijing, 2015.
- [12] N. Sitarum, P. M. Banugade, Effect of double row diffusers on performance and flow field of a centrifugal compressor, International Journal of Emerging Technology and Advanced Engineering. 3(3) (2013) 9–16.
- [13] L. Zhou, Z. Wang, Z. Liu, Investigation on influence of design parameters for tandem cascades diffuser using DOE method, Engineering applications of computational fluid mechanics. 8(2) (2014) 240–251.



International Conference on Industrial Engineering

Development of software for calculation and optimization of diesel operating processes and fuel supply

Malozemov A.A.*

South Ural State University, 76, Lenin Avenue, Chelyabinsk, 454080, Russian Federation

Abstract

The article presents the results of developing software for calculation and optimization of diesel operating processes and fuel injection. The software is intended for calculation and optimization of operating processes and fuel injection for supercharged and naturally aspirated diesel engines, including those running on alternative and mixed fuels, with a multi-phase injection and exhaust gas recirculation, at the start mode and partial loads. The software consists of related modules: user interface for data input, running control and calculation results display, data exchange between modules, a module for one-dimensional calculation of processes in the common rail fuel systems, a module for thermodynamic calculation of operational processes and conjugate calculation of the thermal state of combustion chamber parts using finite element method, a module for three-dimensional calculation and optimization of operations in the combustion chamber using computational fluid dynamic (CFD) method. A distinctive feature of the software is a conjugate calculation of fuel injection, operational processes, and thermal state of the combustion chamber parts. The use of this software can significantly reduce the time required to optimize operational processes, solve problems of engine forcing, reduce fuel consumption and reduce emission rates.

© 2015 The Authors. Published by Elsevier Ltd. This is an open access article under the CC BY-NC-ND license (<http://creativecommons.org/licenses/by-nc-nd/4.0/>).

Peer-review under responsibility of the organizing committee of the International Conference on Industrial Engineering (ICIE-2015)

Keywords: software; diesel; operating process; fuel injection; optimization

1. Introduction

Research Institute for engines (JSC "NIID") with the participation of Bauman Moscow State Technical University and the South-Ural State University has developed software, named as "Bas relief", for calculation and optimization

* Corresponding author. Tel.: +7-351-904-2428; fax: +7-351-245-00-17.

E-mail address: malozemov@gmail.com

of operating processes in piston engine combustion chamber and fuel system of four-stroke diesel engines with and without supercharging, including:

- running on alternative and mixed fuels;
- with multi-stage injection of fuel;
- with exhaust gas recirculation;
- at start-up modes and partial loads.

"Bas relief" include related software modules:

- common graphical user interface for data input, running control and display the results of calculations, data exchange between modules;
- software module for one-dimensional calculation of processes in the common rail fuel systems;
- software module for conjugate thermodynamic calculation of operating processes in the engine combustion chamber and axisymmetric calculation of the combustion chamber parts thermal state by finite element method;
- CFD-module for three-dimensional gas-dynamic calculation of working processes in the engine combustion chamber;
- optimization module.

"Bas relief" software can operate in Linux operating systems (64 bits) and in Windows operating system (64 bits), using the virtualization technology.

Initial data for calculation are entered via the GUI, see Fig. 1.

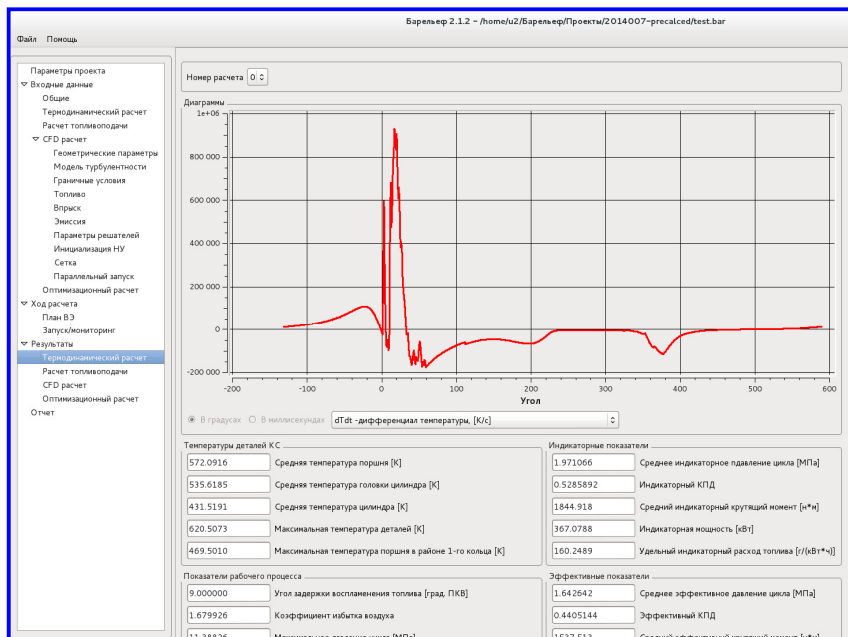


Fig. 1. "Bas relief" software graphical user interface.

For combustion chamber geometry introducing can be use:

- graphical user interface;
- computational grid prepared by using third-party software (for example, ANSYS, KIVA, STAR-CD).

User can prepare a parameterized geometry templates (like AVL ESE diesel software).

The calculation results are displayed in a graphical interface, spatially distributed parameters can be visualized and processed in the free software Paraview or similar.

2. One-dimensional calculation of processes in the common rail fuel systems

In accordance with the concept of building a unified calculation module for developing and optimization processes in cylinders, commensurate with a reasonable complexity of their implementation and feasibility reliable description, mathematical model of the fuel system based on the one-dimensional description of the fuel movement in the long acoustic channels and zero-dimensional description of the processes in the volumes and local hydraulic resistance. All hydraulic, mechanical, electrical, thermodynamic processes described in relation to the conditions of high unsteadiness. The mathematical model used, on the one hand, developed in accordance with the requirements of the specific characteristics adequacy to real fast physical processes, on the other hand - the maximum calculation rate. That is particularly important for time-consuming CFD calculation, must to ensure creating a new generation of fuel systems. Another feature of "Bas relief" software - simultaneous calculation of processes in combustion chamber and in fuel system, that allows to improve fuel supply equipment, as a component of the engine.

Description of the major fuel injection - elastic properties - was carried out using an equation of state for any practically significant fuels which can be used in diesel engines according to the current pressures, temperatures, gas content in the fuel. This form of description allows to describe the two-phase state of the fuel and calculate the properties of mixtures of fuels. In contrast to the widely used estimates of simplified hydraulic resistance pipeline for steady flow and an infinitely long pipeline, in the "Bas relief" software is used correct calculation of hydrodynamic friction for unsteady flow of fuel. It is based on an adequate theoretical concept and unique experimental results.

For modern fuel systems with electronic control applied a detailed calculation of working processes in high-speed motor drives controls. Calculation of the electromagnets includes calculating pulse process in electrical circuits, fast magnetization reversal, calculation of motion parts with the electromagnetic, mechanical, hydrodynamic effects.

The conjugate calculation of fuel hydrodynamic and torsional dynamics of high pressure fuel pump parts allows to analyze the emergence and development not resonant torsional vibrations in the drive. Thus, it is possible to calculate the amplitude loads are repeatedly exceeding quasistatic. Because of this it is possible to design a reliable drive for high pressure fuel pump and not make worse the characteristics of the fuel supply by reason of the torsional vibrations in it.

Comparison of the calculated and experimental diagrams of fuel pressure at the inlet of the nozzle shown on Fig. 2.

3. Thermodynamic calculation of operating processes in the engine combustion chamber and axisymmetric calculation of the combustion chamber parts thermal state

Software module for conjugate thermodynamic calculation of working processes in the engine combustion chamber and axisymmetric calculation of the combustion chamber parts thermal state is used for:

- preliminary optimization of working processes in combustion chamber of diesel engines, including running with alternative fuels, and mixed fuels, with the exhaust-gas recirculation, that can significantly reduce the time of CFD calculations;
- determination of initial and boundary conditions for CFD-module;
- evaluation of the thermal state of the combustion chamber parts.

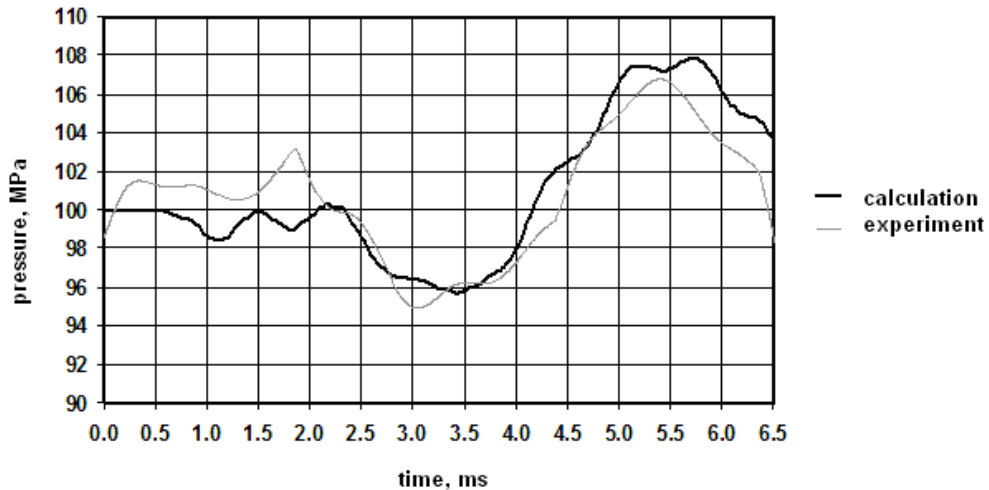


Fig. 2. Comparison of the calculated and experimental diagrams of fuel pressure at the inlet of the nozzle.

This software module is based on:

- system of energy and mass balance ordinary differential equations of the gases in the combustion chamber, to be solved using Adams-Bashforth methods;
- Vibe [1] equation for single zone with two maximums;
- ignition delay period equation;
- equation of gases mass flow through the valve gap in the quasi-stationary formulation;
- Woschni [2] equation to determine the current value of the heat transfer coefficient in the combustion chamber;
- system of equations for calculation of the combustion chamber parts thermal state, based on the finite element method.

4. Computational fluid dynamic

CFD-module is based on open source codes OpenFOAM, and used for:

- calculation and optimization of mixture formation, fuel (including alternative and mixed) ignition and combustion, formation of harmful substances, multiphase injection and exhaust gas recirculation on the different running conditions and engine loads;
- optimization of the combustion chamber shape and characteristics of the fuel injector nozzle, fuel injection strategies.

As the basis of a CFD-modules mathematical model are used:

- fuel breakup submodels: primary - LISA (Linearized Instability Sheet Atomization), secondary - Reitz & Diwakar [3], TAB (Taylor Analogy Breakup), ETAV (Enhanced Taylor Analogy Breakup), Reitz KHRT (Kelvin-Helmholtz & Rayleigh-Taylor) [4];
- submodel of interaction in the spray (O'Rourke [5], N.Nordin [6]);
- submodel of fuel droplets interaction with the combustion chamber walls;
- submodel of fuel droplets motion;
- submodels of heat transfer in fuel spray and the evaporation of the droplets;

- submodels of fuels combustion chemical kinetics (including non-traditional fuels), based on the Arrhenius equation;
- submodel of the physical processes in combustng spray PaSR (Partially Stirred Reactor);
- submodels of nitrogen oxides (Y.Zeldovich) and soot particles (H. Hiroyasu [7]) formation;
- submodel of heat transfer in parts of the diesel engine combustion chamber;
- submodel of turbulent reacting gas flow in the combustion chamber RANS (Reynolds-averaged Navier-Stokes) with standard k- ϵ model or Launder-Sharma k- ϵ model;
- equations of mass, momentum, energy and turbulent parameters conservation.

During software development, the source codes has been modified and supplemented, in particular:

- specified to determine the coefficients of the normal heptane and other fuels thermophysical properties;
- included kinetic mechanism of alternative and mixed fuels combustion;
- included model of soot particles formation (H. Hiroyasu).

Examples of the gas and fuel droplets temperature, concentration of soot and nitrogen oxides calculation are shown in Fig. 3 and Fig. 4.

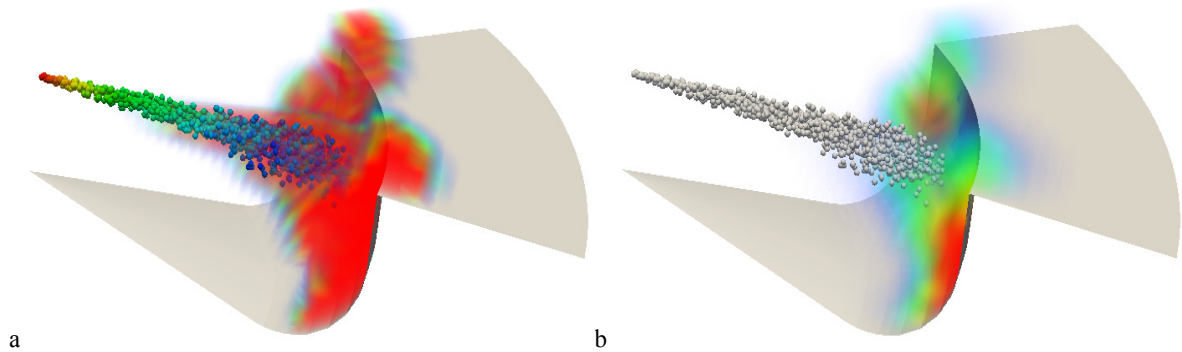


Fig. 3. (a) Temperature of the gas and fuel droplets; (b) concentration of soot.

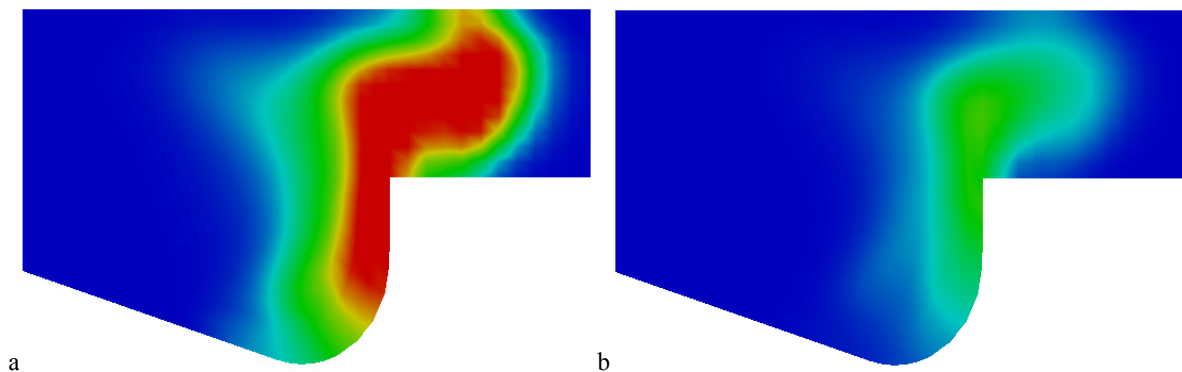


Fig. 4. Concentration of nitrogen oxides: (a) without exhaust gas recirculation; (b) with exhaust gas recirculation.

5. Optimization

Optimization techniques implemented in "Bas relief" software, based on a complex system of energy and environmental efficiency criteria and the algorithm includes:

- the choice of fuel with properties in accordance with the diesel engine running conditions;
- determination of the fuel pressure at the injectors and indicator diagram of gas pressure in the cylinder to determine the parameters of the injection process and the characteristics of fuel combustion in a diesel engine operating cycle;
- determination of basic characteristic of fuel burnout process parameters: duration, timeliness, monotony, specificity and adiabatic.
- definition of the criteria and the rate of control by comparing the actual parameters of the combustion process in a diesel engine operating cycle with optimal;
- selection of diesel engine operating cycle management strategies using required level at the classification scale according to the principles of improving the combustion process;
- determine the effectiveness of diesel engine operating cycle fuel supply optimization using numerical modeling.

6. Conclusion

The developed "Bas relief" software has been verified by the results of new diesel CHTZ 4T371 bench testing, see Fig. 5, compared with the experimental data obtained using a special fuel stand, see Fig. 6, and calculated data obtained with use of AVL Fire software, see Fig. 7.



Fig. 5. Diesel engine CHTZ 4T371 on the HORIBA test bench.



Fig. 6. Comparison of the calculated (top) and experimental (bottom) forms of fuel spray.

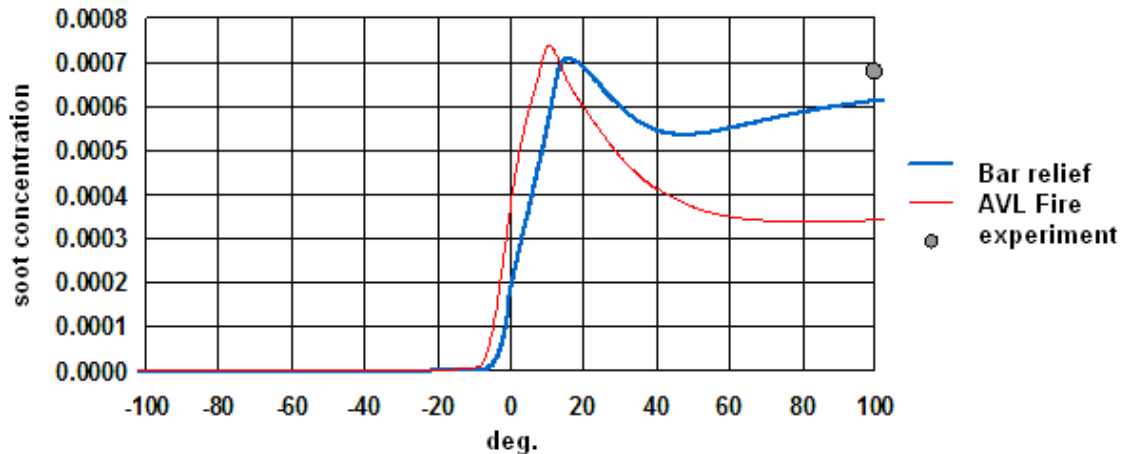


Fig. 7. Mass fraction of soot in the diesel engine CHTZ 4T371 combustion chamber.

"Bas relief" software passed the state registration of copyrights.

"Bas relief" software for calculation and optimization of operating processes in piston engine combustion chamber and fuel system is a single logical unit, which allows to carry out calculations associated impotent diesel engine processes, including fuel supply, injection, spraying, gases movement in the cylinder, fuel evaporation and combustion in the combustion chamber of arbitrary geometry. The value and is unique of "Bas relief" software is a conjugate description of interrelated processes in the diesel engine fuel equipment and cylinder. Using the developed software can significantly reduce the time consuming debugging diesel engine operating processes, help to solve problems engine forcing, fuel consumption and emissions of harmful emissions reducing..

Acknowledgements

This work was performed with methodical and scientific support of AVL List GmbH (Graz, Austria) (Agreement for Use of Simulation Software AVL BOOST, AVL CRUISE, AVL EXCITE and AVL FIRE between SUSU (Chelyabinsk, Russia) and AVL LIST GmbH (Graz, Austria).

References

- [1] Vibe, Brennvlauf und Kreisprozess von Verbrennungsmotoren, VEB-Verlag Technik, Berlin, 1970.
- [2] G. Woschni, A universally applicable equation for the instantaneous heat transfer coefficient in the internal combustion engine. SAE Paper 670931 (1967).
- [3] R.D. Reitz, R. Diwakar, Effect of drop breakup on fuel sprays. SAE Tech. Paper series. 860469 (1986).
- [4] M.A. Patterson, R.D. Reitz, Modeling the Effects of Fuel Spray Characteristics on Diesel Engine Combustion and Emissions, SAE Report No. 980131, SAE International, 1998.
- [5] P.J. O'Rourke, Collective Drop Effect on Vaporizing Liquid Sprays, Ph.D thesis, University of Princeton. (1981).
- [6] N. Nordin Complex chemistry modeling of diesel spraycombustion. Dept. of Thermo and Fluid Dynamics, Chalmers University of Technology, Geoteborg, 2001.
- [7] H Hiroyasu, M Arai, K Naganishi Soot formation and oxidation in diesel engines, SAE paper. 800252 (1980).



International Conference on Industrial Engineering

Variable speed power

Gandzha S.A., Kiessh I.E.*

South Ural State University, 76, Lenin Avenue, Chelyabinsk, 454080, Russian Federation

Abstract

This article shows an application of a double source generator for windmills. It is shown the design and the principle of operation of the electric machine. This machine was modeled with using Solisworks program for creating design and Maxwell program for analyzing of magnet field. The result of modeling is shown too.

© 2015 The Authors. Published by Elsevier Ltd. This is an open access article under the CC BY-NC-ND license (<http://creativecommons.org/licenses/by-nc-nd/4.0/>).

Peer-review under responsibility of the organizing committee of the International Conference on Industrial Engineering (ICIE-2015)

Keywords: brushless electric machine, combine excitation, regulation of magnet flow, electric machine of a double source.

1. Introduction

A common problem encountered with many forms of alternative energy is that the speed of the power source is variable. Windmills are an obvious case, but many other forms of energy produce variable speeds. Flywheel energy storage is the very definition of variable power and variable speed. Small hydropower systems will have variable speeds depending on water flow. Waste gas such as methane from landfills will have variable energy density. Combustion of natural fuels like wood, grass, paper, etc. result in variable amounts of power being produced. Sterling cycle engines operating from different thermal masses will get different amounts of power depending on temperature cycling. Since the power varies a typical conversion system using a prime mover (Internal combustion Engine, turbine, sterling engine etc.) to drive a rotary generator will result in variable speeds.

For a grid connected system variable speed presents a significant problem. The frequency and voltage of the grid is very precisely controlled, a generator that is operating at variable speed normally can not be directly connected to the grid, instead the power must be converted and conditioned to be made acceptable for grid connection. This

* Corresponding author. Tel.: +7-908-812-5819;
E-mail address: gandja_sa@mail.ru

conversion process is expensive in terms of equipment costs, but also in energy cost as there are losses in the conversion process.

For a permanent magnet type alternator, the voltage increases as the speed increases, the frequency of its output also increases. Like the alternator in your automobile, the output of this “wild ac” is usually tamed by converting the out put to direct current (DC), which in the case of the auto is used to charge the battery. This conversion approach works well when the amount of power is relatively small. However we can’t simply connect a battery to the grid, and the grid is where most of the real equipment of the world resides. So an inverter is used to convert the DC power to grid compatible AC power, there is an equipment and an energy cost to these conversions, limiting the economics of this approach to relatively small amounts of power.

For large amounts of power, the standard approach is an AC generator connected to the grid, but that generator is operating at the precise speed, frequency, voltage and phasing necessary to be compatible to the grid. That set of requirements conflicts with the available alternative energy resources; so the authors set about resolving this conflict.

We first started with a design to create a constant voltage over a wide speed range. This was accomplished by using a combination of permanent magnets and electro magnets to create the magnetic fields in the alternator. By using the electro magnets to adjust the magnetic field strength we were able to generate a constant voltage over a broad range of speeds. However because the control is in the low power excitation circuit, we were NOT converting the high power output, thereby avoiding typical power losses in the conversion process. This constant voltage, combined excitation, design was implemented for a battery charging system on diesel powered generator sets. To be clear this constant voltage design is one step toward the solution to an AC grid compatible system.

2. Design and operation principle of a combined excitation constant voltage alternator

The alternator was designed using both permanent magnets and electromagnets to provide the magnetic fields for the primary alternator (fig.1). The use of powerful rare earth magnets reduces the overall size of the unit, while controlling the electro magnets with a low power, low cost, control circuit we were able to maintain a constant output voltage over a wide speed range. In a sense we created an electro dynamic amplifier, where low level signals in the excitation windings become high power outputs in the stator windings of the primary generator [1].

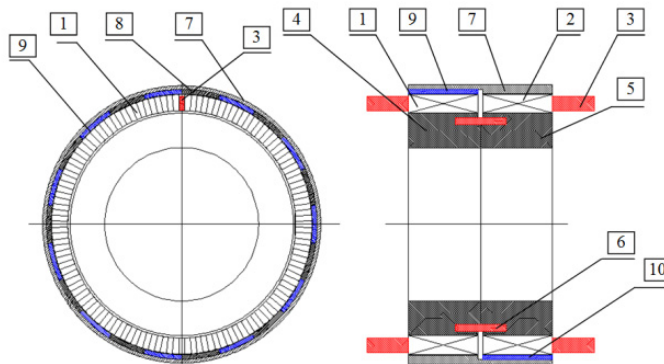


Fig. 1. The cross-section of alternator.

The alternator consists of a stator and a rotor. The stator is comprised of two laminated stacks (1 and 2) The slots in the lam stacks are along the axis. Multi-phase winding (3) is installed in the slots. Laminated stacks are pressed on the laminated core (4 and 5). A stationary excitation winding (6) is located between sections of the laminated core. Rotor (7) of alternator is located outside stator. It has large poles and permanent magnets (8 and 10.) Permanent magnets and poles alternate around the circle. They form two rings over lam stacks (1 and 2.) The rings are located so that the permanent magnet (9) is located opposite the pole (8) in the axial direction. Magnets (9 and 10) have radial magnetization. In one ring the magnets have “south” magnetization (9) on the surface directed to the package, in another ring the “north” magnetization (10.)

Operation:

With DC excitation in winding (6) a magnetic flux is created that follows the magnetic circuit comprised of: laminated stack (1), air gap, large pole(8) of the first ring, back iron of the rotor, large pole (8) of the second ring, air gap, laminated stack (2), section of laminated core(5), section of laminated core (4).

Magnetic flux generated by magnets, is looped by the following way: laminated package (1), air gap, “south” magnet (9), back of rotor, “north” magnet (10), air gap, laminated package (2), part of laminated core (5), part of laminated core (4).

Magnetic fields from the rare earth magnets are increased or decreased by the direction and amplitude of the fields from the electro magnets, the result is the ability to control the output. Voltage over a wide speed range.

Building upon the concepts developed for this constant voltage generator, we found that we could excite the input with a synthesized AC wave, and produce a frequency in the output that could be controlled as needed to be compatible with the grid. Initial experiments used slip ring assemblies and external equipment to produce the PWM synthesized waves. For a practical implementation, we propose a design where the electronics and feedback are incorporated into the rotor assembly. This approach eliminates the brushes and slip rings. However funding is required to complete the development and produce the prototypes.

The stator of the motor generator is of standard construction, with iron laminations and copper coils in a three phase arrangement. These windings are directly tied to the grid.

The rotor is a wound construction with three phase windings. These windings are excited by a typical three phase PWM type drive. When in motor mode, the PWM signals are phased to take power from the grid until the motor gets the flywheel up to speed. During this acceleration ramp, the voltage applied to the motor windings is adjusted to compensate for the BEMF being generated by the motor. When the unit is in generator mode, the phasing is such that power is feeding into the grid, and the PWM drive is maintaining the voltage at a level that is compatible with the grid.

A version of this type alternator has been built and tested as part of a diesel powered generator system. However the unit built only produced a constant voltage. The frequency and phasing functions are at this time theoretical, we believe they are feasible, but a device has not been built and tested.

Why is this different than other approaches? *Note that the power extracted from the flywheel is not being converted in the electronics;* it is being modulated using much lower amounts of current. In effect we have created an electro mechanical amplifier, where the majority of the current is carried in the stator windings, and a much lower current is being controlled by the electronics in the rotor of the alternator.

As with all technologies there is a price to pay: The recovery time of bringing the flywheel back up to speed is going to be significantly longer than the time it takes to extract the power from the flywheel, because the amount of power the electronics can deliver to the rotor is less.

3. Principles of operation

The basic idea is to employ two sources of power to excite a the field windings for an induction type generator, by using this approach brushes are eliminated while the ability to retain a constant voltage output over a wide speed range is accomplished [2,3].

A rotating machine is driven by a prime mover such as a flywheel. There are two sections to this electro dynamic machine. The first section is a standard brushless device with permanent magnets, coils and a rectifier circuit. The purpose of this brushless section is to provide power to the rotor of the alternator without the use of brushes and slip rings. This power is modulated by electronics using a set of coils in the induction alternator to provide the proper voltage, frequency and phasing needed for output directly tied to the grid from the alternator stator. The rotating stator of the alternator is a wire wound rotor of typical construction for motors or generators, but it incorporates some mechanical changes to the laminations to accommodate the frequency shifts needed.

In effect we create an electro mechanical amplifier, where the low power excitation wave generated by the electronics gets a large power increase as the result of the electro dynamic functions of the rotating alternator. This allows the large currents from the stator windings to be directly fed into the grid, without conversion, thereby avoiding power losses in the electronics. This results in both a cost and efficiency savings.

To accomplish field excitation the permanent magnet alternator provides initial power to the primary alternator field winding, the rotation of the machine creates a larger voltage in the primary alternator stator windings. Some of this output power is fed back into the permanent magnet alternator field coils to create the desired voltage.

A portion of the excitation voltage comes from coils moving past the permanent magnets of the excitation generator, in addition there is a set of electro magnets, that are have controlled currents to increase or decrease the magnetic field as a means of providing a controlled excitation voltage to the primary alternator. Sensors detect rotational speed to allow control of the output voltage.

The electronic controls(fig.2) imbedded into the rotor assembly, provide voltage, frequency and phase shifting so that the output of the primary alternator can be matched the grid, or the unit can operate as a stand alone. Since the excitation wave is adjustable, the speed of rotation can change, yet the power output remains at a fixed frequency and voltage.

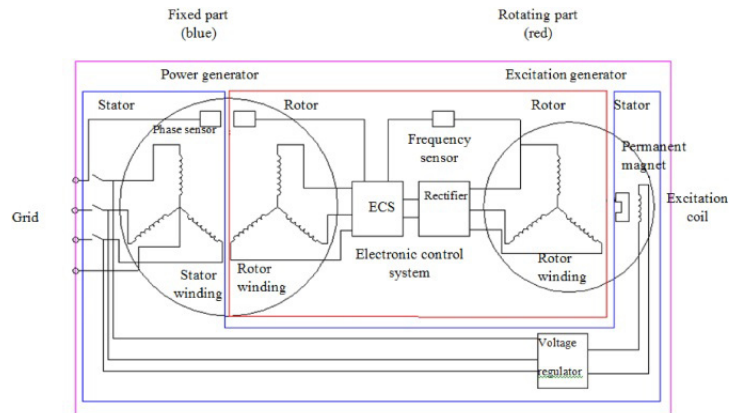


Fig. 2. Electronic control system.

The proposed structure (fig.3) is a stack of flywheel disks, each with their own magnetic support rings. These flywheels may be on a common shaft which drives a large motor generator or there can be a set of parallel axial gap units. It may be desirable to develop both approaches as there will be different markets for different capacity machines.

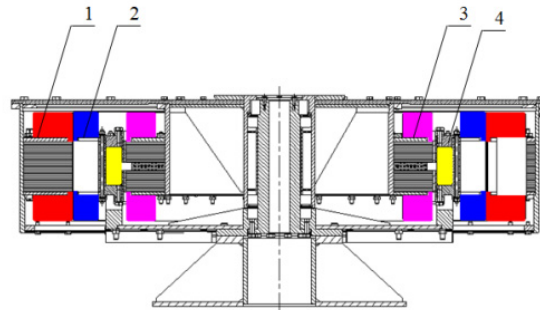


Fig. 3. The assembly of high power generator and excitation generator (1. Rotor of high power generator, 2. Stator of high power generator, 3. Rotor of excitation generator, 4. Stator of excitation generator).

The input to either type motor is 3 phase power from the grid, and output power will be three phase power to the grid. It is very likely that the local utility will require an isolation transformer so we have flexibility in selecting the operating voltages, but we will be constrained by the physical size of conductors. Selection of unit size is going to be a complex exercise as it is difficult to estimate costs without a design and a significant amount of the cost is the design.

Conclusion

Since there are multiple technologies and multiple approaches that can be applied to this technical problem, the authors are confident that technical solutions can be found and implemented. It will only be after a significant amount of the design has been accomplished that it will be possible to do a cost analysis that is anything more than educated guesses.

References

- [1] S.A. Gandzha, A.V. Erlisheva, Starter-generator dly avtonomnih istochnikov pitaniy, *Vestnik uzhno-uralskogo gosudarstvennogo universiteta. Seria "Energetika"*. 6(9) (2005) 84–86.
- [2] S.A. Gandzha, *Primenenie acinchronisirovanih sinhronih generatorov dly vetroenergeticheskikh ustanovok*, ELMASH-2009, *Electroenergetika I electrotehnika. Problemi i perspektivi. Trudi simposiuma.1* (2009) 168–170.
- [3] S.A. Gandzha, R.L. Halstead, Optimal design of brushless axial gap electric machines for low power windmills, *Design World (engineering solution for product manufactures)*. 1 (2012). www.designworldonline.com.



International Conference on Industrial Engineering

Common dateware mechatronic with resolver-to-digital converter

Smirnov Y.S.^a, Safronov V.V.^b, Anisimov Y.O.^{a*}

^a South Ural State University, 76, Lenin Avenue, Chelyabinsk, 454080, Russian Federation

^b Research Institute of Precision Instruments, 51, Dekabristov str., Moscow, 127490, Russian Federation

Abstract

The evolution of mechatronics indicates that Technical Cybernetics (TC) was its progenitor, the parent science of informatics that at the present stage of human development has ensured the transition from an industrial to an information society, information (IT) and cognitive technologies (CT). However, we should recognize that the IT and CT, as catalysts for development and progress, represent only a shell, which acquires the substantive content when solving specific practical problems. In engineering practice, the MS act as such filling, defining the image of the technosphere of the 21st century [1]. A similar example is Common Dateware (CDW) [2] that translates the kinetic energy of an operating mechanism (OM) movement in mechatronics through the Resolvers-to-Digital Converters (RDC) [3], in which the output orthogonal signal resolvers are converted into an analog or digital equivalent of movement, realizing the connection between space and time [4].

© 2015 Published by Elsevier Ltd. This is an open access article under the CC BY-NC-ND license (<http://creativecommons.org/licenses/by-nc-nd/4.0/>).

Peer-review under responsibility of the organizing committee of the International Conference on Industrial Engineering (ICIE-2015)

Keywords: Technical Cybernetics; Information and Cognitive Technologies; Mechatronics; Translating; Kind of Energy; Converting; Digital Equivalent of Displacement

1. Application areas and effectiveness of mechatronics

Outlining in 1954 a new paradigm forecast of TC N.Wiener drew attention to the fact that the computers will be actively used for direct control of the OM [5–7]. This required improving the electromechanics based on electronics, which led to the formation of the term «MECHATRONICS». It is a neologism of the words "Mechanics and Electronics", proposed by the Japanese engineer Tetsuro Moria in 1969.

* Corresponding author. Tel.: +7-904-948-1048.
E-mail address: sys1940@mail.ru

The term «MECHATRONICS» registered as a trademark in 1972 by Yaskawa Electronic (Japan), which is considered one of the world leaders in the development of contactless electric machines with permanent magnets (CMPM) [8]. S. Yaskawa confirms development effectiveness of mechatronics in the XX century, he said in the report "Future Trend in Intelligent Mechatronics Systems" at the Seventh Mechatronics Forum, Sept. 2000 in Atlanta, USA: **"This concept increased productivity in industries such as automotive, computers, communications equipment and enabled global development. This led to the efficiency of mass production. It was focused on material gain. Now we need to take at our disposal the concept of the environment - the full life cycle and "shake off the dust" – our business. As we move from the era of the "closed balanced society" to "open an unbalanced society", management and global standardization are required"**.

These recommendations are relevant to the South Ural region, where it was possible to “shake off the dust” carefully and to give sufficient attention to the improvement of innovations aimed to improve the radiological situation. From this perspective, radiation-resistant MS for robotic vehicles for elimination of consequences of incidents and accidents at the nuclear industries (NI) are of interest [5, 6].

During relatively short existence of mechatronics it has penetrated all spheres of human activity. In industrialized countries mechatronics is a priority for the development of science and technology, determining the level of production, product competitiveness, quality of life, the defense capability and security of the nation. Mechatronics is a vivid example of the impressive results of interdisciplinary cooperation. Besides, mechatronics achievements have the greatest application in mechanical engineering and instrument making, machine tool construction and automotive industry, robotics, aerospace, medical, office and home appliances. The logo shown in Fig. 1a illustrates the application areas. MS for transport engineering and high-rise buildings lifts [9], which significantly increases energy efficiency by energy recovery during coasting, should be noted as the innovative applications.

The actual formation of mechatronics coincides with the withering in the 70s of the last century of TC and with the dawn in the 80's "informatics", which is a neologism of the words "information" and "automatics", introduced in France.

2. Structural Electronization of Mechatronics

Structure of Mechatronics can be presented in the form of the logo (Fig. 1b), reflecting its functions, taking into account the above neologisms, and corresponding the supplementing [4] definition: **"Mechatronics is a computer paradigm of TC, that provides the translating the energy type between mechanics and electronics by converting information through automation"**.

The main feature of the MS structure is the presence of electromechanical (EMC) and automated information (AIC) components carrying, respectively, energy type converting and information forms conversion. Selecting CMPM justified not only by its broad functionality, but also its energy efficiency, contactless, controllability and the ability to eliminate gear which have been used in the electric drive (ED) for over 200 years. The presence of the gear in EMC prevents the establishment of precision MS due to backlash, which, according to the criterion of Miller, doubles the dynamic error. In practice, in continuous operation it is difficult to ensure the gear backlash less than 5' due to wear gearwheels [7, 10].

Electronization, the consequence of which is to increase the effectiveness of the MS, achieved in gearless electricomechatronic system (GEMS), which implemented on the basis of CMPM. Its effectiveness, in turn, is largely dependent on the level and extent of dataware (DW), structural and algorithmic features of GEMS, which are determined by quantitative and qualitative indicators of the DW [11]. Therefore, the choice of the DW structure is an actual problem that typically contains primary measuring sensor (PMS), directly related to the OM and the CMPM rotor. In this respect the advanced design version of the EMC proposed by Danaher Motion and shown in cross section in Fig. 1c is a demonstrative variant [12]. The unit contains a CMPM, in which *resolvers* and clamping sleeve for interfacing with the OM are integrated.



Fig. 1. (a) logo of mechatronics application areas; (b) logo of Mechatronics; (c) EMC

3. Common Dateware of Mechatronic Systems

The equivalents of "authorized" $A_{s\theta}$ and $A_{c\theta}$ signals [8] determining the actual position of the rotor relative to its stator are needed for switching CPM. For analog control the rotor position sensors (RPS) are used based on *reduktosin*, which is a kind of contactless *resolvers*, in which the number of pole pairs coincides with CPM.

Restructuring MS, change of control algorithms of CPM and transformation of displacement components occur as a result of evaluation by the ring transformer (RT) set and actual values of displacement components. Topical question is the question of choosing a device that provides an information exchange between EMC and AIC in MS having high functionality in terms of sustainability, accuracy and high-speed performance. The TC principles for this purpose provide the application of feedback loops [11], representing the analog or digital equivalent of displacement components. For their synthesis one can use special RDC [13], chips with an average degree of integration [14] and digital signal processors (DSP) in conjunction with the ADC and DAC. With the help of the DSP you can compensate the low-frequency drift, stray amplitude modulation and phase shifts of the convertible signals [8].

To suppress the quantization noise is advisable to use tracking converter *resolver* outputs [14], which are referred abroad RDC [3]. They are closed tracking systems with second order astatism, which is in the process of converting the output signals of *resolver* allows sequentially synthesize the analog equivalent of, respectively, the acceleration ε and velocity Ω by analog integration. Subsequent analog-to-digital integration allows synthesizing a digital value equivalent Φ_{θ} of displacement in absolute binary code which changes continuously. Self-organizing design of RDC [14] allows improving the dynamic indicates of conversion under rapidly changing inputs. This eliminates the main drawback inherent to foreign RDC analogues [3]. The recommendations set out in [15] help to improve utilization in mechatronics. High-speed ADCs are used to digitize analog equivalents of velocity Ω and acceleration ε . In the application for the conversion of the microcontroller (MC) digitization is performed by integrated ADC.

The operations necessary to form all components of the common dateware (CDW) to the MS with various embodiments of the PMS are shown in the table 1.

4. Common Dateware Primary Measuring Sensor

Among the PMS, based on the converting of electric power, dynamoelectric *resolvers* are most widely used. They are produced with windings on the stator and rotor. There are *resolvers* without windings toothed rotor (Fig. 2a), which is called the *vernernym resolver* [16] or *reduktosin*. Contactless *resolver* contains a ring transformer (RT) (Fig. 2b) for transmitting to the rotor excitation, which frequency is 0.4 ... 10 kHz. Contactless induction phase shifter type BIF are used (Fig. 2c) when operating at frequencies of 1.5 ... 350 kHz [13-15].

The practice uses of *resolvers* showed that the most effective in terms of improving the accuracy are two reporting PMS with mechanical (see. Fig. 2c) or rather with an electrical reduction. Its principle lies in the fact that

for a small rotation angle of input axis PMS amplitude or phase of the output signal changes for one period, and when turning the rotor at 360° the number of periods is equal to the velocity ratio of the electric reduction (VRER). Multi-pole *resolvers*, *reduktosins* and *inductosyns* are widespread in practice. The conversion error of the PMS is reduced by a factor equal to VRER. Furthermore, there is a weakening influence their technological and manufacturing errors, including irregularities in the air gap [14].

Table 1. Variants of CDW in MS with various PMS.

$\frac{N_\theta}{\pi/\pi}$	The type of primary measuring sensor	The displacement components on the PMS outputs	The operations necessary for the formation of the remaining components of the CDW
1	Coder	Position Gray $N_{\theta G}$ or Barker $N_{\theta B}$ code	Conversion to a binary code Φ_θ and double differentiation for getting Φ_Ω , Φ_v ; generation of $A_{S\theta}$ and $A_{C\theta}$ in the MC or DSP
2	Incremental sensor (IS)	Unitarian code N_θ , marker N_0 at $\theta = 0$	
3	Elektromashina sine-cosine resolver (ESCR)	Analog orthogonal displacement components $U_{S\theta}$ and $U_{C\theta}$	Conversion Φ_θ , Φ_Ω , Φ_v , $A_{S\theta}$ and $A_{C\theta}$ by RDC and ADC
4	Optical absolute encoder (OAE)		Conversion Φ_θ , Φ_Ω , Φ_v , $A_{S\theta}$ and $A_{C\theta}$ y ADC and DSP
5	The detector of the magnetic field (DMF)	Binary Codes Φ_θ , $\Phi_{S\theta}$ and $\Phi_{C\theta}$	Conversion $\Phi_{S\theta}$ and $\Phi_{C\theta}$ DAC in $U_{S\theta}$, $U_{C\theta}$; generation Φ_Ω , Φ_v , $A_{S\theta}$ and $A_{C\theta}$ in DSP or MC

5. Common Dateware Primary Measuring Sensor

Among the PMS, based on the converting of electric power, dynamoelectric *resolvers* are most widely used. They are produced with windings on the stator and rotor. There are *resolvers* without windings toothed rotor (Fig. 2a), which is called the *vernernym resolver* [16] or *reduktosin*. Contactless *resolver* contains a ring transformer (RT) (Fig. 2b) for transmitting to the rotor excitation, which frequency is 0.4 ... 10 kHz. Contactless induction phase shifter type BIF are used (Fig. 2c) when operating at frequencies of 1.5 ... 350 kHz [13-15].

The practice uses of *resolvers* showed that the most effective in terms of improving the accuracy are two reporting PMS with mechanical (see. Fig. 2c) or rather with an electrical reduction. Its principle lies in the fact that for a small rotation angle of input axis PMS amplitude or phase of the output signal changes for one period, and when turning the rotor at 360° the number of periods is equal to the velocity ratio of the electric reduction (VRER). Multi-pole *resolvers*, *reduktosins* and *inductosyns* are widespread in practice. The conversion error of the PMS is reduced by a factor equal to VRER. Furthermore, there is a weakening influence their technological and manufacturing errors, including irregularities in the air gap [14].

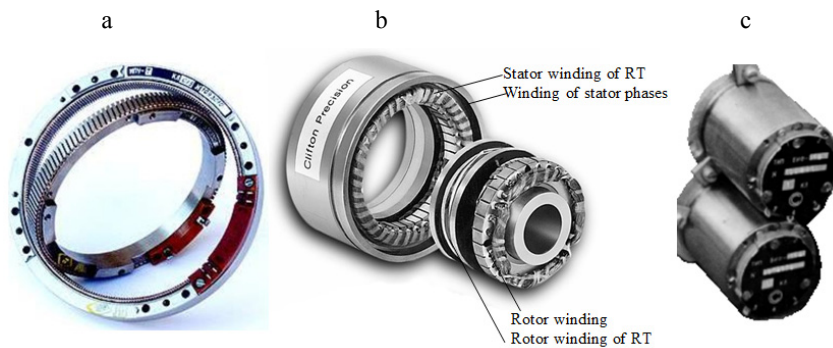


Fig. 2. (a) contactless *reduktosin*; (b) *resolvers*; (c) *phase shifte*

Unlike *reduktosins* (see. Fig. 2a) from *resolvers* (see. Fig. 2b) is that both the primary and two phases of secondary windings located in the stator slots and the rotor is a gearwheel. The ratio between the numbers of teeth of the stator and rotor may be any. The main advantage of *reduktosin* is its contactless. At high rotor speeds of *reduktosin* it becomes possible to use its output signals, the amplitude of which depends on the rotor speed, for tachometry. However, the attenuation of the *reduktosin* output signal at more than multipolar *resolvers*, and in a small area of the stator slot can reach 40. Thus the slope of the tachometer signal is 1 mV/rpm that hinders the formation of a digital equivalent of velocity at low speeds of GEMS [11].

Electronization of PMS led to the creation *inductosyns* whose rotor and stator are discs of isolated (non-conductive) material, arranged coaxially and in parallel at a short distance from each other. Two primary multipole windings and one secondary winding are applied to the discs lithographically. The current powering with a frequency of 2 ... 20 kHz is produced by the method of pulsing or rotating field. The first mode is the amplitude, and the second is phase. Output signals not intended for broadcast over large distances [17].

All kinds of *resolvers* can determine the angle within one pole pitch. To increase the range of conversion one can use two samples or a device that allows you to record the number of pole pitches, fixing zero-crossing of accurate reading signal.

6. Application Features of the PD in Precision Mechatronics Systems

Precision MS requires using PMS with the error less than 20". Their maximum tracking speeds at a resolution of 16 bits reach 1000 rpm and the tracking error of $\pm 2^{\pm 1}$ LSB, which corresponds to ± 7 LSB at a resolution of 16 bits. The most effective method of *resolver's* error compensation is the calibration that was used originally and in the first sample it is allowed to reduce the error from $\pm 50''$ up to $\pm 10''$ [17]. Over the past 60 years it is managed to bring the error to 1" [18]. The resolution 1.5" is attainable for RDC with electric reduction and 14-bit ADC under cyclic arctangent converting [13].

However, because of the PMS error high resolution of conversion does not provide high accuracy. Therefore, the implementation of precision GEMS used structural and algorithmic methods providing for increasing the resolution, repeatability and, in fact, accuracy [16]. As the RDC inferior absolute encoder in high-speed performance and accuracy, they can be used to check the error e_r , which is shown in Fig. 3a. Her character makes it possible to use the Fourier series. Fig. 3b shows the error curve, which decrease on the order after the injection of correction [8].

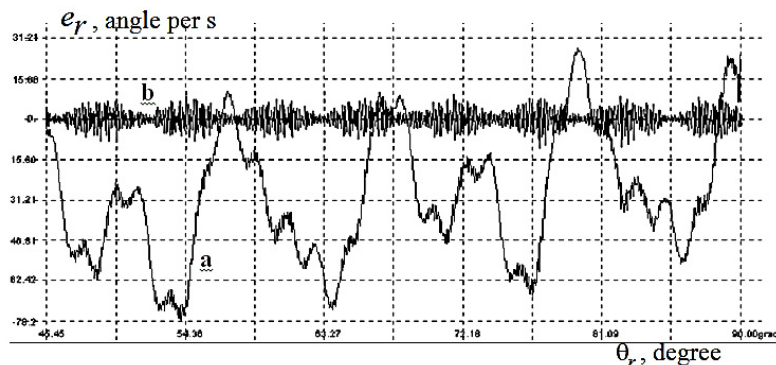


Fig. 3.(a) error curves before correction; (b) error curves after correction

7. Summary and Conclusions

Creating precision positioning devices, which began in the XX century [16], is obliged not to success in creating digital and discrete PMS. It is obliged to continuous improvement of *resolvers* that till now surpass coders and IS in terms of accuracy, resolution, high-speed performance, resistance to external factors, reliability, cost and efficiency of signal processing algorithms.

A common drawback of multi-pole *resolvers* and *reduktosins* is the difficulty of placing multiple windings that significantly increases the complexity of manufacturing contactless electromechanical PMS. Their increased cost is not conducive to widespread use, but their use is justified by the need to obtain a long service life, high reliability and resistance to external influences.

There is an important ability of radiation-resistant *resolvers* to generate output two reporting signals, which parameters allow for interference-free transmission in the phase or amplitude modes, respectively, 3 or 5-wire cable interface from the EMC, located together with the OM in the area of increased radiation, to the distance providing reduction of radiation to values that allow the operation of microelectronics in the MEC. Digital information about the displacement components, formed in the AIC and necessary for controlling the energy converting, returns to the EMC through power circuits. This simplifies the robotization of vehicles operating at high levels of radiation [11].

Attempts to produce complete replacement *resolvers* code sensors did not give the desired effect because of the high cost of manufacturing the code sensors and complexities associated with the transfer of multi-bit digital equivalents of movement required to obtain components of the velocity and acceleration of operations of differentiation in digital processor with extremely high speed and noise immunity in MC.

The application of IS fit into the concept of using a serial interface. This version of the PMS not solved the problem of the dynamics and noise immunity of the formation of velocity and acceleration components. As a further disadvantage, it has a real possibility of data loss during transmission and lack of its self-healing after a power failure. "Sensorless" variants of dateware [19] accumulate these shortcomings of coders and IS. Getting information about the displacement with the help of indirect methods using models of electromechatronic converter can be carried out only approximately, because in most cases on the basis of modern microprocessor only simplified dynamic models of electromechatronic converter can be implemented [20].

High functionality and efficiency make *resolvers* and absolute encoders leaders of PMS mechatronics. They complement each other. The first exhibits higher rates of stability when operating in harsh operating conditions and the second has smaller error. The prospect of format of output orthogonal signals of RDC and OAE is confirmed by successful convergence of nanotechnology in mechatronics. The result of innovation was the emergence of DMF encoders having a space-time communication. Their orthogonal output signals are generated by the induction of the permanent magnet performing the functions of the PMS using Hall-effect or the anisotropic giant tunnel magnetoresonance. Unlike ESCR based on the principle of electro-mechanical energy conversion DMF do not require powering and they are general type sensors. They are not used in the phase format [21]. They do not apply the modulation-demodulation of signals.

References

- [1] E.D. Teryaev, N.B. Filimonov, K.V. Petrin, *Mechatronics as a computer paradigm of development of technical cybernetics*, *Mechatronics, Automation, Control*. 6 (2009) 2–10.
- [2] Y.S. Smirnov, *Common Dateware of Robotics Mechatronic Converters*, *Proc. of the Third ISMCR'93, Italy, Torino*. (1993) 13–18.
- [3] Information on <http://www.analog.com>
- [4] Science. *The great theory*, Issue 1: *The space – it's a matter of time*. Einstein. *Theory of relativity*, De Agostini Publishing, Moscow, 2015.
- [5] Y.S. Smirnov, I.V. Voinov, A.V. Choundeev, *Information technologies and robotics for radioecological training of Agro-Engineers*, 5th Conference on environmental education, Zurich, Switzerland, April, 1999.
- [6] Y.S. Smirnov, *Robototechnical complexes for radioactive accidents aftermath removal*, *Book of abstracts VIII International Symposium «Ural Atomic, Ural Industrial»*. Yekaterinburg. (2000) 37–40.
- [7] A.G. Mikerov, V.V. Djankhotov, *Developing in walking robot servodrives with PMSM*, *Proc. of the International symposium on industrial electronics ISIE 2006*, July 9-13, Montreal, Canada. (2006) 2128–2133.
- [8] A. P. Balkovoy, V.K. Tsatsenkin, *Precision electric drive with brushless motor*, ID MEI, Moscow, 2010.
- [9] A.V. Solovov, *Gearless drive. The eternal pursuit of excellence*, *Equipment. Developments. Technologies*. 5 (2007) 63–64.
- [10] A.G. Mikerov, *Brushless BC torque motors quality Level Indexes for Servo Drive application*, *Proceedings of International Conference JEEE Eurocon 2009*, St. Petersburg, Russia. (2009) 71–79.
- [11] Y.S. Smirnov, *Electromechatronic converters: monograph*, SUSU Publishing, Chelyabinsk, 2013.
- [12] F. Bartos, *High-torque brushless permanent magnet motors*, *Control Engineering Russia*, 2007.
- [13] A.P. Balkovoi, E. Kallenbach, *A low cost RDC*, *Proc. of the 49th International Scientific Colloquium*, Technical University of Ilmenau. (2004) 338–342.
- [14] V.G. Domrachev, V.R. Matveevskiy, Y.S. Smirnov, *Circuitry digital converters movements*, *Energoatomizdat Publishing*, Moscow, 1987.

- [15] V.V. Safronov, Theory and practice using of the encoders based on sine-cosine rotary transformer, *Components and Technologies*, no. 4, 2014, pp. 58–62 (in Russian).
- [16] G. Cronacher, Design, performance and application of the vernier resolver, *The Bell System Technical Journal*, Issue XXXVI, vol. 6, 1957.
- [17] S.A. Vorotnicov, *Robotic systems information devices*, BMSTU Publishing, Moscow, 2005 (in Russian).
- [18] *Torque Motors and Inductive Angle Sensors for Precision Electric Drives and Digital Gearless Tracking Systems*, Catalog SRC of the RF «CSRI Elektropribor», 2002 (in Russian).
- [19] P. Vas, *Sensorless vector and Direct torque control*, Oxford University Press, 1998.
- [20] Y.S. Smirnov, T.A. Kozina, P.B. Serebryakov, Analog-to-digital converters of displacement components based on electromechanical transducers, Vol. 56, Issue 9, 2013, pp. 1026–1030.
- [21] Y.S. Smirnov, T.A. Kozina, E.V. Yurasova, A.V. Sokolov, Analog-to-digital converters of the components of a displacement with the use of microelectronic sine-cosine magnetic encoders, *Measurement Techniques*, Vol. 57, Issue 1, 2014, pp. 41–46.



International Conference on Industrial Engineering

A 6(10) kV cable section reliability assessment model including power distribution network configurations and relay protection circuits

Korzhov A.V.*

South Ural State University, 76, Lenin Avenue, Chelyabinsk, 454080, Russian Federation

Abstract

Urban power distribution network reliability depends on the resource of 6 (10) kV cables, which are its longest element. In the context of long-term operation of the distribution network, it is necessary to know when the cable network must be renewed to avoid damage, with due account of network configurations and regimes. The relevance of retrospective analysis and developing forecast methods is pointed out in the reliability concepts of the electricity industry. A number of statistical models are known. However, the reliability indicators of their operation in the distribution network must be assessed comprehensively to improve the functioning of the existing cable network, taking into account their conditions, network configuration, and relay protection circuits. A model based on the Monte-Carlo method has developed in the LabVIEW software environment so as to estimate the probability of no-failure operation of an urban area cable section, and/or to identify renovations required to reduce the failure rate. The model permits testing different combinations of the failure rate parameters, thus producing "rich" statistical material. Cable line failure rates and urban distribution network configurations are obtained via retrospective analysis. The developed model can be applied to such cable networks.

© 2015 The Authors. Published by Elsevier Ltd. This is an open access article under the CC BY-NC-ND license (<http://creativecommons.org/licenses/by-nc-nd/4.0/>).

Peer-review under responsibility of the organizing committee of the International Conference on Industrial Engineering (ICIE-2015)

Keywords: reliability, power distribution network, power cable, insulation

* Corresponding author. Tel.: +7-922-230-61-03; fax: 8-351-267-92-46.
E-mail address: abk1978@mail.ru

1. Introduction

As the urban distribution networks develop, maintaining operational reliability and optimization of 6 (10) kV cable lines (CL) operation depending on the efficiency and resource conservation criteria becomes a challenge. Our case study of common urban networks schemes (of two cities) shows that the insulation conditions of CL have an impact on each other. This fact is due to the specific configuration of a distribution network and to the location of relay protection and automation devices that act on the head feeder circuit breakers (entire network connected to the switch 2, Fig. 1 (a)) [1,2]. An example of estimation of no-failure operation of a CL with impregnated paper insulation in the circuit of a distribution network feeder is shown in Fig. 1 (b).

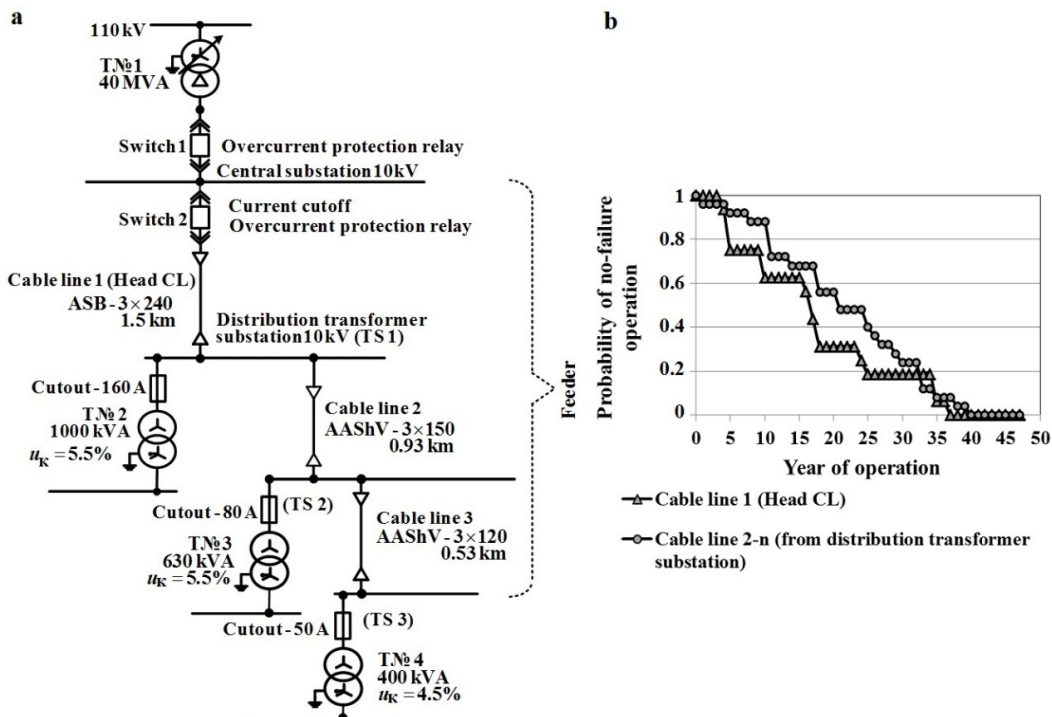


Fig. 1. (a) Example of a distribution network feeder section; (b) Estimation of no-failure operation of a CL in a feeder circuit.

Existing standards of reliability assessment in the Russian Federation and the IEC mandate using several methods: those based on the reference data; according to the reliability of analogues; based on the materials' properties data, available at the time of the calculation; that include forecasting methods; structural methods of calculation; physical methods (experiments) [3,4].

It should be noted that classical methods of calculation of reliability indicators of a feeder with many connected CL (analytical and table-logic method) are hardly applicable in most cases. The first method involves the construction of block diagrams consisting of n interconnected elements, each of which can be in two states – operation or failure. The disadvantage of this method is that cumbersome calculations are unavoidable every time the network configuration is changed (accidents, routine switching, etc.). The number of such configurations in a real network can be high. Table-logic method has similar drawbacks. Thus, these methods do not have the required flexibility when the network configuration is changed. This entails excessive use of computer resources.

Regulatory documents allow the development of calculation methods of reliability indicators for certain objects (identified weak links) that solve various optimization problems, where the reliability indicators serve as objective functions, control parameters or boundary conditions.

Reliability of a CL in a distribution network, taking into account redundancy and relay protection, can be calculated by a program that takes into account the regulatory documents and retrospective analysis of CL operating data.

Several models that estimate reliability and predict damage rate of a CL have already been proposed: statistical models; neural network based model; model using technocenosis approach; probabilistic and statistical approach [5-16]. It is stated in [17] that preliminary cable line data acquisition is necessary for the CL insulation conditions assessment. Otherwise, the data may be misinterpreted. In [18] the existence of several dominant failure processes in cable networks is pointed out. So in addition to the partial discharge analysis, a dielectric analysis should be conducted to determine the actual conditions, taking into account the age of the CL.

2. 2. Virtual model of damage and reliability assessment of a "6(10) kV cable line - distribution network diagram" unit

For the probabilistic estimation of the damage caused by energy curtailment, of the probability of failure-free operation of the feeder consisting of several CL, as well as the estimation of the main reliability indicators (failure rate; mean time to repair, mean time to failure; total number of failures during CL lifetime, steady-state availability; forced outage rate) a model and a program was developed in LabVIEW software environment (S/N: M62X10849) (programming language G). The model provides ability to assess the damage and reliability of the unit "6(10) kV CL – distribution network diagram" using the Monte Carlo method and taking into account the analysis of the CL failure probability and the experiment planning theory. Figure 2 shows the program module that implements the algorithm for a section consisting of 3 CL. For a bigger number of CL in the network the structure of the program and basic modules are identical.

The program consists of several interconnected modules:

- Cable line parameters input module. The following historical operating data is entered: failure rate during three periods (early failure period, operational period, intensive aging period); average time of power supply interruption and damage caused by energy curtailment due to cable insulation breakdown. To account for the circuit connections, distribution network configuration and relay protections criteria are introduced.
- Main calculation module. A random process is generated using Monte-Carlo method, based on historical data and taking into account reliability and possible damage caused by CL failure and the experiment planning theory. Elements from 12 to 20, Fig. 2, generate the random process.
- Result output module.

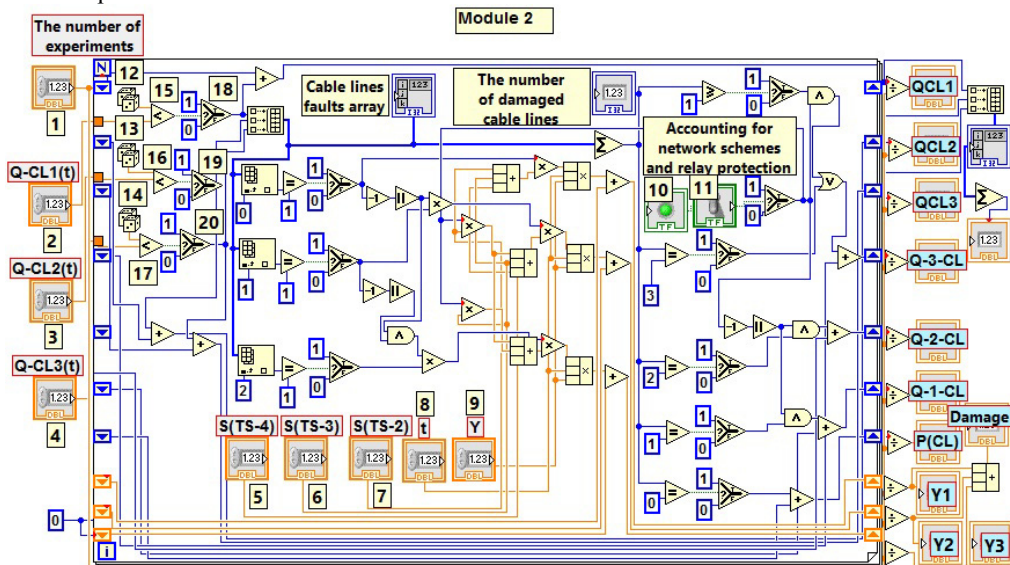


Fig. 2. Diagram of the reliability assessment program of a network section consisting of 3 CL.

3. Sample testing of the virtual model

The program is used when the process is repeated to obtain a representative statistical data that can be analyzed, for example, using the experiment planning theory.

Preliminary studies show that the feeder uptime and possible damage caused by energy curtailment depend nonlinearly on the failure rates of the feeder cable lines (determined by their age, length, operating conditions, insulation conditions) [15-16]. Therefore, according to the mathematical modeling theory, a second order regression equation should be used, and the experiments should be carried out according to the second order plan (Table 1), using a vector representation of variable factors (Fig. 3) [19-20].

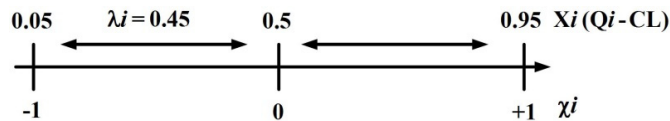


Fig. 3. Vector representation of factors (failure probability of a CL).

In a virtual experiment cable lines with failure probability (Q_1, Q_2, Q_3) of 0.05; 0.5 and 0.95 were used. This was necessary to provide all possible combinations in the experiment matrix (Table 1) that corresponds to the selected second order plan, each experiment was repeated three times. The order of 45 experiments was randomized. Randomization is necessary for a uniform distribution of inaccuracy, it was carried out using a random number generator. Number of realization of experiments is presented in the 2nd column of the Table 1. The experimental results are also presented in Table 1.

The following input data was used for the analysis of the circuit configuration shown in Fig. 1 (a): average statistical downtime 1.2 hours; damage from energy curtailment $Y=1$ c.u. per 1 kWh; number of experiments is equal to the number of hours in one year: 8760 hours. The failure probability parameters are those shown in Fig. 3, with the gradation required for the experiment matrix. It is assumed that the failure of one of CL causes immediate automatic tripping of the whole feeder. If the circuit configuration has redundancy, it is accepted that the breakdown of CL №1 the feeder is disconnected during routine switching, breakdown of CL №2 disconnects transformer substations TS 2 and 3, and breakdown of CL №3 disconnects only transformer substation TS 3.

Table 1. The matrix and virtual experiment results (for a circuit with 3 CL and no redundancy).

Experiment №	Realization №	X1		X2		X3		Y _i – damage			Average value, \bar{Y}	Calculated value, Y
		Phys.	Code.	Phys.	Code.	Phys.	Code.	Y ₁	Y ₂	Y ₃		
1	17, 28, 7	0.05	-1	0.05	-1	0.05	-1	202	204	201	202	258
2	3, 40, 32	0.95	1	0.05	-1	0.05	-1	2321	2312	2308	2314	2284
3	31, 23, 14	0.05	-1	0.95	1	0.05	-1	1246	1240	1236	1241	1210
4	8, 18, 43	0.95	1	0.95	1	0.05	-1	2371	2375	2374	2373	2429
5	27, 12, 30	0.05	-1	0.05	-1	0.95	1	584	599	590	591	561
6	24, 6, 37	0.95	1	0.05	-1	0.95	1	2347	2344	2332	2341	2397
7	33, 2, 29	0.05	-1	0.95	1	0.95	1	1263	1257	1259	1260	1315
8	42, 22, 16	0.95	1	0.95	1	0.95	1	2374	2378	2373	2375	2345
9	26, 5, 38	0.05	-1	0.5	0	0.5	0	824	820	830	825	826
10	13, 15, 21	0.95	1	0.5	0	0.5	0	2356	2353	2358	2356	2354
11	36, 4, 19	0.5	0	0.05	-1	0.5	0	1355	1374	1376	1368	1367
12	1, 34, 9	0.5	0	0.95	1	0.5	0	1810	1818	1816	1815	1816
13	45, 10, 25	0.5	0	0.5	0	0.05	-1	1532	1526	1525	1528	1527
14	20, 44, 35	0.5	0	0.5	0	0.95	1	1645	1627	1636	1636	1636
15	11, 39, 41	0.5	0	0.5	0	0.5	0	1576	1598	1603	1592	1582

The coefficients of the regression equation were calculated using L-matrix that corresponds to the experiment matrix [20]. The second order regression equation $Y = f(Q1, Q2, Q3)$, taking into account accounting the feeder configuration and relay protection with redundancy, is as follows:

$$Y = 1581.9 + 764 \cdot \frac{Q1 - 0.5}{0.45} + 224.7 \cdot \frac{Q2 - 0.5}{0.45} + 54.5 \cdot \frac{Q3 - 0.5}{0.45} + 8.3 \cdot \left[\frac{Q1 - 0.5}{0.45} \right]^2 - 201.7 \cdot \frac{Q1 - 0.5}{0.45} \cdot \frac{Q2 - 0.5}{0.45} - 47.3 \cdot \frac{Q1 - 0.5}{0.45} \cdot \frac{Q3 - 0.5}{0.45} + 9.6 \cdot \left[\frac{Q2 - 0.5}{0.45} \right]^2 - 49.4 \cdot \frac{Q2 - 0.5}{0.45} \cdot \frac{Q3 - 0.5}{0.45} - 0.03 \cdot \left[\frac{Q3 - 0.5}{0.45} \right]^2$$

Where, Y is the damage, Q1, Q2, Q3 is the probability of failure cable line 1, 2, 3.

Table 2 shows an example of assessing the impact of the renovation of cable lines on the cable section failure probability. In Table 2 the probability of failure of three CL (QCL№1, QCL№2, QCL№3) is taken as a source of historical data, and the results of the calculation are the probability of failure of one (Q-1-CL), two (Q-2-CL) or three CL simultaneously (Q-3-CL), the probability of failure of the whole feeder (Q feeder) and damage (Y, c.u.).

Table 2. An example of assessment of a virtual experiment results.

	1 historical situation				2 historical situation (CL №2 renovated)			
Configuration and redundancy taken into account	QCL№1	QCL№2	QCL№3	Y, (c.u.)	QCL№1	QCL№2	QCL№3	Y, (c.u.)
	0.29	0.51	0.48		0.29	0.01	0.48	878
	Q-1-CL	Q-2-CL	Q-3-CL	1236	Q-1-CL	Q-2-CL	Q-3-CL	Effect, %
Configuration taken into account	0.43	0.32	0.07		0.49	0.14	0.001	29
	QCL№1	QCL№2	QCL№3	Y, (c.u.)	QCL№1	QCL№2	QCL№3	Y, (c.u.)
	0.29	0.51	0.48	1987	0.29	0.01	0.48	1538
	Q feeder			Q feeder			Effect, (%)	
	0.82			0.63			23	
	3 historical situation (CL №3 renovated)				4 historical situation (CL №1 renovated)			
Configuration and redundancy taken into account	QCL№1	QCL№2	QCL№3	Y, (c.u.)	QCL№1	QCL№2	QCL№3	Y, (c.u.)
	0.29	0.51	0.01	1161	0.01	0.51	0.48	752
	Q-1-CL	Q-2-CL	Q-3-CL	Effect, (%)	Q-1-CL	Q-2-CL	Q-3-CL	Effect, (%)
Configuration taken into account	0.50	0.15	0.002	6	0.50	0.24	0.002	39
	QCL№1	QCL№2	QCL№3	Y, c.u.	QCL№1	QCL№2	QCL№3	Y, (c.u.)
	0.29	0.51	0.01	1600	0.01	0.51	0.48	1832
	Q feeder		Effect, (%)	Q feeder			Effect, (%)	
	0.66		20	0.75			8	

The obtained results show that not accounting for the circuit configuration, relay protection and redundancy leads to errors in prediction of the probability of failure-free operation of the feeder. It can be noted that in the case of redundancy in the network the damage from energy curtailment is reduced most by replacing the CL №1, despite the fact that it is not the oldest. Without redundancy, the CL №2 must first be updated. Our analysis shows that in more complex schemes the renovation stage assessment is not always obvious.

4. Conclusions

An algorithm and a program are proposed for the evaluation of cable network section reliability, taking into account historical data.

The program allows carrying out various experiments and getting rich statistical data to assess the functional relationships of the probability of no-failure of a feeder that consists of several cable lines with different historical failure data.

The dependencies of reliability indicators of a distribution network configuration, established as a result of virtual experiments, allows estimation of how much the cable network needs to be upgraded to reduce the possible damage.

References

- [1] A.V. Korzhov, A method of selection of relay protection and zoned automatic reclosing in a 6 (10) kV cable network for insulation resource saving and better working conditions, *Industrial Power Engineering*. 2 (2013) 10–16.
- [2] A.V. Korzhov, The influence of electric and magnetic fields of 6 (10) kV power cable lines on the partial discharge intensity in insulation at various operating conditions, *Cables and Wires*. 1(332) (2012) 16–21.
- [3] Analysis techniques for system reliability – Procedure for failure mode and effects analysis (FMEA), IEC 60812, 2006.
- [4] Reliability in engineering. Management of reliability. Reliability test conditions and statistical criteria and methods for evaluating the results, GOST R 27.607, National Standards, Moscow, 2013.
- [5] A.H. Musin, V.K. Korkhonen, The statistical model of the 10 kV urban cable lines damageability, *Industrial Power Engineering*. 8 (1991) 23–24.
- [6] A.H. Musin, M.A. Musin, A computer information system for the 6-10 kV urban electric networks, *Industrial Power Engineering*. 9 (1997) 11–13.
- [7] A.H. Musin, The estimation of the 6-10 kV urban electric network cables insulation defects life span, *Industrial Power Engineering*. 6 (1998) 10–11.
- [8] A.H. Musin, A model of maintenance process of urban 6-10 kV power supply systems, *Industrial Power Engineering*. 10 (1998) 20–22.
- [9] A.H. Musin, Managing urban 6-10 kV power supply systems accident risks, *Industrial Power Engineering*. 11 (1998) 26–30.
- [10] V.G. Litvinov, A.L. Myzin, K.E. Sagidov, V.I. Rybakova, The analysis and forecasting of the damageability of cable lines using artificial neural networks, *Proceedings of the Russian scientific and practical conference Technologies of power system control in XXI century*, NGTU Publishing, Novosibirsk. (2006) 39–44.
- [11] B.I. Kudrin, G.M. Lebedev, A. Gaponenko, Ranked analysis of technocenosis "3-10 kV cable network of «West Siberian Metallurgical Plant»", *Industrial power engineering*. 3 (2007) 21–28.
- [12] G.M. Lebedev, D.M. Meshkov, Forecasting failures of 6-10 kV cable lines using technocenosis approach, *Electrics*. 11 (2006) 27–29.
- [13] G.M. Lebedev, Improving the 6-10 kV cable lines operation efficiency in power supply systems on the basis of non-invasive diagnostics, *AutoAbstract of the thesis of the doctor of technical sciences*, Moscow, 2007.
- [14] V.F. Sitnikov, V.A. Skopintsev, Probabilistic and statistical approach to the resource assessment of in-service grid equipment, *Electricity*. 11 (2007) 9–15.
- [15] A.V. Korzhov, A.I. Sidorov, E.Y. Yurchenko, A.B. Nikolaevsky, A mathematical model of power cable lines insulation damageability in urban electrical networks, *Power stations*. 8 (2008) 40–47.
- [16] A.V. Korzhov, A.I. Sidorov, The methods and models for assessing the insulation conditions and electrosecurity of 6 (10) kV electrical cable lines in urban electric networks: monograph, SUSU Publishing, Chelyabinsk, 2009.
- [17] E. Gulski, E.J. Sinambela, P. Cichecki et al., Optimal partial discharge diagnosis of medium voltage power cables, *CIGRE Session (2007)* 1–6.
- [18] E. Gulski, J.J. Smit, P. Cichecki et al., Insulation diagnosis of high voltage power cables, *Proceedings of the 7th International Conference on Insulated Power Cables (2007)* 1–6.
- [19] K. Hartman, E. Letsky, V. Shefer, Experiment Planning in the studies of technological processes. Translated from German by G. Fomina and N. Letskaya, editad by E. Letsky Ph. D, Mir, Moscow, 1977.
- [20] V.V. Nalimov, V.Z. Brodsky, L.I. Brodsky, T.I. Golikova, E.P. Nikitina, L.A. Panchenko, Tables of experimental designs for factorial and polynomial models, Metallurgy Publishing, Moscow, 1982.



International Conference on Industrial Engineering

Automated stand for intelligent actuators regulators setup parameters

Shaykhutdinov D.V.*, Leukhin R.I., Shirokov K.M.

Platov South-Russian State Polytechnic University (NPI), 132, St. Prosvescheniya, Rostov region, Novocherkassk, 346428, Russian Federation

Abstract

Modern electromagnetic actuators, in particular proportional solenoids, are complex mechatronic systems, including both an actuator and its control system. Electromagnetic actuators are often used in control systems of increased liability and therefore continuously evolving. The development of new types of electromagnetic actuators is based on experimental configuring of parameters of regulators and comprehensive product testing. The complexity and the continuous improvement of the currently used magnetic systems require new approaches to the management of high-precision position of the movable elements. This article discusses an integrated approach to research, monitoring, diagnostics and control of DC proportional solenoids. This approach is based on sensorless measuring of the complex flux-ampere characteristics of the electromagnetic system employed detecting malfunctions, and for determining the position of the movable drive member.

© 2015 The Authors. Published by Elsevier Ltd. This is an open access article under the CC BY-NC-ND license (<http://creativecommons.org/licenses/by-nc-nd/4.0/>).

Peer-review under responsibility of the organizing committee of the International Conference on Industrial Engineering (ICIE-2015)

Keywords: flux-ampere characteristic, sensorless control, sensorless diagnostics

1. Introduction

The complexity and the continuous improvement of the currently used magnetic systems requires new approaches to the management of high-precision position of the movable elements [1]. To implement an effective approach in [2] proposed an automated system of automatic control of the production of intelligent actuators [3], a major element of which is stand for the diagnostics and configuration controls. In the development and pilot

* Corresponding author. Tel.: +7-863-525-5240; fax: +7-683-525-5240.
E-mail address: d.v.shaykhutdinov@gmail.com

production of new proportional solenoids DC said stand may be in the form of automated systems for research and complex tests. These operations are designed to enhance process performance design optimization electromagnets, including the use of new materials or materials known in limit operating conditions.

2. Methods, Equipment And Software

For the design of automated systems for research and complex tests proportional magnet DC platform National Instruments is chosen. The basis used industrial computer chassis-based NI PXIe-1078 [4] under the control of a controller NI PXI-8133 [5], with an extra set: NI PXIe-6341 [6], a multimeter NI PXIe-4071 [7] power supply NI PXI-4130 [8]. To control the operation of the electromagnet used specialized board NI sbRIO-9636 [9], which operates on the FPGA and real-time controller. To determine the position of the movable member used proximity sensor type LS5-15 / 10-232-2-V- (12-24) -A [10]. The object of research is a solenoid type KTS P25A00-24.

The developed algorithms for diagnosis and management based on the principles of natural-model testing and measurement sensorless flux-ampere characteristics of electromagnetic systems [11 – 14]. To implement the developed algorithms used programming environment NI LabVIEW [15]. To realize full-scale tests [16 – 20] used software packages GMSH [21] and GetDP [22], is used to calculate the magnetic field finite element method [23].

3. Solution Description

The position of the movable element of the electromagnet x determines the degree of closed magnetic circuit d . Degree of closed magnetic circuit d determines the level of the magnetic flux F at a given value of the magnetomotive force Iw [24]. The level of magnetic flux has a direct relationship with the magnetic flux of the winding ψ . Thus, there is a physical link between flux-ampere characteristic of the electromagnet ψ (Iw) and the position of its movable element x :

$$x \rightarrow d \rightarrow \Phi(Iw) \rightarrow \psi(Iw) .$$

Under the conditions of complexity and uncertainty of the individual parameters of new experimental models of products, traditional methods of developing control systems are not effective. To solve this problem are encouraged to use the controls on the basis of neural networks.

The block diagram of the automated systems for research and complex tests of electromagnets shown in Fig. 1. In Fig. 2 following notation is used: Chassis NI PXIe-1078 - a block that implements the interaction between the individual elements of the system; CBS NI PXI-8133 - Controller of operating system, implements, including modeling functions and training of the neural network; ADC NI PXIe-6341 – conversion block, which provides measurement of flux-ampere characteristics and the control position of the armature of the electromagnet; UKEP NI PXIe-4071 - control device electrical parameters of the electromagnet; DPJ LS5 - anchor position sensor; BP NI PXI-4130 - power supply of the sensor position of the armature; CD FPGA sbRIO-9636 – control device for the actuator; CCS - controlled current source; OR KTS P25A00-24- object of research.

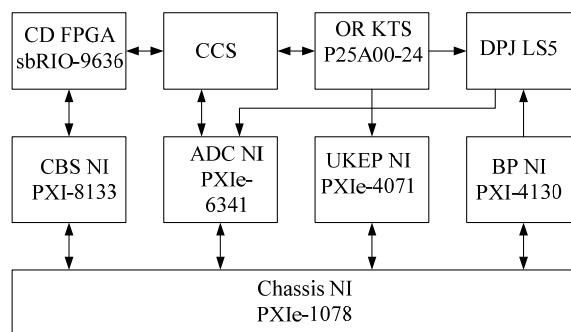


Fig. 1. The block diagram of the automated systems for research and complex tests electromagnets.

The algorithm for the system is shown in Fig. 2.

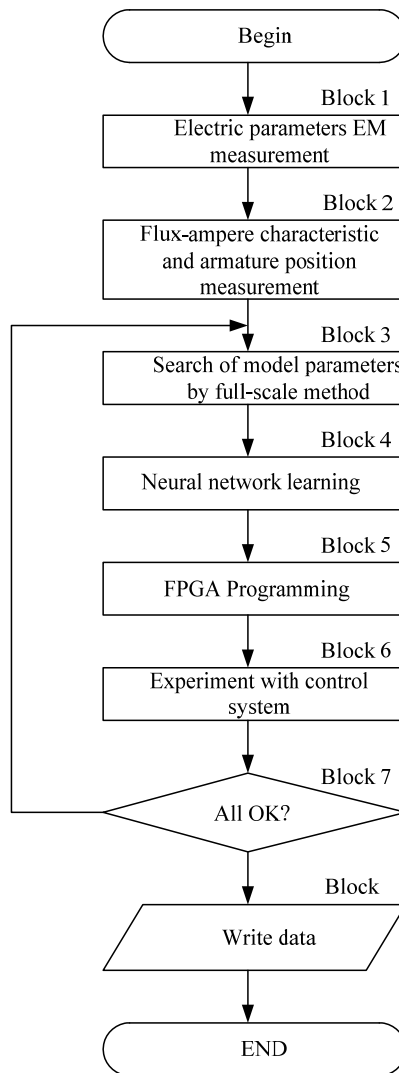


Fig. 2. The algorithm of the automated systems for research and complex tests electromagnets.

The system operates as follows. After connecting the electrical connections to the electromagnet system via UKEP PXIe NI-4071 (Fig. 1) is executed measurement of electrical parameters of its windings (Block 1, Fig. 2). In the second stage (Block 2, Fig. 2) there is a pulsed signal to the working coil of an electromagnet (using CD FPGA sbRIO-9636 by CCS, Fig. 1) is sufficient to carry out a full stroke of the armature, sensorless measuring its flux-ampere characteristics (without installing additional measuring coil - the measured current and voltage at the operating winding ADC NI PXIe-6341 with the following calculation flux-ampere characteristic in CBS NI PXI-8133, Fig. 1) and fixing the position of the armature depending on the time (via DPJ LS5 and CBS NI PXI-8133, Fig. 1). The next step (Block 3, Fig. 2) configures the magnetic and electrical parameters of the model of the electromagnet on the results of the method of full-scale experiment. This model is used as an object of control to adjust the neural network (Block 4, Fig. 2) [25, 26]. In the next step (Block 5, Fig. 2) holds programming CD FPGA sbRIO-9636 (see. Fig. 1) with the resultant adjustment parameters and re-running a full-scale experiment with

parallel registration flux-ampere characteristics and the position of the armature. The control is performed by measuring in real time the flux-ampere characteristic. In the case of obtaining a sufficient precision for the controls (Block 7, Fig. 2), the configuration process ends, and is transmitted for analysis (Block 8, Fig. 2), otherwise the process repeats starting with the model is refined by the method full-scale experiment. The result of the work of neural network [27][28] is shown in Fig. 3.

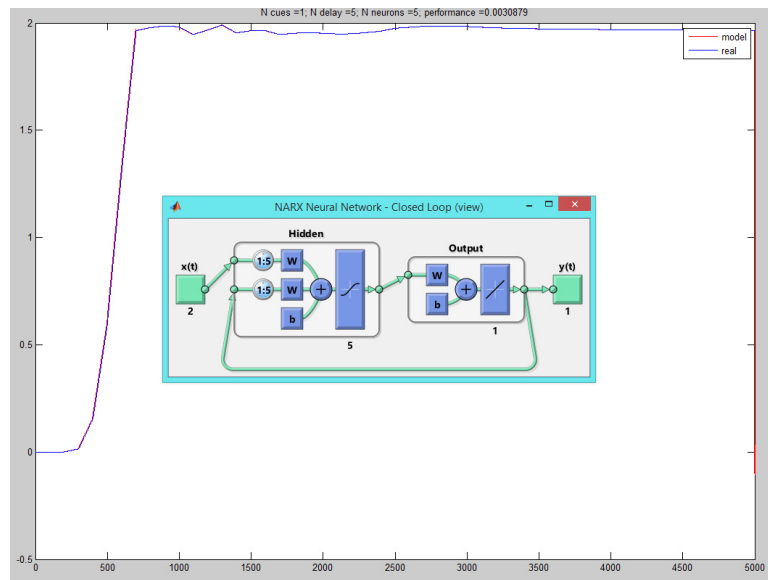


Fig. 3. Structure of the neural network and the result of its work.

Fig. 3 shows the structure of the neural network [29] and the result of its work: determining the position of the movable element of the electromagnet according to the characteristics of flux-ampere.

4. Conclusion

The structure of the automated systems for research and complex tests electromagnets. The algorithm of the system and the computer model of the test object. The scheme settings management system built on the basis of a neural network.

Acknowledgements

The results obtained with the support of the grant RFBR № 15-38-20652 “Development of the theory of predictive methods for sensorless control and diagnosis of electric drives”.

References

- [1] V.I. Dubrov, D.V. Shaykhtudinov, K.M. Shirokov, S.V. Akhmedov, N.I. Gorbatenko, Information-measurement system for stand for testing hydraulic products, 2015 International Siberian Conference on Control and Communications: SIBCON 2015, Omsk, Russia. (2015). <http://www.labview.ru/events/sibcon/sbornik/papers/480ni.pdf>.
- [2] D.V. Shaykhtudinov, N.I. Gorbatenko, K.M. Shirokov, V.V. Grechikhin, A.M. Lankin, Adaptivnaja podsystema avtomaticheskogo upravleniya proizvodstvom intellektualnih electroprivodov, Sovremennye problemi nauki i obrazovania. 1 (2015). <http://www.science-education.ru/125-20095>.
- [3] D.V. Shaykhtudinov, N.I. Gorbatenko, S.V. Akhmedov, R.I. Leukhin, Device For Control Of Magnetic Properties Of Electrical Steel For Industrial Production Management System, 2015 International Siberian Conference on Control and Communications: SIBCON 2015, Omsk, Russia. (2015). <http://www.labview.ru/events/sibcon/sbornik/papers/522ni.pdf>.

- [4] Information on <http://www.ni.com/datasheet/pdf/en/ds-312>.
- [5] Information on <http://www.ni.com/pdf/manuals/372870d.pdf>.
- [6] Information on <http://www.ni.com/datasheet/pdf/en/ds-153>.
- [7] Information on http://www.ni.com/pdf/products/us/cat_NIPXI4071.pdf.
- [8] Information on http://www.ni.com/pdf/products/us/cat_Ni_4130.pdf.
- [9] Information on <http://www.ni.com/pdf/manuals/373378c.pdf>.
- [10] Information on <http://www.prizmasensors.ru/production/ls5>
- [11] N. Gorbatenko, M. Lankin, D. Shaykhutdinov, K. Gazarov, A. Kolomiets, Electromagnetic induction system for testing ferromagnetic shape memory alloys, Proceedings of the 6th International Forum on Strategic Technology, IFOST. (2011) 194–196.
- [12] D.V. Shaykhutdinov, N.I. Gorbatenko, K.M. Shirokov, Facility for Measuring Magnetic Parameters of Articles from Sheet Electrical Steel on the Basis of National Instruments Technologies, Metal Science and Heat Treatment. 56 (2015) 618–620.
- [13] N.I. Gorbatenko, V.V. Grechikhin, D.V. Shaikhutdinov, Measuring and Actuating Devices Based on Shape Memory Ferromagnets, Metal Science and Heat Treatment. 56 (2015) 609–613.
- [14] A.M. Lankin, M.V. Lankin, N.I. Gorbatenko, D.V. Shaykhutdinov, Determination of weber-ampere characteristic for electrical devices based on the solution of harmonic balance inverse problem, International Journal of Applied Engineering Research. 10(3) (2015) 6509.
- [15] D. Trevis, LabVIEW dlia vseh (LabVIEW for all), DM Press, Moscow, 2005.
- [16] N.I. Gorbatenko, Naturno-modelnie ispitania izdelij iz ferromagnitnih materialov (Full-scale tests of device of ferromagnets materials), SKNC VSh, Rostov n/Don, 2001.
- [17] D.V. Shaykhutdinov, N.I. Gorbatenko, Sh.V. Akhmedov, M.V. Shaykhutdinova, K.M. Shirokov, Experimental and Simulation Tests of Magnetic Characteristics of Electrical Sheet Steel, Life Science Journal. 10(4) (2013). http://www.lifesciencesite.com/lj/life1004/361_22173life1004_2698_2702.pdf.
- [18] D. Shaykhutdinov, N. Gorbatenko, V. Grechikhin, K. Shirokov, V. Dubrov, Development of the computer-based stand for research of the voltage generation effect of the magnetic shape memory material, Research Journal of Applied Sciences. 10(4) (2015) 170–172.
- [19] D. Shaykhutdinov, N. Gorbatenko, G. Aleksanyan, V. Grechikhin, K. Shirokov, V. Dubrov, M. Lankin, Development of a computer-based stand for testing algorithms of electrical impedance tomography, Research Journal of Applied Sciences. 10(4) (2015) 173–175.
- [20] A.M. Lankin, M.V. Lankin, N.I. Gorbatenko, D.V. Shaykhutdinov, Determination of Weber-Ampere Characteristics of Electric Devices Using Solution of Inverse Problem of Harmonic Balance, Modern Applied Science. 9(8) (2015) 247–261.
- [21] Information on <http://geuz.org/gmsh/>
- [22] Information on <http://www.geuz.org/getdp/>
- [23] S.I. Trushin, Metod konechnih elementov (Finite element method), Izdatelstvo Associacii stroitelnih vuzov, Moscow, 2008.
- [24] I.A. Ovchinnikov, Electromechanicheskie i mehatronnie sistemi (Electromechanical and mechatron systems), Korona-Print, Moscow, 2012.
- [25] S. Haykin, Neural Networks: A Comprehensive Foundation: second ed., Prentice Hall, 1999.
- [26] M. Mohri, Murphy, Foundations of Machine Learning, The MIT Press, 2012.
- [27] H. Cartwright, Artificial Neural Networks, Springer-Verlag New York, 2015.
- [28] G.A. Rovithakis, A. Manolis, Christodoulou. Adaptive Control with Recurrent High-order Neural Networks, Theory and Industrial Applications, Springer-Verlag London, 2000.
- [29] K. Patan, Artificial neural networks for the modelling and fault diagnosis of technical processes, Springer-Verlag Berlin Heidelberg, 2008.



International Conference on Industrial Engineering

High precision device for diameter rebar control in reinforced concrete products

Ahmedov S.V.^{*}, Stetsenko I.A., Grushko I.S.

Platov South-Russian State Polytechnic University (NPI), 132, St. Prosvescheniya, Rostov region, Novocherkassk, 346428, Russian Federation

Abstract

Modern construction projects are complex engineering structures that vary in purpose, materials, height, the regulatory period of service, purpose and features of operation. Often there is a need for reconstruction of old buildings and structures. All this requires the development of technologies, methods, and special equipment for the inspection of buildings and constructions, quality control not only in the course production but also at the construction site. The use of control devices allows solving problems of contractors non-compliance with the requirements of the project and the consequences of incorrect assembly, which in turn may lead not only to economic losses but also to the damage caused to the health and lives of people. In this article, we have designed a device for measuring the diameter of reinforcement concrete structures. For modeling of individual components of the electronic part of device the system NI Multisim is used. For modeling of electromagnetic sensors for developed the device for measuring the diameter of the reinforcement concrete structures the program Maxwell SV is used.

© 2015 The Authors. Published by Elsevier Ltd. This is an open access article under the CC BY-NC-ND license (<http://creativecommons.org/licenses/by-nc-nd/4.0/>).

Peer-review under responsibility of the organizing committee of the International Conference on Industrial Engineering (ICIE-2015)

Keywords: Valves, control valve diameter, viagratobuy Converter, NI Multisim, Maxwell SV

1. Statement of the problem

Modern construction projects are complex engineering structures that vary in purpose, materials, height, the regulatory period of service, purpose and features of operation. Often there is a need for reconstruction of old buildings and structures [1]. All this requires the development of technologies, methods, and special equipment for inspection of buildings and constructions, quality control not only on production but also on the construction site.

^{*} Corresponding author. Tel.: +7-863-525-52-40;
E-mail address: iimt-srstu@mail.ru

The use of control devices allows to solve problems of non-compliance by contractors with the requirements of the project and the consequences of incorrect assembly, which in turn may lead not only to economic loss but also damage the health and lives of people. Today there are several types of quality control of building structures. One of the main nondestructive testing (NDT)[2], which allows the measurement of the physical parameters of the objects without destroying them[3 – 5].

Methods of nondestructive testing are widely used and applied not just in the construction field, but also in many other fields due to its versatility. At the moment, for measurement of geometric parameters of conductive objects are devices, which are based on direct contact with the test object, and the device based on noncontact measurement method [6].

2. A description of the method

Description metadataresolver an NDT method based on the analysis of the interaction of electromagnetic field eddy current probe with the electromagnetic field of eddy currents induced in the test object [7 – 10]. Eddy currents are excited in the object by the transducer, which is used as an inductive coil fed by alternating sinusoidal or pulsed current [11]. The basis of the eddy current technique is the induction of electric current in a conducting material. When an alternating excitation current is a vector in the complex plane. The inductive interaction of the coil with the object of control is determined by the system of Maxwell's equations [12] describing the electromagnetic field in a predetermined space and having the form (1):

$$\begin{cases} \text{rot} \bar{H} = \bar{J}_{\text{full}} \\ \text{rot} \bar{E} = -\partial \bar{B} / \partial t \end{cases} \quad (1)$$

where \bar{H} and \bar{E} - vectors of magnetic and electric fields [13][14], respectively; \bar{B} - the magnetic induction vector; t - time; \bar{J}_{full} - the vector of density of the total current defined by the expression (2):

$$\bar{J}_{\text{full}} = \bar{J}_{\text{cond}} + \bar{J}_{\text{off}} + \bar{J}_{\text{tran}} + \bar{J}_{\text{third}} \quad (2)$$

where \bar{J}_{cond} - the density vector of conduction current, \bar{J}_{off} - displacement, \bar{J}_{tran} - migration and \bar{J}_{third} - third party.

3. Block diagram of the device measuring the diameter of reinforcement concrete structures

Block diagram of the device is shown in Fig. 1.

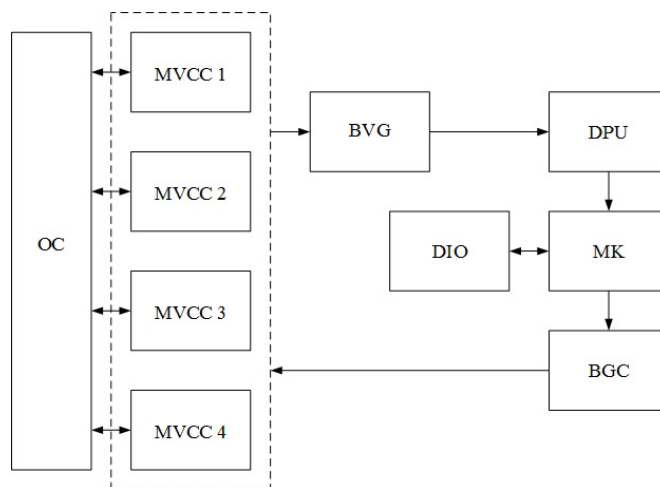


Fig. 1. Block diagram of the device.

The flow diagram shows: DIO – device I / o, designed to set the control parameters and the subsequent output of the received results of measurement of the diameter of the valve; MK – microcontroller block, which is used to generate the excitation signal, the management control process and perform the data processing before output; as block gain current (BGC) is used as a current source controlled by the output voltage of the microcontroller; MVCC matrix eddy-current transducers that communicate with the control object; BVG – gain block voltage – response; DPU – digital processing unit – set analog-to-digital converters [15, 16].

During operation of the device, the microcontroller sets the setpoint frequency current in the generator, the signal is amplified and fed to the switch, where the signal is distributed according to a given algorithm in certain sections of the matrix eddy-current transducers under the influence of the excited coil, an external electromagnetic field interacting with the electromagnetic field of eddy currents induced in the test object this field. The received signals of the measuring coils are amplified and digitized through the switch and to the microcontroller where they are processed and displayed [17 – 19].

4. A schematic diagram of the device

The figure 2 shows a schematic diagram of the signal amplifier and waveform outputted to the virtual oscilloscope

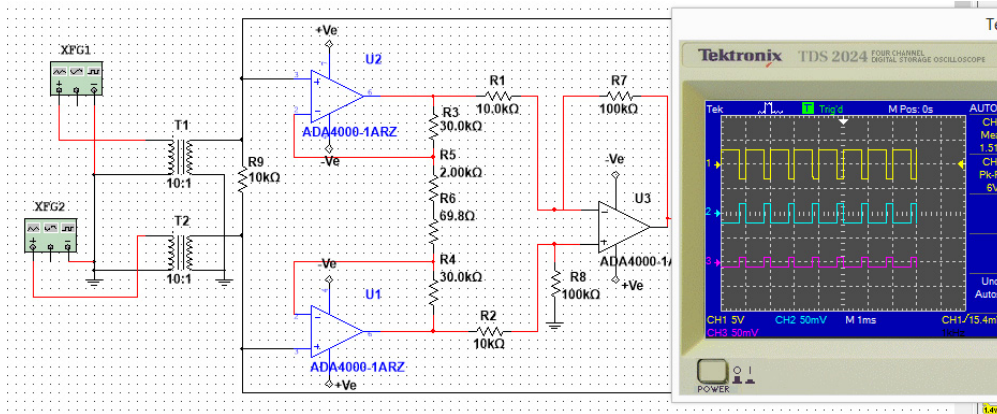


Fig. 2. A schematic diagram of the device.

5. Building a 3D model in the medium Maxwell SV

Building a 3D model of one block of the matrix of eddy current transducer and the relative location of the valve stem with respect to the transducer, in the medium of computer modeling Maxwell SV and set the basic parameters

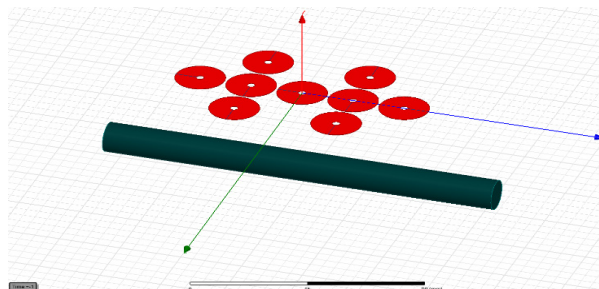


Fig. 3. 3D model of the object in the environment of Maxwell SV.

of the model [20] [21]. The relative dimensions of the coils and the depth of the reinforcement have been described above. The resultant block model matrix eddy current converter is shown in Fig. 3.

The result of the simulation is shown in Fig. 4:

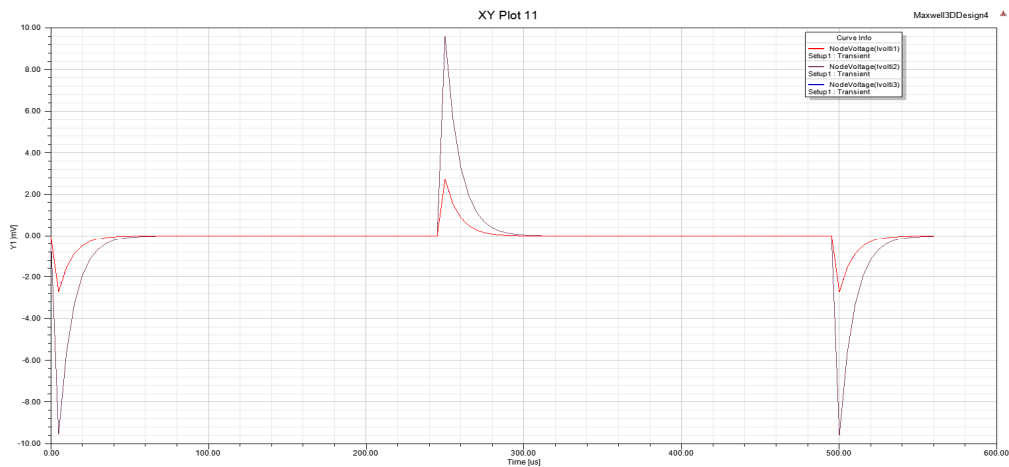


Fig. 4. Result of the simulation.

6. Conclusion

Using the described eddy current methods, it is possible to measure the diameter of the reinforcement of reinforced concrete structures of the electromechanical transducer contactless eddy current type with the appropriate configuration of the electromagnetic field and winding structures.

Acknowledgements

The project became the winner of the youth program Participant research scientific-innovation competition "P.R.S.I.C.". Project #4477GU1/214.

References

- [1] V.S. Vladimirov, V.V. Zharinov, Equations of mathematical physics, FIZMATLIT, 2004.
- [2] V.I. Matveev, Radio wave control, second ed., Engineering, Moscow, 2006.
- [3] Sh.V. Ahmedov, D.V. Shaikhutdinov, N.I. Gorbatenko, Y.R. Krevchenko, To select appropriate functioning of the device highly accurate measurement of the valve parameters, Modern problems of science and education. 1 (2015). URL: <http://www.science-education.ru/121-18963>.
- [4] Sh.V. Akhmedov, D.V. Shaikhutdinov, N.D. Narakidze, N.I. Gorbatenko, Device for controlling the parameters of reinforcement in concrete structures, Engineering and scientific applications based on technologies NI NIDays, Proceedings of XIII International Scientific-practical conference. (2014) 326–328.
- [5] Locator rebar in concrete Profoscope, Company Proceq Rus LLC. Information on URL: <http://www.proceq.com/ru/produkcija/kontrol-betona/lokator-sterzhnei-armatury-v-betone/profoscope.html?pqf=5>
- [6] The system of X-Scan Hilti PS 1000, Company HILTI. Information on URL: <https://www.hilti.ru/r5042>
- [7] N.I. Gorbatenko, M. Lankin, D.V. Shaikhutdinov, K. Gazarov, A. Kolomiets, Electromagnetic induction system for testing ferromagnetic shape memory alloys, Proceedings of the 6th International Forum on Strategic Technology, IFOST 2011. (2011) 194–196.
- [8] D.V. Shaikhutdinov, N.I. Gorbatenko, K.M. Shirokov, Facility for Measuring Magnetic Parameters of Articles from Sheet Electrical Steel on the Basis of National Instruments Technologies, Metal Science and Heat Treatment. 56 (2015) 618–620.
- [9] N.I. Gorbatenko, V.V. Grechikhin, D.V. Shaikhutdinov, Measuring and Actuating Devices Based on Shape Memory Ferromagnets, Metal Science and Heat Treatment. 56 (2015) 609–613.
- [10] A.M. Lankin, M.V. Lankin, N.I. Gorbatenko, D.V. Shayhutdinov, Determination of weber-ampere characteristic for electrical devices based on the solution of har-monic balance inverse problem, International Journal of Applied Engineering Research. 10(3) (2015) 6509.

- [11] I.R. Kuzeev, Electromagnetic diagnostics equipment petrochemical and refining industries, 2001.
- [12] U. Tietze, K. Schenk, Semiconductor circuitry. twelfth ed., Trans. with it, DMK Press, Moscow, 2007.
- [13] P. Horowitz, W. Hill, The Art of Electronics, Trans. with angl, seventh ed., BINOM, Moscow, 2014.
- [14] ADA4000-1, Company Analog Devices. Information on URL: http://www.analog.com/media/en/technical-documentation/data-sheets/ADA4000-1_4000-2_4000-4.pdf
- [15] GOST 14014-91. Instruments and measuring transducers Digital voltage, current, resistance.
- [16] A. Alekseev, S. Shumilin, Microcontroller 1886VE6 for analog systems, Components and Technologies. 9 (2009).
- [17] R.R. Bikkenin, M.N. Chesnokov, Theory of electrical communication, Electronics and telecommunications, Academy, 2010.
- [18] M. Kirin, Fomina's description Multisim. URL: <http://www.phtf.spb.ru/files/electronics/Multisim/manual.pdf>
- [19] E.V. Komarov, A.D. Pokrovsky, V. Sergeev, A.Ya. Shikhin, Testing of magnetic materials and systems, The energy goatomizdat, Moscow, 1984.
- [20] GOST 26.020-80, Fonts for measurement and automation. Faces and basic dimensions, Moscow
- [21] GOST 10316-78, Getinaks foil and glass fiber.



International Conference on Industrial Engineering

Increasing the efficiency of power resource management as a solution of issues of the power supply system stability

Kondrashova Y.N., Gazizova O.V., Malapheev A.V.*

Nosov Magnitogorsk State Technical University, Lenina Av. 38, Magnitogorsk, 450000, Russia

Abstract

The paper considers issues of enhancing the resulting stability of the meshed power supply systems containing distributed generation facilities under conditions of large iron and steel enterprises. An improved software suit for studying emergency and post-emergency conditions has been developed; it provides an opportunity to enhance efficiency of the condition control and power resource usage by reducing the downtime of the electric equipment and enhancing the reliability of the whole power supply.

© 2015 Published by Elsevier Ltd. This is an open access article under the CC BY-NC-ND license (<http://creativecommons.org/licenses/by-nc-nd/4.0/>).

Peer-review under responsibility of the organizing committee of the International Conference on Industrial Engineering (ICIE-2015)

Keywords power supply system; resulting stability; transient modes; asynchronous power; distributed generation facilities; reliability of electric equipment.

1. Introduction

At present we are experiencing the increase of the additional power units of industrial loads within the power supply systems resulting in energy emergency and determining benefit of building and expanding the base of the distributed generation facilities at the main segments featuring concentrated load. It complicates transient emergency and post-emergency conditions stipulating the need for study of static, dynamic and resulting stability issues. This problem is relevant since emergencies caused by stability loss lead to large-scale damage, outage, lost output and life hazard.

A number of studies concern static stability, including [1] which considers special aspects of static stability under conditions of the industrial meshed system for generators and high-voltage motor load.

* Corresponding author. Tel.: +7-902-897-4557;
E-mail address: G389@mail.ru

The issues of dynamic stability are presented in papers [2, 3] on the example of acquisition of dynamical characteristics of the complex load.

Within the meshed power supply systems applying the distributed generation one of the severe accident types is a short circuit accompanied by switching to the operation isolated from the power system and following resynchronization. That is why the forecasting emergency and post-emergency conditions should be performed with development of a new improved algorithm of computing transient modes at occurrence of short circuits in the power supply system with auxiliary power plants accompanied by switching to the isolated operation with possibility of resynchronization with the power system.

The performed analysis of studies dealing with estimation of the resulting stability of the electric power systems and systems of electric power supply of industrial enterprises has revealed the absence of the exact analytical dependencies which could be used for practical calculation and reflect the pattern of the transient process under way within the complex multi-machine system at the resynchronization; the proposed methods of asynchronous mode study are not useful at determining change of power balance in the power supply system and changes of the average voltage and frequency levels in comparison with the pre-emergency ones; methods enabling calculation of the three-phase short circuit with following recovery of the parallel operation within the meshed systems have also not developed yet. At present, there are no exact analytical descriptions of events occurring at the generator resynchronization which could reflect behavior details especially in the complex system.

In connection with the above, it should be noted that in order to increase efficiency of the power resource usage and management of modes of the power supply systems the forecasting transient conditions and estimation of resulting stability at short circuits and their trips are required.

2. Increasing efficiency of power resource management

At the study of the resulting stability the calculation of asynchronous operation of the synchronous generators and high-voltage motors is essential. Analysis of the asynchronous power changes are of special interest at the computing transient processes accompanied by the switch of auxiliary power plants to the non-parallel operation with the power systems [4, 5]. At the operation being parallel with the power system the frequency is generally maintained which is close to the rated one; at any transient process the change of the rotor rotation frequency will be followed by generation (at the synchronous generators) or consumption (synchronous motors) of asynchronous power in relation to the infinite power unit. During short circuit rates of the generator rotors are non-uniformly increased. That is why the switch to the non-parallel operation after trip of the damaged element occurs with different rotation rates. Furthermore, the rate of the generator rotors starts changing in the result of the appearing power imbalance due to the downtime of communication with the power system [6]. To maintain the normal unit operation generators and electric drives should be synchronized. Synchronizing process provides an additional electromagnetic torque associated with presence of the asynchronous power. At the separate operation each generator provides its inherent power corresponding to its own rotation frequency. Relating to it, all other generators provide or receive some asynchronous power depending on the rate ratio of the considered generator pair. At the other side, the ongoing generator will also provide (receive) some asynchronous power related to other generators. Mutual sliding of the relevant generator related to the others is determined as follows (1):

$$S_{i,j} = \frac{\omega_{(n-1)}^{(i)} - \omega_{(n-1)}^{(j)}}{\omega_{(n-1)}^{(i)}}. \quad (1)$$

Mutual sliding of other generator related to that one at issue (2):

$$S_{j,i} = \frac{\omega_{(n-1)}^{(j)} - \omega_{(n-1)}^{(i)}}{\omega_{(n-1)}^{(j)}}, \quad (2)$$

where j – number of the relevant generator and $\omega_{(n-1)}$ – rate at $n-1$ -the calculation interval.

Under conditions considered emergency control automatics including the non-synchronous automatic restarting (NAR) is used for parallel operation recovery. At its operation the conditions of resynchronization of axillary power

plant generators take place which may be followed by great current and voltage changes in different points of the electric network. In the mode of non-parallel operation resynchronization may be delayed due to the significant angle deviations; this may result in instability of other generators of the power supply system.

2.1. Description of the Developed Algorithm

In order to achieve the purposes and tasks set the ingenious software suit [7] has been developed that is based on algorithms for computing steady-state modes with the sequential equivalent method, transient processes with the sequential interval method and for calculation of emergency and post-emergency conditions with the modified sequential equivalent method [8]. The developed software suit enables computing the following options: steady modes of the meshed power supply systems of different configuration, static and dynamic characteristics of consumers of different design, static stability with the successive charging method, dynamic stability under possible emergency situations at designing normal and maintenance operating configurations within the electric networks of large industrial enterprises with auxiliary power plants [9], transient modes at short circuits providing analysis of processes at emergency separation from the power system and recovery of the parallel operation. So, the software suit is designed for calculation and analysis of the temporal angle alteration and estimation of resulting stability at the switch to the non-parallel operation in order to forecast emergency and post-emergency conditions with the aim of enhancing efficiency of mode control of the meshed power supply systems containing distributed generation facilities.

2.2. Example of the Program Application

As a target of research the power supply system of the large iron and steel works containing distributed generation facilities, namely, cogeneration unit (CU) and electricity works (EW) has been selected.

The considered power supply system (PSS) of the large iron and steel works is one of the biggest, so special approach is required in this case, since this PSS with its inherent features is an intermediate link between other PSSs and the power systems. To realize maintenance modes deep redundancy is provided which contributes to low equipment loading. At this, presence of the high power sources assists support of the voltage levels in the maintenance modes. Thus, maintenance works may be carried out without process flow disruption at short circuits. At the parallel operation of the communication substations and power system the PSS is running with the highest stability but voltage reduction at any communication substation results in the same effect in all nodes, Great number of synchronous generators with power range from 4 to 60 MW may cause mutual sweeping and instability of the whole system if at least one of them gets instable. Total capacity of the power stations amounts 623 MW, at this: cogeneration unit (CU) – 330 MW, EW – 201 MW. Presence of high power electric units within the limited industrial area and short communication channels between power supplies establish specific operation conditions for the whole electric power system at issue. There are high short-circuit powers and low residual voltages in the electric networks; that accounts for difficult operation conditions for relay protection and emergency automation.

To study conditions of switch to non-parallel operation of the power stations and analyze transient modes with accompanying recovery the developed software suit has been applied; it provides the following calculation results and transient process curves with changing mutual angle alteration of the auxiliary power station generators. At the switch to non-parallel operation the main stability indexes are not inherent but mutual angles of generators relative to each other. At the study of conditions resulting in switch of the CU station under load to non-parallel operation after short-circuit and following recovery of parallel operation with the power system the following results have been obtained: unit frequency at non-parallel operation – 50.136 Hz, voltage at the point of connection with the power system at the moment of NAR operation – 93 kW, after successful resynchronization – 114.81 kW, at this, 110 kW bus short-circuit duration – 0.5 s, recovery time after two cranks (Fig. 1) – 2 s.

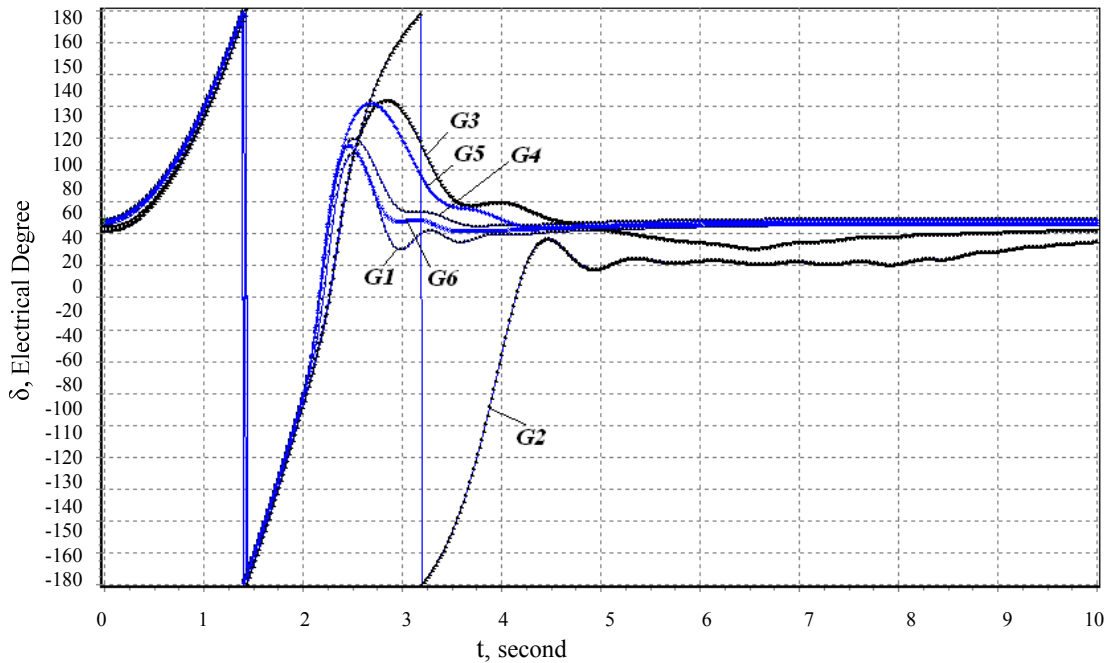


Fig. 1. Generators' mutual angles relative to CU turbo-generator 3 at CU non-parallel operation under conditions of short-circuit at the switchgear -110 kW at $t_{\text{prel.trip}}=0.5$ and $t_{\text{recover}}=2$ s.

Similar calculations and plotting generator mutual angles of the distributed generation facilities have been performed for other layout configurations with separation of the network sections after short circuit. For each mode the critical NAR operating time has been determined.

3. Outcome summary

The study of resynchronization conditions in the distributed generation networks has proven that the emergency control automatic should restart the separated network node at the rotor angle values providing the fastest generator synchronization and elimination of the great electrical surges of stators. At this, generators' initiation influences parallel operation essentially: it occurs either at zero value of the generator angle or at the angle value being equal to the steady one. As the calculations show, the required time moment corresponds to the angle transition through zero. It is due to the fact that the value of the stator current is also close to zero here. The software suit used provides opportunity to determine the most propitious moment for successful resynchronization, thus, to enhance stability of the power supply systems of large industrial enterprises with the aim to reduce downtimes and improve reliability of the power supply system and electrical equipment as well as to increase its remaining lifetime [10]. The software suit is designed to estimate performance of the relay protection and automation devices in regard to the criterion of dynamic stability maintenance at three-phase short-circuits and may be applied by operative and dispatch personnel as a guide tool providing correct solutions.

References

- [1] A.V. Malapheev, B.I. Zaslavets, V.A. Igumenshev, O.V. Bulanova, Yu. N. Rotanova, AC Machine Representation at Computing Dynamical Stability of the Power Supply Systems at Industrial Enterprises with Auxiliary Power Stations, South Ural State University Bulletin, Power Engineering Series (2008), issue 9 no. 11, pp. 3-8.

- [2] A.V. Malapheev, V.A. Igumenshev, B.I. Zaslavets, O.V. Bulanova, Yu. N. Rotanova Modified Sequential Equivalent Method for Calculation of the Complex Power Supply Systems, *Industrial Power Engineering*, (2008), no. 6, pp. 16-22.
- [3] O.V. Bulanova, B.I. Zaslavets, V.A. Igumenshev, A.V. Malapheev, Yu. N. Rotanova, Analysis of Transient Processes in the Power Supply Systems of Industrial Enterprises with Auxiliary Power Stations under Conditions of Switching to Non-Parallel Operation after Short Circuit, *Higher School Bulletin, Electro mechanics*, (2009), no. 1, pp. 60 – 65.
- [4] Yu.N. Rotanova, V.A. Igumenshev, A.V. Malapheev, O.V. Bulanova, Calculation of Dynamical Characteristics of Industrial Synchronous and Asynchronous Motors for Stability Analysis of the Power Supply Systems, *Bulletin of G.I. Nosov Magnitogorsk State Technical University*, (2006), no. 2, pp. 71 – 75.
- [5] O.V. Bulanova, A.V. Malapheev, N.A. Nikolayev, Yu.N. Rotanova, Ju. N. Panova, Determination of Asynchronous Power of Synchronous Generators at Calculation of Electromechanical Transient Processes under Asymmetrical Conditions, *Electrical Engineering*, (2010), no. 8, pp. 24 – 26.
- [6] Yu.N. Rotanova, A.V. Malapheev, O.V. Bulanova, Study of Dynamical Stability of Power Supply Systems of Industrial Enterprises with Auxiliary Power Stations at Separation from the System due to the Short Circuit, *South Ural State University Bulletin. Series: Computer Technologies, Control, Radioelectronics*, (2008), no.17 (117), pp. 72 – 74.
- [7] Yu.N. Rotanova, Stability Improvement of the Power Supply System of Industrial Enterprises with Auxiliary Power Stations at Short Circuits, Ph.D. thesis in Engineering Science: 05.09.03., MSTU, Magnitogorsk, (2008), 174.
- [8] O.V. Bulanova, Mode Control of Industrial Power Stations at Switching to Non-Parallel Operation, Ph.D. thesis in Engineering Science, 05.09.03., MSTU, Magnitogorsk (2007), 175.
- [9] Calculation and Optimization of the Steady-State and Transient Operation Modes of Parallel and Non-Parallel Operation with the Power System, Conditions Of Short-Circuit to Earth with Estimation of Effect on Electric Equipment within the Industrial Power Supply Systems , Certificate of Official Registration of the Software Application, no. 2008610773 V.A. Igumenshev, A.V. Malapheev, O.V. Bulanova, Yu.N. Rotanova, V.V. Zinoviyev. Entered into the Software Register 04.02.2008.
- [10] A.S. Karandaev, Yu.N. Rotanova, G.P. Kornilov, O.I. Karandaeva, V.V. Rovneyko, R.R. Galyamov, Reliability Analysis of the Equipment of the Thermal Power Station at the Introduction of the Frequency Convertors, *South Ural State University Bulletin, Power Engineering Series*, (2009), no.34 (167), pp. 16 – 22.



International Conference on Industrial Engineering

Approaches in a sensor model of error correction in dynamic measurements

Yurasova E.V.^a, Biziaev M.N.^a, Volosnikov A.S.^{a*}

^a South Ural State University, 76, Lenin Avenue, Chelyabinsk, 454080, Russian Federation

Abstract

The article describes three approaches in error correction of dynamic measurements. A sensor model is used in these approaches. The first one is based on the modal control of the dynamic behavior and adapting parameters of a sensor model by direct search. We propose a method of error evaluation in dynamic measurements with a priori information on characteristics of measured signal and noise of the sensor available. The second approach concerns the neural network representation of a sensor. Neural network inverse sensor model and the algorithm for its training by minimizing mean-squared dynamic measurements error criterion are proposed. The third approach is based on the introduction of sliding mode control into the measuring system with modal control of dynamic behavior to achieve the similarity of the sensor model output to the sensor output.

© 2015 Published by Elsevier Ltd. This is an open access article under the CC BY-NC-ND license (<http://creativecommons.org/licenses/by-nc-nd/4.0/>).

Peer-review under responsibility of the organizing committee of the International Conference on Industrial Engineering (ICIE-2015)

Keywords: dynamic measurements error; model of sensor; recovery of sensor input signal; dynamic measuring system; automatic control theory approach; sliding mode control approach; neural networks approach.

1. Introduction

Correction of the dynamic measurements error consists in the solution to problem of a measuring system input signal recovery. This problem is ill-posed and requires the numerical solution to the convolution integral equation [1]–[5]. One of the promising tendencies in the area of modern information-and-measuring equipment development is an intellectualization of such equipment [6]. Characteristic features thereof are the completion of complex measuring procedures using dedicated equipment and means, as well as the development of detectors capable of

* Corresponding author. Tel.: +7-351-267-9001.
E-mail address: volosnikovas@susu.ru

individualizing the processing algorithms, including by adapting change of its own structure and parameters based on accumulated a priori and obtained measuring information [7]. In real information-measuring systems noise characteristics are approximated and may change during measurement. This makes it difficult to process the results of measurement in appropriate way. That is why intellectual measuring systems, adaptable to noise environment, are of practical interest. Discussed in studies [8]–[16] detector with sensor model, existing as real part of its structure, had the model feedback loop coefficients acting as adjustable parameters. Such coefficients was calculated according to the required dynamic error value and remained constant during the experiment data processing. However, there is a possibility in principle to adjust the sensor model feedback loop coefficients during measurement or measurement data processing [17], [18]. In this case the parameter adjustment criterion may serve not only as dynamic error convex functional, but also as dedicated generated signal of dynamic error evaluation, which is a continuous time function, depending on adjustable parameters of the measuring system.

The automatic control theory approach allows the effective improvement of the dynamic measurements accuracy [15], [16]. Along with it, the artificial neural network approach to creation of dynamic models of measuring systems and algorithms for data processing of dynamic measurements is one of promising ways of intelligent measuring systems development.

2. Dynamic behavior modal control approach

2.1. Gradient method of the measuring system dynamic parameters minor adjustment

Let's consider a common case of the measuring system dynamic parameters self-adjustment, when all feedback loops coefficients are subjected to minor adjustment. The method is intended for adjusting the parameters, when the spectral noise density of the measuring channel is constant and unknown, or is slowly changing with a speed not exceeding the speed of the system transient processes.

Self-adjustment criterion of the measuring system dynamic parameters shall adequately reflect noise conversion in the measuring channel, in compliance with a transfer function according to reduced noise term from [15]. The evaluation of the measuring system dynamic error shall be written as follows [16]:

$$e_0(t) = y(t) + V(t) - y_m(t) \quad (1)$$

where $y(t)$ is input signal of the measurement system; $V(t)$ is signal to noise; $y_m(t)$ is input signal of the sensor model.

Or using Laplace transformation, considering the transfer functions of the sensor and the measuring system:

$$e_0(p) = e_{ms}(p)W_D(p) + V(p) \quad (2)$$

where $e_{ms}(p) = U(p) - U^*(p)$ is a Laplace transformation of the measuring system error; $W_D(p)$ is Laplace transformation of the sensor's transfer function.

A signal given below shall be taken for the displacement error of the measuring system and the model output coordinates to self-adjustment criteria:

$$e_1(p) = e_0(p) \frac{W_{ms}(p)}{W_D(p)} = e_{ms}(p) \cdot W_{ms}(p) + V(p) \frac{W_{ms}(p)}{W_D(p)} \quad (3)$$

On condition that $W_{ms}(p) \approx 1$ the signal ensures noise conversion in the error signal with the same degree as its amplification in the output signal of the measuring system. Measure of disagreement of the real system output coordinate motion and the model output shall be the function from the dynamic error evaluation signal – $e_1^*(t)$, in the form as follows [15]:

$$I(t) = F(e_1^*(t)) = (e_1^*(t))^2 \quad (4)$$

where $I(t)$ is a self-adjustment quality criterion, depending on the input signal – $U(t)$, initial displacement of the model and system coordinates, as well as on adjustable dynamic parameters $k_i(t)$, $i=0, n-1$.

Algorithm of small adjustment of the measuring system dynamic parameters $k_i(t)$, $i=0, n-1$ in compliance with the gradient method shall be developed in such manner, that at every instant the feedback loop coefficient change tends to $I(t)$ value decrease as the function $k_i(t)$:

$$\frac{dk_i(t)}{dt} = -\lambda \cdot \frac{\partial I(t)}{\partial k_i(t)} \quad (5)$$

The analysis performed based on Lyapunov's method [15] has demonstrated that the stability of the measuring system, synthesized using a gradient method, is determined by additional feedback loops with coefficients $x_{nm}^0(t), x_{n-1m}^0(t), \dots, x_{1m}^0(t)$, which index depends on the system motion parameters. Value of additional feedback loops is proportional to the adaption speed λ , which control gives possibility of ensuring a measuring system stability.

2.2. Results of computer simulation

To illustrate the possibilities of the dynamic error correction a computer simulation of measuring systems with dynamic error self-adjusting feedback loops coefficients of the sensor model, developed based on the first-order (fig. 1) and the second order sensors was performed. The results of the computer simulation of the dynamic measurement process demonstrate the effectiveness of the designed self-adjusting measuring system. In case of self-adjusting of parameters of the measuring system based on the second sensor with time constant $T = 0.01$ and damping ratio $\zeta = 0.3$, with harmonic input signal – $U(t) = 1 \cdot \sin(10 \cdot t)$ and harmonic noise signal – $V(t) = 0.05 \cdot \sin(100 \cdot t)$, dynamic measurement error has reduced by 84% compared to measurement without additional adjustment.

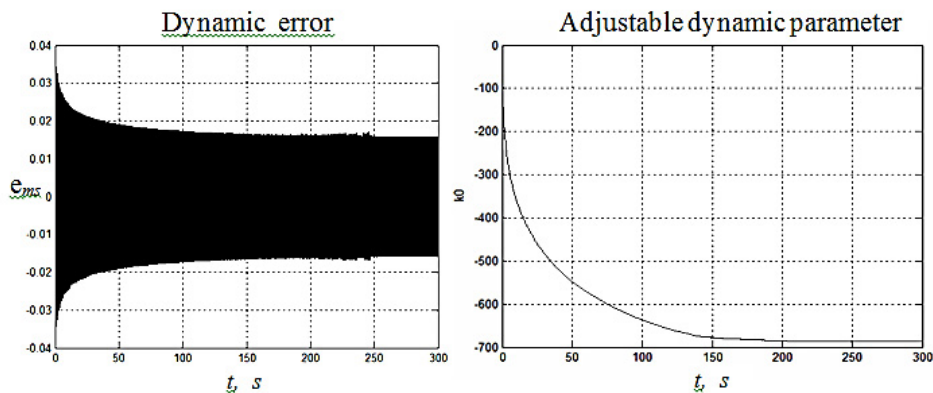


Fig.1. Results of the computer simulation

2.3. Summary

The proposed structure of the measuring system with modal dynamic characteristics control based on sensor model dynamic error and dynamic error assessment channel, as well as self-adjustment algorithm of the measuring system dynamic parameters, based on gradient method, allow to decrease dynamic measurement error by changing

adjustable parameters directly in the process of measurement or at the stage of the measuring experiment data processing.

3. Neural network approach

3.1. Neural network inverse model of a sensor

Let a primary measuring transducer (sensor) is described by the transfer function (TF) as follows:

$$W_s(p) = \frac{Y(p)}{U(p)} = K_0 \frac{\prod_{i=1}^k (T_{2i}^2 p^2 + 2\xi_{2i} T_{2i} p + 1) \prod_{i=k+1}^m (T_{2i} p + 1)}{\prod_{j=1}^q (T_{1j}^2 p^2 + 2\xi_{1j} T_{1j} p + 1) \prod_{j=q+1}^n (T_{1j} p + 1)} \quad (6)$$

where U and Y are the sensor input and output signals respectively; T_{1j} and T_{2i} are time constants; ξ_{1j} and ξ_{2i} are damping coefficients; $i = 1, 2, \dots, m$, $j = 1, 2, \dots, n$ ($m \leq n$); K_0 is the static gain; p is the complex number frequency.

The recovery of the input signal of the sensor with TF (6) is carried out by its measured output signal processing on a basis of the sensor inverse model. This model is presented as the sequential connection of the correcting filter and identical first-order sections, each of which is the neural network inverse model of the following first-order TF:

$$W_1(p) = \frac{1}{pT_1 + 1} \quad (7)$$

The value of the time constant T_1 in the TF (7) is set equal to such a value among time constants T_{1j} in the TF (6), that provides the proximity of step responses of systems with TFs (6) and (7). The TF $W_{cf}(p)$ of the correcting filter is the inverse TF of the sensor, which is supplemented with a certain number ($n_2 - m_2$) of TFs (1) to ensure the stability of the inverse model.

The recovery of the dynamically distorted input signal of the sensor on the basis of its neural network inverse model can be accompanied by the significant increase of the additive noise at the sensor output, as well as the internal noise of the inverse model. For the correct recovery of the input signal of the sensor it is expedient to expand the neural network inverse model, taking into account the presence of the additive noise at the sensor output. This expansion can be implemented as the additional low-pass filtration of the recovered signal by means of the increase of the order of sequential neural network sections in the structure of the inverse model. The block diagram of the d -order section is shown in fig. 2. The algorithm of training sets generation and their length evaluation for the section $C_d[T_1]$ parameters adjustment during the training procedure was proposed [19], [20].

3.2. Results of the experimental data processing

The algorithm for the recovery of dynamically distorted signals on a basis of the proposed neural network inverse model of the sensor was developed. In order to validate experimentally the efficiency of these model and algorithm the dynamic measurement of the temperature was made. The step response of the thermoelectric transducer (thermocouple) «Metran-281» by heating it from 0 °C to 800 °C was obtained.

The result of experimental data processing at $d = 66$ in the form of the plots of the thermocouple measured output $y(t)$ and the thermocouple recovered input $u^*(t)$ is shown in fig. 3.

The obtained result shows that the time of the dynamic temperature measurement decreased from $T_s = 306$ s to $T_d = 60$ s, that is more than 5 times. This validates the efficiency and the effectiveness of the proposed model and the algorithm of the dynamic measurements error correction.

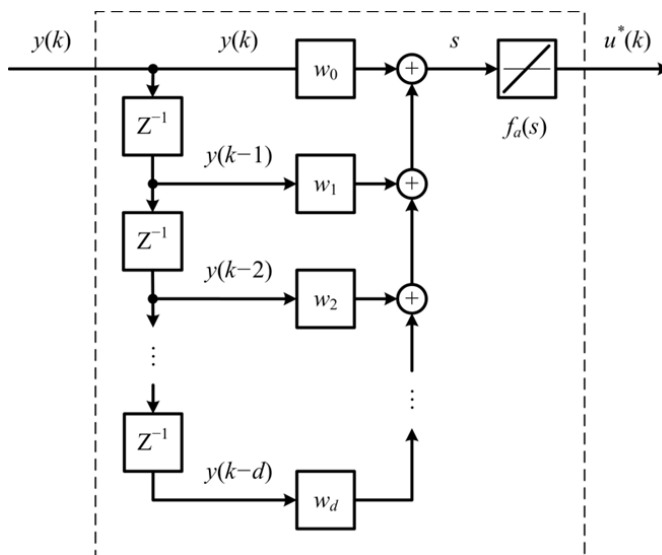


Fig. 2. Block diagram of the d -order section

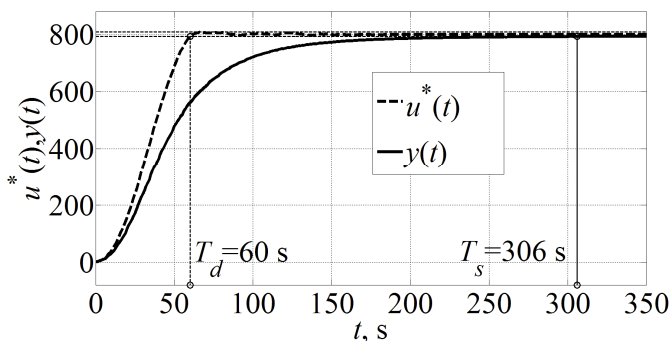


Fig.3. Result of experimental data processing

3.3. Summary

The neural network approach to the recovery of dynamically distorted signals allows the effective correction of the dynamic measurements error caused by the inertia of the sensor and the additive noise at its output.

The considered neural network inverse model of a sensor with filtration of sequentially recovered signal allows the effective improvement of the sensor dynamic behaviour due to deep mathematical processing of measurement data.

The result of experimental data processing validates the improvement of the sensor dynamic behaviour due to the application of the proposed model and the algorithm to the dynamic measurement of the temperature.

4. Conclusions

The proposed structure of the measuring system with modal dynamic characteristics control based on sensor model dynamic error and dynamic error assessment channel, as well as self-adjustment criterion of the measuring system dynamic parameters, based on gradient method, allow to decrease dynamic measurement error by changing

adjustable parameters directly in the process of measurement or at the stage of the measuring experiment data processing.

The neural network approach to the recovery of dynamically distorted signals allows the effective correction of the dynamic measurements error caused by the inertia of the sensor and the additive noise at its output. The considered neural network inverse model of a sensor with filtration of sequentially recovered signal allows the effective improvement of the sensor dynamic behaviour due to deep mathematical processing of measurement data.

Moreover, to ensure the proximity of the sensor model output to the sensor output in the measuring system with modal control of dynamic behavior feedbacks are introduced. It is possible to achieve the proximity of these signals in the measuring system by implementation of sliding mode control [21], [22].

The results of computer modeling and experimental data processing validate the improvement of the sensor dynamic behaviour due to the application of proposed models and algorithms to the dynamic measurements error correction.

References

- [1] G.N. Solopchenko, Ill-posed problems of measuring engineering, *Measuring technique*, 1 (1974) pp. 51-54.
- [2] A.N. Tikhonov, V.Y. Arsenin, *Solution of ill-posed problems*, V.H. Winston & Sons, Washington, 1977.
- [3] A.N. Tikhonov, *Methods of solution to ill-conditioned problems*, Nauka, Moscow, 1979 (in Russian).
- [4] G.I. Vasilenko, *Theory of signals recovery: about reduction to ideal instrument in physics and engineering*, Sov. Radio, Moscow, 1979 (in Russian).
- [5] V.A. Granovskiy, *Dynamic measurements: fundamentals of metrological support*, Energoatomizdat, Leningrad, 1984 (in Russian).
- [6] V.N. Ivanov, G.I. Kavalero, *Theoretical aspects of measuring systems intellectualization*, *Measuring technique*, 10 (1991) pp. 8-10 (in Russian).
- [7] S.N. Vasil'ev, A.K. Zherlov, E.A. Fedosov, B.E. Fedunov, *Intelligent control of dynamic systems*, Fizmatlit: Nauka / Interperiodika, Moscow, 2000 (in Russian).
- [8] V.A. Gamiy, V.A. Koshcheev, A.L. Shestakov, A. s. 1673990 SSSR, *Discoveries and inventions*, 12 (1991) pp. 191 (in Russian).
- [9] A.L. Shestakov, E.V. Soldatkina, *Adaptation algorithm of measuring system parameters by criterion of dynamic error minimum*, *Bulletin of the South Ural State University. Series "Computer Technologies, Automatic Control & Radioelectronics"*, 9 (2001), pp. 33-40 (in Russian).
- [10] A.L. Shestakov, E.V. Soldatkina *Measuring transducer with parameters adaptive to dynamic error criterion*, in: *Information-measuring and control systems and devices proc.*, SUSU Publishing, Chelyabinsk (2000) pp. 126-134. (in Russian).
- [11] A.L. Shestakov, A. s. 1571514 SSSR, *Discoveries and inventions*, 22 (1990) pp. 192 (in Russian).
- [12] A.L. Shestakov, *Dynamic error correction method*, *IEEE Transactions on Instrumentation and Measurement*, 45 (1996) pp. 250–255.
- [13] A.L. Shestakov, *Modal synthesis of measuring transducer*, *Proceedings of the RAS. Theory and Control Systems*, 4 (1995) pp. 67-75 (in Russian).
- [14] A.L. Shestakov, *Measuring transducer of dynamic parameters with iterative principle to signal recovery*, *Instruments and Control Systems*, 10 (1992) pp. 23-24 (in Russian).
- [15] A.L. Shestakov, *Theory approach of automatic control in dynamic measurements: monograph*, SUSU Publishing, Chelyabinsk, 2013 (in Russian).
- [16] A.L. Shestakov, *Dynamic measurements based on automatic control theory approach*, in: *Advanced Mathematical and Computational Tools in Metrology and Testing X. F. Pavese, W. Bremser, A. Chunovkina, N. Fischer, A.B. Forbes (Eds.)*. World Scientific Publishing Company, Singapore, 2015, pp. 66–77.
- [17] *Methods of classical and modern automatic control theory. Vol. 1: Mathematical models, dynamical characteristics and analysis of automatic control systems*, K.A. Pupkov, N.D. Egupov (Eds.), BMSTU Publishing, Moscow, 2004 (in Russian).
- [18] B.N. Petrov, V.Yu. Rutkovskiy, I.N. Krutova etc. *Principles of construction and design of adaptive control systems*, Mashinostroenie, Moscow, 1972 (in Russian).
- [19] A.S. Volosnikov, A.L. Shestakov, *Neural network dynamic model of measuring system with recovered signal filtration*, *Bulletin of the South Ural State University. Series "Computer Technologies, Automatic Control & Radioelectronics"*, 14 (2006) pp. 16-20 (in Russian).
- [20] A.S. Volosnikov, A.L. Shestakov, *Dynamic measurements error correction on the basis of neural network inverse model of a sensor*, *Proc. of 21st IMEKO World Congress, Aug. 30 – Sept. 4, 2015, Prague, Czech Republic*, pp. 2082-2087.
- [21] A.L. Shestakov, M.N. Bizyaev, *Dynamically distorted signals recovery of testing measuring systems by sliding mode control approach*, *Proceedings of RAS. Energetics*, 6 (2004) pp. 119-130 (in Russian).
- [22] A.L. Shestakov, M.N. Bizyaev, *dynamic measurement transducer with sliding mode control*, *Bulletin of the South Ural State University. Series "Computer Technologies, Automatic Control & Radioelectronics"*, 4 (2003) pp. 35-41 (in Russian).



International Conference on Industrial Engineering

On dynamic temperature distributions in the molten bath of the magnesite ores

Igizianova N.A.*, Igizianova A.Y.

South Ural State University, Slatoust, Russian Federation

Abstract

The relevance of this article is due to the enormous value of refractories in the national economy. Refractory materials are the materials produced of mineral raw materials and are capable of retaining their functional properties under a variety of conditions at high temperatures without significant deformations; such materials are used for metallurgical processes, furnace designing, and high-temperature units. There is solved a partial differential equation of parabolic type, non-linear in the second derivatives. The solution is carried out by using the MATLAB software. The article presents the results of researching temperature distribution in conductive magnesite melt, depending on the current leads location.

© 2015 The Authors. Published by Elsevier Ltd. This is an open access article under the CC BY-NC-ND license

(<http://creativecommons.org/licenses/by-nc-nd/4.0/>).

Peer-review under responsibility of the organizing committee of the International Conference on Industrial Engineering (ICIE-2015)

Keywords: refractory materials, fused periclase, thermoelectric processes, the molten liquids; distribution of temperature, the numerical method of nets, software tools.

1. The role and place of refractories in the national economy

Refractory materials have increased strength at high temperatures and chemical inertness. In composition, the refractory materials are ceramic mixture of refractory oxides, silicates, carbides, nitrides, borides, there are mostly non-metallic material having fire resistance not less than 1580 °C [1].

Refractory products occupy a leading position in the production of many materials and construction of thermal units. Without refractories there is impossible construction of the thermal units: reheating furnaces, furnaces, boilers, heat generators, heat storage, various energy and chemical plants, nuclear and laser devices. Moreover, the space

* Corresponding author. Tel.: +7-963-078-47-83;
E-mail address: nadine-66@mail.ru

exploration - the flight of rockets and the existence of man in the cosmos - is also impossible without refractories. The situation on the Russian market is as a whole defined by specialized refractory plants, producing 70-75% of refractory products and materials in the country. [2].

Refractory materials and products ensure an efficient operation of the main production units and machines in most branches of modern industry. In many cases the function and performance of entire process systems due to quality and performance properties of refractories. This primarily relates to the ferrous and nonferrous metallurgy, energy, chemical industry and so on. They are widely used in the production of iron and steel for lining of technological units, tanks for storage and transportation of liquid metal furnaces for heating billets and so forth. Progress in the creation of new types of highly refractory materials has substantially developed technological schemes of production and casting, increase energy-saving effect and ensure the stability of the steel systems in general. It is obvious that the use of new types of highly refractory products allows to significantly reduce unit costs per tonne of steel, increase the productivity of the main metallurgical facilities and, most importantly, the reliability of their work. [3] Production of high strength materials, to which, in particular, relates fused periclase carried out in industrial furnaces steelworks in aggregates with high (over 1000 °C) temperature conditions.

Basic thermoelectric processes that determine the quality of the product - melted periclase occur in non-metallic high-temperature liquid medium through which electrical current is passed. The problems of the distribution of electricity and energy generation in liquid non-metallic high-temperature environments are being paid insufficient attention. And the opportunity to save energy by improving periclase production technology makes this task even more urgent and promising.

2. The thermoelectric aspects of production technology

Caustic magnesite "melts" at 3000 °C and higher in electric arc furnaces that operate on a three-phase alternating current and comprise a casing of 2 sections, set on a trolley with a rotating platform. Furnace transformers are powered by 8000 kW · A with voltages from 90 to 260 V with the same steps. The system includes three electric smelting furnace electrode with a diameter of 457 mm, which are moved by a hydraulic actuator. All operating data is properly measured using a computerized data retrieval system.

Magnesite (6 mm) and a return are supplying into the furnace (Fig. 1) at a controlled rate. The electrode clamp descends to the bottom of the furnace shell as long as the layer of caustic magnesite small holes are not formed. Three graphite rod with a diameter of not less than 30 mm are placed on a layer of the starting material at the bottom of the shell so that they form a triangle with each end of each rod penetrating into preformed recesses (the angles of graphite to be aligned with three electrodes). When the electrodes are lowered and relate graphite, power is supplied, an arc is ignited, and under each electrode form baths of molten feedstock, which begin to increase towards other baths. After combining all the baths in one bath its size will be sufficient to allow an electric current independently; voltage can be increased to the working level.

The operating voltage is set, and the current is adjusted by setting the height of the electrodes over the molten bath. The automatic control system controls a current and a voltage, and continuously adjusts the height of the electrodes to ensure continuous operation. The diameter of the molten magnesite bath under the electrodes continues to grow to such an extent until the edges will not be at a distance of 300 - 400 mm from the furnace shell. After that it requires a constant supply of raw materials to the furnace, which is regulated by an automatic feeding system. Feedstock surrounding layer solidifies and forms a cover for the molten magnesite. This layer forms an insulating crust layer and consists of a partially melted and sintered material and impurities. During the melting cycle the feed rate is adjusted to maintain the unmelted raw material also on top

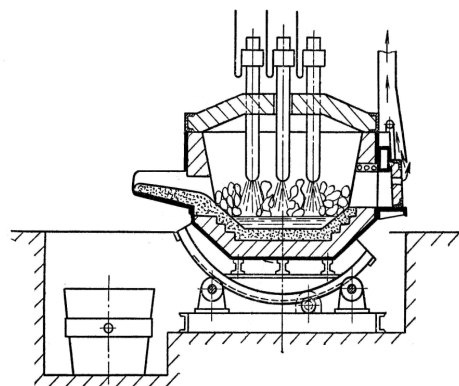


Fig. 1. Scheme of an electric arc smelting furnace.

of the bath, which reduces energy consumption. In the process of melting the electrodes gradually raise by means of an automatic control system to maintain the liquid bath of fused magnesium oxide in the arc covered with a thin layer of feed material until a large ingot of the molten composition [4].

In the process of melting the raw material undergoes complex physical and chemical transformations. Due to the inhomogeneous temperature conditions, nonequal crystal growth and effects of gravity during the periclase melting occurs a noticeable differentiation of melt components, and the separate block areas are enriching with magnesium oxide, whereas the impurities accumulate in the crust, in the central zone and in the melting dust. The smelted block has heterogeneous chemical composition, density, macro and microstructure. Heterogeneity due to its zonal structure, determined by the degree of melting of the material, by conditions of crystallization in a variety of areas, by the migration of impurity oxides, and by other factors [5].

3. Estimations of temperature fields and the main results

The purpose of this paper is to provide dynamic allocation of thermal energy generated by an electric current, around the perimeter of the molten bath at the different mutual arrangement of electrodes and to identify the optimal conditions to achieve an uniform distribution of heat and therefore to save electricity.

A period of the immediately melting is usually more than half of the length of entire melting process, it wastes 60-80% of the total electricity consumed for melting. The main task of this period is to heat up a raw material to the melting point, to maintain this temperature until complete melting of raw materials and provide the required overheating of the bath. Electric mode is unstable at the beginning, it released in a small volume under the electrodes an enormous power, as resulting it formed in a charge melt. The larger is an area of melt contact with the electrode, the greater is current.

The mixing of the liquid magnesite causes the intense heat exchange in a magnesite bath. The energy equation

$$\frac{\partial T_m}{\partial \tau} + \frac{\partial T_m}{\partial x} v_x + \frac{\partial T_m}{\partial y} v_y + \frac{\partial T_m}{\partial z} v_z = \frac{\lambda_m}{c_m \rho_m} \cdot \Delta T_m + \frac{1}{c_m \rho_m} E^2 \cdot \sigma_m \quad (1)$$

gives the amount of heat, expressed in the temperature characteristic T and carried through the layer of liquid magnesite.

Here are τ time; v_x, v_y, v_z - vector components of the linear velocity of the liquid magnesite; $\lambda_m, c_m, \rho_m, \sigma_m$ - respectively, thermal conductivity, heat capacity, density and specific electroconductivity of liquid magnesite; Δ - Laplace operator; E - electric field intensity.

The boundary and initial conditions have being add: $T(0) = T_0, T|_B = T(\tau)$;

- the density of a heat flux, transferred from the liquid surface into the environment as a function of time: $q = \alpha(T_e - T_f)$; α is a heat transfer coefficient;
- the heat transfer between the liquid surface and the environment:

$$\left(\frac{\partial T}{\partial n}\right)_c = -\frac{\alpha}{\lambda}(T_e - T_f).$$

In practice, for assessing the thermal flux passing through the liquid magnesite, the complex process of heat transfer through the layer of liquid magnesite can be replaced by the equivalent thermal conductivity process. Here was the coefficient of thermal conductivity λ_m included in the formula of the coefficient of thermal diffusivity a , replaced by a coefficient of effective heat conductivity $\lambda_{m,ef}$, taking into consideration the transfer of heat from the moving particles of magnesite. To assess this parameter there was carried out an experiment on the example of the electroslog process [6]. We have the following estimates of the parameters in equation (1):

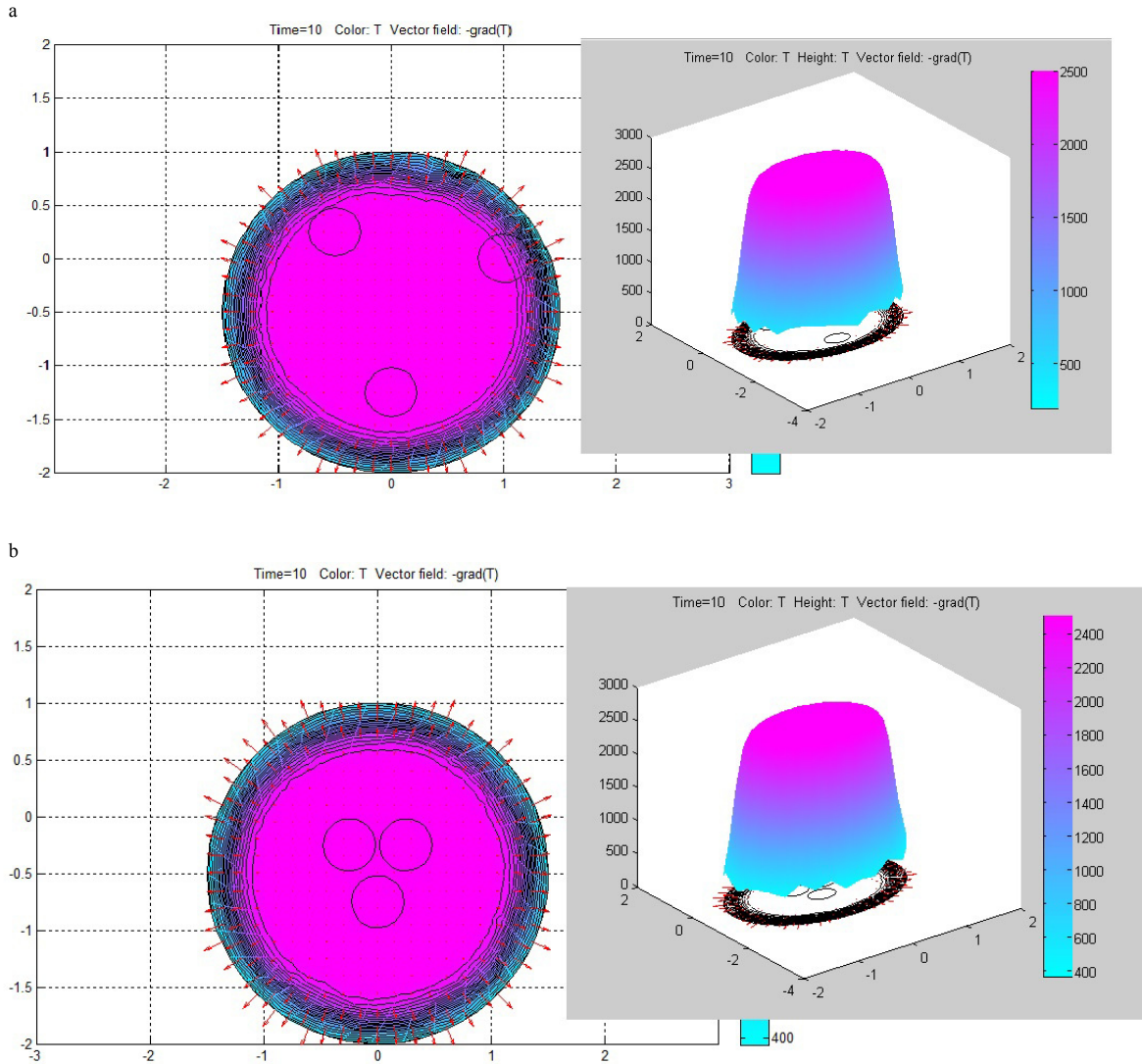
$$\lambda = 1.16 \frac{\text{W}}{\text{m}\cdot\text{K}}, \rho = 0.8 \cdot 10^3 \frac{\text{kg}}{\text{m}^3}, c_v = 1.05 \frac{\text{J}}{\text{kg}\cdot\text{K}}, E = 0.1 \frac{\text{V}}{\text{m}}, \sigma = 10^7 (\text{Om} \cdot \text{m})^{-1},$$

and it takes the form for surface of a magnesite melt:

$$\frac{\partial T}{\partial \tau} + \frac{\partial T}{\partial x} v_x + \frac{\partial T}{\partial y} v_y = 1.38 \cdot 10^{-3} \Delta T + 119, \tag{2}$$

forming a boundary value task of thermal field distribution $\bar{T}(x_i)$ in space of liquid nonmetallic high-temperature environments with the boundary conditions $T(0) = 0^{\circ}C$, $T|_{x=0} = 2500^{\circ}C$.

Capabilities of the analytical solutions are very limited, although there are a number of special methods, so dominant is a numerical method of nets, and as an option - a method of central differences with the calculation of approximation of a heat flow function in the nodes of the partition grid, as well as the method of adaptive grids using a suitable control function [7]. Implementation of such problems of mathematical modeling is possible as an individual by means of software and with the existing software tools: MatCad, Derive, Maple, MatLab and others. They allow you to find both analytical and numerical solutions of ordinary differential equations and partial differential equations with graphically visualization of solutions. The stated boundary value task was solved with the assistance of the software tool MatLab [8] (Fig. 2).



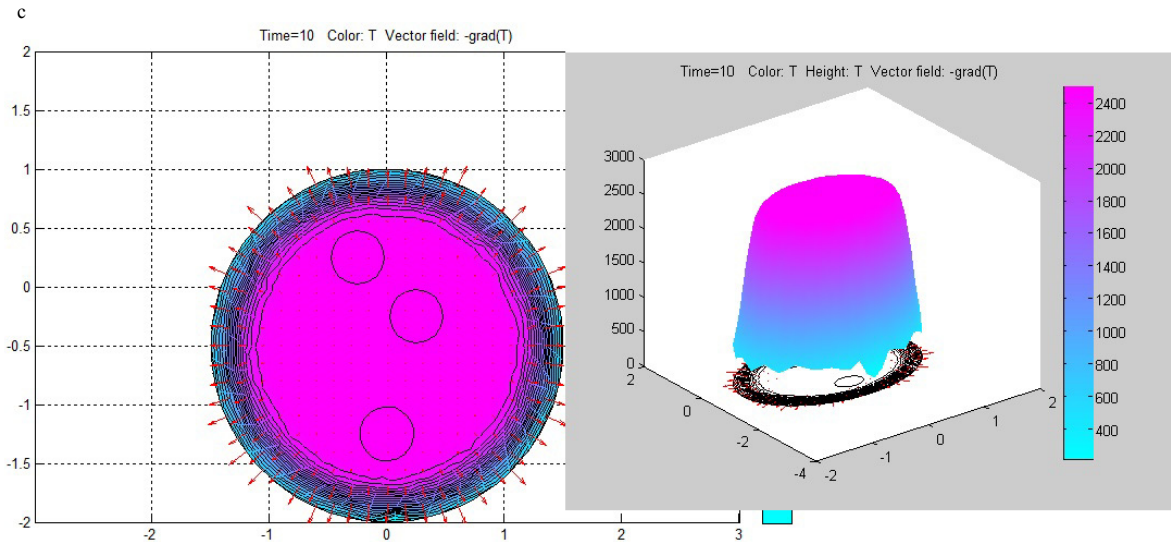


Fig. 2. The temperature distribution over the surface of a magnesite bath in the steady process of remelting depending on the the electrodes locations (a) evenly; (b) centered; (c) chaotic.

As a result of conducted in the experiment researches, we can conclude confirmation an assumptions about a significant anisotropy of energy field in the magnesite melt, as well as in the electroslag field, due to high temperature gradients [9]. The pattern of the energy field distribution practically does not depend on the location of current sources on the molten bath perimeter, apparently due to its relatively small size. However, a sharp temperature drop from 2500°C in the middle of the object to 400°C towards a periphery says about points to the need a thoroughly mixing of magnesite powder during the melting because at temperatures below 2000°C melting process melting does not happen.

References

- [1] K.K. Strelou, P.S. Mamykin, Technology of refractories, "Metallurgy", Moscow, 1978.
- [2] The development prospects of Russian enterprises for the production of refractory materials, Management of economic systems (electronic scientific journal), 2013. URL: <http://www.uecs.ru/ekonomicheskij-analiz/item/2215-2013-06-24-06-41-56>.
- [3] World market: where moves the refractory industry, Metal of Ukraine and of the world. 2015. URL: <http://ukrmet.dp.ua/2015/06/15/mirovoj-rynok-kuda-dvizhetsya-ogneupornaya-otrasl.html>.
- [4] O.N. Popov, D.G. Ribalkin, V.A. Sokolov, Production and application of melt-molded refractories, Metallurgy, Moscow, 1985.
- [5] K.V. Simonov, Y. G. Gaponov, The impact of the brucite meltregime on a quality of periclase, Refractories. 4 (1982) 15–23.
- [6] G.S. Marinsky, V.L. Shevtsov, B.I. Medovar, The thermal processes at electroslag remelting, Science Dumka, Kiev, 1978.
- [7] A.D. Polyaniin, V.F. Zaitsev, A.I. Zhurov, Methods for the solving nonlinear equations of mathematical physics and mechanics: a tutorial, FIZMATLIT, Moscow, 2009.
- [8] N.Y. Golden, The use of MATLAB in the scientific and academic work: teaching and learning materials, Nizhny Novgorod, 2006.
- [9] N.A. Igizyanova, Features of termoelectrodynamic processes in hightemperature liquid non-metallic environments, Vacuum Electron Sources Conference (IVESC): Materials of the 10th international conference. - St. Petersburg: IEEE, Print ISBN: 978-1-4799-5770-5, INSPEC Accession Number: 14565865. (2014). DOI: 10.1109 / IVESC.2014.6891998.



International Conference on Industrial Engineering

Surface as an object of computer geometric modelling

Korotkiy V.A., Usmanova E.A., Khmarova L.I.*

South Ural State University, 76, Lenin Avenue, Chelyabinsk, 454080, Russian Federation

Abstract

The geometric model of a surface is formed taking into consideration the set of functional, structural, technological, economic, and aesthetic requirements. These requirements are formulated in terms of geometry and are expressed through the surface parameters. The surface is modeled with the help of either the kinematic method or the two-dimensional interpolation method. In accordance with the kinematic method, the surface is formed as a continuous one-parameter set of curves which forms the simulated surface. The kinematic method studied in the article is based on the curves of the second order with variable eccentricity. In order to control the shape of the constructed surface, directing ruled surfaces are used. The authors develop a computer program which determines the eccentricity of the forming curves depending on the boundary conditions. The program allows plotting a curve of the second order assigned by the arbitrary set of five coplanar points and tangents. When modeling a surface passing through a close circuit, this circuit is mapped in four-dimensional space. The abovementioned mapping gives a larger control over the shape of the surface. It is shown that the kinematic method of computer surface modeling has more technological advantages compared to the interpolation method.

© 2015 Published by Elsevier Ltd. This is an open access article under the CC BY-NC-ND license (<http://creativecommons.org/licenses/by-nc-nd/4.0/>).

Peer-review under responsibility of the organizing committee of the International Conference on Industrial Engineering (ICIE-2015)

Keywords: The curve of the second order, kinematic way to simulate the surface, directing curve, forming curve, frame of the surface, four-dimensional space.

1. Introduction

The surface properties are dependent on the properties of the lines which form this surface. For instance, when designing streamlined surfaces circular rational curves are used [1, 2]. One of the main ways of modeling is a method of forming the kinematic surface [3, 4]. Curves of the second order can be used for forming a frame of a surface [5]. The main instrument of modern CAD modeling of curves and surfaces are NURBS-curves [6, 7].

* Corresponding author. Tel.: +7-351-267-92-60.

E-mail address: khmarovali@susu.ac.ru

If there are no special requirements to the surface straight or curved lines of the second order can be used for its modelling. Therefore, the author represents the actual task of developing a method of computer simulation of geometric surfaces with curves of the second order.

Algorithms for constructing the curves of the second order which pass through the given points and which are tangent to the given lines are known from the course of projective geometry [8, 9]. Some algorithms are practically implemented in the programs [10, 11]. Full solution to the problem of constructing the curve of the second order is considered in [12, 13, 14]. The program of constructing the curves of the second order is implemented in the Autocad graphic editor in the Autolisp language [15]. Kinematic method of constructing a surface is considered in descriptive geometry [16]. Additional modeling capabilities appear in the process of mapping the surface on a four-dimensional space [17, 18].

2. Task Assignment

The rectangular spatial close circuit ABCD is given, the front segments AB and CD are the arcs of the curves of the second order. The side segments AD and BC are the arbitrary smooth curves (Fig. 1). It is required to construct a continuous smooth surface based on this contour.

To solve the problem it is proposed to use two different ways of modeling. According to the first method, the curve m which is called the forming curve slides along the segments AD and BC gradually changing their shape from arc AB to arc CD [19, 20]. Another way of modeling is based on mapping of the ABCD surface on four-dimensional space.

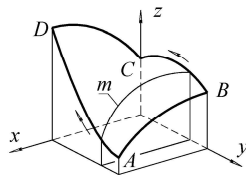


Fig. 1. The support contour

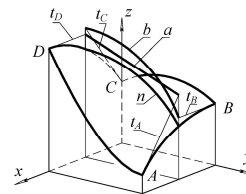


Fig. 2. The determinant of the surface

We require that the forming curve m is a curve of the second order. The curve of the second order has five degrees of freedom on a plane; therefore, to control the shape of the forming curve five conditions should be specified. Suppose, for example, the surface must pass through the convex forming curve n the plane of which is parallel to the plane of the side segments of the circuit (Fig. 2). We shall indicate the following support ruled surfaces: conoid η (AD, a) and cylindroid ψ (BC, b). The simulated surface is tangent to conoid η at points of the section AD and to cylindroid ψ - at the points of the segment BC.

The forming curve n and two adjoining ruled surfaces η , ψ completely define the surface which is based on the four-bar contour. Setting an arbitrary value y corresponds to two points on the side segments of the contour, two tangents at these points and a point on the forming curve n . The five elements (three points and two tangents) define a single second-order curve. This curve is the desired forming curve m at a given value of the coordinate y . Thus, the constructed surface is not determined by a two-parameter set of points but with a one-parameter set of curves of the second order.

We consider three options of forming the surface - with a convex (Fig. 3a), a rectilinear (Fig. 3b) and a concave (Fig. 3c) additional directing curve n the plane of which is parallel to the plane of the side segments of the supporting contour. In accordance with the considered algorithms there appears a continuous smooth surface formed by a one-parameter set of curves of the second order.

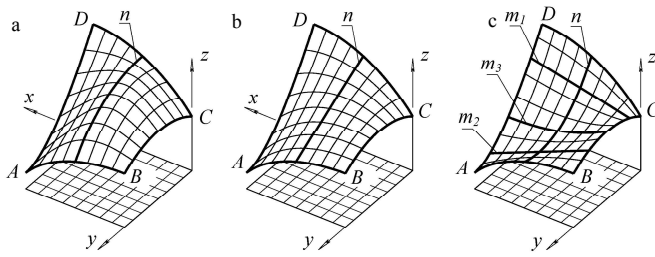


Fig. 3. (a) the surface on the closed circuit convex guide; (b) the surface on the closed circuit straight guide; (c) the surface on the closed circuit concave guide

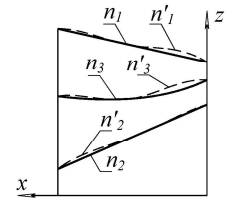


Fig. 4. Comparison of profiles

The task can be solved by means of a two-dimensional interpolation (loft) available in a graphically-oriented CAD. We compare the results of geometric modeling obtained by using loft computational procedure and by the considered algorithm. For the comparison we choose the surface with a concave directive curve. We compare the surface profiles in sections which pass through the forming curves $n1, n2, n3$ (Fig. 4). According to the proposed algorithm, the surface comprises rectilinear forming curves $n1, n2$. But loft computational procedure generates a surface where instead of rectilinear forming curves there arise noticeable oscillations $n1', n2'$ which should be considered as structural defect of the model.

3. Examples of Kinematic Surfaces

With the help of the considered algorithm we can obtain geometric models of various architectural shells based on arbitrary flat or spatial contour (Fig. 5). The shell which is based on a flat contour and intersects the segments of the ellipse e and the hyperbole g includes the watershed line n .

The form of the shell varies with the position of the directive curve BC and AC (Fig. 5a). Oval surface which is based on the arc of the ellipse e is formed by the curve of the second order m which slides along the directive curve n (Fig. 5b). The surface on a rectangular contour is formed by the movement of the forming curve the shape of which is changed from a triangle with a vertex A to the arc of the circle (Fig. 5c).

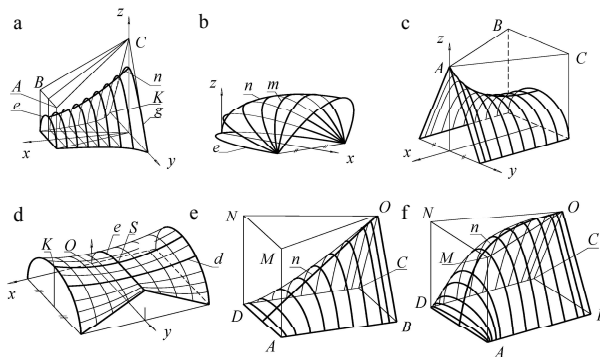


Fig. 5. (a-b) shell on a random basis; (c-f) shell on a rectangular base

Suppose it is required to pull the shell on the spatial contour consisting of a circle, a triangle, a segment of a straight line, and directive lines d, e (Fig. 5d). In this case part of the surface is formed by a second-order curve and changes shape from an arc to a straight line.

Fig. 5, d, e shows a shell resting on a rectangular base. Carcasses of all surfaces, as shown in Fig. 5, are formed by arcs of curves of the second order.

If the shell is based on a flat triangular or quadrangular foundation its frame can be formed by two families of curves of the second order [21, 22]. Suppose it is required to construct a smooth shell on a rectangular base (Fig. 6a). The surface is formed at parallel movement of the forming line along the directive watershed line lying in plane xz . The arc of an ellipse is used as a watershed line. The image of the line changes its shape from an elliptical arc to a segment of the line. The surface is formed by two families of ellipses and may be called an elliptical dome.

An elliptical dome on a rectangular foundation is described by an algebraic equation of the fourth order

$$\frac{x^2}{a_0^2} + \frac{y^2}{b_0^2} + \frac{z^2}{c_0^2} - \frac{x^2 y^2}{a_0^2 b_0^2} = 1, \quad (1)$$

where a_0, b_0, c_0 are the dimensions of the dome. In the section of the dome with the plane $z = 0$ we obtain two pairs of parallel lines $x = a, y = b$ which correspond to a rectangular base.

The shell with a foundation in the shape of a right triangle contains three families of elliptic forming lines and is described by an algebraic equation of the third order

$$xy^2 - xy + x^2 y + \frac{\delta}{\varepsilon} z^2 = 0, \quad (2)$$

where a_0, b_0, c_0 are the dimensions of the dome. In the section of the dome with the plane $z = 0$ we obtain two pairs of parallel lines $x = a, y = b$ which correspond to a rectangular base.

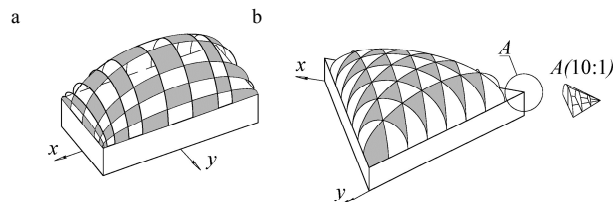


Fig. 6. (a) elliptical dome on a rectangular base; (b) elliptical dome on triangular base

The shell with a foundation in the shape of a right triangle contains three families of elliptic forming lines and is described by an algebraic equation of the third order

$$xy^2 - xy + x^2 y + \frac{\delta}{\varepsilon} z^2 = 0, \quad (3)$$

where the coefficients δ and ε are determined by the ratio of the base and the height of the dome (Fig. 6b).

4. Surface in a Four-Dimensional Space

The single-valuedness of the construction of a two-dimensional surface in four-dimensional space R^4 is achieved thanks to the following properties of this space [23, 24-26].

Property 1. Two planes of the general position in the space R^4 not nested in one hyperplane intersect in one point.

Property 2. If the plane is perpendicular to the hyperplane xyt the orthogonal projection of this plane on xyt is degenerated into a straight line.

By assigning the nodal points of the support contour $ABCD$ with the arbitrary coordinates on the axis t we obtain the hyperepure which consists of two three-dimensional projections of the contour on the front $\Gamma(xyz)$ and horizontal $\Gamma'(xyt)$ hyperplanes (Fig. 7). Surface is a two-parameter set of points, so in R^4 two beams of intermediary planes should be set. According to property 1, any pair of planes intersects at one point. A two-dimensional set of points of the intersection of the intermediary planes in R^4 determine the surface which passes through the reference contour $ABCD$.

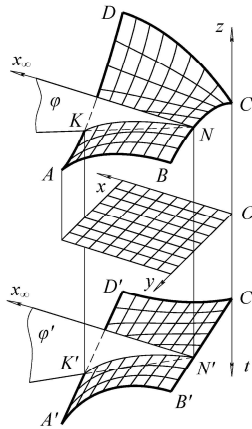


Fig. 7. The surface in the R^4

If one of the links of the four-link circuit has been degenerated into a point then the considered algorithm maintains its constructive certainty. Suppose it is required to create a graphical computer model of the triangular freely stretched sail canvas ABC (Fig. 8a). By assigning the nodes A, B, C with the arbitrary coordinate values along the axis t we obtain the hyperepure of the three-link contour in a four-dimensional space (Fig. 8b).

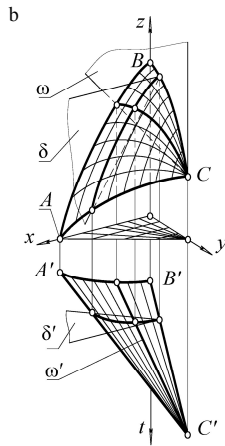


Fig. 8. Four-dimensional model of a sail: a – prototype; b – model

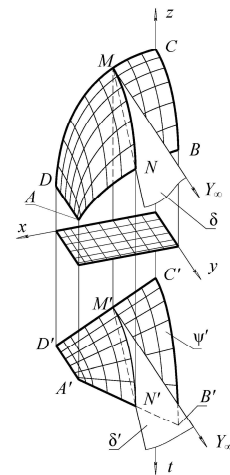


Fig. 9. Four-dimensional model of a surface ship

Suppose it is required to build a unit of a shipboard surface which is limited by the deck line BC , the keel line AD , and frame timbers CD and AB (Fig. 9). We deliver the $ABCD$ contour in the space R^4 giving the nodes arbitrary coordinates on the axis t . We also set the correspondence φ_1 between the points of the links AB and CD by the intermediary hyperplanes of the level $x = const$, and the correspondence φ_2 between the points of the links BC and AD by using hyperplanes of the level $y = const$. Pairs of points correspondent in φ_1 determine the beam of planes δ which range from the deck to the keel. Pairs of points correspondent in φ_2 determine a beam of planes ω which range between frame timbers AB and CD . The set of points of intersection of the planes δ and ω in R^4 determine the desired surface.

Thus, if the deck line is defined as a curve of the second order the surface may be formed by the movement of the curve of the second order MN in accordance with the directive curves of the frame timbers AB and CD .

5. Conclusion

A method of computer modeling of geometric surfaces with curves of the second order as the major formative element is proposed. Algorithms of modeling are based on kinematic representation of a surface in the space of three or four measurements. For a constructive implementation of the proposed algorithm a program of construction of a curve of the second order which passes through the given point and tangent to the set of lines are given.

References

- [1] G. S. Ivanov, Designing of technical surfaces, Moscow, Mechanical engineering, 1987.
- [2] Ya.L. Geronimus, Geometrichesky device of the theory of synthesis of flat mechanisms, Moscow, Publishing house of physical and mathematical literature, 1962.
- [3] G. S. Ivanov, Theoretical fundamentals of descriptive geometry: manual, Moscow, Mechanical engineering, 1998.
- [4] A.V. Bubennikov, Descriptive geometry: manual, Moscow, The higher school, 1985.
- [5] V. E. Mikhaylenko, V.S. Obukhov, A.L. Podgorny., Formoobrazovaniye of covers in architecture: monograph, Kiev, Budivelnik, 1972
- [6] N. N. Golovanov, Geometrical modeling: scientific publication, Moscow, Publishing house of physical and mathematical literature, 2012.
- [7] E.V. Shikin, L.I. Pliss, Curves and surfaces on the computer screen: manual, Moscow, Dialogue MEFPh, 1996
- [8] N. A. Glagolev, Projective geometry: manual, Moscow, The higher school, 1963.
- [9] O. A. Volberg, Main ideas of projective geometry: manual, Moscow, State educational and pedagogical publishing house, 1949.
- [10] <http://dww.no-ip.org> (date of the address 01.09.2015).
- [11] <http://www.kde.org> (date of the address 01.09.2015).
- [12] V. A. Korotkiy, Projective construction horsemen: manual, Chelyabinsk, Publishing center SUSU, 2010.
- [13] V. A. Korotkiy, Projective construction horsemen, set by five valid elements, Depp. in VINITI 19.01.2010, 13-B2010.
- [14] V. A. Korotkiy, Synthetic algorithms of creation of a curve of the second order, in Messenger of computer and information technologies, 2014, No. 11, pp. 20-24.
- [15] V. A. Korotkiy, Creation of the curve of the second order passing through these points and the concerning these straight lines, Certificate about the state registration of the computer program No. 2011611961 of 04.03.2011.
- [16] V. A. Korotkiy, L. I. Khmarova, I.V. Butorina, Descriptive geometry: abstract of lectures, Chelyabinsk, Publishing center SUSU, 2013.
- [17] V.P. Bolotov, Geometrichesky and a program complex of interactive graphic programming in SAPR, Thesis ... Dr.Sci.Tech. – Vladivostok: Publishing house of DVGU, 1993.
- [18] D. V. Voloshinov, Constructive geometrical modeling. Theory, practice, automation: monograph, Saarbrucken, Lambert Academic Publishing, 2010.
- [19] V. A. Korotkiy, E. A. Usmanova, Curves of the second order in problems of a shaping of architectural covers, in News of HIGHER EDUCATION INSTITUTIONS, Construction series, 2014, No. 9-10 (669-670), pp. 101-107.
- [20] V. A. Korotkiy, E. A. Usmanova, Architectural cover on the closed contour, in Messenger SUSU, Construction and Architecture series, 2015, T. 15, No. 2, pp. 47-51.
- [21] V. A. Korotkiy, Elliptic dome on the triangular or quadrangular base, in Volga scientific magazine, 2015, No. 1, pp. 96-102.
- [22] V. A. Korotkiy, E. A. Usmanova, Application of curves of the second order for designing of smooth frame and mesh surfaces, in Messenger SUSU, Construction and Architecture series, 2014, T. 14, No. 3, pp. 45-48.
- [23] V.A. Peklich, The Highest descriptive geometry: manual, Moscow, Publishing house of DIA, 2000.
- [24] V. A. Korotkiy, Computer modeling of figures of four-dimensional space, in Messenger of computer and information technologies, 2014, No. 7, pp. 14-20.
- [25] V. A. Korotkiy, Geometrical modeling of a surface by means of its display to four-dimensional space, in Omsk scientific bulletin, "Devices, Machines and Technologies" series, 2015, No. 1 (137), pp. 8-12.
- [26] V. A. Korotkiy, E. A. Usmanova, L. I. Khmarova, Geometrical designing of covers in the way of an exit in four-dimensional space, in Messenger SUSU, Construction and Architecture series, 2014, T. 14, No. 2, pp. 48-51.



International Conference on Industrial Engineering

Algorithms for constructing resource-saving cutting machines

Makarovskikh T.^{a,b}, Savitskiy E.^a

^aSouth Ural State University, 76, Lenin Avenue, Chelyabinsk, 454080, Russian Federation

^bUral Federal University, pr. Mira, 19, Yekaterinburg, 620002, Russian Federation

Abstract

ICP and ECP technologies for cutting sheet material belong to so called resource-saving technologies. Those allow to overlap the outlines of cut-off details. This article describes mathematical models of cutoff using these technologies and algorithms for cutter routing considering some technological restrictions.

© 2015 The Authors. Published by Elsevier Ltd. This is an open access article under the CC BY-NC-ND license (<http://creativecommons.org/licenses/by-nc-nd/4.0/>).

Peer-review under responsibility of the organizing committee of the International Conference on Industrial Engineering (ICIE-2015)

Keywords: algorithm; hamiltonian trail; cutting problem; routing; plane graph; Eulerian trail.

1. Introduction

It was 1949 when the first publications on linear programming appeared. In 1951 the first issue of [1] appeared. This monograph dealt with problems of using the methods of linear programming for optimal guillotine cutting. The development of enterprise automation lead to appearance of technological equipment with numerical programming control (NPC) used for cutting off the details from a sheet material such as the machines of gas (oxygen), plasma, laser, and EDM cutting. The new technologies allow cutting the details by any trajectory with sufficient accuracy.

If we remove the requirement to cut off only by looping straight cuts then we may significantly reduce the waste of material. This fact became the impulse for a great number of papers on non-guillotine cutting and its optimisation by different enterprises and on the different stages of automation. The detailed review of cutting problems, algorithms, and their solution methods is presented in the paper by A. Filippova [2]. The exact methods of rectangular cutting are used in papers by V. Kartak [3], A. Petunin, R. Devil and his colleagues [4]. A great number of researches work on meta-heuristic methods, i.e. such randomized methods for local searching of optimal solution using algorithmic schemes constructed as an analogue of the nature or technical processes allowing the arbitrary deterioration of the current solution (estrangement from locally optimal solutions) to move to a new searching locality [5]. Some of these algorithms for cutting-and-packing problems are developed by A. Ermachenko and T. Sirazetdinov [6]. The interest to these problems led to appearing the communities uniting the researchers from all

over the world engaged in these problems, for example, ESICUP (EURO Special Interest Group on Cutting and Packing) [7].

Unlike the guillotine cutting plan the non-guillotine one does not define the program for cutting. The constructing of cutting automaton control program for a given cutting plan is a separate problem. In their paper [8] J. Hoeft and W.S. Palekar allow the following classification of routing problems for a sheet cutting.

- General Travelling Salesman Problem (GTSP). The cutter successively goes by a contour of each detail. The incut for each contour is given.
- Continuous Cutting Problem (CCP). The details are cut off consequently. The incut point may be at any part of a contour, and pass to another contour is realized only after the current one is cut off. As well as GTSP this technology does not allow combination of fragments of cutting contours.
- Endpoint Cutting Problem (ECP). The instrument incuts and goes to another cutting plan fragment in the given points of a contour frontier. The combination of contours is allowed. This leads to partial cutting of some contours. To realize this technology one needs represent the cutting plan by a plane graph each component of which be a half-Eulerian graph with odd degree vertices incident to outer face. In this case the route for cutting of each component leads to a problem of OE-trail constructing [9]. The sequence of passing of components is defined by solution of a generalized TSP on the digraph of possible transitions between these components with precedence constraints taking into account the nesting of components into contours of other components. As far as due to combination of fragments of contours the number of components is less than the number of details, then the size of ECP salesman problem in common is less than size of GTSP.
- Intermittent Cutting Problem (ICP). The common case of cutting problem when combining of contours is allowed, and there are no constraints on the choice of incut points. To realize this technology one needs the representation of cutting plan as a plane graph. Unlike ECP components are not to be Eulerian. The construction on a path to cut off each component is reduced to construction on ordered Eulerian covering for the given component by OE-trails [10, 11]. The order of routing of the components is defined by a solution of generalized salesman problem on the digraph of allowed transitions between components with precedence constraints according to the nesting of one components to contours of another ones. The derstriction of component to be Eulerian allow rise their number by overlapping fragments of contour parts and, consequently, decrease the number of components. Hence, the size of ICP salesman problem is not greater than size of ECP salesman problem.

So, ECP and ICP technologies allow to reduce the material waste, the length if a hot cutting, and the length of idle paths due to opportunity of borders of cut details combination. Problems of reducing of material waste and maximal combination of cutting fragments is solved of the stage of cutting plan design. The aim of this paper is to present the mathematical models for routing problem of details cutting and algorithms of defining such paths satisfying technological restrictions. Using of ECP and ICP technologies in a system of technological support of cutting process for a plane details means the following stages.

- Cutting plan design be the definition of such a variant of cut details placement on a rectangular sheet or strip that allow to minimize waste and maximize the length of combined contours of cut-off details [1–3, 6].
- Cutting plan abstracting to a plane graph. To define the sequence of details cutting one does not need any information on the detail shape that is why all the curves without selfintersections and contiguities on a plane representing the shape of details are interpreted as graph edges, and all points of intersections and contiguities are to be graph vertices. To analyze the technological restrictions satisfaction one needs introduce the additional functions on set of vertices, faces, and edges of a graph received.
- Constructing of optimal paths with restrictions on the edges order. These restrictions directly imply technological restrictions on the order of details cutting such as part cut off a sheet does not require additional cuts [12], there are no intersections of cuts [13], the length of idle passes should be minimized [12], the number of incut points should be minimal [14] etc.
- Design of control program for a cutting process using the path defined by algorithm of abstracted routing problem solution. Here the reverse replacement of abstract edges of plane graph by a system of commands to a cutting automaton holds. This replacement allows the movement by curves on a plane according to the detail shape.

- The stages of cutting plan design and interpretation of defined path as commands to a cutting automaton are to be common for all technologies and well known. This paper is devoted to peculiarities of the second and third stages realization for ESP and ICP technologies.

Let's introduce the following nomenclature for abstracting the cutting plan to a planar graph.

Nomenclature

S	plane (model of a cutting sheet)
G	plane graph (model of a cutting plan)
f_0	outer face of graph G
$V(G)$	the set of vertices of graph G
$E(G)$	the set of edges of graph G
$F(G)$	the set of faces of graph G
$ M $	number of elements of set M
$Int(J)$	the union of all components SJ without outer face (any part of graph $J \subseteq G$ the theoretical-set union of its inner faces); may be interpreted as a part cut off a sheet

2. Abstracting of Cutting Plan to a Planar Graph

Let plane S be a model of a cutting sheet then the model of cutting plan be a plane graph G having outer face f_0 on S . The set of graph G components that are non-homeomorphic to a circle let be the points of contiguity of three or more cutting plan fragments, and corresponding fragments be the edges incident to this vertex. Let the component homeomorphic to a circle be a loop. To represent the image of cutting plan as a plane graph $G = (V, F, E)$ one needs to define the following functions for each edge $e \in E(G)$ [15]:

- $v_1(e), v_2(e)$ be vertices incident to edge e ;
- $f_k(e)$ be a face placed at right when one is moving by edge e from vertex $v_k(e)$ to vertex $v_{3-k}(e), k = 1, 2$;
- $l_k(e)$ be the edge incident to face $f_{3-k}(e)$ and $v_k(e), k = 1, 2$;
- $r_k(e)$ be the edge incident to face $f_k(e)$ and $v_k(e), k = 1, 2$.

There is no problem to get these functions. In fact they are used on a stage of graph G design by a cutting plan. The space complexity of this representation is equal to $O(|E| \log_2 |V|)$. As functions mentioned earlier constructed on graph $G = (V, F, E)$ edges define incident vertices for each edge, incident faces and adjacent edges the following statement holds.

Statement 1. Functions $v_k(e), f_k(e), l_k(e), k = 1, 2$ constructed on graph $G = (V, E)$ edges define plane graph $G = (V, E)$ up to homeomorphism.

So with the use of known coordinates of inverse images of graph $G = (V, F, E)$ vertices and placing the fragments of cutting plan being the inverse images of graph $G = (V, F, E)$ edges any path in graph $G = (V, E)$ may be interpreted as a trajectory of cutter moving.

Lets introduce the following definitions of rank for graph $G = (V, E)$ elements to formalize the technological restrictions on the order of cutting.

Definition 1. Let rank of edge $e \in E(G)$ be a value of function $rank : E(G) \rightarrow \mathbb{N}$ defined recursively:

- let $E_1(G) = \{e \in E(G) : e \subset f_0\}$ be a set of edges bounding outer face f_0 of graph $G(V, E)$ then $(\forall e \in E_1(G))(rank(e) = 1)$;
- let $E_k(G) = \left\{ e \in E \setminus \left\{ \bigcup_{l=1}^k E_l \right\} \right\}$ be a set of rank 1 edges for graph $G_k \left(V, E \setminus \left(\bigcup_{l=1}^k E_l \right) \right)$ then $(\forall e \in E_k(G))(rank(e) = k)$.

Definition 2. Let rank of vertex $v \in V(G)$ be a function $rank : V(G) \rightarrow \mathbb{N}$ value:

$$rank(v) = \min_{e \in E(v)} rank(e)$$

where $E(v)$ be a set of edges incident to vertex $v \in V$.

The rank of edge defines its remoteness from outer face and defines the minimal number of faces to be crossed to get from outer face f_0 to this edge. This allows to define the rank and use graph $G'(F, V, E)$ topologically dual to graph $G(V, F, E)$. The set of vertices of G' be the set F of graph G faces, and edges of G' be define the existence of a non-zero length bound between two faces, i.e. there exist edge $e \in E(G)$.

For all $f \in F(G)$ the distance between f and outer face f_0 in graph G' may be defined by constructing of a tree $T_{G'}^{f_0}$ of shortest paths to $f_0 \in F$ in graph G' . The existence of functions $l_k : E(G) \rightarrow E(G), k = 1, 2$ in representation of G allows define rank functions by time not more than $O(|E| \log_2 |V|)$ [9]. As fragments cut by a cutting plan are the inverse images of faces then the requirement to a sequence of faces passing guaranteeing the lack of cutting the cut-off fragments can be easily formalized in the terms of graph G' . Let \prec be the partial order on $F(G)$ induced by tree $T_{G'}^{f_0}$ of shortest paths to vertex $f_0 \in F : (f_i \prec f_j) \Leftrightarrow (f_j \text{ belongs chain of } T_{G'}^{f_0} \text{ between } f_i \text{ and } f_0)$.

Statement 2. *The order of passing the faces is to be allowed if and only if it is the extension of partial order \prec .*

3. Routing Problems for Plane Graphs

While constructing control manipulating systems by the means of graphs one may map the different elements of manipulator trajectory. Here arise the routing problems with different restrictions, for example, routes in which the next edge is defined by the given cyclic order on the set of edges incident to a current vertex [13, 16]; routes in which some edges should be passed in a predefined order [16]; routes satisfying the restriction of ordered enclosing (OE-routes) [9]. Let any route in plane graph G be considered as a part of a graph with all vertices and edges belonging to this route. This allows formalization of claim to a cutter movement path as a condition of lack of intersection of inner faces of any paths initial part in a given plane graph G with edges of its other part [15]. Let such a route be called as a route with ordered enclosing [11] (or for short OE-route).

Definition 3. *Let a trail $C = v_1 e_1 v_2 e_2 \dots v_k$ of plane graph G be an OE-trail if for any its initial part $C_l = v_1 e_1 v_2 e_2 \dots e_l, l \leq (|E|)$ the condition $\text{Int}(C_l) \cap E = \emptyset$ holds.*

It is proved in [17] that plane Eulerian graphs have Eulerian trails of class OE. This result is also correct for half-Eulerian graphs when one of odd degree vertices is adjacent to outer face. The specified trails solve the routing problem for components being Eulerian and half-Eulerian graphs. If a connected graph G is not Eulerian and contains $2k$ odd degree vertices then according to Listing-Luke theorem it is possible to cover graph by k edge-disjoint trails. We need additional definitions to formalize technological claims.

Definition 4. *Let the ordered sequence of edge-disjoint OE-trails*

$$C^0 = v^0 e_1^0 v_1^0 e_2^0 \dots e_{k_0}^0 v_{k_0}^0, C^1 = v^1 e_1^1 v_1^1 e_2^1 \dots e_{k_1}^1 v_{k_1}^1, \dots, C^{m-1} = v^{m-1} e_1^{m-1} v_1^{m-1} e_2^{m-1} \dots e_{k_{m-1}}^{m-1} v_{k_{m-1}}^{m-1}$$

covering graph G and such that

$$(\forall m : m < n), \left(\bigcup_{l=0}^{m-1} \text{Int}(C^l) \right) \cap \left(\bigcup_{l=m}^{n-1} C^l \right) = \emptyset$$

be called OE-cover.

Routes realizing OE-cover represent the ordered set of OE-trails and contain additional idle passes (edges) between the end of current trail and beginning of the next one. Constructing of OE-cover for graph G solves the given routing problem [10]. The most interesting are covers with minimal number of trails and their length because the transition from one trail to another one corresponds to an idle pass of a cutter.

Definition 5. *Let minimal cardinality ordered sequence of edge-disjoint OE-trails for plane graph G be called Eulerian cover with ordered enclosing (Eulerian OE-cover).*

Let's consider algorithms of OE-routing.

3.1. Constructing of OE-route for a Connected Graph

The easiest case is to construct OE-route for a plane Eulerian graph. This problem can be solved by algorithm *OE-Trail*. The proof of its effectiveness is presented in papers [9] and [15]. These papers also contain the proof that computing complexity of this algorithm does not exceed $O(|E(G)| \cdot \log_2 |V(G)|)$. Let's admit that if graph G to be Eulerian then the first vertex v_0 of Eulerian trail may be any vertex incident to outer face. If graph to be half-Eulerian (i.e. it has two vertices of odd degree) then the necessary condition of Eulerian OE-trail existence means existence of odd degree vertex in the set of vertices adjacent to outer face. If both odd degree vertices are adjacent to

outer face then any of them can be chosen as v_0 . If one of these odd degree vertices does not adjacent to outer face then it should be taken as v_0 . If connected graph G is not Eulerian then it contains $2k$ ($k > 1$) of odd vertices. In this case OE-route will contain k edge-disjoint trails. The problem of constructing of such routes can be solved by algorithm *OE-Router*. The proof of its effectiveness is considered in papers [10, 17]. There is also a proof that computing complexity of algorithm does not exceed the value $O(|E(G)| \cdot \log_2 |V(G)|)$. The drawback of algorithm *OE-Router* is non-optimality of idle passes between the ends of trails. Obviously, the minimal estimation of idle passes length is equal to the length of edges forming a minimal weight matching M on the set of odd vertices. If plane graph G being an image of cutting plan is connected and does not contain any bridges incident to outer face then it is possible to construct an OE-route with edges of matching M and only them being the additional ones. The problem of constructing of such a route can be solved by algorithm *M-OE-Router*.

Algorithm M-OE-Router

Input: connected plane graph G , specified by functions $v_k(e), f_k(e), l_k(e)$, $e \in E(G)$, $k = 1, 2$; vertex $v_0 \in V(G)$ incident to outer face; matching M on the set of odd degree vertices.

Output: almost ordered set C of OE-trails of graph G being the OE-cover of graph G .

Intermediate data: for each $v \in V(G)$ the queue $Q(v)$ of incident edges $e \in E(V)$ ordered by decreasing of ranks; vertices $u, v \in V(G)$; edge $e \in E(G)$; a symbol $\#$ of trail ending; for each vertex $v \in V(G)$ mark

$$\text{Odd}(v) = \begin{cases} \text{true}, & \text{if } v \in V_{\text{Odd}}, \\ \text{false}, & \text{if } v \notin V_{\text{Odd}}; \end{cases}$$

Step 0. *<Initialization>* $v := v_0$; $C \ll v_0$; for all $v \in V(G)$ define the value of mark $\text{Odd}(v)$.

Step 1. *<Marking>* Define the ranks of all edges, vertices and faces of graph G . For each vertex $v \in V(G)$ form a queue $Q(v)$.

Step 2. If $\text{Odd}(v)$ go to Step 3, otherwise go to Step 4.

Step 3. If $Q(v) = \emptyset$ go to Step 7, otherwise go to Step 5.

Step 4. If $Q(v) = \emptyset$ then Stop, otherwise go to Step 6.

Step 5. If $\text{rank}(v) \leq \text{rank}(M(v))$ go to Step 7, otherwise go to Step 6.

Step 6. Run the following operators:

$e \ll Q(v)$; /* move the first element from queue $Q(v)$ to variable e */

$v := u : e = \{v, u\}$; $C \ll e \ll u$; /* the next edge and vertex of a trail */

go to Step 2.

Step 7. Run the following operators:

$u = M(v)$; /* the next vertex u is a mate of vertex v */

$\text{Odd}(u) := \text{Odd}(v) := \text{false}$; /* delete vertices u, v from list V_{Odd} */

$C \ll v \ll \# \ll u$; $v := u$; /* ending the current trail and beginning the new one */

go to Step 2.

End of algorithm *M-OE-Router*

The proof of this algorithm effectiveness for plane graphs without bridges is given in paper [18]. At the same paper it is shown that computing complexity of algorithm does not exceed the value $O(|E(G)| \cdot \log_2 |V(G)|)$. Let's admit that connected plane graphs being the images of cutting plans do not contain any bridges. Hence, algorithm *M-OE-Router* constructs a route with minimal length of additional edges for them.

3.2. Constructing of OE-route for a Disconnected Graph

Frequently the cutting plan contains details with wholes, sometimes even some details are situated in these wholes etc. Hence, plane graph being the homeomorphic image of such a cutting plan is being disconnected. The solution of routing problems for each component using methods of section 2 allows find the cyclic OE-route for them. The restrictions on the order of components are defined due to Statement 2.

Definition 7. Let face $f \in F(G)$ be separating if graph G' , $\{f\}$ be disconnected.

Let graph \tilde{G} is being received of graph G by adding bridges between components at separating faces. Obviously, the obtained graph \tilde{G} is plane connected graph and it is possible to get OE-route $M(\tilde{G})$ for it. This OE-route

$M(G)$ can be obtained of route $M(\tilde{G})$ if all vertices incident to injected bridges are to be the ends of trails and beginnings of the next ones (i.e. these bridges are to be the idle passes).

Let's consider the way of constructing the bridges connecting graph G and having minimal summary length.

Algorithm *Bridging*

Input: plane disconnected graph G .

Output: plane connected graph \tilde{G} and set B of added bridges.

Step 0. $\tilde{G} := G$; $B = \emptyset$.

Step 1. Define set C_f of separating faces.

Step 2. Run steps 3–6 for each separating face $f \in C_f$, and stop after that.

Step 3. Find set $S(f)$ of all components of graph G incident to face f .

Step 4. Construct the full abstract graph T . Its vertices are the components $S(f)$, and lengths of its edges are equal to distances between the corresponding components.

Step 5. Define the minimal spanning tree $T(T)$ of T .

Step 6. Add edges of MST to graph $\tilde{G} : E(\tilde{G}) := E(\tilde{G}) \cup E(T(T))$, $B := B \cup E(T(T))$.

End of algorithm *Bridging*.

The plane graph \tilde{G} received by algorithm *Bridging* contain bridges that is why algorithm *OE-Router* can be implemented for it. By complication of steps 5 and 6 of algorithm *Bridging* it is possible to reduce the length of idle passes due to using of algorithm *M-OE-Router*. Indeed, if for abstract graph T we use minimal weight hamiltonian cycle $H(T)$ instead of spanning tree $T(T)$ then the resulting graph \tilde{G} will not contain any bridges and using algorithm *M-OE-Router* for it allow to get the OE-route with minimal length of idle passes.

4. Conclusion

The considered mathematical models and algorithms for routing problem of plane graphs are to solve the problem of definition the allowed sequence of cutting the plan using ECP and ICP technologies. These technologies allow combination of cut-off details bounds. The use of these technologies allows to reduce the waste of material, the length of hot cut, and the length of idle passes.

References

- [1] L. Kantorovich, V. Zalgaller, Rational Cutting of Industrial Materials, Nevskiy Dialekt, 2012.
- [2] A. Filippova, Yu. Valiakhmetova, L. Karamova, Ufa Scientific School by E. A. Mukhacheva: Applied Operational Research Problems, Vestnik USATU. 6 (2013) 83–87.
- [3] V. Kartak, A Problem of Packing the Rectangles: the Exact Algorithm on the Base of Matrix Representation, Vestnik USATU: Control, Computers and Informatics. 4(22) (2007) 104–110.
- [4] R. Dewil, P. Vansteenwegen, D. Cattrysse, M. Laguna, T. Vossen, An improvement heuristic framework for the laser cutting tool path problem, International Journal of Production Research. 53(6) (2015) 1761–1776.
- [5] Yu. Kochetov, Probability Methods of Local Search for Discrete Optimization Problems, in: Discrete Mathematics and its Applications. Issue of Lectures of Scientific Schools for Young Scientists on Discrete Mathematics and its Applications. (2000) 87–117.
- [6] A. Ermachenko, T. Sirazetdinov, Decision making under uncertainty, Vestnik of USATU. (2000) 35–39.
- [7] Information on <http://www.fe.up.pt/esicup>
- [8] J. Hoefl, U.S. Palekar, Heuristics for the plate-cutting travelling salesman problem, IIE Transactions. 29(9) (1997) 719–731.
- [9] A.V. Panyukov, T.A. Panioukova, The Algorithm for Tracing of Flat Euler Cycles with Ordered Enclosing, Proceedings of Chelyabinsk Scientific Center. 14(9) (2000) 18–22.
- [10] T. Panyukova, Eulerian Cover with Ordered Enclosing for Flat Graphs, Electronic Notes in Discrete Mathematics. 28 (2007) 17–24.
- [11] A.V. Panyukov, T.A. Panyukova, Chain sequences with ordered enclosing, J. of Comp. and Syst. Sciences Int. 46(1) (2007) 83–92.
- [12] T. Panyukova, Optimization of Resources for Technological Support of Cutting Process, App. Informatics. 3(39) (2012) 20–32.
- [13] H. Fleischner, Eulerian Graphs and Related Topics. Part 1, Ann. Discrete Mathematics. 50(2) (1991).
- [14] M. Verhoturov, P. Tarasenko, Mathematical support of problem of optimization the path of a cutter for plane figure cutting on the base of chain cut, Vestnik USATU: Control, computers and informatics. 2(27) (2008) 123–130.
- [15] T.A. Panioukova, A.V. Panyukov, Algorithms for Construction of Ordered Enclosing Traces in Planar Eulerian Graphs, The International Workshop on Computer Science and Information Technologies' 2003, Proceedings of Workshop. (2003) 134–138.
- [16] H. Fleischner, L.W. Beineke, R.J. Wilson, Selected Topics in Graph Theory. Part 2, Academic Press, 1983.
- [17] T. Panyukova, Trails with Ordered Enclosing in Plane Graphs, Discrete Anal. and Oper. Research. 2(13) (2006) 31–43.
- [18] T. Panyukova, Optimal Eulerian Covers for Plane Graphs, Discrete Analysis and Operation Research. 2(18) (2011) 64–74.



International Conference on Industrial Engineering

Research of spectral influence of vibration impact on the human spine

Palatinskaya I.P.^{*}, Pirogova N.C.

South Ural State University, 76, Lenin Avenue, Chelyabinsk, 454080, Russian Federation

Abstract

The article proposes the model of vibration influence on motor transport operators. The research was conducted in order to determine some aspects of spectral distribution of the vibro loaded condition of a backbone of an operator on departments of a backbone and of equivalent tension. As a vibration external influence the sinusoidal signal corresponding to maximum-permissible values of vibration accelerations for transport vibration of category 1 depending on compound frequencies of octava strips in the range from 1 Hz to 63 Hz was researched. We created a dynamic biomechanical "costal" 3D model of the "head + backbone" system of a motor transport operator, using 'Solidworks' 3D-software, and taking into account anthropometric parameters of a body pose, structural, functional and biomechanical characteristics of cervical, chest and lumbar segments of a backbone.

© 2015 The Authors. Published by Elsevier Ltd. This is an open access article under the CC BY-NC-ND license (<http://creativecommons.org/licenses/by-nc-nd/4.0/>).

Peer-review under responsibility of the organizing committee of the International Conference on Industrial Engineering (ICIE-2015)

Keywords: vibroloading, spine human, modeling, the amplitude-frequency characteristics

1. Introduction

With the growth of opportunities of modern computing means, the great attention, both in the technical scientific directions, and in medical, is given to computer modeling of the biomechanical processes happening in a human body [1...3], which real statement is often complicated because of complexity or impossibility of carrying experiments out in public.

^{*} Corresponding author. Tel.: +7-351-904-26-75;
E-mail address: palatinskaya@mail.ru

This article is devoted to the research of amplitude-frequency distributions of vibroloading on a backbone of the person at impact of the general vibration of the category 1 "transport" on the developed virtual "costal" 3D model of biodynamic system "the head + a backbone" of a person operator of auto transport devices.

2. Relevance

Reduction of vibration impacts from technical devices on the person operator is an actual world problem. From systematic contact of the person with the vibrating equipment the vibro illness which leads to full disability as a result can arise and develop [4]. According to the Ministry of Labour and Social Protection of Russia adverse working conditions are the reason of high level of operational injuries and occupational diseases [5]. By the available estimates of the International Labour Organization (ILO), 2,34 million people die from the accidents and diseases connected with work [6]. The vast majority of them – about 2,02 million – dies of various occupational diseases. From 6300 daily occurring fatal cases connected with work 5500 come because of occupational diseases.

In distribution of the occupational diseases revealed at working in the Russian Federation according to statistical data of Federal Medical Biological Agency, more than 50% illnesses are vibrodiseases of lumbar-sacral radikulopathy [6]. The main share of the workers exposed to such diseases are drivers of various motor transportation devices who are exposed to continuous impact of the general transport vibration [6]. Among the causes leading to occurrence of occupational diseases due to exposure of vibration, are still: constructive defects of transport facilities and imperfections of workplaces of drivers.

The hygienic assessment of permanent and non-permanent general transport vibration effecting on humans, according to [7...10] is carried out primarily considering the spectral analysis of a rating parameter, then the integrated assessment of the frequency of rating parameter, and ends with the integrated assessment considering the time of equivalent vibration exposure (energy) level of rating parameter..

In the spectral analysis the rating parameters are maximum permissible levels of average square values of vibro speed and vibration acceleration or their logarithmic levels depending on compound frequency in the range of 1 ... 63 Hz [7, 8], at the integrated assessment within given frequency range - adjusted value of velocity and acceleration or their logarithmic levels, while integrated assessment of vibration considering the time of its impact on the equivalent level - equivalent to adjusted value of vibration velocity or acceleration or their logarithmic level.

Thus, the developed rough estimate of vibration impact on the operator doesn't allow to reveal distribution of vibroloading on a body of the person, and, therefore, to reveal vibration sensitivity of different departments of a backbone of the person. Obtaining such data would allow to establish a criteria for a choice of economically reasonable ways of decrease a vibroloading of the person operator of transport devices.

3. Formulation of the problem

Developing the dynamic 3D-model of the human body, we build on the operation requirements, depending on the purpose of research, anthropometric accuracy and biomechanical capabilities [11...14].

Anthropometric parameters of the human body-transport operator devices is determined by its working posture [33], see Fig. 1.

The analysis of the literature connected with a structure, physiology and anatomy of a body of the person [15...17], allowed to define structural, functional and biomechanical characteristics of cervical, chest and lumbar - sacral departments of a backbone of a body of the person, see Table 1.



Fig. 1. Working pose of the person operator of motor transportation devices: 1 – height of a spine column, 2 – head height.

According to medical researches an impact of the general vibration leads to the direct microinjuring of a backbone owing to considerable axial loads of intervertebral disks, local overloads in a vertebral and motive segment that leads to a degeneration of disks [18]. Therefore the spine column consisting of bodies of vertebrae and intervertebral disks was originally constructed and then shoots of vertebrae, which purpose of inclusion in the presented model – transfer of the inertial properties corresponding to a real backbone are simply simulated.

Table 1. Properties of materials of vertebrae and intervertebral disks on departments

Department	Element	Quantity	Module Ship's boy of E, MPa	Poisson's coefficient, μ	Density ρ , kg/m ³
The cervical	Vertebrae	7	350	0.3	2020
	Intervertebral disks	5	105	0.4	1102
Chest department	Vertebrae	12	350	0.3	2020
	Intervertebral disks	11	81	0.4	1096
Lumbar department	Vertebrae	5	350	0.3	2020
	Intervertebral disks	4	57	0.4	1090

4. Theoretical part

Creation of 3D-model of biodynamic system "(the head + a backbone) of a person operator of motor transportation devices", was carried out on [19] algorithm offered in work: the formation of information model, design it in a three-dimensional solid model (the software package of SolidWorks), and then importing it and the subsequent simulation in Ansys Mechanical vibronagruzhennosti.

The basis for the construction of the costal model [12] served as X-ray and MRI images of several people male (mean age 30-40 years), see Fig. 2.

System "(head + spine) of a human operator of transport devices is built a three-dimensional model of the human vertebral column in the package of 3D-modeling Solidworks [20]. The "head" of the operator, as shown in Figure 2, is replaced by a material point. It is reasonable that the stress-strain state is seen in the spine. From the "head" of the operator need only inertial characteristics and the coordinates of the center of gravity.

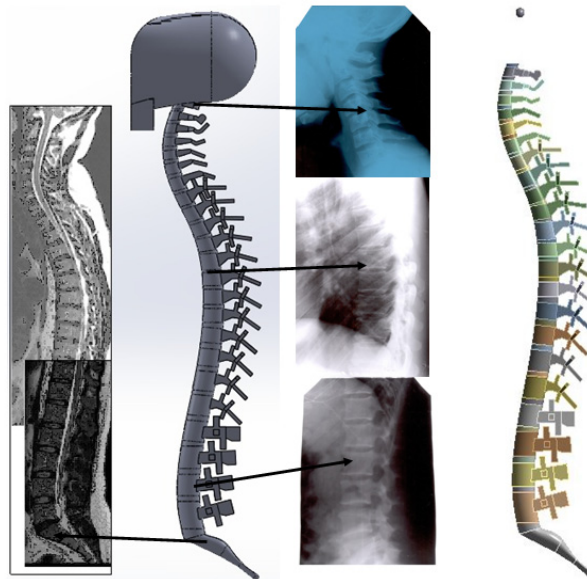


Fig. 2. The calculation model of the spine, built in 3D-modeling package Solidworks.

These characteristics are mass and moments of inertia, they were automatically calculated in the Workbench and can be applied to a material point.

The main assumptions accepted in research:

- only the backbone consisting of vertebrae and intervertebral disks is considered. The soft tissues of the person surrounding it aren't considered;
- the weight of the head is accepted 3,2 kg [17].
- the behavior of vertebrae and intervertebral disks submits to the linear law;
- external influence is necessary sinusoidal: $a(t) = \sin(\omega t)$.

5. Results of experimental studies

On the constructed final and element model calculations of the intense deformed condition of a spine column of the operator who is under the influence of the general vibration of 1 category in frequency range 1 ... 90 Hz were carried out. Parameters of external vibration influence were maximum permissible sizes of the vertical and horizontal vibration accelerations corresponding to compound frequencies of octava strips of f_{sg} (see Table 2) [7]. The studies were conducted using harmonic analysis among AnsysWorkbench.

Results of computer modeling are given in fig. 3, 4.

Table 2.Limit values of vibration transport jobs [7]

f_{sg} , Hz	1,0		2,0		4,0		8,0		16,0		31,5		63	
frequency Range	0,88–1,4		1,4–2,8		2,8–5,6		5,6–11,2		11,2–22,4		22,4–45,0		45,0–90,0	
The coordinate axes	Z ₀	X ₀ , Y ₀	Z ₀	X ₀ , Y ₀										
vibration acceleration,	1,10	0,40	0,79	0,45	0,56	0,79	0,63	1,60	1,10	3,20	2,20	6,30	4,50	13,00

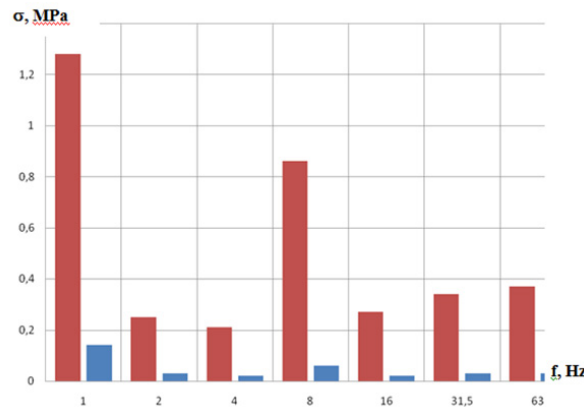


Fig. 3. Histogram distribution of the maximum and minimum values of equivalent stress in the spine, depending on the frequency of the exciting effects.

5. Conclusion

The analysis of results of modeling of impact of transport vibration on the person operator's body at the normalized frequencies (see Table 2) allowed to draw the following conclusions.

The maximum values of equivalent tension in a spine column are revealed on $f_{sg}=1\text{Hz}$ and $f_{sg}=8\text{ Hz}$ (see Fig. 3).

It coincides with data of pilot studies [21], on - which in the range of 2 ... 14 Hz are located resonant frequencies of a spine column of the person. Therefore, the developed "costal" model allows to conduct researches of influence of vibration on the person operator of motor transportation devices.

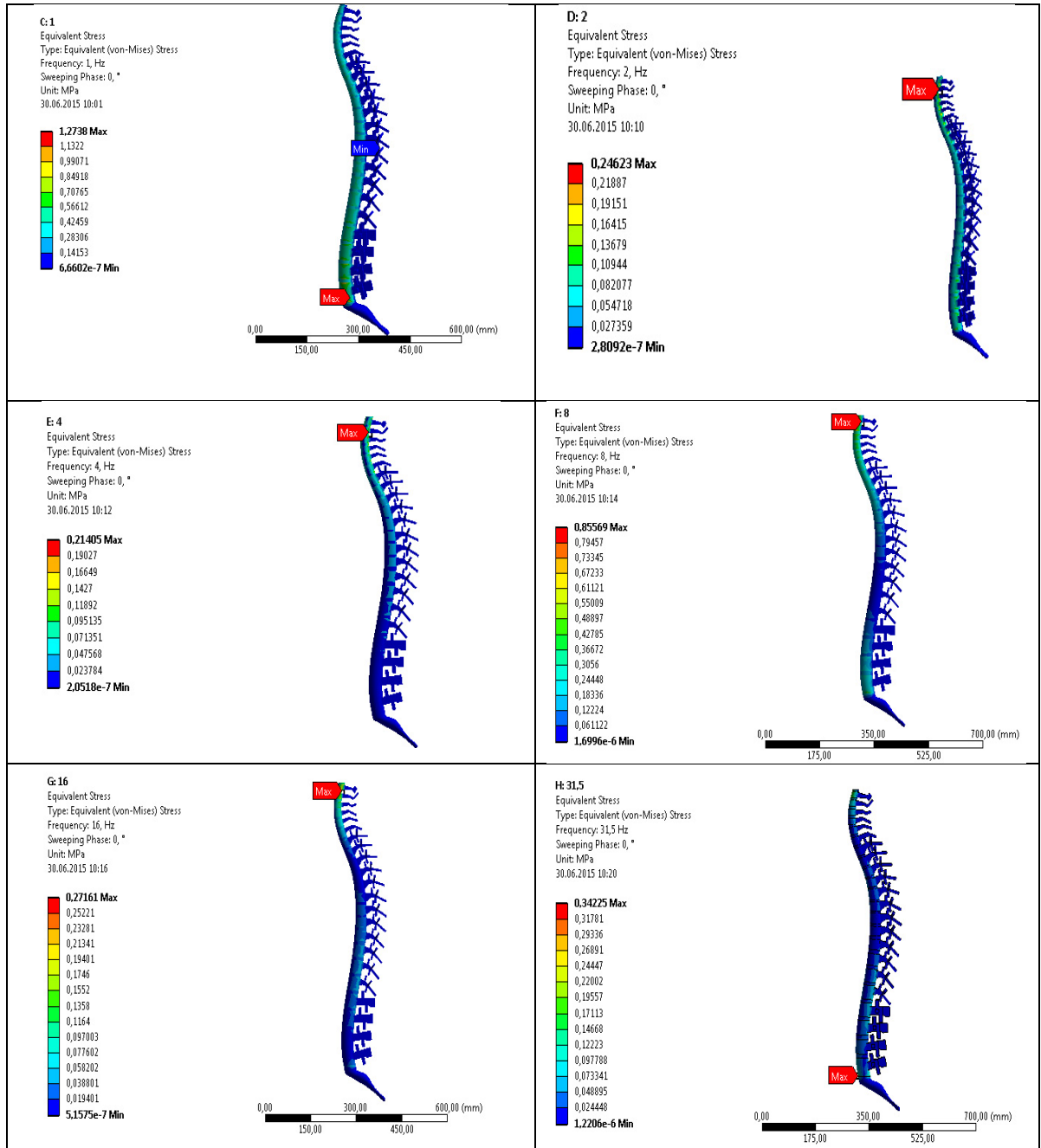


Fig. 4. Fields equivalent stresses in the spine resulting in oscillations at frequencies of 1, 2, 4, 8, 16, 31.5 Hz.

Vibration sensitivity of cervical, chest and lumbar departments of a backbone of the person is approximately identical at compound frequencies of 1 Hz and 2 Hz. It also coincides with data of pilot studies [21, 8, 9] that confirms applicability developed the modeli.avtotransportnykh of devices.

At other studied frequencies (see Fig. 4), it was revealed that vibration sensitivity of each department of a backbone is various. The bigger response at low frequencies (see Fig. 4) is the share on cervical, and then of lumbar department. The obtained data on cervical department are confirmed by that in a design of a chair of the driver the additional basic surface is put into practice – a head restraint [13, 14] which reduces the involuntary movement by the head of the person operator. However in normative documents of the Russian Federation the requirement of existence of a basic surface for the head of a chair of the driver of production transport is absent [22]. There are also no requirements for ergonomics of a support at a chair in the field of lumbar department of the operator.

Thus, results of modeling of the intense deformed condition of a backbone of the person operator revealed need of the accounting of distribution of the vibroloaded state on departments of a backbone at design of a chair of the driver in new motor transportation equipment.

References

- [1] G.J. Steina, P. Muckaa, B. Hinzb, R. Bluthner, Measurement and modelling of the y-direction apparent mass of sitting human body-cushioned seat system, *Journal of Sound and Vibration*. 322 (2009) 454–474.
- [2] H. Ayaria, M. Thomasa, S. Dorea, O. Serrus, Evaluation of lumbar vertebra injury risk to the seated human body when exposed to vertical vibration, *Journal of Sound and Vibration*. 321 (2009) 454–470.
- [3] Li-Xin Guoa, Ming Zhangb, Zhao-Wen Wangc, Yi-Min Zhanga, Bang-Chun Wena, Jin-Li Li, Influence of anteroposterior shifting of trunk mass centroid on vibrational configuration of human spine, *Computers in Biology and Medicine*. 38 (2008) 146–151.
- [4] V.V. Kosarev, S.A. Babanov, Professional diseases: Studies. Grant, High school textbook: INFRA-M, Moscow, 2011.
- [5] About a condition of sanitary and epidemiologic wellbeing nasele-a niya in the Russian Federation in 2014, Federal Service for the Oversight of Consumer Protection and Welfare, State report, Moscow, 2015.
- [6] Information on www.ilo.org/publns
- [7] CN 2.2.4/2.1.8.566-96, The sanitary norms of industrial vibration, vibration of residential and public buildings, Information prod. center, Moscow, 1997.
- [8] GOST 31191.1-2004 (ISO 2631-1:1997), Vibration and shock. Measurement and evaluation of human exposure to whole-body vibration, Part 1. General requirements, Standartinform, Moscow, 2008.
- [9] GOST ISO 8041-2006, Vibration. Human response to vibration. Measuring instrumentation, Standartinform, Moscow, 2008.
- [10] GOST 12.4.094-88 SSBT, Occupational safety standards system. Method for determination of dynamical characteristics of human body under vibration action, Publishing house of standards, Moscow, 2003.
- [11] GOST R ISO 15536-2-2010, Ergonomics. Computer manikins and body templates, Part 1, General requirements, Standartinform, Moscow,
- [12] GOST R ISO 15536-2-2010, Ergonomics. Computer manikins and body templates, Part 1, Verification of functions and validation of dimensions for computer manikin systems, Standartinform, Moscow, 2011.
- [13] GOST R EN 614-1-2003, Safety of machinery. Ergonomic design principles, Part 1, Terms, definition and general principles, IPK Publishing house of standards, Moscow, 2004.
- [14] GOST 12.2.049-80, Occupational safety standards system. Industrial equipment, General ergonomic requirements, Publishing house of standards, Moscow, 2002.
- [15] V.A. Berezovsky, Biophysical characteristics of tissues of the person: reference book, Sciences. thought, Kiev, 1990.
- [16] Information on <http://www.mc-profi.ru/pozvonochnik-heloveka.html>
- [17] M.R. Sapin, Human anatomy, Musculoskeletal device. Internals (digestive and respiratory systems), Alliance-in, Moscow, 2000.
- [18] N.A. Mukhin, V.V. Kosarev, S.A. Babanov, V.V. Fomin, Professional diseases, Geotar-media, Moscow, 2013.
- [19] I.P. Palatinskaya, N.Yu. Dolganina, Sozdaniye of dynamic biomechanical model of lumbar department of the person operator of motor transportation devices, Prospects of development of science and education". The TTU of Akkad. M. S. Osimi bulletin, Dushanbe. 2(26) (2014) 86–92.
- [20] I.P. Palatinskaya, N.S. Pirogova, S.P. Samoylov, Features of creation of the virtual phantom of a backbone of the operator of motor transportation devices, Health and safety in the third millennium, Collection of materials VI of the International scientific and practical conference, Chelyabinsk, YuUrGU. (2015) 206–212.
- [21] K.V. Frolov, Vibrations in equipment: reference book, Protection against vibration and blows, Moscow, Mechanical engineering. 6 (1981) 366–373.
- [22] GOST ISO 10326-1-2002, Vibration. Laboratory method for evaluating vehicle seat vibration, Part 1. Basic requirements Standartinform, Moscow, 2007



International Conference on Industrial Engineering

Diagnosing electromagnets for weber-ampere characteristic of the operating cycle

Grechihin V.V., Lankin M.V., Lankin A.M.*

Platov South-Russian State Polytechnic University (NPI), 132, St. Prosvescheniya, Rostov region, Novocherkassk, 346428, Russian Federation

Abstract

The article describes a method of determining the weber-ampere characteristics electrotechnical AC devices with moving parts of the magnetic circuit, in particular electromagnets. The solution of the inverse problem of harmonic balance and the method of natural-model tests allow obtaining weber-ampere characteristic of the electromagnets, in which it is possible not only to determine the state of the electromagnet, and the type of fault. The technique is based on the previously conducted studies to obtain weber-ampere characteristics of electrotechnical devices to a fixed part of the magnetic circuit. The relevance of the proposed method is based on the possibility of diagnosing electromagnets both in production and in the course of their operation. The method provides a weber-ampere characteristic of the operating cycle with electromagnets error does not exceed 3%.

© 2015 Published by Elsevier Ltd. This is an open access article under the CC BY-NC-ND license

(<http://creativecommons.org/licenses/by-nc-nd/4.0/>).

Peer-review under responsibility of the organizing committee of the International Conference on Industrial Engineering (ICIE-2015)

Keywords: weber-ampere characteristic the operating cycle, the harmonic balance method of natural-model testing, diagnostics.

1. Introduction

All electromagnetic AC device are movable and the fixed part of the magnetic circuit and at least one working coil. During the operation of electromagnets AC operating coil current flows, a working magnetic flux in the stationary part of the magnetic circuit that drives the movable part. The magnetic flux determined by the design, the mutual arrangement of the working parts of the magnetic core and the coil, as well as the number of turns in it and the magnitude of the flowing current. During the working cycle of the AC electromagnet movable part moves relative to the stationary magnetic circuit, which also leads to a change in magnetic flux. The conclusion is that, as

* Corresponding author. Tel.: +7-919-879-4398.

E-mail address: lankinjohn@rambler.ru

an integral characteristic of containing not only information about the operating parameters of AC electromagnets, but also the quality of its individual parts is weber-ampere characteristic of the operating cycle.

2. Determination of weber-voltage characteristics of an electromagnet

The method of determining the weber-ampere characteristics of electromagnets is inversion harmonic balance method of natural-model tests [1-9], the unifying dimension of the physical object and the modeling of the object. The method allows to determine the shape of the weber-ampere characteristic, the known flowing through the coil of the electromagnet current, given in the form of a Fourier series:

$$i(t) = \sum_{m=1}^n I_{(2m-1)} \sin((2m-1)\omega t) \quad (1)$$

where $I_{(2m-1)}$ – amplitude $(2m-1)$ harmonic current and the known shape and amplitude U_a the voltage applied to the coil of an electromagnet:

$$u(t) = U_a \sin(\omega t) \quad (2)$$

Seeking weber-ampere characteristic of the electromagnet, given approximated by the expression:

$$\Phi(i) = \sum_{m=1}^n k_{(2m-1)} i^{2m-1} \quad (3)$$

where Φ – value of the magnetic flux, $k_{(2m-1)}$ – the coefficients of the approximating expression weber-ampere characteristic, $m = (1, n)$, n – the number of terms in the approximated by, i – the current flowing through the coil of the electromagnet.

In our case, there is an electromagnet with an unknown weber-ampere characteristic, known laws of variation of voltage (2) applied to the electromagnet, and the current flowing through it (1). It is required to determine the coefficients $k_{(2m-1)}$ expression (3), approximating weber-ampere characteristic.

The equation of the circuit of the electromagnet:

$$u(t) = Ri + \frac{d\Phi}{dt}$$

Rewrite it, taking into account the known laws of current change (1) and voltage (2):

$$U_a \sin \omega t = R \left(\sum_{m=1}^n I_{(2m-1)} \sin((2m-1)\omega t) \right) + \frac{d \sum_{m=1}^n k_{(2m-1)} \sum_{m=1}^n (I_{(2m-1)} \sin((2m-1)\omega t))^{2m-1}}{dt} \quad (4)$$

Experiments with electrical devices without moving parts of the magnetic circuit, which as a method to determine the weber-ampere characteristics of the electrical device used an algorithm natural-model test, which consists in the following: on the electrical unit is supplied sinusoidal voltage and using the current and voltage sensors, measurements of input (voltage) and the output (current) electrical signaling device, then received data is sent to a personal computer, where model inputs are set to obtain the output data model, and using optimization algorithm seeking matching the output of the electrical device and its model. When coincidence output is based on the latest iteration of the resulting weber-ampere characteristic. As a basis for constructing optimization algorithm of the control program using the simplex method of optimization. The program implements the electromagnet, and an optimization program based on a simplex-planning [10].

Algorithm natural-model tests in the case of an electromagnet, having in his part of the movable parts of the magnetic circuit is as follows. At not disassembled from the electrical product AC electromagnet supplied a sinusoidal voltage whose amplitude is changed stepwise from zero up to the nominal and back (Fig. 1). This makes the duty cycle electromagnet, overcoming the resistance of the actuators connected to it.

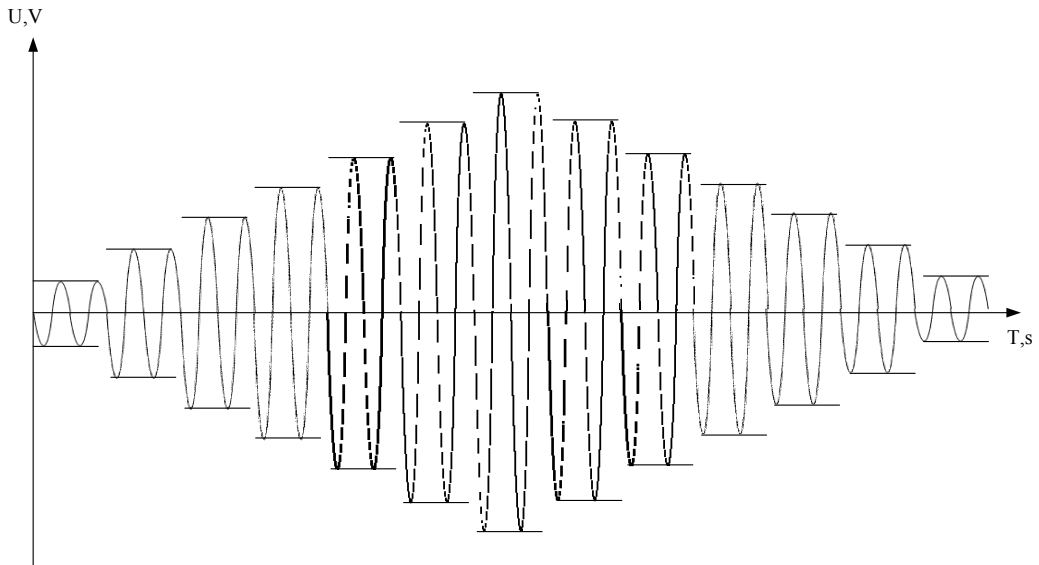


Fig. 1. Step-varying sinusoidal voltage.

At each stage of the voltage measured by the private weber-ampere characteristic and the current amplitude. Fixing the location of the endpoints of private weber-ampere characteristics of the resulting weber-ampere characteristic of the operating cycle (Figure 2, a) and b).

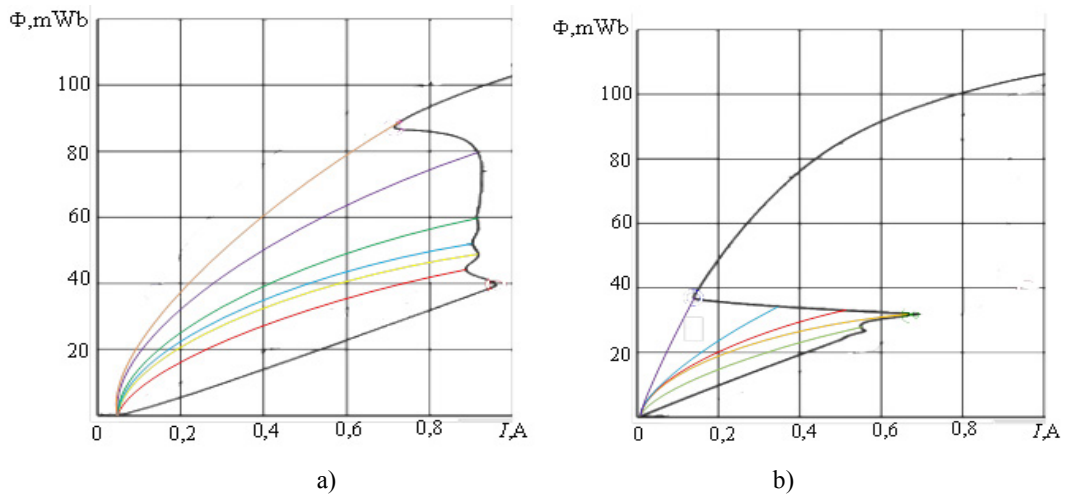


Fig. 2. The method of obtaining weber-ampere characteristic: a) direct and b) reverse branch.

The research showed that the mean obtained by weber-ampere characteristics of the operating cycle of electromagnets AC can determine the type of fault (Fig. 3 – 6).

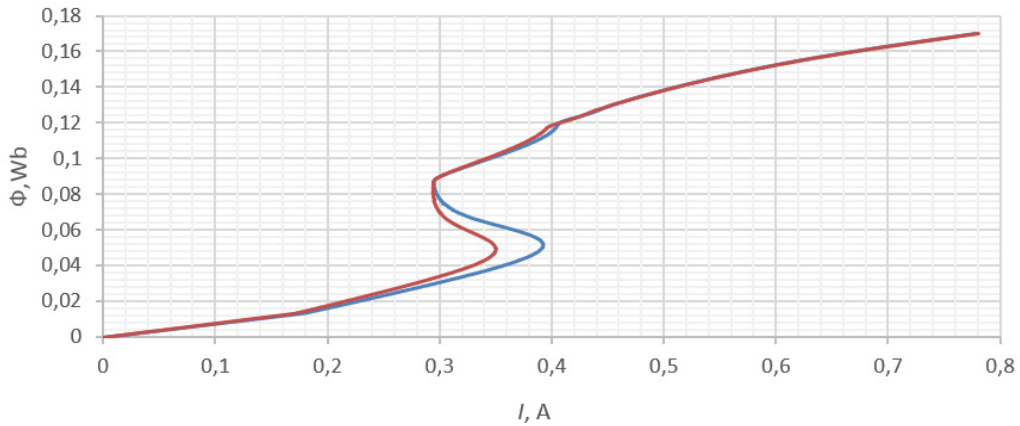


Fig. 3. Weber-ampere characteristics of the operating cycle of electromagnets AC defects, clogging on the upper surface of the armature.

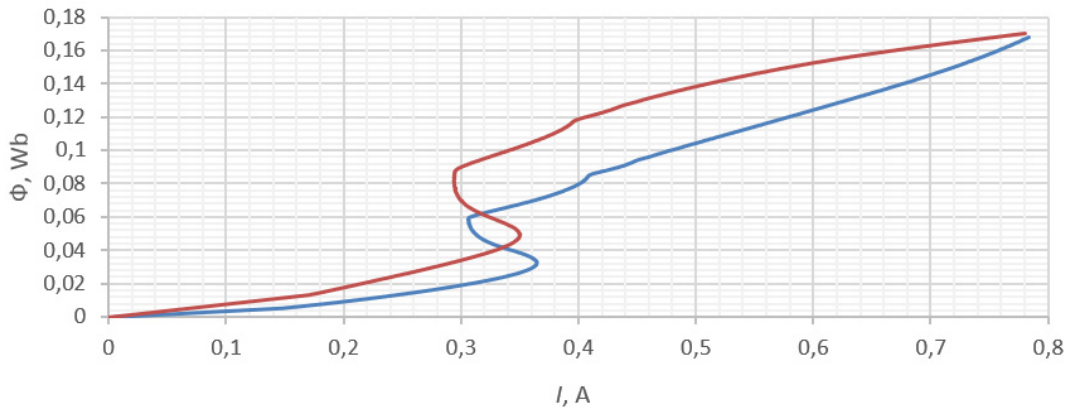


Fig. 4. Weber-ampere characteristics of the operating cycle of electromagnets AC defects, interturn short-circuit.

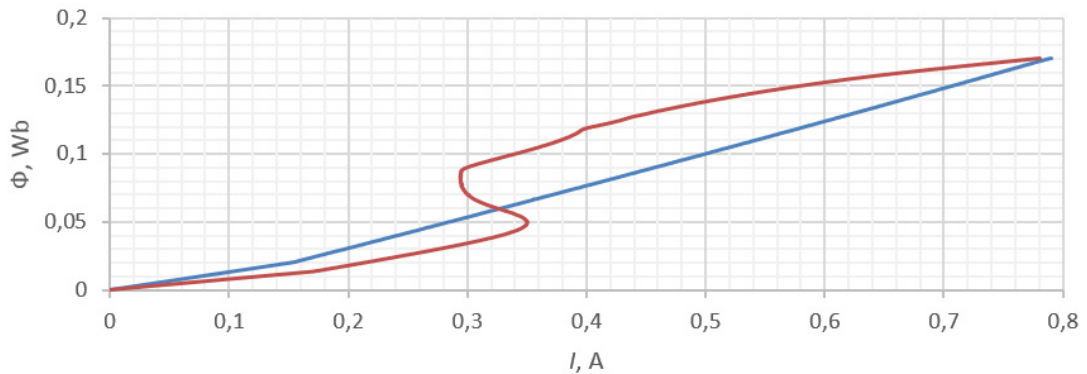


Fig. 5. Weber-ampere characteristics of the operating cycle of electromagnets AC defects, sticking of the armature in the initial position.

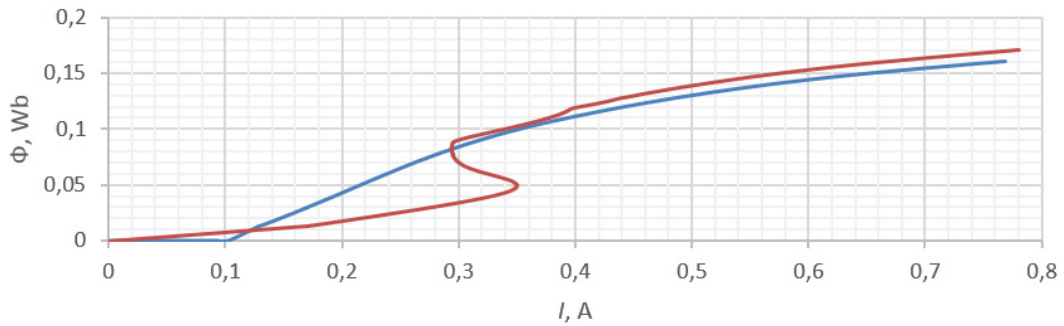


Fig. 6. Weber-ampere characteristics of the operating cycle of electromagnets AC defects, stuck in the extended position of the armature.

The mathematical analysis of the inverse problem of harmonic balance, held computing and natural experiments using a mathematical model and a number of electrical devices (solenoid, motor and toroidal transformer). The results of which suggest that the proposed method provides a measurement of current-voltage characteristics of electrical characteristics of the device with an error not exceeding 3% [11]. A study [7, 8], the effect of measurement errors on the accuracy of harmonic current method of determining the weber-ampere characteristics. The values of harmonic currents varied in the range of $\pm 4,4\%$, the additional error getting weber-ampere characteristics did not exceed 1%.

3. Conclusions (Summary)

The proposed method can diagnose electrical devices AC magnetic moving parts such as solenoids, relays, AC etc. The relevance of the proposed method is the possibility of the diagnosis of electromagnets as in production [12] and in the course of their operation. The method provides a weber-ampere characteristic of the operating cycle with electromagnets error does not exceed 3%.

The results obtained with the support of № 1.2690.2014 / K "Methods for solving inverse problems of diagnosis of complex systems (engineering and medicine) on the basis of natural-model experiment" performed under the project of the state task using equipment NBI "Diagnosis and energy-efficient electrical equipment " South-Russian State Technical University (NPI) of the MI Platov.

References

- [1] A.M. Lankin, M.V. Lankin, The method of measuring weber-ampere characteristics electrotechnical devices, Modern problems of science and education. 1 (2014). URL: <http://www.science-education.ru/115-12186>.
- [2] A.M. Lankin, M.V. Lankin, N.D. Narakidze, The method of measuring weber-ampere characteristics based on solving the inverse problem MGB, Modern problems of science and education. 4 (2014). URL: <http://www.science-education.ru/118-13942>.
- [3] A.M. Lankin, M.V. Lankin, V.A. Kucherov, O.A. Naugol'nov, Algorithm natural-model tests for the diagnosis of electrical systems, Modern problems of science and education. 1 (2015). URL: <http://www.science-education.ru/125-19975>.
- [4] A.M. Lankin, M.V. Lankin, The method of measuring weber-ampere characteristics electrotechnical devices, Modern problems of science and education. 1 (2014). URL: <http://www.science-education.ru/115-12186>.
- [5] A.M. Lankin, M.V. Lankin, Getting weber-voltage characteristics using the method of harmonic balance, The Second International Conference on Eurasian scientific development Proceedings of the Conference. (2014) 264–270.
- [6] N.I. Gorbatenko, A.M. Lankin, M.V. Lankin, D.V. Shayhutdinov, Determination Of Weber-Ampere Characteristic For Electrical Devices Based On The Solution Of Harmonic Balance Inverse Problem, International Journal of Applied Engineering Research. 10(3) (2015) 6509–6519.
- [7] A.M. Lankin, M.V. Lankin, The solution of the inverse problem of harmonic balance in natural-model experiment definition weber-ampere characteristics of electro-technical products: monograph, Book Crossing, Moscow, 2015.
- [8] M.V. Lankin, A.M. Lankin, The devices measure electrical products WAC AC: monograph, LAP LAMBERT, Saarbruecken, 2015.
- [9] A.M. Lankin, M.V. Lankin, N.I. Gorbatenko, D.V. Shayhutdinov, Determination of Weber-Ampere Characteristics of Electric Devices Using Solution of Inverse Problem of Harmonic Balance, Modern Applied Science. 9(8) (2015) 247–261. DOI:10.5539/mas.v9n8p247.

- [10] V.A. Kucherov, A.M. Lankin, M.V. Lankin, L.G. Tarasova, Program planning simplex, Computer technology in science, business, social and economic processes, collection of scientific articles on materials of the 15th International Scientific and Practical Conference, South-Russian State Technical University (NPI) of the MI Platov. (2015) 52–56.
- [11] A.M. Lankin, M.V. Lankin, RU № 2015610308. (2015)
- [12] D.V. Shajhutdinov, N.I. Gorbatenko, K.M. Shirokov, V.V. Grechihin, A.M. Lankin, Adaptive subsystem automatic production control intelligent electric, Modern problems of science and education. 1 (2015). URL: <http://www.science-education.ru/125-20095>.



International Conference on Industrial Engineering

The solution of the harmonic balance method of electrical devices natural-model tests inverse problem

Gorbatenko N.I., Lankin M.V., Lankin A.M.*

Platov South-Russian State Polytechnic University (NPI), 132, St. Prosvescheniya, Rostov region, Novocherkassk, 346428, Russian Federation

Abstract

This article suggests the solution to the inverse problem of harmonic balance by the method of full-scale-model testing to obtain hysteresis weber-ampere characteristics of electrical devices. During the testing of AC electrical devices quite often it is necessary to obtain a hysteresis weber-ampere characteristic. When the magnetic material is magnetized by the alternating field, hysteresis loop that characterizes the energy consumption per cycle of magnetization reversal is expanding due to the appearance of eddy current losses and loss by aftereffect. The aim of the study is to develop a method for determining the hysteresis weber-ampere characteristics on the basis of the solution to the inverse problem of harmonic balance for electrical devices. The technique is based on the previously conducted studies to obtain weber-ampere characteristics of electrical devices, as well as the weber-ampere characteristics of the operating duty cycle of AC electrical devices.

© 2015 Published by Elsevier Ltd. This is an open access article under the CC BY-NC-ND license

(<http://creativecommons.org/licenses/by-nc-nd/4.0/>).

Peer-review under responsibility of the organizing committee of the International Conference on Industrial Engineering (ICIE-2015)

Keywords: weber-ampere characteristic, harmonic balance method, natural-model tests.

1. Introduction

This article describes the solution of the inverse problem of harmonic balance method of natural-model tests for hysteresis weber-ampere characteristics of electrotechnical devices. During diagnostics AC electrical devices often need to receive the hysteretic weber-ampere characteristic. When the magnetization of the magnetic material to the alternating field hysteresis loop that characterizes the energy consumption per cycle of magnetization reversal is

* Corresponding author. Tel.: +7-919-879-4398.

E-mail address: lankinjohn@rambler.ru

expanding due to the appearance eddy current losses and loss-effect. The aim of the study is to develop a methodology for determining the hysteresis weber-ampere characteristics based on the inversion harmonic balance for electrotechnical devices. The technique is based on the previously conducted studies to obtain weber-ampere characteristics of electrotechnical devices, as well as the weber-ampere characteristics of the operating cycle of electrotechnical devices AC.

Automatic control systems enable the production of more efficient use of materials and operating parameters of electrotechnical devices (ED). It is not possible to create a process control system without effective methods and control of products [1]. From studies [2] it is known that the weber-ampere characteristic (WAC) ED AC allows to determine the efficiency of ED and the type of fault.

2. Determination hysteresis wac ed

WAC obtained during the flow of alternating current by the working winding ED will have a hysteresis. When measuring a WAC should take into account two things: the distortion of the curve, and the phase shift between the magnetic flux Φ and the current in the coil I , produced this stream. The relationship between Φ and I determined by the shape and dynamic loop, so the sinusoidal variation of one of the variables considered in the general case, the second will not change sinusoidally (will harmonics).

The lag phase flow curve of the current curve is due to the influence of eddy currents and magnetic viscosity. Angle of lag δ called the angle of losses [3].

To account for the effects of distortion curve shape and the presence of the phase shift depending $\Phi = f(I)$ when magnetizing alternating field Arkadyev [4], it was suggested that the real dynamic loop equivalent ellipse, which satisfies the equation in the coordinates Φ and I .

$$i(t) = I_{max} \sin(\omega t) \quad (1)$$

$$\Phi(t) = \Phi_{max} \sin(\omega t - \delta) \quad (2)$$

If you type in the component stream $\Phi_{max1} = \Phi_{max} \cos\delta$, is in phase with the direction I , and component $\Phi_{max2} = \Phi_{max} \sin\delta$, lagging on 90° the direction I , when [5] Φ_{max1} associated with reversible processes of transformation of energy during magnetization reversal, and Φ_{max2} – with irreversible. The expression (2) takes the form:

$$\Phi(t) = \Phi_{max1} \sin(\omega t) - \Phi_{max2} \cos(\omega t) \quad (3)$$

We propose a method of determining the loop $\Phi = f(I) + \Phi_{max2} \cos(\omega t)$ which takes into account its hysteresis. To do this, we will implement the decision of the inverse problem of harmonic balance method of natural-model tests [6 – 11], the unifying dimension of the physical object and the modeling of the object. The method allows to determine the shape of the loop $\Phi = f(I) + \Phi_{max2} \cos(\omega t)$, the known flowing through the coil current of the electrical device, given in the form of Fourier series:

$$i(t) = \sum_{m=1}^n I_{(2m-1)} \sin((2m-1)\omega t) \quad (4)$$

where $I_{(2m-1)}$ – amplitude $(2m-1)$ harmonic current and the known shape and amplitude U_a the voltage applied to the coil of electrical products:

$$u(t) = U_a \sin(\omega t) \quad (5)$$

The reversible component of the hysteresis weber-ampere characteristic of electrical products, set approximating expression:

$$\Phi(i) = \sum_{m=1}^n k_{(2m-1)} i^{2m-1} \tag{6}$$

where Φ – value of the magnetic flux, $k_{(2m-1)}$ – the coefficients of the approximating expression weber-ampere characteristic, $m = (1, n)$, n - number of terms in the approximated by, i – the current flowing through the coil of electrical products.

The problem is formulated as follows. There are electrical devices with known hysteresis WAC known laws of variation of voltage (5) applied to the nonlinear inductance and current flowing through it (4). It is required to determine the coefficients $k_{(2m-1)}$ expression (6), approximating hysteresis weber-ampere characteristic and the amplitude of the irreversible flow component Φ_{max2} .

The equation of the circuit of the electrical device:

$$u(t) = Ri + \frac{d\Phi}{dt}$$

Rewrite it, taking into account the known laws of current change (4) and voltage (5):

$$U_a \sin \omega t = R \left(\sum_{m=1}^n I_{(2m-1)} \sin((2m-1)\omega t) \right) + \frac{d \sum_{m=1}^n k_{(2m-1)} \sum_{m=1}^n (I_{(2m-1)} \sin((2m-1)t\omega))^{2m-1}}{dt} + \Phi_{max2} \sin(\omega t) \tag{7}$$

The experiments, which as a method for the determination of the hysteresis weber-ampere characteristics of the algorithm used natural-model tests with regard to our problem is this: the electromagnet is supplied sinusoidal voltage and using the current and voltage sensors, measurements of the input (power) and output (current) signals of the electromagnet, then received data is sent to a personal computer, where the data model, the input and data output model, and using an optimization algorithm seeking coincidence output electromagnet and its model. When coincidence output is based on the latest iteration of the resulting weber-ampere characteristic. As a basis for constructing optimization algorithm of the control program using the simplex method of optimization [12]. The program implements the electrical device [13, 14, 15], and an optimization program based on a simplex-planning [13, 14, 15].

3. Realization of natural-model experiment to determine the hysteresis WAC ED

A series of experiments confirming the successful implementation of the method. Fig. 1 shows graphs of current forms on the first iteration of the simplex optimization.

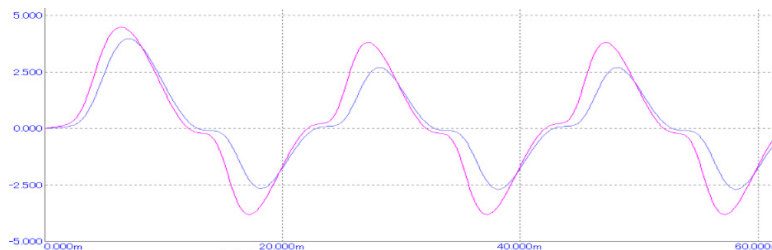


Fig. 1. The shape of the current produced in the physical object in the emulator and the first iteration of the simplex optimization.

From Fig. 1 shows that the current shape of the physical object and emulation have significant differences as hysteresis WAC Fig. 2.

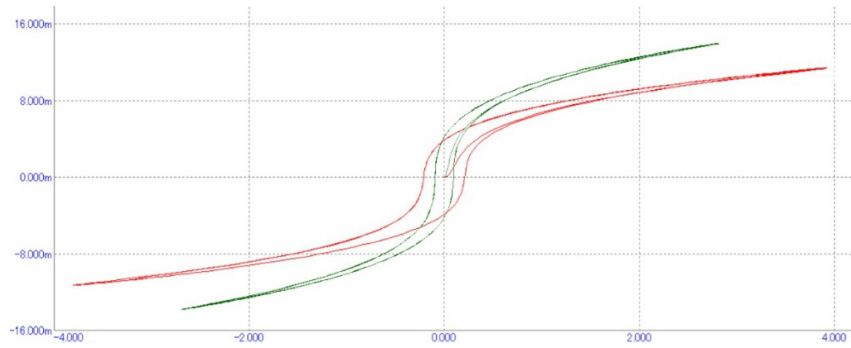


Fig. 2. Hysteresis WAC physical object (1) and Emulator (1) after the first iteration of the simplex optimization.

Optimization program was carried out 34 iterations, resulting in the current waveform obtained in the emulator (2) approaching the current physical form of the model (1) (Fig. 3).

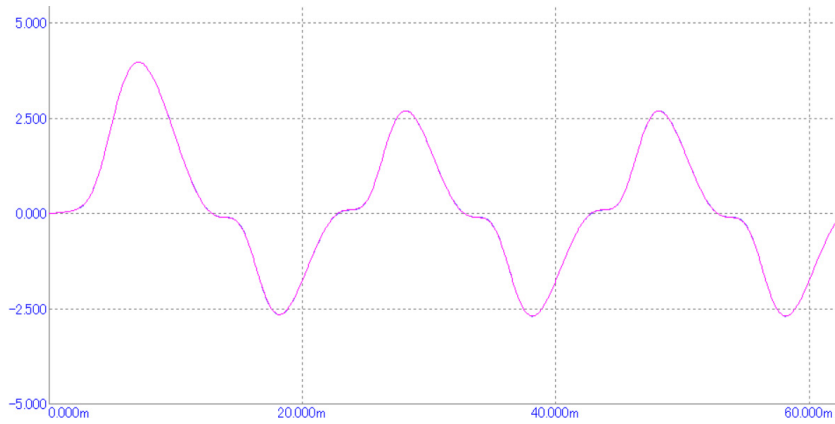


Fig. 3. Current form obtained at the physical object and the emulator on the last iteration.

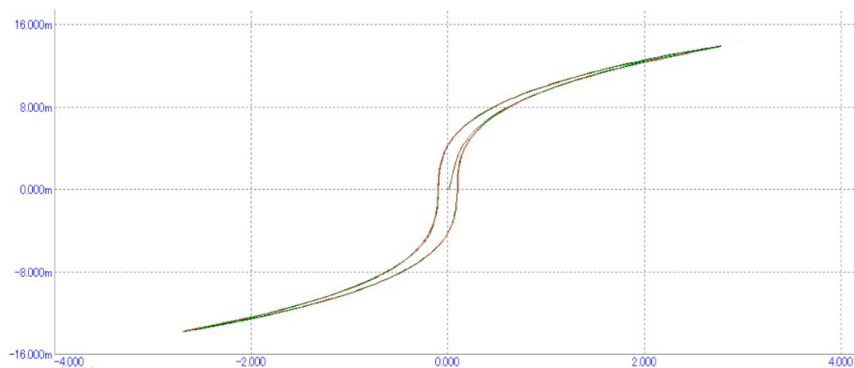


Fig. 4. WAC obtained at the last iteration and on the physical object.

A study [13, 14, 15, 16], the effect of measurement errors on the accuracy of harmonic current method of determining the weber-ampere characteristics. The values of harmonic currents varied in the range of $\pm 4,4\%$, the additional error getting weber-ampere characteristics did not exceed 1%.

4. Conclusions (Summary)

The proposed method is relevant for the monitoring systems and its possible use for magnetic hysteresis characteristics of electrical devices such as during their production and during their operation. The method provides a description of the electrical device with the error does not exceed 3%.

The results obtained with the support of № 1.2690.2014 / K "Methods for solving inverse problems of diagnosis of complex systems (engineering and medicine) on the basis of natural-model experiment" performed under the project of the state task using equipment NBI "Diagnosis and energy-efficient electrical equipment " South-Russian State Technical University (NPI) of the MI Platov.

References

- [1] D.V.Shajhutdinov, N.I. Gorbatenko, K.M. Shirokov, V.V. Grechihin, A.M. Lankin, Adaptive subsystem automatic production control intelligent electric, Modern problems of science and education. 1 (2015). URL: <http://www.science-education.ru/125-20095>.
- [2] A. Gadyuchko, E. Kallenbach, Magnetische Messung - Neue Wege der Funktionsprüfung bei der Herstellung von Magnetaktoren, Innovative Klein- und Mikroantriebstechnik. (2010) 59–64.
- [3] A.A. Preobrazhenskij, E.G. Bishard, Magnetic materials and elements, Higher, Moscow, 1986.
- [4] V.K. Arkad'ev, Electromagnetic processes in metals, Main editorial energy literature, Moscow-Leningrad, 1936.
- [5] K.M. Polivanov, Ferromagnetic: Basic theory of technical applications, Energoizdat, Leningrad, 1957.
- [6] A.M. Lankin, M.V. Lankin, The method of measuring weber-ampere characteristics electrotechnical devices, Modern problems of science and education. 1 (2014). URL: <http://www.science-education.ru/115-12186>.
- [7] A.M. Lankin, M.V. Lankin, N.D. Narakidze, The method of measuring weber-ampere characteristics based on solving the inverse problem MGB, Modern problems of science and education. 4 (2014). URL: <http://www.science-education.ru/118-13942>.
- [8] A.M. Lankin, M.V. Lankin, V.A. Kucherov, O.A. Naugol'nov, Algorithm natural-model tests for the diagnosis of electrical systems, Modern problems of science and education. 1 (2015). URL: <http://www.science-education.ru/125-19975>.
- [9] A.M. Lankin, M.V. Lankin, The method of measuring weber-ampere characteristics electrotechnical devices, Modern problems of science and education. 1 (2014). URL: <http://www.science-education.ru/115-12186>.
- [10] A.M. Lankin, M.V. Lankin, Getting weber-voltage characteristics using the method of harmonic balance, The Second International Conference on Eurasian scientific development Proceedings of the Conference. (2014) 264–270.
- [11] N.I. Gorbatenko, A.M. Lankin, M.V. Lankin, D.V. Shayhutdinov, Determination Of Weber-Ampere Characteristic For Electrical Devices Based On The Solution Of Harmonic Balance Inverse Problem, International Journal of Applied Engineering Research. 10(3) (2015) 6509–6519.
- [12] V.A. Kucherov, A.M. Lankin, M.V. Lankin, L.G. Tarasova, Program planning simplex, Computer technology in science, business, social and economic processes, collection of scientific articles on materials of the 15th International Scientific and Practical Conference, South-Russian State Technical University (NPI) of the MI Platov. (2015) 52–56.
- [13] A.M. Lankin, M.V. Lankin, The solution of the inverse problem of harmonic balance in natural-model experiment definition weber-ampere characteristics of electro-technical products: monograph, Book Crossing, Moscow, 2015.
- [14] M.V. Lankin, A.M. Lankin, The devices measure electrical products WAC AC: monograph, LAP LAMBERT, Saarbruecken, 2015.
- [15] A.M. Lankin, M.V. Lankin, N.I. Gorbatenko, D.V. Shayhutdinov, Determination of Weber-Ampere Characteristics of Electric Devices Using Solution of Inverse Problem of Harmonic Balance, Modern Applied Science. 9(8) (2015) 247–261. DOI:10.5539/mas.v9n8p247.
- [16] A.M. Lankin, M.V. Lankin, RU № 2015610308. (2015)



International Conference on Industrial Engineering

Aspects of production technology for the environment friendly free-machining steel with tin

Ryabov A.V.*

South Ural State University, 76, Lenin Avenue, Chelyabinsk, 454080, Russian Federation

Abstract

The paper describes a new lead-free environmentally friendly free-machining structural steel alloyed containing ~ 0.25 % tin. The following quality characteristics of cast and hot-worked steel are determined: mechanical properties; austenite grain size; contamination with non-metallic inclusions. The results of atomic emission analysis showed that tin is uniformly distributed in the ingot and forged rods. Tin in this amount does not have detrimental effect on mechanical properties after heat treatment, and the values of ultimate and yield tensile strength, characteristics of plasticity and toughness satisfy standard requirements for the base steel. Austenite grain size is not greater than ASTM number 8. Nitrogen and oxygen content is at the same level or lower than that in the analogous steels. The production of lead-free environmentally friendly free-machining structural steel is not accompanied with pollution of working area with harmful substances in amounts exceeding maximum permissible concentrations, unlike lead-bearing steels.

© 2015 The Authors. Published by Elsevier Ltd. This is an open access article under the CC BY-NC-ND license (<http://creativecommons.org/licenses/by-nc-nd/4.0/>).

Peer-review under responsibility of the organizing committee of the International Conference on Industrial Engineering (ICIE-2015)

Keywords: free-machining steels; machinability; alternative lead-free steels; ecological aspects of steel production; tin

1. Introduction

For many years lead-bearing steels, or their substitutes containing selenium or tellurium are preferred as materials for machine working operations due to their high machinability [1–5]. However, in recent years there arises a tendency towards rejection of the use of these low-melting elements for environmental reasons and because of their

* Corresponding author.

E-mail address: avrmetall@yandex.ru

negative effect on hygiene and sanitary conditions for the working personnel. Beside that, serious shortcomings of the free-machining steels presently in use are low recovery and non-uniform distribution of machinability-enhancing additives in the ingot [6–8], which makes it difficult to obtain stable properties in different heats of the steel, complicates engineering design and decreases the yield in metal forming operations [9–12].

The listed aspects of application of traditional machinability-enhancing additives evidence the necessity of searching for alternative components that may increase steel machinability. Analysis of thermodynamic properties of elements and assessment of possible complication of steelmaking technology concerned with their application show that tin may be one of such components.

The purpose of this work is to estimate the potential of alloying steel with tin for increasing its machinability. Main tasks of the study are to determine effects of tin on steel quality and its distribution in steel ingot, as well as the analysis of environmental conditions in melting tin-bearing steel.

2. Materials and Methods

The object of the study was AO30KhM steel [13]. The steel was melted in a 80 kg induction furnace. Tin was added in the form of pure metal. After casting the ingots were hot forged to obtain 20 mm square rods. Chemical composition of the studied steel AO30KhM containing tin and analog steels used for comparison (lead-bearing steel AS30KhM and 30KhM steel without machinability-enhancing additives) is shown in Table 1.

Chemical composition was determined with X-ray spectrum, and concentration of tin with atomic emission analysis. Mechanical properties of forged and heat-treated steel were determined according to GOST 9012-59, 1497-84 and 9454-78. Austenite grain size was determined according to GOST 5639-82. Contamination with non-metallic inclusions was estimated according to GOST 1778-70.

Table 1. Chemical composition of the studied steels, wt. %

Designation	C	Mn	Si	P	S	Ni	Cu	Cr	Mo	Sn	Pb
30KhM	0.27	0.45	0.26	0.015	0.009	0.12	0.09	0.88	0.16	0.005	–
AS30KhM	0.29	0.44	0.24	0.014	0.010	0.16	0.09	0.91	0.15	–	0.25
AO30KhM	0.28	0.49	0.25	0.016	0.008	0.18	0.06	0.89	0.17	0.245	–

3. Results and discussion

Atomic emission analysis showed a rather uniform distribution of tin in the ingot and forged rods (see Table 2).

Mechanical properties were determined in 20 mm square rods at ambient temperature after the following heat treatment: heating to 860 °C, 20 min; oil quenching; tempering at 550 °C, 1 hour, and water cooling. Results of mechanical tests (see Table 3) showed that addition of tin increases hardness, yield strength and tensile strength of heat treated steel. This is explained by solid solution hardening caused by tin atoms dissolved in iron lattice. Unlike most machinability-enhancing elements, tin has high solubility in iron (up to 17.7 wt. % at 900 °C [14]), and at present concentrations forms a solid solution with iron. Though some works, particularly [15], notice a possibility of precipitation of non-ferrous impurities on a substrate of oxides and sulphides, the studies of excess phases using characteristic X-ray radiation in scanning electron microscope with thermal field emission and energy dispersion analyzer could not reveal the presence of tin in free form [16]. On the other way, tin decreases relative elongation δ and reduction in area ψ in tensile tests, as well as impact toughness KCU (see Table 3). The key reason is thought to be tin segregation at grain boundaries. A thin layer with concentration of tin 2–3 orders of magnitude greater than average tin concentration in solid solution localized at grain boundaries causes intercrystalline failure, which results in a decrease of impact toughness and an increase of cleavage fraction on fracture surface [17]. But tin in the amounts of 0.05–0.25 wt. % does not seriously damage mechanical properties of the studied steel in heat-treated condition, and the values of strength, plasticity and toughness characteristics satisfy requirements of GOST 4543-71 standard for the base steel 30KhM.

At the same time tin improves the conditions of chip formation in metal machining with high-speed steel tools [18]. Enhancing of deformation and fracture of surface layer of metal in the cutting zone are due to Rehbinder effect, i.e. decrease of strength, plasticity and strain hardening coefficient caused by adsorption. Tin adsorption in interdendrite regions and at grain boundaries gives rise to internal effect. Thus the work of new surface formation decreases, and initiation and propagation of microcracks at lattice defects or dislocation bundles [19, 20] is enhanced. This results in brittle intercrystalline failure and abrupt fall of strength of the workpiece material.

Analysis of contamination of the steel with non-metallic inclusions showed that in all heats no plastic silicates, point nitrides and stringer nitrides were found. Amount of point oxides did not exceed class 0.5. This is characteristic for aluminium-killed steels without titanium. In 20 mm square rods maximum class of sulphide content was 4.0, of point oxides 0.5, of stringer oxides 3.0 and of brittle and deformable silicates 5.0 and 2.5 correspondingly (see Table 4). These levels of non-metallic inclusion content are typical for structural steels melted in open electric arc furnaces with basic lining and are not changed by the presence of low-melting and low-boiling elements.

Nitrogen and oxygen content was also at the same level as in analog steels (see Table 5). The steel with tin has austenite grain size finer than ASTM number 8 (see Table 6).

Production of lead-free environmentally friendly tin-bearing free-machining structural steel is not accompanied by pollution of the air in the working area with harmful substances in amounts exceeding maximum permissible concentrations, unlike leaded steels.

Table 2. Distribution of tin in the billet of AO30KhM steel, wt. %

Location of samples	Ingot top	Ingot middle	Ingot bottom
Centre	0.245	0.256	0.241
1/2 radius	0.247	0.241	0.249
Surface	0.245	0.245	0.248

Table 3. Mechanical properties of heat-treated steels

Steel	[Sn], %	$\sigma_{0.2}$, MPa	σ_b , MPa	δ , %	ψ , %	KCU, J/cm ²	HB (hot-forged)
30KhM (requirements of GOST 4543-71)	–	≥ 730	≥ 930	≥ 11.0	≥ 45	≥ 78	–
AS30KhM	0.25 Pb	970	1020	13.0	51.0	85	320
AO30KhM	0.05	969	1081	12.8	53.7	107	302
	0.10	951	1075	15.2	56.3	95	321
	0.15	980	1094	13.2	54.7	87	329
	0.20	1002	1120	13.2	53.6	82	329
	0.245	1001	1125	13.2	52.8	82	332

Table 4. Contamination of steels with non-metallic inclusions (maximum/average class)

Steel	Type of non-metallic inclusions				
	Sulfides	Point oxides	Stringer oxides	Brittle silicates	Deformable silicates
30KhM	4.00 / 3.06	0.50 / 0.50	2.00 / 1.17	5.00 / 1.95	4.50 / 2.78
AS30KhM	3.50 / 2.78	0.50 / 0.50	4.00 / 1.78	3.50 / 1.50	3.00 / 1.50
AO30KhM	4.00 / 3.00	0.50 / 0.50	3.00 / 2.00	5.00 / 1.89	2.50 / 1.22

Table 5. Content of oxygen and nitrogen in 20 mm square rods, wt. %

Steel	[Sn], %	Ingot top		Ingot middle		Ingot bottom	
		Oxygen	Nitrogen	Oxygen	Nitrogen	Oxygen	Nitrogen
30KhM	0.005	0.0045	0.010	0.0045	0.011	0.0048	0.012
AS30KhM	0.25 Pb	0.0044	0.010	0.0045	0.012	0.0043	0.011
AO30KhM	0.245	0.0048	0.010	0.0055	0.009	0.0060	0.009

Table 6. Content of tin, aluminium and austenite grain size

Steel	[Sn], %	[Al], %	ASTM grain size number
30KhM	0.005	0.04	8
AS30KhM	0.25 Pb	0.04	7
AO30KhM	0.245	0.04	8–9

4. Conclusion

- Atom emission analysis showed uniform distribution of tin in the ingot and forged rods.
- Tin in amounts up to 0.25 % does not have detrimental effect on mechanical properties of the studied steel after heat treatment. Strength, plasticity and toughness characteristics satisfy requirements of the standard for the base and the lead-bearing steel.
- The lead-free environmentally friendly tin-bearing free-machining structural steel has austenite grain size finer than ASTM number 8.
- Nitrogen and oxygen content in the steel is at the same or lower level compared to analog steels.
- Production of lead-free environmentally friendly tin-bearing free-machining structural steel compared to the leaded steel is not accompanied by pollution of the air in the working area with harmful substances in amounts exceeding maximum permissible concentrations.

Acknowledgements

The study was performed in the framework of the Federal Target Program “Research and Development in Priority Directions of Scientific-Technological Complex of Russia for 2014–2020 years”, contract No. 14.574.21.0054, unique project identifier RFMEFI57414X0054.

References

- [1] Y.Y. Wei, Z.Q. Liu, Q.L. An, M. Chen, Study on the machinability of free-cutting steels 1214 and 12L15 with coated tool, *Advanced Materials Research*. 426 (2012) 151–154.
- [2] D. Wu, Z. Li, Study of free cutting austenitic stainless steel containing sulfur, rare earths and bismuth, *Kang T'ieh/Iron and Steel (Peking)*. 48 (2011) 78–82.
- [3] Z. Li, D. Wu, W. Lv, Application of rare earth elements in lead-free "green steel", *Advanced Materials Research*. 518-523 (2012) 687–690.
- [4] T.J. Zhang, Effective, controlled method to add sulfur into molten steel to produce free cutting steel for automobile, *Applied Mechanics and Materials*. 364 (2013) 558–562.
- [5] Z. Li, D. Wu, L. Wei, Z. Zheng, S. Kang, Investigations on Low Environmental Impact Machining Processes of Free Cutting Austenitic Stainless Steels. *Applied Mechanics and Materials*. 377 (2013) 112–116.
- [6] Jipeng Han, Yang Li, Zhouhua Jiang, Yongchao Yang, Xiuxiu Wang, Lin Wang, Kaiting Li, Summary of the Function of Sn in Iron and Steel, *Advanced Materials Research*. 773 (2013) 406–411.
- [7] Di WU, Zhuang LI, Study on the Machinability of Free Cutting Non-Lead Austenitic Stainless Steels, *Advanced Materials Research*. 430–432 (2012) 306–309.
- [8] M.C. Somani, L.P. Karjalainen, J.H. Bianchi, On the Recrystallisation Characteristics and Kinetics of a 9SMn28 Free Cutting Steel. *Advanced Materials Research*. 558-559 (2012) 333–338.

- [9] A.V. Ryabov, A.M. Panfilov, N.S. Semenova, The X-Ray–TV Investigation of Behaviour of a Bismuth Sample Introduced to Molten Steel, *Modern Applied Science*. 9 (2015) 252–259.
- [10] Zhang Yongjun, Han Jingtao, Wang Huifeng, Graphitization Kinetic of Hypoeutectoid Graphitized Free Cutting Steel, *Advanced Materials Research*. 143-144 (2012) 508–511.
- [11] A.V. Ryabov, I.V. Chumanov, Study and Possibility of making new easy to cut corrosion-resistant steel, *Russ. Metall. (Metall.)*. 12 (2012) 1065–1067.
- [12] S. Hosohara, Y. Miki, K. Senda, H. Nishi, Jap. Patent 2002,194,419. (2002)
- [13] A.V. Ryabov, O.K. Tokovoi and I.V. Chumanov, RU. Patent 2,470,0862. (2012)
- [14] M. Hashimura, K. Miyanishi, A. Mizuno, Development of Low-Carbon Lead-Free Free-Cutting Steel Friendly to Environment, *Nippon Steel technical report*. 96 (2007) 45–49.
- [15] V.G. Zinchenko, V.E. Roshchin, N.V. Malkov, Influence of technology of modifying the content and distribution of harmful impurities in the forging ingots, *Electrometallurgy*. 2 (2007) 11–15.
- [16] M.S. Nikitin, A.V. Ryabov, Analysis of effect of tin additions on the composition of non-metallic inclusions in structural steels, *Bulletin of the SUSU Series “Metallurgy”*. 39 (2012). 43–46.
- [17] N.P. Lyakishev, *The phase diagrams of binary metallic systems*, Mechanical engineering, Moscow, 1997.
- [18] E.T. Stephenson, The effect of tin on the toughness of some common steels, *Metallurgical Transactions A*. 11 (1980) 517–524.
- [19] M.S. Nikitin, A.V. Ryabov, Analysis of effectiveness of tin addition for improving chip formation in machining structural steels, *Bulletin of the SUSU Series “Metallurgy”*. 1 (2013) 214–217.
- [20] A.Ya. Zaslavskiy, *Modern Free-Machining Steels. Composition, Inclusions, Properties*, SUSU Publ., Chelyabinsk, 2005.



International Conference on Industrial Engineering

Growth and distribution disperse particles in liquid-phase interaction of the system Fe-TiC

Chumanov I.V., Anikeev A.N.*

South Ural State University, 76, Lenin Avenue, Chelyabinsk, 454080, Russian Federation

Abstract

From the practical point of view, systems consisting of heat-proof dispersed particles evenly distributed in the metal matrix are a promising subject of studies that investigate hard alloy and carbide steel fabrication processes that take place during disintegration of supersaturated solid solutions. Titanium carbide combined with a binder metal represents a dispersed particle/metal matrix system. Such combination of components leads to enhanced material's properties, such as high resistance to wear, abrasive wear, burrs, radiation and etc. A problem arises when a technology to fabricate such compounds is being developed. That is to forecast compound's structural properties, especially the average size of carbide particles and a pattern of particles distribution according to their size. This article provides a theoretical study of the solubility of titanium carbide in the melt iron.

© 2015 Published by Elsevier Ltd. This is an open access article under the CC BY-NC-ND license

(<http://creativecommons.org/licenses/by-nc-nd/4.0/>).

Peer-review under responsibility of the organizing committee of the International Conference on Industrial Engineering (ICIE-2015)

Keywords: dispersed phases, titanium carbide, phase distribution.

1. Introduction

One of the principal objectives of research in the metal industry and machine building is the development and introduction of metal saving technologies [1] that could be used to fabricate new metallic materials with enhanced characteristics and new functional properties. From this perspective, powder metallurgy and foundry appear to be the most interesting technologies [2]. The technologies mentioned above are easy-to-use and allow fabrication of

* Corresponding author.

E-mail address: banikeev-ml@mail.ru

materials with properties similar to those of final products; consequently, they considerably decrease expenditures on further mechanical processing [3, 4].

Studies that investigate high-ductile metallic materials deliberately combined with heat-proof and high-resistance fillers have become especially relevant over the recent years [5-7]. Such combination of components leads to enhanced material's properties, such as high resistance to wear, abrasive wear, burrs, radiation and etc..

Reinforcing agents with hardness that considerably differs from that of the substrate can not only decrease friction loss, but also increase load range [8].

From the practical point of view, systems consisting of heat-proof dispersed particles evenly distributed in the metal matrix are a promising subject of studies that investigate hard alloy and carbide steel fabrication processes that take place during disintegration of supersaturated solid solutions.

Titanium carbide combined with a binder metal represents a dispersed particle/metal matrix system. A problem arises when a technology to fabricate such compounds is being developed. That is to forecast compound's structural properties, especially the average size of carbide particles and a pattern of particles distribution according to their size.

Titanium carbide characteristics include low electrical resistance and high melting point, high hardness, high heat-conductivity and high resistance to wear in inimical environments [9].

2. Theoretical analysis

Liquid-phase interaction of titanium carbides with molten metal (steel) at high temperatures causes carbide particles to coalesce (coagulate). Carbide particles dissolve in the metal matrix and recrystallize. It's generally accepted that the gradient of solution compounds' chemical potential around the particles with different curve radius is a condition required for recrystallization. The curve ensures the presence of quasi-stationary diffusion flows [10-14]. A diffusion equation that is solved considering boundary conditions and mass balance results in the following formula that depicts dependence of the average radius of a particle (r) on time:

$$r^2 = k\tau, \quad (1)$$

where k – is constant [10,11].

The paper [11] notes that, despite the parabolic law followed by a great number of systems, some deviations from the law have been registered and they can be described by processes taking place at phase boundaries [10-12].

The parabolic law of coalescence is derived from the diffusion equation if boundary conditions are set for semi-infinite samples[11] or if continuous substance flow across the phase boundary is ensured [10]. It's also assumed that the diffusion coefficient doesn't depend on time. The paper [11] states that if coalescence doesn't obey the parabolic law, it should be questioned whether the diffusion equation is applicable to the process or whether the boundary conditions have been set correctly. The study[13] supposes that if dissolved substance concentration is low, new particles are not produced and some particles coalesce at the expense of others. Diffusion flow velocity at particle's surface equals its average radius variation rate when mass balance in the volume is ensured; and it can be formulated by

$$\bar{r}^3 = \frac{4\sigma D}{9} \tau, \quad (2)$$

where r – is the average radius of a particle; σ – is surface energy; D – stands for diffusion coefficient and refers to time.

The paper [13] suggests that particles coalesce because of combined diffusion and does not consider processes at phase boundaries. The paper [14] states that test results on thorium oxide coalescence in nickel matrix is described well by the equation (2). That leads to the conclusion that thorium diffusion in the nickel matrix controls coalescence. Instead, if boundaries expansion is controlled by phase boundary processes, the equation (1) is realized.

As we have stated above, stable diffusion flows are caused by the fact that the curved phase boundary dissolved substance next to it unbalanced. The curve can be described with the Thompson order formula:

$$\frac{C_r}{C_\infty} = \frac{(1+2\sigma M)}{\rho N_a r k T}, \quad (3)$$

where σ – is surface energy, M – is molecular mass, ρ – stands for particle's density, N_a – is the Avagardo number, r – refers to particle's radius, k – is the Boltzmann constant and T – is temperature.

See below calculations for titanium monocarbide in molten ferrum: $\sigma = 0.7 \text{ J/m}^2$ [15], $T = 1773 \text{ K}$, $M = 60$, $\rho = 4900 \text{ kg/m}^3$, $r = 10 \text{ }\mu\text{m}$, $N_a = 6.02 \cdot 10^{23} \text{ mol}^{-1}$, $R = 1.38 \cdot 10^{-23} \text{ J/K}$. The equation (3) results in $c_r / c_\infty = 1.2 \cdot 10^{-4}$. Therefore, it's possible to conclude that the increase in concentration doesn't significantly depend on the phase boundary curve. Therefore, it's not probable that direct diffusion flows will appear in a system consisting of molten metal and hard particles tens of microns in size. However, coalescence (diffusion) takes place in systems like Fe-TiC.

3. Computations

The current paper sets an objective to define particle's size/time dependence taking into consideration the following conditions. Let us suppose that particles with limited solubility are found in the volume of another phase. The function $\varphi(r, \tau)$ of distribution in accordance with particles' size characterizes the whole amount of particles. A particular amount of particles with the mass $m(\tau)$ will dissolve and concentration fields of dissolved substance will be formed between particles. The system will tend to minimize the phase boundary. Atoms of dissolved substance can accidentally jump onto hard particles. Having shifted onto a hard particle, an atom incorporates into its molecular structure, hence increasing the particle's mass by dV . The probability that an atom shifts onto a coalescing particle is

$$\rho(r) = \int_r^\infty \varphi(r, \tau) dr.$$

$\varphi(r, \tau)$ function is normalized the following way

$$\int_0^\infty \varphi(r, \tau) dr = N(\tau),$$

where $N(\tau)$ is the amount of particles in the said volume. If w the volume of atom, v is atom jump frequency and C_a refers to dissolved substance concentration in the matrix (at. %), then

$$\left[\tilde{N}_a w \int_0^\tau \varphi(r, \tau) v d\tau \right] d\tau = dV, \quad v d\tau = dr$$

or

$$\tilde{N}_a w v \int_0^\tau \varphi(r, \tau) v d\tau = 3\alpha \pi r^2 \frac{dr}{d\tau}, \quad (4)$$

where v – is the velocity of particle coalescence and α – is the particles coefficient.

Mass balance condition is

$$\alpha\pi\rho\int_0^r\varphi(r,\tau)r^3v d\tau = m_0 - m(\tau), \quad (5)$$

where ρ – is substance density and m_0 – refers to the particle's initial mass.

Differentiation of the equations (4) and (5) with respect to time results in the following system

$$\begin{aligned} \tilde{N}_a w v \varphi(r, \tau) v &= 3\alpha\pi \left[2r \left(\frac{dr}{d\tau} \right)^2 + r^2 \frac{d^2r}{d\tau^2} \right] \\ \alpha\pi\rho r^3 \varphi(r, \tau) v &= -\frac{dm(\tau)}{d\tau}, \quad v = \frac{dr}{d\tau}. \end{aligned} \quad (6)$$

Let's suppose that dissolved substance mass variation with respect to time corresponds with the change in particle's volume, i.e.

$$-\frac{dm(\tau)}{d\tau} = 3\alpha\pi\rho r^2 \frac{dr}{d\tau}.$$

Then, having excluded the system (6) φ from the first two equations, we formulate the following

$$\frac{d^2r}{d\tau^2} + \frac{2}{r} \left(\frac{dr}{d\tau} \right)^2 - \frac{C_a w v}{\alpha\pi r^3} \cdot \frac{dr}{d\tau} = 0. \quad (7)$$

If the equation (7) is solved for $\frac{dr}{d\tau}$ provided that $\frac{dr}{d\tau} = 0$ and $r=r_0$ it gives

$$\frac{dr}{d\tau} = \frac{1}{Kr^2} \ln \frac{r}{r_0}, \quad K = \frac{\alpha\pi}{C_a w v}. \quad (8)$$

To formulate $r = r(\tau)$, in quadratures, we replace $\ln \frac{r}{r_0}$ function with its average value on the interval $[r_0 ; r_m]$, where r_m is the size of a particle that could be built up of all the particles of the system.

$$\ln \frac{r}{r_0} = \frac{1}{r_m - r_0} \int_{r_0}^{r_m} \ln \frac{r}{r_0} dr = C(r_m, r_0) = \text{const}.$$

Then

$$\frac{dr}{d\tau} = \frac{\tilde{N}(r_m, r_0)}{Kr^2}. \quad (9)$$

If we integrate the equation (9) upon conditions that $r(\tau) = r(0)$ and $\tau = 0$, we develop the following formula

$$r^3 = \frac{3C(r_m, r_0)}{K} \tau + r^3(0). \quad (10)$$

Thus, the paper has suggested a possible mechanism of hard particle coalescence in liquid matrix and, having accepted a number of assumptions, derived an average particle's radius/time dependence (equation 10).

Modelling of dispersedly reinforced materials also requires the ability to define the function of dispersed particles distribution according to their size during Fe-TiC liquid-phase sintering. To fulfill the task, one needs to use the equation (8), formula of radius (r) variation velocity for heat-proof particles in the metal matrix.

Let's suggest that we investigate particle size variation that takes place after the liquid phase has been produced and particles have relocated in the matrix.

Let's define τ as a time period measured from the moment when dispersed phase started to appear in the matrix, t is a time period measured from the moment when, at least, some dispersed particles started to coalesce (dissolve). ($\tau \neq t$) is generally true.

We will be looking for a distribution function formulated the following way

$$\varphi(d, \tau) = f(\tau)\psi(r) \quad (11)$$

Let's write down an equation of continuity [16] for $\varphi(r, \tau)$ in the space of sizes

$$\frac{\partial \varphi(r, \tau)}{\partial \tau} + \frac{\partial}{\partial r}(\varphi(r, \tau) - v) = 0.$$

If we use the equation (11), we derive the following

$$\frac{df(\tau)}{d\tau} \psi(r) + f(\tau) \frac{d\psi(r)}{dr} v + f(\tau)\psi(r) \frac{dv}{dr} = 0. \quad (12)$$

Using the equation (8), let's transform the formula (12)

$$\frac{df(\tau)}{d\tau} \psi(r) + f(\tau) \frac{d\psi(r) \ln\left[\frac{r}{r_0}\right]}{dr Kr^2} + f(\tau)\psi(r) \frac{(1 - 2 \ln\left[\frac{r}{r_0}\right])}{Kr^3} = 0. \quad (13)$$

Solve the equation (13) using the Fourier transform

$$\begin{aligned} \frac{df(\tau)}{f(\tau)d\tau} &= B, \\ \frac{d\psi(r) \ln\left[\frac{r}{r_0}\right]}{\psi(r)\hat{E}r^2 dr} - \frac{(1 - 2 \ln\left[\frac{r}{r_0}\right])}{Kr^3} &= \hat{A}, \end{aligned} \quad (14)$$

where $B = \text{const}$. Integration of the system (14) results in

$$\begin{aligned} f(\tau) &= C_1 \exp(B\tau), \\ \psi(r) &= \frac{C_2 r^2 \exp(-\hat{A}\hat{E} \int r^2 dr / \ln[r/r_0])}{\ln[r/r_0]}. \end{aligned}$$

It follows that

$$\varphi(r, \tau) = \frac{C r^2 \exp\left(-\hat{A} \hat{E} \int \frac{r^2 dr}{\ln[r/r_0]}\right) \exp(\hat{A} \tau)}{\ln[r/r_0]}, \quad (15)$$

where $C=C_1$, $C_2 = \text{const}$. The equation (15) can give us C if we normalize $\varphi(r, \tau)$, for instance, to 1

$$\tilde{N} = \int_r^\infty \varphi(r, \tau) dr = 1$$

It follows that

$$\begin{aligned} \varphi(r, \tau) &= \frac{r^2 \exp(-\hat{A} \hat{E} \int \frac{r^2 dr}{\ln[r/r_0]})}{\hat{O} \ln[r/r_0]} \\ \hat{O} &= \int_r^\infty \varphi(r, \tau) dr. \end{aligned} \quad (16)$$

It is necessary to accept that $B > 0$ in the distribution function (16). B value determines the position of the distribution function's maximum in the space of sizes. If particles are coalescing, the distribution function's maximum will be shifting towards large sizes and the average distance ($2l$) between particles' centers will be increasing.

The increase in time (t) triggers the increase in r and $2l$, which causes the exponent to exert less influence on the equation (16). Therefore, there have to be an inverse relationship between B and $2l$ or B and t . Let's estimate the distance between the centers of dispersed particles. Let's suppose that a particular volume of substance includes the N number of spherical particles with the average size defined as r . If the volume of one particle is defined as $V = (4\pi r^3)/3$, the volume of the system occupied by a particle is $V_1 = 1/N$ and the total volume of all the particles is defined as $V_2 = (4N\pi r^3)/3$. Therefore, $V_3 = (1/N) - (4\pi r^3)/r$ is the interstitial volume occupied by one particle (a sphere surrounding a particle). The sphere volume can be formulated as $V_4 = 4\pi(l^3 - r^3)/3$, where l is a half of the distance between the centers of two adjacent particles. Furthermore, $N = C_v / (1,3\pi r^3)$ where C_v is the volume fraction of the dispersed phase. If we equal V_3 to V_4 and replace N with the formula mentioned above, we conclude that $l^3 - r^3 = r^3[l / (C_v - 1)]$ or $l = r / C_v^{1/3}$. Hence, the width of the spherical zone will be defined as

$$\delta = l - r = r \left(\frac{l}{C_v^{1/3}} - 1 \right).$$

To assess B - t dependence from the geometrical point of view, we accept that particles start to interact as soon as concentration fields of separate particles in the matrix have intersected $\delta/2$, i.e. when an even concentration field of dissolved substance has been established by some point in time marked as tl . We accept that concentration field of every particle is spherical. Hence, $B \approx 1/1,5 \delta$. Considering $r=r(t)$, we conclude that

$$\hat{A} = \frac{\tilde{N}_v^{1/3}}{1,5r(t)(1 - \tilde{N}_v^{1/3})}$$

Let's accept that $r(t) = t$ is approximately true, then

$$\hat{A} = \frac{\tilde{N}_v^{1/3}}{1,5t(1 - \tilde{N}_v^{1/3})} \quad (17)$$

If we input time (t) during which constant temperature was maintained in the system, we can evaluate B using the equation (17) and, consequently, we can use the equation (16) to define the function of dispersed particles

distribution in accordance with their size ($\varphi(r, \tau)$).

Acknowledgments

Work was executed under the projects №14.Z56.15.7690-MK, and supported by the Ministry of Education № 11.1470.2014/K.

References

- [1] V.N. Borisov, O.V. Pochukaeva, The innovative technological development of mechanical engineering as a factor in improving innovative obrbatyvayushey industry, Studies on Russian Economic Development, issue 3(2009), 37–45.
- [2] I.V. Chumanov, V.I. Chumanov, A.N. Anikeev, Hardening of metallic materials dispersed refractory particles, Problems of ferrous metallurgy and materials science, № 1(2010), 24–29.
- [3] V.I. Chumanov, A.N. Anikeev, R.R. Garifulin, I.V. Chumanov, Hardening of the Surface Layers of a Hollow Billet Formed by Centrifugal Casting, Russian Metallurgy (Metally). – Vol. 12(2010), 1125–1128.
- [4] H. Saito, Effect of Co content and WC grain size on wear of WC cemented carbide, № 2(2006), 126–132.
- [5] C. Allen, The wear of ultrafine WC-Co hard metals, 2001, 604–610.
- [6] P. Shipway, Dependens of microscale abrasion mehanism of WC-Co hardmetals on abrasion type, 2005, 44–51.
- [7] I.V. Chumanov, V.I. Chumanov, A.N. Anikeev, Preparation of precipitation-strengthened hollow billets for rotary dispersers, Metallurgist, 2011, 540-543.
- [8] W.T. Griffiths, Aircraft Production – №9 (1947), 444–447.
- [9] Yu.G. Gurevich, V.K. Narva, N.R. Fraga, Carbidoosteels, Metallurgy, Moscow 1988.
- [10] B.Ya. Lobov, The kinetic theory of phase transitions, Metallurgy, Moscow 1969.
- [11] K.P. Gurov, B.A. Kartashkin, Yu.E. Ugaste, Interdiffusion of metal in multiphase systems, Science, Moscow 1981.
- [12] S. Sarian, H.W. Weart, Kinetics of coarsening of spherical particles in a liquid matrix, J. Appl. Phys., 37 (1966), 1675–1681
- [13] E.M. Livshits, P.P. Pitaevskii, Physical Kinetics, Science, Moscow 1979.
- [14] B.S. Bockstein, S.Z. Bockstein, A.A. Zhukhovitskii, Thermodynamics and kinetics of diffusion in solids, Metallurgy, Moscow 1974.
- [15] G.V. Samsonov, I.M. Vinitzky, Refractory compounds: Catalog, Metallurgy, Moscow 1976.
- [16] Ya.B. Zeldovich, A.D. Myshkis, Elements of mathematical physics, Science, Moscow, 1973.



International Conference on Industrial Engineering

Fabrication of functionally graded materials by introducing wolframium carbide dispersed particles during centrifugal casting and examination of FGM's structure

Chumanov I.V., Anikeev A.N., Chumanov V.I.*

South Ural State University, 76, Lenin Avenue, Chelyabinsk, 454080, Russian Federation

Abstract

The paper describes procedures developed for disperse powders introduction into metal melts. We propose to fabricate functionally graded materials by introducing WC particles into liquid metal during mould filling in centrifugal casting machine. A number of experimental studies have been conducted, samples with different WC content have been fabricated and their structure has been examined. The research has revealed that WC particles were distributed unevenly along the width of the samples with the highest concentration in the outer zone of the cylindrical samples. The particles considerably influenced macro- and microstructure causing its grade to decrease from 2 to 9.

© 2015 The Authors. Published by Elsevier Ltd. This is an open access article under the CC BY-NC-ND license (<http://creativecommons.org/licenses/by-nc-nd/4.0/>).

Peer-review under responsibility of the organizing committee of the International Conference on Industrial Engineering (ICIE-2015)

Keywords: wolframium carbide, low-carbon steel, centrifugal casting, functionally graded materials (FGMs).

1. Introduction

Functionally graded materials (FGMs) with preset properties are increasingly used in machines and mechanisms in petrochemical, gas and machine building industries. Efficient design procedures that can ensure predicted interdependence of composition, structure, mechanical and physical properties provide new opportunities and fields for FGM practical application [1].

Introduction of carbide, oxide and nitride dispersed particles during mould filling is one of the methods of FGM fabrication. FGMs can be classified into materials made of fine disperse powders that have been pressed and

* Corresponding author.

E-mail address: chumanoviv@susu.ac.ru

sintered, as well as into materials reinforced with disperse powders (their content doesn't exceed 20 %) that were introduced into a melt at various stages of production [2]. The current paper does not focus on materials made of fine disperse powders since a great number of studies have been dedicated to that subject [3-10]. This study contains a detailed examination of methods used to fabricate so-called dispersedly reinforced materials with disperse powder content of up to 20 %.

2. Method

Experts of the General Metallurgy Department of the South Ural State University developed and patented a new method of FGM production: disperse powder is added to molten while a centrifugal casting mould is being filled [11]. The method is based on difference in density of reinforcing carbides and a reinforced metal. If the density of a thermally-resistant dispersed particle differs from the density of the melt in which it's been introduced, the centrifugal force influencing the particle isn't balanced with the gravity force. Thus, a particle is pushed towards the inner or outer edge of a sample. Once the particle faces the solidification front, the molten metal presses it to the front. Therefore, the particle cannot surface and gets captured by growing dendrites. Particles with a density higher than melt's density (e.g. wolframium carbides, $\rho=15,6 \text{ g/cm}^3$) are pushed towards the outer zone, meanwhile, particles with lower density (e.g. silicon carbides, $\rho=3,2 \text{ g/cm}^3$) move towards the inner zone of a sample.

Experimental casting was performed to test the proposed method. Low-carbon steel was used as a reinforced metal (C 0.17–0.24%; Si 0.17–0.37%; Mn 0.35–0.65%; S \leq 0.040%; P \leq 0.035) and WC powder was taken for reinforcement Table 1.

Table 1. Amount of carbides in experimental samples

Cast number	1					2			
Sample number	1	2	3	4	5	6	7	8	
WC content, g	0	40	80	120	0	120	240	360	
WC content, % (mass percentage)	0	0.4	0.8	1.2	0	1.2	2.4	3.6	

3. Results

Eight hollow cylindrical samples were fabricated for the study. Their dimension were the following: outer diameter of 140 mm, inner diameter of 55 mm, length of 140 mm. Molten metal was heated up to 1650 °C and poured into a rotating mould (1200 rpm) with a graphite core.

Samples for metallographic examinations were cut out from the cylinders (Fig.4). The cylinders were roughly divided into 3 zones Fig. 1: 1 – the outer zone, 2 – ½ of a cylinder width, 3 – the inner zone.

The prepared samples were treated for 10 sec. with the following reagent: 3 ml of HCl; 0.2 g of $\text{CuCl}_2 \cdot 2\text{H}_2\text{O}$; 3 g of FeCl_2 ; 0.1 g of SnCl_2 ; 10 ml of ethanol; 100 ml of water. The samples were examined to find out whether their macrostructure from the outer to the inner zone had changed Fig. 2.



Fig. 1. Fabricated cylinders and cut-out samples: 1 – outer zone, 2- ½ of the width, 3 – inner zone.

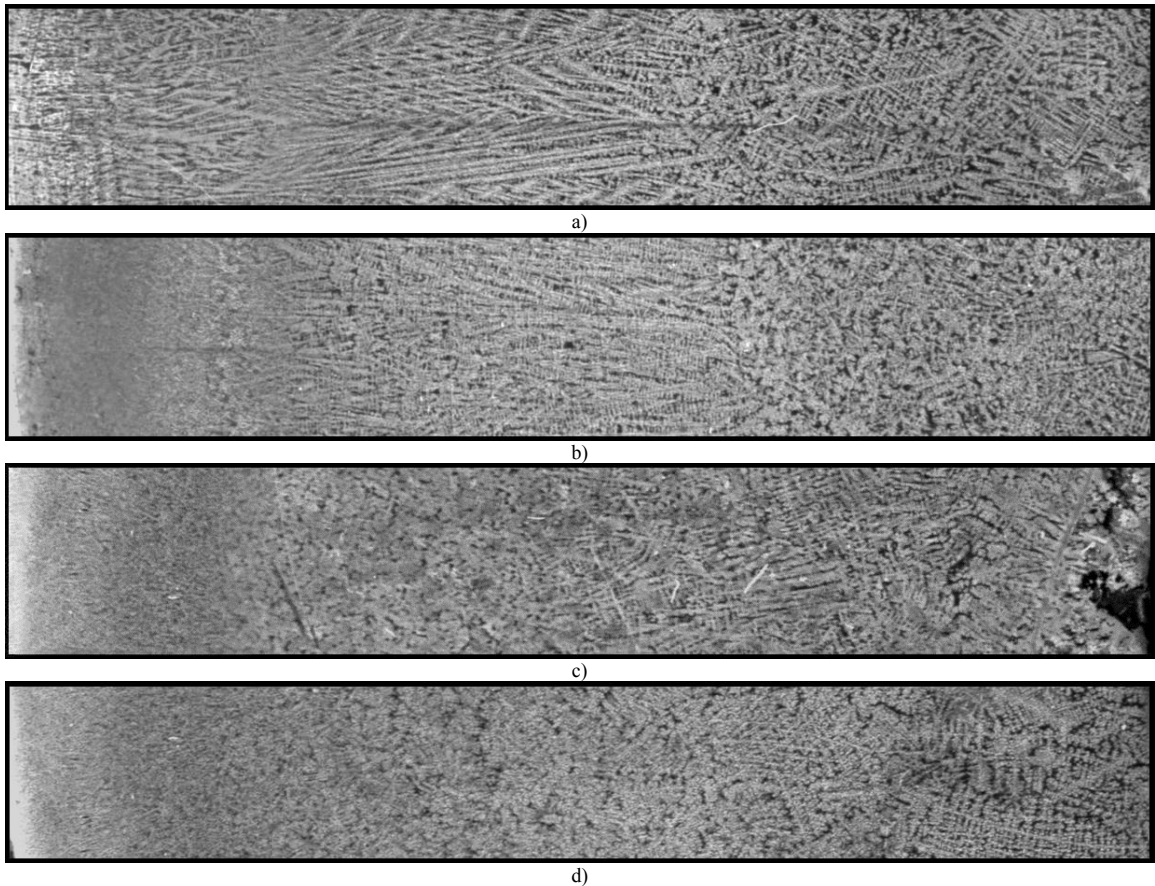


Fig. 2. Macrostructure from the outer to the inner zone: A – sample without dispersed particles, B – 120 g of WC added, C – 240 g of WC added, D – 360 g of WC added.

Macrostructure analysis of samples without reinforcing agents showed that the structure of polished cross-sections was uneven and coarse and the length of crystals was considerable. $3/5$ of the samples were composed of dendrites, monad axils were easily distinguished and twofold axels were thin and densely positioned at the outer edge, grew thicker and got less dense to the inner edge. $2/5$ of the samples' width (at the inner edge) were composed of non-oriented equiaxed crystals. Thus, we may suggest that $3/5$ of the samples' width was composed of fringe crystals because, firstly, the heat was directed towards the outer edge and then solidification conditions changed.

Macrostructural analysis of reinforced samples showed that, despite different reinforcing agent concentration, the outer zone of the examined samples was composed of fine equiaxel grains with dendrites positioned at an angle to each other. It is easy to distinguish clusters of dendrite crystals that are uniform in size and are positioned at angles to each other. The width of the zone composed of equiaxel grains depend on disperse powder concentration: it occupies $1/4$ of the sample #4 (120 g of WC), $1/2$ of the sample #7 (240 g of WC) and $3/4$ of the sample #8 (360 g of WC).

To examine changes in microstructure, the samples were ground, polished and treated for 10 seconds with nitric acid (HNO_3), 4 % in ethanol. Their microstructure was inspected under Axio Observer. Z1m microscope with 100x-200x zoom.

Introduction of the reinforcing agent considerably influenced the samples' structure: the higher concentration of the agent, the more intense microatomization took place. Changes in grain grade were calculated by measuring the lengths of circle chords and are presented by the table 2.

Table 2. Results of dendrites cross-section examination

Zone of examination	Inner zone		½ of width		Outer zone	
	Dendrite cross-section, μm	Grain grade	Dendrite cross-section, μm	Grain grade	Dendrite cross-section, μm	Grain grade
1	156	2	60.9	5	48.6	5–6
2	39.9	6	30.3	7	18.5	8
3	25.2	7	23.5	7	15.9	8–9
4	28.5	7	23.9	7–8	12.9	9
5	38.7	6	34.2	6–7	23.6	8
6	39.3	6	35.3	6–7	20.2	8
7	30.3	7	22.3	7–8	17.9	8
8	25.5	7	19.6	8	15.5	9

Dispersed particles distribution was inspected under JEOL JSM–6460 LV scanning electron microscope. It showed that WC particles were fixed in the microstructure of the solidified samples #2, #3, #4, #6, #7 and #8. WC grains of the samples were considerably smaller in size (0.1–0.94 μm) than initial particles of WC powder (4–65 μm) Fig.3.

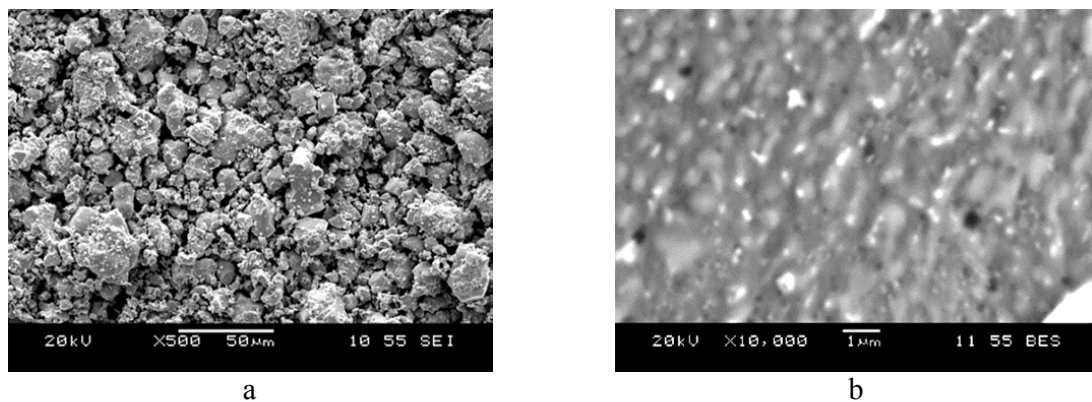


Fig. 3. WC grains: a – before experimental study (x500), b – in fabricated samples (x10000).

WC concentration is uneven along the samples' width with the highest rate at the outer edge, a lower rate in the central zone and almost zero concentration at the inner edge.

Uneven distribution is characteristic to all the other samples reinforced with WC. WC concentration distribution was thoroughly examined in accordance with the following method: different cross-sections of a sample were examined with the same zoom and the number of particles per square micron ($\text{p}/\mu\text{m}^2$) was counted. The "table 3" present WC concentration distribution along the samples' width.

Table 3. WC concentration distribution along the cross-section

Sample number	Dispersed particles concentration distribution		
	Inner zone, $\text{p}/\mu\text{m}^2$	½ of sample's width, $\text{p}/\mu\text{m}^2$	Outer zone, $\text{p}/\mu\text{m}^2$
1	0	0	0
2	0	0	0.4
3	0	0	0.6
4	0	0	2.5
5	0	0	0
6	0	0	2.8
7	0.5	2.6	5.1
8	3.4	3.5	5.1

4. Discussion

Files The developed method of FGM fabrication in based on difference in density between introduced carbides and a metal. Our anticipations about particles distribution have been indirectly supported by the following facts:

- a change in grain grade depending on the quantity of introduced particles;
- a significant difference in samples' microstructure from the outer to inner edge.

Our anticipations have been directly proved by examination performed with an electron microscope. As a result, data on WC concentration from the outer to the inner edge of the samples has been accumulated "Table 3". The fact that particles concentration is different at the outer and the inner edge of the samples proves our hypothesis that particles' distribution depends on their density.

It's worth noting that there is a certain WC "saturation point" for a material fabricated in accordance with the proposed method. This conclusion resulted from examination of the samples #7 and #8 that had been fabricated with different WC content, but showed the same rate of WC concentration at the outer edge. If the number of introduced particles increases, their distribution becomes limited: in the sample #8, WC concentration rates are almost equal in the inner and central zones.

Since dispersed particles influence mechanical properties of the reinforced material and they are distributed unevenly over the volume of the samples, we can claim that the fabricated material is functionally graded. It's worth saying that the proposed method is a promising way of FGM production since the number of carbides, oxides, nitrides and other compounds is plentiful and there are several thousands of steel grades that can be reinforced with dispersed particles. It's possible to fabricate materials with different preset properties varying along the width depending on steel composition, dispersability and particles density. Thus, a fabricated FGM will have a continuous structure without an easily distinguished interface which, otherwise, becomes a stress point.

However, the abundance of reinforcing particles/reinforced metal combinations requires additional examination of particles/metal reaction rates, particles dissolution rates, particles wetting with metal and etc.

Acknowledgements

Work was executed under the projects №14.Z56.15.7690-MK, and supported by the Ministry of Education № 11.1470.2014/K.

References

- [1] Materials Information Society. Handbook ASMI, Powder Metallurgy, Vol. 7, 9-10th Edition, New-York, 2002.
- [2] A.G Krasnobayev, Designing of structure of composite materials on the basis of iron with the set functional properties: thesis of Candidate of Technical Sciences, Rostov-on-Don, 2005.
- [3] M.N. Putintseva, Research of process of electroerosive dispersing of wolframo-cobalt firm alloys: thesis Candidate of Technical Sciences, 2003.
- [4] V.A. Butterfish, G.A. Baglyuk, S.G. Napara-Volgina, R.V. Yakovenko, Hardening of the fast-wearing-out surfaces non wolfram firm alloys and containing carbide steels, The strengthening technologies and coverings. 1 (2007) 42–47.
- [5] I.N. Sevostyanova, N.L. Savchenko, S.N. Kulkov, A structural and phase condition of a sheaf and behavior at friction of composites of WC-(Fe-Mn-C), Metallurgy. 2 (2005) 377–384.
- [6] B.B. Akimov, Research of tribotechnical properties of hard-alloy composite materials on the basis of TiC with the binding phase TiNi, Friction and wear. 2 (2005) 197–199.
- [7] H. Saitoa, A. Iwabuchib, T. Shimizu, Effect of Co content and WC grain size on wear of WC cemented carbide, Wear. 261 (2006) 126–132.
- [8] C. Allen, M. Sheen, J. Williams, V.A. Pugsley, The wear of ultrafine WC-Co hard metals, 13th International Conference on Wear of Materials. 250(1-12) (2001) 604–610.
- [9] C. Allen, M. Sheen, J. Williams, V.A. Pugsley, The wear of ultrafine WC-Co hard metals, 13th International Conference on Wear of Materials. 250(1-12) (2001) 604–610.
- [10] P.H. Shipway, J.J. Hogg, Dependence of microscale abrasion mechanisms of WC-Co hardmetals on abrasion type, Wear. 259 (2005) 44–51.
- [11] V.I. Chumanov, I.V. Chumanov, D.A. Pyatygin, R.R. Garifulin, O.J. Vershinin, A.N. Anikeev, Russian Federation Patent 2008128677/02. (2010).



International Conference on Industrial Engineering

Study of Zirconium Carbide Contact Angle

Anikeev A.N., Chumanov I.V.*

South Ural State University, 76, Lenin Avenue, Chelyabinsk, 454080, Russian Federation

Abstract

This article is devoted to the study of zirconium carbide angle of wettability. An experiment to determine the angle of wettability was carried out in two different ways, being contact and contactless. In the conclusion of the experiment we examined the microstructure of the obtained contact areas on the metal and the substrate and held spectral analysis sessions.

© 2015 The Authors. Published by Elsevier Ltd. This is an open access article under the CC BY-NC-ND license (<http://creativecommons.org/licenses/by-nc-nd/4.0/>).

Peer-review under responsibility of the organizing committee of the International Conference on Industrial Engineering (ICIE-2015)

Keywords: angle, zirconium carbide, high temperatures.

1. Introduction

A promising direction onnyh-producing composition of materials having high mechanical properties, is the introduction into the structure of the metal particulate carbides, oxides or nitrides. Input particles, to a greater or lesser extent, interac-interaction with the melt. The degree of this interaction depends on the property purchased material. Thus, the aim of this work is theoretical and practical study of the process and products of the interaction of zirconium with karyuida mild steel.

* Corresponding author.

E-mail address: anikeev-ml@mail.ru

2. Research Methodology

A case study of the contact angle of zirconium carbide was carried out in high-temperature research Centre research Institute of foundry ("Foundry Research Institute", Krakow, Poland). Research the study was conducted at the experimental complex (Fig. 1). This research facility is designed to evaluate the complex characteristics of materials at high temperatures, including for studying the wettability of materials by various methods. The complex allows testing of different materials under conditions of controlled temperature (up to 2000 °C) under vacuum (up to 10⁻¹⁰ hPa) or in a protective atmosphere [1].

Of fine zirconium carbide was obtained on the substrate, the formation of which was carried out in the press for pressing samples at 180 °C and a pressure of 300 bar. Received support for research has not been polished. As a wetting material samples were used metal, following chemical composition (Table 1).

The study of the kinetics of the interaction were performed using contact and non-contact methods of heating in an argon atmosphere.



Fig. 1. . Experimental facility designed to evaluate the complex characteristics of materials at high temperatures, including for the study of wettability of different materials techniques

Table 1. The chemical composition of images of low carbon steel metal

Item	<i>C</i>	<i>Mn</i>	<i>Si</i>	<i>W</i>	<i>Fe</i>
The content, %	0.217	0.301	0.221	0.069	basis

3. The course of the experimen

The work is done in the framework of the state task of the Ministry of education No. 11.1470.2014/K, and is also supported by the Agreement No. 14.z56.15.7690-MK. Heating the substrate of zirconium carbide with the metal samples was performed for 3 hours until the-temperature of 1600 °C at a speed of 495 °C/hour in an argon atmosphere (degree amendments 99,9992%), at a pressure of 850-900 mbar. The first sample of low carbon steel were used as substrate. The second sample was in a separate mini-camera (metering device (drops-nice), having the shape of the tip is not in contact with the substrate "Fig.2 a". The whole process of heating and melting of the metal was recorded by high speed camera (2000 frames/sec).

During the experiment it was found that the active interaction of the metal with the material of the substrate does not occur even when the temperature reaches 1450 °C at which the sample begins to melt. After melting, the heating process is the formation of droplets of liquid metal on the substrate. When the temperature at 1550 °C, the formation process stops and a drop of liquid metal remains unchanged during subsequent heating "of Fig. 2 b", showing a contact angle equal to 50.

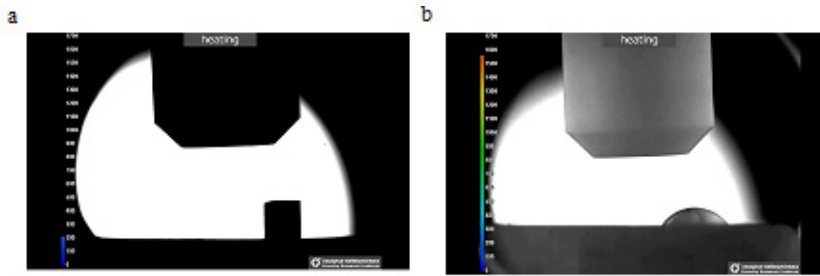


Fig. 2. (a) kinetics of high-temperature interaction of low carbon steel sample with the substrate ZrC in an argon atmosphere according to the method of contact heating start of heating; (b) kinetics of high-temperature interaction of low carbon steel sample with the substrate ZrC in an argon atmosphere according to the method of contact heating formed drop of molten metal (T=1540 °C). Facility designed to evaluate the complex characteristics of materials at high temperatures, including for the study of wettability of different materials techniques

When the temperature reached 1600 °C, from a camera located within the chamber that produces heat, the substrate was squeezed out a drop of molten metal formed during the heating process. The experiment showed that after squeezing droplets of metal on a substrate, formation of droplets, and finally the formed droplet has a contact angle equal to 400 “of Fig. 3”.

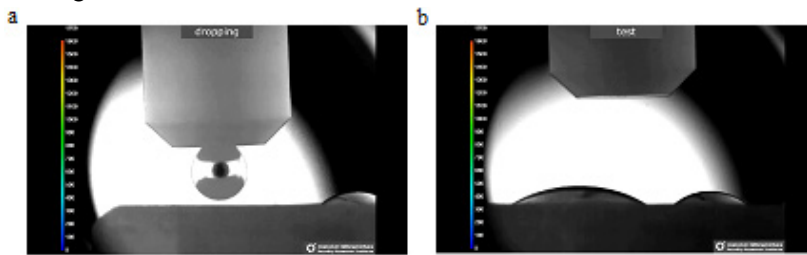


Fig. 3. (a) kinetics of high-temperature interaction of low carbon steel sample with the substrate ZrC in an argon atmosphere according to the method of contactless heating start of heating; (b) kinetics of high-temperature interaction of low carbon steel sample with the substrate ZrC in an argon atmosphere according to the method of contactless heating formed drop of molten metal (T=1540 °C).

4. Study of substrates

Research products of the interaction of substrates zirconium carbide and mild steel was carried out by scanning electron microscope Hitachi TM3000. In the process the study examined the area of contact of each of the samples taken photos of their microstructures. The resulting photographs clearly show the boundary of the drop contact metal and the substrate “Fig. 4”. With the substrate selected spectra from the region of contact with metal scrap “table. 2”, as well as areas recontacterai with metal “table 3”.

Table 2. The composition of the spectrum with the area of contact of the metal with the substrate

Item	Zr	C	Fe
The content, %	91.8	7.8	0.4

Table 3. The composition of the spectrum with the area of contact of the metal with the substrate

Item	Zr	C
The content, %	92.8	7.2

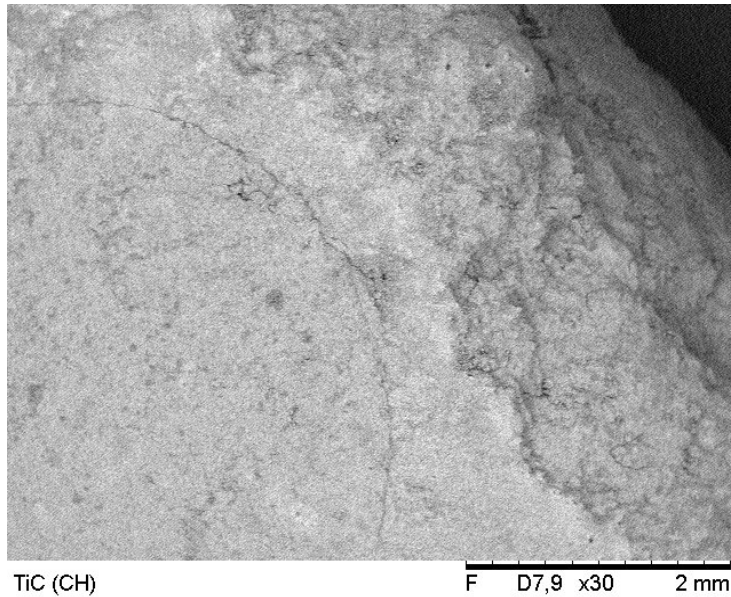


Fig. 4. The image of the microstructure of ZrC (clean surface+contact area) after experiments, the increase in 30 times

5. Conclusion

The results show that despite the use of different techniques to study the interaction of zirconium carbide, the results differ slightly. Edge angles in both cases are significantly less than the 800, which means good wettability of zirconium carbide. However, when the contactless method of heating contact angle less than 100 at contact heating. The study of the substrates showed that direct interaction of substrates and metal are clearly identified Zirconia grain. The iron content in this area shows that a small degree was the interaction of the metal with the substrate. The results indicate that when creating new composite materials, based on the introduction of dispersed particles of ZrC, thanks to the wetting angle of less than 80 and low interaction of the particles with the metal particles will be contacted by the melt, but will not dissolve in the water. The results of the experiment indicate that the contact heating method has an error in the measurement of the contact angle presumably because of the resulting products of the reaction of the metal with the substrate.

Acknowledgements

Work is performed within the state task of the Ministry of education No. 11.1470.2014/K, and is also supported by Agreement No. 14.z56.15.7690-MK.

References

- [1] A.N. Anikeev, I.V. Chumanov, Study wettability if tungsten carbide metal melt, *Electrometallurgy*. 1(1) (2014) 32.
- [2] A.N. Anikeev, I.V. Chumanov, Study wettability if tungsten carbide metal melt, *Electrometallurgy*. 2(2) (2014) 34.
- [3] I.V. Chumanov, A.N. Anikeev, V.I. Chumanov, Preparation of precipitation-strengthened hollow billets for rotary dispersers, *Metallurgist*. 55(5-6) (2011) 439–443.
- [4] N. Sobczak, R. Nowak, W. Radziwill, Experimental complex for investigations of high temperature capillarity phenomena, *Materials Science and Engineering A*. 495(1-2) (2008) 43–49.
- [5] N. Sobczak, Some methodological aspects of high temperature capillarity phenomena investigations, *Transactions of the Foundry Research Institute*. 44(4) (1994) 221–238.



International Conference on Industrial Engineering

Mathematical model of the vehicle in MATLAB Simulink

Radionova L.V., Chernyshev A.D.*

South Ural State University, 76, Lenin Avenue, Chelyabinsk, 454080, Russian Federation

Abstract

The article presents the creation mathematical model of the vehicle. Authors used the software MATLAB Simulink for building model. The article also discloses calculation of forces action on the car. Authors considering of the car as a plane-parallel motion solid body. The block diagram of the mathematical model of the vehicle are presented in the article.

© 2015 The Authors. Published by Elsevier Ltd. This is an open access article under the CC BY-NC-ND license (<http://creativecommons.org/licenses/by-nc-nd/4.0/>).

Peer-review under responsibility of the organizing committee of the International Conference on Industrial Engineering (ICIE-2015)

Keywords: Mathematical model, vehicle, MATLAB Simulink, plane-prallel motion,block diagram

1. Introduction

Currently designers when they design any complex technical devices should be create mathematical model this devise. Mathematical model is needed for verification and research it. Mathematical model allows reducing costs of design this devise. The vehicle is no exception.

2. Mathematical modeling

Moving of the vehicle considering as plane-parallel motion of the solid body in this article. (fig.1.). This assumption is made to simplify the system of equations describing the motion. The motion of the vehicle can be describe by the following system differential equations:

* Corresponding author. Tel.: +7-912-476-2921.
E-mail address: fis6en@gmail.com

$$\begin{cases} \vec{a} = \frac{1}{m} (\sum_{i=1}^4 \vec{P}_{fi} + \sum_{i=1}^4 \vec{R}_i + \vec{P}_w) \\ J_z \frac{d\omega_z}{dt} = \sum_{i=1}^4 M_{nki} + \sum_{i=1}^4 M(\vec{R}_i) + \sum_{i=1}^4 M(\vec{P}_{fi}) \end{cases} \quad (1)$$

where \vec{a} - the acceleration vector of the mass center of the car; m - vehicle weight; \vec{P}_{fi} - the vector of the force of resistance of straight-ahead of wheel; \vec{R}_i - the vector of force of confusion wheel with the ground; \vec{P}_w - the vector of force of air resistance; J_z - moment of inertia of the vehicle; M_{nki} - the moment of resistance to rotation.

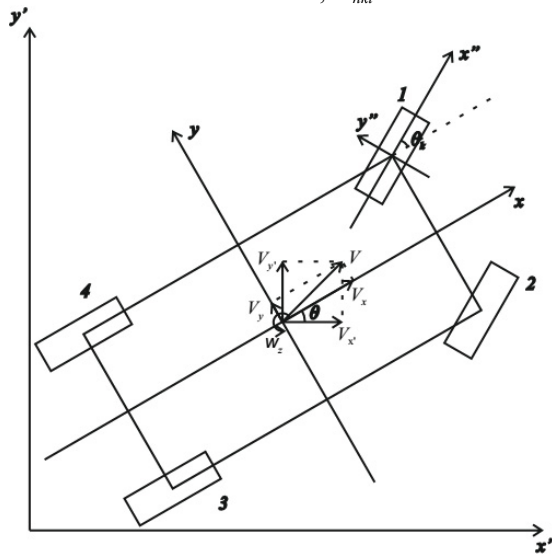


Fig. 1. The design scheme of the car.

x, y, z - axis moving coordinate system; x', y', z' - axis of stationary coordinate system; θ - the angle of rotation of the vehicle around the axis of the vehicle; \vec{V} - the velocity vector of the center of the vehicle; ω_z - angular velocity of turning of a vehicle.

The acceleration in plane-parallel moving is

$$\vec{a} = \frac{d\vec{V}}{dt} + \omega_z \vec{V} \quad (2)$$

where dV/dt - the relative velocity of the center of mass derivative of the vehicle.

For fig. 1 projections of the speeds in coordinate system x', y', z' :

$$\begin{cases} V_{x'} = \frac{dy'}{dt} = V_x \cos \theta - V_y \sin \theta \\ V_{y'} = \frac{dx'}{dt} = V_x \sin \theta + V_y \cos \theta \end{cases} \quad (3)$$

Considering that

$$\omega_z = d\theta / dt \quad (4)$$

then combining (1-4) we can write the following system of equations

$$\left\{ \begin{aligned}
 a_x &= \frac{dV_x}{dt} - \omega_z V_y = \frac{1}{m} \left(\sum_{i=1}^4 P_{fxi} + \sum_{i=1}^4 R_{xi} + P_{wx} \right) \\
 a_y &= \frac{dV_y}{dt} + \omega_z V_x = \frac{1}{m} \left(\sum_{i=1}^4 P_{fyi} + \sum_{i=1}^4 R_{yi} + P_{wy} \right) \\
 J_z \frac{d\omega_z}{dt} &= \sum_{i=1}^4 M_{nki} + \sum_{i=1}^4 M(\bar{R}_i) + \sum_{i=1}^4 M(\bar{P}_{fi}) \\
 V_{x'} &= \frac{dy'}{dt} = V_x \cos \theta - V_y \sin \theta \\
 V_{y'} &= \frac{dx'}{dt} = V_x \sin \theta + V_y \cos \theta \\
 \omega_z &= \frac{d\theta}{dt}
 \end{aligned} \right. , \tag{5}$$

where a_x, a_y – the projection of the acceleration of the center of mass of the vehicle in coordinate axes x, y, z ; $P_{fxi}, P_{fyi}, R_{xi}, R_{yi}, P_{wx}, P_{wy}$ – the projection of the forces acting on the vehicle in coordinate axes x, y, z .

This system of equations allows determines the position, velocities and acceleration of the vehicle. This system of equations was creating in MATLAB Simulink. The inputs are the calculated values of the projections of the forces. The outputs are position, projections of the vehicle, acceleration, angular velocity, angle of rotation of the vehicle. Then this outputs value are used for calculation of the forces.

One of the wheels are considered for calculation of forces (fig. 2). For calculation forces, we used [2].

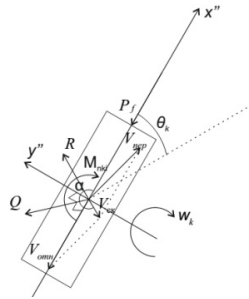


Fig. 2. The design scheme of the car:

The moment and the force of the rolling resistance depend of the properties of the tire and surface of a road. And it proportional to value of normal reactions Q_i . Normal reactions can be find of the system of equations:

$$\left\{ \begin{aligned}
 Q_1 - Q_2 + Q_3 - Q_4 &= 0 \\
 Q_1 + Q_2 + Q_3 + Q_4 &= mg \\
 Q_1 x_1 + Q_2 x_2 + Q_3 x_3 + Q_4 x_4 &= -m a_x H_z \\
 Q_1 y_1 + Q_2 y_2 + Q_3 y_3 + Q_4 y_4 &= -m a_y H_z
 \end{aligned} \right. , \tag{6}$$

where x_i, y_i – position of wheel in $x-y$; H_z – height, which is the center of mass of the vehicle.

The first equation is based on the assertion that the ends of the vectors normal reactions lie in one plane, and the second is derived from the condition that the sum of the normal reactions and weight of the car, the third and fourth equating moments.

The vector of slipping velocity \vec{V}_{sl} of the bottom point of wheel in the coordinate system $x'' - y''$ is determined by:

$$\vec{V}_{sl} = \vec{V}_c + \vec{V}_r, \quad (7)$$

where \vec{V}_c - the vector of the carrying velocity in $x''-y''$; \vec{V}_r - the vector of relating velocity in $x''-y''$.

The vector of the carrying velocity:

$$\vec{V}_c = \vec{V} + \vec{\omega} \times \vec{\rho}, \quad (8)$$

where $\vec{\omega}$ - the vector angular velocity; $\vec{\rho}$ - the radius vector defining the position of the moving coordinate system. The projection of \vec{V}_c , V_{cx} and V_{cy} in $x-y$:

$$\begin{cases} V_{cx} = V_x - \omega_z y_k \\ V_{cy} = V_y + \omega_z x_k \end{cases} \quad (9)$$

The projection of \vec{V}_c in $x''-y''$:

$$\begin{cases} V_{cx} = (V_x - \omega_z y_k) \cos \theta_k + (V_y + \omega_z x_k) \sin \theta_k \\ V_{cy} = -(V_x - \omega_z y_k) \sin \theta_k + (V_y + \omega_z x_k) \cos \theta_k \end{cases} \quad (10)$$

The projection of \vec{V}_r in $x''-y''$:

$$\begin{cases} V_{rx} = \omega_k r_k \\ V_{ry} = 0 \end{cases} \quad (11)$$

where ω_k - angular velocity of wheel; r_k - dynamic radius.

Then projection of \vec{V}_{sl} in $x''-y''$:

$$\begin{cases} V_{slx} = (V_x - \omega_z y_k) \cos \theta_k + (V_y + \omega_z x_k) \sin \theta_k - \omega_k r_k \\ V_{sly} = -(V_x - \omega_z y_k) \sin \theta_k + (V_y + \omega_z x_k) \cos \theta_k \\ V_{sl} = \sqrt{V_{slx}^2 + V_{sly}^2} \end{cases} \quad (12)$$

The coefficient of sliding of the model "with a rectangular imprint" [3] for calculating the interaction with the wheel bearing surface:

$$S = \frac{V_{sl}}{\omega_k r_k} \quad (13)$$

The force of interaction of the wheels to the road:

$$R = \mu_s Q, \quad (14)$$

where μ_s - tire – terrain interaction coefficient

$$\mu_s = \mu_{s\alpha \max} \left(1 - e^{-\frac{S}{S_0}}\right) \left(1 + e^{-\frac{S}{S_1}}\right), \quad (15)$$

where S_0 and S_l - constant parameters of the curve shape; μ_{samax} – coefficient of the tire – terrain interaction at complete slip:

$$\mu_{s\alpha \max} = \frac{\mu_{sx \max} \mu_{sy \max}}{\sqrt{\mu_{sx \max}^2 \sin^2 \alpha + \mu_{sy \max}^2 \cos^2 \alpha}}, \quad (16)$$

where here $\mu_{sx \max}$ and $\mu_{sy \max}$ – friction ellipse parameters (it determined empirically)

$$\begin{cases} \sin \alpha = \frac{V_{sly}''}{V_{sl}} \\ \cos \alpha = \frac{V_{slx}''}{V_{sl}} \end{cases}, \quad (17)$$

The projections of the tire – terrain interaction force in the road plane are calculated in the following way:

$$\begin{cases} R_x'' = -R \cos \alpha \\ R_y'' = -R \sin \alpha \end{cases}, \quad (18)$$

Then it in x - y :

$$\begin{cases} R_x = R_x'' \cos \theta_k - R_y'' \sin \theta_k \\ R_y = R_x'' \sin \theta_k + R_y'' \cos \theta_k \end{cases}, \quad (19)$$

The force of resistance rectilinear motion:

$$P_f = fQ, \quad (20)$$

where here f – tire rolling resistance coefficient:

Vector P_f is oppositely to projection $\overline{V_c}''$ in x'' , then P_f in x - y definition by:

$$\begin{cases} P_{fx} = -P_f \frac{V_{cx}}{|V_{cx}''|} \cos \theta_k \\ P_{fy} = -P_f \frac{V_{cy}}{|V_{cy}''|} \sin \theta_k \end{cases}. \quad (21)$$

Assume that $\overline{P_w}$ is opposite to \overline{V} , then:

$$P_w = c_x F q_v, \quad (22)$$

where c_x - the coefficient of aerodynamics; F – the frontal area of the vehicle;

$$F = k_F B H, \quad (23)$$

where $k_F=0,25-0,45$ – the coefficient of frontal shape of a vehicle; B and H – track and height of a vehicle;

$$q_v = \rho_a V^2 / 2, \quad (24)$$

where ρ_a - density of air.

Slipping of the footprint is causes of the steering force. With acceptable accuracy for find a moment of resistance to rotation, the following system of equations may be used:

$$\left\{ \begin{array}{l} M_{nki} = \frac{M_{nk \max}}{1 + 0,15 \frac{R_{nki}}{b_k}}, \\ M_{nk \max} = 0,375 \mu_{s\alpha \max} Q \sqrt{\frac{\pi l_k b_k}{4}}, \end{array} \right. \quad (25)$$

where $M_{nk \max}$ – moment of resistance for turn wheel while standing still, l_k и b_k – the length and the width of the contact, R_{nki} – the turning circle.

A block diagram of a mathematical calculation of forces and moments acting on the wheel of the car and the car itself based on (6-25) are creating in MATLAB Simulink. Inputs are values of velocity, the angular velocity of rotation of the car, wheel speed, angle of rotation of the wheels. Outputs are values of projection of \vec{P}_w , P_f , R , M_{nki} .

Individual drive each wheel allows you to fully realize the advantages of the electric drive. To power the motors of electric transmission converters can be used as described in [6, 7]. This transmission allows individually controlled for each wheel traction characteristics. It allows form the optimal mode of operation, to minimize the movement of the wheels to skid and the slip and create quick to implement active safety systems. This transmission definition by:

$$\left\{ \begin{array}{l} J_{k1} \frac{d\omega_{k1}}{dt} = M_{d1} - M_{r1} \\ J_{k2} \frac{d\omega_{k2}}{dt} = M_{d2} - M_{r2} \\ J_{k3} \frac{d\omega_{k3}}{dt} = M_{d3} - M_{r3} \\ J_{k4} \frac{d\omega_{k4}}{dt} = M_{d4} - M_{r4} \end{array} \right. \quad (26)$$

where J_{ki} - moment of inertia of the i-th wheel-motor; M_{di} – traction moment of i-th wheel-motor, M_{ri} – the moment of resistance i-th wheel.

On the fig. 3 we presented block diagram of the mathematical model of vehicle.

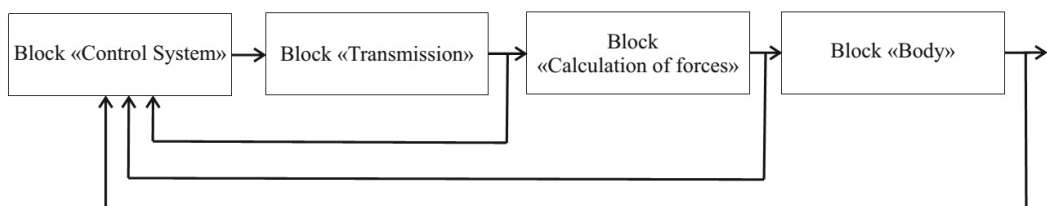


Fig. 3. Block diagram of the mathematical model of vehicle

The block «Control System» is the control system. It form control of traction moment of each wheel and form control of active safety system. The block «Transmission» is model of electric transmission with individual electric drive of each wheel (26). The block «Calculation of forces» make calculation of forces (6-25). And block «Body» is model of moving vehicle as plane-parallel moving solid body (5).

3. Conclusion

The developed mathematical model can synthesize the system of direct torque control on each wheel, depending on the strength of the interaction of wheel support surface, active safety systems and test their performance.

References

- [1] S.M. Marokhin Predicting mobility characteristics of a special-purpose vehicle equipped with active safety systems. [Prognozirovanie kharakteristik podvizhnosti spetsavtomobilya, osnashchennogo sistemami aktivnoy bezopasnosti: avtoref. diss. kand. tekhn. nauk], Ph.D. thesis abstract. Moscow, 2005, 146 p.
- [2] G.A. Smirnov Teoriya dvizheniya kolesnykh mashin: ucheb. dlya vuzov. – 2-e izd., pererab. i dop. [Theory of the wheeled vehicles motion: study guide. – second edition]. Moscow, Mashinostroenie, 1990, 352 p.
- [3] Yu.L. Rozhdestvenskiy, K.Yu. Mashkov Generation of the reaction forces in a flexible wheel rolling on the rigid road [O formirovani reaktiv pri kachenii uprugogo kolesa po nedeformiruemomu osnovaniyu], Trudy MVTU [BMSTU proceedings], 1982, no. 390, pp. 56–64.
- [4] D.R. Ellis Upravlomost avtomobila, Mashinostroenie, Moscow, 1975, 216 p.
- [5] S.V. Potoskuev Povishenie skorosti vipilnenia manevrov avtomobila s pomochiu prinuditelnogo zadania sootnoshenia skorostey vrashenia koles, Izvestia visshih uchebnykh zavedeniy, 2014, no. 5, pp. 12–20
- [6] A.A. Radionov, A.S. Maklakov, E.A. Karyakina, New control method of back to back converter, 2015 International Siberian Conference on Control and Communications, SIBCON 2015 - Proceedings, (2015). DOI: 10.1109/SIBCON.2015.7147135
- [7] A.S. Maklakov, A.A. Radionov, EMC evaluation of three level NPC converter based on space vector PWM, Proceedings of the 2015 IEEE North West Russia Section Young Researchers in Electrical and Electronic Engineering Conference, ElConRusNW 2015, (2015) 236–240. DOI: 10.1109/ElConRusNW.2015.7102269



International Conference on Industrial Engineering

Analysis of thermal state of power transformer of captive power plant

Kondrashova Yu.N., Khramshin R.R., Nikolaev A.A., Shurygina G.V.*

Nosov Magnitogorsk State Technical University, Lenina Av. 38, Magnitogorsk, 455000, Russia

Abstract

It has been proven that the introduction of the systems for continuous control of the power transformer technical state predetermines the need for improvement of the methods for calculation of the thermal modes, insulation wear and remaining service life of the equipment. Disadvantages of the existing methods recommended by domestic and foreign regulatory documents are noted. It is appeared to be practically to consider parameters of the environment, thermal mode retention and non-linearity of the thermal characteristics. The structure of algorithm for calculating temperature charts according to the load parameters with regard to the influence of the above factors is proposed. The developed software is briefly specified, too. The ultimate purpose is to develop and study the improved model for thermal characteristic calculation designed for the systems of on-line monitoring transformer technical state.

© 2015 The Authors. Published by Elsevier Ltd. This is an open access article under the CC BY-NC-ND license (<http://creativecommons.org/licenses/by-nc-nd/4.0/>).

Peer-review under responsibility of the organizing committee of the International Conference on Industrial Engineering (ICIE-2015)

Keywords: Power transformer; technical state; thermal mode; the hottest spot; temperature; useful lifetime; algorithm; software program; analysis

1. Introduction

It is famously urgent to create robust methodological procedures for calculation and forecast of the remaining transformer component lifetime. This is due to the issue of the necessary renewal of the great number of transformers due to their operating life. That is why it is practically important to substantiate objectively the priority and time sequence of this reorganization of the electric power industry. Furthermore, important diagnostic

* Corresponding author. Tel.: +73519431256.

E-mail address: AED174@mail.ru

characteristics in the on-line monitoring systems introduced at high-voltage power transformers are temperature values, remaining lifetime and servicing life of insulation [1]. In this regard, the issues of the accurate calculation of temperature of the hottest spot according to the transformer load parameters become more critical and essential.

Regulatory documents define principal items of the methodology and algorithms for calculation of the transformer's thermal modes [2]. However, the proposed algorithms have essential disadvantages reducing calculation accuracy. So, the thermal model of the cooling system suggested in GOST 14209-97 does not consider the following physical features being specific for unsteady thermal modes:

- temperature of the transformer components changes during unsteady processes according to the non-linear dependencies;
- winding temperature has its own heat retention and changes due to the non-linear dependency;
- temperature of the cooling medium influences the thermal mode of the power transformer with due regard to the time constant of its heating.

[3] shows that during monitoring transformer parameters at the temperature determination θ_h it is reasonable to take into account a time lag of the thermal processes in the winding and winding-oil section at presence of step changes of great amplitude in the load current trending. The above suggests elaborating existing methods and improving analysis algorithms aimed to the elimination of these disadvantages.

2. Main Part

At operation of the oil-filled power transformers one face the problem which is connected with temperature θ_h of the hottest spot of the winding insulation; it has an adverse effect on the insulation condition and may result in its fatal failure. That is why the temperature θ_h should be continuously monitored at the transformer operation. Direct measurement of this temperature has not become a frequent practice; consequently, it is determined due to the temperature rise in the upper oil layers.

To calculate temperature θ_h it is proposed to apply the heat equation of the winding sections neighboring to the hottest spot of insulation. Initial data for calculating θ_h are: current of the winding, temperature of the transformer oil upper layers and type of cooling (natural or forced one). In the mode of the stationary load of the transformer the formulas substantiated in [2] are used: For natural cooling (ON):

$$\theta_h = \theta_a + \Delta\theta_{br} \left[\frac{1 + RK^2}{1 + R} \right]^x + H_{qr} K^y, \quad (1)$$

For forced cooling (OF):

$$\theta_h = \theta_a + \Delta\theta_{br} \left[\frac{1 + RK^2}{1 + R} \right]^x + H_{qr} K^y + 2(\Delta\theta_{imr} - \Delta\theta_{br}) K^y, \quad (2)$$

where θ_a – temperature of the cooling medium; $\Delta\theta_{br}$ – oil temperature rise in the bottom winding part; $\Delta\theta_{imr}$ – average oil temperature rise; K – load ratio; H_{qr} – heat gradient of the hottest spot; R – loss rate; x – oil exponent; y – winding exponent.

2.1. Temperature Calculation in the Unsteady Thermal Mode

From formulas (1) and (2) it follows that the change of the transformer load results in changing the difference between temperatures of the hottest spot and upper oil layers. These dependencies do not reflect transient processes occurring at the change of this temperature but they may be obtained with the model as per [3].

During monitoring transformer parameters at the temperature determination it is reasonable to take into account a time lag of thermal processes in the winding and winding-oil section at presence of step changes of great amplitude

in the load current trending. Any alteration of the load modes should be considered as a step function. The rectangular load chart applied at the analysis of the thermal modes consists of one upward step and, after a while, the next descending step. For the steadily changing load the step function is applied to the lower time spans. Oil temperature rise (e.g. in the bottom part) at the end of time span t is determined with the formula

$$\Delta\theta_{bt} = \Delta\theta_{bi} + (\Delta\theta_{bu} - \Delta\theta_{bi})(1 - e^{-t/\tau_0}) \quad (3)$$

where $\Delta\theta_{bi}$ – initial oil temperature rise in the bottom part; $\Delta\theta_{bu}$ – long-term oil temperature rise in the bottom part at the load applied at this time span; τ_0 – oil time constant.

Any load alteration leads to change of the winding and oil temperature difference which attains a new value with the characteristic time constant of the winding. According to the recommendations of GOST 14109-97, this constant is not used at the calculations. The value of the load ratio K^p in expressions (1) and (2) is assumed to attain a new value immediately.

Relative insulation wear (or relative life reduction) caused by transformer loading for a definite time period is characterized with the following expressions:

$$L = \frac{I}{t} \int_{t_1}^t V dt \quad \text{or} \quad L = \frac{I}{N} \sum_{n=1}^N V_j, \quad (4)$$

where: L – wear ratio for the period; n – order number of the time period; N – number of intervals in the period; V_j – wear ratio for the n -th interval.

2.2. Description of the Developed Algorithm

In the algorithm of the developed software program the following corrections of the thermal model of power transformers are introduced:

- in the iterative methods of the thermal mode calculation the rate of change of winding ohm resistances depending on the calculated temperature value is considered;
- at the thermal mode calculation with due regard to the heating time constant the ambient temperature is considered;
- load is calculated for each load mode of the transformer.

The structure of the developed algorithm for calculation of thermal modes is shown in Fig. 1. Load ratios at the set chart and with regard to the changes of the ambient medium temperature, set temperature limit of the hottest spot and wear are calculated with iterative methods [2].

The maximum temperature value of the hottest spot and the relative wear ratio are calculated for the set load chart. If the maximum temperature value is not exceeded and the wear ratio is less than assumed limit value, the calculation is repeated at the increased value of factor F applied to each particular load K_1, K_2, \dots, K_n at constant time intervals t_1, t_2, \dots, t_n . The factor F is increased stepwise with increment of 1% for each iteration process till one of the limits is reached. If at the initial calculation the relative wear ratio is higher than the assumed value the calculation is repeated using value F decreased to 2%.

Load factor increase and temperature limit tolerances may be selected differently, depending on the transformer type and load parameters. Account must be taken of the fact that at the hottest spot temperature range between 100 and 140°C, after the load ratio having been increased by 2%, the maximum temperature of the hottest spot will rise by more than 2°C, while the relative wear ratio will be increased by about 25%.

The programming and computed suite "Calculation of the Transformer Wear" based on Delphi XP framework has been developed with the use of TChart graphical component. [4]. Checking in respect of permissible heating and wear of insulation forms the basis of the software application. The application is designed for modelling thermal processes in the power transformers in order to solve the following tasks: running control of the permissible loads; calculation of the allowable regular and hazardous overloads; determination of the load capacity resulting from the alteration of the

operation conditions or design parameters of the power supply components; modernization of the power-supply systems. All calculations are carried out relying on procedures set by IEC 354-91, GOST 14109-97.

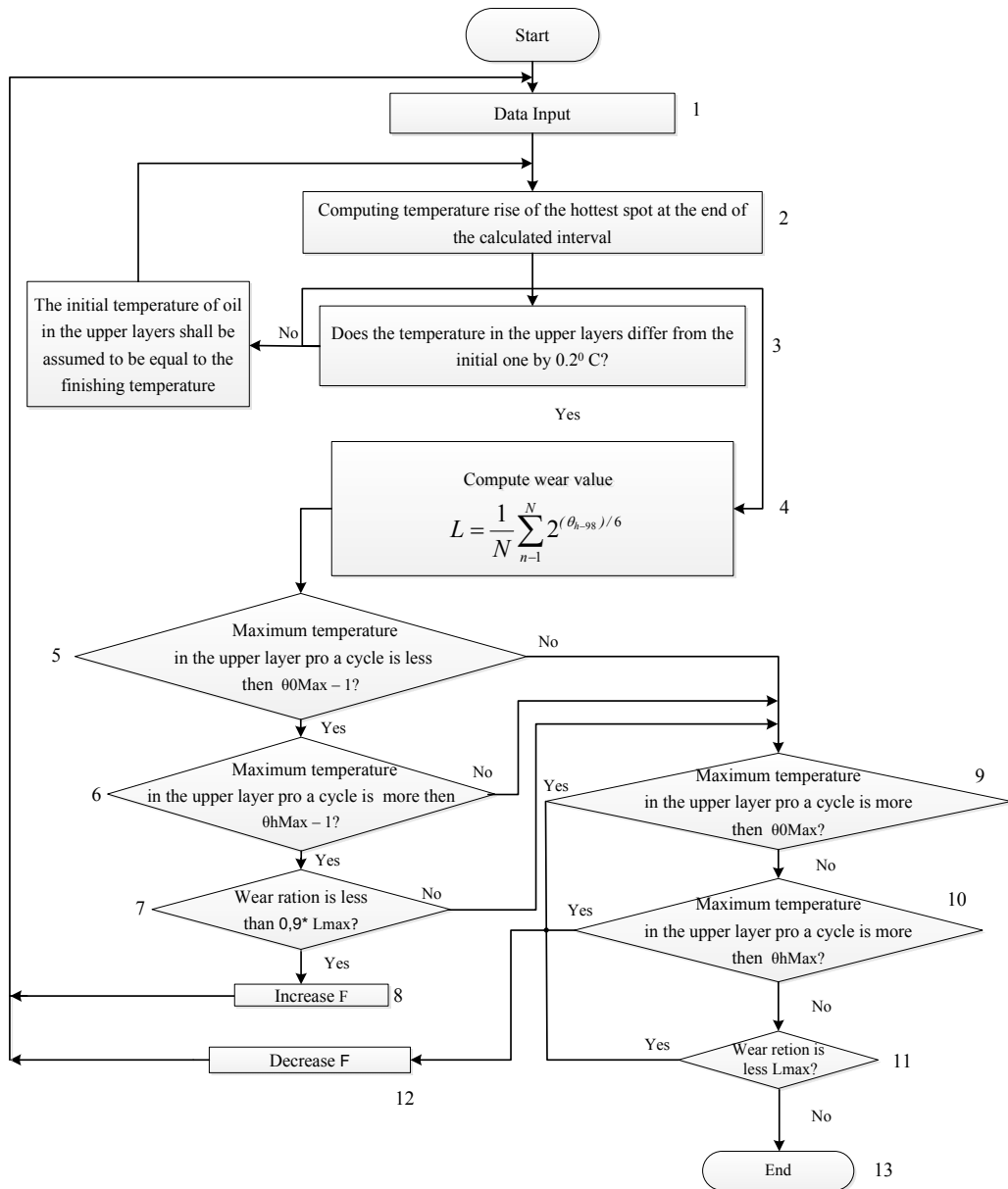


Fig. 1. Structural chart of the temperature calculation algorithm.

The main initial data are the transformer load chart and additional parameters used at the computing. For each load chart the software program calculates:

- temperature in the upper layers in °C;
- temperature of the hottest spot in °C;
- relative wear in relative units.

2.3. Example of the Program Application

Fig. 2 shows timing diagrams of changing active power P and reactive power Q of TDMS 63000/100000/110U1 transformer. The graphs are plotted for typical winter 24 hours under conditions of transformer operation at one of the operating transforming substations.

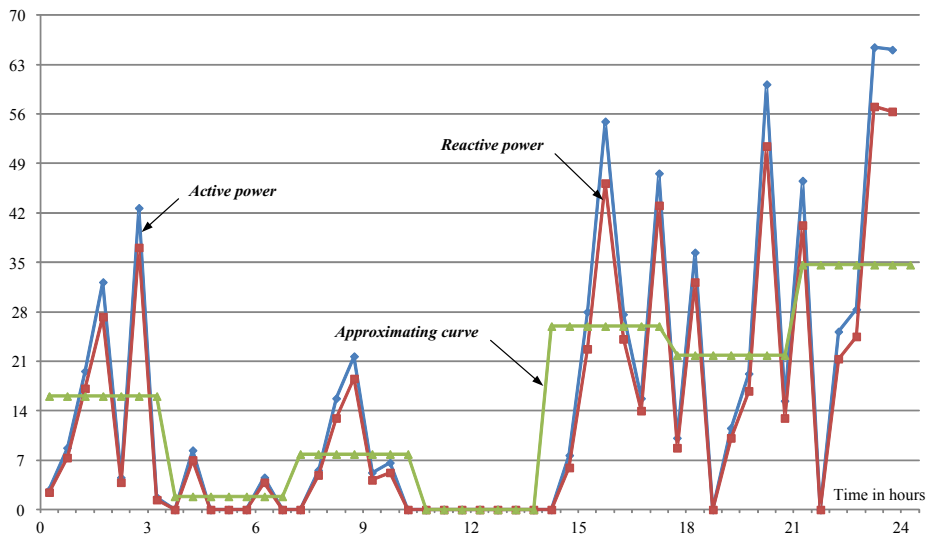


Fig. 2. Graph of transformer load change within 24 hours.

According to the methodology considered in [2], the dependency approximation by a polygonal line has been performed. Fig. 3 shows the step graph of the duty load change plotted due to the approximating curve. Here, eight levels with constant loads are emphasized one of which corresponds to zero load. Values of load and running time at each step are entered into the software application.

Fig. 3, b shows graphs of dependence of the hottest spot of transformer windings at the change of its load as per Fig. 3, a. Curves calculated by means of the developed program are displayed as solid lines while those plotted according to the algorithm as per GOST 14209-97 are displayed with dashed lines. Temperature values exceeding the oil upper layer temperature are being changed practically synchronously with the change of the transformer load current. At moments of loading jerks, the calculation of temperature θ_h due to the proposed model gives the most accurate values as compared to the known methods.

The results obtained correspond to the results published by foreign authors [5, 6] wherefore they may be recognized to be satisfactory.

3. Conclusion

The program developed provides the following options:

- computing and forecasting maximum temperatures with due regard to the ambient temperature changes as well as transformer load change in winter and summer time;
- considering thermal characteristics of transformers of various power with different cooling systems;
- visualizing the temperature of the hottest spot and oil in the upper layers as well as transformer wear behavior;
- calculating relative annual insulation wear based on the transformer's hottest spot temperature change within 24 hours and one year;
- providing controlling personnel with current information.

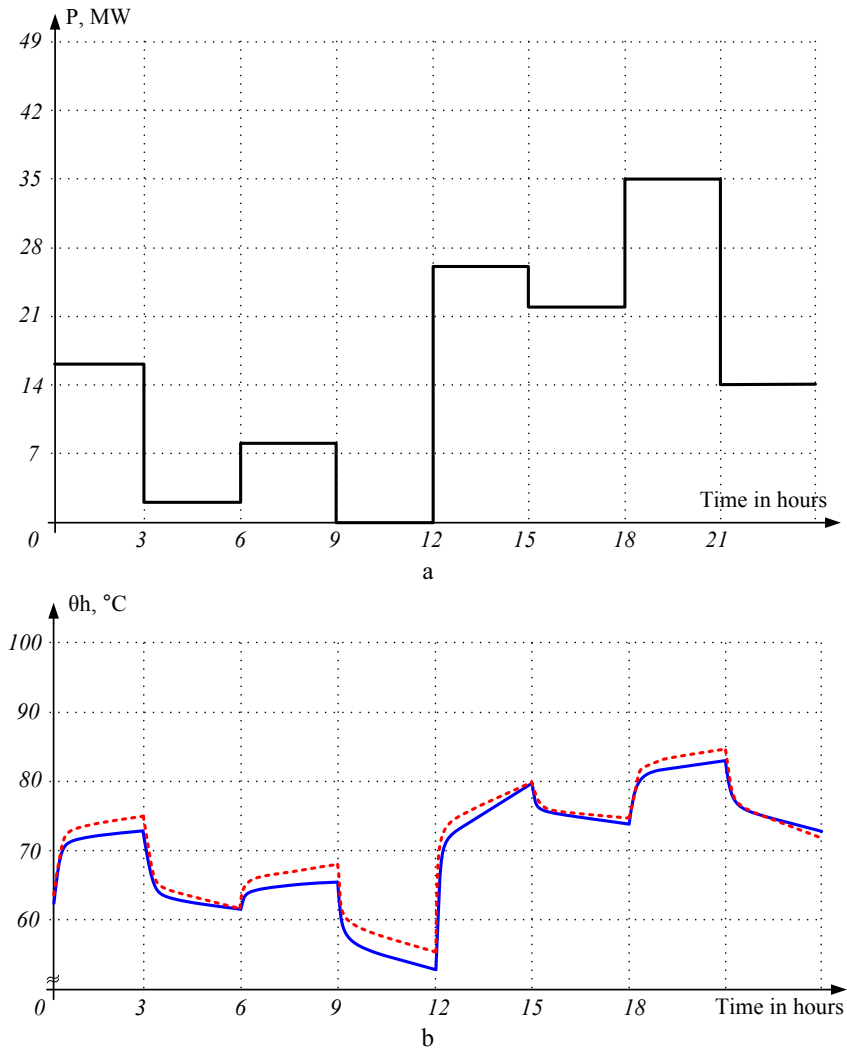


Fig. 3. Graph of transformer load change within 24 hours.

The developed algorithm enables computing thermal modes of the transformer as well as analyzing thermal state in the on-line monitoring mode. For this purpose it is integrated into software algorithms of the monitoring systems being introduced at the transformers [7, 8]. It provides increased efficiency of the technical state control [9,10].

Software of the transformer monitoring system should also include thermal models. This is a prerequisite for provision of the most accurate account of the transformer operational state enabling early fault detection. It is reasonable to develop systems which identify faults by means of comparing measuring results with the values "predicted" with models [11-13]. This is a way to specify transformer loads bearing in mind environmental conditions and to reduce electric power losses due to the load optimization.

Acknowledgements

Work is performed within the state job number 2014/80 of the Ministry of Education and Science of the Russian Federation.

References

- [1] A.S. Karandaev, S.A. Evdokimov, V.R. Khramshin, R.A. Lednov, Diagnostic functions of a system for continuous monitoring of the technical condition of the transformers of arc steelmaking furnaces, *Metallurgist*. 58(7-8) (2014) 655–663. DOI 10.1007/s11015-014-9972-5.
- [2] GOST RU 14209-97 (IEC 354-91). Power Oil Transformer Load Manual.
- [3] Mohammad Tolou ASKARI, M. Z. A Ab. KADIR, Mehdi IZADI, On the trend of improvement of thermal model for calculating the TOT and HST, *Przegląd Elektrotechniczny*, ISSN 0033-2097, R. 88 NR 12a/2012. 297–301.
- [4] A.S. Karandaev, S.A. Evdokimov, An.A. Nikolaev, V.R. Khramshin, Ju.N. Kondrashova, A.A. Nikolaev, Certificate RU of official registration of the software application 2014618972. (2014).
- [5] D. Susa, M. Lehtonen, H. Nordman, Dynamic thermal modeling of power transformers. *IEEE transactions on power delivery*. 20 (2005) 197–204.
- [6] D. Susa, H. Nordman, A simple model for calculating transformer hot-spot temperature, *IEEE transactions on power delivery*. 24 (2009) 1257.
- [7] A.S. Karandaev, S.A. Evdokimov, V.R. Khramshin, A.A. Sarlybaev, System for real-time monitoring of the technical state of a transformer on an ultrahigh-power electric-arc steelmaking furnace, *Metallurgist*. 58(9-10) (2014) 872–879. DOI:10.1007/s11015-015-0010-z.
- [8] A.S. Karandaev, S.A. Evdokimov, V.R. Khramshin, O.I. Karandaeva, Information and measuring system for electric arc furnace transformer monitoring, 12th International Conference on Actual Problems of Electronic Instrument Engineering (APEIE-2014), Novosibirsk. 1(2014) 273–279. DOI 10.1109/APEIE.2014.7040896.
- [9] A.S. Karandaev, V.R. Khramshin, S.A. Evdokimov, Yu.N. Kondrashova, O.I. Karandaeva, Methodology of calculation of the reliability indexes and life time of the electric and mechanical systems. *Proceedings of 2014 International Conference on Mechanical Engineering, Automation and Control Systems (MEACS)*. (2014) 6. DOI 10.1109/MEACS.2014.6986866.
- [10] V.R. Khramshin, A.S. Evdokimov, S.A. Evdokimov, A.S. Karandaev, Development and industrial introduction of systems for monitoring technical state of the rolling mills' electrical equipment. *Proceedings of the 2015 IEEE NW Russia Young Researchers in Electrical and Electronic Engineering Conference (EConRusNW)*. (2015) 208–213. DOI 10.1109/EConRusNW.2015.7102264.
- [11] V.R. Khramshin, S.A. Evdokimov, An.A. Nikolaev, Ar.A. Nikolaev, A.S. Karandaev, Monitoring technical state of the power transformers is a necessary condition of the smart-grid technology introduction within the industrial electric networks, *Proceedings of the 2015 IEEE NW russia young researchers in electrical and electronic engineering conference (EConRusNW)*, St. Petersburg. (2015) 214–220. DOI 10.1109/EConRusNW.2015.7102265.
- [12] A.S. Maklakov, A.A. Radionov, Integration prospects of electric drives based on back to back converters in industrial smart grid, 2014 12th International Conference on Actual Problems of Electronic Instrument Engineering, APEIE 2014 – Proceedings. (2014) 770–774. DOI: 10.1109/APEIE.2014.7040790
- [13] A.A. Radionov, A.S. Maklakov, V.R. Gasiyarov, Smart Grid for main electric drive of plate mill rolling stand, *Proceedings of 2014 International Conference on Mechanical Engineering, Automation and Control Systems, MEACS 2014*. (2014). DOI: 10.1109/MEACS.2014.6986842



International Conference on Industrial Engineering

Viscosity characteristics of hydrocarbons at high pressures

Rednikov S.N.*

South Ural State University, 76, Lenin Avenue, Chelyabinsk, 454080, Russian Federation

Abstract

This article discusses the characteristics of thermal-hydraulic properties of fluids, depending on the fineness of the system. The authors are the main physical and chemical phenomena occurring in the technical hydrocarbons with the impact on them of the conditions of the working process of hydraulic system. The results make it possible to take into account the maximum possible number of factors that influence the rheological properties of the medium. In the paper, problems of measurement of viscosity and changes of temperature of hydrocarbons under the pressure of more than 150 MPa are considered.

© 2015 The Authors. Published by Elsevier Ltd. This is an open access article under the CC BY-NC-ND license (<http://creativecommons.org/licenses/by-nc-nd/4.0/>).

Peer-review under responsibility of the organizing committee of the International Conference on Industrial Engineering (ICIE-2015)

Keywords: viscosity, temperature, hydrocarbons structural viscosity, molecular weight distribution, rheology of hydrocarbons, rotational viscometer.

Introduction

Flowing of hydrocarbons at high pressures may be accompanied by polymerization and depolymerization processes, in such circumstances the viscosity of fluids cannot be longer described as a monotonic dependence on temperatures and pressures [1, 3, 4, 5, 7, 8, 11, 12]. The viscosity of the most liquids in a wide temperature range varies according to the dependencies Williams-Landell-Ferry, Fulcher-Vogel, Eyring and others [6, 10, 15, 18, 19, 22]. These relationships are decreasing functions of temperature and pressure, satisfactory to describe the flows of dropping liquids that are the most common in nature and used in engineering, in particular, liquid metals, melts of natural minerals, polymers. The flow characteristics of such liquids well studied and are being intensively specified.

* Corresponding author.

E-mail: srednikov@mail.ru

Thus, viscosity characteristics of hydrocarbons in a pressure range less than 150 MPa are researched enough [1, 3, 6]. The researching of hydrocarbons at pressures above 150 MPa and during phase transitions that cause both vitrification and crystallization [10, 11] is difficultly due to phases that differ greatly in viscosity. In addition, when designing viscometers at pressures above 200 MPa the changes of the properties of structural materials [12, 13, 14], the parameters of measuring devices [2, 17, 21], the medium chemical activity [16,18,20] and other factors caused by the pressure growing are to be taken into consideration.

Influencing mechanical fields on a liquid, with the task pressure of the certain values, the structure of substance can be transferred in a firm condition at room and even the raised temperatures. It is takes necessary into account, that the temperature of mechanical transition in a firm condition settles down above, depends on a mode of growth of pressure. In a mode of high speeds and pressure, the temperature of mechanical transition in a firm condition is higher, in comparison with a mode of low speeds and pressure, therefore the temperature of structural transition in a firm condition of substance can be considered, as limiting value mechanical transition in the firm condition appropriate to indefinitely slow growth of pressure. At presence at polymers, ability of transition in a condition of volumetric transition in a firm condition in conditions of atmospheric pressure, definition for them temperature of structural transition in a firm condition at which sharp change of a thermal capacity of the substance is observed, caused by significant change of dynamic viscosity and its transition in a super plastic condition is possible. Polymers intensively lose the stability at the temperatures close to values of their temperatures of structural transition in a firm condition, and in conditions of lower temperatures there are minor alterations of properties, thus: the structure, a thermal capacity and other physical parameters change insignificantly. Changes of characteristics of polymers are possible and temperatures of structural transition in a firm condition, a so-called structural relaxation are lower.

Being based on theories of phase transition, physical conditions of polymers are described, kinetic energy of particles, a modular condition of system and a relative positioning of particles in space, a phase condition of system. At change of intensity of thermal movement of particles and energy of intermolecular interaction, owing to increase or downturn of values of thermodynamic parameters, temperature or pressure, there is a change of a modular condition of system. In spite of the fact that substances can be in four modular conditions, such as firm, liquid, gaseous and as plasma, it is considered, that for polymers last two conditions are not realized, and change of a relative positioning of particles at increase or downturn of values of thermodynamic parameters results in change of a phase condition of substance. Hence, phase conditions: Crystal or amorphous in which there can be polymers, differ from each other only a relative positioning of particles: atoms, molecules and their order. Reception of firm structures of amorphous substance becomes possible, at all values of temperatures, below temperatures structural стеклования will represent the firm elastic bodies as molecular regroupings are lower than this temperature do not occur, hence, viscous and deformations are not realized. And also it provided that time of action of growth of pressure becomes less time of a relaxation, liquid polymer starts to react to influence of growth of pressure is similar to a firm body that is not, true phase transition. Considering multi-variant approach of the possible reasons of formation of the given structures and even it a probable combination of some processes, протекавших in system simultaneously or consistently, the establishment of combinations and which sequences demands the realization, more developed additional researches. Distinctions in the received structures and their difference from initial structure that specifies an opportunity of occurrence of similar effects, in working processes of various technical hydrocarbons are obvious. Also at the visual analysis of structures becomes, the various spectrum of absorption of light the received samples in a seen spectrum is obvious, hence, it is possible to assert, that samples have differences in a chemical compound. It is possible to explain the given effect the certain numerical values энергий molecular and intermolecular communications. Therefore, at increase of energy of system, it is necessary to expect break only those existing communications, whose energy do not exceed values of energy to the transferred system on means of influence of the mechanical power field, similar is observed and during formation of new communications.

To study the viscosity characteristics of liquids we used a rotary coaxial-cylinder viscosimeter with a movable inner cylinder, i.e. Serle measuring. The rotary speed of this viscometer is controlled by an operator, and as it will be shown further, the shear rate is linearly related to it. In other words, it is a CR-rheometer. To drive the viscometer we used a collector-free engine powered with constant current to vary gradually the rotation frequency from 0 up to 7000 rev/min.

The engine is controlled by an electronic speed regulator to change the rotation speed due to the pulse-width modulation of the phase voltage and the voltage synchronization with the engine rotation without any additional

sensors. The viscosity of the investigated liquid is calculated due to the power consumed by the engine. When measured the unit of coaxial cylinders is placed in a sealed container with the researched liquid, which is pressed up to 198 MPa with a multi-applicator. The design of the measuring unit is shown in Figure 1. The thermocouple is applied for revealing character of influence of allocation of heat in a measuring cell. Application of this method at research of characteristics at work with a high pressure is unacceptable. [3.] At experiments of the liquids connected to researches with high pressures the quality monitoring of external thermal fields for definition of rise in temperature of a working environment [1] was used. Calculation of temperature of a researched liquid in the chamber of a high pressure, is carried out leaning on results of gaugings of temperature fields of an external surface of the device. Process of heat exchange was considered as process of transfer of heat through a multilayered wall from a material with known heat conductivity under the boundary conditions characterized in constant factor of transfer of heat in an environment and varied temperature of the researched environment inside the device. Knowing factor of heat conductivity of a material of the case, his dependence on pressure, initial distribution of temperatures in installation, geometry of the device, we can defines value of temperature of the liquid at any moment.

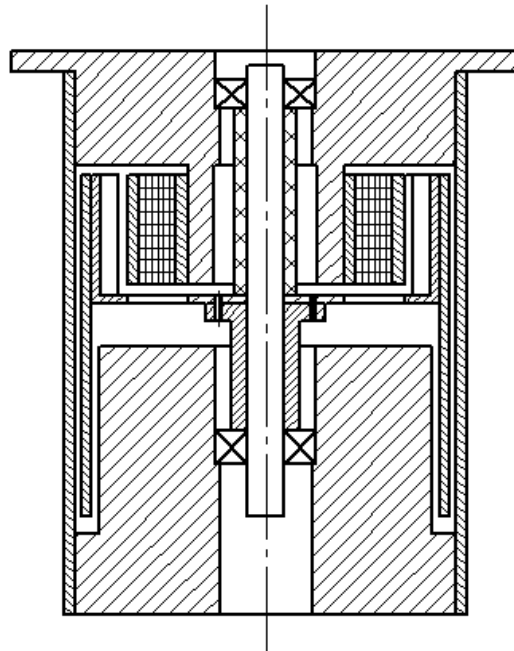


Figure 1. The measuring unit design

The used rotational viscometer has the following characteristics:

- the viscosity of the fluids is 0.005...0.1 Pa·sec;
- the shear rate is 5000...30000 sec⁻¹;
- the pressure of researched liquids is 0.1...200 MPa;
- the temperature of researched liquids is 15...25⁰C;
- the researched liquids are non-conductive hydrocarbons;
- the power supply voltage is measured with the ±0,1% accuracy;
- the current consumed is ± 0,8%;
- the rotor rotations are ± 0,1%.

FINDINGS

We measured the viscosity of some hydraulic fluids within the shear rate range available for the considered installation and at different pressures. The results are shown in Figures 2-4.

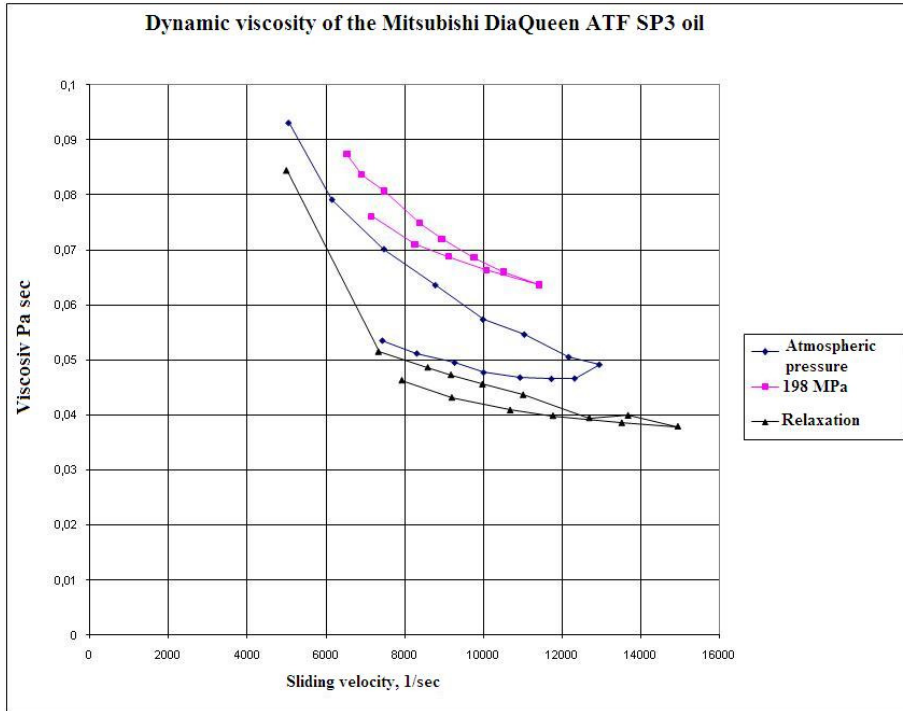


Figure 2. The viscosity curves of the semisynthetic oil Mitsubishi DiaQueen ATF SP3 at the initial temperature 24.0°C. The diagram “Relaxation” shows the viscosity curve immediately after the sudden depressurization from 198 MPa to the atmospheric pressure.

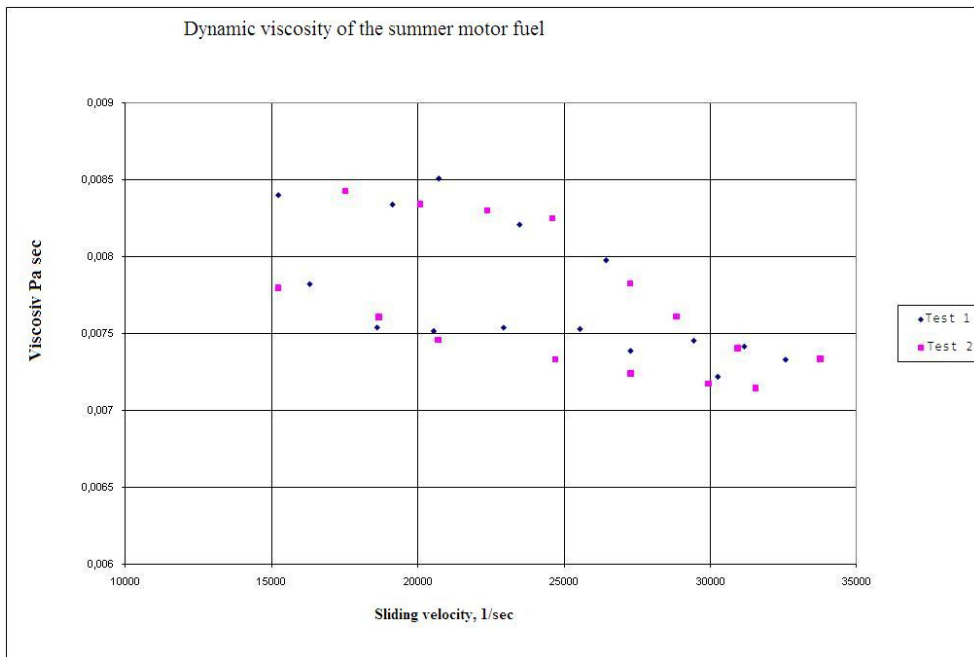


Figure 3. The viscosity curve of summer diesel fuel at the initial temperature of 24.0°C and the atmospheric pressure.

The measurements for the curve “Test 2” were done 10 minutes after the measurements for “Test 1”.

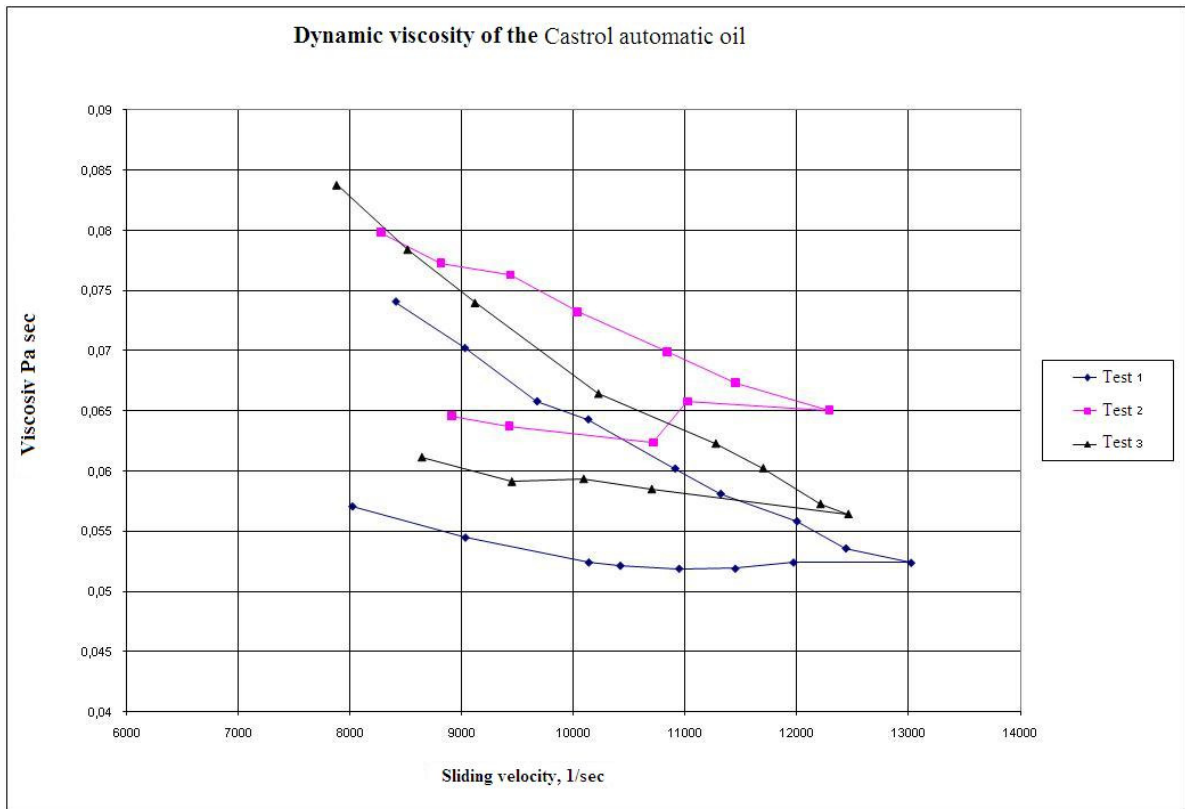


Figure 4. The viscosity curve of the semisynthetic oil for automatic transmission Castrol automatic at the initial temperature 24.0°C. The diagram “Test 1” is for the atmospheric pressure, the diagram “Test 2” shows the pressure immediately after the sudden depressurization from 198 MPa to the atmospheric pressure and the diagram “Test 3” is for the pressure 20 minutes after the depressurization.

Conclusions

The results show the possibility of using the examined viscometer for experimental studying the viscosity characteristics of hydrocarbon liquids at high pressures, with the relaxation effects being revealed in hydrocarbon systems.

References

1. Barenblatt G.I., Gorodtsov V.A., Kalashnikov V.N. *Turbulentnost' anomal'nykh zhidkosti* [Turbulence of abnormal liquids], in: *Teplo I massa perenos* [Heat and mass transfer], Minsk, Science and Technology, 1968, pp.3-23.
2. Belkin I.M., Vinogradov G.V., Leonov A.I. *Rotatsionnye pribory. Izmerenie vyazkosti i fiziko-mekhanicheskikh kharakteristik materialov* [Rotational instruments. Measuring the viscosity and physical and mechanical properties of materials], Moscow, Machine-building, 1967, 272 p.
3. Astarita J., Maruchchi J. *Osnovy gidromekhaniki nen'yutonovskikh zhidkosti* [Hydromechanic basics of non-Newtonian fluids], Moscow, Mir, 1978, 309 p.
4. Vinogradov G.V., Malkin A.Ya. *Reologiya polimerov* [Polymeric rheology], Moscow, Chemistry, 1977, 438 p.
5. Likhachev E.R. The dependence of water viscosity on temperature and pressure [Zavisimost' vyazkosti vody

ot temperatury i davleniya], *Tekhnicheskaya fizika [Technical Physics]*, 2003, V.73, no.4. pp. 135-136.

6. Ostapenko A.A. Effect of the electric field on the dynamic viscosity of liquid dielectrics [Vliyaniye elektricheskogo polya na dinamicheskuyu vyazkost' zhidkikh dielektrikov], *Zhurnal tekhnicheskoi fiziki [Technical Physics]*, 1998, V.68, no.1e, pp. 40-43.

7. Fabelinskii I.L. About macroscopic and molecular shear viscosity [O makroskopicheskoi i molekulyarnoi sdvigivoi vyazkosti], *Uspekhi fizicheskikh nauk [Advances of Physical Sciences]*, 1997, V.167, no.7e, pp. 721-731.

8. Fogelson R.L., Likhachev E.R. Viscosity temperature dependence [Temperaturnaya zavisimost' vyazkosti], *Zhurnal tekhnicheskoi fiziki [Technical Physics Journal]*, 2001, V.71, no.8, pp. 128-131.

9. Frenkel Ya.I., *Kineticheskaya teoriya zhidkosti* [Kinetic theory of liquids], Leningrad, Nauka, 1975, 592 p.

10. Grishin A.P., Rebinder P.A., Alexandrova E.A., Markina Z.N. About crystallization, structural solidification and hysteresis in paraffin solution with added surface active substances [O kristallizatsii, strukturnom zastyvanii i gisterезise v rastvorakh parafina s dobavkami poverkhnostno-aktivnykh veshchestv], Moscow, DAN SSSR, 1970, V. 194, no.4, pp. 850-853.

11. Skorodumov, V.F. Thermodynamic aspects of glass molding [Termodinamicheskiye aspekty steklovaniya pod davleniyem], *Zhurnal fizicheskoi khimii [Journal of Physical Chemistry]*, 1994, V.68, no.12, pp. 2254-2256.

12. Tsiklis, D.S. *Tekhnika fiziko-khimicheskikh issledovaniy pri vysokikh davleniyakh* [The technique of physico-chemical studies at high pressures], Moscow, Chemistry, 1965, 416 p.

13. Bridgman P.V., *Issledovaniya bol'shikh plasticheskikh deformatsii i razryva* [Studies of large plastic deformations and fractures], Moscow, Mir, 1955, 467 p.

14. Bridgman P.V., *Fizika vysokikh davlenii* [Physics of high pressures], Moscow, ONTI, 1935, 256 p.

15. Ioselevich V.A., *Mikro i makro dinamika polimernykh rasstvorov* [Micro and macro hydrodynamics of polymer solutions], Moscow, 1987, V.2, pp. 146-163.

16. Pervushin V.E. *K otsenke vliyaniya teploty vnutrennego treniya na harakteristiki strukturnogo techeniya vyazkoplastichnoi zhidkosti v krugloi trube* [To assess the impact of heat on the internal friction of the structural characteristics of the viscoplastic fluid flow in a round pipe], Moscow, 1974, no.3, pp.79-85.

17. *Reologiya. Teoriya i praktika.* [Rheology. Theory and practice], Ed by F.Eyring, Moscow, Foreign Literature Publishing House, 1962, 921 p.

18. Rebinder P.A. *Fiziko-khimicheskaya mekhanika dispersnykh struktur* [Physico-chemical mechanics of disperse structures, in: *Fiziko-khimicheskaya mekhanika dispersnykh struktur* [Physical-chemical mechanics of disperse structures], Moscow, Nauka, 1966, pp. 3-6.

19. Remezov C.B. *Strukturno-reologicheskie svoystva dispersnykh sistem s nepolyarnoi dispersionnoi sredoi* [Structurally rheology of disperse systems with a nonpolar dispersion medium]. extended abstract of Dr. Sci. (Chemistry), Moscow, MGU, 1996, 21 p.

20. Froysheter G.B., Danilevich S.Y., Radionova N.V. *Techeniye i teploobmen nen'yutonovskikh zhidkosti v trybakh* [Flow and heat exchange of non-Newtonian fluids in pipes], Kiev, 1990, 216 p.

21. Harin V.I. *Interpretatsiya dannykh rotatsionnoi viskozimetrii vyazko-uprugih tiksotropnykh zhidkosti* [Interpretation of rotational viscometry viscoelastic thixotropic liquids], Moscow, Proceedings of Academy of Sciences of the USSR, 1987, V. 293, no.4, pp. 823-827.

22. Yahno O.M., Dubovitsky V.F. *Osnovy reologii polimerov* [Rheology fundamentals of polymers], Kiev, 1976, 185 p.



International Conference on Industrial Engineering

Fatigue life prediction of engineering structures under multivariable random loading using structural model

Abyzov A.A.* , Berezin I.I., Sadakov O.S.

South Ural State University, 76, Lenin Avenue, Chelyabinsk, 454080, Russian Federation

Abstract

The article describes the case of multivariable random loading, which occurs when the caterpillar suspension component acts as a set of loads of independent random processes. In the danger zone details of the changes in the components of the stress tensor are independent random processes. As an example of parts operating at such a loading the author discusses tracked vehicle road arm. Presently, there are no standard techniques for the estimation of fatigue life under random multivariable loading currently available. The article describes the method of estimating the fatigue life for this type of load, based on the calculation of microplastic deformation. It uses a structural model of the material, based on the description of the deformation diagram of dependence by Ramberg-Osgood. To identify the model of accumulation of damage conventional mechanical and fatigue characteristics of the material were used. Accounting for natural dispersion of fatigue characteristics allowed to get the result as a function of the probability of failure-free operation. The validity of the approach is confirmed by comparing the calculation results with the experimental data. The practical application of the technique is illustrated by the example of predicting the durability and reliability of heavily loaded parts of the high-speed caterpillar vehicle.

© 2015 The Authors. Published by Elsevier Ltd. This is an open access article under the CC BY-NC-ND license (<http://creativecommons.org/licenses/by-nc-nd/4.0/>).

Peer-review under responsibility of the organizing committee of the International Conference on Industrial Engineering (ICIE-2015)

Keywords: Multivariable loading; Random process; Microplastic deformation; Structural model of the environment; Fatigue failure;

1. Introduction

When designing a machine, designed to work in heavy accidental load, forecasting of the resource of heavy-duty machines is performed on the basis of the calculation of the fatigue life of its parts [1, 2, 3].

* Corresponding author. Tel.: +7-351-267-92-61; fax: +7-351-267-93-06.
E-mail address: abyzovaa@susu.ac.ru

In the case of a linear stress state, this problem is solved quite simply. Using spectral density of stress changes obtain probability distributions high, convert them into loading units, and then on the basis of hypotheses of summation of fatigue damages, the average values of the components resource[4] are determined. There is also another possible approach, according to which the process is carried out directly by the known methods (for n cycles, "rain- flow", etc.) and the subsequent calculation of the accumulated damage is carried out. Existing theories also make possible to obtain a probability function of failure-free operation in the presence of information about the spread of fatigue characteristics of the material.

The most difficult case is when a heavy duty parts are under plane or volumetric stress states. There are many methods for calculating fatigue strength for a one-parameter loading, when the stress tensor components are stationary random processes with proportional change in values. In these cases it is possible to bring down using conventional hypothesis the amplitude of the principal stress in the danger zone details to the equivalent amplitude of a linear stress state[5].

In engineering practice, there are cases of multi-parameter loading when part loads are cyclically varying forces with random amplitudes and points of application. For example, caterpillar tractor supporting surface during movement of the machine on the track undergo combination of random loads. During operation of engineering machines these loads accompanied by random loads acting on the operating parts. This situation is possible when the components of the stress tensor vary in phase, but with different for each loading cycle ratio factor. Principal planes remain unmoved within a single load, randomly changing its position from cycle to cycle. Methods of estimation of durability for this case is offered in [6, 7, 8, 9, 10].

2. Methods

The case of multi-parameter loading, in which the components of the stress tensor in a dangerous point of part vary randomly for independently is the most difficult. Standard methods of estimation of fatigue life for this type of loading is not currently available.

Examples of parts that implement this type of load in dangerous locations, is the tracked vehicle road arm[3] (Fig. 1, a). The forces acting on each of the rollers may be presented in the form of three components (Fig. 1, b) in the coordinate system x - y - z , associated with the the machine body. The alpha as well as vertical (F_z)_ and longitudinal (F_x) components of the load constantly change over time in the course of driving on the road, having irregularities. When driving on the curved ways there is of a transverse component F_y occur. Examples of such a processes are shown in Fig. 2, a.

During the movement angle α is continuously changes over time, so for further calculations, it is necessary to convert the forces acting on the roller to force components: P_X, P_Y, P_Z, M_X, M_Z , fixed with respect to the road arm body (Fig. 1, c):

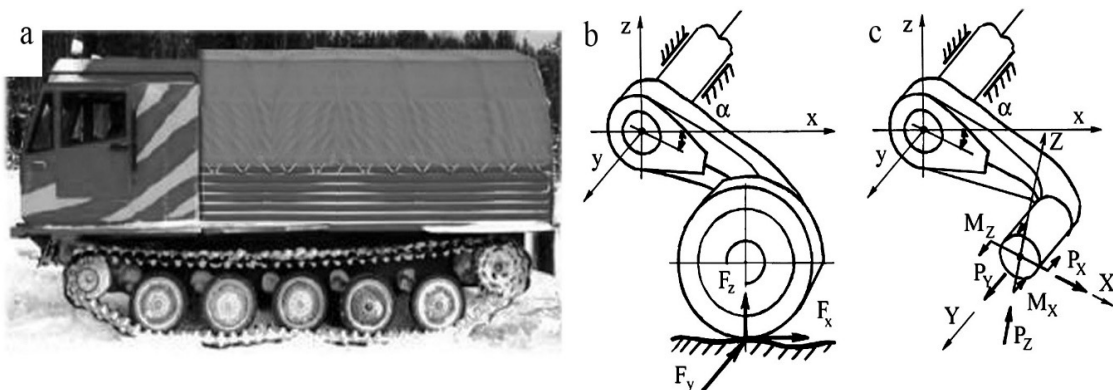


Fig.1. (a) tracked vehicle; (b) the forces acting on the roller; (c) the forces acting on the road arm.

$$P_Z(t) = F_x(t) \sin(\alpha(t)) + F_z(t) \cos(\alpha(t)), \quad P_X(t) = -F_z(t) \sin(\alpha(t)) + F_x(t) \cos(\alpha(t)),$$

$$P_Y(t) = F_y(t), \quad M_X(t) = F_y(t)R \cos(\alpha(t)), \quad M_Z(t) = F_y(t)R \sin(\alpha(t)).$$

where, R is the radius of the support roller.

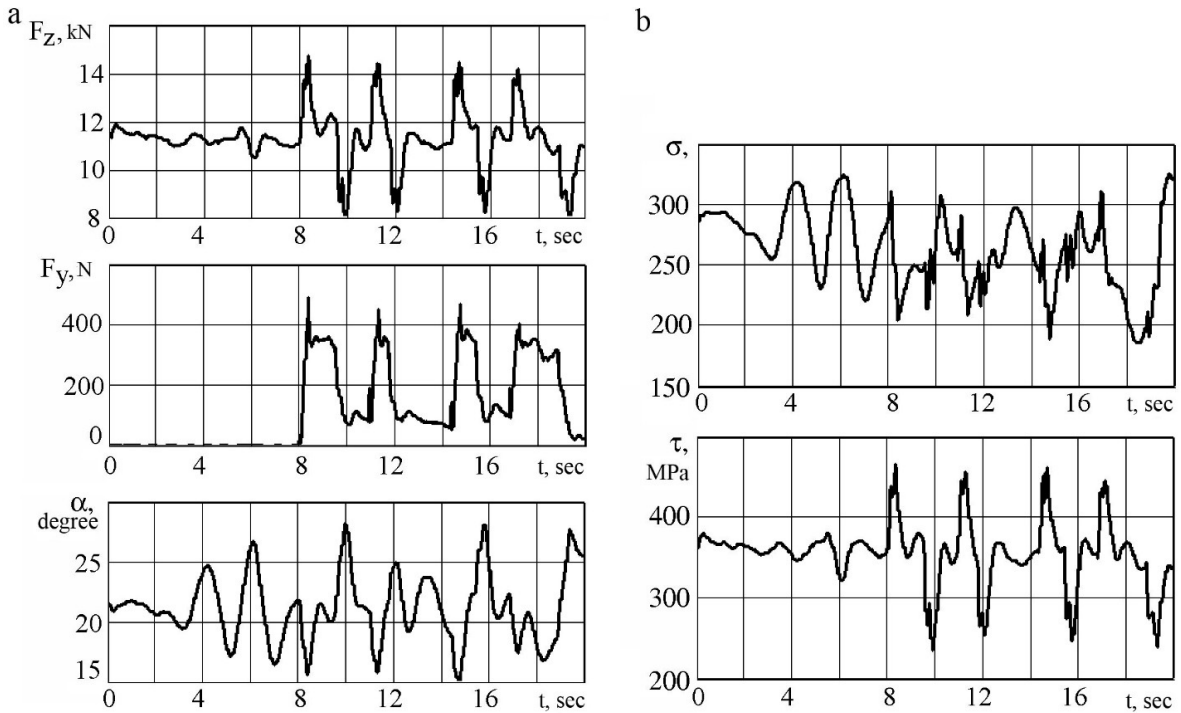


Fig.2. (a) processes of change of forces; (b) processes of change of stress.

Calculation of the momentary stress values can be made using standard finite element method. Firstly, define the components of a stress state in the most loaded zone $\sigma_{\xi n}, \sigma_{\eta n}, \tau_{\xi \eta n}$ under action of single forces of P_X, P_Y, P_Z, M_X, M (ξ and η – axis lying in plane on the n - th finite element). The current value of stress components is defined as a linear combination:

$$\sigma_{\xi n}(t) = \sigma_{\xi n}^{P_X=1} \cdot P_X(t) + \sigma_{\xi n}^{P_Y=1} \cdot P_Y(t) + \sigma_{\xi n}^{P_Z=1} \cdot P_Z(t) + \sigma_{\xi n}^{M_X=1} \cdot M_X(t) + \sigma_{\xi n}^{M_Z=1} \cdot M_Z(t),$$

$$\sigma_{\eta n}(t) = \sigma_{\eta n}^{P_X=1} \cdot P_X(t) + \sigma_{\eta n}^{P_Y=1} \cdot P_Y(t) + \sigma_{\eta n}^{P_Z=1} \cdot P_Z(t) + \sigma_{\eta n}^{M_X=1} \cdot M_X(t) + \sigma_{\eta n}^{M_Z=1} \cdot M_Z(t),$$

$$\tau_{\xi \eta n}(t) = \tau_{\xi \eta n}^{P_X=1} \cdot P_X(t) + \tau_{\xi \eta n}^{P_Y=1} \cdot P_Y(t) + \tau_{\xi \eta n}^{P_Z=1} \cdot P_Z(t) + \tau_{\xi \eta n}^{M_X=1} \cdot M_X(t) + \tau_{\xi \eta n}^{M_Z=1} \cdot M_Z(t).$$

As an example, Fig. 2, b presents fragments of the processes of change of normal and shear stress in the most dangerous points of the cross section of the balancer. Analysis of the processes of change of the stress state components indicated that they are different, although correlated stochastic processes.

In this paper the method of estimation of fatigue life in general under multi-parameter loading is developed. The method is based on the use of structural model of material and the model of damage accumulation [11, 12], originally developed for the low cycle fatigue. The original idea of the model is that fatigue is associated with the micro- plastic deformations. The increment of the accumulated damage is given by:

$$d\omega = K v^\beta d\lambda. \tag{1}$$

where, K and β constant coefficients defined in the construction of the model, $d\lambda$ - Odkvist's parameter, $\nu = p^*/r^*$, p^* - plastic deformation rate after the last reverse, r^* - the intensity of the elastic deformation.

The values of $d\lambda$ and ν are obtained from the solution of the boundary value problem with the help of the structural models of the material. It is assumed that the elementary volume of construction works like a set of subelements, the yield surface in deviatoric space described by Mises spheres of different radiuses. Deformation of all sub-elements are considered the same and is equal to deformation of element. For non-deformed body centers of yield surface are at the origin. In the process of deformation of the material takes place displacement of the point e , corresponding to the current strain. When it reaches any yield surface and seeks to go beyond it, there is a displacement of the center of the surface so that the point e is on the surface all the time. This shift represents a change of inelastic deformation dp_k . The corresponding calculation method is described in [11]. In the process of the material deformation the calculation of $d\lambda$ is carried out by the equation $d\lambda = \langle \Delta p_k \rangle$. The value of ν at each step of loading is determined as a function of the number of shifted yield surfaces [13- 15].

This approach allows the calculation of the accumulated damage at arbitrary trajectory of the point corresponding to the current value of the deformation, including the multi-parameter loading. In the case of high-cycle fatigue instead of the plastic deformation should be regarded microplastic deformation responsible for the accumulation of damage. To calculate microplastic deformation may be used deformation diagram described by Ramberg-Osgood relation [16]:

$$r = Ap^m .$$

where, A and m is the constants factors (material properties), r and p is the intensity of the elastic and plastic deformation. Parameters A and m can be determined by conventional mechanical properties - yield strength and tensile strength.

To identify the model of damage accumulation (1) usually equate the damage calculated by the model and Coffin relation. To obtain adequate results in this case the parameters of this relation should be determined based on material properties at high cycle fatigue. The procedure for the model identifying using the mechanical and fatigue characteristics of the material (yield strength, elastic modulus, Poisson's ratio, endurance limit, the basic number of cycles and the slope of Woehler diagram) is given in [17-19]. Comparison of the durability calculated by the model with experimental data for the cases of uniaxial and plane stress state demonstrated their satisfactory agreement [20, 21].

Characteristic of fatigue strength characterized by a large scattering, that is why in the settlement of the resource assessment it is necessary to evaluate its deviation from the mean. To solve this problem can be used a variety of approaches, such as the Monte Carlo method. In [22], a method that allows using this model of damage accumulation and takes into account the scattering of the endurance limit as a function of reliability is considered.

3. Conclusion

The proposed method was used to solve a number of practical problems. One of them is forecasting the durability and reliability of heavily loaded parts of tracked amphibious all-terrain vehicle TM-120. Road arm of this machine have enlarged cross overhang. To reduce the weight, they are in the form of thin-walled welded structures. These features dramatically increase their stress intensity. In this connection, field tests of TM-120 prototypes shoed frequent fatigue failures of the road arm in the region of its head. To avoid its failure the design of the road arm have been changed: there were introduced reinforcing strips, internal barriers and ribs.

To evaluate the effectiveness of these changes a comparative study of the durability of the original design and reinforced variation of the road arm have been carried out. Simulation of motion was carried out for the conditions of the standard test site. Estimation of fatigue life was carried out using the proposed model of damage accumulation.

Fig. 3 represents functions of failure-free operation of the initial and modified road arm. As a initial data the fatigue characteristics of steel 30KhGSA, having a coefficient of variation of endurance limit 0.1 were used. Analysis of the obtained results shows that gamma-lifetime $\gamma = 90\%$ of the new road arm design increased about 3 times. That is in satisfactory agreement with the test operation of the modernized tracked amphibious all-terrain vehicle.

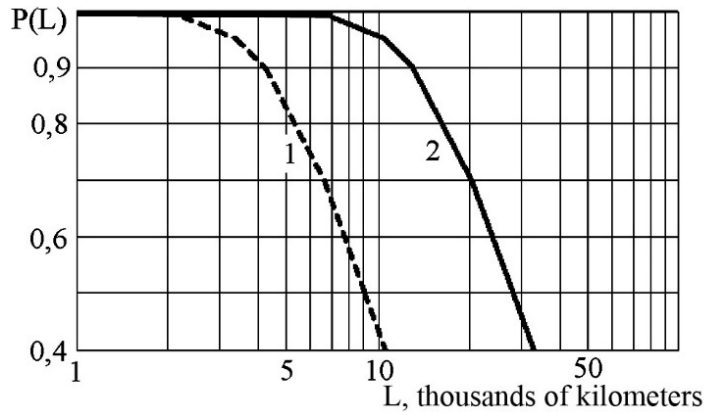


Fig.3. Functions of failure-free operation: 1- initial road arm, 2- modified road arm.

References

- [1] I.Ia. Berezin, A.A. Abyzov, Process modeling simulation of resource use at trial of mobile technology, Technique and technology of construction and operation of highways: Sb.nauch.tr. MADI (TU); UV MADI (TU). (2000) 56–74. (in Russian).
- [2] V.A. Savochkin, A.A. Dmitriev, Statistical vehicle dynamics and traction tracked vehicles, Mashinostroenie, Moscow, 1993. (In Russian).
- [3] A.A. Abyzov, I.Ia. Berezin, V.I. Byvaltsev, The use of simulation techniques to assess the endurance test of the resource elements of heavy-duty propulsion fast tracked vehicles Environmental Engineering in transport-road complex: Coll. scientific. tr. MADI (STU). (2002) 143–154. (in Russian).
- [4] V.P. Kogaev, Strength calculations for voltages variable in time, Mashinostroenie, Moscow, 1993. (in Russian).
- [5] G.S. Pisarenko, A.A. Lebedev, Deformation and strength of materials under complex stress state, Science Dumka, Kiev, 1976. (in Russian).
- [6] I.Ia. Berezin, The estimated longevity of details in unsteady complex stress state Tr. PRF. 139 (1974) 25–29 (in Russian).
- [7] V.G. Sergeev, I.Ia. Berezin, Calculation of the resource components operating in conditions of irregular loading and plane stress, Knowing machines. 4 (1980) 67–73. (in Russian).
- [8] I.Ia. Berezin, D.A. Gokhfeld, V.G. Sergeev, Prediction of durability and residual life of fatigue failure criteria, XI International Colloquium "mechanical fatigue". (1991) 27–40. (in Russian).
- [9] A.S. Gusev, V.V. Nikonov, S.S. Dmitrichenko I.M. Ilinich, On the calculation of the fatigue life under plane stress, Knowing machines. 2 (1979) 81–86. (in Russian).
- [10] A.S. Gusev, Fatigue resistance and survivability of structures under random loads, Mashinostroenie, Moscow, 1989. (in Russian).
- [11] D.A. Gokhfeld, O.S. Sadakov, Plasticity and creep under variable loadings, Mashinostroenie, Moscow, 1984. (in Russian).
- [12] D.A. Gokhfeld, K.M. Kononov, V.B. Poroshin, O.S. Sadakov, Coupled Mathematical Models for Cyclic Inelastic Deformation and Damage Accumulation Processes Trans. 10th Int. Conf. on Structural Mechanics in Reactor Technology. L (1989) 19–24.
- [13] A.A. Abyzov, O.S. Sadakov, Use of a structural model for the assessment of fatigue multiparameter random impact, Vestnik IuUrGU. Serii: Matematika. Fizika. Khimiia. 2 (2005) 73–79. (in Russian).
- [14] A.A. Abyzov, O.S. Sadakov, The effect of the first invariant of the stress on low-cycle fatigue, Vestnik IuUrGU. Serii: Matematika. Fizika. Khimiia. 2 (2005) 69–72. (in Russian).
- [15] A.A. Abyzov, O.S. Sadakov, N.O. Felk, Model accumulation of fatigue damage in the history of any stress, Identification and verification. Vestnik IuUrGU. Serii: Matematika. Fizika. Khimiia. 6 (2005) 72–76. (in Russian).
- [16] D.A. Gokhfeld, L.B. Getsov, K.M. Kononov, The mechanical properties of steels and alloys in unsteady loading, Directory, Ural Branch of Russian Academy of Sciences, Ekaterinburg, 1996. (in Russian).
- [17] A.A. Abyzov, I.Ia. Berezin, O.S. Sadakov, Calculation of the resource parts at random regardless multiparameter loading, Vestnik IuUrGU. Serii: Mashinostroenie. 11 (2006) 30–36. (in Russian).
- [18] A.A. Abyzov, I.Ia. Berezin, O.S. Sadakov, Application of the simulation test to the calculation of the resource undercarriage transport vehicles, Vestnik IuUrGU. Serii: Mashinostroenie. 11 (2006) 122–129. (in Russian).

- [19] A.A. Abyzov, Predicting the reliability of structures under random loading independent multi-parameter, Proceedings "Problems of Security". (2007) 62–64. (in Russian).
- [20] P.A. Pavlov, A.K. Malikbekov, Cycle fatigue of carbon steels in the plane stress, Message 1, Problems of strength. 1 (1986) 55–60. (in Russian).
- [21] P.A. Pavlov, A.K. Malikbekov, Cycle fatigue of carbon steels in the plane stress, Message 2, Problems of strength. 8 (1986) 41–45 (in Russian).
- [22] A.A. Abyzov, The estimated fatigue life of chassis components for random loading multiparameter, Actual problems of protection and safety. Proceedings of the 16th All-Russian scientific-practical conference, Armored machinery and armament, Saint Petersburg, NGOs Spetsmaterialy. 3 (2013) 189–195. (in Russian).



International Conference on Industrial Engineering

Modeling of operation processes and reliability assurance of engineering machines under the multivariable time-varying random loading

Berezin I.I., Halturin V.K., Abyzov A.A.*

South Ural State University, 76, Lenin Avenue, Chelyabinsk, 454080, Russian Federation

Abstract

The article describes the case of multivariable random loading, which occurs when the caterpillar suspension component acts as a set of loads of independent random processes. In the danger zone details of the changes in the components of the stress tensor are independent random processes. As an example of parts operating at such a loading the author discusses tracked vehicle road arm. Presently, there are no standard techniques for the estimation of fatigue life under random multivariable loading currently available. The article describes the method of estimating the fatigue life for this type of load, based on the calculation of microplastic deformation. It uses a structural model of the material, based on the description of the deformation diagram of dependence by Ramberg-Osgood. To identify the model of accumulation of damage conventional mechanical and fatigue characteristics of the material were used. Accounting for natural dispersion of fatigue characteristics allowed to get the result as a function of the probability of failure-free operation. The validity of the approach is confirmed by comparing the calculation results with the experimental data. The practical application of the technique is illustrated by the example of predicting the durability and reliability of heavily loaded parts of the high-speed caterpillar vehicle.

© 2015 The Authors. Published by Elsevier Ltd. This is an open access article under the CC BY-NC-ND license (<http://creativecommons.org/licenses/by-nc-nd/4.0/>).

Peer-review under responsibility of the organizing committee of the International Conference on Industrial Engineering (ICIE-2015)

Keywords: Multivariable loading; Random process; Microplastic deformation; Structural model of the environment; Fatigue failure;

* Corresponding author. Tel.: +7-351-267-92-61; fax: +7-351-267-93-06.
E-mail address: abyzovaa@susu.ac.ru

1. Introduction

The competitiveness of engineering products is largely determined by the level of scientific and technical support for design activities, in particular by means of introduction into engineering of calculation-experimental methods to ensure machines reliability in the early stages of design.

The approach to the problem is illustrated by research processes of operational loading and the formation of fatigue damage of industrial tractor carrier system, as a part of the bulldozer [1 – 6].

2. Methods

The first phase of methodology implementation includes an analysis of force and kinematic processes obtained during field test of machines in various conditions. Figure 1, a, b shows an oscillogram of random loading process of T-10M tractor body caused by rig and ground during work as a bulldozer, cultivator and movement. Processing of oscillograms allows to classify investigated processes and determine their spectral characteristics and statistical characteristics (Fig. 2, a, b).

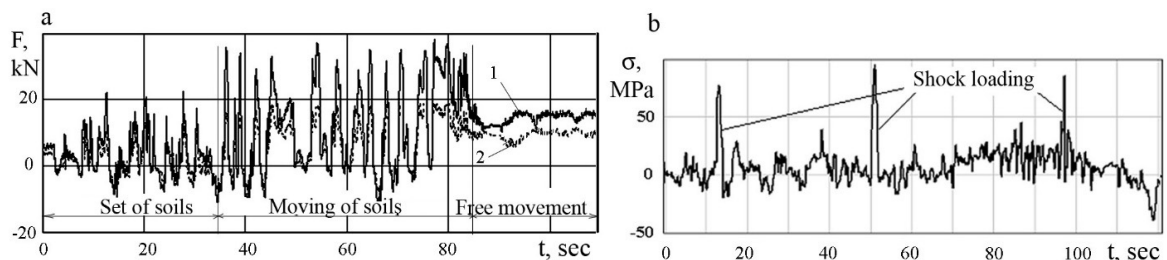


Fig.1. Experimental data: (a) the process of changing loads; (b) the process of changing stress.

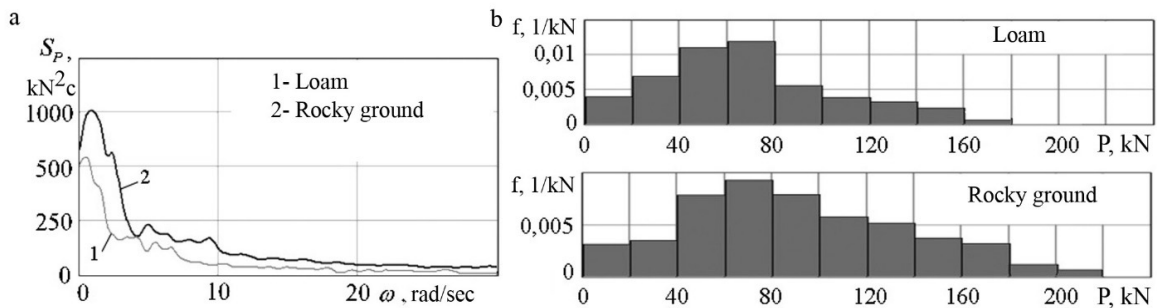


Fig.2. Statistical characteristics of loads: (a) the spectral density function, (b) the histogram peaks.

The field tests allowed to identify a number of special machine's operating modes and the corresponding mechanisms of interaction of its elements, such as:

1. Analysis of experimental data has revealed the cyclical load change during bulldozer work. This is due to technological process during which increasing amount of ground causes resistance and skidding increase and tractor's velocity drops. In order to prevent the tractor stop (extreme slippage) the driver needs lifting the blade every 5 ... 10 sec. The result is a cyclical loading, which becomes the main factor determining the fatigue life of parts and details of carrier system of the tractor.
2. Field tests have revealed the load mechanism of carriage system of the tractor as a random pulse stream (Fig. 1, b), due to semi-rigid suspension of industrial tractor in difficult conditions (working in a stone quarry, rolled back

at higher speeds, etc.), where as a result of suspension strikes there is a abrupt redistribution of forces between the frame and its parts. This is fundamentally changing scheme of machine parts interaction, in particular, the case of the steering clutch operates in a cyclical changing of restrained torsion, which stress is 3-5 times higher than the value of the operating stress [7].

The second phase of the approach includes modeling of work of bulldozer and loosening unit. Peculiarities identified during field tests, particularly of dynamic processes, should be included in mathematic model, in particular:

- the existence of two coupled effects, the first is power effect by operating element and kinematic by chassis system;
- the significant non-linearity of a semi-rigid suspension system of the industrial tractor due to the variability of its structure;
- account of cyclical workloads associated with the phenomenon of extreme slippage of the bulldozer and other.

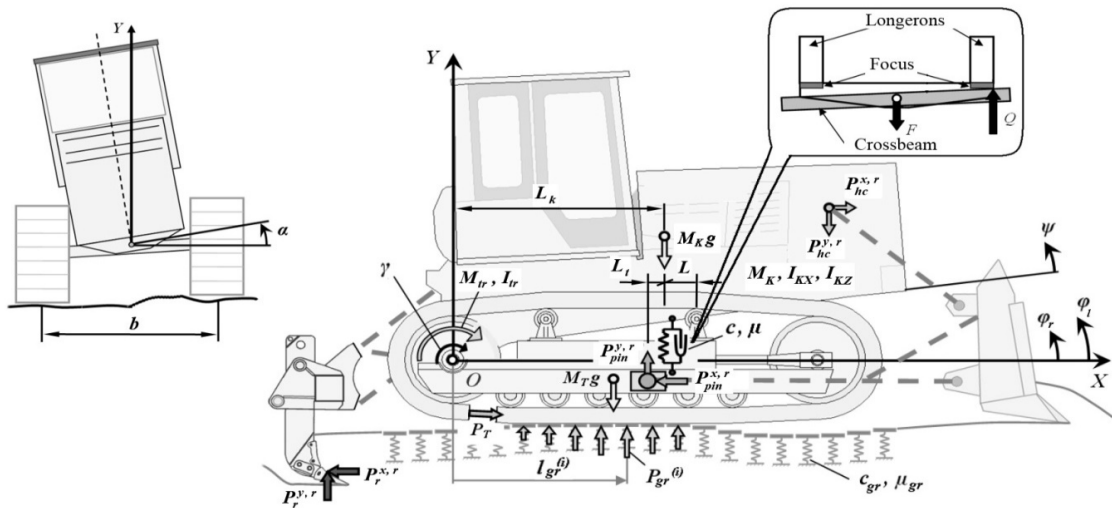


Fig.3. The diagram of a mathematical model.

Figure 3 shows a diagram of a mathematical model describing the dynamics of the tractor [8, 9]. The system of Lagrange differential equations for generalized coordinates $X, Y, \psi, \phi_l, \phi_r, \alpha, \gamma$:

$$\begin{aligned}
 (2M_T + M_K) \ddot{X} &= P_{hc}^{x,r}(t) + P_{hc}^{x,l}(t) - P_{pin}^{x,r}(t) - P_{pin}^{x,l}(t) + P_T \\
 M_T \left[2(\ddot{Y} + g) + 0,5L_T(\ddot{\phi}_l + \ddot{\phi}_r) \right] + M_K \left[\ddot{Y} + g + 0,5L_K \ddot{\psi} \right] &= \\
 = P_{pin}^{y,r}(t) + P_{pin}^{y,l}(t) - P_{hc}^{y,r}(t) - P_{hc}^{y,l}(t) + \sum_i P_{gr,r}^{(i)}(h) + \sum_i P_{gr,l}^{(i)}(h), \\
 0,5M_K L_K \left[\ddot{Y} + g + 0,5L_K \ddot{\psi} \right] + J_{K_z} \ddot{\psi} - cL^2 \left[a/L + 0,5(\phi_l + \phi_r) - \psi \right] - \mu L^2 \left[0,5(\phi_l + \phi_r) - \psi \right] &= \\
 = -\left(P_{hc}^{y,r}(t) + P_{hc}^{y,l}(t) \right) x_K - \left(P_{hc}^{x,r}(t) + P_{hc}^{x,l}(t) \right) y_K, \\
 0,5M_T L_T \left[\ddot{Y} + g + 0,5b\ddot{\alpha} + 0,5L_T \ddot{\phi}_l \right] + J_{T_z} \ddot{\phi}_l + 0,5cL^2 \left[a/L + 0,5(\phi_l + \phi_r) - \psi \right] + 0,5\mu L^2 \left[0,5(\phi_l + \phi_r) - \psi \right] &=
 \end{aligned}$$

$$\begin{aligned}
 &= P_{pin}^{y,l}(t)hx_T - P_{pin}^{x,l}(t)y_T + \sum_i P_{gr,l}^{(i)}(h)l_{gr}^{(i)}, \\
 &0,5M_T L_T [\ddot{Y} + g - 0,5b\ddot{\alpha} + 0,5L_T\ddot{\phi}_r] + J_{Tz}\ddot{\phi}_r + 0,5cL^2 [a/L + 0,5(\phi_l + \phi_r) - \psi] + 0,5\mu L^2 [0,5(\dot{\phi}_l + \dot{\phi}_r) - \dot{\psi}] = \\
 &= P_{pin}^{y,r}(t)x_T - P_{pin}^{x,r}(t)y_T + \sum_i P_{gr,r}^{(i)}(h)l_{gr}^{(i)}, \\
 &M_T b [0,25L_T(\ddot{\phi}_l - \ddot{\phi}_r) + 0,5b\ddot{\alpha}] + [J_{Kx} + 2J_{Tx}] \ddot{\alpha} = \\
 &= 0,5b \left(P_{hc}^{y,r} + P_{pin}^{y,l} + \sum_i P_{gr,l}^{(i)}(h) \right) - 0,5b \left(P_{hc}^{y,l} + P_{pin}^{y,r} + \sum_i P_{gr,r}^{(i)}(h) \right), \quad J_{pr}\ddot{\gamma} = M_{tr}i_{tr} - P_T r_{vk},
 \end{aligned}$$

where, a is the static deflection of the housing under the weight of the tractor, J_{Kx} , J_{Kz} is the moments of inertia of the structure of the tractor about its center of gravity, I_{Kx} , I_{Kz} is the moments of inertia track roller relative to its center of gravity, I_{pr} is given to the drive wheel moment of inertia of the rotating masses and progressively moving the tractor engine and transmission, x_k , y_k , x_b , y_l is the coordinates of the attachment points of the hydraulic cylinder and dozer blade.

The system of differential equations integrated numerically with the help of a specially developed computer program.

At the third stage there is transformation of random generalized coordinates into loads acting on specific details of the construction [10, 11]. These processes are used as a initial data for finite element modeling and implementation of random processes and components of the stress tensor changes in potentially dangerous areas of structures [12, 13, 14].

Consistency between the calculated and experimental results is illustrated by the example of research of strength of T-10M tractor body steering clutches. According to mass operation, a significant reduction in the reliability of the tractor was due to the formation of fatigue cracks in the upper sheet body, leading to its depressurization, stiffness reduce and wear increase of transmission parts. Mathematic model accounting significant nonlinearity properties of semi-rigid suspension of industrial tractor revealed stress peaks of significant magnitude and frequency of the suspension in the area of origin of fatigue cracks.

Figure 4 shows the finite element model and distribution of equivalent stresses on the surface of the upper plate body of steering clutches in moment of shock loading in the suspension. Figure 5 shows pieces process of moving a caterpillar tractor across short high obstacles (movement in the stone quarry on collapsible soil). Comparison of the oscillograms obtained in field tests (Fig. 5, a) with a results of computer simulation (Fig. 5, b) confirms the adequacy of proposed mathematic models and the possibility of its use for predicting fatigue life of heavy-duty components of the machines.

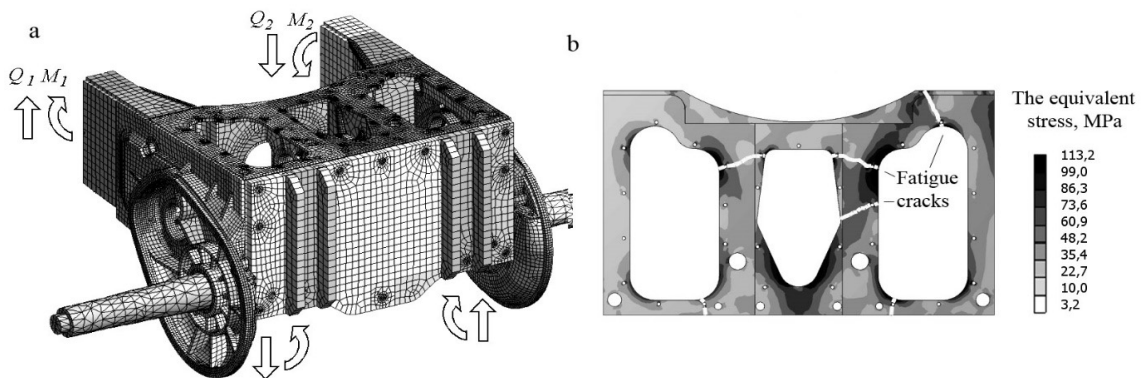


Fig.4. (a) the finite element model; (b) distribution of equivalent stresses.

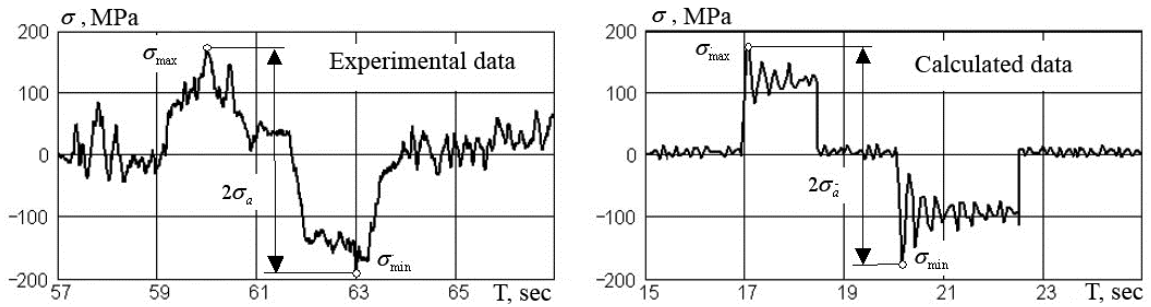


Fig.5. (a) the finite element model; (b) distribution of equivalent stresses.

The final stage involves predicting providing required service life for heavy duty elements of the carriage system according to the criterion of fatigue failure, for which the method of calculation of linear summation of damage was used [15, 9]. The calculation technique involves: account of changes of the components of the stress tensor with the help of complete cycles method [16, 17]; the calculation of equivalent amplitudes of stresses; determination of the law of distribution of equivalent amplitudes; parameter of loads input, and finally forecasting of the probability of failure-free function operation to the random nature of the loading and scattering of fatigue properties of materials [18, 19, 20]. The average predicted resource of the tractor steering clutches body provided by the proposed method is only 3100 hours (Fig. 6, a). This result agrees well with the data of the mass operation.

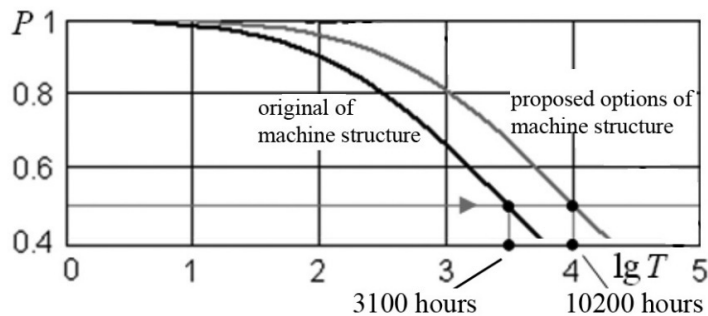


Fig.6. Functions of failure-free operation.

3. Conclusions

The effectiveness of the proposed approach is adjustment possibility of newly designed and modernized products, both at the stage of investigation of dynamic process, and at the stage of reasoned choice of materials and technology. For example, analysis of modeling results revealed that the increase the gap between the stops of equalizing beams and frame girders significantly reduces the magnitude and probability of stress peaks in the housing of steering clutches at the moment of impact in the suspension. Figure 6, a, b shows the function of failure-free operation for original and the proposed options of machine structure, which is predicting three-fold increase of average service life of steering clutches by the criterion of fatigue failure.

References

- [1] V.I. Balovnev, Modeling of the interaction with the environment of working road construction machinery, Mashinostroenie, Moscow, 1994 (in Russian).
- [2] G.M. Kutkov, Traction dynamics tractors, Mashinostroenie, Moscow, 1980 (in Russian).

- [3] U.V. Ginzburg, Industrial tractors, Mashinostroenie, Moscow, 1986 (in Russian).
- [4] I.B. Barsky, V.J. Anilovich, G.N. Kutkov, The dynamics of the tractor, Mashinostroenie, Moscow, 1973 (in Russian).
- [5] J.Y. Wong, Theory of ground vehicles, third ed., John Wiley & Sons, 2001.
- [6] M.G. Bekker, Theory of land locomotion, University of Michigan Press, 1956.
- [7] I.Ia. Berezin, V.I. Kostyuchenko, V.K. Halturin, Providing strength reliability of road construction equipment on the basis of modeling operating processes, Vestnik IuUrGU. Seriya: Mashinostroenie. 12(23-123) (2008) 32–40 (in Russian).
- [8] V.K. Halturin, Operational loading and modeling the dynamics of a caterpillar bulldozerno- loosening unit, Traktory i sel'khoz mashiny. 2 (2013) 16–19 (in Russian).
- [9] V.K. Halturin, Ensuring the reliability of the elements of the support system the Industrial tractor T-10M, Traktory i sel'khoz mashiny. 4 (2013) 42–45 (in Russian).
- [10] J.S. Bendat, A.G. Piersol, Random data analysis and Measurement Procedures, John Wiley & Sons. 1986.
- [11] K.C. Kapur, L.R. Lamberson, Reliability in engineering design, John Wiley & Sons, 1977.
- [12] S.S. Dmitrichenko, O.A. Rusanov, Experience of strength calculations, Designing, and finishing of welded metal mobile machines, Traktory i sel'khoz mashiny. 1 (2006) 8–13 (in Russian).
- [13] S.S. Dmitrichenko, Y.S. Borisov, O.A. Rusanov, Calculation of the strength of the frame with the rear axle of the industrial tractor, Traktory i sel'khoz mashiny. 7 (1999) 23–26 (in Russian).
- [14] O.A. Rusanov, Analysis of the structural strength machines with Num-represented methods, Traktory i sel'khoz mashiny. 2 (2002) 32–37 (in Russian).
- [15] V.V. Bolotin, Predicting resource of machines and structures, Mashinostroenie, Moscow, 1984 (in Russian).
- [16] V.T. Troshchenko, L.A. Sosnovsky, Fatigue resistance of metals and spla Islands, Reference Vol. 1, 2, Naku. Dumka, Kiev, 1987.
- [17] V.P. Kogaev, Strength calculations for stresses variable in time, Mashinostroenie, Moscow, 1993(in Russian).
- [18] V.A. Svetlitskiy, Statistical mechanics and the theory of reliability, Izd MSTU, Moscow, 2002 (in Russian).
- [19] A.S. Gusev, Probabilistic methods in mechanics of machines and structures, Izd MSTU, Moscow, 2000 (in Russian).
- [20] A.S. Gusev, V.A. Svetlitskiy, The calculation of structures when random actions, Mashinostroenie, Moscow, 1984 (in Russian).



International Conference on Industrial Engineering

Modernization of the turbocharger lubrication system of an internal combustion engine

Aleksey Plaksin^a, Alexander Gritsenko^b, Konstantin Glemba^{a,b,*}

^aSouth Ural state agrarian University, Chelyabinsk 454080, Russia

^bSouth Ural State University, 76, Lenin Avenue, Chelyabinsk, 454080, Russian Federation

Abstract

One of the most widespread methods to increase the power of internal-combustion engines (ICEs) is turbocharging. But turbochargers used for 70% of engines have a number of essential disadvantages: their low service reliability as up to 30% of engine failures are caused by turbochargers; their high price; their cost-demanding reconditioning caused by high labour inputs and considerable downtime periods of machine-tractor units; losses due to long downtime periods of machine-tractor units. ICE life reducing usual for those equipped with turbochargers is due to frequent high-temperature overloads abnormal for turbochargers. To reduce the thermal factor of turbocharger elements and the running-out durability can be possible when using a hydraulic accumulator and a braking device. Thus, a test bench is manufactured for examining the turbocharger with the proposed elements. As a result, we manage to avoid semidry and dry friction to extend the turbocharger life, with the rotor slowing time being reduced on average up to 30–35% as compared with the normal (load-free) rotor slowing time. Thus, a hydraulic accumulator combined with a braking device can reduce turbocharger failures up to 10–15%.

© 2015 The Authors. Published by Elsevier Ltd. This is an open access article under the CC BY-NC-ND license (<http://creativecommons.org/licenses/by-nc-nd/4.0/>).

Peer-review under responsibility of the organizing committee of the International Conference on Industrial Engineering (ICIE-2015)

Keywords: Internal combustion engine (ICE); turbocharging, turbocharger; hydraulic accumulator; braking device; engine life; running-out.

* Corresponding author. Tel.: +7-351-262-1347.
E-mail address: alexgrits13@mail.ru

1. Introduction

Experts and specialists consider a further increase in the reliability of turbochargers to be possible due to more advanced manufacturing technologies and design changes of turbochargers, namely: integrated correctors for fuel supply can cause a reliability increase up to 10–25 %; bearing assembly improvements – up to 15–20%; the modernization of the ICE lubrication system – up to 5-7%; the use of new structural materials – up to 10-13%; the heat removal improvement from the turbocharger case – up to 10–20%; the reduced vibration of the turbocharger elements – up to 2–5%; the reduced thermal factor of the turbocharger elements – up to 5–10%. According to practical application of engines equipped with turbochargers, the main indicator of their reliability is known to be the wear resistance factor of the bearing assembly. The most common failure of turbochargers is known to be the shaft (rotor) seizure [1–10].

Thus, we compared and analysed the factors that determine and affect the operational reliability of turbochargers, with the conclusions about the reasons causing their main failures (seizures) being formulated. They are the exceeded limit values of dynamic and thermal parameters when turbochargers operate in critical conditions leading to irregular processes in friction couples; the oil coking in the turbocharger oil distributing lines; the misalignments of the axes and the element openings of the turbine; the increase of the turbocharger oil consumption; the turbocharger case deformations reducing the clearances; the local overheating of parts when the ICE is stopped; the intensive wear of the turbocharger bearing caused by the lubricant lacking after the ICE stops; the insufficient supply of the lubricating oil (oil starvation) in turbochargers [1–25].

According to the research results the following tasks were set: to analyse the causes of reduced operational reliability of turbochargers; to develop the design of a test bench with a hydraulic accumulator and a braking device; to determine experimentally the relationship between the parameters of the turbocharger braking process and the back pressure. To improve the operational reliability of turbochargers it is necessary to lubricate and cool the bearings during the rotor slowing time and to limit it by a braking device. The thorough analysis of scientific papers, literature and design concepts makes it possible to hypothesize how to improve the operational reliability of engine turbochargers due to lubricating the bearings after the engine stops, with a hydraulic accumulator and a braking device to reduce the slowing time being used. Thus, the aim is to improve the operational reliability of turbochargers of motor-tractor engines by lubricating friction couples after the engine stops and reducing the slowing time with a braking device.

2. Methods

2.1 Theoretical research

The equation for the turbocharger rotor rotations can be generally written as [1, 4, 11, 24 and 25]:

$$J \frac{d\omega}{dt} = M_T - M_C - M_R \quad (1)$$

Where $J \times d\omega/dt$ is the inertia moment of the moving rotor masses, (N m); J is the rotor inertia moment about the axis, (kg m^2); $d\omega/dt$ is the rotor angular acceleration (negative acceleration), (rad/s^2); M_T is the turbine effective moment, (N m); M_C is the compressor-driving moment, (N m); M_R is the moment of mechanical resistance to the rotor rotations, (N m).

When the air isn't supplied to the turbine, M_C and M_T are equal to zero, the equation of the turbocharger rotor rotations when the rotor slows down can be written as:

$$J \frac{d\omega}{dt} = -M_{Slow} \quad (2)$$

Where M_{Slow} is the braking torque, (N m).

When braking the compressor operation mode can be determined graphically by the system characteristics combined with the complete compressor characteristics, i.e. the dependence of the total pressure P_T , the capacity N and the output efficiency (Fig. 1), with the intersection point being the compressor operating point and determines the pressure value and the compressor capacity.

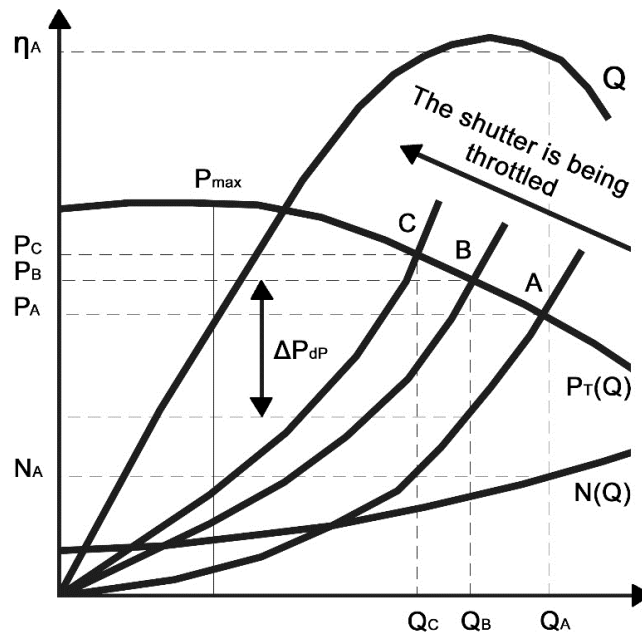


Fig. 1. The turbocharger head-capacity characteristic and the regulation lines.

When the shutter is open, the system head curve is flat, and the operation mode is determined by the point A. This point corresponds to the performance Q_A and the pressure P_A . Due to the obtained capacity we can find the capacity N_A and the efficiency η_A . When the shutter is closed, the resistance (the back pressure) increases, and the system head curve becomes more abrupt, with the operating point moving from the position A into the position B and then into the position C. These points define new parameters of the compressor operation, and thus of the entire turbocharger. Fig. 1 shows that the throttling mode is caused by a reduced compressor operation. The turbocharger shaft power due to throttling is reduced, and the rotor slows down quickly and smoothly. For example, the throttling up to the point B causes the reduced pressure on the throttle ΔP_{dp} [3].

2.2. Research methods

A new rational design is aimed at increasing the turbocharger operation reliability. The lubrication system of the ICE turbocharger comprises the main oil distributing line, with a pressure line to connect the main oil distributing line with the turbocharger bearing, a hydraulic accumulator, and a braking device, additionally installed and connected to the main oil line. There is also an electronic control unit necessary for the lubrication system. Between the air cleaner and the turbocharger impeller in the connecting pipe there are sensors for controlling the air flow and its temperature, they are also connected to the electronic control unit. Between the air pipe and the outlet pipe there is a bypass pipe in the direction of the turbocharger wheel. This bypass pipe is necessary for supplying the cooled air running out to the turbocharger turbine wheel. On the turbocharger main case there is an electromagnetic valve-injector connected to the hydraulic accumulator to supply oil running out to the turbocharger bearing when the engine is stopped. At the outlet of the turbocharger bearing there is an oil-temperature sensor connected to the electronic control unit.

The braking device is designed with two vane-type shutters connected to the main oil distributing line through the pressure line. The system operates in the following way. The electromagnetic valve-injector lets the oil move

into in the turbocharger bearing after the electronic control unit has signaled about the ICE stop, and the turbocharger operates in the rotor slowing down mode. The oil through the turbocharger bearings passes onto the output oil-temperature sensor mounted in a drain oil line. The output oil-temperature sensor send signals to the electronic control unit, which controls the lubricating oil flow for directing it to enter or bypass the oil cooler (due to the oil temperature). When the engine stops, the controlled valve injector opens because of the electronic sensors of the crankshaft position and the turbocharger revolutions, but continues to lubricate and to cool the turbocharger bearings. This device ensures avoiding heat strokes and, as a result, breakages of the turbocharger turbine components. The proposed technical device helps to avoid the oil coking in the turbocharger lubrication system pipelines in case of ICE sudden (emergency) stops when loaded at the turbocharger rotor slowing down mode. This method implies both adjustable (by volume, time and temperature) oil inlets into the turbocharger bearing, and regulated supplies of compressed air onto the turbine wheel input. As the supplied air has a temperature of about 100°C , it cools the turbine components down to $600\text{--}700^{\circ}\text{C}$, with the operating reliability of the bearings being increased as well as the integrity of the rotor, the case and the turbocharger as a whole being achieved [6].

3. Results

To confirm the theoretical background we researched the slowing time of TKR-11 turbochargers [4–8] at four different modes, with the experimental results being shown in Fig. 2 – the dependence of the rotating speed of the TKR turbocharger rotor on the slowing time.

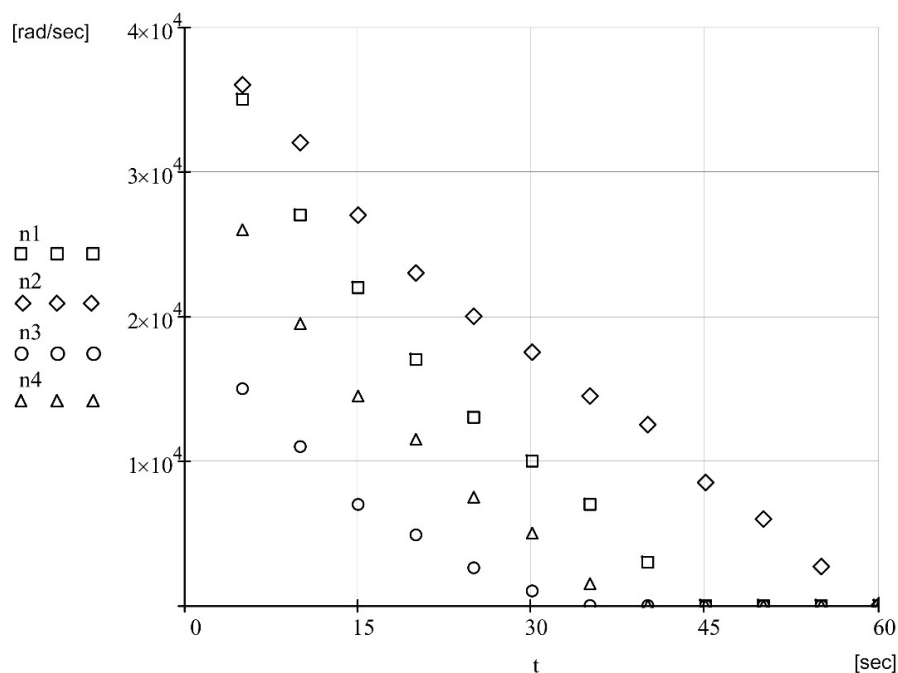


Fig. 2. The dependence of the rotating speed n_1 , n_2 , n_3 , n_4 [rad/sec] on the slowing time t [sec], where 1 is the normal rotor slowing; 2 is the rotor slowing with an operating accumulator; 3 is the rotor slowing with an operating braking device; 4 is the rotor slowing with an operating accumulator combined with a braking device.

To determine the normal rotor slowing down we calculated the first derivative of the TKR rotor rotating speed and obtained the dependence of the TKR rotor slowing down on its slowing time, Fig. 3.

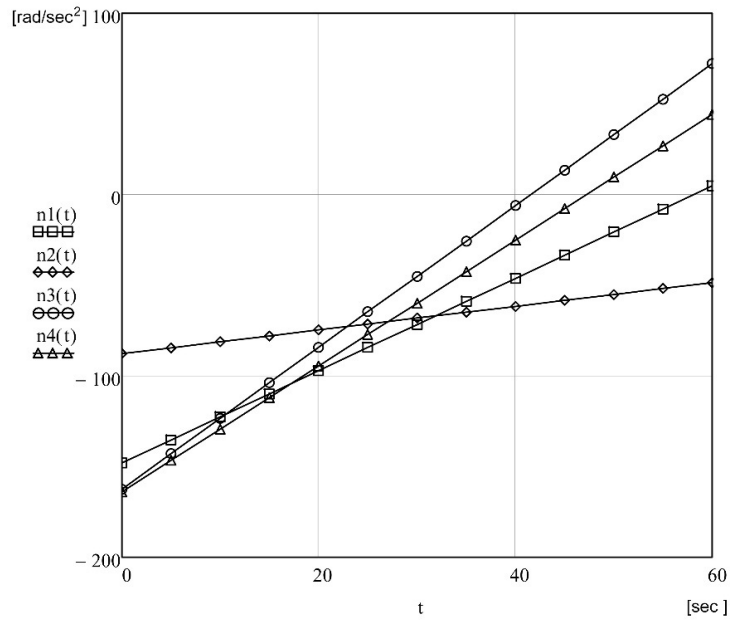


Fig. 3. The dependence of the rotor slowing down $n1(t)$, $n2(t)$, $n3(t)$, $n4(t)$ [rad/sec²] on the slowing time t [sec].

To determine the resistance moment to the TKR rotor rotation we multiplied the slowing values by the TKR rotor inertia moment. Thus, we obtained the dependence of the braking torque on the slowing time, Fig. 4.

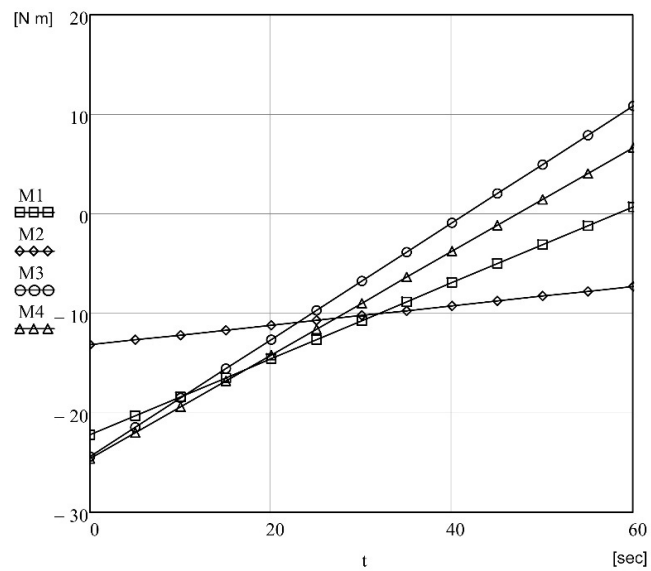


Fig. 4. The dependence of the braking torque $M1$, $M2$, $M3$, $M4$ [N m] on the slowing time t [sec].

4. Conclusion

Having analysed the data in Fig. 2, 3, 4, the following findings can be emphasized.

A hydraulic accumulator used in the lubrication system of the ICE turbocharger ensures the regular lubricating and cooling of the rotor bearings when the engine crankshaft rpm drop, as well as it stops in case of its overload at the rotor slowing down mode.

A braking device makes it possible to reduce the rotor slowing time for preventing oil starvation and dry friction of the rotor bearing.

The hydraulic accumulator combined with a braking device minimizes the risk of dry friction and emergency failures of the turbocharger. A hydraulic accumulator combined with a braking device are proved to reduce the turbocharger rotor slowing time on average up to 30–35% as compared with the normal (load-free) rotor slowing time (the 4th line in Fig. 2, 3, 4). This can reduce turbocharger failures up to 10–15% and downtime periods of machine-tractor units used in growing. The estimated economic effect is 50–80 thousand rubles per one season when operating units are used with various tractors.

References

- [1] A.M. Plaksin, A.V. Gritsenko, S.E. Bisenov, K.V. Glemba, K.I. Lukomsky, Diagnosing exhaust systems of internal combustion engines by monitoring the resistance of the exhaust pipe, *Fundamental research*. 8(2) (2014) 322–326.
- [2] A.M. Plaksin, A.V. Gritsenko, A.Yu. Burtsev, K.V. Glemba, K.I. Lukomsky, Extending the life of turbochargers automotive engineering application of the accumulator in the lubrication system, *Fundamental research*. 6(4) (2014) 728–732.
- [3] A.M. Plaksin, A.V. Gritsenko, A.Yu. Burtsev, K.V. Glemba, K.I. Lukomsky, Increasing the reliability of automotive turbocompressors when using accumulators, the *Bulletin of KrasGAU*. 8 (2014) 176–180.
- [4] A.V. Gritsenko, Development of methods for test diagnosing the performance of power systems and lubrication systems of internal combustion engines (experimental and industrial implementation exemplified by internal combustion engine of cars): Dr. Sci. (Eng.) Dissertation, Chelyabinsk, 2014.
- [5] A.M. Plaksin, A.V. Gritsenko, A.Yu. Burtsev, K.V. Glemba, A method of providing the operability of a diesel engine turbocompressor when using a autonomous lubricating-braking device, the *Bulletin of KrasGAU*. 6 (2015) 89–93.
- [6] A.M. Plaksin, A.V. Gritsenko, A.Yu. Burtsev, The results of experimental studies of the slowing time of the TCR-11 turbocompressor rotor, *AIC of Russia*. 70 (2014) 130–135.
- [7] A.V. Gritsenko, A.Yu. Burtsev, Technical and economic efficiency when introducing a modernized turbocompressor lubrication system. *AIC of Russia*. 72(2) (2015) 39–45.
- [8] A.Yu. Burtsev, A.M. Plaksin, A.V. Gritsenko, Operational reliability growth of tractor diesel turbochargers, *AIC of Russia*. 72(1) (2015) 23–25.
- [9] A.V. Gritsenko, A.M. Plaksin, A.Yu. Burtsev, Researching the running-out of the TCR-11 turbocompressor rotor, *Russian Agricultural and Food Policy*. 1 (2015) 52–55.
- [10] A.V. Gritsenko, A.M. Plaksin, I. Ganiev, A.Yu. Burtsev, F.A. Gafarov, The method and the bench for diagnosing the TCR-11 turbocompressor, *Vestnik of Tajik State Technical University by name of M.Osimi*. 4 (2014) 92–97.
- [11] A.V. Gritsenko, Diagnosing the crank mechanism bearings of an internal combustion engine according to pressure pulsations in the central oil pipeline: Cand. Sci. (Eng.) Dissertation. Chelyabinsk, 2009.
- [12] S.S. Kukov, A.V. Gritsenko, Diagnosing the lubrication systems of internal combustion engines, *Mechanization and Electrification of Agriculture*. 1 (2009) 33–34.
- [13] A.V. Gritsenko, Diagnosing internal combustion engines according to oil pressure, *Mechanization and Electrification of Agriculture*. 1 (2013) 22–24.
- [14] A.V. Gritsenko, K.V. Glemba, O.N. Larin, Diagnosing the main and connectingrod bearings of the crank mechanism, *Bulletin of the South Ural State University: Collection of scientific works*, South Ural State University Publishing House, Chelyabinsk. 4(1) (2014) 63–71.
- [15] A.V. Gritsenko, S.S. Kukov, K.V. Glemba, The methods of improving the accuracy when diagnosing crankshaft bearings, *AIC of Russia*. 57 (2010) 51–56.
- [16] V.K. Glemba, K.V. Glemba, Extending the life of sliding bearings of an internal engine crankshaft, *AIC of Russia*. 57 (2010) 34–35.
- [17] S.S. Kukov, A.V. Gritsenko, Diagnostics of the main bearings of the crank mechanism according to the central oil pipeline pressure, the *Bulletin of KrasGAU*. 3 (2009) 143–147.
- [18] S.S. Kukov, A.V. Gritsenko, Diagnostics of the main bearings of the crank mechanism according to the central oil pipeline pressure, *Mechanization and Electrification of Agriculture*. 3 (2009) 34–35.
- [19] A.G. Karpenko, K.V. Glemba, V.A. Belevitin, *Motor-car exploitation materials: textbook*, Chelyabinsk State Pedagogical University Publishing House, Chelyabinsk, 2014.
- [20] A.V. Gritsenko, Development of the means and methods of diagnosing by partial parallel redundant elements and by excluding unnecessary diagnostic operations and diagnostic parameters, the *Bulletin of KrasGAU*. 7 (2012) 120–125.
- [21] S.S. Kukov, A.V. Gritsenko, RF Patent 2,399,898. (2010)
- [22] V.K. Glemba, RF Patent 85,958. (2009)
- [23] D.Ya. Nosyrev, A.A. Svechnikov, Y.Y. Stanovova, Definition of the technical condition of a turbocharger and a driven centrifugal supercharger, *Vestnik Rostovskogo Gosudarstvennogo Universiteta Putey Soobshcheniya*. 3 (2010) 59–63.
- [24] A.F. Malahovetsky, Improving the reliability of automotive engine turbochargers by reducing their thermal factor: Cand. Sci. (Eng.) Dissertation. Saratov, 2005.
- [25] S.V. Potapov, Increasing the life of thoroughly reconditioned tractor diesel engines by using hydraulic accumulators in their lubrication systems: Cand. Sci. (Eng.) Dissertation. Chelyabinsk, 1999.



International Conference on Industrial Engineering

Development of scientific bases of the dynamics of machines as a section of applied mechanics

Dobrov I.V.*

National metallurgical academy of Ukraine, Gagarin Avenue, 4, Dnepropetrovsk, 49600, Ukraine

Abstract

The characteristic of the inertia forces within the classification of forces during solving the problems of the mechanics of machines was given. This characteristic is based on the simultaneous and unconditional compliance with the laws of Newton and the law of the energy conservation. It is proved that every potential field of motion of a physical body corresponds to a potential velocity field and the poles of these fields are located in the same point in space. For an absolutely rigid body moving with a variable velocity the inertia force is the internal potential force and potential of the inertia force is the velocity of the physical body.

© 2015 The Authors. Published by Elsevier Ltd. This is an open access article under the CC BY-NC-ND license

(<http://creativecommons.org/licenses/by-nc-nd/4.0/>).

Peer-review under responsibility of the organizing committee of the International Conference on Industrial Engineering (ICIE-2015)

Keywords: mechanics, applied mechanics, the mechanics of machines, classification of forces, the force of inertia.

1. Introduction

All variety of problems solved in mechanics¹ as a science “...the motion of the substance” [2] “... is based on a number of basic physical concepts such as time, space, simultaneity, mass, force” [2]. However, there are incorrect results from the point of view of classical mechanics in terms of non-compliance of the solution to the law of conservation of energy and one of Newton's laws when solving a number of problems of dynamics of machines by the methods of mathematical modeling [3-6]. This is primarily connected with the violation of the fundamental ideas during determining the various forces in mechanical systems taking into account the energy changes during mechanical work performing. Nowadays the question whether forces of inertia real or not is still actual [5-11].

* Corresponding author. Tel.: +38056-471501.

E-mail address: igordobrov@yahoo.com

Without force of inertia no analysis of the dynamics of modern high-speed machines is made. Moreover, there are a clear definition of the inertial force², methods of calculation and use for the determination of machines dynamics but the question whether forces of inertia real of not remains open [4-9,12].

2. The problem formulation

The paper proposes to consider a question about the forces of inertia in mechanics of machines, their definition and classification from the point of view of Applied Mechanics as a branch of the mechanics associated with the solution of engineering (practical) problems while moving and deforming the certain mechanical systems in a limited region of space for a certain period of time when using certain sources of mechanical energy with “non-living” source [13]. This point of view with the correct solution of problems of mechanics of machines (Applied Mechanics) [12] based on the fundamental principles of Classical Mechanics described in the three laws of Newton [3] concerning the law of conservation of energy [14,15] and based on the following conditions [13,16,17]:

- the force P^3 (fig. 1) can be balanced by another force only;

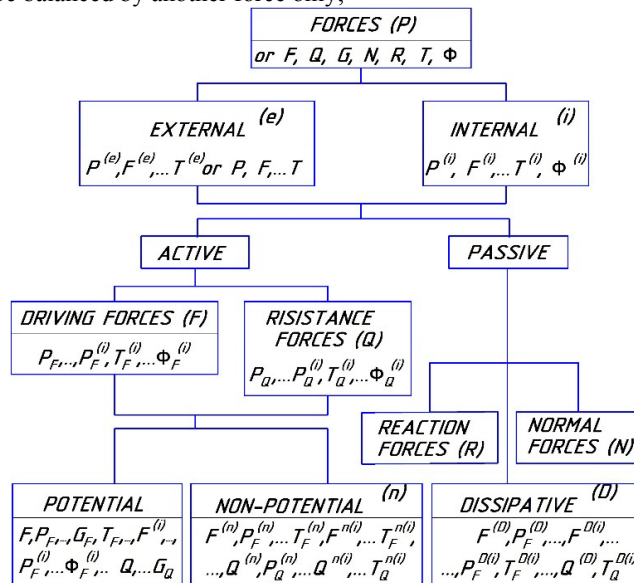


Fig. 1. Classification of forces in Applied Mechanics: $F=P_F$ - driving force, $Q=P_Q$ - resistance force; $G=P_G$ - gravitational force, $N=P_N$ - normal force, $R=P_R$ - reaction force, $\Phi=P_\Phi$ - force of inertia, $T=P_T$ - force of friction.

- the force can't be applied to the body⁴, if the body does not resist to this force;
- the force (P) can perform the mechanical work ($A_P=P s_P$) connected with displacement of the point of application (s_P) if the source of energy of force E_P can change its own mechanical energy ($\Delta E_P \neq 0$);
- change of the mechanical energy of the source of the force is the work produced by the force by moving the point of application of force respectively to that position which places its energy source;

¹ “Mechanics is an area of science about mechanical movement and mechanical interaction of physical bodies” [1].
² “Force of inertia is a force that equals to the product of the mass of a particle and its acceleration. This force is directed opposite to the acceleration” [1].
⁴ Here and hereinafter the term “body” (“part of a body”) is a physical object, the volume of it V_m ($\Delta V_m < V_m$) is finite and can be less than any certain small amount of space ΔV_n ($\Delta V_m < \Delta V_n \rightarrow 0$).

- to the body moving with the certain velocity can't be applied external driving force more than in the certain period of time provides the source of energy of that force during displacement of the point of application with velocity equal to the velocity of the movable body.

It is proposed [16,17] classification of forces (see fig. 1 and table 1) to solve the problems of mechanics of machines (Applied Mechanics). It is based on the normative terminology of [1,17] and the scientific literature [3-5, 13-15, 18-19].

Table 1. Characteristics of forces of Applied Mechanics.

Force (P) is vector quantity which is a measure of the mechanical action of one physical body on another.	
External force is a force acting on any physical body of mechanical system from the side which does not belong to this system. The source energy of external force located beyond the limits of the system of bodies.	Internal force is a force acting on any physical body (point of the body) of a mechanical system from the side of another physical bodies (body point) belonging to the considered mechanical system (the body). The source of energy of internal force is placed inside of this system of bodies.
Active forces perform mechanical work ($A_P \neq 0$) connected with displacement and (or) deformation of the body on which these forces act.	
Driving force (P_F or F , G_F , Φ_F , T_F) is a force the point of application of which to the movable body is moving in the direction of the line of action of force on the body ($A_F > 0$).	Resistance force (P_Q or Q , G_Q , Φ_Q , T_Q) is a force the point of application of which to the movable body is moving in the direction opposite to the direction of action of force on the body ($A_Q < 0$).
Potential force - is a force with fixed point of application ($s_p = s \neq 0$) respectively to the surface (volume) of this body ($v_m \neq 0$) and the direction of action of this force does not change. Non-potential force ($F^{(n)}$, $Q^{(n)}$) is a force the point of application of which to the movable body is moving respectively to the point of surface (volume) of this body ($s_p \neq s$, $s \neq 0$, $s_Q \neq s$) and (or) the direction of action of this force changes its position in space ($0 < A_F^{(n)} < A_F$, $0 > A_Q^{(n)} > A_Q$).	
Passive forces acting on body do not perform mechanical work ($A_P = 0$) that needs for displacement and (or) deformation of this body: Dissipative force ($P^{(D)}$) is a force acting on body in such a way that point of application of this force moves ($s_p \neq s = 0$) relatively to the surface (volume) of the fixed body on which it acts; reaction force (R) is a force acting on a fixed body and the point of application of which does not move ($s_p = s = 0$) respectively to the point of surface (volume) of this body; normal force (N) is a force acting on body in the direction perpendicular to the direction of motion of this body.	

3. Resolving the problem

The condition of linear motion with acceleration of the body m is defined by the Newton's second law⁵

$$P(t) \sim \Delta(m(t)v(t)) \quad (1)$$

For the absolutely rigid body $m(t) = \text{const}$ the equation (1) can be represented as

⁵ "Lex II: Mutationem motus proportionalem esse vi motrici impressae, et fieri secundum lineam rectam qua vis illa imprimitur". This was translated quite closely in Motte's 1729 translation as: "Law II: The alteration of motion is ever proportional to the motive force impress'd; and is made in the direction of the right line in which that force is impress'd". The author highlighted in bold the word of Newton which indicates that Newton's second law defines only a quality relationship between the change of the linear momentum and applied driving force.

$$P(t)k(t) = m\Delta v(t), \quad (2)$$

where $k(t)$ is a coefficient of proportionality which equals $k(t)=t$ [17-19] and represents the duration of action of the driving force in the direction of the line along which the linear momentum of the body m changes. If $t \rightarrow dt$ then $\Delta v(t) \rightarrow dv$ and equation (2) will look like this

$$P(t) = m \frac{dv(t)}{dt} = m \frac{d\dot{x}(t)}{dt} \quad (3)$$

Considering $\dot{x}(t) = \phi(\ddot{x}(t), t)$ from (3) must be

$$P(t) = m(\ddot{x}t + \ddot{x}) \quad (4)$$

Analysis of (4) shows:

$$P(t) = \begin{cases} m \cdot (\ddot{x}t + \ddot{x}) \neq const \Leftarrow (\ddot{x} \neq 0); \\ m\ddot{x} = const \Leftarrow (\ddot{x} = 0). \end{cases} \quad (5)$$

Non uniform linear motion of body m with constant acceleration ($\ddot{x} > 0$) or deceleration ($\ddot{x} < 0$) is possible at constant value and direction of the driving force P_F only. The equation (5) determined from the Newton's second law does not give the characteristics of the driving force⁶ and this requires additional analysis of the equation (5). In the work [18] at $\ddot{x} = const$ received an equation which in the mentioned above notation will be represented in the form

$$P = \pm m\ddot{x} \quad (6)$$

With the correct solution of problems of Applied Mechanics in the right side of equation (6) can be the force balancing the external force P only. If such an external force is absent then to balance the external force P in the equation (6) can be internal force of the body m only. In conditions of non uniform motion according to [1] such a force is the force of inertia

$$\pm m\ddot{x} = \mp \Phi \quad (7)$$

Let us investigate (fig. 2) the process of linear motion of body with mass $m = \rho V_m = \rho lhb$ (ρ - density, lhb - sizes of the body m) with width $b=l$ on the horizontal surface "without friction" (with rollers r) with acceleration $a_m = \ddot{x} > 0$ (fig. 2, a) while this body is driving by the external force $P_F = F$ applied to the body m at the point A on the surface of the body ($F_A = F_A^{(e)}$). Another case: the motion of the body with deceleration $a_m = \ddot{x} < 0$ (fig. 2, b) while this body is driving by the external resistance force $P_Q = Q^{(e)}$ applied to the body m at the point B ($Q^{(e)} = Q_B^{(e)}$). To characterize the parameters of the forces of the body m under the influence of external forces we will use a fixed coordinate system XOY which is connected directly (x_{EF}) or indirectly with fixed source of energy of external driving force $E_F^{(e)}$ (fig. 2, a) or resistance force $-E_Q^{(e)}$ (x_{EQ} on the fig. 2, b). To characterize the internal forces acting in the body m with length l we will use moveable coordinate system $X'O'Y'$ with axis $O'Y'$ that goes through the center mass of body m (in the middle of length l with $m(x') = m(x) = const$ parallel to the axis OY and axis $O'X'$ in the direction of

⁶ In Newton's second law is not indicated the characteristics of the driving force which can be either an external force or internal. The change of linear momentum of the body in the direction of line of action of the driving force can be either with a plus sign (movement with an acceleration) and with a minus sign (movement with a deceleration).

velocity v_m of motion of body m . The relationship between the coordinate systems is determined by the equation

$$x = x_{o'} \pm x' \tag{8}$$

where $x_{o'}$ – coordinate of centre of mass of the body m in the coordinate system XOY ; $x'=x_{o'}$ – coordinate of material point of the body (element of the body $dm=(m/l)dx$). This coordinate defines the position of dm in the coordinate system $X'O'Y'$ (fig. 2, a, b). It does not matter for the kinematics of the body (element of the body) whether it is an external force or a component of the internal force acting on the body (element of the body). If the vectors of these forces at any given period of time are equal (Newton's second law) from (8) and fig. 2, a must be

$$\vec{F}^{(e)} = \vec{F}_A^{(e)} = \vec{F}^{(e)}(x_A) = \vec{F}^{(i)}(x'_A) \tag{9}$$

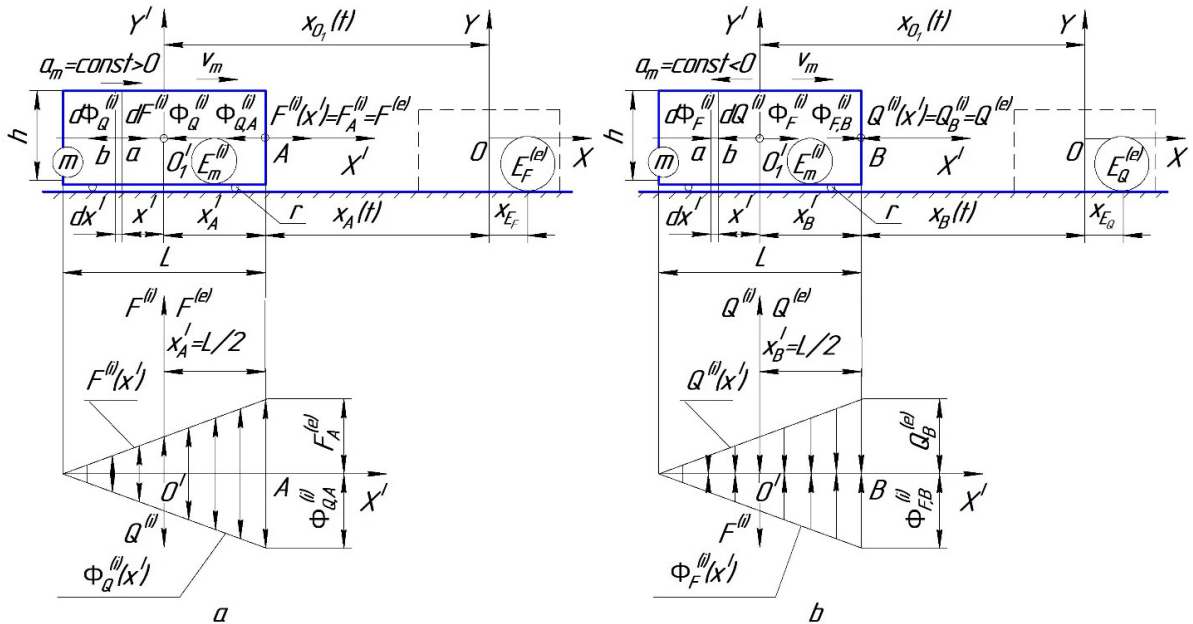


Fig. 2. (a): the scheme of action of forces at non uniform linear motion of the body m with constant acceleration; (b): the scheme of action of forces at non uniform linear motion of the body m constant deceleration

In its turn the influence of the internal driving force $F^{(i)}(x'_A)$ in accordance with Newton's third law⁷ will be balanced by the internal resistance force $\Phi_0^{(i)}(x'_A)$ [9]

$$\vec{F}^{(i)}(x'_A) = -\Phi_0^{(i)}(x'_A) = -\Phi_{Q,A}^{(i)} \tag{10}$$

To determine the law of distribution of the internal forces in the body m let us select (fig. 2, a) at a distance x' from center of mass of this body element dm . The forces $-\Phi_0^{(i)}=F^{(i)}(x')=F^{(e)}(x')$ and $F^{(e)}(x+dx)=F^{(i)}(x'+dx)=-$

⁷ “Lex III: Actioni contrariam semper et æqualem esse reactionem: sive corporum duorum actiones in se mutuo semper esse æquales et in partes contrarias dirigi”. This was translated quite closely in Motte's 1729 translation as: “Law III: The alteration of motion is ever proportional to the motive force impress'd; and is made in the direction of the right line in which that force is impress'd”.

$\Phi_0^{(i)}(x'+dx')$ (on fig. 2, *a* these forces are not shown) will act on the side surfaces of this element in points *b* and *a* accordingly to the equation (10). Consequently the condition of motion of element *dm* with uniform acceleration (fig. 2, *a*):

$$\begin{cases} d\bar{F}^{(i)}(x^l) = d\bar{F}^{(e)} = \text{const} > 0; \\ d\bar{\Phi}_Q^{(i)}(x^l) = -d\bar{F}^{(i)}(x^l) = \text{const} < 0. \end{cases} \quad (11)$$

From (11) taking into account the boundary conditions (9) we obtain (diagram of forces on the fig. 2, *a*)

$$\begin{cases} \bar{F}^{(i)}(x^l) = \frac{\bar{F}^{(e)}}{l} \left(\frac{l}{2} + x^l \right) > 0; \\ \bar{\Phi}_Q^{(i)}(x^l) = -\frac{\bar{\Phi}_Q^{(i)}}{l} x^l = -\bar{F}^{(i)}(x^l) < 0, \end{cases} \quad (12)$$

where $\bar{\Phi}_Q^{(i)} = -\bar{a}_m \int_{-0,5l}^{0,5l} \frac{m}{l} dx^l = -\bar{a}_m m$ force of inertia, internal resistance force of absolutely rigid body *m* while moving with constant acceleration respectively to the center of mass of this body in the coordinate system $X'O'Y'$:

$$x_\phi^l = \frac{\int_{-0,5l}^{0,5l} \Phi_Q^{(i)}(x^l) x^l dx^l}{\bar{\Phi}_Q^{(i)}} = 0 \quad (\text{fig. 2, } a).$$

The work of driving internal force during $t=\Delta t$ with the displacement $x_{\phi}^l(t) = \frac{\ddot{x}(\Delta t)^2}{2}$ of body *m* equals

$$A_F^{(e)}(\Delta t) = \int_0^{x_{\phi}^l(t)} \int_{-0,5l}^{0,5l} F^{(i)}(x^l) dx^l dx = F^{(e)} x_{\phi}^l(t) = A_F^{(e)}(\Delta t) \quad (13)$$

and it is provided by the change of work of the source of energy $E_F^{(e)}$ [2]

$$A_F^{(e)}(\Delta t) = -\Delta E_F^{(e)}. \quad (14)$$

In its turn the work of internal resistance force $\Phi_Q^{(i)}$ equals

$$A_{FQ}^{(i)}(\Delta t) = \int_0^{x_{\phi}^l} \int_{-0,5l}^{0,5l} F_Q^{(i)}(x^l) dx^l dx = -\frac{m(\Delta v_m)^2}{2} = -A_F^{(e)}(\Delta t) \quad (15)$$

and provides the change of the internal mechanical energy $E_m^{(i)}$ of the body *m*

$$A_{\Phi_Q}^{(i)}(\Delta t) = -\Delta E_m^{(i)} = \frac{m(\Delta v_m)^2}{2}. \quad (16)$$

This also based on the law of conservation of energy in the process of motion of the body *m* with constant acceleration.

$$\Delta E_F^{(e)} + \Delta E_m^{(i)} = 0. \quad (17)$$

It is easy to get an equation for the motion of element dm with constant deceleration (fig. 2, b):

$$\begin{cases} d\bar{Q}^{(i)}(x^l) = d\bar{Q}^{(e)} = \text{const} < 0; \\ d\bar{\Phi}_F^{(i)}(x^l) = -d\bar{Q}^{(i)}(x^l) = \text{const} > 0, \end{cases} \quad (18)$$

These equations (18) define the characteristics (diagram) of distribution of internal forces during motion of the body m with constant deceleration (fig. 2, b)

$$\begin{cases} \bar{\Phi}_F^{(i)}(x^l) = \frac{\bar{\Phi}_F}{l} \left(\frac{l}{2} + x^l \right) > 0, \\ \bar{Q}^{(i)}(x^l) = -\bar{\Phi}_F^{(i)} < 0 \end{cases} \quad (19)$$

and make it possible to get equations

$$\begin{cases} A_{\Phi_F}^{(i)}(\Delta t) = \frac{m(\Delta v_m)^2}{2} > 0; \\ A_{\Phi_Q}^{(i)}(\Delta t) = -A_{\Phi_F}^{(i)}(\Delta t) = -A_Q^{(e)} < 0, \end{cases} \quad (20)$$

which provide the law of conservation of energy during that kind of motion

$$A_{\Phi_F}^{(i)}(\Delta t) = -\Delta E_m^{(i)} = \Delta E_Q^{(e)} = -A_Q^{(e)}. \quad (21)$$

In accordance with [2] for potential force “the equation for elementary work must be the total differential of some scalar function...”. Taking into account that the kinetic energy of the body m is a scalar function we will receive:

$$d\left(\frac{m\dot{r}^2}{2}\right) = m\dot{r}d\dot{r} = m\ddot{r}dr = \begin{cases} \Phi_F^{(i)} dr = dA_{\Phi_F}^{(i)} > 0 \text{ npu } \ddot{r} < 0 \text{ и } dE_m^{(i)} < 0; \\ -\Phi_Q^{(i)} dr = -dA_{\Phi_Q}^{(i)} < 0 \text{ npu } \ddot{r} > 0 \text{ и } dE_m^{(i)} > 0, \end{cases} \quad (22)$$

where $r=r(x,y,z)$ - the radius vector defines the position of the body m (centre of gravity of the body) in the coordinate system $XOYZ$; $dA_{\Phi_F}^{(i)}$ and $dA_{\Phi_Q}^{(i)}$ - elementary works of the force of inertia during motion with constant deceleration and constant acceleration of the body m respectively; $dE_m^{(i)}$ - elementary change of internal (kinetic) energy of the body m in the process of motion with variable velocity.

From the equations (10)-(22) and table 1 it is received that the force of inertia of a rigid body is an internal potential force that resists the external force. This external force provides motion of the inertial mass body with variable velocity⁸. The source of energy of the force of inertia is kinetic energy. This kinetic energy is an internal energy of the moveable physical body and the potential of the force of inertia is a velocity⁹ of this body.

⁸ It should be noted that the force of inertia for plastically deformable body is not a potential force because the condition (22) is not fulfilled [20].

⁹ “Depending on velocity potential...was primarily used (and erroneously) by Weber W. in classical electrodynamics where postulated forces depending on velocity. German mathematician Schering E. was probably the first who seriously tried to use such a force in mechanics (see GÖtt. Abh. 18, 3,1873). For example, in the first edition Whittaker E.”Analytical dynamics” published in

To confirm this let us prove the Theorem.

If in any space there is the potential function $U(x,y,z)$ then in this space there is the potential function $V(\dot{x},\dot{y},\dot{z})$ and the pole of the force field $U(x,y,z)$ is a pole of the force field $V(\dot{x},\dot{y},\dot{z})$.

The proof of the Theorem.

If potential forces are acting on moveable body then according to the law of conservation of mechanical energy

$$E = \Pi + T = \text{const} , \quad (23)$$

where $\Pi = -U(x,y,z) = -U(r)$ - potential energy (Π) of force field $U(x,y,z) = U(r)$ interacting with the body with center of mass m located in the point of space $U(x,y,z)$ defined by the radius vector $r = \sqrt{x^2 + y^2 + z^2} \gg l$ (l - maximum linear size of the body) in the coordinate system $XOYZ$ with the centre O located in the pole of the force field $U(x,y,z)$; $T = \frac{mv^2}{2} = -V(m, \dot{x}(x), \dot{y}(y), \dot{z}(z)) = -V(m, \dot{r}(r))$ - kinetic energy of the body m in the coordinate system $XOYZ$:

The equation (23) can be represented:

$$E(x, y, z, \dot{x}, \dot{y}, \dot{z}) = U(x, y, z) + V(\dot{x}, \dot{y}, \dot{z}) = \text{const} . \quad (24)$$

Consequently

$$dE = \Delta U + \Delta V = 0 . \quad (25)$$

From (16,17), (20–22), (25) we will receive

$$dE = (P_x^{(e)} + \Phi_x)dx + (P_y^{(e)} + \Phi_y)dy + (P_z^{(e)} + \Phi_z)dz = 0 , \quad (26)$$

where $P_x^{(e)} = \frac{\partial U}{\partial x}$, $P_y^{(e)} = \frac{\partial U}{\partial y}$, $P_z^{(e)} = \frac{\partial U}{\partial z}$ - graphical projections onto a coordinate axes $XOYZ$ of the potential force $P^{(e)} = P^{(e)}(m,r) = \text{grad}U$; $\Phi_x = \frac{\partial V}{\partial \dot{x}}$, $\Phi_y = \frac{\partial V}{\partial \dot{y}}$, $\Phi_z = \frac{\partial V}{\partial \dot{z}}$ - graphical projections onto a coordinate axes $XOYZ$ of the force of inertia $\Phi = \Phi(m, \dot{r}(r)) = \text{grad}V$.

The equation (26) with $dx \neq 0$, $dy \neq 0$ and $dz \neq 0$ has a solution if $\text{grad}U = -\text{grad}V$.

Consequently fields $U(x,y,z)$ and $V(\dot{x},\dot{y},\dot{z})$ have the same pole. End of proof.

The Theorem gives us the idea that potential of the force $P^{(e)}$ is the position of the point of application of this force respectively to the pole of the force field $U(x,y,z)$ (source of energy of the force $P^{(e)}$) and the potential of the force of inertia $\Phi^{(i)}$ is a velocity of the body m respectively to the source of energy of external force acting on this body.

Let us consider an example. The body m in the form of a particle having an electric charge moves in an electrostatic field of the body $M \gg m$ (fig. 3).

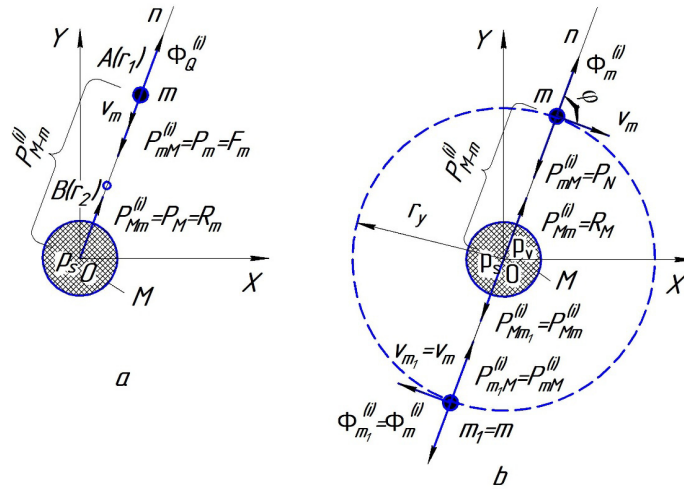


Fig. 3. (a): energy parameters of the body m without external resistance in the uniform potential field linear motion; (b) – energy parameters of the body m without external resistance in the uniform potential field uniform rotation

Without forces of resistance to motion of the body m in the uniform potential field of the body M this body can perform two kinds of movement (fig. 3, a and fig. 3, b).

- The linear motion of the body m with acceleration. This motion directed along the normal On to the center of mass of the body M located in the pole p_s of the linear force field at the intersection of the axes OX and OY (fig. 3, a). The internal force $P_{M-m}^{(i)}$ acts on these bodies. The components of this force are forces $\bar{P}_{Mm}^{(i)}$ and $\bar{P}_{mM}^{(i)} = -\bar{P}_{Mm}^{(i)}$ acting on the body M from the side of the body m and on the body m from the side of the body M respectively. It can be written $\bar{P}_{Mm}^{(i)} = \bar{P}_M$ and $\bar{P}_{mM}^{(i)} = \bar{P}_m^{(e)} = \bar{F}_m$ for each of these bodies accordingly to the mentioned above classification. In this case accelerations of the bodies M and m : $\bar{a}_M = \frac{\bar{P}_M}{M} \approx 0$; $\bar{P}_M = \bar{R}_M$; $\bar{a}_m = \frac{\bar{F}_m}{m}$; $\bar{\Phi}_Q^{(i)} = -\bar{a}_m m = -\bar{F}_m$. The force F_m performs the work $A_F = F_m(r_1 - r_2) > 0$ during motion of the body m from the point $A(r_1)$ to the point $B(r_2 < r_1)$. This work changes the potential energy of the body m . The change of this energy: $\Delta\Pi = F_m(r_2 - r_1) = -A_F$. At the same time at the motion of the body m with constant acceleration from the point $A(r_1)$ to the point $B(r_2 < r_1)$ the velocity of this body increases: $\Delta v_m = \sqrt{2a_m(r_1 - r_2)}$ and change of the kinetic energy of the body m : $\Delta T = \frac{m(\Delta v_m)^2}{2} = F_m(r_1 - r_2) > 0$. The characteristics of motion of the body m in the potential force field are provided by the following condition

$$\Delta E_p = F_m(r_2 - r_1) = A_F. \tag{27}$$

and up to the moment of the contact of the bodies M and m this condition corresponds with the law of conservation of energy (23). The mechanical energy or its part transforms from one form to another at the moment of interaction between bodies M and m but this question in the present article is not considered.

- Let us consider the motion of the body m (fig. 3, b) along the circumference of a circle which is the level of the potential field $U(r)$ with pole p_s and radius r_y . This motion at the same time is a motion with constant velocity

v_m along the circumference of a circle which is the level of the potential field $V(\dot{r})$ with pole p_v . The force of inertia $\Phi_m = m \frac{v_m^2}{r_y}$ acts on the body m . The angle between the force vector and the vector of velocity of the body is $\varphi = 0,5\pi$. The work of the force of inertia during period of time t : $A_\Phi = \Phi_m^{(i)} v_m t \cos \varphi = 0$. The same way the work of the force $P_{mM}^{(i)} = P_N$ balancing the force of inertia equals zero. In this case $\Delta E_p = 0$ and $\Delta T = 0$. Consequently $\Delta E = 0$ and the condition (27) is met irrespectively to the duration of motion of the body m in the potential field of the body M . In its turn the action of force $P_N = -\Phi_m^{(i)}$ defines the value of the force $P_{Mm}^{(i)} = -P_N$. It is necessary to balance the force $P_{Mm}^{(i)} = R_M$ by the force $R_{M1} = -R_M$ to provide a constant position of the center of mass of the body M in the coordinate system XOY . This constant position is achieved by the rotation of the body $m_1 = m$ along the circumference of a circle with radius r_y with constant velocity $v_{m_1} = v_m$ at diametrically opposite locations of these bodies.

Conclusion

- The force of inertia of absolutely rigid body relatively to this body is an internal potential force acting during change of kinetic energy of the body and balancing the resultant force of the external forces (external force) applied to the rigid body at the process of its motion with acceleration.
- Kinetic energy is an internal mechanical energy of the moveable body. This energy provides the work of forces of inertia while acting unbalanced external forces (external force) on this body. The potential of the force of inertia is the velocity of motion of the body at the current time.
- Each of the potential field of displacement of the physical body corresponds to the field of velocities. The poles of these fields are located in the same point of space and force functions of the fields have opposite signs.

References

- [1] Theoretical Mechanics. Terminology. Notation of quantities: the collection of recommended terms, Science, Moscow, 1984.
- [2] V.G. Nevzglyadov, Theoretical Mechanics, State edition of physical and mathematical literature, Moscow, 1959.
- [3] Isaac Newton, The Principia, Mathematical principles of natural philosophy, Printed for Benjamin Motte, London, 1729.
- [4] H. Goldstein, Classical Mechanics, second ed., Addison-Wesley, 1980.
- [5] A.G. Loytzyanskiy, A.I. Lur'ye, The course of theoretical mechanics, Dynamics, Science, Moscow, 1983.
- [6] S.E. Khaykin, The physical foundations of mechanics, Science, Moscow, 1971.
- [7] V.V. Dobronravov, The foundations of analytical mechanics, University press, Moscow, 1976.
- [8] A.Yu. Ishlinskiy, The classical mechanics and the forces of inertia, Science, Moscow, 1987.
- [9] L.V. Kirpichev, The lectures about the mechanics, The State Scientific and Technical Publishing House, Moscow, 1933.
- [10] L.I. Sedov, Lectures related to the basics of mechanics and physics, Knowledge, Moscow, 1983.
- [11] A.N. Bogolyubov, E.Ya. Antonyuk, S.A. Fedosova, Sergey Nikolaevich Kozhevnikov (1906–1988), edited by Bessonov A.P, Science, Moscow, 1998.
- [12] N.I. Kolchin, M.S. Movnin, The mechanism and machine theory, State Publishing House of Literature of shipbuilding, Leningrad, 1962.
- [13] I.V. Dobrov, The physical foundations of the processes of external friction at solving tasks of applied mechanics, Friction and Lubrication in Machines and Mechanisms. 7 (2007) 3–10.
- [14] M.V. Lomonosov, S.R. Mikulinskiy (chairman), Selected works, Academy of Sciences of the USSR, Institute of History of Science and Technology. 1 535.
- [15] Hermann von Helmholtz Über die Erhaltung der Kraft, Druck und Verlag von G. Reimer, Berlin, 1847.
- [16] L. Eüler. The foundations of dynamics of a point. The first chapters from «Mechanics» and from «Theory of movement of rigid bodies». Translation from Latin by V.S. Gokhman and S.P. Kondrat'yev, edited with foreword and notes by V.P. Egorshin, ONTI-NKTP-SSSR, Moscow, 1938.
- [17] The mechanism and machine theory. Terminology. Notation of quantities: the collection of recommended terms, Science, Moscow, 1984.
- [18] D'alamber Zh. Dinamika, Translation from French, Gostekhteorizdat, Moscow, 1950.
- [19] Joseph Louis Lagrange, Mécanique Analytique, fourth ed., Paris: Gauthier-Villars et fils, Translation from French by V.S. Gokhman, edited with notes by L.G. Loytzyanskiy and A.I. Lur'ye. Second edition, The State Scientific and Technical edition, Moscow, 1950.
- [20] I.V. Dobrov, The energy method of definition of the influence of the forces of inertia on the drawing conditions in the monolithic cone die, Mechanical eng: net electronic journal. 3 (2015) 32–39.



International Conference on Industrial Engineering

Diesel Engine operating cycle optimization with simulation of combustion process by double-Wiebe function

Kamaltdinov V.G.*, Lysov I.O., Nikiforov S.S.

South Ural State University, 76, Lenin Avenue, Chelyabinsk, 454080, Russian Federation

Abstract

The model and the program for analysis of the operating cycle with two fuel combustion laws according to Wiebe I.I. are developed. The calculation of the transport diesel engine with the Common-Rail system for gasoline direct injection is performed. The optimal heat generation law for the maximum pressure reduction in the cylinder and the improvement of indicator values of the diesel engine is specified.

© 2015 The Authors. Published by Elsevier Ltd. This is an open access article under the CC BY-NC-ND license (<http://creativecommons.org/licenses/by-nc-nd/4.0/>).

Peer-review under responsibility of the organizing committee of the International Conference on Industrial Engineering (ICIE-2015)

Keywords: diesel engine, calculation, operating cycle, indicator values, maximum combustion pressure, simulation, double-Wiebe function, combustion process, combustion type factor, initial period, main period, fuel rate

1. Introduction

The fuel combustion process in heavy transport diesel engines has two significant periods. It's most pronounced at the diesel engines with the Common-Rail system for gasoline direct injection. The existing mathematical models of the combustion process with one combustion law according to I.I. Wiebe [1,2] are in appreciable error in determination of the maximum heat generation rate in the initial period of the process. That's why in most cases the models with two combustion laws according to I.I. Wiebe are applied for modeling of the operating cycle of heavy transport diesel engines [3,4, etc.]. They enable one to indicate duration of significant periods and peculiarities of changing the heat generation rate in them. The known mathematical models yield different results during the

* Corresponding author. Tel.: +7-951-777-00-11; +7-967-863-40-18.
E-mail address: vkamaltdinov@yandex.ru

evaluation of the spent fuel rate in the initial and main periods of the combustion process. Thus, the need for introduction of a new parameter, namely a fuel rate, which takes part in the fuel combustion in the initial period, from the general cyclic fuel supply have become imminent. A new model and the program for calculation of the operating cycle with two fuel combustion laws according to I.I. Wiebe in transport diesel engines with the Common-Rail injection system has been developed at the Department of Internal-Combustion Engines of South Ural State University.

2. New model of the combustion process calculation in the diesel engine

The new mathematical model of the combustion process calculation in the transport diesel engines with the accumulator fuel delivery system is based on the following formula:

$$x = \Phi \times \left\{ 1 - \exp \left[-c \left(\frac{\varphi_{1p}}{\varphi_{z1p}} \right)^{m_{1p}+1} \right] \right\} + (1 - \Phi) \times \left\{ 1 - \exp \left[-c \left(\frac{\varphi_{2p}}{\varphi_{z2p}} \right)^{m_{2p}+1} \right] \right\}$$

where Φ is a fuel rate, which takes part in combustion in the initial period, from the general cyclic supply; φ_{1p} , φ_{2p} is angle of crankshaft rotation, the beginning of burning out in the initial and main periods; φ_{z1p} , φ_{z2p} is duration of the initial and main periods of the combustion process; m_{1p} , m_{2p} is indicators of the type of initial and main periods of the combustion process.

According to the form this mathematical model is similar to the combustion process model developed by N. Kojima [3]. But in the new model the start of the main period is not connected with the start of the fuel combustion in the initial phase. It enables one if necessary to simulate the start of heat generation in the main period earlier than in the initial one. It expands the opportunities to take into consideration special characteristics of the fuel injection, its distribution in the combustion chamber and its preparation for ignition in heavy diesel engines with the Common-Rail injection system.

The fuel burnup in each period is specified independently by its type indicators, the start and the duration of the combustion process, as well as by the fuel rate, which takes part in each period of the combustion. The change of these parameters enables one to simulate different combustion laws depending on the set restraints on parameters of the operating cycle. The total rate of the fuel combustion in the cylinder is determined by composition of combustion rates in the initial and main periods. If $\Phi=0$ or $\Phi=1$, the combustion rate has one maximum according to the combustion law of I.I. Wiebe. If the value of Φ lies in the range from 0 to 1, the combustion rate has two maximums, typical for the working process of modern transport diesel engines with the Common-Rail injection system (Fig. 1).

The calculation of diesel working cycle is produced step-by-step from the point 1 (the beginning of the step) to the point 2 (the end of the step) by well-known method [5]. Herewith, the following equation for definition of the pressure in the diesel cylinder on each step of the calculation is used [5]:

$$p_2 = \frac{\frac{2(\Delta Q_{comb} - \Delta Q_{well})}{m} + p_1 \left(v_1 \frac{k+1}{k-1} - v_2 \right)}{v_2 \frac{k+1}{k-1} - v_1}$$

where ΔQ_{comb} , ΔQ_{well} – fuel burn energy and heat transfer through the wells of cylinder head, piston and sleeve consequently; m – gas mass in the cylinder; p , v – pressure and specific volume of gas in cylinder; $k=C_p/C_v$ – the indicator of adiabat.

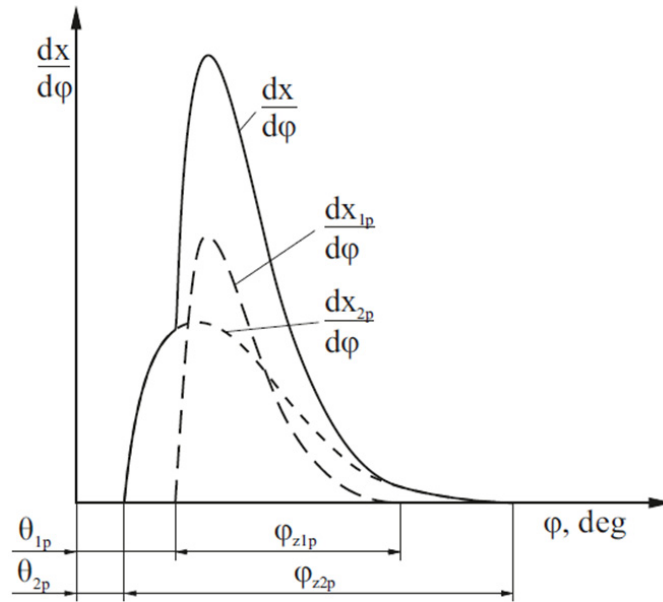


Fig. 1. Differential characteristic of fuel burn: θ_{1p} , θ_{2p} – angle of crankshaft rotation, the beginning of burning out in the initial and main periods; $dx/d\phi$, $dx_{1p}/d\phi$, $dx_{2p}/d\phi$ – the fuel burn speed is summarized, in the initial and main periods consequently

The fuel burn energy on the step of working cycle calculation (from the point 1 to the point 2) is defined by a well-known expression:

$$\Delta Q_{comb} = \Delta m_{comb} \cdot \xi \cdot H_u$$

where Δm_{comb} – fuel mass which has burned on the calculation step from the point 1 to the point 2; ξ – effective combustion ratio; H_u – the lowest fuel heat content.

Heat transfer through the wells of cylinder head, piston and sleeve is calculated according to the Newton-Richmann law:

$$\Delta Q_{well} = \frac{\alpha_1 F_1 (T_1 - T_w) \Delta \phi}{6n}$$

where α_1 – the coefficient of heat transfer from the working fuel to the wells; F_1 и T_w – square and the temperature of the cylinder volume surface at the beginning of the calculation step; T_1 – the gas temperature at the beginning of the calculation step; n – the rate of crankshaft rotation; $\Delta \phi$ – the angle of the crankshaft turn per calculation step.

The described mathematical model is taken as a basis of the methods and algorithm of “Working cycle calculation program of the “Double-Wiebe function” diesel” engineering software. With the help of this program the influence of F-value, indicators of combustion characteristics, the beginning and duration of the combustion process in the initial and main periods on the diesel engine working cycle indicators were defined.

There are results of diesel working cycle calculation with different fuel share values taking part in the combustion in the initial period are given on the Figure 2. The increase of this share from 0,1 to ~0,3 when the other parameters are unchangeable leads to essential improvement of the indicator values and essential increase of the maximum gas pressure in the diesel cylinder. The best indicator values are gotten when $\Phi=0,38$: average cycle indicator pressure $p_i=1,801$ MPa, fuel flow indicated density $g_i=177,7$ gramm/kilowatt-hour, indicated efficiency $\eta_i=0,4793$. The maximum pressure in the cylinder p_{max} equals to 18,1 MPa. The further increase of F till 0,45 leads to the degradation of indicator values and the growth of maximum pressure in cylinder p_{max} to 18,8 MPa.

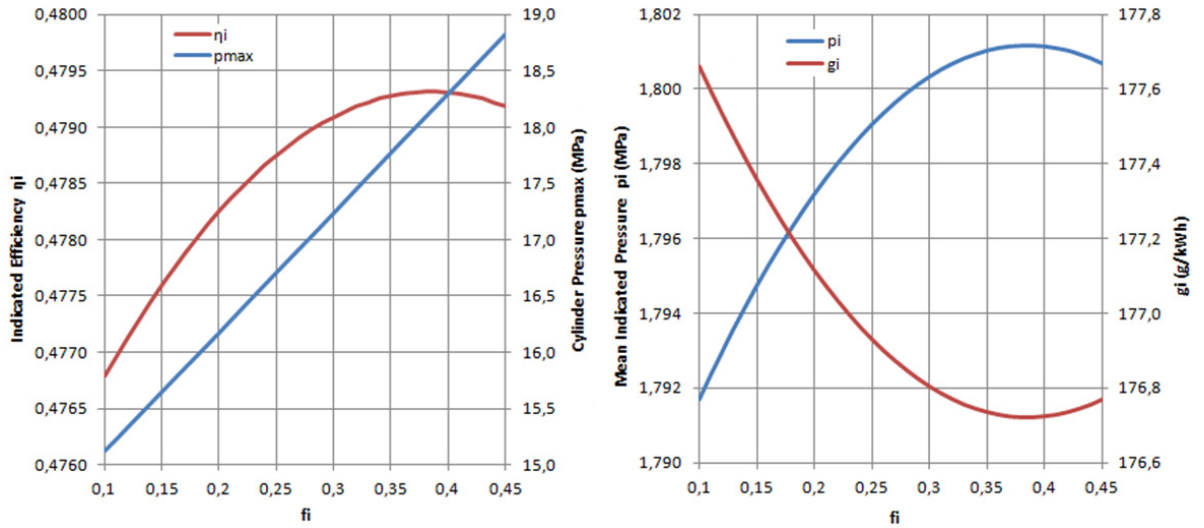


Fig. 2. Dependence of parameters p_{max} , η_i , p_i , g_i on fraction of fuel Φ (f_i)

Fig. 3 shows measurement charts of the in-cylinder pressure and heat release rate at different values of the proportion of fuel involved in combustion at the initial stage. Here it is seen that the larger the proportion of fuel is the higher the maximum heat release rate in the initial period and the smaller the maximum heat release rate in the main period are. This results in an increase of pressure rise rate and the increase of the maximum pressure in the cylinder.

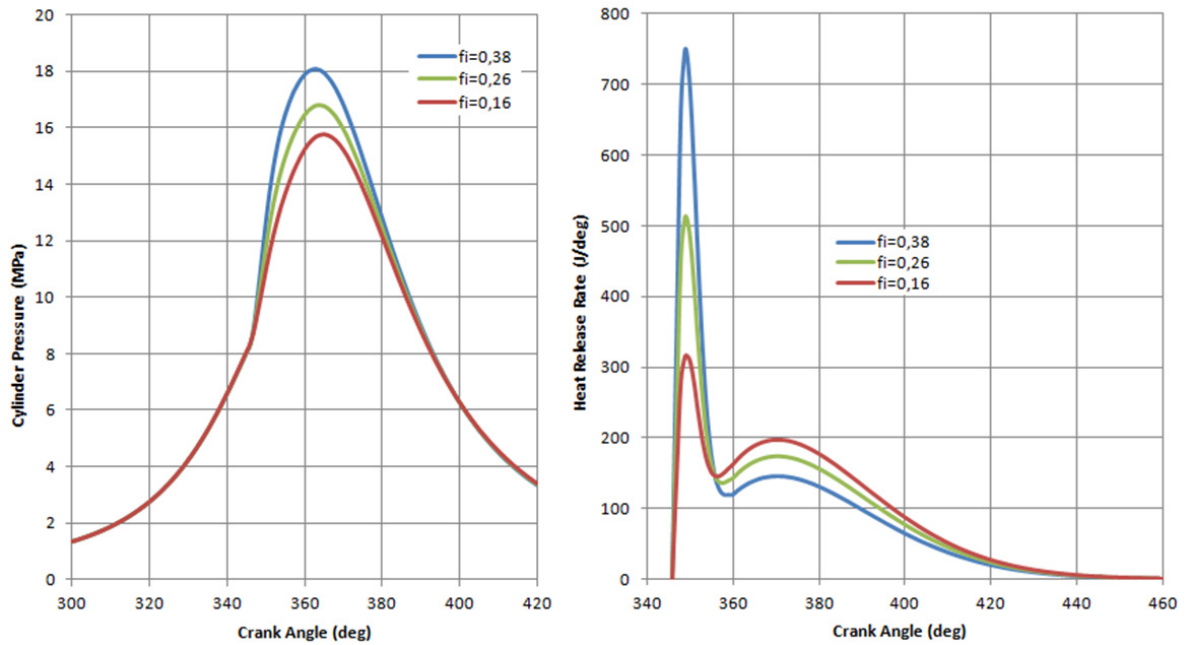


Fig. 3. Charts of pressure change P in the cylinder and heat release rate Q at different Φ (f_i)

Obviously in a real transport diesel with fuel-handling system fuel the fraction of fuel involved in combustion in the initial stage depends on pilot fuel injection. The greater the portion of the fuel in the pilot fuel injection is the greater the value of the fraction of fuel is Φ . Thus, the use of the developed program allows to plan the amount of fuel in the pilot fuel injection at the stage of design.

Fig. 4 shows the results of calculating the working cycle of a diesel at different rates of the combustion character in the initial m_1 and main m_2 periods. The increase of m_1 from 0,1 to 1,1 (while other parameters remain constant) leads to a slight improvement of indicator values and preservation of the same maximum gas pressure in the cylinder of a diesel. That means that the law of fuel combustion in the initial period does not affect the performance of a diesel. This is due to the short duration of the initial period of the combustion.

The increase of m_2 from 0,1 to 1,1 (while other parameters remain constant) leads to a significant deterioration of the indicator values (indicated coefficient of efficiency η_i and indicated mean pressure are reduced by $\sim 11\%$) and reduction of the maximum gas pressure in the cylinder of a diesel from 19,6 to 14,4 MPa (by $\sim 26.5\%$). That means that the law of fuel combustion in the main period significantly affects the performance of a diesel. This is due to the long duration of the main period of the combustion.

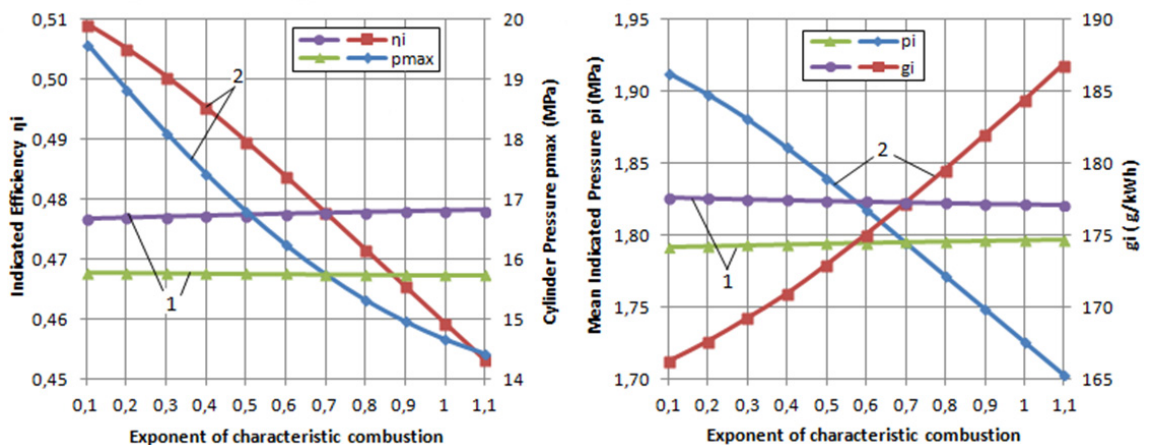


Fig. 4. Influence of values of combustion character m_1 (1) and m_2 (2) on parameters P_{max} , η_i , P_i , g_i

3. Conclusions

According to the results of the performed work the author makes the following conclusions:

1. The model and calculation program of the working cycle with two laws of combustion by Ivan Ivanovich Wiebe for transport diesel engines with the Common-Rail system of direct injection has been developed.
2. The novelty of the model of combustion process is the introduction of a new parameter – the fraction of fuel which is involved in the combustion of fuel in the initial period from the total cyclic delivery. The fact that the start of the main combustion period is not associated with the start of the combustion in the initial phase has also become an innovation in the field.
3. Best indicator values have been obtained when the fraction of fuel involved in combustion in the initial period has had the value of about 0,38.
4. The value of the indicator of the combustion character in the initial period almost has no effect on the indicator values of a diesel engine and the maximum pressure in the cylinder.
5. The value of the indicator of the combustion character in the main period significantly affects the indicator values of a diesel and the maximum pressure in the cylinder.
6. The given model of the combustion process allows to perform search engineering calculations for transport diesel engines with the accumulator fuel-handling system and to plan the value of a pilot fracture of fuel at the stage of design.

Acknowledgements

The given work is written with the support of the Federal Target Program “Research and Development in Priority Areas of the Development of Scientific and Technological Complex of Russia for 2014-2020”.

References

- [1] I. I. Wiebe, *Novoe o rabochem cikle dvigatelej*. [New on the Working Cycle of Engines]. Moscow, Mashgiz Publ., 1962. 272 p.
- [2] I.I. Wiebe, *Brennverlauf und Kreisprozess von Verbrennungsmotoren*, VEB Verlag Technik, Berlin, 1970.
- [3] T. Murayama, N. Kojima, Y. Satomi, A simulation of diesel engine combustion noise, SAE Technical Paper 760552 (1976) 16 p.
- [4] E. A. Lazarev, *Osnovnyie printsipy, metody i effektivnost sredstv sovershenstvovaniya protsessa sgoraniya topliva dlya povysheniya tehnikeskogo urovnya traktornyih dizeley: monografiya*. [Fundamentals Principles, Methods, and Effectiveness of the Means of Improvement of Combustion Process for the Raise of the Technological Level of Tractor Diesel Engines: Monograph]. Chelyabinsk: South Ural St. Univ. Publ. (2010) 288.
- [5] V. G. Kamaltdinov, *Utochnennaya metodika rascheta parametrov rabocheho tela na puskovyih rezhimah dizelya*. [Refined Methods of Calculation of Parameters of a Working Body on Starting Operating Mode of Diesel Engines]. *Dvigatelistroenie*. (2008) (232-2), 31–34.



International Conference on Industrial Engineering

Comparative analysis of "NGTU – Electro" electric car movement processes modeling in MATLAB Simulink and AVL Cruise software

Ilimbetov R.Yu. *, Popov V.V., Vozmilov A.G.

South Ural State University, 76, Lenin Avenue, Chelyabinsk, 454080, Russian Federation

Abstract

The article describes the factors of environmental pollution by road, the decision is supported by the Government of the Russian Federation. Presents the perspectives of the transition from the traditional internal combustion engine vehicles to electric vehicles and hybrid. It sets out the current state of the sales of light commercial vehicles in the Russian market. Possible perspectives of computer simulation in the automotive industry. The description of the programs MATLAB Simulink and AVL Cruise, used in electric motion simulation based on the Gazelle. Program allow you to make the technical characteristics of vehicles to choose driving cycle to make changes to existing designs components and assemblies, to simulate the process of driving. The comparative results of the simulation of electric vehicle Gazel test cycle, the intensity of acceleration, characterized by a mechanical-drive motor . The findings are explained, according to the results of the comparative simulation programs MATLAB Simulink and AVL Cruise.

© 2015 The Authors. Published by Elsevier Ltd. This is an open access article under the CC BY-NC-ND license (<http://creativecommons.org/licenses/by-nc-nd/4.0/>).

Peer-review under responsibility of the organizing committee of the International Conference on Industrial Engineering (ICIE-2015)

Keywords: environment, emissions, electric vehicle, modeling.

1. Introduction

In our country according to the Ministry of Natural Resources and Environmental Protection of the Russian Federation of 42% of pollution of the atmosphere it is the share of emissions of motor transport, and in the large cities (Moscow, St. Petersburg) to 80-90% [1].

* Corresponding author. Tel.: +7-968-111-9556; fax: +7-351-267-96-55.

E-mail address: ilimbay@yandex.ru

The order of the Government of the Russian Federation of 27.12.2010 No. 2446 - approved a state program "Energy saving and increase of power efficiency on transport by the period till 2020". According to this resolution, a share of cars with the hybrid power plant and electric cars among the sold new cars in the territory of the Russian Federation there have to be not less than 1,4% in 2012 (35 000 pieces a year) and by 2020 to increase to 4,6% (115 000 pieces a year) [2].

Since the end of the XX century the transition tendency from the traditional car with the internal combustion engine (ICE) to the hybrid car was outlined. It should be noted that broad use of hybrid cars essentially doesn't solve, and only softens a fuel consumption problem by individual vehicles and emissions of CO₂. Therefore such type of the power plant is considered as the temporary, intermediate stage on the way of creation and development of production of electric cars [3,4,5,6].

Now actively cars on hydrogen fuel, fuel elements, and also electric cars are developed and take root into mass production. According to data of researches of JSC MOESK for 2012 presented in figure 1 it is visible that the maximum number of emissions of CO₂ is the share of cars with DVS (more than 150 g / 100 to km) and the most minimum is the share of electric cars that is 70% less in comparison with petrol DVS [7,8,9].

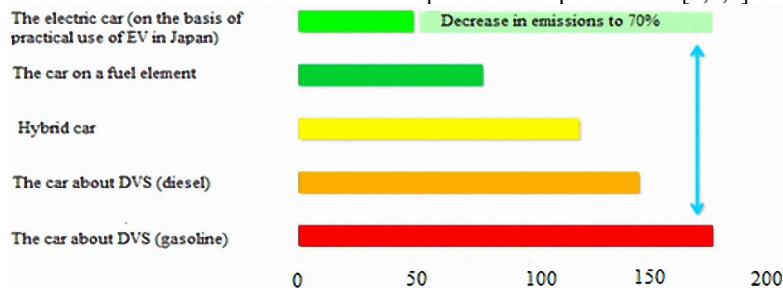


Fig1. – Emissions of CO₂ of of electrotransport and process of production of the electric car

Ecological indicators of electrotransport taking into account emissions of harmful substances in environment (according to MGTU of "MAMI") were reduced in table 1.

Table 1 - Comparison on indicators of emissions of the fulfilled gases of cars from DVS and the electric car[10]

Comparative figure	Electric car Mitsubishi 1-MIEV (13,5 kWph/100km)	Mitsubishi Colt 1,1 1 (55kW)	Chevrolet Spark 1 1 (50 kW)	Toyota Camry 3,5 1 (205 kW)
Emission CO ₂ , g/100km	9.06	20.2 (+22%)	16.9 (+28%)	37.5 (+23%)
Emission NO _x , g/100km	9.52	18.0 (+125%)	18.1 (+126%)	26.8 (+235%)
Emission CO, g/100km	0	182,2 (+81%)	182.4 (+82%)	253.1 (+153%)
Expenditure kgu.t./100km	4.65	19.5 (+87%)	19.8 (+87%)	36.7 (+87%)
Power consumption Wph/km	135	904.2 (+41%)	917 (+41%)	1705 (+41%)

The analysis of the table 1pokazyvayet that the electric car is on average 50% more blank and for 80% energoeffektivny than the analogs with an internal combustion engine.

Thus, the analysis shows that one of the actual directions of development of the motor transport is creation of electric cars which most as much as possible meet requirements of vehicles for settlements.

On release of easy commercial cars, Russia is one of world leaders. In figure 2 the chart characterizing a condition of the automobile market in Russia in 2011 is provided [11].

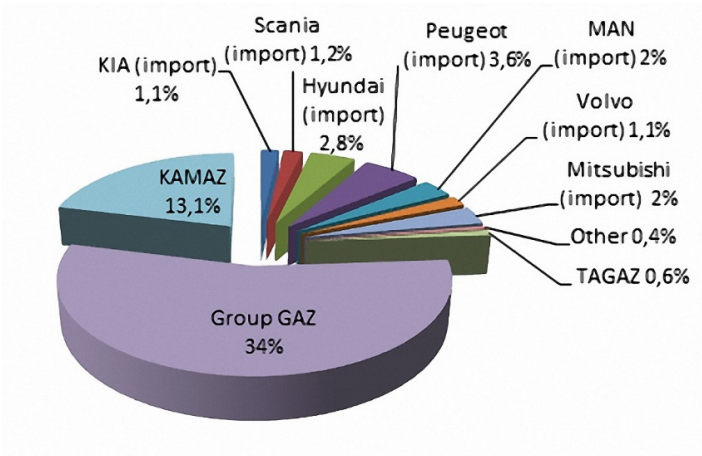


Fig. 2 – The market of commercial transport in Russia

According to this chart cars of the GAS brand occupies the leading position in the Russian market. The main cars released by GAZ Group, as we know, is the Gazelle models which following the results of 2007 more than 170 thousand cars of this brand were sold that made about 95% of realization of GAZ Group [12].

2. Review of programs

All Now at design of the motor transport computer modeling which allows "to glance" in the future of possible results of the designed mechanisms and machines is widely used. For design of modern cars, their knots and units the most suitable programs are: MATLAB Simulink and AVL Cruise [13,14].

The MATLAB Simulink software product with use of the SimPowerSystems module contains ready models of many components used in transformers, engines and libraries of specific models in figure 3.

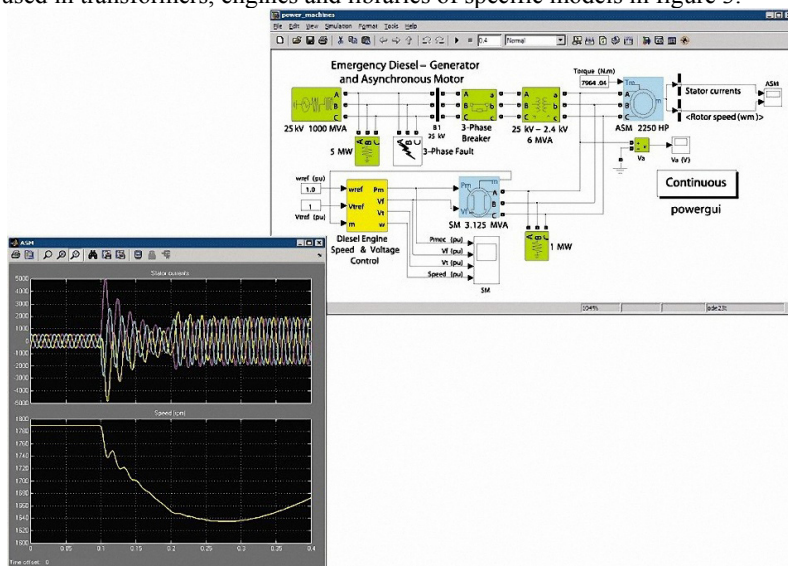


Fig. 3. SimPowerSystems module window

By means of this module of the program, perhaps to realize the following opportunities: modeling of electrical power systems; modeling of individual components; possibilities of simulation [15,16,17]. Thus it has the shortcomings such as: lack of separate modules of mechanical elements with the subsequent modeling in figure 4.

The program AVL complex is highly specialized, it is directed on the solution of tasks in the field of automotive industry. The complex is capable to count separately all knots and units of the car, their interaction and a control system. Has full library of knots of the car for modeling: automobile and trucks, buses, motorcycles, hybrid and electric cars [18,19,20].

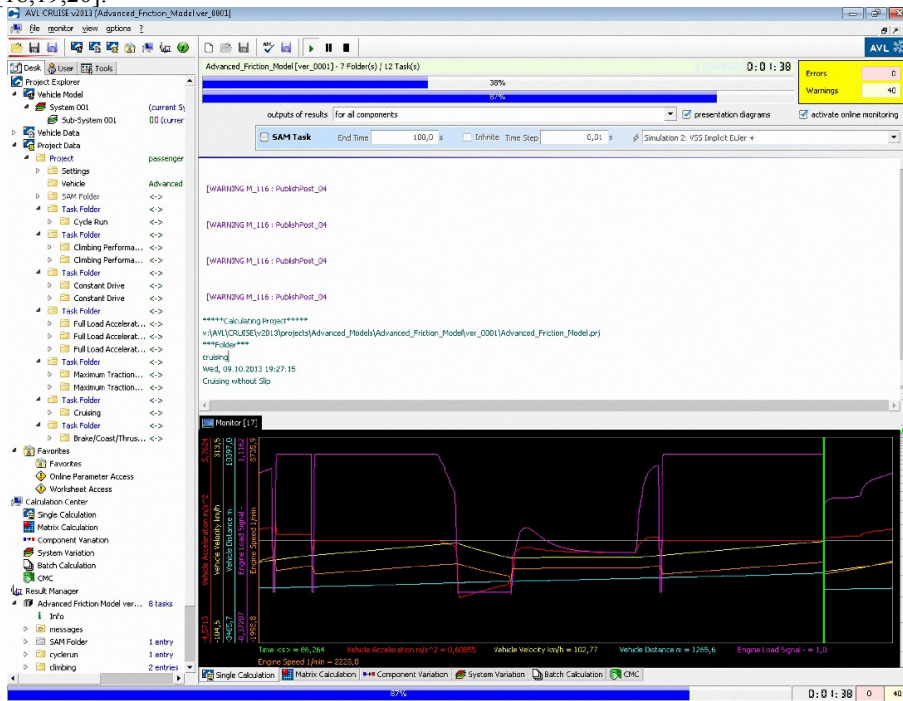


Fig. 4. A window of model of the 3-wheeled motorcycle in the AVL Cruise program

3. Results

For modeling and comparison of the received results in the MATLAB Simulink and AVL Cruise programs the electric car "NGTU-Elektro" on the basis of brand of the car the Gazelle was taken.

For an assessment of power expenses (power efficiency) of the electric car it is expedient to carry out modeling of the movement in city conditions of the cycle UDC for automobile and easy commercial cars with a full weight up to 3,5 t. figure 5[8,9,13].

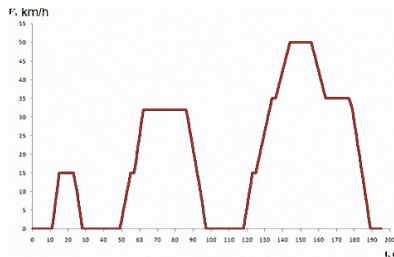


Fig. 5 – Schedule of the simple European city cycle Udcrisunok.

In figures 6-7 comparative results of imitating modeling of the movement of the car with the electric drive in the conditions of the city cycle UDC are shown.

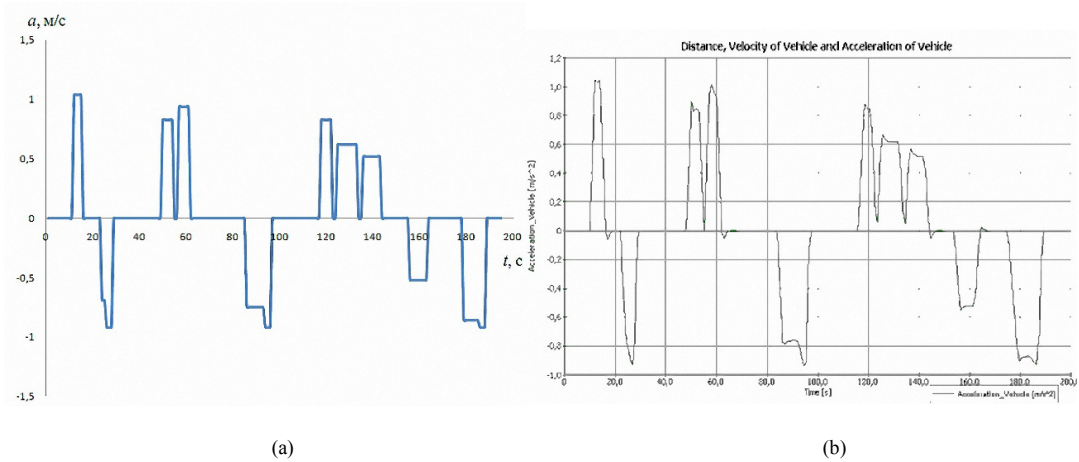


Fig. 6 (a) MATLAB Simulink; (b) AVL Cruise

From figure 7 it is visible that when modeling processes of the movement of the electric car intensity of dispersal and braking in the city cycle UDC coincide.

Power and torque on an electric motor shaft, necessary for the movement in a city cycle allows to estimate energy losses (figure 7, 8).

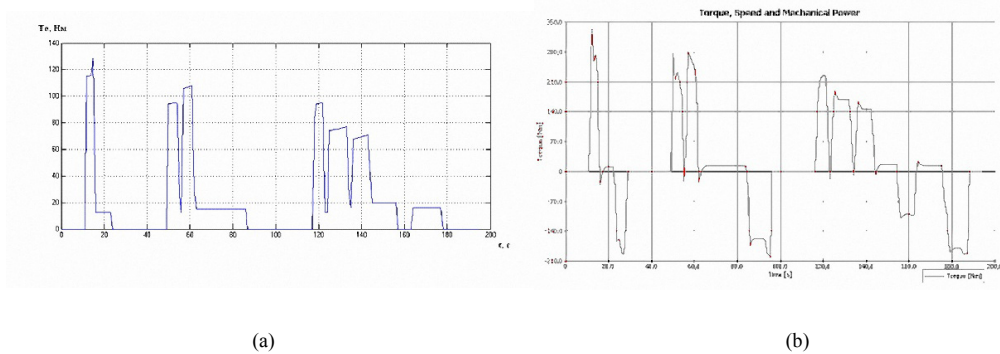


Fig. 7 (a) MATLAB Simulink; (b) AVL Cruise

In a torque curve form (figure 8), we observe coincidence of schedules of modeling, it is also visible that when modeling at the AVL Cruise program there is a negative size. It specifies that at reduction in the rate of the movement of the electric car a gazelle, the electric motor passes into the braking generator mode for charging of the high-voltage battery. However value of the moment on an electric motor shaft in the AVL Cruise and MATLAB Simulink program differ no more than for 50%. It is connected, first of all, with different methods of calculation and inertial masses in the presented programs of modeling.

Results of modeling of dependence of change of power on an electric motor shaft from time of the movement showed us that the received values of curves in the MATLAB Simulink and AVL Cruise programs, have full coincidence (figure 8).



Fig. 8 – (a) MATLAB Simulink; (b) AVL Cruise

In table 2 comparative results of modeling of the movement of the electric car on the basis of make of the car the Gazelle are presented in the MATLAB Simulink and AVL Cruise program.

Table 2 – Comparative results of modeling of the movement of the electric car in the MATLAB Simulink and AVL Cruise program

Technical parameters	Program MATLAB Simulink	AVLCruise Program
Full weight, kg	3500	3500
The mass of the chassis (including the driver), no more	2200	2200
Electric motor type	synchronous with permanent magnets	
Electric motor	UQM PowerPhase 200 SPM286-149-2	
Maximum (peak) power (engine / generator), kW	200	
Maximum (peak) torque, Nm	850	
Maximum frequency of rotation, rpm	5700	
Rated entrance voltage direct current, V	250...425	250
Tension of a direct current for ensuring the maximum power, V	360...425	360
Minimum working tension direct current, V	240	240
WinstonBattery battery	Lithium - iron-phosphatic	
Main transfe	Transfer number-5,125	
Tires	225/75R16 110R	
The received results of modeling		
Run on one charging in city traffic conditions at a full load of the electric car, km	145	145

Analyzing these tables 2 it is visible that at equal basic data of the electric car Gazelle, the MATLAB Simulink and AVL Cruise program in the course of computer modeling show similar results of the passable way the vehicle on one charging of the high-voltage battery.

Thus, computer modeling of the movement in city conditions (in the cycle UDC) the electric car Gazelle showed that the received results in the MATLAB Simulink and AVL Cruise programs have identical values on power on an electric motor shaft, and the main thing on the passable way on one charging of the high-voltage battery.

However there are also divergences in the course of modeling of a torque on a shaft of the traction electric motor (UQM Power Phase 200) with a difference no more than 50%. Is the main reason for it different techniques of mathematical calculation of empirical models of inertial mass of the vehicle.

authors are required to complete the Procedia exclusive license transfer agreement before the article can be published, which they can do online. This transfer agreement enables Elsevier to protect the copyrighted material for the authors, but does not relinquish the authors' proprietary rights. The copyright transfer covers the exclusive rights to reproduce and distribute the article, including reprints, photographic reproductions, microfilm or any other

reproductions of similar nature and translations. Authors are responsible for obtaining from the copyright holder, the permission to reproduce any figures for which copyright exists.

4. Conclusion

Any computer modeling as the mathematical tool allows to optimize process of programming of new technical ideas, including in mechanical engineering area. However comparing results of modeling of two computer MATLAB Simulink and AVL Cruise programs on the example of the electric car Gazelle, we observe that there are results, both full coincidence, and partial. That is, in the future we need to conduct comparative theoretical and practical researches for optimization of computer modeling.

References

- [1] I.E. Levitin, Transport and Environment: national approach, Transport of the Russian Federation. 2011. № 6 (37). S. 4-5.
- [2] The guarantor "of information - legal portal» - URL: <http://www.garant.ru/products/ipo/prime/doc/55070341/> (23.09.2015).
- [3] R.Yu. Ilimbetov, E.V. Solomin, A.M. Astapenko, A.V. Bakanov, Use of electro-mechanical transmissions in commercial vehicles in order to improve environmental performance, International Journal of Alternative Energy and Ecology. 2013. № 5-1 (125). S. 88-93.
- [4] L.A. Kukarskikh, The impact of motor transport on the environment and the state of public health, Herald of the Voronezh State Technical University. 2008. V. 4. № 4. C. 56-60.
- [5] Shenghui C. The development and future outlook of HEV, Mechanics of machines, tools and materials. 2008. № 2 (3). S. 42-47.
- [6] V.A. Rakov, Evaluation of the global car fleet of hybrid cars, Motor Company. 2012. № 8. C. 27-30
- [7] State contract № 14.740.11.0403 on 20.09.2010 under the Federal Program "Scientific and scientific-pedagogical personnel of innovative Russia" for 2009-2013. Report on the scientific - research work on the theme: the creation of environmentally friendly urban gear with electric promising sources and energy storage code "2010-1.1-217-140-012."
- [8] K. Hamada, Evolution of Hybrid Vehicle Electric System and its Support Technologies, Toyota Motor Corporation. APEC 2007. System Design. Feb 2007.
- [9] S. Sysoev, Fuel economy, efficiency, environment - attributes of new vehicles, engines and systems, Components and technologies. 2009. № 95. C. 29-36.
- [10] "MOESK" debunks myths about electric vehicles - URL: <http://gisee.ru/articles/experience/38678/> (22.09.2015).
- [11] A.A. Khilus, Current state and prospects of development of the Russian automotive market, Russian Foreign Economic Herald. 2015. T. 2015. № 6. S. 100-111.
- [12] The Group "GAS": diversified automaker URL: - http://data.investfunds.ru/stocks_comments/3689/2008-03-13_GAZ.pdf (23.09.2015).
- [13] R.Yu. Ilimbetov, V.V. Dernov, Computer modeling of electromechanical transmission truck Ural – 4320, Science SUSU: mater.66 th Scientific. Conf. Section of Technical Sciences in 2 volumes. Chelyabinsk: SUSU izd.tsentr, 2014. pp 241-247.
- [14] R.Yu. Ilimbetov, V.V. Popov, A.V. Bakanov, I.V. Kirpichnikov, Computer simulation of the motion of a car with serial combine power plant, ChGAA bulletin. 2014. Vol 70. pp 71-77.
- [15] Description of the MATLAB Simulink module SimPowerSystems URL: - <http://matlab.ru/products/simpowersystems> (23.09.2015).
- [16] Sim Power Systems URL: - http://matlab.ru/products/simpowersystems/simpowersystems_rus.pdf (23.09.2015).
- [17] Electrical Power Systems Simulation URL: - <http://www.mathworks.com/products/simpower/> (23.09.2015).
- [18] AVL CRUISE 2014.0 URL: - <http://rutracker.org/forum/viewtopic.php?T=4867044> (09/23/2015)
- [19] Software for simulation of powertrains: Know-how AVL to increase the share of research in the early stages of design - URL: - http://www.aps-c.ru/publications/AVL_simulation_technologies_with_FM.pdf (23.09.2015).
- [20] AVL CRUISE 2013 URL: - http://ebookeye.org/AVL-CRUISE-2013-Build-1100-32bit-64bit_2343378.html (23.09.2015).



International Conference on Industrial Engineering

The usage of 156 mm diameter continuous cast billets on “140” pipe-rolling plant for pipe production

Sherkunov V., Korsakov A.*

South Ural State University, 76, Lenin Avenue, Chelyabinsk, 454080, Russian Federation

Abstract

The research on the possibility of unification of piercing and reeling mills rolls for screw rolling for both decreasing and increasing the diameter of crude pipes was conducted. In the result the possibility was confirmed. The technology of wide range of sizes “140” pipe-rolling plant 156 mm diameter continuous casting pipe production was developed to use one roll design on piercing mill and one roll design on reeling mill instead of two roll designs for each therefore decreasing the amount of sizing mills grooves.

© 2015 Published by Elsevier Ltd. This is an open access article under the CC BY-NC-ND license (<http://creativecommons.org/licenses/by-nc-nd/4.0/>).

Peer-review under responsibility of the organizing committee of the International Conference on Industrial Engineering (ICIE-2015)

Keywords: continuous cast billet, piercing, reeling, rolls, point, diameter decreasing, diameter increasing, unification of mills.

1. Introduction

Due to the change of usage continuous cast billets for seamless pipe production the problem of 89-121mm diameter on “140” pipe-rolling plant pipe production from 156 mm diameter continuous casting occurred.

The main problem is that existing 120 mm and less diameter pipe production technologies use under 150 mm and less diameter continuous cast and rolled billet.

2. Some time ago

In order to solve this problem a new prospective technology was developed. This technology allows gradual

* Corresponding author.

E-mail address: bkorsakov174@gmail.com

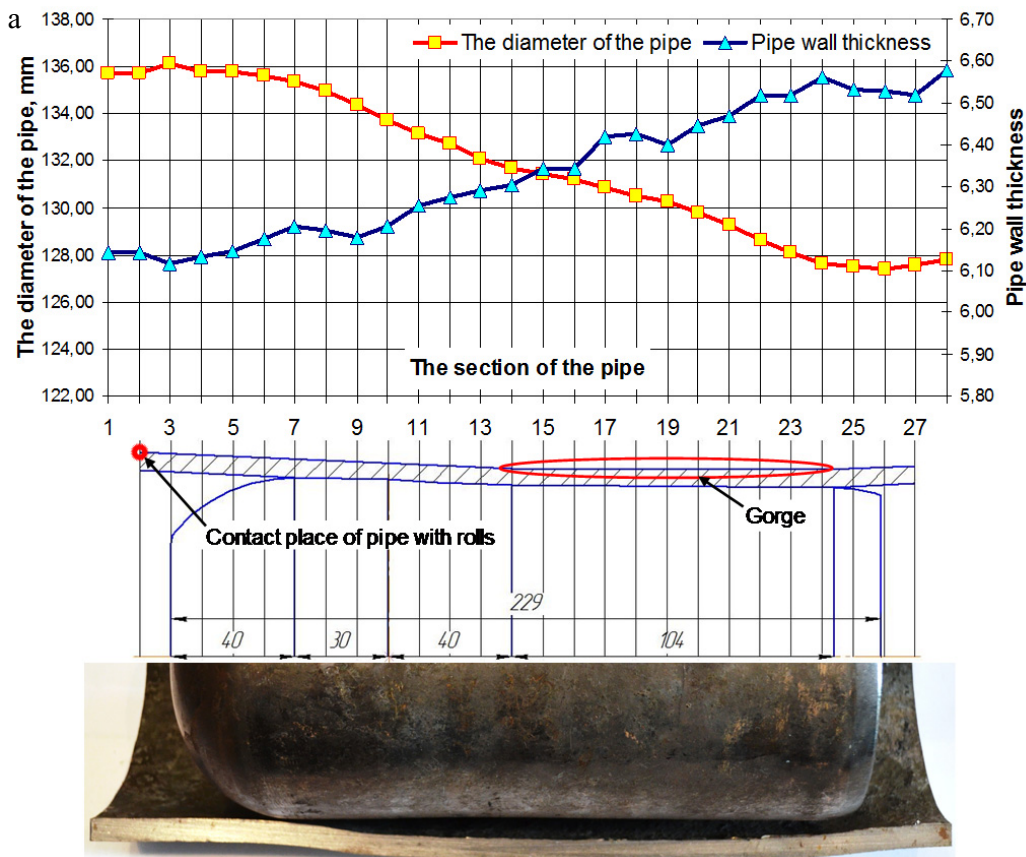
The main characteristic of two different crude pipe reeling schemes (Fig. 2) is the usage of different point types: 1 – inverted cone point (Fig. 2-a) is for a crude pipe diameter decreasing. The point position is in deformation zone in the inlet cone and roll pitch point area; 2 – right cone point (Fig. 2-b) is for a crude pipe diameter increasing. The point position is in pitch point and in the outlet cone. A point of a crude pipe engagement with both rolls has no big differences.

5. Experimental research

“Sinarskiy pipe plant” made an experimental run research both decreasing and increasing an outside crude pipe diameter at the same roll groups. A 136-6mm diameter crude pipe was put into reeling mill deformation zone and rolled in different norms. (Fig. 3).

As it is showed on the Fig. 3, depending on the point type both decrease and increase of the crude pipe diameter can be reached with the same type of roll: the maximum diameter decrease is 89 mm (with the thickening of pipe wall up to 0.05 mm – Fig. 3a).

The maximum diameter increase is up to 14 mm (with the thinning of pipe wall up to 0.4 mm Fig. 3b). This figures can be used for development of point-to-point technology of wide size range of 156mm diameter seamless pipe production on “140” pipe-rolling plant.



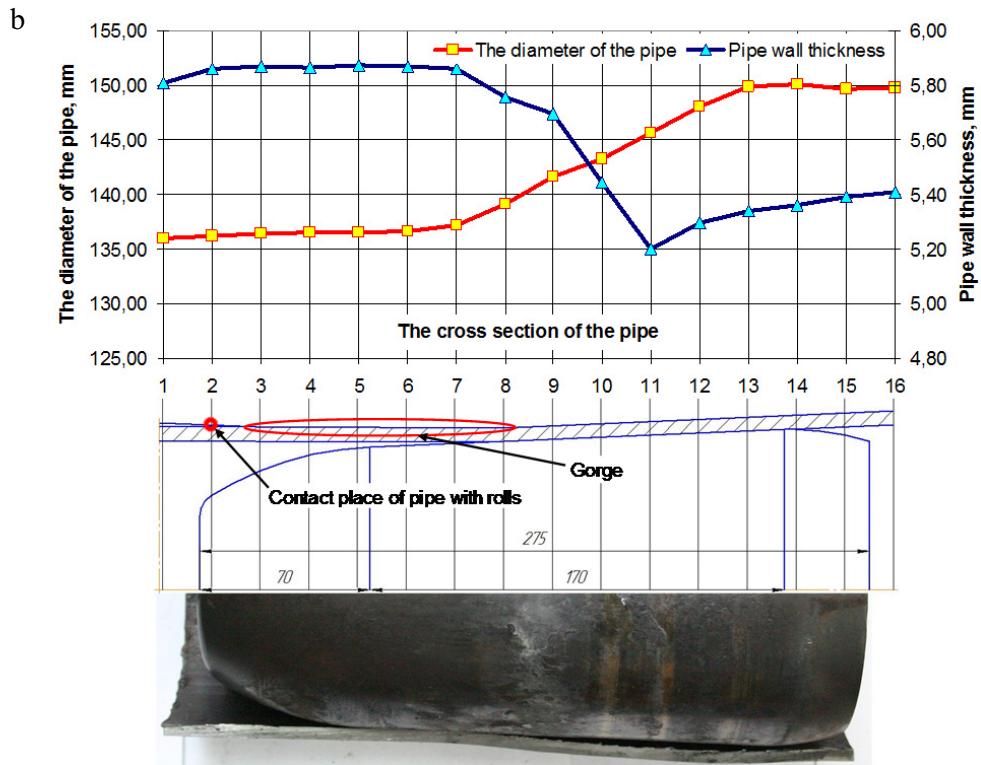


Fig. 3. Experimental research of two different crude pipe reeling schemes.

6. New technology

Taking into account the results of experimental and theoretical studies, border-line conditions and kinematic characteristics of the rolling process a new technology of wide size range of 156mm diameter seamless pipe production on “140” pipe-rolling plant was developed (Fig. 4) to improve the quality of pipe inner surface using piercing mill point with increased diameter spout and to improve the precision of pipe thickness using reeling mill point with combination of back taper and parallel section.

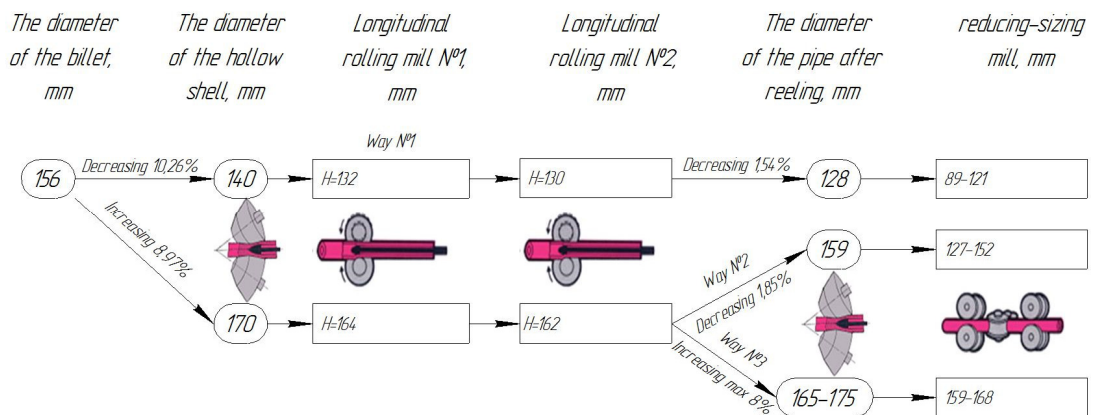


Fig. 4. New technology of “140” pipe-rolling plant 156mm diameter seamless pipe production wide size range.

Summary

The main advantages of the developed technology are a billet standard size amount reduction from 4 to one, a piecing mill roll design reduction from 2 to 1, a reeling mill roll design reduction from 2 to 1, a longitudinal rolling mill groove reduction from 3 to 2.

References

- [1] Pysmintsev I.J., Kurjatnikov A.V., Korol A.V., Korsakov A.A. and others *Sposob vintovoy proshivki litoj zagotovki* [Method of helical piercing of cast billet]. Patent RF, no. 2489220, 2013.
- [2] Pysmintsev I.J., Kurjatnikov A.V., Korol A.V., Korsakov A.A. and others *Sposob proizvodstva goryachekatanykh trub* [Methods of hot-rolled pipe production]. Patent RF, no. 2489221, 2013.
- [3] Kurjatnikov A.V., Korol A.V., Korsakov A.A. Research of pipe sizing process on three-roll screw rolling mill TPA “140” AT JSC “Sinarsky pipe plant”. Bulletin of the South Ural State University Serial “Metallurgy”, 2013, vol. 13. No. 1, pp. 160-164 (in Russia).



International Conference on Industrial Engineering

Involute helical-bevel gearing

Lopatin B.A.^{a*}, Plotnikova S.V.^a, Khaustov S.A.^b

^aZlatoust branch of the "South Ural State University" (National Research University), Turgeneva 16, Zlatoust, Russia, 456209

^bResearch Office, Cardiff University, Queen's Buildings, Cardiff, UK, CF24 3AA

Abstract

This paper describes helical-bevel gearing (HBG). The helical-bevel gearing commonly includes a cylindrical and a bevel gear. The tooth profiles can be either spur or helical. The involute HBG provides an opportunity to design a broad variety of gear trains, unobtainable by the use of conventional types of gears. The article defines methods of their generation, a contact shape and points out advantages of various arrangements of gears, diagrams of an external helical-bevel gearing skew axis, hypoid gearing, intersecting axes, parallel axes. The expediency of the use of such gear in a machine drive is justified.

© 2015 Published by Elsevier Ltd. This is an open access article under the CC BY-NC-ND license (<http://creativecommons.org/licenses/by-nc-nd/4.0/>).

Peer-review under responsibility of the organizing committee of the International Conference on Industrial Engineering (ICIE-2015)

Keywords: helical-bevel gearing; involute bevel gear; TCA; synthesis of gears.

1. Introduction

In the design of modern mechanical drives, successful solutions can be obtained by using non-conventional gearing, which includes helical-bevel gearing [1, 2]. The helical-bevel gearing (HBG) commonly includes a cylindrical and a bevel gears. The tooth profiles can be either spur or helical. The helical-bevel gearing can transfer torque between the shafts at an arbitrary disposition (Fig. 1) [3, 4].

The generation of the HBG by a rack-cutter produces involute flanks of the bevel gear teeth due to the fact that the axis of the machining engagement L is parallel to the gear axis (Fig. 2). That type of the gears is called an involute-bevel gear. It is characterized by the linearly changing displacement of the rack-cutter [5]. In this case, the HBG is involute. The generation of the HBG by a hob is impossible due to the difference of the machining kinematics and the actual meshing of the gears in the HBG. The generation of the non-involute internal and external HBG by a hob shown in [4, 6, 7, 8].

* Corresponding B.A. Lopatin. Tel.: +7-951-242-7871
E-mail address: lopatinba@rambler.ru

2. Methods of teeth profile generation and contact shape

Depending on the type of the generating tools and the kinematic arrangements of the manufacturing process, the profile of the teeth of the bevel gear of the helical-bevel gearing can be involute or non-involute.

3. Advantages of involute helical-bevel gearing

The involute HBG provides an opportunity to design a broad verity of gear trains, unobtainable by the use of conventional types of gears. The explanation of main arrangements as follows.

3.1 Skew axes HBG

The gearing shown at Fig. 1 (a) can only exist if:

$$\cos \Sigma = \cos(\beta_1 + \beta_2) \cos \delta \tag{1}$$

The center distance:

$$a_w = \left(\frac{mz_1}{\cos \beta_1 \cos \delta} + \frac{mz_2}{\cos \beta_2} \right) \frac{\sin(\beta_1 + \beta_2) \cos \delta}{\sin \Sigma}; \tag{2}$$

where δ is a taper angle of the HBG, m is a module, z_1 and z_2 are numbers of teeth of the gears, β_1 and β_2 are base helix angles.

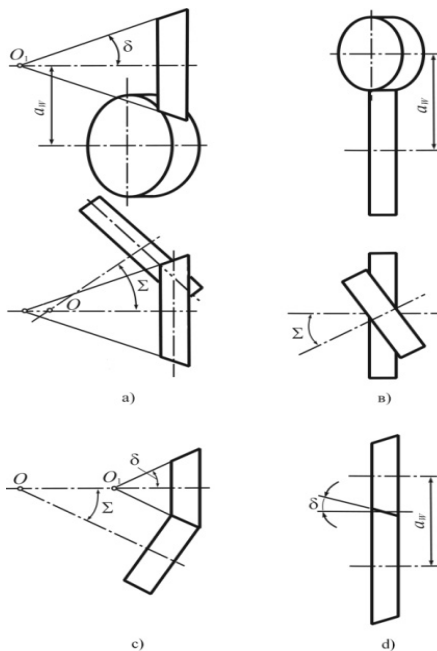


Fig. 1. Diagrams of an external helical-bevel gearing: a) skew axis (Σ is the angle between axes); b) hypoid gearing (special case when bevel gear becomes cylindrical); c) intersecting axes; d) parallel axes (special case when $\Sigma=0$).

Advantages:

1. This type of gearing allows reducing dimensions of the transmission due to an ability to position the gears arbitrarily with a respect to the line of shortest distance between the centers for the given cross-angle. As it can be seen in Fig. 3, the axial dimensions of the conventional transmission A are greater than the dimensions of the HBG transmission A₁.

2. The skew axes HBG gives an opportunity to set the contact area dimensions and shape on each side of the tooth by assigning appropriate helix angles. The contact can be designed as a linear one-sided meshing by evaluating helix angles as follows [4]:

HBG is involute. The generation of the HBG by a hob is impossible due to the difference of the machining kinematics and the actual meshing of the gears in the HBG. The generation of the non-involute internal and external HBG by a hob shown in [4, 6, 7, 8].

$$\operatorname{tg} \alpha \cdot \sin(\beta_1 + \beta_2) = \operatorname{tg} \delta \cdot \cos \beta_1, \tag{3}$$

where α is a profile angle.

For δ and β_1 as above:

$$\cos \beta_2 = \frac{\operatorname{tg} \alpha}{\sin \delta} \sqrt{(\cos^2 \delta - \cos^2 \Sigma)} \tag{4}$$

where $\Sigma > \delta > \arcsin(\sin \Sigma \cdot \sin \alpha)$.

3. It possible to set an appropriate meshing backlash by axial translation of the bevel gear, which is very important to adjust a kinematic precision.

The linear contact HBG is irreversible, because contact only occurs on the one side of the tooth profile.

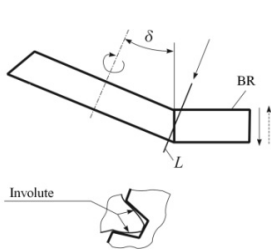


Fig. 2. HBG generation by a rack-cutter (BR).

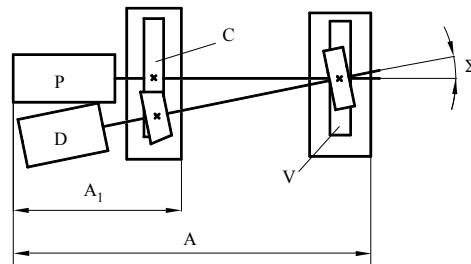


Fig. 3 Arrangement advantages of the HBG: D – electric motor; P – receiver; V – hypoid gearing; C – HBG.

3.2 Intersecting axes HBG

If the skew axes helical-bevel gear ensured a mutual arrangement of the initial surfaces when they are produced in the initial transfer plane coincide with each other, they become a bevel gearing (see. Fig. 1, c). An obvious condition for the formation of such is:

$$\beta_1 = -\beta_2; \delta = \Sigma. \tag{5}$$

There are some options:

- a) transmission, composed of involute helical-bevel and helical gears $\beta_1 = -\beta_2$; $\delta \neq 0$;
- b) transmission composed of spur and bevel gears $\beta_1 = \beta_2 = 0$; $\delta_1 \neq 0$.

Advantages of the transmission.

1. When using helical-bevel gear with intersecting axes can be obtained bevel gear with an arbitrarily small interaxial angle Σ , which is implemented is not possible for conventional bevel gears due to lack of technological equipment for the production of gears with a large cone distance.
2. As for the transmission with skewed axes, a backlash in an engagement can be adjusted by axial displacement of the bevel gear.
3. Due to a highly localized contacts, the transmission is not very sensitive to any errors in an assembling and a manufacturing.

In the transmission with intersecting axes of the working surfaces the degree of localization increases with the increase of the axial angle Σ . Therefore, the power drive is advisable to desing only at small interaxial angles ($\Sigma < 15^\circ$).

3.3 Parallel axes HGB

If both gears are involute bevel the parallel axes transmission can be designed (see. Fig. 1, d) [10].

This gears shall have equal taper angles $\delta_1 = \delta_2 = \delta$, set by the codirectional cones and by the angles of inclination of the tooth line $\beta_1 = -\beta_2$, which are equal by magnitude but in the opposite directions.

In this case, the teeth flanks are involute helicoids, equal by magnitude and antitropic with a respect to the helical lines on the main cylinder.

Advantages of the transmission:

Due to the linearity of the contact, the load capacity of the transmission is very high.

Due to the curvilinear boundaries of the field of engagement and the overlap factor of 1.2 ... 1.5 times higher (even for spur gears) than for conventional cylindrical gears, the smoothness of the transmission is increased.

By the axial displacement of the gears it is possible to change the center distance of the transmission, or to reduce or even eliminate backlash between the teeth if the center distance is fixed, which is important to increase the kinematical precision.

By an appropriate selection of angles δ and β , a zero axial force can be obtained. In this case, one of the teeth profiles is an involute helicoid and another one is a linearly extruded involute. Therefore, $\sin \beta = \text{tg } \alpha \text{ tg } \delta$.

If the tooth angles on a pitch cylinders are of the same sign for both sides of the teeth, it is possible to obtain a one-way transmission, which have an option of a free running. The transmission is legit for the condition ($\sin \beta > \text{tg } \alpha \cdot \text{tg } \delta$) [10].

Summary

Involute helical-bevel gears can be designed for any position of the shaft axes (skew, intersecting or parallel axis). In that HBG have a number of layout, operational and technical advantages relative to transmissions made up of conventional spur and bevel gears.

The most efficient use of HBG is at small interaxial angles ($\Sigma < 20^\circ$) and taper angles of the bevel gear ($\delta < 15^\circ$), the width of which is limited to values of the coefficients of the displacement of its faces.

One of the significant advantages of involute HBG is that the gears can be made by the same mechanical units and with the same precision as the conventional spur gears. Therefore, the HBG can be used in any precise heavy loaded transmissions.

References

- [1] F.L. Litvin, *A Fientes Gear Geometry and Applied Theory*, second ed., Cambridge University Press, Cambridge, 2004.
- [2] Y.S. Davidov, *Non-involute gearing*, Mashizd, Moscow, 1950.
- [3] B.A. Lopatin, O.N. Tsukanov, *Helical-bevel gearing*, *Mezhdunarodnij Jurnal eksperimentalnogo obrazovaniya*. 11 (2012) 34–36.
- [4] B.A. Lopatin, O.N. Tsukanov, *Helical-bevel gears: monograph*, SUSU, Chelyabinsk, 2005.
- [5] O.N. Tsukanov, *Ground rules of design of helical-bevel gearing in homogeneous coordinates*, SUSU, Chelyabinsk, 2011.
- [6] F.I. Plekhanov, B.A. Lopatin, RF Patent 2550598. (2015).
- [7] B.A. Lopatin, O.N. Tsukanov, S.V. Plotnikova, *Helical-bevel gears in transmissions*, *Vestnik mashinostroeniya*. 8 (2003) 7–9.
- [8] B.A. Lopatin, O.N. Tsukanov, E.A. Poluektov, *Angular adjustment electromechanical drive in aerospace industry*, *Vestnik mashinostroeniya*. 2 (2009) 14–16.
- [9] I.A. Bolotovskij, *Handbook of involute and worm gear geometry*, second ed., Mashinostroenie, Moscow, 1986.
- [10] B.A. Lopatin, S.V. Plotnikova, *Cilingrical gear formed by helical-bevel gearing*, *Nauka I obrazovanie v zhizni sovremennogo obshestva*. 8 (2015) 120–121.



International Conference on Industrial Engineering

Calculation and Choice of Grip Parameters for Garbage Truck Manipulator

Zubov V.V.^a, Domnitskiy A.A.^b, Kargin R.V.^{c*}

^a *Ul. Voroshilova, d. 17, kv. 12, Shakhty, 346500, Russia*

^b *Ul. Biriulevskaia, d. 58, korpus 2, kv. 455, Moscow, 115547, Russia*

^c *Ul. Proletarskaia, d. 245, Shakhty, 346500, Russia*

Abstract

Around the world the issue related to municipal solid waste (MSW) management ranks second in urban economy system. For the most part the actual researches deal with the improvement of MSW recycling, neutralization, utilization and burying processes. The garbage trucks are initial unit in a processing chain of MSW utilization. As to the garbage trucks operation management issues the researches are carried out on the enhancement of designs, maintenance and repair system, models and methods of work route schedules development. The free oscillations of the vehicle frame are not taken into account in the fundamentals of garbage trucks engineering design.

As part of the fulfilled research the process modeling of side mechanized loading of solid waste in the garbage truck body, taking into account the vehicle frame free oscillations, is carried out. As result the constructive and connecting sizes of a new grip design to ensure minimum stresses and moments generation in «grip-container-grip» system are determined.

© 2015 The Authors. Published by Elsevier Ltd. This is an open access article under the CC BY-NC-ND license (<http://creativecommons.org/licenses/by-nc-nd/4.0/>).

Peer-review under responsibility of the organizing committee of the International Conference on Industrial Engineering (ICIE-2015)

Keywords: garbage truck; manipulator; grip; load; moment; modeling; parameters optimization

1. Introduction

The problem of municipal solid waste (MSW) management is a priority worldwide, ranking second in the urban economy taking into account costs and investments after the water and canalization sector [1]. In order to protect the

* Corresponding author. Tel.: +7-928-621-8455.

E-mail address: kargin-r-v@mail.ru

natural environment, air and water resources the researches are carried out in the world and domestic practice in the field of ecology, economics, engineering and technology of MSW management [2-12]. The special mobile units, named garbage trucks are initial unit in the process chain of solid waste disposal. The garbage trucks with mechanized body side-loading are the most widely used [13]. The garbage trucks operating efficiency depends on the organization and improvement of the three main processes: collection and disposal of MSW, as well as maintenance and repair (M&R) of garbage truck [14]. The M&R system is being improved in the direction of periodicity technical impacts optimization taking into account the technical reliability indices and operating conditions by the criterion of minimum unit costs for maintaining and restoring a state of serviceability [15]. The researchers are conducted to enhance models and methods for developing route schedules garbage trucks with a view to optimize the process of MSW disposal [16-18]. As concerns the MSW collection, the researchers are aimed at improving garbage trucks and grippers designs [19-24].

2. Methods

At present, the engineering design fundamentals of machines for MSW collection and disposal are based on the known positions of theoretical mechanics, theory of strength of materials, theory of mechanisms and machines, and theory of vehicles. The current method for calculating manipulator includes characterization of estimated positions, kinematic and dynamic analysis of system and strength design calculation [25]. The process of MSW collection (loading process of containers in truck body), despite the outrigger availability, is oscillatory type, related to the base vehicle sprung mass. This gives rise to generation of loads of dynamic nature in the manipulator structure elements and the grip, and peak values significantly higher than the estimated, which are currently determined, without considering vehicle frame free oscillations [26].

For the purpose of description and accounting of truck oscillations in operating mode the design scheme, the differential equations of oscillations of vehicle frame and manipulator with container using the Lagrange's equations of the second kind are composed; the dependence of vehicle frame's oscillation angle in one operational cycle of manipulator is obtained. In order to determine the amplitude-frequency characteristics the equation of manipulator oscillations taking into account vehicle frame oscillations in one operational cycle is developed and the dependence of changes in lifting angle of manipulator in one operational cycle under different loading of body is obtained [27].

The researches on garbage trucks reliability [28] have shown that a substantial proportion of attached implements refusals ($\approx 50\%$) can be accounted for steel structures and hydraulic system, of which about 80% accrue to the boom, manipulator grip and their drive.

In order to reduce the acting efforts in the grip structural elements, as well as improve its work reliability and prevent deformation of container walls a grip construction is developed [29, 30], which provides picking up under the container bottom.

For determining the loads generated in the grip elements of new design the calculation models are developed (Fig. 1), the equilibrium equations in the «grip-container-grip» system (1, 2) are composed and modeling of efforts in the grip structural elements in one operational cycle of manipulator as a function of the angle of oscillation of the vehicle frame is carried out. The results modeling show that when using the proposed grip design the loads occurring in «grip-container-grip» system diminish in different phases of manipulator operation cycle from 1,2 to 5,5 times in comparison with the serial grip. Maximum loads occur on hydraulic cylinder rods, which increase when rising container weight. The garbage weight change does not affect the value and amplitude of loads, but their frequency response varies only [27].

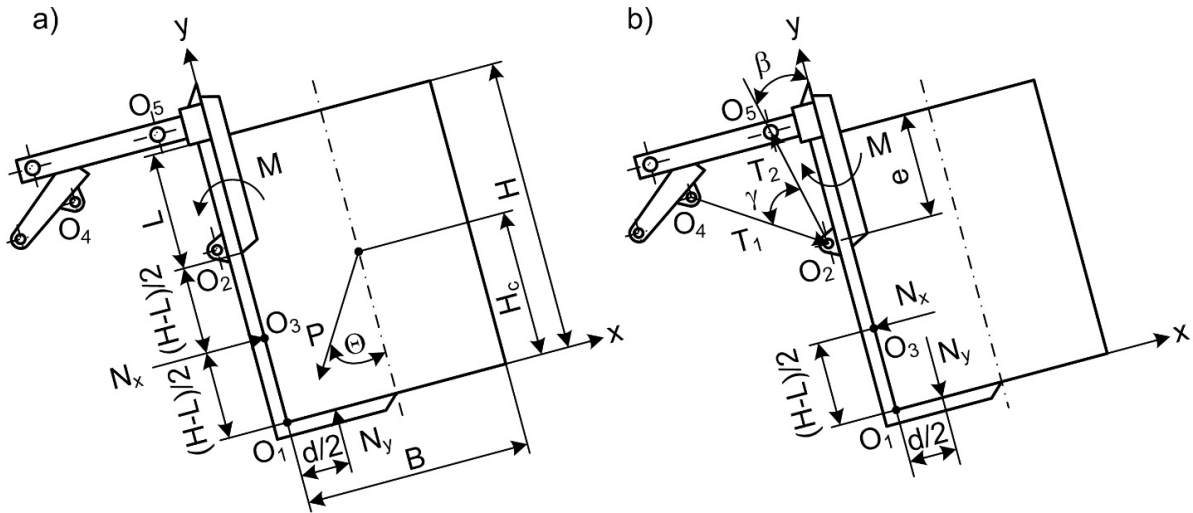


Fig. 1. (a) calculation models of forces in «grip-container-grip» system on the side of grip to container; (b) calculation models of forces in «grip-container-grip» system on the side of container to grip

$$\begin{cases} \sum F_{kx} = 0; & N_x - P \cdot \sin \Theta = 0, \\ \sum F_{ky} = 0; & N_y - P \cdot \cos \Theta = 0, \\ \sum m_{O_1} = 0; & P \cdot \frac{B}{2} \cdot \cos \Theta - N_y \cdot \frac{d}{2} - P \cdot H_c \cdot \sin \Theta + N_x \cdot \frac{H-L}{2} - M = 0. \end{cases} \quad (1)$$

$$\begin{cases} \sum F_{kx} = 0; & -N_x - T_2 \cdot \sin \beta + T_1 \cdot \sin(\beta + \gamma) = 0, \\ \sum F_{ky} = 0; & -N_y + T_2 \cdot \cos \beta - T_1 \cdot \cos(\beta + \gamma) = 0, \\ \sum m_{O_2} = 0; & M + N_x \cdot \left(\frac{H+L}{2} - e \right) + N_y \cdot \frac{d}{2} = 0, \end{cases} \quad (2)$$

where N_x , N_y – normal pressure on container wall and bottom, respectively, H ; P – container weight, H ; Θ – manipulator lifting angle, rad; B – container width, m; d – pick-up length at container bottom, m; H_c – height of center of container masses, m; H – container height, m; L – length of grip plate plunged into a container, m; T_1 – effort at hydraulic cylinder rod of clamp, H ; T_2 – effort at control hydraulic cylinder rod, H ; β – inclination angle of control hydraulic cylinder to Y axis, rad; γ – angle between the axes of hydraulic cylinders, rad; e – distance from top edge of container to attachment point of hydraulic cylinders rods, m.

3. Results

The «grip-container-grip» system reliability is not influenced primarily by loads acting in it, but by torque moments. The moment values depend on constructional and mounting dimensions. Considering the H and B container sizes as known, let « e » linear dimension be defined from moment equation of the system (2).

$$e = \frac{B}{2} \operatorname{ctg} \Theta + H - H_c \quad (3)$$

In case of constant sizes of a container «e» value is a function of lifting angle of manipulator in one operational cycle. Modeling of «e» parameter under complete garbage truck load shows that according to equilibrium condition of moments many values cannot be realized because they exceed container dimensions for height (Fig. 2,a). After 2,5 seconds of work «e» parameter takes on a value, which corresponds to the level of container bottom. At the end of cycle «e» value is reduced to a value corresponding to height of center of gravity of complete container (Fig. 2,b). It should be noted that on a section from H to H_c «e» values for full and empty garbage trucks differ by less than 1%.

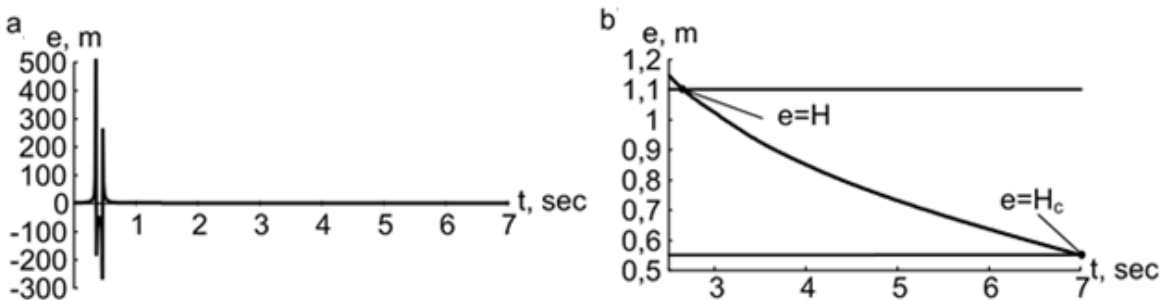


Fig. 2. Distance from top edge of container to attachment point of hydraulic cylinders rods

Modeling of torque moments in «container-grip» system can be carried out as a function of «e» value based on design constraints for maximum values of N_x and N_y, that corresponds to full container loading in full garbage truck (Fig. 3). Minimal moments values occur when the attachment point of hydraulic cylinders rods (O₂) coincides with the application point of force N_x (O₃), that is,

$$e = (H + L)/2 \tag{4}$$

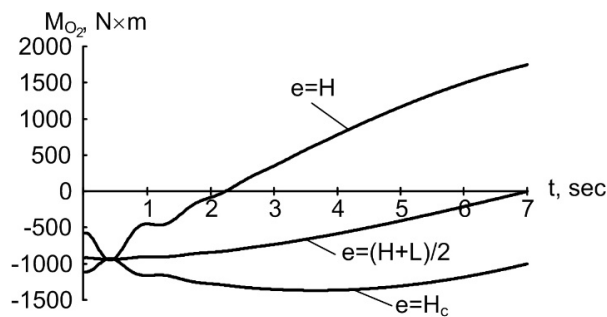


Fig. 3. Torque moment in «container-grip» system

In this case, the torque moment in the system only occurs under the effect of force N_y. With decreasing «e» value the moments are increased and its rise causes in addition the moment to change direction of action during operational cycle.

The «e» value does not only affect the torque values. The angles of inclination of hydraulic cylinders β and γ to the axis Y depend from it. These angles determine the effort values on their rods. The increasing of «e» value leads to a decrease of the angles β and γ, at that, the efforts on rods of hydraulic cylinders T₁ (Fig. 4,a) and T₂ (Fig. 4,b) are increased.

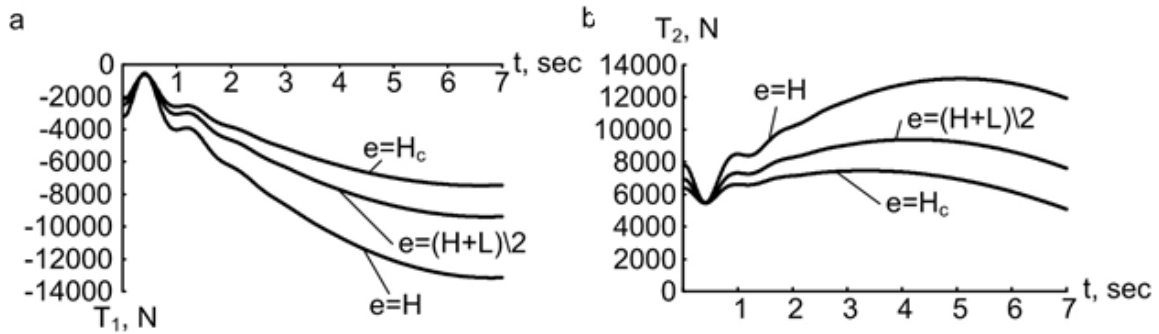


Fig. 4. Efforts at grip hydraulic cylinders

With a view to ensuring in the system «container-grip» the effects of minimum moments and minimum stresses on rods of hydraulic cylinders «e» values must be different when other factors being equal. This condition cannot be satisfied because the attachment point of hydraulic cylinders rods (O_2) cannot structurally change its position during operation. In observance of the conditions of generation of minimum moments, as well as stresses it is necessary to make changes to the layout scheme of grip so that the attachment point of rods of hydraulic cylinders (O_2) has the same height as the attachment point of force N_x (O_3); in addition, it is required to shift the attachment points of casing shells of hydraulic cylinders O_4 and O_5 in the direction of increasing angles β and γ .

The generation of moments in «container-grip» system is influenced by «e» value, as well as by length of the pick-up under the container bottom d . The modeling results (Fig. 3) are obtained on the assumption that $d=B/2$. Taking into account the condition (4), the equation of the moment becomes

$$M = -N_y \cdot \frac{d}{2} \quad (5)$$

The equation (5) shows that with the increase of d the growth of torque values will occur (Fig. 5,a). For ensuring minimum torque d value should be positive, tend to minimum, but should not be equal to 0, since in this case the grip design and calculation schemes of forces and moments change (as an example $d_{\min} = 0,05$ m).

The length of the pick-up under the bottom of the container d influences the moments generation not only in the «container-grip» system, but also in the «grip-container» system. The estimation of d value influence on generation of a moment bending the container wall can be done by means of the moment equilibrium equation of the system (1). The modeling results show that in the «grip-container» system the growth of a moment occurs when reducing d value (Fig. 5,b). In this respect, for the range of d value variation, except d_{\max} , the torque changes the direction of its action during operating cycle of manipulator.

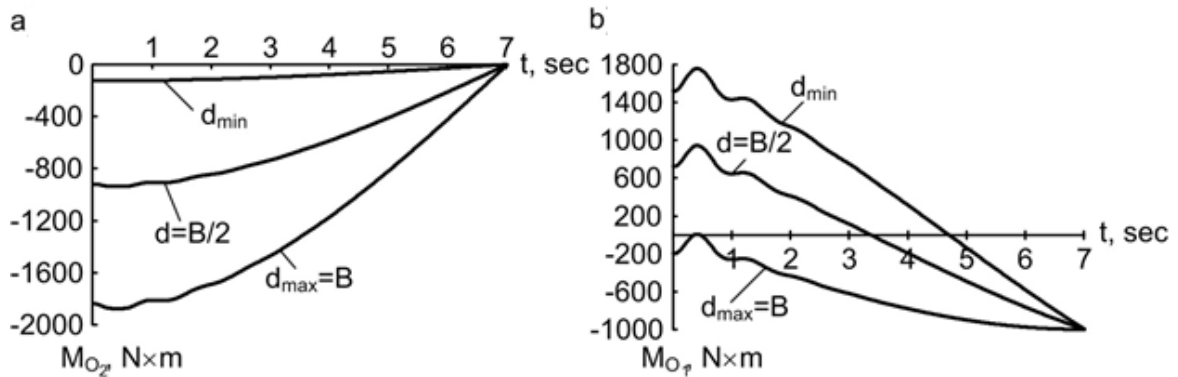


Fig. 5. Torque moments in the «grip-container-grip» system

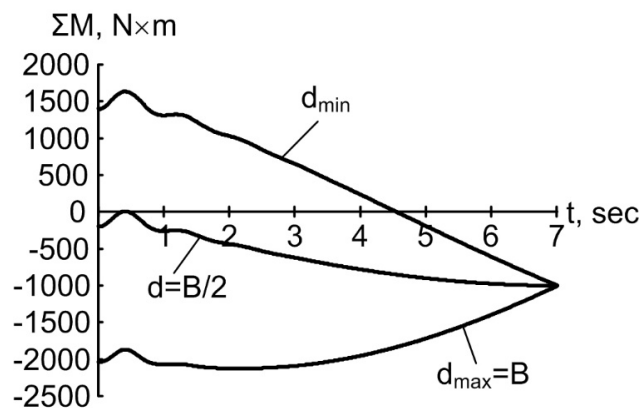


Fig. 6. Sum of moments in the «grip-container-grip» system

The «grip-container-grip» system is influenced by two moments: M_{O1} and M_{O2} that during operating cycle of a manipulator can either counterbalance or amplify the effect of each other (Fig. 6). At d_{max} both moments are in effect in the same direction, amplify the effect of each other and in the system the maximum total moment occurs. At d_{min} at the end of operating cycle of manipulator the system has a minimum total moment, but in the beginning of a cycle its value is close to the maximum, while during the operating cycle the change in the direction of its action occurs. The $d=B/2$ value is optimal in terms of generation of the total moment, which does not change direction of its effect and takes minimum values for the most part of operating cycle in this case.

References

- [1] D. Vilson, Solid Waste Utilization. Translated from English, Strojizdat, Moscow, 1985.
- [2] V.G. Sister, A.N. Mirnyj, Modern technologies of municipal solid waste neutralization and utilization, Academy of Municipal Economy named after K.D. Pamfilov, Moscow, 2003.
- [3] D.V. Stalinski, A.Z. Ryzhavsckij, A.V. Dunaev, A.Ju. Pirogov, D.B. Birjukov, S.L. Stasevskij, A.V. Zimogljad, A.A. Azarnov, RF Patent 2455567. (2010).
- [4] V.D. Nazarov, M.V. Nazarov, I.N. Minigazimov, K.L. Chertes, D.E. Bykov, R.I. Hangil'din, RF Patent 2406578. (2009).
- [5] F.D. Mubarakshina, A.A. Guseva, Modern problems and technologies of waste recycling in Russia and abroad. Proceedings of Kazan State University of Architecture and Engineering. 4 (2011) 91–99.

- [6] I.M. Bernadiner, A.A. Koval'chuk, Municipal Solid Waste Utilization by Air–Steam Gasification Method. Perm National Research Polytechnic University Bulletin, Applied Ecology, Urban Planning. 2 (2014) 81–96.
- [7] O.B. Barysheva, Ju.H. Habibullin, Research on Processes of Municipal Solid Waste Incineration Using Numerical Methods, Proceedings of Kazan State University of Architecture and Engineering. 2 (2013) 315–319.
- [8] Ja.I. Filimonov, Recycling and Incineration in Europe: Prospects for Development, Municipal Solid Wastes. 6 (2012) 59–62.
- [9] I.A. Barcev, O.V. Trofimov, I.S. Docenko, Analysis of Strategies of Municipal Solid Wastes Disposal and Recycling in the Russian Federation. Management of Economic Systems: an Electronic Scientific Journal. 9 (2013) 34.
- [10] N.I. Pljaskina, V.N. Haritonova, Plasma Technology of Solid Waste Disposal: The Promotion of Innovation in the Market, Innovations. 12 (2014) 67–79.
- [11] G.M. Dolgih, S.N. Okunev, S.N. Strizhkov, Ecological Technologies and Equipment: Introduction of Innovative Environmentally Friendly Technologies for MSW Disposal in Kriolitzone, Ecological Bulletin of Russia. 1 (2012) 29–33.
- [12] A.N. Tugov, V.F. Moskvichev, About the Feasibility of Plasma Technology Using for MSW Thermal Utilization, Municipal Solid Wastes. 10 (2014) 40–45.
- [13] R.V. Kargin, Classification of Machines for Collecting and Removing Hard Everyday Waste Products, News of Higher Educational Institutions, North Caucasus Region, Technical Sciences. 2 (2011) 69–74.
- [14] R.V. Kargin, The efficiency enhancement of the garbage trucks operation system, News of Higher Educational Institutions, North Caucasus Region, Technical Sciences. 5 (2011) 93–96.
- [15] A.S. Nosenko, R.V. Kargin, M.S. Altunina, Y.A. Shemshura, Regularity of Forming a Garbage-Carriers Resources among Repairments Taking into Consideration the Exploitation Regimes, Izvestiya vuzov. Severo - Kavkazskii region. Technical Sciences. 5 (2010) 89–94.
- [16] E.S. Severova, Transportation of municipal solid waste, Cargo and passenger motor transport fleet. 11 (2006) 46–47.
- [17] V.A. Korchagin, S.A. Ljapin, N.M. Moiseeva, Improving the Efficiency of the Motor Transport System of Municipal Solid Waste Disposal for Processing and Recycling, MADI Bulletin. 2 (2007) 80–83.
- [18] R.V. Kargin, A.A. Domnitskiy, Traffic Routing of Road Trucks for Waste Collecting and Removal, Roads and Bridges. 28 (2012) 92–102.
- [19] Rivard Daniel, FR Patent 2590241. (1987).
- [20] G.M. Belocerkovskij, D.A. Bashev, S.B. Karjakin, RU Patent 2381163. (2010).
- [21] A.S. Nosenko, R.V. Kargin, I.V. Kargina, A.A. Domnitskiy, RU Patent 2450943. (2012).
- [22] Jakob Naab, RU Patent 2107014. (1998).
- [23] V.K. Nabrovenkov, G.L. Ratner, G.N. Smirnov, A.N. Tolmachev, V.I. Farafonov, V.A. Zotov, K.M. Ippolitov, RU Patent 2166469. (2001).
- [24] V.I. Lisin, A.I. Paramonov, A.T. Ljubaev, L.N. Labzina, RU Patent 2177901. (2002).
- [25] A.B. Ermilov, Calculation and Design of Special Vehicles for Municipal Solid Waste Collection and Disposal, MADI, Moscow, 1983.
- [26] R.V. Kargin, O.S. Miroshnitchenko, Constructions and Working Processes of the Manipulators of Body Garbage Carries, News of Higher Educational Institutions, North Caucasus Region, Technical Sciences. 6 (2010) 75–78.
- [27] R.V. Kargin, O.S. Miroshnitchenko, I.V. Kargina, Dynamic Analysis of Body Garbage Truck Handler, Engineering journal of Don. 1(4) (2012). <http://www.ivdon.ru/magazine/issue/105?page=4>.
- [28] R.V. Kargin, V.I. Zhigulsky, Reliability of Body Garbage Trucks, Truck. 2 (2012) 37–40.
- [29] A.S. Nosenko, R.V. Kargin, M.S. Altunina, O.S. Miroshnitchenko, RF Patent 2400417. (2010).
- [30] R.V. Kargin, Development of Body Garbage Truck Construction, Scientific and Technical Volga Region Bulletin. 1 (2011) 116–120.



International Conference on Industrial Engineering

Implementing Formal Evaluations of Design Decisions Similarity for Upgrading Machine Components Pre-Production

Aleksandr I. Kondakov*

Moscow State Technical University Named after N.E. Bauman, 5, 2-nd Baumana street, Moscow, 105005, Russian Federation

Abstract

Automation level of design decisions support for machines components pre-production does not exactly meet today's requirements. Today pre-production in general is characterized by low level of formalization of relationships and connections, forming in it. Formal quantitative evaluations, allowing effective evaluation and implementation of portability (similarity) of design decisions are poorly used. Research, aimed on revealing and using for pre-production efficiency the upgrading of relations and quantitative formal estimations of the structural and technological design decisions similarity, is quite actual. Presented work demonstrates scientific-methodical approach to determining and using for machines components pre-production of quantitative estimations of the structural and technological design decisions similarity on the basis of the components models decomposition to complexes of surfaces, united by forms forming technologies similarity. We have found stable relations between quantitative estimations of the structural and technological similarity of the compared components. Document includes proved applications for evaluating design decisions similarity when preparing production: directional forming groups of technologically similar components; evaluation of production system technological potential and of possibility of effective producing of specified nomenclature components in such system; designing technical (technological) complexes for producing machines components.

© 2015 The Authors. Published by Elsevier Ltd. This is an open access article under the CC BY-NC-ND license (<http://creativecommons.org/licenses/by-nc-nd/4.0/>).

Peer-review under responsibility of the organizing committee of the International Conference on Industrial Engineering (ICIE-2015)

Keywords: design decisions, pre-production, structural decision, technological decision, support, similarity, component

* Corresponding author. Tel/fax.: +7-499-263-6508.
E-mail address: kondakov1950@mail.ru

1. Introduction

Machines structures complication, operating quality requirements growth, rugged competition on the market of machines demand severe reduction of producing-and-technological parts of their service life under increasing quality of taken and implemented structural and technological design decisions [1,2]. It is not possible without using Decision Support Systems [3].

Modern decision support systems for machines producing are far from perfection and perform only informational functions [4]. Creating full systems of the mechanical facilities preparation intellectual support is work for the future. It is reasoned by insufficiently developed methodological base of decisions forming during pre-production and its implementing and by specialty of used technological knowledge and rules. Problem of technological designing objects structures synthesis automation is not solved [5, 6]. Technological designing automation systems are systems only of operational level. Existing methods of classification and simulating subjects of production process, for example, components, have critical weaknesses.

Today machines pre-production is characterized by low level of formalization of relationships and connections, forming in it. There are no quantitative evaluations, allowing objective evaluation and implementation of portability (similarity) of design decisions. Structural and technological decisions relationships are not studied enough. Lack of these relationships quantitative evaluations, for example, has lead to low efficiency of implementing cluster analysis [7] in forming groups of technologically similar goods (components). All mentioned above demonstrates actuality of research, aimed on revealing and using for pre-production efficiency the upgrading of relations and quantitative formal estimations of the structural and technological design decisions similarity.

2. Formalization and comparison of structural decisions

Decision is considered as structural when its full implementation in production and technological cycle leads to producing physical (material) object, corresponding with its producing purpose. It is considered as dominating design decision for machines pre-production, not depending of the good life circle structure – consecutive [2] or changed according to the concurrent engineering method [8, 9]. Formed structural decision is implemented in the form of the production subject, for example, (hereinafter) component, model, usually imported from the CAD system. Model is the information source for forming following design decisions. But usually model, received from CAD, contains redundant information and of a little use for technological pre-production automation. It is necessary to reasonably decrease dimension description for component as production subject. Component model decomposition to complexes of surfaces, united by forms forming technologies similarity [10] solves this task quite well.

Technological complex (*T*-complex) – system of different type surfaces that can be processed jointly during continuous moving of the tool according to set path, or can be processed by set of successively used tools when implementing elementary complex processing route. Each complex is assigned with finite class of technological methods, which, depending of supposed production conditions and quality requirements, can be used separately or jointly as operations for producing surfaces, forming the *T*-complex.

Each *T*-complex is characterized by classes of:

- Types of surfaces, forming the complex.
- Technological parameters (production or operational quality parameters) of the surfaces, forming it.
- External parameters, assuring connecting this complex with other complexes.

Component model (*D*) is presented as:

$$D \equiv \langle \{TK\}, G_{TK} \rangle, \quad (1)$$

where $\{TK\}$ – class of identifiers of the pointed *T*-complexes, determining component model content; G_{TK} – network of relations for the *T*-complexes, included into component model and determining component structure. *T*-complexes catalogue and components models decomposing rules were worked out [10]. In case there are no means of

automated T -complexes generating in the component model, subjective decomposition is possible. Performed studies have proved low influence of the decomposition subjectivity on content of design decisions, taken on the basis of such decomposition [11].

Quantitative evaluation of components D_B and D_C models similarity is possible under following compatibility conditions, indicated below:

- Identity of functions, performed by compared components in assembly units (machines).
- Compared components belonging to one range of overall dimensions and dimensions of functional (operating) surfaces.
- Belonging to one class per adopted classifier.
- Similarity of material groups and its main features (technological and operational).
- Similarity of main production and operational quality parameters.

Independent evaluations of components D_B and D_C models similarity can be obtained:

- a) by content of T -complexes, forming the models $(S_{B,C})_K^{TK}$;
- b) by T -complexes relations structure in components models $(S_{B,C})_K^G$.

Both evaluations quantitatively can be determined by following formulae:

$$(S_{B,C})_K^* = \frac{2m}{b+c}, \quad (2)$$

Where $(S_{B,C})_K^*$ – value of chosen evaluation $(S_{B,C})_K^{TK}$ or $(S_{B,C})_K^G$ of components D_B and D_C models structural similarity. For evaluation $(S_{B,C})_K^{TK}$: m – quantity of identical T -complexes in components D_B and D_C models; b and c – quantity of T -complexes in components D_B and D_C models accordingly. For chosen evaluation $(S_{B,C})_K^G$: m – quantity of identical T -complexes relations in components D_B and D_C models; b and c – quantity of relations in components D_B and D_C compared networks, accordingly.

In G_{TK} relations networks, used for evaluation of compared components structural similarity, components processed surfaces T -complexes are considered as nodes, and T -complexes conditionally shown relations – as ribs. There is no intent to show components spatial structure, but only obvious relations (contacts) of T -complexes. We have worked out system of rules, allowing well-defined generating networks of T -complexes relations even for complex components without symmetry axis [13].

There are quantitative relations between structural similarity evaluations. They are determined by compared components classes. In particular, for compared general purpose hydro cylinders components, being rotary bodies:

$$(S_{*,*})_K^G \approx 0,75 \dots 0,83 (S_{*,*})_K^{TK}, \quad (3)$$

with relative error not more than 10 % [13]. Structural similarity evaluations values are within 0 1 range. When in (2) $b > c$, maximum value of any D_B and D_C -components models structural similarity evaluation is equal to

$$(S_{A,B})_K^* = \frac{2m}{b+c}. \quad (4)$$

The larger evaluation value is, the higher structural decisions similarity is.

3. Formalization and comparing technological decisions

Any decision, implemented during pre-production or production, related to determining or changing production subject condition and aimed on assuring production release, is considered technological. Technological object of appropriate functional class (EQUIPMENT, TECHNOLOGICAL METHOD, TECHNOLOGICAL PROCESS, TOOL, etc.) is always the object of the technological decision.

Each object of technological decision can be presented in predicate form [14]:

$$R(A_0, A_1, A_2, \dots, \{A_{ij}\}, \dots, A_S), \quad (5)$$

where R – predicate word, determining functional class of the object; A_0 – identifier of the object copy (main attribute); A_1, \dots, A_S – object attributes; $\{A_{ij}\}$ – class of the uniform object attributes. Predicate of the indicated structure determines specific copy (B) of class R object in case attributes specific values are determined, and they correspond with values for determined object copy:

$$B = R(a_0^B, a_1^B, a_2^B, \dots, \{a_{ij}^B\}, \dots, a_S^B), \quad (6)$$

where $a_0^B, a_1^B, \dots, \{a_{ij}^B\}, \dots, a_S^B$ – object B attributes values.

Two objects (B) and (C) of one functional class (R) are identical, if:

$$\begin{aligned} a_0^B \neq a_0^C; a_1^B \equiv a_1^C; a_2^B \equiv a_2^C; \dots; \\ \{a_{ij}^B\} \equiv \{a_{ij}^C\}; \dots; a_S^B \equiv a_S^C. \end{aligned} \quad (7)$$

In case even one identity law (from indicated) is not fulfilled, objects are not identical. Non-identical objects of one functional class can be similar [15].

Objects B and C of same functional class are similar per metric (actual or integral-valued) attribute a_i , if

$$|a_i^B - a_i^C| \leq d_i, \quad (8)$$

where d_i – remote function value (actual or integral figure).

In case object B and C are presented only by metric attributes, than their similarity evaluation:

$$S_{B,C} = \frac{p_{B,C}}{n}, \quad (9)$$

where $p_{B,C}$ – quantity of attributes of objects, for which similarity condition is generated; n – object attributes general quantity ($n=b=c$).

Objects B and C of same functional class (R) are similar per symbol attribute a_i , if

$$a_i^B \equiv a_i^C. \quad (10)$$

In case of same quantity of attributes, similarity evaluation is determined per (8).

Actual technological objects are presented by metric and symbol attributes. Attributes quantity in compared objects can be different ($b \neq c$).

Objects B and C similarity evaluation is determined per (2), where b and c – attributes quantity, accordingly, for objects B and C ; m – quantity of attributes pairs for compared objects, for which similarity conditions (7) and (8) are met. Generally $b \neq c$. Presented evaluation takes into account only list of technological objects attributes. Their structure (relations of their elements) is not considered.

Depending of functional class of the decision object and performed technological task, determined technological objects can be considered as unstructured or as structured.

Unstructured technological objects don't have internal structure and are presented by lists of attributes. Their composition similarity evaluation is determined per (2). Only same-name or uniform attributes can be compared.

Following can be determined for structured technological objects:

- composition similarity evaluation ($S_{B,C}^C$);
- structure similarity evaluation ($S_{B,C}^{CT}$).

Composition similarity evaluation is determined same as above. When evaluating structure similarity you should take into account not only parameters (features, values) of the element, but also its location (relations) in the object as a system.

In general

$$(S_{B,C})_T^{CT} \approx 0.65 \dots 0.8 (S_{B,C})_T^C. \quad (11)$$

When solving practical tasks it is more reasonable to use composition similarity evaluations (as more simple to determine).

Example: Compared technological objects – routing technological processes of *B* and *C* components manufacturing, presented by technological operations sequences.

Process *B*:

- Milling-centering
- Turning-screw-cutting
- Turning-screw-cutting
- Turning with CNC
- Turning with CNC
- Turning with CNC
- Turning with CNC
- Vertical-milling
- Vertical-milling
- Turning-screw-cutting
- Turning-screw-cutting
- Round-grinding
- Round-grinding

Process *C*:

- Turning-screw-cutting
- Turning-screw-cutting
- Horizontal-milling
- Vertical-drilling
- Splined-milling
- Turning with CNC
- Turning with CNC
- Round-grinding
- Round-grinding

Composition similarity evaluation:

$$(S_{B,C})_T^C = \frac{2 \cdot 7}{13 + 9} \approx 0.63. \quad (12)$$

evaluation of structure similarity (process *C* was taken for comparison as basic structure):

$$(S_{B,C})_T^{CT} = \frac{2 \cdot 5}{13 + 9} \approx 0.45. \quad (13)$$

Composition and structure similarity evaluation can be determined for any technological objects under corresponding levels of presenting them as systems.

4. Relations and implementing of design decisions similarity evaluations

It was experimentally revealed presence of stable relations between quantitative evaluations of structural and technological similarity, linearly approximated according to least spreads method with relative error not more than 10 % for components of one group [13]. In particular, for main components of hydro cylinders:

- pistons:

$$(S_{**})_T^C = 0.169(S_{**})_K^{TK} + 0.83 ; \quad (14)$$

- rear covers:

$$(S_{**})_T^C = 0.509(S_{**})_K^{TK} + 0.347 ; \quad (15)$$

- stems:

$$(S_{**})_T^C = 0.054(S_{**})_K^{TK} + 0.849 \quad (16)$$

- front covers:

$$(S_{**})_T^C = 0.436(S_{**})_K^{TK} + 0.587 . \quad (17)$$

In (14)...(17) $(S_{**})_T^C$ means evaluation of composition similarity for routed technological processes of producing any two components of this group; $(S_{**})_K^{TK}$ means evaluation of structural similarity of T -complexes composition for same components. Dependences (14) ... (17) allow predict supposed values of evaluations for technological similarity of specified component and component being supposed analogue. At allows automation of searching analogue technological processes, requiring minimum adjustments when converting into unit processes of manufacturing specified components [13], [16].

Quantitative evaluations of similarity of compared components structures or manufacturing them technological processes are measures of similarity of such processes and have numeral approved practical applications, facilitating upgrade of machines components pre-production:

- Directional forming groups of technologically similar components [17, 18]. Similarity evaluation is the value of a function of components membership in one group.
- Evaluation of production system technological potential and of possibility of effective producing of specified nomenclature components in such system. [19].
- Designing technical (technological) complexes for producing machines components [20].

Discussed information forms part of an original theory of taking design decisions [21], being the basis of the similarly-named course of study.

5. Conclusions

- Automation level of design decisions support for machines components pre-production does not meet today's requirements. Research in the field of relations and possibilities of using quantitative, formally determined evaluations of structural and technological design decisions similarity during pre-production is quite actual.
- Using formally determined (according to suggested approach) evaluations of structural and technological design decisions similarity leads to increasing pre-production effectiveness by means of: directional search of closest analogue processes, objective forming of technologically similar components groups, and objective evaluating technological possibilities of the production system.

References

- [1] F.P. Miller, J. Mebrewster, A.F. Vandome, Product lifecycle management, 2010.
- [2] A.F. Kolchin, M.V. Ovsyannikov, A.F. Strelakov, and S.V. Sumarokov, Production Life Circle Management., Anakharsis, Moscow, 2002.
- [3] R.A. Sprague, Framework for the Development of Decision Support Systems, MIS Quarterly. 4(4) (1980) 1–25.
- [4] E. Turban, J.E. Aronson, Decision Support Systems and intelligent Systems., Ting – Peng Liang, 2008.
- [5] M.L. Kheiphetch, B.P. Chemisov, Intelligent Production: Current Situation and Development Prospects., Novopolotsk, PSU, 2002.
- [6] A.S. Vasiliev, A.M. Dal'ski, Yu.M. Zolotarevski, and A.I. Kondakov, Directional Forming of Machine Building Industry Products Features., Mashinostroenie, Moscow, 2005.
- [7] H. Spath, Cluster Dissection and Analysis : Theory, Fortran Programs, Examples., Halsted Press, New York, 1985.
- [8] A. Rosenblatt, G. Watson, Concurrent Engineering/A. Rosenblatt., IEEE Spectrum. (1991) 22–37.
- [9] Landon C.G.Miller, Concurrent Engineering Design :Integrating the Best Practices for Process Improvement., Society of Manufacturing Engineers, 1993.
- [10] A.I. Kondakov, Forming Innovative Basis for Designing Routed Processes of Components Production, Reference Book. Engineering Magazine. 3 (2001) 15–20.
- [11] R.B. Meshkob, Technological modelling of parrallel designing of engineering, J. Bulleting if Computer and IT Technologies. 4 (2008) 43–45.
- [12] A.V. Zaitsev, Automation of Decisions Support for Hydro cylinders Pre-production, J. Higher Educational Institutes News. Machine Constructio. 6 (2012) 59–65.
- [13] A.I. Kondakov, A.V. Zaitsev, Implementing Similarity Evaluations for Finding Analogue Processes of Machines Components Production, J. Reference Book. Engineering Magazine. 7 (2012) 13–20.
- [14] A.I. Kondakov, A.S. Vasiliev, Theory of Making Design Decisions, J, Reference Book. Engineering Magazine. 8 (2014) 50–55.
- [15] A.I. Kondakov, Structural Succession and Similarity of Technological Processes, J. MSTU Bulletin. Machine Construction. 2 (1997) 89–95.
- [16] A.I. Kondakov, A.V. Zaitsev, Similarity of Components Manufacturing Unit Processes and Their Closest Analogue Processes, J. Higher Educational Institutes News. Machine Construction. 5 (2013) 39–42.
- [17] A.I. Kondakov, Forming Technologically Similar Components Groups when Assuring Full Load of Production Systems, J. MSTU Bulletin. Machine Construction Series. 3 (2001) 117–126.
- [18] A.I. Kondakov, Using Decisions Similarity when Reforming Machine Construction Production, J. Mechanical Engineer. 11 (2003) 41–46.
- [19] A.I. Kondakov, K.S. Gorlyshev, Express-evaluation of Possibility of Producing Goods in Production System with Fixed Structure, J. Machine Constructing Industry Bulletin. 5 (2002) 53–56.
- [20] A.I. Kondakov, V.V. Gali, Using Design Decisions Relations when Developing Technological Complexes, J. Reference Book. Engineering Magazine. 8 (2013) 14–17.
- [21] A.I. Kondakov, A.S. Vasiliev, Theory of Taking Design Decisions: Summary of Lectures., Moscow, Publishing House Specter, 2015.



International Conference on Industrial Engineering

Justification of an adaptive working body of a cable excavator

Isakov V.S^{a*}, Maksimov V.P., Maksimov Y.V^b.

^a *Platov South-Russian State Polytechnic University (NPI), 132, St. Prosvescheniya, Rostov region, Novocherkassk, 346428, Russian Federation*

^b *LLC "Rostselmash", Rostov-on-Don, Russia (344029, Rostov-on-Don, Menzhinsky Str. 2), Russia*

Abstract

The article deals with the advantages and disadvantages of cable backhoe excavators in comparison with the hydraulic ones. It was stated that the main cause of the slow performance of rope excavators was a rigid attachment of the bucket to the handle. The authors of the article conduct the synthesis of the structure of rotation mechanism of the bucket, which does not require additional drive. The authors also developed the design of cable excavator bucket rotation mechanism where the bucket rotation is carried out with the help of additional kinematic connection of variable length between the bucket and the handle or the bucket and the boom and implementing the internal forces due to the mutual arrangement of the boom and the arm. The authors consider the trajectory of the working process, where the rotation of the handle is carried out relative to the boom while turning the bucket relative to the handle. The parameters of the mechanism influencing the position of the bucket during the digging relative to the horizon are stated. The authors report the algorithm of search optimization of rotation mechanism geometrical parameters providing the required law of the bucket rotation with the given constraints.

© 2015 Published by Elsevier Ltd. This is an open access article under the CC BY-NC-ND license (<http://creativecommons.org/licenses/by-nc-nd/4.0/>).

Peer-review under responsibility of the organizing committee of the International Conference on Industrial Engineering (ICIE-2015)

Keywords: cable excavator, structural synthesis, the rotation mechanism of the bucket.

INTRODUCTION

Increased productivity of universal shovels is among the most important areas to increase the production efficiency of earthworks in the construction process of the structures for various purposes. Excavators with cable suspension of working equipment with their reliability, ease of maintenance, without sophisticated repair facilities, and low price for both the excavators and spare parts are also very popular among the shovels with the backhoe as a working equipment [1]. Thus cable excavators have significant advantages over the hydraulic ones working with abrasive formations and under extreme temperature conditions, proved by their exploitation experience [2, 3]. The main

*Tel +7(8635)255-649 e-mail: kafedra_sdkm@mail.ru

disadvantage of cable excavators equipped with backhoe is the decrease of performance due to the loss of soil in different parts of the working trajectory. The existence of such losses is due to the rigid mounting of the bucket to the handle. Despite the well-known attempts to eliminate this disadvantage by introducing the additional kinematic units [4], the task of ensuring the possibility of rotation relative to the handle of the bucket has not found a final decision, however, the very hypothesis of a possible control while turning the handle of the bucket by means of more rigid rod connecting the bucket and the boom is promising and needs further study.

Estimation of competitiveness of different types of shovels is based on arguments ultimately influencing on minimization of the costs. Thus, the arguments, directly connected with the performance, are considered to be defining. [5] Consequently, the preservation of the total amount of soil in the areas out of the slaughter and unloading increases efficiency and, consequently, the competitiveness of cable excavators with the backhoe working body. In this case, the source of innovation in the modernization process is to develop a scheme of additional manipulation of the bucket (including adaptation trajectory of the backhoe to external conditions both at the loading and the unloading site).

Since all single-cable excavators have a common structural scheme of backhoe working equipment, then further analysis of working processes will be carried out on the example of the most common in-class excavator ЭО-4112 with a bucket capacity of 0.65 m³. The analysis showed that at an acceptable cycle of operation equals to 18 sec., the actual operational efficiency due to the pouring out of 30% of the soil from the bucket back to the mine face is considerably lower than technical. This is due to the inability of the existing structure to ensure the rational position of the bucket relative to the horizon in all sections of the working trajectory.

Main text

The aim of the study is to substantiate and develop the structure and design of non-power mechanism providing the rotation of the bucket relative to the handle.

The structure of the rotation mechanism of the bucket, in accordance with [6], is understood as a set of elements and relations between them, i.e., a collection of links and mobile connections. In this case, the geometric structure of rotation mechanism can be described by the shape and size of its units, their location and hinge connection between them.

As a result of studying the structure of linkages it was established that the solution to the problem of the bucket rotation is possible through the use of intense loops. These mechanisms are widely presented in [6]. Further studies [7, 8] will allow solving the problem of redistribution of power factor in parallel links of mechanisms and machines, and loading the circuits in the various modes.

In [9], the authors describe a method of conceptual design of excavators working bodies on the basis of which they developed a structural scheme of the mechanism of rotation of the cable excavator bucket (Fig. 1), which is protected by the patent of the Russian Federation. [10]

A distinctive feature of the proposed structure of the rotation mechanism is alternating the use of additional kinematic connection (in the form of cylinders) of the bucket to the handle or the bucket to a boom that allows to realize the forces occurring in a closed loop boom, arm, bucket and additional cylinders to rotate the bucket relative to the handle. The presence of the structure units (cylinders) of variable length in each individual period of the cycle of operation causes the variable structure of the mechanism, the operation of which is possible only when incorporated into the structure of one of two additional bonds, while the other, excessive in this case is turned off. The units of variable length must provide intermediate fixation on the length defined by an external control. Such link has no fundamental significance in terms of its kinematic design. It can be various devices. For this particular study the choice of hydraulic cylinders (without drive) is due to a set of indicators such as minimum cost, availability of standard equipment, ease of operation, positioning accuracy, ability to control and measurement of process parameters.

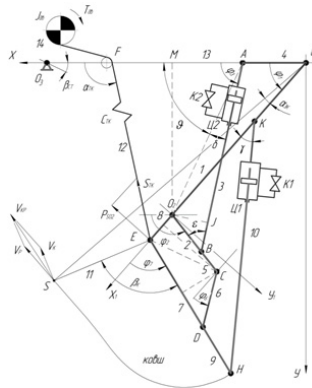


Fig.1. The scheme of the bucket rotation mechanism

The proposed mechanism of the bucket rotation consists of two adjacent four-member mechanisms: O_1ABO_2 and O_2CDE supplemented with the member KH, where the role of the fixed member for the first mechanism O_1ABO_2 (member 4) is played by the boom, and the leading element is handle 1 (member O_1O_2). Member 1 is rotated with an angular velocity ω_1 by pulling cable 12 wound on the main winch drum driven by a motor (T_{δ}). The fixed member O_2CDE for the second mechanism is a handle (member 8), and the leading is member 5 (O_2C) which is an extension of member 2 (O_2B) of first mechanism O_1ABO_2 . Members AB and KH in this mechanism are members (hydraulic cylinders without drive) of variable length, that under the control of taps K1 and K2 are able to: - fix the length of the corresponding member when the tap is closed and declutch the member from the structure as a redundant one when it's opened.

The process of digging with cable excavators with rotating bucket is characterized by a certain order; each stage of the work is completed by an event that initiates the transition. Transition is the transfer of control from one state of activity to another. Fig. 2 is a diagram of activities of the working body. Decomposition of the state of activity is carried out by the swimming paths that divide the diagram into vertical zones, each of which represents a zone of responsibility of the corresponding equipment. The line of synchronization is used for the description of parallel processes. Diagram of activities can be the basis for the creation of a control system that can adapt the work process to the specific conditions, providing the trajectory of the bucket with the maximum preservation of the soil in the bucket.

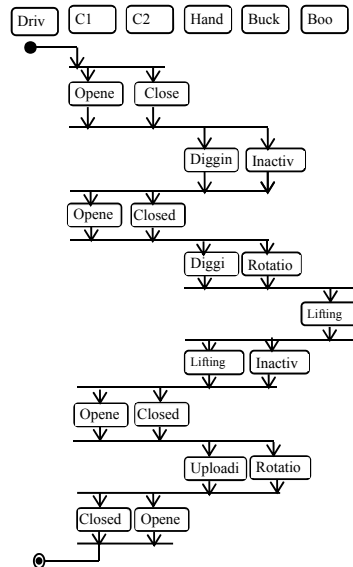


Fig. 2. Activity diagram of the working body

Obviously, the efficiency and effectiveness of the mechanism in the proposed scheme depends on a combination of

rational design (geometric) parameters of two adjacent four-member mechanisms. To determine them we need analytical parameters of the bucket rotation mechanism in a function of the angle of handle rotation (the leading member 1), which are derived from the kinematic analysis in [11].

For brevity, let's specify the length of the members as the following:

$O_1O_2 = l_1; O_2B = l_2; AB = l_3; AO_1 = l_4; O_2C = l_5; CD = l_6; ED = l_7; EO_2 = l_8; EH = l_9; HK = l_{10}; EF = l_{12}; O_1F = l_{13}; O_1E = l_{14}; ES = l_{15}$.

The length of eight members forming a steering gear ($l_1...l_8$) appears for the optimized parameters. Restrictions for parameters are determined firstly by the definite (for the particular cable excavator) sizes of boom, arm, bucket, and secondly - the sizes, providing the strength for hinge joints themselves. In this case, the task of finding a rational parameters is formulated as a problem of multiparametric constrained optimization and mathematically can be described by the expression [12]

$$J = extr(\vec{X}) = \varphi_7 = f(l_1, l_2, \dots, l_8) \rightarrow min \quad (1),$$

where (\vec{X}) - vector of controlled (optimized) parameters with imposed restrictions $\vec{\varphi}(\vec{X}) > 0$; and $\vec{\psi}(\vec{X}) = 0$. (2)

Analytical dependence obtained in [11] does not establish a direct link between controlled parameters and objective function (1) and constraints (2), making it difficult to determine the point of extremum. Search optimization should be applied in such a situation, its essence is [12] that the evaluation of the point of extremum \vec{X}^* in the range of control parameters is carried out in successive steps, leading from the starting point \vec{X}_0 through some intermediate point showing \vec{X}_k in a given ε - neighborhood of the point of extremum \vec{X}^* . The transition from point \vec{X}_k to point \vec{X}_{k+1} is one of successive steps (iterations) for calculating the values of output parameters.

After finding the set of significant solutions that conditionally characterize Pareto set we should select the final version. This latter procedure is usually performed by the decision-makers on the basis of their own experience and informal analysis.

Fig. 3 shows a flowchart of a search parameter optimization of bucket rotation mechanism.

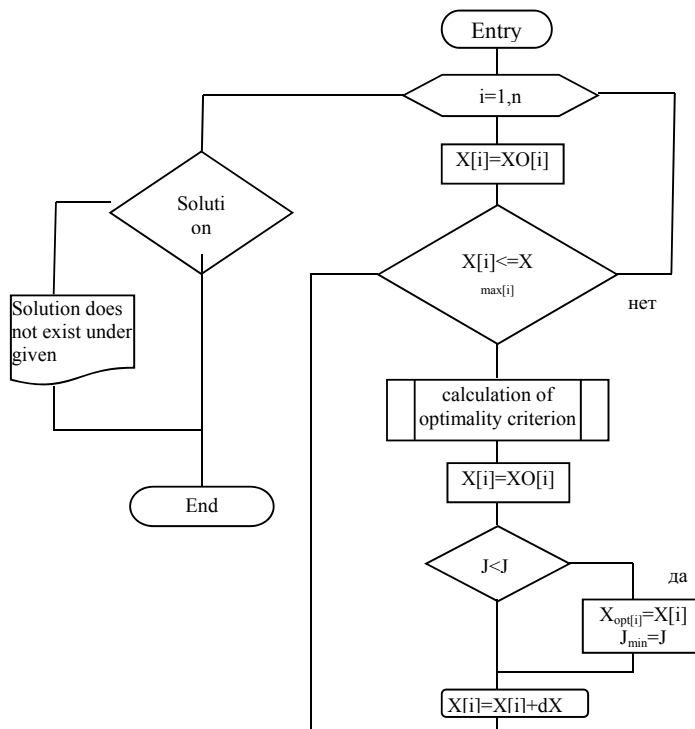


Figure 3. Control-flow chart of search optimization

The search of parameter values lying in the specified limits is realized in the cycle \vec{X}_p . The calculation of optimality criterion and the search of extreme value of the criteria is performed:

$$J = extr(\vec{X}).$$

The cycle of the point of extremum calculation is carried out in all the tolerance range with the step dX . Upon reaching the extreme value of the criteria, the parameter value of the point of extremum is stored.

With the regard to the type of excavator ЭО 4112 the range of restrictions on the amount of members in the rotation mechanism according to the diagram in Figure 1 is identified with specific dimensions: - Boom (the distance from the axis of the handle attachment to the diverting pulley traction rope); - Handle (the distance from the axis of its attachment to the boom to bucket hinge); - Bucket (the length of the upper wall, the distance from the hinge to the front edge). In this case the rotation mechanism should provide the angle of the bucket rotation equal to 90^0 ($\varphi_7^{max} = 90^0$) in the range of handle rotation angle of $90...45^0$ and efforts in member I3 (cylinder C2) must not exceed five standard units, where the unit is the digging force applied to the front edge of the bucket. The latter condition corresponds to the average values of hydraulic excavators.

Digging force is determined by the well-known formula of Dombrowsky N.G. [13] taking into account the special aspects in the process of digging with the cable excavators with rotating bucket. [14]

As a result of calculations with the help of the above mentioned algorithm, the values of rational parameters of the rotation mechanism of the bucket (l_1, l_2, \dots, l_8) are determined. The lengths of the links that define the point of attachment of link l_{10} (hydraulic cylinder) are selected constructively.

In accordance with the results of the research a special experimental setup of the working body has been designed to verify that the proposed structure of the rotation mechanism of cable excavator bucket is functional. Experiments were carried out in a specialized room of the department of "Handling, construction and road machines" in South-Russia State Polytechnical University (NPI. Main geometrical parameters of the experimental setup of the working body are corresponding parameters of the cable excavator EO-4112 in a ratio of 1:7. The conducted experimental studies confirmed its performance and high efficiency in terms of the bucket rotation and maintaining weight load in the bucket when lifting from the bottom.

Conclusion

The performed synthesis of structure and a series of experiments on the mathematical and physical models prove the performance and efficiency of the developed non-power control system of turning the rope excavator bucket.

REFERENCES

1. V.S. Isakov On the prospects of using shovels with a rope suspension / V.S. Isakov Y.V. Maksimov // New technology of motion control of technological objects: The 9th Intern. scientific and engineering. konf.- Novocherkassk: Lik, 2008. - Vol.1 - p. 59-62.
2. P.A. Chemetov Operating experience of cable and hydraulic excavators in a borrow of Muruntau [electronic resource] / P.A. Chemetov, S.K. Rubtsov A.G. Shlikov // Mining. - 2005. - № 5; - Access: URL: <http://www.mining-media.ru/ru/article/karertekh/1227-opyt-ekspluatatsii-kanatnykh-i-gidravlicheski-kh-ekskavatorov-v-usloviyakh-karera-muruntau>
3. H.R. Kölsch Predicting the resource of hydraulic pumps and hydraulic motor drives of mining shovels when operating at low temperature / H.R. Kölsch, G.S. Brodsey // Mining Equipment and Electromechanics. -2008. -№11. - p. 35-37.
- 4 V.S. Isakov Kinematics of digging shovel with rope pennant / V.S. Isakov, Y.V. Maksimov // New technology of motion control of technological objects: The 9th Intern. scientific and engineering. konf.- Novocherkassk: Lik, 2008. - Vol. 1. - p. 55-58.
5. K.P. Mandrovsky Estimation of competitiveness of construction shovels / K.P. Mandrovsky // Road Empire. - 2007. - № 5. - p. 50-52.
6. I.I. Artobolevsky Theory of mechanisms and machines: textbook / I.I. Artobolevsky. - 4th ed., rev. and add. - M.: Publishing House Alliance, 2012. - 640 p.
7. V.S. Isakov On the formation of closed strained hydromechanical circuit structures / V.S. Isakov // News of Higher Educational Institutions. North-Caucasus. region. Spec. Release. Actual problems of engineering. 2006. - p. 55-58.
8. V.S. Isakov The use of intense closed kinematic loops in the working mechanisms of excavators / V.V. Isakov Y.V. Maksimov // Modern trends of the Russian system of higher education: Mater. Conf. Tver, May 14-16, 2008 - Tver: TSTU, 2008. p. 8-9.
9. V.P. Maksimov The conceptual design of innovative working bodies of cable excavators [electronic resource] / V.P. Maksimov, Y.V. Maksimov // Don Engineering Bulletin, 2013. № 4. - Access: [htt://www/ivdon.ru/magazine/archive/n4y2013/2183](http://www/ivdon.ru/magazine/archive/n4y2013/2183).
10. RF Patent 2450106, IPC E02F 3/42. Operating equipment of bucket excavator / V.S. Isakov Y.V. Maksimov, G.M. Simileysky; 15.10.2010 stated; publ. 10.05.2012, Bull. № 13. - 8 p., II.
11. Y.V. Maksimov The kinematic study of the bucket rotation mechanism of cable excavator [electronic resource] / Y.V. Maksimov // Don Engineering Bulletin, 2013. № 4. - Access: <http://www/ivdon.ru/magazine/archive/n4y2013/2174>.
12. V.P. Tarasik Mathematical modeling of technical systems: Textbook for High Schools. - Minsk: Design PRO, 2004. - 640 p.
13. N.G. Dombrowski Escavators / N.G. Dombrowski. - M.: Engineering, 1969. - 318p.
14. Y.V. Maksimov Mathematical modeling of the digging process with cable excavators with rotating bucket [electronic resource] / Y.V. Maksimov V.P. Maksimov // Modern problems of science and education. - 2014. - № 2; - Access: URL: <http://www.science-education.ru/116-12285>.



International Conference on Industrial Engineering

Analysis of a doubly fed induction motor in electric drives of pumping stations

Bochkarev I.V.*

Kyrgyz State Technical University named after I. Razzakov, Mira av. 66, Bishkek, 720044, Kyrgyzstan

Abstract

The investigation of a doubly fed induction motor in electric drives of pumping stations is conducted in this paper. The effect of non-sinusoidal rotor supply is considered in the analysis as well. The current total harmonic distortion (THD) is evaluated with respect to the selected voltage modulation in a thyristor frequency converter (TFC) as well as on motor duty cycle. A novel method of reactive power regulation with constant rotor current $I_2=I_{2n}=\text{constant}$ is proposed. It is shown that the proposed method considerably improves motor performance in the whole operation range. The proposed analytical method is verified with laboratory measurements.

© 2015 Published by Elsevier Ltd. This is an open access article under the CC BY-NC-ND license

(<http://creativecommons.org/licenses/by-nc-nd/4.0/>).

Peer-review under responsibility of the organizing committee of the International Conference on Industrial Engineering (ICIE-2015)

Keywords: pumping station; centrifugal pump; doubly fed induction motor; slip power; frequency converter; current THD; efficiency.

1. Introduction

An uninterrupted water supply is often required for efficient and continuous work of many industrial processes. Many industries, such as metallurgical and metalworking plants, are also one of the major consumers of water. The pumping stations used for supplying water to the plants are energy-demanding and thus by improving their performance, a more efficient operation of the entire plant can be achieved.

The today's electric drives in pumping stations employ squirrel cage induction motors. Further, in the vast majority of pumping stations, the motors operate at constant speed. The power and pressure are changed by

* Corresponding author. Tel.: +0312-56-15-58.

E-mail address: elmech@mail.ru

switching on and off the pumps or by adjusting the valves. These control methods are not desirable as far as the energy efficiency of the system is concerned [1].

2. Problem description

The conducted investigation showed that the speed of pumps normally varies in the range of 50-100% of its nominal value. For this speed range, the use of doubly fed induction motors (DFIM) can particularly be advantageous for improving the system efficiency. The DFIM is a type of induction motor with wound rotor whose stator terminals are directly connected to a 6/10 kV grid, while rotor is connected to the grid through a frequency converter. In the cascade regulation, only the slip power, proportional to a DFIM slip and stator power, is being controlled. Furthermore, the inverter employed in the system operates at low voltages, i.e. below 1000 V. This can be applied in electric drives with nearly any power rating without increasing complexity of the inverter topology.

Additionally, by controlling the reactive power flow through stator, the high efficiency of an entire system can be achieved. Due to the mentioned reasons, these types of systems applied in pumps are particularly beneficial as compared to the frequency control of squirrel cage induction motors

Fig.1 depicts an electric circuit of a centrifugal pump connected to grid. The stator winding of the DFIM is directly connected to the grid, while rotor is connected through a rectifier (R), an inverter (Inv), and a step-down transformer (Tr). The step-down transformer is introduced in the system to adjust the high voltage of the grid (3.6, 10 kV) to the low-voltage supplied to the rotor winding. To smoothen the current waveform and improve operation of the inverter, an adjustable inductor AI is added between the inverter and rectifier sides of the frequency converter.

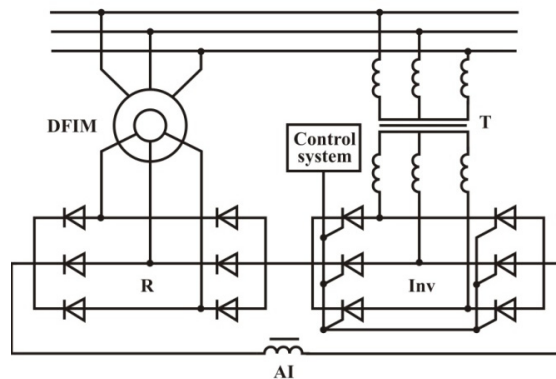


Fig. 1. An electric circuit of a centrifugal pump connected to the grid.

The rotor slip power is controlled by adjusting the back electromagnetic force (EMF) which is obtained by selecting an appropriate firing angle of thyristors β . In such a way, in the studied centrifugal pump with doubly fed induction motor, the voltage is rectified by means of a rectifier R, the waveform is further smoothened with varying inductor AI and finally modulated back a 50 Hz AC. The slip power is fed back to the grid through a transformer Tr.

Due to the applied signal modulation, the output inverter voltage contains high-order harmonics. The presence of these harmonics can lead to an increased copper and iron loss of motor as well as transformer.

This can eventually lead to the unwanted overheating and can negatively affect the entire system efficiency. To make the voltages and currents more sinusoidal, different inverter topologies can be applied (e.g. with higher number of pulses), low-pass filters, and various methods of modulation. The total harmonic distortion (THD) of current and voltage waveforms should be obtained before selection of the modulation method. The most common duty cycle of a motor in the centrifugal pump is a continuous cycle with nearly constant load. Therefore, the conducted investigation covers only the steady state conditions of the motor and converter.

3. Result discussion

The frequency, phase and voltage amplitude control can be realized in power converters employing fully-controlled thyristors. Pulse width modulation (PWM) is one of the most common methods to control the output voltage. In this arrangement the switching function of the thyristors are modulated, rather than input voltage as in a typical PWM regulation [2]. To make distinction, this modulation method is referred to as PWMS.

The Fourier transformation is applied to derive analytical expressions describing currents in DFIM.

In [3] the output voltage U_2 of the frequency converter with PWMS is defined as

$$U_2 = \frac{3\sqrt{3}}{\pi} U_{p.m} \left[\frac{r}{2} \sin \omega_2 t + \sum_{k=1}^{\infty} (-1)^{Pk} \frac{\cos[(Pk \pm 1) \arccos(\frac{r}{2})]}{Pk \pm 1} \sin [Pk \omega_1 + (Pk \pm 1) \omega_2] t \right] \tag{1}$$

where $U_{p.m}$ – peak voltage of U_2 ; P – the number pulsation of the frequency converter; ω_1, ω_2 – input and output frequency on the frequency converter; $r = 2\pi U_2 K_T / (3\sqrt{3} U_1)$ – depth of voltage regulation; K_T – transformation ratio of a transformer.

The amplitude of the first harmonic of the output voltage is defined as

$$A_1 = \frac{3\sqrt{3}}{\pi} U_{p.m} \frac{r}{2}. \tag{2}$$

Fig. 2 depicts the variation of the output voltage of the frequency converter with time. Further, the input voltage of the power converter can be represented as a vector in the synchronous coordinate system. The following is defined:

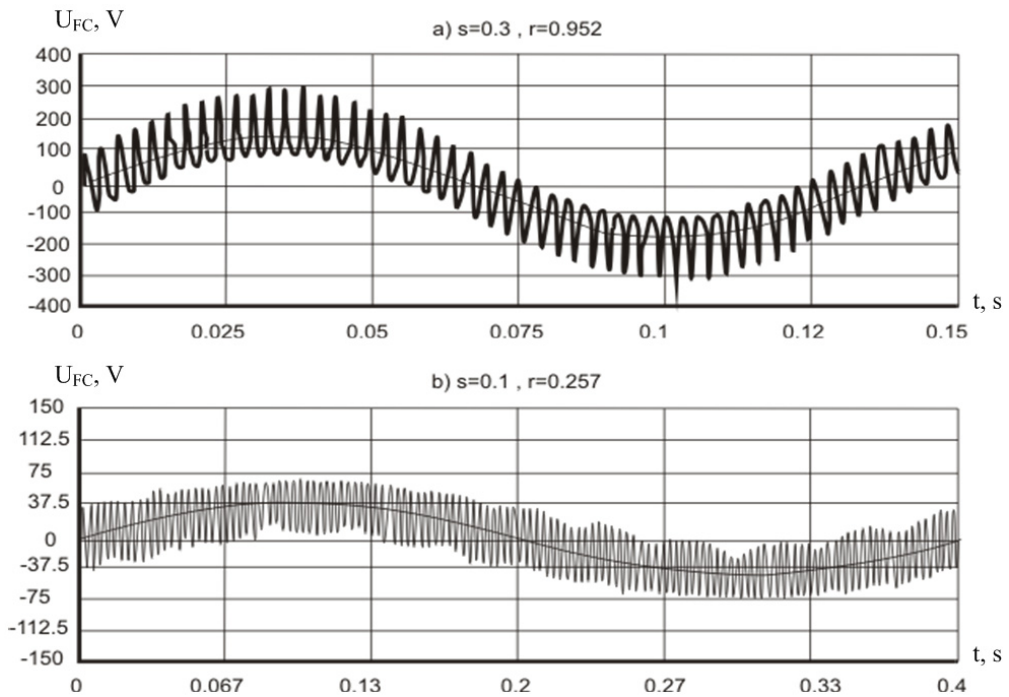


Fig. 2. Output voltages in power converter in various modes of operation of a centrifugal pump.

$A_{pn} = \frac{3\sqrt{3}}{\pi} U_{p.m} (-1)^{Pn} \frac{\cos[(Pn+1)\arccos(\frac{r}{2})]}{Pn+1}$; $A_{nm} = \frac{3\sqrt{3}}{\pi} U_{p.m} (-1)^{Pn} \frac{\cos[(Pn-1)\arccos(\frac{r}{2})]}{Pn-1}$ - magnitudes of voltage harmonic of a positive sequence (with frequency $Pk\omega_1 + (Pk+1)\omega_2$) and negative sequence (with frequency $Pk\omega_1 + (Pk-1)\omega_2$).

Then the projections on the synchronous axes x, y of the voltage vector of U_2 can be obtained as

$$\begin{cases} U_{2x} = \sum_{n=1}^{\infty} (A_{pn} + A_{nm}) \sin[Pn(\omega_1 + \omega_2)t] \\ U_{2y} = -A_1 - \sum_{n=1}^{\infty} (A_{pn} - A_{nm}) \cos[Pn(\omega_1 + \omega_2)t] \end{cases} \quad (3)$$

As the power rating of the motors used in the pumping stations is usually quite high, the phase stator winding resistance can be neglected $r_1 = 0$. In (3), the projections of the current vector on synchronous axes is defined as:

$$i_{1xp} = -k_s \sum_{n=1}^{\infty} \frac{A_{pn}}{r_2^2 + \omega_{2pn}^2 L_2^2 \sigma^2} [r_2 \sin(Pn(\omega_1 + \omega_2)t) - \omega_{2pn} L_2 \sigma \cos(Pn(\omega_1 + \omega_2)t)]$$

$$i_{1xn} = -k_s \sum_{n=1}^{\infty} \frac{A_{nm}}{r_2^2 + \omega_{2nm}^2 L_2^2 \sigma^2} [r_2 \sin(Pn(\omega_1 + \omega_2)t) + \omega_{2nm} L_2 \sigma \cos(Pn(\omega_1 + \omega_2)t)]$$

$$i_{1yp} = k_s \sum_{n=1}^{\infty} \frac{A_{pn}}{r_2^2 + \omega_{2pn}^2 L_2^2 \sigma^2} [\omega_{2pn} L_2 \sigma \sin(Pn(\omega_1 + \omega_2)t) + r_2 \cos(Pn(\omega_1 + \omega_2)t)]$$

$$i_{1yn} = k_s \sum_{n=1}^{\infty} \frac{A_{nm}}{r_2^2 + \omega_{2nm}^2 L_2^2 \sigma^2} [\omega_{2nm} L_2 \sigma \sin(Pn(\omega_1 + \omega_2)t) - r_2 \cos(Pn(\omega_1 + \omega_2)t)]$$

where L_2 – equivalent rotor inductance.

The projection of the rotor current vector is defined as:

$$i_{2xp} = \sum_{n=1}^{\infty} \frac{A_{pn}}{r_2^2 + \omega_{2pn}^2 L_2^2 \sigma^2} [r_2 \sin(Pn(\omega_1 + \omega_2)t) - \omega_{2pn} L_2 \sigma \cos(Pn(\omega_1 + \omega_2)t)]$$

$$i_{2xn} = \sum_{n=1}^{\infty} \frac{A_{nm}}{r_2^2 + \omega_{2nm}^2 L_2^2 \sigma^2} [r_2 \sin(Pn(\omega_1 + \omega_2)t) + \omega_{2nm} L_2 \sigma \cos(Pn(\omega_1 + \omega_2)t)]$$

$$i_{2yp} = -\sum_{n=1}^{\infty} \frac{A_{pn}}{r_2^2 + \omega_{2pn}^2 L_2^2 \sigma^2} [\omega_{2pn} L_2 \sigma \sin(Pn(\omega_1 + \omega_2)t) + r_2 \cos(Pn(\omega_1 + \omega_2)t)]$$

$$i_{2yn} = -\sum_{n=1}^{\infty} \frac{A_{nm}}{r_2^2 + \omega_{2nm}^2 L_2^2 \sigma^2} [\omega_{2nm} L_2 \sigma \sin(Pn(\omega_1 + \omega_2)t) - r_2 \cos(Pn(\omega_1 + \omega_2)t)]$$

Inversed transformation of the derived equations gives the instantaneous values of the DFIM currents in the real coordinate systems. In Fig. 3 the stator and rotor currents of a DFIM employed in a centrifugal pump with power

frequency and PWM is shown (with slip $S = 0,3$ and depth of voltage regulation $r = 0,95$). The calculations are conducted for a 6-puls power converter. The electrical motor considered in the analysis is a doubly fed induction motor, which is based on an induction motor AK-13-59-94 rated $P = 1200$ kW, $U = 3000$ V, $n_l = 1500$ rpm.

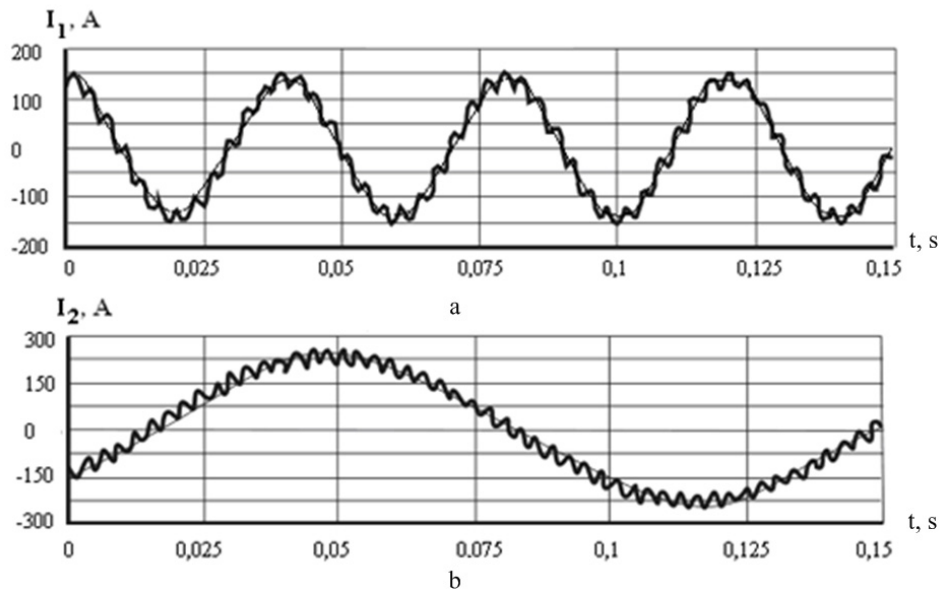


Fig. 3. Stator (a) and rotor (b) currents of the DFIM when supplied through power converter with PWM regulation.

The harmonic content and the magnitudes of high-harmonic currents to large extent are decided by the slip, depth of regulation of the first harmonic voltage, or in other words, by the control parameters of the DFIM: voltage U_2 and phase δ , which are supplying the rotor through frequency converter. Usually, the voltage vector U_2 is lagging voltage U_1 by angle δ . Then the voltage components can be defined as:

$$U_{1x} = U_1; \quad U_{1y} = 0; \quad U_{x2} = U_2 \cos \delta; \quad U_{y2} = U_2 \sin \delta. \quad (4)$$

The conducted analysis has shown that the DFIM can normally be regulated by the following rules:

- reactive power on the stator side is equal to zero $Q_1 = 0$. The benefits of this method can be explained as follows: as the slip frequency f_s much smaller than the grid frequency f_l , then for the same flux density the power needed on the rotor side much smaller as compared to the stator;
- reactive power consumed on the rotor side is equal to zero $Q_2 = 0$. The most evident advantage of this method is that the frequency converter can be selected with the smallest rating possible;
- minimizing the electromagnetic power losses in the system $\Delta P = \min$. This method is achieved by controlling the reactive component of the rotor and stator currents.

The values of U_2 and δ , which corresponds to a given operation mode can be defined by solving equations for active and reactive components of the currents as well as the electromagnetic torque in DFIM. For example, to satisfy condition at which the stator reactive power is equal to zero $Q_1 = 0$, the values U_2 and δ can be derived by solving the equation for the imaginary part of the stator current $I_{1y}(U_2, \delta, s) = 0$ with the electromagnetic torque defined according to [4]:

$$M = \frac{C_n H_c + \left(\frac{1-s}{1-s_n} \right)^2}{\eta_{TM}(\omega, H_c)} \sqrt{1 - \frac{H_c}{H_0} \left(\frac{1-s_n}{1-s} \right)^2}, \quad (5)$$

where H_c – pumping pressure head, which equals to the pressure drop between the inlet and outlet of the pipe; H_0 – the pump head when the valve is closed $Q = 0$; $C_n = 1 - 1/H_0$ – coefficient; s – rotor slip; $\eta_{TM}(\omega, H_c)$ – efficiency; ω – angular frequency of the pump in relative units.

By solving these two equations together, the values U_2 and δ , which satisfy the requirements in terms of pressure head and reactive power Q_l can be found.

In DFIM, for the same flux density the power from rotor side is needed much smaller as compared to the stator. Therefore, one more way to control reactive power that assures the highest system efficiency of the centrifugal pump for all duty cycles can be defined. This can be achieved by keeping the rotor current equal to its nominal value: $I_2 = I_{2n} = \text{constant}$. To achieve that the reactive rotor current I_{2y} should satisfy the following condition for whole frequencies

$$I_{2y} = \sqrt{I_{2n}^2 - I_{2x}^2}, \quad (6)$$

where I_{2x} – active component of the rotor current.

The current THD is calculated for all operational frequencies in order to determine the influence that non-sinusoidal output voltage of the frequency converter has on entire as shown in Fig. 4. The THD value K_u in the frequency interval varies from 0,990 to 0,998, which is much smaller as compared to rectangular modulation of the output voltage of the frequency converter.

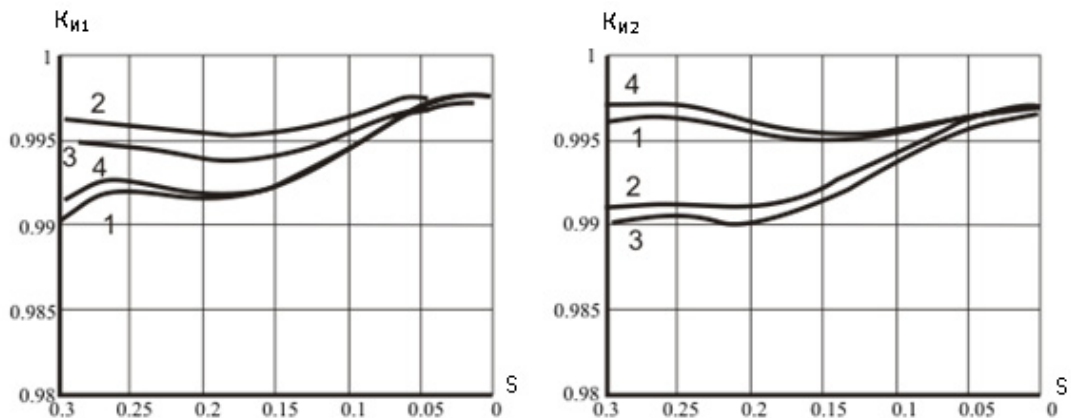


Fig. 4. Stator current THD (a) and rotor current THD (b) with PWM: 1 – $Q_l = 0$; 2 – $Q_2 = 0$; 3 – $\Delta P = \min$; 4 – $I_2 = I_{2n}$.

Therefore, it is confirmed that for such a low current THD has a negligible effect on system efficiency.

Due to interaction of the main magnetic flux of the machine with the fluxes created by the high-frequency components of the rotor current at PWM regulation, the torque ripple are produced. It is possible to obtain the torque ripple by considering only interaction of high-frequency components with the fundamental components. The results of conducted analysis are summarized in Fig. 5.

The electromagnetic torque pulsations with PWM has a more advanced harmonic content, but their frequencies $Pk\omega_1 + (Pk \pm 1)\omega_2$ are much higher as compared to the rectangular voltage modulation. The most significant harmonics with the 6-pulse frequency converter have frequency of 600 Hz, which are damped by the motor inertia, even at no load.

To confirm the obtained analytical expressions, the results have been confirmed with laboratory measurement. The measurement results are summarize in Fig. 6. The DFIM is made of an induction motor with wound rotor AOK2-51-6 rated 4 kW, nominal speed 950 rpm, with a possibility for dual supply. The efficiency measurements are shown in Fig. 6. It can be observed that the difference between calculated and measured values does not exceed 11%, which can suggest the obtained results for practical implementation.

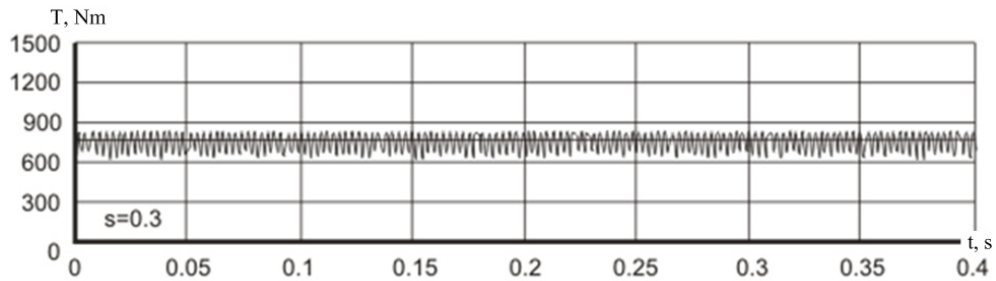
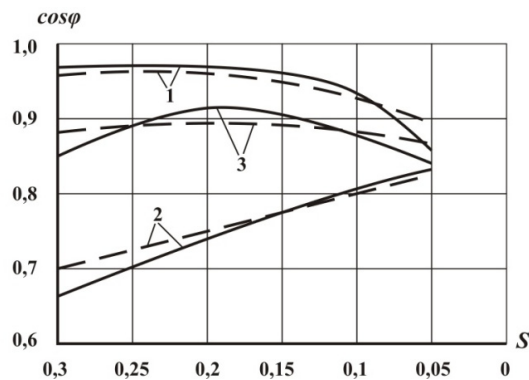


Fig. 5. Pulsating electromagnetic torque in DFIM.

Fig. 6. Efficiency: 1 – $I_2 = I_{2n} = \text{constant}$; 2 – $\Delta P = \text{min}$; 3 – $Q_1 = 0$; (____ analytical values; ---- experimental values).

4. Conclusions

1. The more effective operation of centrifugal pumps can be achieved by replacing the outdated electrical motors with modern motors that have higher efficiency and which can regulate the head pressure of a pump by controlling their rotation speed. One of the potential motor technologies in centrifugal pumps can be considered the doubly fed induction motor (DFIM).

2. The high harmonics of the rotor currents due to the operation of a frequency converter with fully-controlled thyristors have generally rather limited effect on motor efficiency and torque ripple.

3. The highest system efficiency of the DFIM in the whole operation range of the centrifugal pump is achieved by keeping the rotor current constant and equal to its nominal value: $I_2 = I_{2n} = \text{constant}$.

References

- [1] B.S. Leznov, Energy saving and regulated in the electric pump and blower systems, Moscow: Energoatomizdat, 2006, 360 p.
- [2] E.E. Parfenov, Features of electromagnetic processes, calculation of parameters and characteristics of the controlled electrical machines, asynchronous valve cascade, Research turbo- and hydro generators, Leningrad: Nauka, 1976, pp.146–154.
- [3] O.Z. Popkov, Basics converters. Stand-alone inverters, Moscow: MEI Publishing, 2003, 64 p.
- [4] I.V. Bochkarev, K.K. Kelebaev, Energy characteristics of double engine power to drive centrifugal pumps, Problems of Automation and Control: Scientific and technical journal, National Academy of Sciences. – Bishkek: Ilim, 2010, pp. 149–153.



International Conference on Industrial Engineering

Development of control algorithms in Matlab/Simulink

Martyanov A.S.*, Solomin E.V., Korobatov D.V.

South Ural State University, 76, Lenin Avenue, Chelyabinsk, 454080, Russian Federation

Abstract

The progress in the development of computing machinery and software leads to new opportunities in design and research of different hardware. One of the popular instruments for scientists and engineers is MATLAB/Simulink software package which allows not only making complex mathematical calculations but also various hardware simulations. Simulink library contains a wide spectrum of computer devices and modules models. However, the existing data bank content in some cases does not correspond with the software user requirements. The present paper describes the opportunities of MATLAB/Simulink resources expansion by building extra computer models based on S-Function module usage.

© 2015 The Authors. Published by Elsevier Ltd. This is an open access article under the CC BY-NC-ND license (<http://creativecommons.org/licenses/by-nc-nd/4.0/>).

Peer-review under responsibility of the organizing committee of the International Conference on Industrial Engineering (ICIE-2015)

Keywords: MATLAB, Simulink, S-Function, simulation, control system.

1. Introduction

Digital control systems prevalence more and more in the World. At the same time, engineers and scientists develop and improve such aids of design and analysis as software support for mathematic modeling and computational analysis, high-level languages, software development as well as hardware-controlled capabilities of computing machinery.

The usage of simulation approaches on the R&D stage of control system development enables not only the significant shortage of research, development and experiment expenses but reduces the development time.

Today there are many software packages intended for simulation (MATLAB, Scilab, VISSIM) [1]. However, there is a lack of computation models and approaches that would simplify the research of features of the machinery

* Corresponding author.

E-mail address: martyanov_andrey@mail.ru

on the early stages of its development [2].

2. Problem definition

Research of the development process efficient improvement and development of complex object control systems with the help of mathematic modelling, numerical methods and software packages using the multipurpose controller as a sample [3,4]. The system model should support the programming with the high-level language to provide the transferability of control program on the target system. The widely distributed and well known by scientists and engineering organizations MATLAB/Simulink software package for mathematic computation from Mathworks Incorporation, is used as the instrument for research and development [5,6].

3. Theoretical base

MATLAB solver is a component of the Simulink software solver. The Simulink buildup for the solver was developed by Mathworks Incorporation to simplify the modeling process of different systems. This product provides an extensive library of solvers, each of which determines the time of the next simulation step and applies numerical methods to make mathematic operations with different objects (numbers, vectors, matrices) as well as to solve the sets of ordinary differential equations that represent the model. In the process of solving this initial value problem, the solver also satisfies the accuracy requirements specified by operator. In addition, the Simulink library provides the big library of different device models with mathematic description documentation. However during the development of control system not only control object models are required, but also the model of controlling device which complexity varies from task to task which in turn generates a challenge of universal approach for the development of controlling device model. The building structures could be simplified significantly in this case and would not contain the long line of repetitive blocks [7, 8].

Operator may generate individual blocks and combine them in libraries for the further usage in Simulink. There are generally two approaches: graphical and programming. Graphical approach allows the building of the model from standard Simulink blocks for simulating the control system functions [9]. This approach is not universal [10-12], as the transfer of the development results on the target control system requires time-consuming operations for adaptation of developing control device features to the results of computer model built. Programming approach is more universal due to the capability of building a computer model of the device, which is based on the features, and algorithms of control device operation [13, 14]. In turn the operation of this device should be supported by the software written on the high-level language suitable both for computer model control and target device.

The task is to build a user block simulating the operation of control system in accordance with the built-in algorithm using the programming code of target system with microprocessor control

Experimental procedure The S-Function block is provided by Simulink for capability of building the user block with different properties. This block should be supplied with the description of its operation and associated with the program written on the high-level language. The description of the operation of the block could be made on “C” language which will allow a simple transfer of this program on the target device.

As a sample of building a computer model with the help of S-Function, we used a battery charger. The general view of the model is presented on Fig.1.

The model contains the following main blocks:

3 phase source – three phase electric energy source for charging device;

3 phase load – block simulating the loading of electric grid and containing current and voltage sensors for each phase, and controlled resistors for loading simulation;

Controller – block with the functions of battery charger controller, containing S-Function block communicating with control program on the high-level language;

Battery array – the array of battery elements simulating the behaviour of a real battery and generating a signals carrying information about the battery status for charging controller;

Scope – software-based oscilloscope for registering different signals during numerical experimental testing;

Solver Configuration – block of numerical experiment parameter adjustment required for correct models

operation.

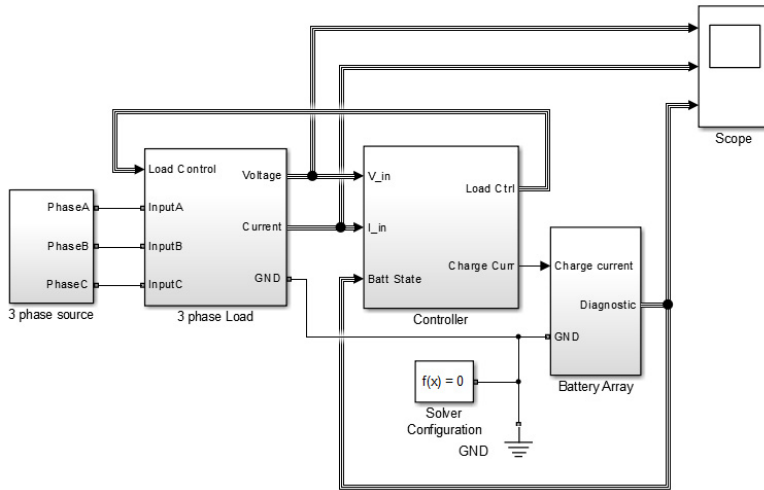


Fig. 1. General view of the model.

Thereby the base of controlling device is the «Controller» block receiving the measured system parameters from sensors and forming the control signals. The structure chart of this block is presented on Fig. 2.

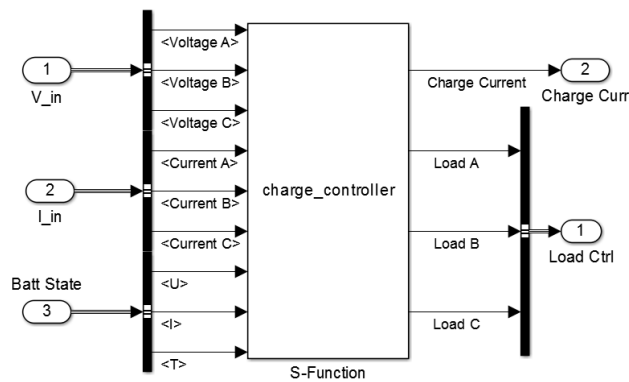
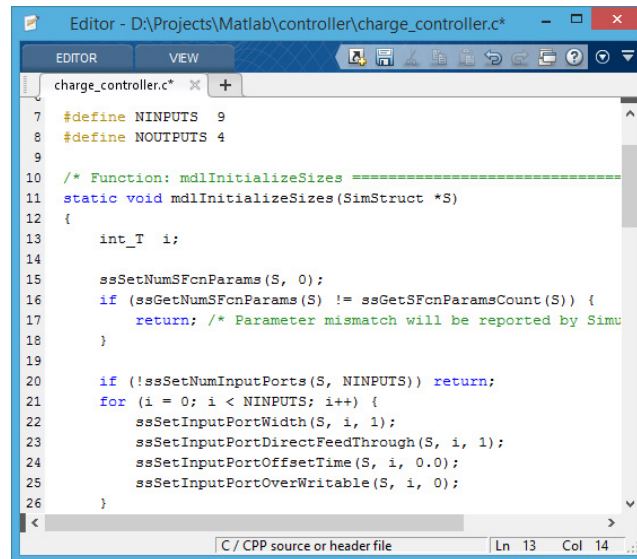


Fig. 2. Structure chart of control device.

The structure chart of control device shows that the controlling device is based on the S-Function block built with the help of software written on the high-level language.

MATLAB/Simulink software environment has the built-in file editor for editing the source text of the initial software without using the off-site programs. The editor window is presented on Fig.3.



```

Editor - D:\Projects\Matlab\controller\charge_controller.c*
charge_controller.c* x +
7 #define NINPUTS 9
8 #define NOUTPUTS 4
9
10 /* Function: mdlInitializeSizes =====
11 static void mdlInitializeSizes(SimStruct *S)
12 {
13     int_T i;
14
15     ssSetNumSFcnParams(S, 0);
16     if (ssGetNumSFcnParams(S) != ssGetSFcnParamsCount(S)) {
17         return; /* Parameter mismatch will be reported by Simu
18     }
19
20     if (!ssSetNumInputPorts(S, NINPUTS)) return;
21     for (i = 0; i < NINPUTS; i++) {
22         ssSetInputPortWidth(S, i, 1);
23         ssSetInputPortDirectFeedThrough(S, i, 1);
24         ssSetInputPortOffsetTime(S, i, 0.0);
25         ssSetInputPortOverWritable(S, i, 0);
26     }

```

Fig. 3. Program text editor window.

The text of the program presents the C-code containing “C” language operators and functions as well as a callback-functions with macro commands communicating with Simulink data types and running the commands and functions of this package. The callback functions data are activated not by C-file itself but with Simulink environment. Macro commands of callback functions have a prefix “ss” and directed on the operation with the SimStruct structure containing all information used for modelling. These macro commands support the communicating of the program with the computer model during the numerical experimental testing. In addition to the callback functions C-file may contain the instructions activating the interface functions available in Matlab package. These operations are controlled by functions with “mex” prefix.

4. Results and conclusions

The usage of S-Function technology may help to build any required block which logic and operation algorithm is written on the high-level language. The part of code, describing the block operation, may be transferred on the target system, which simplifies the development of software of control system operating under microprocessor control.

The proposed approach of S-Function block usage is being universal for building any block for computer model, without limitation of researcher or developer by the finite Simulink library block set.

The given approach helps to increase the efficiency of the process of design and development the control systems of complex objects using the mathematic modelling, numerical methods and software packages.

The practical result of the research is the computer model of the multi-functional battery-charging device intended for the virtual testing of control system parameters under different charging strategies and control algorithms.

Research was supported in part by R.F. Ministry of Education under Grant 14.577.21.0154 dated of 28.11.2014 (unique identifier is RFMEFI57714X0154).

References

- [1] V.P. D'yakonov, VisSim + Mathcad + MATHLAB. Vizual'noe matematicheskoe modelirovanie, SOLON-Press, Moscow, 2004.
- [2] A.S. Mart'yanov, E.V. Solomin, Razrabotka matematicheskoy modeli vetroenergeticheskoy ustanovki moshchnost'yu 3 kVt proizvodstva OOO «GRTs-Vertikal' v pakete Matlab, Al'ternativnaya energetika i ekologiya, NIIES. 5 (2011) 41–44.
- [3] A.S. Mart'yanov, E.V. Solomin, Kontroller zaryada vetroenergeticheskoy ustanovki, Mezhdunarodnyy nauchnyy zhurnal «Al'ternativnaya energetika i ekologiya». 1(81) (2010) 106–109.

- [4] A.S. Mart'yanov, Regulirovanie moshchnosti v vetroenergeticheskoy ustanovke, Nauchnyy poisk: materialy tret'ey nauchnoy konferentsii aspirantov i doktorantov. *Tekhnicheskie nauki*. 2 (2011) 206–209.
- [5] I.M. Kirpichnikova, A.S. Mart'yanov, E.V. Solomin, Modelirovanie generatora vetroenergeticheskoy ustanovki, *Elektrotehnika*. 10 (2013) 46–49.
- [6] A.S. Mart'yanov, Modelirovanie potrebleniya elektroenergii, Nauka YuUrGU: materialy 65-oy Nauchnoy konferentsii. *Sektsiya tekhnicheskikh nauk*. (2013) 174–177.
- [7] V.I. Karlashchuk, Universal'noe zaryadnoe ustroystvo dlya li-ion akkumulyatorov, *Vestnik rossiyskogo universiteta druzhby narodov. Seriya: Inzhenernye issledovaniya*. (2014) 22–26.
- [8] D.N. Ovsyannikov, V.N. Oskolkov, Razrabotka struktur skhem zaryadnykh ustroystv model'nogo ryada, *Vestnik permskogo natsional'nogo issledovatel'skogo politekhnicheskogo universiteta. Seriya Elektrotehnika, informatsionnye tekhnologii, sistemy upravleniya, Permskiy natsional'nyy issledovatel'skiy politekhnicheskiiy universitet*. (2012) 262–266.
- [9] J. Yan, G. Xu, H. Qian, Model Predictive Control-Based Fast Charging for Vehicular Batteries, Shenzhen Institutes of Advanced Technology. The Chinese Academy of Science. Shenzhen. *Energies*. 4 (2011) 1178–1196. DOI:10.3390/en4081178.
- [10] J. Deng, C.C. Mi, R. Ma, S. Li, Design of LLC Resonant Converters Based on Operation-Mode Analysis for Level Two PHEV Battery Chargers. *IEEE/ASME Transactions on Mechatronics*. (2014). DOI: 10.1109/TMECH.2014.2349791.
- [11] S.Q. Ali, D. Mascarella, G. Joos, Integrated battery charger for delta connected machines in plug-in hybrid electric vehicles, Conference Paper, Electrical and Computer Engineering Department, McGill University Montreal, Canada. IEEE Peterborough Section, IEEE Toronto Section Publisher: Institute of Electrical and Electronics Engineers Inc. DOI: 10.1109/CCECE.2014.6901072.
- [12] M.A. Tabari, A. Yazdani, Stability of a dc distribution system for power system integration of plug-in hybrid electric vehicles, *IEEE Transactions on Smart Grid*. 5(5) (2014) 2564–2573. DOI: 10.1109/TSG.2014.2331558.
- [13] Y. Huang, J.J. Ye, X. Du, L.Y. Niu, Simulation study of system operating efficiency of EV charging stations with different power supply topologies, Conference Paper, *Applied Mechanics and Materials*. 494-495 (2014) 1500–1508. DOI: 10.4028/www.scientific.net/AMM.494-495.1500.



International Conference on Industrial Engineering

Wind turbine asynchronous generator control algorithms

Smolin V.I., Topolskaya I.G.*

South Ural State University, 76, Lenin Avenue, Chelyabinsk, 454080, Russian Federation

Abstract

The aspects of mass usage of 7-15 meters diameter wind turbines (WT) on 5-15 kW uninterrupted power supply in the continental region conditions at 3-10 m/s dominant wind speeds and 4-6 m/s average annual wind speed is discussed. A method of generating the desired power characteristics of WT, taking into account the differential chart of wind flow distribution and electric energy consumption structure is proposed. We have studied the control algorithms of frequency-controlled asynchronous generator wind turbine to provide the braking of rotor in the modes of partial loading, stabilizing the nominal power and full stop. The approach is illustrated by the analysis of combined mechanical characteristics of the wind turbine and the generator. We discuss the control system of a wind turbine with gain-frequency control of the generator and automatic distribution of generated power between the consumers of self-contained power grid and the static energy storage. We propose the methods of optimization for the generator operating modes based on the theory of three phase electromechanical converters generalized energy flow theory.

© 2015 The Authors. Published by Elsevier Ltd. This is an open access article under the CC BY-NC-ND license (<http://creativecommons.org/licenses/by-nc-nd/4.0/>).

Peer-review under responsibility of the organizing committee of the International Conference on Industrial Engineering (ICIE-2015)

Keywords: wind turbine, self-contained power grid; uninterrupted power supply; asynchronous generator; algorithms gain-frequency control; electric energy balance control.

1. Introduction

The medium and large power modern wind turbines (WT) are being developed on high nominal wind speed $V_{0N} = 11...13$ m/s, typical for the coastal regions [1...6]. However the continental part of Russia is limited by 3...10 m/s dominant annual wind flow range in the most regions, and average annual wind speed doesn't exceed 4...6 m/s [7, 8]. Since the wind energy depends on the third wind speed degree, these WT cannot operate efficiently

* Corresponding author. Tel.: +7-904-978-03-30.

E-mail address: topolskaiaig@susu.ac.ru

everywhere. The mass application in Russia could be forecasted for autonomous WT with 7...15 meters diameter, generating $P_N = 5...15$ kW nominal power [7] on the areas of low wind speeds, providing uninterrupted power supply of consumers [9, 10] together with energy static storage (GB). Actually, the talk is about the back off to the wide usage of power devices with outline dimensions of wind-mills, but developed on principally new base for the small energy demands.

Autonomous WTs have as a rule, limited abilities of getting and flattening the impulse energy flow. To support the grid power on nominal level, it's necessary for WT parameters and control system to meet the requirements of providence the positive energy balance in accordance with the differential characteristics of local area wind flows as well as consumption structure. Let's discuss the said problem in more details.

2. Theory

2.1. Desired Power Characteristic of Wind Turbine

On Fig. 1 we showed a differential characteristic of wind flow, typical for earlier mentioned continental regions.

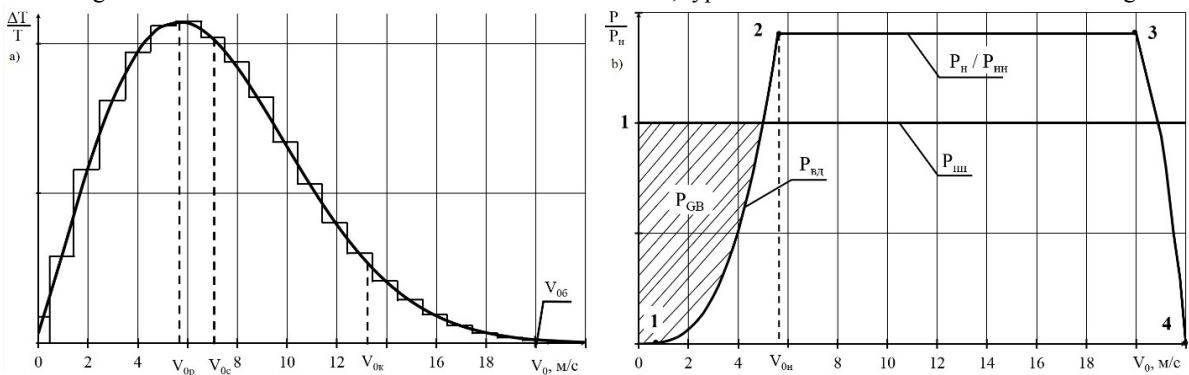


Fig. 1. Characteristic of WT: a — differential characteristic of wind flow; b — desired power characteristics: P_{nn} — autonomous grid, $P_{n\lambda}$ — wind turbine, P_{GB} — accumulating batteries; V_{0p} , V_{0c} , V_{0k} , V_{06} — operating, average, root-mean-cube and cut off speeds.

It could be determined experimentally in the place of estimated WT location with the help of wind speed sensor equipped by electronic clocks. The clock measure and accumulate the timing intervals $\Delta T_i / T$, during which the wind speed is within the appropriate range $V_{0i} + \Delta V_i$ within the period of research T [11]. Differential characteristic helps to estimate objectively the season and annual distribution of wind flows and experimentally determine the operating, average, root-mean-cube and/or cut-off speed [12].

Let's consider that the integral chart of electric energy consumption of some company during the research period T , contains the constant component P_{nn} . This part of energy could be selected as a nominal for autonomous local grid of WT. The company should get the missing electric energy from backbone network grid. We predict that the energy generated by WT, would be less expensive and the payback period is acceptable.

Power characteristic of WT (Fig. 1b) should meet the statistic distribution of local wind flows. Nominal speed of rotor V_{0h} could be selected from the range $V_{0p} \dots V_{0c}$. Reduction of nominal speed relatively the operating one, may lead to significant increase of rotor diameter, and economically failing increase of capital and operating expenditure comparing with the battery price benefits. The tasks of providing the resource and protection of wind rotor (WR) to be solved in power stabilizing mode on P_n level and in-time cut off (stop of WR). The selection of cut off (storm) speed V_{06} should be justified by differential characteristic of wind flows. The power P_{GB} in calm area is provided by GB discharge. The charge should return back on wind speeds exceeding V_{0h} . Energy balance of autonomous grid on partial loading modes (1-2) is provided by combined operation of WT and GB: $W_{nn} = W_{GB} + W_{WT}$. In nominal power stabilizing modes (2-3) the WT operates as a sole energy source: $W_{WT} = W_{nn} + W_{GB}$. In the modes (3-4) of short time storm wind speeds the electric supply of autonomous grid is provided by discharge of GB: $W_{nn} = W_{GB}$. Accumulating

batteries shouldn't be progressively discharged during the WT usage. Deficit of charge could be determined daily, weekly, monthly, depending on the type of GB and under the condition that battery state of charge will be recovered. The system of GB recharge should provide the automatic refilling of energy in backbone network grid failure situations.

2.2. Mechanical Characteristics of Wind Rotors

WT rotors are being described in most papers by aerodynamic characteristic in the form of dependences of relative rotating torque \bar{M} and power coefficient C_p on rotor tip speed ratio Z [13, 14]. Electromechanical energy converters are presented as a rule, by mechanical characteristics in the form of dependences of rotating or braking torque on angular velocity [15]. To comprehensively analyse the WT rotor it's necessary to cast the characteristics of devices to the same base, for instance by re-calculating the aerodynamic characteristics of WR to mechanical characteristics of electric generator. The sample of such re-calculation based on aerodynamic characteristics data of four bladed WR [13], is presented in Fig. 2.

Relative angular velocity of non-loaded WR when $V_{0H} = \text{const}$, is taken as one. Under the load the velocity of WR will decrease and in critical mode (Ω_k, \bar{M}_k) the action of aerodynamic forces is qualitatively changing. Further braking of the WR causes the reduction of braking torque and WR stops (\bar{M}_0 — initial or starting torque). Power characteristic of WR has the demonstrable maximum, which could be a base for nominal power P_H determination. Relative angular velocity of WR in the mode of normal loading $\Omega_n = 0,5...0,6$ is closed to theoretical, equal $2/3$.

Let's get back to the WT characteristics (see Fig. 1). The task of WT operation efficiency increase in mode (1-2) of low wind potential, can be solved by improvement of aerodynamic characteristics of WR and duty optimizing of generator power take off. The extremum on power characteristic of WR, causes the determined preconditions for generator control by criteria of maximum power take off. Characteristics of WR in low speed wind flow range, are shown in Fig. 3.

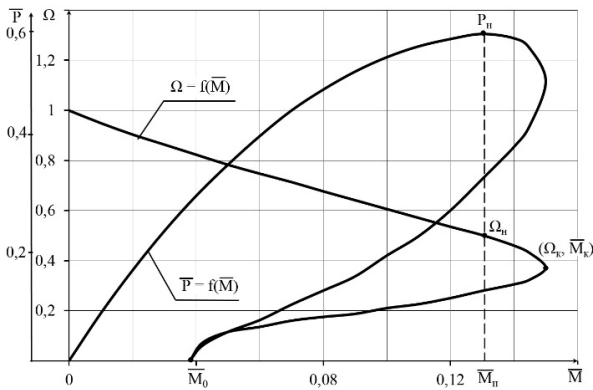


Fig. 2. Dependence of angular velocity $\Omega = \omega_0/\omega$ and power $\bar{P} = \Omega \cdot \bar{M}$ on torque \bar{M} of four bladed WR on $V_{0H} = \text{const}$: ω_0, ω — angular velocities in idling mode and loaded WR.

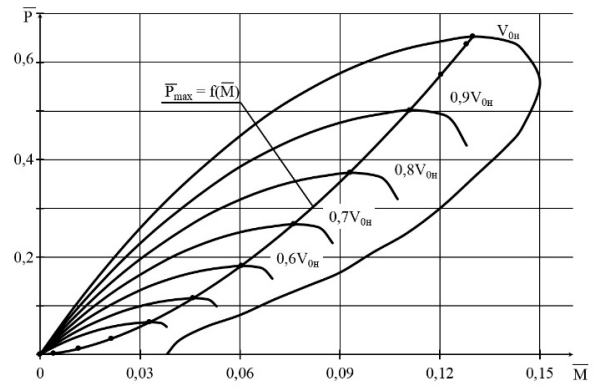


Fig. 3. Dependence of WT relative power on torque \bar{M} on small wind speeds.

The re-calculation of these values from nominal characteristic (V_{0H}) on another (V_{0i}) was made in assumption that the power coefficient C_p is constant and the incoming flow is reducing in a cubic dependence on wind speed: $P_{0i} \approx V_{0i}^3$. Extremums of power characteristics allow determining the function of optimal control $\bar{P}_{max} = f(\bar{M})$. Information data base of generator control is enough to determine the electromagnetic torque by algorithmic method [16, 17], based on the control of energy conversions in electric machine. Using this approach we can avoid the application of expensive sensors of braking torque. The task would be even more simple if the control law would be presented in function as a dependence on rotor angular velocity: $\bar{P}_{max} = f(\Omega)$. The argument can be determined with the help of two sensors: wind speed V_0 ($V_0 \sim \omega_0$) and rotor angular velocity ω . The main problem is stipulated in

this case by the dynamics of the control process. Instantaneous wind speed has impulse nature comparing with the inertia of rotor. Thus the information channel of the speed Ω should be filtered.

If the wind speed exceeds the nominal, the power of rotor should be limited. The Stall (Stahl) method of control solves this task by profiling the stationary blades of rotor [18]. The exemplary mechanical characteristics with aerodynamic stabilizing, are shown in Fig. 4.

When the wind speed increases $V_{0i} > V_{0n}$, the mechanical characteristics of rotor become more soft. And the coordinates of point A_H (Ω_n, \bar{M}_n) remain constant in general, in the wide range of wind flows. Extra stabilizing of duty point with the help of control system, allows decreasing the requirements for the accuracy of fabrication of blades.

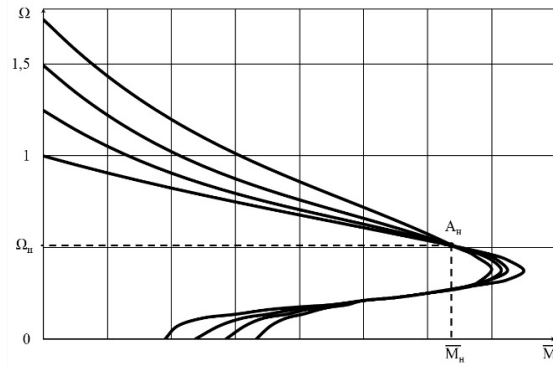


Fig. 4. Mechanical characteristics of rotor with aerodynamic stabilizing.

To stop the rotor, it's necessary to apply braking torque \bar{M}_{0i} to the rotor (see Fig. 4), not exceeding the nominal value. The task of rotor stop can be also solved by turning the electric machine into the motor reversible mode. Braking by generator allows the decreasing of requirements for the design of electromagnetic brake.

3. Results and discussion

3.1. Joint Analysis of Duties of Rotor and Generator

Let's discuss the opportunity of usage of the braking modes of WR with the help of asynchronous generator (AA) with amplitude-frequency control. Let's combine the mechanical characteristic of WR with analog characteristics of asynchronous electric machine of corresponding power, operating in braking mode. We would combine the characteristics by transferring the WR characteristic from the first quarter of coordinate map into the second one, which characterizes the operation of electric machines in generator mode (Fig. 5). The said analysis is qualitative, without analysing any specific parameters of WR or AA.

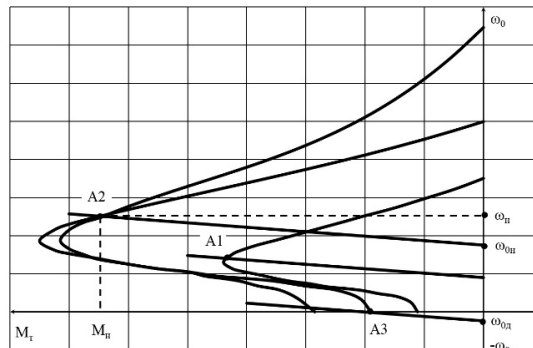


Fig. 5. Combined characteristics of Wind Turbine: A1 – mode of partial loading, A2 – mode of stabilizing of nominal power, A3 – mode of stop.

In the modes of partial loading (A1) and stabilizing of nominal power (A2) the control of AA should be handled by software in accordance with the law of optimal power takeoff obtained experimentally or by modeling [19]. AA control system should have a corresponding technical means.

To turn the rotor into the braking mode, it's necessary to shortly increase the braking torque up to critical \bar{M}_k and further smoothly decreasing the torque in accordance with the rotor angular velocity reduction [16]. The full stop with the help of electric machine in generator mode is impossible. It's necessary to have an external source of braking torque generated by turning the AA into the generator mode (A3) [20]. The AA control system should contain the reversible converter of frequency with amplitude-frequency control in the low speed area.

3.2. WT Control System

The desired power characteristics of WT can be realized by control system (Fig. 6), containing the earlier marked basic components.

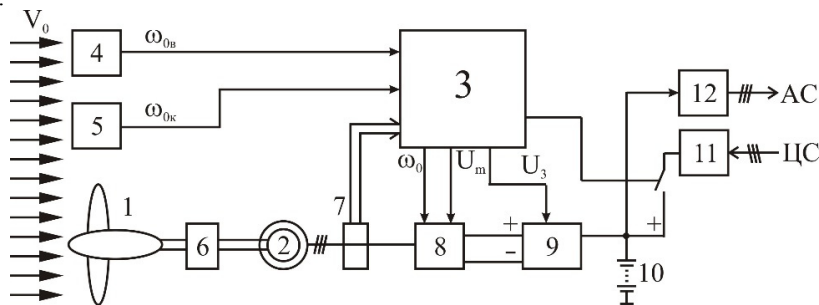


Fig. 6. Functional chart of WT control system: 1 – wind turbine, 2 – asynchronous generator, 3 – controller, 4 – wind speed sensor, 5 – wind rotor sensor, 6 – reduction unit, 7 – measuring converters of phase currents and voltages, 8 – reversible frequency converter, 9 – converter, 10 – batteries (GB), 11 – external charging device (compensator of charge for GB), 12 – voltage autonomous inverter, I – self-contained power grid, II – central power grid.

Controller keeps in memory the main parameters of power characteristics and function of control $P_{max} = f(\bar{M})$ or $P_{max} = f(\Omega)$, obtained as the result of testing or modeling of wind rotor. Using the information about current wind speed V_0 and angular velocity ω of wind rotor, the controller controls the power of AA, adjusting it in accordance with the tabular P_{max} . Reversible frequency converter based on the autonomous voltage inverter, should solve two tasks simultaneously during the control process: generate a synchronous frequency and amplitude of AA three-phase voltage [21].

Among the main tasks to be handled by controller, there is a function of support of positive energy balance of autonomous grid of WT. Converter is functionally connected with the controller, and should provide the automatic distribution of AA power between consumers of autonomous grid and accumulating battery module. Static energy storage compensates deficit of generator power in low speed modes. The recovery of energy balance of WT autonomous grid should be realized with the help of external charging device controlled by controller.

Control of three phase electric machine in generator mode can be implemented by the known methods [22...24] of theory of alternating current drive. New opportunities in implementation of required AA braking modes would give out the control algorithms based on the theory of generalized energy flow of three phase electromechanical converters, in particular amplitude control of torque and energy efficient AA control under criteria of constant overloading ability.

4. Conclusion

We discussed the aspects of mass usage of 7-15 meters diameter wind turbines (WT) on 5-15 kW uninterrupted power supply in conditions of continental regions with 3-5 m/s dominant wind flow range and 4-6 m/s average annual wind speed. We proposed the method of generating the desired WT power characteristic taking into account

a differential chart of wind flow distribution and electric energy consumption. We formulated the task of research of control algorithms for frequency controlled asynchronous generators WT, to provide the braking of wind rotor in modes of partial loading, nominal power stabilizing and full stop. The solution of the problem was illustrated by the analysis of combined mechanical characteristics of wind rotor and generator. We showed that the application of Stall method of aerodynamic stabilizing of rotor nominal power provides the ability of using the braking mode without increase of generator dimensions. We discussed the system of WT control with gain-frequency control of generator and automatic distribution of generated power between the consumers of local grid and the static energy storage. We proposed methods of optimizing the generator duties on the base of theory of generalized energy flow of three phase electromechanical converters.

References

- [1] Information on http://www.gwec.net/wp-content/uploads/2013/02/GWEC-PRstats-2012_english.pdf.
- [2] V.P. Kharitonov, Self-contained wind turbine, GNU VIESKh Publ., Moscow, 2006.
- [3] Yu.N. Petrenko, S.A. Stankevich, Development of a Control Algorithm that Provides the Highest Possible Power output of Wind Turbine with Energy Storage, *Electronics, Automation and Measuring Technology*. (2011) 47–52.
- [4] V.S. Krivtsov, A.M. Oleynikov, A.I. Yakovlev, *Inexhaustible energy*. Bk. 1. Wind turbine, KhAI Publ., Kharkiv, 2003.
- [5] Information on <http://cdn.intechweb.org/pdfs/16255.pdf>.
- [6] S.A. Sinkevich, Yu.N. Petrenko, The Use of Fuzzy Logic Controller to Control the Wind Turbine, *Information Technology and Systems 2012: Proc. of the Int. Scientific Conference*. (2012) 66–67.
- [7] E.A. Muravleva, S.P. Rudobashta, Efficiency Electricity Farmhouse Based on a Small Wind Turbine Power, *Vestnik FGOU VPO MGAU*. 1 (2013) 24–27.
- [8] V.V. Yelistratov, Monitoring the Development of Renewable Energy in the World and Russia, *Akademiya energetiki*. 2 (2008) 22–44.
- [9] E.V. Solomin, I.M. Kirpichnikova, A.S. Martyanov, The Iterative Approach to the Design and Optimization of Vertical Axis Wind Turbines, *Proc. of the VII Int. Scientific Conference of Young Scientists "Electrical. Electrotechnology. Energy"*. (2015) 92–95.
- [10] S.V. Kozlov, A.N. Kudryashov, E.V. Solomin, An Analysis of the Effectiveness of Energy Storage Systems, *International Scientific Journal "Alternative Energy and Ecology"*. 6(170) (2015) 10–23.
- [11] V.E. Belyakov, System of Automated Simulation of Wind Turbines, *Generation of the Future: Looking for young scientists*. (2014) 391–395.
- [12] S.N. Udalov, *Renewable energy*, Publ. NGTU, Novosibirsk, 2009.
- [13] P.P. Bezrukikh, *Wind power*, Publ. «ENERGY», Moscow, 2010.
- [14] V.P. Kharitonov, *Fundamentals of wind Energy*, Publ. GNU VIESKH, Moscow, 2010.
- [15] A.N. Kindryashov, A.S. Martyanov, E.V. Solomin, Electric cars wind turbines with a vertical axis of rotation, *International Scientific Journal "Alternative Energy and Ecology"*. 1/2(118) (2013) 59–62.
- [16] V.I. Smolin, D.V. Topolsky, N.N. Gudaev, Measurement of a Torque of the Electrical Machines According to Their Electrical Parameters, *EPE Conference'97, Proceedings*. 3 (1997).
- [17] I.G. Topolskaya, D.V. Topolskiy, V.I. Smolin, Non-contact Inspection Method Shock in Wind Turbines, *International Scientific Journal "Alternative Energy and Ecology"*. 10(78) (2009) 69–73.
- [18] I. Munteanu, A.I. Bratcu, N.-A. Cutululis, E. Ceanga, *Optimal Control of Wind Energy Systems*, *Advances in Industrial Control*, Springer-Verlag London, 2008.
- [19] I.M. Kirpichnikova, A.S. Martyanov, E.V. Solomin, Simulation of Wind Turbine Generator, *Electrical engineering*. 10 (2013) 46–50.
- [20] G.I. Volovich, E.V. Solomin, D.V. Topolskiy, I.G. Topolskaya, On the Development of Automation in the Energy from Renewable Energy Sources, *International Scientific Journal "Alternative Energy and Ecology"*. 9(131) (2013) 59–64.
- [21] V.I. Smolin, I.G. Topolskaya, The Theory of Generalized Energy Flow Three-phase Electromechanical Transducers in Control Electric, *Proc. of the VIII Int. (XI All-Russian) Conference on Automated Electric AEP 2014*. (2014) 111–115.
- [22] F. Blasche, The Principle of Field-orientation as Applied to the New Transvektor Closed-loop Control System for Rotating-field Machines, *Siemens Review*. 34 (1972) 217–220.
- [23] M. Depenbrock, Direct Self-control of Inverter-fed Induction Machine, *IEEE Transactions on Power Electronics*. 3 (1988) 420–429.
- [24] R.E. Betz, B.J. Cook, Instantaneous Power Control of Induction Machines, *Journal of Electrical & Electronics Engineering*. 1 (2001) 57–63.



International Conference on Industrial Engineering

Adaptive units and control systems of power semiconductor converters on the basis of integrating scanning conversion

Dudkin M.M., Tsytovich L.I., Nesterov A.S.*

South Ural State University, 76, Lenin Avenue, Chelyabinsk, 454080, Russian Federation

Abstract

One of the possible solutions leading to higher interference immunity and electromagnetic compatibility of control systems of power semiconductor converters (SC) due to the usage of integrating scanning conversion is given. Integrating adaptive synchronizing units, phase shifting devices and analog-digital converters, which are distinguished by a high interference immunity to the external interference signals, accuracy and ability to adapt to the changing parameters of mains voltage are considered. It has been shown that integrating scanning conversion in the base of construction of control systems of power semiconductor converters contributes to a high level of interference immunity and adaptation of SC to the inconsistent parameters of mains voltage in the stationary and autonomic-based power-supply systems, outgoing with this considerably the analogous indicators of the commercial power converters of home-made and imported production with the control systems constructed on the principle of momentary values sampling of information coordinate.

© 2015 The Authors. Published by Elsevier Ltd. This is an open access article under the CC BY-NC-ND license (<http://creativecommons.org/licenses/by-nc-nd/4.0/>).

Peer-review under responsibility of the organizing committee of the International Conference on Industrial Engineering (ICIE-2015)

Keywords: integrating scanning converter, control system, power semiconductor converter, interference immunity

1. Introduction

The integral part of modern automatic control systems of electric drive and automatic control engineering are regulated semiconductor converters (SC) (regulated rectifiers, frequency converters, pulse-duration converters, regulators of AC voltage and so on), with the help of which modulating control of output coordinates of operating

* Corresponding author. Tel.: +7-351-267-9321; fax: +7-351-267-9321.

E-mail address: dudkinmax@mail.ru

units is carried out. However, in some cases the following factors interfere with the work of commercial SC:

- external interference in the channels of information transmission of control systems, induced directly by the power semiconductor converters themselves operating in discrete (pulse) mode [1, 2];
- switching and pulse distortions of mains voltage [3, 4], appearing due to the changing character of operation of power devices, welding equipment and high-power relay-contact devices in particular and also power SC and their interference with each other;
- instability of amplitude and frequency of mains voltage [4], which is more typical for semiconductor electric drives and process installations, the supply of which is realized from the limited power-supply systems.

The factors specified above worsen the quality level of control process, switch to emergency-mode on technological objects and increase expenses on output products as a result.

The reason of such situations is low interference immunity of the units of SC control systems, where synchronizing units (SU), phase-shifting units (PSU) and analog-digital converters (ADC) play a special role.

This demands the necessity to construct devices and SC control systems having high interference immunity and ability to adapt their characteristics in the instable conditions of power-supply parameters.

2. Theoretical studies

Nowadays comparator synchronizing units have found great acceptance in SC control systems [5], which in most practical cases represent cascade application of a smoothing filter (F), for example, the aperiodic one of the first order and a relay element (RE) with switching thresholds symmetrical to the zero level $\pm b$ (fig. 1a). The drawback of such solution is obvious – when amplitude ΔA_S and/or frequency Δf_S of mains voltage is changed, the specified synchronization angle $\Delta \alpha_S$ is also significantly changed, that is proved by the space of static condition $\Delta \alpha_S = f(\Delta A_S, \Delta f_S)$ (Fig. 2a). Here $\Delta \alpha_S = (\alpha_S^* / \alpha_S) - 1$ – the rated fault of the synchronization angle α_S^* relative to the initial synchronization angle α_S while external disturbance is out, which is taken to be equal to -30 el. degrees; $\Delta A_S = (A_S / A_{S,N}) - 1$, $\Delta f_S = (f_S / f_{S,N}) - 1$ – the rated amplitude A_S and frequency f_S faults of mains voltage $X_S(t)$ relative to their nominal values $A_{S,N}$ and $f_{S,N}$ correspondingly; $\alpha_F = \alpha_S - \alpha_{RE}$ – delay angle, implemented by the aperiodic filter F and is taken to be equal to -20 el. degrees.

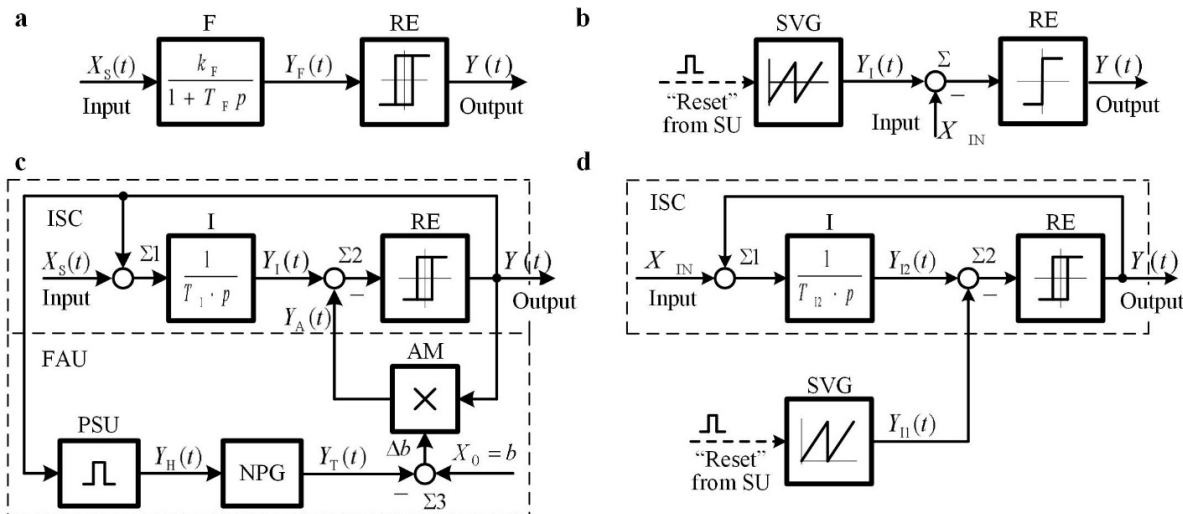


Fig. 1. (a-b) block diagram of comparator; (c-d) adaptive integrating synchronizing and phase-shifting units correspondingly.

It is worth noting that a comparator SU (Fig.1a) can adapt to the amplitude and frequency of mains voltage only in absence of a filter F at the input and a hysteresis loop by a RE, but at expense of considerable fall of interference immunity of a device, for example, to switching and pulse disturbance of mains voltage.

For regulation of the control angle or time of on-state of power keys comparator phase-shifting units or pulse modulators [5], consisting of a sawtooth-voltage generator SVG, a summer Σ and a relay element RE (comparator) (Fig. 1b) are applied in the commercial SC. Their principle of operation is based on sampling of instantaneous values of a control signal, when the input signal X_{IN} is directly compared with the sawtooth voltage $Y_I(t)$ and formation of control response in the moment of their equality.

Comparator PSU (Fig. 1b) and also the SU constructed on the same operating principal (Fig.1 a) are not able to adapt to frequency changes $\Delta \bar{f}_s$ of mains voltage (Fig. 2 b) as a result of deviation of the sawtooth-voltage amplitude at the output of the SVG from its initial value. While at positive deviations of mains frequency $\Delta \bar{f}_s > 0,1$ and $\bar{X}_{IN} < 0$ switching breakdown is observed in PSU, when its output signal takes one of static conditions, for example, of the logical zero. Here $\Delta \bar{\alpha}_c = (\alpha_c^* / \alpha_c) - 1$ – rated fault of the control angle at the change of frequency $\Delta \bar{f}_s$ of mains voltage; $\bar{X}_{IN} = |X_{IN} / A|$ – the rated value of the control signal X_{IN} relative to the amplitude A at the output of the SVG.

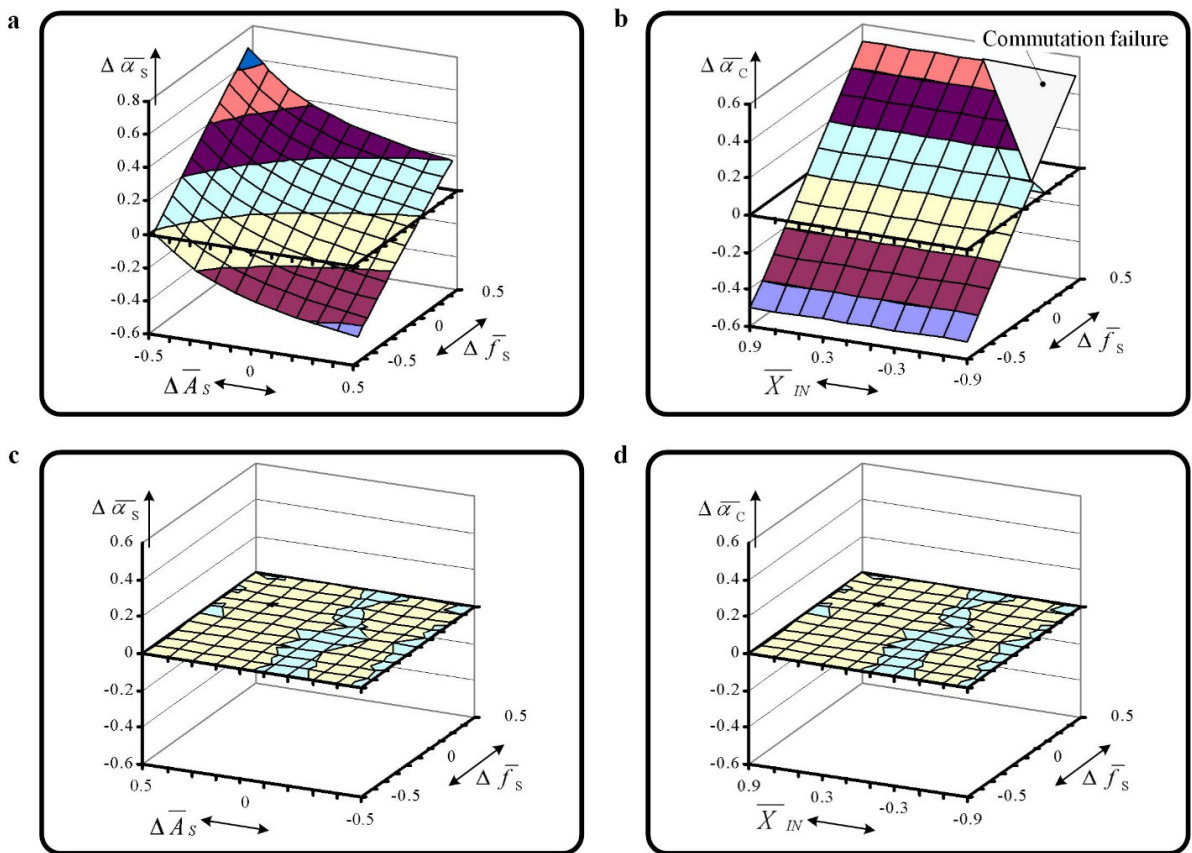


Fig. 2. (a-b) spaces of static condition of comparator correspondingly at unstable amplitude and frequency of mains voltage; (c-d) spaces of adaptive integrating synchronizing and phase-shifting units correspondingly at unstable amplitude and frequency of mains voltage.

Besides, the PSU constructed on sampling of instantaneous values of a control signal have low interference immunity to the signals of external disturbance from the information input, because in the field of frequencies of slow discretization ($\bar{F} > 0,5$) they form low-frequency constituents \bar{F}_H comparable by their level with the amplitude

\bar{A}_D of the harmonic wave of disturbance, that is proved by the space of spectral condition $\bar{A}_H = f(\bar{F}_H, \bar{F}, \bar{A}_D = 0,1)$ (Fig. 3a), taken in the presence of a digital filter at the output of the system. As a result of this a converted low-frequency signal at the output of the PSU appears in the field of operating frequencies of the SC control system, which leads to its nonoperability or considerable fall of quality level of the control process [6, 7]. Here $\bar{A}_H = |A_H/A|$, $\bar{F}_H = |f_H / f_0|$ – the rated values of the amplitude A_H and frequency f_H of the harmonics at the output of the PSU relative to the amplitude A and the carrier frequency of the sawtooth-voltage generator f_0 ; $\bar{A}_D = |A_D/A|$, $\bar{F} = |f_D / f_0|$ – the rated value of the amplitude A_D and frequency f_D of the harmonic wave of disturbance correspondingly.

Hereby, the analysis of studies has shown that in real-life environment of commercial operation determined by unstable parameters of mains voltage and a high level of disturbance in information transmission channels, the application of comparator synchronizing and phase-shifting units (Fig. 1a, b) in commercially produced SC leads to their static accuracy worsening and also emergency situations on industrial facilities, for example, because of main inverter triggering in thyristor rectifiers.

One of the most effective ways to improve statistical and dynamic accuracy of the SC control systems as well as their interference immunity are the ways of integrating and scanning conversion [6, 8-10].

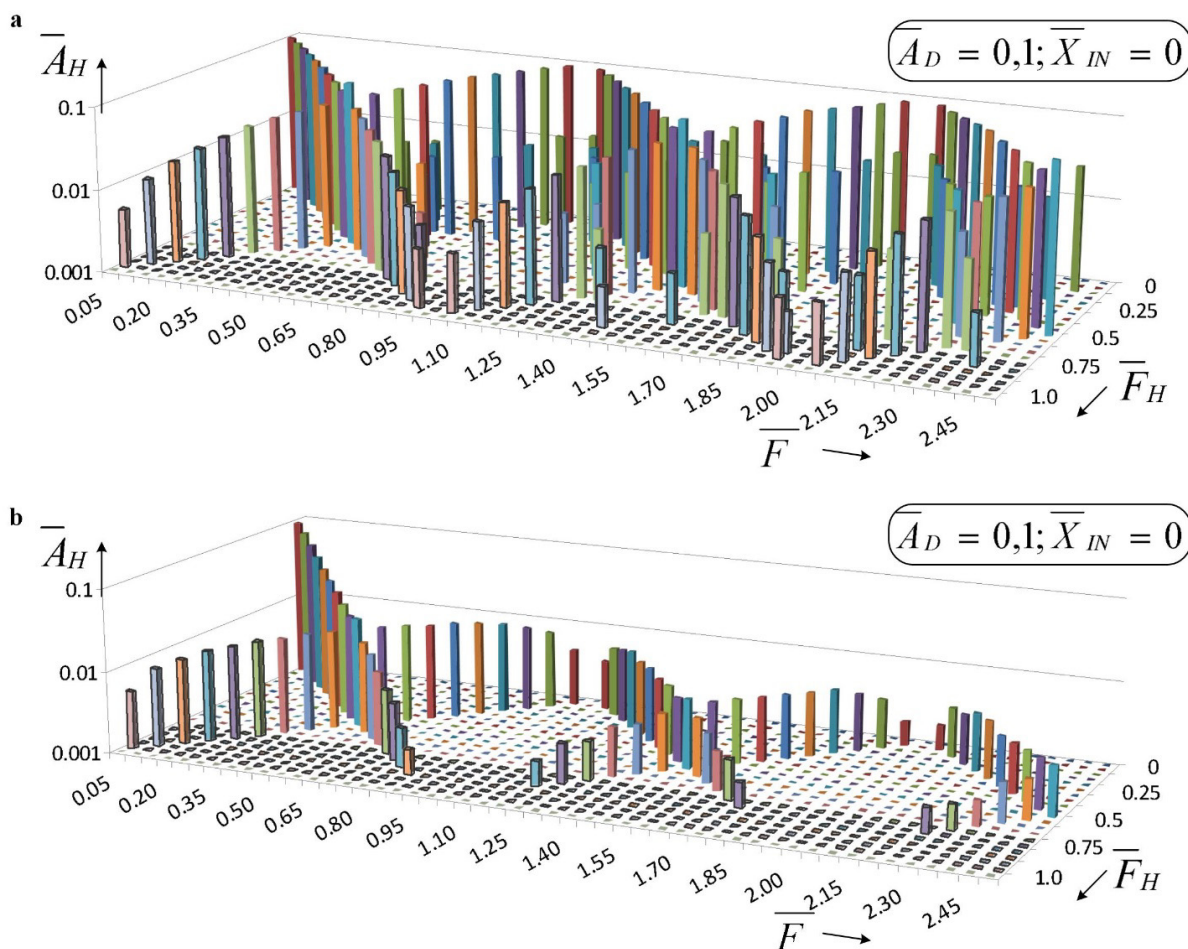


Fig. 3. (a) the spaces of spectral condition of phase-shifting units with sampling of instantaneous values of a control signal; (b) the spaces of spectral condition of integrating units with influence of the harmonic wave of disturbance on the information input in a wide frequency range.

In Fig. 1c,d the new structures of adaptive integrating SU and PSU have been represented [11, 12], in the basis of which a closed integrating scanning converter (ScC) lies, consisting of summers $\Sigma 1$ - $\Sigma 2$, integrator I with a constant of integral action time T_I and a relay element RE with switching thresholds $\pm b$ symmetrical in relation to the zero level. The introduced units operate in the mode of external synchronization when forced switches with frequency of synchronization action are set at their output. In addition to that the mains voltage $X_S(t)$ is applied directly as a synchronization signal in the adaptive integrating SU (Fig. 1c) and the sawtooth voltage $Y_{I1}(t)$ formed by the SVG and synchronized, for example, with the main with the help of pulse “RESET” from the output of SU is applied in the integrating PSU (Fig. 1d).

The results of the research have showed the following:

- the adaptive integrating SU and PSU adapt totally to deviations of amplitude and frequency of mains voltage, that is proved by the space of static condition $\Delta\bar{\alpha}_S = f(\Delta\bar{A}_S, \Delta\bar{f}_S)$ and $\Delta\bar{\alpha}_C = f(X_{IN}, \Delta\bar{f}_S)$ (Fig. 2c, d), providing a zero value of faults of the synchronization angle $\Delta\bar{\alpha}_S$ and control angle $\Delta\bar{\alpha}_C$. The adaptation to mains frequency in the integrating SU is reached due to the frequency adjustment unit FAU (Fig.1c), consisting of an amplitude modulator AM, a summer Σ , a phase-to-voltage converter of the direct-voltage transducer and a narrow-pulse generator NPG;
- the adaptive integrating PSU has high interference immunity to the signals of external disturbance from the information input as it has a low level of harmonics \bar{A}_H in the field of frequencies of slow discretization (at the average by an order less than for the PSU with sampling of instantaneous values of a control signal), which falls with the growth of a frequency \bar{F} of a signal of harmonic interference (Fig. 3a, b). This is the result of a closed-structure character of the PSU and the presence of the integrator in the direct control channel.

In digital control systems of SC the problem of their interference immunity and service ability depends not only on the SU and PSU but on the quality of transformation of an analog coordinate to a digit that requires the application of integrating ways of analog-to-digital conversion in the channels “Sensor – ADC”. With this purpose the clocked integrating AD converters with pulse-width [13] and synphased pulse-frequency-amplitude modulation [14] have been introduced. Their distinctive characteristic is that they operate synchronously in the frequency of SC discretization [15] suppressing wholly current or voltage ripples of a power converter and also blocking interference with frequencies equal or multiple of the frequency of discretization of the SC. Besides, the proposed AD converters provide a constant rate of transmission even during changes of the frequency of the clock pulses outgoing because of the unstable frequency of mains voltage.

3. Practical studies

With the application of the adaptive integrating SU, PSU and AD converters the power semiconductor converters of multiple functionality for electric drives and process installations of direct and alternating current for industrial and special purposes, including those operating with the main of limited power, for example, with diesel- or wind-generator stations, characterized by a high level of switching interference and a wide range of amplitude and frequency changes of mains voltage, have been theoretically and experimentally studied. The developed semiconductor converters include:

- single- and three-phase reversible and nonreversible thyristor-controlled rectifiers [6, 16] and also a reversible pulse width converter [6] for DC electric drives;
- thyristor voltage adjusters for a reduced-current start of induction motor drives of various categories and power [6, 17, 18];
- a pulse-width-frequency AC voltage regulator for technological installations of inertial devices, for example, temperature control systems [19];
- a single-phase active compensating filter for improvement of energy data of power-supply systems [20].

The developed SC have shown a high level of performance criteria in a whole series of emergency situations, where the commercial converters with the control systems constructed on the principle of momentary values sampling of information coordinate simply fall out of service. Therefore, for example, the semiconductor converters with the adaptive integrating control system can operate in amplitude deviations within limits no less $\pm 50\%$ and frequency ± 25 Hz and also switching interference with mains voltage till 100% for 25 el. degrees. In commercial SC similar indicators should not exceed $\pm(10...15)\%$ by amplitude and $\pm 0,6$ Hz by frequency and the level of switching interference of the main is 100% for 3-5 el. degrees. An admissible level of interference at the information input in the adaptive integrating control system is by an order higher than in the known systems. In dynamic modes of operation during smooth variations of both amplitude and mains voltage frequency the developed SC provide error-free operation at amplitude deviations within one period of mains voltage and frequency within a second in the limits $\pm 11\%$ and $\pm 6\text{Hz/s}$ correspondingly.

4. Conclusions

- It has been established as the result of the research that integrating scanning conversion is an effective way to improve technical characteristics of devices and control systems of power SC and also the means of their adaptation to disturbance from the power-supply source.
- It has been shown that the integrating SU and PSU as opposed to the known comparator units have the ability to adapt to amplitude and frequency deviations of mains voltage in a wide range and also have high interference immunity to external disturbance.
- The usage of the clocked integrating AD converters in the SC control systems permits in the channel “Sensor – ADC” to suppress wholly current or voltage ripples of a power converter and also block by this interference with control channels with frequencies equal or multiple of the frequency of discretization of the SC.
- The substantial advantage of integrating scanning conversion when constructing SC control systems has been theoretically and experimentally proved, that provides a high “safety factor” of the developed semiconductor converters at their operation both with stationary and autonomic systems of power-supply characterized by a high level of switching disturbance and a wide range of amplitude and frequency variations of mains voltage. To the list of such objects drilling rigs and sets, the systems of sea location, autonomic transfer objects and so on are referred.

References

- [1] O.I. Osipov, Yu.S. Usynin, *Promyshlennyye pomekhi i sposoby ikh podavleniya v ventil'nykh elektroprivodakh postoyannogo toka*, Energiya, Moscow, 1979.
- [2] H.W. Ott, *Noise reduction techniques in electronic systems*, second ed., John Wiley & Sons, New York, 1988.
- [3] E. Khabiger, *Elektromagnitnaya sovmestimost'. Osnovy ee obespecheniya v tekhnike*, Energoatomizdat, Moscow, 1995.
- [4] GOST 32144-2013. *Elektricheskaya energiya. Sovmestimost' tekhnicheskikh sredstv elektromagnitnaya. Norma kachestva elektricheskoy energii v sistemakh elektroobrazovaniya obshchego naznacheniya*, Standartinform, Moscow, 2013.
- [5] M.P. Kazmierkowski, R. Krishnan, F. Blaabjerg, *Control power electronic*, Academic Press, USA, 2002.
- [6] M.M. Dudkin, L.I. Tsytoich, *Elementy informatsionnoy elektroniki sistem upravleniya ventil'nymi preobrazovatelyami*, Izdatel'skiy tsentr YuUrGU, Chelyabinsk, 2011.
- [7] M.M. Dudkin, *Integriruyushchie fazosdvigayushchie ustroystva kak odin iz sposobov povysheniya pomekhoustoychivosti ventil'nykh preobrazovateley*, Trudy mezhdunarodnoy XIV nauchno-tekhnicheskoy konferentsii «Elektroprivody peremennogo toka». (2007) 31–34.
- [8] M.M. Dudkin, L.I. Tsytoich, O.G. Brylina, *Spectral characteristics of scanning converters with pulse-width and pulse-frequency-width modulations*, Russian Electrical Engineering. 84(10) (2013) 549–555.
- [9] L.I. Tsytoich, M.M. Dudkin, A.V. Kachalov, *Integriruyushchie razvertyvayushchie preobrazovateli s povyshennoy temperaturnoy stabil'nost'yu kharakteristik*, Pribory i sistemy. Upravlenie, kontrol', diagnostika. 10 (2010) 38–43.
- [10] L.I. Tsytoich, M.M. Dudkin, S.P. Lokhov, O.G. Brylina, *About the dynamics of some methods of integrating conversion of analog signal into digital code*, Vestnik YuUrGU. Seriya «Energetika». 13(1) (2013) 80–91.
- [11] M.M. Dudkin, RF Patent 2,513,024. (2012)
- [12] L.I. Tsytoich, M.M. Dudkin, A.V. Kachalov, R.M. Rakhmatullin, RF Patent 2,373,624. (2008)
- [13] L.I. Tsytoich, O.G. Brylina, M.M. Dudkin, R.M. Rakhmatullin, A.V. Tyugaev, RF Patent 2,496,228. (2012)
- [14] L.I. Tsytoich, M.M. Dudkin, A.V. Kachalov, R.M. Rakhmatullin, RF Patent 2,429,563. (2009)
- [15] L.I. Tsytoich, O.G. Brylina, M.M. Dudkin, R.M. Rakhmatullin, A.V. Tyugaev, *Analog-digital converter with integrating in-phase*

- amplitude-frequency-pulse modulation for switched drive systems, Russian Electrical Engineering. 84(5) (2013) 244–249.
- [16] L.I. Tsytoich, R.M. Rakhmatullin, M.M. Dudkin, A.V. Kachalov, Reversivnyy tiristornyy preobrazovatel' dlya sistem upravleniya s pitaniem ot seti s nestatsionarnymi parametrami, Prakticheskaya silovaya elektronika. 2(34) (2009) 35–41.
- [17] L.I. Tsytoich, S.I. Shkalikov, M.M. Dudkin, Tiristornyy preobrazovatel' s integriruyushchim ustroystvom dlya myagkogo puska asinkhronnykh elektrodvigately, Problemy energetiki: izvestiya vysshikh uchebnykh zavedeniy, Izdatel'stvo KGEU, Kazan'. 7-8 (2005) 57–65.
- [18] M.M. Dudkin, Tiristornyy regulyator napryazheniya s adaptivnoy integriruyushchey sistemoy upravleniya dlya plavnogo puska asinkhronnykh elektrodvigately, Vestnik YuUrGU. Seriya «Energetika». 14(2) (2014) 36–43.
- [19] M.M. Dudkin, O.G. Brylina, L.I. Tsytoich, A.V. Tyugaev, Chastotno-shirotno-impul'snyy adaptivnyy regulyator peremennogo napryazheniya s integriruyushchey sistemoy upravleniya, Vestnik YuUrGU. Seriya «Energetika». 13(2) (2013) 45–52.
- [20] M.M. Dudkin, Energoberegayushchie tekhnologii v ispytatel'nykh standakh s ispol'zovaniem odnofaznykh obratimnykh preobrazovately, Vestnik YuUrGU. Seriya «Energetika». 13(1) (2013) 5–18.



International Conference on Industrial Engineering

Traction electric drive with the field regulated reluctance machine

Shishkov A.N., Belousov E.V., Grigoryev M.A.*

South Ural State University, 76, Lenin Avenue, Chelyabinsk, 454080, Russian Federation

Abstract

The field regulated reluctance machine is the future for automotive transport electric drives. In this machine, stator current is switched in the function of a rotor position. The massive salient rotor of the electric machine does not contain windings. The stator is fulfilled in the body and iron of the serial ac induction motor. The stator winding sections, which positioned over interpolar space, serve as an excitation winding and others sections, which positioned over the rotor poles, the role of an armature winding. In most cases, the optimal winding current waveform is distinct from the sine waveform. The ideal rectangular waveform is used for a case of separate current sources for each phase. At the rotation of the motor, each stator section winding pass from the "excitation" zone to the "armature" zone. The stator has a finite number of phases. If the stator currents are switched, the part phase, in which there is a switching of an armature current, is in a zone of excitation, and another - in a zone of an armature. It causes additional losses in the rotor, because the rotor is fulfilled massive (not laminated). To calculate the losses first of all it is necessary to determine the factors, which impact their value, and then, to estimate the degree of influence each of them has on the switching losses value. Such factors include the form of the stator core, the form of the current in phase windings, and the number of stator winding phases. The calculation of losses is executed by the method of winding functions. The experimental data is provided from a breadboard model of the 20 kW drive.

© 2015 The Authors. Published by Elsevier Ltd. This is an open access article under the CC BY-NC-ND license (<http://creativecommons.org/licenses/by-nc-nd/4.0/>).

Peer-review under responsibility of the organizing committee of the International Conference on Industrial Engineering (ICIE-2015)

Keywords: urban trams with a low floor, field regulated reluctance machine, losses in the motor, power circuit schemas.

1. Introduction

The urban trams with a low floor are comfortable for passengers, and with a high floor – more cheaply and more

* Corresponding author. Tel.: +7-351-223-6713.
E-mail address: grigorevma@susu.ac.ru

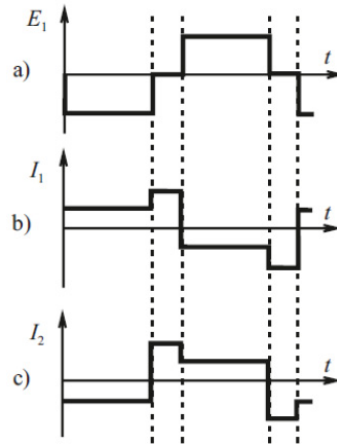


Fig. 2. Graphs of EMF (a) and currents in works of FRRM in motor (b) and generator (c) modes

3. Losses in the stator copper

The different modification are compared by value of a criteria q , which make possible evaluate efficiency of use the electric motor by torque at the different laws of commutations.

Dependence value of parameter q from different criteria: the kind of current in a phase coils, quantity of phases in a stator coils are shown in table 1.

Efficiency of increase quantity of phases is decreased after $m > 6$.

Trapeze should be recognized at the best form of current. For example, parameter q is increased from 0,1 to 0,2 at $m = 6$, if sine is changed on the trapezium [3, 9].

Table1. Values of parameters q

Form of a current	Quantity of phases m						
	3	4	5	6	7	8	9
Trapeziform	0,78	0,83	0,87	0,89	0,91	0,92	0,93
Rectangular	0,72	0,75	0,79	0,8	0,81	0,82	0,83
Sine	0,73	0,76	0,78	0,785	0,791	0,792	0,794

4. Losses in the rotor

Criteria are regarded, which affected on the values of commutation losses: dependence of ripple amplifier of flux to its value (A_F / F). The relation is shown of relative ripple amplifier of flux from quantity of phases m of a stator coil of FRRM in the fig. 3. Curve 1 (fig. 3) is stepped configuration form of phase current in the stator coil of FRRM. Ripple of flux is from 5% to 24%. Curve 2 (fig.3) is trapeziform of phase current. Ripple of flux is from 1% to 7%. Curve 3 (fig.3) is sine form of phase current in the coil. Minimum flux ripples and losses are achieved by choice these forms in the rotor steel [4, 12].

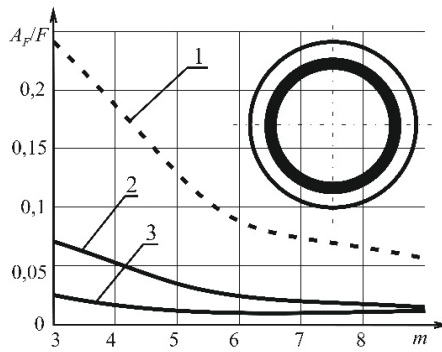


Fig. 3. Relative ripple flux from quantity of phases

5. Experimental values of losses

Observed dependence of losses in steel and mechanical losses for variable values of the flux and motor speed for FRRM. The experiment was underway no load. Frequency rectifier ABB ACS 600 is provided supply for motor [5]. Nominal rating power of FRRM was about 20kW. The stator coil fulfilled from three phases. Amount the flux be maintained by law (1):

$$\frac{U_{LIN}}{f_{SUP}} = \text{const} \tag{1}$$

Losses is equal $P_0 = 600 \text{ W}$ in the steel in the nominal point, if frequency $f_{SUP} = 50 \text{ Hz}$ and linear voltage is equal $U_1 = 250 \text{ V}$.

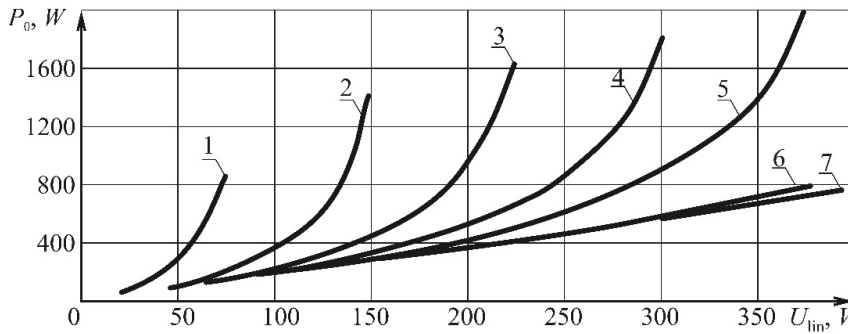


Fig. 4. Losses in the steel and mechanical losses in linear voltage function under supply of FRRM from F_1 for different frequency (1 – 10 Hz; 2 – 20 Hz; 3 – 30 Hz; 4 – 40 Hz; 5 – 50 Hz; 6 – 75 Hz; 7 – 100 Hz)

According computation losses is equal $P_{st,h} = 600 \text{ W}$. The mechanical losses is composed $P_{MECH} = 60 \text{ W}$, which was achieved by approximation curve 5 (fig. 4) on the zero linear voltage. Losses in steel rotor:

$$P_{ROT} = P_0 - P_{st,h} - P_{MECH} = 600 - 240 - 60 = 300W$$

6. Power circuits schemas

Schemas with individual current sources (fig. 5) more simplified used for supply FRRM. The reference current is used in the function of a shaft position of FRRM, which changed in time by a law is shown in fig. 2, c. The drawback of the schemas is the great number of switchers which equal $4m$. Possible variant using the schema of electric drive with attention possibility of the serial three-phase voltage inverters, in which stator coil are assembled in two three-phase stars, dislocated on the 30 electric degrees from each other. In schema would be used two bridge inverters $UZ1$ and $UZ2$, in the case of FRRM is designed of the six-phase (fig. 6). In the electric drives it is more useful with small and average power than schema (fig. 5) with smaller number of keys. In the high-power electric drives it is more applies because not required parallel connection of keys at the big current [6, 15].

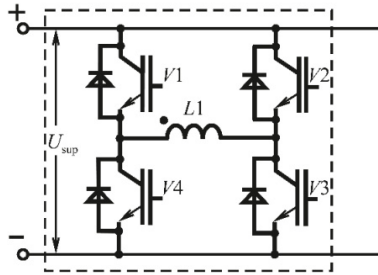


Fig. 5. Bridge circuit supply the phase of FRRM

The offered schemas are allowed use all power operation modes of electric drive.

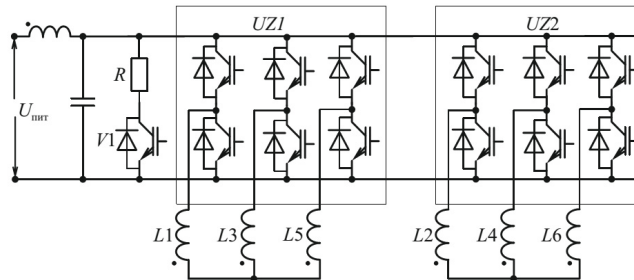


Fig. 6. Schema with two bridge inverter

7. Control circuits

The variant of two zone speed control is offered how control scheme (fig. 7). Here the reference is conducted from output of the speed regulator AR and inverter A3 via unit of creation of phase current A5 on the armature coil currents (voltage $+U_{RS}$ and $-U_{RS}$). No regulation reference is conducted from outputs AU and inverter A4 on the excitation current (voltage $+U_E$ and $-U_E$). Requires magnitude of the speed rotation is supported of the electric drive by a speed loop [7, 11].

Creation unit of phase currents is give a drive pulses on the switchers of autonomous voltage inverters $UZ1$, $UZ2$.

Voltage are reduced on an output AU and magnetic flux of a stator because, increase of a motor velocity, higher of a reference magnitude, and constant amplitude of the stator voltage [8].

8. Conclusion

The experimental tests of engineering sample have shown, the rotor of motor have a great mechanical stiffness, so drive can be designed a small diameter and long length.

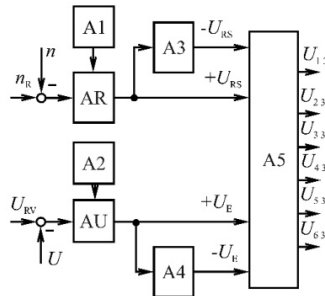


Fig. 7. Functional schema for control electric drive based on the two zone speed control

Trapeze form current in phase coil is optimally in relation achieve maximum electromagnetic torque under minimum losses in the stator coil of FRRM.

For decreased switching losses can be recommended Based on the research findings of electric drive with FRRM supply stator coil with sine current source [13, 14].

References

- [1] M.A. Grigoryev, A.N. Gorozhankin, S.I. Kinas, E.V. Belousov, Dynamic parameters of active rectifiers, Russian Electrical Engineering. 85(10) (2014) 638–640.
- [2] A.N. Shishkov, D.A. Sychev, A.E. Bychkov, N.Yu. Sidorenko, The DET-400 Tractor Traction Electric Drive, Russian Electrical Engineering. 10 (2014) 24–26. (in Russ.).
- [3] M.A. Grigoryev, S.I. Kinas, A mathematical model of the synchronous reluctance machine with independent control along the excitation line. Russian Electrical Engineering. 85(10) (2014) 645–648.
- [4] Yu.S. Usynin, M.A. Grigor'ev, A.N. Shishkov, Electric drive with a field-regulated reluctance machine. Russian Electrical Engineering. 84(3) (2013) 149–154.
- [5] M.A. Grigoryev, Specifics of power circuit arrangements of semiconductor converters for power supply to synchronous reluctance machines. Russian Electrical Engineering. 85(10) (2014) 601–603.
- [6] S.P. Gladyshev, Yu.S. Usinin, M.A. Grigoryev, A.N. Shishkov, A.E. Bychkov, Switching losses in the rotor of the field regulated reluctance machine, SAE Technical Papers, 2010.
- [7] M.A. Grigoryev, A control system for an electric drive with a synchronous reluctance machine with separate excitation, Russian Electrical Engineering. 84(10) (2013) 560–565.
- [8] A.N. Gorozhankin, A.N. Shishkov, D.A. Sychev, S.I. Kinas, E.V. Belousov, A direct torque control system for synchronous electric drives, Russian Electrical Engineering. 10 (2014) 29–32. (in Russ.).
- [9] Yu.S. Usinin, S.P. Gladyshev, M.A. Grigoryev, A.N. Shishkov, A.E. Bychkov, The losses in control electric drives of transport mechanisms at different controlled laws, SAE Technical Papers, 2011.
- [10] U.S. Usinin, M.A. Grigorjev, K.M. Vinogradov, A.N. Gorojankin, S.P. Gladyshev, Weight and dimensional parameters of a power drive for electrical vehicle, SAE Technical Papers, 2009.
- [11] Yu.S. Usinin, S.P. Gladyshev, M.A. Grigoryev, A.V. Valov, A.E. Bychkov, Pulse vector control of wound rotor induction motor, SAE Technical Papers, 2010.
- [12] Y.S. Usinin, M.A. Grigorjev, K.M. Vinogradov, A.N. Gorozhankin, S.P. Gladyshev, The electric drive of a tram with an average floor, SAE Technical Papers, 2008.
- [13] Yu.S. Usinin, S.P. Gladyshev, M.A. Grigoryev, A.N. Shishkov, A.E. Bychkov, E.V. Belousov, Electric drive of an industrial tractor, SAE Technical Papers, 2013.
- [14] Yu.S. Usynin, M.A. Grigoryev, K.M. Vinogradov, Electric drives and generators with field regulated reluctance machine, Electrical Technology Russia. 3 (2007) 21–26. (in Russ.).
- [15] Yu.S. Usinin, S.P. Gladyshev, M.A. Grigoryev, A.N. Shishkov, A.E. Bychkov, K.M. Vinogradov, Pulse vector control of wound rotor induction motor, SAE Technical Papers, 2010.



International Conference on Industrial Engineering

Mass-dimensional parameters of traction drive

Zhuravlev A.M., Sychev D.A., Savosteenko N.V.*

South Ural State University, 76, Lenin Avenue, Chelyabinsk, 454080, Russian Federation

Abstract

A traction electric drive is used for an industrial tractor. The motor consists of a generator, a controlled rectifier, autonomous inverters, and two onboard motors. The key feature of the introduced electric drive is the use of field regulated independent excitation reluctance machine as a generator and traction motors. These electric machines have the following performance specifications: the generator and motor design is brushless; and simple, the rotor has high mechanical stiffness that increases reliability at high rate and overloads. There are no turns on the rotor; the motor is designed for simplicity of manufacture. The drives have increased effectiveness in terms of the effect of a "cold" rotor frame; the motors have high torque overloads power (up to 4-6 times the values of nominal torque). The turns of the motor and the generator are one-layered with full pitch capability of current and voltage. The drive manipulation is based on the transistors. The interval of the torque regulation is 1:10 resulting in permanent power for the drive [1]. This motor is used not only as a traction drive, but because of the simplicity of a frame it may be used for other devices where high load working cycles are required for operation.

© 2015 The Authors. Published by Elsevier Ltd. This is an open access article under the CC BY-NC-ND license (<http://creativecommons.org/licenses/by-nc-nd/4.0/>).

Peer-review under responsibility of the organizing committee of the International Conference on Industrial Engineering (ICIE-2015)

Keywords: traction electric drive, field regulated reluctance machine, traction characteristics, estimation of mass dimensional parameters

1. Introduction

Today different electric drive systems are applied actively in independent high-horsepower feed systems such as sea crafts, river boats, rock handlers, tractors, etc. They have certain benefits in comparison to only mechanical systems. In these systems, electricity is generated by a diesel-generator set. The output parameter of generator is being three-phase power. It can use typical synchronous and induction motors or to a new frame electrical machines.

* Corresponding author. Tel.: +7-351-223-6713.

E-mail address: grigorevma@susu.ac.ru

Power supply for such motors is increased to 1, 3, and 6 kV to loss reduction and decrease their size. For AC motors speed regulation can use a high voltage cascade frequency rectifier. The quantity of frequency rectifiers and its configuration are depends on the motor's power and its voltage level. In this article, for an industrial tractor is used the traction motor. The electric drive is consist of the generator, the controlled converter, the two autonomous inverters, two onboard drives. A key feature of the electric drive is the use of synchronous reluctance (reactive) machines with independent excitation as the generator and traction motors [2].

2. Industrial tractor electric drive

Introduced is one of the versions of the traction electric drive of the transport machine (fig. 1), composed of: a gas-turbine engine GTE, electrical generator G (alternator), the controlled rectifier CR on the output of the generator, two autonomous inverters AI1 and AI2, two onboard motors M1 and M2, and onboard mechanical transmissions MT1 and MT2 on driving wheels of tracks T1 and T2.

The major engine (GTE) is diesel engine (280-300 rad/s) or a gas-turbine engine. The gas-turbine engine GTE and a rotor of generator G are install on a common axis. The generator and gas-turbine engine are bond as complete unit. In the next modification, between shaft of a diesel engine and shaft of electric generator G is used an intermediate speed increasing gear box in this case is applied the diesel engine. Angular speed of the rotor increases up to 1000 rad/s because of the speed-increasing gearbox [3].

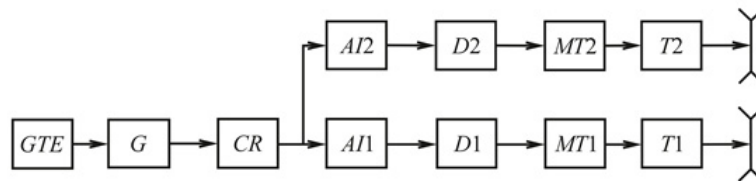


Fig. 1. The block diagram of the traction electric drive.

The generator is accomplish based on the synchronous reluctance machine with independent excitation. The G has the next rating: efficiency 0.9, the number of stator phases, $m = 3$, there are three-phase star connected output windings.

The controlled rectifiers (CR) are imagined three transistor bridges and linked to the output stator coils of the electric generator.

Input circuits of each bridge are linked to one of the three-phase stator coil. The secondary rectifier's circuits are linked in parallel and build up a direct current voltage circuit.

The autonomous inverters AI1, AI2 are complete on the base of the transistors as the three-phase bridge circuits. Onboard motors M1 and M2 are supplied from the convertors. The nominal parameters of the inverters: the voltage on the direct current side $V_d = 1000V$, an entrance current (I_d), 2000, the number of inverter bridges three. Each bridge is a three-phase circuit.

The nominal parameters of the motors M1, M2: rated speed 1000 rad /s, number of stator phases 3. The stator coils have connection like a Y (star). There are three stars are potentially separated. The nominal efficiency is 0.9. The maximal rotor speed is 1500 rad/s [4].

The traction electric drive can be used of the field regulated reluctance machines FRRM (fig. 2) as the generator G and the traction motors M1, M2 and this is a major feature. The field regulated reluctance machines are imagined as highly perspective modification of machines with the high torques [5]

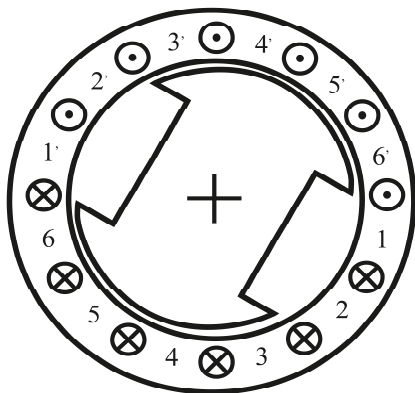


Fig. 2. Machine cross section area.

- A major feature of the electrical machines:
- A simple completely a no-touch frame of the drive;
 - The rotor has high or very high mechanical stiffness that increases availability of the motor at the high speeds and the high overloads;
 - There are no coils on the rotor;
 - High flexibility to production the motor. By experimental evaluation, its price should be lower than the asynchronous (induction) short-circuited electric motor by 15 ... 20 %;
 - Increased efficiency because of a "cold" rotor;
 - High overloads on the torque up to 4 ... 6;
 - Capacitance of the capacitor is minimal in the direct current part of the frequency converter.
- The coil of the motor is complete as single-layered with full pitch. The current and voltage waveforms optimally interfaced with converter switchers [6].

3. Principle of operation

In the salient poles synchronous machine, the part of an excitation coil in the stator slots can execute the coils if they are opposite to an inter-polar interval of a rotor; secondly, this coil has a full pitch.

So, if current is passed via coils 1 – 1’ and 2 – 2’, positioned over an inter-polar space (fig. 2), it will produce a flux along magnetic axis of the machine. Electromagnetic torque is created if a current is passed via coils 3 – 3’, 4 – 4’, 5 – 5’ and 6 – 6’, positioned over poles of the rotor.

The currents I_F are positioned in the field winding, over inter-polar space of the rotor, and the currents I_A are positioned in the armature coil over poles of a rotor, can be adapted independently and are switched as a function the rotor position. Via these coils it is not need to pass a sine wave current. It appears that a rectangular waveform of current is a more effective, the same as in slots of the direct current motor. The motor is operated in multiphase; a current and an electromotive force for each sequent phase are move at π/m electric degrees, where there are m phases.

In the electric drive, the coil of a stator coil consistently serves as the armature windings and the excitation windings. If the electric machine would be operated in a generator mode, commutation keys, linked to the armature coils, work in a natural commutation mode [7].

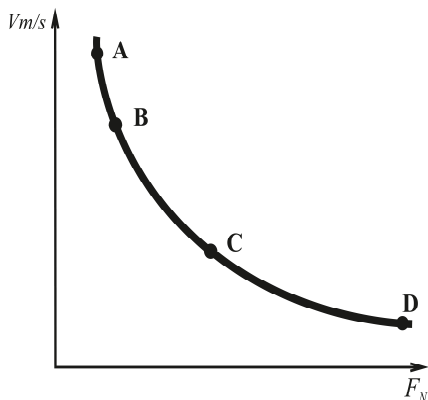


Fig. 3. Traction characteristic.

4. Traction characteristic

The traction characteristic of the transport machine is shown in fig. 3. It is corresponded to a constant power mode on a shaft of a driving wheel. In a constant power mode the operating range of the pull force is 0. The specific characteristic points are: Point A is a point of the maximal speed of the transportation vehicle. It is $v_A = 19$ m/s. Points B, C, and D are conformed of the conditions to a mode of constant power of the electric drive.

Point B is the upper limit of a constant power range, $v_B = 13.4$ m/s. Point D is the lower limit of a constant power range $v_D = 1,34$ m/s. Point D is

conformed to the greatest possible short-term traction force generate by the electric drive which is equal to the weight of the transportation vehicle. The point C is conformed to a long-term typical operation of the electric motors M1, M2 and the generator, G. In this point, speed $v_C = 5.36$ m/s [8].

5. Choice of rated data of electric motor

On the traction characteristic in the point A developing maximum velocity of the drive equal $n_A = 1500$ rad/s, point B conform to a velocity of 1060 rad/s, at point C, it is 425 rad/s, and at point D, it is 106 rad/s. In this situation, the velocity of the drives will be like the velocity of the generator. Acceleration speed of the motors because of the broad band of the torque control in a constant power mode. Under specific conditions, point C is conformed to long-term typical operation. Out of the electric drives in spaces A, B, and C happens because of decrease of the motor flux and nominal stator voltage. Work in the space of C and D happens at a nominal flux, and at the decrease stator voltage and an increased stator current [9, 14].

6. Estimation of mass dimensional parameters of electric machine and converters

According to references, electric machines of general purpose industrial grade series with air cooling have special property within the limits of 1.0 ... 1.5 Nm/kg, but if they have low angular rate (within the limits of 1000 ... 1500 rev/min) their special power parameters are low 5 ... 7 kg/kW. According to that data [10], electric machines of specific transport vehicle, with oil cooling, have special conditions of torque 0.6 ... 1.5 Nm/kg and of power about 2 kg/kW. Starting with initial conditions, it is possible assume that the weight of generator G is relatively small. Advanced scheme of the power circuits is shown on Figure 4.

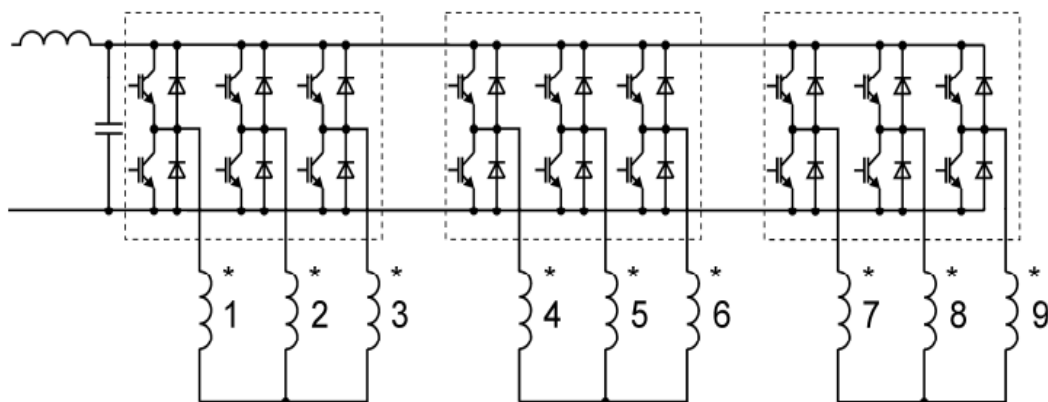


Fig. 4. Power circuits of "Autonomous inverter - Motor".

7. Control system of the electric drive

In the electric drive of an industrial tractor, the control system is operates in two zones of control [11]. The nominal power of the pull electric motor is $P_N = 250$ kW. The band of the torque control is equal 10. The first band of the torque regulation, by variation the motor magnetic flux, is equal 4, and the second band of regulation, by variation the motor armature current the decrease of the electromotive force, is equal 2.5. The profile power of the traction motor (in fractions of the mechanical profile power) is equal 6. But, if the motor regulation would be realize by only variation the motor magnetic flux, the profile power would be equal 10. In the torque regulation mode is achieved dramatic decline in dimension of the power profile of the motor because, first, there were two-zones of torque regulation and, secondly, because of the advantageous curve form density configuration of the pull force on the transports, when very high overloads are presented as for a short time. In electric drives of industrial tractors,

with mode for regulation of the conditions of the control system, it is also possible to impulse - vector control [12, 15].

8. Conclusions

An electric drive using synchronous reluctance machines with independent excitation is a strong competitor in regulated alternating current electric drives, because, it has the possibility for large overload torques, effective use of active materials, and easy system control [13].

An intense process invention that included attention on the semiconductor elements could result in an industrial tractor applicable to a wide variety of products.

References

- [1] Yu.S. Usynin, M.A. Grigor'ev, A.N. Shishkov, Electric drive with a field-regulated reluctance machine, *Russian Electrical Engineering*. 84(3) (2013) 149–154.
- [2] S.P. Gladyshev, Yu.S. Usin, M.A. Grigoryev, A.N. Shishkov, A.E. Bychkov, Switching losses in the rotor of the field regulated reluctance machine, *SAE Technical Papers*, 2010.
- [3] M.A. Grigoryev, A control system for an electric drive with a synchronous reluctance machine with separate excitation, *Russian Electrical Engineering*. 84(10) (2013) 560–565.
- [4] Yu.S. Usin, S.P. Gladyshev, M.A. Grigoryev, A.V. Valov, A.E. Bychkov, Pulse vector control of wound rotor induction motor, *SAE Technical Papers*, 2010.
- [5] U.S. Usin, M.A. Grigor'ev, K.M. Vinogradov, A.N. Gorojankin, S.P. Gladyshev, Weight and dimensional parameters of a power drive for electrical vehicle, *SAE Technical Papers*, 2009.
- [6] Y.S. Usin, M.A. Grigor'ev, K.M. Vinogradov, S.P. Gladyshev, Generator for vehicle applications, based on the field regulated reluctance machine, *SAE Technical Papers*, 2008.
- [7] Y.S. Usin, M.A. Grigor'ev, K.M. Vinogradov, A.N. Gorojankin, S.P. Gladyshev, The electric drive of a tram with an average floor, *SAE Technical Papers*, 2008.
- [8] Y.S. Usin, S.P. Gladyshev, M.A. Grigor'ev, A.N. Shishkov, A.E. Bychkov, E.V. Belousov, Electric drive of an industrial tractor, *SAE Technical Papers*, 2013.
- [9] Y.S. Usin, S.P. Gladyshev, M.A. Grigor'ev, A.N. Shishkov, A.E. Bychkov, K.M. Vinogradov, Pulse vector control of wound rotor induction motor, *SAE Technical Papers*, 2010.
- [10] A.N. Shishkov, D.A. Sychev, A.E. Bychkov, N.Yu. Sidorenko, The DET-400 Tractor Traction Electric Drive, *Russian Electrical Engineering*. 10 (2014) 24–26. (in Russ.)
- [11] M.A. Grigor'ev, A.N. Gorozhankin, S.I. Kinas, E.V. Belousov, Dynamic parameters of active rectifiers, *Russian Electrical Engineering*. 85(10) (2014) 638–640.
- [12] A.N. Gorozhankin, A.N. Shishkov, D.A. Sychev, S.I. Kinas, E.V. Belousov, A direct torque control system for synchronous electric drives, *Russian Electrical Engineering*. 10 (2014) 29–32. (in Russ.)
- [13] M.A. Grigor'ev, S.I. Kinas, A mathematical model of the synchronous reluctance machine with independent control along the excitation line. *Russian Electrical Engineering*. 85(10) (2014) 645–648.
- [14] Yu.S. Usin, S.P. Gladyshev, M.A. Grigoryev, A.N. Shishkov, A.E. Bychkov, The losses in control electric drives of transport mechanisms at different controlled laws, *SAE Technical Papers*, 2011.
- [15] M.A. Grigoryev, Specifics of power circuit arrangements of semiconductor converters for power supply to synchronous reluctance machines, *Russian Electrical Engineering*. 85(10) (2014) 601–603.



International Conference on Industrial Engineering

The algorithm of economically beneficial overhead wires cross section selection using corrected transmission lines mathematical models

Kornilov G.P., Panova E.A., Varganova A.V.*

Platov South-Russian State Polytechnic University (NPI), 132, St. Prosvescheniya, Rostov region, Novocherkassk, 346428, Russian Federation

Abstract

The paper presents an unparalleled electric power system operating mode optimization algorithm aimed to economically beneficial overhead wires cross section selection with respect to electricity rate, electric power system elements price, reliability problem. The algorithm in question allows eliminating the limitation on the maximum allowable wires cross section with the help of corrected transmission lines mathematical models.

© 2015 Published by Elsevier Ltd. This is an open access article under the CC BY-NC-ND license

(<http://creativecommons.org/licenses/by-nc-nd/4.0/>).

Peer-review under responsibility of the organizing committee of the International Conference on Industrial Engineering (ICIE-2015)

Keywords: electric power system engineering; optimization; wires cross section; method of coordinatewise optimization; equivalent circuit; mutual inductance.

1. Introduction

To date due to the load rise a lot of existing electric power systems (EPS) need to be reconstruct-ed. Also new electric power supply systems are being constructed for a new objects. So the problem of sustainable EPS scheme selection is raised. The conditions of economically advantageous EPS variant choice are system scheme, wires cross section, voltage level, measure of reliability, number of back-up power sources, the number and points of installation of compensating devices. The above mentioned factors in turn determine power, electricity and voltage losses, investments into the EPS under reconstruction or engineering.

* Corresponding author. Tel.: +79193246719.

E-mail address: aleksanra-khlamova@yandex.ru

The first step of power system engineering is a loads computation resulting in transformers and wires selection. At the moment according to the Electrical Installations Code the choice of wires cross section is executed on the basis of economic current density. But such a way does not allow to take into account the above mentioned factors in terms of modern EPS. Thus in the [1] reliability of overhead electric transmission lines (OHL) accountance and in [2] the question of reactive power compensation are considered. Moreover the choice of economically advantageous EPS scheme variant, wires cross section in particular, is executed using direct search method that lengthen dramatically the process of EPS engineering on its first steps.

Consequently the algorithm of optimal OHL wires cross section selection should be elaborated. The algorithm in question is supposed to be materialized using coordinatewise optimization method in combination with penalty function approach.

2. Optimization algorithm

Basing on the preplanned EPS scheme and calculated parameters of its operation mode using the methods of matrix math providing certain wires cross section variants the optimal ones are chosen.

To understand the approach of optimal power flow in power systems there are a lot of views. At the [3] authors using the gradient-type interaction prediction approach to define the optimal control problems. The article [4] presents a gravitation search method to find an optimal power flow in a distribution network. The other way in response to this problem is the use of differential evolution method [5]. Power supply systems are described with multi-objective function. In order to address the multi-objective optimal power flow at the [6, 7] algorithms of evolutionary programming, genetic algorithm, and particle swarm optimization are considered. The other way is described at [8].

Authors of this paper offer to solve the problem of multi-objective optimization using coordinatewise optimization method [9, 10].

The optimally criterion is the minimum of EPS construction and operation costs (C) with respect to the electric power supply interruption costs. So target function is computed according to (1)

$$\min C(I + OC_{\Delta P} + IC), \quad (1)$$

where C – aggregate costs, RUR; I - investments into the EPS, RUR; $OC_{\Delta P}$ - cost of power transmission, RUR; IC - electric power supply interruption costs, RUR.

When calculating investments according to (2) it is necessary to take into account wires cost, OHL construction costs, climate region and investments into the switching equipment.

$$I = I_{OHL} + I_{SE}, \quad (2)$$

where I_{OHL} – investments into the OHL construction costs, RUR; I_{SE} - investments into the switching equipment, RUR.

The cost of power transmission is calculated according to (3)

$$OC_{\Delta P} = \sum_{i=1}^n \Delta P_i \cdot \tau_i \cdot \beta_i, \quad (3)$$

where n – number of EPS regions; ΔP_i – power losses, kW; τ_i – the using time of power losses, h; β_i – electricity rate, RUR/kWh.

Power losses are calculated with respect to EPS operation mode parameters. Electricity cost is offended by the power supply organization. The using time of power losses according to [2] is to be computed using the following empirical equation (4).

$$\tau = \left(0.124 + \frac{T_{\max}}{10000} \right)^2 \cdot 8760, \quad (4)$$

where T_{\max} – maximum load utilization time, h [2].

Supply interruption costs are defined by the reliability of the chosen scheme by (5) formula, specifically by the main reliability targets and per unit economical damage, mentioned in [11]:

$$IC = [(pud_s + pud_p \cdot T_{r,t}) \cdot w_t] \cdot p, \quad (5)$$

where pud_s – per unit sudden economical damage, RUR/unit; pud_p – per unit productivity economical damage, RUR/unit·h; $T_{r,t}$ – EPS total recovery time, h; w_t – total failure rate, 1/year; p – average annual productivity, unit·kWh.

Dependent (6) and independent (7) limitations are kept in mind. The first are voltages in EPS nodes, power flows in OHL. The second are loads, admissible voltage losses, permissible continuous current in EPS elements, amount of power given by the power source.

$$\begin{cases} I_{adm} \geq I_{\max}, \\ U_{adm} = \frac{U_n \cdot 100\%}{U_{nom}} \leq \pm 5\% U_{nom}. \end{cases} \quad (6)$$

where I_{adm} and I_{\max} – admissible and maximum conductor current, A; U_n – node voltage, kV; U_{adm} – admissible voltage losses of EPS, kV; U_{nom} – nominal voltage of EPS, kV.

$$\begin{cases} S_{load} = \text{const}, \\ P_{\min} \leq P_{gen} \leq P_{\max}. \end{cases} \quad (7)$$

where S_{load} – power load, kVA; P_{gen} – load-supplying capacitance, kW; P_{\min} and P_{\max} – minimum and maximum power output, kW.

Also it is necessary to mention the power balance of EPS (8)

$$P_{gen} = P_{load} + \Delta P. \quad (8)$$

3. Corrected transmission lines mathematical models

Power flow and losses computation results are defined mostly by the mathematical models of OHL. The away of OHL modeling depends mostly on the aims of the mode computation. Thus the most widely spread way to represent the OHL in the power system steady-mode calculation is the use of their specific parameters [12, 13]. Another way of OHL modeling implies the calculation of lines conductors mutual inductance and capacitance [14]. This model is more accurate, but the scope of its application often limited to the EPS out-of-balance operating conditions computation [15] and place of damage determination in 110 kV network [16].

The modeling of OHL by the specific electric parameters leads to the underprediction of specific impedance and as a result to the overestimation of power losses. The use of such an approach in EPS engineering and optimal wires cross section choice could result in wrong decision. The authors of the paper suggest to use in EPS under engineering operating mode forecast analysis aimed to its optimization the specific U-shaped equivalent circuit (fig. 1) taking into account not only the model of phase wires, but also their relative position on the OHL tower.

The U-shaped equivalent circuit given in the paper allows to compute OHL parameters as lumped, which keeps the calculation process simple comparing to the use of distributed parameters [17].

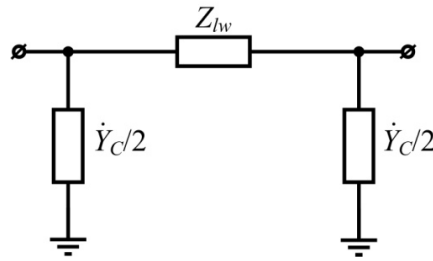


Fig. 1. U-shaped equivalent circuit of OHL.

Lengthwise impedance is formed by the impedance of “wire-ground” conductor \dot{Z}_L and mutual inductance between phase wires of one and the same circuit \dot{Z}_M which diminish equivalent lengthwise impedance. The active part of “wire-ground” impedance is the sum of wire resistance r_w and r_g resistance which takes into account the losses of active power because of current flow in the ground and equals $0.05 \text{ } \Omega/\text{km}$ [18]. Reactive part of above mentioned impedance depends on the equivalent return conductor depth in the ground D_g , which equals 935 m, and equivalent conductor radius $\rho_{c,e}$ (9):

$$\rho_{c,e} = k \cdot \rho_w, \quad (9)$$

where ρ_w – real wire radius; k – factor, considering the inner magnetic field of the conductor and equals 0.779 for solid round cross section conductors made of nonmagnetic materials, 0.95 for aluminium steel supported conductor, 0.82 for aluminium steel supported conductor with two or three lay-ups.

Mutual inductance impedance depends on the r_g , equivalent return conductor depth in the ground D_g and geometric mean distance between the phase wires D_m , which for the single-circuit OHL is:

$$D_m = \sqrt[3]{D_{L1L2}D_{L2L3}D_{L3L1}}. \quad (10)$$

Taking into consideration all the above mentioned information specific lengthwise impedance is:

$$\dot{Z}_{lw} = r_w + i0,1451 \lg \frac{D_m}{\rho_{c,e}}. \quad (11)$$

To calculate the capacitance of OHL the important initial condition is capacitance between phase conductors and ground which with respect to the method of electrical images [19, 20] is:

$$C = 1/(\alpha_{own} - \alpha_{mut}), \text{ F/km} \quad (12)$$

where α_{own} – own potential coefficient (13), α_{mut} – mutual potential coefficient (14).

With the knowledge of the distance between phase conductor and its electrical image S_{pp} it is possible to calculate own potential coefficient:

$$\alpha_{own} = 41.4 \cdot 10^6 \cdot \lg \left(\frac{\sqrt[3]{S_{L1L1}S_{L2L2}S_{L3L3}}}{\rho_w} \right). \quad (13)$$

Mutual potential coefficient is calculated with the help of distance between the conductor of one phase and electrical image of another $S_{pp'}$:

$$\alpha_{mut} = 41.4 \cdot 10^6 \cdot \lg \left(\sqrt[3]{\frac{S_{L1L2} S_{L1L3} S_{L2L3}}{D_{L1L2} D_{L1L3} D_{L2L3}}} \right). \quad (14)$$

Putting (13) and (14) into (12) the equation for calculation of capacitance between OHL wires and ground is formed:

$$C = \frac{0.241 \cdot 10^{-6}}{\lg \frac{D_m \sqrt[3]{S_{L1L1} S_{L2L2} S_{L3L3}}}{\rho_w \sqrt[3]{S_{L1L2} S_{L1L3} S_{L2L3}}}}. \quad (15)$$

Specific capacitive admittance of OHL:

$$\dot{Y}_C = i2\pi fC. \quad (16)$$

References

- [1] I.R. Abdulveleev, G.P. Kornilov, A.N. Shemetov, Automated calculation of mechanical efforts of overhead power transmission lines in emergency modes, *Electrical equipment: operation and maintenance*. 7 (2014) 30–38.
- [2] A.A. Gerasimenko, V.T. Fedin, *Transmission and distribution*, KNORUS, Moscow, 2012.
- [3] N. Sadati, M.H. Ramezani, Optimization of large-scale systems using gradient-type interaction prediction approach, *Electrical Engineering*. 91 (2009) 301–312.
- [4] J. Radosavljević, M. Jevtić, N. Arsić, D. Klimenta, Optimal power flow for distribution networks using gravitational search algorithm, *Electrical Engineering*. 96 (2014) 335–345.
- [5] A.A. Abou El Ela, M.A. Abido, S.R. Spea, Optimal power flow using differential evolution algorithm, *Electrical Engineering*. 91 (2009) 69–78.
- [6] S. Kahourzade, A. Mahmoudi, H.B. Mokhlis, A comparative study of multi-objective optimal power flow based on particle swarm, evolutionary programming, and genetic algorithm, *Electrical Engineering*. 97 (2015) 1–12.
- [7] K. Fraundorfer, H. Glavitsch, R. Bacher, *Optimization in planning and operation of electric power systems*, Lecture Notes of the SVOR/ASRO Tutorial Thun, Switzerland, 1992.
- [8] P.E. Gill, W. Murray, M.A. Saunders, M.H. Wright, *Sparse matrix methods in optimization*, Society for Industrial and Applied Mathematics. 5(3) (1984) 562–589.
- [9] Xin-She Yang, *Engineering optimization*, New Jersey, John Wiley and Sons, 2010.
- [10] S.A-H Soliman, A-A.H. Mantawy, *Modern optimization techniques with applications in electric power systems*, Springer-Verlag New York, 2012.
- [11] A.N. Shemetov, *ERCOT electric reliability*, NSTU, Magnitogorsk, 2007.
- [12] K. Fraundorfer, H. Glavitsch, R. Bacher, *Optimization in Planning and Operation of Electric Power System*, Lecture Notes of the SVOR/ASRO Tutorial Thun, Physica-Verlag Heidelberg, Switzerland, 1993.
- [13] F. Kiessling, P. Nefzger, J.F. Nolasco, U. Kaintzyk, *Overhead Power Lines. Planning, Design, Construction*, Springer-Verlag Berlin Heidelberg, 2003.
- [14] A.E. Guile, W. Paterson, *Electrical power systems*, second ed., Pergamon Press, Oxford, 1977.
- [15] J. M. Nahman, Zero-sequence representation of overhead lines, *Electrical Engineering*. 65(4) (1982) 209–217.
- [16] M.Sh. Misrikhanov, V.A. Popov, R.V. Medov, D.Yu. Kostyunin, Error of the Method of Determination of the Place of Damage of Overhead Lines Due to Ignored Phase Differences in Its Parameters, *Power Technology and Engineering*. 36(6) (2002) 363–366.
- [17] O.V. Gazizova, A.A. Abdulkhalikova, Transmission capacity research of feed power lines of large industrial power unit, *Electrotechnical systems and complexes*. 2(23) (2014) 48–52.
- [18] *Emergency procedure of protective relay, Short-circuit current calculation for protective relaying and automation of 110-750 kV network*, Energiya, Moscow, 1979.
- [19] P. Zhou, *Numerical Analysis of Electromagnetic Fields*, Springer Berlin Heidelberg, 1993.
- [20] A.L. Shenkman, M. Zarudi, *Circuit Analysis for Power Engineering Handbook*, Springer US, 1998.

International Conference on Industrial Engineering

Correction of rotor rotation irregularity of permanent magnet synchronous motor in a controlled synchronous mode

Voronin S.G., Kurnosov D.A., Korobotov D.V.* , Kulmukhametova A.S.

South Ural State University, 76, Lenin Avenue, Chelyabinsk, 454080, Russian Federation

Abstract

While the permanent magnet synchronous motor (PMSM) operation in the synchronous mode rotor speed average value coincides with current frequency in the windings by definition. However instantaneous value of rotation speed can differ from the average one significantly in the process of oscillations occurring in the PMSM rotor and stator electromechanical system. This article describes a refined mathematical model of permanent magnet synchronous motor (PMSM) operating in the synchronous rotation mode allowing to explore rotor speed oscillations arising in the synchronous mode. On the basis of the mathematical model the article provides a theoretical foundation and the example of specific implementation of one of the oscillation damping ways of the PMSM rotor with permanent-magnet excitation in the synchronous mode by introducing a current feedback to the impact on the stator phase voltage. The transfer function of the compensating device, affecting the voltage phase on the motor windings and providing a significant reduction of PMSM rotor rotation irregularity is synthesized on the basis of matrix transfer function of interrelationship between output variables and input signals.

© 2015 The Authors. Published by Elsevier Ltd. This is an open access article under the CC BY-NC-ND license (<http://creativecommons.org/licenses/by-nc-nd/4.0/>).

Peer-review under responsibility of the organizing committee of the International Conference on Industrial Engineering (ICIE-2015)

Keywords: permanent magnet synchronous motor, oscillations damping, synchronous operating mode of PMSM ;

1. Task description

It is comparatively simple to implement the vector control system with the help of permanent-field synchronous motors if it has a rotor angular position sensor with fine resolution. If however such sensor is absent due to structural and space limitations, then only indirect rotational positional sensing on signals of current and voltage sensors is

* D.A. Kurnosov. Tel.: +7-912-479-5600
E-mail address: kurnosovda@susu.ac.ru

possible. The complex algorithms involving lots of computing resources are used for it [1, 2]. Meanwhile in some cases when a resistive torque on a motor shaft is changing insignificantly, it is possible to implement a simplified form of vector control – so called controlled synchronous operating mode [3]. While implementation such mode three-phase sinusoidal voltage is energized on a motor stator winding as in a classical synchronous motor. It provides a steady vector rotation of stator field. In order to leave the rotor motor in the synchronous mode, signals from rotor position discrete sensor (RPS) are used, for instance, based on Hall sensors installed in the motor air gap. The coarse control of rotor angular position to stator is carried out according to the signals from discrete RPS. If this angular deviation reaches some critical value, motor source voltage is changed in the way that to bring this deviation to required value [4]. In a steady mode when there are no grand disturbances, motor rotor is rotating at a speed of stator field rotation. However as it is known, the rotor of a synchronous motor is apt to oscillations for which reason in many cases a damping winding is installed on it in order to remove these oscillations. In motors with permanent-magnet excitation such winding significantly complicates the rotor configuration and not always solves oscillability problem as well as degrades general dynamic properties of the motor. This article provides a theoretical foundation and the example of specific implementation of one of the oscillation damping ways of the PMSM rotor in the synchronous mode by introducing a current feedback to the impact on the stator phase voltage.

2. Refinement of synchronous motor mathematical model in a small oscillation mode

We get a block scheme of PMSM in the synchronous rotation mode from a simplified mathematical motor model presented in [5,6] taking a commutating angle as variable ($\theta=var$) in it. Then a block scheme gets a view of Fig. 1.

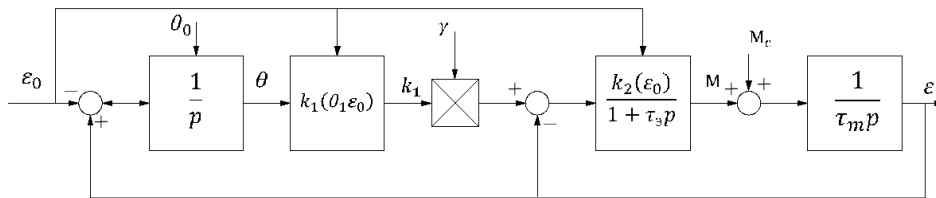


Fig. 1. Block scheme of PMSM in the synchronous rotation mode.

Fig. 1 shows: ϵ_0 is preselected synchronized relative rotor speed, where ideal unload speed (ω_0) as $\theta=0$ is taken as basis speed value; p is operator of differentiation; $\tau_e = \omega_0 L/R$ is relative electromagnetic constant of phase winding; L, R is respectively total inductance and active resistance of phase winding; τ_m is relative value of electromechanical time constant equal to product of absolute constant (T_m) and idle speed; coefficients $k_1(\theta, \epsilon_0)$ and $k_2(\epsilon_0)$ are determined from equations 1, 2:

$$k_1(\theta, \epsilon_0) = \cos\theta + \epsilon_0 \tau_e \sin\theta, \tag{1}$$

$$k_2(\epsilon_0) = 1/[1 + (\epsilon_0 \tau_e)^2]. \tag{2}$$

As it is seen from the block scheme, the PMSM model is non-linear both towards to input signals and to output variables. This circumstance significantly complicates the analysis of dynamic and static modes of PMSM. Let us conduct linearization of mathematical model. We should implement a standard method of linearization with Taylor expansion of non-linear functions in the vicinity of reference trajectory and truncation till linear terms [7]. As a result of quite cumbersome transformations we get a linearized block scheme of PMSM as Fig. 2.

Compared to the scheme on Fig. 1 the regulation possibility of phase to neutral voltage by actuating signal γ is taken into consideration in this block scheme. Besides, it is denoted:

$$k_3(\bar{\theta}, \bar{\gamma}, \bar{\epsilon}_0) = \bar{\gamma}(\bar{\epsilon}_0 \tau_e \cos\bar{\theta} - \sin\bar{\theta}), \tag{3}$$

$$k_4(\bar{\varepsilon}, \bar{\theta}, \bar{\gamma}, \bar{\varepsilon}_0) = \frac{\tau_e [\bar{\gamma} \sin \bar{\theta} - \bar{\gamma} \bar{\varepsilon}_0 \tau_e (2 \cos \bar{\theta} + \bar{\varepsilon}_0 \tau_e \sin \bar{\theta}) + 2 \bar{\varepsilon}_0 \bar{\varepsilon} \tau_e]}{[1 + (\bar{\varepsilon}_0 \tau_e)^2]}$$

$$\bar{\theta} = \bar{\vartheta} + \bar{\theta}_0.$$

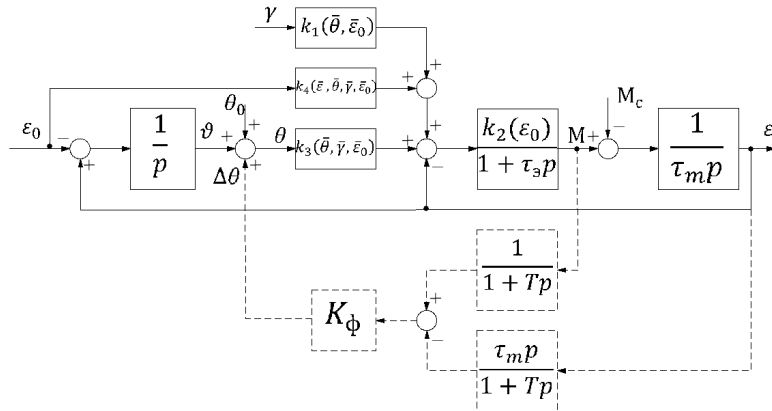


Fig. 2. Linearized block scheme of PMSM in the synchronous rotation mode.

The reference coordinate values are marked by dashes on top relative to which linearization is being implemented.

Linearized model presented in state space can be written over as (equations are written in deviations relative to system reference trajectory):

$$\begin{aligned} \dot{x} &= Ax + Bu, \\ y &= Cx + Du. \end{aligned}$$

Here in addition to state vectors $x = (\mu, \varepsilon, \vartheta)^T$ and input signals $u = (\gamma, \theta_0, \varepsilon_0, \mu_c)^T$ vector of output variables is introduced $y = (\mu, \varepsilon, \theta)^T$. For matrixes A, B, C and D it is correctly

$$A = \begin{bmatrix} -1 & -1 & \bar{\gamma} [\bar{\varepsilon}_0 \tau_e \cos \bar{\theta} - \sin \bar{\theta}] \\ \tau_e & \tau_e [1 + (\bar{\varepsilon}_0 \tau_e)^2] & \tau_e [1 + (\bar{\varepsilon}_0 \tau_e)^2] \\ 1 & 0 & 0 \\ \tau_m & 1 & 0 \\ 0 & 1 & 0 \end{bmatrix},$$

$$B = \begin{bmatrix} \frac{\cos \bar{\theta} + \bar{\varepsilon}_0 \tau_e \sin \bar{\theta}}{\tau_e [1 + (\bar{\varepsilon}_0 \tau_e)^2]} & \frac{\bar{\gamma} [\bar{\varepsilon}_0 \tau_e \cos \bar{\theta} - \sin \bar{\theta}]}{\tau_e [1 + (\bar{\varepsilon}_0 \tau_e)^2]} & \frac{\bar{\gamma} \sin \bar{\theta} - \bar{\gamma} \bar{\varepsilon}_0 \tau_e [2 \cos \bar{\theta} + \bar{\varepsilon}_0 \tau_e \sin \bar{\theta}] + 2 \bar{\varepsilon}_0 \bar{\varepsilon} \tau_e}{[1 + (\bar{\varepsilon}_0 \tau_e)^2]^2} & 0 \\ 0 & 0 & 0 & -\frac{1}{\tau_m} \\ 0 & 0 & -1 & 0 \end{bmatrix},$$

$$C = \begin{bmatrix} 1 & 0 & 0 \\ 0 & 1 & 0 \\ 0 & 0 & 1 \end{bmatrix},$$

$$D = \begin{bmatrix} 0 & 0 & 0 & 0 \\ 0 & 0 & 0 & 0 \\ 0 & 1 & 0 & 0 \end{bmatrix}.$$

The state vector and output vector views will be as follows

$$\begin{aligned}x(p) &= (pE - A)^{-1}Bu(p), \\y(p) &= [C(pE - A)^{-1}B + D]u(p).\end{aligned}$$

The association matrix between output variables and input signals under zero initial conditions is called a matrix transfer function and designated as

$$W(p) = C(pE - A)^{-1}B + D. \quad (4)$$

It is represented by a matrix with the following components:

$$W(p) = \begin{bmatrix} W_{11}(p) & W_{12}(p) & W_{13}(p) & W_{14}(p) \\ W_{21}(p) & W_{22}(p) & W_{23}(p) & W_{24}(p) \\ W_{31}(p) & W_{32}(p) & W_{33}(p) & W_{34}(p) \end{bmatrix}, \quad (5)$$

where $W_{ij}(p) = y_i(p)/u_j(p)$ is scalar transfer functions, tying two coordinates. For instance, $W_{11}(p)$ ties an electromagnetic motor torque μ with actuating signal θ_0 and it is as follows

$$W_{12}(p) = \frac{\mu(p)}{\theta_0(p)} = \frac{\tau_m p^2 \bar{\gamma} (\sin \bar{\theta} - \bar{\varepsilon}_0 \tau_e \cos \bar{\theta})}{[1 + (\bar{\varepsilon}_0 \tau_e)^2] (\tau_e \tau_m p^3 + \tau_m p^2) + p + \bar{\gamma} (\sin \bar{\theta} - \bar{\varepsilon}_0 \tau_e \cos \bar{\theta})}.$$

Other transfer functions will differ only in numerator, tying other coordinates.

The matrix transfer function (5) can be used both for analytic survey of dynamic processes and for compensating devices synthesis. Its analysis allows to express different strategies of valve electric drive control for all its operating modes. Let us deal with one of it.

3. The practical implementation of corrective action in the electric motor drive

Let us study a synchronous operating mode of PMSM. For improving accuracy of speed control while load fluctuations we introduce into control law a component, depending on the electromagnetic torque variation. Such additional feedback in relation to supported speed rate and amount of load should correct either amplitude (γ) or phase (θ_0) of PMSM source voltage. Let us implement the latest correction variant. Technically such implementation is quite simple. Information about load torque value of the motor can be obtained with the help of reduced observer [8] in accordance with equation

$$\hat{\mu}_c(p) = W_\varepsilon(p)\varepsilon(p) + W_\mu(p)\mu(p),$$

where $W_\varepsilon(p)$, $W_\mu(p)$ is corrective transfer functions by corresponding variables. The latest can be chosen in the following view

$$W_\varepsilon(p) = \frac{-\tau_m p}{1 + Tp}, \quad W_\mu(p) = \frac{1}{1 + Tp}.$$

Here time constant T is entitled to setting.

Based on this information the compensating device generates the actuating signal in the form of phase shift of basic impulses, stating the frequency of motor source voltage. Then, phase of motor source voltage by signals of the compensating device can be shifted inertialess back and forth, changing the angle current value θ . On the block scheme (Fig. 2) a functional implementation of the compensating device is shown by dotted lines. At the same time

a phase-shifting device is accepted as inertialess with the transfer factor $K\phi$. It is obvious that changing the view and parameters values $W(p)$ we can effect dynamic properties of the electric motor drive.

Below on Fig. 3 the results of valve electric drive operation modelling in the synchronous mode with the additional correction are presented. Modelling was conducted with following initial data: $\gamma = 1$, $\varepsilon_0 = 0.5$, $\tau_e = 0.1$, $\tau_m = 5$, $T = 0.01$. At the time $t=80$ load torque rise was carried out ($\Delta\mu_c = +0.4$), and at the time $t=110$ loss of load torque was performed ($\Delta\mu_c = -0.4$). On Fig. 3 the diagrams of speed $\varepsilon(t)$, of load torque $\mu_c(t)$ and of commutating angle variations $\theta_0(t)$ are presented.

For illustrative purposes on one fig. 3 two speed performance curves are given: the one – without introduction of the additional correction (without feedback), the other – with introduction into control loop of PMSM the corrective feedback up to moment variation (with feedback). The introduction of this feedback while altering the load torque to 0.4 ea. causes commutating angle alternation approximately to 0.6 ea. The diagrams demonstrate a high efficiency of such additional corrective feedback, velocity error is reduced from 33% to 1.7%, i.e. approximately in twenty times.

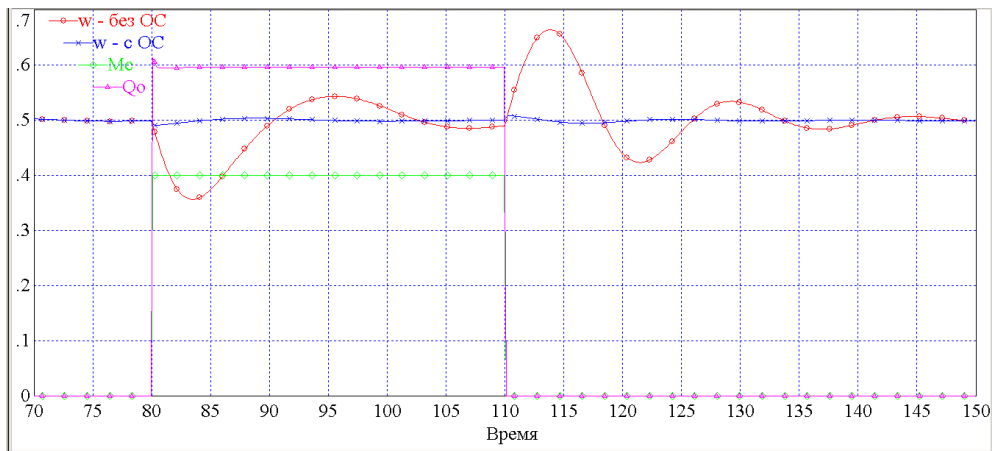


Fig. 3. The results of permanent-magnet synchronous motor operation modelling in a synchronous mode.

As a result of optimal adjustment of such feedback, which can be carried out by involvement of corresponding matrix components (5), it is possible to achieve a practical invariance of valve electric drive to load torque variations.

Acknowledgment

This work was supported in part by R.F. Ministry of Education under Grant 14.577.21.0154 of 28.11.2014 (RFMEFI57714X0154).

References

- [1] C. Busca, Open loop low speed control for PMSM in high dynamic application, Denmark, Aalborg university, 2010.
- [2] S.G. Voronin, D.A. Kurnosov, A.S. Kul'mukhametova, Vector control of permanent-magnet synchronous motors, Russian Electrical Engineering 84, Issue 10, pp 581–585.
- [3] D.V. Korobotov, A.S. Kulmukhametova, A.A. Shevchenko, Controlled synchronous mode in a ventilator, Electrical equipment and systems: collection of scientific papers. 20 (2012) 79–82.
- [4] A.S. Kulmuhametova, D.V. Korobotov, Implementation of vector control and synchronous mode SMPM, Proceedings of the International Scientific and Technical Conference in 3 tons "State and Prospects of Electrotechnology". 3 (2013) 111–113.
- [5] S.G. Voronin, D.V. Korobotov, R.T. Kiyakpaev, A.S. Kulmuhametova, Dynamic models of the electric motors at different combinations of parameters, Proceedings of the Academy of Electrical Sciences. 2011 58–63.

- [6] S.G. Voronin, D.A. Kurnosov, P.O. Shaburov, A.S. Kulmuhametova, Mathematical model of dynamic processes in the electric drive of valves, "Electrical Equipment and Systems ": collection of scientific papers. 20 (2012) 132–140.
- [7] N.D. Yegupova, Methods of classical and modern control theory: Analysis and statistical dynamics of automatic control systems, Moscow, 2000.
- [8] S.G. Voronin, D.A. Kurnosov, D.V. Korobotov, P.O. Shaburov, A.S. Kul'mukhametova, Electromagnetic and Resistance Torque on a Synchronous Motor Shaft with Permanent Magnet Excitation, Russian Electrical Engineering. 83(2) 61–63.

International Conference on Industrial Engineering

Effect of different winding switching methods on regulating and energetic characteristics of synchronous motor with permanent magnet excitation

Voronin S.G., Kurnosov D.A., Korobatov D.V., Kulmukhametova A.S.*

South Ural State University, 76, Lenin Avenue, Chelyabinsk, 454080, Russian Federation

Abstract

The article contains evaluation of effect of different winding switching methods for synchronous motor with permanent magnet excitation (SMPM) on energetic efficiency, possibility of enlarging the ranges of working speeds and torques, adaptation of regulating characteristics with the aim of using it in particular electric drive. The evaluation is performed at similar values of relative speed and relative inductance. The conditions, which make sensible the usage of 120-degree or 180-degree switching, meanwhile all considered SMPM characteristics are not worse than those under vector control, are defined. It is proved, that there is a possibility to minimize engine's energy consumption by regulating switching angle, as well as change it's mechanical characteristics. In particular, it is possible to get mechanical SMPM characteristic, typical for direct-current motor with series excitation, suitable for usage in electric traction drive.

© 2015 The Authors. Published by Elsevier Ltd. This is an open access article under the CC BY-NC-ND license (<http://creativecommons.org/licenses/by-nc-nd/4.0/>).

Peer-review under responsibility of the organizing committee of the International Conference on Industrial Engineering (ICIE-2015)

Keywords: Synchronous Motor with Permanent Magnet, windings switching methods, vector control, electromagnetic efficiency.

1. Introduction. Task statement.

When choosing type and principle of motor drive construction they mostly are guided by providing preset range of operation speeds, torques and minimizing of energy usage. For the purposes of getting the best energy indicators the most perspective are SMPM. There are various ways of switching the windings SMPM. For example, discrete

* D.A.Kurnosov. Tel.: +7-912-479-5600
E-mail address: kurnosovda@susu.ac.ru

switching, when stator field vector is rotating discretely through stator bore according to the signals of rotor position sensor (RPS). There is also a vector control, when field vector is rotating gradually. The mentioned above ways of motor power admit the changing of stator field vector magnitude and of its angular position relative to the rotor field. This fact determines the possibility of the influence on the energy characteristics as well as on the adjusting properties of the drive.

Discrete switching the SMPM windings leaves open the possibility of cheap technical solutions in comparison with vector control, which is more expensive. Formation algorithms of stator field are resource-intensive (they can only be performed with process-specific microcontrollers). That is why arises the problem of comparative evaluation of different ways of switching the SMPM winding according to the energetic efficiency, the possibility to enlarge the range of working speeds and torques, and improvement of adjusting properties. The article describes the problem solution and gives recommendations, which give the possibility to choose SMPM power rationally on a certain electric drive.

2. Methods of SMPM characterization in steady-state

SMPM under vector control can be characterized as a synchronous motor, powered by harmonic voltage source with fixed value of torque angle (θ) [1,2], which is called switching angle in SMPM theory. Then to define electromagnetic and working power in steady-state we can use expressions, acknowledged in synchronous machine theory. Particularly, if we assume that SMPM stator is having permanent-magnet excitation and the difference of magnetic reactance along the axis d and q can be neglected, equations of relative values of electromagnetic (P_e) and working (P_w) powers can be written as [3]:

$$P_e = \frac{v \cdot (\cos(\theta) + v \cdot \xi \cdot \sin(\theta) - v)}{1 + \xi^2}, \quad (1)$$

$$P_w = \frac{v \cdot (\xi \cdot \sin(\theta) - \cos(\theta)) + 1}{1 + \xi^2}, \quad (2)$$

where $v = K\Phi\omega/U$ is relative motor speed, ω is instantaneous speed of armature rotation, Φ is instantaneous flux value, K is structural factor, which is defined by $K = pN/2a$, where p is a number of pairs of poles, N , a is respectively, number of active wires and number of parallel paths of armature winding; $\xi = \omega L/R$ is parameter defined by the SMPM construction, where L, R is magnetic and active reactance of winding.

Electromagnetic efficiency (η) will be defined by ratio of electromagnetic and working power

$$\eta = P_e/P_w. \quad (3)$$

Under discrete switching of three-phase SMPM there are two ways of switching: 180-degree and 120-degree [4,5]. In the first instance on every interswitching interval (ISI) there are three phase winding connected to power supply bus lines, in the second – just two phase windings. Electromagnetic processes, and thus the energy performance of the motor at various ways of switching the windings are different. Mathematical models that describe these processes, are now well-established [4,6–8]. For performance analysis of working characteristics, defining electromagnetic and working powers, as well as efficiency any of them can be chosen. We used the model described in the reference [6].

3. Comparative evaluation of switching methods in SMPM according to efficiency characteristics

Comparative evaluation of all SMPM switching methods, mentioned above was made at similar values of ξ and v . Depending on the switching method, electromagnetic power and electromagnetic efficiency of SMPM were calculated either according to the expressions (1-3), or to the models, given in [4,6–8]. According to the calculations were built some ratios of those variables and switching angle θ at $\xi = [0.5; 0.05]$ and $v = [0.5; 0.8]$, shown in Fig. 1.

From comparison of the given ratios we can deduce:

1. The highest efficiency for motors with relatively low inductance of winding ($\xi < 1$) we get at 120-degree

switching. Vector control is slightly inferior. The worst variant is 180-degree switching.

2. At $\xi > 1$ ratios of $\eta(\theta)$ and $Pe(\theta)$ for SMPM with vector control and 180-degree switching are practically the same and have their maximum in electromagnetic power and efficiency.

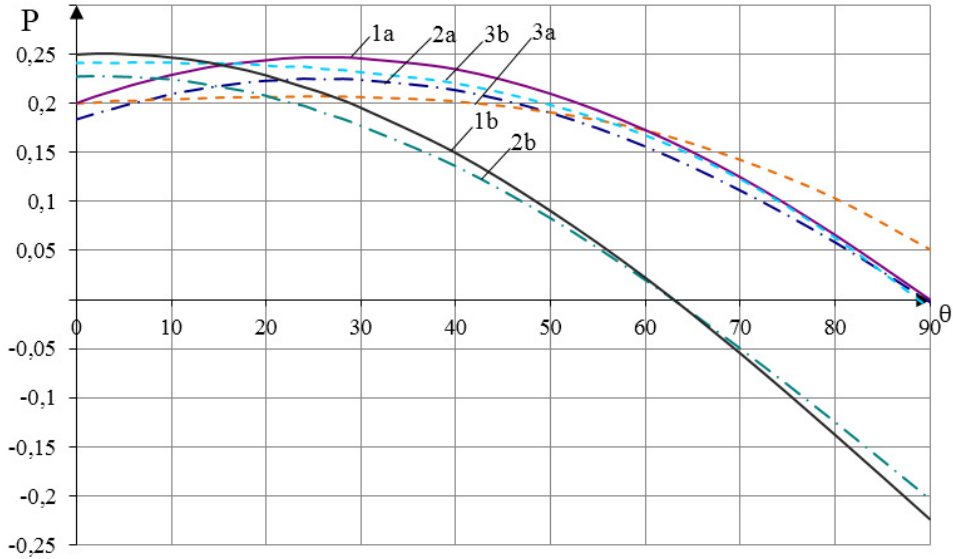


Fig. 1. Ratio of electromagnetic power Pe and switching angle θ at $v = 0.5$ for $\xi = [0.5; 0.05]$, where 1a – Pe under vector control for $\xi = 0.5$; 1b – for $\xi = 0.05$; 2a – Pe at 180-degree switching for $\xi = 0.5$; 2b – for $\xi = 0.05$; 3a – Pe at 120-degree switching for $\xi = 0.5$; 3b – for $\xi = 0.05$

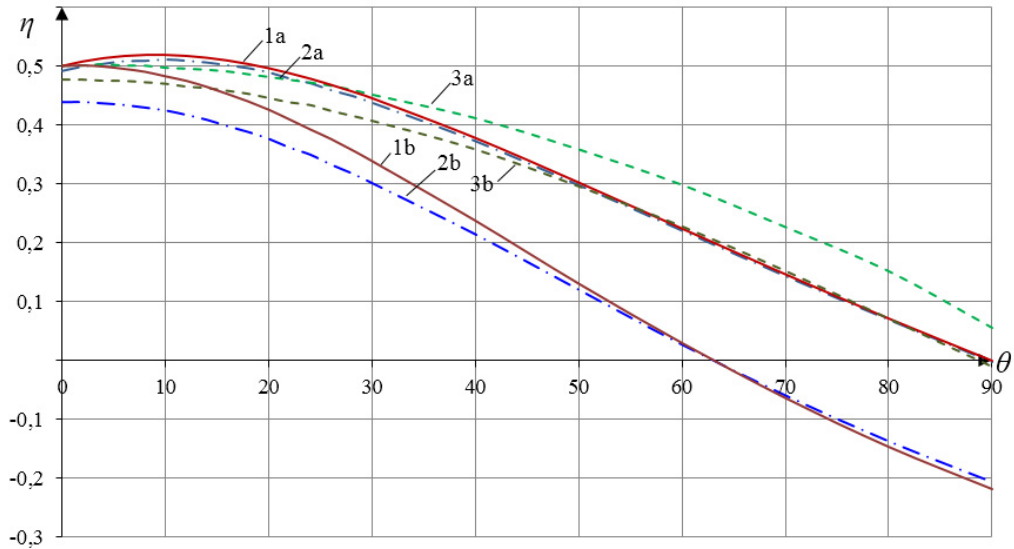


Fig. 2. Ratio of electromagnetic efficiency and switching angle θ at $v = 0.5$ for $\xi = [0.5; 0.05]$, where 1a – efficiency under vector control for $\xi = 0.5$; 1b – for $\xi = 0.05$; 2a – efficiency at 180-degree switching for $\xi = 0.5$; 2b – for $\xi = 0.05$; 3a – efficiency at 120-degree switching for $\xi = 0.5$; 3b – for $\xi = 0.05$

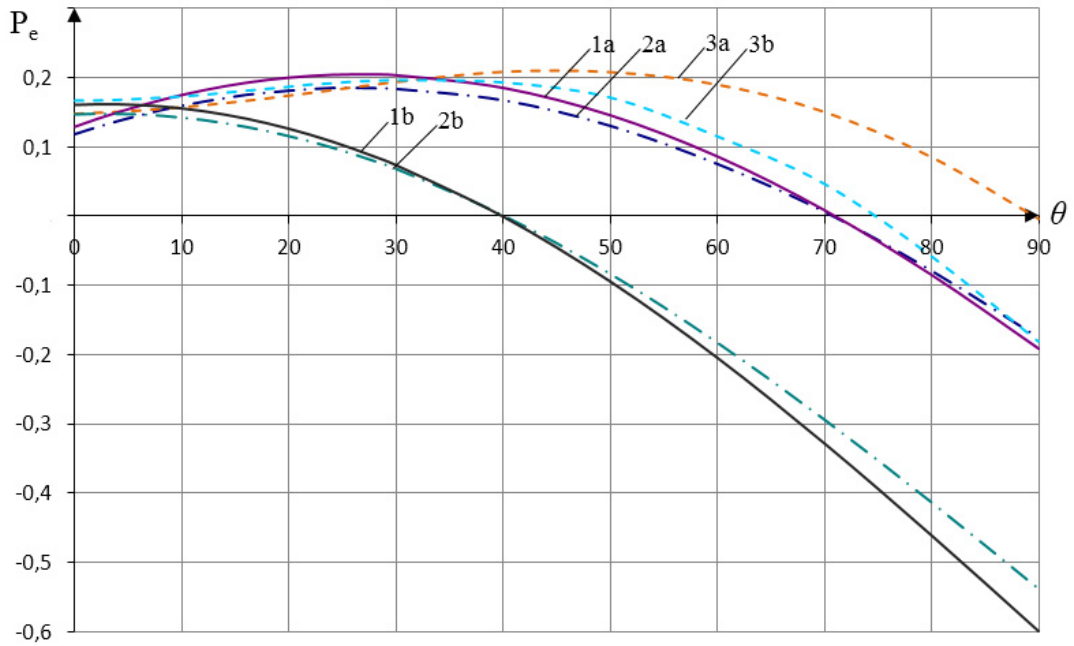


Fig. 3. Ratio of electromagnetic power P_e and switching angle θ at $v = 0.8$ for $\xi = [0.5; 0.05]$, where 1a – P_e under vector control for $\xi = 0.5$; 1b – for $\xi = 0.05$; 2a – P_e at 180-degree switching for $\xi = 0.5$; 2b – for $\xi = 0.05$; 3a – P_e at 120-degree switching for $\xi = 0.5$; 3b – for $\xi = 0.05$

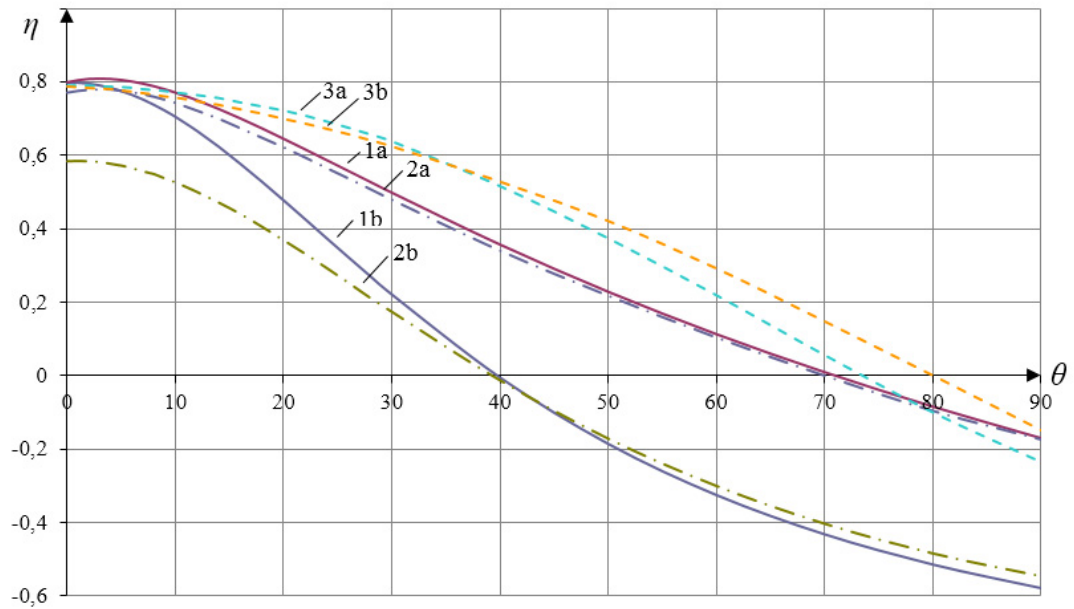


Fig. 4. Ratio of electromagnetic efficiency and switching angle θ at $v = 0.8$ for $\xi = [0.5; 0.05]$, where 1a – efficiency under vector control for $\xi = 0.5$; 1b – for $\xi = 0.05$; 2a – efficiency at 180-degree switching for $\xi = 0.5$; 2b – for $\xi = 0.05$; 3a – efficiency at 120-degree switching for $\xi = 0.5$; 3b – for $\xi = 0.05$

From comparison of the given ratios we can deduce:

1. The highest efficiency for motors with relatively low inductance of winding ($\xi < 1$) we get at 120-degree switching. Vector control is slightly inferior. The worst variant is 180-degree switching.

2. At $\xi > 1$ ratios of $\eta(\theta)$ and $Pe(\theta)$ for SMPM with vector control and 180-degree switching are practically the same and have their maximum in electromagnetic power and efficiency.

3. For the characteristics under consideration at 120-degree switching the value of electromagnetic power and efficiency decreases with increasing of θ with the changing of switching angle from 0 to $\pi/2$. Therefore, the optimal value for switching angle in this switching method is $\theta = 0$ both for the electromagnetic power and efficiency.

It may be noted that for the certain values of parameters and rotation speed, the current of the section, disconnected from the power supply does not have time to decay to zero during one ISI. As a result, 120-degree switching ceases to differ from 180-degree switching by nature of electromagnetic processes and can be described by the same ratios. The equation of conditions determination for transfer from 120-degree switching to 180-degree is shown in [5] and in adopted system of relative units can be represented as

$$C_1 \cdot (1 - b) - C_2 \cdot b = 0 ,$$

where:

$$C_1 = (1 - b) + \frac{(v')^2 \cdot \xi}{1 + (v' \cdot \xi)^2} \cdot \left(\left[\frac{1}{v' \cdot \xi} \cdot \cos \theta - \sin \theta \right] \cdot b - \left[\frac{1}{v' \cdot \xi} \cdot \cos \left(\frac{\pi}{3} - \theta \right) - \sin \left(\frac{\pi}{3} - \theta \right) \right] \right);$$

$$C_2 = (1 - b) + \frac{(v')^2 \cdot \xi}{1 + (v' \cdot \xi)^2} \cdot \left(\left[\frac{1}{v' \cdot \xi} \cdot \cos \left(\frac{2\pi}{3} + \theta \right) - \sin \left(\frac{2\pi}{3} + \theta \right) \right] \cdot b - \left[\frac{1}{v' \cdot \xi} \cdot \cos \left(\frac{\pi}{3} + \theta \right) - \sin \left(\frac{\pi}{3} + \theta \right) \right] \right);$$

$$b = e^{-\frac{\pi}{3 \cdot \xi \cdot v}}; \quad v' = \frac{6}{\pi} \cdot v .$$

4. Definition of switching angle, corresponding to maximum value of electromagnetic torque and efficiency

When using 180-degree switching or vector control, the value of switching angle (θ^{\max}), corresponding to maximum value of electromagnetic efficiency, can be defined by well-known proportion [9]

$$\theta^{\max} = \arctg(\xi) . \tag{4}$$

It can be used to set regulating point of switching angle in dynamic modes, when it is important to provide maximum torque for the engine to finish transient process as soon as possible.

Analytic dependence for switching angle in relation to roll speed, which corresponds to maximum electromagnetic efficiency of the given SMPM, can't be define in elementary functions. Therefore, it is rational to use approximate fitting ratios. For their development there were several numerical experiments, which resulted in switching angle values θ_M , corresponding to the maximum value of electromagnetic efficiency and efficiency values in range of parameters $v = (0.1, \dots, 0.9)$ and $\xi = (0.1, \dots, 1.5)$. As a result of this experiment with the help of least-square method, some approximate ratios, linking θ_M , v and ξ became available. Polynomials of the second and third order were taken as basic functions for approximation [10]

$$\theta(v, \xi) = C_1 + C_2 \cdot v + C_3 \cdot \xi + C_4 \cdot v \cdot \xi + C_5 \cdot v^2 + C_6 \cdot \xi^2 + C_7 \cdot v^2 \cdot \xi + C_8 \cdot v \cdot \xi^2 + C_9 \cdot v^3 + C_{10} \cdot \xi^3 .$$

As a result of the calculation, it is managed to present polynomial of the second order as

$$\theta(v, \xi) = 7.15 - 28.11 \cdot v + 40.19 \cdot \xi - 34.54 \cdot v \cdot \xi + 21.67 \cdot v^2 - 5.40 \cdot \xi^2 . \tag{5}$$

Here sum squared error, calculated by method [11], is equal to $\Delta = 103.21$, relative error $\delta = 0.54\%$.

Accordingly, to obtain a third order polynomial

$$\theta(v, \xi) = 1.85 - 15.13 \cdot v + 56.44 \cdot \xi - 75.69 \cdot v \cdot \xi + 26.55 \cdot v^2 - 14.86 \cdot \xi^2 + 18.84 \cdot v^2 \cdot \xi +$$

$$+13.95 \cdot v \cdot \xi^2 - 13.3 \cdot v^3 - 1.03 \cdot \xi^3 \quad (6)$$

Here we have $\Delta=20,154$, $\delta=0,24\%$.

For evaluation of ratios (5) and (6) in whole working range of parameters there calculations were made and ratios $\theta_M = f(\xi)$ were built at different values of v , shown in Fig. 5 (dashed lines – calculated by expression (5), dash-dotted – by expression (6)). Analogical ratios, deduced by searching θ_M , at the known numerical values of v and ξ by expressions (1–3) are shown by solid lines. Comparison of these curves shows that it is possible to find θ_M by the expressions (5) or (6) with sufficient accuracy for optimization of the drive energy performance.

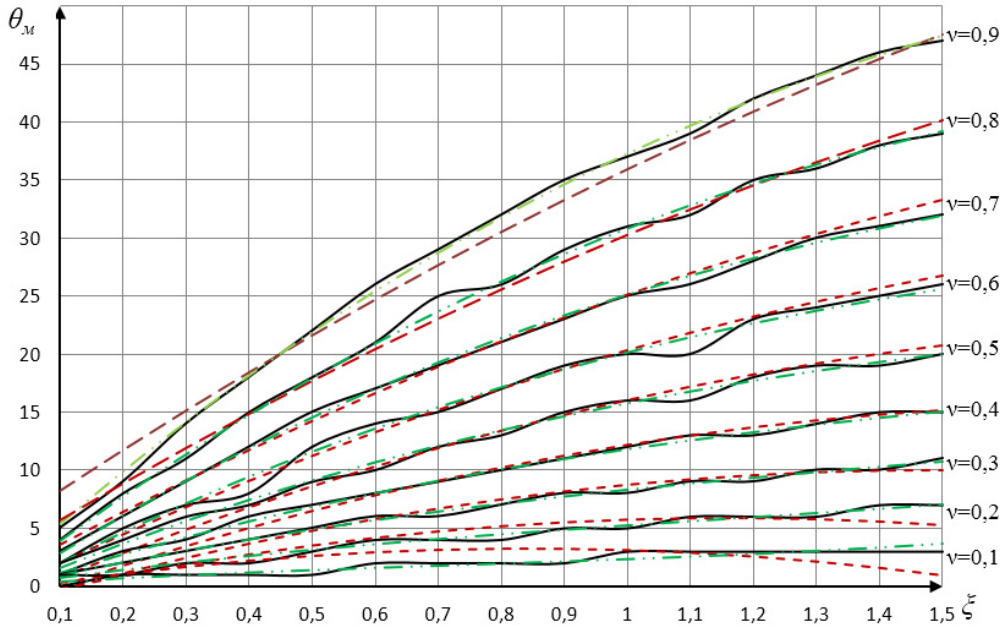


Fig. 5. Set of approximate ratios, allowing to choose the optimal switching angle θ_M in whole stator rotation speed range (v) for SMPM of the set construction (parameter - $\xi = \omega L/R$) according to the criterion of maximum electromagnetic efficiency in cases of vector control or 180-degree switching

5. SMPM regulating characteristics under vector control by changing of switching angle

As was noted before, when using vector control it is possible to regulate not only the stator field vector magnitude while it is rotating steadily, but also it's angular position in the respect of stator field vector. Such possibility allows to change the type of mechanical characteristic of the motor and it's working range of rotation speeds.

Fig. 6 illustrates SMPM mechanical characteristics at changing θ , defined by ratio (3) for different values of ξ . The curves illustrate, that by regulating of switching angle type of mechanical characteristics can be substantially changed from ones, corresponding to independent excitation motor to those, corresponding to series-wound motor. It is obvious, that according to requirements for the electric drive it is possible to regulate angle θ independently according to any unspecified law, which is chosen with regard to those requirements.

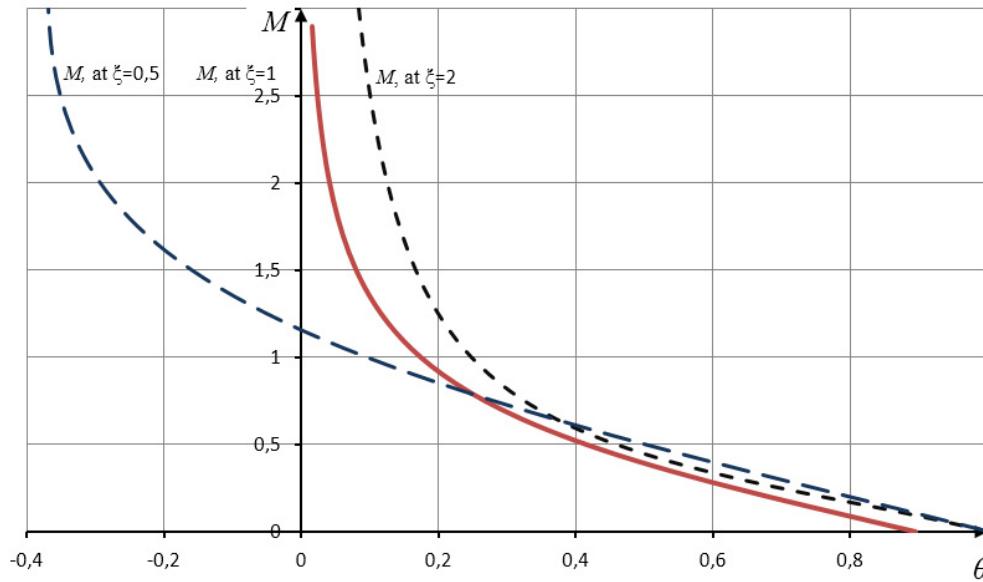


Fig. 6. SMPM mechanical characteristics at changing switching angle θ

6. Conclusion

In engines, having relatively low inductance values of armature winding, while using discrete switching from the point of energetic characteristics it is sensible to use 120-degree switching, which has characteristics not worse than those under vector control. In this case the most effective is neutral switching ($\theta=0$), providing maximum electromagnetic efficiency for the given speed and electromagnetic torque value, which is very close to maximum.

In case of a big relative inductance value, 120-degree switching is turning into 180-degree, that is why it is sensible to program engine work for this switching from the very beginning. At this value of angle θ , corresponding to the maximum efficiency and maximum torque will be different. For the definition of the first one of them, we can use expression (4), for the second one – expression (5) or (6). Those ratios can be used for realization of vector control of electric drive.

When using vector control, regulating SMPM switching angle, with the changing of rotation speed there is a possibility not only to minimize engine's energy consumption, but also change it's mechanical characteristics from ones, corresponding to independent excitation motor to those, corresponding to series-wound motor.

Acknowledgment

This work was supported in part by R.F. Ministry of Education under Grant 14.577.21.0154 of 28.11.2014 (RFMEFI57714X0154).

References

- [1] C. Busca, Open loop low speed control for PMSM in high dynamic application, Denmark, Aalborg university, 2010.
- [2] S.G. Voronin, D.A. Kurnosov, D.V. Korobotov, P.O. Shaburov, A.S. Kul'mukhametova, Electromagnetic and Resistance Torque on a Synchronous Motor Shaft with Permanent Magnet Excitation, Russian Electrical Engineering. 83(2) 61–63.
- [3] F.M. Yuferov, M.M. Kacman, Electriccheskie mashini avtomaticheskikh system, Moscow, 1979.
- [4] I.E. Ovchinnikov, Ventilnye Electriccheskie Dvigateli i Privody na ih Osnove, 2012.
- [5] V.A. Lifanov, S.G. Voronin, B.G. Shumikhin, Issledovanie pulsaciy momenta tikhokhodnikh beskontaktnykh dvigateley postoyannogo toka s diskretnym datchikom pologeniya rotora, Elektrichestvo [Electricity].11 (1977) 54.

- [6] N.P. Advolodkin, V.G. Garashenkov, N.N. Lebedev, N.E. Ovchinnikov, *Upravlyaemye beskontakthye elektroprivody postoyannogo toka* [Contactless controlled DC drives], Leningrad, 1984.
- [7] S.G. Voronin, D.V. Korobotov, R.T. Kiyakpaev, A.S. Kulmukhametova, Dynamic processes of brushless DC motor with different combinations of parameters, *Izvestiya Akademii Elektrotekhnicheskikh Nauk.* (2011)58–63.
- [8] V.F. Samoseyko, *Theoretical Foundations of Motor Control*, 2007.
- [9] E.A. Lodochnikov, Yu.M. Yuferov, *Mikrodvigateli dlya system avtomatiki* [Micromotors for Automation Systems], Moscow, 1969.
- [10] Yu.V. Linnik, *The method of least squares and the foundation of mathematics and statistical theory of observation processing*, Moscow, 1962.
- [11] S.A. Ayvazyan, *Applied Statistics. Foundations of Econometrics*, Moscow, 2001.



International Conference on Industrial Engineering

The solution for the electrodynamic problem on the alternative test site border fencing construction to conduct special studies of technical means

Antyasov I.S.*

South Ural State University, 76, Lenin Avenue, Chelyabinsk, 454080, Russian Federation

Abstract

The article deals with the solution of the electrodynamic problem on the border enclosing structure anechoic chamber in a rigorous formulation in an infinite region of space. The proposed solution comprises two stages. The first is calculated on the basis of experimental studies of complex permittivity and permeability of radio absorbing material using Nicolson-Ross-Weir model. The second evaluates channel Floquet transmission and reflection coefficients for the walls in an infinite plane. The articles shows the obtained dependence of the transmission coefficient on the mesh structure for the combination of the mesh structure and the dielectric plate.

© 2015 The Authors. Published by Elsevier Ltd. This is an open access article under the CC BY-NC-ND license (<http://creativecommons.org/licenses/by-nc-nd/4.0/>).

Peer-review under responsibility of the organizing committee of the International Conference on Industrial Engineering (ICIE-2015)

Keywords: anechoic chamber; Floquet channel; electromagnetic radiation; mesh structure; dielectric permittivity ; magnetic permeability.

1. Introduction

For carrying special investigations bench (SI) of side electromagnetic radiation and interference (PEMIN) technical devices (TD) in accordance with the regulations and methods necessary to have an alternative measurement area (AMA). AMA can be called a "semi-anechoic" chamber, as it differs from the anechoic chamber (AC), the presence of ground plates on the lower boundary of the chamber [1]. To AMA some requirements on the coefficient of anechoic and shielding effectiveness of external industrial interference [2, 3, 4]. For this purpose a series of tests carried out on the suitability of the built AMA [5]. Construction of AMA is quite costly and requires a

* Corresponding author. Tel.: +7-351-2679285.
E-mail address: antyasov@gmail.com

comprehensive approach to address identified problems [6], achieved in different ways: geometry, size, use of radioabsorbing materials (RM), shielding materials, interference suppression filters [7]. All walls of AMA (except for the lower) have a multilayer structure shown in Fig. 1 (with an indication of the direction of incidence of the electromagnetic wave \vec{E}^i by TD).

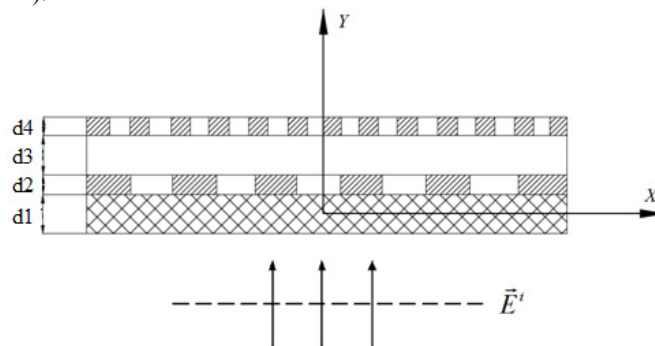


Fig. 1. Structure of walls of AMA, where d1 – thickness RM; d2, d4 – thickness of mesh screens; d3 – the thickness of the air layer.

In order to assess suitability of the use of AMA, scheduled to build, simulate electromagnetic processes taking place inside the room AMA and on its boundary. Considering that applied shielding fine screen [8] and RM, ideal modeling of AMA with all the elements of its construction requires a considerable amount of computational operations (in the frequency range from tens of kilohertz to several gigahertz, the minimum linear dimensions of the site - the order of several meters, mesh size - a few tenths of a millimeter).

The possibilities of experimental modeling AMA is very limited: the quality of the measurements in the required frequency range [2] difficult to achieve because of the problem unformed front of wave (the far zone is formed at a considerable distance) and background electromagnetic noise (low signal to noise ratio). Deserves special attention RM: manufacturers, as a rule, do not indicate exhaustive characteristics of materials, and are limited to specifying the reflection losses at perpendicular incidence of the wave [9]. These data do not allow us to estimate the coefficients of transmission and absorption because for understanding the full picture of electrodynamic processes occurring in the material, it is necessary to know the permittivity, permeability and conductivity of the material.

For simplicity the model simulations AMA is carried out in two stages: the general problem is solved in the volume in the optical approximation and is based on the solution of the electrodynamic problem on the border enclosing structure AMA in a rigorous formulation in an infinite region of space.

The solution of the electrodynamic problem is done in two stages: first, the calculation of complex permittivity and permeability RM (based on his experimental studies), and secondly, the calculation of transmission and reflection coefficients on the basis of modeling walls of AMA in an infinite plane.

2. Permittivity and permeability of RM

Preliminary assessment of the permittivity and permeability performed capacitive (low frequency) and waveguide (high-frequency) method [12] for the investigated RM, which is used as the ferrite tile absorber [9].

In the measurements capacitance method sample was placed between the plates of the capacitor and determines the change in capacitance and dielectric loss tangent with the introduction of RM to the condenser. Obtained the following results measured at a frequency of 100 kHz:

$$\text{without RM: } C=10,4 \text{ pF, tg } \delta = 0,066;$$

$$\text{with RM: } C=78,7 \text{ pF, tg } \delta = 0,02;$$

$$\Delta C=68,3 \text{ pF, } \Delta \text{tg } \delta = 0,046.$$

By measuring the transmission and reflection coefficients in the waveguide at a frequency of 8.4 GHz, the dielectric constant of the sample RM estimated. In accordance with the method of the scattering matrix of attenuation coefficient β [10] totaled

$$\beta = \frac{|S_{12}|^2}{1 - |S_{11}|^2} = 0,035 = -14,6 \text{ dB},$$

where $|S_{11}|=0,316$ – reflection coefficient, $|S_{12}|=0,0316$ – transmission coefficient.

According to the manufacturer, RM has a significant permeability, which can also must take into account at modeling of the electromagnetic wave passing through the wall AMA.

Thus, there is attenuation in the material at different frequencies, which indicates the presence of loss and the need to incorporate the permittivity and permeability in complex form.

There are various methods for measuring permittivity and permeability [12] coaxial probe, a method of "free space", a cavity resonator, the method of parallel plate waveguide and coaxial transmission line. Variant with coaxial probe is not suitable, because investigated RM has permeability. Use of the method "free space" is limited because of the need to use low-frequency antennas and RM big sample size. Application of the waveguide method and method of "cavity resonator" is limited to a narrow range of frequencies. The capacitive method is not applicable due to the substantial errors caused by low quality factor of the investigated RM.

The most suitable from the viewpoint of applicability is the method of the coaxial transmission line, which provides broadband measurements from 100 MHz to 8 GHz [11]:

$$D + d < \frac{2}{\pi} \lambda,$$

where D – large diameter line, d – the diameter of the inner shaft.

An advantage of the method is the use of a T-wave type coinciding with type of waves in free space, and the applicability of the method for magnetic materials. Thus, the coefficients of transmission T and reflection R , measured in a coaxial transmission line, can be applied to calculations in the free space. [12, 13]

Calculations of complex permittivity and permeability on the basis of found T and R можно сделать на основе модели Nicolson-Ross-Weir [14]. This requires the manufacture of a toroid RM thickness d , set coaxial transmission line and to measure the parameters of the scattering matrix. The characteristic impedance of the material is of the form

$$Z = \sqrt{\frac{\mu_r}{\epsilon_r}} Z_0,$$

where μ_r , ϵ_r – relative permittivity and permeability of material, Z_0 – characteristic impedance of the free space.

The reflection coefficient of the surface of the RM has the form

$$R = \frac{Z - Z_0}{Z + Z_0} = \frac{\sqrt{\mu_r/\epsilon_r} - 1}{\sqrt{\mu_r/\epsilon_r} + 1} \quad (1)$$

The transmission coefficient for a finite thickness can be written as

$$T = \exp[-j \frac{\omega}{c} d \sqrt{\mu_r \epsilon_r}], \quad (2)$$

where ω – circular frequency, d – thickness of the material.

The coefficients of the scattering matrix S_{11} and S_{21} has the form:

$$S_{21}(\omega) = \frac{(1-R^2)T}{1-T^2R^2}, \quad S_{11}(\omega) = \frac{(1-T^2)R}{1-T^2R^2}$$

Introducing variables

$$V_1 = S_{21} + S_{11}, \quad V_{21} = S_{21} - S_{11}, \quad X = \frac{1 - V_1 V_2}{V_1 - V_2},$$

reflection and transmission coefficients can be written as

$$R = X \pm \sqrt{X^2 - 1}, \quad T = \frac{V_1 - R}{1 - V_1 R}.$$

With regard to (1) and (2) receive

$$\frac{\mu_r}{\varepsilon_r} = \left(\frac{1+R}{1-R}\right)^2 = C_1, \quad \mu_r \varepsilon_r = -\left\{\frac{c}{\omega d} \ln\left(\frac{1}{T}\right)\right\}^2 = C_2$$

then

$$\mu_r = \sqrt{C_1 C_2}, \quad \varepsilon_r = \sqrt{\frac{C_2}{C_1}}$$

Model Nicolson-Ross-Weir is widely recognized method of calculation of the electromagnetic characteristics of the materials from the measured scattering matrix elements and well applicable for materials with both small and large losses. [15, 16]

3. Wall of AMA in infinite area

Direct simulation walls of AMA to a cascade of relatively large mesh with a mesh of 20 mm and 18 mm and the diameter of the wire, respectively, 2 and 1,8 mm, revealed a general problem of modeling - limited computing resources. The problem was solved for the walls of the size of 3000 * 5000 mm among computer-aided design (CAD) CST STUDIO on a PC with quad-core processor i7, RAM 16 GB and solid-state hard disk drive 1 hour 7 minutes. The large costs of calculation related to the fact that the definition of radiating elements mesh screens requires a large dimension, since the geometry of the cascade return period of two screens large enough. The calculation time for volumetric the room 3*4*5 m and mesh wire diameter of 10 mm and 40 mm cell in the range of 1 GHz to more than 2 days of continuous operation. The situation is exacerbated when registered in the RM with complex permittivity and permeability. Thus, the solution of the problem with this approach is not possible.

The measured value of the transmission coefficient in a waveguide for copper mesh 0,56x0,56 mm with of the wire diameter 0,15 mm at a frequency of 8,4 GHz totaled -39,7 dB, and taking into account the intrinsic attenuation 5 dB in a waveguide, totaled -44,7 dB. The calculated value of the coefficient in CAD CST STUDIO: -39,79 dB. The difference can be explained by non-ideal of the meshes (GOST[17] allows deviation in cell size 6 %) and the geometry of its placement in the waveguide. Hence the experimental error can be estimated at 6-10%, and therefore, requires a method to simulate with a high accuracy.

The wall of the AMA is a periodic structure, since the two asymmetrical meshes can make the common repetition period. Therefore, the natural method of analysis of infinite periodic structures is the use of periodicity conditions that reduce the problem of an infinite structure of the analysis of one period [18]. For this purpose use of Floquet channel, which is a part of the space bounded by the vertical walls on which you installed periodic boundary conditions.

The electric field intensity for the half- space $Z > 0$ in a rectangular channel of Floquet is given [18,19]:

$$E(x, y, z) = \sum_n \sum_m a_{n,m} e^{-ik_n x - i\beta_m y - n_m z},$$

where $k_n = k_0 + 2\pi n/L_x$, $\beta_m = \beta_0 + 2\pi m/L_y$, $n_m = \sqrt{k^2 - k_n^2 - \beta_m^2}$, $L_{x,y}$ – periods of repetition structure of the axes OX and OY, $a_{n,m}$ – amplitude n,m harmonics, k – the wave number of free space.

Constant k_0, β_0 are given the incident field, which is a plane wave:

$$k_0 = k \sin \theta \cos \varphi, \quad \beta_0 = k \sin \theta \sin \varphi,$$

where θ – meridional angle of incidence of the plane wave, φ – the azimuthal angle of incidence.

In the case of perpendicular incidence for the far zone is only the fundamental harmonic Floquet with parameters $n=m=0$.

To verify the possibility of using Floquet channels studied common mesh structures [17] with the CAD CST STUDIO. Calculations of the transmission coefficient for the mesh, placed in a coaxial line with outer and inner radii, respectively, 16 и 7 mm, and for an infinite network structure by using a predetermined channels Floquet demonstrate good agreement, characterized by less than 1 dB. The difference can be explained by the peculiarities of the geometry of the current distribution on the border of meshes adjunction and the coaxial line (fig. 2).

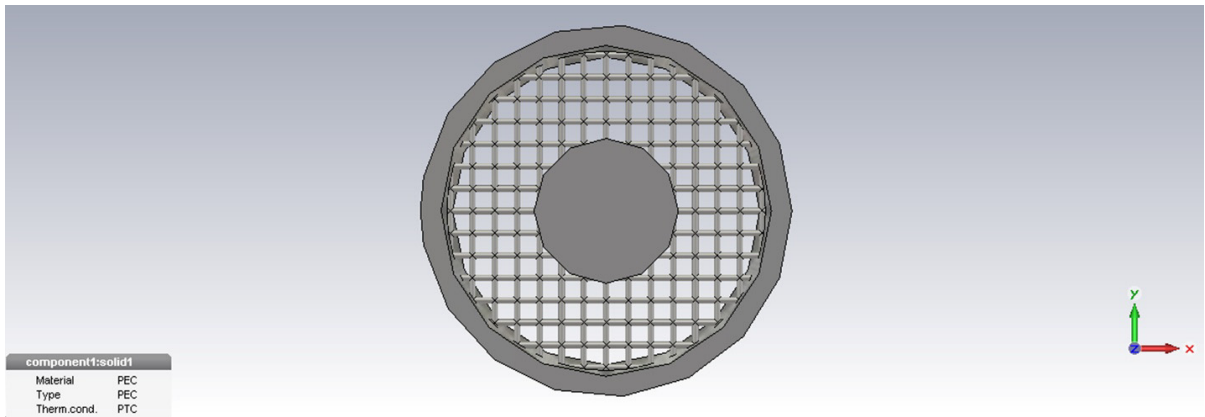


Fig. 2. Scheme of meshes in a coaxial line.

Comparing the the transmission coefficient for meshes 1 cell size 0,8 mm and a diameter of 0,32 mm, calculated in the coaxial line and using Floquet channels received permanent differences 0,38 dB in the entire frequency range (table 1). Calculations were carried out for a length of coaxial transmission line 100 mm installed in the middle of a mesh, and channel Floquet ports installed accordingly at a distance 50 mm before the meshes and 50 mm after the meshes.

Table 1. The transmission coefficient for the mesh 1.

Frequency, GHz	0,2	0,4	0,6	0,8	1	1,2	1,4	1,6	1,8
Floke, dB	68,819	62,799	59,277	56,778	54,84	53,226	51,917	50,757	49,734
Klp, dB	68,434	62,414	58,893	56,394	54,457	52,875	51,536	50,377	49,353
Difference, dB	0,385	0,385	0,384	0,384	0,383	0,351	0,381	0,38	0,381

Analogous measurements for the mesh 2 with a cell 0,9 mm and diameter 0,36 mm in the coaxial transmission line using channels Floquet show constant difference 0,15 dB (table 2).

Table 2. The transmission coefficient for the mesh 2.

Frequency, GHz	0,2	0,4	0,6	0,8	1	1,2	1,4	1,6	1,8
Floke, dB	67,796	61,776	58,254	55,755	53,816	52,233	50,894	49,734	48,711
Klp, dB	67,948	61,923	58,406	55,907	53,969	52,386	51,047	49,886	48,863
Difference, dB	0,152	0,147	0,152	0,152	0,153	0,153	0,153	0,152	0,152

For a cascade meshes (fig. 3) with the distance between them 50mm and the start of counting phase Floquet 1000 mm transmission coefficient totaled -107,90 dB at 1 GHz.

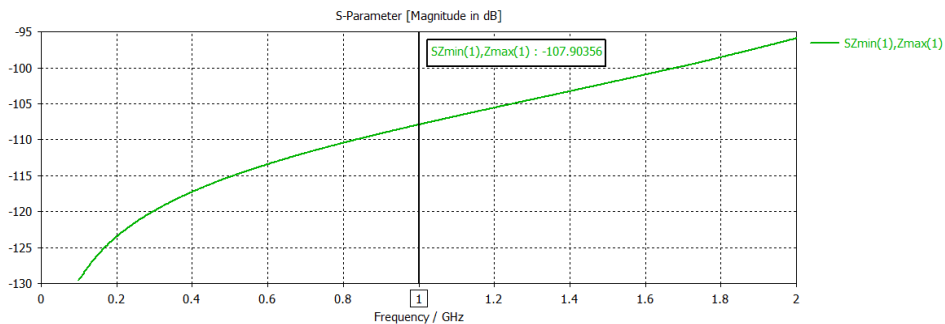


Fig. 3. Transmission coefficient for a cascade meshes in the channel Floquet.

The foregoing results agree well with the values of the transmission coefficient obtained at the decision with use of model the transmission line.[20]

For the validation of of calculations using a Floquet channels carried out researches the transmission coefficient (on power) for a combination of wire mesh (lumen 15 mm, radius 0.3 mm) and a dielectric plate ($\epsilon/\epsilon_0=3.6-0.2i$, thickness 4 mm) depending on the distance h among them at a frequency of 9,375 GHz. The simulation results (fig. 4) have a good agreement with the calculated data obtained by the averaged boundary conditions [21]. Revealing of the difference can be explained by to CAD using the method of finite integrals without the use of averages.

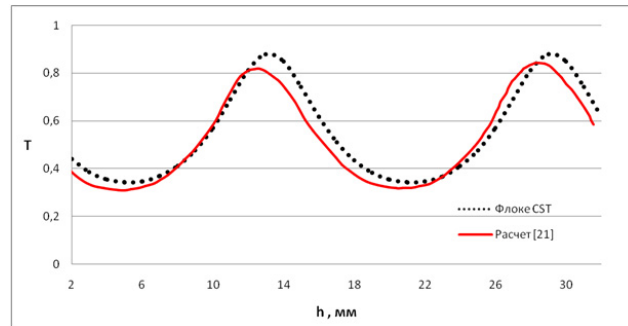


Fig. 4. The transmission coefficient calculated, using the channels Floquet and [21].

Results of calculating the transmission coefficient depending on the thickness of the dielectric plate shown in fig. 5. Increasing the thickness of the material affects the ambiguous change in transmission coefficient: it can be seen that, firstly, at frequencies greater than 4,62 GHz (the wavelength in the material is 34 mm) the transmission coefficient increases with increasing thickness, secondly, at a frequency of about 7 GHz (the wavelength in the material is 22 mm) the transmission coefficient for the thickness of 10mm is greater than for other thicknesses. These effects can be explained by resonance phenomena related to the wavelength in the material.

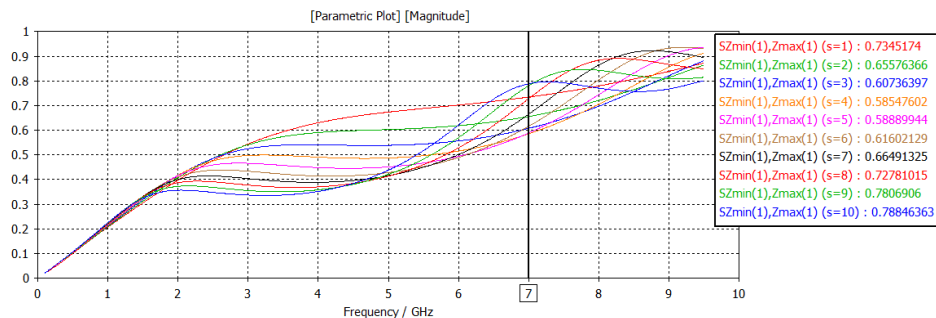


Fig. 5. The transmission coefficient in the range of frequencies at different thicknesses of the dielectric plate.

It is necessary be noted that the the transmission coefficient decreases with increasing thickness of material only at frequencies below 3,5 GHz, which is about a quarter of the wavelength in the material which is related to the wavelength in the free space ratio $\lambda = \lambda_0 / \sqrt{\epsilon_r \mu_r}$. Hence, knowing the permittivity and permeability, it is possible to determine the optimal thickness of RM.

Research transmission coefficient for different cell sizes allow to make conclude that the resonance phenomena occur at frequencies corresponding to 1/8 multiple of wavelength. This is associated to the number of faces of the cell: 4 faces * 1/8 wavelength = 1/2 wavelength.

Research of the transmission coefficient as a function of the distance between the meshes to reveal the presence of resonance at 1/2 wavelength, and the degradation is observed, starting with 1/4 wavelength.

Conclusions

Thus, the determination of complex permittivity and permeability of the material is possible with use of model Nicolson-Ross-Weir by analyzing the dependence of the coefficients of transmission and reflection in a coaxial transmission line. With known material parameters multilayer structure walls of AMA can be modeled in the a rigorous formulation using Floquet channels. In order to assess suitability of the use of AMA, the planned for construction, buildings volume model in the optical approximation, from which are issued the necessary recommendations to the requirements of the customer.

This work was financially supported by the Ministry of Education and Science of the Russian Federation in the framework of an integrated project under the contract №02.G25.31.0046

References

- [1] Antyasov I.S., Sokolov A.N. Features of the construction of the shielded room to study the properties of the electromagnetic field. // Bulletin of the Ural Federal District. Security in the information sphere. - Chelyabinsk Univ. Centre SUSU, 2014. — № 1(15) - P. 8-12.
- [2] GOST R 51320 – 99. Radio disturbance. Test methods of technical equipment - industrial noise sources. - Enter. 1999-22-12. - M.: Russian State Standard, 1999. – 27 pp.
- [3] GOST R 50414 – 92. Compatibility of technical equipment. The equipment for the tests. Shielded chambers. Classes, basic parameters, technical requirements and test methods. – Enter. 1992-26-11. – M.: Russian State Standard, 1992. – 28 pp.
- [4] GOST R 51318.16.1.4 – 2008. Compatibility of technical equipment. Requirements for equipment for measuring industrial radio interference and immunity and methods of measurement. Part 1-4. The equipment for measuring industrial radio interference and noise immunity. Devices for measuring the emitted interference and the test for resistance to radiated radio noise.– Enter. 2008-12-25. – M.: Russian State Standard, 2009. – 75 pp.
- [5] Antyasov I.S., Voytovych N.I., Sokolov A.N. Features of the validation of alternative test site to conduct special studies of technical means // Bulletin of the Ural Federal District. Security in the information sphere. - Chelyabinsk Univ. Centre SUSU, 2014. — № 1(11).
- [6] Antyasov I.S., Voytovych N.I., Sokolov A.N. Comprehensive shielding the alternative test site to conduct special research techniques. // Vestnik of SUSU. Computer technology, management, electronics. — Chelyabinsk Univ. Centre SUSU, 2014. — № 2(14) – C. 61-69.
- [7] Anechoic chamber microwave / Mitsmaher M. Yu, Torgovanov V.A. - M.: Radio and Communications, 1982. – 128 pp.
- [8] Antyasov I.S., Sokolov A.N. The use of mesh materials in an alternative screening test site to conduct special studies of technical equipment // Safety information space: a collection of the works of XIII All-Russian scientific-practical conference of students, graduate students and young scientists.. – Chelyabinsk: South Ural State University Publishing Center, 2015. – P. 8 – 13.
- [9] Technical description 390-5.1. C-RAM FT The ferrite tile absorber. http://www.eltm.ru/editor/upload-files/C-RAM_FT___390-5.1_.pdf
- [10] E.L. Ginston. The measurements at centimeter wavelengths. 1960 - 620 pp.
- [11] Frantsuzov A.D. Electrodynamic fundamentals of calculation and design of screens and microwave devices. 1979 - 98 pp.
- [12] Fundamentals of measuring the dielectric properties of materials. Application Notes. Agilent Technologies. 2010. — 32 pp.
- [13] Valitov R.A., Sretensky V.N. Radio measurements at microwave frequencies. 1951. - 392 pp.
- [14] Nicolson A. M. and Ross G. F. // IEEE Trans. Instrum. Meas. – 1970. – V. IM-19. – No. 4. – P. 377–382.
- [15] Maxim V. Akhterov. MICROWAVE ABSORPTION IN NANOSTRUCTURES. A thesis submitted in partial satisfaction of the requirements for the degree of BACHELOR OF SCIENCE in APPLIED PHYSICS. 10.06.2010
- [16] E.J. Korovin, V.I. Suslyaev, I.P. Hlunovsky, E.V. Chebotarev. Measurement of electromagnetic parameters of carbon nanostructures in the range 0,01-18 GHz // News of higher educational institutions. Physics. 2012. T. 55, № 9/2.
- [17] GOST 3826 - 82. The wire gauze with square cells. Technical conditions. - Enter. 1984-01-01. - M.: Publisher IPC Standards, 2003. - 8 pp.
- [18] Kurushin A.A. "Using Floquet channels to simulate a periodic nanostructure" // "JOURNAL OF OF RADIO ELECTRONICS" N 11, 2010
- [19] P. Montgomery, "Scattering by an Infinite Periodic Array of thin Conductors on a Dielectric Sheet", IEEE Trans on Ant Prop, Vol Ap - 23, No. 1, Jan 1975.
- [20] Antyasov I.S. "Evaluating the effectiveness of electromagnetic screen in the construction of alternative test site to conduct special studies of technical means" // All-Russia scientific-technical conference "Automated control systems and information technology", Perm, 15.05.2015.
- [21] Numerical methods of the theory of diffraction: Coll. articles. Trans. from English. / - M.: Mir, 1982. - 200c.



International Conference on Industrial Engineering

Application of Technical and Economic Criterion of Equipment Control with Sucker Rod Pump

Sadov V.B.^{a*}, Plotnikova N.V.^b

¹Rabotnits, 72-24, Chelyabinsk, 454084, Russia

²Gryazeva, 8, Chelyabinsk, 454082, Russia

Abstract

An approach to the synthesis of control algorithms of equipment with drive sucker rod pump is given on the basis of the analysis of the existing control principles. This approach uses the criterion including technical and economic component of oil production. Connections with diagnostic system of equipment in the control process are described. The principles of restrictions formation on control when using this criterion are given on the basis of operation results of embedded diagnostic system. The information system in the control structure of oil production is shown with application of the synthesized criterion, components of this system are described. This approach to the control synthesis of oil production can be extended onto some other types of equipment of oil production.

© 2015 The Authors. Published by Elsevier Ltd. This is an open access article under the CC BY-NC-ND license (<http://creativecommons.org/licenses/by-nc-nd/4.0/>).

Peer-review under responsibility of the organizing committee of the International Conference on Industrial Engineering (ICIE-2015)

Keywords: equipment with the drive sucker rod pump, control, an information structure of control system.

1. Introduction

Recently, questions of industrial automation in oil branch often connect with implementation of "smart" deserted technologies, "intellectual slits" which control systems are able to select itself the modes of oil pumping from a slit depending on the slit parameters and external conditions. The main aims of control systems of oil production are the

* Corresponding author. Tel.: +7-902-600-18-77.
E-mail address: sv_2005@inbox.ru

decrease of the extraction cost of a unit of production and the general direct and indirect costs on slits exploitation. It means increase of coefficient of the oil recovery, reduction of coefficient of the pumping equipment depreciation, etc. Different control algorithms are used for control of installations with the drive sucker rod pump (DSRP) in an automatic mode. Value of "residue" on a plunger dinamogramm in case of insufficient fluid influx to slit is used as criterion in control systems of Lufkin Automation SAM Well Manager Variable Speed Drive firm. Practically it means that the system is retained in the mode on the boundary where the quantity of the moves is maximum for an accurate identification of defect appearance "insufficient fluid influx in a slit", determined at the plunger dinamogramm. The results of research of control stations of Lufkin firm [1] show that the power consumed by equipment decreases by 20%, exploitation costs of slits and equipment decrease by 25%, and production increases and equipment downtimes decrease only by 1-4% in case of use of the Lufkin Controller Well Manager RPC controller.

There are control systems of drives of Danfoss firm of the mechanized oil production of SALT (Sensor less Artificial Lift Technology) on technology without sensors where load data when using the frequency controlled drive for regulation of the pump delivery are used. Load is analyzed during regulation and the speed of the movement decreases or increases when it is necessary [2]. Thus both drive sucker rod pumps, and screw and submersible electrocentrifugal pumps can be used as pumps.

The main drawback of the given control algorithms of pump equipment is the lack of the direct link with main goals of control systems of oil production. It doesn't allow to change the level of oil production depending on the current parameters of the extracting equipment and economic components of oil production.

2. Synthesis of control algorithm of pump equipment

Synthesis of algorithms and control systems depends on a field of system application [3].

There is a method [4] in which the maximum of the criterion including components of production level, expenses on the electric power and exploitation of the deep equipment and drive sucker rod pump is defined for formation of level of the current production for borehole equipment with DSRP

$$G = q - k_1 \cdot (n + \alpha \cdot n^2) - k_2 \cdot n, \quad (1)$$

where q – the value of the current production in a unit of time (current productivity of a slit) or its assessment;

n – the current quantity of the double moves per minute of the drive of the drive sucker rod pump;

$M = k_1 \cdot (n + \alpha \cdot n^2)$ – the value characterizing the expenses on the electric power in a unit of time;

$D = k_2 \cdot n$ – the value characterizing the expenses on exploitation of the deep equipment and the drive of the drive sucker rod pump in recalculation per unit of time.

The scaling coefficients k_1 and k_2 have the dimensions resulting economic components in dimension of the current production in a time unit.

Constants k_1 , k_2 , α can be received on the basis of expert estimations. They can change depending on the price of oil (the oil production price), price of electricity, the price and the cost of exploitation of the deep and pump equipment.

It should be noted that it is necessary to consider the restrictions on the controlling variable (quantity of the double moves) because of characteristics of the DSRP drive and characteristics of an oil well, oil layer and the pumped-out liquid under search of a maximum of criterion (1). It is necessary to use diagnostic system in the controller of the control system of a well oil production. The conclusions about restrictions on the controlling variable and opportunity or expediency of further work of pump equipment (for example, during the diagnostics of a break of a rods column) in certain cases are drawn by the results of operation of this diagnostic system.

For example, during algorithm work the restriction of quantity of the double moves was 6 and step was changed from 4 to 4,5 double moves as a result of the work of adaptive algorithm. Thus the diagnostic system gave out the result "insufficient inflow of liquid to a well" for this value. It is necessary to change the restriction of quantity of the double moves to the value 4,5 as the increase of moves quantity relative to this value is inefficient. It is necessary to act similarly if insufficient inflow of liquid to a well hasn't been revealed during the work of the algorithm, but the

current restriction of the moves quantity is less than technological one and the outlet after the boundary of the current restriction of the quantity of the double moves has taken place. It is expedient to build the diagnostic system using the results of the dinamograms and vattmetrograms assessment because these approaches are most studied.

3. Synthesis of information system of equipment of oil production

As a rule, modern control systems have communication with shop information system. In most cases this communication has one-sided character: in spite of the fact that requests and answers from shop information system go diversely, information moves from a control system to shop, and from shop there are only requests for data acquisition, for example, of dinamograms and vattmetrograms data, equipment work parameters, etc.

If criteria of oil production control (1) are used during control information exchange in the direction shop information system – the control system of oil production becomes expedient. In this direction it is possible to transfer information which will lead to change the oil production parameters or even to change the modes of oil production. It is connected with the terms "intellectual field" and "intellectual well" which, obviously, shouldn't be autonomous and have to be closely connected with each other at the solution of the general problem of minimization of expenses on production of one ton of oil and various private tasks solved at each control level. Correction of those information streams which exist now in structure of control of oil production is required.

It is expedient to break all information system into groups with definition of connections between them. This structure is presented in figure 1 [5].

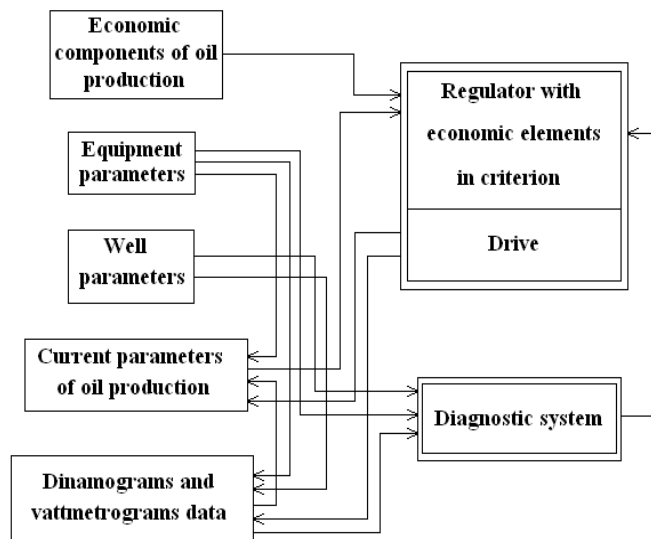


Fig. 1. Information connections in a control system of DSRP.

Information groups in the system are shown in the figure at the left. Modules of hardware-software part of a control system are shown on the right by double lines. We will consider components of this system. The block of economic components of oil production contains only coefficients of the expenses entering in the control criterion in the automatic mode and is connected with the control system regulator. The values of criterion change during change of data of this block and the control system respectively reacts on it by change of the control action (in our case the quantity of the double moves changes).

The block of equipment parameters is individual for each type of the DSRP and contains such values as length of the move of the polished rod, the area of the piston of a hydraulic cylinder at the gidrofikational drive, etc. These parameters influence on the parameters of the block of the current parameters of oil production (for example, an

estimation of the value of the current productivity of equipment), on the block of dinamograms and vattmetrograms data (for example, on the calculated values of points of the plunger dinamogram received from the estuarial data), and on the diagnostic system (for example, during estimation of the current loading in a column of rods).

The block of the well parameters contains such values as depth of immersion of the pump, level and characteristics of the pumped-out liquid, characteristics of the pump and a column of rods, etc. Parameters of this block influence on the diagnostic system (for example, during estimation of the minimum value of load of a column of rods), on the block of dinamograms and vattmetrograms data (for example, on the calculated values of points of the plunger dinamogram received from the estuarial data).

The block of the current parameters of oil production contains the current data of equipment operation (for example, the current measured quantity of the double moves) and estimated data of results of oil production (for example, exploitation productivity). Parameters of this block influence on operation of the regulator as, for example, the value of productivity estimation is included into the value of criterion of automatic control of exploitation.

The block of dinamograms and vattmetrograms data contains the dinamograms data (estuarial and, perhaps, plunger, received as a result of calculation) and archives of these data for its subsequent output via connection channels or to internal devices of indication. Dinamograms and, perhaps, vattmetrograms are used for the delivery of results of quality estimation of oil production and the equipment of a well in diagnostic system. Such information division into groups will allow to use the uniform structural units at data transmission from/in a control system of the drive regardless of DSRP drive type. Filling of blocks will depend on the type of DSRP drive and, perhaps, on pump type.

4. Conclusion

The new method of synthesis of control of the oil production equipment with the drive sucker rod pump is given. This approach is suitable as well in the case of use of pumps of other type, for example, of the electrocentrifugal.

References

- [1] I.F. Zubairov, Intellectual well – increase of efficiency of the mechanized production, *J. Engineering Practice*. 5 (2011) 84–89.
- [2] Information on http://www.danfoss.com/NR/rdonlyres/90BCF710-9C97-4F9C-9EF5-F9274DA9A842/0/salt_broschyura.pdf
- [3] N.V. Plotnikova, Formulation of synthesis problem of quasistationary stochastic system, *J. Bulletin of the South Ural State University, Ser. Computer Technologies, Automatic Control, Radio Electronics*. 3 (2009) 68–71.
- [4] V.B. Sadov, A.L. Shestakov, Automatic control of equipment of the borehole sucker rod pump, *J. Oil Economy*. 1 (2015) 98–101.
- [5] V.B. Sadov, Synthesis of information system of installation of the borehole sucker rod pump, *Proc. of IV Int. Sci. Conf., Topical Issues of Development of Science in the World*. (2015) 51–53.



International Conference on Industrial Engineering

The structure of the surface roughness, treated by surface plastic deformation to facilitate its calculation

Telkov I.A. *

Murom Institute of Vladimir State University, Orlovskaya Street, 602264, Murom, Russia

Abstract

This paper describes the laws of structuring surface roughness at surface plastic deformation for the purpose of revised calculation of operating modes at the technological process design stage. It derives a formula of roughness profile that allows calculating its general parameters. These formulas are obtained without the action of inertial forces in the reciprocating movement of the tool.

© 2015 The Authors. Published by Elsevier Ltd. This is an open access article under the CC BY-NC-ND license (<http://creativecommons.org/licenses/by-nc-nd/4.0/>).

Peer-review under responsibility of the organizing committee of the International Conference on Industrial Engineering (ICIE-2015)

Keywords: surface plastic deformation, surface roughness, roughness structure, equalization of rough surface, reciprocating of the tool.

1. Introduction

Present-day methods of surface plastic deformation are characterized by high intensification of modes, which is achieved on the account of newer design-engineering methods application. In these circumstances one of the general directions of processing performance improvement and durability of the tools is calculation and provision of qualitative indicators of the surface at maximum possible intensity of processing at design stage. The solution of these issues for processing of parts of materials has special importance, the processing of which is characterized by increased aptitude to vibrations occurrence. These products that are made of nonferrous metals and alloys with high requirements to roughness of the processed surface $Ra=0.05 \div 0.08$ microns of high uniformity. For similar

* Corresponding author. Tel.: 8-492-347-7282; fax: 8-492-347-7128.
E-mail address: telkoviv@yandex.ru

calculations it is necessary to use the models, which take into account the physical phenomena at contact of tool and blank. Current models are either bulky for practical application or too simple and have insufficient accuracy [1, 2, 3].

2. Results and Discussion

On movement of indenter along the treatable surface, the microprofile is formed with parameters that depend on numerous factors is formed. We will mark its height as h_1 .

The indenter with every subsequent revolution of the blank distorts previously formed grooves, by squeezing them in direction that is opposite to the feed (fig.1, a). The higher the pressure at the contact zone and plasticity of the processed material, the larger the plastic displacement zone and to greater degree the distortion of the microprofile takes place. The newly formed microrelief (fig.1, b), section 1), has form, which differs from the form of segments of circle - that is similar to the form of sinuous line indents (fig.1, b), section 2).

The relief that is obtained on the surface we will approximate with the help of the function of the following form:

$$f(t) = h_1(1 - |\sin \omega t|) . \quad (1)$$

Period of sin function is equal to the time of two revolutions of part; therefore, its frequency ω is equal to half angular frequency of revolution of part. I. e. $\omega = \pi n$.

Then the function 1, which describes the formation of the profile of the surface roughness, can be rewritten as follows:

$$f(t) = h_1(1 - |\sin(\pi n t)|) . \quad (2)$$

To determine the component, due to vibration of the tool and work surface, we make the following assumptions:

- tool makes vibrations with respect to work surface with constant average amplitude A and frequency ω ;
- average work rotational speed n is constant;
- average feed at burnishing s is constant.

Relative vibrations of tool and blank can be represented in the form of harmonic function that is confirmed by oscillograms of radial displacement of deforming tool, having a harmonic character and which are described mathematically by sinuous line with amplitude that is equal to the maximum radial-motion variation δ_{\max} :

$$y(t) = A \sin(\omega t + \psi_0) . \quad (3)$$

where: t - time; ω - radian frequency; ψ_0 - phase displacement.

The value ψ_0 will be determined by the displacement of maximum of radial-motion variation for revolution of part. It is determined by the characteristics of the bearings of spindle assembly. Spindle assembly of the most machine tool stations is made on ball bearings that have some eccentricity due to the deviation of the real size of the balls from the rated one upward or downward. As a result, the maximum of radial-motion variation of bearing falls on its side, from which the ball of smaller diameter is placed. Schematically the ball bearing is shown in fig. 3.

In figure: D_1 - diameter of raceway of the outer ring of the bearing; D_2 – diameter of raceway of the inner ring of the bearing; δ - eccentricity that produces the radial-motion variation of the rolling bearing and, accordingly, the spindle. Point A corresponds to the maximum of radial-motion variation.

When you rotate the spindle on 1 turn, the point, corresponding to the maximum of radial-motion variation will move only on certain angle, i.e. the one will be delayed with respect to the rotation of the spindle on angle: λ . The angle, on which the maximum of value of radial-motion variation for 1 revolution of blank will move, will be determined as follows.

Frictional sliding in rolling bearings gives the size of order: 0.0004 ... 0.0005. So, we accept rolling motion of the balls in the bearing without frictional slipping. Then the point of contact of ball and raceways of the inner ring of the bearing for 1 revolution will pass a distance that is equal to the length of the inner ring raceway of inner ring - πD_2 . The point of contact of ball and raceway of the outer ring of the bearing for one revolution of the spindle will pass the same distance - πD_2 , that is less than the length of the raceway of the outer ring (as $\pi D_2 < \pi D_1$).

The point of contact of ball and raceway of the outer ring of the bearing is moved through an arc, the length of which is equal to the product of the rotation angle of the contact point (λ , rad) and the radius of the raceway ($0.5D_1$). It is possible to write down:

$$\pi D_2 = 0,5\lambda D_1 \quad \text{Or} \quad \lambda = 2\pi D_2 / D_1 . \quad (4)$$

Value of angle ψ_0 will be:

$$\psi_0 = 2\pi - \lambda = 2\pi(1 - D_2 / D_1)(rad) . \quad (5)$$

Under real conditions, the determine the parameters of bearings and value ψ_0 is not difficult one. The position of the tool tip after 1 revolution (see Fig. 3, a), after 2, 3, revolutions (see fig. 3, b, c) can be determined if we know the value of the eccentricity - of radial-motion variation and parameters of bearings of spindle assembly. After number of revolutions that is equal to i , the tool tip is returned to the initial position, corresponding to the maximum radial-motion variation (see Fig. 3 d). In longitudinal section of the blank (per generatrix) from revolution to revolution the tool tip moves along sinuous line. (see fig. 3, e).

Wavelength ℓ that occurs on generatrix depends on both feed and the angle value ψ_0 . It may be that the value ℓ will be much less of base length on which the determination of surface roughness parameters is carried out. It can be determined by the number of revolutions, for which the point of maximum of radial-motion variation will return to the starting point and the one shall be calculated according to formula:

$$\ell = s \frac{2\pi}{\psi_0} = \frac{s}{1 - D_2 / D_1} . \quad (6)$$

When burnishing with feed about 0.02 mm/rev and at ratio $D_2 / D_1 \approx 0.6$ (for ball bearings of medium and heavy series), we obtain the following value of the wave: $\ell \approx 0.05$ mm. On standard base length of several of these segments can be fitted.

Taking into account the angular frequency $\omega = 2\pi n$, oscillation equation (3) can be rewritten as follows:

$$y(t) = h_2 \sin(2\pi n(t - 1 + D_2 / D_1)) . \quad (7)$$

Amplitude h_2 - is additional summary penetration from action of inertial forces and friction forces in the area of contact of tool and blank. Equation of profile of roughened surface can be written:

$$L = f(t) + y(t) = h_1(1 - |\sin(\pi n t)|) + h_2 \sin(2\pi n(t - 1 + D_2 / D_1)) . \quad (8)$$

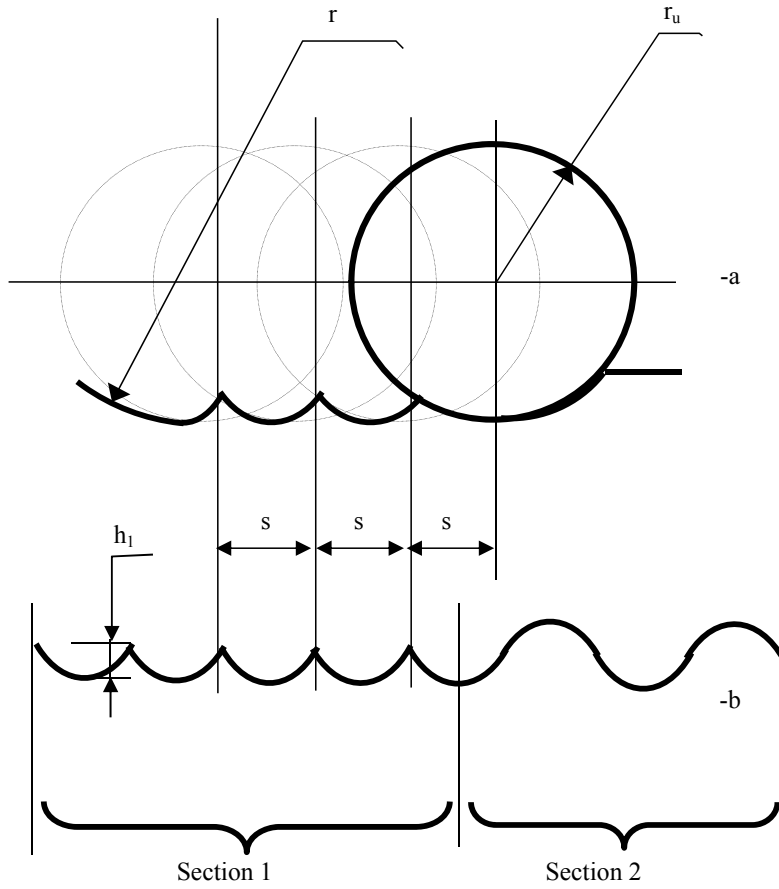


Fig. 1 Scheme of microrelief formation at burnishing

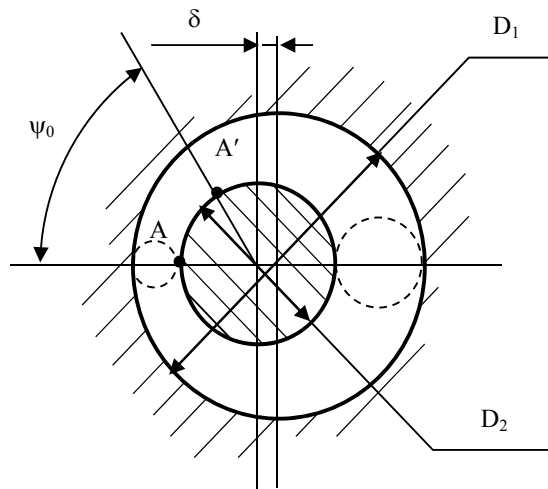


Fig. 2. Diagram of shifting of maximum of spindle radial error motion

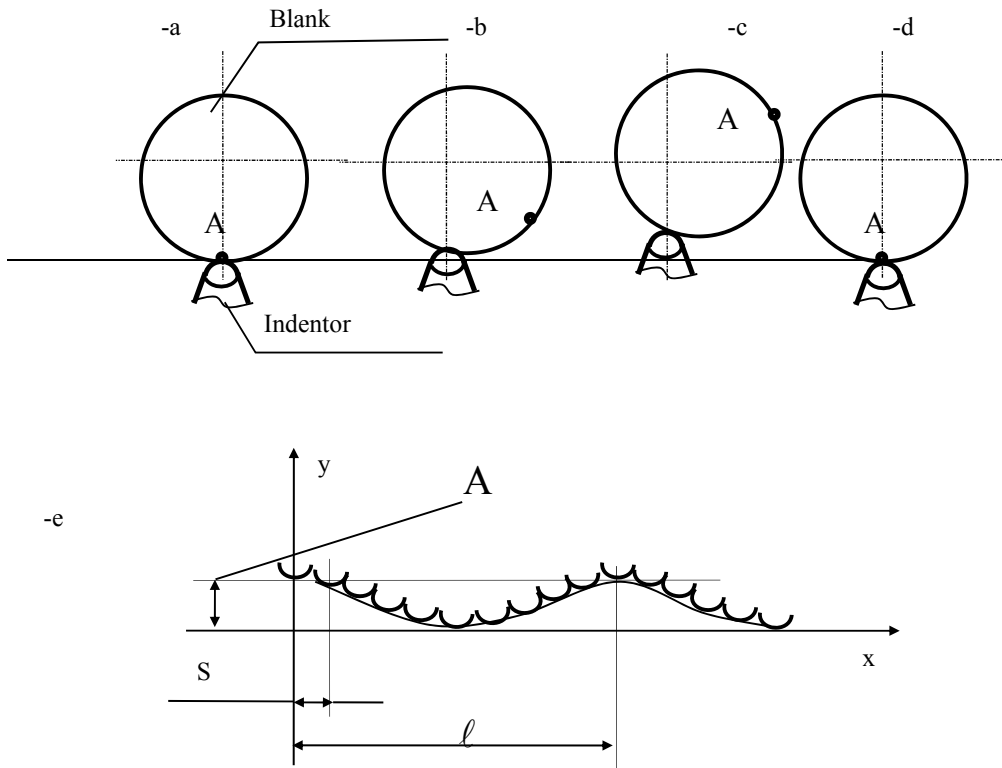


Fig. 3 The dynamics of tool tip motion in transverse -a, -b, -c, -d and longitudinal -e cross sections at reciprocating vibrations of the tool.

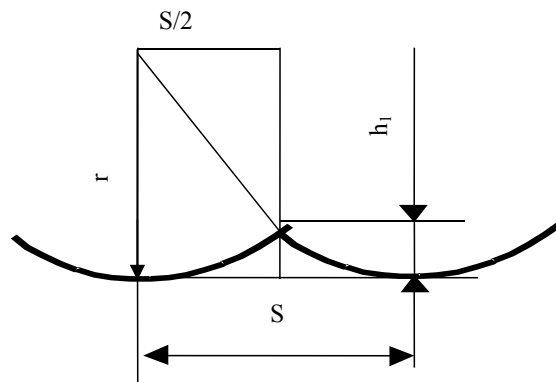


Fig. 4 Profile of ironed surface

Parameter: Ra shall be found as follows:

$$\left. \begin{aligned} Ra &= \frac{1}{\ell} \int_0^{\ell} |y| dx = \frac{1}{\ell} \int_0^{\ell} |L| d\ell = \frac{1}{t_0} \int_0^{t_0} |f(t) + y(t)| dt \\ Ra &= \frac{1}{t_0} \int_0^{t_0} \left[h_1 (1 - |\sin(\pi n t)|) + h_2 \sin(2\pi n (t - 1 + k_{CK} D_2 / D_1)) \right] dt \end{aligned} \right\} \quad (9)$$

where: t_0 - is time of passing by indenter of base length ℓ_0 , on which the integration is carried out.

As a result, with consideration of the roughness of the deforming tool, the formula for finding of the value of the roughness parameter: Ra at burnishing processing will be rewritten as follows:

$$Ra = \varepsilon \frac{1}{t_0} \int_0^{t_0} \left[h_1 (1 - |\sin(\pi n t)|) + h_2 \sin(2\pi n (t - 1 + k_{CK} D_2 / D_1)) \right] dt + kRa_U, \quad (10)$$

where: Ra_U - the value of the roughness of the working tool, which is reproduced on the surface of the machined blank.

ε - coefficient, taking into account the additional distortion of the shape of original groove at subsequent revolutions of the blank; k - coefficient, taking into account the changes of the profile of the surface that is processed as result of intensive wave formation at low feed rates.

At preparation of the surfaces with relatively low requirements to the parameter of surface roughness: Ra , the value Ra_U can be omitted. But when providing the roughness parameter:

$Ra = 0.1$ mm and less, the value of tool roughness has the more significant impact, the smaller the parameter Ra will be.

3. Conclusions

- It was obtained the equation of rough surface when processing with surface plastic deformation, per which you can determine the basic parameters of the roughness at the design stage of the technological process.
- In obtained model the impact of the cross-wave generation, dynamic and inertial phenomena that are characteristic ones for intensive treatment are considered.
- The model is simple enough for practical application.

References

- [1] Serop Kalpakjian, S.R. Schmid, Manufacturing Engineering and Technology, Prentice Hall, 2010.
 [2] Fritz Klocke, Wilfried König, Fertigungsverfahren, Verein Deutscher Ingenieure, Springer London, Limited, 2007.
 [3] A.M. Dalsky, A.G. Kosilova, R.K. Meshcheriakova, A.G. Suslov, Directory technologist-Machinist, Mechanical Engineering, Moscow, 2001.



International Conference on Industrial Engineering

Dynamic and technological traction drive parameters optimization

Sychev D.A., Naumovich N.I., Khayatov E.S.*

South Ural State University, 76, Lenin Avenue, Chelyabinsk, 454080, Russian Federation

Abstract

The article considers the electric traction drive with the field regulated reluctance machine (*FRRM*). The *FRRM* operating principle and main benefits equal with induction machine and synchronous reluctance machine (*SRM*) are introduced, disadvantages are noted. Electric drive is determined as point in the static regime, transient schema analysis, which considers electrical, electromechanical and mechanical operations of electric traction drive, introduced in the first phase of optimization. The second step is expounded how a mode of increasing the velocity of the drive. The third phase is linked with the optimization *FRRM* properties with over-torque. Therefore, drive is received which meet the standards of the traction with improved weight and dimension parameters, overload capability. Weight-size characteristics optimization are evaluation the most appropriate parameters of the control system and the motor. The clarification drawing are shown in the article.

© 2015 The Authors. Published by Elsevier Ltd. This is an open access article under the CC BY-NC-ND license (<http://creativecommons.org/licenses/by-nc-nd/4.0/>).

Peer-review under responsibility of the organizing committee of the International Conference on Industrial Engineering (ICIE-2015)

Keywords: electric traction drive, field regulated reluctance machine

1. Introduction

Electric traction drive is introduced the performance part of the facility of all electric or hybrid traction engine. Was laid on the broad band of to the power equipment, regulation system characteristics and output performance of the full electromechanical complex. As traction engine drives are often operating in heavy mode, it is need to form energy efficiency criterion of the drive in different method.

The available solutions of the electric drives based on the induction motor or *SRM* do not responding such demands. Inductions motors have the optimized structure design, coil productivity, isolation materials and power

* Corresponding author. Tel.: +7-351-223-6713.

E-mail address: grigorevma@susu.ac.ru

feed. Although, the reload value are not high. The current loading is growth and complex the *SRM* design can be achieved the nominal torque equal to 1.1 of the induction drive nominal torque [1].

A series of scientific paper are associated with the optimization of the motor element. However, the introduced solution is aimed to the bridge *m*-phase inverters supply with the bounded quantity of phases.

The fresh approach gave of the electric drive engineering for updating overload and weight-size dimension. The «valve-inverter – motor» multipurpose optimization would be done with account for specific electric traction drive requirements such as high overloads application opportunity (e.g. for outrunning or for starting with heavy goods); as minimal sizes (e.g. for urban electric transport with low floor for comfortable passenger drop-off and pick-up), by the example of the field regulated reluctance machine (*FRRM*) [2].

2. Idea and operating principles of the *FRRM*

FRRM is the synchronous reluctance machine where the stator coil can be operate as excitation coil if the winding is above the interpolar interval and it is a full step coil. Such motor is operated as the reverse *DC* machine. Stator coils can be supplied by the autonomous sources or by the usual multiphase controlled power converters, e.g. based on the full bridge circuit.

As the rotor may be made solid, high mechanical rigidity of the shaft can be reached. Drive can be done in the like stator frame as the asynchronous motor, and using the same stator line current load *FRRM* produced torque greater by 20...35 %. Because of geometric neutral is deliberated displacement to the pole edge, the drive can generate overload torque up to 4...10 nominal values [3, 7].

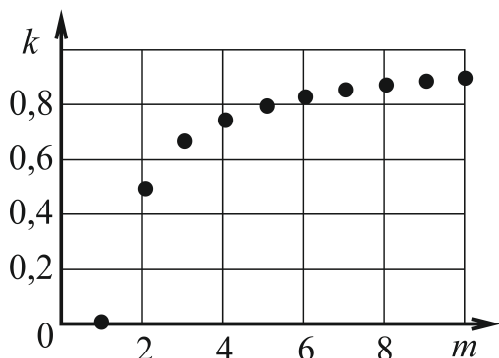


Fig. 1. Electromagnetic torque ripple rate as a function of number of phases of the *FRRM*

Although, these values would be reduced with decreasing quantity of phases of the machine. The pulsations of electromagnetic torque are coming out. The pulsations of speed as a dependent of the quantity of phases are presented on figure 1. The quantity of power semiconductor switches and total power are incremented with growth of quantity of phases. The compromise with according to the economical, mass-weight, energy value is the application of six-phase machine [4].

3. Electric drive weight-size parameters optimization

In general, the task of the weight-size characteristics optimization can be explained with the next condition:

$$q = \min \Delta P_{OV} (T_r, n_{max}, T_{max}),$$

where ΔP_{OV} is the electric drive power loss, T_r is the nominal motor torque, n_{max} is the high motor velocity, and T_{max} is the high drive torque.

The main limitation in this problem should be the heat engine:

$$P_{HE} = \text{const.}$$

The electric traction drive it is possible to separated velocity-torque curve into 3 part for optimizing (fig. 2, a): 1 – constant power part (*A-N-B* curve), 2 – high velocity part (horizontal part is crossing via the *A* point), and 3 – high limiting torque part (vertical part is crossing the *B* point).

If the traction drive is used, e.g. electric drive of a tractor, *A* and *B* points would be limited by the technological operation requirements – high torque is the slipping torque. If during the drive engineering, it is need to analyzing the position of the points, such characteristics of the power facilities as drive power, gear reduction rate, must be visibility. As rule, this comes if high overloads or speed broadband is hard to actualize by of electric drive [5, 15].

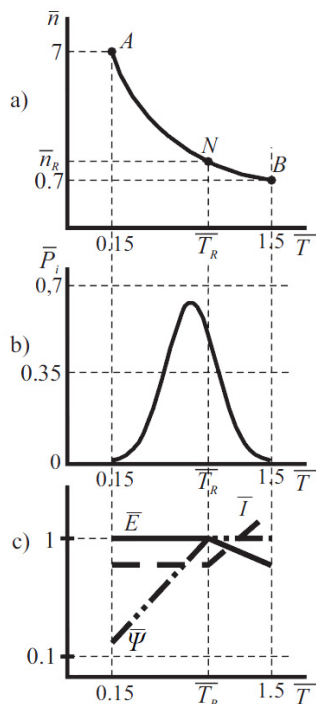


Fig.2. Drive phase motion path (a), load distribution function (b), static characteristics (c)

1b. For each specific case this graph would be different. Employ the *NB* curve and the frequency function graph the torque *RMS* meaning can be calculated. This meaning is utilized to choose the electromechanical converter by power [6].

Velocity control by changing voltage is not effective, because the semiconductor converter power should be overvalued. For this cause, it is better to utilize operating systems with field reduction. This can decreased total capacity of the facilities to 40 percent if the considerable torque overloads would be about short time, as it is in the electric traction drive.

The location of *N* point is calculated by to criterion of electric loss minimum. The logic of switching the electric drive control system can be proposed for the first space to the second space: the diapason that has calculations of armature coil electric loss is chosen. *EMF E*, current *I*, flux Ψ are presented as an operation of torque on fig. 2, c to explain the evaluation process. This optimization algorithm can be reduced weight-size characteristics to 20% [7, 13].

5. Optimization in transient of the electric drive

The problem of definition the scheme and controller characteristics is significant, because when the drive operated close to the limited area of the speed-torque curve, self-excited fluctuation can happen by to the considerable loop fault signals.

Fig. 3 represents the electric traction drive block schema. This is a multiple circuit control system. Speed control

4. Optimization on the steady-state mode

The *A-N-B* curve (fig. 2, a) is border and it is bounded by the diesel generator power. There are two parts of the curve: *AN* – voltage *V* and current *I* are permanent values, magnetic flux is variable with the torque; *NB* – voltage *V* reduced, current *I* increases the according law:

$$P_{el} = VI = \text{const}.$$

The *A-N-B* curve position changes with varying the gear reduction rate. The first section can be divided on the electric traction drive with the FRRM for the basic task of better motion path selection on the task of providing maximum torque and speed of the drive. In relation to measure of minimizing the weight-size characteristics of the motor, it is worth to employ max reduction speed gear box, but it is need to correspond nominal motor velocity and instrument velocity.

Limit of heat can be introduced as next equation if the current and torque are linear graphs:

$$T_r < \sqrt{\frac{1}{T_0} \int T^2(t) dt},$$

where T_r is the nominal motor torque; $T(t)$ is the traction torque time curve; T_0 is the overall cycle time. Load chart for electric traction drives is traditional mounted with frequency function P_i , which is presented on fig.

- [2] Yu.S. Usynin, M.A. Grigor'ev, A.N. Shishkov, Electric drive with a field-regulated reluctance machine, *Russian Electrical Engineering*. 84(3) (2013) 149–154.
- [3] M.A. Grigoryev, A.N. Gorozhankin, S.I. Kinas, E.V. Belousov, Dynamic parameters of active rectifiers, *Russian Electrical Engineering*. 85(10) (2014) 638–640.
- [4] A.N. Gorozhankin, A.N. Shishkov, D.A. Sychev, S.I. Kinas, E.V. Belousov, A direct torque control system for synchronous electric drives, *Russian Electrical Engineering*. 10 (2014) 29–32.
- [5] S.P. Gladyshev, Yu.S. Usinin, M.A. Grigoryev, A.N. Shishkov, A.E. Bychkov, Switching losses in the rotor of the field regulated reluctance machine, *SAE Technical Papers*, 2010.
- [6] A.N. Shishkov, D.A. Sychev, A.E. Bychkov, N.Yu. Sidorenko, The DET-400 Tractor Traction Electric Drive, *Russian Electrical Engineering*. 10 (2014) 24–26. (in Russ.)
- [7] Yu.S. Usinin, S.P. Gladyshev, M.A. Grigoryev, A.N. Shishkov, A.E. Bychkov, E.V. Belousov, Electric drive of an industrial tractor, *SAE Technical Papers*, 2013.
- [8] M.A. Grigoryev, A control system for an electric drive with a synchronous reluctance machine with separate excitation, *Russian Electrical Engineering*. 84(10) (2013) 560–565.
- [9] U.S. Usinin, M.A. Grigor'ev, K.M. Vinogradov, A.N. Gorozhankin, S.P. Gladyshev, Weight and dimensional parameters of a power drive for electrical vehicle, *SAE Technical Papers*, 2009.
- [10] Yu.S. Usinin, S.P. Gladyshev, M.A. Grigoryev, A.N. Shishkov, A.E. Bychkov, The losses in control electric drives of transport mechanisms at different controlled laws, *SAE Technical Papers*, 2011.
- [11] Yu.S. Usinin, S.P. Gladyshev, M.A. Grigoryev, A.N. Shishkov, A.E. Bychkov, K.M. Vinogradov, Pulse vector control of wound rotor induction motor, *SAE Technical Papers*, 2010.
- [12] M.A. Grigoryev, S.I. Kinas, A mathematical model of the synchronous reluctance machine with independent control along the excitation line. *Russian Electrical Engineering*. 85(10) (2014) 645–648.
- [13] Y.S. Usinin, M.A. Grigor'ev, K.M. Vinogradov, S.P. Gladyshev, Generator for vehicle applications, based on the field regulated reluctance machine, *SAE Technical Papers*, 2008.
- [14] M.A. Grigoryev, Specifics of power circuit arrangements of semiconductor converters for power supply to synchronous reluctance machines. *Russian Electrical Engineering*. 85(10) (2014) 601–603.
- [15] Y.S. Usinin, M.A. Grigor'ev, K.M. Vinogradov, A.N. Gorozhankin, S.P. Gladyshev, The electric drive of a tram with an average floor, *SAE Technical Papers*, 2008.



International Conference on Industrial Engineering

Energoinformatics of a gearless mechatronic systems

Smirnov Y.S., Yurasova E.V., FunkT.A.*

South Ural State University, 76, Lenin Avenue, Chelyabinsk, 454080, Russian Federation

Abstract

Energoinformatics is a complex science studying energy-information exchange (interaction) in various animate and inanimate systems [1]. Its research areas include mechatronics, with its subject being computer-controlled mechanical movements [2]. A mechatronic system (MS) is a closed automatic control system (ACS) with artificial intelligence. The structural, algorithmic and dataware support provides the functioning synergistic effect manifested in increasing energy efficiency, accuracy, and resource capacity in comparison with the analogues based on electric machines of other types [3–5]. The intellectual nature of the integration of mechanical and electronic components is determined by the fact that they do not just complement each other, but constitute a unit with completely new features and options to influence the operating mechanism (OM) [6]. In turn, these properties create sufficient and necessary conditions for the microprogramming usage. In order to control electric power changes, a discrete commutation is used and combined with pulse-width modulation and variations of the commutation angle of contactless electric machines with permanent magnets (CMPMs). The development of CMPM industry helped to create gearless electromechatronic systems (GEMS).

© 2015 The Authors. Published by Elsevier Ltd. This is an open access article under the CC BY-NC-ND license (<http://creativecommons.org/licenses/by-nc-nd/4.0/>).

Peer-review under responsibility of the organizing committee of the International Conference on Industrial Engineering (ICIE-2015)

Keywords: energoinformatics; mechatronic system; synergy; intellectualization; energy efficiency; operating mechanism; gearless electromechatronic systems

1. Energy Carriers of Mechatronic Systems

When designing a MS, it should be noted that it changes the type of energy necessary for its OM functioning. It largely determines the ACS efficiency, performance and metrological characteristics. Devices with liquid (water, oil) or gases (air, nitrogen, etc.) energy carriers which are fed under pressure from a generator (a pump, a

* Corresponding author. Tel.: +7-351-267-9001.
E-mail address: urasova2004@gmail.com

compressor) to circulate in a closed system are used to design MSs. Hydraulic and pneumatic MS allow generating great force. However, they require special sources of high pressure liquid or compressed gas. Using a hydraulic drive environment protection problems because of pollution due to leakages of energy carriers [7].

When using a pneumatic actuator such problems do not occur. Pneumatic MSs occupy an intermediate position between electrical and hydraulic MSs in terms of weight horsepower. Pneumatic MSs are insensitive to radiation and temperature changes. Maintenance of pneumatic parts does not require highly skilled personnel. But there are some disadvantages: on the one hand the absence of lubrication and on the other hand the presence of water vapour in the air, with this vapour being removed with difficulty. The air movement at high velocity causes noise. In such MSs the air compressibility leads to a tendency to fluctuations that are difficult to suppress. Thus, the requirements for the personnel of pneumatic and hydraulic mechatronic units significantly increase.

The need for additional changing of thermal or electric energy with the help of a pump or a compressor reduces the MS energy efficiency. This fact along with the complexity of the interface between the microelectronic and hydraulic (or pneumatic) components slights the advantages of the liquid or gas used as an energy carrier. Electromechatronics allows solving the problem of electronization of energy changing into the OM mechanical movements to improve the electric drive (ED) [5].

2. Gearless Electromechatronics

Electromechatronic changers (EMTC) for movements are MS basic modules necessary for changing the types of energy and the forms of information into the OM functional movement. The ED traditional structure used for a similar purpose is based on digital microelectronics and computer technology. A significant increase in the ED efficiency can be achieved through its electronization. The gear excluding became a revolutionary step though gears were used in EDs over the last 200 years, and the CMPM use increases the flexibility of mechanical movement controlling. A stepping, vent, synchronous or moment electric motor or a constant current generator[8] can be used depending on the CMPM dateware level [5]. This ED is usually called direct or gearless, and in foreign technical and scientific literature it is called as «Direct drive» or «Direktantrieb» [4].

In addition to the gear excluding a further increase in the efficiency of energy changes into movements gives the process intellectual properties and the synergy inherent in mechatronics. Thus, we had to increase the level of the MS dateware up to the highest one, i.e. to its self-organization concerning not only the whole system but also its components [5]. In its turn, this self-organization demanded independent flexible changes of the techniques and algorithms of the CMPM controlling necessary for time optimization of movements and changes.

To increase the efficiency of the energy changes in CMPMs with the calibrated controlling [3–5] the digital equivalents of the movement components should be generated. Time diagrams of these components are shown in Fig. 1, where (a) is the value θ , (b) is the velocity Ω , (c) is the acceleration ε , (d) is the jump ρ .

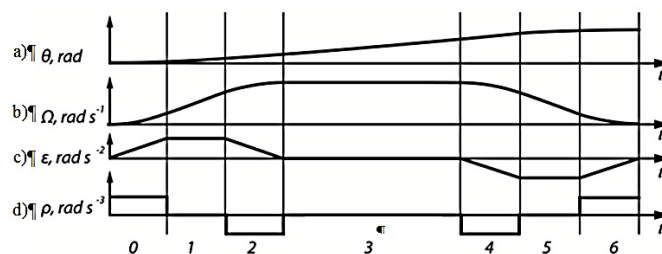


Fig. 1. Time diagrams of the movement components.

The gear excluding from precision electromechatronics is an obligatory step for any long-lasting MS operation. Simplifying its electromechanical component (EMC) leads to complicating of its microelectronic component (MEC). This is caused by the need to increase the effectiveness of structural, algorithmic and dateware support of the process of changing the energy type and information forms to control the OM functional movement.

3. Gearless Electromechatronic Systems Operating Element Selection

Applied mechatronics in most cases is based on electromechanics which is most effective for generating driving forces by changing electrical energy into mechanical energy.

The EMTC output parameters are largely determined by an operating element included in the EMC. Today due to their advantages over other electric machines, CMPMs are most widely used in GEMSs. Their use, in addition to the well-known [5] significant advantages, is preferable because of the fact that during the manufacturing process it is possible to not only exclude an unreliable and interfering unit with a sliding current collector, but also to use a winding-free rotor with high-performance magnets [9]. In Russia two series of structurally interchangeable CMPMs are manufactured: the DBM series made according to the interior permanent magnet (IPM) technology, and the DBMV series manufactured according to the surface permanent magnet (SPM) technology [5, 10, 11].

A significant advantage of the IPM technology is its mechanically strong, well-balanced rotor. Interior permanent magnets cannot fail and fall out. They are screened from external influences not only with the help of the CMPM case but also the rotor design itself. The IPM technology is a compromise between ultra-smooth and super-power CMPMs with more technological flat rare-earth magnets. They are known to be the most expensive part of CMPMs. The SPM technology typically requires less magnetic material, and particularly for powerful CMPMs. It is the SPM technology advantage. Due to the simple design and little use of magnets the SPM technology is more economical. Normally, you should seek for a compromise between production costs and technological advantages. For example, when using the IPM technology the torque caused by noise of the CMPM start is only 0.05% of the rated torque, it is much better than using the SPM technology. This advantage becomes determinant in case of high requirements to precision and movement smoothness [5, 12].

It should be noted that the GEMS high operational rates are due not only because of using high-performance CMPMs, but also because of using original devices to control them. The dateware of the energy type changes obtained by changing the analog information of movements at the primary measuring changer (PMC) output into the digital equivalents of its components plays an important role [13, 14].

4. Synthesis of Movement Components

The efficiency of a precision GEMS is improved by using a MS self-organizing structure which is based on cognitive technologies (CTs) and provides the assessment of a current situation and an ability to make an independent decision for changing the control method of the electric machine and the commutation algorithm of its windings. Thus, it is necessary to use both structural and algorithmic methods of improving the MS efficiency which is largely dependent on the level and extent of the dateware of the positioning process [5]. The creation of the local feedback of the CMPM rotor position changes its operation mode, and it operates as a vent or moment electric motor. For precision MS it is necessary to control the value, velocity and acceleration of movements, i.e. to generate its analog or digital equivalents of movement components (see Fig. 1).

The mechatronic common dateware (MCD) [15] is preferable, with the resolver in it [4, 14, 16] being used as a PMC. Its output signals contain the information about the value of the movement vector, its velocity and acceleration. It is noteworthy that the convergence of the MS nanotechnological [17] into the informational ones resulted in creating magnetic field sensors (MFSs) where unipolar or multipolar magnets are used as primary detectors [18]. These magnets affect the microelectronic elements of a secondary changer through a gap [9].

The resolver and the MFS operating in an amplitude regime has a chronotope nature, i.e. the space-time correlation [19]. The MFS calibration is performed by teaching with a precision CMPM. It uses an electromechanical resolver with electric reduction as a PMC to ensure a sufficient metrological supply when converting analog signals through a microcontroller (MC) [20].

5. Gearless Electromechatronic System Microcontrolling

The minimax strategy of the mechatronic approach made it possible to generate the GEMS structure (Fig. 2) which uses the PMC output signals of the MC in the MEC, and the EMC changes the energy varying the CMPM

means and its control algorithms in a closed system. The closure of the main and local circuits and the velocity feedback with the MCD is achieved through the *PMC* based on the resolver.

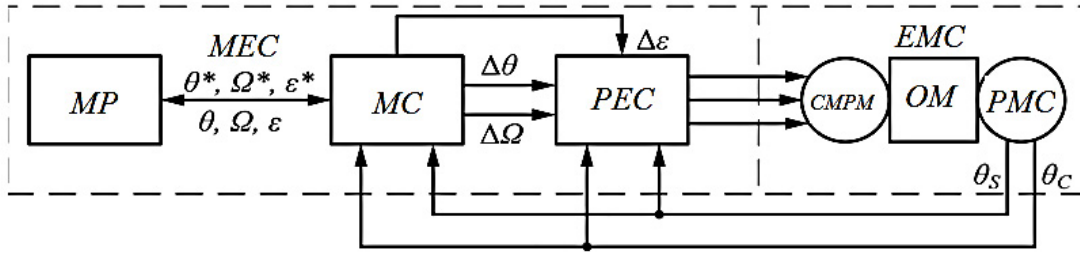


Fig. 2. GEMS. Block diagram of the microcontrolling

A microprocessor (*MP*) forms the movement trajectory caused by the *OM* by setting the moving components θ^* , Ω^* , ε^* that come into the *MC*. Thus, at its output the current values of the *OM* deviation movement are generated at $\Delta\theta$, $\Delta\Omega$ and $\Delta\varepsilon$. They arrive at the polyregime electronic commutator (*PEC*). The second inputs of *PEC* and *MC* receive quadrature signals θ_s and θ_c from the *PMC* output which contain information about the *OM* current state, its velocity and acceleration. The digital equivalents of the current values of magnitude θ , velocity Ω and acceleration ε of displacement after the formation in the *MC* and enter the *MP*.

Generation of the required values of velocity and acceleration in the *CMPM* is achieved by varying the current in the *CMPM* control winding and the angle of their commutation. "Angular advance" [5] allows compensating the electromagnetic delay that occurs in the *CMPM* control winding. This increases the rotor speed at a fixed point at the *OM* outlet.

The *CMPM* starting torque is proportional to $\sin(\gamma - \theta)$ where γ is the rotation angle of the stator vector field, and θ is the value of the rotor rotation angle averaged over the commutation period, i.e. $\psi = \gamma - \theta - 90^\circ$. The average value of the starting torque at $\psi = 0^\circ$ is more than the one at $\psi = 45^\circ$. However, with the rotor increasing velocity Ω , this ratio is reversed due to the electromagnetic delay in the *CMPM* defined with its electromagnetic time constant.

The *CMPM* mechanical characteristics with the commutation angles $\psi = 0^\circ$ and 45° are shown in Fig. 3a. It implies that when changing the neutral commutation angle in a self-organizing *CMPM* with $\psi = 0^\circ$ into the advancing one with $\psi = 45^\circ$ at the threshold velocity Ω_T , the resulting mechanical characteristics will have the starting torque value μ_{nyc} , corresponding to a neutral commutation and the idling velocity Ω_{xx} – to the advancing one.

From all points of view the most effective turned out to be the *CMPM* controlling when the commutation angle is changed simultaneously into the advancing or lagging one and the value of supply voltage through PDM with the ratio γ . The *CMPM* mechanical characteristic is $\mu = f(\gamma, \Omega)$. The controlling characteristics are shown in Fig. 3b.

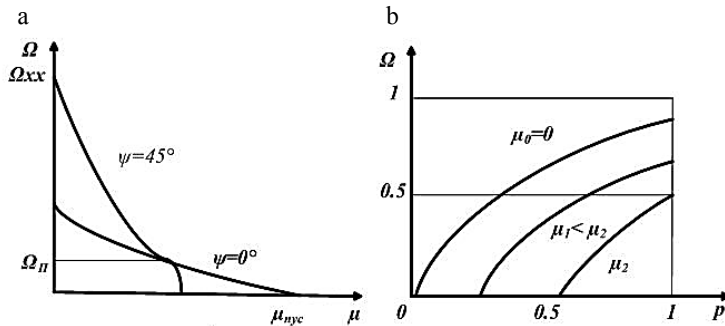


Fig. 3. The *CMPM* mechanical (a) and control (b) characteristics.

The dual *CMPM* controlling enhances smooth movement with its limiting value being reached through the quadrature controlling, with the MCD being created to provide it. The mechatronic approach to the proper MCD creating provides a quasi-harmonic commutation with the PDM being controlled by digital orthogonal components of the PEC output movement.

6. Conclusion

Having evaluated the energoinformational exchange [1] between EMC and MEC in the *CMPM* we can draw the following conclusions:

- The MCD high degree when generating digital equivalents of movements allows implementing the quasioptimal movement controlling. EMC electromechanic simplification requires a certain MEC complexity which determines the level of the MS intelligence.
- The widespread MC introduction in developments allows substituting hardware implementation of algorithmic, structural and dateware support for the appropriate software to increase the GEMS efficiency.
- The MCD high level and extent lead not only to improving the GEMS energy efficiency but also to implementing the changes in its structure depending on the movement data changes, i.e. its value or its velocity and acceleration.
- The increase of GEMS indicators is achieved when using a MS self-organizing structure that provides the CT-based assessment of a current situation and an independent decision on changing the *CMPM* controlling method and the commutation algorithm of its controlling windings.
- When self-organizing, both structural and algorithmic methods turn to be involved to increase the MS efficiency which is to a large extent dependent on the MCD level and degree of the GEMS energy changing.

References

- [1] Energoinformatic. Grand Encyclopaedia, Terra, Moscow, 2006.
- [2] Y.S. Poduraev, *Mechatronics: Fundamentals, Methods, Application*, Mashinostroenie Publishing, Moscow, 2006.
- [3] B. Drury, *The Control Techniques Drives and Controls: Handbook*, second ed., EMERSON. JET, 2009.
- [4] A. P. Balkovoy, V.K. Tsatsenkin, *Precision electric drive with brushless motor*, ID MEI, Moscow, 2010.
- [5] Yu.S. Smirnov, *Electromechatronic converters: monograph*, SUSU Publishing, Chelyabinsk, 2013.
- [6] K.A. Pupkov, V.G. Konkov, *Intelligent system*, BMSTU Publishing, Moscow, 2003.
- [7] T. Isii, I. Simoyama, Kh. Inoue, *Mechatronics*, Mir Publishing, Moscow, 1988.
- [8] Y.S. Smirnov, D.A. Katsay, T.A. Funk, Y.O. Anisimov, Information supply features of the Gearless electromechatronics converters, materials of Conference «Information Technologies in Management», St. Petersburg. (2014) 729–737.
- [9] F. Bartos, Technology of embedded magnets for brushless servo motors, *Control Engineering, Russia*, 2006.
- [10] A.G. Mikerov, V.V. Djankhotov, Developing in walking robot servodrives with PMSM, Proc. of the International symposium on industrial electronics ISIE 2006, Montreal, Canada. (2006) 2128–2133.
- [11] A.G. Mikerov, Brushless BC torque motors quality level indexes for servo drive application, Proceedings of International Conference JEEE Eurocon 2009, St. Petersburg. (2009).
- [12] F. Bartos, High-torque brushless permanent magnet motors, *Control Engineering Russia*, 2007.
- [13] V.G. Domrachev, Digital-to-analog positioning systems. *Electromechatronic converters*, Energoatomizdat Publishing, Moscow, 1990.
- [14] V.G. Domrachev, V.R. Matveevskiy, Y.S. Smirnov, *Circuitry digital converters movements*, Energoatomizdat Publishing, Moscow, 1987.
- [15] Y.S. Smirnov, Common Dateware of robotics mechatronic converters, Proc. of the Third ISMCR'93, Italy, Torino. (1993) 13–18.
- [16] Y.S. Smirnov, T.A. Kozina, P.B. Serebryakov, The Analog-Digital converters of displacement components based on electromechanical transducers, *Measuring Techniques*. 9 (2013) 40–43.
- [17] E.D. Teryaev, N.B. Filimonov, Nanomechatronics: Status, Problems and Prospects, *Mechatronics, Automation, Control*. 106(1) (2010) 2–14.
- [18] Y.S. Smirnov, T.A. Kozina, E.V. Yurasova, A.V. Sokolov, Analog-to-digital converters of the components of a displacement with the use of microelectronic sine-cosine magnetic encoders, *Measurement Technique*. 57(1) 42–46.
- [19] Science. The great theory, Issue 1: The space – it's a matter of time. Einstein. Theory of relativity, De Agostini Publishing, Moscow, 2015.
- [20] Y.S. Smirnov, E.V. Yurasova, T.A. Kozina, Multifunctional phase displacement transducer, XII Russian Meeting on the Management, Moscow, Russia. (2014) 7171–7182.



International Conference on Industrial Engineering

Calculative and experimental analysis of natural and critical frequencies and mode shapes of high-speed rotor for micro gas turbine plant

Pirogova N.S., Taranenko P.A.*

South Ural State University, 76, Lenin Avenue, Chelyabinsk, 454080, Russian Federation

Abstract

The Micro gas turbine plant (MGTP) is used for the decentralized supply to the external electric power consumers. Its nominal and heat capacity are 100 kW and 200 kW respectively. Its critical part is a rotor with the operating speed of 65,000 rpm. It consists of two subsystems: a turbocharger rotor (TCR) and a rotor of the starter-generator (SGR) connected by elastic coupling. One of the design requirements for the rotor is the absence of critical speed in the $\pm 30\%$ operating speed range.

In this article the natural and the critical frequencies of the rotor are analyzed.

Its natural frequencies evaluated for the whole rotor system and for each of the two subsystems individually. For the TCR such an assessment was obtained through the finite element method (FEM) calculation. Due to the complexity of the SGR design, its natural frequencies were estimated and proved experimentally using LMS modal analysis technology. Also a study of the influence of bearings stiffness on the natural frequencies of the rotor was conducted to identify its acceptable range.

The study of the critical speeds of the MGTP rotor was performed in two stages by calculation: an analytical and numerical solution of the test problem obtained firstly in order to confirm the accuracy of FEM calculation in the Ansys Workbench package followed by the critical speeds evaluated through the FEM calculation on solid 3D model.

Based on the obtained results, some recommendations on the design of the rotor elements are given to ensure the natural frequencies are in the restrained region.

© 2015 The Authors. Published by Elsevier Ltd. This is an open access article under the CC BY-NC-ND license (<http://creativecommons.org/licenses/by-nc-nd/4.0/>).

Peer-review under responsibility of the organizing committee of the International Conference on Industrial Engineering (ICIE-2015)

Keywords: Micro gas turbine plant, natural frequencies, natural shapes, critical frequencies, bearings stiffness, finite element method, Campbell diagram.

* Corresponding author. Tel.: +7-351-272-37-44;
E-mail address: taranenkopa@susu.ac.ru

1. Introduction

Nomenclature

MGTP	Micro gas turbine plant
TCR	Turbocharger rotor
SGR	Rotor of the starter-generator
SGR	Rotor of the starter-generator
FEM	Finite element method

Low-powered micro gas turbine plants are utilized in industrial enterprises, medical centres; on main gas lines, oil pipe lines, gas distribution stations; in power-hungry regions of Extreme North, Siberia, Far East; to replenish electrical shortage caused with natural disasters and other emergency situations.

The most important part of the MGTP is rotor; its operational frequency is 65,000 rpm. It consists of turbocharger rotor (TCR) and starter-generator rotor (SGR) connected by elastic coupling (Fig. 1).

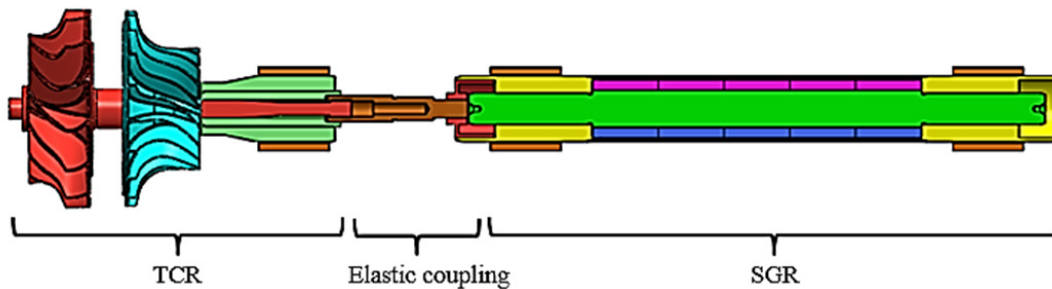


Fig. 1. The MGTP rotor

One of the requirements to high-speed rotor is exclusion of falling its critical speeds in the range of $\pm 30\%$ of operating speed (45,500–84,500 rpm) [5]. Thus, there rises an objective to develop a rotor with critical speeds, which do not fall in the prohibited range. Works [1, 2, 6, 7, 17-20] are devoted to the same matter.

2. Methods

2.1. Evaluation of natural frequencies and shapes of MGTP rotor

The evaluation is performed through the finite element method (FEM) in the package Ansys Workbench. Natural frequencies were calculated at free-free boundary conditions. Natural frequencies of bending vibrations of the rotor in the range from 0 to 120,000 rpm (2,000 Hz) are represented in table 1, frequencies and shapes of torsional and longitudinal vibrations are not considered.

As it is seen from the table 1, frequencies corresponding to the third and fourth bending shape lie in the prohibited range 45,500–84,500 rpm.

Table 1. The results of calculating natural frequencies and shapes of the MGTP rotor at its lateral vibrations

Mode number	Mode shape	Natural frequency
1 – 4		0 Hz (0 rpm)
7	First bending	78 Hz (4,692 rpm)
8		87 Hz (5,196 rpm)
11	Second bending	489 Hz (29,322 rpm)
12		499 Hz (29,910 rpm)
14	Third bending	1,165 Hz (69,900 rpm)
17		1,453 Hz (87,180 rpm)
15	Fourth bending	1,302 Hz (78,120 rpm)
16		1,378 Hz (82,680 rpm)

2.2. Evaluation of natural frequencies of MGTP rotor subsystems

To analyze natural frequencies and shapes which fell in the prohibited range it is decided to evaluate natural frequencies of TCR and SGR separately.

The evaluation of natural frequencies of the TCR rotor is performed through FEM. The first bending frequency corresponds to the shape of vibrations which is not dangerous for the TCR. The second shape of bending vibrations is the most interesting. However, the frequency, which corresponds to it, is 2,228 Hz (133,680 rpm), and it is far outside the range 45,500–84,500 rpm. Thus, TCR is characterized with rather high bending stiffness.

Due to complexity of the SGR [21] construction its natural frequencies were determined experimentally.

2.3. The experimental evaluation of natural frequencies and shapes of the SGR

In the course of the experiment the rotor was hung on flexible ropes (Fig.2). Vibration excitation was set with a hammer. The experiments took place in the module of Impact Testing of package LMS Test.Lab 13A utilizing the technology of experimental modal analysis [3]. The results of the experiment are given in table 2.

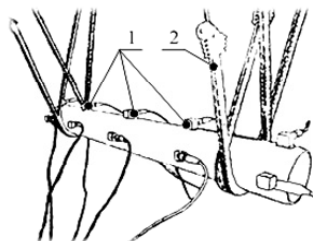


Fig. 2. The experimental unit: 1 – one-component accelerometers x10; 2 – flexible ropes x4

In accordance with the results of the experiment the equivalent model of the rotor of the starter-generator is built with natural frequencies and shapes close to the results of the experiment. The model is built by criteria of equality of masses, lengths and first natural bending frequencies of an equivalent model and its real prototype (Fig. 2) [13, 14, 15]. The results of calculation of natural frequencies on the equivalent model of the SGR are represented in table 3.

Thus, the equivalent model of the SGR is built where both first and second natural frequency and shape of bending vibrations.

Table 2. Experimental bending mode shapes and natural frequencies of SGR

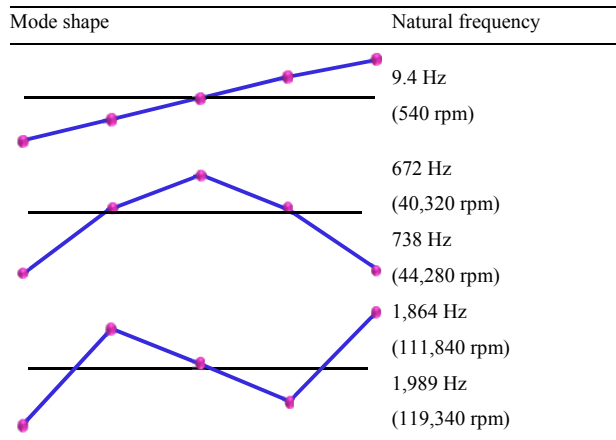


Table 3. Experimental and calculated natural frequencies of SGR

Experiment (Fig. 4, Table 2)	Equivalent rotor (FEM solution)
738 Hz	737 Hz
1,989 Hz	2,032 Hz

3. Results and discussions

3.1. The evaluation of influence of bearings stiffness on critical speeds of the rotor of MGTP

A simplified beam FEM model of the rotor (Fig.3) is arranged in the package Ansys Mechanical APDL, and calculation of critical speeds of a rotor [4] is performed in a wide range of stiffness of the assembly [16].

As calculation shows (Fig. 4), at bearings stiffness less than 10^6 N/m, flexible assemblies have almost no influence on critical speeds and shapes of the rotor, so it can be considered on free-free conditions. Thus, to meet the requirements by critical speeds it is necessary to use bearing assemblies where stiffness does not exceed 10^6 N/m.

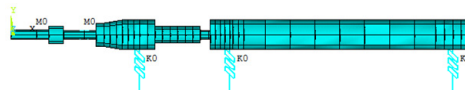


Fig. 3. Beam model of rotor for MGTP

3.2. The calculation of natural frequencies of the MGTP rotor with equivalent SGR

The calculation of natural frequencies of the MGTP rotor is performed in the condition of free hanging (which corresponds to bearings assemblies with stiffness less than 106 N/m) on considering the equivalent model of the SGR. The calculation showed that natural frequencies of the model do not correspond to the design requirements. The conclusion was made that it caused by torsional stiffness.

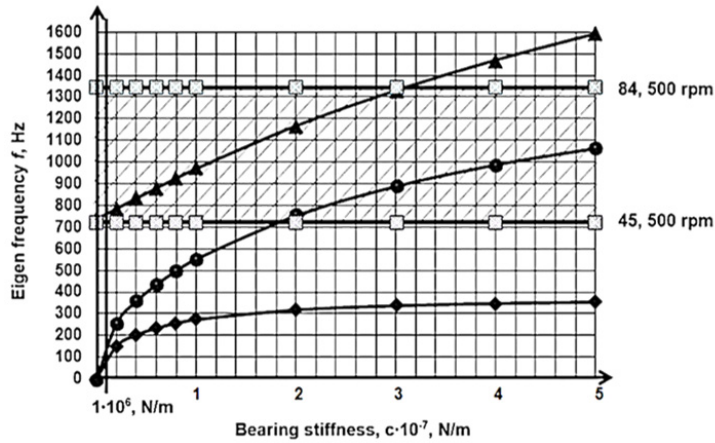


Fig. 4. Influence of bearings stiffness on critical speeds of the rotor of MGTP

The several models were suggested with various elastic connections. The best of them is a MGTP model construction where TCR and SGR are connected with a torsion bar with two membranes (Fig. 5). Natural frequencies and shapes of MGTP rotor with selected version of flexible connection and an equivalent model of SGR are represented in table 4.

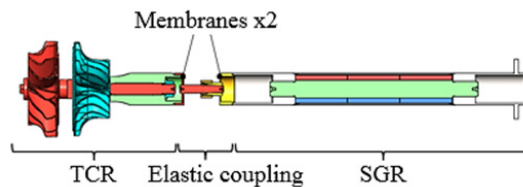


Fig. 5. Model of MGTP rotor with proposed design of elastic coupling

Table 4. Calculated natural frequencies and mode shapes of MGTP rotor

Mode number	Mode shape	Natural frequency
First Bending		51 Hz (3,079 rpm)
		52 Hz (3,129 rpm)
Second Bending		308 Hz (18,453 rpm)
		309 Hz (18,532 rpm)
Third Bending		730 Hz (43,783 rpm)
		731 Hz (43,818 rpm)
Fourth Bending		1,497 Hz (89,808 rpm)
		1,498 Hz (89,862 rpm)
Fifth Bending		1,767 Hz (105,996 rpm)
		1,767 Hz (106,014 rpm)

3.3. Evaluation of critical speeds of 3D model of the MGTP rotor

The problem was resolved through FEM calculation in Ansys Workbench package. Resulting from this solution concerning determination of critical speeds of MGTP rotor Campbell diagram was made [8, 9, 10, 11, 12] (fig. 6). The values of critical speeds of MGTP rotor are given in table 5. Comparison of the results represented in tables 4 and 5 shows that the first, second and third critical speeds of the rotor which are found taking into consideration gyroscopic moment (table 5), are by 7%, 5% and 4% higher than the corresponding natural frequencies (table 4). The calculated critical speeds of rotor (table 5) fall out of the range $\pm 30\%$ of operational speed (45,500–84,500 rpm) which meets the requirements to the construction.

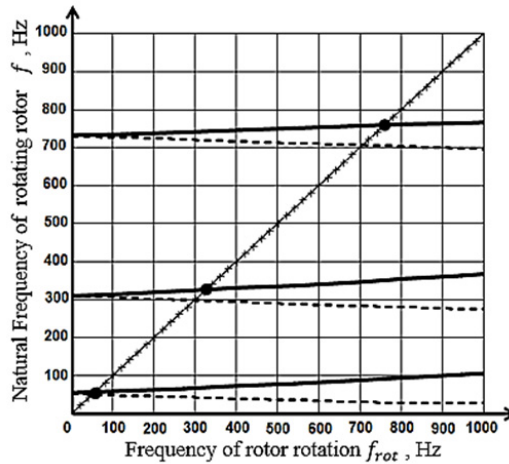


Fig 6. Campbell diagram

Table 5. Critical speeds of MGTP rotor

Number of bending mode	Direct precession	Inverse precession
1	54.4 Hz (3,263 rpm)	49.5 Hz (2,970 rpm)
2	324.2 Hz (19,450rpm)	295.8 Hz (17,746 rpm)
3	757.5 Hz (45,451 pm)	705.4 Hz (42,325 rpm)

4. Conclusion

Thus, based on calculation and experimental approach the recommendations for the construction of MGTP rotor are developed: bearings stiffness must not exceed 10^6 N/m; the rotor of turbocharger and the rotor of starter-generator must be connected with flexible element with low bending stiffness; the design of elastic connection should grant critical speeds of the rotor fall out of the range $\pm 30\%$ of operational speed (45,500–84,500 rpm).

Acknowledgements

The work was conducted with the financial support of the Ministry of Education and Science of the Russian Federation in the framework of the complex project «Establishing Production of New Generation Micro Turbine Units Range» according to the contract no. 02.G25.31.0078 d.d. 23.05.2013.

References

- [1] Y.-B. Lee, S.-B. Cho, T.-Y. Kim, C. H. Kim, T. H. Kim, Rotordynamic performance measurement of an oil-free turbo-compressor supported on gas foil bearings. The 8th IFToMM International Conference on Rotor Dynamics. (2010) 420–426.
- [2] K.-S. Kim, B.-C. Cho, M.-H. Kim, Rotordynamic characteristics of 65kw micro turbine with compliant air foil bearings. The 8th IFToMM International Conference on Rotor Dynamics. (2010) 799–803.
- [3] V. Kheylen, P. Lammens, P. Sas, Modal'nyy analiz: teoriya i ispytaniya [Modal analysis: theory and testing], Moscow Novatest Publ., Moscow, 2010.
- [4] V.L. Bidermam, Teoriya mekhanicheskikh kolebaniy, Moscow, 1980.
- [5] Normy prochnosti aviatsionnykh gazoturbinnnykh dvigateley grazhdanskoj aviatsii, Moscow, CIAM Publ., 2004.
- [6] B.A. Ponomarev, V.V. Gavrilov, Problems of making auxiliary gas turbine engines with gas bearing rotors, Bulletin of the Samara State Aerospace University. Aeronautical engineering and rocketry. 1 (2009) 41–45.
- [7] Yu.M. Temis, M.Yu. Temis, A.M. Egorov, V.V. Gavrilov, V.N. Ogorodov, Rotor in gas bearings dynamics experiment-calculated investigation, Bulletin of the Samara State Aerospace University. 3(27) (2011) 174–182.
- [8] A.G. Kostyuk, Dinamika i prochnost' turbomashin [Dynamics and strength of turbomachines], Moscow, CIAM Publ., 2004.
- [9] D.V. Khronin, Teoriya i raschet kolebaniy v dvigatelyakh letatel'nykh apparatov [Theory and calculation of oscillations in engines flight vehicles], Moscow, 1970.
- [10] Dzh.P. Den-Gartog, Mekhanicheskie kolebaniya [Mechanical oscillations], Moscow, 1960.
- [11] A.S. Kel'zon, Yu.P. Tsimanskiy, V. I. Yakovlev, Dinamika rotorov v uprugikh oporakh [Dynamics of rotors in the elastic supports], Moscow, 1982.
- [12] A. Muszynska, Rotordynamics, CRC Press, 2005.
- [13] V.I. Krylov, Priblizhennoe vychislenie integralov [An approximate calculation of integrals], Moscow, 1967.
- [14] O.K. Sliva, Metod sosredotochennykh parametrov i ego primeneniye v issledovanii kolebaniy rabochikh lopatok turbomashin [Lumped parameter method and its application in the study oscillations of rotor blades of turbomachines]: PhD dissertation. Kharkov, 1967.
- [15] P.A. Taranenko, Dinamika rotora turbokompressora na podshipnikakh skol'zheniya s plavayushchimi vtulkami [The dynamics of the turbocharger rotor on bearings with floating rings]: PhD dissertation. Chelyabinsk, 2011.
- [16] Yu.B. Nazarenko, A.Yu Potapov, Removal of critical speeds of rotors of gas turbine engines by regulating bearing stiffness.1(91) 14–16.
- [17] D. Chiang Hsiao-Wei, Hsu Chih-Neng, Jeng Wes, Tu Shun-Hsu, Li Wei-Chen, A Microturbine Rotor-Bearing System Analysis. ASME Turbo Expo 2002: Power for Land, Sea, and Air Volume 4: Turbo Expo 2002, Parts A and B Amsterdam. 4 (2002).
- [18] Hong Do-Kwan, Joo Daesuk, Woo Byung-Chul, Jeong Yeon-Ho, Koo Dae-Hyun, Ahn Chan-Woo, Cho Yun-Hyun, Performance verification of a high speed motor-generator for a microturbine generator. International Journal of Precision Engineering and Manufacturing. 14(7) 1237–1244.

- [19] T. Waumans, P. Vleugels, J. Peirs, F. Al-Bender, D. Reynaerts, Rotordynamic behaviour of a micro-turbine rotor on air bearings: modelling techniques and experimental verification, Proceedings of ISMA, 2006.
- [20] SongJu-ho, Kim Daejong, Bump-Type Foil Bearing Structural Stiffness: Experiments and Predictions, Journal of Tribology. (2007) 628–639. DOI: 10.1115/1.2736455.
- [21] N.S. Pirogova, P.A. Taranenko, Calculated-experimental analysis of the natural and critical frequencies and mode shapes high-speed of rotors micro gas turbine unit, Bulletin of the South Ural State University. Ser. Mechanical Engineering Industry,15(3) (2015) 37–47 (in Russ.).



International Conference on Industrial Engineering

Development of methods for determining the locations of large industrial goods during transportation on the basis of RFID

Provotorov A., Privezentsev D., Astafiev A.*

Russian Federation, 602264 Murom, Vladimirskaya oblast (region), Orlovskaya, 23

Abstract

Errors in products motion control lead to great financial and time treats. That's why nowadays large-scale industrial enterprises widely implement the automated monitoring systems of industrial products movement in all stages of the production process. Decisions on the monitoring systems market often allow to automate only areas where the routes are clearly defined and objects move consistently. In other areas such as product storages or shipment manual methods of monitoring objects often dominate such as visual inspection or using hand-held label readers. One of approaches to automate products motion control is a radio frequency identification one.

© 2015 The Authors. Published by Elsevier Ltd. This is an open access article under the CC BY-NC-ND license (<http://creativecommons.org/licenses/by-nc-nd/4.0/>).

Peer-review under responsibility of the organizing committee of the International Conference on Industrial Engineering (ICIE-2015)

Keywords: identification, RFID tags; manufactured product; storage area; location;

1. Formulation of a practical problem

To put a practical problem it is necessary to consider the process of transportation and storing of a typical industrial enterprise. During storage large industrial production goes through three main stages: reception to the warehouse, storage, shipment from the warehouse. The movement of industrial products is often made by bridge cranes or mobile loaders. In most cases the technique used for goods transportation is not equipped with means of position determining so the organization of products motion control at the warehouse with staff resources is unreachable. In general, the process of industrial products storage can be represented as follows (Figure 1)

* Corresponding author. Tel.: +7-9190169450.

E-mail address: alanwake@mail.ru

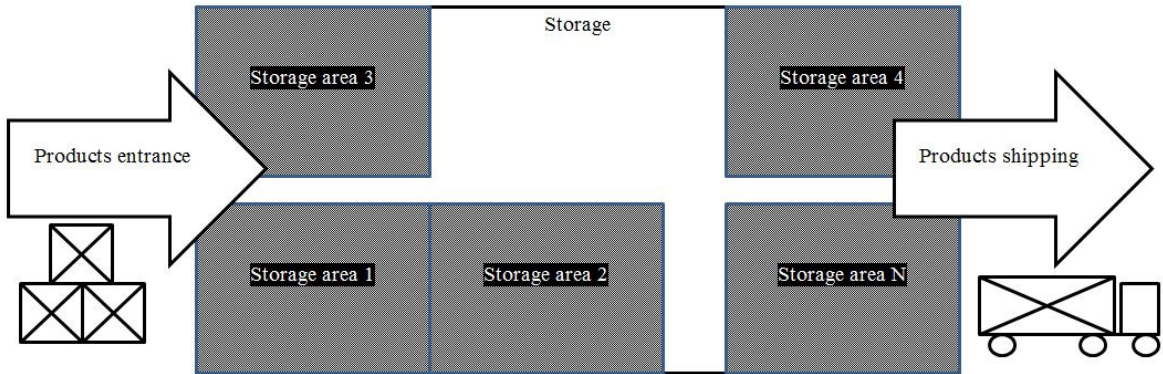


Figure 1 - industrial products storage scheme

The process of industrial products storage can be represented by the following set of operations:

- Reception of industrial products.
- Storage of goods received in storage areas.
- Shipment of industrial products.

During storage following common errors may appear:

- incorrect placement of the product on admission;
- incorrect movement between storage areas;
- shipment of incorrect product.

The appearance of such errors leads to significant time and financial treats.

So, the practical purpose of the research is to develop methods for determining the location of large industrial products during transportation on the basis of RFID and vision systems to improve the efficiency and reliability of storage.

2. Overview of analogues

Due to the fast development of RFID technology a large number of scientists are using it to solve the typical problems [4-6]. For example, a team of researchers Soo-Cheol Kim, Young-Sik Jeong, Sang-Oh Park applied RFID technology to locate a person in a building by covering him RF readers. The mobile phone serves as a label. The achievements are described in detail in the publications «RFID-based indoor location tracking to ensure the safety of the elderly in smart home environments» (2013), «An indoor location tracking based on mobile RFID for smart exhibition service» (2014) [7-9]. Another trend of RFID using is security at industrial objects. Kwangsoo Kim and Myungsik Kim scientists in «RFID-based location-sensing system for safety management» (2012) examined using of RFID tags for the dangerous areas analysis for the presence of workers there [10-11]. For example, the workers localization under the boom of the crane. Arijit Sengupta and Shu Z. Schiller scientists in «FlexRFID: A design, development and deployment framework for RFID-based business applications» (2010) used the RFID technology for automated checkpoint system where the barrier automatically receives employee ID arrived up to it and determines whether access is allowed. [12] The team of Ruey-Shun Chen, Mengru Arthur Tu and Jung-Sing Jwo

scientists in «An RFID-based enterprise application integration framework for real-time management of dynamic manufacturing processes» (2010) uses RFID for enterprise solutions building of dynamic processes management [13].

The realizability of these projects indicates that selected target can be achieved by the using of international experience and developed methods and approaches.

3. Development of methods for determining the location of large industrial products during transportation on the basis of RFID and vision systems

To automate the storage it is necessary to research two main cases in which identification is needed: products transportation to the storage area and the items capture from the storage area for onward transportation (Figure 2).

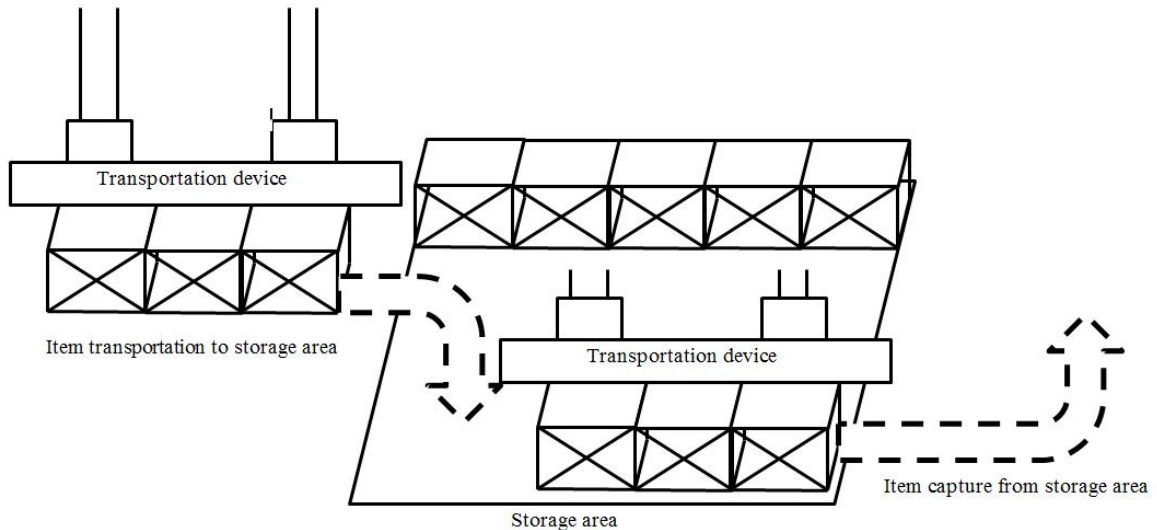


Figure 2 - operations with goods in storage area

To determine the location of large-sized industrial products during transportation it is proposed to use RFID methods. To this aim a RFID reader is mounted on conveyor device and storage areas are equipped with labels. This approach allows to determine which of the storage areas transporting device is located. The storage areas labeling scheme is shown at Figure 3.

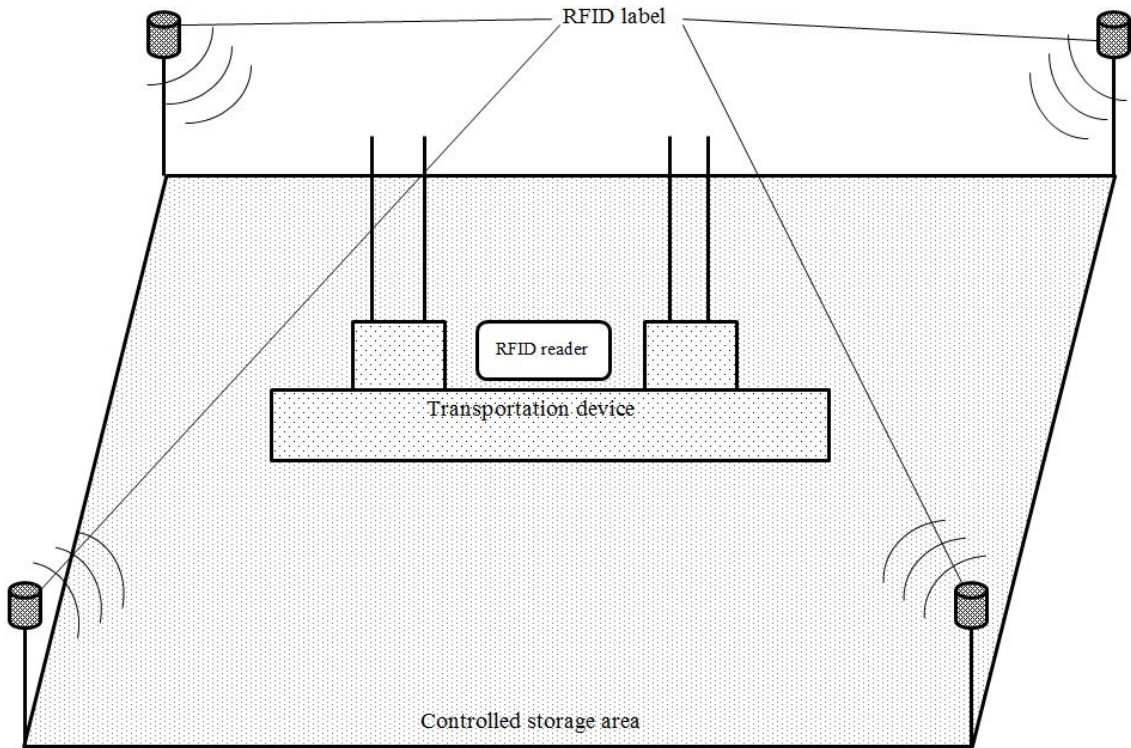


Figure 3 - storage areas labelling scheme

For the transported goods identification RFID-tags of industrial products are using what allows to determine with high accuracy which products are transporting at the moment, from which storage area and where.

4. Conclusion

During laboratory research the developed method of identification showed the 99.6% accuracy, the object identification speed is 0.3-0.7 seconds.

Currently it is planned to introduce the developed technique in the Welding workshop №3 JSC "Vyksa metallurgical factory" to control the movement of large-diameter pipes.

The developed method implementation allows to significantly reduce the speed of goods identification in transit and the number of errors associated with its incorrect movement.

References

- [1] A. Orlov, A.V. Astafjevs, A.V. Provotorov, Methodology and algorithms for automatic two-stage video identification of rolling billets, *Automation in the industry*. 10 (2013) 53–57.
- [2] A.V. Astafjevs, A.V. Provotorov, A.A. Orlov, Analysis of visual monitoring of the production process at the industrial enterprises, *Herald NSUEM*. 1 (2011) 26–32.
- [3] B.A. Alpatov, P.V. Babayan, O.E. Balashov, A.I. Stepashkin, Method of automatic detection and tracking of objects. *Image processing and management*, Radio Engineering, Moscow, 2008.

- [4] I.N. Trapeznikov, A.L. Prior, A.A. Noskov, E.A. Aminov, Combined algorithm for detecting car registration plates, *Electromagnetic waves and electronic systems*. 18(12) (2013) 32–37.
- [5] J.C. Chen, C.-H. Cheng, PoTsang B. Huang, K.-J. Wang, C.-J. Huang, T.-C. Ting. Warehouse management with lean and RFID application: a case study, *Int J Adv Manuf Technol*. 69 (2013) 531–542. DOI 10.1007 / s00170-013-5016-8.
- [6] V.V. Kumar, F.T.S. Chan, A superiority search and optimisation algorithm to solve RFID and an environmental factor embedded closed loop logistics model, *Int J Prod Res*. 49(16) (2010) 4807–4831. DOI: 10.1080 / 00207543.2010.503201.
- [7] S.-C. Kim, Y.-S. Jeong, S.-O. Park, An indoor location tracking based on mobile RFID for smart exhibition service, *J Comput Virol Hack Tech*. 10 (2014) 89–96. DOI 10.1007 / s11416-014-0200-4.
- [8] S.-C. Kim, Y.-S. Jeong, S.-O. Park, RFID-based indoor location tracking to ensure the safety of the elderly in smart home environments, *Pers Ubiquit Comput*. 17 (2013) 1699–1707. DOI 10.1007 / s00779-012-0604-4.
- [9] Jo.M. Youn, H.Y. Cha, S.-H. Choo, Mobile RFID tag detection influence factors and prediction of tag detectability, *IEEE Sens. J*. 9(2) (2009) 112–119.
- [10] K. Kwangsoo, K. Myungsik, RFID-based location-sensing system for safety management. 16 (2012) 235–243. DOI 10.1007 / s00779-011-0394-0.
- [11] L.M. Ni, Y. Liu, Y.C. Lau, A.P. Patil, Indoor location sensing using active RFID, *ACM Wireless Networks*. 10(6) (2004) 701–710.
- [12] Arijit Sengupta, Shu Z. Schiller, FlexRFID: A design, development and deployment framework for RFID-based business applications, *Inf Syst Front*. 12 (2010) 551–562. DOI 10.1007 / s10796-009-9217-5.
- [13] Ruey-Shun Chen, Mengru Arthur Tu and Jung-Sing Jwo, An RFID-based enterprise application integration framework for real-time management of dynamic manufacturing processes, *Int J Adv Manuf Technol*. 50 (2010) 1217–1234. DOI 10.1007 / s00170-010-2573-y.



International Conference on Industrial Engineering

Improvement of the automated control systems for the development of the metallurgy

Antipov K.V., Maslakov M.P., Yurenko K.I.*

North Caucasian Institute of Mining and Metallurgy (State Technological University), str. Nikolaeva 44, city Vladikavkaz, 362021, Russia

Abstract

Innovative ways and hindrance to the metallurgical industry development of Russia are identified in the article. The authors lighted the emergency situations dependence on the human and technological factors. Three-level organizational structure of the automated management and control system of production of metallurgical enterprises is described in the article. The necessity in additional smart information systems for the metallurgical enterprise automated control system to warn emergency situations is substantiated by the authors. The interplay structure of Automated Control Systems, Emergency Warning Systems and computer information management systems for the metallurgical enterprises is demonstrated in the paper. Functionality of the system and the role of its components in the Emergency Warning System (EWS) are defined in the paper. The final analysis of the research shows the way of preventing emergency situations efficiency confirmed by the positive results of the experimental studies at the joint-stock company " Electrozinc" (Vladikavkaz city).

© 2015 Published by Elsevier Ltd. This is an open access article under the CC BY-NC-ND license (<http://creativecommons.org/licenses/by-nc-nd/4.0/>).

Peer-review under responsibility of the organizing committee of the International Conference on Industrial Engineering (ICIE-2015)

Keywords: metallurgical industry; safety; emergencies; information management system the prevention of accidents.

1. Introduction

Over the last decades, Russian metallurgical enterprises are the major suppliers of steel products in the world market. The main advantage that causes the Russian metallurgical enterprises export success is in the fact that the high quality of its products satisfies the world standards requirements. Experts predict high production growth in the

* Corresponding author. Tel.: +7-904-445-46-78

E-mail address: ki-yurenko@yandex.ru

Russian metallurgical industry in 2030. The world economy forecast for the following decade assumes two scenarios of sustainable rise in production of the Russian metallurgical companies [1].

The first scenario is based on the existing enterprises principles and suggests the non-ferrous metals production growth in 2030 is able to be increased by 40% [2]. The second scenario involves the metallurgical industry innovative development that can make possible to increase the production in 2030 by more than 48%. The second scenario is definitely more efficient because it determines the long-term development of the metallurgical industry and embraces the industrial sector of economic development programs of the country [7,17]. Such programs follow both Russian and international laws in the fields of labour and environmental safety at the metallurgical enterprises. However, there are definitely some challenges on the path of innovative development of the steel industry. They are:

- facilities and equipment wear and tear high percentage;
- lack of the necessary number of highly skilled specialists;
- ore composition heterogeneity, etc.

These factors not only lead to negative economic and technical results but also cause emergencies with serious social and environmental aftereffects.

Thus, one of the key tasks of innovative development of the steel industry is to work out intellectual information management systems that improve conditions of labor and environmental safety, both within the enterprise and the surrounding areas.

In this light, the aim of our work is the development of smart information systems for improving the metallurgical enterprises enterprise Industrial control system (ICS).

2. Improvement of the metallurgical enterprise Industrial control system(ICS) along with its functionality perfection

Today, the responsibility for the technological processes management has considerably increased and management information systems (MIS) such as SCADA are partially in charge of the production safety. These systems, SCADA trace mode v.6 in particular allows them to be upgraded. This fact in its turn allows us to consider it as the most perspective way to manage in complex automated systems due to the possibility of modernization [3, 14, 15, 16].

The study of such systems have shown a tendency to reduce the accident rate at the metallurgical enterprises, caused by technical failures and accidents of growth due to the influence of the human factor, as shown in Figure 1.

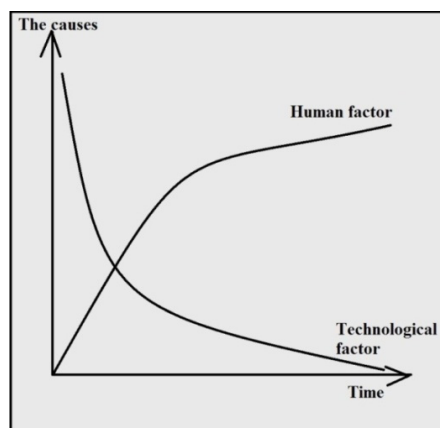


Fig. 1. Dependence of the number of accidents on the human and technological factors.

The complicity of the metallurgical enterprise technological processes management is caused by the large amount of equipment, the technological process continuity, the instability of technological parameters, etc. For this reason, the decision-making concerning the object management can be seriously hampered and its effectiveness may be reduced [4,13,18]. The key role in organizing the three-tier management process (Figure 2) plays the administrative level on the basis of the information processed by Management Information System (MIS) at the hardware and software level. It should be summarized that the used IMS do not provide personnel with the possible ways to get out of the negative situation. It is important that the interaction with the enterprise MIS system is performed by the system that processes the information from the very beginning, i.e. from the technological level and it provides emergency situations prevention.

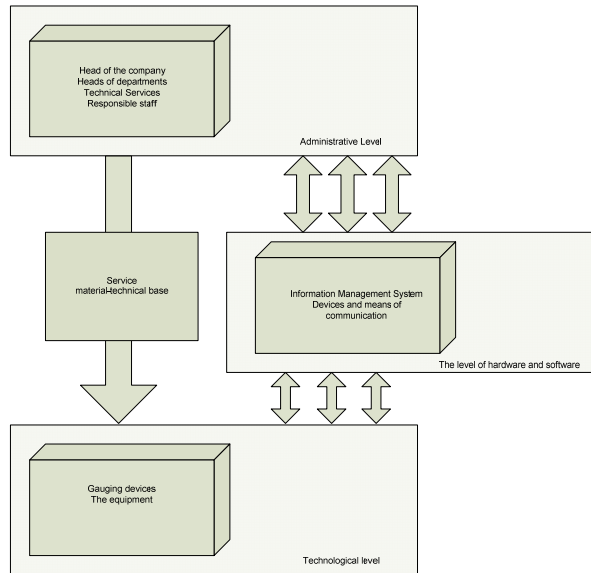


Fig. 2. Three-tier organization of the metallurgical enterprise management.

It is discovered by the authors that the principle of openness bases of SCADA Systems [19,20], allows to introduce additional modules without significant human and financial costs, designed to solve the following problems:

- Increase the economic and environmental assessment of the enterprise;
- Reduction of the environmental costs;
- Maintenance of the stable operation of equipment and chemical composition of raw materials within the standards;
- Safeguarding of the enterprise high rating on a domestic and international markets.

These tasks are proposed to be solved by the Smart Advanced Warning System (AWS) development and its integration into the ICS of the metallurgical enterprise. The generalized structure of the Technological Processes ICS and AWS is presented in Figure 3

During the AWS development process the complex man-machine systems creation experience for other industries, including the transport safety and the glass manufacture, was taken into consideration.[8,9,10,11,12]. AWS allows to evaluate current production situation and to demonstrate effective solutions connected with the impact on the technological situation, including the pre-emergency and emergency ones.

The developed AWS has smart properties and provides the substantial improvement of the overall automation of metallurgical enterprises.

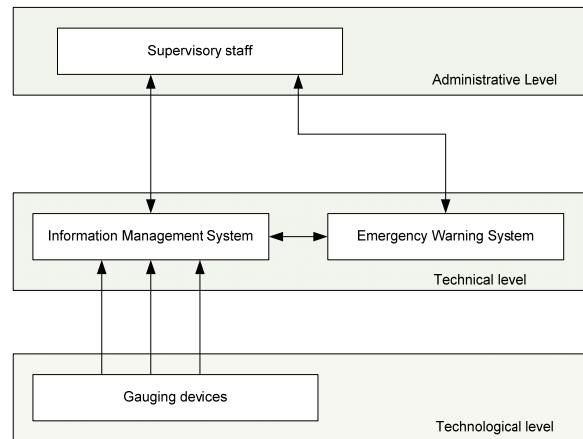


Fig. 3. Generalized structure of the metallurgical enterprise Technological Processes ICS and AWS.

AWS provides several procedures:

- Formation of the negative situations database and knowledge- base of the enterprise. Obviously, the number of negative situations can be great.

As a result, it is assumed to define more often emerging and potentially negative situations by using the checklist method. The method is based on the opinion of the expert group proposed by the authors and is discussed in the literature [5]. To evaluate the risk of each situation the critical factor is proposed [6].

- Processing of information on the basis of the AWS units such as:
 - Situation evaluation unit, which is required to determine the current production situation;
 - Situations classification unit where the situations are subdivided into classes. Each class definitely or with some priorities determines different ways to impact on the situation;
 - Preliminary decisions processing unit selects the best of several alternative solutions;
 - Decision selecting unit provides the choice of only one managerial decision to overcome the situation. The AWS algorithm and analysis of the individual AWS units are discussed in [4].

3. Conclusion (findings)

Summarizing the results of the studies it should be noted that the proposed AWS processes the technological data and then provides authorized personnel with the information. The information is then used to eliminate the negative impact of the situation and helps to reduce the number of accidents at the enterprise by 10%. This is proved by the accident rate A_v .

$$A_v = \frac{m(t)}{M(t)} \rightarrow \min, \quad \text{при } M(t) > 0 \quad m(t) < M(t), \text{ then } 0 \leq A_v \leq 1, \quad (1)$$

where $m(t)$ - the number of accidents caused by violations of technological regime in the definite period of time t ($m(t) \geq 0$); $M(t)$ - the total number of negative situations in the same period of time t .

The obtained results effectiveness is confirmed by the experimental research carried out at the JSC "Electrozinc" (Vladikavkaz). As a result of experimental works in the first half of 2015, the accident rate A_v in the zinc leaching area was 0.034, it is by 9.8% less than during the same period of the previous year when AWS was not used.

AWS provides the significant economic impact, mainly due to the decrease of emergency situations, reducing staff and time for repair and restoration of the management technical facilities. AWS also provides the improvement of the ecology in the areas surrounding the enterprise.

Obviously, ICS for metallurgical enterprises obtaining the functions of AWS will be widely used not only at the so called "dangerous industrial enterprises" but in the transport industry in order to create new on-board systems for safe locomotives management and control.

Acknowledgements

This article is based on the results of the experimental data obtained while working on the project Russian Foundation for Basic Research (RFBR) № 15-37-50393 (The contest of young scientists' research projects carried out under the supervision of PhDs at the scientific organizations of the Russian Federation).

References

- [1] Forecast of long-term socio-economic development of the Russian Federation for the period up to 2030. Information on http://www.consultant.ru/document/cons_doc_LAW_144190/?frame=9.
- [2] Order of the Ministry of Industry and Trade of the Russian Federation "On utver-Suppress the strategy of development of ferrous metallurgy of Russia for 2014 - 2020 and on the trans-prospects to 2030 and the Development Strategy of nonferrous metallurgy of Russia for 2014 - 2020 and in the future up to 2030 "from 05.05.2014g.
- [3] Y. Artiushin, I.Y. Svyatenko, I.M. Teterin, N.G. Topolsky, Analysis of the activities of operators of automated control systems in crisis situations Megapay-foxes, Technology technospheric bezopasnosti: (e-zine). 5(27) (2009). <http://agps-2006.narod.ru/ttb/2009-5/13-05-09.ttb.pdf>.
- [4] K. Antipov, B.D. Khastsaev, Development subsystem warning avaryinyh B ations in the leaching of zinc // Technology technospheric bezopasnosti (electron-throne Journal). 6(46) (2012). <http://ipb.mos.ru/ttb/2012-6/2012-6.html>.
- [5] Guidance documents 03-418-0. Guidelines for risk analysis of hazardous production facilities. Resolution Gosgortekhnadzor Russia on July 10, 2001 N 30.
- [6] K. Antipov, Application subsystem emergency warning system in situatsiy-me control the leaching of zinc // Sustainable razviti-e mountain territory. 2(16) (2013) 57–62.
- [7] Resolution of the Government of the Russian Federation "On approval of the state-term program" The development of industry and increase its competitiveness ", 2014.
- [8] K.I.Yurenko, A.N. Abaykin, Architecture and features of the implementation of the system is removed-term monitoring of a technical condition of the new generation of locomotives, Bulletin of the Russian Research and Design Institute of electric locomotive "VELNII". 2(60) (2010) 82–88.
- [9] K.I. Yurenko, E.I. Fandeyev, Hardware-software complex for modeling and automated train control, Math. Universities. North Caucasus region. Technical science. 2 (2012) 26–31.
- [10] M.P. Maslakov, N.A. Kotov, Simulation of processes in the glass industry in order to identify emergencies, Technology technospheric security (e-zine). 3(31) (2010).
- [11] A.G. Dedegkaev, M.P. Maslakov, Modeling process of glass-foot manufacturing modified Petri nets (for example, of "Irtsteklo"), Sustainable development of mountain areas. 4(14) (2012) 35–39.
- [12] R. Machado, M. Anderson, Emergency Situations in Nightclubs: A Discussion on How to Improve the Fire Safety Strategies Through The Use of Evacuation Modeling Analysis, 2011.
- [13] N.N. Radaev, S.I. Borid'ko, Effectiveness indicators for measures taken to decrease the risk of emergency situations at potentially dangerous objects Atomic Energy. 100(6) (2006).
- [14] I. Garitano, R. Uribeetxeberria, U. Zurutuza, A Review of SCADA Anomaly Detection Systems, 2011.
- [15] L. Guoling, Y. Zhenyu, J. Wenfeng, A Method of Remote Interactive Control in Electricity SCADA System Based on Internet Advances in Mechanical and Electronic Engineering, 2012.
- [16] N. Mayadevi, S. Ushakumari, S.S. Vinodchandra, Erratum to: SCADA-based Operator Support System for Power Plant Equipment Fault Forecasting Journal of The Institution of Engineers (India): Series B, 2015.
- [17] O.S. Sukharev, E.N. Strizhakova, Industrial policy and development priorities of Russian industrial systems. 15(252) 2014.
- [18] D.V. Nemchinov, O.M. Protalinsky, Reducing the risk of emergencies at the production facility. Management, Computer Science and Informatics. ASTU. 1 (2009).
- [19] Piotr Bazydło, Roman Szewczyk, Integrated SCADA Checkweigher System, Measuring Techniques and Systems. 3 (2015).
- [20] Ryszard Jakuszewski, Programming of Industrial Object Simulators in Proficy HMI/SCADA iFIX System Man-Machine Interactions 3, Advances in Intelligent Systems and Computing. 242 (2014).